ANNUAL ISSUE 2009

PROGRESS IN PHYSICS

"All scientists shall have the right to present their scientific research results, in whole or in part, at relevant scientific conferences, and to publish the same in printed scientific journals, electronic archives, and any other media." — Declaration of Academic Freedom, Article 8

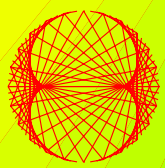

ISSN 1555-5534

The Journal on Advanced Studies in Theoretical and Experimental Physics, including Related Themes from Mathematics

PROGRESS IN PHYSICS

A quarterly issue scientific journal, registered with the Library of Congress (DC, USA). This journal is peer reviewed and included in the abstracting and indexing coverage of: Mathematical Reviews and MathSciNet (AMS, USA), DOAJ of Lund University (Sweden), Zentralblatt MATH (Germany), Scientific Commons of the University of St. Gallen (Switzerland), Open-J-Gate (India), Referativnyi Zhurnal VINITI (Russia), etc.

To order printed issues of this journal, contact the Editors. Electronic version of this journal can be downloaded free of charge:
http://www.ptep-online.com
http://www.geocities.com/ptep_online

Postal address

Chair of the Department
of Mathematics and Science,
University of New Mexico,
200 College Road,
Gallup, NM 87301, USA

This journal is powered by LaTeX

A variety of books can be downloaded free from the Digital Library of Science:
http://www.gallup.unm.edu/∼smarandache

ISSN: 1555-5534 (print)
ISSN: 1555-5615 (online)

Standard Address Number: 297-5092
Printed in the United States of America

JANUARY 2009 **VOLUME 1**

CONTENTS

Information for Authors and Subscribers

Progress in Physics has been created for publications on advanced studies in theoretical and experimental physics, including related themes from mathematics and astronomy. All submitted papers should be professional, in good English, containing a brief review of a problem and obtained results.

All submissions should be designed in LaTeX format using *Progress in Physics* template. This template can be downloaded from *Progress in Physics* home page http://www.ptep-online.com. Abstract and the necessary information about author(s) should be included into the papers. To submit a paper, mail the file(s) to the Editor-in-Chief.

All submitted papers should be as brief as possible. We usually accept brief papers, no larger than 8–10 typeset journal pages. Short articles are preferable. Large papers can be considered in exceptional cases to the section *Special Reports* intended for such publications in the journal. Letters related to the publications in the journal or to the events among the science community can be applied to the section *Letters to Progress in Physics*.

All that has been accepted for the online issue of *Progress in Physics* is printed in the paper version of the journal. To order printed issues, contact the Editors.

This journal is non-commercial, academic edition. It is printed from private donations. (Look for the current author fee in the online version of the journal.)

The "Scattering of the Results of Measurements" of Processes of Diverse Nature is Determined by the Earth's Motion in the Inhomogeneous Space-Time Continuum. The Effect of "Half-Year Palindromes"

Simon E. Shnoll

Institute of Theor. and Experim. Biophysics, Russian Acad. of Sciences, Pushchino, Moscow Region, 142290, Russia
and Department of Physics, Moscow State University, Moscow 119992, Russia

E-mail: shnoll@mail.ru; shnoll@iteb.ru

As obtained in this experimental research, the sequence of the shapes of histograms (the spectra of the amplitudes of fluctuations), measured during an astronomical day from 6 h to 18 h of the local time, is very similar (with high precision of probability) to the sequence of the histogram shapes obtained during an astronomical night from 18 h to 6 h of the local time a half of year later in exact. We call the effect that the sequences of the histogram shapes in the same half of day measured a half of year later are similar after inversion the "effect of half-year palindromes". This means that the shapes of histograms are stable characteristics of a given region of space.

In the previous work [32], we considered the phenomenon of "palindromes", which stands for a high probability of similar histograms to be found upon comparison of two data series: first, representing the results of measurements of ^{239}Pu α-decay over astronomical day (since 6 to 18 h by local, longitude, time) and, second, measured over astronomical night (since 18 to 6 h, in continuation of the first series) and *inverted*. "Inverted" means that the order of histograms in the second series is reversed. The palindrome effect implies that (1) the shape of histograms depends on the spatial region passed by the axially rotating Earth over the period of measurements, and (2) the properties of this spatial region are not shielded by the Earth: whether in the daytime or nighttime, the histograms corresponding to the same spatial region are similar. In the course of the Earth's motion along the circumsolar orbit, i.e., upon its translocation into new spatial regions, histogram shapes change; the effect of palindromes, however, will manifest itself every new day.

A remark *It should be stressed that the shape of histograms depends on many factors: rotation of the Earth about its axis; motion of the Earth along the sircumsolar orbit; relative positions of the Earth, Moon and Sun; axial rotation of the Sun; motion of the Moon along the circumterrestrial orbit. In the past years, we revealed and described, more or less, most of these factors. It seems there is an hierarchy of causes (factors) that determine histogram shape. Among them, the axial rotation of the Earth and, correspondingly, the near-day periods in the change of histogram shapes are of primary importance. Because of such a multifactorness, the number of histogram shapes related to the effect of any single factor may amount to only a part of the total. In the case of palindrome effects, for example, this number is about 15–20% of the total possible shapes.*

As supposed by M. N. Kondrashova, the palindrome effect should also be revealed upon comparing histograms that have a half-year interval between them, i.e., histograms that correspond to the measurements made when the Earth was at the opposite ends of a diameter of the circumsolar orbit [33]. This supposition agrees with our earlier observation on similarity between the series of daytime histograms obtained on the days of vernal equinox and the series of nighttime histograms taken in the periods of autumnal equinox. However, in those experiments the "daytime" and "nighttime" terms were not associated with the rotational and translational motion of the Earth about its axis and along the circumsolar orbit, so the results were poorly reproducible. With the terms "daytime" and "nighttime" strictly defined (since 6 to 18 h and since 18 to 6 h by local time, respectively), the supposition was proved for different seasons, equinoctial periods and solstices. The daytime series of vernal equinox, for example, are highly similar to the inverse daytime and noninverse nighttime series of autumnal equinox.

Thus, there are "half-day" and "half-year" palindrome effects. This is illustrated in Figure 1.

The effect of "half-day" palindromes consists in the high probability of a series of nighttime histograms to be similar to the *inverse* series of daytime histograms measured on the same day (equally, noninverse daytime series are similar to the inverse nighttime ones). For example, the sequence "1-2-3-4-5" of the series of nighttime histograms is similar to the sequence "5-4-3-2-1" of the series of daytime histograms.

The effect of "half-year" palindromes results from the Earth's motion at two opposite points of the circumsolar orbit being directed oppositely during the same half of the day. This effect consists in the high probability of a series of nighttime histograms at a certain point of the circumsolar orbit to be similar to the *noninverse* series of daytime histograms at the opposite point of the orbit (the same holds true upon comparing a nighttime (daytime) series to the inverse nighttime (daytime) series at the opposite point of the orbit).

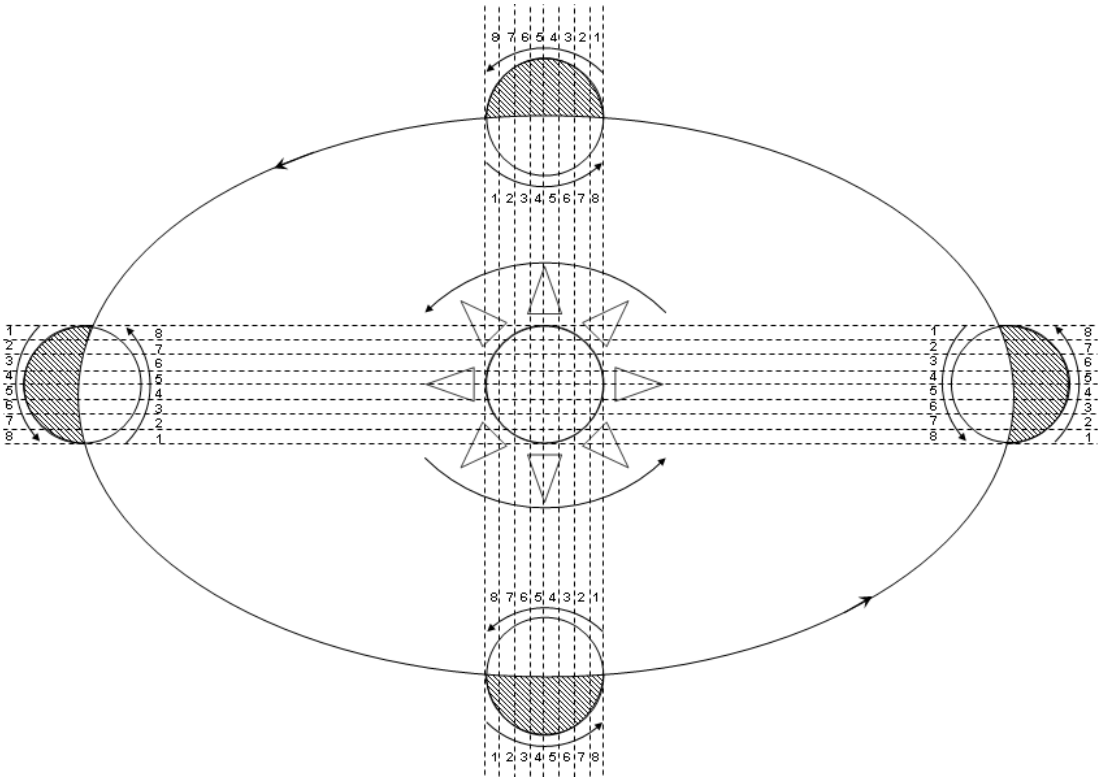

Fig. 1: A scheme illustrating "palindrome effects". With the Sun in the centre, the scheme shows four positions of the Earth on the circumsolar orbit. Both the Earth and the Sun are rotating counterclockwise; motion of the Earth along the circumsolar orbit is counterclockwise as well. As seen in the Figure, the Earth's rotational motion in the nighttime is co-directional to its motion along the circumsolar orbit and to rotation of the Sun. In the daytime, the direction of these motions is opposite. Hence, in the case of "backward" motion (in the daytime), the object measured passes in the inverse order the same spatial regions that it has passed in the direct order in the nighttime.

The half-year palindromes indicate, first of all, that certain features of the space continuum keep for a long time: after half a year we observe similar histograms. Obviously, a daytime picture of the stellar sky will correspond to the nighttime one after six months. The daytime series resembling the nighttime ones after half a year also means that the factors determining the shape of histograms are not shielded by the Earth.

As follows from these effects,

(1) the shape of histograms does not depend on the direction that a spatial region is scanned in during the Earth's motion (from right to left or vice versa);

(2) factors that determine histogram shape are not shielded by the Earth: both in the day- and nighttime, series of histograms turn out similar and dependent only on the region (vector) of space passed by the object measured at that moment;

(3) the shape of histograms is determined by the spatial regions being scanned in the course of rotational and translational motion of the Earth; in other words, the shape of histograms is a specific characteristic, which reflects peculiarities of the spatial region scanned during the measurement.

The fine structure of histograms resembles interferrential pictures [3–5, 15–17, 25]. This analogy may have a real significance: every spatial region is a result of interference of many gravitational waves, and the interferrential picture emerging can be reflected somehow in the shape of histograms.

Discovering the half-year palindromes, in addition to the half-day ones, allows us to consolidate all the previous findings and unify our views on the phenomenon of "macroscopic fluctuations", which stands for regular changes in the fine structure of sampling distributions (histograms) calculated from the results of measurements of processes of diverse (any) nature [2–16].

Now there is a good explanation for the high probability of a certain histogram shape to appear regularly, on a daily and yearly basis. The similarity of histograms obtained at different geographical points at the same local time becomes evident too.

As follows from all the data collected, our old conclusion — that alterations in the histogram shape are caused by the motion of the object studied along with the rotating and translocating Earth relatively to the "sphere of fixed stars" ("siderial day" and "sidereal year" periods) and the Sun ("solar day" and "near-27-day" periods) — is correct. The shape

of histograms also depends on motion of the Moon about the Earth and changes in the relational positions of the Earth, Moon and Sun [10, 23–29]. Supplemented with the results of experiments, in which α-activity was measured with a collimator-based setup [24, 26–28], these data indicate, on the one hand, a sharp anisotropy of our world and, on the other hand, a relative stability of characteristics of the space continuum.

Discussion

In some way, the data presented above can be considered as a completion of the series of experiments that was started more than 50 years ago (the first paper was published in 1958 [1]). Over this period, the results obtained have been reviewed several times, and all the necessary references are provided in the correspondent reviews [3, 4, 12, 14, 15, 17, 25, 31]. Nevertheless, a brief consideration of the course of those studies would not be out of place.

The subject of this series of experiments was, basically, the "scatter of results", which will inevitably accompany any measurements. For most scientific and practical purposes, this "scatter" is a hindrance, impeding accurate evaluation of the parameters measured. To overcome undesirable influence of data scattering, researchers use a well-known and widely approved apparatus of statistical analysis, specifically designed to process the results of measurements. Different processes (of different nature) will be characterized by their own specific amplitude of data scattering, and they have even been classified according to this attribute. In biological processes, for example, the scatter (its mean-square estimate) can reach tens percent of the value measured. In chemical reactions, the scatter — if not resulted from trivial causes — would be smaller and amounts to several percent. In purely physical measurements, the scatter can be as small as several tenth or hundredth percent. There is a saying, popular in the scientific circles, that "biologists measure 'bad' processes with 'bad' devices, chemists measure 'bad' processes with 'good' devices, and physicists measure 'good' processes with 'good' devices". In fact, the relative amplitude of this unavoidable scatter of results is determined by deep causes, and among them is the subjection of the quantities (objects) measured to cosmophysical regularities. In this sense, the figurative "bad-good" assessment of natural processes changes its sign: the "best" (most sensitive) are biological processes; chemical processes are "somewhat worse"; and "much worse" (least sensitive) are processes like quantum generation or natural oscillations of piezoelectric quartz. From this viewpoint, a valuable and important process to study is radioactive decay, in which relative dispersion is equal, according to Poisson statistics, to $\sqrt{N}$, where N is the quantity measured.

Free of trivial errors, the scatter of the results of measurements has, usually, a purely stochastic character and, hence, will be described by a smooth, monotonously decreasing at both ends distribution, like Gaussian or Poisson functions. In reality, however, never do experimenters obtain such a smooth distribution. Whether the experimental distribution fits a theoretical one is decided by applying fitting criteria based on central limit theorems. These criteria are integral; they neglect the fine structure of distributions, which is considered casual.

The main result of our works consists in proving non-randomness of the fine structure of sample distributions (i.e., histograms) constructed with the highest possible resolution. The proof is based on the following facts:

1. There is a high probability that at the same place and time, the fine structure of distributions obtained for different, independent processes will be similar;
2. The phenomenon is universal and independent of the nature of the process studied. Whether biochemical reactions or radioactive decay — if measured at the place and time, they will show similar histograms;
3. There exists a "near-zone effect", meaning that neighbour histograms calculated for non-overlapping segments of a time series of the results of measurements would be more similar than random far-apart histograms;
4. In the course of time, the shape of histograms changes regularly: similar histograms appear with periods equal to the sidereal and solar days, "calendar" and "sidereal" years [21];
5. At the same local time, similar histograms will appear at different geographical points: this is a so-called "effect of local time". This phenomenon was observed at both large and small distances between the objects measured. "Large distances" means that the measurements were carried out in different countries, in the Arctic and Antarctic, and on the board of ships sailing round the world. "Small distances" can be as short as 10 cm, as in V. A. Pancheluga's experiments with noise generators [27–30];
6. The "palindrome effects" discussed here and in the previous work [32] round off the set of proofs.

All these pieces of evidence were collected in the experiments with quite stochastic, according to the accepted criteria, processes.

The high quality of the apparatus for continuous, 24-hour measurements of α-activity constructed by I. A. Rubinstein enables us to collect long, non-non-interrupted data series for many years. On the basis of these data, accurate evaluation of the yearly periods has been made. A key step was conducting long-term measurements with I. A. Rubinstein's collimator-equipped detectors, which isolated beams of α-particles emitted in certain directions. Those experiments gave evidence that the shape of histograms depends on the spatial vector of the process. The sharpness of this dependence implies a sharp

anisotropy of the space continuum [20, 22, 25].

In addition to the effects listed above, we have also found regularities that have been attributed to the relative positions of the Earth, Moon and Sun [10, 23, 26, 28, 32].

The whole set of these results is in agreement with the scheme in Figure 1.

Thus, the regularities found in the "scatter of results" of various measurements reflect important features of our world. The fine structure of histograms — spectra of amplitudes of fluctuations of the results of measurements of processes of diverse nature — is the characteristic of the inhomogeneous, anisotropic space-time continuum.

Acknowledgements

I am very much obliged to M. N. Kondrashova and V. P. Tikhonov for valuable discussions, psychological and financial support. I thank I. A. Rubinstein and V. A. Pancheluga for fruitful collaboration and joint research. I express sincere gratitude to my colleagues from the Department of Biophysics of Physical Faculty of Moscow State University (Head of the Department, Prof. V. A. Tverdislov) and from the Laboratory of Physical Biochemistry at the Institute of Theoretical and Experimental Biophysics RAS (Head of the Laboratory, Prof. D. P. Kharakoz). Many thanks to D. D. Rabounski for valuable discussions and comments on the text of our manuscripts. I am also grateful to Director of the Institute of Theoretical and Experimental Biophysics RAS, Corresponding Member of Russian Academy of Sciences G. R. Ivanitsky for his everlasting patience and goodwill.

I thank T. A. Zenchenko and K. I. Zenchenko for their help in conducting measurements and maintaining a computer archive of experimental results.

Submitted on September 08, 2008
Accepted on September 19, 2008

References

1. Shnoll S.E. On the self-arbitrary transits in the molecules of actomysine from one state into another tate in the solution. *Trans. Med. Chem.*, 1958, v. 4, no. 6, 443–454.
2. Shnoll S.E., Namiot V.A., Zhvirblis V.E., Morozov V.N., Temnov A.V., and Morozova T.Ya. Possible common nature of macroscopic fluctuations of the rates of biochemical and chemical reactions, electrophoretic mobility of the cells and fluctuations in measurements of radioactivity, optical activity and flicker noise. *Biophysics*, 1983, v. 28(1), 164–168.
3. Shnoll S.E. Discrete amplitude spectra (histograms) of macroscopic fluctuations in processes of various nature. *Itogi Nauki i Techniki*, *Molecular Biology Series*, ed. V. P. Skulachev, 1985, v. 5, Moscow, VINITI, 130–200.
4. Udaltzova N.V., Kolombet V.A., and Shnoll S.E. A possible cosmophysical origin of macroscopic fluctuations in various processes. Puschino, ONTI NtsBI, 1987.
5. Shnol S.E., Udaltzova N.V., Bodrova N.B. The possible gravitational nature of factor influensing discrete macroscopic fluctuations. In: *Proc. First Intern. Congress on Geo-cosmic Relations*, Wageningen, Netherlands, 1989.
6. Udaltzova N.V., Kolombet V.A. and Shnol S.E. The possible gravitational nature of factor influensing discrete macroscopic fluctuations. In: *Proc. First Intern. Congress on Geo-cosmic Relations*, Wageningen, Netherlands, 1989, 174–180.
7. Shnol S.E., Udaltzova N.V., and Bodrova N.B. Macroscopic fluctuations with discrete structure distributions as a result of universal causes including cosmophysical factors. In: *Proc. First Intern. Congress on Geo-cosmic Relations*, Wageningen, Netherlands, 1989, 181-188.
8. Shnoll S.E. Correlation of the shape of macroscopic fluctuations amplitude spectra with position of the Moon relative to the horizon. *Biophysics*, 1989, v. 34(5), 911–912.
9. Shnoll S.E., Udaltsova N.V., Kolombet V.A., Namiot V.A., and Bodrova N.B. Patterns in the discrete distributions of the results of measurements (cosmophysical aspects). *Biophysics*, 1992, v. 37(3), 378–398.
10. Shnoll S.E. The form of the spectra of states realized in the course of macroscopic fluctuations depends on the rotation of the Earth about its axis. *Biophysics*, 1995, v. 40(4), 857–866.
11. Shnoll S.E., Agulova L.P., Zaikin A.N., Zenchenko T.A., Pozharskii E.V., and Konradov A.A. On the similarity of histograms fine structure for synchronized time series of different nature processes at different locations. *Annales Geophysicae*, Supplement 1 to Volume 16 Part 1 Society Symposia, Solid Earth Geophysics & Geodesy, 1998, C312.
12. Shnoll S.E., Kolombet V.A., Pozharski E.V., Zenchenko T.A., Zvereva I.M., and Konradov A.A. Realization of discrete states during fluctuations in macroscopic processes. *Physics-Uspekhi*, 1998, v. 162(10), 1129–1140.
13. Shnoll S.E., Pozharski E.V., Zenchenko T.A., Kolombet V.A., Zvereva I.M., Konradov A.A. Fine structure of distributions in measurements of different processes as affected by geophysical and cosmophysical factors. *Phys. Chem. Earth A*, 1999, v. 24, no. 8, 711–714.
14. Shnoll S.E., Zenchenko T.A., Zenchenko K.I., Pozharski E.V., Kolombet V.A., and Konradov A.A. Regular variation of the fine structure of statistical distributions as a consequence of cosmophysical agents. *Physics-Uspekhi*, 2000, v. 43(2), 205–209.
15. Shnoll S.E. Discrete distribution patterns: arithmetic and cosmophysical origins of their macroscopic fluctuations. *Biophysics*, 2001, v. 46(5), 733–741.
16. Shnoll S.E., Zenchenko T.A., Zenchenko K.I., Fedorov M.V., and Konradov A.A. The non-random character of fine structure of various measurement result distributions as a possible consequence of cosmophysical and arithmetical causes. *Gravitation & Cosmology*, 2002, v. 8, Supplement, 231–232.
17. Shnoll S.E. Paradoxes and problems of the interpretation of the acroscopic fluctuations phenomenon. *Russian Chem. J.*, 2002, v. 46, no. 3, 3–8.
18. Fedorov M.V., Belousov L.V., Voeikov V.L, Zenchenko T.A., Zenchenko K.I., Pozharski E.V., Konradov A.A., and

Shnoll S.E. Synchronous changes in dark current fluctuations in two separate photomultipliers in relation to the Earth's rotation. *Astrophysics & Space Science*, 2003, no. 1, 105–112.

19. Shnoll S.E., Rubinstein I.A., Zenchenko K.I., Zenchenko T.A., Konradov A.A., Shapovalov S.N., Makarevich A.V., Gorshkov E.S., and Troshichev O.A. Dependence of "macroscopic fluctuations" on geographic coordinates (by the data of Arctic and Antarctic expeditions). *Biophysics*, 2003, v. 48(5), 1123–1131.
20. Shnoll S.E., Zenchenko K.I., Berulis I.I., Udaltsova N.V., Zhirkov S.S., and Rubinstein I.A. The dependence of "macroscopic fluctuations" on cosmophysical factors. Spatial anisotropy. *Biophysics*, 2004, v. 49(1), 129–139.
21. Shnoll S.E., Zenchenko K.I., and Udaltsova N.V. Cosmophysical effects in the structure of daily and yearly periods of changes in the shape of histograms constructed from the measurements of 239-Pu alpha-activity. *Biophysics*, 2004, v. 49, Suppl. 1, 155–164; arXiv: physics/0504092.
22. Shnoll S.E., Zenchenko K.I., Berulis I.I., Udaltsova N.V., and Rubinstein I.A. Fine structure of histograms of alpha-activity measurements depends on direction of alpha particles flow and the Earth rotation: experiments with collimators. arXiv: physics/0412007.
23. Shnoll S.E., Zenchenko K.I., Shapovalov S.N., Gorshkov E.S., Makarevich A.V., and Troshichev O.A. The specific form of histograms presenting the distribution of data of alpha-decay measurements appears simultaneously in the moment of New Moon in different points from Arctic to Antarctic. arXiv: physics/0412152.
24. Shnoll S.E., Rubinshtejn I.A., Zenchenko K.I., Shlekhtarev V.A., Kaminsky A.V., Konradov A.A., and Udaltsova N.V. Experiments with rotating collimators cutting out pencil of alpha-particles at radioactive decay of Pu-239 evidence sharp anisotropy of space. arXiv: physics/0501004; *Progress in Physics*, 2005, v. 1, 81–84.
25. Shnoll S.E. Changes in fine structure of stochastic distributions as a consequence of space-time fluctuations. *Progress in Physics*, 2006, v. 2, 39–45.
26. Shnoll S.E. and Panchelyuga V.A. On the characteristic form of histograms appearing at the culmination of Solar eclipse. arXiv: physics/0603029.
27. Kaminsky A.V. and Shnoll S.E. The study of synchronous (by local time) changes of the statistical properties of thermal noise and alpha-activity fluctuations of a 239-Pu sample. arXiv: physics/0605056.
28. Shnoll S.E. and Pancheluga V.A. Cosmo-physical effects in the time series of the GCP network. arXiv: physics/0605064.
29. Panchelyuga V.A., Kolombet V.A., Pancheluga M.S., and Shnoll S.E. Local-time effect on small space-time scale. In: *Space-Time Structure*, collected papers, Moscow, Tetru, 344–350.
30. Panchelyuga V.A., Kolombet V.A., Pancheluga M.S., and Shnoll S.E. Experimental investigation of the existence of a local-time effect on the laboratory scale and the heterogenety of space-time. *Progress in Physics*, 2007, v. 1, 64–69.
31. Shnoll S.E. Fine structure of the statistic distribution as a result of the spatial and gravitational anisotropy of our world. *Russian Chem. J.*, 2007, v. 51, no. 1, 150–157.
32. Shnoll S.E., Panchelyuga V.A., and Shnoll A.E. The palindrome effect. *Progress in Physics*, 2008, v. 2, 151–153.
33. Kondrashova M.N. Private communication, 2008.

The Length of the Day: A Cosmological Perspective

Arbab I. Arbab

Department of Physics, Faculty of Science, University of Khartoum, P.O. 321, Khartoum 11115, Sudan
and Department of Physics and Applied Mathematics, Faculty of Applied Sciences and Computer,
Omdurman Ahlia University, P.O. Box 786, Omdurman, Sudan

E-mail: aiarbab@uofk.edu; arbab_ai@yahoo.com

We have found an empirical law for the variation of the length of the Earth's day with geologic time employing Wells's data. We attribute the lengthening of the Earth's day to the present cosmic expansion of the Universe. The prediction of law has been found to be in agreement with the astronomical and geological data. The day increases at a present rate of 0.002 sec/century. The length of the day is found to be 6 hours when the Earth formed. We have also found a new limit for the value of the Hubble constant and the age of the Universe.

1 Introduction

According to Mach's principle the inertia of an object is not a mere property of the object but depends on how much matter around the object. This means that the distant universe would affect this property. Owing to this, we would expect a slight change in the strength of gravity with time. This change should affect the Earth-Moon-Sun motion. It is found that the length of the day and the number of days in the year do not remain constant. From coral fossil data approximately 400 million years (m.y.) ago, it has been estimated that there were little over 400 days in a year at that time. It is also observed that the Moon shows an anomalous acceleration (Dickey, 1994 [1]). As the universe expands more and more matter appears in the horizon. The expansion of the universe may thus have an impact on the Earth-Moon-Sun motion. Very recently, the universe is found to be accelerating at the present time (Peebles, 1999 [2], Bahcall *et al.*, 1999 [3]). To account for this scientists suggested several models. One way to circumvent this is to allow the strength of gravity to vary slightly with time (Arbab, 2003 [4]). For a flat universe, where the expansion force is balanced by gravitational attraction force, this would require the universe to accelerate in order to avoid a future collapse. This can be realized if the strength of the gravitational attraction increases with time (Arbab, 1997 [5], 2003 [4]), at least during the present epoch (matter dominated). One appropriate secure way to do this is to define an effective Newton's constant, which embodies this variation while keeping the "bare" Newton's constant unchanged. The idea of having an effective constant, which shows up when a system is interacting with the outside world, is not new. For instance, an electron in a solid moves not with its "bare" mass but rather with an effective mass. This effective mass exhibits the nature of interaction in question. With the same token, one would expect a celestial object to interact (couple) with its effective constant rather than the normal Newton's constant, which describes the strength of gravity in a universe with constant mass. We, therefore, see that the expansion of the universe affects indirectly (through Newton's constant) the evolution of the Earth-Sun system. Writing an effective quantity is equivalent to having summed all perturbations (gravitational) affecting the system. With this minimal change of the ordinary Newton's constant to an effective one, one finds that Kepler's laws can be equally applicable to a perturbed or an unperturbed system provided the necessary changes are made. Thus one gets a rather modified Newton's law of gravitation and Kepler's laws defined with this effective constant while retaining their usual forms. In the present study, we have shown that the deceleration of the Earth rotation is, if not all, mainly a cosmological effect. The tidal effects of the Earth deceleration could, in principle, be a possible consequence, but the cosmological consequences should be taken seriously.

The entire history of the Earth has not been discovered so far. Very minute data are available owing to difficulties in deriving it. Geologists derived some information about the length of the day in the pats from the biological growth rhythm preserved in the fossil records (e.g., bi-valves, corals, stromatolites, etc.). The first study of this type was made by the American scientist John Wells (1963 [7]), who investigated the variation of the number of days in the year from the study of fossil corals. He inferred, from the sedimentation layers of calcite made by the coral, the number of days in the year up to the Cambrian era. Due to the lack of a well-preserved records, the information about the entire past is severely hindered. The other way to discover the past rotation is to extrapolate the presently observed one. This method, however, could be very misleading.

2 The model

Recently, we proposed a cosmological model for an effective Newton's constant (Arbab, 1997 [5]) of the form

$$G_{\text{eff}} = G_0 \left(\frac{t}{t_0} \right)^{\beta}, \tag{1}$$

where the subscript "0" denotes the present value of the quantity: G_0 is the normal (bare) Newton's constant and t_0 is the present age of the Universe. Here G_{eff} includes all perturbative effects arising from all gravitational sources. We remark here that G_0 does not vary with time, but other perturbations induce an effect that is parameterized in G_{eff} in the equation of motion. Thus, we don't challenge here any variation in the normal Newton's constant G_0. We claim that such a variation can not be directly measured as recently emphasized by Robin Booth (2002 [7]). It can only be inferred from such analysis. We remark here that β is not well determined ($\beta > 0$) by the cosmological model. And since the dynamics of the Earth is determined by Newton's law of gravitation any change in G would affect it. This change may manifest its self in various ways. The length of day may attributed to geological effects which are in essence gravitational. The gravitational interaction should be described by Einstein's equations. We thus provide here the dynamical reasons for these geological changes. We calculate the total effect of expansion of the universe on the Earth dynamics.

The Kepler's 2nd law of motion for the Earth-Sun system, neglecting the orbit eccentricity, can be written as

$$G_{\text{eff}}^2\left[(M+m)^2 m^3\right] T_{\text{eff}} = 2\pi L_{\text{eff}}^3, \tag{2}$$

where m, M are the mass of the Earth and the Sun respectively; L_{eff} is the orbital angular momentum of the Earth and T_{eff} is the period (year) of the Earth around the Sun at any time in the past measured by the days in that time. T_{eff} defines the number of days (measured at a given time) in a year at the epoch in which it is measured. This is because the length of day is not constant but depends on the epoch in which it is measured. Since the angular momentum of the Earth about the Sun hasn't changed, the length of the year does not change. We however measure the length of the year by the number of days which are not fixed. The length of the year in seconds (atomic time) is fixed. Thus one can still use Kepler's law as in (2) (which generalizes Kepler's laws) instead of adding other perturbations from the nearby bodies to the equation of motion of the Earth. We, however, incorporate all these perturbations in a single term, viz. G_{eff}. Part of the total effect of the increase of length of day could show up in geological terms. We calculate here the total values affecting the Earth dynamics without knowing exactly how much the contribution of each individual components.

The orbital angular momentum of the Earth (around the Sun) is nearly constant. From equation (2), one can write

$$T_{\text{eff}} = T_0\left(\frac{G_0}{G_{\text{eff}}}\right)^2, \tag{3}$$

where $T_0 = 365$ days and $G_0 = 6.67\times10^{-11}\ \text{N}\,\text{m}^2\text{kg}^{-2}$.

Equations (1) and (3) can be written as

$$T_{\text{eff}} = T_0\left(\frac{t_0}{t_0 - t_p}\right)^{2\beta}, \tag{4}$$

where t_0 is the age of the universe and t_p is the time measured from present time backward. This equation can be casted in the form

$$x = \ln\left(\frac{T_{\text{eff}}}{T_0}\right) = 2\beta\ln\left(\frac{t_0 - t_p}{t_0}\right), \tag{5}$$

or equivalently,

$$t_0 = \frac{t_p}{\left(1 - \exp(-x/2\beta)\right)}. \tag{6}$$

To reproduce the data obtained by Wells for the number of days in a year (see Table. 1), one would require $\beta = 1.3$ and $t_0 \backsimeq 11\times10^9$ years. This is evident since, from (Arbab, 2003 [4]) one finds the Hubble constant is related to the age of the Universe by the relation,

$$t_0 = \left(\frac{2+\beta}{3}\right) H_0^{-1} = 1.1\, H_0^{-1}, \tag{7}$$

and the effective Newton's constant would vary as

$$G_{\text{eff}} = G_0\left(\frac{t_0 - t_p}{t_0}\right)^{1.3}. \tag{8}$$

This is an interesting relation, and it is the first time relation that constrained the age of the Universe (or Hubble constant)from the Earth rotation. However, the recent Hipparcos satellite results (Chaboyer *et al.*, 1998 [8]) indicate that the age of the universe is very close to 11 billion years. Hence, this work represent an unprecedented confirmation for the age of the universe. One may attribute that the Earth decelerated rotation is mainly (if not only) due to cosmic expansion that shows up in tidal deceleration. Thus, this law could open a new channel for providing valuable information about the expansion of the Universe. The Hubble constant in this study amounts to $H_0 = 97.9\ \text{km s}^{-1}\text{Mpc}^{-1}$. However, the Hubble constant is considered to lie in the limit, $50\ \text{km s}^{-1}\text{Mpc}^{-1} < H_0 < 100\ \text{km s}^{-1}\,\text{Mpc}^{-1}$. Higher values of H_0 imply a fewer normal matter, and hence a lesser dark matter. This study, therefore, provides an unprecedented way of determining the Hubble constant. Astronomers usually search into the space to collect their data about the Universe. This well determined value of β is crucial to the predictions of our cosmological model in Arbab, 2003 [4]. We notice that the gravitational constant is doubled since the Earth was formed (4.5 billion years ago).

From (3) and (8) one finds the effective number of days in the year (T_{eff}) to be

$$T_{\text{eff}} = T_0\left(\frac{t_0}{t_0 - t_p}\right)^{2.6}, \tag{9}$$

and since the length of the year is constant, the effective length of the day (D_{eff}) is given by

$$D_{\text{eff}} = D_0\left(\frac{t_0 - t_p}{t_0}\right)^{2.6}, \tag{10}$$

so that

$$T_0\, D_0 = T_{\text{eff}}\, D_{\text{eff}}. \tag{11}$$

Time*	65	136	180	230	280	345	405	500	600
solar days/year	371.0	377.0	381.0	385.0	390.0	396.0	402.0	412. 0	424.0

*Time is measured in million years (m.y.) before present.

Table 1: Data obtained from fossil corals and radiometric time (Wells, 1963 [7]).

Time*	65	136	180	230	280	345	405	500	600
solar days/year	370.9	377.2	381.2	385.9	390.6	396.8	402.6	412.2	422.6
length of solar day (hr)	23.6	23.2	23.0	22.7	22.4	22.1	21.7	21.3	20.7
Time*	715	850	900	1200	2000	2500	3000	3560	4500
solar days/year	435.0	450.2	456.0	493.2	615.4	714.0	835.9	1009.5	1434.0
length of solar day (hr)	20.1	19.5	19.2	17.7	14.2	12.3	10.5	8.7	6.1

*Time is measured in million years (m.y.) before present.

Table 2: Data obtained from our empirical law: equations (9) and (10).

We see that the variation of the length of day and month is a manifestation of the changing conditions (perturbation) of the Earth which are parameterized as a function of time (t) only. Thus, equation (7) guarantees that the length of the year remains invariant.

3 Discussion

The Wells's fossil data is shown in Table 1 and our corresponding values are shown in Table 2. In fact, the length of the year does not change, but the length of the day was shorter than now in the past. So, when the year is measured in terms of days it seems as if the length of the year varies. Sonett *et al.* (1996 [9]) have shown that the length of the day 900 m.y. ago was 19.2 hours, and the year contained 456 days. Our law gives the same result (see Table 2). Relying on the *law of spin isochronism* Alfvén and Arrhenius (1976 [10]) infer for the primitive Earth a length of day of 6 hours (p.226). Using coral as a clock, Poropudas (1991 [11], 1996 [12]) obtained an approximate ancient time formula based on fossil data. His formula shows that the number of days in the year is 1009.77 some 3.556 b.y. ago. Our law shows that this value corresponds rather to a time 3.56 b.y. ago, and that the day was 8.7 hours. He suggested that the day to be 5–7 hours at approximately 4.5 b.y. ago. Ksanfomality (1997 [13]) has shown that according to the principle of isochronism all planets had an initial period of rotation between 6–8 hours. However, our model gives a value of 6 hours (see Table 2). Berry and Baker (1968 [14]) have suggested that laminae, ridges and troughs, and bands on present day and Cretaceous bivalve shells are growth increments of the day and month, respectively. By counting the number of ridges and troughs they therefore find that the year contains 370.3 days in the late Cretaceous. According to the latest research by a group of Chinese scientists (Zhu *et al.* [15]), there were 15 hours in one day, more than 540 days, in a year from a study of *stromatolite* samples. We however remark that according to our law that when the day was 15 hours there were 583 days in a year 1.819 billion years ago. The difference in time could be due to dating of their rock.

Recently, McNamara and Awramik (1992 [16]) have concluded, from the study of *stromatolite*, that at about 700 m.y. ago the number of days in a year was 435 days and the length of the day was 20.1 hours. In fact, our model shows that this value corresponds more accurately to 715 m.y. ago. Vanyo and Awramik (1985 [17]) has investigated *stromatolite*, that is 850 m.y. old, obtained a value between 409 and 485 days in that year. Our law gives 450 days in that year and 19.5 hours in that day. This is a big success for our law. Here we have gone over all data up to the time when the Earth formed. We should remark that this is the first model that gives the value of the length of the day for the entire geologic past time.

The present rate of increase in the length of the day is 0.002 m s/century. Extrapolating this astronomically determined lengthening of the day since the seventeenth century leads to 371 days in the late Cretaceous (65 m.y. ago) Pannella (1972 [18]). The slowing down in the rotation is not uniform; a number of irregularities have been found. This conversion of Earth's rotational energy into heat by tidal friction will continue indefinitely making the length of the day longer. In the remote past the Earth must have been rotating very fast. As the Earth rotational velocity changes, the Earth will adjust its self to maintain an equilibrium (shape) compatible with the new situation. In doing so, the Earth should have experienced several geologic activities. Accordingly, one would expect that the tectonic movements (plate's motion) to be attributed to this continued adjustment.

We plot the length of day (in hours) against time (million years back) in Fig. (1). We notice here that a direct extrapolation of the present deceleration would bring the age of the Earth-Moon system t a value of 3.3 billion years. We observe that the plot deviates very much from straight line. The plot curves at two points which I attribute the first one to emergence of water in huge volume resulting in slowing down the rotation of the Earth's spin. The second point is when water becomes abundant and its rate of increase becomes steady.

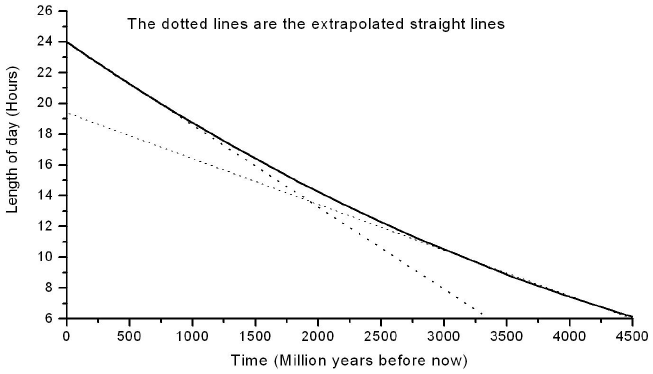

Fig. 1: The variation of length of day versus geological time.

These two points correspond to 1100 m.a. and 3460 m.a., and their corresponding lengths of day are 18.3 and 8.9 hours, respectively. As the origin of life is intimately related to existence of water, we may conclude that life has started since 3.4 billion years ago, as previously anticipated by scientists.

4 Conclusion

We have constructed a model for the variation of length of the day with time. It is based on the idea of an effective Newton's constant as an effective coupling representing all gravitational effects on a body. This variation can be traced back over the whole history of the Earth. We obtained an empirical law for the variation of the length of the day and the number of days in a year valid for the entire past Earth's rotation. We have found that the day was 6 hours when the Earth formed. These data pertaining to the early rotation of the Earth can help paleontologists to check their data with this findings. The change in the strength of gravity is manifested in the way it influences the growth of biological systems. Some biological systems (rythmites, tidalites, etc.) adjust their rhythms with the lunar motion (or the tide). Thus any change in the latter system will show up in the former. These data can be inverted and used as a geological calendar. The data we have obtained for the length of the day and the number of days in the year should be tested against any possible data pertaining to the past's Earth rotation. Our empirical law has been tested over an interval as far back as 4500 m.y. and is found to be in consistency with the experimental data so far known. In this work we have arrived at a generalized Kepler's laws that can be applicable to our ever changing Earth-Moon-Sun system.

Acknowledgements

I wish to thank the University of Khartoum for providing research support for this work, and the Abdus salam International Center for Theoretical Physics (ICTP) for hospitality where this work is carried out.

Submitted on September 21, 2008 / Accepted on September 26, 2008

References

1. Dickey J.O. et al. *Science*, 1994, v. 265, 482.
2. Peebles J. *Nature*, 1999, v. 398, 25.
3. Bahcall N.A. *et al. Science*, 1999, v. 284, 1481.
4. Arbab A.I. *Class. Quantum. Gravit.*, 2003, v. 20, 93.
5. Arbab A.I. *Gen. Relativ. Gravit.*, 1997, v. 29, 61.
6. Wells J.W. *Nature*, 1963, v. 197, 948.
7. Booth R. arXiv: gr-qc/0203065.
8. Chaboyer B. *et al. Astrophys. J.*, 1998, v. 494, 96.
9. Sonett C.P., Kvale E.P., Chan M.A. and Demko T.M. *Science*, 1996, v. 273, 100.
10. Alfvén H. and Arrhenius G. Evolution of the solar system, NASA, Washington, USA, 1976.
11. Poropudas H.K.J. 1991, http://www.cs.colorado.edu/∼lindsay/creation/coral-clocks.txt.
12. Poropudas H.K.J. *Harrastelijan ajatuksia päivän, kuukauden ja vuoden pituudesta muinaisina aikoina. Geologi*, 1996, v. 4–5, 92.
13. Ksanfomality L.V. *Astrophys. Space Sci.* 1997, v. 252, 41.
14. Berry W.B. and Barker R.M. *Nature* 1968, v. 217, 938.
15. Zhu S.X., Huang X.G. and Xin H.T. *Proceedings of the 80th Anniversary of the Chinese Geological Society*, Geology Publishing House, Beijing, 2002.
16. McNamara K.J. and Awramik S.M. *Sci. Progress*, 1992, v. 76, 345.
17. Vanyo J.P. and Awramik S.M. *Precambrian Research*, 1985, v. 29, 121.
18. Pannella G. *Astrophys. Space Sci.*, 1972, v. 16, 212.

A Quantum Theory of Magnetism

Stephan Gift

Department of Electrical and Computer Engineering
University of the West Indies, St Augustine, Trinidad and Tobago

E-mail: stephan.gift@sta.uwi.edu

In this paper, a new Quantum Theory of Magnetic Interaction is proposed. This is done under a relaxation of the requirement of covariance for Lorentz Boost Transformations. A modified form of local gauge invariance in which fermion field phase is allowed to vary with each space point but not each time point, leads to the introduction of a new compensatory field different from the electromagnetic field associated with the photon. This new field is coupled to the magnetic flux of the fermions and has quanta called magnatons, which are massless spin 1 particles. The associated equation of motion yields the Poisson equation for magnetostatic potentials. The magnatons mediate the magnetic interaction between magnetic dipoles including magnets and provide plausible explanations for the Pauli exclusion principle, Chemical Reactivity and Chemical Bonds. This new interaction has been confirmed by numerical experiments. It establishes magnetism as a force entirely separate from the electromagnetic interaction and converts all of classical magnetism into a quantum theory.

1 Introduction

Quantum Electrodynamics (QED) is the most accurate theory available. The associated electromagnetic interaction, which is embodied in Maxwell's equations, is universally viewed as a unification of the electric force and the magnetic force. Such an interpretation, however, encounters difficulty when applied to a rather basic situation. Specifically, consider two electrons with parallel spins that are arranged spatially alongside each other ($\uparrow\ \uparrow$). From the theory of QED based on the Gordon decomposition [1, see p. 198], the electric charge of the electron along with its spin results in an electromagnetic interaction between the two particles which is made up of a dominant electric (Coulomb) repulsion and a weaker attractive magnetic component. That the magnetic component is attractive is stated explicitly by Fritzsch in his discussion of chromomagnetic forces among quarks [2, see p. 170]). This explains why orthopositronium, where the particle (electron and positron) spins are parallel and hence the magnetic component of the electromagnetic interaction is repulsive, has a higher energy state than parapositronium where the particle spins are anti-parallel and the magnetic component of QED is attractive. However, from the classical theory of magnetism, the magnetic moment of the two electrons results in a magnetic repulsion between the electrons rather than an attraction [3]. The commonplace occurrence of two bar magnets interacting with each other presents a further problem for the electromagnetic interaction since magnets, in general, carry a net zero charge and therefore cannot interact by exchanging photons. These examples appear to call into question the universally adopted practice of interpreting the magnetic force as part of the electromagnetic interaction and suggest the need for some level of re-examination. In attempting to address these problems associated with the magnetic interaction, we observe that according to the relativistic world-view, all physical laws of nature must have the same form under a proper Lorentz transformation [4]. With respect to quantum field theories, this means that the field equations describing the various interactions of elementary particles must be Lorentz-covariant, a requirement that places certain restrictions on the allowed interaction models. Lorentz covariance is however not an observed law of nature but is rather a mathematical requirement that is assumed to apply universally. We wish to relax the restrictions imposed by this condition and therefore advance the following postulate:

Postulate 1

Not all interactions are covariant under Lorentz boost transformations. On the basis of this conjecture, we develop a new model of the magnetic interaction. Postulate 1 is the only assumption used in this development and is no more far-fetched than any of the several assumptions of the widely considered superstring theory for which there is no firm supporting evidence and which includes (i) strings rather than particles as fundamental entities, (ii) supersymmetry, the interchangeability of fermions and bosons and (iii) 9 dimensional rather than 3 dimensional spatial existence! On the other hand, the validity of our model and the likely correctness of the postulate are demonstrated by the significant extent to which the consequences of the model accord with or provide plausible explanations for observed phenomena. In particular, the model achieves the following:

- It predicts the existence of a new massless vector particle different from the photon that satisfies the wave

equation for magnetic fields. This particle mediates the magnetic interaction between magnetic dipoles thereby establishing the magnetic interaction as one separate from the electromagnetic interaction and converts all of classical magnetism into a quantum theory.

- It provides plausible explanations for a wide range of hitherto unexplained phenomena including phenomena associated with the Pauli exclusion principle, chemical reactivity and chemical bonds.

2 The electromagnetic interaction

At present, it is believed that the interaction of the electromagnetic field with charged point-like (Dirac) particles is governed by the Principle of Minimal Interaction [4]; all charged particles have only current-type interactions with the electromagnetic field given by $j^\mu A_\mu$ where A_μ is the 4-vector potential of the electromagnetic field and j^μ is the 4-vector current. The minimal concept implies that all electromagnetic properties can be described by this interaction and that no other interactions are necessary. The interaction involves both the charge of the particle and its magnetic moment resulting from its spin magnetic moment (SMM) derived from the Dirac theory and the quanta of the 4-vector electromagnetic field are spin 1 photons. Consider a "spinless" Dirac particle. For such a particle, the SMM is zero and hence electromagnetic interaction is only via the charge with the associated electric field being mediated by the 4-vector A_μ [5]. If on the other hand, the charge of the Dirac particle with spin goes to zero, the SMM again goes to zero and the interaction between the 4-vector A and the uncharged particle disappears. Roman [4, see p. 436] used the proton-photon interaction in the form $j^\mu A_\mu$ and the absence of a neutron-photon interaction (since the neutron is uncharged) to account for the experimental fact that the electromagnetic interaction destroys the isotropy of isospin space, an effect that Sakurai [6] considered as "one of the deepest mysteries of elementary particle physics".* It seems therefore that for neutrons, where the electric charge is zero but the magnetic moment is non-zero, interaction cannot be of the type $j^\mu A_\mu$ i.e. the associated magnetic field is not mediated by the 4-vector A_μ . The well-known absence of interaction between (relatively stationary) electric charges and magnets does perhaps suggest that different mediating quanta are involved in these interactions. We note from the electrodynamic equation $B = \nabla \times A_k$ that, unlike the electric field E that requires both the 3-vector potential A_k and a scalar potential ϕ for its definition, the magnetic field B is completely defined by A_k, which we know, satisfies [3]

$$\Box A_k = \mu J_k. \tag{2.1}$$

*Using this same nucleon-photon interaction, Roman also proved that the electromagnetic interaction conserves the third component of isospin, T_3, a known experimental fact.

where J_k is current density, and which, as established by the Aharonov-Bohm Effect [7], has independent physical existence. We therefore ask, is the 3-vector A_k a magnetic interaction field that is separate from the 4-vector A_μ electromagnetic interaction field?

It is generally believed that all interactions are mediated by gauge fields and hence if A_k is an interaction field, then it should result from the gauge invariance principle [5]. According to this principle, changing the phase of a fermion locally creates phase differences, which must be compensated for by a gauge field if these differences are not to be observable. In other words, a gauge field results from fermion field phase changes. The electromagnetic field of QED and the gluon field of QCD (quantum chromodynamics) are examples of such compensating fields. Reversing this rule, we suggest that an independently created gauge field should produce local phase changes in the fermion field through interaction, i.e. fermion field phase changes should result from a gauge field. We believe that this is precisely what is demonstrated by the Aharonov-Bohm Effect [7]. Here, a 3-vector field A_k independently generated by an electric current, directly produces phase changes in a beam of electrons, in a region where the associated magnetic field B is zero. It follows, we believe, that A_k can be produced by an appropriate fermion field phase change, and that it represents an interaction field.

In order to model A_k as a gauge field, an appropriate conserved quantity, like electric charge, which will determine the strength of the coupling of A_k to the fermion, must be identified. In this regard, we note that an extensive quantum field theory describing magnetic monopoles carrying magnetic charges has been developed [8]. The quanta of this field theory are the quanta associated with the gauge field A_μ of QED, namely photons, which in this theory couple to both electric charge and magnetic charge. However magnetic monopoles have not been found despite strenuous efforts and therefore this theory remains unverified. Towards the development of a new theory having A_k as the gauge field, we adopt an approach sometimes employed in magnetostatics [3, see p. 325] and define a magnetic charge ν which, though physically unreal, is treated as the source of magnetic flux for the purposes of the development.

3 A gauge theory of magnetism

For a fermion with magnetic moment μ_m, we define [3]

$$\nu = \nabla \cdot \mu_m. \tag{3.1}$$

where we refer to ν as magnetic charge and regard it as the source of the magnetic flux associated with the magnetic moment μ_m. Now consider the Lagrangian density $L(x)$ of the fermion field $\psi(x)$ given by

$$L(x) = \bar{\psi}(x)(i\gamma^\mu \partial_\mu - m)\,\psi(x)\,. \tag{3.2}$$

L is clearly invariant under the transformation

$$\psi^{'}(x) = e^{-i\nu a}\psi(x)\,, \tag{3.3}$$

where α is a constant and ν is the magnetic charge of the fermion. From Noether's theorem [4], it follows that the magnetic charge is conserved i.e.

$$\partial_t \nu = \partial_t \left\{ \sum \nu_i \int \bar{\psi}_i \gamma^0 \psi_i d^3x \right\} = 0. \tag{3.4}$$

In practical terms, this means that magnetic flux is conserved. Thus, like electric charge, the conservation of magnetic charge (flux) can be viewed as a consequence of the invariance of the fermion Lagrangian density under the global transformation (3.3). Towards the generation of A_k through local phase changes, we recall that the electromagnetic field is the gauge field which guarantees invariance of the Lagrangian density under space-time local $U(1)$ gauge transformations, i.e. α is a function of space $\bar{x}$ and time t. Here, noting that the electron interference pattern produced by A_k in the Aharonov-Bohm effect varies spatially as A_k is changed, we let the parameter α, in (3.3) be a function of space $\bar{x}$, $\alpha = \alpha(\bar{x})$ i.e. it may have different values at different points in space but continues to be the same at every time t. Considering a neutron field ψ_n say, (3.3) becomes

$$\psi^{'}(x) = e^{-i\nu\alpha(\bar{x})}\psi(x). \tag{3.5}$$

Under this space-local transformation, the Lagrangian density is not invariant. Invariance is achieved by the introduction of a 3-vector massless field A_k, $k = 1, 2, 3$, such that

$$L = \bar{\psi_n}(i\gamma^\mu\partial_\mu - m)\,\psi_n - \nu\,\bar{\psi}_n\gamma^k\psi_n A_k\,, \tag{3.6}$$

where $A_k \to A_k + \frac{\partial\alpha(\bar{x})}{\partial\bar{x}}$ as

$$\psi_n \to e^{-i\nu\alpha(\bar{x})}\,\psi_n\,. \tag{3.7}$$

The quantity $\bar{\psi}_n\gamma^k\psi_n$ varies like a vector under space rotation and space inversion but not under a Lorentz boost. However, under postulate 1, such a term is allowed in the interaction. Hence, by demanding space-local invariance, a 3-vector field A_k is introduced. When we add to the fermion Lagrangian density a term representing kinetic energy of A_k [4], we arrive at the equation of motion for A_k given by

$$\Box A_k = \nu\,\bar{\psi}_n\gamma^k\psi_n\,. \tag{3.8}$$

This is a 3-vector Klein-Gordon equation whose associated quanta have spin 1 charge 0 and mass 0. Variation of (3.6) with respect to ψ_n gives

$$(i\gamma^\mu\partial_\mu - m)\psi_n = -\,\nu\,\gamma^k A_k\psi_n\,, \tag{3.9}$$

which is the modified Dirac equation in the presence of the field A_k. Analogous to the electromagnetic case, we associate the quantity $\nu\bar{\psi}_n\gamma^k\psi_n$ with current density J_k such that

$$\Box A_k = \mu J_k\,, \tag{3.10}$$

where μ is the permeability constant. This is equation (2.1) of classical electrodynamics. In the case of magnetic material, the equivalent current density is referred to as magnetization or Amperian current density J_m [3, see p. 315] given by

$$J_m = \nabla\times M\,, \tag{3.11}$$

where M is the magnetic dipole moment/unit volume or magnetization . Equation (3.10) is the well-known wave equation for magnetic potentials. [3]. If the magnetic charge distribution is time-independent, the wave equation (3.10) reduces to

$$\nabla^2 A_k = -\,\mu J_k\,. \tag{3.12}$$

Equation (3.12) is the Poisson equation for magnetostatic potentials that contains all of classical magnetism. It leads, under appropriate conditions, to the inverse square law for magnetic poles as well as an inverse higher-order law for magnetic dipoles given by

$$F = \frac{3\mu\mu_1\mu_2}{4\pi r^4}\,, \tag{3.13}$$

where the dipoles are parallel and spatially opposite each other $\uparrow\uparrow$ [4, see p. 311, problem 19.10]. Thus, J_k is the source of the potential A_k and we interpret A_k as the magnetic gauge field with quanta of spin 1, mass zero, charge zero and odd parity which we shall call magnatons. It is the gauge field which guarantees invariance under space-local $U(1)$ gauge transformations. The conservation of magnetic charge is directly associated with the universality of the magnetic coupling constant for all particles with a magnetic moment and the strength of the coupling is the magnetic charge (flux) of the particle. Thus, while for electrically charged particles the interaction with an electromagnetic field — the Quantum Electrodynamic Interaction or electromagnetic interaction — is mediated by the photon and involves the electric charge and the associated SMM, the interaction of a "magnetically charged" particle with a magnetic field is mediated by the magnaton and involves the particle's magnetic moment. This is a new quantum interaction, which we shall refer to as the Quantum Magnetodynamic Interaction or magnetic interaction. It is in general different from the magnetic component of the electromagnetic interaction. To demonstrate this difference, consider again two electrons with parallel spins ($\uparrow\uparrow$). Recall, from the theory of QED, (e.g. [1, see p. 198]), that the electric charge of the electron along with its spin results in an electromagnetic interaction between the two particles which is made up of a dominant electric repulsion and a weaker attractive magnetic component. In the new theory, the magnetic moment of the two electrons results in a magnetic repulsion given by (3.13) consistent with the classical theory of magnetism and different from the magnetic component of the electromagnetic force, which is attractive. Since the potential of the magnetic interaction is of the form $1/r^3$, its effect will not generally be noticed in QED interactions

where the potential is of the form $1/r$, but becomes dominant at short distances. Experimentally, in electron-positron high-energy scattering for example, there are indeed sharp resonances as well as novel asymmetries in the angular distributions, which cannot be accounted for in the QED perturbation theory, which Barut [9] has considered to be possibly of magnetic origin. In fact, Barut points out that in perturbation theory, the short distance behaviour of QED is completely unknown since the forces involved change completely at high energies or short distances. We believe that it is the magnetic interaction mediated by the magnaton, which becomes effective at short distances, that is the operative mechanism. We conclude then that the observed magnetic interaction between magnetic dipoles and magnets is mediated not by photons as is widely believed, but by magnatons. Because magnatons are massless vector particles, the associated magnetic field is long-range and results in interactions that are both attractive and repulsive, all in agreement with observation.

4 Application of the quantum magneto-dynamic interaction

The quantum magnetodynamic interaction effectively converts all of classical magnetism into a quantum theory and is therefore supported by 400 years of scientific discovery in magnetism, started by Gilbert in 1600. We expect new detailed predictions from the theory because of its quantum mechanical nature but defer this substantial exercise. Instead, we examine simple and direct tests of the model and show that it offers plausible explanations in precisely those areas where there are no simple answers. The larger the number of applications where it provides a persuasive account, the greater will be our confidence in its correctness and consequently our preparedness to engage in more detailed analysis. In the following sub-sections, three areas are discussed: The Pauli exclusion principle, chemical reactivity and chemical bonds.

4.1 The Pauli Exclusion Principle

The Pauli Exclusion Principle is an extremely important principle in science [10]. It is the cornerstone of atomic and molecular physics and all of chemistry. It states that two electrons (or other fermions) cannot have the same spatial wave function unless the spins are anti-parallel ($\uparrow\downarrow$) i.e. apart from the electric repulsion, parallel spin electrons tend to repel each other while anti-parallel spin electrons tend to attract each other. The operative force of attraction/repulsion is unknown. It cannot be the magnetic component of the electromagnetic force since it has the wrong sign and because of the inability to identify this so-called "Pauli Force", the tendency is to label this behaviour a "quantum-mechanical effect, having no counterpart in the description of nature according to classical physics" [10, see p. 564]. We suggest that the tendency for parallel spin electrons to repel each other and anti-parallel spin electrons to attract each other arises as a result of the quantum magnetodynamic interaction. The magnetic moment of an electron is aligned with its spin, making it effectively a tiny magnet. Therefore, parallel spin electrons will experience mutual repulsion according to equation (3.13) arising from the exchange of magnatons, while anti-parallel spin electrons will experience mutual attraction. This, of course, is consistent with classical magnetism represented by (3.13).

Periodic Table of Elements

An immediate application of the magnetic attraction between anti-parallel spin electrons is in the energy levels of atoms. The attractive magnetic force in the anti-parallel spin electrons accounts for the anti-parallel pairing of electrons in atomic orbitals where the electrons are close together, this leading to the Periodic Table of elements. We further suggest that the attractive component of the long-range electromagnetic force between parallel spin electrons accounts for the experimental fact that unpaired electrons in different atomic orbitals having the same energy are parallel spin-aligned.

Solidity of matter

In solids, inter-atomic and inter-molecular forces are in general considered to be manifestations of the electromagnetic interaction between the constituents, and the electric (Coulomb) component plays the dominant role. This interaction provides an attractive force that holds the constituent atoms in a regular lattice. This is very evident in solids such as sodium chloride. For small inter-atomic distances such that the orbitals of inner electrons overlap, a repulsive force component arises. This repulsive force at short distances is called the repulsive core and is a general feature of atomic interaction. It prevents the interpenetration of atoms and thereby provides the solidity of matter [11]. The repulsive core is attributed to the Pauli Exclusion Principle and Gillespie explains this as follows [12, see p. 69]: "... because of the Pauli principle, in any region of space around a nucleus in which there is a high probability of finding a pair of electrons of opposite spin, there is only low probability of finding any other electrons. Since most molecules have an equal number of electrons of opposite spin, no other electrons can penetrate into each other to a significant extent." Again no force is identified and in fact Gillespie refers to the unknown Pauli forces as apparent forces that are not real. We propose that the quantum magnetodynamic interaction between the magnetic fields of the orbiting anti-parallel electron pairs in the various atoms is the missing component in Gillespie's explanation and that this along with the electric force prevents collapse in solids. The magnetic interaction neutralizes the associated magnetic field of the anti-parallel pair such that there is no magnetic interaction (which could be attractive) between the pair and the magnetic field of other electrons. As a result the electric field of the pair repels other electrons and prevents them from

penetrating to any significant extent. This, we suggest, is responsible for the solidity of matter with the magnetic neutralization being a critical feature of the process. The existence of the magnetic interaction in the repulsive core mechanism is supported by Earnshaw's theorem [13] according to which a system of only interacting electric charges cannot be stable.

4.2 Chemical reactivity

Chemical reaction generally involves the union or separation of atoms. While the Coulomb force is a dominant feature of this activity, we suggest that the primary basis of chemical reactivity is the magnetic interaction. This interaction explains why atoms and molecules with unpaired electrons in the valence shell like the alkali metals, the halogens and free radicals, tend to be highly reactive. The unpaired electrons in such substances have a magnetic field that interacts with the magnetic field of unpaired electrons of other atoms and molecules. The hydroxyl radical (OH) is an example of an odd electron molecule or free radical having an unpaired electron. It is extremely reactive because the radicals can combine with each other or with odd electron carriers, each contributing an electron to form pairs with the constituents drawn together and bound by the magnetic interaction. The magnetic interaction causes unpaired electrons to be points of high reactivity and hence free radicals have no more than a fleeting existence at room temperature [14]. The presence of this magnetic field in substances with unpaired electrons is evident in nitric oxide, boron and oxygen, all of which have one or more unpaired valence electron and are paramagnetic. Liquid oxygen will actually cling to a magnet. On the other hand, atoms and molecules with paired electrons like the noble gases of Group 8 on the Periodic Table tend to be unreactive. This occurs because the paired electrons in such substances are anti-parallel in spin alignment and this results in a substantial neutralization of the overall magnetic field associated with the pair. Since this magnetic field is being proposed as the agent responsible for promoting reactions, such substances would be expected to be less chemically reactive, as is observed. Because of this unavailability of unpaired electrons, the atoms of the members of Group 8 all exist singly.

Experimental confirmation

Important numerical experiments carried out by Greenspan [15] provide strong confirmation of this magnetic interaction and the attraction it produces between anti-parallel electron pairs. This researcher found that classical dynamical calculations for the ground-state hydrogen molecule using a Coulombic force between the bond electrons along with spectroscopic data yielded a vibrational frequency of 2.20×10^{14} Hz, which was a significant deviation from the experimentally determined value of 1.38×10^{14} Hz. By assuming the force between the electrons to be fully attractive rather than fully repulsive, Greenspan obtained the correct vibrational frequency. This approach was successfully tested for the following ground-state molecules: H_2^1, H_2^2, H^1H^2, H^1H^3, and Li_2^7. In all, these cases, deterministic dynamical simulations of electron and nuclei motions yielded correct ground-state vibrational frequencies as well as correct molecular diameters under the assumption that the binding electrons attract. In another paper [16] Greenspan showed that the assumption of electron attraction also yields the correct vibrational frequencies and average molecular diameters for ground-state molecules Li_2^7, B_2^{11}, C_2^{12}, and N_2^{14}. Obtaining correct ground-state results for both vibrational frequencies and average molecular diameters in this large number of molecules was most unexpected and is an extremely strong indication of the correctness of the magnetic interaction model proposed in this paper.

4.3 Chemical bonds

Chemical bonding is due to the attraction of atoms for the electrons of other atoms toward their unfilled orbitals. We suggest that the basis of this attraction is the magnetic interaction between the unpaired electrons associated with these unfilled orbitals. Here we consider ionic bonds, covalent bonds and the concept of the rule-of-two that is central to chemistry.

Ionic bonds

In ionic bonds, donor atoms such as sodium tend to lose electrons easily while acceptor atoms such as chlorine tend to acquire additional electrons. When atoms of these two kinds interact, a re-arrangement of the electron distribution occurs; an electron from the donor atom migrates to the acceptor atom thereby making the acceptor atom negatively charged and the donor atom positively charged. The Coulomb interaction between these ions then holds them in place in the resulting crystal lattice. [11]. In this explanation of the formation of an ionic bond, while the role of the Coulomb force is clear, it is not clear what makes the electron from the donor atom migrate to the acceptor atom. We suggest that apart from the action of the electric force, the migration of the electron from a donor atom to an acceptor atom during a chemical reaction results from the magnetic interaction. As the chemicals are brought together, the electron of the donor atom is close enough to interact with the electron of the acceptor atom via their magnetic fields. The operative quantum magnetodynamic interaction causes the electron of the donor atom and the electron of the acceptor atom to be drawn together in an anti-parallel spin alignment consistent with magnetic attraction. The resulting magnetically bound pair becomes attached to the acceptor atom because of its greater electric attraction (electronegativity), precisely as observed.

Covalent bonds

While some bonds are ionic, the majority of chemical bonds have a more or less covalent character. This bond is the foundation of organic chemistry and is the basis of the chemistry of life as it binds DNA molecules together. According to the current understanding [11], atoms with incomplete shells

share electrons, with the electrons tending to concentrate in the region between the atoms. This concentration of electrons exerts a Coulombic attraction on the positive nuclei of the two atoms and this gives rise to a covalent bond. What is not evident in this explanation though is why the shared electrons cluster between the atoms, despite their mutual electric repulsion. The accepted approach is to solve the Schrodinger equation arising from the application of wave mechanics to the system and on this basis attempt to show that the electrons occupy the region where they are observed to cluster. This approach to the explanation of the nature of the covalent bond has been described by Moore [17] as the most important application of quantum mechanics to chemistry. However, this quantum-mechanical method is at best only an approximation as the only atoms that can be described exactly by wave mechanics are hydrogenic (single-electron) atoms such as H, He^{+1} and Li^{+2}. As a result, most of the claimed predictions are really systematized experimental facts as pointed out by Luder [18]. Moreover, wave mechanics does not identify the force that causes the clustering. The quantum magnetodynamic interaction offers an immediate explanation for this clustering: the two electrons involved in a covalent bond always have opposite spin arising from the interaction of the associated magnetic fields and this results in magnetic attraction between them, and hence the clustering. The strong directional characteristic of covalent bonds is a significant indicator of the magnetic nature of the bond, and the close proximity of the associated electron orbitals is consistent with dominant magnetic interaction. The general saturable nature of this bond and the empirical fact that an electron pair cannot normally be used to form more than one covalent bond arise because the intensity of the magnetic field of the anti-parallel electron pair constituting the bond is significantly reduced due to the anti-parallel alignment. This reduction in reactivity resulting from magnetic field neutralization in the anti-parallel pair has already been observed in the noble gases where only electron pairs exist.

To illustrate covalent bond formation based on the magnetic interaction, we examine the covalent bonds in hydrogen gas (like atoms) and hydrogen chloride (unlike atoms). The hydrogen atom has one electron in the 1s orbital. Consider the approach of two hydrogen atoms in the formation of a hydrogen molecule. If the electron spins are parallel (triplet state), then there will be magnetic (and electric) repulsion between the electrons as their orbitals overlap. This repulsive state with spin-aligned electrons in triplet state hydrogen atoms is spectroscopically detectable, thus confirming the overall correctness of this description. Magnetic repulsion along with electric repulsion between the nuclei prevents the formation of a stable molecule. If the electron spins are anti-parallel (singlet state), then for sufficient electron orbital overlap, the resulting magnetic attraction between the electrons is enough to overcome the electric repulsion between them (as well as between the nuclei), and the electrons cluster in a region between the two nuclei. The electric force of attraction between this electron cluster and the two nuclei establishes the covalent bond and a stable hydrogen molecule H_2 results. It is an observed fact [19] that atomic hydrogen is highly unstable as the atoms tend to recombine to form H_2 molecules. We attribute this to the action of the magnetic interaction between the unpaired electrons as described. Similar action occurs in chlorine and oxygen molecules. As a second example, consider the formation of hydrogen chloride from an atom of hydrogen and an atom of chlorine. Hydrogen has one unpaired electron in the K shell in a spherical orbital and chlorine has seven valence electrons in the M shell, 2 filling the 3s orbital and 5 in the 3p orbitals comprising 3 orthogonal dumbbell-shaped orbitals about the nucleus. Two of these 3p orbitals are filled with paired electrons while the remaining 3p orbital has a single unpaired electron. When a hydrogen atom and a chlorine atom approach, the spherical orbital of the hydrogen overlaps with the unfilled elliptical orbital of the chlorine and the magnetic interaction between the unpaired electrons in these two orbitals causes these 2 electrons to cluster between the 2 atomic nuclei in an anti-parallel spin formation. The elliptical shape of the chlorine's 3p orbital is altered in the process. This magnetic interaction between these unpaired elections establishes the covalent bond and the consequent formation of hydrogen chloride (HCl). The arrangement is shown in Figure 1.

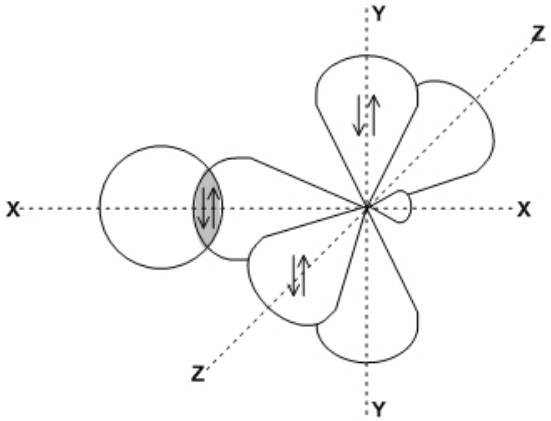

Fig. 1: Covalent bond formation in hydrogen chloride: the s orbital of the hydrogen atom overlaps with a p orbital of the chlorine atom.

The bound electrons are situated closer to the chlorine atom because of its higher electronegativity though they are not completely transferred to the chlorine atom as in sodium chloride. This imbalance causes the HCl molecule to be polar with a positive pole near the hydrogen atom and a negative pole near the chlorine atom. Thus, both the ionic bond and the covalent bond involve a magnetically bound (anti-parallel spin-aligned) electron pair that is attracted to two positively charged atomic nuclei by Coulomb forces. The relative strength of these two electric forces in a specific bond determines the exact position of the electron pair between

the atomic nuclei and hence its location along the bonding continuum represented by pure covalent (H_2)-polar covalent (HCl)-ionic (NaCl) bonding.

Rule-of-two

The "rule of two" [12] is a central concept in chemistry that is more significant than the well-known "rule-of-eight" or stable octet for which there are many exceptions. It is recognition of the observational fact that electrons are generally present in molecules in pairs, despite their mutual electric repulsion. We attribute this tendency to electron pair formation to the magnetic attraction between the two anti-spin aligned electrons forming the pair as verified by the Greenspan data. The new magnetic interaction therefore explains the universal "rule-of two" simply and naturally.

5 Conclusion

In this paper, we have proposed a new magnetic interaction — quantum magneto-dynamics or QMD — that is mediated by massless spin 1 quanta called magnatons. These mediators are different from photons, the quanta of the electromagnetic interaction in QED. QMD is associated with the magnetic moment of the fermions and accounts for all magnetic interactions between magnets. Magnatons are massless vector particles that give the magnetic field its long-range attractive/repulsive character. They satisfy the Poisson equation of classical magnetism and are, we believe, the transmission agents in the Aharanov-Bohm effect. QMD provides plausible explanations for various hitherto unexplained phenomena including the Pauli exclusion principle, chemical reactivity and chemical bonds. It explains the "Pauli Force" that leads to electron pairing in atomic orbitals. It also explains covalent bonds which are the foundation of organic chemistry as well as the "rule of two" according to which electrons are present in molecules in pairs with only a few exceptions, despite their mutual electric repulsion. Greenspan [15, 16] has confirmed this attractive magnetic force between anti-parallel spin aligned electrons for several molecules in important numerical experiments. The effects of QMD are not evident in low-energy QED interactions because the potential of the magnetic interaction is of the form $1/r^3$ but become dominant at high energies or short distances. The extent to which the new quantum theory of magnetism accords with observation and its success in providing simple answers in several areas where relativistic models provide none all strongly suggest that the theory may be right and that a more detailed investigative programme should be pursued. Issues that need to be explored include:

1. The renormalizability of the new interaction to enable calculations;
2. Quantitative application of the magnetic interaction to the Pauli Exclusion phenomenon, chemical reactivity and chemical bonds;
3. Application to molecular geometry;
4. Analysis of the new interaction in order to reveal new quantum mechanical phenomena such as may occur in electron-positron high-energy scattering [9], polarised proton-proton collisions [20] and elastic electron-neutron scattering [5].

We have been led to this new interaction by breaking away from the excessively restrictive idea of Lorentz covariance. An alternative modification of U(1) gauge invariance explored in ([21], where we demand that the Lagrangian density be invariant under a time-local (rather than space-local) $U(1)$ gauge transformation $\psi \to \psi' = U\psi$ with U being time-dependent (rather than space-dependent), generated a scalar spin0 field (rather than a 3-vector spin1 field) which we identify as the gravitational field (instead of the magnetic field). This field satisfies a wave equation, which contains the Poisson equation for gravitational potentials and hence 300 years of Newtonian gravitation. This is a further indication that the basic approach may be valid. In future research, therefore, we intend to pursue the modified gauge invariance approach used in this paper and demand that nucleon interaction be invariant under an isotopic gauge transformation $\psi \to \psi' = U\psi$ with U being a space-dependent isospin rotation $U(\vec{x})$. The hoped-for result is massless rho-mesons which when unified with the spin1 magnatons are given mass through spontaneous symmetry breaking thereby yielding massive rho-mesons. Such an approach in [22] involving a time-dependent isospin rotation $U(t)$ and unification with spin0 gravitons yielded pi-mesons!

Acknowledgements

This paper supersedes Ref. [23]. The author would like to thank Dr Frederick Campayne formerly of the Physics Department of the University of the West Indies for extensive assistance in the preparation of this paper.

Submitted on July 18, 2008 / Accepted on September 25, 2008

References

1. Renton P. Electroweak interactions. Cambridge University Press, London, 1990.
2. Fritzsch H. Quarks — the stuff of matter. Allen Lane Penguin Books, London, 1983.
3. Wangsness R. K. Electromagnetic fields. Wiley, New York, 1986.
4. Roman P. Theory of elementary particles. North-Holland Publishing Company, Amsterdam, 1960.
5. Halzen F. and Martin A.D. Quarks and leptons. Wiley and Sons, New York, 1985.
6. Sakurai J.J. Theory of strong interactions. *Annals of Physics*, 1960, v. 11, 1.
7. Ryder L.H. Quantum field theory. Cambridge University Press, London, 1985.

8. Blagojevic M. and Senjanovic P. *Physics Reports*, 1988, v. 157, 233.
9. Barut A.O. Electromagnetic interactions and particle physics. In: *Frontiers of Fundamental Physics*, ed. M. Barone and F. Selleri, Plenum Press, New York, 1994.
10. French A.P. and Taylor E.F. An introduction to quantum physics. W.W. Norton & Co. Inc., New York , 1978.
11. Ohanian H.C. Modern physics. Prentice-Hall of India Private Ltd., New Delhi, 1994.
12. Gillespie R.J. and Popelier P.L.A. Chemical bonding and molecular geometry. Oxford University Press, Oxford, 2001.
13. Gottfried K. and Weisskopf V.F. Concepts of particle physics. Volume I, Clarendon Press, New York, 1984.
14. Ryschkewitsch G.E. Chemical bonding and the geometry of molecules. Van Nostrand, New York, 1963.
15. Greenspan D. Electron attraction as a mechanism for the molecular bond. *Physics Essay*, 1992, v. 5, 250.
16. Greenspan D. On electron attraction in the diatomic bond. *Physics Essays*, 1992, v. 5, 554.
17. Moore W.J. Physical chemistry. Longman, London, 1972.
18. Luder W.F. The electron-repulsion theory of the chemical bond. Reinhold Publishing Corporation, New York, 1967.
19. Tilley D.R. and Tilley J. Superfluidity and superconductivity. Institute of Physics Publishing, Philadelphia, 1990.
20. Krisch A.D. Collisions between spinning protons. *Scientific American*, v. 32, August 1987.
21. Gift S.J.G. A negation of Einstein's General Theory of Relativity and a return to Newtonian gravitation. *Physics Essays*, 2001, v. 14, no. 4, 320–328.
22. Gift S.J.G. A unified theory of spin 0 nuclear interactions. *Speculations in Science and Technology*, 1998/1999, v. 21, no. 3, 143–154.
23. Gift S.J.G. A unified theory of spin 1 nuclear interactions. Part 1: magnetism. *Hadronic Journal Supplement*, 2002, v. 17, no. 3, 377–415.

The Planck Vacuum

William C. Daywitt

National Institute for Standards and Technology (retired), Boulder, Colorado, USA
E-mail: wcdaywitt@earthlink.net

This paper argues that there is a polarizable vacuum state (the Planck vacuum) that is the source of the quantum vacuum; the free particles; the gravitational, fine structure, and Planck constants; the gravitational field and the spacetime of General Relativity; the Maxwell equations and the Lorentz transformation; and the particle Compton relations and the quantum theory.

1 Introduction

This is an unusual paper that needs to be put into perspective to be understood because the definitions contained herein evoke preconceived ideas that get in the way of the reader. For example, the words "bare charge" mean something very specific to the quantum-field-theory specialist that evoke notions of renormalization and Feynman diagrams. The definition of these words given here, however, mean something quite different; so this preface is intended to provide a setting that will make the paper easier to understand.

About ten years ago the author derived the gravitational ($G = e_*^2/m_*^2$), Planck ($\hbar = e_*^2/c$), and also fine structure ($\alpha = e^2/e_*^2$) constants in a somewhat confused and mixed-up manner. Although their derivation at that time left something to be desired, the simple elegance and connectedness of these three fundamental equations has provided the motivation behind the search for their explanation. Thus it was the "leading" of these three constants that resulted in the paper that is about to be read. The intent at the beginning of the investigations was not some urge to discover a grand theory that unifies diverse areas of physics, although the search for the physics behind the constants appears to be doing just that.

The Planck vacuum (PV) state is envisioned as an infinite, invisible (not directly observable), omnipresent, uniform, and homogeneous negative energy state somewhat analogous to the Dirac "sea" in quantum mechanics. The quantum vacuum, on the other hand, consists of virtual particles that appear and disappear at random in free space, the space where free particles and the rest of the universe are observed. The source of this quantum vacuum is assumed to be the PV, where the fields of the quantum vacuum are analogous to non-propagating induction fields with the PV as their source. The PV is also assumed to be the source of the free particles.

The charge of the Planck particle is called the bare charge, and it is this bare charge that is the true, unscreened, charge of the electron and the rest of the charged elementary particles. The polarizability of the PV is shown to be responsible for the fact that the observed electronic charge e has a smaller magnitude than the bare charge e_*.

The PV theory is not derived from some pre-existing theory, e.g. the quantum field theory — it is assumed to be the source of these pre-existing theories. The simple calculations in the paper lead to the above constants and from there to the many suggestions, assumptions, speculations, and hand-waving that necessarily characterize the PV theory at this early stage of development. It is expected, however, that the theory will eventually lead to a "sea change" in the way we view fundamental physics. So let's begin.

The two observations: "investigations point towards a compelling idea, that all nature is ultimately controlled by the activities of a single *superforce*", and "[a living vacuum] holds the key to a full understanding of the forces of nature"; come from Paul Davies' popular 1984 book [1] entitled *Superforce: The Search for a Grand Unified Theory of Nature*. This living vacuum consists of a "seething ferment of virtual particles", and is "alive with throbbing energy and vitality". Concerning the vacuum, another reference [2] puts it this way; "we are concerned here with virtual particles which are created alone (e.g., photons) or in pairs (e^+e^-), and with the vacuum — i.e., with space in which there are no real particles". This modern vacuum state, as opposed to the classical void, is commonly referred to as the quantum vacuum (QV) [3]. The virtual particles of this vacuum are jumping in and out of existence within the constraints of the Heisenberg uncertainty principle ($\Delta E \Delta t \sim \hbar$); i.e., they appear for short periods of time (Δt) depending upon their temporal energy content (ΔE), and then disappear. The QV, then, is an ever-changing collection of virtual particles which disappear after their short lifetimes Δt, to be replaced by new virtual particles which suffer the same fate, ad infinitum.

Among other things, the following text will argue that the source of the QV is the Planck vacuum (PV) [4] which is an omnipresent degenerate gas of negative-energy Planck particles (PP) characterized by the triad (e_*, m_*, r_*), where e_*, m_*, and r_* ($\lambda_*/2\pi$) are the PP charge, mass, and Compton radius respectively. The charge e_* is the bare (true) electronic charge common to all charged elementary particles and is related to the observed electronic charge e through the fine structure constant $\alpha = e^2/e_*^2$ which is one manifestation of the PV polarizability. The PP mass and Compton radius are equal to the Planck mass and length [5] respectively. The zero-point (ZP) random motion of the PP charges e_* about

their equilibrium positions within the PV, and the PV dynamics, are the source of both the QV and the free particles. The PV is held together by van der Waals forces. In addition to the fine structure constant, the PV is the source of the gravitational ($G = e_*^2/m_*^2$) and Planck ($\hbar = e_*^2/c$) constants. The non-propagating virtual fields of the QV are assumed to be real fields appearing in free space which are analogous to induction fields with the PV as their source.

A charged elementary particle is characterized by the triad (e_*, m, r_c), where m and r_c are the particle's mass and Compton radius. The field *intrinsic* to the particle is the bare Coulomb field $e_*\mathbf{r}/r^3$, where $\mathbf{r}$ is the radius vector from the particle to the field point. All other fields, classical or quantum, associated with the particle and its motion arise from this fundamental field and its interaction with the PV.

Section 2 traces the concept of the PV from the first observation of the initial paragraph after the preface to the derivation of the fine structure, gravitational, and Planck constants; to the Compton relation of the PP; and to the free-space permittivities. A rough heuristic argument shows the binding force of the vacuum to be van-der-Waals in nature.

The ultimate PV-curvature force is derived in Section 2 from Newton's gravitational equation. This ultimate force is shown in Section 3 to be tied to the Riemannian spacetime of General Relativity (GR) which, therefore, is related to the real physical curvature of the PV. As a consequence, GR describes the *spacetime* curvature of the PV.

Using the Coulomb field of the bare charge, the polarizability of the PV, and an internal feedback mechanism intrinsic to the PV; Section 4 derives the relativistic electric and magnetic fields associated with the charge, and infers the Lorentz transformation and constancy of the speed of light from the results.

The electromagnetic vacuum (EV) consists of the virtual photons mentioned in the first paragraph which lead collectively to the ZP electromagnetic field with which Section 5 argues that the EV has its origin in the PV.

A free charged particle distorts the PV in two ways. Its bare Coulomb field polarizes the vacuum, and its mass exerts a van-der-Waals attractive force on the PPs of the PV. Section 6 shows how these two vacuum-distorting forces lead to the quantum mechanics and, by inference from Section 5, to the quantum field theory (QFT).

Section 7 summarizes and comments on the ideas presented in Sections 1 through 6.

2 Planck particle and vacuum

The idea from Davies' first observation that a single superforce controls all of nature is interpreted here to mean that the ultimate strengths of nature's fundamental forces are identical, whether those forces are actually realizable or just asymptotically approachable. The static Coulomb and gravitational forces between two like, charged elementary particles are used in this section to derive the fine structure constant, the ultimate Coulomb force, the ultimate gravitational force, the gravitational constant, and the ultimate PV-curvature force. Using a new expression (4) for the gravitational force, and the results from the above; the Compton relation of the PP, and the free-space permittivities (the dielectric constant and magnetic permeability) are derived. These derivations utilize three normalization constants to isolate the ultimate forces. The three constants correspond to charge normalization (e_*), mass normalization (m_*), and length normalization (r_*). These constants start out as normalization constants, but end up defining a new fundamental particle (the PP) and a fundamental vacuum state (the PV).

The static Coulomb force between two like, charged particles can be expressed in the following two forms:

$$F_{\text{el}} = \frac{e^2}{r^2} = \alpha \left(\frac{r_*}{r}\right)^2 F_*' \,, \tag{1}$$

where r is the distance between particles, $\alpha \equiv e^2/e_*^2$, and $F_*' \equiv e_*^2/r_*^2$. If e_* is assumed to be the maximum particle charge (the electronic charge unscreened by a polarizable vacuum state), and r_* is assumed to be some minimum length ($r_* < r$ for all r); then F_*' is the ultimate Coulomb force.

The static gravitational force of Newton acting between two particles of mass m separated by a distance r can be expressed in the following forms:

$$-F_{\text{gr}} = \frac{m^2 G}{r^2} = \frac{m^2}{m_*^2}\left(\frac{r_*}{r}\right)^2 F_* \,, \tag{2}$$

where G denotes Newton's gravitational constant, and $F_* \equiv m_*^2 G/r_*^2$. If m_* is the maximum elementary particle mass, and r_* is the minimum length, then F_* is the ultimate gravitational force as m_*/r_* is the maximum mass-to-length ratio.

Adhering to the idea of a single superforce implies that the force magnitudes F_*' and F_* must be equal. This equality leads to the definition of the gravitational constant

$$G = \frac{e_*^2}{m_*^2} \tag{3}$$

in terms of the squared normalization constants e_*^2 and m_*^2.

The gravitational force in (2) can also be expressed as

$$-F_{\text{gr}} = \frac{(mc^2/r)^2}{c^4/G} \tag{4}$$

by a simple manipulation where c is the speed of light. The ratio mc^2/r has the units of force, as does the ratio c^4/G. It can be argued [6] that c^4/G is a superforce, i.e. some kind of ultimate force. The nature of the two forces, mc^2/r and c^4/G, is gravitational as they emerge from Newton's gravitational equation; but their meaning at this point in the text is unknown. As an ultimate force, c^4/G can be equated to the ultimate gravitational force F_* because of the single-superforce

assumption. Equating c^4/G and F_* then leads to

$$\frac{c^4}{G} = \frac{m_* c^2}{r_*} \tag{5}$$

for the ultimate force c^4/G. It is noteworthy that the form $m_* c^2/r_*$ of this force is the same as that ratio in the parenthesis of (4), which must be if c^4/G is to represent an ultimate force of the form mc^2/r. That (5) is an ultimate force is clear from the fact that m_* is the ultimate particle mass and r_* is the minimum length, roughly the nearest-neighbor distance between the PPs constituting the PV.

Invoking the single-superforce requirement for the ultimate force c^4/G from (5) and the ultimate Coulomb force F'_* leads to

$$\frac{m_* c^2}{r_*} = \frac{e_*^2}{r_*^2} \tag{6}$$

or

$$r_* m_* c = \frac{e_*^2}{c} \equiv \hbar\,, \tag{7}$$

where e_*^2/c defines the (reduced) Planck constant. Furthermore, if the reasonable assumption in made that the minimum length r_* is the Planck length [5], then m_* turns out to be the Planck mass [5]. Noting also that (7) has the classic form of a Compton relation, where r_* is the Compton radius ($\lambda_*/2\pi$), it is reasonable to assume that the triad (e_*, m_*, r_*) characterizes a new particle (the PP). Thus the Compton radius r_* of the PP is $r_* = e_*^2/m_* c^2$.

The units employed so far are Gaussian. Changing the units of the first equation in (7) from Gaussian to mks units [7] and solving for ϵ_0 leads to

$$\epsilon_0 = \frac{e_*^2}{4\pi r_* m_* c^2} \qquad \text{[mks]} \tag{8}$$

where ϵ_0 is the electric permittivity of free space in mks units. Then, utilizing $\epsilon_0 \mu_0 = 1/c^2$ leads to

$$\mu_0 = 4\pi\, \frac{r_* m_*}{e_*^2} \qquad \text{[mks]} \tag{9}$$

for the magnetic permittivity. The magnitude of μ_0 is easy to remember — it is $4\pi\times10^{-7}$ in mks units. Thus $r_* m_*/e_*^2$ in (9) had better equal 10^{-7} in mks units, and it does (e_* in Gaussian units is obtained from (3) and G, or from (7) and $\hbar$; and then changed into mks units for the calculation).

Shifting (8) and (9) out of mks units back into Gaussian units leads to

$$\epsilon = \frac{1}{\mu} = \frac{e_*^2}{r_* m_* c^2} = 1 \tag{10}$$

for the free-space permittivities in Gaussian units. Considering the fact that the free-space permittivities are expressed exclusively in terms of the parameters defining the PP, and the speed of light, it is reasonable to assume that the free-space vacuum (the PV) is made up of PPs. Furthermore, the negative-energy solutions to the Klein-Gordon equation or the Dirac equation [3], and the old Dirac hole theory [3], suggest that a reasonable starting point for modeling the PV may be an omnipresent gas of negative-energy PPs.

The PV is a monopolar degenerate gas of charged PPs. Thus the PPs within the vacuum repel each other with strong Coulombic forces, nearest neighbors exerting a force roughly equal to

$$\frac{e_*^2}{r_*^2} = \left(\frac{5.62\times10^{-9}}{1.62\times10^{-33}}\right)^2 \sim 10^{49} \quad \text{[dyne]} \tag{11}$$

where r_* is roughly the nearest-neighbor distance. The question of what binds these particles into a degenerate gas naturally arises. The following heuristic argument provides an answer. Using the definition of the gravitational constant ($G = e_*^2/m_*^2$), the gravitational force between two *free* PPs separated by a distance r can be written in the form

$$-\frac{m_*^2 G}{r^2} = -\frac{e_*^2}{r^2} \tag{12}$$

leading to a total gravitational-plus-Coulomb force between the particles equal to

$$(-1+\alpha)\,\frac{e_*^2}{r^2} \tag{13}$$

where the Coulomb force ($\alpha e_*^2/r^2$) comes from (1). This total force is attractive since the fine structure constant $\alpha \approx 1/137 < 1$. The total force between two PPs *within* the PV must be roughly similar to (13). Thus it is reasonable to conclude that the vacuum binding force is gravitational in nature.

3 General Relativity

Newton's gravitational force acting between two particles of mass m_1 and m_2 separated by a distance r can be expressed as

$$F_{\text{gr}} = -\frac{(m_1 c^2/r)(m_2 c^2/r)}{c^4/G} = \\ = \frac{(-m_1 c^2/r)(-m_2 c^2/r)}{-m_* c^2/r_*}\,, \tag{14}$$

where (5) has been used to obtain the second expression. Although the three forces in the second expression must be gravitational by nature as they come from the gravitational equation, their meaning is unclear from (14) alone.

Their meaning can be understood by examining two equations from the GR theory [5], the Einstein metric equation

$$G_{\mu\nu} = \frac{8\pi T_{\mu\nu}}{c^4/G} = \frac{8\pi T_{\mu\nu}}{m_* c^2/r_*} \tag{15}$$

and the Schwarzschild equation

$$ds^2 = -\left[1-2n(r)\right]c^2 dt^2 + \frac{dr^2}{\left[1-2n(r)\right]} + r^2\, d\Omega^2 \tag{16}$$

where the n-ratio is

$$n(r) \equiv \frac{mc^2/r}{c^4/G} = \frac{mc^2/r}{m_* c^2/r_*} \tag{17}$$

and where $G_{\mu\nu}$ is the Einstein curvature tensor, $T_{\mu\nu}$ is the energy-momentum density tensor, ds is the Schwarzschild line element, and dt and dr are the time and radius differentials. The remaining parameter in (16) is defined in [5]. The line element in (16) is associated with the curvature of spacetime outside a static spherical mass — in the particle case the equation is only valid outside the particle's Compton radius [8]. For a vanishing mass ($m = 0$), the n-ratio vanishes and the metric bracket $[1-2n(r)]$ reduces to unity; in which case (16) describes a flat (zero curvature or Lorentzian) spacetime.

As mc^2/r in (16) and (17) is a spacetime-curvature force, (14) implies that m_1c^2/r and m_2c^2/r are PV curvature forces. The ultimate curvature force m_*c^2/r_* appears in the denominators of (14), (15), and (17). Thus it is reasonable to conclude that the theory of GR refers to the *spacetime*-curvature aspects of the PV. The forces m_1c^2/r and m_2c^2/r are attractive forces the masses m_1 and m_2 exert on the PPs of the PV at a distance r from m_1 and m_2 respectively.

According to Newton's third law, if a free mass m exerts a force mc^2/r on a PP within the PV at a distance r from m, then that PP must exert an equal and opposite force on m. However, the PP at $-r$ exerts an opposing force on m; so the net average force the two PPs exert on the free mass is zero. By extrapolation, the entire PV exerts a vanishing average force on the mass. As the PPs are in a perpetual state of ZP agitation about their average "r" positions, however, there is a residual, random van der Waals force that the two PPs, and hence the PV as a whole, exert on the free mass.

Puthoff [9] has shown the gravitational force to be a long-range retarded van der Waals force, so forces of the form mc^2/r are essentially van der Waals forces. The ZP electromagnetic fields of the EV are the mechanism that provides the free-particle agitation necessary to produce a van der Waals effect [9]. But since the source of the EV is the PV (see Section 5), the PV is the ultimate source of the agitation responsible for the van-der-Waals-gravitational force between free particles, and the free-particle-PV force mc^2/r.

4 Maxwell and Lorentz

The previous two sections argue that curvature distortions (mass distortions) of the PV are responsible for the curvature force mc^2/r and the equations of GR. This section argues that polarization distortions of the PV by free charge are responsible for the Maxwell equations and, by inference, the Lorentz transformation. These ends are accomplished by using the bare Coulomb field of a free charge in uniform motion, a feedback mechanism intrinsic to the PV [10], and the Galilean transformation; to derive the relativistic electric and magnetic fields of a uniformly moving charge.

The bare Coulomb field $e_*\mathbf{r}/r^3$ intrinsic to a free bare charge e_* polarizes the PV, producing the Coulomb field

$$\mathbf{E}_0 = \frac{e\mathbf{r}}{r^3} = \frac{e}{e_*}\,\frac{e_*\mathbf{r}}{r^3} = \alpha^{1/2}\,\frac{e_*\mathbf{r}}{r^3} = \frac{e_*\mathbf{r}}{\epsilon'\,r^3} \qquad (18)$$

observed in the laboratory, and creating the effective dielectric constant $\epsilon'\ (\equiv e_*/e = 1/\sqrt{\alpha})$ viewed from the perspective of the bare charge, where α is the fine structure constant. In terms of the fixed field point (x, y, z) and a charge traveling in the positive z-direction at a uniform velocity v, the observed field can be expressed as

$$\mathbf{E}_0 = \frac{e\,[x\widehat{\mathbf{x}} + y\widehat{\mathbf{y}} + (z - vt)\,\widehat{\mathbf{z}}]}{[x^2 + y^2 + (z - vt)^2]^{3/2}}\,, \qquad (19)$$

where the charge is at the laboratory-frame origin $(0, 0, 0)$ at time $t = 0$. This expression assumes that the space-time transformation between the charge- and laboratory-coordinate frames is Galilean.

The observed field produces an effective dipole at each field point. When the charge moves through the vacuum, the dipole rotates about the field point and creates an effective current circulating about that point. The circulating current, in turn, produces the magnetic induction field*

$$\mathbf{B}_1 = \boldsymbol{\beta} \times \mathbf{E}_0 = \frac{e\beta\,(z - vt)}{r^3}\,\boldsymbol{\phi}\,, \qquad (20)$$

where $\beta = v/c$, $\boldsymbol{\beta} = \beta\,\widehat{\mathbf{z}}$, $\boldsymbol{\phi}$ is the azimuthal unit vector, and $r^2 = x^2 + y^2 + (z - vt)^2$ is the squared radius vector $\mathbf{r} \cdot \mathbf{r}$ from the charge to the field point. The field $\mathbf{B}_1$ is the first-step magnetic field caused by the bare charge distortion of the PV.

An iterative feedback process is assumed to take place within the PV that enhances the original electric field $\mathbf{E}_0$. This process is mathematically described by the following two equations [10]:

$$\nabla \times \mathbf{E}_n = -\frac{1}{c}\frac{\partial \mathbf{B}_n}{\partial t} \qquad (21)$$

and

$$\mathbf{B}_{n+1} = \boldsymbol{\beta} \times \mathbf{E}_n\,, \qquad (22)$$

where $n\ (= 1, 2, 3\ldots)$ indicates the successive partial electric fields $\mathbf{E}_n$ generated by the PV and added to the original field $\mathbf{E}_0$. The successive magnetic fields are given by (22). Equation (21) is recognized as the Faraday equation.

The calculation of the final electric field $\mathbf{E}$, which is the infinite sum of $\mathbf{E}_0$ and the remaining particle fields $\mathbf{E}_n$, is conducted in spherical polar coordinates and leads to [10]

$$\mathbf{E} = \frac{(1 - \lambda)\,\mathbf{E}_c}{\left(1 - \beta^2 \sin^2\theta\right)^{3/2}}\,, \qquad (23)$$

where λ is the infinite sum of integration constants that comes from the infinity of integrations of (21) to obtain the $\mathbf{E}_n$, and θ is the polar angle between the positive z-direction and the radius vector from the charge to the field point. The field $\mathbf{E}_c$ is the observed static field of the charge, i.e. equation (19) with $v = 0$. The final magnetic field is obtained from $\mathbf{B} = \boldsymbol{\beta} \times \mathbf{E}$.

*The polarization vector $\mathbf{P} = \chi_e\mathbf{E}_0 = (\epsilon' - 1)\mathbf{E}_0/4\pi$ rotating about a field point in the PV produces an effective current proportional to $\beta \sin\theta$ which leads to the magnetic induction field $\mathbf{B}_1 = \boldsymbol{\beta} \times \mathbf{E}_0$.

Finally, the constant λ can be evaluated from the conservation of electric flux [10] (the second of the following equations) which follows from Gauss' law and the conservation of bare charge e_* (the first equation):

$$\int \mathbf{D}\cdot\mathbf{dS} = 4\pi e_* \longrightarrow \int \mathbf{E}\cdot\mathbf{dS} = 4\pi e \tag{24}$$

where $\mathbf{dS}$ is taken over any closed Gaussian surface surrounding the bare charge, and where $\mathbf{D} = \epsilon'\,\mathbf{E} = (e_*/e)\,\mathbf{E}$ is used to bridge the arrow. Inserting (23) into the second equation of (24) and integrating yields

$$\lambda = \beta^2 \tag{25}$$

which, inserted back into (23), leads to the relativistic electric field of a uniformly moving charge [7]. The relativistic magnetic field is $\mathbf{B} = \boldsymbol{\beta}\times\mathbf{E}$. The conservation of electric flux expressed by the second equation of (24) is assumed as a postulate in [10]. The first equation shows that the postulate follows from Gauss' law and the conservation of bare charge.

The relativistic field equations $\mathbf{E}$ and $\mathbf{B}$ for a uniformly moving charge are derived above from the Coulomb field $e_*\mathbf{r}/r^3$ of the bare charge in (18), an assumed PV feedback dynamic given by (21) and (22), and the *Galilean* transformation. Of course, the relativistic equations can also be derived [7] from the Coulomb field $e\mathbf{r}/r^3$ (where $r^2 = x^2+y^2+z^2$) of the observed electronic charge e at rest in its own coordinate system, and the *Lorentz* transformation. It follows, then, that the Lorentz transformation is a mathematical shortcut for calculating the relativistic fields from the observed charge e $(= e_*\sqrt{\alpha})$ without having to account directly for the polarizable PV and its internal feedback dynamic. Furthermore, it can be argued that the constancy of the speed of light c from Lorentz frame to Lorentz frame, which can be deduced from the resulting Lorentz transformation, is due to the presence of the PV in the photon's line of travel.

If there were no polarizable vacuum, there would be no rotating dipole moments at the field points (x, y, z); and hence, there would be no magnetic field. A cursory examination of the free-space Maxwell equations [7] in the case where the magnetic field $\mathbf{B}$ vanishes shows that the equations reduce to $\nabla\cdot\mathbf{E} = 4\pi\rho_*$, and to the equation of continuity between e_* and its current density. Thus it can be argued that the Maxwell equations owe their existence to the polarizable PV.

5 Electromagnetic vacuum

The EV is the photon part of the QV mentioned at the beginning of the Introduction, i.e. the virtual photons that quickly appear and dissappear in space. This section argues that the EV has its origin in the PV.

The virtual photons of the EV lead to the ZP electric field (see [9] for detail)

$$\mathbf{E}_{zp}(\mathbf{r},t) = \mathrm{Re}\sum_{\sigma=1}^{2}\int d\Omega_k \int_0^{k_{c*}} dk\, k^2\, \widehat{\mathbf{e}}_\sigma\{A_k\}\times \times \exp\left[i\left(\mathbf{k}\cdot\mathbf{r}-\omega t+\Theta\right)\right] \tag{26}$$

the spectrum of which Sakharov [11] has argued must have an upper cutoff wavenumber k_{c*} that is related to the "heaviest particles existing in nature". In the present context, the heaviest particles existing in nature are clearly PPs. Puthoff [9, 12] has calculated the wavenumber to be $k_{c*} = \sqrt{\pi c^3/\hbar G}$, which can be expressed as $k_{c*} = \sqrt{\pi}/r_*$ by substituting the constants $\hbar = e_*^2/c$ and $G = e_*^2/m_*^2$ and using the PP Compton relation. The cutoff wave number is characteristic of the minimum length r_*, the Compton radius of the PP, associated with the PV.

The amplitude factor in (26) is [9]

$$A_k = \left(\frac{\hbar\omega}{2\pi^2}\right)^{1/2} = e_*\left(\frac{k}{2\pi^2}\right)^{1/2}, \tag{27}$$

where $\hbar = e_*^2/c$ and $k = \omega/c$ are used to obtain the second expression. This result implies that bare charges are the source of the ZP field, for if e_* were zero, the amplitude factor would vanish and there would be no field. It is reasonable to assume that these bare charges reside in the PV.

Equation (26) can be expressed in the more revealing form

$$\mathbf{E}_{zp}(\mathbf{r},t) = \left(\frac{\pi}{2}\right)^{1/2}\frac{e_*}{r_*^2}\,\mathbf{I}_{\mathrm{zp}}(\mathbf{r},t)\,, \tag{28}$$

where $\mathbf{I}_{\mathrm{zp}}$ is a random variable of zero mean and unity mean square; so the factor multiplying $\mathbf{I}_{\mathrm{zp}}$ in (28) is the root-mean-square ZP field. Since m_*c^2/r_*^3 is roughly the energy density of the PV, the ZP field can be related to the PV energy density through the following sequence of equations:

$$\frac{m_*c^2}{r_*^3} = \frac{e_*^2/r_*}{r_*^3} = \left(\frac{e_*}{r_*^2}\right)^2 \approx \langle\mathbf{E}_{\mathrm{zp}}^2\rangle\,, \tag{29}$$

where the PP Compton relation is used to derive the second ratio, and the final approximation comes from the mean square of (28). The energy density of the PV, then, appears to be intimately related to the ZP field. So, along with the k_{c*} and the A_k from above, it is reasonable to conclude that the PV is the source of the EV.

6 Quantum theory

A charged particle exerts two distortion forces on the collection of PPs constituting the PV, the curvature force mc^2/r and the polarization force e_*^2/r^2. Sections 2 and 3 examine the PV response to the curvature force, and Section 4 the response to the polarization force. This section examines the PV response to both forces acting *simultaneously*, and shows that the combination of forces leads to the quantum theory.

The equality of the two force magnitudes

$$\frac{mc^2}{r} = \frac{e_*^2}{r^2} \quad\Longrightarrow\quad r_c = \frac{e_*^2}{mc^2} \tag{30}$$

at the Compton radius r_c of the particle appears to be a fundamental property of the particle-PV interaction, where m is the particle mass. This derivation of the Compton radius shows the radius to be a particle-PV property, not a property solely of the particle.

The vanishing of the force difference $e_*^2/r_c^2 - mc^2/r_c = 0$ at the Compton radius can be expressed as a vanishing tensor 4-force [7] difference. In the primed rest frame ($\mathbf{k}' = \mathbf{0}$) of the particle, where these static forces apply, this force difference $\Delta F'_\mu$ is ($\mu = 1, 2, 3, 4$)

$$\Delta F'_\mu = \left[\mathbf{0},\ i\left(\frac{e_*^2}{r_c^2} - \frac{mc^2}{r_c}\right)\right] = [0,\ 0,\ 0,\ i\,0]\,, \qquad (31)$$

where $i = \sqrt{-1}$. Thus the vanishing of the 4-force component $\Delta F'_4 = 0$ in (31) is the source of the Compton radius in (30) which can be expressed in the form $mc^2 = e_*^2/r_c = (e_*^2/c)(c/r_c) = \hbar\omega_c$, where $\omega_c \equiv c/r_c = mc^2/\hbar$ is the Compton frequency associated with the Compton radius r_c. As an aside: the transformation of the force difference (31) to the laboratory frame using $\Delta F_\mu = a_{\mu\nu}\Delta F'_\nu$ leads to a $\Delta F_3 = 0$ from which the de Broglie radius ($\lambda_d/2\pi$), $r_d \equiv r_c/\beta\gamma = \hbar/m\gamma v$, can be derived.

In what follows it is convenient to define the 4-vector wavenumber tensor

$$k_\mu = (\mathbf{k}, k_4) = (\mathbf{k}, i\,\omega/c)\,, \qquad (32)$$

where $\mathbf{k}$ is the ordinary vector wavenumber, and $i\omega/c$ is the frequency component of k_μ. This tensor will be used to derive the particle-vacuum state function, known traditionally as the particle wavefunction.

The vanishing of the 4-force component $\Delta F'_4$ from (31) in the rest frame of the particle leads to the Compton frequency ω_c. Thus from (32) applied to the prime frame, and $\mathbf{k}' = \mathbf{0}$, the equivalent rest-frame wavenumber is $k'_\mu = (\mathbf{0}, i\,\omega_c/c)$.

The laboratory-frame wavenumber, where the particle is traveling uniformly along the positive z-axis, can be found from the Lorentz transformation $k_\mu = a_{\mu\nu}k'_\nu$ [7] leading to

$$k_z = \gamma k'_z - i\beta\gamma k'_4 \quad \text{and} \quad k_4 = i\beta\gamma k'_z + \gamma k'_4\,, \qquad (33)$$

where

$$a_{\mu\nu} = \begin{pmatrix} 1 & 0 & 0 & 0 \\ 0 & 1 & 0 & 0 \\ 0 & 0 & \gamma & -i\beta\gamma \\ 0 & 0 & i\beta\gamma & \gamma \end{pmatrix} \qquad (34)$$

is used, $\beta = v/c$ and $\gamma^2 = 1/(1-\beta^2)$, and where the x- and y-components of the wavenumbers vanish in both frames. With $k'_z = 0$ and $k'_4 = i\omega_c/c$, the laboratory-frame wavenumber from (32) and (33) becomes

$$k_\mu = (0,\ 0,\ \beta\gamma\omega_c/c,\ i\gamma\omega_c/c) = (0,\ 0,\ p/\hbar,\ iE/c\hbar)\,, \qquad (35)$$

where $p = m\gamma v$ and $E = m\gamma c^2$ are the relativistic momentum and energy of the particle. The second parenthesis in (35) is derived from the first parenthesis and $\omega_c = mc^2/\hbar$, from which $k_z = p/\hbar$ and $k_4 = iE/c\hbar = i\omega_z/c$ emerge.

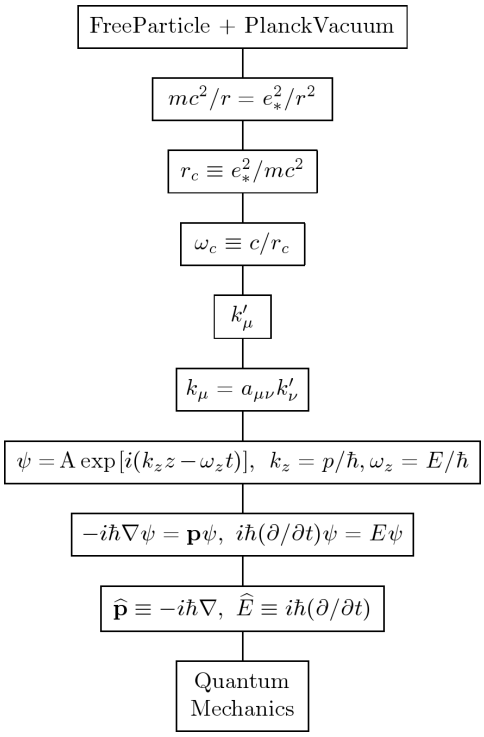

Fig. 1: The flow-diagram traces the particle-vacuum interaction to the Compton radius r_c and the Compton frequency ω_c. From there, the corresponding four-vector wavenumber k'_μ and the Lorentz transformation lead to the particle-vacuum wavefunction ψ, the gradient and time derivative of which then yield the momentum and energy operators, and the quantum mechanics.

The relativistic momentum p and energy E in $k_z = p/\hbar$ and $\omega_z = E/\hbar$ characterize the classical particle motion, and suggest the simple plane-wave

$$\psi = \mathrm{A}\exp\left[i(k_z z - \omega_z t)\right] = \mathrm{A}\exp\left[i(pz - Et)/\hbar\right] \qquad (36)$$

as a suitable state function to characterize the wave behavior of the particle-PV system. This laboratory-frame state function reduces to the state function $\psi = \mathrm{A}\exp\left(-imc^2 t/\hbar\right)$ in the particle rest frame where $v = 0$. The $S(z,t) \equiv pz - Et$ in the exponent of (36) are particular solutions (for various non-vanishing m) of the free-particle, relativistic Hamiltonian-Jacobi equation [8, p.30] although this fact is not used here in deriving the state function.

Since $-i\hbar\nabla\psi = \mathbf{p}\psi$ and $i\hbar(\partial/\partial t)\psi = E\psi$ from (36), it is clear that the momentum ($\widehat{\mathbf{p}} \equiv -i\hbar\nabla$) and energy ($\widehat{E} \equiv i\hbar(\partial/\partial t)$) operators have their origin in the vacuum perturbation caused by the two forces mc^2/r and e_*^2/r^2 as these two forces are responsible for the wavefunction (36). Once the operators $\widehat{\mathbf{p}}$ and $\widehat{E}$ are defined, the quantum mechanics follows from the various classical (non-quantum) energy equations of particle dynamics. A flow-diagram of the preceding calculations is given in Figure 1.

The preceding calculations leading from the particle-PV interaction to the quantum mechanics are straightforward. Tracing the QFT [12] of the massive particles to the PV is less clearcut however. Nevertheless, as Section 5 shows the PV to be the source of the EV, it is easy to conclude that the PV must also be the source of the massive-particle-vacuum (MPV) part of the QV, and thus the QFT.

7 Summary and comments

This paper presents a new theory in its initial and speculative stage of development. Sections 2 through 6: show that the fine structure constant, the gravitational constant, and the Planck constant come from the PV; derive the free-space permittivities in terms of the PP parameters, showing that the free-space vacuum and the PV are one and the same; show that the previously unexplained force mc^2/r is a curvature force that distorts both the PV and the spacetime of GR, and that GR describes the spacetime aspects of the PV; show the PV to be the source of the Maxwell equations and the Lorentz transformation; show that the QV has its origin in the PV; show that the PV is the source of the Compton relations ($r_c mc = \hbar$) and the quantum theory.

The Compton radius r_c ($= e_*^2/mc^2$) is traditionally ascribed to the particle, but emerges from the PV theory as a particle-PV interaction parameter. Inside r_c ($r < r_c$) the polarization force dominates ($e_*^2/r^2 > mc^2/r$) the curvature force, while outside the reverse is true. Both the EV and MPV parts of the QV are omnipresent, but inside r_c the MPV is responsible for the particle *Zitterbewegung* [3, p.323] caused by "exchange scattering" taking place between the particle and the MPV, resulting in the particle losing its single-particle identity inside r_c.

The development of the PV theory thus far is fairly simple and transparent. The theory, however, is fundamentally incomplete as particle spin is not yet included in the model. Calculations beyond the scope and complexity of those here are currently underway to correct this deficiency.

Even in its presently incomplete state, the PV theory appears to offer a fundamental physical explanation for the large body of mathematical theory that is the vanguard of modern physics. The predictive ability of the QFT, or the modern breakthroughs in astrophysics made possible by GR, are nothing less than spectacular; but while the equations of these theories point toward a fundamental reality, they fall short of painting a clear picture of that reality. Most students of physics, for example, are familiar with the details of the Special Theory of Relativity, and a few with the differential tensor calculus of GR. In both cases, however, the student wonders if there is a real physical space related to these mathematically-generated spacetimes, or whether these spacetimes are just convenient schematic diagrams to help visualize the mathematical artifacts in play. The present paper argues that there is indeed a real physical space associated with spacetime, and that space is the free-space PV.

Submitted on September 22, 2008 / Accepted on September 26, 2008

References

1. Davies P. Superforce — the search for a grand unified theory of Nature. Simon and Schuster, New York, 1984, 5 and 104.
2. Zel'dovich Y.B. and Novikov I.D. Stars and relativity. Dover Publications, Inc., New York, 1996, 73.
3. Milonni P.W. The quantum vacuum — an introduction to Quantum Electrodynamics. Academic Press, New York, 1994.
4. Daywitt W.C. A model for Davies' universal superforce. *Galilean Electrodynamics*, 2006, Sept./Oct., 83. In this reference, the PP and the PV are referred to as the super-particle and super-particle vacuum respectively.
5. Misner C.W., Throne K.S., and Wheeler J.A. Gravitation. W.H. Freeman and Co., San Francisco, 1973.
6. Heaston R.J. Identification of a superforce in the Einstein field equations. *Journal of the Washington Academy of Sciences*, 1990, v. 80, no. 1, 25–36. Heaston R.J. Einstein's great oversight. *Galilean Electrodynamics*, 1991, Mar./Apr., 23.
7. Jackson J.D. Classical electrodynamics. John Wiley & Sons, Inc, 1st ed., 2nd printing, NY, 1962.
8. Landau L.D. and Lifshitz E.M. The classical theory of fields. Addison-Wesley Pub. Co., revised 2nd ed., Mass., 1962. See the first footnote on p. 329. It is accepted knowledge that the line element ds does not apply to the elementary particles because the gravitational radius $r_0 = 2mG/c^2$ "of the particle" is many orders of magnitude less than the particle's Compton radius. This argument is specious because r_0 does not belong to the particle; for particles it is a misleading construct derived from setting the curvature-force ratio $2(mc^2/r)/(c^4/G)$ equal to unity at $r = r_0$. Writing the force ratio as $2(m/m_*)^2/(r/r_c)$ instead indicates that, like other classical (non-quantum) equations, the usefulness of the Schwarzschild line element to the elementary particles (the connection to the metric, how the particles perturb spacetime, etc.) is where $r > r_c$.
9. Puthoff H.E. Gravity as a zero-point-fluctuation force. *Phys. Rev. A*, 1989, v. 39, no. 5, 2333–2342.
10. Pemper R.R. A classical foundation for electrodynamics. MD Thesis, U. of Texas, El Paso, 1977. Barnes T.G. Physics of the future — a classical unification of physics. Institute for Creation Research, California, 1983, 81.
11. Sakharov A.D. Vacuum quantum fluctuations in curved space and the theory of gravitation. *Soviet Physics — Doklady*, 1968, v. 12, no. 11, 1040.
12. Ryder L.H. Quantum field theory. 2nd ed., Cambridge University Press, New York, 1996.

The Source of the Quantum Vacuum

William C. Daywitt

National Institute for Standards and Technology (retired), Boulder, Colorado, USA
E-mail: wcdaywitt@earthlink.net

The quantum vacuum consists of virtual particles randomly appearing and disappearing in free space. Ordinarily the wavenumber (or frequency) spectrum of the zero-point fields for these virtual particles is assumed to be unbounded. The unbounded nature of the spectrum leads in turn to an infinite energy density for the quantum vacuum and an infinite renormalization mass for the free particle. This paper argues that there is a more fundamental vacuum state, the Planck vacuum, from which the quantum vacuum emerges and that the "graininess" of this more fundamental vacuum state truncates the wavenumber spectrum and leads to a finite energy density and a finite renormalization mass.

1 Introduction

The quantum vacuum (QV) [1] consists of virtual particles which are created alone (photons) or in massive particle-antiparticle pairs, both of which are jumping in and out of existence within the constraints of the Heisenberg uncertainty principle ($\Delta E \Delta t \sim \hbar$); i.e., they appear in free space for short periods of time (Δt) depending upon their temporal energy content (ΔE) and then disappear. So the QV is an ever-changing collection of virtual particles which disappear after their short lifetimes Δt to be replaced by new virtual particles that suffer the same fate, the process continuing ad infinitum. The photon component of the QV is referred to here as the electromagnetic vacuum (EV) and the massive-particle component as the massive particle vacuum (MPV).

The quantum fields ascribed to the elementary particles are considered to be the "essential reality" [2] behind the physical universe; i.e., a set of *fields* is the fundamental building block out of which the visible universe is constructed. For example, the vector potential for the quantized electromagnetic field can be expressed as [1, p. 45]

$$\mathbf{A}(\mathbf{r},t) = \sum_{s=1}^{2}\sum_{\mathbf{k}} \left(\frac{2\pi c\hbar}{kV}\right)^{1/2} \times \\ \times \left[a_{\mathbf{k},s}(t)\exp\left(i\mathbf{k}\cdot\mathbf{r}\right) + \text{h.c.}\right]\mathbf{e}_{\mathbf{k},s}\,, \tag{1}$$

where the first sum is over the two polarizations of the field, $k = |\mathbf{k}|$, $V = L^3$ is the box-normalization volume, $a_{\mathbf{k},s}(t)$ is the photon annihilation operator, *h.c.* stands for the Hermitian conjugate of the first term within the brackets, and $\mathbf{e}_{\mathbf{k},s}$ is the unit polarization vector. This is the quantized vector potential for the EV component of the QV. The vector potential satisfies the periodicity conditions

$$\mathbf{A}(x+L, y+L, z+L, t) = \mathbf{A}(x,y,z,t) \tag{2}$$

or equivalently

$$\mathbf{k} = (k_x, k_y, k_z) = (2\pi/L)(n_x, n_y, n_z)\,, \tag{3}$$

where the n_i can assume any positive or negative integer or zero. Since the Planck constant $\hbar$ is considered to be a primary constant, the field in (1) is a fundamental field that is not derivable from some other source (e.g. a collection of charged particles). This paper argues that $\hbar$ is not a primary constant and thus that there is a more fundamental reality behind the quantum fields.

The most glaring characteristic of the EV (and similarly the MPV) is that its zero-point (ZP) energy [1, p. 49]

$$\sum_{s=1}^{2}\sum_{\mathbf{k}}\frac{\hbar\omega_k}{2} = c\hbar\sum_{\mathbf{k},s}\frac{k}{2} \tag{4}$$

is infinite because of the unbounded nature of the $\mathbf{k}$ ($|k_i| < \infty$) in (3). The sum on the right side of the equal sign is an abbreviation for the double sum on the left and $\omega_k = ck$. Using the well-known replacement

$$\sum_{\mathbf{k},s} \longrightarrow \sum_{s}\left(\frac{L}{2\pi}\right)^3\int d^3k = \frac{V}{8\pi^3}\sum_{s}\int d^3k \tag{5}$$

in (4) leads to the EV energy density

$$\frac{c\hbar}{V}\sum_{\mathbf{k},s}\frac{k}{2} = \frac{c\hbar}{2\pi^2}\int_0^\infty k^3\,dk = \infty\,, \tag{6}$$

where the infinite upper limit on the integral is due to the unbounded $\mathbf{k}$ in (3).

The present paper does two things: it identifies a charged vacuum state (the PV [3]) as the source of the QV; and calculates a cutoff wavenumber (based on an earlier independent calculation [4]) for the integral in (6). The PV model is presented in the Section 2. In a stochastic-electrodynamic (SED) calculation [4] Puthoff derives the particle mass, the cutoff wavenumber (in terms of the speed of light, the Planck constant, and Newton's gravitational constant), and the gravitational force. The Puthoff model is reviewed in Section 3 and the resulting cutoff wavenumber changed into a form more useful to the present needs by substituting derived relations [3] for the Planck and gravitational constants.

Section 4 argues that the QV has its source in the PV. It accomplishes this result by comparing the PV and QV energy densities. The reader is asked to excuse the course nature of the comparisons used to make the argument. Section 5 comments on the previous sections and expands the PV theory somewhat.

The de Broglie radius is derived in Appendix A to assist in the calculations of Section 4. The derivation is superficially similar to de Broglie's original derivation [5], but differs essentially in interpretation: here the radius arises from the two-fold perturbation the free particle exerts on the PV.

2 Planck vacuum

The PV [3] is an omnipresent degenerate gas of negative-energy Planck particles (PP) characterized by the triad (e_*, m_*, r_*), where e_*, m_*, and r_* $(\lambda_*/2\pi)$ are the PP charge, mass, and Compton radius respectively. The charge e_* is the bare (true) electronic charge common to all charged elementary particles and is related to the observed electronic charge e through the fine structure constant $\alpha = e^2/e_*^2$ which is a manifestation of the PV polarizability. The PP mass and Compton radius are equal to the Planck mass and length respectively. In addition to the fine structure constant, the particle-PV interaction is the ultimate source of the gravitational $(G = e_*^2/m_*^2)$ and Planck $(\hbar = e_*^2/c)$ constants, and the string of Compton relations relating the PV and its PPs to the observed elementary particles and their bare charge e_*

$$r_* m_* c^2 = \cdots = r_c m c^2 = \cdots = e_*^2 , \tag{7}$$

where the charged elementary particles are characterized by the triad (e_*, m, r_c), m and r_c being the mass and Compton radius $(\lambda_c/2\pi)$ of the particle. Particle spin is not yet included in the theory. The ZP random motion of the PP charges e_* about their equilibrium positions within the PV, and the PV dynamics, are the source of both the free particles and the QV.

The Compton relations (7) have their origin in the two-fold perturbation of the PV by the free particle which polarizes and "curves" (in a general relativistic sense) the PV. The particle-PV interaction is such that the polarization force (e_*^2/r^2) and the curvature force (mc^2/r) are equal at the Compton radius r_c [3]:

$$\frac{e_*^2}{r^2} = \frac{mc^2}{r} \quad \longrightarrow \quad r_c m c^2 = e_*^2 , \tag{8}$$

where the second equation can be expressed in its usual form $r_c mc = \hbar$. The requirement that the force equality in (8) hold in any Lorentz frame leads to the momentum $(\widehat{\mathbf{p}} = -i\hbar\nabla)$ and energy $(\widehat{E} = i\hbar\partial/\partial t)$ operators and to the de Broglie radius (Appendix A). The so-called "wave-particle duality" of the particle follows from the coupling of the free particle to the (almost) continuous nature of the PV whose continuum supports the wave associated with the wave property ascribed to the particle.

3 Puthoff model

One of the charges in the product e_*^2 terminating the chain of Compton relations (7) belongs to the free particle while the other represents the magnitude of the PP charges making up the PV. The fact that the bare charge is common to all the charged elementary particles depicted by (7) suggests that perhaps e_* is massless, and that the mass m in the particle triad (e_*, m, r_c) results from some reaction of the charge to the ZP fields. In a seminal paper [4] Puthoff, in effect, exploits the idea of a massless charge to derive the particle mass, the wavenumber k_{c*} truncating the spectrum of the ZP fields, and the Newtonian gravitational force. This section reviews Puthoff's SED calculations and casts them into a form convenient to the present needs. Some minor license is taken by the present author in the interpretation behind equations (12) and (13) concerning the constant A.

The Puthoff model starts with a particle equation of motion (EoM) for the mass m_0

$$m_0 \ddot{\mathbf{r}} = e_* \mathbf{E}_{zp} , \tag{9}$$

where m_0, considered to be some function of the actual particle mass m, is eliminated from (9) by substituting the damping constant

$$\Gamma = \frac{2e_*^2}{3c^3 m_0} \tag{10}$$

and the electric dipole moment $\mathbf{p} = e_* \mathbf{r}$, where $\mathbf{r}$ represents the random excursions of the charge about its average position at $\langle \mathbf{r} \rangle = 0$. The force driving the particle charge is $e_* \mathbf{E}_{zp}$, where $\mathbf{E}_{\mathrm{zp}}$ is the ZP electric field (B5). Equation (9) then becomes

$$\ddot{\mathbf{p}} = \frac{3c^3\Gamma}{2} \mathbf{E}_{\mathrm{zp}} , \tag{11}$$

which is an EoM for the charge that, *from here on*, is considered to be a new equation in two unknowns, Γ and the cutoff wavenumber k_{c*}. The mass m of the particle is then defined via the stochastic kinetic energy of the charge whatever that may be. A reasonable guess is the kinetic energy of the discarded mass m_0

$$mc^2 \sim \left\langle \frac{m_0 \dot{\mathbf{r}}^2}{2} \right\rangle = \frac{\langle \dot{\mathbf{p}}_2^2 \rangle}{3c^3\Gamma} \tag{12}$$

realizing that, at best, this choice is only a guide to predicting what parameters to include in the mass definition. The dipole variation $\dot{\mathbf{p}}_2$ is explained below. The simplest definition for the mass is then

$$m \equiv \frac{1}{c^2} \frac{A \langle \dot{\mathbf{p}}_2^2 \rangle}{3c^3\Gamma} , \tag{13}$$

where A is a constant to be determined, along with Γ and k_{c*}, from a set of three experimental constraints.

The three constraints used to determine the three constants Γ, k_{c*}, and A are: 1) the observed mass m of the particle; 2) the perturbed spectral energy density of the EV caused by radiation due to the random accelerations experienced by the particle charge e_* as it is driven by the random force

$e_*\mathbf{E}_{\rm zp}$; and 3) Newton's gravitational attraction between two particles of mass m.

The dipole moment $\mathbf{p}$ in (11) can be readily determined using the Fourier expansions [6]

$$\mathbf{p}(t) = \int_{-\infty}^{\infty} \widetilde{\mathbf{p}}(\Omega) \exp\left(-i\Omega t\right) d\Omega/(2\pi)^{1/2} \qquad (14)$$

and

$$\mathbf{E}_{\rm zp}(\mathbf{r},t) = \int_{-\infty}^{\infty} \widetilde{\mathbf{E}}_{zp}(\Omega) \exp\left(-i\Omega t\right) d\Omega/(2\pi)^{1/2}, \qquad (15)$$

where $\widetilde{\mathbf{p}}(\Omega)$ and $\widetilde{\mathbf{E}}_{zp}(\Omega)$ are the Fourier transforms of the dipole moment vector $\mathbf{p}$ and the field $\mathbf{E}_{\rm zp}$ respectively.

The mass of the particle is defined via the planar motion of the charge normal to the instantaneous propagation vector $\mathbf{k}$ in (B5) and results in (Appendix B)

$$\left\langle \dot{\mathbf{p}}_2^2 \right\rangle = 2\left\langle (\widehat{\mathbf{x}}\cdot\dot{\mathbf{p}})^2 \right\rangle = \frac{3\hbar c^5 \Gamma^2 k_{c*}^2}{2\pi}\,, \qquad (16)$$

where $\widehat{\mathbf{x}}$ is a unit vector in some arbitrary x-direction and the factor 2 accounts for the 2-dimensional planar motion. When the average (16) is inserted into (13), the constant

$$\Gamma = \frac{2\pi m}{A\hbar k_{c*}^2} \qquad (17)$$

emerges in terms of the two as yet unknown constants A and k_{c*}.

Acceleration of the free bare charge e_* by $\mathbf{E}_{\rm zp}$ generates electric and magnetic fields that perturb the spectral energy density of the EV with which $\mathbf{E}_{\rm zp}$ is associated. The corresponding average density perturbation is [4]

$$\overline{\Delta\rho'(k)} = \frac{\hbar c^3 \Gamma^2 k}{2\pi^2 R^4} = \frac{2m^2 c^3 k}{A^2 \hbar k_{c*}^4 R^4}\,, \qquad (18)$$

where (17) is used to obtain the final expression, and where R is the radius from the average position of the charge to the field point of interest. An alternative expression for the spectral energy perturbation

$$\Delta\rho(k) = \frac{\hbar k}{2\pi^2 c^3}\left(\frac{mG}{R^2}\right)^2 \qquad (19)$$

is calculated [4] from the spacetime properties of an accelerated reference frame undergoing hyperbolic motion, and the equivalence principle from General Relativity. Since the two perturbations (18) and (19) must have the same magnitude, equating the two leads to the cutoff wavenumber

$$k_{c*} = \left(\frac{2\pi c^3}{A\hbar G}\right)^{1/2}\,, \qquad (20)$$

where G is Newton's gravitational constant.

The final unknown constant A in (20) is determined from the gravitational attraction between two particles of mass m calculated [4] using their dipole fields and coupled EoMs, resulting in Newton's gravitational equation

$$F = -\frac{\hbar c^3 \Gamma^2 k_{c*}^2}{\pi R^2} = -\frac{2m^2 G}{AR^2}\,, \qquad (21)$$

where (17) and (20) are used to obtain the final expression. Clearly $A = 2$ for the correct gravitational attraction, yielding from (20) and (17)

$$k_{c*} = \left(\frac{\pi c^3}{\hbar G}\right)^{1/2} \quad \left[= \frac{\pi^{1/2}}{r_*}\right] \qquad (22)$$

and

$$\Gamma = \frac{\pi m}{\hbar k_{c*}^2} = \frac{mG}{c^3} \quad \left[= \left(\frac{r_*}{r_c}\right)\frac{r_*}{c}\right] \qquad (23)$$

for the other two constants. The expressions in the brackets of (22) and (23) are obtained by substituting the PV expressions for the gravitational constant ($G = e_*^2/m_*^2$), the Planck constant ($\hbar = e_*^2/c$), and the Compton relation in (8). The bracket in (22) shows, as expected, that the cutoff wavenumber in (B5) is proportional to the reciprocal of the Planck length r_* (roughly the distance between the PPs making up the PV). The bracket in (23) shows the damping constant Γ to be very small, orders of magnitude smaller than the Planck time r_*/c. The smallness of this constant is due to the almost infinite number ($\sim 10^{99}$ per cm^3) of agitated PPs in the PV contributing simultaneously to the ZP field fluctuations.

An aside: zitterbewegung

SED associates the *zitterbewegung* with the EV [7, p. 396], i.e. with the ZP electric and magnetic fields. In effect then SED treats the EV and the MPV as the same vacuum while the PV model distinguishes between these two vacuum states. Taking place within the Compton radius r_c of the particle, the particle *zitterbewegung* can be viewed [1, p. 323] as an "exchange scattering" between the free particle and the MPV on a time scale of about $r_c/2c$, or a frequency around $2c/r_c$. The question of how the particle mass derived from the averaging process in (13) can be effected with the charge appearing and disappearing from the MPV at such a high frequency naturally arises. For this averaging process to work, the frequency of the averaging must be significantly higher than the *zitterbewegung* frequency. This requirement is easily fulfilled since $ck_{c*} \gg 2c/r_c$. To see that the averaging frequency is approximately equal to the cutoff frequency ck_{c*} one needs only consider the details of the average $\left\langle (\widehat{\mathbf{x}}\cdot\dot{\mathbf{p}})^2 \right\rangle$ in (13) which involves the integral $\int_0^{k_{c*}} k\,dk \approx \int_0^{10^{33}} k\,dk$. Ninety-nine percent of the averaging takes place within the last decade of the integral from 10^{32} to 10^{33} (the corresponding frequency ck in this range being well beyond the Compton frequency c/r_c of any of the observed elementary particles), showing that the effective averaging frequency is close to ck_{c*}.

4 EV and MPV with truncated spectra

The non-relativistic self force acting on the free charge discussed in the previous section can be expressed as [1, p. 487]

$$e_*\mathbf{E}_{\text{self}} = \frac{2e_*^2}{3c^3}\frac{d\ddot{\mathbf{r}}}{dt} - \ddot{\mathbf{r}}\,\delta m \tag{24}$$

where the radiation reaction force is the first term and the renormalization mass is

$$\delta m = \frac{4e_*^2}{3\pi c^2}\int_0^{k_{c*}} dk \tag{25}$$

assumed here to have its wavenumber spectrum truncated at k_{c*}. An infinite upper limit to the integral corresponds to the box normalization applied in Section 1 to equation (3) where $|n_i| < \infty$ is unbounded. However, if the normal mode functions of the ZP quantum field are assumed to be real waves generated by the collection of PPs within the PV, then the number of modes n_i along the side of the box of length L is bounded and obeys the inequality $|n_i| \leqslant L/2\sqrt{\pi}\,r_*$, where r_* is roughly the separation of the PPs within the PV. Thus the cutoff wavenumber from the previous section ($k_{c*} = \sqrt{\pi}/r_*$) that corresponds to this n_i replaces the infinite upper limit ordinarily assumed for (25). So it is the "graininess" ($r_* \neq 0$) associated with the minimum separation r_* of the PPs in the PV that leads to a bounded k_i and n_i for (3), and which is thus responsible for the finite renormalization mass (25) and the finite energy densities calculated below.

Electromagnetic vacuum

Combining (4) and (5) with a spectrum truncated at k_{c*} leads to the EV energy density [1, p. 49]

$$\frac{c\hbar}{V}\sum_{\mathbf{k},s}\frac{k}{2} = \frac{2c\hbar}{8\pi^3}\int d^3k\,\frac{k}{2} = \frac{c\hbar}{4\pi^3}\int d\Omega_k\int_0^{k_{c*}} dk\,k^2\,\frac{k}{2} =$$

$$= \frac{4\pi c\hbar}{4\pi^3}\int_0^{k_{c*}} dk\,k^2\,\frac{k}{2} = \frac{c\hbar}{2\pi^2}\frac{k_{c*}^4}{4} = \frac{c\hbar}{8r_*^4} = \frac{1}{8}\frac{e_*^2/r_*}{r_*^3}\,, \tag{26}$$

where the 2 in front of the triple integral comes from the sum over $s = 1, 2$; and where $k_{c*} = \sqrt{\pi}/r_*$ and $c\hbar = e_*^2$ are used to obtain the final two expressions. If the energy density of the PV (excluding the stochastic kinetic energy of its PPs) is assumed to be roughly half electromagnetic energy ($\sim e_*^2/r_*$) and half mass energy ($\sim m_*c^2$), then

$$\frac{e_*^2/r_* + m_*c^2}{r_*^3} = 2\frac{e_*^2/r_*}{r_*^3} \tag{27}$$

is a rough estimate of this energy density. Thus the energy density (26) of the EV (the virtual-photon component of the QV) is at most one sixteenth ($1/16$) the energy density (27) of the PV. Although this estimate leaves much to be desired, it at least shows the EV energy density to be less than the PV energy density which must be the case if the PV is the source of the EV.

Massive particle vacuum

The energy density of the ZP Klein-Gordon field is [1, p. 342]

$$\frac{\langle 0|H|0\rangle}{V} = \frac{1}{2V}\int d^3k E_k\,\delta^3(0) =$$

$$= \frac{\delta^3(0)}{2V}\int d\Omega_k\int_0^{k_{c*}} dk\,k^2 E_k = \frac{1}{4\pi^2}\int_0^{k_{c*}} k^2 E_k\,dk =$$

$$= \frac{e_*^2}{4\pi^2}\int_0^{k_{c*}} k^2\left(k_c^2 + k^2\right)^{1/2} dk\,, \tag{28}$$

where $\delta^3(0) = V/8\pi^3$ is used to eliminate $\delta^3(0)$ and $E_k = e_*^2\sqrt{k_c^2 + k^2}$ comes from (A5). Equation (28) leads to

$$\frac{\langle 0|H|0\rangle}{V} = \frac{e_*^2 k_c}{4\pi^2}\int_0^{k_{c*}} k^2\left[1 + \left(\frac{k}{k_c}\right)^2\right]^{1/2} dk =$$

$$= \frac{e_*^2/r_c}{4\pi^2}\int_0^{k_{c*}} k^2\left[1 + (r_c k)^2\right]^{1/2} dk =$$

$$= \frac{e_*^2/r_c}{4\pi^2 r_c^3}\int_0^{r_c k_{c*}} x^2(1 + x^2)^{1/2} dx =$$

$$= \frac{1}{16}\frac{e_*^2/r_*}{r_*^3}\left(1 + \frac{r_*^2}{\pi r_c^2} + \cdots\right) \approx \frac{1}{16}\frac{e_*^2/r_*}{r_*^3}\,, \tag{29}$$

where $k_c = 1/r_c$ is used in the first line. The final integral is easily integrated [8] and leads to the expansion in the second-to-last expression. The final expression follows from the fact that the second ($r_*^2/\pi r_c^2 \sim 10^{-40}$) and higher-order terms in the expansion are vanishingly small (the ratio $r_*/r_c \sim 10^{-20}$ is used as a rough average for the ratio of the Compton radii of the PP and the observed elementary particles). So the energy density in (29) is one thirty-second ($1/32$) of the PV energy density in (27).

The k^2 term under the radical sign in (28) corresponds to the squared momentum of the massive virtual particles contributing to the average vacuum density described by (28). The second term in the large parenthesis of (29) is approximately the relative contribution of the virtual-particle mass to the overall energy density as compared to the coefficient in front of the parenthesis which represents the energy density of the virtual-particle kinetic energy. Thus the kinetic energy of the virtual particles in the MPV dominates their mass energy by a factor of about 10^{40}.

5 Conclusion and comments

The conclusion that the PV is the source of the quantum fields is based on the fact that $\hbar$ ($= e_*^2/c$) is a secondary constant, where one of the e_*s in the product e_*^2 is the particle charge and the other is the charge on the PPs making up the PV; and that the amplitude factor A_k in the ZP electric field (B5) is proportional to the charge on the PPs in the PV. The ubiquitous nature of $\hbar\omega = e_*^2 k$ in the quantum field equations,

whether k is an electromagnetic wavenumber or a de Broglie wavenumber, further supports the conclusion.

The Compton relations (7) and the Puthoff model in Section 3 both suggest that the particle charge e_* is massless. To be self-consistent and consistent with the Puthoff model, the PV model for the Compton relations must assume that the Compton radius $r_c = r_c(m) = e_*^2/mc^2$ is larger than the structural extent of the particle and the random excursions of the charge leading to the mass (13).

The PV theory has progressed to this point without addressing particle spin — its success without spin suggesting perhaps that spin is an acquired, rather than an intrinsic, property of the particle. A circularly polarized ZP electric field may, in addition to generating the mass in (13), generate an effective spin in the particle. This conclusion follows from a SED spin model [7, p. 261] that uses a circularly polarized ZP field in the modeling process — in order to avoid too much speculation though, one question left unexplored in this spin model is how the ZP field acquires the circular polarization needed to drive the particle's spin. Perhaps the ZP field acquires its circular polarization when the magnetic field probing the particle (a laboratory field or the field of an atomic nucleus) induces a circulation within the otherwise random motion of the PP charges in the PV, these charges then feeding a circular polarization back into the ZP electric field $\mathbf{E}_{\text{zp}}$ of the EV, thus leading to the particle spin.

Appendix A de Broglie radius

A charged particle exerts two distorting forces on the collection of PPs constituting the PV [3], the polarization force e_*^2/r^2 and the curvature force mc^2/r. The equality of the two force magnitudes at the Compton radius r_c in (8) is assumed to be a fundamental property of the particle-PV interaction. The vanishing of the force difference $e_*^2/r_c^2 - mc^2/r_c = 0$ at the Compton radius can be expressed as a vanishing tensor 4-force [9] difference. In the primed rest frame of the particle where these static forces apply, this force difference $\Delta F'_\mu$ is ($\mu = 1, 2, 3, 4$)

$$\Delta F'_\mu = \left[\mathbf{0},\ \ i\left(\frac{e_*^2}{r_c^2} - \frac{mc^2}{r_c}\right)\right] = [\,0,\ 0,\ 0,\ i\,0\,]\,, \tag{A1}$$

where $i = \sqrt{-1}$. Thus the vanishing of the 4-force component $\Delta F'_4 = 0$ in (A1) is the source of the Compton relation in (8) which can be expressed in the form $mc^2 = e_*^2/r_c = (e_*^2/c)(c/r_c) = \hbar\omega_c$, where $\omega_c \equiv c/r_c = mc^2/\hbar$ is the Compton frequency corresponding to the Compton radius r_c.

The 4-force difference in the laboratory frame, that is $\Delta F_\mu = a_{\mu\nu}\Delta F'_\nu = 0_\mu$, follows from its tensor nature and the Lorentz transformation $x_\mu = a_{\mu\nu}\, x'_\nu$ [9], where $x_\mu = (x, y, z, ict)$,

$$a_{\mu\nu} = \begin{pmatrix} 1 & 0 & 0 & 0 \\ 0 & 1 & 0 & 0 \\ 0 & 0 & \gamma & -i\beta\gamma \\ 0 & 0 & i\beta\gamma & \gamma \end{pmatrix} \tag{A2}$$

and $\mu, \nu = 1, 2, 3, 4$. Thus (A1) becomes

$$\begin{aligned} \Delta F_\mu &= \left[0,\ 0,\ \beta\gamma\left(\frac{e_*^2}{r_c^2} - \frac{mc^2}{r_c}\right),\ i\gamma\left(\frac{e_*^2}{r_c^2} - \frac{mc^2}{r_c}\right)\right] = \\ &= \left[0,\ 0,\ \left(\frac{e_*^2}{\beta\gamma r_d^2} - \frac{mc^2}{r_d}\right),\ i\left(\frac{e_*^2}{\gamma r_L^2} - \frac{mc^2}{r_L}\right)\right] = \\ &= [\,0,\ 0,\ 0,\ i0\,] \end{aligned} \tag{A3}$$

in the laboratory frame. The equation $\Delta F_3 = 0$ from the final two brackets yields the de Broglie relation

$$p = \frac{e_*^2/c}{r_d} = \frac{\hbar}{r_d} = \hbar k_d \tag{A4}$$

where $p = m\gamma v$ is the relativistic particle momentum, $r_d \equiv r_c/\beta\gamma$ is the de Broglie radius, and $k_d = 1/r_d$ is the de Broglie wavenumber.

Using (8) and (A4), the relativistic particle energy can be expressed as

$$\begin{aligned} E_{k_d} &= \left(m^2c^4 + c^2p^2\right)^{1/2} = \\ &= \left(e_*^4k_c^2 + c^2\hbar^2k_d^2\right)^{1/2} = e_*^2\left(k_c^2 + k_d^2\right)^{1/2}, \end{aligned} \tag{A5}$$

where $mc^2 = e_*^2/r_c$, $k_c = 1/r_c$, and $c\hbar = e_*^2$ are used to obtain the final two expressions.

The equation $\Delta F_4 = 0$ from (A3) leads to the relation $p = \hbar/r_L$, where $r_L \equiv r_c/\gamma$ is the length-contracted r_c in the ict direction. The Synge primitive quantization of flat spacetime [10] is equivalent to the force-difference transformation in (A3): the ray trajectory of the particle in spacetime is divided (quantized) into equal lengths of magnitude $\lambda_c = 2\pi r_c$ (this projects back on the "ict" axis as $\lambda_L = 2\pi r_L$); and the de Broglie wavelength calculated from the corresponding spacetime geometry. Thus the development in the previous paragraphs provides a physical explanation for Synge's spacetime quantization in terms of the two perturbations e_*^2/r^2 and mc^2/r the free particle exerts on the PV.

Appendix B Charge EoM with the self force

Combining (24) and (25) leads to the charge's self force

$$e_*\mathbf{E}_{\text{self}} = \frac{2e_*^2}{3c^3}\left(\frac{d\ddot{\mathbf{r}}}{dt} - \omega'_*\ddot{\mathbf{r}}\right) \tag{B1}$$

with $\omega'_* \equiv 2c/\sqrt{\pi}\, r_*$. Adding (B1) to the right side of (9) then yields the x-component of the charge's acceleration corresponding to (11):

$$\ddot{x} = \Gamma\left(\frac{d\ddot{x}}{dt} - \omega'_*\ddot{x}\right) + \frac{3c^3\Gamma}{2e_*}\,\widehat{\mathbf{x}}\cdot\mathbf{E}_{\text{zp}} \tag{B2}$$

which can be solved by the Fourier expansions

$$x(t) = \int_{-\infty}^{\infty} \widetilde{x}(\Omega)\exp\left(-i\Omega t\right) d\Omega/(2\pi)^{1/2} \tag{B3}$$

and

$$E_x(\mathbf{r}, t) = \int_{-\infty}^{\infty} \widetilde{E}_x(\Omega)\exp\left(-i\Omega t\right) d\Omega/(2\pi)^{1/2} \tag{B4}$$

where $E_x \equiv \widehat{\mathbf{x}}\cdot\mathbf{E}_{\text{zp}}$, and where the ZP electric field $\mathbf{E}_{\text{zp}}$ is assumed to have an upper cutoff wavenumber k_{c*} [3, 4]:

$$\begin{aligned} \mathbf{E}_{zp}(\mathbf{r}, t) = \text{Re}\sum_{\sigma=1}^{2}\int d\Omega_k \int_0^{k_{c*}} dk\, k^2\,\widehat{\mathbf{e}}_\sigma(\mathbf{k})A_k \times \\ \times\ \exp\left[\,i\left(\mathbf{k}\cdot\mathbf{r} - \omega t + \Theta_\sigma(\mathbf{k})\right)\right], \end{aligned} \tag{B5}$$

where Re stands for "real part of"; the sum is over the two transverse polarizations of the random field; the first integral is over the solid angle in k-space; $\widehat{\mathbf{e}}_\sigma$ is the unit polarization vector; $A_k = \sqrt{\hbar\omega/2\pi^2} = e_* \sqrt{k/2\pi^2}$ is the amplitude factor which is proportional to the bare charge e_* of the PPs in the PV; $\omega = c\,k$; and Θ_σ is the random phase that gives $\mathbf{E}_{\text{zp}}$ its stochastic character.

The inverse Fourier transform of E_x from (B4) works out to be

$$\widetilde{E}_x(\Omega) = \left(\frac{\pi}{2}\right)^{1/2} \sum_{\sigma=1}^{2} \int d\Omega_k \int_0^{k_{c*}} dk\, k^2\, \widehat{\mathbf{x}} \cdot \widehat{\mathbf{e}}_\sigma(\mathbf{k}) A_k \times \\ \times \left\{ \delta(\Omega - \omega) \exp\left[\, i\,(\mathbf{k}\cdot\mathbf{r} + \Theta_\sigma(\mathbf{k}))\right] + \right. \\ \left. + \, \delta(\Omega + \omega) \exp\left[-i\,(\mathbf{k}\cdot\mathbf{r} + \Theta_\sigma(\mathbf{k}))\right] \right\} \tag{B6}$$

in a straightforward manner, where $\delta(\Omega - \omega)$ and $\delta(\Omega + \omega)$ are Dirac delta functions. Equation (B6) is easily checked by inserting it into (B4) and comparing the result with $\widehat{\mathbf{x}} \cdot \mathbf{E}_{\text{zp}}$ from (B5).

Calculating $\ddot{\mathbf{x}}$ and $d\ddot{\mathbf{x}}/dt$ from (B3) and inserting the results, along with (B4), into (B2) leads to the inverse transform

$$\widetilde{x}(\Omega) = -\frac{\left(3c^3\Gamma/2e_*\right)\, \widetilde{E}_x(\Omega)}{(1 + \Gamma\omega'_*)\Omega^2 + i\,\Gamma\Omega^3} \tag{B7}$$

for $x(t)$. Then inserting (B7) into (B3) yields

$$x(t) = -\left(\frac{3c^3\Gamma}{2e_*}\right) \text{Re} \sum_{\sigma=1}^{2} \int d\Omega_k \int_0^{k_{c*}} dk\, k^2\, \widehat{\mathbf{x}} \cdot \widehat{\mathbf{e}}_\sigma(\mathbf{k}) A_k \times \\ \times \frac{\exp\left[\, i\,(\mathbf{k}\cdot\mathbf{r} - \omega t + \Theta_\sigma(\mathbf{k}))\right]}{(1 + \Gamma\omega'_*)\omega^2 + i\,\Gamma\omega^3} \tag{B8}$$

for the random excursions of the charge.

Differentiating (B8) with respect to time while discarding the small Γ terms in the denominator leads to the approximation

$$\dot{x}(t) = \left(\frac{3c^3\Gamma}{2e_*}\right)\, \text{Re} \sum_{\sigma=1}^{2} \int d^3k\, \widehat{\mathbf{x}} \cdot \widehat{\mathbf{e}}_\sigma(\mathbf{k}) \times \\ \times \frac{A_k\, i\omega \exp\left[\, i\,(\mathbf{k}\cdot\mathbf{r} - \omega t + \Theta_\sigma(\mathbf{k}))\right]}{\omega^2} \tag{B9}$$

for the x-directed velocity, from which the dipole average (16)

$$\left\langle \dot{\mathbf{p}}_2^2 \right\rangle = 2 \left\langle (\widehat{\mathbf{x}} \cdot \dot{\mathbf{p}})^2 \right\rangle = 2e_*^2 \left\langle \dot{x}^2(t) \right\rangle = \frac{3\hbar c^5 \Gamma^2 k_{c*}^2}{2\pi} \tag{16}$$

follows, where $e_*^2 = c\hbar$ is used to eliminate e_*^2, and

$$\int d^3k \;=\; \int d\Omega_k \int_0^{k_{c*}} dk\, k^2 \tag{B10}$$

is used to expand the triple integral during the calculation.

Differentiating (B8) twice with respect to the time leads to the dipole acceleration that includes the charge's self force:

$$\ddot{\mathbf{p}} = \frac{3}{2} \left(\frac{r_*}{r_c}\right)^2 r_c c^2\, \text{Re} \sum_{\sigma=1}^{2} \int d\Omega_k \int_0^{k_{c*}} dk\, k^2\, \widehat{\mathbf{e}}_\sigma(\mathbf{k}) \times \\ \times \frac{A_k \exp\left[\, i\,(\mathbf{k}\cdot\mathbf{r} - \omega t + \Theta_\sigma(\mathbf{k}))\right]}{1 + \Gamma\omega'_* + i\,\Gamma c k}\,, \tag{B11}$$

which differs from (11) only in denominator on the right side of (B11). The last two terms in the denominator are orders of magnitude smaller than one: $\Gamma\omega'_* < r_*/r_c \sim 10^{-20}$ and $\Gamma c k < \Gamma c k_{c*} = \sqrt{\pi}\, r_*/r_c \sim 10^{-20}$. Thus the charge's self force is not a significant consideration in the definition (13) of the particle's mass.

Submitted on September 22, 2008 / Accepted on September 30, 2008

References

1. Milonni P.W. The quantum vacuum — an introduction to Quantum Electrodynamics. Academic Press, New York, 1994.
2. Weinberg S. The search for unity — notes for a history of Quantum Field Theory. *Daedalus*, v. 106, 1977, 17.
3. Daywitt W.C. The planck vacuum. *Progress in Physics*, 2009, Jan., v. 1, 20.
4. Puthoff H.E. Gravity as a zero-point-fluctuation force. *Phys. Rev. A*, 1989, v. 39, no. 5, 2333–2342.
5. de Broglie L. Une tentative d'interprétation causale et non linéaire de la mécanique ondulatoire. Gauthier-Villars, Paris, 1956. See Ch. 12.
6. Haisch B., Rueda A., Puthoff H.E. Inertia as a zero-point-field force. *Phys. Rev. A*, v. 49, no. 2, 1994, 678–695. Section III and Appendix A of this reference point out a small problem with the calculations in Section III of ref. [4]. The problem is easily corrected by using Fourier expansions in Section III of [4].
7. de la Peña L., Cetto A.M. The quantum dice — an introduction to Stochastic Electrodynamics. Kluwer Academic Publishers, Boston, 1996.
8. Dwight H.B. Tables of integrals and other mathematical data. The Macmillan Co., 3rd ed., NY, 1947. See equation 232.01.
9. Jackson J.D. Classical Electrodynamics. John Wiley & Sons, 1st ed., 2nd printing, NY, 1962.
10. Synge J.L. Geometrical Mechanics and de Broglie Waves. Cambridge University Press, 1954. See pp.106–107.

A Unified Theory of Interaction: Gravitation, Electrodynamics and the Strong Force

Pieter Wagener

Department of Physics, Nelson Mandela Metropolitan University, Port Elizabeth, South Africa
E-mail: Pieter.Wagener@nmmu.ac.za

A unified model of gravitation and electromagnetism is extended to derive the Yukawa potential for the strong force. The model satisfies the fundamental characteristics of the strong force and calculates the mass of the pion.

1 Introduction

A unified theory of interaction, as it is generally understood, implies a description of the four fundamental forces — gravitation, electromagnetism, the strong interaction and the weak force — in terms of a single mathematical formulation. It has been shown [1–3] that a unified model of gravitation and electromagnetism can be derived by starting from a Lagrangian for gravitation,

$$L = -m_0(c^2 + v^2)\exp R/r\,, \tag{1}$$

where

m_0 = *gravitational rest mass* of a test body moving at velocity $\mathbf{v}$ in the vicinity of a massive, central body of mass M,

$\gamma = 1/\sqrt{1 - v^2/c^2}$,

$R = 2GM/c^2$ is the Schwarzschild radius of the central body.

This Lagrangian characterizes the *dynamics* of a system.

Applying the canonical equations of motion, the following conservation equations follow:

$$E = mc^2 e^{R/r} = \text{total energy} = \text{constant}\,, \tag{2}$$

$$L^2 \equiv M^2 e^{2R/r} = \text{constant}, \tag{3}$$

$$L_z \equiv M_z e^{R/r} = e^{R/r} m_0 r^2 \sin^2\theta\,\dot{\phi}, \tag{4}$$

$$= z \text{ component of } \mathbf{L} = \text{constant},$$

where $m = m_0/\gamma^2$ and

$$\mathbf{M} = (\mathbf{r} \times m_0\mathbf{v}) \tag{5}$$

is the total angular momentum of the test body.

The *kinematics* of the system is determined by assuming the local and instantaneous validity of special relativity (SR). This leads to a Lagrangian characterizing the kinematics of the system,

$$L = -\tilde{m}_0 c^2 \sqrt{1 - v^2/c^2}\,\exp(r_e/r)\,. \tag{6}$$

giving the following conservation equations:

$$E_e = \tilde{m} c^2 e^{r_e/r} = \text{constant}, \tag{7}$$

$$L^2 \equiv M^2 \exp(2r_e/r) = \text{constant}, \tag{8}$$

$$L_z \equiv M_z \exp(r_e/r) = \text{constant}, \tag{9}$$

where

$$r_e = R/2\,, \tag{10}$$

$$\tilde{m} = \gamma\tilde{m}_0\,, \tag{11}$$

$$\mathbf{M} = \mathbf{r} \times \tilde{m}\mathbf{v}\,. \tag{12}$$

For the hydrogen atom, R = Schwarzschild radius of the proton, r_e = classical electron radius = $R/2 = -e^2/\tilde{m}_0 c^2$, while $\tilde{m}_0$ is the *relativistic* or *kinematical* rest mass of the electron and $\mathbf{M}$ is the total angular momentum of the orbiting electron.

We also note that

$$E_e = \tilde{E}\, e^{r_e/r}\,, \tag{13}$$

where $\tilde{E} = \tilde{m}c^2$ is the total relativistic energy.

The common factor between the gravitational and electromagnetic interactions is the radius constant, $R = 2r_e$. These two radii are related in terms of electromagnetic masses $\tilde{m}$ by $N_p \approx 10^{40}$, one of the numbers of Dirac's Large Number Hypothesis (LNH).

2 Basic properties of nuclear interaction

Any theory of the strong interaction must satisfy certain basic properties of the force. They are:

(1) the force is charge independent,

(2) it only acts over a range $\sim 10^{-13}$ cm,

(3) the form of its potential is

$$-\frac{Q^2}{r}\,\exp(-r/r_q)\,,$$

(4) where the coupling constant $Q^2/\hbar c \sim 1$–15,

(5) r_q is related to the mass of a pion by $r_q \sim h/m_\pi c$.

The above items describe the fundamental properties of the strong force and we shall limit ourselves to showing how these are accommodated in our model.

3 Derivation of an energy relation for the strong interaction

The energy equation (2) can be rearranged in a unique form for $r \approx R$ as follows:

$$\begin{aligned} E &= mc^2 \exp(R/r)\,, \\ &\approx mc^2(1+R/r)\,, \\ &= mc^2(r/R+1)R/r\,, \\ &\approx mc^2 R/r \exp(r/R)\,. \end{aligned} \tag{14}$$

The mathematical condition for the approximate equality of (2) and (14) is found by equating the two equations:

$$\begin{aligned} \exp(R/r) &\cong R/r \exp(r/R) \\ \Rightarrow R/r &\cong \exp\left[(R^2-r^2)/rR\right]. \end{aligned} \tag{15}$$

The approximate equality of the two exponential forms therefore holds uniquely for $r^2 \cong R^2$.

Repeating the above procedure for the electromagnetic energy (7) we find

$$E_e \approx \widetilde{m}c^2 r_e/r \exp(r/r_e)\,. \tag{16}$$

We rewrite the classical electron radius r_e as

$$\widetilde{m}_{e0}c^2 = -e^2/r_e\,, \tag{17}$$

where we now write $\widetilde{m}_{e0}$ for the electromagnetic rest mass of the electron.

Substituting (17) in (16) gives

$$E \approx -\widetilde{m}c^2 \left(\frac{e^2}{\widetilde{m}_{e0}c^2}\right)\frac{1}{r} \exp\left[r/(-e^2/\widetilde{m}_{e0}c^2)\right]. \tag{18}$$

Defining

$$r_q = |r_e|\,, \tag{19}$$

(18) can be written as

$$E \approx -\widetilde{m}c^2 \frac{r_q}{r} \exp(-r/r_q) \tag{20}$$

$$= -\frac{Q^2}{r} \exp(-r/r_q)\,, \tag{21}$$

where Q^2 is defined as

$$Q^2 = \widetilde{m}c^2 r_q = \widetilde{E} r_q\,. \tag{22}$$

Eq.(21) has the form of the Yukawa potential. The corresponding gravitational form is given by (14).

3.1 Model for the strong interaction

It was seen that a Yukawa-type potential exists at $r = R$ for gravitational interaction as well as at $r = r_e = R/2$ for electromagnetic interaction. The two related energy equations are respectively (14) and (16). Since our model postulates the concurrent action of gravitation and electromagnetism we have to find a model for the nuclear force that reconciles both these equations simultaneously.

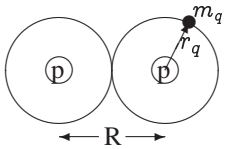

Fig. 1: Model of a deuteron. Two protons are separated at a distance R from each other. A particle of mass $\widetilde{m}_q$ and charge $-e$ moves in a figure eight pattern alternatively about each of them at a radius of $r = r_q = |r_e|$ from each proton.

Consider the model of a deuteron depicted in Figure 1.

The two protons are bound by a gravitational force according to the energy given by (2). Each proton moves in the gravitational field of the other, with the total kinetic energy expressed in terms of their reduced mass. The form of this energy is not relevant at this stage. At the same time, a charged particle of mass $\widetilde{m}_q$ moves at a radius of $r = r_q$ alternately about each proton, causing alternative conversions from proton to neutron and vice-versa. Only this hybrid form simultaneously and uniquely satisfies both the conditions for the two Yukawa-type potentials. This is possible, as can be seen from Figure 1, because $R = 2r_q$.

We provisionally call the charged, orbiting particle a q-particle.

3.2 Determination of the mass $\widetilde{m}_q$

The mass $\widetilde{m}_q$ cannot be determined independently without using some boundary condition. For gravitation, the Newtonian form in the weak-field limit was used, and for electromagnetism the condition for bound motion was applied. Both conditions are derived from observation. In this case we apply the experimental value for Q^2 and assume

$$\frac{Q^2}{\hbar c} \approx 1\,. \tag{23}$$

The q particle orbiting the protons spends half of its period about each proton. In considering the proton-q particle electromagnetic interaction, we must therefore assume that the mass $\widetilde{m}_q$ is spread over both protons. Its electromagnetic energy $\widetilde{E}$ is therefore equal to $\widetilde{m}_q c^2/2$ for a single proton-q particle interaction.

Applying this condition to (22) and using (17) we get

$$\begin{aligned} Q^2 &= \widetilde{E} r_q\,, \\ &= \frac{1}{2}\widetilde{m}_q c^2 \frac{e^2}{\widetilde{m}_{e0}c^2}\,, \\ &= \frac{\widetilde{m}_q \alpha \hbar c}{2\widetilde{m}_{e0}}\,, \end{aligned} \tag{24}$$

where $\alpha = e^2/\hbar c$ is the fine-structure constant.

The condition $Q^2/\hbar c = 1$ then yields

$$\widetilde{m}_q = \frac{2\widetilde{m}_{e0}}{\alpha}\,. \tag{25}$$

The mass $\tilde{m}_q$ is therefore equal to the mass of the π^- meson, namely

$$\tilde{m}_q = 274\,\tilde{m}_{e0} = \tilde{m}_\pi\,. \tag{26}$$

We henceforth refer to the q particle as the π^- meson or pion, and use $\tilde{m}_\pi$ for $\tilde{m}_q$, and $\tilde{m}_0$ for $\tilde{m}_{e0}$.

3.3 Comparison with characteristics of the strong interaction

In Section 2 we listed the characteristics of the strong interaction. Comparing these with the results of our model we find:

1. The attractive force between the nucleons is gravitational and therefore charge independent. It must be remembered that the gravitational force acts on the *gravitational masses* of the protons, which are reduced to the magnitude of the electromagnetic masses by the LNH factor;
2. The strong interaction appears in its unique form at $r = R = 2r_q \approx 10^{-13}$ cm;
3. The Yukawa potential is given by (21);
4. The value of the coupling constant had to be assumed to calculate the mass of the orbiting particle;
5. The expression for r_q follows from (17), (25) and $\alpha = e^2/\hbar c$:

$$r_q = \frac{e^2}{\tilde{m}_0 c^2} = \frac{2e^2}{\alpha\,\tilde{m}_\pi c^2} = \frac{2\hbar}{\tilde{m}_\pi c}\,. \tag{27}$$

4 Discussion

The above derivations are in accord with Yukawa's model of nucleon interaction through the exchange of mesons. Eq.(21) confirms the experimental result that nuclear forces only act in the region $r \cong r_q \cong 10^{-13}$ cm. Conversely, forces that only manifest in this region are describable by the Yukawa potential, which is a unique form for *both* the gravitational and electrodynamic energy equations in this region. In terms of our unified model it implies that nuclear forces only appear different from the gravitational force because experimental observations at 10^{-13} cm confirm the form of the Yukawa potential.

One of the main obstacles to the unification of gravity and the strong force has been the large difference in their coupling constants. The foregoing derivations overcomes this difficulty by the special form of the energy equations at distances close to the Schwarzschild radius.

Since the strong force appears to be a special form of gravity at small distances it explains why the strong force, like gravity, is attractive. The occurrence of repulsion at the core of the nucleus is presently little understood and if this is to be explained in terms of our model one would have to look at the form of the general energy equation in the region $r < r_q$.

It was previously shown [2, 3] how gravitational and electromagnetic energies could respectively be expressed as a power series in R/r or r_e/r. However, the form of (21) shows that this cannot be done for the energy arising from nuclear forces since $r \approx r_q$.

Our analysis of the three fundamental forces shows that the forces are all manifestations of one fundamental force, manifesting as universal gravitation. Electrodynamics arises as a kinematical effect and the nuclear force as a particular form at a distance equal to the classical electron radius. The weak force is not yet accommodated in this model, but analogously it is expected to be described by the energies of (2) and (7) in the region $r < R$.

Submitted on September 24, 2008 / Accepted on September 30, 2008

References

1. Wagener P.C. Principles of a theory of general interaction. PhD thesis, University of South Africa, 1987.
2. Wagener P.C. A classical model of gravitation. *Progress in Physics*, 2008, v. 3, 21–23.
3. Wagener P.C. A unified theory of interaction: gravitation and electrodynamics. *Progress in Physics*, 2008, v. 4, 3–9.

The Logarithmic Potential and an Exponential Mass Function for Elementary Particles

Klaus Paasch

Waldstrasse 20, 22889 Tangstedt, Germany
E-mail: klauspaasch@aol.com

The assumption that elementary particles with nonzero rest mass consist of relativistic constituents moving with constant energy pc results in a logarithmic potential and exponential expression for particle masses. This approach is put to a test by assigning each elementary particles mass a position on a logarithmic spiral. Particles then accumulate on straight lines. It is discussed if this might be an indication for exponential mass quantization.

1 Introduction

The approach of fitting parts of elementary particle mass spectra involving logarithmic potentials has been subject to research in the past decades. In this paper the simple assumption of relativistic constituents moving with constant energy pc in a logarithmic potential is discussed. A similar approach has already been presented in one of the early papers by Y. Muraki et al. [1], where the additional assumption of circular quantized orbits results in an empiric logarithmic mass function with accurate fits for several meson resonance states.

Besides the basic assumption of constant energy pc of the constituents and a resulting logarithmic potential, however, the physical approach in this paper differs and results in an exponential mass function with elementary particle masses proportional to ϕ^n, where n are integers. ϕ is a constant factor derived and thus not empirical chosen to fit particle masses.

The mass function results in points on a logarithmic spiral lining up under a polar angle φ and being separated by the factor ϕ. Elementary particle masses following this exponential quantization thus would, when placed on the spiral, be found on straight lines. Even slight changes of the value ϕ would change the particle distribution on the spiral significantly. Linear distributions for particle masses on the spiral thus would give hints if the logarithmic potential is an approach worth being further investigated to explain the wide range of elementary particle masses.

2 Physical approach

Elementary particles with mass m consist of confined constituent particles, which are moving with constant energy pc within a sphere of radius R. For this derivation it is not essential to define further properties of the constituents, e.g. if they are rotating strings or particles in circular orbits.

The only assumption made is that the force F needed to counteract a supposed centrifugal force $F_Z \propto c^2/R$ acting on each constituent is equal or proportional to pc/R, thus $F = F_Z = a_1/R$, regardless of the origin of the interaction. The potential energy needed to confine a constituent therefore is

$$E = \int \frac{a_1}{R}\, dR = a_1 \int \frac{1}{R}\, dR = a_1 \ln \frac{R}{R_a}\,, \qquad (2a)$$

where R_a is the integration constant and a_1 a parameter to be referred to later. The center of mass of the elementary particle as seen from the outside and thus the mass that is assigned to the system is

$$m = \frac{\hbar}{cR}\,. \qquad (2b)$$

The logarithmic potential energy in Eq. (2a) is assumed to be proportional to m/R, yielding

$$E = \frac{a_2 m}{R}\,. \qquad (2c)$$

Both parameters a_1 and a_2 are supposed not to be a function of R, but to depend on constituent particle properties and coupling constants, resp. For example, a_1/a_2 could be set equal c^2/γ (γ is the gravitational constant), but such a constraint is not required. Inserting m from Eq. (2b) into Eq. (2c) yields

$$E = a_2 \frac{\hbar}{cR^2}\,. \qquad (2d)$$

The angular momentum of the system is assumed to be an integer multiple n of $\hbar$, with a ground state of radius R_0.

$$E_n = a_2 \frac{\hbar}{cR_n^2} = a_2 \frac{(n+1)\hbar}{cR_0^2}, \quad n = 0, 1, 2 \ldots \qquad (2e)$$

From Eq. (2a) and Eq. (2e) it follows that

$$\ln \frac{R_a}{R_n} = -(n+1)\frac{R_a^2}{R_0^2} \quad \text{with} \quad R_a = \left(\frac{a_2\hbar}{a_1 c}\right)^{\frac{1}{2}}, \qquad (2f)$$

assigning the integration constant R_a a value. For $n = 0$ the value for R_n is set to R_0, allowing to calculate the ratio R_a/R_0 using Eq. (2f)

$$x = e^{-x^2} \quad \text{with} \quad x = \frac{R_a}{R_0}\,,$$

and with defining $\phi = 1/x$ resulting in

$$\phi = 1.53158. \qquad (2g)$$

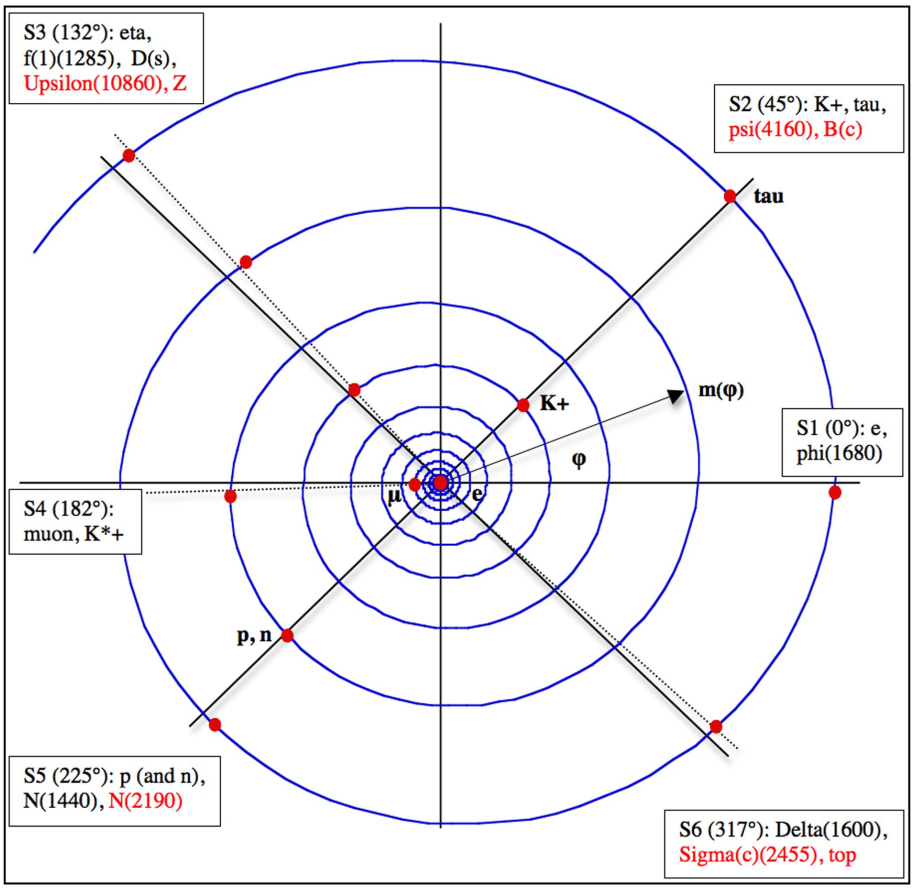

Fig. 1: The masses of elementary particles placed on the spiral and listed for each resulting sequence starting from the center. The solid lines are seperated by 45°. The red dot in the center is the electron at 0°. The outer limit of the spiral at 135° is about 2 GeV. Particles allocated on a sequence, but with masses too large for this scale are marked red in the attached listings of sequence particles. The top for example is far outside on S6 at 317°.

Since $\ln\phi = 1/\phi^2$ it follows that

$$R_n = R_a e^{(n+1)\ln\phi}\,. \tag{2h}$$

With Eq. (2b) and Eq. (2f) R_a can be written as

$$R_a = R_0\alpha\,, \tag{2i}$$

where

$$R_0 = \frac{\hbar}{m_0 c} \quad \text{with} \quad \alpha = m_0\left(\frac{a_2 c}{a_1\hbar}\right)^{\frac{1}{2}}$$

and inserting R_a into Eq. (2h) yields

$$R_n = R_0 e^{k\varphi_n} \quad \text{where} \quad k = \frac{1}{2\pi}\ln\phi\,, \tag{2j}$$

and

$$\varphi_n = 2\pi(n+1) + \varphi_s \quad \text{and} \quad \varphi_s = 2\pi\,\frac{\ln\alpha}{\ln\phi}\,.$$

Eq. (2j) applies to particle masses by inserting R_n into Eq. (2b). Thus with

$$m_n = \frac{\hbar}{R_n c} \quad \text{and} \quad m_0 = \frac{\hbar}{R_0 c}$$

it follows that

$$m_n = m_0 e^{k\varphi_n}\,. \tag{2k}$$

In Eq. (2k) $-k$ is substituted by k, which just determines to start with m_0 as the smallest instead of the biggest mass and thus turning the spiral from the inside to the outside instead vice versa. This has no influence on the results. m_n are elementary particle masses and points on a logarithmic spiral lining up at an angle φ_s as defined in Eq. (2j). These points are referred to as a particle sequence $S(\varphi_s)$. The angle φ_s should not be the same for all elementary particles since it is a function of the parameters a_1 and a_2.

To determine whether elementary particle masses tend to line up in sequences first of all a logarithmic spiral

$$m(\varphi) = m_0 e^{k\varphi}$$

with continues values for φ is calculated. m_0 is the initial mass and thus starting point of the spiral at $\varphi = 0$. The starting point $m_0 = m(\varphi = 0)$ is set so that as a result the electron is placed at the angle $\varphi = 0$.

One turn of the spiral $m(\varphi) \to m(\varphi + 2\pi)$ corresponds to multiplying $m(\varphi)$ by ϕ, yielding $m(\varphi)\phi = m(\varphi + 2\pi)$. Spiral points lining up at the same polar angle φ differ by a factor ϕ.

In a second step for each elementary particle mass pro-

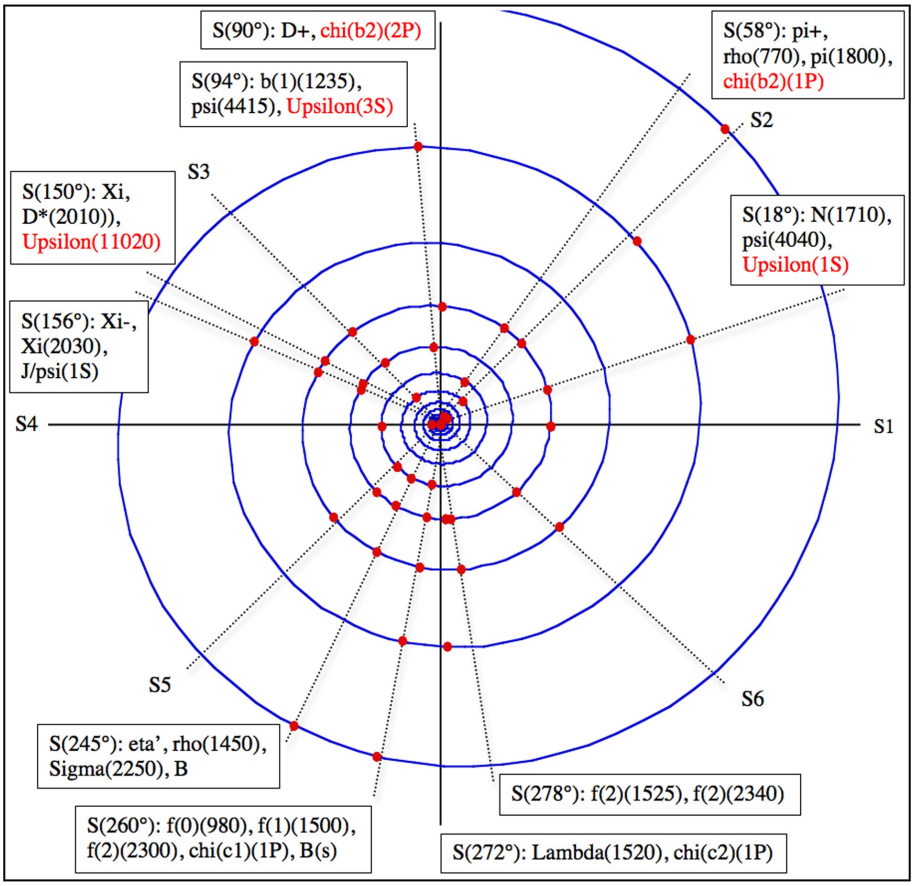

Fig. 2: Additional sequences shown within a mass range of 6.5 GeV. See Fig. 1 for listings of S1-S6.

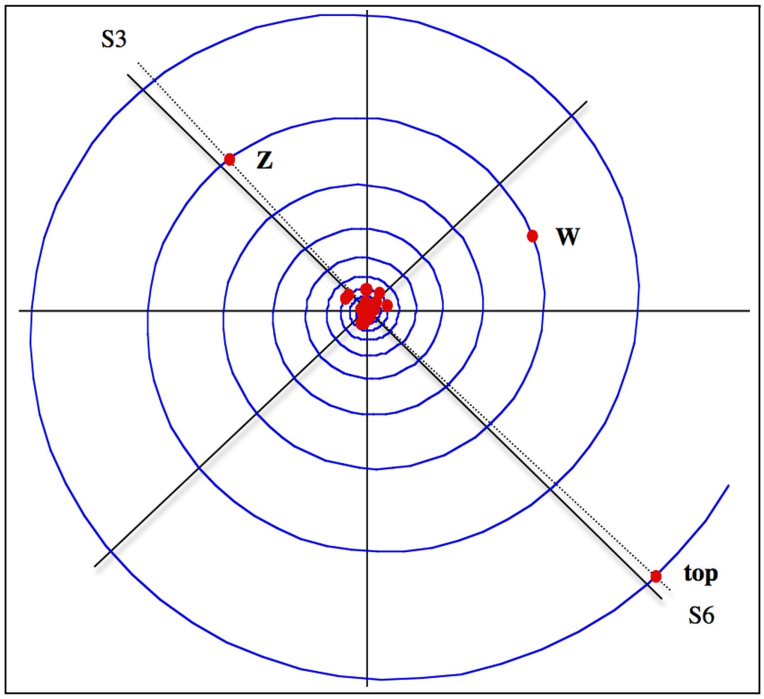

Fig. 3: At a mass range of 175 GeV the Z and top align with S3 and S6, resp., as listed in Fig. 1.

vided by the PDG table 2004 [2, 3] the resulting angle φ_s in the logarithmic spiral is calculated using Eq. (2k) with m_0 as the electron mass and φ_s as defined in Eq. (2j). This results in polar coordinates (m_n, φ_s) and thus a point on the spiral for each elementary particle.

After all elementary particles are entered as points into the spiral it is analyzed if sequences $S(\varphi_s)$, thus particle masses m_n lining up in the spiral in the same direction φ_s are found.

3 Results

The results for particle sequences are shown step by step for mass ranges from 2 GeV to 175 GeV to provide a clear overview. Elementary particles which are part of a sequence, but out of the shown mass range and thus not displayed as red dots in the spiral are marked red in the list of sequence particles, which is attached to each sequence.

All allocations of elementary particle masses to sequences are accurate within at least $\Delta m/m = 4\times10^{-3}$. All sequence positions are fitted and accurate within $\varphi_s \pm 0,5^\circ$.

Fig. 1 shows the results within a mass range of 2 GeV from the center to the outer limit of the spiral. The position of the electron is set to 0° as the starting point of the spiral, the muon then is found to be at 182°. Also on these sequences are the phi (1680) and the K* (892), resp.

The K+, tau, psi (4160) and B (c) are at 45°. The proton, N (1440) and N (2190) opposite at 225°. The eta, f (1)(1285), D (s), Upsilon (10860), Z-boson are at 132° and the Delta (1600), Sigma (c)(2455) and the top opposite at 317°, resp. Calculating the Planck mass with $m_{pl} = (\hbar c/\gamma)^{1/2}$ results in a position on sequence S6.

In Fig. 2 additional sequences within a mass range of 6.5 GeV are shown, e.g. the pi+, rho (770), pi (1800) and chi (b2)(1P) are aligned at S (58°).

Also the f (0)(980), f (1)(1500), f (2)(2300), chi (b2)(1P) and B (s) are aligned precisely in a sequence at 260°. The f (2)(1525) and f (2)(2340) align at 278°.

Other sequences are as follows, at 150° (Xi, D* (2010), Upsilon (11020)), at 156° (Xi-, Xi (2030), J/psi (1S)) and at 245° (eta', rho (1450), Sigma (2250), B). Also the psi (4040), psi (4415), Upsilon (1S) and Upsilon (3S) are found in sequences.

A picture of the mass range of elementary particles at 175 GeV is shown in Fig. 3, with the Z and top aligning in the sequences S3 and S6, resp., as listed in Fig. 1.

4 Discussion and conclusion

In this simple model the mass distribution of elementary particles strongly depends on the derived quantization factor ϕ. Even slight changes $\Delta\phi/\phi \approx 5\times10^{-4}$ disrupt the particle sequences. Thus of interest are the symmetric sequences S1-S6 with precise positions for the electron, muon, kaon, proton and tau. Also the eta, K (892), D (s), B (c), Upsilon (10860), Z and top are placed on these sequences. Other sequences align particles like f's, pi's and Xi's.

The existence of more than one sequence implies that α in Eq. (2i), i.e. the ratio of parameters a_1 and a_2, has several values within the elementary particle mass spectrum.

Randomly chosen values for ϕ other than the derived one do not provide symmetric and precise results, but rather uniform distributions, as should be expected. The results of the precise and specific sequences in the derived logarithmic spiral still might be a pure coincidence. But they also could be an indication for constituent particles moving in a logarithmic potential, resulting in an exponential quantization for elementary particle masses. Then the results would suggest the logarithmic potential to be considered an approach worth being further investigated to explain the wide range of elementary particle masses.

Submitted on November 27, 2008
Accepted on October 06, 2008

References

1. Muraki Y., Mori K., Nakagawa M. Logarithmic mass formulae for elementary particles and a new quantum number. *Lettere al Nuovo Cimento*, 1978, v. 23, no. 1, 27–31.
2. NIST, National Institute of Standards and Technology (http://physics.nist.gov).
3. Particle Data Group (http://pdg.lbl.go).

A Note of Extended Proca Equations and Superconductivity

Vic Christianto*, Florentin Smarandache†, and Frank Lichtenberg‡

*Sciprint.org — a Free Scientific Electronic Preprint Server, http://www.sciprint.org
E-mail: admin@sciprint.org
†Chair of the Dept. of Mathematics, University of New Mexico, Gallup, NM 87301, USA
E-mail: smarand@unm.edu
‡Bleigaesschen 4, D-86150 Augsburg, Germany
E-mail: novam@nlp-nicoletta.de

It has been known for quite long time that the electrodynamics of Maxwell equations can be extended and generalized further into Proca equations. The implications of introducing Proca equations include an alternative description of superconductivity, via extending London equations. In the light of another paper suggesting that Maxwell equations can be written using quaternion numbers, then we discuss a plausible extension of Proca equation using biquaternion number. Further implications and experiments are recommended.

1 Introduction

It has been known for quite long time that the electrodynamics of Maxwell equations can be extended and generalized further into Proca equations, to become electrodynamics with finite photon mass [11]. The implications of introducing Proca equations include description of superconductivity, by extending London equations [18]. In the light of another paper suggesting that Maxwell equations can be generalized using quaternion numbers [3, 7], then we discuss a plausible extension of Proca equations using biquaternion number. It seems interesting to remark here that the proposed extension of Proca equations by including quaternion differential operator is merely the next logical step considering already published suggestion concerning the use of quaternion differential operator in electromagnetic field [7, 8]. This is called Moisil-Theodoresco operator (see also Appendix A).

2 Maxwell equations and Proca equations

In a series of papers, Lehnert argued that the Maxwell picture of electrodynamics shall be extended further to include a more "realistic" model of the *non-empty vacuum*. In the presence of electric space charges, he suggests a general form of the Proca-type equation [11]:

$$\left(\frac{1}{c^2}\frac{\partial}{\partial t^2} - \nabla^2\right) A_\mu = \mu_0 J_\mu, \qquad \mu = 1, 2, 3, 4. \quad (1)$$

Here $A_\mu = (A, i\phi/c)$, where A and ϕ are the magnetic vector potential and the electrostatic potential in three-space, and:

$$J_\mu = (j,\ ic\bar{\phi})\,. \quad (2)$$

However, in Lehnert [11], the right-hand terms of equations (1) and (2) are now given a new interpretation, where $\bar{\phi}$ is the nonzero electric charge density in the vacuum, and j stands for an associated three-space current-density.

The background argument of Proca equations can be summarized as follows [6]. It was based on known definition of derivatives [6, p. 3]:

$$\left.\begin{aligned} \partial^\mu &= \frac{\partial}{\partial x^\mu} = \left(\frac{\partial}{\partial t}; \frac{\partial}{\partial x}, \frac{\partial}{\partial y}, \frac{\partial}{\partial z}\right) = \left(\partial^0; -\nabla\right) \\ \partial_\mu &= \frac{\partial}{\partial x^\mu} = \left(\partial^0; \nabla\right) \end{aligned}\right\}, \quad (3)$$

$$\partial_\mu a^\mu = \frac{\partial a^0}{\partial t} + \nabla \vec{a}\,, \quad (4)$$

$$\partial_\mu \partial^\mu = \frac{\partial^2}{\partial t^2} - \frac{\partial^2}{\partial x^2} - \frac{\partial^2}{\partial y^2} - \frac{\partial^2}{\partial z^2} = \partial_0^2 - \nabla^2 = \partial^\mu \partial_\mu\,, \quad (5)$$

where ∇^2 is Laplacian and $\partial_\mu \partial^\mu$ is d'Alembertian operator. For a massive vector boson (spin-1) field, the Proca equation can be written in the above notation [6, p. 7]:

$$\partial_\mu \partial^\mu A^\nu - \partial^\nu (\partial_\mu A^\mu) + m^2 A^\nu = j^\nu. \quad (6)$$

Interestingly, there is also a neat link between Maxwell equations and quaternion numbers, in particular via the *Moisil-Theodoresco D* operator [7, p. 570]:

$$D = i_1 \frac{\partial}{\partial x_1} + i_2 \frac{\partial}{\partial x_2} + i_3 \frac{\partial}{\partial x_3}\,. \quad (7)$$

There are also known links between Maxwell equations and Einstein-Mayer equations [8]. Therefore, it seems plausible to extend further the Maxwell-Proca equations to biquaternion form too; see also [9, 10] for links between Proca equation and Klein-Gordon equation. For further theoretical description on the links between biquaternion numbers, Maxwell equations, and unified wave equation, see Appendix A.

3 Proca equations and superconductivity

In this regards, it has been shown by Sternberg [18], that the classical *London equations* for superconductors can be written in differential form notation and in relativistic form, where

they yield the Proca equations. In particular, the field itself acts as its own charge carrier [18].

Similarly in this regards, in a recent paper Tajmar has shown that superconductor equations can be rewritten in terms of Proca equations [19]. The basic idea of Tajmar appears similar to Lehnert's extended Maxwell theory, i.e. to include *finite photon mass* in order to explain superconductivity phenomena. As Tajmar puts forth [19]:

> "In quantum field theory, superconductivity is explained by a *massive photon*, which acquired mass due to gauge symmetry breaking and the Higgs mechanism. The wavelength of the photon is interpreted as the London penetration depth. With a nonzero photon mass, the usual Maxwell equations transform into the so-called Proca equations which will form the basis for our assessment in superconductors and are only valid for the superconducting electrons."

Therefore the basic Proca equations for superconductor will be [19, p. 3]:

$$\nabla \times \bar{E} = -\frac{\partial \bar{B}}{\partial t}\,, \tag{8}$$

and

$$\nabla \times B = \mu_0 \bar{j} + \frac{1}{c^2}\frac{\partial \bar{E}}{\partial t} - \frac{1}{\lambda^2}\bar{A}\,. \tag{9}$$

The Meissner effect is obtained by taking curl of equation (9). For non-stationary superconductors, the same equation (9) above will yield second term, called London moment.

Another effects are recognized from the finite Photon mass, i.e. the photon wavelength is then interpreted as the London penetration depth and leads to a photon mass about 1/1000 of the electron mass. This furthermore yields the Meissner-Ochsenfeld effect (shielding of electromagnetic fields entering the superconductor) [20].

Nonetheless, the use of Proca equations have some known problems, i.e. it predicts that a charge density rotating at angular velocity should produce huge magnetic fields, which is *not observed* [20]. One solution of this problem is to recognize that the value of photon mass containing charge density is different from the one in free space.

4 Biquaternion extension of Proca equations

Using the method we introduced for Klein-Gordon equation [2], then it is possible to generalize further Proca equations (1) using biquaternion differential operator, as follows:

$$(\diamondsuit\bar{\diamondsuit})A_\mu - \mu_0 J_\mu = 0\,, \qquad \mu = 1,2,3,4, \tag{10}$$

where (see also Appendix A):

$$\diamondsuit = \nabla^q + i\nabla^q = \left(-i\,\frac{\partial}{\partial t} + e_1\,\frac{\partial}{\partial x} + e_2\,\frac{\partial}{\partial y} + e_3\,\frac{\partial}{\partial z}\right) + \\ + i\left(-i\,\frac{\partial}{\partial T} + e_1\,\frac{\partial}{\partial X} + e_2\,\frac{\partial}{\partial Y} + e_3\,\frac{\partial}{\partial Z}\right). \tag{11}$$

Another way to generalize Proca equations is by using its standard expression. From d'Alembert wave equation we get [6]:

$$\left(\frac{1}{c^2}\frac{\partial}{\partial t^2} - \nabla^2\right) A_\mu = \mu_0 J_\mu\,, \qquad \mu = 1,2,3,4, \tag{12}$$

where the solution is Liennard-Wiechert potential. Then the Proca equations are [6]:

$$\left[\left(\frac{1}{c^2}\frac{\partial}{\partial t^2} - \nabla^2\right) + \left(\frac{m_p c}{\hbar}\right)^2\right] A_\mu = 0\,, \quad \mu = 1,2,3,4, \tag{13}$$

where m is the photon mass, c is the speed of light, and $\hbar$ is the reduced Planck constant. Equation (13) and (12) imply that photon mass can be understood as charge density:

$$J_\mu = \frac{1}{\mu_0}\left(\frac{m_p c}{\hbar}\right)^2. \tag{14}$$

Therefore the "biquaternionic" extended Proca equations (13) become:

$$\left[\diamondsuit\bar{\diamondsuit} + \left(\frac{m_p c}{\hbar}\right)^2\right] A_\mu = 0\,, \qquad \mu = 1,2,3,4. \tag{15}$$

The solution of equations (12) and (12) can be found using the same computational method as described in [2].

Similarly, the generalized structure of the wave equation in electrodynamics — *without* neglecting the finite photon mass (Lehnert-Vigier) — can be written as follows (instead of eq. 7.24 in [6]):

$$\left[\diamondsuit\bar{\diamondsuit} + \left(\frac{m_p c}{\hbar}\right)^2\right] A^a_\mu = R A^a_\mu\,, \quad \mu = 1,2,3,4. \tag{16}$$

It seems worth to remark here that the method as described in equation (15)-(16) or ref. [6] is not the only possible way towards generalizing Maxwell equations. Other methods are available in literature, for instance by using topological geometrical approach [14, 15].

Nonetheless further experiments are recommended in order to verify this proposition [23,24]. One particular implication resulted from the introduction of biquaternion differential operator into the Proca equations, is that it may be related to the notion of "active time" introduced by Paine & Pensinger sometime ago [13]; the only difference here is that now the time-evolution becomes nonlinear because of the use of 8-dimensional differential operator.

5 Plausible new gravitomagnetic effects from extended Proca equations

While from Proca equations one can expect to observe gravitational London moment [4,22] or other peculiar gravitational shielding effect unable to predict from the framework of General Relativity [5, 16, 22], one can expect to derive new gravitomagnetic effects from the proposed extended Proca equations using the biquaternion number as described above.

Furthermore, another recent paper [1] has shown that given the finite photon mass, it would imply that if m is due to a Higgs effect, then the *Universe is effectively similar to a Superconductor.* This may support De Matos's idea of dark energy arising from superconductor, in particular via *Einstein-Proca* description [1, 5, 16].

It is perhaps worth to mention here that there are some indirect observations [1] relying on the effect of Proca energy (assumed) on the galactic plasma, which implies the limit:

$$m_A = 3\times10^{-27}\ \text{eV}. \tag{17}$$

Interestingly, in the context of cosmology, it can be shown that Einstein field equations with cosmological constant are approximated to the second order in the perturbation to a flat background metric [5]. Nonetheless, further experiments are recommended in order to verify or refute this proposition.

6 Some implications in superconductivity research

We would like to mention the Proca equation in the following context. Recently it was hypothesized that the creation of superconductivity at room temperature may be achieved by a resonance-like interaction between an everywhere present background field and a special material having the appropriate crystal structure and chemical composition [12]. According to Global Scaling, a new knowledge and holistic approach in science, the everywhere present background field is given by oscillations (standing waves) in the universe or physical vacuum [12].

The just mentioned hypothesis how superconductivity at room temperature may come about, namely by a resonance-like interaction between an everywhere present background field and a special material having the appropriate crystal structure and chemical composition, seems to be supported by a statement from the so-called ECE Theory which is possibly related to this hypothesis [12]:

> "... One of the important practical consequences is that a material can become a superconductor by absorption of the inhomogeneous and homogeneous currents of ECE space-time ..." [6].

This is a quotation from a paper with the title "ECE Generalizations of the d'Alembert, Proca and Superconductivity Wave Equations ..." [6]. In that paper the Proca equation is derived as a special case of the ECE field equations.

These considerations raises the interesting question about the relationship between (a possibly new type of) superconductivity, space-time, an everywhere-present background field, and the description of superconductivity in terms of the Proca equation, i.e. by a massive photon which acquired mass by symmetry breaking. Of course, how far these suggestions are related to the physical reality will be decided by further experimental and theoretical studies.

7 Concluding remarks

In this paper we argue that it is possible to extend further Proca equations for electrodynamics of superconductivity to biquaternion form. It has been known for quite long time that the electrodynamics of Maxwell equations can be extended and generalized further into Proca equations, to become electrodynamics with finite photon mass. The implications of introducing Proca equations include description of superconductivity, by extending London equations. Nonetheless, further experiments are recommended in order to verify or refute this proposition.

Acknowledgement

Special thanks to Prof. M. Pitkanen for comments on the draft version of this paper.

Submitted on September 01, 2008 / Accepted on October 06, 2008

Appendix A: Biquaternion, Maxwell equations and unified wave equation [3]

In this section we're going to discuss Ulrych's method to describe unified wave equation [3], which argues that it is possible to define a unified wave equation in the form [3]:

$$D\phi(x) = m_\phi^2 \cdot \phi(x), \tag{A.1}$$

where unified (wave) differential operator D is defined as:

$$D = \left[(P - qA)_\mu \left(\bar{P} - qA\right)^\mu\right]. \tag{A.2}$$

To derive Maxwell equations from this unified wave equation, he uses free photon expression [3]:

$$DA(x) = 0, \tag{A.3}$$

where potential A(x) is given by:

$$A(x) = A^0(x) + jA^1(x), \tag{A.4}$$

and with electromagnetic fields:

$$E^i(x) = -\partial^0 A^i(x) - \partial^i A^0(x), \tag{A.5}$$

$$B^i(x) = \in^{ijk} \partial_j A_k(x). \tag{A.6}$$

Inserting these equations (A.4)-(A.6) into (A.3), one finds Maxwell electromagnetic equation [3]:

$$\begin{aligned} &-\nabla \bullet E(x) - \partial^0 C(x) + ij\nabla \bullet B(x) - \\ &- j(\nabla x B(x) - \partial^0 E(x) - \nabla C(x)) - \\ &- i(\nabla x E(x) + \partial^0 B(x)) = 0. \end{aligned} \tag{A.7}$$

For quaternion differential operator, we define quaternion Nabla operator:

$$\begin{aligned} \nabla^q \equiv c^{-1}\frac{\partial}{\partial t} + \left(\frac{\partial}{\partial x}\right) i + \left(\frac{\partial}{\partial y}\right) j + \left(\frac{\partial}{\partial z}\right) k = \\ = c^{-1}\frac{\partial}{\partial t} + \vec{i}\cdot\vec{\nabla}. \end{aligned} \tag{A.8}$$

And for biquaternion differential operator, we may define a diamond operator with its conjugate [3]:

$$\diamondsuit\bar{\diamondsuit} \equiv \left(c^{-1}\frac{\partial}{\partial t} + c^{-1}\, i\,\frac{\partial}{\partial t}\right) + \{\vec{\nabla}\}* \qquad (A.9)$$

where Nabla-star-bracket operator is defined as:

$$\{\vec{\nabla}\}* \equiv \left(\frac{\partial}{\partial x} + i\,\frac{\partial}{\partial X}\right) i + \\ + \left(\frac{\partial}{\partial y} + i\,\frac{\partial}{\partial Y}\right) j + \left(\frac{\partial}{\partial z} + i\,\frac{\partial}{\partial Z}\right) k\,. \qquad (A.10)$$

In other words, equation (A.9) can be rewritten as follows:

$$\diamondsuit\bar{\diamondsuit} \equiv \left(c^{-1}\,\frac{\partial}{\partial t} + c^{-1}\, i\,\frac{\partial}{\partial T}\right) + \left(\frac{\partial}{\partial x} + i\,\frac{\partial}{\partial X}\right) i + \\ + \left(\frac{\partial}{\partial y} + i\,\frac{\partial}{\partial Y}\right) j + \left(\frac{\partial}{\partial z} + i\,\frac{\partial}{\partial Z}\right) k\,. \qquad (A.11)$$

From this definition, it shall be clear that there is neat link between equation (A.11) and the Moisil-Theodoresco D operator, i.e. [7, p. 570]:

$$\diamondsuit\bar{\diamondsuit} \equiv \left(c^{-1}\,\frac{\partial}{\partial t} + c^{-1}\, i\,\frac{\partial}{\partial t}\right) + (D_{xi} + iD_{Xi}) = \\ = \left(c^{-1}\,\frac{\partial}{\partial t} + c^{-1} i\,\frac{\partial}{\partial T}\right) + \left[i_1\,\frac{\partial}{\partial x_1} + i_2\,\frac{\partial}{\partial x_2} + i_3\,\frac{\partial}{\partial x_3}\right] + \\ + i\left[i_1\,\frac{\partial}{\partial X_1} + i_2\,\frac{\partial}{\partial X_2} + i_3\,\frac{\partial}{\partial X_3}\right]. \qquad (A.12)$$

In order to define biquaternionic representation of Maxwell equations, we could extend Ulrych's definition of *unified differential operator* [3,17,21] to its biquaternion counterpart, by using equation (A.2) and (A.10), to become:

$$\{D\}* \equiv \left[\left(\{P\}* - q\{A\}*\right)_{\mu}\,\left(\{\bar{P}\}* - q\{A\}*\right)^{\mu}\right], \qquad (A.13)$$

or by definition $P = -i\hbar\nabla$, equation (A.13) could be written as:

$$\{D\}* \equiv \left[\left(-\hbar\{\vec{\nabla}\}* - q\{A\}*\right)_{\mu}\left(-\hbar\{\vec{\nabla}\}* - q\{A\}*\right)^{\mu}\right], \qquad (A.14)$$

where each component is now defined in term of biquaternionic representation. Therefore the biquaternionic form of the *unified wave equation* [3] takes the form:

$$\{D\} * \phi(x) = m_{\phi}^{2} \cdot \phi(x)\,, \qquad (A.15)$$

which is a wave equation for massive electrodynamics, quite similar to Proca representation.

Now, biquaternionic representation of free photon fields could be written as follows:

$$\{D\} * A(x) = 0\,. \qquad (A.16)$$

References

1. Adelberger E., Dvali G., and Gruzinov A. Photon-mass bound destroyed by vortices. *Phys. Rev. Lett.*, 2007, v. 98, 010402.
2. Christianto V. and Smarandache F. Numerical solution of radial biquaternion Klein-Gordon equation. *Progress in Physics*, 2008, v.1.
3. Christianto V. *Electronic J. Theor. Physics*, 2006, v. 3, no. 12.
4. De Matos C. J. arXiv: gr-qc/0607004; Gravio-photon, superconductor and hyperdrives. http://members.tripod.com/da_theoretical1/warptohyperdrives.html
5. De Matos C.J. arXiv: gr-qc/0609116.
6. Evans M.W. ECE generalization of the d'Alembert, Proca and superconductivity wave equations: electric power from ECE space-time. §7.2; http://aias.us/documents/uft/a51stpaper.pdf
7. Kravchenko V.V. and Oviedo H. On quaternionic formulation of Maxwell's equations for chiral media and its applications. *J. for Analysis and its Applications*, 2003, v. 22, no. 3, 570.
8. Kravchenko V.G. and Kravchenko V.V. arXiv: math-ph/0511092.
9. Jakubsky V. and Smejkal J. A positive definite scalar product for free Proca particle. arXiv: hep-th/0610290.
10. Jakubsky V. *Acta Polytechnica*, 2007, v. 47, no. 2–3.
11. Lehnert B. Photon physics of revised electromagnetics. *Progress in Physics*, 2006, v. 2.
12. Lichtenberg F. Presentation of an intended research project: searching for room temperature superconductors. August, 2008, http://www.sciprint.org; http://podtime.net/sciprint/fm/uploads/files/1218979173Searching_for_Room_Temperature_Superconductors.pdf
13. Paine D.A. and Pensinger W.L. *Int. J. Quantum Chem.*, 1979, v.15, 3; http://www.geocities.com/moonhoabinh/ithapapers/hydrothermo.html
14. Olkhov O.A. Geometrization of classical wave fields. arXiv: 0801.3746.
15. Olkhov O.A. *Zh. Fiz. Khim.*, 2002, v. 21, 49; arXiv: hep-th/0201020.
16. Poenaru D. A. Proca (1897–1955). arXiv: physics/0508195; http://th.physik.uni-frankfurt.de/∼poenaru/PROCA/Proca.pdf
17. Ulrych S. arXiv: physics/0009079.
18. Sternberg S. On the London equations. *PNAS*, 1992, v. 89, no. 22, 10673–10675.
19. Tajmar M. Electrodynamics in superconductors explained by Proca equations. arXiv: 0803.3080.
20. Tajmar M. and De Matos C.J. arXiv: gr-qc/0603032.
21. Yefremov A., Smarandache F. and Christianto V. Yang-Mills field from quaternion space geometry, and its Klein-Gordon representation. *Progress in Physics*, 2007, v. 3.
22. Gravitational properties of superconductors. http://functional-materials.at/rd/rd_spa_gravitationalproperties_de.html
23. Magnetism and superconductivity observed to exist in harmony. Aug. 28, 2008, http://www.physorg.com/news139159195.html
24. Room temperature superconductivity. Jul. 8, 2008, http://www.physorg.com/news134828104.html

Phase Transitions in Even-Even Palladium Isotopes

Sohair M. Diab

Faculty of Education, Phys. Dept., Ain Shams University, Cairo, Egypt

E-mail: mppe2@yahoo.co.uk

The positive and negative parity states of the even-even palladium isotopes were studied within the frame work of the interacting boson approximation model (IBA-1). The energy spectra, potential energy surfaces, electromagnetic transition probabilities, back bending and staggering effect have been calculated. The potential energy surfaces show smooth transition from vibrational-like to gamma-soft and finally to rotational-like nuclei. Staggering effectle, has been observed between the positive and negative parity states in palladium isotopes. The agreement between theoretical predictions and experimental values are fairly good.

1 Introduction

The region of neutron-excess nuclei at mass $A \cong 100$ is an area of interest to many authors because of the observation of the phase transitions. Three phase transitional regions are well known where the structure changes rapidly. Nd-Sm-Gd and Ru-Pd regions where the change is from spherical to well deformed nuclei when moving from lighter to heavier isotopes. But, Os-Pt regions the change is from well deformed to γ-soft when moving from lighter to heavier isotopes.

The structure of these transitional nuclei has been the subject of many experimental and theoretical studies. Experimentally, levels of ^{102}Pd were populated from the decay of ^{102}Ag populated in the ^{89}Y (^{16}O,3n) reaction [1] and their properties were studied through γ spectroscopy. Also, measurements were performed using an array of eight HPGe detectors on gamma multiplicity gated on proton spectra of $^{102\text{-}104}$Pd which have been measured [2] in the ^{12}C + ^{93}Np reaction E(^{12}C) = 40 MeV, at backward angles.The cross-section along with the angular momentum and excitation energy are populated.

Theoretically, the transitional regions and phase transitions in palladium isotopes have been analyzed in the frame work of the IBA-2 model [3–7]. From the analysis of energies, static moments, transition rates, quadrupole moments and mixing ratios, they were able to identify states having large mixed - symmetry components.

Cranked Strutinsky Method [8], Geometric Collective Model [9] (GCM) and the Relativistic Mean Field Theory [10] have examined palladium series of isotopes to find examples displaying the characteristics of E(5) critical point behavior [11]for the shape transition from spherical vibrator to a triaxially soft rotor.

In this article, we carried out a microscopic study of the Yrast and negative parity states, electromagnetic transition rates, $B(E1)$, $B(E2)$, potential energy surfaces, $V(\beta,\gamma)$, for $^{100\text{-}116}$Pd nuclei employing the interacting boson model.

2 Interacting boson approximation model (IBA-1)

2.1 Level energies

IBA-1 model [12–14] was applied to the positive and negative parity states in even-even $^{100\text{-}116}$Pd isotopes. The Hamiltonian employed [15] in the present calculation is:

$$\begin{aligned} H &= EPS \cdot n_d + PAIR \cdot (P \cdot P) + \\ &+ \frac{1}{2} ELL \cdot (L \cdot L) + \frac{1}{2} QQ \cdot (Q \cdot Q) + \\ &+ 5OCT \cdot (T_3 \cdot T_3) + 5HEX \cdot (T_4 \cdot T_4) , \end{aligned} \tag{1}$$

where

$$P \cdot p = \frac{1}{2} \left[\begin{array}{l} \left\{ (s^\dagger s^\dagger)_0^{(0)} - \sqrt{5} (d^\dagger d^\dagger)_0^{(0)} \right\} x \\ \left\{ (ss)_0^{(0)} - \sqrt{5} (\tilde{d}\tilde{d})_0^{(0)} \right\} \end{array} \right]_0^{(0)} , \tag{2}$$

$$L \cdot L = -10\sqrt{3} \left[(d^\dagger \tilde{d})^{(1)} x \, (d^\dagger \tilde{d})^{(1)} \right]_0^{(0)} , \tag{3}$$

$$Q \cdot Q = \sqrt{5} \left[\begin{array}{l} \left\{ (S^\dagger \tilde{d} + d^\dagger s)^{(2)} - \dfrac{\sqrt{7}}{2} (d^\dagger \tilde{d})^{(2)} \right\} x \\ \left\{ (s^\dagger \tilde{d} + + \tilde{d}s)^{(2)} - \dfrac{\sqrt{7}}{2} (d^\dagger \tilde{d})^{(2)} \right\} \end{array} \right]_0^{(0)} , \tag{4}$$

$$T_3 \cdot T_3 = -\sqrt{7} \left[(d^\dagger \tilde{d})^{(2)} x \, (d^\dagger \tilde{d})^{(2)} \right]_0^{(0)} , \tag{5}$$

$$T_4 \cdot T_4 = 3 \left[(d^\dagger \tilde{d})^{(4)} x \, (d^\dagger \tilde{d})^{(4)} \right]_0^{(0)} . \tag{6}$$

In the previous formulas, n_d is the number of boson; $P \cdot P$, $L \cdot L$, $Q \cdot Q$, $T_3 \cdot T_3$ and $T_4 \cdot T_4$ represent pairing, angular momentum, quadrupole, octupole and hexadecupole interactions between the bosons; EPS is the boson energy; and $PAIR$, ELL, QQ, OCT, HEX is the strengths of the pairing, angular momentum, quadrupole, octupole and hexadecupole interactions.

nucleus	EPS	$PAIR$	ELL	QQ	OCT	HEX	$E2SD(eb)$	$E2DD(eb)$
^{100}Pd	0.6780	0.000	0.0095	−0.020	0.0000	0.0000	0.1020	−0.3817
^{102}Pd	0.5840	0.000	0.0115	−0.0200	0.0000	0.0000	0.1270	−0.3757
^{104}Pd	0.5750	0.0000	0.0225	−0.0200	0.0000	0.0000	0.1210	−0.3579
^{106}Pd	0.5630	0.0000	0.0230	−0.0200	0.0000	0.0000	0.1220	−0.3609
^{108}Pd	0.5180	0.0000	0.0235	−0.0200	0.0000	0.0000	0.1170	−0.3461
^{110}Pd	0.4950	0.0000	0.0235	−0.0200	0.0000	0.0000	0.1110	−0.3283
^{112}Pd	0.4950	0.0000	0.0235	−0.0200	0.0000	0.0000	0.08770	−0.2594
^{114}Pd	0.52200	0.0000	0.0235	−0.0200	0.0000	0.0000	0.0612	−0.1810
^{116}Pd	0.5700	0.0000	0.0216	−0.0200	0.0000	0.0000	0.0742	−0.2195

Table 1: Parameters used in IBA-1 Hamiltonian (all in MeV).

2.2 Electromagnetic transition rates

The electric quadrupole transition operator [15] employed in this study is:

$$T^{(E2)} = E2SD \cdot (s^{\dagger}\tilde{d} + d^{\dagger}s)^{(2)} + \\ + \frac{1}{\sqrt{5}} E2DD \cdot (d^{\dagger}\tilde{d})^{(2)} . \qquad (7)$$

The reduced electric quadrupole transition rates between $I_i \to I_f$ states are given by

$$B(E_2, I_i - I_f) = \frac{[< I_f \parallel T^{(E_2)} \parallel I_i >]^2}{2I_i + 1} . \qquad (8)$$

3 Results and discussion

3.1 The potential energy surfaces

The potential energy surfaces [16], $V(\beta, \gamma)$, as a function of the deformation parameters β and γ are calculated using:

$$\begin{aligned} & E_{N_{\Pi}N_{\nu}}(\beta,\gamma) = <N_{\pi}N_{\nu};\beta\gamma\,|H_{\pi\nu}|N_{\pi}N_{\nu};\beta\gamma> \\ & = \zeta_d(N_{\nu}N_{\pi})\beta^2(1+\beta^2) + \beta^2(1+\beta^2)^{-2}\times \\ & \times \left\{ kN_{\nu}N_{\pi}[4 - (\bar{X}_{\pi}\bar{X}_{\nu})\beta\cos 3\gamma] \right\} + \\ & + \left\{ [\bar{X}_{\pi}\bar{X}_{\nu}\beta^2] + N_{\nu}(N_{\nu}-1)\left(\frac{1}{10}c_0 + \frac{1}{7}c_2\right)\beta^2 \right\} , \end{aligned} \qquad (9)$$

where

$$\bar{X}_{\rho} = \left(\frac{2}{7}\right)^{0.5} X_{\rho} \quad \rho = \pi \text{ or } \upsilon . \qquad (10)$$

The calculated potential energy surfaces, $V(\beta,\gamma)$, are presented in Fig. 1. It shows that $^{100-110}$Pd are vibrational-like nuclei while ^{112}Pd is a γ-soft where the two wells on the oblate and prolate sides are equal. ^{114,116}Pd are prolate deformed and have rotational characters. So, ^{112}Pd is thought to be a transitional nucleus forming a zone between soft vibration side and nearly deformed nuclei in the other side.

3.2 Energy spectra

The energy of the positive and negative parity states of palladium series of isotopes are calculated using computer code PHINT [17]. A comparison between the experimental spectra [18–26] and our calculations for the ground state and $(-ve)$ parity states are illustrated in Fig. 2. The model parameters given in Table 1 are free parameters and adjusted to reproduce as closely as possible the excitation energy of the $(+ve)$ and $(-ve)$ parity levels. The agreement between the calculated levels energy and their correspondence experimental values for all nuclei are slightly higher for the higher excited states. We believe this is due to the change of the projection of the angular momentum which is due mainly to band crossing.

Unfortunately there is no enough measurements of electromagnetic transition rates $B(E1)$ or $B(E2)$ for these series of nuclei. The only measured $B(E2, 0_1^+ \to 2_1^+)$'s are presented, in Table 2 for comparison with the calculated values. The parameters $E2SD$ and $E2DD$ are displayed in Table 1 and used in the computer code NPBEM [17] for calculating the electromagnetic transition rates after normalization to the available experimental values.

No new parameters are introduced for calculating electromagnetic transition rates $B(E2)$, (Table 1), and $B(E1)$, (Table 2), of intraband and interband. The values of the ground state band are presented in Fig. 3 and show bending at $N = 64$ which means there is an interaction between the $(+ve)$ ground state and the $(-ve)$ parity states.

The moment of inertia I and angular frequency $\hbar\omega$ are calculated using equations (11, 12):

$$\frac{2J}{\hbar^2} = \frac{4I - 2}{\Delta E(I \to I - 2)} , \qquad (11)$$

$$(\hbar\omega)^2 = (I^2 - I + 1)\left[\frac{\Delta E(I \to I - 2)}{(2I - 1)}\right]^2 . \qquad (12)$$

The plots in Fig. 4 show upper bending at $I^+ = 12$ and lower bending at $I^+ = 14$ for $^{100\text{-}116}$Pd. It means, there is a crossing between the ground and the $(-ve)$ parity states.

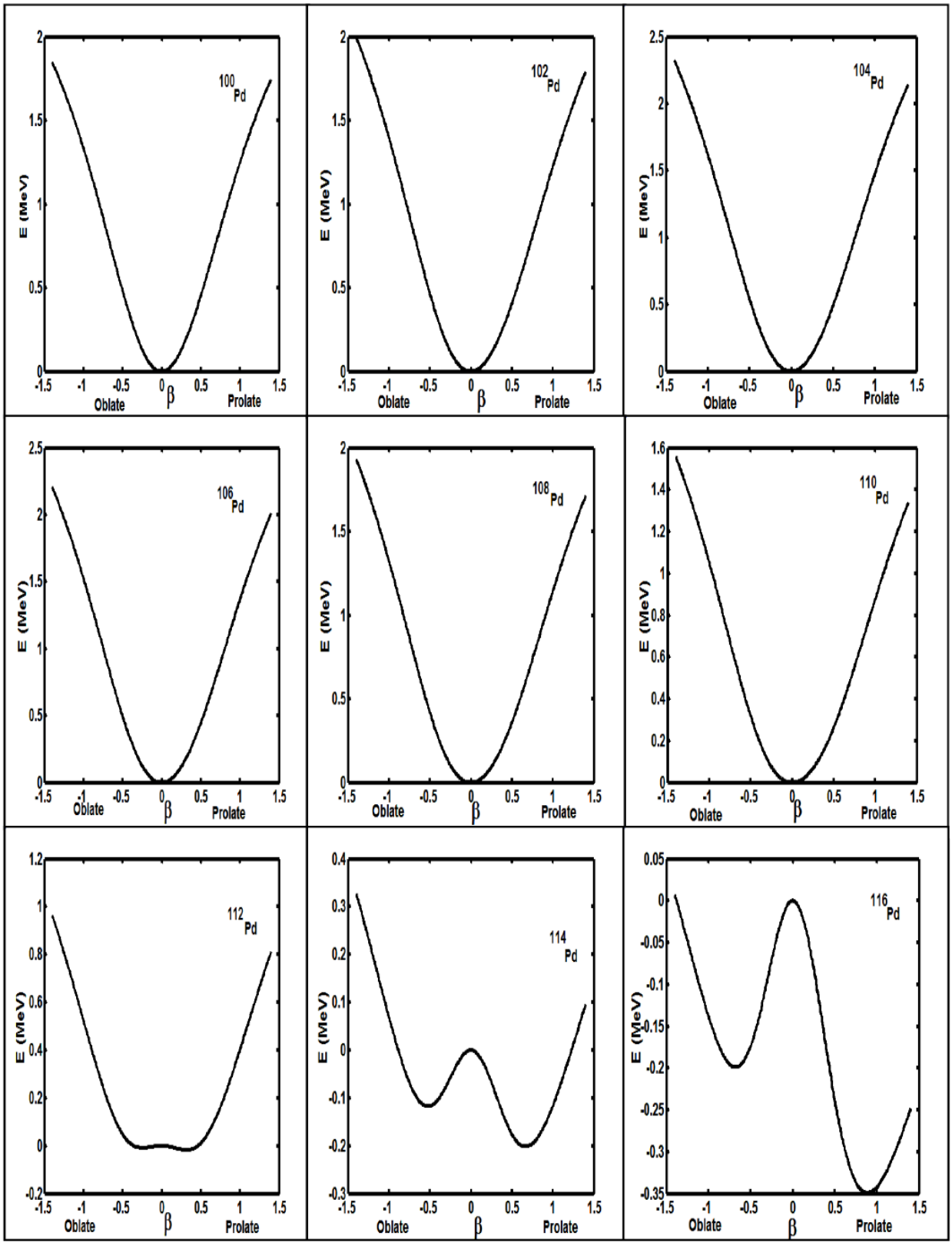

Fig. 1: Potential energy surfaces for $^{100\text{-}116}$Pd nuclei.

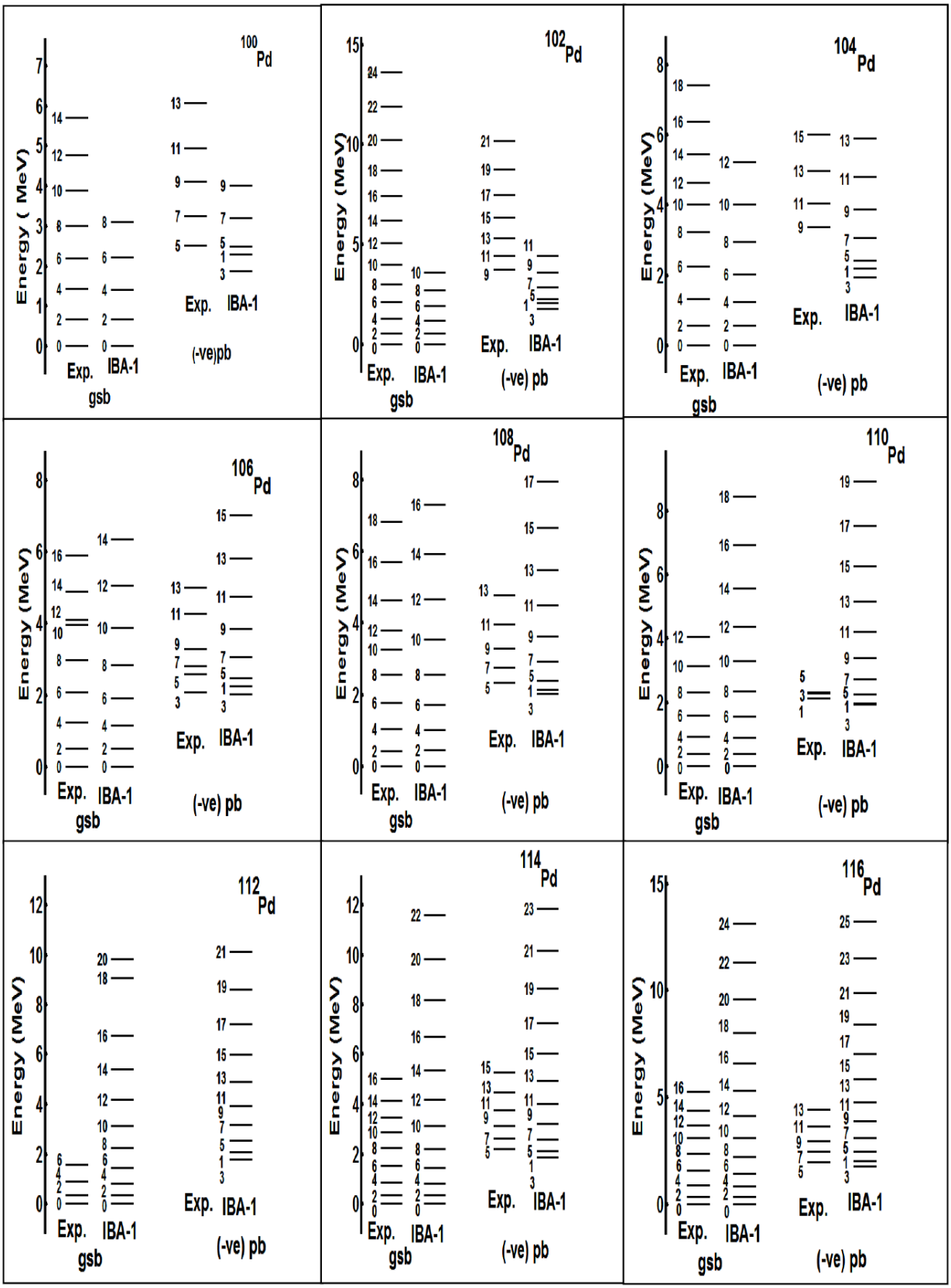

Fig. 2: Comparison between exp. [18–26] and theoretical (IBA-1) energy levels.

I_i^+ I_f^+	^{100}Pd	^{102}Pd	^{104}Pd	^{106}Pd	^{108}Pd	^{110}Pd	^{112}Pd	^{114}Pd	^{116}Pd
0_1 Exp*. 2_1	——	0.460(30)	0.535(35)	0.660(35)	0.760(40)	0.870(40)	0.660(11)	0.380(20)	0.620(18)
0_1 Theor. 2_1	0.2275	0.4657	0.5317	0.6663	0.7672	0.8631	0.6640	0.3804	0.6237
2_1 0_1	0.0455	0.0931	0.1063	0.13333	0.1534	0.1726	0.1328	0.0761	0.1247
2_2 0_1	0.0001	0.0004	0.0007	0.0013	0.0023	0.0034	0.0029	0.0017	0.0028
2_2 0_2	0.0199	0.0395	0.0449	0.0582	0.0738	0.0925	0.0785	0.0481	0.0819
2_3 0_1	0.0000	0.0000	0.0000	0.0000	0.0001	0.0004	0.0007	0.0006	0.0010
2_3 0_2	0.0286	0.0669	0.0822	0.1051	0.1126	0.1100	0.0704	0.0356	0.0576
2_3 0_3	0.0045	0.0082	0.0095	0.0128	0.0180	0.0270	0.0260	0.0166	0.0292
2_4 0_3	0.0012	0.0044	0.0074	0.0129	0.0234	0.0423	0.0462	0.0317	0.0570
2_4 0_4	0.0335	0.0602	0.0640	0.0755	0.0744	0.0702	0.0398	0.0182	0.0279
4_1 2_1	0.0702	0.1545	0.1846	0.2396	0.2943	0.3265	0.2535	0.1463	0.2429
4_1 2_2	0.0071	0.0137	0.0156	0.0202	0.0249	0.0300	0.0245	0.0150	0.0264
4_1 2_3	0.0117	0.0278	0.0346	0.0449	0.0492	0.0492	0.0323	0.0168	0.0277
6_1 4_1	0.0711	0.1756	0.2236	0.3011	0.3635	0.4188	0.3244	0.1878	0.3153
6_1 4_2	0.0098	0.0177	0.0195	0.0241	0.0273	0.0304	0.0233	0.0139	0.0244
6_1 4_3	0.0062	0.0191	0.0261	0.0353	0.0384	0.0380	0.0250	0.0131	0.0218
8_1 6_1	0.0476	0.1559	0.2225	0.3180	0.3950	0.4613	0.3599	0.2102	0.3574
8_1 6_2	0.0107	0.0184	0.0197	0.0236	0.0252	0.0266	0.0198	0.0116	0.0205
8_1 6_3	——	0.0094	0.0169	0.0253	0.0288	0.0295	0.0201	0.0109	0.0185
10_1 8_1	——	0.0969	0.1835	0.2936	0.3849	0.4629	0.3679	0.2183	0.3769
10_1 8_2	——	0.0178	0.0187	0.0219	0.0224	0.0229	0.0166	0.0096	0.0171

Table 2: Values of the theoretical reduced transition probability, $B(E2)$ (in $e^2\,b^2$).
*Ref. 27.

I_i^- I_f^+	^{100}Pd	^{102}Pd	^{104}Pd	^{106}Pd	^{108}Pd	^{110}Pd	^{112}Pd	^{114}Pd	^{116}Pd
1_1 0_1	0.0009	0.0020	0.0033	0.0052	0.0091	0.0148	0.0213	0.0255	0.0259
1_1 0_2	0.1290	0.1248	0.1299	0.1314	0.1340	0.1360	0.1369	0.1379	0.1384
3_1 2_1	0.1268	0.1228	0.1235	0.1246	0.1309	0.1414	0.1530	0.1605	0.1617
3_1 2_2	0.0267	0.0361	0.0395	0.0443	0.0501	0.0566	0.0645	0.0719	0.0771
3_1 2_3	0.0006	0.0018	0.0030	0.0053	0.0108	0.0190	0.0268	0.0311	0.0335
3_2 2_1	0.0093	0.0031	0.0016	0.0012	0.0014	0.0028	0.0053	0.0079	0.0099
3_2 2_2	0.0912	0.0278	0.0190	0.0153	0.0136	0.0146	0.0172	0.0196	0.0193
3_2 2_3	0.1132	0.2103	0.2247	0.2243	0.2172	0.2109	0.1827	0.1686	0.1599
5_1 4_1	0.2660	0.2582	0.2578	0.2576	0.2637	0.2747	0.2873	0.2959	0.2979
5_1 4_2	0.0260	0.0392	0.0457	0.0530	0.0604	0.0670	0.0736	0.0801	0.0861
5_1 4_3	0.0002	0.0010	0.0018	0.0032	0.0058	0.0088	0.0111	0.0125	0.0137
7_1 6_1	0.415*	0.4035	0.4005	0.3982	0.4025	0.4121	0.4236	0.4319	0.4341
7_1 6_2	0.0163	0.0325	0.0419	0.0515	0.0598	0.0663	0.0722	0.0781	0.0844
9_1 8_1	0.5714	0.5561	0.5489	0.5439	0.5454	0.5524	0.5617	0.5689	0.5709
9_1 8_2	——	0.0187	0.0318	0.0436	0.0533	0.0604	0.0664	0.0725	0.0792
11_1 10_1	——	0.7143	0.7015	0.6933	0.6914	0.6950	0.7017	0.7073	0.7088

Table 3: Values of the theoretical reduced transition probability, $B(E1)$ (in $\mu\,e^2 b$).

This fact has confirmed by studying the staggering effect to palladium isotopes which presented in Fig.5.

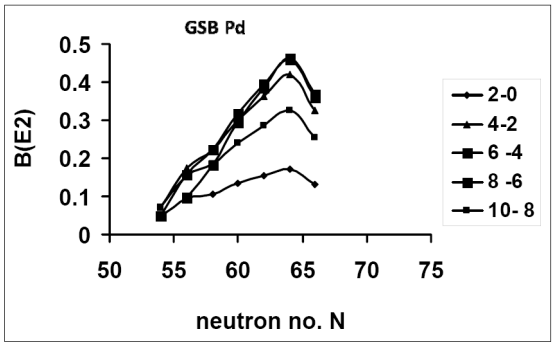

Fig. 3: The calculated $B(E2)$'s for the ground state band.

3.3 The staggering

The presence of $(+ve)$ and $(-ve)$ parity states has encouraged us to study staggering effect [28–30] for $^{100\text{-}116}$Pd series of isotopes using staggering function equations (15, 16) with the help of the available experimental data [18–26].

$$Stag(I) = 6\Delta E(I) - 4\Delta E(I-1) - 4\Delta E(I+1) + \Delta E(I+2) + \Delta E(I-2), \quad (13)$$

with

$$\Delta E(I) = E(I+1) - E(I). \quad (14)$$

The calculated staggering patterns are illustrated in Fig. 5 which show an interaction between the $(+ve)$ and $(-ve)$ parity states of $^{100\text{-}104}$Pd and $^{112\text{-}1116}$Pd nuclei at $I^+ = 12$. Unfortunatelly, there is no enough experimental data are available for $^{106\text{-}110}$Pd to study the same effect.

3.4 Conclusions

IBA-1 model has been applied successfully to $^{100\text{-}116}$Pd isotopes and we have got:

1. The levels energy are successfully reproduced;
2. The potential energy surfaces are calculated and show vibrational-like to $^{100-110}$Pd, γ-soft to ^{112}Pd and rotational characters to $^{114\text{-}116}$Pd isotopes where they are mainly prolate deformed nuclei;
3. Electromagnetic transition rates $B(E1)$ and $B(E2)$ are calculated;
4. Upper bending for $^{100\text{-}106}$Pd has been observed at angular momentum $I^+ = 12$ and lower bending at $I^+ = 14$ for all palladium isotopes;
5. Electromagnetic transition rates $B(E1)$ and $B(E2)$ are calculated;and

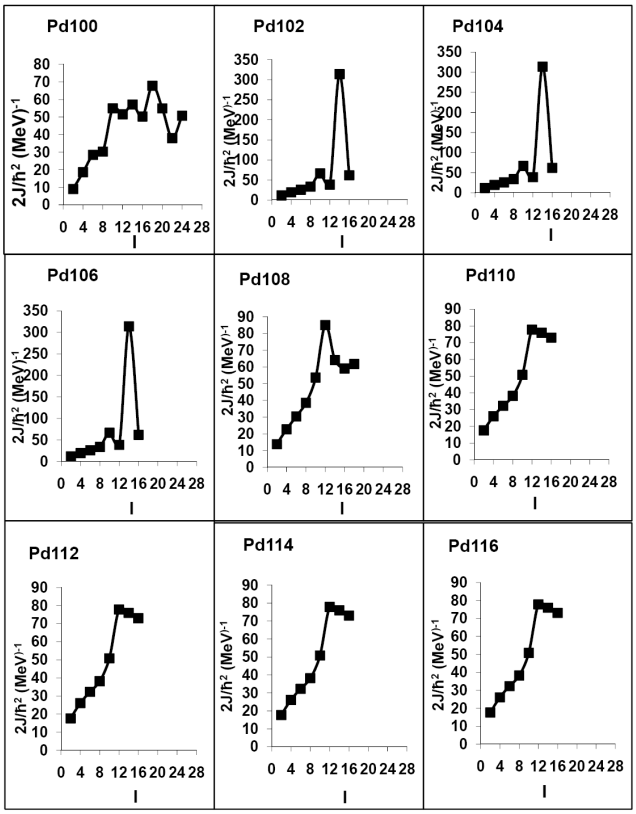

Fig. 4: Angular momentum I as a function of $2J/\hbar^2$.

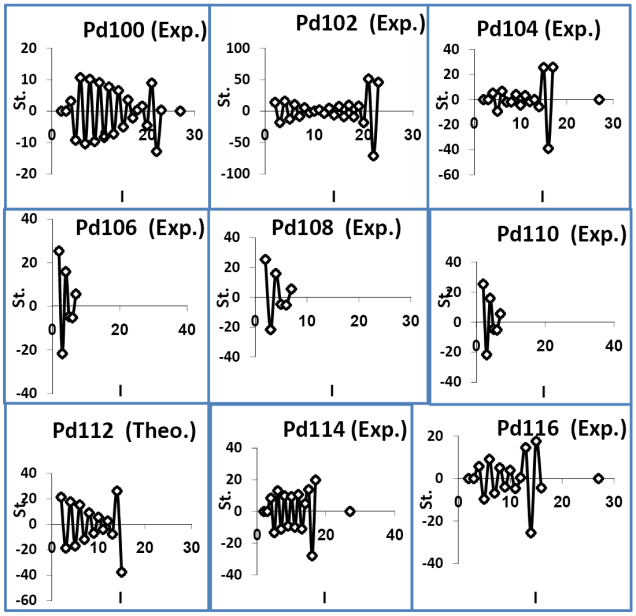

Fig. 5: $\Delta I = 1$, staggering patterns for $^{100\text{-}116}$Pd isotopes.

6. Staggering effect and beat patterns are observed and show an interaction between the $(-\mathtt{ve})$and $(+\mathtt{ve})$ parity states at $I^{+}=12$ for palladium isotopes except for $^{106\text{-}110}$Pd where scarce experimental data are available.

Submitted on September 02, 2008
Accepted on October 17, 2008

References

1. Zamfir N. V., Capiro M. A., Casten R. F., Barton C. J., Beausang C. W., Berant Z., Bernner D. S., Chou W. T., Cooper J. R., Hecht A. A., Krucken R., Newman H., Novak J. R., Pietralla N., Wolf A. and Zyromski K. E. *Phys. Rev. C*, 2002, v. 65, 044325.
2. Mitra A., Chakrabarty D. R., Datar V. M.,Kumar S., Mirgule E. T., Oza H. H., Nanal V., Pillay R. G. *Nucl. Phys. A*, 2006, v. 765, 277.
3. Bharti A. and Khosa S. K. *Phys. Rev. C*, 1996, v. 53, 2528.
4. Giannatiempo A., Nannini A. and Sona P. *Phys. Rev. C*, 1998, v. 58, 3316.
5. Giannatiempo A., Nannini A. and Sona P. *Phys. Rev. C*, 1998, v. 58, 3335.
6. Pan F. and Draayer J. P. *Nucl. Phys. A*, 1998, v. 636, 156.
7. Garcia-Ramos J. E., De Coster C., Fossion R. and Heyde K. *Nucl. Phys. A*, 2001, v. 688, 735.
8. Chasman R. R. *Phys. Rev. C*, 2001, v. 64, 024311.
9. Caprio M. A. *Phys. Rev. C*, 2003, v. 68, 054303.
10. Fossion R., Bonatsos D. and Lalazissis G. A. *Phys. Rev. C*, 2006, v. 73, 044310.
11. Clark R. M., Cromaz M., Deleplanque M. A., Descovich M., Diamond R. M., Fallon P., Lee I. Y., Macchiavelli A. O., Mahmud H., Rodriguez-Vieitez E., Stephens F.S., and Ward D. *Phys. Rev. C*, 2004, v. 69, 064322.
12. Arima A. and Iachello F. *Ann. Phys. (N.Y.)*, 1976, v. 99, 253.
13. Arima A. and Iachello F. *Ann. Phys. (N.Y.)*, 1978, v. 111, 201.
14. Arima A. and Iachello F. *Ann. Phys. (N.Y.)*, 1979, v. 123, 468.
15. Feshband H. and Iachello F. *Ann. Phys.*, 1974, v. 84, 211.
16. Ginocchio J. N. and Kirson M. W. *Nucl. Phys. A*, 1980, v. 350, 31.
17. Scholten O. *The programm package PHINT (1980) version, internal report KVI-63, Gronigen: Keryfysisch Versneller Institut*.
18. Balraj Singh *Nucl. Data Sheets*, 2008, v. 109, 297.
19. Frenne D. D. and Jacobs E. *Nucl. Data Sheets*, 1998, v. 83, 535.
20. Blachot J. *Nucl. Data Sheets*, 2007, v. 108, 2035.
21. Frenne D. D. and Negret A. *Nucl. Data Sheets*, 2008, v. 109, 943.
22. Blachot J. *Nucl. Data Sheets*, 2000, v. 91, 135.
23. Frenne D. D. and Jacobs E. *Nucl. Data Sheets*, 2000, v. 89, 481.
24. Frenne D. D. and Jacobs E. *Nucl. Data Sheets*, 1996, v. 79, 639.
25. Blachot J. *Nucl. Data Sheets*, 2002, v. 97, 593.
26. Blachot J. *Nucl. Data Sheets*, 2001, v. 92, 455.
27. Raman S., de Nestor C. W. and Tikkanen P. *Atomic Data and Nucl. Data Tab.*, 2001, v. 78, 1.
28. Minkov N., Yotov P., Drenska S. and Scheid W. *J. Phys. G*, 2006, v. 32, 497.
29. Bonatsos D., Daskaloyannis C., Drenska S. B., Karoussos N., Minkov N., Raychev P. P. and Roussev R. P. *Phys. Rev. C*, 2000, v. 62, 024301.
30. Minkov N., Drenska S. B., Raychev P. P., Roussev R. P.and Bonatsos D. *Phys. Rev. C*, 2001, v. 63, 044305.

The Apparent Lack of Lorentz Invariance in Zero-Point Fields with Truncated Spectra

William C. Daywitt

National Institute for Standards and Technology (retired), Boulder, Colorado, USA
E-mail: wcdaywitt@earthlink.net

The integrals that describe the expectation values of the zero-point quantum-field-theoretic vacuum state are semi-infinite, as are the integrals for the stochastic electrodynamic vacuum. The unbounded upper limit to these integrals leads in turn to infinite energy densities and renormalization masses. A number of models have been put forward to truncate the integrals so that these densities and masses are finite. Unfortunately the truncation apparently destroys the Lorentz invariance of the integrals. This note argues that the integrals are naturally truncated by the graininess of the negative-energy Planck vacuum state from which the zero-point vacuum arises, and are thus automatically Lorentz invariant.

1 Introduction

Sakharov [1] hypothesized that Newton's gravitational constant is inversely proportional to a truncated integral over the momenta of the virtual particles in the quantum vacuum [2] (QV), and that the cutoff wavenumber "...determines the mass of the heaviest particles existing in nature..." according to a suggestion by M. A. Markov. Inverting the Markov suggestion, the Planck vacuum (PV) model [3, 4] assumes that these "heaviest particles" are the Planck particles (PPs) constituting the degenerate negative-energy PV state, and that it is the separation between these PPs that leads to the cutoff wavenumber. Puthoff [4, 5] furthers the Sakharov argument by calculating the cutoff wavenumber to be

$$k_{c*} = \left(\frac{\pi c^3}{\hbar G}\right)^{1/2} \quad \left[= \frac{\pi^{1/2}}{r_*}\right], \tag{1}$$

where G is Newton's gravitational constant and r_* is the Planck length. The ratio in the bracket is derived by substituting the constants $\hbar = e_*^2/c$, $G = e_*^2/m_*^2$, and the Compton relation $r_* m_* c^2 = e_*^2$ from the PV model, where m_* is the Planck mass and e_* is the bare (true) charge common to the charged elementary particles.

It is accepted knowledge that the truncation of the vacuum integrals destroys their Lorentz invariance. For example, a stochastic electrodynamic version of the zero-point (ZP) electric field can be expressed as [5]

$$\mathbf{E}_{zp}(\mathbf{r},t) = \mathrm{Re}\sum_{\sigma=1}^{2}\int d\Omega_k \int_0^{k_{c*}} dk\, k^2\, \mathbf{e}_\sigma(\mathbf{k})\, A_k \times$$
$$\times \exp\left[\, i\left(\mathbf{k}\cdot\mathbf{r} - \omega t + \Theta_\sigma(\mathbf{k})\right)\right], \tag{2}$$

where the cutoff wavenumber k_{c*} apparently destroys the Lorentz invariance of the field. The accepted Lorentz-invariant version of (2) replaces k_{c*} by ∞. By giving the cutoff wavenumber an interpretation different from a momentum wavenumber, however, this note argues that (2) is Lorentz invariant as it stands. The next section presents this argument.

The virtual-particle field consists of virtual photons and massive virtual-particle pairs, the collection being the QV. It is assumed that the structure of the PV and the ZP agitation of its PPs are responsible for the structure of the virtual-particle field, the corresponding average of the photon field being the ZP electric field in (2). While the negative-energy PV is assumed to be invisible (not directly observable), it offspring the QV appears in free space and interacts with the free particles therein. The argument in the next section assumes this perspective.

2 Cutoff wavenumber

The set of orthogonal modes associated with a continuous medium contains an infinite number of eigenfunctions. If the medium is quasi-continuous like the PV, however, the number is finite. Using this fact, the development of the ZP electric field is reviewed below to show that the cutoff wavenumber is associated with the number of PPs per unit volume in the PV and is not fundamentally a momentum wavenumber for the QV fields. Thus being associated with the PP density, the cutoff wavenumber is not dependent upon the free-space Lorentz frames observing the QV.

The ZP electric field can be expressed as [6, p.73]

$$\mathbf{E}_{\mathrm{zp}}(\mathbf{r},t) = \left(\frac{8\pi^3}{V}\right)^{1/2} \times$$
$$\times\ \mathrm{Re}\sum_{\sigma}\sum_{\mathbf{n}} \mathbf{e}_{\mathbf{k},\sigma} A_k \exp\left[\, i\left(\mathbf{k}\cdot\mathbf{r} - \omega t + \Theta_{\mathbf{k},n}\right)\right], \tag{3}$$

where the first sum is over the two polarizations of the field, $k = |\mathbf{k}|$, $V = L^3$ is the box-normalization volume, $\mathbf{e}_{\mathbf{k},\sigma}$ is the polarization vector,

$$\pi^2 A_k^2 = \frac{\hbar\omega}{2} = \frac{e_*^2 k}{2} \tag{4}$$

yields the amplitude factor A_k which is proportional to the bare charge e_* of the PPs in the PV, and Θ_σ is the random phase that gives $\mathbf{E}_{\rm zp}$ its stochastic character. The two ratios in (4) are the ZP energy of the individual field modes. The field satisfies the periodicity condition

$$\mathbf{E}_{\rm zp}(x+L,\ y+L,\ z+L,t) = \mathbf{E}_{\rm zp}(x,y,z,t) \qquad (5)$$

or equivalently

$$\mathbf{k} = (k_x, k_y, k_z) = (2\pi/L)(n_x, n_y, n_z) = (2\pi/L)\,\mathbf{n}\,, \quad (6)$$

where $k = (2\pi/L)\,n$, and where ordinarily the n_i can assume any positive or negative integer and zero.

An unbounded mode index n_i in (6) leads to the infinite energy densities and renormalization masses that plague both the quantum field theory and the stochastic electrodynamic theory. However, if the normal mode functions of the ZP field are assumed to be waves supported by the collection of PPs within the PV [4], then the number of modes n_i along the side of the box of length L is bounded and obeys the inequality $|n_i| \leqslant (L/2\pi)\,k_{c*} = L/2\sqrt{\pi}\,r_*$. So it is the "graininess" ($r_* \neq 0$) associated with the minimum separation r_* of the PPs that leads to a bounded k_i and n_i for (6), and which is thus responsible for finite energy densities and renormalization masses [4]. Unfortunately this truncation of the second sum in (3) leads to apparently non-Lorentz-invariant integrals for the "continuum" version of that equation developed below.

Using the replacement [6, p.76]

$$\sum_\sigma \sum_{\mathbf{n}} f(\mathbf{k_n}, \mathbf{e}_{\mathbf{n},\sigma})\, a_{\mathbf{n},\sigma} \longrightarrow \qquad (7)$$

$$\longrightarrow \left(\frac{V}{8\pi^3}\right)^{1/2} \sum_\sigma \int d^3k f(\mathbf{k}, \mathbf{e}_\sigma(\mathbf{k}))\, a_\sigma(\mathbf{k}) \qquad (8)$$

in (3) and truncating the field densities at $k_{c*} = \sqrt{\pi}/r_*$ leads to [4, 5]

$$\begin{aligned}\mathbf{E}_{\rm zp}(\mathbf{r},t) &= \mathrm{Re}\sum_\sigma \int d^3k\, \mathbf{e}_\sigma(\mathbf{k})\, A_k \times \\ &\times \exp\left[\, i\,(\mathbf{k}\cdot\mathbf{r} - \omega t + \Theta_\sigma(\mathbf{k}))\,\right] = \\ &= \mathrm{Re}\sum_\sigma \int d\Omega_k \int_0^{k_{c*}} dk\, k^2\, \mathbf{e}_\sigma(\mathbf{k})\, A_k \times \\ &\times \exp\left[\, i\,(\mathbf{k}\cdot\mathbf{r} - \omega t + \Theta_\sigma(\mathbf{k}))\,\right], \end{aligned} \qquad (9)$$

where $d\Omega_k$ is the k-space solid-angle differential. As shown below in (10) and(11) this cutoff wavenumber k_{c*} is fundamentally related to the number of PPs per unit volume constituting the PV.

The ZP electromagnetic energy density of the QV calculated from (8) is

$$\frac{\langle \mathbf{E}^2_{\rm zp}\rangle}{4\pi} = \int_0^{k_{c*}} \frac{e_*^2 k}{2} \cdot \frac{k^2\,dk}{\pi^2}\,, \qquad (10)$$

where the first ratio under the integral sign is the ZP energy of the individual modes. The second ratio is the number of modes per unit volume between k and $k + dk$; so the number of modes in that range is $k^2 V\,dk/\pi^2$. If the total number of PP oscillators (with three degrees of freedom each) in the volume V is N, then the total number of modes in V is [7]

$$\int_0^{k_{c*}} \frac{k^2 V\,dk}{\pi^2} = 3N\,, \qquad (11)$$

which provides an estimate for N/V. Integrating (10) gives

$$\frac{N}{V} = \frac{k_{c*}^3}{9\pi^2} \quad \left[= (9^{1/3}\pi^{1/6} r_*)^{-3} \approx \frac{1}{(2.5\,r_*)^3}\right] \qquad (12)$$

for the number of PPs per unit volume. The equation outside the brackets shows that k_{c*} is proportional to the cube root of this PP density. The ratio in the bracket shows that the average separation of the PPs is approximately 2.5 times their Compton radii r_*, a very reasonable result considering the roughness of the calculations.

From (11) the previous paragraph shows that the cutoff wavenumber k_{c*} in (8) and (9) is associated with the mode counting in (10) taking place within the invisible PV. Since the number of these PV modes is not influenced by the free-space Lorentz frame observing the QV, the k_{c*} in (8) and (9) must be independent of the Lorentz frame. Thus (8) and (9) are Lorentz invariant as they stand since k_{c*} is frame independent and the integrands are already Lorentz invariant [8]. That is, when viewed from different Lorentz frames, the wavenumber k_{c*} remains the same; so the integrals are Lorentz invariant.

3 Review and comments

From the beginning of the ZP theory the medium upon which calculations are based is the free-space continuum with its unbounded mode density. So if the spectral density is truncated, the ZP fields naturally lose their Lorentz-invariant character because the truncation and the Lorentz viewing frames exist in the same space. This contrasts with the development in the preceding section where the truncation takes place in the invisible PV while the viewing is in the free space containing the QV.

One way of truncating in free space without losing Lorentz invariance [9, 10] is to assume that the so-called elementary particles are constructed from small sub-particles called partons, so that the components of the parton driving-field $\mathbf{E}_{\rm zp}$ with wavelengths smaller than the parton size ($\sim r_*$) are ineffective in producing translational motion of the parton as a whole, effectively truncating the integral expressions at or near the Planck frequency c/r_*. The parton mass turns out to be

$$m_0 = \frac{2}{3}\left(\frac{m_*^2}{m}\right) = \frac{2}{3}\left(\frac{r_c}{r_*}\right) m_* \sim 10^{20}\, m_* \qquad (13)$$

where m_* is the Planck mass, m is the particle mass, and r_c is the particle Compton radius. The parenthetical ratio in the second expression is roughly 10^{20} for the observed elementary particles; i.e., for the observed particles, the parton mass is about twenty orders of magnitude greater than the Planck mass.

It is difficult to explain the inordinately large $(10^{20}m_*)$ parton mass in (12) that is due to the equation of motion

$$m_0\ddot{\mathbf{r}} = e_*\mathbf{E}_{\rm zp} \tag{14}$$

at the core of the Abraham-Lorentz-Dirac equation used in [9], where $\ddot{\mathbf{r}}$ is the acceleration of the mass about its average position at $\langle\mathbf{r}\rangle = 0$. Equation (13) is easily transformed into the equation of motion

$$e_*\ddot{\mathbf{r}} = \frac{3c^3\Gamma}{2}\,\mathbf{E}_{\rm zp} \tag{15}$$

for the charge e_*, where $\ddot{\mathbf{r}}$ is the charge acceleration. If the time constant Γ is treated as a constant to be determined from experiment [4, 5], then solving (14) leads to

$$\Gamma = \left(\frac{r_*}{r_c}\right)\frac{r_*}{c} \sim 10^{-20}\,\frac{r_*}{c}\,, \tag{16}$$

where r_*/c is the Planck time. Unlike the m_0 in (12) and (13), this inordinately small time constant can be accounted for: it is due to the large number ($N/V \sim 10^{97}$ per cm^3) of agitated PPs in the PV contributing simultaneously to the ZP field fluctuations described by (8). It is noted in passing that the size of the parton ($\sim r_*$) is not connected to its mass m_0 by the usual Compton relation (i.e., $r_*m_0c^2 \neq e_*^2$) as is the case for the PP ($r_*m_*c^2 = e_*^2$).

Acknowledgement

The author would like to thank Dr. Cynthia Whitney, the editor of *Galilean Electrodynamics*, for allowing this and the previous two papers in the Planck Vacuum Series to be published in the present journal.

Submitted on October 02, 2008 / Accepted on October 17, 2008

References

1. Sakharov A.D. Vacuum quantum fluctuations in curved space and the theory of gravitation. *Soviet Physics — Doklady*, 1968, v. 12, no. 11, 1040.
2. Milonni P.W. The quantum vacuum — an introduction to Quantum Electrodynamics. Academic Press, New York, 1994.
3. Daywitt W.C. The Planck vacuum. *Progress in Physics*, 2009, Jan., v. 1, 20.
4. Daywitt W.C. The source of the quantum vacuum. *Progress in Physics*, 2009, Jan., v. 1, 27.
5. Puthoff H.E. Gravity as a zero-point-fluctuation force. *Phys. Rev. A*, 1989, v. 39, no. 5, 2333–2342.
6. de la Peña L. and Cetto A.M. The quantum dice — an introduction to stochastic electrodynamics. Kluwer Academic Publishers, Boston, 1996.
7. Dekker A.J. Solid state physics. Prentice-Hall, N.J., Sixth Printing, 42, 1962.
8. Boyer T.H. Derivation of the blackbody radiation spectrum without quantum assumptions. *Phys. Rev.*, 1969, v. 182, no. 5, 1374–1383.
9. Haisch B., Rueda A., Puthoff H.E. Inertia as a zero-point-field force. *Phys. Rev. A*, 1994, v. 49, no. 2, 678–695. If the parton equation of motion (12) in [9] were to use the bare charge e_* rather than the observed electronic charge e, the equations would be free of the fine structure constant $\alpha\,(=e^2/e_*^2)$. For example equation (111), $m_0 = (2\alpha/3)(m_*^2/m)$, would become $m_0 = (2/3)(m_*^2/m)$.
10. Rueda A. Behavior of classical particles immersed in the classical electromagnetic zero-point field. *Phys. Rev. A*, 1981, v. 23, no. 4, 2020.

On the Tidal Evolution of the Earth-Moon System: A Cosmological Model

Arbab I. Arbab

Department of Physics, Faculty of Science, University of Khartoum, P.O. 321, Khartoum 11115, Sudan
and Department of Physics and Applied Mathematics, Faculty of Applied Sciences and Computer,
Omdurman Ahlia University, P.O. Box 786, Omdurman, Sudan

E-mail: aiarbab@uofk.edu; arbab_ai@yahoo.com

We have presented a cosmological model for the tidal evolution of the Earth-Moon system. We have found that the expansion of the universe has immense consequences on our local systems. The model can be compared with the present observational data. The close approach problem inflicting the known tidal theory is averted in this model. We have also shown that the astronomical and geological changes of our local systems are of the order of Hubble constant.

1 Introduction

The study of the Earth-Moon-Sun system is very important and interesting. Newton's laws of motion can be applied to such a system and good results are obtained. However, the correct theory to describe the gravitational interactions is the general theory of relativity. The theory is prominent in describing a compact system, such as neutron stars, black hole, binary pulsars, etc. Einstein theory is applied to study the evolution of the universe. We came up with some great discoveries related to the evolution of the universe. Notice that the Earth-Moon system is a relatively old system (4.5 billion years) and would have been affected by this evolution. Firstly, the model predicts the right abundance of Helium in the universe during the first few minutes after the big bang. Secondly, the model predicts that the universe is expanding and that it is permeated with some relics photons signifying a big bang nature. Despite this great triumphs, the model is infected with some troubles. It is found the age of the universe determined according to this model is shorter than the one obtained from direct observations. To resolve some of these shortcomings, we propose a model in which vacuum decays with time couples to matter. This would require the gravitational and cosmological constant to vary with time too. To our concern, we have found that the gravitational interactions in the Newtonian picture can be applied to the whole universe provided we make the necessary arrangement. First of all, we know beforehand that the temporal behavior is not manifested in the Newton law of gravitation. It is considered that gravity is static. We have found that instead of considering perturbation to the Earth-Moon system, we suggest that these effect can be modeled with having an effective coupling constant (G) in the ordinary Newton's law of gravitation. This effective coupling takes care of the perturbations that arise from the effect of other gravitational objects. At the same time the whole universe is influenced by this setting. We employ a cosmological model that describes the present universe and solves many of the cosmological problems. To our surprise, the present cosmic acceleration can be understood as a counteract due to an increasing gravitational strength. The way how expansion of the universe affects our Earth-Moon system shows up in changing the length of day, month, distance, etc. These changes are found in some biological and geological systems. In the astronomical and geological frames changes are considered in terms of tidal effects induced by the Moon on the Earth. However, tidal theory runs in some serious difficulties when the distance between Earth and Moon is extrapolated backwards. The Moon must have been too close to the Earth a situation that has not been believed to have happened in our past. This will bring the Moon into a region that will make the Moon rather unstable, and the Earth experiencing a big tide that would have melted the whole Earth. We have found that one can account for this by an alternative consideration in which expansion of the universes is the main cause.

2 Tidal theory

We know that the Earth-Moon system is governed by Kepler's laws. The rotation of the Earth in the gravity field of the Moon and Sun imposes periodicities in the gravitational potential at any point on the surface. The most obvious effect is the ocean tide which is greater than the solid Earth tide. The potential arising from the combination of the Moon's gravity and rotation with orbital angular velocity (ω_L) about the axis through the common center of mass is (Stacey, 1977 [1])

$$V = -\frac{Gm}{R'} - \frac{1}{2}\,\omega_L^2 r^2\,, \tag{1}$$

where m is the mass of the Moon, and from the figure below one has

$$\left.\begin{aligned} R'^2 &= R^2 + a^2 - 2aR\cos\psi \\ r^2 &= b^2 + a^2\sin^2\theta - 2ab\cos\psi \end{aligned}\right\}, \tag{2}$$

where $\cos\psi = \sin\theta\cos\lambda$, $b = \frac{m}{M+m}R$, while a is the Earth's radius.

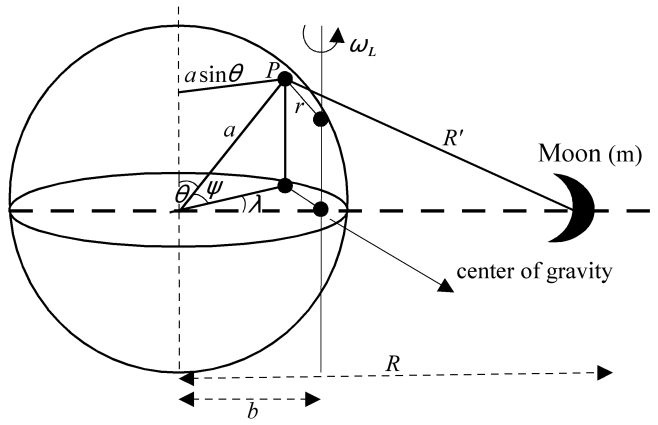

Fig. 1: The geometry of the calculation of the tidal potential of the Moon and a point P on the Earth's surface.

From Kepler's third law one finds

$$\omega_L^2 R^3 = G(M+m)\,, \tag{3}$$

where M is the Earth's mass, so that one gets for $a \ll R$

$$V = -\frac{Gm}{R}\left(1+\frac{1}{2}\frac{m}{M+m}\right) - \\ -\frac{Gma^2}{R^3}\left(\frac{3}{2}\cos\psi - \frac{1}{2}\right) - \frac{1}{2}\omega_L^2 a^2 \sin^2\theta\,. \tag{4}$$

The first term is a constant that is due to the gravitational potential due to the Moon at the center of the Earth, with small correction arising from the mutual rotation. The second term is the second order zonal harmonics and represents a deformation of the equipotential surface to a prolate ellipsoid aligned with the Earth-Moon axis. Rotation of the Earth is responsible for the tides. We call the latter term tidal potential and define it as

$$V_2 = -\frac{Gma^2}{R^3}\left(\frac{3}{2}\cos\psi - \frac{1}{2}\right). \tag{5}$$

The third term is the rotational potential of the point P about an axis through the center of the Earth normal to the orbital plane. This does not have a tidal effect because it is associated with axial rotation and merely becomes part of the equatorial bulge of rotation. Due to the deformation an additional potential $k_2 V_2$ (k_2 is the Love number) results, so that at the distance (R) of the Moon the form of the potential due to the tidal deformation of the Earth is

$$V_T = k_2 V_2 = k_2\left(\frac{a}{R}\right)^3 = -\frac{Gma^5}{R^6}\left(\frac{3}{2}\cos\psi - \frac{1}{2}\right). \tag{6}$$

We can now identify ψ with ϕ_2: the angle between the Earth-Moon line and the axis of the tidal bulge, to obtain the tidal torque (τ) on the Moon:

$$\tau = m\left(\frac{\partial V_T}{\partial\psi}\right)_{\psi=\phi_2} = \frac{3}{2}\left(\frac{Gm^2a^5k_2}{R^6}\right)\sin 2\phi_2\,. \tag{7}$$

The torque causes an orbital acceleration of the Earth and Moon about their common center of mass; an equal and opposite torque exerted by the Moon on the tidal bulge slows the Earth's rotation. This torque must be equated with the rate of change of the orbital angular momentum (L), which is (for circular orbit)

$$L = \left(\frac{M}{M+m}\right)R^2\omega_L\,, \tag{8}$$

upon using (3) one gets

$$L = \frac{Mm}{M+m}(GR)^{\frac{1}{2}}\,, \qquad L = \frac{MmG^{\frac{2}{3}}}{(M+m)^{\frac{1}{3}}}\,\omega_L^{-\frac{1}{3}}\,. \tag{9}$$

The conservation of the total angular momentum of the Earth-Moon system (J) is a very integral part in this study. This can be described as a contribution of two terms: the first one due to Earth axial rotation ($S = C\omega$) and the second term due to the Moon orbital rotation (L). Hence, one writes

$$J = S + L = C\,\omega + \left(\frac{Mm}{M+m}\right)R^2\omega_L\,. \tag{10}$$

We remark here to the fact that of all planets in the solar system, except the Earth, the orbital angular momentum of the satellite is a small fraction of the rotational angular momentum of the planet. Differentiating the above equation with respect to time t one gets

$$\tau = \frac{dL}{dt} = \frac{L}{2R}\frac{dR}{dt} = -\frac{dS}{dt}\,. \tag{11}$$

The corresponding retardation of the axial rotation of the Earth, assuming conservation of the total angular momentum of the Earth-Moon system, is

$$\frac{d\omega}{dt} = -\frac{\tau}{C}\,, \tag{12}$$

assuming C to be constant, where C is the axial moment of inertia of the Earth and its present value is ($C_0 = 8.043\times 10^{37}$ kg m^{-3}). It is of great interest to calculate the rotational energy dissipation in the Earth-Moon system. The total energy (E) of the Earth-Moon system is the sum of three terms: the first one due to axial rotation of the Earth, the second is due to rotation of the Earth and Moon about their center of mass, and the third one is due to the mutual potential energy. Accordingly, one has

$$E = \frac{1}{2}C\,\omega^2 + \frac{1}{2}R^2\omega_L^2\left(\frac{Mm}{M+m}\right) - \frac{GMm}{R}\,, \tag{13}$$

and upon using (3) become

$$E = \frac{1}{2}C\omega^2 - \frac{1}{2}\frac{GMm}{R}\,. \tag{14}$$

Thus

$$\frac{dE}{dt} = C\omega\,\frac{d\omega}{dt} - \frac{1}{2}\frac{GMm}{R^2}\frac{dR}{dt}\,, \tag{15}$$

using (8), (11) and (12) one gets

$$\frac{dE}{dt} = -\,\tau\,(\omega - \omega_L)\,. \tag{16}$$

3 Our cosmological model

Instead of using the tidal theory described above, we rather use the ordinary Kepler's and Newton law of gravitational. We have found that the gravitation constant G can be written as (Arbab, 1997 [2])

$$G_{\text{eff}} = G_0 f(t)\,, \tag{17}$$

where $f(t)$ is some time dependent function that takes care of the expansion of the universe. At the present time we have $f(t_0) = 1$. It seems as if Newton's constant changes with time. In fact, we have effects that act as if gravity changes with time. These effects could arise from any possible source (internal or external to Earth). This variation is a modeled effect due to perturbations received from distant matter. This reflects the idea of Mach who argued that distant matter affects inertia. We note here the exact function $f(t)$ is not known exactly, but we have its functional form. It is of the form $f(t) \propto t^n$, where $n > 0$ is an undetermined constant which has to be obtained from experiment (observations related to the Earth-Moon system). Unlike Dirac hypothesis in which G is a decreasing function of time, our model here suggests that G increases with time. With this prescription in hand, the forms of Kepler's and Newton's laws preserve their form and one does not require any additional potential (like those appearing in (5) and (6)) to be considered. The total effect of such a potential is incorporated in G_{eff}. We have found recently that (Arbab, 1997 [2])

$$f(t) = \left(\frac{t}{t_0}\right)^{1.3}\,, \tag{18}$$

where t_0 is the present age of the universe, in order to satisfy Wells and Runcorn data (Arbab, 2004 [3]).

3.1 The Earth-Sun system

The orbital angular momentum of the Earth is given by

$$L_S = \left(\frac{M}{M + M_\odot}\right) R_E^2 \Omega\,, \tag{19}$$

or equivalently,

$$\left.\begin{aligned} L_S &= \left(\frac{M M_\odot}{M + M_\odot}\right)(G_{\text{eff}} R_E)^{\frac{1}{2}} \\ L_S &= \left(\frac{M M_\odot}{M + M_\odot}\right)^{\frac{1}{3}} \left(\frac{G_{\text{eff}}^2}{\Omega}\right)^{\frac{1}{3}} \end{aligned}\right\}, \tag{20}$$

where we have replace G by G_{eff}, and Ω is the orbital angular velocity of the Earth about the Sun. The length of the year (Y) is given by Kepler's third law as

$$Y^2 = \left(\frac{4\pi^2}{G_{\text{eff}}(M_\odot + M)}\right) R_E^3\,, \tag{21}$$

where R_E is the Earth-Sun distance. We normally measure the year not in a fixed time but in terms of number of days. If the length of the day changes, the number of days in a year also changes. This induces an apparent change in the length of year. From (20) and (21) one obtains the relation

$$L_S^3 = N_1 G_{\text{eff}} Y^2\,, \tag{22}$$

and

$$L_S^2 = N_2 G_{\text{eff}} R_E\,, \tag{23}$$

where N_1, N_2 are some constants involving (m, M, $M_\odot$). Since the angular momentum of the Earth-Sun remains constant, one gets the relation (Arbab, 2009 [4])

$$Y = Y_0 \left(\frac{G_0}{G_{\text{eff}}}\right)^2\,, \tag{24}$$

where Y is measured in terms of days, $Y_0 = 365.24$ days. Equation (23) gives

$$R_E = R_E^0 \left(\frac{G_0}{G_{\text{eff}}}\right)\,, \tag{25}$$

where $R_E^0 = 1.496\times10^{11}$ m. To preserve the length of year (in terms of seconds) we must have the relation

$$D = D_0 \left(\frac{G_{\text{eff}}}{G_0}\right)^2\,, \tag{26}$$

so that

$$Y_0 D_0 = Y D = 3.155\times10^7 \text{ s}\,. \tag{27}$$

This fact is supported by data obtained from paleontology. We know further that the length of the day is related to ω by the relation $D = \frac{2\pi}{\omega}$. This gives a relation of the angular velocity of the Earth about its self of the form

$$\omega = \omega_0 \left(\frac{G_0}{G_{\text{eff}}}\right)^2\,. \tag{28}$$

3.2 The Earth-Moon system

The orbital angular momentum of the Moon is given by

$$L = \left(\frac{M}{M + m}\right) R^2 \omega_L \tag{29}$$

or,

$$\left.\begin{aligned} L &= \left(\frac{Mm}{M + m}\right)(G_{\text{eff}} R)^{\frac{1}{2}} \\ L &= \left(\frac{Mm}{M + m}\right)^{\frac{1}{3}} \left(\frac{G_{\text{eff}}^2}{\omega_L}\right)^{\frac{1}{3}} \end{aligned}\right\}, \tag{30}$$

where we have replace G by G_{eff}, and ω_L is the orbital angular velocity of the Moon about the Earth. However, the length of month is not invariant as the angular momentum of the Moon has not been constant over time. It has been found found by Runcorn that the angular momentum of the Moon 370 million years ago (the Devonian era) in comparison to the present one (L_0) to be

$$\frac{L_0}{L} = 1.016 \pm 0.003\,. \tag{31}$$

The ratio of the present angular momentum of the Moon (L) to that of the Earth (S) is given by

$$\frac{L_0}{S_0} = 4.83\,, \tag{32}$$

so that the total angular momentum of the Earth-Moon system is

$$J = L + S = L_0 + S_0 = 3.4738\times10^{34}\ \text{Js}\,. \tag{33}$$

Hence, using (17) and (18), (28), (30) and (31) yield

$$\left.\begin{aligned} L &= L_0\left(\frac{t}{t_0}\right)^{0.44} \\ \omega &= \omega_0\left(\frac{t_0}{t}\right)^{2.6}, \quad \omega_L = \omega_{0L}\left(\frac{t}{t_0}\right)^{1.3} \end{aligned}\right\}, \tag{34}$$

where $t = t_0 - t_b$, t_b is the time measured from the present backward. The length of the sidereal month is given by

$$T = \frac{2\pi}{\omega_L} = T_0\left(\frac{t_0}{t}\right)^{1.3}\,, \tag{35}$$

where $T_0 = 27.32$ days, and the synodic month is given by the relation

$$T_{sy} = \left(\frac{T}{1-\frac{T}{Y}}\right)\,. \tag{36}$$

We notice that, at the present time, the Earth declaration is -5.46×10^{-22} rad/s^2, or equivalently a lengthening of the day at a rate of 2 milliseconds per century. The increase in Moon mean motion is 9.968×10^{-24} rad/s^2. Hence, we found that $\dot{\omega} = -54.8\,\dot{n}$, where $n = \frac{2\pi}{\omega_L}$. The month is found to increase by 0.02788/cy. This variation can be compared with the present observational data.

From (34) one finds

$$\omega\,\omega_L^2 = \omega_0\,\omega_{0L}^2\,. \tag{37}$$

If the Earth and Moon were once in resonance then $\omega = \omega_L \equiv \omega_c$. This would mean that

$$\left.\begin{aligned} \omega_c^3 &= \omega_0\,\omega_{0L}^2 = 516.6\times10^{-18}\ (\text{rad/s})^3 \\ \omega_c &= 8.023\times10^{-6}\ \text{rad/s} \end{aligned}\right\}. \tag{38}$$

This would mean that both the length of day and month were equal. They were both equal to a value of about 9 present days. Such a period has not been possible since when the Earth was formed the month was about 14 present days and the day was 6 hours! Therefore, the Earth and Moon had never been in resonance in the past.

Using the (11) and (34) the torque on the Earth by the Moon is (Arbab, 2005 [4, 5])

$$\tau = -\frac{dL}{dt} = -\frac{dS}{dt}\,, \qquad \tau = -\tau_0\left(\frac{t}{t_0}\right)^{0.56}\,, \tag{39}$$

where $\tau_0 = 3.65\times10^{15}$N m. The energy dissipation in the Earth is given by

$$P = \frac{dE}{dt}\,, \quad \frac{dE}{dt} = \frac{d}{dt}\left(\frac{1}{2}\,C\,\omega^2 - \frac{1}{2}\,\frac{G_{\text{eff}}\,Mm}{R}\right), \tag{40}$$

where R, ω is given by (30) and (34).

We remark that the change in the Earth-Moon-Sun parameters is directly related to Hubble constant (H). This is evident since in our model (see Arbab, 1997 [2]) the Hubble constant varies as $H = 1.11\,t^{-1}$. Hence, one may attribute these changes to cosmic expansion. For the present epoch $t_0 \sim 10^9$ years, the variation of ω, ω_L and D is of the order of H_0 (Arbab, 2009 [4,5]). This suggests that the cause of these parameters is the cosmic expansion.

Fossils of coral reefs studied by John Wells (Wells, 1963 [7]) revealed that the number of days in the past geologic time was bigger than now. This entails that the length of day was shorter in the past than now. The rotation of the Earth is gradually slowing down at about 2 milliseconds a century. Another method of dating that is popular with some scientists is tree-ring dating. When a tree is cut, you can study a cross-section of the trunk and determine its age. Each year of growth produces a single ring. Moreover, the width of the ring is related to environmental conditions at the time the ring was formed. It is therefore possible to know the length of day in the past from palaeontological studies of annual and daily growth rings in corals, bivalves, and stromatolite. The creation of the Moon was another factor that would later help the planet to become more habitable. When the day was shorter the Earth's spins faster. Hence, the Moon tidal force reduced the Earth's rotational winds. Thus, the Moon stabilizes the Earth rotation and the Earth became habitable. It is thus plausible to say that the Earth must have recovered very rapidly after the trauma of the Moon's formation. It was found that circadian rhythm in higher animals does not adjust to a period of less than 17–19 hours per day. Our models can give clues to the time these animals first appeared (945–1366 million years ago).

This shortening is attributed to tidal forces raised by the Moon on Earth. This results in slowing down the Earth rotation while increasing the orbital motion of the Moon. According to the tidal theory explained above we see that the tidal frictional torque $\tau \propto R^{-6}$ and the amplitude of tides is $\propto R^{-3}$. Hence, both terms have been very big in the past when R was very small. However, even if we assume the rate $\frac{dR}{dt}$ to have been constant as its value now, some billion years ago the Earth-Moon distance R would be very short. This close approach would have been catastrophic to both the Earth and the Moon. The tidal force would have been enough to melt the Earth's crust. However, there appears to be no evidence for such phenomena according to the geologic findings. This fact places the tidal theory, as it stands, in great jeopardy. This is the most embarrassing situation facing the tidal theory.

4 Velocity-dependent Inertia Model

A velocity — dependent inertial induction model is recently proposed by Ghosh (Gosh, 2000 [8]) in an attempt to surmount this difficulty. It asserts that a spinning body slows down in the vicinity of a massive object. He suggested that part of the secular retardation of the Earth's spin and of the Moon's orbital motion can be due to inertial induction by the Sun. If the Sun's influence can make a braking torque on the spinning Earth, a similar effect should be present in the case of other spinning celestial objects. This theory predicts that the angular momentum of the Earth (L'), the torque (τ'), and distance (R') vary as

$$\left.\begin{aligned} L' &= \frac{mM}{(M+m)^{\frac{1}{3}}}\, G_{\text{eff}}^{\frac{2}{3}}\, \omega_L^{-\frac{1}{3}} \\ \tau' &= -\frac{L'}{3\omega_L}\,\dot{\omega}_L \\ \dot{R} &= -\frac{2}{3}\,\frac{R}{\omega_L}\,\dot{\omega}_L \end{aligned}\right\}. \qquad (41)$$

The present rate of the secular retardation of the Moon angular speed is found to be $\frac{d\omega_L}{dt} \equiv \dot{\omega}_L \approx 0.27\times10^{-23}$ rad s^{-2} leaving a tidal contribution of $\approx -0.11\times10^{-23}$ rad s^{-2}. This gives a rate of $\frac{dR}{dt} \equiv \dot{R} = -0.15\times10^{-9}$ m s^{-1}. Now the apparent lunar and solar contributions amount to $\approx 2.31\times10^{-23}$ rad s^{-2} and $\approx 1.65\times10^{-23}$ rad s^{-2} respectively. The most significant result is that $\frac{dR}{dt}$ is negative and the magnitude is about one tenth of the value derived using the tidal theory only. Hence, Ghosh concluded that the Moon is actually approaching the Earth with a vary small speed, and hence there is no close-approach problem. Therefore, this will imply that the tidal dissipation must have been much lower in the Earth's early history.

Acknowledgements

I wish to thank the University of Khartoum for providing research support for this work, and the Abdus salam International Center for Theoretical Physics (ICTP) for hospitality where this work is carried out.

Submitted on October 12, 2008 / Accepted on October 17, 2008

References

1. Stacey F. Physics of the Earth. Earth tides. J. Wiley & Sons Inc., New York, 1977.
2. Arbab A.I. *Gen. Relativ. & Gravit.*, 1997, v. 29, 61.
3. Arbab A.I. *Acta Geodaetica et Geophysica Hungarica*, 2004, v. 39, 27.
4. Arbab A.I. *Progress in Physics*, 2009, v. 1, 8.
5. Arbab A.I. *Astrophys. Space Sci.*, 2008, v. 314, 35.
6. Arbab A.I. *Acta Geodaetica et Geophysica Hungarica*, 2005, v. 40, 33.
7. Wells J.W. *Nature, 1963, v. 197, 948.*
8. *Gosh A. Origin of inertia: extended Mach's principle and cosmological consequences. Apeiron Pibl., 2000.*

Parameters for Viability Check on Gravitational Theories Regarding the Experimental Data

Emilija G. Celakoska* and Kostadin Trenčevski†

*Faculty of Mechanical Eng., Sts. Cyril and Methodius Univ., P.O.Box 464, 1000 Skopje, Macedonia
E-mail: cemil@mf.edu.mk

†Faculty of Natural Sci. and Math., Sts. Cyril and Methodius Univ., P.O.Box 162, 1000 Skopje, Macedonia
E-mail: kostatre@iunona.pmf.ukim.edu.mk

Parameterized post-Newtonian formalism requires an existence of a symmetric metric in a gravitational theory in order to perform a viability check regarding the experimental data. The requirement of a symmetric metric is a strong constraint satisfied by very narrow class of theories. In this letter we propose a viability check of a theory using the corresponding theory equations of motion. It is sufficient that a connection exists, not necessarily a metrical one. The method is based on an analysis of the Lorentz invariant terms in the equations of motion. An example of the method is presented on the Einstein-Infeld-Hoffmann equations.

1 Introduction

The parameterized post-Newtonian (PPN) formalism is a tool used to compare classical theories of gravitation in the limit of weak field generated by objects moving slowly compared to c. It is applicable only for symmetric metric theories of gravitation that satisfy the Einstein equivalence principle.

Each parameter in PPN formalism is a measure of departure of a theory from Newtonian gravity represented by several parameters. Following the Will notation [1], there are ten parameters: $\gamma, \beta, \xi, \alpha_1, \alpha_2, \alpha_3, \zeta_1, \zeta_2, \zeta_3, \zeta_4$; γ is a measure of space curvature; β measures the nonlinearity in superposition of gravitational fields; ξ is a check for preferred location effects, i.e. a check for a violation of the strong equivalence principle (SEP) whether the outcomes of local gravitational experiments depend on the location of the laboratory relative to a nearby gravitating body; α_1, α_2, α_3 measure the extent and nature of preferred-frame effects, i.e. how much SEP is violated by predicting that the outcomes of local gravitational experiments may depend on the velocity of the laboratory relative to the mean rest frame of the universe; $\zeta_1, \zeta_2, \zeta_3, \zeta_4$ and α_3 measure the extent and nature of breakdowns in global conservation laws. The PPN metric components are

$$g_{00} = -1+2U-2\beta U^2-2\xi\Phi_W+(2\gamma+2+\alpha_3+\zeta_1-2\xi)\,\Phi_1+ \\ +2\,(3\gamma-2\beta+1+\zeta_2+\xi)\,\Phi_2+2\,(1+\zeta_3)\,\Phi_3+ \\ +2\,(3\gamma+3\zeta_4-2\xi)\,\Phi_4-(\zeta_1-2\xi)\,A-(\alpha_1-\alpha_2-\alpha_3)w^2U- \\ -\alpha_2\,w^iw^jU_{ij}+(2\alpha_3-\alpha_1)\,w^iV_i+O(\epsilon^3)\,, \qquad (1.1)$$

$$g_{0i} = -\tfrac{1}{2}\,(4\gamma+3+\alpha_1-\alpha_2+\zeta_1-2\eta)\,V_i- \\ -\tfrac{1}{2}\,(1+\alpha_2-\zeta_1+2\xi)\,W_i- \\ -\tfrac{1}{2}\,(\alpha_1-2\alpha_2)\,w^iU-\alpha_2w^jU_{ij}+O(\epsilon^{5/2})\,, \qquad (1.2)$$

$$g_{ij} = (1+2\gamma U)\,\delta_{ij}+O(\epsilon^2)\,, \qquad (1.3)$$

where w^i is the coordinate velocity of the PPN coordinate system relative to the mean rest-frame of the universe and U, U_{ij}, Φ_W, A, Φ_1, Φ_2, Φ_3, Φ_4, V_i and W_i are the metric potentials constructed from the matter variables and have similar form as the Newtonian gravitational potential [1, 2].

The theories that can be compared using PPN formalism are straightforward alternatives to GR. The bounds on the PPN parameters are not the ultimate criteria for viability of a gravitational theory, because many theories can not be compared using PPN formalism. For example, Misner et al. [3] claim that Cartan's theory is the only non-metric theory to survive all experimental tests up to that date and Turyshev [4] lists Cartan's theory among the few that have survived all experimental tests up to that date. There are general viability criteria [5] for a gravitational theory: (i) is it self-consistent? (ii) is it complete? (iii) does it agree, to within several standard deviations, with all experiments performed to date?

For a symmetric metric theory, the answer of (iii) is consisted in checking the PPN parameters. But, for a non-symmetric or a non-metric theory there is not a convenient method. So, we propose a method for checking (iii) even in the cases when the PPN formalism can not be applied such as non-symmetric metric and non-metric theories. It is based on a Lorentz invariance analysis of all terms in the equations of motion of the corresponding theory. Since there is no general equations of motion formula for all theories, we give an example of the method on the Einstein-Infeld-Hoffmann (EIH) equations. However, the general principle of the method can be applied to any other theory in which the equations of motion can be derived, no matter whether the theory includes a metric or not.

2 Lorentz invariant terms in the EIH equations

Given a system of n bodies, the equations of motion of the j-th body is

$$\frac{d^2\vec{r}_j}{dt^2}=\sum_{i\neq j}\frac{(\vec{r}_i-\vec{r}_j)Gm_i}{r_{ij}^3}\left[1-\frac{3}{2c^2}\frac{[\dot{\vec{r}}_i\cdot(\vec{r}_j-\vec{r}_i)]^2}{r_{ij}^2}-\right.$$
$$-\frac{2(\beta+\gamma)}{c^2}\sum_{k\neq j}\frac{Gm_k}{r_{jk}}-\frac{2\beta-1}{c^2}\sum_{k\neq i}\frac{Gm_k}{r_{ik}}+\frac{1}{2c^2}(\vec{r}_i-\vec{r}_j)\,\dot{\vec{v}}_i-$$
$$\left.-\frac{2(1+\gamma)}{c^2}\,\dot{\vec{r}}_i\dot{\vec{r}}_j+\gamma\Big(\frac{v_j}{c}\Big)^2+(1+\gamma)\Big(\frac{v_i}{c}\Big)^2\right]+$$
$$+\frac{1}{c^2}\sum_{i\neq j}\frac{Gm_i}{r_{ij}^3}\big((\vec{r}_j-\vec{r}_i)\cdot\big((2+2\gamma)\,\dot{\vec{r}}_j-(1+2\gamma)\,\dot{\vec{r}}_i\big)\big)\times$$
$$\times(\dot{\vec{r}}_j-\dot{\vec{r}}_i)+\frac{3+4\gamma}{2c^2}\sum_{i\neq j}\frac{Gm_i}{r_{ij}}\,\dot{\vec{v}}_i\,, \qquad (2.1)$$

where $\vec{r}_s$ is the radius-vector of the s-th body, $\vec{v}_s=\dot{\vec{r}}_s$ is the velocity of the s-th body and upper dot marks the differentiation with time. Formula (2.1) can be rearranged in the form

$$\frac{d^2\vec{r}_j}{dt^2}=\sum_{i\neq j}\frac{(\vec{r}_i-\vec{r}_j)Gm_i}{r_{ij}^3}\left[1-\frac{3}{2c^2}\frac{[\dot{\vec{r}}_i\cdot(\vec{r}_j-\vec{r}_i)]^2}{r_{ij}^2}+\right.$$
$$+\frac{1}{c^2}\sum_{k\neq i}\frac{Gm_k}{r_{ik}}+\frac{1}{2c^2}(\vec{r}_i-\vec{r}_j)\,\dot{\vec{v}}_i-\frac{2}{c^2}\,\dot{\vec{r}}_i\dot{\vec{r}}_j+\Big(\frac{v_i}{c}\Big)^2\Big]+$$
$$+\frac{1}{c^2}\sum_{i\neq j}\frac{Gm_i}{r_{ij}^3}\big((\vec{r}_j-\vec{r}_i)\cdot(2\dot{\vec{r}}_j-\dot{\vec{r}}_i)\big)(\dot{\vec{r}}_j-\dot{\vec{r}}_i)+$$
$$+\frac{3}{2c^2}\sum_{i\neq j}\frac{Gm_i}{r_{ij}}\,\dot{\vec{v}}_i+\gamma\left[\sum_{i\neq j}\frac{(\vec{r}_i-\vec{r}_j)Gm_i}{r_{ij}^3}\times\right.$$
$$\times\left(-\frac{2}{c^2}\sum_{k\neq j}\frac{Gm_k}{r_{jk}}+\frac{1}{2c^2}(\vec{r}_i-\vec{r}_j)\,\dot{\vec{v}}_i+\frac{1}{c^2}(\dot{\vec{r}}_i-\dot{\vec{r}}_j)^2\right)+$$
$$+\frac{2}{c^2}\sum_{i\neq j}\frac{Gm_i}{r_{ij}^3}\big((\vec{r}_j-\vec{r}_i)\cdot(\dot{\vec{r}}_j-\dot{\vec{r}}_i)\big)(\dot{\vec{r}}_j-\dot{\vec{r}}_i)+$$
$$\left.+\frac{2}{c^2}\sum_{i\neq j}\frac{Gm_i}{r_{ij}}\,\dot{\vec{v}}_i\right]-\beta\,\frac{2}{c^2}\left[\sum_{i\neq j}\frac{(\vec{r}_i-\vec{r}_j)Gm_i}{r_{ij}^3}\times\right.$$
$$\left.\times\left(\sum_{k\neq j}\frac{Gm_k}{r_{jk}}+\sum_{k\neq i}\frac{Gm_k}{r_{ik}}\right)\right]. \qquad (2.2)$$

The second and the third term are of order c^{-2} and each of them is Lorentz invariant, neglecting the terms of order c^{-4} and smaller, i.e. they take same values in all inertial systems. So, (2.2) means

$$\frac{d^2\vec{r}_j}{dt^2}=\sum_{i\neq j}\left\{-\frac{(\vec{r}_j-\vec{r}_i)Gm_i}{r_{ij}^3}\left[1-\frac{3}{2}\frac{[\vec{v}_i\cdot(\vec{r}_j-\vec{r}_i)]^2}{r_{ij}^2c^2}+\right.\right.$$
$$\left.+\frac{v_i^2}{c^2}-2\,\frac{\vec{v}_i\cdot\vec{v}_j}{c^2}\right]+\frac{Gm_i}{r_{ij}^3c^2}\,(\vec{v}_j-\vec{v}_i)\big[(\vec{r}_j-\vec{r}_i)\cdot\vec{v}_j\big]\Big\}+$$
$$+\ \text{Lorentz invariant terms.} \qquad (2.3)$$

Every single Lorentz invariant term in (2.2), i.e. in (2.3), can be replaced by a term proportional to the corresponding Lorentz invariant term, so

$$\frac{d^2\vec{r}_j}{dt^2}=\sum_{i\neq j}\left\{-\frac{(\vec{r}_j-\vec{r}_i)Gm_i}{r_{ij}^3}\left[1-\frac{3}{2}\frac{[\vec{v}_i\cdot(\vec{r}_j-\vec{r}_i)]^2}{r_{ij}^2c^2}+\right.\right.$$
$$\left.+\frac{v_i^2}{c^2}-2\,\frac{\vec{v}_i\cdot\vec{v}_j}{c^2}\right]+\frac{Gm_i}{r_{ij}^3c^2}\,(\vec{v}_j-\vec{v}_i)[(\vec{r}_j-\vec{r}_i)\cdot\vec{v}_j]+$$
$$+A\,\frac{(\vec{r}_i-\vec{r}_j)Gm_i}{r_{ij}^3}\,\frac{(\vec{v}_i-\vec{v}_j)^2}{c^2}+B\,\frac{(\vec{r}_i-\vec{r}_j)Gm_i}{r_{ij}^3c^2}\times$$
$$\times[(\vec{r}_i-\vec{r}_j)\cdot\dot{\vec{v}}_i]+C\,\frac{Gm_i}{r_{ij}c^2}\,\dot{\vec{v}}_i+D\,\frac{Gm_i}{r_{ij}^3c^2}\,(\vec{v}_j-\vec{v}_i)\times$$
$$\times[(\vec{r}_j-\vec{r}_i)\cdot(\vec{v}_j-\vec{v}_i)]+E\sum_{k\neq i,j}\frac{(\vec{r}_i-\vec{r}_j)Gm_i}{r_{ij}^3}\,\frac{Gm_k}{r_{ki}c^2}+$$
$$\left.+F\sum_{k\neq i,j}\frac{(\vec{r}_i-\vec{r}_j)Gm_i}{r_{ij}^3}\,\frac{Gm_k}{r_{kj}c^2}\right\}. \qquad (2.4)$$

The bounds on the parameters A, B, C, D, E and F can be determined directly from the experimental data. Now, the viability check of any gravitational theory regarding the agreement on the experimental data would be consisted in checking how the theory fits in the bounds of the new parameters.

3 Conclusion

In this letter we introduced a new approach of viability check of gravitational theories regarding the experimental data, based on the analysis of the Lorentz invariance of the equations of motion. An example is given for the EIH equations. This method can be applied on any theory that has a connection regardless it is metrical or not. The bounds of the new parameters can be determined directly from the experimental data.

Submitted on October 27, 2008 / Accepted on October 30, 2008

References

1. Will C.M. Theory and experiment in gravitational physics. Cambridge University Press, New York, 1993.
2. Will C.M. The confrontation between General Relativity and experiment. *Living Rev. Relativity*, 2006, v.9.
3. Misner C.W., Thorne K.S., and Wheeler J.A. Gravitation. W. H. Freeman and Company, San Francisco, 1973.
4. Turyshev S.G. Testing gravity in the solar system. *Alternative Gravities and Dark Matter Workshop Royal Observatory*, Edinburgh, Scotland, 20–22 April 2006; http://star-www.st-and.ac.uk/ ∼hz4/workshop/workshopppt/turyshev.pdf
5. Ni W.-T. Theoretic frameworks for testing relativistic gravity IV. *Astrophys. Journal*, 1972, v. 176, 769–796.

An Asymptotic Solution for the Navier-Stokes Equation

Emilio Casuso Romate and John E. Beckman
Instituto de Astrofísica de Canarias, E-38200 La Laguna, Tenerife, Spain
E-mail: eca@iac.es

We have used as the velocity field of a fluid the functional form derived in Casuso (2007), obtained by studying the origin of turbulence as a consequence of a new description of the density distribution of matter as a modified discontinuous Dirichlet integral. As an interesting result we have found that this functional form for velocities is a solution to the Navier-Stokes equation when considering asymptotic behaviour, i.e. for large values of time.

1 Introduction

The Euler and Navier-Stokes equations describe the motion of a fluid. These equations are to be solved for an unknown velocity vector $\vec{u}(\vec{r},t)$ and pressure $P(\vec{r},t)$, defined for position $\vec{r}$ and time $t \geqslant 0$. We restrict attention here to incomprenssible fluids filling all real space. Then the Navier-Stokes equations are: a) Newton's law $\vec{f} = m\vec{a}$ for a fluid element subject to the external force $\vec{g}$ (gravity) and to the forces arising from pressure and friction, and b) The condition of incompressibility. A fundamental problem in the analysis is to find any physically reasonable solution for the Navier-Stokes equation, and indeed to show that such a solution exists. Many numerical computations appear to exhibit blowup for solutions of the Euler equations (the same as Navier-Stokes equations but for zero viscosity), but the extreme numerical instability of the equations makes it very hard to draw reliable conclusions (see Bertozzi and Majda 2002 [1]). Important progress has been made in understanding weak solutions of the Navier-Stokes equations (Leray 1934 [2], Khon and Nirenberg 1982 [3], Scheffer 1993 [4], Schnirelman 1997 [5], Caffarelli and Lin 1998 [6]). This type of solutions means that one integrates the equation against a test function, and then integrates by parts to make the derivatives fall on the test function. In the present paper we test directly the validity of a solution which was obtained previously from the study of turbulence.

2 Demonstration of validity of the asymptotic solution

We start from the Navier-Stokes equation for one-dimension:

$$\frac{\partial u_x}{\partial t} + u_x \frac{\partial u_x}{\partial x} = \nu \frac{\partial^2 u_x}{\partial x^2} - \frac{\partial P}{\partial x} + g\,, \tag{1}$$

where ν is a positive coefficient (viscosity) and g means a nearly constant gravitational force per unit mass (an externally applied force).

Taking from Casuso, 2007 [7], the functional form derived for the velocity of a fluid

$$u_x = -\sum_k \frac{\sin(x_k t)}{it^2}\, e^{it(x+k)} + \text{const}, \tag{2}$$

where $-x_k \leqslant x + k \leqslant x_k$, k describe the central positions of real matter structures such as atomic nuclei and x_k means the size of these structures. Assuming a polytropic relation between pressure P and density ρ via the sound speed s we have:

$$P = s^2\rho = \frac{s^2}{\pi}\sum_k \int \frac{\sin(x_k t)}{t}\, e^{it(x+k)} dt\,. \tag{3}$$

Puting equations (2) and (3) into equation (1) we obtain:

$$A + B = C + g\,, \tag{4}$$

where

$$A = -\sum_k \left[\frac{\cos(x_k t)}{it^2}\, x_k + \frac{(x+k)}{t^2}\sin(x_k t) + 2\frac{\sin(x_k t)}{t^3} \right] e^{it(x+k)}\,, \tag{5}$$

$$B = \left[-\sum_k \frac{\sin(x_k t)}{it^2}\, e^{it(x+k)} + \text{const} \right] \times \left[-\sum_k \frac{\sin(x_k t)}{t}\, e^{it(x+k)} \right]\,, \tag{6}$$

$$C = \nu \left[-\sum_k i \sin(x_k t)\, e^{it(x+k)} \right] - \frac{is^2}{\pi}\sum_k \int \sin(x_k t)\, e^{it(x+k)}\, dt\,. \tag{7}$$

Now taking the asymptotic approximation, at very large time t, we obtain

$$\nu \sin(x_k t)\, e^{it(x+k)} = -\frac{s^2}{\pi}\int \sin(x_k t)\, e^{it(x+k)} dt + g\,, \tag{8}$$

and differentiating and taking only the real part, we have

$$x_k \cos(x_k t) = -\frac{s^2}{\pi\nu}\sin(x_k t)\,, \tag{9}$$

which is the same as

$$-\frac{x_k \pi\nu}{s^2} = \tan(x_k t) \tag{10}$$

then, in the limiting case (real case) $x_k \to 0$ and, again at very

large time t, we have the solutions

$$x_k t = 0, \pi, 2\pi, 3\pi, \ldots, n\pi \tag{11}$$

with n being any integer number. So we have demonstrated that the equation (2) is a solution for the Navier-Stokes equation in one dimension.

Now, for the general case of 3-dimensions we have to generalize the functional form which describes the nature of matter in Casuso, 2007 [7], in the sense of taking a new form for the density

$$\rho = \frac{1}{\pi} \sum_k \int \frac{\sin(r_k t)}{t}\, e^{it(r+k)}\, dt\,, \tag{12}$$

where $r = \sqrt{x^2 + y^2 + z^2}$, and applying the continuity equation

$$\frac{\partial \rho}{\partial t} = -\frac{\partial}{\partial x}(\rho u_x) - \frac{\partial}{\partial y}(\rho u_y) - \frac{\partial}{\partial z}(\rho u_z). \tag{13}$$

Using the condition of incompressibility included in Navier-Stokes equations

$$\mathrm{div}\vec{u} = 0 \tag{14}$$

and assuming isotropy for the velocity field $u_x \simeq u_y \simeq u_z$, we have

$$u_x = u_y = u_z = -\frac{r}{\pi(x+y+z)} \times \\ \times \sum_k \frac{\sin(r_k t)}{it^2}\, e^{it(r+k)} + \mathrm{const}, \tag{15}$$

where $-r_k \leqslant r + k \leqslant r_k$. Including this expression for the velocity in the 3-dimensional Navier-Stokes main equation (taking into account the condition $\mathrm{div}\vec{u} = 0$)

$$\frac{\partial}{\partial t} u_x = \nu \left[\frac{\partial^2}{\partial x^2} + \frac{\partial^2}{\partial y^2} + \frac{\partial^2}{\partial z^2} \right] u_x - \frac{\partial P}{\partial x} + g\,, \tag{16}$$

we obtain

$$-\frac{r}{\pi(x+y+z)} \sum_k e^{it(r+k)} \times \\ \times \left[\frac{r_k \cos(r_k t)}{it^2} + \frac{(r+k)\sin(r_k t)}{t^2} - \frac{2\sin(r_k t)}{it^3} \right] = \\ = \nu \Delta u_x - \frac{\partial P}{\partial x} + g\,, \tag{17}$$

where Δ means $\frac{\partial^2}{\partial x^2} + \frac{\partial^2}{\partial y^2} + \frac{\partial^2}{\partial z^2}$. Again taking the approximation of very large time, we have

$$\frac{\partial P}{\partial x} = g\,, \tag{18}$$

i.e.

$$i\,\frac{s^2 x}{\pi r} \sum_k \int \sin(r_k t)\, e^{it(r+k)} dt = g\,. \tag{19}$$

Taking the partial derivative with respect to time we obtain

$$i\,\frac{s^2 x}{\pi r} \sum_k \sin(r_k t)\, e^{it(r+k)} = 0 \tag{20}$$

or (which is the same),

$$e^{it(r+k)} \sin(r_k t) = 0\,, \tag{21}$$

i.e.

$$\left(\cos[(r+k)t] - i\sin[(r+k)t]\right) \sin(r_k t) = 0\,. \tag{22}$$

Taking only the real part

$$\sin(r_k t)\cos[(r+k)t] = 0\,. \tag{23}$$

So, we have two solutions: (a) $r_k t = 0, \pi, 2\pi, \ldots, n\pi$, and (b) $(r+k)t = \frac{\pi}{2}, 3\frac{\pi}{2}, \ldots, (2n+1)\frac{\pi}{2}$. We must note that the solution (a) is similar to the 1-dimension solution.

3 Conclusions

By using a new discontinuous functional form for matter density distribution, derived from consideration of the origin of turbulence, we have found an asymptotic solution to the Navier-Stokes equation for the three dimensional case. This result, while of intrinsic interest, may point towards new ways of deriving a general solution.

Acknowledgements

This work was partially supported by grant AYA2007-67625-C02-01 of the Spanish Ministry of Science and Technology.

Submitted on November 10, 2008 / Accepted on November 14, 2008

References

1. Bertozzi A. and Majda A. In: *Vorticity and Incompressible Flows*, C.U.P., 2002.
2. Leray J. *Acta Math. J.*, 1934, v. 63, 193.
3. Khon R. and Nirenberg L. *Comm. Pure & Appl. Math.*, 1982, v. 35, 771.
4. Scheffer V. *J. Geom. Analysis*, 1993, v. 3, 343.
5. Shnirelman A. *Comm. Pure & Appl. Math.*, 1997, v. 50, 1260.
6. Caffarelli L. and Lin F.-H. *Comm. Pure & Appl. Math.*, 1998, v. 51, 241.
7. Casuso E. *IJTP*, 2007, v. 46, 1809.

On PT-Symmetric Periodic Potential, Quark Confinement, and Other Impossible Pursuits

Vic Christianto* and Florentin Smarandache†

*Sciprint.org — a Free Scientific Electronic Preprint Server, http://www.sciprint.org
E-mail: admin@sciprint.org

†Department of Mathematics, University of New Mexico, Gallup, NM 87301, USA
E-mail: smarand@unm.edu

As we know, it has been quite common nowadays for particle physicists to think of six impossible things before breakfast, just like what their cosmology fellows used to do. In the present paper, we discuss a number of those impossible things, including PT-symmetric periodic potential, its link with condensed matter nuclear science, and possible neat link with Quark confinement theory. In recent years, the PT-symmetry and its related periodic potential have gained considerable interests among physicists. We begin with a review of some results from a preceding paper discussing derivation of PT-symmetric periodic potential from biquaternion Klein-Gordon equation and proceed further with the remaining issues. Further observation is of course recommended in order to refute or verify this proposition.

1 Introduction

As we know, it has been quite common nowadays for particle physicists to think of six impossible things before breakfast [1], just like what their cosmology fellows used to do. In the present paper, we discuss a number of those impossible things, including PT-symmetric periodic potential, its link with condensed matter nuclear science, and possible neat link with Quark Confinement theory.

In this regards, it is worth to remark here that there were some attempts in literature to generalise the notion of symmetries in Quantum Mechanics, for instance by introducing CPT symmetry, chiral symmetry etc. In recent years, the PT-symmetry and its related periodic potential have gained considerable interests among physicists [2, 3]. It is expected that the discussions presented here would shed some light on these issues.

We begin with a review of results from our preceding papers discussing derivation of PT-symmetric periodic potential from biquaternion Klein-Gordon equation [4–6]. Thereafter we discuss how this can be related with both Gribov's theory of Quark Confinement, and also with EQPET/TSC model for condensed matter nuclear science (aka low-energy reaction or "cold fusion") [7]. We also highlight its plausible implication to the calculation of Gamow integral for the (periodic) non-Coulomb potential.

In other words, we would like to discuss in this paper, whether there is PT symmetric potential which can be observed in Nature, in particular in the context of condensed matter nuclear science (CMNS) and Quark confinement theory.

Nonetheless, further observation is of course recommended in order to refute or verify this proposition.

2 PT-symmetric periodic potential

It has been argued elsewhere that it is plausible to derive a new PT-symmetric Quantum Mechanics (PT-QM; sometimes it is called pseudo-Hermitian Quantum Mechanics [3, 9]) which is characterized by a PT-symmetric potential [2]

$$V(x) = V(-x)\,. \tag{1}$$

One particular example of such PT-symmetric potential can be found in sinusoidal-form potential

$$V = \sin\varphi\,. \tag{2}$$

PT-symmetric harmonic oscillator can be written accordingly [3]. Znojil has argued too [2] that condition (1) will yield Hulthen potential

$$V(\xi) = \frac{A}{\left(1 - e^{2i\xi}\right)^2} + \frac{B}{\left(1 - e^{2i\xi}\right)}\,. \tag{3}$$

Interestingly, a similar periodic potential has been known for quite a long time as Posch-Teller potential [9], although it is not always related to PT-Symmetry considerations. The Posch-Teller system has a unique potential in the form [9]

$$U(x) = -\lambda \cosh^{-2} x\,. \tag{4}$$

It appears worth to note here that Posch-Teller periodic potential can be derived from conformal D'Alembert equations [10, p.27]. It is also known as the second Posch-Teller potential

$$V_\mu(\xi) = \frac{\mu(\mu-1)}{\sinh^2\xi} + \frac{\ell(\ell+1)}{\cosh^2\xi}\,. \tag{5}$$

The next Section will discuss biquaternion Klein-Gordon equation [4, 5] and how its radial version will yield a sinusoidal form potential which appears to be related to equation (2).

3 Solution of radial biquaternion Klein-Gordon equation and a new sinusoidal form potential

In our preceding paper [4], we argue that it is possible to write biquaternionic extension of Klein-Gordon equation as follows

$$\left[\left(\frac{\partial^2}{\partial t^2}-\nabla^2\right)+i\left(\frac{\partial^2}{\partial t^2}-\nabla^2\right)\right]\varphi(x,t)= \\ =-m^2\varphi(x,t)\,, \quad (6)$$

or this equation can be rewritten as

$$\left(\diamondsuit\bar{\diamondsuit}+m^2\right)\varphi(x,t)=0 \quad (7)$$

provided we use this definition

$$\diamondsuit=\nabla^q+i\nabla^q=\left(-i\frac{\partial}{\partial t}+e_1\frac{\partial}{\partial x}+e_2\frac{\partial}{\partial y}+e_3\frac{\partial}{\partial z}\right)+ \\ +i\left(-i\frac{\partial}{\partial T}+e_1\frac{\partial}{\partial X}+e_2\frac{\partial}{\partial Y}+e_3\frac{\partial}{\partial Z}\right), \quad (8)$$

where e_1, e_2, e_3 are *quaternion imaginary units* obeying (with ordinary quaternion symbols $e_1=i$, $e_2=j$, $e_3=k$):

$$i^2=j^2=k^2=-1\,, \quad ij=-ji=k\,, \quad (9)$$

$$jk=-kj=i\,, \quad ki=-ik=j\,, \quad (10)$$

and quaternion *Nabla operator* is defined as [4]

$$\nabla^q=-i\frac{\partial}{\partial t}+e_1\frac{\partial}{\partial x}+e_2\frac{\partial}{\partial y}+e_3\frac{\partial}{\partial z}\,. \quad (11)$$

Note that equation (11) already included partial time-differentiation.

Thereafter one can expect to find solution of *radial* biquaternion Klein-Gordon Equation [5, 6].

First, the standard Klein-Gordon equation reads

$$\left(\frac{\partial^2}{\partial t^2}-\nabla^2\right)\varphi(x,t)=-m^2\varphi(x,t)\,. \quad (12)$$

At this point we can introduce polar coordinate by using the following transformation

$$\nabla=\frac{1}{r^2}\frac{\partial}{\partial r}\left(r^2\frac{\partial}{\partial r}\right)-\frac{\ell^2}{r^2}\,. \quad (13)$$

Therefore by introducing this transformation (13) into (12) one gets (setting $\ell=0$)

$$\left(\frac{1}{r^2}\frac{\partial}{\partial r}\left(r^2\frac{\partial}{\partial r}\right)+m^2\right)\varphi(x,t)=0\,. \quad (14)$$

By using the same method, and then one gets radial expression of BQKGE (6) for 1-dimensional condition as follows [5, 6]

$$\left(\frac{1}{r^2}\frac{\partial}{\partial r}\left(r^2\frac{\partial}{\partial r}\right)-i\frac{1}{r^2}\frac{\partial}{\partial r}\left(r^2\frac{\partial}{\partial r}\right)+m^2\right)\varphi(x,t)=0\,. \quad (15)$$

Using Maxima computer package we find solution of equation (15) as a new potential taking the form of sinusoidal potential

$$y=k_1\sin\left(\frac{|m|\,r}{\sqrt{-i-1}}\right)+k_2\cos\left(\frac{|m|\,r}{\sqrt{-i-1}}\right), \quad (16)$$

where k_1 and k_2 are parameters to be determined. It appears very interesting to remark here, when k_2 is set to 0, then equation (16) can be written in the form of equation (2)

$$V=k_1\sin\varphi\,, \quad (17)$$

by using definition

$$\varphi=\sin\left(\frac{|m|\,r}{\sqrt{-i-1}}\right). \quad (18)$$

In retrospect, the same procedure which has been traditionally used to derive the Yukawa potential, by using radial biquaternion Klein-Gordon potential, yields a PT-symmetric periodic potential which takes the form of equation (1).

4 Plausible link with Gribov's theory of Quark Confinement

Interestingly, and quite oddly enough, we find the solution (17) may have deep link with Gribov's theory of Quark confinement [8, 11]. In his Third Orsay Lectures he described a periodic potential in the form [8, p.12]

$$\ddot{\psi}-3\sin\psi=0\,. \quad (19)$$

By using Maxima package, the solution of equation (19) is given by

$$\left.\begin{aligned} x_1&=k_2-\frac{\int\frac{1}{\sqrt{k_1-\cos(y)}}dy}{\sqrt{6}} \\ x_2&=k_2+\frac{\int\frac{1}{\sqrt{k_1-\cos(y)}}dy}{\sqrt{6}} \end{aligned}\right\}, \quad (20)$$

while Gribov argues that actually the equation shall be like nonlinear oscillation with damping, the equation (19) indicates close similarity with equation (2).

Therefore one may think that PT-symmetric periodic potential in the form of (2) and also (17) may have neat link with the Quark Confinement processes, at least in the context of Gribov's theory. Nonetheless, further observation is of course recommended in order to refute or verify this proposition.

5 Implication to condensed matter nuclear science. Comparing to EQPET/TSC model. Gamow integral

In accordance with a recent paper [6], we interpret and compare this result from the viewpoint of EQPET/TSC model which has been suggested by Prof. Takahashi in order to explain some phenomena related to Condensed matter nuclear Science (CMNS).

Takahashi [7] has discussed key experimental results in condensed matter nuclear effects in the light of his EQPET/TSC model. We argue here that his potential model with inverse barrier reversal (STTBA) may be comparable to the periodic potential described above (17).

In [7] Takahashi reported some findings from condensed matter nuclear experiments, including intense production of helium-4, ^{4}He atoms, by electrolysis and laser irradiation experiments. Furthermore he [7] analyzed those experimental results using EQPET (Electronic Quasi-Particle Expansion Theory). Formation of TSC (tetrahedral symmetric condensate) were modeled with numerical estimations by STTBA (Sudden Tall Thin Barrier Approximation). This STTBA model includes strong interaction with negative potential near the center.

One can think that apparently to understand the physics behind Quark Confinement, it requires fusion of different fields in physics, perhaps just like what Langland program wants to fuse different branches in mathematics.

Interestingly, Takahashi also described the Gamow integral of his STTBA model as follows [7]

$$\Gamma_n = 0.218 \left(\mu^{1/2}\right) \int_{r_0}^{b} \left(V_b - E_d\right)^{1/2} dr \,. \tag{21}$$

Using $b = 5.6$ fm and $r = 5$ fm, he obtained [7]

$$P_{4D} = 0.77, \tag{22}$$

and

$$V_B = 0.257 \text{ MeV}, \tag{23}$$

which gave significant underestimate for 4D fusion rate when rigid constraint of motion in 3D space attained. Nonetheless by introducing different values for λ_{4D} the estimate result can be improved. Therefore we may conclude that Takahashi's STTBA potential offers a good approximation (just what the name implies, STTBA) of the fusion rate in condensed matter nuclear experiments.

It shall be noted, however, that his STTBA lacks sufficient theoretical basis, therefore one can expect that a sinusoidal periodic potential such as equation (17) may offer better result.

All of these seem to suggest that the cluster deuterium may yield a different inverse barrier reversal which cannot be predicted using the D-D process as in standard fusion theory. In other words, the standard procedure to derive Gamow factor should also be revised [12]. Nonetheless, it would need further research to determine the precise Gamow energy and Gamow factor for the cluster deuterium with the periodic potential defined by equation (17); see for instance [13].

In turn, one can expect that Takahashi's EQPET/TSC model along with the proposed PT-symmetric periodic potential (17) may offer new clues to understand both the CMNS processes and also the physics behind Quark confinement.

6 Concluding remarks

In recent years, the PT-symmetry and its related periodic potential have gained considerable interests among physicists.

In the present paper, it has been shown that one can find a new type of PT-symmetric periodic potential from solution of the radial biquaternion Klein-Gordon Equation. We also have discussed its plausible link with Gribov's theory of Quark Confinement and also with Takahashi's EQPET/TSC model for condensed matter nuclear science. All of which seems to suggest that the Gribov's Quark Confinement theory may indicate similarity, or perhaps a hidden link, with the Condensed Matter Nuclear Science (CMNS). It could also be expected that thorough understanding of the processes behind CMNS may also require revision of the Gamow factor to take into consideration the cluster deuterium interactions and also PT-symmetric periodic potential as discussed herein.

Further theoretical and experiments are therefore recommended to verify or refute the proposed new PT symmetric potential in Nature.

Submitted on November 14, 2008 / Accepted on November 20, 2008

References

1. http://www-groups.dcs.st-and.ac.uk/∼history/Quotations/Dodgson.html
2. Znojil M. arXiv: math-ph/0002017.
3. Znojil M. arXiv: math-ph/0104012, math-ph/0501058.
4. Yefremov A.F., Smarandache F., and Christianto V. *Progress in Physics*, 2007, v. 3, 42; also in: *Hadron Models and Related New Energy Issues*, InfoLearnQuest, USA, 2008.
5. Christianto V. and Smarandache F. *Progress in Physics*, 2008, v. 1, 40.
6. Christianto V. *EJTP*, 2006, v. 3, no. 12.
7. Takahashi A. In: *Siena Workshop on Anomalies in Metal-D/H Systems*, Siena, May 2005; also in: *J. Condensed Mat. Nucl. Sci.*, 2007, v. 1, 129.
8. Gribov V.N. arXiv: hep-ph/9905285.
9. Correa F., Jakubsky V., Plyushckay M. arXiv: 0809.2854.
10. De Oliveira E.C. and da Rocha R. *EJTP*, 2008, v. 5, no. 18, 27.
11. Gribov V.N. arXiv: hep-ph/9512352.
12. Fernandez-Garcia N. and Rosas-Ortiz O. arXiv: 0810.5597.
13. Chugunov A.I., DeWitt H.E., and Yakovlev D.G. arXiv: astro-ph/0707.3500.

LETTERS TO PROGRESS IN PHYSICS

LETTERS TO PROGRESS IN PHYSICS

An Explantion of Hubble Redshift due to the Global Non-Holonomity of Space

Dmitri Rabounski
E-mail: rabounski@ptep-online.com

In General Relativity, the change of the energy of a freely moving photon should be the solution to the scalar equation of the isotropic geodesic equations, which manifests the work produced on the photon being moved along the path. I solved the equation in terms of physical observables (Zelmanov, *Physics Doklady*, 1956, v. 1, 227–230), and in the large scale approximation, i.e. with gravitation and deformation neglected in the space, while supposing the isotropic space to be globally non-holonomic (the time lines are non-orthogonal to the spatial section, a condition manifested by the rotation of the space). The solution is $E = E_0 \exp(-\Omega^2 a\, t/c)$, where Ω is the angular velocity of the space (it meets the Hubble constant $H_0 = c/a = 2.3\times10^{-18}\ \mathrm{s}^{-1}$), a is the radius of the Universe, $t = r/c$ is the time of the photon's travel. So a photon loses energy with distance due to the work against the field of the space non-holonomity. According to the solution, the redshift should be $z = \exp(H_0\, r/c) - 1 \approx H_0\, r/c$. This solution explains both the redshift $z = H_0\, r/c$ observed at small distances and the non-linearity of the empirical Hubble law due to the exponent (at large r). The ultimate redshift, according to the theory, should be $z = \exp(\pi) - 1 = 22.14$.

In this short thesis, I show how the Hubble law, including its non-linearity with distance, can be deduced directly from the equations of the General Theory of Relativity.

In General Relativity, the change of the energy of a freely moving photon should be the solution to the scalar equation of isotropic geodesics, which is also known as the equation of energy and manifests the work produced on the photon being moved along the path. In terms of physically observable quantities — chronometric invariants (Zelmanov, 1944), which are the respective projections of four-dimensional quantities onto the time line and spatial section of a given observer — the isotropic geodesic equations are presented with two projections onto the time line and spatial section, respectively [1–3]

$$\left.\begin{aligned} &\frac{d\omega}{d\tau} - \frac{\omega}{c^2}\, F_i c^i + \frac{\omega}{c^2}\, D_{ik} c^i c^k = 0 \\ &\frac{d(\omega c^i)}{d\tau} - \omega F^i + 2\omega \left(D^i_k + A^{i}_{k\cdot}\right) c^k + \omega \triangle^i_{nk} c^n c^k = 0 \end{aligned}\right\},$$

where ω is the proper frequency of the photon, $d\tau$ is the interval of physically observable time, c^i is the vector of the observable velocity of light ($c_k c^k = c^2$), F_i is the gravitational inertial force, A_{ik} is the angular velocity of the space rotation due to the non-holonomity of space (the non-orthogonality of the time lines to the spatial section), D_{ik} is the deformation of space, $\triangle^i_{nk}$ are the three-dimensional Christoffel symbols. Integration of the scalar equation should give a function $E = E(t)$, where $E = \hbar\omega$ is the proper energy of the photon. However, integration of time in a Riemannian space is not a trivial task. This is because the observable interval of time $d\tau = \sqrt{g_{00}}\, dt - \frac{1}{c^2}\, v_i dx^i$ depends on the gravitational potential along the path, on the linear velocity $v_i = -\frac{c\, g_{0i}}{\sqrt{g_{00}}}$ of the rotation of space (due to the non-holonomity of it), and on the displacement dx^i of the observer with respect to his coordinate net during the measurement in process. The result of integration depends on the integration path, so time is not integrable in a general case. We consider the "large scale approximation", where distances are close to the curvature radius of the Universe; so gravitation and deformation are neglected in the space ($g_{00} = 1$ and $D_{ik} = 0$, respectively), and the observer is resting with respect to his coordinate net ($dx^i = 0$). In such a case, integration of time is allowed, and is simple as $d\tau = dt$. We also suppose the isotropic space, the "home space" of photons, to be globally non-holonomic ($v_i \neq 0$). With these, the gravitational inertial force F_i, losing the gravitational potential $\mathrm{w} = c^2\left(1 - \sqrt{g_{00}}\right) = 0$, consists of only the second term, which is due to the space non-holonomity

$$F_i = \frac{1}{\sqrt{g_{00}}} \left(\frac{\partial \mathrm{w}}{\partial x^i} - \frac{\partial v_i}{\partial t} \right) \simeq - \frac{\partial v_i}{\partial t}\,.$$

We consider a single photon travelling in the x-direction ($c^1 = c,\ c^2 = c^3 = 0$). With the "large scale approximation" in a globally non-holonomic isotropic space, and assuming the linear velocity of the space rotation to be $v_1 = v_2 = v_3 = v$, and be stationary, i.e. $\frac{\partial v}{\partial t} = B = \mathrm{const}$, the scalar equation of isotropic geodesics for such a photon takes the form

$$\frac{dE}{dt} = - \frac{B}{c}\, E\,.$$

This is a simplest uniform differential equation of the 1st order, like $\dot{y} = -ky$, so that $\frac{dy}{y} = -k\,dt$ or $d(\ln y) = -k\,dt$. It solves as $\ln y = -kt + \ln C$, so we obtain $y = y_0 e^{-kt}$. As a result, the scalar equation of isotropic geodesics (the equation of energy), in the "large scale approximation" in the globally non-holonomic space, gives the solution for the photon's energy (frequency) and the redshift $z = \frac{\omega_0 - \omega}{\omega}$ as depending on the distance $r = ct$ travelled from the observer

$$E = E_0\, e^{-kt}, \qquad z = e^{kt} - 1\,,$$

such that at small distances of the photon's travel, i.e. with the exponent $e^x = 1 + x + \frac{1}{2}x^2 + \ldots \simeq 1 + x$, takes the form

$$E \simeq E_0\,(1 - kt)\,, \qquad z \simeq kt\,,$$

where $k = \frac{1}{c}B = \frac{1}{c}\frac{\partial v}{\partial t} = \text{const}$. Thus, according to our calculation based on the General Theory of Relativity, a photon being moved in a non-holonomic space loses its proper energy/frequency due to the work produced by it against the field of the space non-holonomity (or the negative work produced by the field on the photon).

It is obvious that, given a stationary non-holonomity of the isotropic space, we can express k through the angular velocity Ω and the curvature radius $a = \frac{c}{H_0}$ of the isotropic space connected to our Metagalaxy (we suppose this is a constant curvature space of sperical geometry), as

$$k = \frac{1}{c}\,\Omega^2 a\,,$$

where H_0 is the Hubble constant. So for the galaxies located at a distance of $r \simeq 630$ Mpc* (the redshift observed on them is $z \simeq 0.16$) we obtain

$$\Omega = \sqrt{\frac{z\,c}{a\,t}} = \sqrt{\frac{z\,c^2}{a\,r}} \simeq 2.4{\times}10^{-18}\ \text{sec}^{-1},$$

that meets the Hubble constant $H_0 = 72 \pm 8{\times}10^5$ cm/sec×Mpc $= 2.3 \pm 0.3{\times}10^{-18}$ sec^{-1} (according to the Hubble Space Telescope data, 2001 [4]).

With these we arrive at the following law

$$E = E_0\, e^{-\frac{H_0 r}{c}}, \qquad z = e^{\frac{H_0 r}{c}} - 1\,,$$

as a purely theoretical result obtained from our solution to the scalar equation of isotropic geodesics. At small distances of the photon's travel, this law becomes

$$E \simeq E_0 \left(1 - \frac{H_0 r}{c}\right), \qquad z \simeq \frac{H_0 r}{c}\,.$$

As seen, this result provides a complete theoretical ground to the linear Hubble law, empirically obtained by Edwin Hubble for small distances, and also to the non-linearity of the Hubble law observed at large distances close to the size of the Metagalaxy (the non-linearity is explained due to the exponent in our solution, which is sufficient at large r).

Then, proceeding from our solution, we are able to calculate the ultimate redshift, which is allowed in our Universe. It is, according to the exponential law,

$$z_{\max} = e^{\pi} - 1 = 22.14\,.$$

In the end, we calculate the linear velocity of the rotation of the isotropic space, which is due to the global non-holonomity of it. It is $\breve{v} = \Omega\, a = H_0\, a = c$, i.e. is equal to the velocity of light. I should note, to avoid misunderstanding, that this linear velocity of rotation is attributed to the isotropic space, which is the home of isotropic (light-like) trajectories specific to massless light-like particles (e.g. photons). It isn't related to the non-isotropic space of sub-light-speed trajectories, which is the home of mass-bearing particles (e.g. galaxies, stars, planets). In other words, our result doesn't mean that the visible space of cosmic bodies rotates at the velocity of light, or even rotates in general. The space of galaxies, stars, and planets may be non-holonomic or not, depending on the physical conditions in it.

A complete presentation of this result will have been held at the *April Meeting 2009 of the American Physical Society* (May 2–5, Denver, Colorado) [5], and also published in a special journal on General Relativity and cosmology [6].

Submitted on October 31, 2008 / Accepted on November 06, 2008

*1 parsec = $3.0857{\times}10^{18}$ cm $\simeq 3.1{\times}10^{18}$ cm.

References

1. Zelmanov A.L. Chronometric invariants and accompanying frames of reference in the General Theory of Relativity. *Soviet Physics Doklady*, MAIK Nauka/Interperiodica, distributed by Springer, 1956, v. 1, 227–230 (translated from *Doklady Academii Nauk USSR*, 1956, v. 107, no. 6, 815–818).
2. Zelmanov A.L. Chronometric invariants: on deformations and the curvature of accompanying space. Translated into English from the preprint of 1944 (Sternberg Astron. Inst., Moscow), American Research Press, Rehoboth (NM), 2006, 232 pages.
3. Zelmanov A.L. On the relativistic theory of an anisotropic inhomogeneous universe. Translated from the manuscript of 1957, *The Abraham Zelmanov Journal*, 2008, v. 1, 33–63 (originally presented, in Russian, at the *6th Soviet Meeting on Cosmogony*, Moscow, 1959).
4. Freedman W.L., Madore B.F., Gibson B.K., Ferrarese L., Kelson D.D., Sakai S., Mould J.R., Kennicutt R.C.Jr., Ford H.C., Graham J.A., Huchra J.P., Hughes S.M.G., Illingworth G.D., Macri L.M., Stetson P.B. Final results from the Hubble Space Telescope Key Project to measure the Hubble constant. *Astrophys. Journal*, 2001, v. 553, issue 1, 47–72.
5. Rabounski D. Hubble redshift due to the global non-holonomity of space. *2009 APS April Meeting*, May 2–5, 2009, Denver, Colorado.
6. Rabounski D. Hubble redshift due to the global non-holonomity of space. *The Abraham Zelmanov Journal*, 2009, v. 2, 11–17.

LETTERS TO PROGRESS IN PHYSICS

A Few Remarks on "The Length of Day: A Cosmological Perspective"

Vic Christianto*, Matti Pitkanen† and Florentin Smarandache‡

*Sciprint.org — a Free Scientific Electronic Preprint Server, http://www.sciprint.org
E-mail: admin@sciprint.org

†Puutarhurinkatu 9 A1, 10960 Hanko, Finland
E-mail: matpitka@luukku.com

‡Department of Mathematics, University of New Mexico, Gallup, NM 87301, USA
E-mail: smarand@unm.edu

An interesting hypothesis concerning the varying length of day has been formulated in this edition, proposed by A.I. Arbab, based on a proposition of varying gravitational constant, G. The main ideas are pointed out, and alternative frameworks are also discussed in particular with respect to the present common beliefs in astrophysics. Further observation is of course recommended in order to refute or verify this proposition.

1 Introduction

An interesting hypothesis has been formulated in this edition, proposed by A. I. Arbab [1,2], based on a proposition of varying gravitational constant, G. The main ideas are pointed out, and alternative frameworks are also discussed in particular because the idea presents a quite different approach compared to the present common beliefs in astrophysics and cosmology, i.e. that the Earth is not expanding because the so-called Cosmological expansion does not take place at the Solar system scale.

2 Basic ideas of Arbab's hypothesis

Arbab's hypothesis is mainly an empirical model based on a set of observational data corresponding to cosmological expansion [1]. According to this model, the day increases at a present rate of 0.002 sec/century. His model started with a hypothesis of changing gravitational constant as follows [1]:

$$G_{\text{eff}} = G_0 \left(\frac{t}{t_0}\right)^{\beta} . \tag{1}$$

We shall note, however, that such a model of varying constants in nature (such as G, etc.) has been discussed by numerous authors. The idea itself can be traced back to Dirac, see for instance [3].

What seems interesting here is that he is able to explain the Well's data [4, 5]. In a sense, one can say that even the coral reef data can be considered as "cosmological benchmark". Furthermore, from this viewpoint one could expect to describe the "mechanism" behind Wegener's idea of tectonic plate movement between continents [6]. It can be noted that Wegener's hypothesis has not been described before in present cosmological theories. Moreover, it is also quite safe to say that: "There has been no consensus on the main driving mechanism for the plate tectonics since its introduction" [7].

It is worth noting here that the idea presented in [1,2] can be considered as quite different compared to the present common beliefs in astrophysics and cosmology, i.e. that the Earth is not expanding because the so-called Cosmological expansion does not take place at the Solar system scale. Apparently in [1] the author doesn't offer any explanation of such a discrepancy with the present beliefs in astrophysics; nor the author offers the "physics" of the causal relation of such an expansion at the Solar system scale. Nonetheless, the empirical finding seems interesting to discuss further.

In the subsequent section we discuss other alternative models which may yield more-or-less similar prediction.

3 A review of other solutions for cosmological expansion

In this regards it seems worth noting here that there are other theories which may yield similar prediction concerning the expansion of Earth. For instance one can begin with the *inhomogeneous scalar field cosmologies* with exponential potential [8], where the scalar field component of Einstein-Klein-Gordon equation can be represented in terms of:

$$\phi = -\frac{k}{2} + \log(G) + \psi . \tag{2}$$

Alternatively, considering the fact that Klein-Gordon equation is neatly related to Proca equation, and then one can think that the right terms of Proca equation cannot be neglected, therefore the scalar field model may be expressed better as follows [9]:

$$(\Box + 1) A_\mu = j_\mu + \partial_\mu (\partial_\nu j^\nu) . \tag{3}$$

Another approach has been discussed in a preceding paper [10], where we argue that it is possible to explain the lengthening of the day via the phase-space relativity as implication of Kaluza-Klein-Carmeli metric. A simpler way to predict the effect described by Arbab can be done by including

equation (1) into the time-dependent gravitational Schrödinger equation, see for instance [11].

Another recent hypothesis by M. Pitkanen [12] is worth noting too, and it will be outlined here, for the purpose of stimulating further discussion. Pitkanen's explanation is based on his TGD theory, which can be regarded as generalization of General Relativity theory.

The interpretation is that cosmological expansion does not take place smoothly as in classical cosmology but by quantum jumps in which Planck constant increases at particular level of many-sheeted space-time and induces the expansion of space-time sheets. The accelerating periods in cosmic expansion would correspond to these periods. This would allow also avoiding the predicted tearing up of the space-time predicted by alternative scenarios explaining accelerated expansion.

The increase of Earth's radius by a factor of two is required to explain the finding of Adams that all continents fit nicely together. Increases of Planck constant by a factor of two are indeed favoured because p-adic lengths scales come in powers of two and because scaling by a factor two are fundamental in quantum TGD. The basic structure is causal diamond (CD), a pair of past and future directed light cones forming diamond like structure. Because two copies of same structure are involved, also the time scale $T/2$ besides the temporal distance T between the tips of CD emerges naturally. CD's would form a hierarchy with temporal distances $T/2^n$ between the tips.

After the expansion the geological evolution is consistent with the tectonic theory so that the hypothesis only extends this theory to earlier times. The hypothesis explains why the continents fit together not only along their other sides as Wegener observed but also along other sides: the whole Earth would have been covered by crust just like other planets.

The recent radius would indeed be twice the radius that it was before the expansion. Gravitational force was 4 time stronger and Earth rotated 4 times faster so that day-night was only 6 hours. This might be visible in the biorhythms of simple bacteria unless they have evolved after that to the new rhythm. The emergence of gigantic creatures like dinosaur and even crabs and trees can be seen as a consequence of the sudden weakling of the gravitational force. Later smaller animals with more brain than muscles took the power.

Amusingly, the recent radius of Mars is one half of the recent radius of Earth (same Schumann frequency) and Mars is now known to have underground water: perhaps Mars contains complex life in underground seas waiting to the time to get to the surface as Mars expands to the size of Earth.

Nonetheless what appears to us as a more interesting question is whether it is possible to find out a proper metric, where both cosmological expansion and other observed expansion phenomena at Solar-system scale can be derived from the same theory (from a Greek word, *theoros* — "to look on or to contemplate" [13]). Unlike the present beliefs in astrophysics and cosmological theories, this seems to be a continuing journey. An interesting discussion of such a possibility of "generalized" conformal map can be found in [14]. Of course, further theoretical and experiments are therefore recommended to verify or refute these propositions with observed data in Nature.*

Submitted on November 01, 2008 / Accepted on November 10, 2008

References

1. Arbab A.I. The length of day: a cosmological perspective. *Progress in Physics*, 2009, v. 1, 8.
2. Arbab A.I. On the tidal evolution of Earth-Moon system: a cosmological model. *Progress in Physics*, 2009, v. 1, 54.
3. Vereshchagi G.V. Physical constant and the Gurzadyan-Xue formula for the dark energy. arXiv: astro-ph/0511131.
4. Wells J.W. Coral growth and geochronometry. *Nature*, 9 March 1963; http://freepages.genealogy.rootsweb.com/∼springport/geology/coral_growth.html
5. Smoot N.C. Earth geodynamic hypotheses updated. *Journal of Scientific Exploration*, 2001, v. 15, no. 3, 465–494.
6. Sollanych M.J. Continental drift and the expansion of the universe. http://www3.bc.sympathico.ca/moon/index.html
7. Choi D. From the Editor, in *New Concepts in Global Tectonics Newsletter*, no. 46, March 2008, 2.
8. Ibanez J. and Olasagasti I. On the evolution of large class solution of inhomogeneous scalar field cosmologies. arXiv: gr-qc/9803078.
9. Speight J.M. Static intervortex forces. arXiv: hep-th/9601355.
10. Christianto V. and Smarandache F. Kaluza-Klein-Carmeli metric from quaternion-Clifford space, Lorentz' force, and some observables. *Progress in Physics*, 2008, v. 4, 144.
11. Christianto V. and Smarandache F. Plausible explanation of quantization of intrinsic redshift from Hall effect and Weyl quantization. *Progress in Physics*, 2006, v. 4, 37.
12. Pitkanen M. Evolution in many-sheeted space-time. 2008, http://www.helsinki.fi/∼matpitka/articles/prebiotic.pdf
13. Goth G.W. A brief etymology of words used in the teaching of physics. http://laser.physics.sunysb.edu/∼wise/wise187/2001/weblinks/physics_words.html
14. Gott J.R. et al. A map of the universe. arXiv: astro-ph/0310571.
15. Arbab A.I. Cosmological models in the generalized Einstein action. *The Abraham Zelmanov Journal*, 2009, v. 2, 3–10.
16. Arbab A.I. On the planetary acceleration and the rotation of the Earth. arXiv: astro-ph/0708.0666.

*At the time of writing, we are informed that Arbab's forthcoming paper will discuss a more comprehensive and theoretical approach of his hypothesis [15]. Our remarks here are limited to his papers discussed in this issue, and also in his earler paper [16].

LETTERS TO PROGRESS IN PHYSICS

Israel L. Bershtein (1908 – 2000) — the Founder of the Theory of Fluctuations in Self-Oscillating Systems

(In Commemorating the 100th Birthday Anniversary)

Gregory B. Malykin

Inst. of Applied Physics, Russian Acad. of Sciences, Ulianova Str. 46, Nizhni Novgorod 603600, Russia
E-mail: malykin@ufp.appl.sci-nnov.ru

Israel L. Bershtein (1908–2000) was one of the famous radio physicists in the world. He had constructed the theory of amplitude and frequency fluctuations for the electromagnetic wave generators working in the radio and optical scales. He also had developed numerous methods for precise measurement of the fluctuations, which also can be applied to ultimate small mechanical displacements. Besides these he was the first person among the scientists, who had registered the Sagnac effect at radiowaves.

Fig. 1: I. L. Bershtein in 1930 (the left corner in the picture), being a 5th grade university student at the Low Current Lab (a common name for a radio laboratory in those years). This photo is interesting from the historical viewpoint, because the background of a radio laboratory of the 1930's.

In November, 2008 we celebrate the 100th Birthday Anniversary of Israel Lazarevich Bershtein, Doctor of Science in Physics and Mathematics, a distinguished radio physicist, the author of theoretical and experimental research methods for fluctuations of radio and optical electromagnetic oscillators. The paper deals with I. L. Bershtein's basic scientific achievements.

I. L. Bershtein started his scientific activities when radiophysics originated and broke new ground, so he took a part in its development. I. L. Bershtein was born on November 22, 1908 in the Mogilyov city of the Russian Empire (nowadays the Republic of Belarus). After graduating from school he studied physics at the Electromechanical Faculty of the Leningrad Polytechnical Institute (1926–1930). A. F. Ioffe, V. F. Mitkevich, D. D. Rozhansky, A. A. Chernyshev, and M. A. Shatelen were among his teachers. A well-known debate concerning the nature of electric current, electric and magnetic fields and also the long-range action problem between V. F. Mitkevich, the full member of the USSR Academy of Sciences, and Ya. I. Frenkel, the corresponding member of the Academy, took a place in 1929–1930 at the Polytechnical Institute. P. Ehrenfest was invited by A. F. Ioffe to participate in two sessions of the debate. I. L. Bershtein took a part in all three sessions of these.

After graduating from the Polytechnical Institute in 1931 I. L. Bershtein was employed at the Central Military Research Radio Laboratory (later — the Frunze Factory). He however preferred scientific activities. In 1930 N. D. Papaleksi, the corresponding member of the Academy, paid attention to the talented student. On his advice I. L. Bershtein addressed Prof. A. A. Andronov who agreed to become his scientific supervisor. In 1933 I. L. Bershtein was enrolled for A. A. Andronov's in-service training postgraduate course. His task was to obtain expressions for amplitude and frequency fluctuations of a self-oscillating system (by the example of valve oscillator) close to its periodic motion. I. L. Bershtein managed to show that frequency fluctuations of the generator "blurred" the infinitely narrow radiation line of an ideal oscillator and it acquired width, while amplitude fluctuations created a rather wide but low "pedestal" of the generation line. Results of this work were recommended to publishing by L. I. Mandelstam, the full member of the Academy, and they were published in *Soviet Physics — Doklady* [1]. Paper [1] considerably exceeded the maximum permissible volume and A. A. Andronov reached an agreement with the Editor-in-Chief S. I. Vavilov, the full member of the Academy, on publishing [1] in total. In 1939 I. L. Bershtein under supervision of A. A. Andronov defended a Ph.D. thesis. The official opponents were M. A. Leontovich and G. S. Gorelik. In 1941 I. L. Bershtein

Fig. 2: I. L. Bershtein in 1938, among the research scientists and professors of the Gorky Physics and Technical Institute (GPTI). In the 1st row (from left to right): unknown person; unknown person; Prof. S. M. Rytov; I. L. Bershtein; Prof. Jakov N. Nikolaev; Kholodenko. In the 2nd row (from left to right): Prof. Alexandra G. Lyubina; Prof. Victor I. Gaponov (the husband of Prof. Maria T. Grekhova, the Director of GPTI, and the father of A. V. Gaponov-Grekhov, the full member of the Academy); unknown person.

published a more detailed statement of the theory of fluctuations in valve oscillator [2]. The original theoretical results he had obtained required experimental validation, however the Fascist Germany aggression upon the USSR forced I. L. Bershtein to postpone his fundamental research.

During the World War II I. L. Bershtein developed radio receiving equipment for the Soviet army and aviation needs. In 1946 I. L. Bershtein stopped his industrial activity and was employed at the Gorky Physics and Technical Institute (GPTI) in G. S. Gorelik's department, and held a post of Assistant Professor and Full Professor of radioengineering at the newly organized Radiophysical Faculty of the Gorky State University. Nevertheless, until 1952 he continued to supervise the development and production of radio equipment at a factory. At that time I. L. Bershtein starts to develop experimental methods for measuring amplitude and frequency fluctuations of valve oscillator. In particular, he was the first person who suggested to process measurement of small phase fluctuations by the so-called method of triangle, based on the interference of the measured and reference signals having an insignificant constant phase shift relative to each other and close amplitude values. The experimental measurement carried out by I. L. Bershtein in [3, 4] completely verified his earlier theoretical results [1, 2]. His paper [4] was awarded the Mandelstam Prize presented to L. I. Bershtein at a session of the USSR Academy of Sciences by N. I. Vavilov, the President of the Academy.

In papers [3, 4] I. L. Bershtein managed to measure the lowest level of periodic phase modulation of the order 10^{-8} rad in the frequency band 1 Hz. This permitted to carry out a very interesting physical experiment, i.e., to measure the Sagnac effect at radio waves employing a cable of the 244 m length coiled round a barrel [5]. The radio wavelength was 10 m and the angular velocity of the barrel's rotation was 1–1.3 revolutions per second. Since the phase difference of counter-running waves caused by the rotation is inversely proportional to the wavelength, it is evident that the Sagnac interferometer sensitivity at radio waves is 10^7 lower than the sensitivity under the other equal conditions expected in the optical range.

I. L. Bershtein's papers on fluctuations and the Sagnac effect [3–5] brought him world-wide popularity. He became a leading Soviet scientist on fluctuation measurement. In 1954 he measured extremely small mechanical displacements employing the interference method, and recorded a displacement of the order 10^{-3} Å (see [6]). (It should be noted that, in 1998, one of I. L. Bershtein's disciples, namely — V. M. Gelikonov, managed to increase the measurement accuracy of mechanical displacements by 4 orders to it. See [7] for detail.) That year I. L. Bershtein defended a Dr.Sci. thesis (his opponents were G. S. Landsberg, Yu. B. Kobzarev, S. M. Rytov, and G. S. Gorelik) and after G. S. Gorelik's departure for Moscow he headed a scientific department in GPTI. In the same time he became a Full Professor at the Radioengineering Faculty of the Gorky State University.

In 1957 I. L. Bershtein and his department were transferred to the Radiophysical Research Institute (RRI), where he studied klystron oscillators and matched their frequencies to the frequencies of a quartz oscillator and an ammonia maser,

Fig. 3: I. L. Bershtein in 1948. This is the time of the upper point of his scientific achievements.

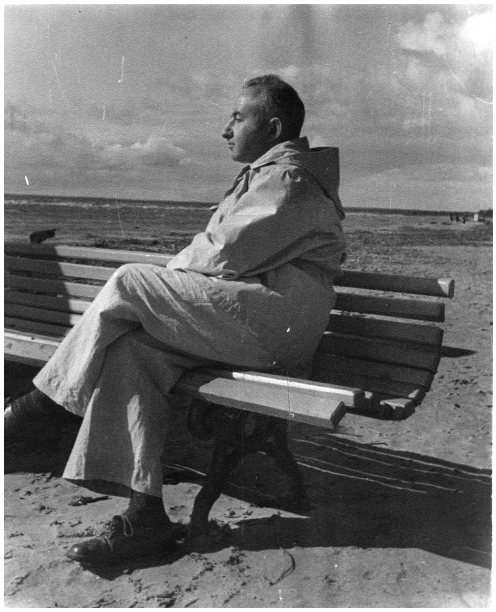

Fig. 4: The mid-60's. I. L. Bershtein being taking relax at the coast of the Black Sea.

then investigated the oscillator fluctuations in AFC system operation. In the mid-60's I. L. Bershtein's department started developing a subject related to the pioneering experimental and theoretical studies in the field of fluctuation processes in gas lasers with Fabry-Pérot and ring resonators, including gas lasers with an absorbing cell used for elaboration of the optical frequency standards. At that time I. L. Bershtein developed a heterodyne method for frequency fluctuation measurement, enabling his disciples Yu. I. Zaitsev and D. P. Stepanov to be first persons in the world who measured frequency fluctuations of a gas laser at the wavelength 0.63 μ [8]. In 1969 I. L. Bershtein was invited to held a lecture on his department's activities at P. L. Kapitsa's workshop in Kapitza's Institute for Physical Problems in Moscow.

In 1970 the so-called polarization resonances in counterrunning waves in an amplifying laser tube at the wavelength 3.39 μ [9] were discovered with the participation of L. I. Bershtein. He also studied the influence of the light backscattering on laser operation and reciprocal capture of the counterrunning wave frequencies in a ring gas laser. The AFC systems for laser generation developed by I. L. Bershtein permitted his disciples to discover new effects in gas lasers with an absorbing cell. The new effects they have discovered were the dynamic self-stabilization of the generation frequency which occurs not only at the centre of the transition line of the absorbing gas, but also at the boundaries of the entire non-uniformly broadened absorption line, the dependence of the self-stabilization coefficient on the modulation frequency [10], and the so-called dispersion resonances they have recorded.

I. L. Bershtein was a member of the Editorial Board of the journal *Soviet Radiophysics* published in RRI for about twenty years (1958–1976).

From 1977 to 1986 I. L. Bershtein headed a research laboratory at the Institute of Applied Physics dealing with fiber-optic interferometers. From 1987 to 1999, being a leading consulting scientist, he continued his studies in the field of fiber-optic gyroscopy and semiconductor radiation sources for fiber optics. I. L. Bershtein died on August 16, 2000.

The life and scientific activity of I. L. Bershtein is a worthy example of service to science. His work in the field of self-oscillating system fluctuations and micro phase metering are the classics of science, and are extremely valuable for radiophysics. He is the author of more than 60 scientific publications and many inventions certified by patents. He was also awarded several prizes provided by the USSR Government [11].

Under careful leading of I. L. Bershtein three persons have got a Ph.D. degree. Those were I. A. Andronova, Yu. I. Zaitsev, and L. I. Fedoseev (the last person was led by I. L. Bershtein commonly with V. S. Troitsky, the corresponding member of the Academy). Many other research scientists were also I. L. Bershtein's disciples: Yu. A. Dryagin, D. P. Stepanov, V. A. Markelov, V. V. Lubyako, V. A. Rogachev. The next generations of research scientists were also I. L. Bershtein's disciples. Those are I. A. Andronova's disciples, namely — I. V. Volkov, Yu. K. Kazarin, E. A. Kuvatova, Yu. A. Mamaev, A. A. Turkin, G. V. Gelikonov, and Yu. I. Zaitsev's disciples — V. M. Gelikonov, V. I. Leonov, G. B. Malykin, and also D. V. Shabanov who was V. M. Gelikonov's disciple, and also L. M. Kukin, who was Yu. A. Dryagin's disciple. I. L. Bershtein patiently transferred all his scientific experience to the aforementioned persons, who are actually his disiples and followers in science.

Fig. 5: I. L. Bershtein at the working desk in his cabinet. This photo, pictured in 1967, is very specific to his nativity of a man who spent his life in science.

The author of this paper would like to thank V. M. Gelikonov, E. G. Malykin, V. I. Pozdnyakova, and N. V. Roudik for their assistance in this paper. This work was partly supported by the Council on President's Grants of the Russian Federation for Leading Scientific Schools (project no. NSh. 1931.2008.2).

Submitted on October 30, 2008 / Accepted on November 14, 2008

References

1. Bershtein I. L. Fluctuations close to periodic motion of self-oscillating systems. *Dokl. Acad. Nauk SSSR* (*Sov. Phys.-Dokl.*), 1938, v. 20, 11–16 (*in Russian*).
2. Bershtein I. L. Fluctuations in a self-oscillating system and determination of natural spread of valve oscillator frequency. *Zh. Tekh. Fiz.* (*Sov. Phys.-Tech. Phys.*), 1941, v. 11, 305–316 (*in Russian*).
3. Bershtein I. L. On valve oscillator fluctuations. *Dokl. Acad. Nauk SSSR* (*Sov. Phys.-Dokl.*), 1949, v. 68, 469–472 (*in Russian*).
4. Bershtein I. L. Amplitude and phase fluctuations in a valve oscillator. *Izv. Acad. Nauk SSSR*, *Ser. Fiz.* (*Bull. Acad. Sci. USSR*, *Phys. Ser.*), 1950, v. 14, 145–173 (*in Russian*).
5. Bershtein I.L. Sagnac experience at radio waves. *Dokl. Acad. Nauk SSSR* (*Sov. Phys.-Dokl.*), 1950, v. 75, 635–638 (*in Russian*).
6. Bershtein I. L. On measurement of extremely small mechanical path difference of two light oscillations. *Dokl. Acad. Nauk SSSR* (*Sov. Phys.-Doklady*), 1954. v. 94, 655–658 (*in Russian*).
7. Gelikonov V.M. Measurment of nanoangström oscillatory displacements by a gas laser with a small natural linewidth. *Radiophysics and Quantum Electronics*, 1998, v. 41, 998–1006.
8. Zaitsev Yu.I. and Stepanov D.P. On frequency fluctuations of a gas laser. *Pis'ma Zh. Exp. Teor. Fiz.* (*JEPT Letters*), 1967, v. 6, 733–737 (*in Russian*).
9. Bershtein I.L. and Rogachev V.A. Faraday rotation due to the interaction of oppositely directed waves in the $3.39\,\mu$. *Radiophysics and Quantum Electronics*, 1970, v. 13, 23–26.
10. Gelikonov V.M., Zaitsev Yu.I., Malykin G.B. On one manifestation of nonstationary saturation of absorbing gas in a standing frequency-modulated wave. *Pis'ma Zh. Tekh. Fiz.* (*Sov. Tech. Phys. Lett.*), 1979, v. 5, 1468–1471 (*in Russian*).
11. Malykin G.B. I. L. Bershtein, his scientific activity. To the 90th birthday anniversary. Institute of Applied Physics Publishers, Nizhny Novgorod, 1998, 20 p.

LETTERS TO PROGRESS IN PHYSICS

Frank Robert Tangherlini — the Founder of an Alternative Relativistic Kinematics

(On the Occasion of His 85th Birthday)

Gregory B. Malykin

Inst. of Applied Physics, Russian Acad. of Sciences, Ulianova Str. 46, Nizhni Novgorod 603600, Russia
E-mail: malykin@ufp.appl.sci-nnov.ru

Already fifty years ago, Frank Robert Tangherlini, an American theoretical physicist, suggested an original procedure which, targeting the synchronization of clocks located in two different inertial reference frames of the space, was different from that Einstein had introduced. As a result of these, Tangherlini had deduced the so-called the Tangherlini transformations, which are a sort of the transformations of the spatial coordinates and time being moved from one inertial reference frame into another one. The Tangherlini transformations differ from the Lorentz transformations (which can be meant classic ones in the theory of relativity) and, in particular, suggest the velocity of light to be anisotropic in a moving inertial reference frame. The Tangherlini transformations being applied provide adequate explanations to all well-known interference experiments checking of the Special Theory of Relativity.

In this paper I have to present, to the scientific community, the life and scientific achievements of Frank Robert Tangherlini, the prominent American theoretical physicist who meets his 85th birthday on Saturday, March 14, 2009. He started his scientific carrier with a blessed theoretical result, known later as the *Tangherlini transformations*, which was shadowed and unknown to the scientific community for about twenty years. I also give here the direct and inversion Tangherlini transformations, and tell the story how his famous PhD thesis [1] containing the transformations, was written, and how he got a PhD degree on the basis of the thesis.

Frank Robert Tangherlini was born on March 14, 1924, in Boston (Massachusetts, USA) in the family of a worker. His father, Emiliano Francesco Tangherlini (1895–1979) was an Italian-born immigrant: being a young boy, Emiliano was carried out from Italy into the USA by his father Luigi, a marble sculptor assistant. In his young years, Emiliano was employed as an instrumental worker at a machine factory, then, in the years of the Great Depression, he happily found some employment at the Boston Shipyard. What is interesting, one of the flats in the house at Beacon Hill near Massachusetts State House, where Emiliano Tangherlini had residence, was owned by the Kennedy family — the great American family which gave John Fitzgerald Kennedy (1917–1963), the thirty-fifth President of the United States. (Also, John Kennedy's grandfather from the mother's side was the Major of Boston city). In 1947–1952, despite the big difference in the age and in the social status of John Kennedy, Emiliano Tangherlini found a friendship from the side of him when walked somewhere in the park near the home. They spent much time together when talking about everything at the walks. Many years later, when becoming the US President, John Kennedy visited Emiliano Tangherlini when doing an official visit to Boston: John Kennedy stopped his car escort, then went to Emiliano Tangherlini through the crowding people who met him on the street, and shacked Emiliano's hand on the public.

The grandfather of Frank Robert Tangherlini from the mother's side, Barnett Rubinovich (he has changed his family name to Robinson when becoming a US citizen), was born in Krolevetz — a small town near Nezhin city of Chernigov Gubernya of the Russian Empire. He immigrated to the USA in the end of the 19th century, and settled in New York city where he later owned a clothes shop. His daughter, Rose (1894–1953) was born a few years later he arrived in the USA. In 1919 Rose changed her religion from Judaism and took Catholic belief, in order to get marry with Emiliano Tangherlini. She was employed as a bookkeeper then, in the years of the Great Depression, as a waitress in order to survive in the hard conditions of the economical crisis.

In June 1941, Frank Robert Tangherlini completed his high school education, by getting a silver medal (he also had got a bronze medal in the field of the world history). Then, in the Autumn of 1941, he became a student at Boston Jesuit College, where he took education in electrical engineering during five semesters. Being a student, he was set free of military service. He actually had a possibility to continue this "free-of-war time" until the actual end of the World War II. Such a behaviour was not in his habit. In July 1943 he volunteered to the US army, and had the basic training during one year at Fort Beining, Georgia. In the Autumn, 1944, he was sent to Liverpool, England. Being in England he, in common with his two close friends, volunteered to a parachute

Fig. 1: Frank Robert Tangherlini with two paratrooper friends in Auxerre, France, Summer 1945. From left to right: Sergeant Frank Tangherlini, Private James Barlow (he died in Connecticut, in October 2007), Private Joe Rhiley (later he was a major in the US Airforce, and was killed in an aviation accident in Japan while on a training mission with a Japanese pilot; there is an airfield in Nebraska, his home state, named after him). Tanghelini called his youngest son Riley (without "h") in honour of his late friend.

training school at Hungerford, Berkshire, 60 miles West from London city. When visiting London in free time, Tangherlini saw the great destruction in the city and many people killed due to the ballistic missiles V-2 launched from the Fascist Germany through the strait. He observed the people, who actually lived at the London underground railways during many weeks without seeing sunshine, in order to survive under the Nazi's air attacks.

A few months later, the paratrooper corps where Tangherlini continued military service was dispatched into France. Tangherlini had got five parachute jumps into the battle, then was a machine-gunner, and participated in many bloody battles in France, Belgium, Germany. In particular, he fought at the Battle for Ardennes, where many Americans were killed. Many his friends-in-battle were killed there. He met the end of the World War II in Europe being a Paratrooper Sergeant. It was in Ulm, Germany, the patrimony of Albert Einstein. His paratrooper corps was moved to Austria, in order to keep the Austrian-Italian border safely. Then they started preparation to a very risky dispatch known as the "jump at Tokyo", which was happily cancelled due to the capitulation of Japan.

Fig. 2: Paratrooper Sergeant Frank Tangherlini (right) and his youngest brother Burt (left). Los Angeles, the Spring of 1946.

In January, 1946, Frank Robert Tangherlini returned to the USA, and retired from military service. He has several military orders from the US Government.

In close time after his coming back to the USA, Tangherlini continued his education. He moved to Harvard University, where he studied sciences in the same grade that Robert Francis Kennedy (the US Attorney General in the future). Tangherlini was graduated as a BSc at Harvard, then — as MSc at the University of Chicago. In the years 1952–1955 he was employed as a research engineer in Convair-General Dynamics Company, San Diego. It was some ierony that his scientific supervisor was a German engineer, who worked for the Fascist Germany at the Peenemunde Rocket Centre during the World War II, and participated in the V-2 launches at London.

In 1959 Tangherlini got a PhD degree from Stanford University. He continued his post-doctorate studies in Copenhagen (1958–1959), at the Institute of Theoretical Physics headed by Niels Bohr. Then Tangherlini continued his studies at the School of Theoretical and Nuclear Physics, the Naples University (1959–1960). In the same time many other physicists, famous in the future, continued their post-doctorates there. They were Francis R. Halpern (1929–1995), Murray Gell-Mann (b. 1929), and the Japanese physicist Susunu Okubo (b. 1930).

In the years 1960–1961 Frank Robert Tangherlini was employed as a research scientist at the Institute of Field Physics, University of North Carolina. In 1961–1964 he was Assistant Professor at Duke University, North Carolina, then in 1964–1966 — Associate Professor at The George Washington University (four blocks from the White House, Washington, DC). In 1966–1967 he was a research scientist at Danish Space Research Institute, Copenhagen, and in the same time

Fig. 3: Some people pictured at the Institute of Theoretical Physics (now — Bohr Institute). Copenhagen, the fall of 1959. Top row: nine persons to the right, the tall person is Sheldon Glashow of the later Glashow-Weinberg-Salam electroweak theory. Just below him slightly to the right is Eugen Merzbacher, the author of a text on quantum mechanics. The second person in the same row, going to the right, is Frank Tangherlini. Go down two rows to the person almost directly below Tangherlini, with a beard, then move one person to the right , that is "Ben" Sidorov (Veniamin A. Sidorov) who later became the full member of the Russian Academy of Sciences and Director of the Accelerator Centre in Novosibirsk. Now go down two more rows to the first row. In the centre is Niels Bohr. Next to him, to your left, is Felix Bloch, whom Tangherlini had for nuclear physics when he was at Stanford. Four persons to the left of Bloch is Aage Bohr, one of Bohr's sons. Next to Aage Bohr, to your left is Ben Mottelson, who worked with Aage Bohr on nuclear physics. Go back to Niels Bohr, and count three persons to your right, that is Leon Rosenfeld who co-laborated with Bohr, particularly later on Complementarity. Finally, the next to the last person on the right is Magnusson. He was from Iceland, and worked with Prof. Møller on the gravitational energy-momentum tensor. Møller himself is not in the photo because he was then Director of NORDITA, a separate institute devoted mainly to assistance in research of Scandinavian physicists.

— a lecturer at the Technical University of Denmark. A long time from 1967 to 1994 he was Associate Professor at the College of the Holy Cross, Worcester (Massachusetts). Commencing in 1994 he is retired. He has residence in San Diego, California, where he is still active in science and sport.

Frank Robert Tangherlini is a member of the American Physical Society, and is also a member of several other civil and sport clubs. He is enthusiastic in tennis and foot racing. In particular, he participated, until the least time, in the annual marathon runs in California. He journalist reports are requested to publish by San Diego Union-Tribune. In 1947 he published a roman [2]. He survives by four children and seven grandchildren (four girls and three boys).

Frank Robert Tangherlini has a wide field of scientific interests: the Special Theory of Relativity, the General Theory of Relativity, relativistic cosmology, Mach's principle, and many others. He authored many publications in the peer review scientific journals. W. K. H. Panofsky (1919–2007) was one of his co-authors in science [3].

In already 1951, Tangherlini paid interest to the possibility of the superluminal objects — the objects whose velocity exceeds the velocity of light. He discussed this problem in 1951–1956 with Hermann Weyl (1885–1955), Gregor Wentzel (1898–1978), Wolfgang Pauli (1900–1958), John Wheeler (1911–2008), Julian Schwinger (1918–1994). He also had a talk with George Gamov (1904–1968), on the connected theme — the ultimate high ratio "signal/noise" which could be possible in radiowaves. All those considerations concerning the principal possibility of superluminal motions have led Tangherlini, in the future, to his own version of the transformations of the spatial coordinates and time being moved from one inertial reference frame into another one, which is different from the Lorentz transformations.

These transformations — at now they are known as the *Tangherlini transformations* — were deduced in 1958 while Frank Robert Tangherlini worked on his PhD thesis, and were

Fig. 4: Frank Tangherlini in 1959 at Copenhagen, after he has defended his PhD thesis where the Tanghelini transformations and the other important results were first introduced into theoretical physics.

the main part of the thesis. Tangherlini himself called these the *absolute Lorentz transformations*.

His PhD supervisor was Sidney D. Drell (b. 1926), who had became the best friend of Andrew D. Sakharow many years later. At the initially stage of the development, Tangherlini had also another supervisor who consulted him: it was Leonard Isaac Shiff (1915–1971), with whom Tangherlini closely co-laborated commencing in 1955.

June of 1958 was met by Tangherlini at Stanford University. He gave a public presentation of his PhD thesis [1] then, in September, he put his thesis on the desk of the Physics Section of the Graduate Division, Stanford University. Positive review on his PhD thesis were given from the side of Sidney D. Drell and Leonard Isaac Shiff, while Albert H. Bouker, the Dean of the Graduate Division, clarified that the PhD thesis is enough ready to be defended. Tangherlini's PhD thesis was considered in the absence of the author himself, because at that time he, in common with Drell, was with Niels Bohr in Copenhagen, in the Institute of Theoretical Physics (this Institute was called later Bohr Institute). On December 9, 1958, Florine H. McIntosh, the Secretary Committee on Graduate Study, informed Tangherlini that his PhD thesis has met a positive reaction from the side of the Committee's members — Joshua L. Soske (Geophysics), chairman, Walter E. Meyerhof (Physics), and Menaham M. Schiffer (Mathematics) — who considered the thesis. On January 9, 1959, Harvey Hall, the Registar of the Committee, provided a hardcopy of the Stanford PhD Diploma to Tangherlini. Later Tangherlini produced a microfilm of his PhD thesis [1], then gave presentations, based on the microfilm, at Copenhagen. In particular he provided the microfilm to several theoretical physicists such as Oscar Klein (1894–1977), who noted that he met a similar method of the synchronization of clocks while he read the lectures at Stockholm [4].

Being in 1959 at Copenhagen, Tangherlini composed a detailed paper on the basis of his PhD thesis, then submitted the paper to *Annals of Physics* (New York). Philip McCord Morse (1903–1985), the founder and first editor of the journal, however declined Tangherlini's paper. He argued that this paper was so large (it was 76 pages of the typewriting) for such a journal, and suggested, in his letter to Tangherlini sent on September 23, 1959, that Tangherlini should truncate it or, alternatively, split into two segregate papers. In his next letter to Tangherlini (September 28, 1959), Morse hoped that the requested version of the paper will be submitted in close time. Unfortunately, there was no chance to do it, because Tangherlini was very hurry of time while his post-doctorate studies at Naples. Undoubtedly, it was a big mistake made by Tangherlini that he ignored such a lucky chance. If that paper would have been published in that time, the end of the 1950's, his theory [1] was wide known to the scientific community so that the next fifty years of his life and scientific carrier were much glorious than it was in his real life.

Meanwhile, a very brief contents of his main scientific results, in particular — the direct and inverse Tangherlini transformations, were published in 1961, in a very short Section 1.3 of his large paper [5] spent on the applications of Mach's principle to the theory of gravitation. This paper got so much attention from the side of the scientific community, that was translated into Chinese by Prof. P. Y. Zhu, the famous Chinese theoretical physicist, then published in China [6]. A short description of Tangherlini's PhD thesis was also given in Appendix to his paper of 1994 [4].

The direct and inverse Tangherlini transformations are introduced on the case, where the clocks, located in two different inertial reference frames, are synchronized with each other by the signals of such a sort that they travel at infinite velocity (for instance, these can be superluminal-speed tachyons, the hypothetical particles). One regularly assumes that such an instant synchronization is impossible in practice. However this becomes real in the case where all clocks of the resting and moving reference frames are located along the same single line. To do it, one can use the so-called "light spot" B. M. Bolotovskiĭ and V. L. Ginzburg suggested [7], because it has to travel at a superluminal phase velocity. (In paper [8], I already considered the problem how two clocks, distantly located from each other, can be synchronized by means of such a "light spot", and also the auxiliary problems connected to it.) In his PhD thesis [1], Tangherlini suggested also another method how to synchronize the clocks: this is so-called the "external synchronization", where the clocks, distantly located from each other, become synchronized in

a resting ("preferred") inertial reference frame, then these already synchronized clocks are used for synchronization of the other clocks, which are located in the moving inertial reference frames distant from each other. With these, each of the moving clocks are synchronized at that moment of time, when they meet the resting clocks. This method of synchronization leads however to the non-equality of different inertial reference frames: the "preferred" inertial reference frame is such that got the first synchronization of the clocks. The direct and inverse Tangherlini transformation are

$$\left.\begin{array}{ll} x' = \gamma(x - vt), & x = \gamma^{-1}x' + \gamma vt', \\ y' = y, & y = y', \\ z' = z, & z = z', \\ t' = \gamma^{-1}t, & t = \gamma t, \end{array}\right\} \quad (1)$$

where v is the velocity (it is directed along the x-axis) of the inertial reference frame K' with respect to the preferred inertial reference frame K, $\gamma = 1/\sqrt{1 - v^2/c^2}$ is the Lorentz-factor, while c is the velocity of light.

It is obvious that the direct Tangherlini transformations have the sequel that time t' of a moving inertial reference frame has to delay in γ times with respect to t that is the same that the transverse Doppler-effect in the Special Theory of Relativity. The direct Tangherlini transformations (1) differ from the Lorentz transformations in only the transformation of time (this is due to the difference in the synchronization method for the clocks in different inertial frames). Proceeding from (1), Tangherlini obtained the velocity of light in vacuum, c', measured in the moving inertial reference frame K' [1]

$$c' = \frac{c}{1 + \frac{v}{c}\cos\alpha'}, \quad (2)$$

where the angle α' is counted from the x'-axis in the moving inertial frame K'. Formula (2) means that the velocity of light in the moving inertial frame K', i.e. the quantity c', is anisotropic to the angle α'. This is a direct result of the synchronization procedure suggested by Tangherlini [1].

Tangherlini's formula (2) gives an explanation to the results obtained in the Michelson-Morley experiment [9] and also in the Kennedy-Thorndike experiment [10], because, according to Tangherlini's formula, the common time of the travel of a light beam toward and backward doesn't depend on the velocity v the inertial reference frame K' moves with respect to the "preferred" inertial reference frame K. Moreover, it is possible to show that the Tangherlini transformations provide an explanation to all interferention experiments checking the Special Theory of Relativity, in particular — Sagnac's experiments [11]. (Read more on the Sagnac effect and explanations of it in my recent papers [12, 13].) It should also be noted that the Lorentz transformations lead to the relation $c' = c$, which differs from Tangherlini's formula (2). Another important sequel of the Tangherlini transformations is that they keep Maxwell's equations to be invariant [1].

Fig. 5: Prof. Frank Robert Tangherlini at the present days. San Diego, California.

First time after Frank Robert Tangherlini suggested these transformations, they met actually no attention from the side of the scientific community. However just the anisotropy of the cosmic microwave background was found in 1977, the scientists have understood that fact that our inertial reference frame, connected to the Earth, moves with a velocity of about 360 km/sec with respect to a "preferred" inertial reference frame, where the microwave background radiation is mostly isotropic so that the common momentum of all space masses of our Universe is zero. After that experimental discovery, many suppositions concerning the anisotropy of the velocity of light were suggested, and the Tangherlini transformations became requested. The first persons who called the Tangherlini transformations in order to explain the Michelson-Morley result in the presence of the anisotropy of the velocity of light were R. Mansouri and R. U. Sexl [14]. Then many papers concerning the Tangherlini transformations were published.

There were several papers produced by the other authors where the Tangherlini transformations were "re-discovered" anew. Just two examples with the papers by S. Marinov, 1979 [15], and by N. V. Kupryaev, 1999 [16]. What is interesting, Frank Tangherlini met Stefan Marinov at the *General Relativity 9th Meeting* in Jena, in 1980. Tangherlini wrote me in his private letter on October 14, 2006, how this happened [17]:

> "I met Marinov under a most curios circumstance: He had put up over doorway of a hall where many of passed through, a poster of about 1/3 meter width and about 2 meter long in which he criticized me, in artistic calligraphy, for not having folloved on my transformation. I

found this very strange behaviour. After all why did't write to me, or arrange a meeting at conference? So I suspect than he was somewhat crazy, although possibly artistically talented. In any crazy, one should't spend too much time on him except as an example of how people in science, just as in every day life, can astray."

During more than the hundred years after the Special Theory of Relativity was constructed, the most researchers were filled in belief that the Lorentz transformations originate in two postulates of the Special Theory of Relativity: the equality of all inertial reference frames, and the isotropy of the velocity of light in all inertial reference frames, including the independence of the velocity of light from the velocity of the source of light. If however using another procedure synchronizing the clocks, we obtain other transformations of the coordinates and time. In particular, if using the procedure synchronizing the clocks through the infinite-speedy signals, as Tangherlini suggested [1], we obtain the Tangherlini transformations. In other word, the synchronizing procedure suggested by Tangherlini leads to the kinematic relativistic transformations of the spatial coordinates and time (1), which are unexpected, but very adequate in the description of the transfer from one inertial reference frame into another one.

In this concern, I would emphasize the very important difference between the Tangherlini transformations and the Lorentz transformations. In the Tangherlini transformations, c' (2) is the velocity of light in the inertial reference frame K' measured by an observer who is located in the inertial reference frame K. An observer located in the inertial reference frame K' will found that $c' = c$. On the contrary, in the Lorentz transformations, given any inertial reference frame (K', K, or any other inertial frame), there is $c' = c$ and, hence, the velocity of light in the inertial frame K, being measured by the observers located in the inertial frames K' and K is always the same. The anisotropy of the coordinate velocity of light $c' = c$ in the inertial reference frame K' is the fee paid for the absolute simultaneity in all inertial reference frames [18].

The author thanks Frank Robert Tangherlini for the complete text of his PhD thesis [1] and the other papers useful to me, and also for friendly discussions. I also thank V. V. Kocharovski, for useful notes, and N. V. Roudik and E. G. Malykin who helped me. Special thank goes to D. Rabounski for assistance. This work was partly supported by the Council on President's Grants of the Russian Federation for Leading Scientific Schools (project no. NSh. 1931.2008.2).

Submitted on November 24, 2008 / Accepted on November 27, 2008

References

1. Tangherlini F.R. The velocity of light in uniformly moving frame. PhD Thesis, Stanford Univ., Sept. 1958, 135 pages.
2. Tangherlini F.R. Catholic girl and atheist: a story of the battle of ideas (the Letters of Paul). Girard (Kansas), Haldeman-Julius, 1947, 58 pages.
3. Lazarus A., Panofsky W.K.H., Tangherlini F.R. Photoproduction of positive pions in Hydrogen in angular range $7^\circ <$ c.m. $< 27^\circ$ and proton energy range 220 Mev $< k <$ 270 Mev. *Phys. Rev.*, 1959, v. 113, 1130–1138.
4. Tangherlini F.R. Light travel times around a closed universe. *Nuovo Cim.*, 1994, v. B109, 929–951.
5. Tangherlini F.R. An inroduction to the General Theory of Relativity. *Suppl. Nuovo Cim.*, 1961, Ser. X, v. 20, 1–86.
6. Tangherlini F.R. An inroduction to the General Theory of Relativity. Transl. by P. Y. Zhu, Shanghai Science & Technology Press, Shanghai, 1979.
7. Bolotovskiĭ B.M., Ginzburg V.L. The Vavilov-Cerenkov effect and the Doppler effect in the motion of sources with superluminal velocity in vacuum. *Soviet Physics Uspekhi*, 1972, v. 15, no. 2, 184–192 (translated from *Uspekhi Fizicheskikh Nauk*, 1972, v. 106, 577–592).
8. Malykin G.B. On the possibility of experimental verifying the second postulate of special relativity. *Physics-Uspekhi*, 2004, v. 47, no. 7, 739–742 (translated from *Uspekhi Fizicheskikh Nauk*, 2004, v. 174, 801–804).
9. Michelson A.A., Morley E.W. On the relative motion of the Earth and the Luminiferous Ether. *Am. J. Sci.*, 1887, Ser. III, v. 34, 333–345.
10. Kennedy R.J., Thorndike E.M. Experimental establishment of the relativity of time. *Phys. Rev.*, 1932, v. 42, 400–418.
11. Sagnac M.G. L'éther lumineux démontré par l'effet du vent relatif d'éther dans un interféromètre en rotation uniforme. *Comptes Rendus des Séances de l'Académie des Sciences*, 1913, t. 157, 708–710.
12. Malykin G.B. The Sagnac effect: correct and incorrect explanations. *Physics-Uspekhi*, 2000, v. 43, no. 12, 1229–1252 (translated from *Uspekhi Fizicheskikh Nauk*, 2000, v. 170, 1325–1349).
13. Malykin G.B. Sagnac effect in a rotating frame of reference. Relativistic Zeno paradox. *Physics-Uspekhi*, 2002, v. 45, no. 8, 907–909 (translated from *Uspekhi Fizicheskikh Nauk*, v. 172, 969–970).
14. Mansouri R., Sexl R.U. A test of Theory of Special Relativity. *General Relativiy and Gravitation*, 1977, v. 8, 497–513; 515–524; 809–814.
15. Marinov S. The coordinate transformation of the absolute space-time theory. *Found. Phys.*, 1979, v. 9, 445–460.
16. Kupryaev N.V. Extended representation of the lorentz transformations. *Russian Physics Journal*, 1999, v. 42, no. 7, 592–597 (translated from *Izvestia VUZov*, *Fizika*, 1999, no. 7, 8–14).
17. Private communication with the author, October 14, 2006.
18. Cavalleri G., Bernasconi C. Invariance of light speed and non-conservation of simultaneity of separate events in prerelativistic physics and vice versa in special relativity. *Nuovo Cim.*, 1989, v. B104, 545–561.

The Journal on Advanced Studies in Theoretical and Experimental Physics, including Related Themes from Mathematics

PROGRESS IN PHYSICS

A quarterly issue scientific journal, registered with the Library of Congress (DC, USA). This journal is peer reviewed and included in the abstracting and indexing coverage of: Mathematical Reviews and MathSciNet (AMS, USA), DOAJ of Lund University (Sweden), Zentralblatt MATH (Germany), Scientific Commons of the University of St. Gallen (Switzerland), Open-J-Gate (India), Referativnyi Zhurnal VINITI (Russia), etc.

To order printed issues of this journal, contact the Editors. Electronic version of this journal can be downloaded free of charge:

http://www.ptep-online.com
http://www.geocities.com/ptep_online

Postal address

Chair of the Department
of Mathematics and Science,
University of New Mexico,
200 College Road,
Gallup, NM 87301, USA

ISSN: 1555-5534 (print)
ISSN: 1555-5615 (online)

Standard Address Number: 297-5092
Printed in the United States of America

APRIL 2009 **VOLUME 2**

CONTENTS

Information for Authors and Subscribers

Progress in Physics has been created for publications on advanced studies in theoretical and experimental physics, including related themes from mathematics and astronomy. All submitted papers should be professional, in good English, containing a brief review of a problem and obtained results.

All submissions should be designed in LaTeX format using *Progress in Physics* template. This template can be downloaded from *Progress in Physics* home page http://www.ptep-online.com. Abstract and the necessary information about author(s) should be included into the papers. To submit a paper, mail the file(s) to the Editor-in-Chief.

All submitted papers should be as brief as possible. We usually accept brief papers, no larger than 8–10 typeset journal pages. Short articles are preferable. Large papers can be considered in exceptional cases to the section *Special Reports* intended for such publications in the journal. Letters related to the publications in the journal or to the events among the science community can be applied to the section *Letters to Progress in Physics*.

All that has been accepted for the online issue of *Progress in Physics* is printed in the paper version of the journal. To order printed issues, contact the Editors.

This journal is non-commercial, academic edition. It is printed from private donations. (Look for the current author fee in the online version of the journal.)

The Neutrino: Evidence of a Negative-Energy Vacuum State

William C. Daywitt

National Institute for Standards and Technology (retired), Boulder, Colorado, USA

E-mail: wcdaywitt@earthlink.net

This note argues that the neutrino is a phonon packet that exists and propagates within the negative-energy Planck vacuum. Simple calculations connect the three neutrinos to their corresponding leptons and show: that the neutrino mass is a ficticious or effective mass; that the neutrino mass cannot be zero; that each of the three neutrinos has a unique mass that determines its velocity; and that flavor (neutrino-type) mixing does not involve mass mixing.

The total energy E of a relativistic particle of rest mass m is

$$E = (m^2c^4 + c^2p^2)^{1/2}, \tag{1}$$

where c is the speed of light, $p = m\gamma v$ is the relativistic momentum, $\gamma^2 = 1/(1-\beta^2)$, $\beta = v/c$, and v is the particle velocity. Rearranging (1) leads to

$$\frac{v}{c} = \left[1 - \left(\frac{mc^2}{E}\right)^2\right]^{1/2}, \tag{2}$$

which can be used to determine the particle mass by measuring its velocity and relativistic energy. For any measurement set (v, E), the same mass will emerge within the measurement accuracy. When this measurement procedure is applied to the neutrino [1, pp. 534–536], however, different masses emerge. Thus the neutrino is not an elementary particle in the usual sense of the term "elementary particle". It is not surprising, then, that the "mystery of neutrino mass" is currently the most important subject of study in neutrino physics [1, p. 180].

The present note argues that the neutrino is a massless phonon packet traveling within the negative-energy Planck vacuum (PV), the primary task being to determine the structure of that packet. Taking the decay of the neutron into a proton and an electron as an example, the heuristic calculations proceed as follows: the sudden appearance of the electron as a decay product sets up a periodic disturbance in the PV from which the packet emerges; it is then assumed that the packet is the same as a phonon packet traveling a linear lattice whose lattice points are separated by a distance equal to the electron's Compton wavelength. Treating the neutrino as a phonon packet tracks the solid state theory remarkably well, but the presentation here is sketchy because of the formal complexity of the latter theory with its "undergrowth of suffixes" as Ziman would put it [2, p. 17]. The more precise details are left to a subsequent paper.

The PV [3] is an omnipresent degenerate gas of negative-energy Planck particles (PP) characterized by the triad (e_*, m_*, r_*), where e_*, m_*, and r_* $(\lambda_*/2\pi)$ are the PP charge, mass, and Compton radius respectively. The vacuum is held together by van-der-Waals forces. The charge e_* is the bare (true) electronic charge common to all charged elementary particles and is related to the observed electronic charge e through the fine structure constant $\alpha = e^2/e_*^2$ which is a manifestation of the PV polarizability. The PP mass and Compton radius are equal to the Planck mass and length respectively. The particle-PV interaction is the source of the gravitational $(G = e_*^2/m_*^2)$ and Planck $(\hbar = e_*^2/c)$ constants, and the Compton relations $(r_* m_* c^2 = r_c mc^2 = e_*^2)$ relating the PV and its PPs to the observed elementary particles, where the charged elementary particles are characterized by the triad (e_*, m, r_c), m and r_c being the mass and Compton radius $(\lambda_c/2\pi)$ of the particle (particle spin is not yet included in the theory). A feedback mechanism in the particle-PV interaction leads to the Lorentz transformation. The zero-point random motion of the PP charges e_* about their equilibrium positions within the PV, and the PV dynamics, are the source of the quantum vacuum [4].

The mean power flux of phonons traveling a linear lattice chain in an elastic medium is [2, p. 15]

$$U = \langle \mathcal{U} \rangle = \left\langle \sum_k \hbar\omega_k v_k a_k^* a_k \right\rangle = \sum_k \hbar\omega_k v_k N_k\,, \tag{3}$$

where $0 \leqslant k \leqslant \pi/r_a$, $\hbar\omega_k$ is the phonon energy for the k-th mode, v_k is the phonon group velocity, a_k^* and a_k are the phonon creation and annihilation operators, and $N_k = \langle a_k^* a_k \rangle$ is the number of phonons per unit length in the kth mode. Restricting k to non-negative values (non-positive values would work just as well) implies that only traveling waves (rather than standing waves) are of interest in the calculations.

The dispersion relation connecting the phonon frequency ω_k and wavenumber k is [2, p. 12]

$$\omega_k = \left(\frac{4g_a}{m}\right)^{\frac{1}{2}} \left|\sin\left(\frac{\phi_{n,k}}{2}\right)\right| = \left(\frac{4g_a}{m}\right)^{\frac{1}{2}} \sin\left(\frac{kr_a}{2}\right), \tag{4}$$

where g_a is the "spring constant". The angle $\phi_{n,k} = 2n\pi + kr_a$, where $n\,(=0, 1, 2, \dots)$ are the positive branches or Brillouin zones of interest and $k_a\,(=2\pi/\lambda_a = 1/r_a)$ is the k-axis scaling factor. The absence of absolute-value bars in the

final expression follows from the fact that $0 \leqslant kr_a \leqslant \pi$. The group velocity

$$v_k = \frac{d\omega_k}{dk} = \left(\frac{r_a^2 g_a}{m}\right)^{1/2} \cos\left(\frac{kr_a}{2}\right) \tag{5}$$

is the velocity of the k-mode phonons. The phonon number N_k is then the number of k-phonons per unit r_a.

For a single phonon packet (a neutrino) traveling the chain, i.e. for a single value of n and k, (3) leads to

$$U_k = \hbar\omega_k \cdot v_k \cdot N_k = E_k \cdot v_k \tag{6}$$

where $\hbar\omega_k$ is the phonon energy of the packet and $E_k \equiv \hbar\omega_k N_k$ is the total energy carried by the packet. The index k corresponds to the type of neutrino (ν_e, ν_μ, or ν_τ) participating in the decay or capture processes.

The PV is an elastic medium and, because a free particle distorts the PV, the sudden appearance or disappearance of a free particle will initiate a corresponding phonon disturbance in that vacuum. In the rest frame of the particle the static distortion force is [3]

$$F(r) = \frac{e_*^2}{r^2} - \frac{mc^2}{r}\,, \tag{7}$$

where m is the particle mass and the first and second forces are the polarization and curvature force respectively. (In the laboratory frame these opposing forces lead to the particle's de Broglie radius [4, Append. A].) The two forces on the right side of (7) are equal at the Compton radius ($r_c = e_*^2/mc^2$) of the particle, the positive polarization force dominating inside this radius ($r < r_c$) and the negative curvature force outside ($r > r_c$). These opposing forces result in a harmonic-oscillator-type disturbance within the PV, the effective "spring constant" of which is easy to derive from (7):

$$\Delta F(x) = \frac{e_*^2}{(r_c + x)^2} - \frac{mc^2}{r_c + x} = \\ = \frac{e_*^2}{r_c^2}\left[-\frac{x}{r_c} + 2\left(\frac{x}{r_c}\right)^2 - \cdots\right] \approx -\frac{e_*^2}{r_c^3}\,x = -g_c x\,, \tag{8}$$

where x is the excursion of the disturbance about its equilibrium position at $x = 0$, and where the particle Compton relation $e_*^2/r_c^2 = mc^2/r_c$ is used in deriving the second expression. For small excursions ($x/r_c \ll 1$) the force reduces to the final expression where $g_c \equiv e_*^2/r_c^3$ is the desired "spring constant".

Using $r_a = r_c$ and $g_a = g_c$ and the Compton radius (it is $r_c = e_*^2/mc^2$) of the free particle (the lepton) in (4) and (5) leads to

$$\hbar\omega_k = \frac{e_*^2}{r_c}\,\frac{\sin(kr_c/2)}{1/2} \approx e_*^2 k \tag{9}$$

and

$$\frac{v_k}{c} = \cos\left(\frac{kr_c}{2}\right) \approx 1 - \frac{1}{2}\left(\frac{kr_c}{2}\right)^2 = 1 - \frac{1}{2}\left(\frac{e_*^2 k/2}{mc^2}\right)^2 \tag{10}$$

to second order in $kr_c/2$. The "spring constant" (g_c) and scaling factor ($k_c = 1/r_c$) tie the m-phonons to the m-lepton that created them, where the prefix "m" stands for the lepton mass in (10). Inserting (9) and (10) into (6) yields

$$U_k = \frac{e_*^2}{r_c}\,\frac{\sin(kr_c/2)}{1/2} \cdot c\cos(kr_c/2) \cdot N_k \tag{11}$$

$$\approx e_*^2 k \cdot c\left[1 - \frac{1}{2}\left(\frac{e_*^2 k/2}{mc^2}\right)^2\right] \cdot N_k \tag{12}$$

for the mean power flux of the lepton-induced neutrino. The magnitude of N_k varies with the needs of the decay or capture process to conserve momentum and energy (and spin, although spin is not included in the present discussion). That is, the PV absorbs the unbalanced momentum and energy of the process.

Using $r_c = e_*^2/mc^2$, (11) and (12) can be put in the more convenient form

$$U_k = mc^2\,\frac{\sin(m_k c^2/2mc^2)}{1/2} \cdot c\cos(m_k c^2/2mc^2) \cdot N_k \tag{13}$$

$$\approx m_k c^2 \cdot c\left[1 - \frac{1}{2}\left(\frac{m_k c^2}{2mc^2}\right)^2\right] \cdot N_k \tag{14}$$

where $m_k \equiv e_*^2 k/c^2$ is a ficticious or effective mass. It is clear from (14) that m_k cannot vanish for then the packet flux U_k would also vanish. The bracket shows that the packet propagates at somewhat less than the speed of light.

It is instructive at this point to compare the particle and phonon-packet models of the neutrino. In the particle model described by (1) and (2), the energy and velocity of the neutrino are

$$E'_\nu = cp'_\nu = m'_\nu c^2 \cdot \beta\gamma \tag{15}$$

and

$$\frac{v'_\nu}{c} = 1 - \frac{1}{2}\left(\frac{m'_\nu c^2}{E'_\nu}\right)^2 \tag{16}$$

for $E'_\nu \gg m'_\nu c^2$. As discussed in the first paragraph, the particle mass m'_ν is a variable mass and, in order to make the equations fit the experimental data, mass and flavor mixing (see below) must be brought *ad hoc* into the particle model, destroying the particle description of the neutrino in the process. From (14) for the packet model

$$E_k = m_k c^2 \cdot N_k \tag{17}$$

and

$$\frac{v_k}{c} = 1 - \frac{1}{2}\left(\frac{m_k c^2}{2mc^2}\right)^2 \tag{18}$$

for small $m_k c^2$. Equation (17) shows that the neutrino energy E_k is the product of the phonon energy $m_k c^2$ and the number of phonons N_k in the packet. Equation (18) shows that the neutrino velocity is determined solely by the neutrino mass m_k and its corresponding lepton mass m.

The three types (or flavors) of neutrinos are the electron (ν_e), muon (ν_μ), and tau (ν_τ) neutrinos and, in the particle model, each flavor is assumed to have one or a combination of three masses (m_1, m_2, m_3) [1, p. 452]. The corresponding three-neutrino mixing (or flavor oscillation) is a phenomenon in which a neutrino created with a particular flavor is later measured to have a different flavor due to a mismatch between the flavor and mass eigenstates of the three neutrinos. In the packet model each neutrino has its own mass as seen in (17) and (18), leading to the more straightforward flavor-oscillation process described below.

The harmonic (quadratic) approximation [2, p. 12] to the Hamiltonian for a linear lattice chain leads to the calculations in equations (3) through (14). For a three-dimensional lattice, the addition of the anharmonic cubic term [2, pp. 130–136] to the quadratic Hamiltonian, along with the effects of the selection rules, lead to a three-phonon process

$$(\mathbf{k}, \mathbf{p}) + (\mathbf{k}', \mathbf{p}') \Longleftrightarrow (\mathbf{k}'', \mathbf{p}'') \tag{19}$$

that can be tied to the three-neutrino mixing phenomenon, where $\mathbf{k}$ and p, etc., are the wavenumber vector and polarization of the three phonons. That is, the only allowed transitions are those in which two phonons combine to give a third, or vise versa. In addition, conservation of energy requires that

$$\hbar\omega_{\mathbf{k},\mathbf{p}} + \hbar\omega_{\mathbf{k}',\mathbf{p}'} = \hbar\omega_{\mathbf{k}'',\mathbf{p}''} \tag{20}$$

and the conservation of wave vector for a *continuous* medium gives

$$\mathbf{k} + \mathbf{k}' = \mathbf{k}'' , \tag{21}$$

where, although the PV is discontinuous at the Planck level ($l \sim r_*$), it is effectively continuous at lengths $l \sim r_c \gg r_*$ where the observed particle Compton radius r_c is concerned. When the phonons are traveling the same straight line, the $\mathbf{k}$s in (19)–(21) can be replaced by their magnitudes. To illustrate the "physical" meaning of (19), consider the equation going from left to right, where the $\mathbf{k}$ and $\mathbf{k}'$ phonons combine to produce the phonon $\mathbf{k}''$: as $\mathbf{k}$ propagates, it distorts the medium in such a fashion as to create an effective "diffraction grating" off of which $\mathbf{k}'$ reflects, destroying the $\mathbf{k}$ and $\mathbf{k}'$ phonons while creating the $\mathbf{k}''$ phonon [2, p. 133].

Equations (19)–(21) are the foundation of the phonon-packet description of flavor mixing which involves three packets (one for each type of neutrino) of the form found in (14). For example, employing (19) from right to left, the neutrino described in (3) through (14) can change into two different neutrinos according to a given probability law [2, eqn.(3.1.6)]. Ignoring polarization and assuming the phonons travel the same straight line, (20) and (21) reduce to

$$m_k c^2 + m'_k c^2 = m''_k c^2 \tag{22}$$

and

$$k + k' = k'' , \tag{23}$$

which are the same equation as $m_k c^2 = e_*^2 k$, etc.. Thus the effective masses of the neutrinos drop out of the mixing process; i.e. there is no mass mixing in the packet description of flavor mixing.

In summary, the ease with which the phonon-packet model of the neutrino, based on the negative-energy PV, describes and explains the experimental data makes a compelling case for that model and for a negative-energy vacuum state. With the inclusion of flavor oscillations and variable neutrino masses, on the other hand, the free-particle model appears to be an exercise more in curve fitting than physical modeling.

Submitted on November 14, 2008 / Accepted on December 01, 2008

References

1. Giunti C., Kim C.W. Fundamentals of neutrino physics and astrophysics. Oxford Univ. Press, Oxford, UK, 2007.
2. Ziman J.M. Electrons and phonons: the theory of transport phenomena in solids. Oxford Press, Oxford, UK, 1972.
3. Daywitt W.C. The planck vacuum. *Progress in Physics*, 2009, v. 1, 20.
4. Daywitt W.C. The source of the quantum vacuum. *Progress in Physics*, 2009, v. 1, 27.

Black Holes and Quantum Gravity from a Planck Vacuum Perspective

William C. Daywitt

National Institute for Standards and Technology (retired), Boulder, Colorado, USA

E-mail: wcdaywitt@earthlink.net

This note explores the question of whether or not the Planck vacuum theory can explain black holes and quantum gravity. It is argued that black holes do not physically exist in nature and that the term "quantum gravity" makes no sense. The importance of the Planck vacuum in constraining the n-ratio in the Schwarzschild line element is noted.

The Planck vacuum (PV) [1] is an omnipresent degenerate gas of negative-energy Planck particles (PP) characterized by the triad (e_*, m_*, r_*), where e_*, m_*, and r_* $(\lambda_*/2\pi)$ are the PP charge, mass, and Compton radius respectively. The vacuum is held together by van der Waals forces. The charge e_* is the bare (true) electronic charge common to all charged elementary particles and is related to the observed electronic charge e through the fine structure constant $\alpha = e^2/e_*^2$ which is a manifestation of the PV polarizability. The PP mass and Compton radius are equal to the Planck mass and length respectively. The particle-PV interaction is the source of the gravitational $(G = e_*^2/m_*^2)$ and Planck $(\hbar = e_*^2/c)$ constants, and the Compton relations $(r_* m_* c^2 = r_c mc^2 = e_*^2)$ relating the PV and its PPs to the observed elementary particles, where the charged elementary particles are characterized by the triad (e_*, m, r_c), m and r_c being the mass and Compton radius $(\lambda_c/2\pi)$ of the particle (particle spin is not yet included in the theory). A feedback mechanism in the particle-PV interaction leads to the Lorentz transformation. The zero-point random motion of the PP charges e_* about their equilibrium positions within the PV, and the PV dynamics, are the source of the quantum vacuum [2]. Neutrinos appear to be phonon packets that exist and propagate within the PV [3].

General relativity describes the spacetime-curvature aspects of the PV [1]. So it is natural to assume that this vacuum state has something to do with black holes, "tunnels in spacetime", and "wormholes connecting different universes" [4, p. 642] if such things do indeed exist.

The Einstein metric equation, and the "Schwarzschild" line element outside a static sphere of mass m, expressed in terms of the PV parameters, are [1]

$$G_{\mu\nu} = \frac{8\pi T_{\mu\nu}}{c^4/G} = \frac{8\pi T_{\mu\nu}}{m_* c^2/r_*} \tag{1}$$

and

$$ds^2 = -\left[1 - 2n_r\right] c^2 dt^2 + \frac{dr^2}{\left[1 - 2n_r\right]} + r^2\, d\Omega^2, \tag{2}$$

where the n-ratio is

$$n_r \equiv n_r(m/r) \equiv \frac{mc^2/r}{c^4/G} = \frac{mc^2/r}{m_* c^2/r_*} \tag{3}$$

with $0 \leqslant n_r < 1$. Here $d\Omega^2 \equiv d\theta^2 + \sin^2\theta\, d\phi^2$.

The force mc^2/r is the distortion or curvature force the mass m exerts on the PV at a distance r from the center of the mass [1]. This curvature force is always smaller than the ultimate curvature force $c^4/G = m_* c^2/r_*$. As $r \to \infty$ the n-ratio vanishes where the metric bracket $[1 - n_r]$ is unity and the spacetime is flat. At the surface of the sun, a white dwarf, or a neutron star, n_r is roughly 0.00001, 0.001, and 0.5 respectively. Only at $m_* c^2/r_*$ is n_r equal to one. Thus the n-ratio is limited to $n_r < 1$ by the nature of the PV.

The metric structure of (2) leads to a black hole with its event horizon at $n_r = 1/2$ and to the corresponding "Schwarzschild radius" $R_s = 2Mc^2/(m_* c^2/r_*)$ [4, pp. 630–636]. From here such ideas as "tunnels" and "wormholes" arise. However, (2) is apparently incorrect [5–8]. For a point mass m at $r = 0$, the original and correct Schwarzschild line element [5] is

$$ds^2 = -\left[1 - 2n(R)\right] c^2 dt^2 + \frac{dR^2}{\left[1 - 2n(R)\right]} + R^2\, d\Omega^2, \tag{4}$$

where

$$R = r[1 + 8n_r^3]^{1/3} \tag{5}$$

and where (4) is only valid for $r > 0$. The metric bracket is now

$$1 - 2n(R) = 1 - \frac{2n_r}{[1 + 8n_r^3]^{1/3}}\,, \tag{6}$$

which is monotonically decreasing from 1 at $n_r = 0$ to $0.0385\ldots$ at $n_r = 1$. Thus, in the allowable range of n_r, the line element ds in equation (4) is well behaved. Again the metric bracket is unity as $r \to \infty$ where both n_r and $n(R)$ vanish.

The velocity of a radial photon starting from infinity and heading toward $r = 0$ can be found by setting $d\Omega^2 = 0$ and $ds = 0$ in (4). Its velocity dr/dt relative to its velocity (c) at infinity is easily shown to be

$$\beta(n_r) = \left(1 + 8n_r^3\right)^{2/3} \left[1 - \frac{2n_r}{\left(1 + 8n_r^3\right)^{1/3}}\right], \tag{7}$$

which yields $\beta(0) = 1$ as it should, and $\beta(1) \approx 1/6$ for a PP $(n_r = 1)$ positioned at $r = 0$.

From the two preceding paragraphs it is clear that nothing singular happens to the Schwarzschild line element of (4) in the allowed range of n_r. Furthermore, the PV theory does not

need to explain the black hole or its "tunneling" and "wormhole" attributes since the black hole does not exist.

The metric gravity discussed above deals with what happens when the curvature force mc^2/r of an isolated mass perturbs the PV. If "electromagnetics" is what happens when the polarization force e_*^2/r^2 of an isolated bare charge e_* perturbs the PV, then it can be shown that electromagnetics leads to the Maxwell equations, the relativistic electric and magnetic fields of a moving charge, and the Lorentz transformation [1]. Both of these phenomena deal with a *single* force acting on the PV. In either case, the terms "quantum gravity" or "quantum electromagnetics" make no sense because the word "quantum" applies to what happens when both forces, mc^2/r and e_*^2/r^2, perturb the PV simultaneously and lead to the Planck constant

$$r_c mc = \frac{e_*^2}{c} = \hbar \tag{8}$$

at $r = r_c$ where the two forces are equal. The standard name for this dual-force perturbation is, of course, "quantum electrodynamics" when dealing with an electron containing both mass and charge. In summary, the search for a theory of "quantum gravity" appears to make no sense.

Submitted on November 14, 2008 / Accepted on December 01, 2008

References

1. Daywitt W.C. The planck vacuum. *Progress in Physics*, 2009, v. 1, 20.
2. Daywitt W.C. The source of the quantum vacuum. *Progress in Physics*, 2009, v. 1, 27.
3. Daywitt W.C. The neutrino: evidence of a negative-energy vacuum state. *Progress in Physics*, 2009, v. 2, 3.
4. Carroll B.W., Ostlie D.A. An introduction to modern astrophysics. Addison-Wesley, San Francisco–Toronto, 2007.
5. Schwarzschild K. On the gravitational field of a mass point according to Einstein's theory. *Sitzungsberichte der Königlich Preussischen Akademie der Wissenschaften zu Berlin*, *Phys.-Math. Klasse*, 1916, 189.
6. Abrams L.S. Black holes: the legacy of Hilbert's error. *Can. J. Phys.*, 1989, v. 67, 919.
7. Crothers S.J. On the general solution to Einstein's vacuum field and its implications for relativistic degeneracy. *Progress in Physics*, 2005, v. 1, 68.
8. Rabounski D. On the current situation concerning the black hole problem. *Progress in Physics*, 2008, v. 1, 101.

On the Generalized Maxwell Equations and Their Prediction of Electroscalar Wave

Arbab I. Arbab and Zeinab A. Satti

Department of Physics, Faculty of Science, University of Khartoum, P.O. 321, Khartoum 11115, Sudan
Department of Physics and Applied Mathematics, Faculty of Applied Sciences and Computer, Omdurman Ahlia University, P.O. Box 786, Omdurman, Sudan

E-mail: aiarbab@uofk.edu; arbab_ai@yahoo.com

We have formulated the basic laws of electromagnetic theory in quaternion form. The formalism shows that Maxwell equations and Lorentz force are derivable from just one quaternion equation that only requires the Lorentz gauge. We proposed a quaternion form of the continuity equation from which we have derived the ordinary continuity equation. We introduce new transformations that produces a scalar wave and generalize the continuity equation to a set of three equations. These equations imply that both current and density are waves. Moreover, we have shown that the current can not circulate around a point emanating from it. Maxwell equations are invariant under these transformations. An electroscalar wave propagating with speed of light is derived upon requiring the invariance of the energy conservation equation under the new transformations. The electroscalar wave function is found to be proportional to the electric field component along the charged particle motion. This scalar wave exists with or without considering the Lorentz gauge. We have shown that the electromagnetic fields travel with speed of light in the presence or absence of free charges.

1 Introduction

Quaternions are mathematical construct that are generalization of complex numbers. They were introduced by Irish mathematician Sir William Rowan Hamilton in 1843 (Sweetser, 2005 [1]). They consist of four components that are represented by one real component (imaginary part) and three vector components (real part). Quaternions are closed under multiplication. Because of their interesting properties one can use them to write the physical laws in a compact way. A quaternion $\widetilde{A}$ can be written as $\widetilde{A} = A_0 + A_1 i + A_2 j + A_3 k$, where $i^2 = j^2 = k^2 = -1$ and $ij = k$, $ki = j$, $jk = i$, $ijk = -1$. A_0 is called the scalar component and A_1, A_2, A_3 are the vector components. Each component consists of real part and imaginary part. The real part of the scalar component vanishes. Similarly the imaginary part of the vector component vanishes too. This is the general prescription of quaternion representation.

In this paper we write the Maxwell equations in quaternion including the Lorentz force and the continuity equation. We have found that the Maxwell equations are derived from just one quaternion equation. The solution of these equations shows that the charge and current densities are waves traveling with speed of light. Generalizing the continuity equation resulted in obtaining three equations defining the charge and current densities. Besides, there exists a set of transformation that leave generalized continuity equation invariant. When these transformations are applied to the energy conservation law an electroscalar wave propagating with speed of light is obtained. Thus, the quaternionic Maxwell equation and continuity equation predict that there exist a scalar wave propagating with speed of light. This wave could possibly arise due to vacuum fluctuation. Such a wave is not included in the Maxwell equations. Therefore, the existence of the electroscalar is a very essential integral part of Maxwell theory. Expressions of Lorentz force and the power delivered to a charge particle are obtained from the quaternion Lorentz force.

Moreover, the current and charge density are solutions of a wave equation travelling with speed of light. Furthermore, we have shown that the electromagnetic field travels with speed of light in the presence and/or absence of charge. However, in Maxwell theory the electromagnetic field travels with speed of light only if there is no current (or free charge) in the medium. We have found here two more equations relating the charge and current that should supplement the familiar continuity equation. These two equations are found to be compatible with Maxwell equations. Hence, Maxwell equations are found to be invariant under these new transformations. This suggests that the extra two equations should be appended to Maxwell equations. Accordingly, we have found an electroscalar wave propagating at the speed of light. The time and space variation of this electroscalar wave induce a charge density and current density even in a source free. The electroscalar wave arises due to the invariance of the Maxwell equations under the new set of transformations. We have shown that such a scalar wave is purely electric and has no magnetic component. This is evident from the Poynting vector that has only two components, one along the particle motion and the other along the electric field direction. We re-

mark that Maxwell equations are still exact and need no modifications. They steadily predict the existence of the a electroscalar wave if we impose the new transformation we obtained in this work.

2 Derivation of Maxwells' equations

The multiplication of two quaternions is given by

$$\begin{aligned}&\widetilde{A}\,\widetilde{B} = (A_0, \vec{A})\,(B_0, \vec{B}) = \\ &= (A_0 B_0 - \vec{A}\cdot\vec{B},\, A_0\vec{B} + \vec{A}\,B_0 + \vec{A}\times\vec{B})\,. \end{aligned} \tag{1}$$

We define the quaternion D'Alembertian operator as

$$\widetilde{\Box}^2 \equiv -|\nabla|^2 = -\widetilde{\nabla}\widetilde{\nabla}^* = \frac{1}{c^2}\frac{\partial^2}{\partial t^2} - \vec{\nabla}\cdot\vec{\nabla}\,, \tag{2}$$

where Nabla and its conjugate are defined by

$$\widetilde{\nabla} = \left(\frac{i}{c}\frac{\partial}{\partial t},\, \vec{\nabla}\right), \qquad \widetilde{\nabla}^* = \left(\frac{i}{c}\frac{\partial}{\partial t},\, -\vec{\nabla}\right). \tag{3}$$

The wave equation of the quaternionic vector potential $\widetilde{A} = (i\frac{\varphi}{c}\,, \vec{A})$ has the form

$$\widetilde{\Box}^{\,2}\widetilde{A} = \mu_0\widetilde{J}, \qquad \widetilde{J} = (ic\rho\,, \vec{J})\,. \tag{4}$$

where ρ is the charge density.

The electric and magnetic fields are defined by (Jackson, 1967 [2])

$$\vec{E} = -\left(\vec{\nabla}\varphi + \frac{\partial\vec{A}}{\partial t}\right), \qquad \vec{B} = \vec{\nabla}\times\vec{A}\,. \tag{5}$$

Using Eqs. (1)–(3), the scalar part of Eq. (4) now reads

$$\begin{aligned}&-\frac{i}{c}\vec{\nabla}\cdot\left(\vec{\nabla}\varphi + \frac{\partial\vec{A}}{\partial t}\right) + \frac{i}{c}\frac{\partial}{\partial t}\left(\frac{1}{c^2}\frac{\partial\varphi}{\partial t} + \vec{\nabla}\cdot\vec{A}\right) - \\ &\qquad - \vec{\nabla}\cdot\left(\vec{\nabla}\times\vec{A}\right) = ic\mu_0\rho\,. \end{aligned} \tag{6}$$

Using Eq. (5) the above equation yields

$$\vec{\nabla}\cdot\vec{B} = 0\,, \tag{7}$$

$$\frac{1}{c^2}\frac{\partial\varphi}{\partial t} + \vec{\nabla}\cdot\vec{A} = 0\,, \tag{8}$$

and

$$\vec{\nabla}\cdot\vec{E} = \frac{\rho}{\varepsilon_0}\,, \tag{9}$$

where $c = \frac{1}{\sqrt{\varepsilon_0\mu_0}}$. This is the Gauss Law and is one of the Maxwell equations.

The vector part of the Eq. (4) can be written as

$$\begin{aligned}&-\frac{i}{c}\left(\vec{\nabla}\times\vec{E} + \frac{\partial\vec{B}}{\partial t}\right) + \left(\vec{\nabla}\times\vec{B} - \frac{1}{c^2}\frac{\partial\vec{E}}{\partial t}\right) - \\ &\qquad - \vec{\nabla}\left(\frac{1}{c^2}\frac{\partial\varphi}{\partial t} + \vec{\nabla}\cdot\vec{A}\right) = \mu\vec{J}\,. \end{aligned} \tag{10}$$

This yields the two equations

$$\vec{\nabla}\times\vec{E} + \frac{\partial\vec{B}}{\partial t} = 0 \tag{11}$$

and

$$\vec{\nabla}\times\vec{B} - \frac{1}{c^2}\frac{\partial\vec{E}}{\partial t} = \mu_0\vec{J}\,. \tag{12}$$

Eqs. (7), (9), (11) and (12) are the Maxwell equations.

By direct cancelation of terms, Eqs. (6) and (10), yield the wave equations of the scalar potential φ and the vector potential $\vec{A}$, viz., $\Box^2\varphi = \frac{\rho}{\varepsilon_0}$ and $\Box^2\vec{A} = \mu_0\vec{J}$.

We thus see that we are able to derive Maxwell equations from the wave equation of the quaternion vector potential. In this formalism only Lorentz gauge is required by the quaternion formulation to derive Maxwell equations. This would mean that Lorentz gauge is more fundamental. It is thus very remarkable that one are able to derive Maxwell equations from just one quaternion equation. Notice that with the 4-vector formulation Maxwell equation are written in terms of two sets of equations.

3 The quaternionic Lorentz force

The quaternionic Lorentz force can be written in the form

$$\left.\begin{aligned}&\widetilde{F} = q\,\widetilde{V}(\widetilde{\nabla}\widetilde{A})\,,\quad \widetilde{V} = (ic\,,\vec{v})\,,\quad \widetilde{F} = \left(i\frac{P}{c}\,,\ \vec{F}\right)\\ &\widetilde{A} = \left(\frac{i\varphi}{c}\,,\vec{A}\right),\ \widetilde{\nabla} = \left(\frac{i}{c}\frac{\partial}{\partial t}\,,\vec{\nabla}\right)\end{aligned}\right\}, \tag{13}$$

where P is the power. The scalar part of the above equation can be written in the form

$$\begin{aligned}&-iqc\left[\left(\vec{\nabla}\cdot\vec{A} + \frac{1}{c^2}\frac{\partial\varphi}{\partial t}\right) + \frac{\vec{v}}{c^2}\cdot\left(\vec{\nabla}\varphi + \frac{\partial\vec{A}}{\partial t}\right)\right] - \\ &- q\,\vec{v}\cdot\vec{\nabla}\times\vec{A} = i\frac{P}{c}\,. \end{aligned} \tag{14}$$

Upon using Eqs. (5) and (8), one gets

$$q\,\vec{v}\cdot\vec{\nabla}\times\vec{A} = 0 \quad\Rightarrow\quad \vec{v}\cdot\vec{B} = 0\,, \tag{15}$$

and

$$P = q\,\vec{v}\cdot\vec{E}\,. \tag{16}$$

This is the usual power delivered to a charged particle in an electromagnetic field. Eq. (15) shows that the charged particle moves in a direction normal to the direction of the magnetic field.

Now the vector component of Eq. (13) is

$$\begin{aligned}&q\left[-\frac{\partial\vec{A}}{\partial t} - \vec{\nabla}\varphi + ic\,\vec{\nabla}\times\vec{A} - \frac{\vec{v}}{c^2}\frac{\partial\varphi}{\partial t} - \right.\\ &\left. - \vec{v}(\vec{\nabla}\cdot\vec{A}) + \vec{v}\times\left(\frac{i}{c}\frac{\partial\vec{A}}{\partial t} + \frac{i}{c}\vec{\nabla}\varphi + \vec{\nabla}\times\vec{A}\right)\right] = \vec{F}\,. \end{aligned} \tag{17}$$

This yields the two equations

$$\vec{F} = q\,\left(\vec{E} + \vec{v}\times\vec{B}\right), \tag{18}$$

and

$$\vec{B}_m \equiv \vec{B} = \frac{\vec{v}}{c^2}\times\vec{E}\,. \tag{19}$$

Eq. (18) is the familiar Lorentz force. Eq. (19) gives a new relation between the magnetic field of a moving charge due to an electric field. Thus, we are able to derive the power and the Lorentz force on a charged particle. This new magnetic field may be interpreted as the magnetic field seen in a frame moving with velocity $\vec{v}$ when $\vec{B}=0$ in the rest frame. It is thus an apparent field. This equation is compatible with Eq. (15), since $\vec{v}\cdot\vec{B}_m = \vec{v}\cdot(\frac{\vec{v}}{c^2}\times\vec{E}) = 0$, by vector property. Moreover, we notice that $\vec{E}\cdot\vec{B}_m = \vec{E}\cdot(\frac{\vec{v}}{c^2}\times\vec{E}) = 0$. This clearly shows that the magnetic field produced by the charged particle is perpendicular to the electric field applied on the particle. Thus, a charged particle when placed in an external electric field produces a magnetic field perpendicular to the direction of the particle motion and to the electric field producing it. As evident from Eq. (19), this magnetic field is generally very small due to the presence of the factor c^2 in the dominator. Hence, the reactive force arising from this magnetic field is

$$\vec{F}_m = q\,\vec{v}\times\vec{B}_m\,, \tag{20}$$

which upon using Eq. (19) yields

$$\vec{F}_m = q\,\vec{v}\times\left(\frac{\vec{v}}{c^2}\times\vec{E}\right). \tag{21}$$

Using Eq. (16) and the vector properties, this can be casted into

$$\vec{F}_m = \frac{P}{c^2}\,\vec{v} - \frac{v^2}{c^2}\,q\,\vec{E}\,. \tag{22}$$

This reactive force acts along the particle motion (longitudinal) and field direction. The negative sign of the second term is due to the back reaction of the charge when accelerates by the external electric field. The total force acting on the charge particle is $\vec{F}_{\rm total} = q(\vec{E} + \vec{v}\times\vec{B}_{\rm total})$, $\vec{B}_{\rm total} = \vec{B} + \vec{B}_m$, $\vec{F}_{\rm total} = q\big(1-\frac{v^2}{c^2}\big)\vec{E} + q\,\vec{v}\times\vec{B} + \frac{P}{c^2}\,\vec{v}$. Notice that when $v \ll c$, this force reduces to the ordinary force and no noticeable difference will be observed. However, when $v \approx c$ measurable effects will be prominent.

4 Continuity equation

The quaternion continuity equation can be written in the form

$$\widetilde{\nabla}\,\widetilde{J} = 0\,, \qquad \widetilde{J} = \left(i\rho c\,,\vec{J}\right), \tag{23}$$

so that the above equation becomes

$$\widetilde{\nabla}\,\widetilde{J} = \left[-\left(\vec{\nabla}\cdot\vec{J} + \frac{\partial\rho}{\partial t}\right), \frac{i}{c}\left(\frac{\partial\vec{J}}{\partial t} + \vec{\nabla}\rho\,c^2\right) + \vec{\nabla}\times\vec{J}\right] = 0\,. \tag{24}$$

which yields the following three equations

$$\vec{\nabla}\cdot\vec{J} + \frac{\partial\rho}{\partial t} = 0\,, \tag{25}$$

and

$$\vec{\nabla}\rho + \frac{1}{c^2}\frac{\partial\vec{J}}{\partial t} = 0\,, \tag{26}$$

so that

$$\vec{\nabla}\times\vec{J} = 0\,. \tag{27}$$

Using the Stockes theorem one can write Eq. (27) to get, $\int\vec{J}\cdot d\vec{\ell} = 0$. Eqs. (26) and (27) are new equations for a flow. Eq. (27) states that a current emanating from a point in spacetime does not circulate to the same point. In comparison with a magnetic field, we know that the magnetic field lines have circulation.

Now take the dot product of both sides of Eq. (26) with $d\vec{S}$, where S is a surface, and integrate to get

$$\int\vec{\nabla}\rho\cdot d\vec{S} + \int\frac{1}{c^2}\frac{\partial\vec{J}\cdot d\vec{S}}{\partial t} = 0\,, \tag{28}$$

or

$$\int\vec{\nabla}\rho\cdot d\vec{S} + \frac{1}{c^2}\frac{\partial I}{\partial t} = 0\,, \qquad I = \int\vec{J}\cdot d\vec{S}\,. \tag{29}$$

But from Stokes' theorem $\int\vec{A}\cdot d\vec{S} = \int\vec{\nabla}\times\vec{A}\cdot d\vec{\ell}$. Therefore, one gets

$$\int\vec{\nabla}\rho\cdot d\vec{S} = \int\vec{\nabla}\times(\vec{\nabla}\rho)\cdot d\vec{\ell} = 0\,, \quad \vec{A} = \vec{\nabla}\rho\,. \tag{30}$$

This implies that $\frac{\partial I}{\partial t} = 0$ which shows that the current is conserved. This is a Kirchoff-type law of current loops. However, Eq. (25) represents a conservation of charge for electric current.

Eq. (27) suggests that one can write the current density as

$$\vec{J} = \vec{\nabla}\Lambda\,, \tag{31}$$

where Λ is some scalar field. It has a dimension of Henry (H). It thus represent a magnetic field intensity. We may therefore call it a magnetic scalar. Substituting this expression in Eq. (26) and using Eq. (42), one yields

$$\nabla^2\Lambda - \frac{1}{c^2}\frac{\partial^2\Lambda}{\partial t^2} = 0\,. \tag{32}$$

This means that the scalar function $\Lambda(r,t)$ is a wave traveling with speed of light.

Now taking the divergence of Eq. (26), one gets

$$\vec{\nabla}\cdot\vec{\nabla}(\rho\,c^2) + \frac{\partial\,\vec{\nabla}\cdot\vec{J}}{\partial t} = 0\,, \tag{33}$$

which upon using Eq. (25) becomes

$$\nabla^2(\rho\,c^2) + \frac{\partial\,\frac{-\partial\rho}{\partial t}}{\partial t} = 0\,, \tag{34}$$

or

$$\frac{1}{c^2}\frac{\partial^2\rho}{\partial t^2}-\nabla^2\rho=0\,, \tag{35}$$

which states the the charge scalar (ρ) is a field propagating with speed of light.

Now take the curl of Eq. (27) to get

$$\vec{\nabla}\times(\vec{\nabla}\times\vec{J})=\vec{\nabla}(\vec{\nabla}\cdot\vec{J})-\nabla^2\vec{J}=0\,, \tag{36}$$

and upon using Eq. (25) and (26) one gets

$$\vec{\nabla}\left(-\frac{\partial\rho}{\partial t}\right)-\nabla^2\vec{J}=\frac{\partial(-\vec{\nabla}\rho)}{\partial t}-\nabla^2\vec{J}=$$
$$=\frac{\partial\frac{1}{c^2}\frac{\partial\vec{J}}{\partial t}}{\partial t}-\nabla^2\vec{J}=0\,, \tag{37}$$

which states that the current density satisfies a wave that propagate with speed of light, i.e.,

$$\frac{1}{c^2}\frac{\partial^2\vec{J}}{\partial t^2}-\nabla^2\vec{J}=0\,. \tag{38}$$

Therefore, both the current and charge densities are solutions of a wave equation traveling with a speed of light. This is a remarkable result that does not appear in Maxwell initial derivation. Notice however that if we take $\frac{\partial}{\partial t}$ of Eq. (12) and apply Eqs. (11) and (9), we get

$$\frac{1}{c^2}\frac{\partial^2\vec{E}}{\partial t^2}-\nabla^2\vec{E}=-\frac{1}{\varepsilon_0}\left(\vec{\nabla}\rho+\frac{1}{c^2}\frac{\partial\vec{J}}{\partial t}\right). \tag{39}$$

Now take the curl of both sides of Eq. (12) and apply Eqs. (11) and (7), we get

$$\frac{1}{c^2}\frac{\partial^2\vec{B}}{\partial t^2}-\nabla^2\vec{B}=\mu_0\big(\vec{\nabla}\times\vec{J}\big)\,. \tag{40}$$

The left hand side of Eqs. (39) and (40) is zero according to Eqs. (26) and (27). Therefore, they yield electric and magnetic fields travelling with speed of light. However, Maxwell equations yield electric and magnetic fields propagating with speed of light only if $\vec{J}=0$ and $\rho=0$ (free space). Because of Eqs. (26) and (27) electromagnetic field travels with speed of light whether the space is empty or having free charges. It seems that Maxwell solution is a special case of the above two equations. Therefore, Eqs. (39) and (40) are remarkable.

Now we introduce the new gauge transformations of $\vec{J}$ and ρ as:

$$\rho'=\rho+\frac{1}{c^2}\frac{\partial\Lambda}{\partial t}\,,\qquad \vec{J}'=\vec{J}-\vec{\nabla}\Lambda\,, \tag{41}$$

leaving Eqs. (25) - (27) invariant, where Λ satisfies the wave equation

$$\frac{1}{c^2}\frac{\partial^2\Lambda}{\partial t^2}-\nabla^2\Lambda=-\left(\vec{\nabla}\cdot\vec{J}+\frac{\partial\rho}{\partial t}\right). \tag{42}$$

These transformations are similar to gauge transformations endorse on the vector potential ($\vec{A}$) and the scalar potential (φ) leaving $\vec{E}$ and $\vec{B}$ invariant. It is interesting to see that the current $\vec{J}$ and density ρ are not unique, however. van Vlaenderen and Waser arrived at similar equations, but they attribute the Λ field to a longitudinal electroscalar wave in vacuum. Thus, even if there is no charge or current density present in a region, the scalar field Λ could act as a source for the electromagnetic field. Such a term could come from quantum fluctuations of the vacuum. This is a very intriguing result. Notice from Eq. (41) that the scalar wave (Λ) distribution induces a charge density, $\rho_{\mathrm{vacuum}}=\frac{1}{c^2}\frac{\partial\Lambda}{\partial t}$, and a current $\vec{J}_{\mathrm{vacuum}}=-\vec{\nabla}\Lambda$. It may help understand the Casimir force generated when two uncharged metallic plates in a vacuum, placed a few micrometers apart, without any external electromagnetic field attract each other(Bressi, *et al.*, 2002 [18]). Notice that this vacuum current and density satisfy the continuity equations, Eqs. (25)–(27). Note that these vacuum quantities could be treated as a correction of the current and charge, since in quantum electrodynamics all physical quantities have to be renormalized. It is interesting that the Maxwell equations expressed in Eqs. (39) and (40), are invariant under the transformation in Eq. (41) provided that $\vec{E}'=\vec{E}$, $\vec{B}'=\vec{B}$. It is thus remarkable to learn that Maxwell equations are invariant under the transformation,

$$\left.\begin{array}{ll}\rho'=\rho+\dfrac{1}{c^2}\dfrac{\partial\Lambda}{\partial t}\,, & \vec{J}'=\vec{J}-\vec{\nabla}\Lambda\\ \vec{E}'=\vec{E}, & \vec{B}'=\vec{B}\end{array}\right\}. \tag{43}$$

We notice from Eq. (42) that the electroscalar wave propagates with speed of light if the charge is conserved. However, if the charge is not conserve then Λ will have a source term equals to the charge violation term. In this case the electroscalar wave propagates with a speed less than the speed of light. Hence, charge conservation can be detected from the propagation speed of this electroscalar wave.

5 Poynting vector

The Poynting theorem, which represents the energy conservation law is given by (Griffiths, 1999 [4])

$$\frac{\partial u}{\partial t}+\vec{\nabla}\cdot\vec{S}=-\vec{J}\cdot\vec{E}\,, \tag{44}$$

where $\vec{S}$ is the Poynting vector, which gives the direction of energy flow and u is the energy density. However, in our present case we have

$$\frac{\partial u_{\mathrm{total}}}{\partial t}+\vec{\nabla}\cdot\vec{S}_{\mathrm{total}}=-\vec{J}'\cdot\vec{E}\,', \tag{45}$$

where $\vec{S}_{\mathrm{total}}=\vec{S}_{\mathrm{em}}+\vec{S}_m$ is the total Poynting vector, $\vec{S}_{\mathrm{em}}=$ $=\frac{\vec{E}\times\vec{B}}{\mu_0}$, and $u_{\mathrm{total}}=\frac{1}{2}\,\varepsilon_0\,E^2+\frac{1}{2\mu_0}(\vec{B}+\vec{B}_m)^2$. Because of Eqs. (15) and (19), the cross term in the bracket vanishes. Hence,

$$u_{\mathrm{total}}=\frac{1}{2}\,\varepsilon_0\left(1+\frac{v^2}{c^2}\right)E^2+\frac{B^2}{2\mu_0}-\frac{1}{2}\,\varepsilon_0\left(\frac{\vec{v}}{c}\cdot\vec{E}\right)^2. \tag{46}$$

This implies that the excessive magnetic field of the charged particles contributes an energy, $u_m = \frac{1}{2}\,\varepsilon_0 \frac{v^2}{c^2}\,E^2 \times$ $\times \left(1 - (\hat{n}\cdot\hat{e})^2\right)$, where $\hat{n}$ and $\hat{e}$ are two unit vectors along the motion of the particle and the electric field. This contribution is generally very small, viz., for $v \ll c$. When the charged particle moves parallel to the electric field, i.e., $\hat{n}\cdot\hat{e} = 1$, its energy density contribution vanishes.

Using Eq. (19), one finds

$$\vec{S}_m = \frac{\vec{E}\times\vec{B}_m}{\mu_0} = \frac{\vec{E}}{\mu_0}\times\left(\frac{\vec{v}\times\vec{E}}{c^2}\right) = \\ = \left(\varepsilon_0 E^2\right)\vec{v} - \left(\vec{E}\cdot\vec{v}\right)\varepsilon_0\,\vec{E}\,. \quad (47)$$

Using the vector identity, $\vec{\nabla}\cdot\left(f\vec{A}\right) = \left(\vec{\nabla}f\right)\cdot\vec{A} + \left(\vec{\nabla}\cdot\vec{A}\right)f$ (Gradstein and Ryzik, 2002 [5]) and Eq. (19), the energy conservation law in Eq. (47) reads

$$\frac{\partial u_{\mathrm{total}}}{\partial t} + \vec{\nabla}\cdot\left(\vec{S}_{\mathrm{em}} + \left(\varepsilon_0 E^2\right)\vec{v}\right) = \\ = -\vec{E}\cdot\vec{\nabla}\left(\Lambda - \varepsilon_0(\vec{E}\cdot\vec{v})\right). \quad (48)$$

The left hand side of the above equation vanishes when

$$\Lambda = \varepsilon_0\left(\vec{E}\cdot\vec{v}\right). \quad (49)$$

Thus, this scalar wave is not any arbitrary function. It is associated with the electric field of the electromagnetic wave. It is thus suitable to call this an electroscalar wave. Eq. (48) with the condition in Eq. (49) states that when Λ is defined as above, there is no work done to move the free charges, and that a new wave is generated with both energy density and having energy flow along the particle direction. Hence,

$$\frac{\partial u_{\mathrm{total}}}{\partial t} + \vec{\nabla}\cdot\left(\vec{S}_{\mathrm{em}} + \left(\varepsilon_0 E^2\right)\vec{v}\right) = 0\,. \quad (50)$$

In such a case, we see that no electromagnetic energy is converted (into neither mechanical energy nor heat). The medium acts as if it were empty of current. This shows that the scalar wave and the charged particle propagate concomitantly. However, in the de Broglie picture a wave is associated with the particle motion to interpret the wave particle duality present in quantum mechanics. Eq. (50) shows that there is no energy flow along along the magnetic field direction. Therefore, this electroscalar wave is a longitudinal wave. The transmission of such a wave does cost extra energy and it avails the electromagnetic energy accompany it. Notice that this scalar wave can be used to transmit and receive wireless signals (van Vlaenderen and Waser, 2001 [6]). It has an advantage over the electromagnetic wave, since it is a longitudinal wave and has no polarization properties. We will anticipate that this new scalar wave will bring about new technology of transmission that avails such properties.

We have seen that recently van Vlaenderen, 2003 [7], showed that there is a scalar wave associated with abandonment of Lorentz gauge. He called such a scalar field, S. We have shown that without such abandonment one can arrive at the same conclusion regarding the existence of such a scalar wave. We have seen that the scalar wave associated with the current $\vec{J}$ travels along the current direction. However, van Vlaenderen obtain such a scalar wave with the condition that $\vec{J} = \vec{B} = 0$. But our derivation here shows that this is not limited to such a case, and is valid for any value of $\vec{E}, \vec{B}$, and $\vec{J}$. We can obtain the scalar wave equation of van Vlaenderen if we apply our transformation in Eq. (41) to Maxwell equations.

Van Vlaenderen obtained a scalar field for $\vec{E} = 0$ and $\vec{B} = 0$. See, Eq. (25) and (26). These equations can be obtained from from Maxwell and continuity equation by requiring an invariance of Maxwell equations under our transformation in Eq. (41) without requiring $\vec{E} = \vec{B} = 0$. Therefore, our Eq. (42) is similar to van Vlaenderen equation, viz., Eq. (35).

Wesley and Monstein [9] claimed that the scalar wave (longitudinal electric wave) transmission has an energy density equals to $\frac{1}{2\mu_0}\,S^2$. However, if the violation of Lorentz condition is very minute then this energy density term will have a very small contribution and can be ignored in comparison with the linear term in the Poynting vector term. Notice, however, that in such a case the van Vlaenderen prediction will be indistinguishable from our theory with a valid Lorentz condition. Hence, the existence of the electroscalar wave is not very much associated with Lorentz condition invalidation. Ignatiev and Leus [10] have confirmed experimentally the existence of longitudinal vacuum wave without magnetic component. This is evident from Eq. (47) that the energy flows only along the particle motion and the electric field direction, without trace to any magnetic component. van Vlaenderen proposed source transformations to generalize electrodynamic force and power of a charge particle in terms of a scalar wave S. Therefrom, he obtain a Poynting vector due to this scalar to be $-\frac{S}{\mu_0}\vec{E}$. These transformations coincide with our new transformation that arising from the invariance of the continuity equations under these transformation. Hence, Eq. (35) of van Vlaenderen would become identical to our Eq. (43), by setting $\Lambda = \frac{S}{\mu_0}$, but not necessarily limited to $\vec{B} = 0$, as he assumed.

We summarize here the quaternion forms of the physical laws which we have studied so far we:

- Maxwell equation: $\widetilde{\square}^2\widetilde{A} = \mu_0\widetilde{J}$;
- Lorentz force: $\widetilde{F} = q\widetilde{V}(\widetilde{\nabla}\widetilde{A})$;
- continuity equation: $\widetilde{\nabla}\widetilde{J} = 0$.

6 Conclusion

I think that a new and very powerful idea drives this work, namely, that all events are nicely represented as a quaternion. This implies that any collection of event can be generated by an appropriate quaternion function. Scalar and vector mix

under multiplication, so quaternions are mixed representation. Every event, function, operator can be written in terms of quaternions. We have shown in this paper that the four Maxwell equations emerge from just one quaternion equation. Moreover, Lorentz force and the power delivered by a charged particle stem from one quaternion equation. The quaternion form of the continuity equation gives rise to the ordinary continuity equation, in addition to two more equations. The invariance of Maxwell equations under our new transformation shown in Eq. (43) ushers in the existence of new wave. This wave is not like the ordinary electromagnetic wave we know. It is a longitudinal wave having their origin in the variation of the electric field. It is called an electroscalar wave, besides that fact that it has a dimension of magnetic field intensity. Thus, in this paper we have laid down the theoretical formulation of the electroscalar wave without spoiling the beauty of Maxwell equations (in addition to Lorentz force). This scalar wave is not like the scalar potential which is a wave with a source term represented by the density that travels at a speed less than that of light. If the electroscalar wave is found experimentally, it will open a new era of electroscalar communication, and a new technology is then required. We remark that one does not need to invalidate the Lorentz condition to obtain such wave as it is formulated by some authors. In this work, we have generalize the continuity equation to embody a set of three equations. These equations imply that both current and density are waves traveling at a speed of light. Urgent experimental work to disclose the validity of these predictions is highly needed.

Acknowledgements

This work is supported by the University of Khartoum and Ahlia University research fund. We appreciate very much this support. Special thanks go to F. Amin for enlightening and fruitful discission.

Submitted on November 28, 2008 / Accepted on December 05, 2008

References

1. Sweetser D.B. Doing physics with quaternions. MIT, 2005. Accessed online: http://world.std.com/∼sweetser/quaternions/ps/book.pdf
2. Jackson J.D. Classical electrodynamics. John Wiley and Sons, 1967.
3. Bressi G., Carugno G., Onofrio R., and Ruoso G. *Phys. Rev. Lett.*, 2002, v. 88, 041804.
4. Griffiths D.J., Introduction to electrodynamics. Prentice-Hall Inc., 1999.
5. Gradstein I.S. and Ryzik I.M Vector field theorem. Academic Press, San Diego (CA), 2002.
6. Van Vlaenderen K.J. and Waser A. *Hadronic Journal*, 2001, v. 24, 609.
7. Van Vlaenderen K.J. arXiv: physics/0305098.
8. Waser A. Quaternions in electrodynamics. AW-verlag, 2000.
9. Monstein C. and Wesley J.P. *Europhysics Letters*, 2002, v. 59, 514.
10. Ignatiev G.F. and Leus V.A. In: *Instantaneous Action at a Distance in Modern Physics: Pro and Contra*, Nova Science, Hauppage (NY), 1999, 203.

On the New Gauge Transformations of Maxwell's Equations

Arbab I. Arbab

Department of Physics, Faculty of Science, University of Khartoum, P.O. 321, Khartoum 11115, Sudan
Department of Physics and Applied Mathematics, Faculty of Applied Sciences and Computer, Omdurman Ahlia University, P.O. Box 786, Omdurman, Sudan

E-mail: aiarbab@uofk.edu; arbab_ai@yahoo.com

We have found new gauge transformations that are compatible with Maxwell's equations and Lorentz gauge. With these transformations, we have formulated the electrodynamic equations that are shown to be invariant. New generalized continuity equations are derived that are also compatible with Maxwell's equations. Moreover, we have shown that the electromagnetic wave travels with speed of light in vacuum or a medium with free charge or current if the generalized continuity equations are satisfied. Magnetic monopoles don't show up in ordinary experiments because the Lorentz force acting on the magnetic charge is zero.

1 Introduction

Maxwell's equations describing the electric ($\vec{E}$) and magnetic ($\vec{B}$) fields reveal that when these fields are written in terms of a vector and scalar potentials, the equations of motion of these potential are generally solutions of wave equation with a source term. However, there is no unique way to define these potentials. A set of new potentials satisfying the Lorentz gauge can be solutions as well. Thus, Maxwell's equations are also invariant under these gauge transformations. Maxwell's equations are invariant under Lorentz transformation. Since the motion of charged particles is governed by the continuity equation, Maxwell's equations determine the motion of the charged particles in conformity with this equation.

Using quaternions, we have recently shown that Maxwell's equations can be written as a single quaternionic equation (Arbab and Satti, 2009 [1]). It is a wave equation. This immediately shows that the electromagnetic fields are waves. Similarly, by writing the continuity equation in a quaternionic form, we have shown that this equation yields three set of equations. We call these equations the generalized continuity equations (GCEs). Besides, we have found that the magnetic field arised from the charge motion (with speed $\vec{v}$) acted by an electric field is given by $\vec{B} = \frac{\vec{v}}{c^2} \times \vec{E}$. Because of this feature, the magnetic monopoles postulated by Dirac (Dirac, 1931 [2]) couldn't show up, because the Lorentz force component acting on this magnetic charge vanishes (Moulin, 2001 [3], Wolfgang, 1989 [4]). Hence, magnetic monopole can only be detected indirectly.

In the present paper, we have introduced new gauge transformations that leave Maxwell's equations, Lorentz gauge and the continuity equations invariant. Moreover, we know that according to Maxwell's theory the electromagnetic fields travel with speed of light in vacuum, i.e., when no free charge or current exists. However, in our present formulation, we have shown that the electromagnetic fields travel with speed of light in vacuum or free charged medium if the GCEs are satisfied.

2 Continuity equation

The flow of any continuous medium is governed by the continuity equation. The quaternionic continuity equation reads, (Arbab and Satti, 2009 [1]),

$$\tilde{\vec{\nabla}}\,\tilde{J} = \left[-\left(\vec{\nabla}\cdot\vec{J} + \frac{\partial\rho}{\partial t} \right) \frac{i}{c} \left(\frac{\partial \vec{J}}{\partial t} + \vec{\nabla}\rho c^2 \right) + \vec{\nabla}\times\vec{J} \right] = 0\,, \quad (1)$$

where

$$\tilde{\vec{\nabla}} = \left(\frac{i}{c}\frac{\partial}{\partial t}, \vec{\nabla} \right), \qquad \tilde{J} = \left(i\rho c, \vec{J} \right). \quad (2)$$

This implies that

$$\vec{\nabla}\cdot\vec{J} + \frac{\partial\rho}{\partial t} = 0\,, \quad (3)$$

$$\vec{\nabla}\rho + \frac{1}{c^2}\frac{\partial\vec{J}}{\partial t} = 0\,, \quad (4)$$

and

$$\vec{\nabla}\times\vec{J} = 0\,. \quad (5)$$

We call Eqs. (3)–(5) the *generalized continuity equations* (GCEs). Equation (5) states the current density $\vec{J}$ is irrotational.

In a covariant form, Eqs. (3)–(5) read

$$\partial_\mu J^\mu = 0\,, \qquad N_{\mu\nu} \equiv \partial_\mu J_\nu - \partial_\nu J_\mu = 0\,. \quad (6)$$

Notice that the tensor $N_{\mu\nu}$ is an antisymmetric tensor. It is evident from Eq. (6) that Eqs. (3)–(6) are Lorentz invariant. Now differentiate Eq. (3) partially with respect to time and use Eq. (4), we obtain

$$\frac{1}{c^2}\frac{\partial^2\rho}{\partial t^2} - \nabla^2\rho = 0\,. \quad (7)$$

Similarly, take the divergence of Eq. (4) and use Eq. (3), we obtain

$$\frac{1}{c^2}\frac{\partial^2 \vec{J}}{\partial t^2} - \nabla^2 \vec{J} = 0\,, \tag{8}$$

where $\rho = \rho(\vec{r}, t)$ and $\vec{J} = \vec{J}(\vec{r}, t)$. Therefore, both the current density and charge density satisfy a wave equation propagating with speed of light. In covariant form, Eqs. (7) and (8) now read

$$\Box^2 J^\nu \equiv \partial_\mu \partial^\mu J^\nu = 0\,. \tag{9}$$

We remark that the GCEs are applicable to any flow whether created by charged particles or neutral ones.

3 Maxwell's equations

We have recently shown that quaternion equation (Arbab and Satti, 2009 [1])

$$\tilde{\Box}^2 \tilde{A} = \mu_0 \tilde{J}\,, \qquad \tilde{A} = \left(i\frac{\varphi}{c},\ \vec{A}\right) \tag{10}$$

yields the Maxwell's equations (Arbab and Satti, 2009 [1])

$$\vec{\nabla}\cdot\vec{E} = \frac{\rho}{\varepsilon_0}\,, \tag{11}$$

$$\vec{\nabla}\times\vec{E} + \frac{\partial \vec{B}}{\partial t} = 0\,, \tag{12}$$

$$\vec{\nabla}\times\vec{B} - \frac{1}{c^2}\frac{\partial \vec{E}}{\partial t} = \mu_0 \vec{J}\,, \tag{13}$$

and

$$\vec{\nabla}\cdot\vec{B} = 0\,. \tag{14}$$

The electric and magnetic fields are defined by the vector potential (A) and the scalar potential (φ) as follows

$$\vec{E} = -\vec{\nabla}\varphi - \frac{\partial \vec{A}}{\partial t}\,, \qquad \vec{B} = \vec{\nabla}\times\vec{A}\,, \tag{15}$$

such that the Lorentz gauge

$$\vec{\nabla}\cdot\vec{A} + \frac{1}{c^2}\frac{\partial \varphi}{\partial t} = 0\,, \tag{16}$$

is satisfied. We know that the electric and magnetic fields are invariant under the following gauge transformations

$$\vec{A}' = \vec{A} - \vec{\nabla}\chi\,, \qquad \varphi' = \varphi + \frac{\partial \chi}{\partial t}\,. \tag{17}$$

The invariance of the Lorentz gauge implies that

$$\frac{1}{c^2}\frac{\partial^2 \chi}{\partial t^2} - \nabla^2 \chi = 0\,. \tag{18}$$

The 4-vector potential, A_μ, can be written as

$$A_\mu = \left(\frac{\varphi}{c}, -\vec{A}\right)\,. \tag{19}$$

In a covariant form, Eq. (17) becomes

$$A'_\mu = A_\mu + \partial_\mu \chi\,. \tag{20}$$

Eq. (15) can be written in a covariant form as

$$F_{\mu\nu} = \partial_\mu A_\nu - \partial_\nu A_\mu\,. \tag{21}$$

In a covariant form, Maxwell's equations, Eqs. (11)–(14), read

$$\partial_\mu F^{\mu\nu} = \mu_0 J^\nu, \qquad \partial_\mu F_{\nu\lambda} + \partial_\nu F_{\lambda\mu} + \partial_\lambda F_{\mu\nu} = 0\,. \tag{22}$$

Notice however that if we take $\frac{\partial}{\partial t}$ of Eq. (12) and apply Eqs. (13) and (14), we get

$$\frac{1}{c^2}\frac{\partial^2 \vec{B}}{\partial t^2} - \nabla^2 \vec{B} = \mu_0\left(\vec{\nabla}\times\vec{J}\right)\,. \tag{23}$$

Now take the curl of both sides of Eq. (12) and apply Eqs. (11) and (13), we get

$$\frac{1}{c^2}\frac{\partial^2 \vec{E}}{\partial t^2} - \nabla^2 \vec{E} = -\frac{1}{\varepsilon_0}\left(\vec{\nabla}\rho + \frac{1}{c^2}\frac{\partial \vec{J}}{\partial t}\right). \tag{24}$$

We remark that, according to our GCEs, the electric and magnetic waves propagate with speed of light whether $\vec{J} = \rho = 0$ or not, as long as Eqs. (4) and (5) are satisfied.

In a covariant form, Eqs. (23) and (24) read

$$\Box^2 F_{\mu\nu} = \mu_0\left(\partial_\mu J_\nu - \partial_\nu J_\mu\right)\,. \tag{25}$$

This can be casted in the form

$$\partial^\alpha\left(\mu_0^{-1}\partial_\alpha F_{\mu\nu} + g_{\nu\alpha}J_\mu - g_{\mu\alpha}J_\nu\right) \equiv \partial^\alpha \mathcal{C}_{\alpha\mu\nu} = 0\,, \tag{26}$$

where

$$\mathcal{C}_{\alpha\mu\nu} = \mu_0^{-1}\partial_\alpha F_{\mu\nu} + g_{\nu\alpha}J_\mu - g_{\mu\alpha}J_\nu\,, \tag{27}$$

where $g_{\mu\nu}$ is the metric tensor. Notice that the current tensor $\mathcal{C}_{\alpha\mu\nu}$ is antisymmetric in the indices μ, ν and is a conserved quantity. Likewise the total momentum and energy of the electrodynamics system (fields + particles) is conserved, we found here that the total current of the system, one arising from the electromagnetic fields and the other from the particles motion, is conserved. The first term in Eq. (27) represents the electromagnetic current, the second term represents the electronic current and the last term represents the vacuum current (with negative sign) as suggested by Eq. (28).

4 New gauge transformations

Now we introduce the current density transformations (CDTs) for $\vec{J}$ and ρ, viz.,

$$\rho' = \rho + \frac{1}{c^2}\frac{\partial \Lambda}{\partial t}\,, \qquad \vec{J}' = \vec{J} - \vec{\nabla}\Lambda\,, \tag{28}$$

leaving the generalized continuity equations (GCEs) invariant. In a covariant form, Eq. (28) reads

$$J_\mu{}' = J_\mu + \partial_\mu \Lambda \,. \tag{29}$$

Applying this transformation in Eq. (6), one finds that

$$\partial_\mu (J^\mu + \partial^\mu \Lambda) = \partial_\mu J^{\mu\,\prime} = 0 \,, \qquad N'_{\mu\nu} = N_{\mu\nu} \,. \tag{30}$$

It is thus evident that the GCEs are invariant under the CDTs. Moreover, the application of the current transformation in the continuity equation, Eq. (3), yields

$$\frac{1}{c^2}\frac{\partial^2 \Lambda}{\partial t^2} - \nabla^2 \Lambda = -\left(\vec{\nabla}\cdot\vec{J} + \frac{\partial \rho}{\partial t}\right) \,. \tag{31}$$

We thus that $\vec{J}$ and ρ in the GCEs are not unique and any new set of $\vec{J}'$ and ρ' will lead to the same GCEs provided that Λ is gauged by Eq. (31). Since the right hand side of Eq. (31) vanishes, Λ is a solution of a wave equation traveling with speed of light in vacuum. This equation is similar to Eq. (18). Notice also that Eqs. (23) and (24) are invariant under the following CDTs

$$\rho' = \rho + \frac{1}{c^2}\frac{\partial \Lambda}{\partial t} \,, \quad \vec{J}' = \vec{J} - \vec{\nabla}\Lambda \,, \quad \vec{E}\,' = \vec{E}, \quad \vec{B}\,' = \vec{B} \,. \tag{32}$$

In a covariant form, these read

$$J'_\mu = J_\mu + \partial_\mu \Lambda \,, \qquad F'_{\mu\nu} = F_{\mu\nu} \,. \tag{33}$$

Now let us introduce new gauge transformations (NGTs) as follows

$$\vec{A}\,' = \vec{A} + \alpha \vec{J} \,, \;\; \varphi' = \varphi + \alpha \rho\, c^2 \,, \;\; \alpha = \mu_0 \lambda^2 \,, \;\; \lambda = \text{const.} \tag{34}$$

In a covariant form, Eq. (34) reads

$$A'_\mu = A_\mu + \alpha\, J_\mu \,, \tag{35}$$

so that the electromagnetic tensor

$$F'_{\mu\nu} = F_{\mu\nu} + \alpha\,(\partial_\mu J_\nu - \partial_\nu J_\mu) \,, \tag{36}$$

using Eq. (6), is invariant under the NGTs and hence, Maxwell's equations are invariant too. Moreover, notice that the Lorentz gauge

$$\vec{\nabla}\cdot\vec{A} + \frac{1}{c^2}\frac{\partial \varphi}{\partial t} = 0 \,, \qquad \text{or} \qquad \partial_\mu A^\mu = 0 \,, \tag{37}$$

is also invariant under the NGTs provided that the continuity equation, Eq. (3), is satisfied. The covariant derivative is defined by

$$D_\mu = \partial_\mu - \frac{ie}{\hbar}\, A_\mu \,. \tag{38}$$

The quantum electrodynamics Lagrangian of a particle of spinor ψ is given by

$$\mathcal{L} = \overline{\psi}\,(i\hbar\, c\, \gamma^\mu\, D_\mu - mc^2)\psi - \frac{1}{4\mu_0} F_{\mu\nu} F^{\mu\nu} \,. \tag{39}$$

so that the Eq. (39) is invariant under the local gauge transformation of the spinor ψ (Bjorken, 1964 [5]). In terms of this derivative, one has

$$F_{\mu\nu} = D_\mu A_\nu - D_\nu A_\mu \,, \tag{40}$$

and Maxwell's equations become

$$D_\mu F^{\mu\nu} = \mu_0 J^\nu, \quad D_\mu F_{\nu\lambda} + D_\nu F_{\lambda\mu} + D_\lambda F_{\mu\nu} = 0 \,. \tag{41}$$

Upon using Eq. (6), Eq. (41) is invariant under NGTs. Applying the NGTs into the above Lagrangian yields

$$\mathcal{L}' = \mathcal{L} + \alpha\, J_\mu J^\mu \,. \tag{42}$$

The current density is defined by $J^\mu = ec\,\overline{\psi}\gamma^\mu\psi$. This extra interaction term has already appeared in the Fermi theory of beta decay. It is written in the form $\frac{G_F}{\sqrt{2}} J_\mu J^\mu$, i.e., $\alpha = \frac{G_F}{\sqrt{2}}$, where G_F is the Fermi constant. We anticipate that this term is related to the mass of the photon (propagator). This term term couldn't be added to the initial Lagrangian because, it breaks the ordinary gauge invariance. However, the NGTs could rise to the mass of the photon. It is something like Higg's mechanism that gives the elementary particles their masses. Such a term may be related to an interaction of two electrons closed to each other like in Cooper pairs in superconductivity. The behavior of superconductors suggests that electron pairs are coupling over a range of hundreds of nanometers, three orders of magnitude larger than the lattice spacing. These coupled electrons can take the character of a boson and condense into the ground state.

5 Symmetrized Maxwell's equation

Dirac was the first to suggest the possibility of a particle that carries magnetic charge. At the present time there is no experimental evidence for the existence of magnetic charges or monopoles. This can be formulated in the context of Maxwell's equations. Maxwell's equations can be written in a symmetric form by invoking the idea of monopole. Let us denote the magnetic charge by q_m and its density and current by ρ_m and J_m, so that symmetrized Maxwell's equations are written as follows

$$\vec{\nabla}\cdot\vec{E} = \frac{\rho_e}{\varepsilon_0} \,, \tag{43}$$

$$\vec{\nabla}\times\vec{E} = -\mu_0 \vec{J}_m - \frac{\partial \vec{B}}{\partial t} \,, \tag{44}$$

$$\vec{\nabla}\times\vec{B} = \mu_0 \vec{J}_e + \frac{1}{c^2}\frac{\partial \vec{E}}{\partial t} \,, \tag{45}$$

and

$$\vec{\nabla}\;\cdot\;\vec{B} = \mu_0 \rho_m \,. \tag{46}$$

Lorentz force will have the form (Moulin, 2001 [3])

$$F = q_e(\vec{E} + \vec{v}\times\vec{B}) + q_m(\vec{B} - \frac{\vec{v}}{c^2}\times\vec{E}) \,. \tag{47}$$

But since (Arbab and Satti, 2009 [1])

$$\vec{B} = \frac{\vec{v}}{c^2} \times \vec{E} \tag{48}$$

the Lorentz force does not affect the magnetic charge whether it exists or not. Hence, the magnetic monopole does not manifest its self via Lorentz force. The magnetic field generated by the charged particle is in such a way that it does not influence the magnetic charge. Note also that the magnetic field created by the charged particle does not do work because $\vec{v} \cdot \vec{B}$. The above symmetrized Maxwell's equations have the duality transformations, i.e., $\vec{E} \to \vec{B}$, $\vec{B} \to -\vec{E}$.

Using the vector identity $\vec{\nabla} \cdot (\vec{A} \times \vec{C}) = \vec{C} \cdot (\vec{\nabla} \times \vec{A}) - - \vec{A} \cdot (\vec{\nabla} \times \vec{C})$, it is interesting to notice that the divergence of Eq. (48) vanishes, viz.,

$$\vec{\nabla} \cdot \vec{B} = \vec{\nabla} \cdot \left(\frac{\vec{v}}{c^2} \times \vec{E} \right) = \\ = \frac{1}{c^2} \left[\vec{E} \cdot (\vec{\nabla} \times \vec{v}) - \vec{v} \cdot (\vec{\nabla} \times \vec{E}) \right] = 0, \tag{49}$$

for a motion with constant velocity, where $\vec{\nabla} \times \vec{v} = 0$ and $\vec{v}$ is perpendicular to $\vec{\nabla} \times \vec{E}$.

6 The Biot-Savart law

We can now apply Eq. (48) to calculate the magnetic field acted on the electron in Hydrogen-like atoms. This magnetic field is produced by the moving electron due to the presence of an electric field created by the nucleus at a distance r, as seen by the electron. Therefore,

$$\vec{B} = \frac{\vec{v}}{c^2} \times \vec{E}\,, \tag{50}$$

where $\vec{E}$ is the electric produced by the nucleus at the electron site. The magnetic field due to a single moving charged particle (q) is given by the Biot-Savart law as

$$\vec{B} = \frac{\mu_0}{4\pi} \frac{q\,\vec{v} \times \vec{r}}{r^3}\,. \tag{51}$$

Comparing Eq. (50) with Eq. (51) and using the fact that $\mu_0 \varepsilon_0 c^2 = 1$, one gets

$$\vec{E} = \frac{q}{4\pi\varepsilon_0} \frac{\vec{r}}{r^3} \tag{52}$$

which is the familiar definition of the electric field of a single charged particle. Hence, Eq. (50) is one variant of Biot-Savart law. This law was not included in the original formulation of Maxwell's theory. Hence, Maxwell's equations were missing this law and thus were incomplete.

Since the electric field produced by the nucleus is perpendicular to the electron velocity, Eq. (50) yields

$$B = \frac{v}{c^2} E\,. \tag{53}$$

But for Hydrogen-like atoms

$$E = \frac{1}{4\pi\varepsilon_0} \frac{Ze}{r^2}\,, \tag{54}$$

so that one has

$$B = \frac{Zev}{4\pi\varepsilon_0 r^2}\,. \tag{55}$$

In terms of the orbital angular momentum (L) where $L = mvr$, one has

$$\vec{B} = \frac{Ze}{4\pi\varepsilon_0 mr^3} \vec{L}\,. \tag{56}$$

However, this is the same equation that is obtained using the Biot-Savart law. This is a remarkable result, and suggests that the relation $\vec{B} = \frac{\vec{v}}{c^2} \times \vec{E}$ is truly fundamental in electrodynamics. This term gives rise to the spin-orbit interaction described by

$$E_{\text{int}} = \frac{1}{4\pi\varepsilon_0} \frac{Ze^2}{m_e^2 c^2 r^3}\, \vec{S} \cdot \vec{L}\,. \tag{57}$$

A factor of $1/2$ correcting the above expression is introduced by Thomas leading to

$$E_{\text{int}} = \frac{1}{8\pi\varepsilon_0} \frac{Ze^2}{m_e^2 c^2 r^3}\, \vec{S} \cdot \vec{L}\,. \tag{58}$$

We now use the Biot-Savart law to demonstrate that $\vec{\nabla} \cdot \vec{B} = 0$. This law is written in the form

$$\vec{B} = \frac{\mu_0}{4\pi} \int \frac{\vec{J}(\vec{r}\,') \times (\vec{r} - \vec{r}\,')}{|\vec{r} - \vec{r}\,'|^3}\, d^3 r'\,. \tag{59}$$

Using the vector identity $\vec{\nabla} \cdot (\vec{A} \times \vec{C}) = \vec{C} \cdot (\vec{\nabla} \times \vec{A}) - - \vec{A} \cdot (\vec{\nabla} \times \vec{C})$, one has

$$\vec{\nabla} \cdot \int \left(\frac{\vec{J}(\vec{r}\,') \times (\vec{r} - \vec{r}\,')}{|\vec{r} - \vec{r}\,'|^3} \right) d^3 r' = \\ = \int \frac{(\vec{r} - \vec{r}\,')}{|\vec{r} - \vec{r}\,'|^3} \cdot \left(\vec{\nabla} \times \vec{J} \right) d^3 r' - \int \vec{J} \cdot \left(\vec{\nabla} \times \frac{(\vec{r} - \vec{r}\,')}{|\vec{r} - \vec{r}\,'|^3} \right) d^3 r'. \tag{60}$$

Because of Eq. (5) and the fact that the curl of any pure radial function is zero, i.e. $\vec{\nabla} \times (f(r)\,\hat{r}) = 0$, the first and the second term vanish, so that above equation yields

$$\vec{\nabla} \cdot \vec{B} = 0\,. \tag{61}$$

Now let us calculate the magnetic field at a distance r from the wire produced by an infinitely long wire carrying a current I . Using Ampere's law, this is given by

$$B = \frac{\mu_0 I}{2\pi r}\,. \tag{62}$$

However, using Eqs. (50) and (51) and the fact that $I\,t = q$ and $\vec{v}$ is perpendicular to $\vec{r}$, one finds that the magnetic

field sets up at a point P at a distance r is *not* instantaneous, but reaches after a passage of time

$$\Delta t = \frac{2r}{v}\,. \tag{63}$$

Placing a detector at a distance r from the wire, one can measured this time experimentally. $2\,r$ is the round trip distance covered by the mediator (photon) traveling with speed v to send the magnetic induction at a point P. This exhibits the causal behavior associated with the wave disturbance. This shows that an effect observed at the point r at time t is caused by the action of the source a distant r away at an earlier or retarded time $t' = t - r/c$.The time r/c is the time of propagation of the disturbance from the source to the point r. Because of this Maxwell's equations satisfy the causality principle. Notice that this magnetic field is not changing with time. This may help understand that photons are emitted and absorbed by electron continuously, asserting that the electromagnetic interaction is exchanged by a mediator, as advocated by the quantum field theory.

7 Concluding remarks

We have shown in this paper the importance of the new gauge transformations, and how they leave Maxwell's equations invariant. These are the continuity equations, the current-density transformations and the current-gauge field transformations. According to Noether's theorem, invariance of a Lagrangian under any transformation will give rise to a conserved quantity. Hence, we trust that there must be some deep connections of these transformations with other electrodynamics phenomena. We emphasize here how the relation $\vec{B} = \frac{\vec{v}}{c^2} \times \vec{E}$ is important in calculating magnetic fields produced by moving charged particle. This equation was missing in the derivation of Maxwell's equations. Note that this field is always perpendicular to the velocity of the particle, i.e., $\vec{v} \cdot \vec{B} = 0$. We have also found that $\vec{B} = \frac{\vec{v}}{c^2} \times \vec{E}$ is equivalent to Biot-Savart law. Thus, the quaternionic form of Maxwell's equations generalizes the ordinary Maxwell's equations and unified the Biot-Savart law with other electromagnetic laws. The magnetic charge (monopole) proposed by Dirac could exist in principle, but it doesn't feel the electromagnetic force. The generalized continuity equations are in agreement with Newton's second law of motion. Moreover, we have obtained the Euler and energy conservation equations from the quaternionic Newton's law. Application of these new gauge transformations in quantum field theory will be one of our future endeavor.

Acknowledgments

I would like to thank F. Amin for the enlightening and stimulating discussion.

Submitted on December 06, 2008 / Accepted on December 13, 2008

References

1. Arbab A.I. and Satti Z.A. *Progress in Physics*, 2009, v. 1, 8.
2. Dirac P.A.M. *Proc. Roy. Soc.*, 1931, v. A133, 60.; Dirac P.A.M. *Phys. Rev.*, 1948, v. 74, 817.
3. Moulin F. *Nuovo Cimento*, 2001, v. 116B, 869.
4. Wolfgang R. *Am. J. Phys.*, 1989, v. 57, 993.
5. Bjorken J.D. and Drell S.D. *Relativistic Quantum Mechanics*, McGraw-Hill Book Company, 1964.

Introducing the Table of the Elements of Anti-Substance, and the Theoretical Grounds to It

Albert Khazan
E-mail: albkhazan@.gmail.com

Herein we study how the Hyperbolic Law acts in the Periodic Table of Elements, in each of the four quadrants of the plane "molecular mass X — contents of element Y". It is shown that the symmetry of the equation $Y = K/X$ is permitted only in the 1st and 2nd quadrants. The negative numerical values on the X-axis, and also $K < 0$, testify that the 2nd quadrant should contain the elements and compounds of anti-substances.

1 Introduction

As can be seen in [1–4], our method has produced hyperbolas located in the first quadrant. At the same time, their second branches have not been investigated from the point of view of the hyperbolic law in the Periodic Table of Elements.

Its essence is reflected in the fact that in any chemical compound with molecular mass X referred to one gram-atom of a defined element K, its maintenance Y represents the equilateral hyperbola $Y = K/X$ whose top is located on the valid axis located in a corner at 45 degrees with respect to the abscissa in the positive direction.

2 Mathematical substantiation. A principle of symmetry

For any element $K > 0$ there is only one hyperbola consisting of two branches (in the first and the third quadrants). Hyperbolas with various values K cannot be imposed against each other. At each point of a hyperbola, there are coordinates according to the equation $XY = K$ where X and Y can have not only positive values, but also negative values. If we identify the set of hyperbolas at various values K, they can wholly fill the area of the rectangular corner XOY (the first quadrant). In mathematics, the two branches of an equilateral hyperbola are symmetric with respect to each other. The valid axis passes through the tops located in the first and third quadrants, and also through the center of symmetry. The normal to it is an imaginary axis, and also an axis of symmetry around which it is possible to combine both quadrants.

3 The comparative analysis of equilateral hyperbolas in the first and third quadrants

Let's consider the hyperbolas of Beryllium, Chromium, Mercury, and the last element identified by us, which we shall call 155 and which is represented in Fig. 1. Apparently, the ordinate of the curves is equal to unity, while the abscissa is 600. The tops of the curves are on the valid axis which is perpendicular to the imaginary axis, while their curvature decreases with the growth of molecular mass. These properties have been considered in detail in our previous works for the first quadrant, in which $Y = K/X$ (where $X > 0, Y > 0$).

If these hyperbolas are constructed in the coordinates $X < 0, Y < 0$, (at $K > 0$), they will take the place of the second branches and settle down in the third quadrant. Hence, the properties of these equilateral hyperbolas, proceeding from mathematical concepts, except for one, can be completely found. It is impossible to combine these curves in two quadrants as the axes X and Y have different names and, accordingly, we see that the scales are caused by chemical conditions.

This discrepancy can be excluded if we take advantage of the factor of scaling $M = 20.2895$ described in a previous work [1]. In a Fig. 2 the same hyperbolas in the coordinates transformed by means of M are shown: $X' = X/M$, $Y' = YM$. Apparently, the form and properties of the hyperbolas after transformation remain unchanged and prove the mathematical principles.

If now around an imaginary axis we make the third and the first quadrants overlap, it is possible to see that there is nearly full concurrence among the curves and valid axes (Fig. 3). However, there is some increase in the ordinates because the abscissa in Fig. 2 possesses a slightly higher value than that of the ordinate, which is easy to notice from the position of circles designating the second branches. It has no basic value since the initial scales of the coordinate axes are naturally various upon their schematic construction. Therefore, the corner of the valid axis seems to be less than 45 degrees though its equation is given by the equality $Y = X$. This fact is due to the scale of coordinate axes only. At identical values of X and Y, the tangent of the corner of an inclination of the valid axis of an equilateral hyperbola is equal to 1, while, at the same time, its top is defined as a root square of K and corresponds to the equality $X_0 = Y_0$.

It is necessary to note also that all the established laws apply extensively to adjacent hyperbolas of the kind given by $Y = 1 - KX$ [2].

4 Discussion of results

On the basis of our results, it is possible to draw a conclusion that the properties of hyperbolas described by $K = XY$, which is in first quadrant, prove to be true. The same holds for those in the third quadrant, where $K = (-X)(-Y)$. Hence,

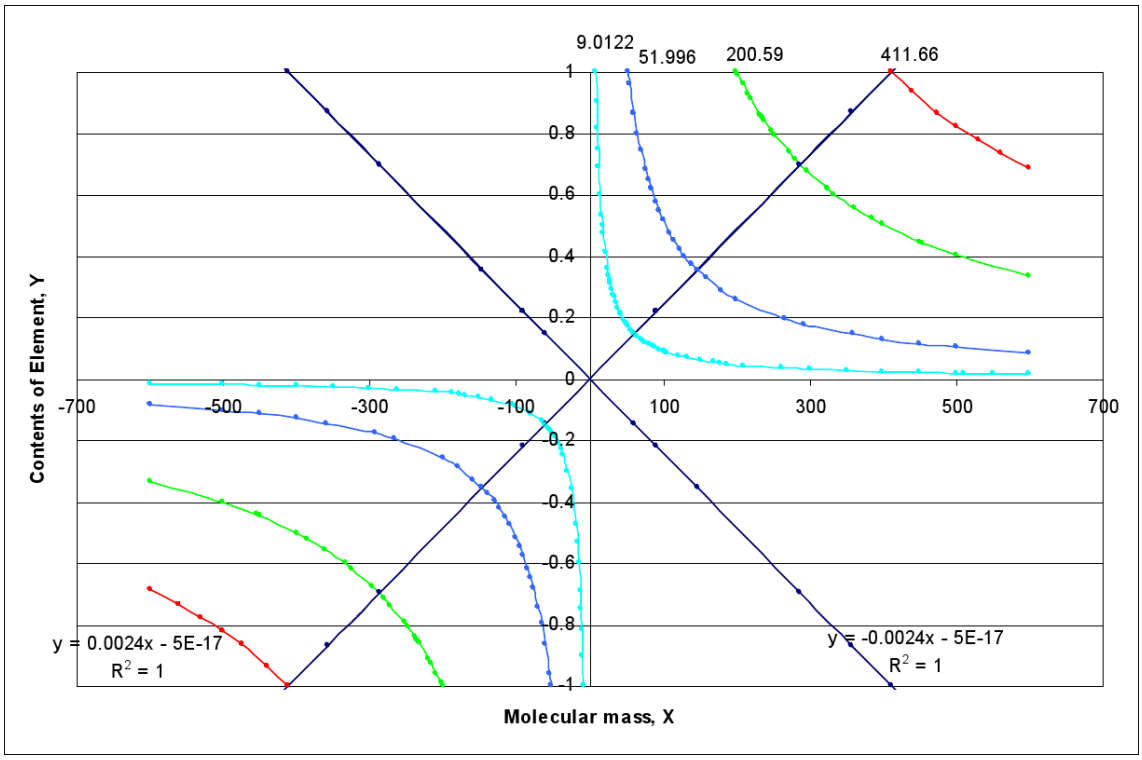

Fig. 1: Dependence of the contents of Be, Cr, Hg, No. 155 from molecular mass of the compounds.

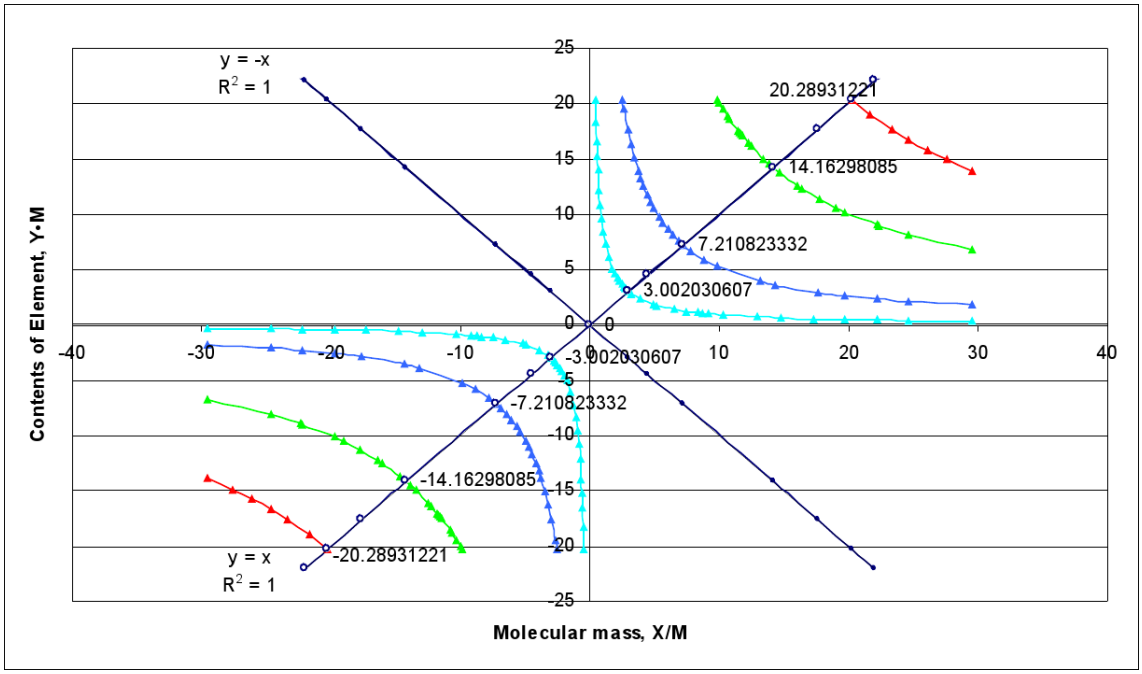

Fig. 2: Dependence of the contents of Be, Cr, Hg, No. 155 from molecular mass of the compounds, using the scaling coefficient M.

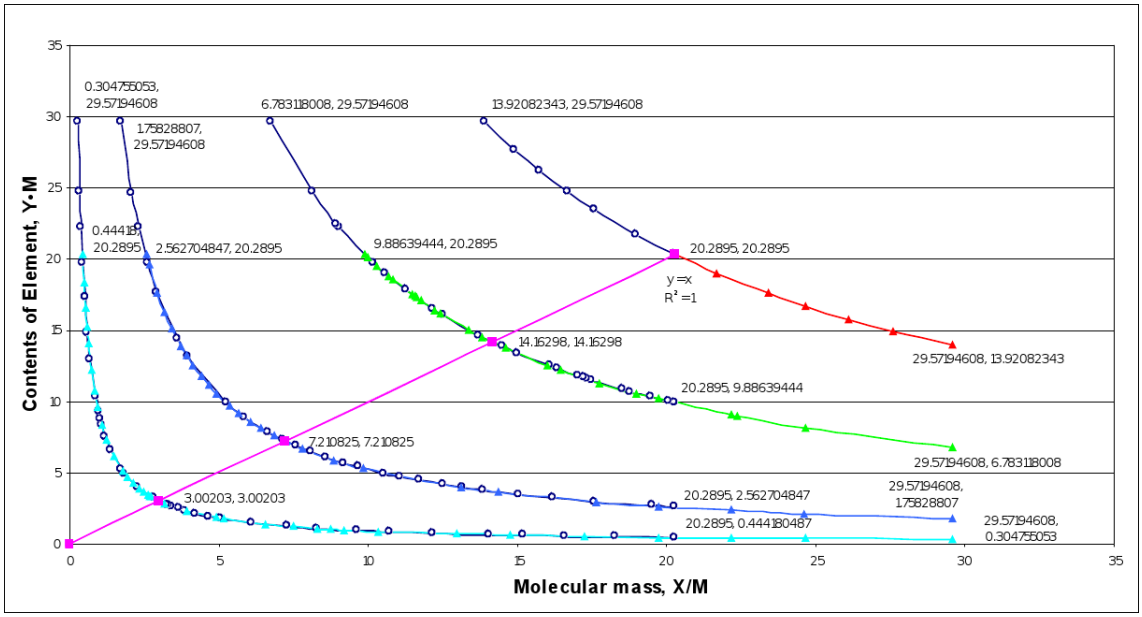

Fig. 3: The scale of the axes X and Y are numerically like each other, while the divisions of the scales are different. So, if a division is 3.075 in the axis X, while it is 1.75 in the axis Y. Under 60, the corner of the real axis gives 45°.

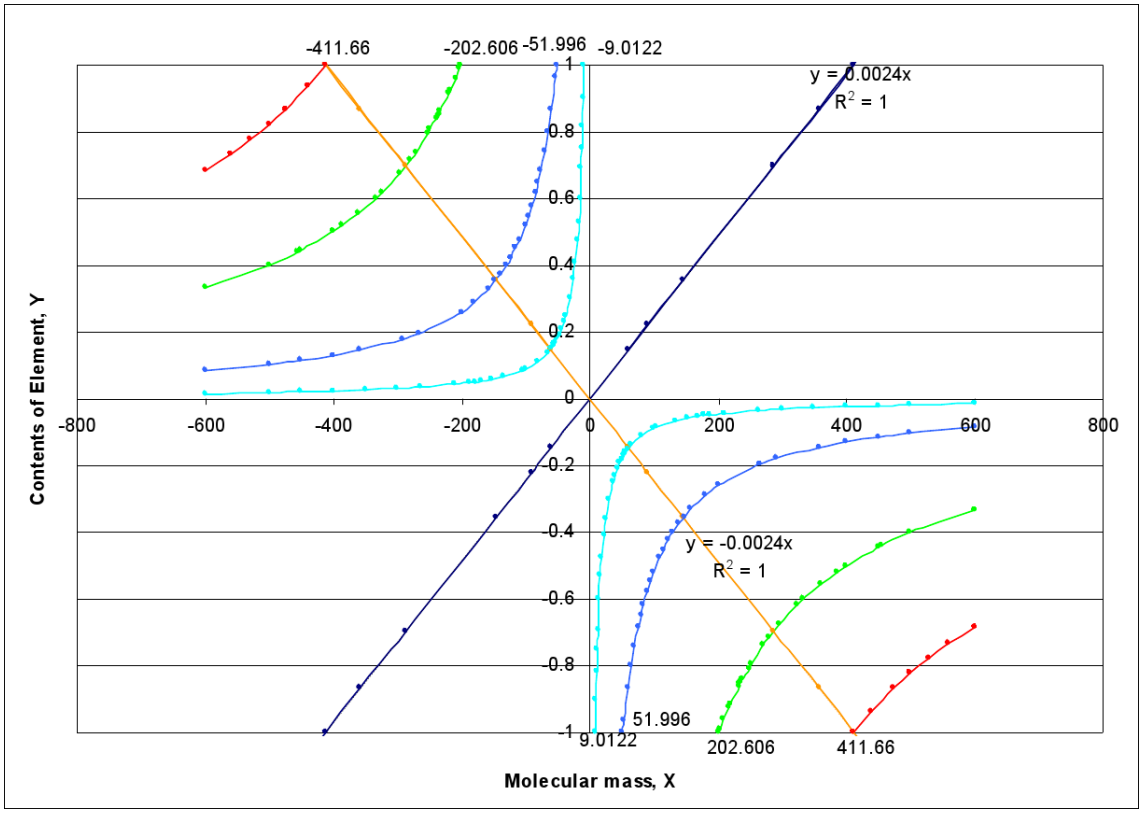

Fig. 4: Dependence of the contents of Be, Cr, Hg, No. 155 from molecular mass of the compounds in the 2nd and 4th quadrants.

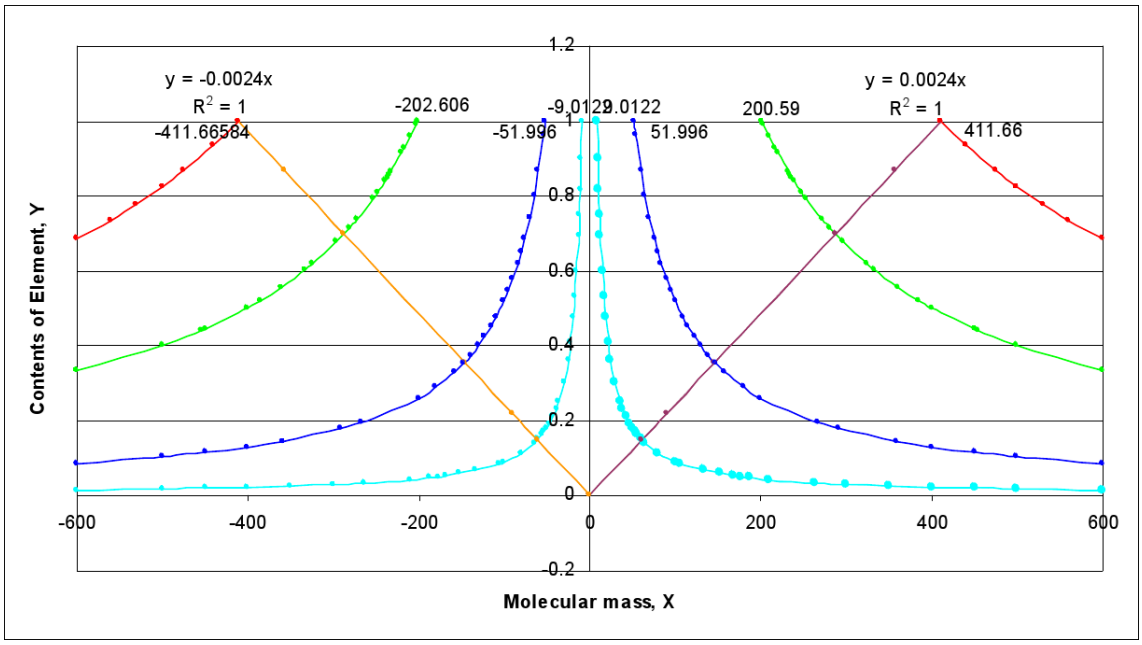

Fig. 5: Dependence of the contents of Be, Cr, Hg, No. 155 from molecular mass of the compounds in the 1st and 2nd quadrants.

1 H -	2A 2											3A 13	4A 14	5A 15	6A 16	7A 17	2 He -
3 Li -	4 Be -	3B 3	4B 4	5B 5	6B 6	7B 7	8	9	10	1B 11	2B 12	5 B -	6 C -	7 N -	8 O -	9 F -	10 Ne -
11 Na -	12 Mg -											13 Al -	14 Si -	15 P -	16 S -	17 Cl -	18 Ar -
19 K -	20 Ca -	21 Sc -	22 Ti -	23 V -	24 Cr -	25 Mn -	26 Fe -	27 Co -	28 Ni -	29 Cu -	30 Zn -	31 Ga -	32 Ge -	33 As -	34 Se -	35 Br -	36 Kr -
37 Rb -	38 Sr -	39 Y -	40 Zr -	41 Nb -	42 Mo -	43 Tc -	44 Ru -	45 Rh -	46 Pd -	47 Ag -	48 Cd -	49 In -	50 Sn -	51 Sb -	52 Te -	53 I -	54 Xe -
55 Cs -	56 Ba -	57-71	72 Hf -	73 Ta -	74 W -	75 Re -	76 Os -	77 Ir -	78 Pt -	79 Au -	80 Hg -	81 Tl -	82 Pb -	83 Bi -	84 Po -	85 At -	86 Rn -
87 Fr -	88 Ra -	89-103	104 Rf -	105 Db -	106 Sg -	107 Bh -	108 Hs -	109 Mt -	110 Ds -	111 Rg -	112 Uub -	113 Uut -	114 Uuq -	115 Uup -	116 Uuh -	117 Uus -	118 Uuo -

Lantanoids (upper row) and Actinoids (lower row)

57 La -	58 Ce -	59 Pr -	60 Nd -	61 Pm -	62 Sm -	63 Eu -	64 Gd -	65 Tb -	66 Dy -	67 Ho -	68 Er -	69 Tm -	70 Yb -	71 Lu -
89 Ac -	90 Th -	91 Pa -	92 U -	93 Np -	94 Pu -	95 Am -	96 Cm -	97 Bk -	98 Cf -	99 Es -	100 Fm -	101 Md -	102 No -	103 Lr -

8th period

119 -	120 -	121 -	122 -	123 -	124 -	125 -	126 -	127 -	128 -	129 -	130 -	131 -	132 -	133 -	134 -	135 -	136 -
137 -	138 -	139 -	140 -	141 -	142 -	143 -	144 -	145 -	146 -	147 -	148 -	149 -	150 -	151 -	152 -	153 -	154 -
155 -																	

s-block	alkaline metals and alkaline earth metals
d-block	transit metals
p-block	metals, metaloids and non-metals
f-block	lantanoids, actinoids
Short dash is signed in the Table for anti-elements	

Table 1: Eight periods of the Table of Substance and Anti-Substance.

the action of the Hyperbolic Law covers also an area of negative values of coordinate axes covering 155.

We recall the construction of hyperbolas at $K < 0$ (Fig. 4). Therefore, it has been established that in the second and the fourth quadrants of the hyperbolas, the same laws hold, which have also been established by us for the first and the third quadrants. It is caused by the fact that the equilateral hyperbolas have equal parameters on the module, but opposite in sign, namely, they are mutually interfaced and so possess identical properties. Therefore, proceeding from the chemical concepts, they can be symmetric only after changing the scale of the axes X, Y. Thus, referring to their congruence, unlike other mathematical conditions: curves coincide in the field of action of the factor M. Outside, its one hyperbola is generated as the abscissa increases, while the second corresponds to the increase in ordinate, not changing the direction of a curve. As it has appeared, absolute symmetry is available only on the axes X and Y.

Because in the third and fourth quadrants, a negative ordinate (a degree of transformation of a substance) cannot occur in Nature, we shall consider only quadrants 1 and 2.

From Fig. 5 it is seen that for $K > 0$ and $K < 0$ the congruence of hyperbolas and their valid axes are imposed against each other.

Corresponding to such symmetry, there is a question about the observation of chemical conditions. In the first quadrant, they have been considered in detail and do not cause doubts. In the second case (at $K < 0$) the abscissa is negative, and the ordinate is positive. Here the degree of transformation Y defined as the mass of an element (of one gram-atom), with respect to the corresponding molecular mass, is given by $Y = K/(-X)$, or, in other words, $K = (-X)Y$. From the point of view of mathematics, this result is fair. At the same time, physicists are in need of further necessary elaboration from the point of view of chemistry.

5 Substances and anti-substances

It is known that a Substance consists of atoms containing protons, neutrons, and electrons. An Anti-Substance differs only by the prefix "anti". In terms of chemical condition, all substances are divided into simple and complex (chemical compounds). They can be organic and inorganic.

As the Hyperbolic Law in the Periodic Table has been proved for hyperbolas of the first quadrant, there arises an idea to apply it also to the second quadrant. As the basis for this purpose, the quadrants are symmetric and the maintenance of elements in connection (Y) has a positive value. The difference consists only in those abscissas with opposite signs. But it is possible only when the molecular mass of a chemical compound has a minus sign. If, in the first quadrant, we arrange all possible hyperbolas around 155 inclusively, nothing prevents us from making the same apply to the second quadrant. Hence, in it there are substances with a minus sign, i.e., anti-substances constructed of anti-particles (similar to the substances in the first quadrant). With respect to mass, they are similar to a proton, neutron and, electron, only with an opposite (minus) sign.

From this it follows that it is possible to construct Table 1 (similar to the Periodic Table [3]) for the elements of anti-substances. For example, the known synthesized elements (their hyperbolas are more exact): anti-hydrogen, anti-deuterium, and anti-helium occupy symmetric places in both quadrants.

6 Conclusions

On the basis of symmetry with application of the Hyperbolic Law in the Periodic Table of Elements, the existence of anti-substances has been indirectly proved. As well, the construction of the various hyperbolas in the second quadrant and in the Table has been shown to be similar to that of the Periodic Table of Substances. It is clear that the third and fourth quadrants cannot be (directly) applied to calculation in the field of chemistry because the negative degree of transformation of substances does not exist.

Hence, it is now possible to draw a conclusion that the Hyperbolic Law established by us in the Periodic Table of Elements is generally true for the characteristics of not only substances, but also those of anti-substances. It also allows us to calculate all nuclear masses up to the last element (anti-element).

Submitted on December 04, 2008 / Accepted on December 23, 2008

References

1. Khazan A. Upper limit in the Periodic System of Elements. *Progress in Physics*, 2007, v. 1, 38–41.
2. Khazan A. Effect from Hyperbolic law in the Periodic Table of Elements. *Progress in Physics*, 2007, v. 2, 83–86.
3. Khazan A. Upper limit of the Periodic Table and synthesis of super heavy elements. *Progress in Physics*, 2007, v. 2, 104–109.
4. Khazan A. The rôle of the element Rhodium in the hyperbolic law of the Periodic Table of Elements. *Progress in Physics*, 2008, v. 3, 56–62.

Aspects of Stability and Quantum Mechanics

Robert Carroll

University of Illinois, Urbana, IL 61801, USA
E-mail: rcarroll@math.uiuc.edu

We comment on some work of Ruslov and Vlasenko indicating how stable Hamiltonian systems can be quantized under certain assumptions about the perturbations.

1 Introduction

In [7] we indicated some results of Rusov and Vlasenko [56, 57] involving Hamiltonian stability and quantization which we summarize here with a somewhat different interpretation. In [56, 57] (which are the same modulo typos and conclusions) one indicates how the work of Chetaev [9–11] (based in particular on classical results of Poincaré [52] and Lyapunov [39]) allow one to relate stability of classical systems to quantum mechanics in certain situations. We review here some of the arguments (cf. also [7, 55, 60] for additional material on the Poincaré-Chetaev equations).

One recalls that holonomic systems involve an agreement of the degrees of freedom with the number of independent variables. Then following [9] consider a holonomic system with Hamiltonian coordinates

$$\frac{dq_j}{dt} = \frac{\partial H}{\partial p_j};\ \frac{dp_j}{dt} = -\frac{\partial H}{\partial q_j} \tag{1.1}$$

and think of perturbations $(\mathbf{1A})$ $q_j = q_j(t) + \xi_j$ and $p_j = p_j(t) + \eta_j$. Denoting then $q_j \sim q_j(t)$ and $p_j \sim p_j(t)$ one has

$$\left.\begin{aligned} \frac{d(q_j+\xi_j)}{dt} &= \frac{\partial H(t, q_i+\xi_i, p_i+\eta_i)}{\partial p_j} \\ \frac{d(p_j+\eta_j)}{dt} &= -\frac{\partial H(t, q_i+\xi_i, p_i+\eta_i)}{\partial q_j} \end{aligned}\right\}. \tag{1.2}$$

Expanding and using (1.1) gives

$$\left.\begin{aligned} \frac{d\xi_j}{dt} &= \sum\left(\frac{\partial^2 H}{\partial p_j \partial q_i}\,\xi_i + \frac{\partial^2 H}{\partial p_j \partial p_i}\,\eta_i\right) + X_j \\ \frac{d\eta_j}{dt} &= -\sum\left(\frac{\partial^2 H}{\partial q_j \partial q_i}\,\xi_i + \frac{\partial^2 H}{\partial q_j \partial p_i}\,\eta_i\right) + Y_j \end{aligned}\right\}, \tag{1.3}$$

where the X_j, Y_j are higher order terms in ξ, η. The first approximations (with $X_j = Y_j = 0$) are referred to as Poincaré variational equations. Now given stability questions relative to functions Q_s of (t, q, p) one writes

$$x_s = Q_s(t, q_i+\xi_i, p_i+\eta_i) - Q_s(t, q_i, p_i) = \\ = \sum\left(\frac{\partial Q_s}{\partial q_i}\xi_i + \frac{\partial Q_s}{\partial p_i}\eta_i\right) + \cdots \tag{1.4}$$

which implies

$$\frac{dx_s}{dt} = \sum\left(\frac{\partial Q'_s}{\partial q_i}\xi_i + \frac{\partial Q'_s}{\partial p_i}\eta_i\right) + \cdots \tag{1.5}$$

where

$$Q'_s = \frac{\partial Q_s}{\partial t} + \sum\left(\frac{\partial Q_s}{\partial q_i}\frac{\partial H}{\partial p_i} - \frac{\partial Q_s}{\partial p_i}\frac{\partial H}{\partial q_i}\right). \tag{1.6}$$

Given $1 \leqslant s \leqslant 2k$ and $1 \leqslant i, j \leqslant k$ one can express the ξ_i, η_i in terms of x_s and write $(\mathbf{1B})$ $(dx_s/dt) = X_s$ (normal form) with $X_s(0) = 0$. For equations $(\mathbf{1B})$ with $1 \leqslant s \leqslant n$, for sufficiently small perturbations ϵ_j, ϵ'_j one assumes there exists some system of initial values x_{s0} with $\sum x_{s0}^2 < A$ for an arbitrarily small A (with perturbations ϵ_j, $\epsilon'_j \leqslant E_j$, E'_j). Further for arbitrarily small E_j, E'_j one assumes it is possible to find A as above such that there exists one or more values ϵ_j, ϵ'_j with absolute values $\leqslant E_j$, E'_j. Under these conditions the initial values of x_s play the same role for stability as the ϵ_j, ϵ'_j and one assumes this to hold. One assumes also convergent power series for the X_s etc. Then Lyapunov stability means that for arbitrary small A there exists λ such that for all perburbations x_{s0} satisfying $\sum x_{s0}^2 \leqslant \lambda$ and for all $t \geqslant t_0$ one has $\sum x_s^2 < A$ (i.e. the unperturbed motion is stable). Next one considers $t \geqslant t_0$ and $\sum x_s^2 \leqslant H$ and looks for a sign definite (Lyapunov) function V (with $V' = \partial_t V + \sum_1^n X_j(\partial V/\partial x_j)$ then sign definite of opposite sign or zero). If such a function exists the unperturbed motion is stable (see [9] for proof).

We pick up the story now in [10] where relations between optics and mechanics are also illuminated (but not considered here). Take a holonomic mechanical system with coordinates q_i and conjugate momenta p_i with n degrees of freedom. Assume the holonomic constraints are independent of time and the forces acting on the system are represented by a potential function $U(q_i)$. Let $(\mathbf{1C})$ $T = \frac{1}{2}\sum_{i,j} g_{ij}p_i p_j$ denote the kinetic energy where the $g_{ij} = g_{ji}$ are not dependent explicitly on time. Hamilton's equations have the form

$$2T = \sum g_{ij}\frac{\partial S}{\partial q_i}\frac{\partial S}{\partial q_j} = 2(U+E) \tag{1.7}$$

where E represents a kinetic energy constant (the sign of U is changed in Section 2). Here the integral of (1.7) is $(\mathbf{1D})$ $S(q_i, \alpha_i) + c$ with the α_i constants and $(\mathbf{1E})$ $||\partial^2 S/\partial q_i \partial \alpha_j|| \neq 0$ while $(\mathbf{1F})$ $E = E(\alpha_i)$. According to the Hamilton-Jacobi theory the general solution of the motion equations is given via $(\mathbf{1G})$ $p_i = \partial S/\partial q_i$ and $\beta_i = -t(\partial E/\partial \alpha_i) + \partial S/\partial \alpha_i$ where the β_i are constants. In order to determine a stable

solution one looks at the Poincaré variations

$$\left.\begin{aligned}\frac{d\xi_i}{dt} &= \sum_j \left(\frac{\partial^2 H}{\partial q_j \partial p_i}\,\xi_j + \frac{\partial^2 H}{\partial p_j \partial p_i}\,\eta_j\right)\\ \frac{d\eta_i}{dt} &= -\sum \left(\frac{\partial^2 H}{\partial q_j \partial q_i}\,\xi_j + \frac{\partial^2 H}{\partial p_j \partial q_i}\,\eta_j\right)\end{aligned}\right\}, \tag{1.8}$$

where H should be defined here via $(\mathbf{1H})$ $H = T - U$. For a stable unperturbed motion the differential equations for Poincaré variations (1.8) must be reducible by nonsingular transformation to a system of linear differential equations with constant coefficients all of whose characteristic values must be zero (recall that the Lyapunov characteristic value $X[f]$ of f is $X[f] = -\overline{\lim_{t\to\infty}}[\log(|f(t)|)/t]$ — cf. [39,40]). In such perturbed motion, because of $(\mathbf{1G})$ one has (recall $p_i \sim \partial S/\partial q_i$)

$$\eta_i = \sum_j \frac{\partial^2 S}{\partial q_i \partial q_j}\,\xi_j \;\; (i = 1, \cdots, n)\,. \tag{1.9}$$

Hence

$$\frac{d\xi_i}{dt} = \sum_{j,s} \xi_s \frac{\partial}{\partial q_s}\left(g_{ij}\frac{\partial S}{\partial q_j}\right) \;\; (i = 1, \cdots, n)\,. \tag{1.10}$$

Note here that (1.8) involves $\sum g_{ij}p_i p_j - U$ so

$$(\bigstar)\;\; \frac{\partial H}{\partial p_i} = \sum g_{ij}p_j; \quad \frac{\partial H}{\partial q_j} = \sum \frac{\partial g_{ij}}{\partial q_j}\,p_i p_j - \frac{\partial U}{\partial q_j}$$

and (1.10) says

$$(\bigstar\bigstar)\;\; \frac{d\xi_i}{dt} = \sum \xi_s \left(\frac{\partial g_{ij}}{\partial q_s}\frac{\partial S}{\partial q_j} + g_{ij}\frac{\partial^2 S}{\partial q_s \partial q_j}\right) = \\ = \sum \xi_s \frac{\partial g_{ij}}{\partial q_s}\frac{\partial S}{\partial q_j} + \sum g_{ij}\eta_j\,.$$

The second term here is $[\partial^2 H/\partial p_i \partial p_j]\,\eta_j$ and we want to identify the term $\xi_s(\partial g_{ij}/\partial q_s)(\partial S/\partial q_j)$ with $\partial^2 H/\partial q_s \partial p_i \xi_s$. However we can see that $\partial U/\partial p_i = 0$ so $\xi_s(\partial^2 H/\partial q_s \partial p_i) = \xi_s(2\partial^2 T/\partial q_s \partial p_i) = \xi_s(\partial g_{ij}/\partial q_s)p_j$ confirming (1.10). Here the q_i, α_i are represented by their values in an unperturbed motion. Now for a stable unperturbed motion let (1.10) be reducible by a nonsingular linear transformation $(\mathbf{1I})$ $x_i = \sum \gamma_{ij}\xi_j$ with a constant determinant $\Gamma = ||\gamma_{ij}||$. If ξ_{ir} $(r = 1, \cdots, n)$ are a normal system of independent solutions of (1.10) then $(\mathbf{1J})$ $x_{ir} = \sum_j \gamma_{ij}\xi_{jr}$ will be the solution for the reduced system. For a stable unperturbed motion all the characteristic values of the solutions x_{ir} $(i = 1, \cdots, n)$ are zero and consequently

$$||x_{sr}|| = C^* = ||\gamma_{sj}||\,||\xi_{jr}|| = \\ = \Gamma\, C \exp\left[\int \sum \frac{\partial}{\partial q_i}\left(g_{ij}\frac{\partial S}{\partial q_j}\right) dt\right]. \tag{1.11}$$

Consequently for a stable perturbed motion (cf. [9,39,40])

$$\sum \frac{\partial}{\partial q_i}\left(g_{ij}\frac{\partial S}{\partial q_j}\right) = 0\,. \tag{1.12}$$

2 Stability approach

Following Rusov and Vlasenko one writes an integral of the Hamilton-Jacobi (HJ) equation in the form $(\mathbf{2A})$ $S = f(t, q_i, \alpha_i) + A$ $(i = 1, \cdots, n)$ with the α_i arbitrary constants. The general solution is then $(\mathbf{2B})$ $p_i = \partial S/\partial q_i$ with $\beta_i = \partial S/\partial \alpha_i$ where the β_i are new constants of integration. The canonical equations of motion are $dq_i/dt = \partial H/\partial p_i$ and $dp_i/dt = -\partial H/\partial q_i$ where H is the Hamiltonian and under perturbations of the α_i, β_i one writes $\xi_i = \delta q_i = q_i - q_i(t)$ and $\eta_i = \delta p_i = p_i - p_i(t)$ and derives equations of first approximation

$$\left.\begin{aligned}\frac{d\xi_i}{dt} &= \sum \frac{\partial^2 H}{\partial q_j \partial p_i}\,\xi_j + \sum \frac{\partial^2 H}{\partial p_j \partial p_i}\,\eta_j\\ \frac{d\eta_i}{dt} &= -\sum \frac{\partial^2 H}{\partial q_j \partial q_i}\,\xi_j - \sum \frac{\partial^2 H}{\partial p_j \partial q_i}\,\eta_j\end{aligned}\right\} \tag{2.1}$$

as in (1.8). By differentiating in t one obtains then $(\mathbf{2C})$ $C = \sum(\xi_s\eta_s' - \eta_s\xi_s')$ where C is a constant. Also for given ξ_s, η_s there is always at least one solution ξ_s', η_x' for which $C \neq 0$. Stability considerations (as in form. 1.1) then lead via $(\bigstar)$ $\eta_i = \sum(\partial^2 S/\partial q_i \partial q_j)\xi_j$ and $(\mathbf{2D})$ $H = \frac{1}{2}\sum g_{ij}p_i p_j + U = T + U$ to

$$\frac{d\xi_i}{dt} = \sum \xi_s \frac{\partial}{\partial q_s}\left(g_{ij}\frac{\partial S}{\partial q_j}\right) \tag{2.2}$$

(note in Section 1 $H \sim T - U$ following [10] but we take now $U \to -U$ to agree with [56, 57] — the sign of U is not important here). According to [56, 57], based on results of Chetaev [10] (as portrayed in Section 1), it results that $L = \sum(\partial/\partial q_i)[g_{ij}(\partial S/\partial q_j)] = 0$ (as in form. 1.12) for stability (we mention e.g. [9–11,39,40,45] for stability theory, Lyapunov exponents, and all that).

REMARK 2.1. One also notes in [56, 57] that a similar result occurs for $(\bullet\bullet)$ $U \to U^* = U + Q$ for some natural Q and the stability condition (1.12) itself provides the natural introduction of quantization (see below). The perturbation relation in (1.9) is irrelevant to this feature (which we did not realize previously) and the quantum perturbations introduced via Q will satisfy the Heisenberg uncertainty principle as desired (cf. [3]). ■

Now one introduces a function $(\mathbf{2E})$ $\psi = A\exp(ikS)$ in (1.12) where k is constant and A is a real function of the coordinates q_i only. There results

$$\frac{\partial S}{\partial q_j} = \frac{1}{ik}\left(\frac{1}{\psi}\frac{\partial \psi}{\partial q_j} - \frac{1}{A}\frac{\partial A}{\partial q_j}\right) \tag{2.3}$$

so that (1.12) becomes

$$\sum_{i,j} \frac{\partial}{\partial q_i}\left[g_{ij}\left(\frac{1}{\psi}\frac{\partial \psi}{\partial q_j} - \frac{1}{A}\frac{\partial A}{\partial q_i}\right)\right] = 0\,. \tag{2.4}$$

On the other hand for the perturbed motion (with $U \to$

$\to U^* = U + Q$) the HJ equation can be written in the form

$$\frac{1}{2k^2}\sum_{i,j} g_{ij}\left[\frac{1}{\psi}\frac{\partial\psi}{\partial q_i} - \frac{1}{A}\frac{\partial A}{\partial q_i}\right]\left[\frac{1}{\psi}\frac{\partial\psi}{\partial q_j} - \frac{1}{A}\frac{\partial A}{\partial q_j}\right] = \\ = \partial_t S + U + Q \quad (2.5)$$

with $\partial_t S$ obtained via (**2E**). Adding (2.4) and (2.5) yields

$$\frac{1}{2k^2\psi}\sum_{i,j}\frac{\partial}{\partial q_i}\left(g_{ij}\frac{\partial\psi}{\partial q_j}\right) - \frac{1}{2k^2 A}\sum_{i,j}\frac{\partial}{\partial q_i}\left(g_{ij}\frac{\partial A}{\partial q_j}\right) - \\ - \frac{1}{k^2 A}\sum_{i,j} g_{ij}\frac{\partial A}{\partial q_j}\left(\frac{1}{\psi}\frac{\partial\psi}{\partial q_i} - \frac{1}{A}\frac{\partial A}{\partial q_i}\right) - \\ - \frac{1}{ikA\psi}\left[A\,\partial_t\psi - \psi\,\partial_t A\right] - U - Q = 0 \quad (2.6)$$

as a necessary stability condition (in the first approximation). Note (2.6) will not contain Q if A is defined via

$$\frac{1}{2k^2 A}\sum_{i,j}\frac{\partial}{\partial q_i}\left(g_{ij}\frac{\partial A}{\partial q_j}\right) + \\ + \frac{i}{kA}\sum_{i,j} g_{ij}\frac{\partial A}{\partial q_j}\frac{\partial S}{\partial q_i} - \frac{1}{ikA}\,\partial_t A + Q = 0 \quad (2.7)$$

which means

$$\left.\begin{aligned} Q &= -\frac{1}{2k^2 A}\sum_{i,j}\frac{\partial}{\partial q_i}\left(g_{ij}\frac{\partial A}{\partial q_j}\right) \\ \partial_t A &= -\sum_{i,j} g_{ij}\frac{\partial A}{\partial q_j}\frac{\partial S}{\partial q_i} \end{aligned}\right\}. \quad (2.8)$$

A discussion of the physical content of (2.8) appears in [56, 57] and given (2.8) the stability condition (2.6) leads to

$$\frac{i}{k}\,\partial_t\psi = -\frac{1}{2k^2}\sum_{i,j}\frac{\partial}{\partial q_i}\left(g_{ij}\frac{\partial\psi}{\partial q_j}\right) + U\psi \quad (2.9)$$

which is of course a SE for $k = 1/\hbar$ (this is the place where quantum mechanics somewhat abruptly enters the picture — see Remark 2.1). In fact for kinetic energy (**2F**) $T = \frac{1}{2m}\left[p_1^2 + \right.$ $\left. + p_2^2 + p_3^2\right]$ (2.9) leads to

$$Q = -\frac{\hbar^2}{2m}\frac{\Delta A}{A};\;\; \partial_t A = -\frac{1}{m}\sum\frac{\partial A}{\partial x_j}\,p_j;\;\; k = \frac{1}{\hbar} \quad (2.10)$$

and (2.9) becomes (note $A = A(q)$)

$$i\hbar\,\partial_t\psi = -\frac{\hbar^2}{2m}\Delta\psi + U\psi\,. \quad (2.11)$$

Going backwards now put the wave following function $\psi = A\exp(iS/\hbar)$ in (2.11) to obtain via (1.12) and (2.8) the Bohmian equations

$$\left.\begin{aligned} \partial_t A &= -\frac{1}{2m}\left[A\Delta S + 2\nabla A\cdot\nabla S\right] = -\nabla A\cdot\frac{\nabla S}{m} \\ \partial_t S &= -\left[\frac{(\nabla S)^2}{2m} + U - \frac{\hbar^2}{2m}\frac{\nabla A}{A}\right] \end{aligned}\right\}, \quad (2.12)$$

where the quantum potential QP is naturally identified.

If one writes now $P = \psi\psi^* = A^2$ then (2.12) can be rewritten in a familiar form

$$\left.\begin{aligned} &\partial_t P = -\nabla P\cdot\frac{\nabla S}{m} \\ &\partial_t S + \frac{(\nabla S)^2}{2m} + U - \\ &\qquad - \frac{\hbar^2}{4m}\left[\frac{\Delta P}{P} - \frac{1}{2}\frac{(\nabla P)^2}{P^2}\right] = 0 \end{aligned}\right\}. \quad (2.13)$$

That P is indeed a probability density is "substantiated" via a least action of perturbation principle attributed to Chetaev [11, 56, 57] which involves (**2G**) $\int Q|\psi^2|dV = \min$ where dV is a volume element with $\int|\psi|^2 dV = 1$ and this condition is claimed to be necessary for stability (one assumes that the influence of perturbative forces generated by Q is proportional to the density of trajectories $|\psi|^2 = A^2$ and dV cannot be a phase space volume element as stated in [56,57]). Write now, using (**2D**)

$$Q = -\partial_t S - U - T = -\partial_t S - U - \frac{1}{2}\sum g_{ij}\frac{\partial S}{\partial q_i}\frac{\partial S}{\partial q_j}\,. \quad (2.14)$$

Then if (**2E**) holds one can show that

$$\frac{1}{2}\sum g_{ij}\frac{\partial S}{\partial q_i}\frac{\partial S}{\partial q_j} = -\frac{1}{2k^2\psi^2}\sum g_{ij}\frac{\partial\psi}{\partial q_i}\frac{\partial\psi}{\partial q_j} + \\ + \frac{1}{2k^2 A^2}\sum g_{ij}\frac{\partial A}{\partial q_i}\frac{\partial A}{\partial q_j} + \frac{ik}{2k^2 A^2}\sum g_{ij}\frac{\partial A}{\partial q_i}\frac{\partial S}{\partial q_j}\,. \quad (2.15)$$

Then for the first term on the right side substitute its value from the first stability condition (2.4), then insert this relation into (2.15) and put the result into the equation (2.14) corresponding to the variational principle; the result is then (2.6) and consequently the resulting structure expression and the necessary condition for stability coincide with (2.8) and (2.9). This leads one to conclude that stability and (Bohmian) quantum mechanics are two complementary procedures of Hamiltonian theory. The authors cite an impressive list of references related to experimental work related to the analysis in [56,57].

3 The quantum potential

From Sections 1–2 we have seen that a stable Hamiltonian system as indicated gives rise to a quantum Schrödinger equation with quantum potential Q. It seems therefore appropriate to examine this in the light of other manifestations of the QP as in e.g. [3–6, 16–19, 24, 26–28, 30, 36, 37, 53]. We note that following [4] one can reverse some arguments involving the exact uncertainty principle (cf. [3,26–28,53]) to show that any SE described by a QP based on $|\psi|^2 = P$ can be modeled on a quantum model of a classical Hamiltonian H perturbed by a term H_Q based on Fisher information, namely

$$H_Q = \frac{c}{2m}\int\frac{(\nabla P)^2}{P}\,dx = \frac{c}{2m}\int P(\delta p)^2, \quad (3.1)$$

where $\delta p = \nabla P/P$. This does not of course deny the presence of "related" $x \sim q$ oscillations $\delta x \sim \delta q$ and in fact in Olavo [49] (cf. also [3]) Gaussian fluctuations in δq are indicated and related to δp via an exact uncertainty relation $(\mathbf{3A})$ $\overline{(\delta p)^2 \cdot (\delta q)^2} = \hbar^2/4$. We note that the arguments establishing exact uncertainty stipulate that the position uncertainty must be entirely characterized by $P = |\psi|^2$ (cf. [3,26–28,53]). Thus the quantum potential generates the quantum perturbations δp and these are essentially unrelated to the $\delta p \sim \eta_i$ of (1.9).

REMARK 3.1. We recall here [29] (cf. also [54]) were it is shown that quantum mechanics can be considered as a classical theory in which a Riemannian geometry is provided with the distance between states defined with natural units determined via Planck's constant (which is the inverse of the scalar curvature). ■

REMARK 3.2. In [2] one shows that non-relativistic quantum mechanics for a free particle emerges from classical mechanics via an invariance principle under transformations that preserve the Heisenberg inequality. The invariance imposes a change in the laws of classical mechanics corresponding to the classical to quantum transition. Some similarities to the Nottale theory of scale relativity in a fractal spacetime are also indicated (cf. [3, 8, 47, 48]). There are relations here to the Hall-Reginatto treatment which postulates that the non-classical momentum fluctuations are entirely determined by the position probability (as mentioned above). In Brenig's work one derives this from an invariance principle under scale transformations affecting the position and momentum uncertainties and preserving the Heisenberg inequality. One modifies the classical definition of momentum uncertainty in order to satisfy the imposed transformation rules and this modification is also constrained by conditions of causality and additivity of kinetic energy used by Hall-Reginatto. This leads to a complete specification of the functional dependance of the supplementary term corresponding to the modification which turns out to be proportional to the quantum potential. ■

REMARK 3.3. We note that in work of Grössing (cf. [6, 24]) one deals with subquantum thermal oscillations leading to momentum fluctuations $(\mathbf{3B})$ $\delta p = -(\hbar/2)(\nabla P/P)$ where P is a position probability density with $-\nabla \log(P) = \beta \nabla \mathcal{Q}$ for $\mathcal{Q}$ a thermal term (thus $P = c\exp(-\beta \mathcal{Q})$ where $\beta = 1/kT$ with k the Boltzman constant). This leads also to consideration of a diffusion process with osmotic velocity $\mathbf{u} \propto -\nabla \mathcal{Q}$ and produces a quantum potential

$$Q = \frac{\hbar^2}{4m}\left[\nabla^2 \tilde{\mathcal{Q}} - \frac{1}{D}\,\partial_t \tilde{\mathcal{Q}}\right] \tag{3.2}$$

where $\tilde{\mathcal{Q}} = \mathcal{Q}/kT$ and $D = \hbar/2m$ is a diffusion coefficient. Consequently (cf. [6] one has a Fisher information $(\mathbf{3C})$ $F \propto \beta^2 \int \exp(-\beta \mathcal{Q}(\nabla \mathcal{Q})^2 d^3x$. As in the preceeding discussions the fluctuations are generated by the position probability density and one expects a connection to (Bohmian) quantum mechanics (cf. [3, 12, 18, 19]). ■

REMARK 3.4. There is considerable literature devoted to the emergence of quantum mechanics from classical mechanics. There have also been many studies of stochastic and hydrodynamic models, or fractal situations, involving such situations and we mention in particular [1, 3–6, 8, 12, 13, 18–20, 23, 24, 26–28, 36, 37, 42–44, 46–49, 53, 58, 59, 61]; a survey of some of this appears in [3]. For various geometrical considerations related to the emergence question see also [14, 15, 25, 30–35, 51, 62] and in connection with chaos we cite e.g. [1, 25, 38, 41, 50, 51, 62, 63]. ■

Submitted on December 12, 2008 / Accepted on December 23, 2008

References

1. Benenti G., Casati G., and Strini G. Principles of quantum computation and information. Vols. 1 and 2. World Scientific, 2007.
2. Brenig L. *Jour. Phys. A*, 2007, v. 40, 4567–4584; arXiv: quant-ph/0608025.
3. Carroll R. Fluctuations, information, gravity and the quantum potential. Springer, 2006; On the quantum potential. Arima Publ., 2007.
4. Carroll R. *Teor. i Mat. Fiz.*, 2007, v. 152, 904–914.
5. Carroll R. *Prog. in Phys.*, 2007, v. 4, 22–24 and 2008, v. 1, 21–24 (preprinted in arXiV: math-ph/0703065 and 0710.4351); *Prog. in Phys.*, 2008, v. 2, 89–90 (preprinted in arXiv: math-ph/0712.3251).
6. Carroll R. arXiv: math-ph/0807.1320 and 0807.4158.
7. Carroll R. arXiv: math-ph/0808.2965.
8. Célérier M. and Nottale L. *Jour. Phys. A*, 2004, v. 37, 931; arXiv: hep-th/0112213 and 0210027.
9. Chetaev N. The stability of motion (Ustoichevost dvizhenia). Permagon, 1961; Theoretical mechanics. Mir-Springer, 1989.
10. Chetaev N. *Soviet Applied Math. and Mech.*, 1958, v. 22, 487–489.
11. Chetaev N. *Soviet Applied Math. and Mech.*, 1956, v. 20, 309–314; 1959, v. 23, 425–433; 1960, v. 24, 6–19, 23–32, 33–34.
12. Crowell L. Quantum fluctuations of spacetime. World Scientific, 2005.
13. Davidson M. *Jour. Math. Phys.*, 1979, v. 20, 1865–1869; arXiv: quant-ph/0112063, 0112076, 0112114, 0112099, 0112157, 0211097, and 0602211; *Annales L. de Broglie*, 2004, v. 29, 661–680.
14. Elitzur A., Dolev S., and Kolenda N. (Eds.). Quo vadis quantum mechanics. Springer, 2005.
15. Elze H. arXiv: gr-qc/0512016; quant-ph/0710.2765.
16. Frieden B. and Gatenby R. Exploratory data analysis using Fisher information. Springer, 2007.
17. Frieden B. Physics from Fisher information. Cambridge Univ. Press, 1998; Science from Fisher information. Springer, 2004.

18. Garbaczewski P. *Entropy*, 2005, v. 7, 253–299; *Jour. Stat. Phys.*, 2007, v. 123, 315–355.
19. Garbaczewski P. arXiv: cond-mat/0202463, 0211362, 0510533, 0706248, 0604538, and 0703147; quant-ph/0612151.
20. Gell-man M. and Tsallis C. Non-extensive entropy. Oxford Univ. Press, 2004.
21. de Gosson M. arXiv: quant-ph/0808.2774; Maslov classes, metaplectic representations, and Lagrangian quantization. Akad. Verlag, 1997.
22. de Gosson M. and Luef F. *Phys. Lett. A*, 2007, v. 364, 453–457.
23. Granik A. arXiv: quant-ph/0801.3311.
24. Grössing G. *Phys. Lett. A*, 2008, v. 372, 4556–4562; *Found. Phys. Lett.*, 2004, v. 17, 343–362; arXiv: quant-ph/0201035, 0205047, 0404030, 0410236, 0508079, and 0806.4462.
25. Gutzwiller M. Chaos in classical and quantum mechanics. Springer, 1990.
26. Hall M. and Reginatto M. *Jour. Phys. A*, 2002, v. 35, 3289–3303; *Fortschr. Phys.*, 2002, v. 50, 646–651; arXiv: quant-ph/0201084.
27. Hall M., Kumar K., and Reginatto M. *Jour. Phys. A*, 2003, v. 36, 9779–9794.
28. Hall M. arXiv: gr-qc/0408098, quant-ph/0007116; *Jour. Phys. A*, 2004, v. 37, 7799 and 9549 (preprinted in arXiv: quant-ph/0404123 and 0406054).
29. Heslot A. *Amer. Jour. Phys.*, 1983, v. 51, 1096–1102; *Phys. Rev. D*, 1985, v. 31, 1341–1348.
30. Hiley B. Quo vadis quantum mechanics. Springer, 2005, pp. 299–324.
31. Holland P. The quantum theory of motion. Cambridge Univ. Press, 1993.
32. 't Hooft G. arXiv: hep-th/0707.4568, quant-ph/0604008.
33. Isidro J., Santander J., and de Cordoba P.F. arXiv: hep-th/0808.2351 and 0808.2717; gr-qc/0804.0169.
34. Isidro J. arXiv: hep-th/0110151, 0204178, 0304175, 0407161, 0411015, and 0510075; quant-ph/0307172, 0310092, and 0407159.
35. Isidro J. and de Gosson M. arXiv: hep-th/0608087; quant-ph/0608093.
36. Kaniadakis G. arXiv: quant-ph/0112049.
37. Kaniadakis G. and Scarfone A. arXiv: cond-mat/0303334.
38. Klages R. Microscopic chaos, fractals, and transport in non-equilibrium statistical mechanics. World Scientific, 2007.
39. Lyapunov A. The general problem of stability of motion. Gostekhizdat, 1950; Princeton Univ. Press, 1947.
40. Malkin I. Theory of stability of motion. Gostekhizdat, 1952; Some problems in the theory of nonlinear oscillations. Gostekhizdat, 1956.
41. Magnitskij N. and Sidorov S. New methods for chaotic dynamics. World Scientific, 2006.
42. Nasiri S. arXiv: quant-ph/0511125.
43. Nasiri S., Sobouti Y., and Taati F. arXiv: quant-ph/0605129.
44. Nelson E. Quantum fluctuations. Princeton Univ. Press, 1985; Dynamical theory of Brownian motion. Princeton Univ. Press, 1967.
45. Nemytskii V. and Stepanov V. Qualitative theory of differential equations. Dover, 1989.
46. Nottale L. Fractal space-time and microphysics: Toward a theory of scale relativity. World Scientific, 1993.
47. Nottale L., Célérier M., and Lehner T. arXiv: hep-th/0407093.
48. Nottale L. and Célérier M. arXiv: quant-ph/0711.2418.
49. Olavo L. *Physica A*, 1999, v. 262, 197–214; 1999, v. 267, 260–302; *Phys. Rev. E*, 2001, v. 64, 036125.
50. Ott E. Chaos in dynamical systems. Cambridge Univ. Press, 2002.
51. Pettini M. Geometry and topology in Hamiltonian dynamics and statistical mechanics. Springer, 2007.
52. Poincaré H. New methods of celestial mechanics. Vols. 1–3. Dover, 1957.
53. Reginatto M. arXiv: quant-ph/9909065; gr-qc/0501030; *Phys. Rev. A*, 1998, v. 58, 1775–1778.
54. Rowe D., Ryman A., and Rosensteel G. *Phys. Rev. A*, 1980, v. 22, 2362–2373.
55. Rumyantsev V. *Soviet Applied Math. and Mech.*, 1996, v. 60, 899–909; 1994, v. 58, 373–386.
56. Rusov V. arXiv: quant-ph/0804.1427.
57. Rusov V. and Vlasenko D. arXiv: quant-ph/08064050.
58. Schuch D. *Inter. Jour. Quant. Chem.*, 1989, v. 23, 59–72; 1992, v. 42, 663–683.
59. Soubouti Y. and Nasiri S. *Inter. Jour. Mod. Phys. B*, 1993, v. 7, 3255–3272.
60. Stanuykovitch P., Kolesnikov S., and Moskovkin V. In: *Problems of Space, Time, and Matter Theory*, Atomizdat, 1968.
61. Tsekov R. *Jour. Phys. A*, 1995, v. 28, L557–L561; 2007, v. 40, 10945–10947; arXiv: quant-ph/07111442, 0803.4409, and 0808.0326.
62. Wyatt R. Quantum dynamics with trajectories. Springer, 2005.
63. Zaslavsky G. Hamilton chaos and fractional dynamics. Oxford Univ. Press, 2005.

On the Physical Model of the Phenomena Registered in the Experiments by Shnoll's Group and Smirnov's Group

Sergey A. Vasiliev

Scientific Research Institute of Exploration Geophysics VNII Geofizika (retired), Moscow 107140, Russia
Permanent address: 38 Nazliu Str., Palio Faliro, Athens 17564, Greece
E-mail: disput22@gmail.com

The study of experimental data leads to the conclusion about the existence of the fields of the Earth as not being of clear physical nature. The structure and properties of these fields on the Earth's surface are studied. These fields turn out to be related to the motions of matter and, in particular, to the internal motions of the Earth itself. Therefore, the fields may include precursors to earthquakes that conform to experiments. The disclosed statistical relations of seismicity with the planet configurations, sunrises and sunsets, and with the pulsar impact becomes logical. Other planets, the Sun and the Moon must possess the same fields.

1 Introduction

Nearly thirty years ago, Meidav and Sadeh [1] discovered the effect of pulsar CP1133 on seismicity that triggered the professionals' interest. Ya. B. Zeldovich immediately apprehended the potential meaning of this phenomenon. According to him, even if that message would be by ten per cent true, he would only engage himself with this issue. According to Weber, the energy of the pulsar gravitational waves is many orders of magnitude lower than that required for the detected pulsar effect on seismicity. The interest in this phenomenon gradually shrank to a nullity, mainly because this phenomenon had not acquired any reasonable interpretation. At about the same time, Ben-Menachem, the famous seismologist, detected a correlation between seismicity and sunrises-sunsets that could not be explained as well. As a consequence, the above Ben-Menachem's discovery was overridden, although he insisted that his experimental results were correct. Recently, Georgian seismologists have found a correlation between the planets' configuration and earthquakes [2]. Moreover, as it turned out, some distant planets rather than neighboring planets play a part in this correlation. T. Chernoglazova has disclosed a strong correlation between earthquakes and the coverings of the planets and the Sun by the Moon (in the sky). A. Ya. Lezdinsh has advanced further. He forecasts the epicenter, the time and the magnitude of the earthquakes at the same time for Kamchatka Peninsula by using the correlation between earthquakes and stellar bodies' positions relative to the Earth and the local horizon plane [3]. This method comes first in the open competition among many methods of earthquake forecast (with maximal magnitude error 0.4 point). At rises and settings, the upper and the lower culminations of the Sun, the Moon and the planets, Smirnov's detector (a specific gyroscope on a magnetic suspension) changes its average angular spin rate by 0.7–1.5% for a short period of time (generally, 1.5–3 minutes) [4–8]*. For instance, at the rises of Jupiter the gravitational effect on the detector is one and half billion times weaker than that of an observer moving around the detector†. However, the device responded to the planet but no to the observer. As in Refs. [1, 2, 3], here we again observe an effect of the planets on the motions in the Earth's region with a lack of the effective energy for such an event, and against all else, much more powerful effects. Smirnov's detector produces as well the anomalous signals, the strong earthquakes precursors for 2–10 days before strong earthquakes [9]. They are quite distinct from other signals due to their unusually high amplitude and extended duration (refer to Figs. 4 and 5 in Ref. [9]). Since Smirnov's detector indicates direction to the signal source as well, the perspective appears to find epicenters of the future strong earthquakes up to thousand kilometers off the detector that demands the labor-consuming but necessary forecast finalizing technique. Smirnov's and Shnoll's detectors respond to the same astronomical phenomena, but Shnoll's one shows variations not in angular velocity but in the G histogram shapes representing macroscopic fluctuations of the rates of physical processes‡. In their experiments, Shnoll's group [10–15] has studied G histograms for processes of different physical nature and different energy saturation, from radioactive decays and chemical reactions to the noises in gravitational antennas. Despite of the great differences in energy saturation of the above processes (forty orders of magnitude) their G histograms taken at the same time tend to look alike§. The effects of the Sun and the Moon on the G histograms have been disclosed. To put it differently, again a certain distant impact on the processes is disclosed in the absence of any accordance between the impact energy and the energies of the processes. According

*Developed by Kurchatov Institute of Atomic Energy and MEPHI.

†For proper calculation of the gravitational effect of planets, account must be taken of free falling of the Earth in an external gravity field.

‡Developed by Institute of Theoretical and Experimental Biophysics, Russian Academy of Science.

§More precisely, a probability increase of similar histograms occurrence is observed. For brevity's sake, this will be referred to as occurrence of similar histograms.

to S. E. Shnoll, the G histograms' shape variations are generated by space-time fluctuations, because, as pointed out, it is the only common factor for such different processes [14]. S. E. Shnoll has drawn attention to the important fact of the energy-free nature of the considered impacts [15]:

> "... The energy variation range for the processes under study equals tens of orders of magnitude. It is therefore clear that the "external force" that causes synchronous alteration of the histogram shapes is of the non-energy nature."

Recently, responding to my request, V. A. Zubov et al. (2008, Germany) have accordingly adjusted the technique of their experiments. As a consequence, their direct physical experiment has confirmed, at last, a significant impact of planets on the living matter on the Earth [20]. For instance, during the upper culmination of the Jupiter, the abrupt pulse variations in the mean molecular weight of potato biomatrix clusters, in terms of the number of the various clusters and their energy irradiation, were observed [20]:

> "During the Jupiter upper culmination the reliable picture of its effect on the potato biomatrix is disclosed. ... the Jupiter effect is unexpectedly strong during its culmination ... the commensurability of the planet and the Moon effects follows from the experimental data".

At least an approximate explanation of the above referred phenomena is in order. A physical model is created below as a logical consequence of the accumulated experimental material. The model allows us to approach the understanding of many of the described, seemingly paradoxical, facts. As long as the detectors are located on the Earth, as the unique planet, the effects of that can be studied in any direction relative to its center, whereas the effects of the other planets, the Sun and the Moon may be investigated on the Earth's orbit only. Shnoll's detector has been used in observations in various geographical regions, including the North Pole and Antarctica regions. Therefore our searching is based on the investigations of Shnoll's detector data and the corresponding impacts, mainly, of the Earth. This paper is based on the Refs. [16, 17].

2 Shnoll's detector data and the principles of their physical modeling

Initially the duration Dt of the histograms G was 1 hour. Presently, it has been reduced to less than a second. Let us denote the histogram with duration Dt confined to the time moment t as $G(t)$*. Let us denote the corresponding histograms from detectors A and B as $G_A(t)$ and $G_B(t)$, respectively. Using the detectors' data, observers can plot the graph of the probability of occurrence of the similar histogram shapes $G_B(t+\delta t^*)$ and $G_A(t)$ depending on the time shift δt^* and then seek a narrow peak (or peaks) of the probability increase and determine such time shift δt, at which a maximum peak occurs. (The peak width is usually equal to a few of the histograms durations Dt.) In what follows, the regularities of appearance of the similar histograms $G_B(t+\delta t)$ and $G_A(t)$ at the above maxima are studied depending on the time shift δt and on the detectors' locations. Let us conditionally denote the similarity of histograms as $G_B(t+\delta t) \approx G_A(t)$, and the coincidence of the histogram shapes as $G_B(t+\delta t) = G_A(t)$. The above equalities refer to the similarity of two histograms taken at the maxima of the aforesaid peaks, in the presence of these peaks, but not with respect to a random similarity of any pair of histograms. For brevity's sake only, the histograms $G_B(t+\delta t)$ and $G_A(t)$ similar at the above maxima denoted below shall simply be referred to as "similar histograms". A series of the cycles and the regularities in the occurrence of similar histograms has been determined. To understand the physical meaning of these cycles and regularities, the physical principles of their modeling should be established (listed below as enumerated notes).

Note 1: As mentioned above, the histogram shape varies with distance effects, at least, of the Sun and the Moon. In physics, the substance that transmits a distance effect is called a "field". Thus let us consider that the histogram shape is changed by some field† F (probably, of electromagnetic or gravitational origin). The field F may be multi-component (i.e. is composed of the sub-fields F_1, F_2, F_3, etc.) and many various sources of the field F may exist. To interpret Shnoll's detectors data, the following postulated rules will be used. The character of the field F impact on the detector is mapped into the histogram shape. The identical histogram shapes (at the maxima of the mentioned peaks) correspond to the identical impact character of the field F_i (where $i = 1, 2, 3, \dots$) from a single source, the histogram shapes at the mentioned maxima are not identical but only similar due to the different effects of the fields from others sources and/or other field components from the same source. Disclosed repetitions of similar histograms correspond to repetitions of the impact character of some field component F_i or of some field F. If one of the Moon, the Sun, and the Earth possesses a field F_i, then all of them possess this field‡. ■

According to Note 1, if the impact of the mentioned component on the detector is much stronger than other impacts, almost an identical histogram shape with almost a hundred percent probability should be observed. The Earth is surrounded by different celestial bodies. Of them, the highest variable impact on the Earth is caused by the Sun and the Moon. Their maximal impact should be expected when they are in the ray aimed at the Earth. Actually, during solar eclipses, several Shnoll's detectors located in different geo-

*For example, the time moment t may be the middle or the beginning of the $G(t)$ histogram.

†In the articles by Shnoll's team, a cloudy notion of some "structures" affecting the histograms is used. This one is used instead of the field notion. This one is not explained [15].

‡The fact that this statement is true becomes clear from the sub-section "About the reasons of the field beginning...".

graphical locations, produce at the same moment almost identical histograms with nearly a hundred percent probability [14]. This confirms the principles postulated in Note 1 and indicates also that the statistical properties of the macroscopic fluctuations, displayed by the histograms, are not random at all, but that they are distantly generated by celestial bodies, i.e. by their some field F. Thus an intensification of the impact of the field F (relative to the background) is displayed by the histograms through probability increase in the maxima of the above peaks. Therefore, through the histograms, one can judge about the character and relative strength of the impact of the field F and can also grade it using the probabilities at the maxima of the peaks. Then the field conception will start to possess the quantitative character. As far as the author knows, such dynamic investigations have not been performed yet. It is useful to perform them through a quantitative study of time and space distribution of the relative impact force, induced by each field component F_i from each source. For this purpose, localized observations at very short distances between the Shnoll detectors are most suitable [11]. According to experimental results, during the solar eclipse the above-mentioned peak's width is much shorter than the eclipse duration. Consequently, interaction between the field F from the Sun and the Moon at their junction is of a strongly marked, very short, splash-like character. Similar events happen during full-moon and new moon times [14].

Note 2: If an impact character on the detector is constant in time, then (in the absence of other impacts), according to Note 1, it induces histograms $G(t)$, whose shape is independent of time: $G_B(t+\delta t^*) = G(t)$ at any δt^*. As a consequence, there is no peak of histogram similarity at some definite time shift δt^*. Therefore, when the character of impact gradually becomes constant, the histogram similarity peak smears out gradually and disappears. Therefore, *the Shnoll technique based on the separation of the histogram similarity peaks is unable to identify impacts of constant character*. In this case, the Shnoll technique *gives the impression of an impact's absence, although the detector itself records both changing and constant impacts*. In the case of constant impact, another technique is required to investigate the near-zero temporal frequencies against the parameter δt^*. When a constant impact is considered in the background of a multiplicity of other changing impacts on the detector, conclusions remain the same, but the histogram shapes become rather similar than coincidental (this, of course, if a constant impact still remains visible in the presence of the other impacts). ■

Let $\{\mathrm{V}_d^m\}$ be the detector's movement parameters, where $m = 0, 1, 2, 3, \ldots$ and V_d^m is the m-th time derivative of the detector's speed V_d, $\mathrm{V}_d^0 \equiv \mathrm{V}_d$. The same set $\{\mathrm{V}_S^m\}$ denotes the movement's parameters of any object S.

Note 3: It is not excluded that the character of the impact on the detector is defined by both the field F and orientation O of some detector motion parameters $\mathrm{V}_{d,a}^m$ (belonging to a set $\{\mathrm{V}_d^m\}$), to be called active, relative to a ray L by which the field F arrives (similar to the case of a magnetic field and a moving electrical charge). The *force and character of the impact* may depend, of course, on the values of the motion parameters. Apparently, the active parameters $\mathrm{V}_{d,a}^m$ represent acceleration and/or acceleration derivative, and/or rate, etc. Let the field F, whose impact character depends also on the orientation O, be called the *second-type field* F_2 and be distinguished from the *first-type field* F_1, whose impact character is independent of the direction of the detector's motion parameter. If there is a dependence of the impacts on the motion parameters, let us consider the following: the Earth's field impact depends on the parameters of the detector's motion relative to the Earth, while the Sun's field impact depends on the parameters of the detector's motion relative to the Sun, etc. To put it differently, the impact of a field from some source depends on the detector's motion parameters relative to this source. The following question arises: whether or not the first and the second-type fields exist? ■

Generally, the experimental data will be studied in reference to a geocentric (GSC) and heliocentric (HSC) systems of coordinates. The GSC does not rotate relative to "motionless" stars. In the GSC, the Earth spins. In the GSC, let us determine the latitude φ and longitude θ of the Earth's surface points relative to the geographical Earth poles in the usual manner, but the meridian $\theta = \text{const}$ and the parallel $\varphi = \text{const}$ do not rotate relative to "motionless" stars. Let two detectors A and B be fixed on the Earth's surface and at time t in GSC have longitudes $\theta_A(t)$ and $\theta_B(t)$ and latitudes $\varphi_A(t)$ and $\varphi_B(t)$, respectively. For definiteness, if the detectors are located at different rotating geographical meridians, let us consider that the detector A is positioned ahead of detector B relative to the Earth's rotation direction. In the GSC system, detectors rotate about the Earth axis, moving along a motionless parallel given by $\varphi = \text{const}$.

According to the experiment [10, 11, 14], as the detector slides along the a motionless parallel $\varphi = \text{const}$, its histograms change, but the following equalities, which express the *effect of local sidereal time*, according to the terminology of experimentalists, stand:

$$G_B(t+\delta t_{ST}) \approx G_A(t) \text{ at } \varphi_A(t) = \varphi_B(t) = \text{const}, \quad (1)$$

$$G_B(t) \approx G_A(t) \text{ at } \theta_A(t) = \theta_B(t)\,, \quad (2)$$

$$G_A(t+T_{ST}) \approx G_A(t)\,, \quad (3)$$

where T_{ST} is the sidereal day, $\delta t_{ST} = t_{ST,A} - t_{ST,B}$, $t_{ST,A}$ and $t_{ST,B}$ are the local *sidereal* times at the locations of the detectors A and B, respectively. Sidereal day, T_{ST}, is the period of rotation of the Earth and the detectors in the GSC system about the Earth axis. In particular, in the GSC, at the moment $(t+T_{ST})$, the detector A returns to the same location, where it was at time t. In the GSC, when the detector is fixed at a geographical point on the Earth's surface, its parameters V_d^m are the same with the respective parameters $\mathrm{V}_d^{SPIN,m}$ of

the detector's fixation point's rotary (spin) motion about the Earth axis:

$$\mathrm{V}_d^m = \mathrm{V}_d^{SPIN,m}. \quad (4)$$

Obviously, the directions (and the values) of the parameters V_d^m of the detectors' rotary motion relative to the "motionless" stars are also repeated with the same period T_{ST} in the GSC system. The velocity V_d and its even order derivatives are directed along the tangent to the local parallel at the detector's location point. The odd-order derivatives of the rate V_d (including acceleration V_d^1) are directed along the local normal to the Earth's axis dropped from the detector's location point to the Earth axis. Therefore, in the GSC system, directions of the parameters V_d^m do not change along the meridians. In the GSC, the local sidereal times $t_{ST,A}$ and $t_{ST,B}$ unambiguously characterize the angle of detectors' rotation about the Earth axis relative to their initial position at the moment $t_{ST,A} = t_{ST,B} = 0$. In the GSC, the difference, δt_{ST}, represents a period of time, after which detector B arrives at the same place, where detector A was at the moment t. Therefore, by virtue of Note 1, the equalities (1)–(3) mean:

Statement 1: There are some fields F, whose summarized impact character at the Earth's surface points depends on the point location in the GSC, but not on time (equalities (1) and (3), and changes in the GSC along the motionless parallels and is constant along the motionless meridians of the Earth (formula 2). ■

For example, the effects (1)–(3) may be explained by the existence of the Earth's own field of the first type, not rotating in the GSC and changing along the motionless parallels but being constant along the motionless meridians of the Earth. The effects (1) and (3) may also be explained by the existence of an external field of the second type F_{2ext}, whose rays L_{2ext} are mutually parallel, and the field itself is constant at the Earth's orbit. According to Note 3, this shall lead to repetitions in the impact character of the field F_{2ext}, when the directions and magnitudes of the vectors V_d^m are repeated. By analogy, according to Note 3, the effect (2) can be caused by the Sun's field F_{2S}, of the second type, because the directions of the Sun rays and the parameters V_d^m along the Earth meridian do not virtually change, and, therefore, the angles between them do not change along this meridian as well. As can be seen, the use of only the local sidereal time effects gives multiple interpretations.

Just as the above, the effect of the *local solar time* has also been discovered experimentally [14] and is split into three equalities (detectors A and B are again fixed at the Earth's surface)

$$G_B(t + \delta t_S) \approx G_A(t) \text{ at } \varphi_A(t) = \varphi_B(t) = \text{const}, \quad (5)$$

$$G_B(t) \approx G_A(t) \text{ at } \theta_A(t) = \theta_B(t), \quad (6)$$

$$G_A(t + T_S) \approx G_A(t), \quad (7)$$

where T_S is the solar day; $\delta t_S = t_{S,A} - t_{S,B}$, $t_{S,A}$ and $t_{S,B}$ are the local *solar* times at the locations of the detectors A and B, respectively. The solar day, T_S, is the period of repetitions of the upper culmination of the Sun. By analogy, the effects of the local lunar time, the local planetary time, etc. may be introduced, but these effects have not been studied experimentally by Shnoll's group. Since the effects (5) and (7) include the local solar time, they obviously relate to the impacts of the Sun. Due to the Earth's motion along its orbit, the direction from the Earth to the Sun changes slightly, approximately by a degree per day. Therefore, the solar day is approximately 4 minutes longer than the sidereal day. The parameters V_d^m of the detector's motion relative to the Sun, i.e., in the HSC system, are composed of the detector's rotation relative to the Earth's axis (spin) and of its motion together with the Earth along its orbit. As a consequence, in the HSC system

$$\mathrm{V}_d^m = \mathrm{V}_d^{SPIN,m} + \mathrm{V}_d^{ORB,m}, \quad (8)$$

where $\mathrm{V}_d^{ORB,m}$ are the orbital motion parameters of the Earth and the detector. Despite the almost full coincidence of the formulae (1)–(3) and (5)–(7), their physical meaning is significantly different. Obviously, the orientation of the parameters $\mathrm{V}_d^{ORB,m}$ in relation to the Sun's ray, L_S, passing through the detector, does not change with time*. The orientation of parameters $\mathrm{V}_d^{SPIN,m}$ relative to the ray L_S, after a solar day T_S, is repeated with high accuracy. This repetition would have been exact, if the angle of the Earth axis to the ray L_S did not change during a solar day T_S, but as is known, it changes a little — by one fourth of a degree per day, approximately. Thereafter, the parameters of the spin motion of the detectors A and B at the times t and $t + \delta t_S$, respectively, have an almost equal orientation relative to the ray L_S. Therefore, by virtue of Note 3, the effects (5) and (7) can be explained by the existence of the Sun's field F_{2S} of the second type, almost or exactly cylindrically symmetrical relatively to the axis passing through the Earth's orbit center, and almost or exactly perpendicular to its plane. If, indeed, such the field F_{2S} does exist, its impact should be repeated almost or exactly everytime, when the orientation of the parameters $\mathrm{V}_d^{SPIN,m}$ relative to the ray L_S is repeated. This is really what happens according to the relations (5) and (7). The same effects could be explained in other ways. For example, by the repetitions of the total impact of the Sun's and Earth's fields, resulting from the repetitions of the angles between the solar ray L_S and the ray L_E of the Earth's own field radiated from the Earth's center or from its rotation axis. It is seen here again that the use of only the local solar time effects gives multiple interpretations.

Which field existence could be determined unambiguously? Let us answer this question using some other experiments. Experiments using collimators have the decisive meaning for answering the above question. As it turns out, the theoretical

*Within the accuracy of the Earth's orbit deviations from a circular orbit.

study of the experiments with collimators predicts many of the effects (1)–(3) and (5)–(7) as well as the results of other experiments. The study is based on the discovery and using of the significant differences of the physical meaning of experimental results obtained by using detectors of different types.

3 The particular rôle of the Shnoll radiation detectors

The effects of the local time (1)–(3), (5)–(7) are confirmed experimentally by the histograms records of processes of different physical nature. For example, there is a version of Shnoll's detector D_α based on the histograms recording of the quantity of the moving α-particles emitted by the compact radioactive source Plutonium-239 (^{239}Pu). Another version of the detector D_{noise} is based on the histograms recording of the noises in semiconductors. Seemingly, it's all the same, which physical process is used, because processes of different physical nature display similar histograms at the same time (see Introduction). Therefore, in the works of Shnoll's group, no difference is made between the physical meaning of the experimental results obtained by the detectors D_α and D_{noise}. However, in practice, the difference is considerable. Without the understanding of this, it is difficult to correctly understand the many valuable experimental results of Shnoll's group. This difference is essentially used below.

The motion parameters V_α^m of the α-particles emitted in different directions are differently oriented in space and, therefore, they are differently affected by the fields of the second type. If fields represented by F_2 exist, the histograms of the α-particles emitted in different directions should be different, i.e., at the level of macroscopic fluctuations an impression of the space anisotropy should be formed. The phenomenon described is, indeed, observed in the experiments with the collimators, which cut off pencils of the α-particles' emission directions [13, 14]. According to the results of all experiments with the collimators, S. E. Shnoll comes to a conclusion [14]:

> "... the shape of histograms depends on the α-particles' emission direction in relation to a particular point of the celestial sphere".

Theoretically, the impact character of the type-two field F_2 on any detector should be depended on the orientation O of the active detector motion parameters $\mathrm{V}_{d,a}^m$ relative to the ray L_2, by which the impact of the field F_2 comes to the detector. However, the points of the Earth equator are rotated by the Earth about its axis at the linear speed $V^{EQV} = 0.465$ km/s. The average speed of the Earth's orbital motion equals $V^{ORB} = 29.765$ km/s. The average kinetic energy of the α-particles emitted by Plutonium-239 equals 5.15 MeV, which corresponds to the α-particle emission speed of $V_\alpha = 15760$ km/s. Obviously, the speeds V^{EQV} and V^{ORB} are negligibly small in comparison with the speed V_α. The act of the α-particle irradiation is so short (tiny parts of a second) that for the acceleration and acceleration derivatives the ratios are very much not in favour of these motions of the Earth. Therefore, I conclude:

> Actually, the impact character of the type-two field F_2 on the detectors D_α is independent of the parameters $\mathrm{V}_d^{SPIN,m}$ and $\mathrm{V}_d^{ORB,m}$. This character depends only on the field F_2 and directions of the α-particles emission (used in the detector D_α) relative to the ray L_2.

In the collimator detector $D_{\alpha K}$, all parameters V_α^m of the α-particles motion are directed along the collimator. Hence, firstly, the detectors D_α are, in fact, inapplicable to the study of the effects on the histogram shapes of the directions and magnitudes of the vectors $\mathrm{V}_d^{SPIN,m}$ and $\mathrm{V}_d^{ORB,m}$. Secondly, the collimator detectors $D_{\alpha K}$ are almost the ideal tool for disclosing the second-type field and for the study of its impact character dependence on the angles between the motion parameters and ray L_2. General scheme of experiments for the disclosing of the field F_2 is simple: the collimator detector $D_{\alpha K}$ voluntarily, but periodically, with some period T, changes its direction relative to the ray L_2. Then, at each repetition of the orientation of the detector $D_{\alpha K}$ relative to the ray L_2, the repetitions of the impact character of the field F_2 and of the histogram similarity must be observed. Here it's all the same, either the collimator is fixed relative to the local horizon plane (LHP) and changes its direction periodically due to the Earth rotation or the detector direction is changed by an experimenter. To determine the direction, for instance, of the ray L_{2ext} of the field F_{2ext}, the collimator $D_{\alpha K}$ should periodically circumscribe a round cone with some cone axis O_K and some constant angle γ_K between the axis and generator of this cone. When the direction of the axis O_K approaches to an unknown direction of the ray L_{2ext}, the peak at the point $\delta t = T$ must gradually spread and disappear completely, when the directions of the axis O_K and ray L_{2ext} coincide. Indeed, when the axis O_K is parallel to the ray L_{2ext}, the angle between the ray L_{2ext} and the collimator is not changed if the latter circumscribes a round cone. Therefore, the impact character of the field F_{2ext} on the collimator's α-particles is permanently constant. Then according to Note 2, the narrow similarity peak disappears. The experiments with rotating collimators have been run in [13]. However, since the above specific rôle of the detectors $D_{\alpha K}$ has been unclear, it has also been impossible to understand what we are to do with the collimators and how we should understand the results of the experiments with the rotated collimators. Therefore, firstly, insufficient attention has been paid to the experiments with the rotated detectors $D_{\alpha K}$. As a result, such experiments has been run very little. Secondly, the results of these experiments have caused bewilderment among their authors [13]:

> "Despite the fact that the results obtained are quite clear, they cause natural bewilderment ... Apparently, explanation of these phenomena requires changes in the general physical concept".

The bewilderment was caused by dependence of the histogram shape on the collimator's direction, disclosed in [13]. Thirdly, the authors of the experiments have come to the main conclusion of the article [13] that the said angular dependence "*point to the sharp anisotropy of the space*". Fourthly, by means of the experiments with the detectors D_α, the impact character and histogram shape dependencies on the directions of the impacted object's motion parameters has not been investigated.

The bewilderment is resolved, if we take into consideration the angular dependence of the type- two field impacts on the moving α-particles, whose existence may be discovered just in the experiments with the rotated collimators. Obviously, not every angular dependence is equivalent to the space anisotropy. Therefore, the problem about the space anisotropy requires further development. If S. E. Shnoll is correct in the statement that changes in the histogram shape are induced by the fluctuations of the space-time properties [14], it is most likely, that the matter is thus: the type-two fields generate the space-time fluctuations; but in the near-Earth region the space is isotropic, and the small space fluctuations are anisotropic (more precisely, they depend on the angles between directions in the space and the ray of any type-two field). By the concourse of the circumstances, the experiments with the rotated collimators [13] coincide with the particular version of the above general scheme of the experiments for the detection of the field F_2 with the following particular parameters: the collimator circumscribes a round cone; the axis O_K is parallel to the Earth axis; $\gamma_K = 90^\circ$ (i.e. the collimator rotated in the local parallel plane $\varphi = \text{const}$); $T = \frac{1}{4}T_{ST}, \frac{1}{3}T_{ST}, \frac{1}{2}T_{ST}, T_{ST}$. These experiments are suitable for the disclosure of the type-two fields of the Sun, the Earth and the sources external to the Solar System. The experiments for the determination of the direction of the ray of the external field F_2 have not been carried out.

Note 4 (on the technology of the experiments): In the plate-type detectors $D_{\alpha P}$, the point-like radioactive source is located so close to the plate P detecting the α-particles that nearly half of all α-particles are detected. In this case, the α-particles are detected at once upon the setting of directions of the emission. This is equivalent to the integral detection of the α-particles by the many differently directed collimator detectors $D_{\alpha K}$. The central direction of the α-particles' entrapment coincides with the line perpendicular to the plate. Let's draw the perpendicular line through the plate center. By symmetry, the directional diagram of the detector $D_{\alpha P}$ is symmetrical relative to this perpendicular line. Therefore, the direction of this perpendicular line characterizes the directivity of the detector $D_{\alpha P}$ and its orientation in space. This perpendicular line we shall name the axis of the detector $D_{\alpha P}$ and we shall denote it as $O_{\alpha P}$. In the experiments, the plate P was always fixed horizontally relative to LHP and, consequently, was turned about the Earth axis together with LHP and the parameters $\mathrm{V}_d^{SPIN,m}$. Hence:

> During the Earth rotation, the spatial orientations of the detector $D_{\alpha P}$, LHP and parameters $\mathrm{V}_d^{SPIN,m}$ are always changed synchronously and equally.

Primarily, the effects of the local time (1)–(3), (5)–(7) was disclosed by the plate-type detector $D_{\alpha P}$ and then confirmed by the noise detector D_{noise}. ■

4 The disclosure and the cylindrical symmetry properties of the type two field F_2

Let F_{2ext} be some second-type field, external in relation to the Solar System, whose ray L_{2ext} and the field F_{2ext} itself are constant within the spatial area covered by the Solar System during the entire period of the experiments. How can we disclose the field F_{2ext} and determine the direction of its ray? In accordance with the above-mentioned general scheme, we should change the direction of the collimator $D_{\alpha K}$ relative to "motionless" stars almost voluntarily but periodically, with a voluntarily chosen period T. Then the collimator's orientation (and the parameters V_α^m of the motion of the α-particles) relative to an unknown but constant direction of the ray L_{2ext} will be repeated with the period T. This will induce the similarity between the histograms $G_K(t)$ of the detector $D_{\alpha K}$ separated in time by period T, i.e., the following equality will be fulfilled:

$$G_K(t+T) \approx G_K(t)\,, \tag{9}$$

which usually has a clear narrow peak by the parameter δt^*. This similarity will be the indicator of the existence of the field F_{2ext}. In realized collimator experiences, the axis O_K is parallel to the Earth axis and, hence, has constant orientation relative to the system of "motionless" stars (which is accurate to small deviations). Therefore these experiences are suitable for the detection of the field F_{2ext}. These experiences were performed at the periods $T = \frac{1}{4}T_{ST}, \frac{1}{3}T_{ST}, \frac{1}{2}T_{ST}, T_{ST}$. For all the mentioned periods, the delineated (by δt^*) narrow peak of the histogram similarity (9) was disclosed [13]. Hence, *the field F_{2ext} exists**. Taking into account the physical model developed here, it is useful to determine the direction of the ray L_{2ext} and the force of the field F_{2ext}, making clear, first of all, whether it comes from the Galactic Plane or from some external source relative to the Galaxy. Many fields, such F_{2ext}, may indeed occur†. Therefore, one may

*At time T_{ST}, the detector returns to the same point in the GSC system. Therefore, if $T = T_{ST}$, the histogram similarity (9) is also caused by the Earth's field of the first type (see below). At $T = \frac{1}{4}T_{ST}, \frac{1}{3}T_{ST}$, the only parameter, which is repeated with the period T, is the collimator orientation relative to "motionless" stars and the ray L_{2ext}. Hence, at $T = \frac{1}{4}T_{ST}, \frac{1}{3}T_{ST}$ the histogram similarity (3) unambiguously occurs due to the existence of the field F_{2ext} that makes sense of the experiments with $T = \frac{1}{4}T_{ST}, \frac{1}{3}T_{ST}$.

†During a single day, the direction of the ray from remote planets relative to "motionless" stars is almost not changed.

expect to get an interesting and informative investigation result.

If the detectors A and B from equalities (1)–(3) and (5)–(7) are the plate-type detectors, $D_{\alpha P}$, let us denote them as $D_{\alpha PA}$ and $D_{\alpha PB}$, respectively. When they are the noise detectors, D_{noise}, let us denote them as D_{noiseA} and D_{noiseB}.

> The existence of the field F_{2ext} explains the effects (1) and (3) in the experiments with the detectors $D_{\alpha P}$, since the orientation of the detector $D_{\alpha PA}$, in relation to the ray L_{2ext}, is repeated after the period T_{ST}, and the orientation of the detector $D_{\alpha PB}$ in relation to the ray L_{2ext} at the moment $t + \delta t_{ST}$ repeats the orientation of the detector $D_{\alpha PA}$ at the moment t (see Note 4 and Section 3).

If we do not neglect the orbital motion, the existence of the field F_{2ext} cannot explain the effects (1) and (3) in the experiments with the noise detector D_{noise} as, by virtue of equality (8), in the times δt_{ST} and T_{ST} there are no the corresponding repetitions of the directions of the detector's parameters V_d^m relative to the ray L_{2ext} because of the Earth's orbital motion. Probably, the effects (1) and (3) are generated in the noise detector by any other field (about this, see Section 5 "The disclosure and constancy of the type-one field F_1 along meridians").

By analogy, the disclosure of the type-two field F_{2S} of the Sun requires a periodical, with voluntarily chosen period T, variation of the orientation of the collimator $D_{\alpha K}$ in relation to the solar ray L_S passing through the detector $D_{\alpha K}$. But in practice, the period of the previous experiments may be used. For example, at $T = \frac{1}{4} T_{ST}$ the collimator is rotated in the plane of the local parallel (and, therefore, in the plane of the local celestial equator) with quadruplicated angular velocity of the Earth. Therefore the collimator almost exactly repeats its orientation in relation to the ray L_S in one forth of the solar day T_S. Indeed, in the experiments, the similarity of the histograms $G_K(t + \frac{1}{4} T_S)$ and $G_K(t)$ have been determined [13]:

$$G_K \left(t + \frac{1}{4} T_S \right) \approx G_K(t) \,. \tag{10}$$

In the time interval $\frac{1}{4} T_S$, nothing but ψ_α^m is repeated where ψ_α^m are the angles between the parameters V_α^m of the motion of α-particles and the solar ray L_S. As a consequence, the effect (10) is the result of the Sun's field impact, moreover, of the type-two field F_{2S}, because its impact depends on the above angles. The same is also confirmed experimentally at the repetition of the above angles during the time intervals $\frac{1}{3} T_S$, $\frac{1}{2} T_S$, and T_S. Thus:

> The Sun's field of the second type F_{2S} and the active motion parameters exist.

Which ones are the active motion parameters? This has not been determined experimentally. At the time lapse of 529600 minutes, i.e., at the time of an integer number of the solar days nearest to the sidereal year $T_{SID} = 525969$ min, the orientations of the detectors $D_{\alpha P}$ and $D_{\alpha K}$ relative to the direction to the Sun are also repeated, and the histogram similarity should occur, too. The required experiments were performed with the plate-type detector $D_{\alpha P}$. The experiments demonstrate [14] the presence of the effect that is the additional confirmation of the existence of the field F_{2S}. The histogram similarity after the time lapse of 529600 minutes was detected accurate to within a minute. At the time of a solar day T_S, the orientation of the detector $D_{\alpha PA}$ relative to the ray L_S is repeated. Under the condition $\varphi_A(t) = \varphi_B(t) =$ const, the orientation of the detector $D_{\alpha PB}$ relative to the ray L_S at the moment $t + \delta t_S$ repeats the orientation of the detector $D_{\alpha PA}$ at the moment t.

> Therefore, the existence of the type-two field F_{2S} of the Sun must lead to the effects (5) and (7) in the experiments with the detectors $D_{\alpha P}$ but only under the condition that the field F_{2S} is accurately, or sufficiently accurately, cylindrically symmetrical about the Earth's orbital axis, at least, in the orbital plane.*

The last condition is fulfilled because the effects (5) and (7) are indeed observed in the experiments with the detector $D_{\alpha P}$. Why is this condition fulfilled? The fact is that the experiment has confirmed (see below) the cylindrical symmetry of the type-two field of the Earth relative to the Earth's rotation axis. As a consequence, the Sun's field F_{2S} should be cylindrically symmetrical about the Sun's rotation axis. The rotation axis of the Sun is approximately normal to the Earth's orbit plane that leads to a sufficiently low deviation of the field F_{2S} from the cylindrical symmetry about the Earth's orbital axis. It is easier to study the field of the second type in the example of the Earth, because in relation to it the experiments are more accessible (with the reason presented below).

> The field F_{2S} induces all effects (5) and (7), and in the experiments with the noise detectors.

Indeed, in the period of a Sun's day T_S, the orientation of the moving parameters $\mathrm{V}_d^m = \mathrm{V}_d^{SPIN,m} + \mathrm{V}_d^{ORB,m}$ of the detector D_{noiseA} relative to the solar ray L_S is repeated. Under the condition $\varphi_A(t) = \varphi_B(t) =$ const, the orientation of the moving parameters of the detector D_{noiseB} relative to the solar ray L_S at moment $t + \delta t_S$ repeats the moving parameters orientation of the detector D_{noiseA} that the last had relative to the ray L_S at the moment t. In this reason, the effects (5) and (7) arise as it will be shown shortly.

Does the Earth has its own field F_{2E} of the second type, cylindrically symmetrical relative to the Earth's rotation axis? The presence of the field F_{2E} may be checked experimentally, for whose purpose let us compose an appropriate experiment.

*The impact character of the field F_{2S} depends on both the said orientations and the field F_{2S} itself. If the field F_{2S} does not possess the said symmetry, it changes along the Earth's orbit, which prevents the occurrence of the effects (5) and (7).

By virtue of the cylindrical symmetry, the field F_{2E}, if it exists, comes from, as it were, from the Earth axis by the ray L_E perpendicular to the Earth axis (in the Earth's areas outlying from its poles). Let us use the noise detector D_{noise}. Then the impact character of the field F_{2E} on the detector should depend on the orientation of the active motion parameters $\mathrm{V}^m_{d,a}$ of the detector relative to the ray L_E passing through the detector. According to Note 3, the motion parameters should be considered in the GSC system.

> In the framework of Shnoll's technique, it is useless to fix a detector D_{noise} on the rotating Earth surface.

This is because in this case they will be moved in the GSC system along the motionless parallels $\varphi = \text{const}$ and have constant orientation and magnitudes of its parameters $\mathrm{V}^m_{d,a}$ relative to the ray L_E passing through the detector. Hence, the impact character of the field F_{2E} on each detector will be constant in time.

> Then, by virtue of Note 2, the Shnoll technique may not determine the existence of the field F_{2E}.*

Therefore, let us detach some detectors from the Earth's surface and begin to move them in the GSC system not in parallel to the motionless parallels $\varphi = \text{const}$. Then in the GSC system, every detector $D_{noise,n}$ $(n = 1, 2, 3, \ldots, N)$ has time-dependent active motion parameters $\mathrm{V}^m_{d,a,n}(t)$. The detector D_n crosses the motionless parallel $\varphi = \text{const}$ at some point Q_n, at some moment of time t_n. Vectors $\mathrm{V}^m_{d,a,n}(t_n)$ are the active motion parameters of the detector $D_{noise,n}$ at the moments t_n of the intersections by the detector of the motionless parallel $\varphi = \text{const}$, that is at the point Q_n. Let the following condition be observed: the points Q_n do not coincide among themselves; the magnitudes and orientations of the active motion parameters $\mathrm{V}^m_{d,a,n}(t_n)$ relative to the ray L_E passing through the detector $D_{noise,n}$ are the same for all detector $D_{noise,n}$. Under the condition, despite the differences between the points Q_n, the field F_{2E} impact character on all detectors at the moments of their crossing of the parallel $\varphi = \text{const}$ must be the same that should generate the appropriate histograms similarity. The histogram of the detector $D_{noise,n}$ timed to moment t will be denoted as $G_n(t)$. As a consequence, the following equality must be observed:

$$G_1(t_1) \approx G_2(t_2) \approx G_3(t_3) \approx \cdots \approx G_N(t_N)\,. \qquad (11)$$

The particular case of the above described experiment with two detectors, that were detached from the Earth's surface and placed on board of the same aircraft flying to the north at a constant speed relative to the Earth's rotating surface, was performed in [12]. In principle, the detectors may be placed on board of different aircrafts, which fly differently, providing that the above conditions is observed. In [12], one detector was located northward from another. In the GSC system, the aircraft is shifted eastward by the Earth rotation. Therefore, in the GSC system, the detectors cross the parallel $\varphi = \text{const}$ at some different points Q_1 and Q_2. Obviously, the above conditions is observed. As a result, in these different points of the parallel, the expressed peak of the histograms $G_1(t_1)$ and $G_2(t_2)$ similarity (11) was really detected, i.e.:

$$G_1(t_1) \approx G_2(t_2)\,, \qquad (12)$$

or, in other words:

> This fact experimentally confirms existence of the field F_{2E} of the Earth.†

If only the field F_{2E} does not change along the meridians, the similar histograms would occur equiprobably at different time shifts within the value $t_2 - t_1$, and the histogram similarity peak (12) would smears out and disappears (see Note 2). Hence, the field F_{2E} changes along the meridians. Not simple but useful is to broaden the experiment, as it is described above, for studying of the impacts' dependence on the values and directions of the detector motion parameters relative to the Earth's axis and the ray L_E passing through the detector.

> It is much simpler to perform these investigations in a laboratory by moving the detector relative to a rotating massive body, because the last must, as it will be seen, also generate the second type field and, since it is clear now how the detector should be moved to study the field impact.

By the opinion of experimenters, this experiment "confirms the hypothesis that the local time effect is induced by systematic motion in a heterogeneous alternating space" [12]. Contrary to the above opinion, this experiment bears no relation to the local time effect, but represents a new, long-awaited result [16], which experimentally confirms the existence of the Earth's field F_{2E} of the second type. The above experiment would relate to the local time effects, if the second detector in GSC enters the same point of the same motionless parallel, where the first detector has occurred before, i.e. if points Q_1 and Q_2 are the same, as required by the local sidereal time effect. By analogy, there is no relation to the local solar time effect.

5 The disclosure and constancy of the type-one field F_1 along the meridians

As is obvious, many in the effects (1)–(3) and (5)–(7) are explainable as results of the disclosure of the type-two fields. However, the existence of the type-two fields cannot explain

*The same also relates to detectors D_α with the orientation fixed relative to the LHP system, because in this case the detector orientation relative to the ray L_E do not change along the parallels.

†Obviously, $t_2 = t_1 + (t_2 - t_1) = t_1 + \tau$, where $\tau \equiv t_2 - t_1$. At any moment t_1, the first detector crosses some parallel $\varphi = \text{const}$. Therefore, in the formula (12), the value t_1 can be changed by the current time t and present it as $G_1(t) \approx G_2(t + \tau)$. In [12], the value τ is constant. The same experiment could be performed with detectors $D_{\alpha K}$ observing constancy of the collimator direction relative to the ray L_E (and in a sufficient resolution power by time).

synchronism along the meridian (2), (6) in the experiments with the detector $D_{\alpha P}$. Actually, as is easy to see, the orientations of the plate-type detectors $D_{\alpha PA}$ and $D_{\alpha PB}$ (perpendicular to the plate) change along the meridians relative to the rays L_S, L_E, L_{2ext} and any other system of the ray mutually parallel within the bounds of the Earth. At the same time, the impact character of the type-two fields on the detectors $D_{\alpha PA}$ and $D_{\alpha PB}$ depends on the above orientations. Therefore, in the experiments with the detectors $D_{\alpha PA}$ and $D_{\alpha PB}$, the type-two fields of the Earth, the Sun and any other external source of them associated with the ray, mutually parallel within the Earth, may not generate the synchronism (2) and (6) on the Earth meridians. By analogy, regarding the orbital motion of the Earth, the existence of the type-two fields may not explain the effects (1) and (3) in the experiments with the noise detector D_{noise}. Hence:

> The different field does exist, the impact character of which is independent of the above orientations.

This field must affect the histograms of any Shnoll detector independently on the orientation of the parameters of its motion or the motions of the α-particles (for example, on the detectors $D_{\alpha P}$, $D_{\alpha K}$ and D_{noise}). The character of its impact depends exclusively on the field itself, on the detector location in this field and, probably, on the magnitudes of the above motion parameters. By definition, this is *the field F_1 of the first type*. The constancy lines of its impact character are the Earth meridians despite of the Earth's motion in space. Hence, this is the self-field F_{1E} of the Earth. If the field F_{1E} impact character would not vary and along the Earth parallels $\varphi = \text{const}$, it would be constants on the Earth's surface. Then there would be no reason for the raise of the probability of the similar histograms occurrences when two detectors are located on the same meridian. But, still, the indicated raise is observed. Hence, the field F_{1E} changes along the Earth parallels $\varphi = \text{const}$.

According to Note 1, the Sun must have its own field F_{1S} of the first type, the impact character of which in the HSC system is constant along of the Sun's meridians, but changes along its parallels motionless in the HSC system. The field F_{1S} should change along the Earth's orbit. If the field F_{1S} is static at a time in the HSC system, the character of its impact on the Earth should depend only on the Earth's location along the Earth's orbit. In the sidereal year T_{SID}, the Earth repeats its location in its orbit. A sidereal year is not equal to an integer of a sidereal day $T_{ST} = 1436$ min since in the sidereal year the Earth makes not an integer of its turnovers about of the Earth axis. Therefore, the detector's motion parameters and the motion parameters of the α-particles, if the detector is the radiation detector, at the moments $t + T_{SID}$ and t are directed differently. It is simple to convince ourselves that the angular difference in the directions on the equator attains approximately 90°. Despite of the indicated difference in the directions, if the Sun has a static field F_{1S}, the impact character of the field F_{1S} on the detectors D_{noiseA} and $D_{\alpha PA}$ should repeat in the sidereal year T_{SID}. Hence, the histogram similarity should be observed at the time T_{SID} under the effect of the field F_{1S} on the detectors. During the searching by S. E. Shnoll's group at about a year's cycle, the required experiment has been carried out but only with the detector $D_{\alpha PA}$ and with the use of many moments of a time t during several sidereal years [14]. In the experiments of Shnoll's group [14], the expressed peak of the similarity among the histograms divided by the interval $T_{SID} = 525969$ min has really been detected to one minute, which in addition experimentally confirms the existence of the first-type fields (of celestial bodies), their variability along motionless parallels and their *static character at a time*.

As we have illustrated earlier, in the GSC system at $\varphi_A(t) = \varphi_B(t) = \text{const}$, the detector D_{noiseB} at the moment $t + \delta t_{ST}$ and the detector D_{noiseA} at the moment $t + T_{ST}$ arrive at the same point where the detector D_{noiseA} was at the moment t and, therefore, arrive at the same point of the field F_{1E}. For this reason, the effects (1) and (3) should be in the experiments with the noise detectors as it is observed. Synchronism along the meridian is observed on the noise detectors. But the magnitudes of the motion parameter $\mathrm{V}_d^{SPIN,m}$ of the noise detector D_{noise} change along the Earth meridians — from zero value at the Earth poles to a maximum value on the Earth equator. Therefore field F_{1E} can generate synchronism along the meridian with the noise detectors only during the event when only the impact force, but not the impact character, of the first-type field F_1 depends on the magnitudes of the detector's motion parameters.

The effects (1) and (3) with the noise detectors are generated also by the exterior field F_{2ext} if it is possible to neglect the active parameters of the orbital motion. Indeed, in this case only the spin motion parameter $\mathrm{V}_d^{SPIN,m}$ of the noise detector D_{noise} relative to the Earth's center plays a rôle. These parameters of the noise detector D_{noiseA} repeat their orientation relative to the ray L_{2ext} at the time T_{ST}. A detector D_{noiseB} at the moment $t + \delta t_{ST}$ repeats the orientation of the parameter $\mathrm{V}_d^{SPIN,m}$ of the detector D_{noiseB}, which it previously had at the moment t. This way, it reduces to the effects (1) and (3). At any fixed moment t, the direction of each parameter $\mathrm{V}_d^{SPIN,m}$ does not change along the meridians. Therefore the field F_{2ext} should generate synchronism along the meridians (2) in the experiments with the noise detector D_{noise} but only if the impact force, but not the impact character, of the second-type field F_2 depends on the magnitudes of the detector's motion parameters (varying along the meridians). The ray coming from each point of the Sun (as well as the ray L_{2ext} of the external field) is practically mutually parallel in the Earth's limit (to five thousandth of a grade). Therefore the Sun's field F_{2S} also generates synchronism along the meridians in the experiments with the noise detector D_{noise} but only under the last condition.

Thus, in all cases, for the appearance of the above syn-

chronism on the noise detectors it is necessary that only the impact force, but not the impact character, of the considered fields depends on the magnitudes of the detector's motion parameters. Synchronism along the meridians on the noise detectors is observed. Hence:

> At least for one of the fields F_1 and F_2, only the impact force, but not the impact character, depends on the magnitudes of the detector's motion parameters.

Now, let's ask ourselves whether it is possible to neglect the active parameters of the orbital motion? Probably — yes, if all active parameters are derivatives of the acceleration. In fact, the first derivative $\mathrm{V}_d^{ORB,2}$ of the detector's orbital acceleration with respect to the Sun makes only five ten-thousandth of the first derivative $\mathrm{V}_d^{SPIN,2}$ of the detector's rotational acceleration with respect to the Earth axis. With respect to the derivatives and the motion relative to the galactic center, a relation is not for the benefit of the latest. From the current experiments with the noise detector, it is not possible to draw a single one-valued conclusion concerning the rôle of the orbital motions as the active parameters have not been discovered.

6 About the reasons of the occurrence of the fields of the first and the second types

The field F_{2E} of the Earth is cylindrically symmetrical relative to the Earth axis. The Earth axis is the axis of its rotation. Hence the field F_{2E} is inseparably linked to the Earth rotation about its axis. If we stop the Earth rotation, the Earth axis loses its physical meaning and disappears and, consequently, the field cylindrically symmetrical relative to the Earth rotation axis loses its sense too. At the stopped Earth rotation, the field no longer has reason to be cylindrically symmetrical relative to the Earth axis. In this case, any other field may exist (with other properties) but not the above field F_{2E}. Consequently:

> The field F_{2E} arises as the result of the Earth rotation*.

The spatial distribution of the impact character of the field F_{1E} (as well as that of the field F_{2E}) is determined by the Earth's rotational characteristics — by its meridians $\theta = \text{const}$ and parallels $\varphi = \text{const}$. In fact, impact character of the field F_{1E} is constant along the Earth meridians $\theta = \text{const}$ and changes along the Earth parallels $\varphi = \text{const}$. So the field F_{1E} is also inseparably linked to the Earth rotation about its axis. At the stopped Earth rotation, the Earth poles, its meridians and parallels lose their physical meaning and disappear and, consequently, the field F_{1E} inseparably linked to the Earth meridians and parallels loses its physical meaning, too. At the stopped Earth rotation, the field has no reason to be linked to the Earth meridians and parallels. In this case, any other field (with others properties) may exist, not the above field F_{1E}. Hence:

> The field F_{1E} also arises as a result of the Earth rotation.

The origination of the field as a result of a material body's rotation may be checked by laboratory experiment. In one of the preceding paper of the author (2004), it is noted:

> "If a sphere or a disk first is rotated and then is stopped in a laboratory, the field generated by the rotation first will appear and then will disappear. Our interest is to register this phenomenon by the Shnoll detector and then study, in a laboratory, the characteristics of this field, its relations with rotation if, of course, the Shnoll detector will be sensitive enough, because the laboratory body mass is negligibly small compared with the masses of planets".

Based on the theory developed here, it is interesting to ask ourselves the following question: what must occur when the body is rotated in a laboratory with the angular velocity ω? As a result of a body's rotation, the fields of the first type, F_{1B}, and the second type, F_{2B}, must be generated. Let the position and the orientation of the detector $D_{\alpha P}$ be constant relative to a body's axis. When $\omega = \text{const}$, the fields F_{1B}, F_{2B} and their the impacts character on the motionless detector are constant in time. At $\omega = \text{const}$, by virtue of Note 2, the Shnoll technique gives no ability to detect impacts of the fields F_{1B}, F_{2B}, and

> An impression of the absence of the impact arises, although the detector itself registers the impacts of alternate and constant character.

If the impact character depends on ω value, upon multiple repetitions of the angular velocity with the period T, the impact character must repeat multiply, too†. Accordingly, the peak of similarity of the detector histograms $G(t)$ separated in time by the period T should occur: $G(t + \delta t) \approx G(t)$ at $\delta t = T$. The first appropriate experiment has already been performed with the detector $D_{\alpha P}$ [18]. The Shnoll detector had been found to be sensitive enough. The rotating massive body was accelerated from the angular velocity $\omega_{min} = 10\,\pi$ rad/s (300 rpm) to $\omega_{max} = 100\,\pi$ rad/s (3000 rpm). The acceleration and deceleration times were about one minute, and the rotation at the constant angular velocity $\omega = \omega_{max}$ lasted for about three minutes. This repeated many times every 5 minutes of the slow rotation at $\omega = \omega_{min} = \text{const}$. Finally, the process periodically repeated every 10 minutes. During

*The Earth rotation forms and, most likely, generates the field F_{2E}. The point is that in all cases known in physics, if the field is formed by some motion, then it is also generated by this motion. These are intimately related to cases of the formation and generation of the magnetic field by moving electric charges, or to cases of the formation and generation of the so-called gravimagnetic, or co-gravitational fields of moving masses. For the consideration below of the field's dependence on motion, it does not matter, that the field is generated or formed by motion. It is important only that the field arises in the definite form as a result of the motion.

†If the impact character is independent of ω, at its voluntary changes the former false impression will be created.

the acceleration, the value of ω was increased from ω_{min} to ω_{max}, and during the deceleration the value of ω was decreased from ω_{max} to ω_{min}. As a consequence, the angular velocity ω multiply repeated, approximately, at the periods $T = 3 - 5$ min and $T = 5 - 7$ min. According to the developed theory, the similarity peaks of the histograms should be observed at these periods. More similar histograms should be observed at $T = 5$ min. But the greatest number of ω repetitions happens within the period $T = 10$ min, where the maximal peak of the histogram similarity should be expected. In accordance with the developed theory, in the first experiment the impression was created [18]:

> "... that the recording system is sensitive not to the presence or absence of the rotor's centrifuge rotation, but to its acceleration or deceleration".

Secondly, the similarity peak of the histograms was detected within the interval $\delta t = 3 - 7$ min with the maximum at the time shift δt about $\delta t = 5$ min (see Fig. 10a in Ref. [18]). In accordance with the process' cyclicity, the highest peak is observed for the shear $\delta t = 10$ min (see Fig. 10a in Ref. [18]). Despite the obviousness, the authors of the work [18] have spoken about the appearance of the "*five-minute period instead of expected ten-min period*". They came to the inexact conclusion because of the application of the Fourier transform to the curve of numbers of the similar histograms with respect to the shear δt between histograms (see Fig. 10b in [18]). However, the maximum at the shear $\delta t = 10$ min already indicates the maximal repetition of the histogram shape separated by the interval $\delta t = 10$ min. Therefore, to detect repetition of the histogram shape in the interval $\delta t = 10$ min no Fourier transform is needed. The Fourier transform indicates another: it indicates that at the time 5 minute the peaks on the above curve repeat. These peaks are present at $\delta t = 5$, 10 and 15 min. As a result, the Fourier transform mixes the physically miscellaneous peaks and gives the spectrum its maximum at the frequency corresponding to the period of the peaks' repetition 5 min. This has no relation to the sought interval of the histogram shape repetition*. Moreover, it may be shown that in the considered experiment, the quasistationary rotation takes place, i.e., the angular acceleration is so low that it does not affect the instantaneous linear velocity, acceleration and accelerational derivative of the rotating body's points. Indeed, let point M rotate at a variable angular velocity ω. Then it is clear that vectors of its linear velocity v, linear acceleration a and accelerational derivative a' in time are defined by the expressions:

$$\mathrm{v} = \big[\omega, \mathrm{r}\big] , \tag{13}$$

$$\mathrm{a} \equiv \mathrm{v}' = \big[\omega, \big[\omega, \mathrm{r}\big]\big] + \big[\omega', \mathrm{r}\big] , \tag{14}$$

$$\mathrm{a}' \equiv \mathrm{v}'' = \big[\omega, \big[\omega, \big[\omega, \mathrm{r}\big]\big]\big] + \big[\omega, \big[\omega', \mathrm{r}\big]\big] + 2\big[\omega', \big[\omega, \mathrm{r}\big]\big] + \big[\omega'', \mathrm{r}\big] , \tag{15}$$

where ω is the angular velocity vector, "prime" is signed for time derivative, square brackets denote vector cross-product, and r is the radius-vector of the point M relative to the axis of rotation. For the stationary rotation case, $|\omega'| = |\omega''| = 0$. Therefore, linear parameters v, a, a' of the stationary rotation are described by the first summands in the right part of the formulas (13)–(15). The rest summands containing ω' and ω'' values describe the correction arising from the rotation's unevenness. For the purpose of estimation, let us suggest that $|\omega'| = \frac{\omega_{max} - \omega_{min}}{60 \text{ sec}} = \frac{3\pi}{2}$ rad/s^2. For example, at $\omega = \omega_{max}$, we get

$$\big|\big[\omega, \big[\omega, \mathrm{r}\big]\big]\big| = (\omega_{max})^2 \, |\mathrm{r}| = (10000\,\pi) \times \pi |\mathrm{r}| , \tag{16}$$

$$\big|\big[\omega', \mathrm{r}\big]\big| = \frac{3\pi}{2} \, |\mathrm{r}| . \tag{17}$$

Therefore, the second sum in (14) is $\frac{10000 \times 2\,\pi}{3} = 20943$ times smaller in absolute magnitude than the first summand, and may be neglected. The linear acceleration a is determined by the first summand and equals that of the stationary case. As is estimated, the same is true for other values of ω and a'. Therefore, it shall be reasonably assumed that the results of this experiment indicate the effects of rotation, but not acceleration or deceleration of rotation. Thus:

> The experiment confirms formation of the field as a result of the body's rotation and discloses the presence of the impact character dependence on the angular velocity. Hence, at least for one of the fields F_1 and F_2, the impact character depends on the magnitudes of the motion parameters of the field source, and, by the principles of relativity and reciprocity, also from the magnitudes of the motion parameters of the detector.

Then we obtain the analogy of an electromagnetic field impact on an electric charge — the electric field's impact does not depend on the velocity of the charge, and a magnetic field's impact depends on the magnitude and direction of the velocity of the charge. If we trust this analogy, there should expectedly be a mutual induction of fields F_1 and F_2. The axis $O_{\alpha P}$ of the detector $D_{\alpha P}$ has been directed to the body's rotational axis in the above circumscribed experiment. In another experiment, the detector has been turned on. Its axis was parallel to the body's rotational axis. As a result, the produced histograms, which form a response to the body's rotation, has disappeared [18]. The impact character of the field F_1 does not depend on the turns of the axis $O_{\alpha P}$ of the detector $D_{\alpha P}$. Therefore the effects of its action cannot disappear at the turns of the detector $D_{\alpha P}$. At the turns of the detector $D_{\alpha P}$, the action of only the field F_2 varies. Hence,

*If a multitude of other variable impacts did not interfere, obviously, the similarity peaks would also be observed at $\delta t = 20, 30, 40$ min, etc. (see Note 1). In this case, the Fourier transform would have physical meaning and give the peak at the frequency corresponding to the period 10 min. The cut-off of the transformed curve at time $\delta t = 26$ min and the said interference, naturally, do not render the peak at the above frequency possible, and simply mix the physically miscellaneous peaks.

the response of the detector in the first experiment is the result of the impact of the field F_2. Consequently:

> The impact character of the field F_2 depends on the magnitudes of the motion parameters of the source and the receiver, and the impact character of the field F_1 does not depend on these magnitudes. Only the impact force of the field F_1 can depend on these magnitudes.

And, the impact of the field F_2 of a rotating body disappears or the impact character of the field F_2 does not depend on the motion parameters of the source when the detector axis $O_{\alpha P}$ is parallel to the rotating body axis. These conclusions are obtained by the supposition that the detector records directly the fields F_1 and F_2 generated by the rotation. However, in it there is some doubt. The rotating body mass is very small in comparison with the masses of the planets. Probably, the rotating body generates the fields $F_1$and F_2 so weakly, that the detector is not capable of registering them. On the contrary, the speed of the variations (changing) of these fields in the experiments are unusually great on planetary scales, i.e., in comparison with the speed of the variations (changing) of such fields of the Earth, or of the remote planets. Therefore, probably, there are enough strong fields of an induction (induced by weak, but sufficiently fast varying fields of the rotating body) which are registered with the detector. Then essential conclusions can vary. Therefore:

> In the development based on such experiences, it is useful experimentally "to study in a laboratory the performance of the investigated field", especially by the collimator detector $D_{\alpha K}$, to investigate in a laboratory the relation between the field's impact force and character on the location and the motion parameters of the source and the detector, to study the effects of the local-time type and a possible mutual induction of fields F_1 and F_2.

In order to detect the field's existence at $\omega = \text{const}$, it is possible to move the detector.

The formation of the field F_{2E} as a result of the Earth rotation gives birth to consequences chain. The field F_{2E} of the entire Earth formed by rotation should be composed of the elementary fields F_{2P} of the material points P of the Earth. The material points P move around the axis of the Earth. Hence, the whole field F_{2E} is composed of its elementary components F_{2P} arising as a result of the cyclic motions of the material points P around the Earth axis (similar to how a magnetic field is generated by the motion of an electric charge). At any fixed moment of time t, a (sample) material point P is located not at all points of its cyclic orbit around the Earth axis, but at some fixed point K of its orbit. At the moment t, at the point K, the field F_{2P} is formed, naturally, not due to the general characteristics of the motion of the material point P on its whole orbit, but due to the local characteristics of its motion at the point K at the moment t, i.e., at least due to some active, parameter $\mathrm{V}^m_{P,a}$ of the motion of the point P from the set $\{\mathrm{V}^m_P\}$, where $m = 0, 1, 2, 3, \ldots$; V^m_P is the m-th derivative of the velocity V_P of the material point P, $\mathrm{V}^0_P \equiv \mathrm{V}_P$. The significant task for the physical experiment is to find out what the parameters of the motion of the (sample) material point are active and how the field F_{2P} depends on them. Now, in general terms, the following can be said: if some component of the field arises as a result of a motion, then its intensity must depend on the motion's intensity, i.e., on the value of the active parameter $\mathrm{V}^m_{P,a}$, and, for the total field F_{2E} of the entire Earth, on the angular velocity of the Earth rotation. The Earth is moving along its orbit around the Sun. Therefore, the motion of the material points P along the Earth orbit must lead to the formation of some field F^{ORB}_{2E}which we shall denote as the *orbital* field of the Earth. We will distinguish it from the Earth's field formed due to its self-rotation about its axis, which is called the *spin* field and denoted as F^{SPIN}_{2E}. Analogously to the orbital motion, the internal motions of the material points of the Earth (the motions of tectonic plates, subcortical melt, water flows, etc.) must lead to the formation of the field F^{IN}_{2E}, which we will denote as the field of the internal motions of the Earth. The Earth is only one of many planets. Then the said must be true for other planets, their satellites, the Sun, the Moon and for other celestial bodies, because all of them consist of material points, have orbital, spin and internal motions, i.e., all celestial bodies must have orbital, spin fields and fields formed by their internal motions. This is in accordance with NOTE 1. Any sample (a motionless one included) of matter consists of physical material particles (molecules, atoms, etc.) which are mobile. Hence, any sample of matter has the same fields. By the same logic, the same consequences chain for the field F_{1E} are obtained. In particular, the field F_{1E} of the entire Earth is composed of elementary field F_{1P} of the material points P of the Earth. Consequently, the above conclusions about relation between the *type-two* fields and the motions of their sources are also true for the *type-one* field. Then the Earth has a spin field, F^{SPIN}_{1E}, and an orbital field, F^{ORB}_{1E}, of the first type, as well as the type-one field F^{IN}_{1E} formed by the internal motions of the Earth. The impact character of the field $F_P = F_{1P} + F_{2P}$ depends on the magnitudes of the active parameters of the motion of the material point P, since for the entire Earth it depends on ω.

7 Conclusions and discussion

From the experimental material accumulated by Shnoll's group, the following physical model is logically succeeded. The Shnoll detector records the fields of two types. The impact character of the second-type field F_2 displayed by the histogram shape depends on the orientation of the active parameters of motion of the object relative to the ray by which the impact arrive at the object. The impact character of the first-type field F_1 does not depend on the above orientation. The motion of the material particles P leads to the simulta-

neous formation of the type-one field F_{1P} and type-two field F_{2P} of the particles. Therefore, the fields F_{1P} and F_{2P} may be considered as the components of the single field $F_P = F_{1P} + F_{2P}$. The intensity of the fields F_{1P} and F_{2P} should depend on the intensity of the motions, i.e., on the active parameters of motion of the particles P. The impact character of the field $F_P = F_{1P} + F_{2P}$ depends on them, too. The material particles of the Earth are moving around the Earth axis and, as a result, form the Earth's total *spin* fields of the first type, F_{1E}^{SPIN}, and the second type, F_{2E}^{SPIN}. In the geocentric coordinate system, GCS, (non-rotating relative to "motionless" stars), the impact character of the field F_{1E}^{SPIN} is constant along the motionless meridians $\theta = \text{const}$ of the Earth but changes along its motionless parallels $\varphi = \text{const}$. The field F_{2E}^{SPIN} is cylindrically symmetrical about the rotation axis of the Earth. Its impact character is constant along the parallels $\varphi = \text{const}$ and changes along the meridians $\theta = \text{const}$. The motion of the Earth's particles, as of a single whole, along the Earth's orbit forms *orbital* fields of the Earth of the first type, F_{1E}^{ORB}, and the second type, F_{2E}^{ORB}.

> The motion of tectonic plates, subcortical melt, water flows, etc. form the fields F_{1E}^{IN} and F_{2E}^{IN} of the Earth's internal motions of both types.

The measure of the relative strength of the considered fields may be the probability of the appearance of similar histograms by the considered field effect. This allows a change over from a qualitative estimation to a quantitative estimation of the field. The Earth is only one of many planets. Other planets, their satellites, the Sun, the Moon and other celestial bodies must have the same fields. The study of the results of the experiments performed with the Shnoll detector has allowed us to uncover the existence of the first and second-type fields of the Earth and the Sun, as well as the field F_{2ext} of the second type external to the Solar system, the ray of which is reciprocally parallel within the Earth's orbit. Any sample (including a motionless one) of matter consists of mobile material particles (molecules, atoms, etc.) and possesses the same fields. According to S. E. Shnoll's opinion [14], his detector, per se, detects fluctuations of local space-time properties. If S. E. Shnoll is right, the physical nature of the above-studied field F displays itself in the form of fluctuations of local space-time properties (just as the gravitational field displays itself in the form of space-time distortion). Then the statistical properties of the body's internal motions should affect the statistical character of the space-time fluctuations, induced by this body. The inverse effect should also take place, i.e., there should be an interaction between the statistical phenomena in the body and in space-time. The studied aggregate field $F = F_1 + F_2$ of the Sun, the Earth, the Moon, planets, and other material bodies should also depend on the microscopic motions of microscopic particles, for instance, on temperature and spin motions of their atoms. Therefore, the aggregate field F of any material body should depend not simply on its mass, but also on its substance, structure and processes occurring in it.

One would think, that it doesn't matter which Shnoll detector is used, since the histograms of the processes of different physical natures are similar and changed synchronously. Nevertheless, in this paper a different physical meaning of the experimental data of the detectors of the different types is determined: the noise detector D_{noise} indicates dependence of the impact character on the active vectorial parameters of the motions of the detector and the points of the Earth, but the detectors D_α, based on the α-decay registration, indicates dependence of the impact character on the active vectorial parameters of the motion of α-particles. Correspondingly, if the dependence of the impact character and the histogram shapes on the directions of motion parameters or on the spatial orientation of the detector is studied, the method for the interpretation of the experiments with the detector D_α must always be different from the method for the interpretation of the experiments with the detector D_{noise}, which has not been taken into account in the works [10–14]. Taking into account the last conclusion, the system of experimental data of the Shnoll detector and the specific rôle of the experiments with the rotating collimator $D_{\alpha K}$, cutting off the pencils of α-particles, become clear. In the framework of the developed physical model, the effects of local time (1), (3), (5), (7) and near-year cycle with the period of 529600 minutes, observed on detectors D_α, are the theoretical consequences of the experiments resulting from performance of the rotated collimator $D_{\alpha K}$, in which the Sun's second-type field F_{2S} and the external field F_{2ext} has been disclosed. Naturally, this is the reason for the recommendation to use the detectors D_α and $D_{\alpha K}$ for studying of the angular diagram of the type-two field impact upon their laboratory generation. In particular, as described in this paper, with the detectors D_α and $D_{\alpha K}$ rotating on different planes, it is desirable to study the character and relative strength of the impact, and the directions of the ray of the type-two field. The laboratory experiments may allow us more reliably to determinate the details of the properties of the fields of both types. For instance, the already performed laboratory experiment has confirmed the theory's conclusions about the field generation by rotation and has disclosed the disappearance of the response of the plate-type detector $D_{\alpha P}$ to the body's rotation within the detector's orientation along the rotational axis [18]. This is in accordance with an experiment, in which the collimator is parallel to the Earth's rotational axis. The Moon rotates about its axis 28 times slower than the Earth. Therefore, the detection and study of the Moon's type-two field may answer the following question: what changes, if the rotational velocity is strongly decreased?

In the nearest future, the influence of macroscopic internal motions of the Earth on the aggregate two-component field F_E of the Earth may gain direct practical importance for the purpose of the detection of hidden water flows, motions of tectonic plates and subcortical melt, forecasting of strong

earthquakes, etc. According to seismology, earthquakes happen as a result of collision in the Earth's crust of large plates floating on the underlying melt. Let us briefly consider earthquakes themselves. During an earthquake, a short-term (pulse) motion and displacement of large masses of the Earth's crust arise. Then, by virtue of our theory, a pulse change of the field of the mentioned masses arises and, therefore, a pulse change of the Earth's field $F_E^{IN} = F_{1E}^{IN} + F_{2E}^{IN}$ arises too. That is why the Smirnov (and Shnoll) detectors should detect earthquakes, being integral recorders of the motions and displacements of masses. The precursors' appearance in indications of the Smirnov detector before 2–10 days of the earthquakes means, apparently, that some pulse changes in the motions or displacements of the large masses of the Earth's crust or subcortical melt happen also and 2–10 days prior to a strong earthquake that may be, for example, due to the mechanism in which the mentioned plates come into sufficiently rigid contact and, as a result, they are sufficiently abruptly decelerated. Therefore, the presence of earthquake precursors in the field F_E is not surprising and seems logical. However, the precursors' strength is unexpected. The Smirnov detector goes off scale, and it requires us to reduce the detector's sensitivity. Now the precursors of strong earthquakes are separated exactly by anomalously high amplitudes (and with the duration increased, approximately, up to 12–13 minutes). The reason of the mentioned anomalous strength of the precursors' amplitudes may be due to the induction of a strong field due to relatively quick changes in the motions and positions of the tectonic plates or melt. Frequently, in physics, the following rule of reciprocity is true: if some physical process generates or changes some field then, vice versa, this field or its changes may influence the behavior of this process. As a result of the seismic motions, the aggregate two-component field is formed and changed. Seemingly, the reciprocity rule is realized in the connection between such fields and earthquakes, i.e., the fields affect the Earth's seismicity. Moreover, if planets, the Sun and the Moon affect the motions on the Earth via their own aggregate two-component field F, which has been disclosed by the Smirnov detector, then there are serious foundations for the supposition that they also affect the Earth's internal motions related to the earthquakes. This is directly confirmed by the detected correlation between microseismicity and planetary motions. In favor of the same, the old data of Ben-Menachem state the correlation between microseismicity and sunrises and sunsets. According to the Smirnov detector's data, the strong splashes of the field F of the Sun and planets occur exactly at risings, settings and culminations. (Incidentally, the Sun's gravitational impact is minimal exactly at sunrises and sunsets.) This also explains the Jupiter splash affecting in living matter immediately at its upper culmination. Actually, the system of such splashes is much wider. In particular, the strong short-term splashes happen at pair-wise connections between planets, the Sun and the Moon on the coelosphere and at their crossing of their network's definite lines, which will be discussed in a separate paper. Therefore, a strong correlation between earthquakes and the connection between the Moon and planets, observed by T. Chernoglazova, becomes natural. The data on the effects of the pulsar on the Earth's seismicity indicate a noticeable long-range action of the considered fields. Generally, the outlined effects of planets and the pulsar on seismicity and terrestrial motions indicate the existence of the long-range action fields.

However, astrophysics firmly states one's position: *planets are unable to impact the Earth*. These are not mere words. Actually, the total energy flow of a field (known or still unknown to us) through its frontal area must be constant and must be spread throughout the frontal area. The frontal area increases with respect to r^2 (in the case of its spherical shape, where r is the distance from the point-source of the field). Finally, the energy-flux density of the field together with the field intensity should decrease with respect to $1/r^2$ or faster. The corresponding numerical estimates lead astrophysics to the said position. However, astrophysics keeps back the following: *the position is correct for the class of energy fields*. Scientific experiments and observations demonstrate the impact of planets and pulsars on the Earth. Therefore, the dilemma arises: either astrophysics is right in the class of energy fields, then consequently there are the fields outside this class (by definition, they are the energy-free fields) or astrophysics is not right. The known physical laws do not prohibit the existence of the energy-free impacts and fields. Moreover, from physics it is known that energy-free impacts exist. These energy-free impacts do not change the energy of the process but merely control its development, for example, turning on and off energy transforms from one of its kind to another [16]. As is mentioned in the Introduction, S. E. Shnoll has disclosed some universal, remote non-energy impact synchronously affecting on processes of different physical nature. That is, some substance — some physical field — does exist, which is transferring these non-energetic impacts. In order not to conflict with the mentioned position of astrophysics and the conservation law of energy, this field itself must be of non-energetic nature. Though the above idea about a non-energetic field is unusual, it should be seriously investigated, as it is the result of experiments and generally recognized scientific views of astrophysics.

At the same time, the developed theory here does not disclose the physical nature of the fields. This theory is valid independently of whether the fields are energetic or energy-free, electromagnetic, gravitational or of any other physical nature. This theory just gives the field properties as the logical consequence of the experimental material and independently of their physical nature. Therefore, as A. A. Artamonov has reasonably noted, this theory may be included as an independent block for any future theory attempting to explain the properties and the physical nature of the considered fields.

In the interrelation between the considered fields and seismicity, significant are not only new prospects in the forecasts

of earthquakes. Most likely, higher importance is attributed to the renovated view on the physical model of evolution and the interdependence between seismic processes themselves and the surrounding cosmos [19]. The renovated view arises also on geopathogenic zones, as on the zones of anomalies of the considered fields since, according to the above theory and other observations, these fields affect the state of living systems, that will be discussed in a special paper.

Acknowledgements

The author is thankful to the following persons: A. S. Alekseev, the full member of Russian Academy of Sciences, A. V. Nikolaev, the corresponding member of Russian Academy of Sciences, V. (N.) P. Tataridou, and also Dr. A. D. Gruzdev. Essential discussions of the problem with these persons have led to valuable advices and their supporting the author's investigations.

Submitted on October 19, 2008 / Accepted on January 09, 2009

References

1. Sadeh Dror and Meidav Meir. Periodisities in seismic response caused by pulsar CP1133. *Nature*, 1972, v. 240, November 17, 136–138.
2. Kiladze R.I., Kachakhidze M.K., Kachakhidze N.K., Kukhnanidze V.D., Ramishvili G.T. Seaching for possible connections between strong earthquakes and astronomic phenomena on the example of seismically active region in Caucasus. *Vulkanologia i Seismologia*, 2005, no. 3, 78–84 (*in Russian*).
3. Lezdinsh A.Ya. Astroseismology. *The Earth Planet System*, *Proceedings of XVI-th Scientific Seminar*, Moscow State University, Moscow, 2008, 221–225 (*in Russian*).
4. Bogdanovich B.Yu., Shchedrin I.S., Smirnov V.N., Egorov N.V. Specific method of mass rotation — the instrument for astrophysical investigations. Preliminary analytical estimates of changes in kinetic energy of rotating mass on coordinate-time position of the Sun and the Moon. *Scientific Session MEPHI-2003*, Moscow, MEPHI, 2003, v. 7, 45–48 (*in Russian*); http://library.mephi.ru/data/scientific-sessions/2003/7/045.html
5. Bogdanovich B.Yu., Egorov N.V., Smirnov V.N. Recording of some phenomena by spatial-temporal geometrizer. *Scientific Session MEPHI-2005*, Moscow, MEPHI, 2005, v. 7, 59 (*in Russian*); http://library.mephi.ru/data/scientific-sessions/2005/t7/0-1-24.doc
6. Bogdanovich B.Yu., Egorov N.V., Kulago A.P., Smirnov V.N. Recording of various orbital configurations of planets in the Solar System by the gravitational interactions detector. *Scientific Session MEPHI-2006*, Moscow, MEPHI, 2006, v. 7, 1–5 (*in Russian*); http://library.mephi.ru/data/scientific-sessions/2006/t7/0-6-5.doc
7. Bogdanovich B.Yu., Smirnov V.N. The peculiarities of experimental works in studies of gravitational interactions. *Inzhenernaya Fizika*, 2006, no. 4, 10–14 (*in Russian*).
8. Smirnov V.N. Gravitational disturbances and physical peculiarities of rotating gyroscope. *Inzhenernaya Fizika*, 2006, no. 5, 22–24 (*in Russian*).
9. Smirnov V.N., Egorov N.V. and Shchedrin S.I. A new detector for perturbations in gravitational field. *Progress in Physics*, 2008, v. 2, 129–133.
10. Shnoll S.E., Kolombet V.A., Pozharskyi E.V., Zenchenko T.A., Zvereva I.M., Kondratov A.A. On realization of discrete states during fluctuations in macroscopic processes. *Physics-Uspekhi*, 1998, v. 168, no. 5, 1129–1140.
11. Panchelyuga V.A., Shnoll S.E. On the dependence of a local-time effect on spatial direction. *Progress in Physics*, 2007, v. 3, 51–54.
12. Panchelyuga V.A. and Shnoll S.E. A study of a local time effect on moving sources of fluctuations. *Progress in Physics*, 2007, v. 3, 55–56.
13. Shnoll S.E., Rubinshtein I.A., Zenchenko K.I., Shlehtarev V.A., Kaminsky A.V., Konradov A.A., Udaltsova N.V. Experiments with rotating collimators cutting out pencil of α-particles at radioactive decay of 239-Pu evidence sharp anisotropy of space. *Progress in Physics*, 2005, v. 1, 81–84.
14. Shnoll S.E. Changes in the fine structure of stochastic distributions as consequence of space-time fluctuations. *Progress in Physics*, 2006, v. 6, 39–45.
15. Shnoll S.E. Macroscopic fluctuations — possible consequence of time-space fluctuations. Arithmetical and cosmophysical aspects. *Rossiyskii Khimicheskii Zhurnal*, 2001, v. XLV, no. 1, 12–15 (*in Russian*).
16. Vasiliev S.A. On some field of the Earth in view of its internal motions. *Degassing of the Earth: Geodynamics, Geofluids, Oil, Gas, and Their Parameters*, *Proceedings of the Conference*, Moscow, April 22–25, 2008, GEOS Publishing House, Moscow, 576–579 (*in Russian*).
17. Vasiliev S.A. On two-component field of the Earth and stellar bodies. *The Earth Planet System*, *Proceedings of XVI-th Scientific Seminar*, Moscow State University, Moscow, 2008, 98–119 (*in Russian*).
18. Panchelyuga V.A., Shnoll S.E. Experimental study of quickly rotating massive body influence on the shape of distribution functions amplitudes of α-decay rate fluctuations. *Hypercomplex Numbers in Geometry and Physics*, 2006. v. 3, no. 1, 102–115.
19. Nikolaev A.V. The pattern of geophysics in XXI century. In: *Problems of Geophysics in XXI Century*, collected papare, book 1, 2003, Moscow, Nauka Publishing House, 7–16 (*in Russian*).
20. Zubov V.A. et al. Private communications. Germany, 2008.

Beta Decay and Quark-Antiquark Non-Parity in Collision-Induced Gravity

Gary C. Vezzoli

Department of Science and Mathematics, Lebanon College, Hanover Street, Lebanon, NH 03766, USA
Senior Research Consultant Physicist, Institute for the Basic Sciences, West Windsor, VT 05089, USA

E-mail: vezzoli2005@yahoo.com

The quark-antiquark interaction, with non-conservation of parity, associated with neutrino-nucleon inelastic scattering, and electron/positron decay consequent to nuclear transmutation and re-materialization, are invoked as the phenomena responsible for heat carry-off. The mechanism is applied to collision-induced gravity, including quantitative justification, using Feynman parton theory. The application to heat dissipation necessarily involves the tri-quark current that associates with weak interactions.

1 Introduction

Parity refers to the operation of studying a system or a sequence of events reflected in a mirror plane [1]. In chemistry and biology, the term "chirality" is used, instead of parity, and refers to a structure that is different from its mirror reflection, and from this property, very important criteria of handedness and broken symmetry arise [2]. In physics, a deeper understanding of the meaning of parity (often called space parity) refers to every real object or process having a mirror image that *obeys the same physical laws* as the original object. It was originally assumed that parity is conserved upon collisions, and this implied that elementary particles have antiparticles, such as neutrinos and antineutrinos, such that the antiparticle subscribed to the *same* physical laws as the particle. This all changed with the publishing of Lee and Yang's seminal work [3] that argued that parity was *not* conserved in weak interactions. One such interaction is radioactive decay, described to arise from what is referred to as the "weak force", contrasting the strong force and electromagnetism both of which are shown to conserve parity in interaction with matter. Experiments by Wu et al. [4] involving the direction of beta decay emitted from Co^{60} in a magnetic field (thus relative to the associated applied magnetic field vector) confirmed that in beta decay, parity is *not* conserved. The relationship between *gravitating* bodies is also a manifestation of weak interactions. In both a field-based wave-mechanical model of gravity, and a particle-based collision-induced model of gravity [5, 6], parity is thus interpreted to be non-conserved.

The theoretical analysis [6], which was based on the interpretations from super K data that the neutrino oscillations between flavors could only occur if the neutrino had a rest mass, was cast in terms of a net transfer of *linear* momentum, but since it is now known that the neutrino always possesses left-handed helicity, and since it is reported that upon inelastic collision between a neutrino at $v \sim c$, and a proton or a neutron, the flavor of the neutrino has a very high probability to change — thus the spin magnetic moment property of the particle changes — the analysis is broadened herein to include *total* angular momentum. The nucleon's spin properties, the neutrino's spin properties, and the neutrino's essentially linear velocity at collision, all then demand the consideration of spin angular momentum *and* linear angular momentum; however, since quark properties must also be considered in an inelastic interaction with protons or neutrons, the orbital angular momentum must also be treated in a full analysis.

A major element of a collision-induced gravity model that has not been yet explained is how the heat generated in the inelastic collision is carried-off from the local neighborhood of the 3D coordinates of the collision. Without fully explaining heat carry-off, such a model is not complete. The major purpose of this current work is to propose to an international forum of readers, a model for the phenomenological basis of this removal of heat, so as to receive feedback and stimulate further work.

In the interest of simplicity in basic modeling, the collision-induced mathematical analysis did *not* treat the effect of a change-in-flavor of the neutrino (flux) consequent to a neutrino-nucleon inelastic collision due, for example, to a collision with nucleons of the moon during a total solar eclipse, which would then generate a change in the collision cross-section that could affect a subsequent collision with another mass body (such as an interaction with a gravity measuring experimental apparatus located at an Earth laboratory). As a more comprehensive knowledge of the properties of the neutrino is emerging, it seems *unlikely* that a collision of a neutrino with a mass particle would *not* cause a change in flavor. Although the original model [6] has been successful [7] in generating the total solar eclipse (occurring March 1997 in China) gravitational anomaly dip signal detected by Wang et al. [8], and elaborated upon by Yang and Wang [9], adjustment parameters are employed to reproduce the signal, especially in the central region of the signal, but the fundamental *functional* basis for these collision-related parameter adjustments is not yet established.

In wave mechanics terms, and in a particle approach, when the spatial coordinates are reflected from coordinates x, y, z through the origin to position $-x$, $-y$, $-z$, non-conservation of parity means that what is physically expected/observed at x, y, z is *not* the same as what is expected/

observed at $-x$, $-y$, $-z$. In the model/theory of collision-induced gravity this has profound importance, and herein is applied to explain the process of heat carry-off after the inelastic scattering net-transfer-of momentum interaction that the collision model invokes as the fundamental cause of gravity. Without solving the heat-carry-off problem, the collision model suffers vulnerability to a potentially critical weakness.

In our original theoretical work [6] we utilized 10^{-38} cm^2 for the collision cross-section of the neutrino with the neutron, as well as for the collision cross-section with the proton — a value now supported by other studies [10] that relate to the Feynman parton model, and about one order of magnitude higher than the values of sigma arising from earlier work [11]. This is an extremely small collision cross-section, and implies a very enormous flux density of particles such that the neutrino could be considered a realistic candidate for the particle that carries the gravity interaction property. The paradox is that even though experiments such as those conducted in the Super K project or related works, report that it is exceedingly difficult to detect a neutrino (as with scintillator counter devices), these calculations and the interpretations of experiments, do not consider that the neutrino is taking part in gravity interactions, and thus is implicitly detected. If the neutrino is indeed responsible for collision-induced gravity, then the equipment and experiment that is being utilized to detect its collisions with nucleons — such as the 50000 gallons of nuclide treated water, and the associated scintillation counters — is itself detecting neutrinos by virtue of the gravitational interactions related to the experiment as a whole.

2 Initial hypothesis

My own interpretation of very important and unique experimental work of the collimated free-falling neutron experiments at Grenoble [12] is that gravitational interactions must be quantized. And my own hypothesis as to the origin of that quantization, and also the origin of the phenomenon that explains the carry-off of heat generated from an inelastic scattering interaction (in which although momentum *is* conserved, energy is *not* — because of the involved heat), is cast in terms of the quantum mechanics of neutrino-nucleon inelastic collision, and this necessarily must involve the quark constituents of the nucleon. (If this were not so, then I see no way in which gravity can be quantized, and no way that collision-induced gravity could pass all of the scrutinizing tests necessary for embracing a model/theory as viable in modern physics.) Thus the hypothesis must include that the quark-antiquark interaction is involved in the heat carry-off phenomenon.

3 Related original experimental results

For the details regarding experimental findings, including the non-constancy of G, that are not explicable through field theory, including General Relativity, see [8, 9, 13–16]. The original data for my own experimental work, measuring a gravitational anomalous dip ($\sim$35 sec) on 18 May 2001 (16:10 hrs EDT) during the lineup of Earth-Sun-Jupiter's magnetosphere, and Saturn is given in Fig. 1 [16]. This signal was measured using two close-proximity dual-cable suspended Newton cradle pendula. The inter-pendula distance was interrogated with a 100 mw He-Ne cw laser. A change in the very short length-scale inter-pendula distance caused a change in the scattered laser radiation which was detected by a light-detecting diode. The output of the diode detector was fed into a Goerz 7800 chart recorder in the Y vs t mode, and also into a computer using an analogue-to-digital converter. All apparatus was mounted on an optical bench floating on inner tubes, and within a screened enclosure to preclude stray signals. Isolation transformers and RC filters were employed to minimize effects of transients. The operational amplifiers were employed on an offset scale for highest sensitivity so that the magnitude of the dip in gravity, which is shown in Fig. 1, is a relative measurement in arbitrary units. To my best estimate, the decrease in gravity due to the syzygy is of the order of a few microgals (see caption to Fig. 1). At the time of the measurement of the anomalous dip shown in Fig. 1, by use of a telescope attached to the experimental apparatus, I could clearly see the two pendula separating slightly due to the weakened gravity because of the presence of the Sun, Jupiter's magnetosphere, and Saturn that had moved between the deep space source of neutrinos and the Earth-laboratory.

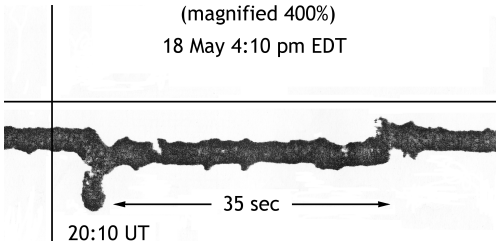

Fig. 1: Original raw data [16] of anomalous dip in gravity detected by use of laser scattering between two gravitating dual-cable suspended pendula, during the planetary line-up/syzygy of 18 May 2001: Earth/Sun/Jupiter's-magnetosphere/Saturn. The leading edge of the signal when expanded is a parabolic dip very similar to the initial parabolic dip detected by Wang et al. [8] for the 1997 total solar eclipse in China. The trailing edge is a parabolic bump, not analogous to any reported data known to the author. I interpret the above signal as due to occulting by the chromosphere-photosphere 1000 km zone of the Sun associated with an enormous change in temperature (from 10,000 to 1,000,000 degrees) and a major change in density, characteristic of the corona region.

The work of Refs. [8, 9, 13–16] strongly argue that G is *not* a constant, and this has been readily shown by the work of Gershteyn et al. at the Massachusetts Institute of Technology, reporting [17] that G varies at least 0.054% as a function of the orientation of the vector between the two gravitating

Cavendish spheres and the direction to large stars, and also that G is periodic with the sidereal year This histogram periodicity can only develop, in my judgment, if gravity is based on external impinging particles such that once per sidereal year the bulk of the Earth is interrupting the flux of gravity-bearing particles some of which never reach the measuring instrumentation (the Cavendish spheres). More precise examination of data of highly controlled robotically measured experiments such as that of Ref. [17] should be capable of measuring indications of periodicity of G on a monthly and daily basis as well. My own work determined the value of G (measured in 2007 in New England) as $G = 6.692 \pm 0.10 \times 10^{-11}$) cubic meters per kg sec^2 [18]. This work was accomplished with a fixed 16 pound spherical composite non-conducting resting mass located on a micro-moveable track, and a close-proximity 3 gram cork pendulum suspended from a nylon fiber. The inter-mass distance was interrogated by a HeNe cw laser, the radiation of which was scattered by the gravitating masses, and detected by a light-detecting diode and/or a solar cell, the output of which was fed into an oscilloscope.

The spatial and temporal patterns of the scattered laser light were measured as the massive sphere was slowly moved, by a servo-mechanism, toward the oscillating cork pendulum, which caused the frequency of oscillation of the cork pendulum to change slightly. By measuring this change in frequency (Δf) as a function of distance between the gravitating masses, we could determine the change in interacting energy, and determine the change in the associated force between the gravitating masses. We tested for any charge concentrations on the gravitating masses, and observed none. The theoretical analysis for the massive-sphere/pendulum interaction can employ either a Newtonian approach or a Lagrangian approach, yielding the same results. From these analyses we could extract the value of G. Our work also showed that our value of G changed somewhat if a film of water replaced air as the inter-mass medium, and changed again, if the temperature of that water was altered from 22°C to about 60°C.

Both our work and the highly accurate laser-cooling interferrometric Pb micro-mass work of Fixler et al. at Stanford (published earlier in 2007), giving $G = 6.693 \times 10^{-11}$ [19], is at significant variance from the accepted averaged value of 6.67, and thus indicates that corrections must be made to those determinations based on using the standard accepted value of G. As a function of collision parameters [6], G is expected to change with time, and with location of the position of measurement in the galaxy, and in the universe.

Our earlier measurements showed that G changes as a function of temperature according to $G = G_0(1 + aT)$, where a is a micro-valued constant in accord with measurements taken much earlier in England, and also changed as a function of phase (increasing as ice melts to water) and as a function of shape (increasing as a loop of 1 mil diameter Cu wire underwent multi-convolutions of the loop to approximate a sphere such as a spool of wool) [16,18].

4 Theoretical discussion

The parton model, advanced by Richard Feynman, postulates that the nucleon is composed of point-like constituents, referred to as partons. The partons share the total momentum of the nucleon by constituting variable fractions of the total momentum, designated (within the Feynman model) by the variable x. The probability, $f(x)$, of the parton to carry momentum does *not* depend upon the process in which it is engaged, or the nucleon energy, but is an intrinsic property. This, in my own interpretation, is fundamental to collision-induced gravity — namely that the carrying and transferring of momentum is an intrinsic property of the neutrino-nucleon interaction, and this is why, at least in part, the gravitation interaction is weak. The partons are composed of the three quarks (referred to as the valence quarks), but also includes the quark-antiquark pairs emerging from vacuum point energy, explicable by the uncertainty principle as well as involving gluons which are quanta of the strong force of quark interactions. The question naturally arises of how a *weak force* non-parity-conserving interaction can affect *strong* force quanta. Because the momenta of quarks (and of gluons) are added to give proton momentum, and from implication of the collision-induced gravity theory, I wish to postulate herein that there exists a constraint, and although strong forces/interactions are necessary to break quark-quark bonds and break apart the nucleus, weak forces are sufficient to change, for example, a d-quark (down-quark) to u-quark (up quark) which involve a transmutation of a neutron to a proton, and which gives rise to a quark-antiquark interaction, otherwise quantum mechanical selection rules could not emerge. Justification for this postulate is given subsequently.

It is thus proposed herein, based on my own interpretation of what is necessitated and implied in collision-induced gravity model and theory, that

> ... the within-nucleon transition of a d-quark to a u-quark, or the reverse, is associated with the formation of an antiquark, without the requirement of GeV energies necessary to break apart the nucleus.

(Because of the broken parity, I believe that further analysis and research must be conducted to determine/understand any thermal properties that might be associated with the antiquark).

The laws of quantum mechanics as applied to the wave function that is associated with the quark-antiquark system, imply that for a quark and antiquark, having angular momentum, L, the parity is established by:

$$P = (-1)(L + 1),$$

where L is an integer. Thus, in an even function, parity is conserved, but if the applicable function is an odd function, then parity is *not* conserved.

The amount of orbital angular momentum, L, and the spin angular momentum, S, of the quark-antiquark system is constrained by quantum mechanics as integers. Parity (P) depends only upon relative orbital angular momentum between objects, however, charge conjugation (C) depends upon both the orbital angular momentum and the combined spin states of the quark and antiquark. If the sum of $L+S$ is an odd integer, then the wave function changes sign when charge conjugation is effectuated upon a collision between a neutrino and a nucleon. From the analysis, there are a set of allowed states $J(PC)$ for a quark and an antiquark in net spin 0 and 1 coupled to orbital angular momentum, L, and total spin $J=L+S$. It is within the context of allowed $J(PC)$ states whereby gravity is, I believe, quantized.

Since the neutron is believed to be spherically symmetric, having a much simpler topology than the proton (which appears to be peanut or torus shaped depending upon respectively whether the quark spin aligns with the proton spin or opposite to it), and since the magnetic moment of the neutron is opposite in direction to that of the highest magnetic moment neutrino flavor — the tau neutrino which has a magnetic moment two orders of magnitude higher than the electron neutrino and/or the muon neutrino — the neutrino-neutron inelastic interaction is first analyzed herein. (I believe that the change of shape of the proton, associated with the alignment relationship of the spin of the quark emphasizes the importance of the quark-antiquark interaction, as related to gravitation.)

The inelastic scattering interaction between the neutrino and the neutron can be described as:

$$\nu(0)+\mathrm{n}(0) \longrightarrow \mathrm{p}^{+}+\mathrm{e}^{-}+\nu_{[\mathrm{anti}]}(0),$$

where ν refers to the neutrino, p refers to the proton, e refers to the electron, 0 means charge neutrality, and $^{+}$ and $^{-}$ refer to positive and negative charge, and "anti" refers to an anti-particle. The above represents a nuclear transmutation creating an element of atomic number $Z+1$, from an element of atomic number, Z, however the transiently created element having $N-1$ neutrons, yet essentially unchanged atomic weight A. This process must be associated with the creation of heat, and kinetic energy cannot be conserved. This neutrino-interaction generating a $Z+1$ atom must decay to the stable Z atomic number atom, and the created heat cannot be allowed to build up, thus must be transported from the system. The reverse-direction reaction, namely

$$\mathrm{p}^{+}+\mathrm{e}^{-}+\nu_{[\mathrm{anti}]}(0) \longrightarrow \mathrm{n}(0)+\nu(0)$$

must also be valid in the description of collision-induced gravity*. This then indicates that if the neutrino or the antineutrino perturbs the proton, then the electron can become unstable and collapse into the proton, and combine with the proton to form a neutron (by changing the direction of one quark).

The reaction that then represents the decay of the unstable $Z+1$ state is normally written:

$$^{A}_{Z}X_{N} \longrightarrow {}^{A}_{Z-1}Y_{N+1}+\mathrm{e}^{+}+\nu\,,$$

where X and Y designate different elemental atoms that differ by one proton, or by a single quark in the up-flavor (X), rather than the down-flavor (Y).

The equivalent reaction for the decay of the unstable state after the interaction between the neutrino and the proton is written as:

$$^{A}_{Z}X_{N} \longrightarrow {}^{A}_{Z+1}Y_{N-1}+\mathrm{e}^{-}+\boldsymbol{\nu}\,,$$

where $\boldsymbol{\nu}$ represents the antineutrino. The above represents beta decay.

> In summary of the above, it is postulated that the generated heat is carried off by the neutrino, and the antineutrino, ejected with changed energy, that are produced, respectively, in the above nuclear decay reactions, and do so according to quantum mechanical selection rules that emerge from the quark-antiquark non-conservation of parity interaction.

It is herein proposed that the Feynman work indicating that the cross-section for the neutrino-nucleon interaction can be described through the quark distribution functions, $d\sigma/dxdy$, which expressed in terms of momentum of the u-quark and the d-quark, is fundamental to explain collision-induced gravity. The work clearly shows that more momentum is transferred by quarks than be antiquarks.

The calculation yields that

$$\sigma_{\nu}=1.56\left(Q\pm\frac{Q}{3}\right)\times 10^{-38}\ \mathrm{cm}^{2}/\mathrm{GeV},$$

where Q represents the momentum integral (for the integrated cross-section). This gives sigma $\nu=0.74\pm 02\times 10^{-38}$ cm^2/GeV for the neutrino, and for the antineutrino, sigma $\nu_{[\mathrm{anti}]}=0.28\pm 0.01\times 10^{-38}$ cm^2/GeV. Therefore σ is linearly *energy dependent for both the neutrino and the anti-neutrino*, and, thus, so is the heat carry-off phenomenon. This also suggests that more heat is carried off by neutrinos than antineutrinos, and this must be because of the structural differences between the proton and the neutron, and differences in their collision cross-sections with respect to neutrinos.

The implication of a collision-induced gravity is that since gravity is statistical, and that the net change of momentum involves a flux of externally impinging particles, and certainly more than a single proton or neutron, and thus a collective effect of protons and neutrons interacting with external particles (neutrinos), such interactions will always be at least slightly different regarding the number of total particles involved. This implies that no two measurements, taking place

*Otherwise, if the inelastic collision with the neutrino, only involved neutrons, then hydrogen (consisiting of one proton, one electron, and zero neutrons) would not be observed to possess weight.

at two different time, of any experimental parameter will ever yield exactly the same value — this possibly related to some of the physical roots of the Uncertainty principle. Both the entity being measured, and the entity doing the measuring, are constantly changing to at least some infinitesimal level because of the stochastic properties of a particle-based gravity. This implies, for example, that typical Poisson statistics are not simply an instrument to assess statistical error in measurements, and standard deviation, but are a fundamentally related to the statistical properties of gravity.

Before this paper can attain closure, it is necessary to furnish scholarly support for my postulate that the quark-antiquark interaction (necessary for establishing the quantum mechanical selection rules that give rise to heat carry-off) can arise from weak interactions. As a career condensed matter basic research physicist, who for the past ten years has been working in gravitation measurements, and interpretations thereof aimed at an understanding of the fundamental cause of gravity — not being a theoretical particle physicist — I had to recruit the assistance from others upon realizing reaching a potential impasse in endeavoring to explain heat carry off — that impasse being explaining how a weak interaction can affect the tri-quark current. I was graciously assisted [20], and the following italicized material is a condensed version of this assistance which is highly cogent to my work.

> The non-conservation of parity of hadronic interactions is closely related to the interaction current of neutrino couplings. Key to understanding this relationship is the unification between leptonic neutrinos and gluons. This manifests at *lower* energy values of particle couplings and is observed in decay patterns of the high-quark meson complexes, such as the top- and bottom-quarks, but these are resonant energies of the up-quark and the down-quark. The proton-neutron interconversion acts to cause a mixing of wave functions and the exchange of a mesonic mediator. This is known as Yukawa coupling, and it is the Yukawa meson that carries the antiquark which couples to an up-quark of the proton. These couplings necessarily relate to the Heisenberg zero-point energy (ZPE) metric background.

In our measurement of G, cited earlier herein, the method which we employed, involving ultra-close-length/scale gravitating bodies, interrogated by cw laser scattering (as a function of the temperature of the coupling medium of air or water), inescapably had to involve the Casimir effect and ZPE — albeit a classical or mixed version of the Casimir effect. It seems that fundamental studies of the physics of the quark-antiquark interaction must involve ZPE.

> The net result is that the strong gluonic coupling can be assumed by the weak antineutrino coupling in terms of a neutral weak-interaction current. The current arises from the triquark complex of a nucleon, and thus can re-circulate; therefore the original nucleon (such as the neutron in the $\nu + \mathrm{n}$ inelastic interaction) can be re-materialized. The associated long decay times are ideal for heat carry-off. The significant point to this is that the quark-antiquark coupling (designated ud') is transmuted into a temporary diquark selfstate (designated ud) following a simple exchange of the state-antistate couplings of the neutral pions (designated dd' and uu').

My experimental results indicate that as related to gravitational interactions, the above couplings collectively are associated with time-constants, or relaxation times, of the order of a fraction of a millisecond. The results of the above analysis, and the available CERN Proton Synchrotron data on the neutrino and the antineutrino, and on the quark and the antiquark, indicate that the input-output physics of the neutrino-nucleon inelastic scattering process yields only a relatively small fraction of the input energy being converted to heat. This is because of values of masses and velocities before and after the inelastic collision do not change substantially. I estimate that the maximum heat energy would be about 15% of the input neutrino energy, and this depends upon the exit velocity of the antineutrino. Detailed quantitative calculated results giving the heat carry-off in electron volts, as a function of input energy in electron volts, will be eventually forthcoming as theoretical intra-nucleus thermodynamic codes become more detailed and comprehensive.

5 Conclusion and interpretation

I conclude that my conjecture/postulate that for d-quark/u-quark neutrino-inelastic- collision-induced transmutations, and consequent quark-antiquark interactions, the strong gluon energies are *not* required for neutral currents, and the weak gluon-neutrino interaction is sufficient, is supported by current accepted theory. Although the above analysis includes very complex internal nuclear processes, and although as scientists we search for elegant simplicity in explanations of nature, it seems to me that to provide an understanding of the heat carry-off phenomenon in inelastic neutrino-nucleon scattering, the invoking of these very complex workings within the nucleon is necessary.

Acknowledgements

The author wishes to express appreciation to Dr. W. Stanley, Professor X. Yang, and members of the Yahoo physics group forums for years of valuable discussions that relate to this work. Gratitude is also expressed to the administration and faculty of Lebanon College who have been supportive of my research, and to Sandra Smalling who has edited and assembled graphics related to thousands of items of data and thousands pages of publications and reports. Appreciation is

also extended to Dr. John Gedye (dec), Frank Lucatelli, Dr. Robert Zamenhof, Robert Morgan, Professor C. Blatchley, Mr. Julian Leon, Ms. Leanne Mortell, Dr. Richard Chrystal, Dr. Traci Jensen, and Dr. Dave Spero for intensive discussions and/or administrative support over the course of the past ten years.

Submitted on January 05, 2009 / Accepted on January 09, 2008

References

1. Bertulani C. Nuclear physics. Princeton University Press, 2007, p. 8, 9, 195, 196. See also Kaku M. and Thompson J. Beyond Einstein. Anchor, Random House, New York, 1995.
2. The new physics. Edited by P. Davies, Cambridge University Press, 1989, p. 400–405.
3. Lee T. and Yang C. *Phys. Rev.*, 1956, v. 104, 256–259.
4. Wu C. et al. *Phys. Rev.*, 1957, v. 105, 1413–1416.
5. The original work on push gravity is attributed to le Sage, and analyzed by Laplace.
6. Stanley W. and Vezzoli G. Induced gravity model based on external impinging neutrinos: calculation of G in terms of collision phenomena and inferences to inertial mass and atomic quantization. arXiv: astro-ph/0102109.
7. Stanley W. and Vezzoli G. Unpublished manuscript.
8. Wang Q., Yang X., Wu C., Guo H., Liu H., and Hua C. Precise measurement of gravity variation during a total solar eclipse. *Phys. Rev. D.*, 2000, v. 62, 041101R.
9. Yang X. and Wang Q. Gravity anomaly during the Mohe total solar eclipse and new constraint on gravitational shielding parameter. *Astrophysics and Space Science*, 2002, v. 285, 245–253; also: Yang X. Private communications. 2005–2007.
10. Kudryabtsev V. Lectures "The Development of Particle Physics". *Phys. Lett.*, 1986, v. 170B, 79–89. This work treats the Feynman parton theory.
11. Work originally done at Princeton University, 1959.
12. Nesvishevsky V.N. et al. Quantum states of neutrons in Earth's gravitational field. *Nature*, 2002, v. 413, 297–299.
13. Alais M. Movement of paracanonical pendulum and total solar eclipse of 30 June 1954, 1957. *Proceedings of the French Academy of Sciences*, 1959, v. 18, 46–49.
14. Saxl E. and Allen M. 1970 solar eclipse as "seen" by a torsion pendulum. *Phys. Rev. D*, 1971, v. 3(4), 823–825.
15. Mishra D. and Rao M. Total solar eclipse of October 224, 1995 in Dhorajii, Saurashtra. *Current Science*, 1997, v. 72(11), 783–786.
16. Vezzoli G. C. Gravitational data during the syzygy of May 18, 2001 and related studies. *Infinite Energy*, 2004, v. 9(53), 18–27.
17. Gershteyn M. et al. *Gravitation and Cosmology*, 2002, v. 3(32) 243–247. This work is regarded by the author as of profound significance, and relates to analogous sidereal year, lunar month, and solar day, periodicity in properties of radioactive decay of Pu-239, observed and reported by S. E. Schnol' for decades; see Letters authored by myself and Schnol' in *Progress in Physics*, 2008, v. 2. I have observed similar diurnal periodicity in related experiments using Po-210 during Jupiter eclipsing quasar J0842+1835, 7–11 Sept 2002 (see Ref. 16).
18. Vezzoli G.C. Experimental research incondensed matter physics arguing for modifications in mainstream concepts: considerations of the significance of a physics of collisions, shape and spin, regarding charge as a paradigm, relationship to subtle energy physics and far-from-equilibrium physics as well as zero point energy. *Infinite Energy*, 2007.
19. Fixler J. et al. Atom interferometer measurement of the Newtonian constant of gravity. *Science*, 2007, v. 315, 74–77.
20. John Shadow (Moderator: Yahoo Groups, Theoretical Physicist); Hans Schatten (Theoretical Physicist) and Tony Bedmenseder (Quantum Relativity Theoretical Physicist). Private communications.

The Mass of the Universe and Other Relations in the Idea of a Possible Cosmic Quantum Mechanics

Ioannis Iraklis Haranas* and Michael Harney†

*Department of Physics and Astronomy, York University, 314A Petrie Building, North York, Ontario, M3J-1P3, Canada
E-mail: ioannis@yorku.ca

†841 North 700 West, Pleasant Grove, Utah, 84062, USA
E-mail: michael.harney@signaldisplay.com

Recent observations confirm that galactic red-shifts might be quantized and hint a possible new form of quantum mechanics, which could probably explain these observed properties of the galaxies. This brief note investigates some expressions for the mass of the universe M_U, which were obtained with the help of the definition of the new cosmic Planck's constant $\hbar_g$.

Introduction

After it was found that the recession velocities for single and double galaxies appear to be quantized [1] then a new quantum of action was also derived to yield [2, 3]:

$$\hbar_g = \frac{\left(1+\sqrt{3}\right)^2 M}{H} V^2 \cong 7.0\times10^{74}\ \text{erg}\times\text{s}, \qquad (1)$$

where $V = 12$ km/s, $M = 10^{44}$ g, and $H = 1.7\times10^{-18}$ s^{-1}. Using Weinberg's relation for the mass of an elementary particle [4] we can now expect to obtain the mass of the universe if Planck's constant in (2) has been substituted by the new maximum value of the new cosmic quantum of action $\hbar_g$ [5]. Therefore we have

$$M_U = \left[\frac{\hbar_g^2 H}{Gc}\right]^{1/3}. \qquad (2)$$

If we now solve for the new defined quantum of action $\hbar_g$ in equations (2), and also use (1) we obtain that the mass of the universe is given by:

$$M_U = \left(1+\sqrt{3}\right)^4 \left[\frac{v^4}{GHc}\right]. \qquad (3)$$

Relation (3) was obtained after treating the universe as the "ultimate superparticle" following Weinberg's idea [4], and using his relation for the mass of an elementary particle. If now assume that velocity v corresponds to the radial velocity of the individual "particle" galaxies we can further assume that their velocities are those of the expansion of the universe's horizon, and will be equal to speed of light c, so that we obtain:

$$M_U = \left(1+\sqrt{3}\right)^4 \left[\frac{c^3}{GH}\right]. \qquad (4)$$

Substituting for the known values of constants in (4), and using $H = 1.7\times10^{-18}$ s^{-1} we obtain for the mass of the universe to be

$$M_U = 1.326\times10^{58}\ \text{g}. \qquad (5)$$

The mass of the universe found here is actually higher than the universes's actuall mass of 7.5×10^{55} g as given in [6] That could also be due to the contribution of the numerical term that enters the calculations from the definition of the cosmic $\hbar_g$. Since not all the objects in the universe are within such a great cosmic distances to allow $v \approx c$, this could also mean that the cosmic quantum mechanics idea could apply to the universe at very early times when the objects were closer together. To ensure numerically the value of the mass of the universe from (3) a galaxy would have to have a radial velocity $v = 0.254c = 7.640\times10^9$ cm/s. Objects of this redshift are observationally quite frequent. Quasistellar objects or quasars hold the record for redshifts up to $z = 5$ [7]. Therefore it could be that at those cosmic distances that quasars exist qualifies them for possible candidates of cosmic quantum mechanics, which somehow could be effecting their physics. Now suppose that this superparticle universe contains a number of particles in an Euclidean sphere of radius c/H_0 then, following Narlikar [8] we have that:

$$N = \frac{c^3}{2m_pGH}. \qquad (6)$$

Using (6) and (4) we can also obtain for the mass of the universe:

$$M_U = \left(1+\sqrt{3}\right)^4 [2m_pN] = 1.86\times10^{58}\ \text{g}, \qquad (7)$$

and where m_P is the mass of the proton, 1.672×10^{-24} g, and $N \approx 10^{80}$ is the total number of particles in the universe.

Let us now consider relation (4) and from that let us try to obtain the mass of the "super-particle" universe at very early times, and near Planck time. For that a very early Hubble constant should be taken into account. Since the age of the universe in general is equal to the inverse of the Hubble constant, then $\frac{1}{H_p} = t_p = \frac{\hbar}{m_{pl}c^2}$ we finally have after simplifying that

$$M_U = \left(1+\sqrt{3}\right)^4 m_{pl} = 1.114\times10^{-3}\ \text{g}. \qquad (8)$$

Now let us define the maximum value of the cosmological constant Λ which is defined below [9]

$$\Lambda_{max} = \frac{c^3}{G\hbar} \approx 10^{66}\ \mathrm{cm}^{-2} \quad (9)$$

and occurs during the quantum era of the early universe and using (1) we can now obtain the corresponding $\Lambda_{max}(\hbar_g)$ under cosmic quantum mechanics and so we have

$$\Lambda_{max}(\hbar_g) = \frac{c^3}{G\hbar_g} = 5.782\times10^{-37}\ \mathrm{cm}^{-2}. \quad (10)$$

Using now (10) together with (4) we can also write for the mass of the universe

$$M_U = \left(1+\sqrt{3}\right)^4 \left[\frac{\Lambda_{max}(\hbar_g)}{H}\right]\hbar_g = \\ = 1.894\times10^{-17}\hbar_g = 1.325\times10^{58}\ \mathrm{g}. \quad (11)$$

From the above we see that the mass of the universe becomes a multiple of the cosmic $\hbar_g$, or in other words the mass of the universe is now quantized in units of the cosmic $\hbar_g$. That could probably indicate that if cosmic quantum mechanics is in effect in the universe, basic quantities like mass, energy, or angular momentum could also be quantized, in an analogy with ordinary quantum mechanics.

Next if we try to obtain the cosmic quantum mechanical equivalent of Planck time by again substituting $\hbar \to \hbar_g = 7\times10^{74}$ ergs we have:

$$t_{pl_{cos}} = \sqrt{\frac{\hbar_g G}{c^5}} = 4.383\times10^{7}\ \mathrm{s}. \quad (12)$$

This period is well into the radiation era of the universe which lies between $10\ \mathrm{s} \leqslant t \leqslant 10^{12}$ s [10]. Next we can obtain the possible maximum cosmic Planck time for $\hbar_g = 2.228\times10^{94}$ ergs

$$t_{pl_{cos}} = \sqrt{\frac{\hbar_g G}{c^5}} \approx \frac{1}{H_0} = 2.472\times10^{17}\ \mathrm{s}. \quad (13)$$

The time found in (13) is almost the value of the Hubble constant today. This is the matter era of the universe. For the value of time in (13) a temperature close to the microwave background should be calculated. Therefore we have:

$$T = \frac{1.5\times10^{12}}{t^{2/3}} = 3.808\ \mathrm{K}. \quad (14)$$

Next a relation can be derived which connects the mass of the "super-particle universe" to its gravitational energy under the cosmic $\Lambda_{max}(\hbar_g)$. In general the energy of a hadron particle is given by [11]:

$$E_{grav} = \frac{Gm^3c^2}{\hbar^2} \cong NH_0. \quad (15)$$

Therefore (4) becomes:

$$M_U = \left(1+\sqrt{3}\right)^4 \left[\frac{\Lambda_{max}(\hbar_g)}{H_0^2}\right] E_{grav}(\hbar_g) = \\ = 1.114\times10^{1} E_{grav}(\hbar_g) = 1.894\times10^{57}\ \mathrm{g}. \quad (16)$$

Conclusions

A relation for the mass of the universe has been derived in the grand scheme of a possible quantum mechanics, an idea that emanates from a probable redshift quantization in observational data. The mass of the universe has been found to depend on three fundamental quantities: i.e. the speed of light, the gravitational constant, and the Hubble parameter. Its numerical value is almost two hundred times higher than the actual mass of the universe. From that another expression for the mass of the universe at very early times has also been retrieved. The mass of the universe at Planck time seems to be slightly larger than the Planck mass by a factor of a hundred. Next making use of a max quantum cosmic cosmological term (lambda) we obtained the mass of the universe, which now appears quantized in the units of cosmic $\hbar_g$. Also the Planck cosmic quantum mechanical time equivalent was obtained for the two different values of $\hbar_g$. The first lies in the radiation era of the universe, and the second in the matter era, being almost the same in magnitude with today's Hubble parameter, from which a temperature of 3.8 K is obtained. Finally the mass of universe was obtained in relation to its gravitational energy. Hence it might be that a relation between ordinary and cosmic quantum mechanics based on the results found might exists, a relation between microcosm and macrocosm an idea, which had been suspected for long.

Submitted on December 13, 2008 / Accepted on January 09, 2009

References

1. Cocke W. and Tifft W. *Astrophysical Journal*, 1984, v. 287, 492.
2. Dersarkissian M. *Lett. Nuovo Cimento*, 1984, v. 40, 390.
3. Dersarkissian M. *Lett. Nuovo Cimento*, 1985, v. 43, 274.
4. Weinberg S. Gravitation and cosmology. John Wiley, New York, 1972.
5. Haranas I. *Journal of Theoretics*, 2001, v. 3, no. 2, 2001.
6. Padmanabhan T. Structure formation in the Universe. Cambridge University Press, Cambridge, 1993.
7. Antwrp.gsfc.nasa.gov/apod/ap981211.html
8. Narlikar J. Introduction to cosmology. Cambridge University Press, Cambridge, 1993, p. 272.
9. Sivaram C. and de Sabbata V. *Astrophysics and Space-Science*, 1991, v. 176, 145–148, 1991.
10. Ohanian H.C. and Ruffini R. Gravitation and space-time. 2nd edition, Norton & Co., 1994.
11. Johri V.B. The early Universe. Hadronic Press, Instituto Per La Ricerca Di Base, Italy, 1996, p. 33.

A Planck Vacuum Cosmology

William C. Daywitt

National Institute for Standards and Technology (retired), Boulder, Colorado, USA

E-mail: wcdaywitt@earthlink.net

Both the big-bang and the quasi-steady-state cosmologies originate in some type of Planck state. This paper presents a new cosmological theory based on the Planck-vacuum negative-energy state, a state consisting of a degenerate collection of negative-energy Planck particles. A heuristic look at the Einstein field equation provides a convincing argument that such a vacuum state could provide a theoretical explanation for the visible universe.

1 Introduction

Cosmology, taken as a whole, is the study of the origin and evolution of the universe [1, p. 1144]. The universe is the visible (observable by whatever means) universe that exists in free space. At present there are two major competing cosmologies that theoretically describe the real observed universe, the big-bang cosmology [2] and the quasi-steady-state cosmology [3], the big-bang cosmology being considered by most cosmologists as the major one of the two. Both cosmologies claim some type of Planck state as the origin for their calculations; in the big-bang case it is a point source at time zero in which an explosion takes place, subsequently creating the expanding universe; while in the quasi-steady-state case a background field called the "creation field" creates free Planck particles (PP) on a quasi-continuous basis that immediately decay into a large number of particles, subparticles and fields.

The present paper presents a new cosmological model called the Planck-vacuum (PV) cosmology. The PV (briefly described in Appendix A) is an omnipresent negative-energy state that is assumed to be the Planck state that is the foundation for the visible universe, its expansion, and also its eventual contraction. The addition of the PV to the visible universe in a cosmological model requires a name to distinguish the combination from the visible universe of standard cosmology. The name used here is "cosmos" and includes, correspondingly, the PV and the visible universe. As might be expected, this new model differs significantly from the two models mentioned in the preceding paragraph.

We begin with a brief look at the standard Einstein metric equation

$$G_{\mu\nu} = \frac{8\pi G}{c^4} T_{\mu\nu} = \frac{8\pi}{m_* c^2 / r_*} T_{\mu\nu} \qquad (1)$$

where $G_{\mu\nu}$ and $T_{\mu\nu}$ are the Einstein and energy-momentum tensors, and G and c are the gravitational and speed-of-light constants. The force $m_* c^2 / r_*$ in the denominator of the final expression is the ultimate curvature force that can be applied to the spacetime of General Relativity or to the PV [4]. Compared to this force, the relative curvature force the sun, a white dwarf, or a neutron star exert on spacetime and the PV is 0.00001, 0.001, and 0.5 respectively. With the help of Appendix A, the Einstein equation can also be expressed in the form

$$\frac{G_{\mu\nu}/6}{1/r_*^2} = \frac{T_{\mu\nu}}{\rho_* c^2} \qquad (2)$$

where r_* is the Compton radius of the PP and ρ_* is its mass density. The ratio $1/r_*^2$ can be thought of as the PP's Gaussian curvature. In this latter form both sides of the equation are dimensionless. As the curvature force, the mass density, and the Gaussian curvature are intimately related to the PPs in the negative-energy PV, it is easy to conclude that the Einstein equation and General Relativity must also be intimately related to that vacuum state.

The PV-cosmology modeling begins in the next section which concerns the expansion of the cosmos. Since little is known about the PV at the present time, however, the calculations in that section and the one following it are a bit sketchy and of a cursory nature.

The PV cosmology must address the question of how PPs from the PV are injected into free space to populate the visible universe with the particles and fields upon which the larger components of the universe are built. A scenario for this injection process that somewhat parallels the quasi-steady-state theory of PP creation is presented in Section 3, the main difference being that in the quasi-steady-state model the PPs evolve from "creation fields" while in the present theory they spring directly from the negative-energy PV state.

A comments Section 4 closes the main text of the paper. Appendix A gives a brief description of the PV theory to date and Appendix B compares the PV to the cosmological-constant term in the Einstein field equation.

2 Cosmological expansion

The mass density of the degenerate PV state in the PV cosmology is roughly equal to the PP mass density

$$\rho_* \equiv \frac{m_*}{4\pi r_*^3/3} \approx 10^{94} \ [\mathrm{gm\ cm^{-3}}] \qquad (3)$$

where m_* and r_* are the PP mass and Compton radius respectively. If we somewhat arbitrarily take the universal

mass density as $\rho_m \sim 10^{-30}$ [gm cm^{-3}], then the ratio $\rho_m/\rho_* \sim 10^{-124}$ is vanishingly small. Thus it is unreasonable to expect that the visible universe can effect the expansion or contraction of the cosmos as it does for the universe in the big-bang and quasi-steady-state cosmologies. This fact leads to the conclusion that the expansion of the universe must be determined by that of the PV itself.

The expansion of a homogeneous and isotropic universe is characterized by the expansion factor S $(= S(t))$ in the Robertson-Walker line element [3, p. 111]

$$ds^2 = c^2dt^2 - S^2\left[\frac{dr^2}{1-kr^2} + r^2d\theta^2 + r^2\sin^2\theta\, d\phi^2\right] \quad (4)$$

where (t, r, θ, ϕ) are comoving coordinates, and where $k=+1$, $k=-1$, and $k=0$ denote a universe with a positive, negative, or zero curvature respectively. The Robertson-Walker metric is used to determine the "kinematic" properties of the universe for any given S, the dynamics of the expansion only appearing implicitly in the time dependence of S. For example, (4) can be used to derive the standard expressions for the redshift z [3, pp.112-113] and the Hubble constant H [3, pp.118–119]:

$$1 + z = \frac{1}{S} \quad (5)$$

$$H = \frac{\dot{S}}{S} \quad (6)$$

without specifying the particular dynamics of the expansion. Thus these relations are equally valid in the big-bang, quasi-steady-state, and PV cosmological models.

To determine the dynamics of the expansion factor in the big-bang and quasi-steady-state cosmologies, some form of the Einstein equation (2) is used. Both models start by calculating the Einstein tensor $G_{\mu\nu}$ from the metric coefficients of the Robertson-Walker line element (4). The standard big-bang cosmology then assumes various energy-momentum tensors for the right side of (2) to derive the Friedmann equations for S in the various phases of the expanding universe [2, pp.48–50]. An early version of the quasi-steady-state model modifies the numerator on the right side of (2) to include a "creation field" for generating PPs, then derives Friedmann-like equations for the expansion-factor dynamics [3, pp.322–324]. As the expansion-factor dynamics in the PV-cosmology model is determined by the expansion of the PV itself, however, it isn't clear what part the Einstein and Friedmann-like equations may or may not play in the research surrounding the PV cosmology.

There is no compelling evidence that the constants governing the fundamental laws of physics were once different from their present values [1, p. 1056]. This statement bares significantly on the nature of the PV expansion — it implies, in effect, that the PV expands by an increase in its content rather than a change in its properties. Assume that the number density of the PPs in the PV decreases as the PV expands for example. Then the density of the virtual fields of the quantum vacuum [5] would also decrease because the PV is the source of the quantum vacuum [6]. This in turn would decrease the magnitude of the dominant Bethe term [7, p. 208] in the $2S_{1/2} - 2P_{1/2}$ Lamb shift of atomic hydrogen as the Bethe term is proportional to the density of the virtual fields [5, p. 91]. Thus the 2S-2P transition frequency of the atom would decrease as the PV expands, contradicting the assumption in the first sentence of the paragraph.

3 Planck Particle creation

It is assumed that a sufficiently stressed PV will release one or more of its PPs into the visible universe in a manner resembling a mini-big-bang outburst. "[This] requirement is in agreement with observational astrophysics, which in respect of high-energy activity is all of explosive outbursts, as seen in the QSOs, the active galactic nuclei, etc. The profusion of sites where X-ray and γ-ray activity is occurring are in the present [quasi-steady-state] theory sites where the creation of matter is currently taking place" [3, p. 340]. It is then assumed that the new free-space PP decays into a number of secondary particles. The lifetime of the free PP is assumed to be governed by the time required ($t_* = r_*/c \sim 10^{-44}$ sec) for the internal PP fields (traveling at the speed of light) to decay within the confines of the PP Compton radius r_*.

It is too early in the PV-cosmology theory to present any substantial analysis concerning the details of the activity mentioned in the previous paragraph. We are left, then, with a heuristic description of the PP-creation process in terms of the Einstein field equation. Taking the (covariant) divergence of (2) gives

$$G^{\mu\nu}_{\ ;\nu} \equiv 0 \qquad \Longrightarrow \qquad T^{\mu\nu}_{\ ;\nu} = 0 \quad (7)$$

showing that the standard Einstein equation provides no mechanism for creating PPs due to the vanishing divergence of the energy-momentum tensor. Assume that at some point x^α $(\alpha = 0, 1, 2, 3)$ in empty spacetime ($T^{\mu\nu} \approx 0$ before x^0) a PP is ejected from the PV into the free space of the visible universe. In the standard action (see Appendix A)

$$\mathcal{A} = \frac{1}{2c}\left(\frac{\rho_* c^2}{1/r_*^2}\right)\int \frac{R}{6}\sqrt{-g}\, d^4x + m_a c\int ds_a \quad (8)$$

whose variation yields (2), the world lines are considered to be continuous in the full range $0 < |x^\alpha| < \infty$. At the point x^α where a PP is created, however, the PP world line begins. It is possible to modify (8) in that case so its variation leads to the modified Einstein equation [3, p. 323]

$$\frac{G^{\mu\nu}/6}{1/r_*^2} = \frac{T^{\mu\nu}_{(m_*)} + \mathcal{T}^{\mu\nu}_{(pv)}}{\rho_* c^2} \quad (9)$$

where, as interpreted here, the calligraphic tensor in the nu-

merator at the right is associated with processes taking place within the PV.

The free-PP creation represented by (9) is explained physically as an interchange of energy and momentum between the PV and the PP injected into the visible universe. The divergence of (9) now leads to

$$T^{\mu\nu}_{(m_*);\nu} = -\mathcal{T}^{\mu\nu}_{(pv);\nu} \tag{10}$$

which is meaningful only if the right side of the equation leads to a positive free-space PP energy [3, p. 325]; i.e. only if the 0-0 component of the PV energy-momentum tensor is negative. That this tensor component is negative follows from the fact that the PV state is a negative-energy state. Thus we have

$$T^{00}_{(m_*)} = -\mathcal{T}^{00}_{(pv)} = +\rho_* c^2 \tag{11}$$

as

$$\mathcal{T}^{00}_{(pv)} = -\rho_* c^2 \tag{12}$$

since the PP mass-energy density of a PP *within* the PV is $-\rho_* c^2$.

4 Sundary comments

It is assumed that the origin of the light nuclei and the cosmic microwave background in the PV-cosmology model are essentially the same as those discussed in the quasi-steady-state model [3, pp.350-358].

Both the big-bang and the quasi-steady-state cosmologies are based on field theory, the big-bang cosmology on the quantum field theory of the early universe [2] and the quasi-steady-state cosmology on the so-called "creation fields". The choice of a field-theoretic approach reflects, of course, the current paradigm that fields are the fundamental building blocks of the particles and subparticles out of which the observed universe is constructed. With the advent of the PV theory, however, these fields now have a charged source (the PPs within the PV) as their origin. It is this charged source that is the foundation of the PV cosmology presented here.

The action integrals in (A8) of the appendix tie the creation field $\mathcal{C}_\mu$ of the quasi-steady-state theory [3, p. 321] directly to the PPs in the PV.

The calculations in Appendix B show that the PV cannot be identified with the cosmological-constant term in the Einstein field equation.

Appendix A: The Planck Vacuum

The PV [4] is a uni-polar, omnipresent, degenerate gas of negative-energy PPs which are characterized by the triad (e_*, m_*, r_*), where e_*, m_*, and r_* $(\lambda_*/2\pi)$ are the PP charge, mass, and Compton radius respectively. The vacuum is held together by van der Waals forces. The charge e_* is the bare (true) electronic charge common to all charged elementary particles and is related to the observed electronic charge e through the fine structure constant $\alpha = e^2/e_*^2$ which is a manifestation of the PV polarizability. The PP mass and Compton radius are equal to the Planck mass and length respectively. The particle-PV interaction is the source of the gravitational $(G = e_*^2/m_*^2)$ and Planck $(\hbar = e_*^2/c)$ constants, and the string of Compton relations

$$r_* m_* = \cdots = r_c m = \cdots = e_*^2/c^2 = \hbar/c \tag{A1}$$

relating the PV and its PPs to the observed elementary particles, where the charged elementary particles are characterized by the triad (e_*, m, r_c), m and r_c being the mass and Compton radius $(\lambda_c/2\pi)$ of the particle (particle spin is not yet included in the theory). The zero-point random motion of the PP charges e_* about their equilibrium positions within the PV, and the PV dynamics, are the source of the quantum vacuum [6] [5]. Neutrinos appear to be phonon packets that exist and propagate within the PV [8].

The Compton relations (A1) follow from the fact that an elementary particle exerts two perturbing forces on the PV, a curvature force mc^2/r and a polarization force e_*^2/r^2:

$$\frac{mc^2}{r} = \frac{e_*^2}{r^2} \qquad \Longrightarrow \qquad r_c = \frac{e_*^2}{mc^2} \tag{A2}$$

whose magnitudes are equal at the particle's Compton radius r_c.

Equating the first and third expressions in (A1) leads to $r_* m_* = e_*^2/c^2$. Changing this result from Gaussian to MKS units yields the free-space permittivities [4]

$$\epsilon_0 = \frac{1}{\mu_0 c^2} = \frac{e_*^2}{4\pi r_* m_* c^2} \quad [\mathrm{mks}] \tag{A3}$$

where $\mu_0/4\pi = r_* m_*/e_*^2 = r_c m/e_*^2 = 10^{-7}$ in MKS units. Converting (A3) back into Gaussian units gives

$$\epsilon = \frac{1}{\mu} = \frac{e_*^2}{r_* m_* c^2} = 1 \tag{A4}$$

for the permittivities.

A feedback mechanism in the particle-PV interaction leads to the Maxwell equations and the Lorentz transformation. General Relativity describes the spacetime-curvature aspects of the PV. The ultimate curvature force [4]

$$\frac{c^4}{G} = \frac{m_* c^2}{r_*} \tag{A5}$$

that can be exerted on spacetime and the PV is due to a free PP, large astrophysical objects exerting a curvature force equal to Mc^2/R, where M and R are the mass and radius of the object. Equation (A5) leads to the important ratio

$$\frac{c^4}{8\pi G} = \frac{1}{6}\,\frac{\rho_* c^2}{1/r_*^2} \tag{A6}$$

where $\rho_* \equiv m_*/(4\pi r_*^3/3)$ is the PP mass density and $1/r_*^2$ is its Gaussian curvature.

Using (A6), the Einstein-Hilbert action $\mathcal{A}_g$ can be expressed as

$$\mathcal{A}_g = \frac{c^3}{16\pi G}\int R\,\sqrt{-g}\,d^4x = \\ = \frac{1}{2c}\left(\frac{\rho_* c^2}{1/r_*^2}\right)\int \frac{R}{6}\,\sqrt{-g}\,d^4x \tag{A7}$$

leading to the total PP-creation action [3, p. 321]

$$\mathcal{A} = \frac{1}{2c}\left(\frac{\rho_* c^2}{1/r_*^2}\right)\int \frac{R}{6}\sqrt{-g}\,d^4x + m_a c\int ds_a + \\ + \frac{f}{2c}\int C_\mu C^\mu \sqrt{-g}\,d^4x - \int C_\mu\, da^\mu, \tag{A8}$$

which includes the usual inertial second term, and the third and fourth creation-field terms containing C_μ. The effect of the PV PPs on this equation is clearly evident in the parenthesis of the first term which is the ratio of the PP's mass-energy density to its Gaussian curvature.

Appendix B: Cosmological constant

The Einstein equation including the cosmological constant Λ is

$$\frac{(G_{\mu\nu} + \Lambda g_{\mu\nu})/6}{1/r_*^2} = \frac{T_{\mu\nu}}{\rho_* c^2}, \tag{B1}$$

which can be expressed as

$$\frac{G_{\mu\nu}/6}{1/r_*^2} = \frac{T_{\mu\nu} + \mathcal{T}_{\mu\nu}}{\rho_* c^2}, \tag{B2}$$

where

$$\mathcal{T}_{\mu\nu}^{(vac)} \equiv -\frac{1}{6}\frac{\rho_* c^2}{1/r_*^2}\,\Lambda g_{\mu\nu} \tag{B3}$$

leads to

$$\rho_{vac} c^2 \equiv \frac{\mathcal{T}_{00}}{g_{00}} = -\frac{1}{6}\frac{\rho_* c^2}{1/r_*^2}\,\Lambda \tag{B4}$$

which is often seen as the "vacuum energy".

From (B4)

$$\frac{\rho_{vac}}{\rho_*} = -\frac{1}{6}\frac{\Lambda}{1/r_*^2} \tag{B5}$$

the ratio being negative for a positive Λ. If the vacuum density ρ_{vac} is identified as the PP mass density ρ_*, then

$$\Lambda = \frac{6}{r_*^2} \approx 2.3 \times 10^{66}\,[\mathrm{cm}^{-2}]\,. \tag{B6}$$

As Λ should be close to zero, it is clear that the PV is not related to the cosmological constant.

Submitted on December 31, 2008 / Accepted on January 13, 2009

References

1. Carroll B.W., Ostlie D.A. An introduction to modern astrophysics. Addison-Wesley, San Francisco—Toronto, 2007.
2. Kolb E.W, Turner M.S. The early universe. Westview Press, 1990.
3. Narlikar J.V. An introduction to cosmology. Third edition, Cambridge Univ. Press, Cambridge, UK, 2002.
4. Daywitt W.C. The planck vacuum. *Progress in Physics*, 2009, v. 1, 20.
5. Milonni P.W. The quantum vacuum — an introduction to quantum electrodynamics. Academic Press, New York, 1994.
6. Daywitt W.C. The source of the quantum vacuum. *Progress in Physics*, 2009, v. 1, 27.
7. Grandy W.T. Jr. Relativistic quantum mechanics of leptons and fields. Kluwer Academic Publishers, Dordrecht-London, 1991.
8. Daywitt W.C. The neutrino: evidence of a negative-energy vacuum state. *Progress in Physics*, 2009, v. 2, 3.

An Alternative Hypothesis for Special Relativity

Horst Eckardt

Alpha Institute for Advanced Study (AIAS) and Telesio-Galilei Association (TGA)
E-mail: horsteck@aol.com

An alternative theory being analogous to Einstein's special theory of relativity is presented. While Einstein based his theory on the relativity principle of motion and constancy of the velocity of light, this theory assumes an absolute frame of reference and a general length contraction. Both concepts are taken from general relativity and applied to an asymptotically flat space. This results in a transformation group being different from the Lorentz transformation and a Eucledian addition theorem of velocitites. The results are in accordance with experiments and long known discrepancies between special relativity and experimental findings are resolved as well as paradoxa being introduced by Einstein's original theory. Physical facts being unintelligible before can be interpreted in the light of the alternative theory.

1 Introduction

The theory of special relativity of Albert Einstein is essentially based on the constancy of the velocity of light in all inertial frames of reference. Einstein introduced this as a physical principle or axiom in order to explain the negative outcome of the experiments of Michelson and Morley who tried to prove the existence of a drift velocity of the earth in a hypothetical ether. However, in the last years a number of experiments came up showing that the velocity of light is not an incontrovertible constant. For example Nimtz [5, 6] has realised a transfer of information by microwaves by speeds faster than light. His explanations are wound and based on quantum effects (tunnelling) which should not appear in systems with exclusively macroscopic dimensions. Most convincing would be an explanation by classical physics which is also the basis of electromagnetic signal transmission. Another important development is the re-interpretation of the Michelson-Morley experiments [10, 11] which show that they had not been evaluated in the right way. When doing this, earlier inconsistencies are resolved and an absolute motion of the earth against the space background is detected. This revolutionary insight has not been recognized in the scientific public so far. Therefore re-thinking about the concepts of special relativity is required.

A second fundament of modern physics is the principle of relativity. Besides the reasonable assumption that laws of nature work in the same way in all reference frames not being accelerated to one another, it is postulated that the transformation between reference frames is always of the same form. It is assumed that all frames of reference be of equal kind. This consideration does not take into account that the universe is structured by masses which define reference points for physical processes. The whole universe is impleted with gravitational and electromagnetic fields. This also holds for the "empty" ranges between galaxies and galaxy clusters since the particle density is non-vanishing in interstellar space to today's knowledge. So we can say that in certain areas of the cosmos we can neglect the influence of cosmic fields, but normally we use the visible beacons (earth, sun, centers of galaxies) to define reference frames. The cosmos as a whole is described by general relativity and Mach's principle which states that the masses define the space. Without masses there is no space at all. Crothers [4] has pointed out that there is no smooth transition from general to special relativity:

> "Special Relativity is merely an augmentation to Minkowski space by the arbitrary insertion of mass and energy into Minkowski space with the constrained kinematic features of Minkowski space applied to those masses and energies".

This view is corroborated by newer advanced theories like Einstein-Cartan-Evans theory [18] where space is not empty but filled with the background or "vacuum" potential. Without potential there is no space, in accordance with Mach's principle. So it should become clear that general relativity (or any similar advanced theory) is necessarily required to define a basis for all physics. One can abstract then from these foundations and concentrate on other problems, for example experiments of particle collisions, without taking care of these basic premises. When it comes to define the frames of reference, however, the state of motion relative to the absolutely defined environment is important again.

All these arguments become much more intelligible if we assume that the space between massive particles has a state of motion. This sounds like introducing the old ether idea from the nineteenth century. Our knowledge has only little improved since then. The ether was abolished by Einstein, but indirectly re-introduced by himself in his theory of general relativity. It is possible to define an "objective" frame of reference constituted by existing masses. Considering Einstein-Cartan-Evans theory, space is not empty but itself a medium which for example has optical properties [18]. We can extend the comparison with usual media by assigning a state of

motion to the space itself. Masses "swim" in this space and therefore reflect its movement. Conversely, the fields created by the masses determine the surrounding space in a fed-back manner. Both entities cannot be considered independently from each other.

In Einstein-Cartan-Evans theory, the covariance principle is the most general description base of physics, indicating that all laws of nature are independent of the coordinate system or reference frame. Our physical environment is defined by the objectively existing structure which is defined by masses, charges and fields. These are adequately described in an objective manner by laws of nature being independent from subjective human receptions.

In this article we try to modify Einstein's axioms of special relativity in such a way that constancy of light velocity is not required to be introduced axiomatically. It will be shown that this is an artifact of measurement. Instead of this axiom we demand for an absolute frame of reference. As a consequence, we will arrive at transformation laws similar to Einstein's which depend on the absolute reference frame but change asymptotically to Einstein form in certain important application cases. In particular we will obtain a different addition theorem of velocities allowing for superluminal speed. The well known Lorentz transformation and symmetry will evolve not to be valid in our new framework. A more general four-dimensional affine transformation will take its place which has mathematical group properties as well. We will end with a short discussion of the experiments mentioned it this introduction in the light of the new theory.

2 Problems in experimental proofs of Special Relativity

In the well-known experiment of Michelson and Morley, which was repeated several times at the beginning of the twentieth century (see a review in [11]), it was apparently shown that the velocity of light c is the same in all directions relative to the earth orbit. This was considered to be a proof that this velocity is a general constant in nature under all circumstances. We will critically analyse this in the following.

Firstly we have to comment that this is valid only in special relativity, i.e. for unacceletated motion. In general relativity c depends on the gravitational field (or on all fields in case of unified field theories). This dependence is well proven experimentally. Therefore we should state that constancy of c is only valid in vacuo with neglection of all fields.

Secondly we inspect the way in which measurements of the speed of light were done. These were carried out by interferometers where the runtime of light rays was compared between rays having been reflected in different directions. If there is a directional dependence on propagation speed, a characteristic interferometric pattern should occur if the apparatus is rotated. Within assumed experimental uncertainties, no such pattern was observed. Since the length of the apparatus was not changed it was concluded that the velocity of light was the same in all directions. What not has been considered in this explanation is the effect of length contraction. According to Einstein's special relativity, the measured length changes with the same factor as the measured time, if the frame of reference is changed by modifying relative speed between observer and object. For the experiments of Michelson-Morley type this means that the run-time of light as well as the interferometer length change, as soon as the apparatus is rotated relative to a hypothetical absolute direction of motion ("ether wind"). The compression factor is the same for length and time, therefore we obtain for two directions with length l and l' and run-time t and t':

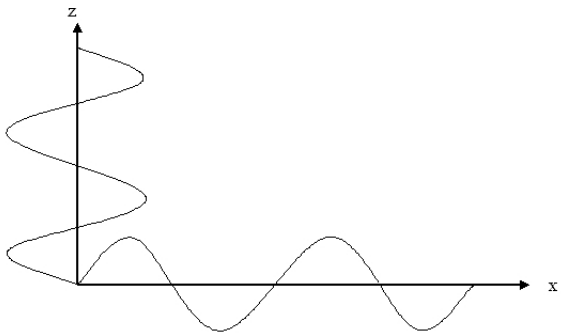

Fig. 1: Length contraction in experiments of Michelson Morley type.

$$c = \frac{l}{t} = \frac{l'}{t'} = \text{const.} \qquad (1)$$

According to Fig. 1 the number of wave trains is the same irrespective of the compression factor. No wonder the value of c is constant. This type of experiments does not prove the details of the Lorentz transformation.

The re-evaluation of experiments of Michelson-Morley type by Cahill et al. [10, 11] has revealed that the evaluation of experimental data was done by erroneously assuming no length contraction. As explained above, taking length contraction into account leads to a meaningless null experiment. This is the outcome of modern laser interferometer spectroscopy in vacuo. However, the older experiments were performed by interferometers in air or helium. Therefore the refraction index is different from unity (although nearby). Doing the evaluation with respection of length contraction as well as refractive index effects leads indeed to a non-null result. Surprisingly, all the older experiments, evaluated in this way, then prove a velocity of the earth orbit relative to the space background of 365 km/s within error bars, see Fig. 2 taken from [10, 11]. This is the most significant experimental hint for the physical relevance of a background field. However, it must be added that the most precise value in Fig. 2, measured from the constant background radiation by the COBE satellite, is controversial. Robitaille [17] has argued that the background radiation is an earth-made effect due to the black body radiation of the oceans. Further satellite missions will clear this up.

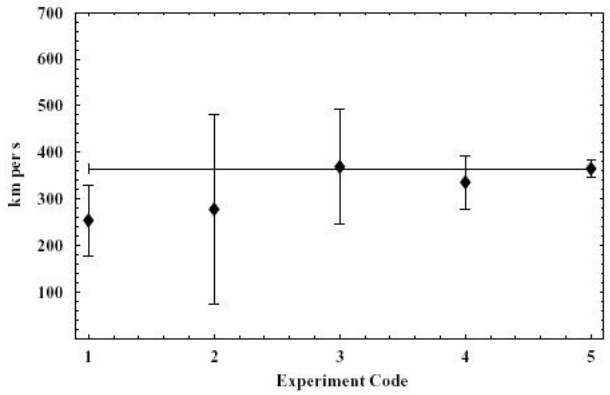

Fig. 2: Speed of earth orbit (reproduction from [10]) in km/s, determined from various Michelson interferometer experiments (1)–(4) and COBE (5): (1) Michelson-Morley (noon observations), (2) Michelson-Morley (18h observations), (3) Illingworth, (4) Miller, Mt.Wilson, and finally in (5) the speed from the COBE satellite observation of the CBR (Constant Background Radiation) microwave spectrum dipole term.

A third problem concerns the interpretation of length contraction and time dilation. Originally Einstein believed that these changes are virtual, i.e. are only measured values of an observer moving relative to another system. The scales of the real objects never change. Later after upcoming of general relativity it became clear that scales have to change in reality because the gravitational field is real in the sense that it evokes real, measurable forces. So it was implicitly assumed that also the scale changes of special relativity have to be real. This however is a severe philosophical problem since two observers measuring the same object would obtain different values for identical physical properties of the object. This discrepancy has not been addressed in literature until today and reflects inconsistencies in the transition from general to special relativity.

3 Length contraction

Since length contraction is the central property of this theory as well as Einstein's special relativity, we will give an explanation how this can be interpreted as a geometric property of fast moving circular or spherical objects. We assume a simple model of matter where atoms are built from an atomic nucleus and orbiting electrons moving in spherical orbits. An observer may travel relative to such an atom with velocity $-v$, and the orbital tangential velocity of an electron may be v_e (near to speed of light). Then the observer sees the electron moving on a curve which is a cycloid or trochoid, see Fig. 3. The form of the curve depends on the ratio of radii a/b, where a is the radius of the "rolling" circle and b is the radius of the path of the electron. For the uniform velocity v we have

$$v = \omega a \tag{2}$$

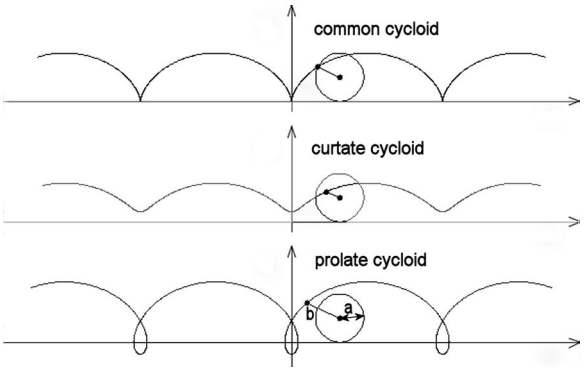

Fig. 3: Several forms of trochoids, also called common cycloid, curtate cycloid and prolate cycloid [19].

with ω being the angular velocity of angle ϕ rotating in time t:

$$\phi = \omega t\,. \tag{3}$$

For the x and y coordinates the parameter form of the cycloid is given by

$$x = a\phi - b\sin\phi\,, \tag{4}$$

$$y = a - b\cos\phi\,. \tag{5}$$

In the rest frame of the atom we have

$$v_e = \omega b \tag{6}$$

for the rotating electron. This equation determines the angular velocity ω. The same ω has to be used in formula (2). The roll radius a is determined then by the relative velocity v. If an observer tries to measure the diameter of a moving atom, he will see the reduced thickness of the cycloidal loop. For $v = v_e$ we obtain $a = b$, the diameter goes to zero. For $v > v_e$ there is only an unharmonic wave left and there is no measurable diameter of an atomic structure.

The diameter can be calculated quantitatively as follows. The x values for the diameter are defined by a vertical tangent of the cycloid, i.e.

$$\frac{dx}{d\phi} = 0\,, \tag{7}$$

which is according to Eq. (4):

$$a - b\cos\phi_0 = 0 \tag{8}$$

or

$$\phi_0 = \arccos\left(\frac{a}{b}\right). \tag{9}$$

Inserting ϕ_0 into (4) gives for the x values where the diameter is being measured

$$x_0 = a\,\arccos\left(\frac{a}{b}\right) - b\,\sqrt{1-\frac{a^2}{b^2}}\,. \tag{10}$$

Since we have

$$x\left(\phi = 0\right) = 0 \tag{11}$$

the value x_0 describes the radius of the atom measured from an observer frame with relative speed v. The well-known square root term is contained in this expression. To obtain this term exclusively we have to tentatatively modify Eq. (4) by replacing a by another parameter a_1. Then we obtain from (10):

$$x_0 = a_1 \arccos\left(\frac{a}{b}\right) - b\sqrt{1-\frac{a^2}{b^2}} \qquad (12)$$

and in the limit $a_1 \to 0$ the observed radius of the atom becomes

$$r = |x_0| = b\sqrt{1-\frac{a^2}{b^2}}\,, \qquad (13)$$

which with help of (2) and (6) can be rewritten to

$$r = b\sqrt{1-\frac{v^2}{v_e^2}}\,, \qquad (14)$$

which is the experimentally found expression for length contraction. So at least qualitatively we can explain length contraction from the geometric effect of relative circular motion.

4 Special Relativity according to Einstein

We describe shortly the axiomatic foundation of special relativity as given by H. Ruder [1]. All physical conclusions follow from the Lorentz transformation. This can be derived from three postulates or axioms:

1. Homogeneity and isotropy of space;
2. Principle of relativity;
3. Constancy of light velocity.

The first axiom is foundational for all physics. The three-dimensional space free of masses has no places which are singled out from others and all directions are equivalent. From classical mechanics we know that these properties lead to the conservation laws of energy and angular momentum. Both statements are equivalent. Therefore axiom 1 is unsurrendable.

The relativity principle states that all inertial frames are equivalent for describing the laws of physics. A difference by measurement is not detectable. The prerequisite is that a global, absolute reference frame does not exist. This is at variance with general relativity as well as newer experiments explained in section 2. The relativity principle would be valid only if space were exactly homogeneous, i.e. free of matter. Then, according to general relativity and Mach's principle, the space would not exist at all. Therefore the relativity principle is a simplifying assumption which we will abandon in the following.

In the same way we do not claim absolute constancy of light velocity (c) in all reference frames. From general relativity it follows that this velocity is not constant but dependent on the strength of the gravitational and other fields. One has to negate this assumption even in special relativity as soon as optical refraction plays a role where the transmission speed of waves is $v = c/n$ with n being the index of refraction. c can only be considered to be a value of light propagation in vacuo with absence of fields of every kind. Another way of circumventing the a priori assumption of a constant c is to measure the transformation law for the proper time of fast moving systems. In this way the well-known Myon experiment can be interpreted for example [1]. It comes out that the transformation law can be cast in a mathematical form containing a constant c which "may have something to do" with light propagation in vacuo. We conclude that only the first axiom has withstood a critical analysis.

5 Modified Special Relativity according to this hypothesis

We will derive now the alternative theory resting upon the three fundamental assumptions:

1. Homogeneity and isotropy of space;
2. Existence of an absolute frame of reference;
3. Physical length contraction.

The first axiom has already been discussed. The second can be constituted by the fact that a more general theory, which does not presuppose inertial systems, allows a referencing system bound to the masses of the universe. Therefore it makes no sense to ignore this fact. If an absolute frame of reference is of physical relevance, it will have an effect. This is not so obvious from general relativity, because the gravitational field is no more effective outside the range of galaxies. It would be more plausible to have a principle of close-ranging or local interaction. In this class of principles belong the ether theories. Already Einstein talked of an "ether space" which was immaterial to his opinion. Sometimes new ether theories come up as for example by Schmelzer [2] where the ether has the property of mediating the principle "actio = reactio". An absolute frame of reference can be related to this ether. It is analogous to a medium for sound waves and the concept of non-homogeneity and the refraction index of wave propagation are applicable. This shows that an ether concept can be added to general relativity, if not already existing in it. An attempt to incorporate it into technical applications was made by Meyl [3].

The ether concept is not necessary when we base our considerations on a unified field theory like Einstein-Cartan-Evans theory [18]. Then space itself is a medium which shows optical properties and a local structure which is defined by the vacuum or background potential. The new interpretation of Michelson-Morley experiments is compatible with this concept.

As a third prerequisite we assume length contraction first introduced by Fitzgerald and Lorentz. As explained above this contraction is required to give consistent results of the

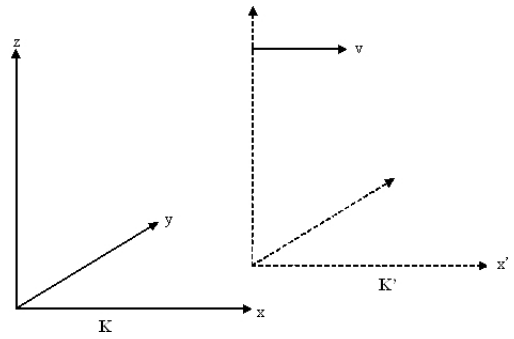

Fig. 4: Reference frames at rest (K) and with relative motion (K').

interferometric experiments. If a body moves with velocity v relative to the background, all lengths are shortened by a factor of

$$\gamma = \sqrt{1 - \frac{v^2}{c^2}}. \tag{15}$$

This contraction is real and not an artifact of measurement. According to the considerations above this is an effect of relative motion. This factor also appears in electrodynamics where it describes the transformation law between electromagnetic fields. Matter exists on an electromagnetic basis. Consequently, this factor also appears in relativistic quantum mechanics. We will see in the next section that length contraction has an effect on time measurements so that local ("proper") times of moving systems are impacted in the same way.

6 Derivation of the alternative theory

6.1 The transformation equations

In the following we will derive the transformation law between different reference frames. We will first give the transformation law of special relativity in the most general case as described in [1]. The result of the first axiom can be used directly because it is identical in Einstein's and our theory. We define a coordinate system K at rest and a system K' moving with velocity v relative to K. The system K is the absolute rest frame as for example measured by experiment. Coordinate axes are chosen so that all axes between K and K' are in parallel, and motion is in x direction of system K. Then we can restrict consideration to one dimension. According to [1] the transformation law between K and K' then has the general form

$$x' = b(v)(x - vt) \tag{16}$$

$$x = b'(v')(x' + v't') \tag{17}$$

where $b(v)$ and $b'(v')$ are functions of the velocity. The second axiom has already been respected by assuming K to be at absolute rest. It should be noted that v is not an arbitrary relative velocity between any two frames but the velocity between the rest frame and another one.

Since the relativity principle is not valid it makes a difference if we transform from the resting to the moving system or backward. The functions b and b' therefore are different. b is defined by length contraction according to the third axiom. Since length contraction is real there is no symmetry between both systems. All length scales in moving systems are larger than in the rest system. The length l of a moving system measured from the rest system then is

$$l_0 = l\sqrt{1 - \frac{v^2}{c^2}}\,. \tag{18}$$

All scales are shrinking, i.e. for measuring the same length (the measured value read from a scale) in K' more scale units have to be used than in K if measurement is done when K' flies by in K. The length Δl (in units of K or K' respectively) transforms then as

$$\Delta l' = \frac{\Delta l}{\sqrt{1 - \frac{v^2}{c^2}}} \tag{19}$$

and the function b from (16) is defined by

$$b = \frac{1}{\sqrt{1 - \frac{v^2}{c^2}}}\,. \tag{20}$$

By backtransformation from K' to K we have to obtain the original length again, therefore

$$b' = b^{-1} = \sqrt{1 - \frac{v^2}{c^2}}\,. \tag{21}$$

If K' moves with v, observed from K, then K moves with $-v$ observed from K'. This is the only place where the relativity principle remains valid. The sign of v however does not play a role in (20). The reversal of the sign of v has already been taken into account in Eqs. (16, 17). Therefore we can assume $v = v'$ in the following.

As already mentioned, the length contraction also leads to a change in time scales as we can see from insertion of (16) into (17) (or vice versa) with regard of b and b':

$$t' = bt = \frac{t}{\sqrt{1 - \frac{v^2}{c^2}}}\,. \tag{22}$$

In total we arrive at the complete non-symmetric set of transformation equations

$$x' = \frac{x - vt}{\sqrt{1 - \frac{v^2}{c^2}}}\,, \tag{23}$$

$$t' = \frac{t}{\sqrt{1 - \frac{v^2}{c^2}}}\,, \tag{24}$$

$$x = (x' + vt') \sqrt{1 - \frac{v^2}{c^2}}\,, \tag{25}$$

$$t = t' \sqrt{1 - \frac{v^2}{c^2}}\,. \tag{26}$$

So far we have considered only two inertial frames with one of them being at (absolute) rest. In case of several frames moving arbitrary to one another, none of them can be assumed to be the rest frame. Let us define two frames K' and K'' whose coordinate origins move with speeds v_1 and v_2 relative to the rest frame K. then we have for the length contraction in both frames:

$$\Delta l' = \frac{\Delta l}{\sqrt{1 - \frac{v_1^2}{c^2}}}\,, \tag{27}$$

$$\Delta l'' = \frac{\Delta l}{\sqrt{1 - \frac{v_2^2}{c^2}}}\,. \tag{28}$$

Setting them in relation to each other directly gives

$$\frac{\Delta l'}{\Delta l''} = \sqrt{\frac{c^2 - v_2^2}{c^2 - v_1^2}} \tag{29}$$

or

$$\Delta l'' = \Delta l' \sqrt{\frac{c^2 - v_1^2}{c^2 - v_2^2}}\,. \tag{30}$$

Only in case $v_1 << v_2$ this approximately results in the expression being know from special relativity:

$$\Delta l'' = \frac{\Delta l'}{\sqrt{1 - \frac{v_2^2}{c^2}}}\,, \tag{31}$$

where v_2 is approximately the relative velocity between frames K' and K''. To derive the complete transformation law between K' and K'' we first write the transformation of both frames from the rest frame:

$$x' = \frac{x - v_1 t}{\sqrt{1 - \frac{v_1^2}{c^2}}}\,, \tag{32}$$

$$t' = \frac{t}{\sqrt{1 - \frac{v_1^2}{c^2}}}\,, \tag{33}$$

$$x'' = \frac{x - v_2 t}{\sqrt{1 - \frac{v_2^2}{c^2}}}\,, \tag{34}$$

$$t'' = \frac{t}{\sqrt{1 - \frac{v_2^2}{c^2}}}\,. \tag{35}$$

Mutual insertion then gives the direct transformation

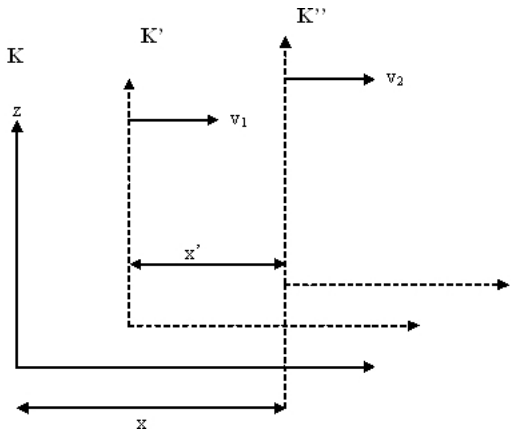

Fig. 5: Reference frames for addition theorem of velocities.

$K' \to K''$ as well as the reverse transformation $K'' \to K'$:

$$x'' = (x' - (v_2 - v_1)t') \sqrt{\frac{c^2 - v_1^2}{c^2 - v_2^2}}\,, \tag{36}$$

$$t'' = t' \sqrt{\frac{c^2 - v_1^2}{c^2 - v_2^2}}\,, \tag{37}$$

$$x' = (x'' + (v_2 - v_1)t'') \sqrt{\frac{c^2 - v_2^2}{c^2 - v_1^2}}\,, \tag{38}$$

$$t' = t'' \sqrt{\frac{c^2 - v_2^2}{c^2 - v_1^2}}\,. \tag{39}$$

Thus we have arrived at the general transformation laws between arbitrary frames of reference. For the back transformation the square root terms change to their inverse, and the sign of the vt term changes. These expressions cannot be reduced to a simple dependence on the speed difference $v = v_2 - v_1$. They depend on the absolute speeds of the inertial systems against the rest frame. Space and time coordinates transform with the same factor.

6.2 The addition theorem of velocities

We consider three coordinate systems K, K' and K'' . Frame K' is moving with velocity v_1 relative to the rest frame K and K'' with velocity v_2 relative to K'. We will compute now with which velocity v_3 then K'' moves relative to K (Fig. 5). At time $t = t' = t'' = 0$ all three coordinate origins shall coincide, so we have

$$x = v_3 t\,, \tag{40}$$

$$x' = v_2 t'\,. \tag{41}$$

The transformation equations (25–26) then with (41)

yield the connection between $x(x', t')$ and $t(t')$:

$$x = (x' + v_1 t')\sqrt{1 - \frac{v_1^2}{c^2}} = (v_2 t' + v_1 t')\sqrt{1 - \frac{v_1^2}{c^2}}\,, \quad (42)$$

$$t = t'\sqrt{1 - \frac{v_1^2}{c^2}}\,. \quad (43)$$

By applying (40) the resulting velocity of K'' is

$$v_3 = \frac{x}{t} = v_1 + v_2\,. \quad (44)$$

This is the addition theorem. The velocities add as vectors, in contrast to special relativity where we have the Einsteinian addition theorem (see Table 1). According to the latter, the sum of two velocities cannot exceed velocity of light. In this theory velocities add as vectors as in the Galilean transformation. The experimental consequences will be discussed in the subsequent section.

Now let's consider how velocities transform between frames directly. We assume that in K' and K'' the same movement (for example of a mass) is measured locally by the velocities

$$v' = \frac{x'}{t'} \quad (45)$$

and

$$v'' = \frac{x''}{t''}\,. \quad (46)$$

By inserting (36, 37) into (46) we find

$$v'' = v' - (v_2 - v_1)\,. \quad (47)$$

Velocities transform according to the Galilean transformation. In particular there is no limiting velocity.

7 Consequences

7.1 Comparison with Special Relativity

Both theories show a high degree of similarity, but there are some essential differences (see Table 1). In Einsteinian relativity the transformations are the same in both directions which is a consequence of the relativity principle. In the alternative theory the contraction factor reverses. This follows from the fact that this theory is based on an absolute frame of reference. This will be further discussed below.

There is a principal difference in the time transformations. In the alternative theory time is stretched by the same factor as length. In Einstein's relativity there is an additional term containing the space coordinate. So there is a coupling between space and time which ensures the basic axiom of constancy of c. In our theory space and time are decoupled, leading to a different metric. The coupling between space and time coordinates can be interpreted as follows. Consider two clocks in the rest frame, one at the coordinate origin and the other at location $x = x_0$, $y = 0$, $z = 0$. In Einstein's theory clocks must be synchronized. When the first clock registers an event at $x = 0$, $t = 0$, this will be seen at x_0 only after a delay which for light signals is $t_0 = x_0/c$. This delay of the measuring process is "built in" into special relativity and explains the appearance of the term $(v/c^2)x'$ in the time transformation $t(t')$ in Table 1.

This Theory	Special Relativity
Coordinate Transformation	
$x' = \dfrac{x - vt}{\sqrt{1 - \frac{v^2}{c^2}}}$	$x' = \dfrac{x - vt}{\sqrt{1 - \frac{v^2}{c^2}}}$
$x = (x' + vt')\sqrt{1 - \dfrac{v^2}{c^2}}$	$x = \dfrac{x' + vt'}{\sqrt{1 - \frac{v^2}{c^2}}}$
$y' = y$	$y' = y$
$z' = z$	$z' = z$
$t' = \dfrac{t}{\sqrt{1 - \frac{v^2}{c^2}}}$	$t' = \dfrac{t - \frac{v}{c^2}x}{\sqrt{1 - \frac{v^2}{c^2}}}$
$t = t'\sqrt{1 - \dfrac{v^2}{c^2}}$	$t = \dfrac{t' + \frac{v}{c^2}x'}{\sqrt{1 - \frac{v^2}{c^2}}}$
Addition Theorem of Velocities	
$v_3 = v_1 + v_2$	$v_3 = \dfrac{v_1 + v_2}{1 + \frac{v_1 v_2}{c^2}}$

Table 1: Comparison of theories.

In contrast to this, the alternative theory does not make any assumptions about measuring processes. Since there is no upper limit of relative velocities, it should be possible to construct an apparatus which measures a global time without significant delay. Such experiments have been discussed in section 1. Alternative methods of clock synchronization have been introduced by Tangherlini [7–9] who proposed a concept of a preferred frame similar to this work. He based his work (already done before 1958 [7]) on a partially instantaneous synchronization of clocks and arrived at transformation equations similar, but not identical, to ours. This corroborates that the measuring term x_0/c built into Einstein's theory is artificial. Tangherlini was not aware at that time of the anisotropy of c found experimentally in later years, for example by Cahill. Therefore he assumed full Lorentz invariance (i.e. isotropy) in each inertial frame. He *defined* the special form of time transformation so that it was consistent with his assumptions on clock synchronization. This is an essential difference to our work where the time transformation follows *by calculation* from the space transformation. Tangherlini obtained different values of c in each frame and a non-linear, direction dependent formula which relates these values to one another. In contrast, our calculation gives a vectorial addition

of all speeds including the signal transmission speed and relative frame speed. This is because we do not assume Lorentz invariance in each frame as Tangherlini did. Compared with the experiments of Cahill, our results are in accordance with them, but Tangherlini's are not.

Also in special relativity there is no real need for integrating signal transmission times into the transformation formulas. In addition, there are signal transmission speeds smaller than c, therefore it cannot be seen why experiments carried out with transmission velocity c should play a dominant role. If the space distance between clocks is known (and it can be measured of course), there is no problem to calculate the time of events at the other clock positions. This is like introducing time zones around the globe. We exactly know what time it is in other parts of the world without making any measurement. Occurrence of events at the same time can be defined by using the time of the rest frame.

While the Lorentz transformation represents a rotation in fourdimensional space, the transformation introduced by this theory has lower symmetry, it can be considered to be an affine mapping, i.e. a translation with stretching of scales. The transformation exhibits group properties as does the Lorentz transformation. This is shown in Appendix A in detail. We therefore conclude that the transformation introduced in this work can be used similarly to the Lorentz transformation as a basic property of higher developed theories, for example general relativity.

7.2 Comparison with known problems of Einsteinian theory

There are several interpretation problems in conventional special relativity. When comparing two frames being in motion to one another, the length rods of the other system appear shortened, seen from the system where the observer resides. This follows from the symmetry of the transformation law (Lorentz transformation). When the speed of one system is adopted to that of the other system, the difference in rod length disappears. At least Einstein has assumed that the scale change is a measuring artifact and not real.

Time dilation is regarded differently. In the well known twin paradoxon it is assumed that the integral taken over the coordinate time is identical to the real elapsed time, the scale change is considered to be a real effect as is done in general relativity. There is a contradiction in the interpretation. Contrary to this, the alternative theory assumes the scale changes always to be real. Since all length changes are related to the rest frame, there is no "symmetry" between measurements when one moving system measures quantities in another. For the twin paradoxon this means that the twin having higher absolute speed ages faster than the other one. Both twins can calculate the age of the other twin and come to the same result. All contradictions are removed.

The change of the time coordinate deserves further comments. As is generally known the Lorentz transformation is a rotation in four dimensions, therefore the length of vectors is an invariant as can be expressed by

$$x^2 + y^2 + z^2 - c^2t^2 = x'^2 + y'^2 + z'^2 - c^2t'^2. \qquad (48)$$

From this the differential invariance condition of the Minkowski metric follows:

$$dx^2 + dy^2 + dz^2 - c^2dt^2 = dx'^2 + dy'^2 + dz'^2 - c^2dt'^2. \qquad (49)$$

To the knowledge of the author, experimental tests of special relativity, however, are not based on the invariance principle but on the coordinate transformations where the proper time of a moving system is computed by integrating the equation

$$d\tau = dt\sqrt{1 - \frac{v^2}{c^2}}\,. \qquad (50)$$

Considering the time transformation for special relativity in Table 1, this equation should generally read

$$d\tau = \left(dt - \frac{v}{c^2}\,dx\right)\sqrt{1 - \frac{v^2}{c^2}}\,. \qquad (51)$$

It is questionable if this formula ever has been tested experimentally. Experimenters always used setups where the simplified Eq. (50) was sufficient. These types of checks of special relativity have been made with very high precision. For testing the Lorentz transformation thoroughly, however, use of Eq. (51) would be required.

We conclude this section with a hint to relativistic mechanics which is also based on Eq. (50). Therefore the alternative theory gives the same results as special relativity, as far as the lab system can be identified within sufficient precision with the absolutely resting system. When experiments with light are performed, this is the case. Relativistic mechanics would look differently if experiments were performed in a fast moving lab relative to earth.

7.3 Comparison with newer experiments and final remarks

As a last point we bring to mind the experiments of Cahill et al. [10, 11] mentioned in sections 1 and 2. The authors stress that older experiments of Michelson-Morley type were two-way experiments, that means the distances in the interferometer were passed twice by light rays, in contrary directions. Thus a lot of information gets lost, and such experiments in vacuo are even meaningless as already mentioned. With use of modern electronics, one-way experiments have been carried out by Cahill et al. It could be shown that light velocity is indeed different in both directions compared to the motion of the earth relative to the space background. Even fluctuations in the background velocity were found. There is a full analogy to sound waves in media, with effects of speeds relative to the observer and of the refraction index. Similar experiments were carried out be de Witte [12]. Further independent

confirmations are required. There are certain measurements of Marinov [15, 16] which seem not to be consistent with Cahill's results, but it is not clear if the evaluation method of Marinov is compatible with that of Cahill and this work.

The concept of the refraction index can be used to produce superluminal processes by deploying special optical media with a refraction index $n < 1$. Obviously, the experiments of Nimtz [5, 6], who has transmitted audio data with superluminal speed, can be explained in this way. Since the input data (a symphony of Mozart) was recognized as such after the transmission, it is clear that useful signals can be transmitted with such a speed. The old argument that a "phase velocity" $v > c$ cannot transport any information no longer holds. Thus our above statements are corroborated that a global time can be defined experimentally. Thornhill [14], and later Cahill [13], have further shown that Maxwell's equations, which are taken as an irrevocable proof that the Lorentz transform is incorporated in nature, can be formulated Galilei-invariant. Advanced theories like Einstein-Cartan-Evans theory [18] introduced a background potential and optical properties of space itself. Einstein's area is overcome. We conclude with a citation from Cahill [13]:

> "The Special Relativity formalism asserts that only relative descriptions of phenomena between two or more observers have any meaning. In fact we now understand that all effects are dynamically and observationally relative to an ontologically real, that is, detectable dynamical 3-space. Ironically this situation has always been known as an "absolute effect". The most extraordinary outcome of recent discoveries is that a dynamical 3-space exists, and that from the beginning of Physics this has been missed — that a most fundamental aspect of reality has been completely overlooked".

Appendix A: Proof of group properties

The transformation equations can be written in vector form with four-dimensional vectors and a transformation matrix:

$$\begin{pmatrix} x'' \\ y'' \\ z'' \\ t'' \end{pmatrix} = \begin{pmatrix} \alpha & 0 & 0 & -\alpha\beta \\ 0 & 1 & 0 & 0 \\ 0 & 0 & 1 & 0 \\ 0 & 0 & 0 & \alpha \end{pmatrix} \begin{pmatrix} x' \\ y' \\ z' \\ t' \end{pmatrix} \tag{A-1}$$

with

$$\alpha := \sqrt{\frac{c^2 - v_1^2}{c^2 - v_2^2}}\,, \qquad \beta := v_2 - v_1\,. \tag{A-2}$$

This is — in contrast to the Lorentz transformation — not a rotation in 4-space but a linear transformation (stretching) with a translation. The determinant is α^2, not unity as for the Lorentz transformation. Straight lines remain in parallel. The inverse transformation of (A-1) is

$$\begin{pmatrix} x' \\ y' \\ z' \\ t' \end{pmatrix} = \begin{pmatrix} \alpha^{-1} & 0 & 0 & \alpha^{-1}\beta \\ 0 & 1 & 0 & 0 \\ 0 & 0 & 1 & 0 \\ 0 & 0 & 0 & \alpha^{-1} \end{pmatrix} \begin{pmatrix} x'' \\ y'' \\ z'' \\ t'' \end{pmatrix} \tag{A-3}$$

as can be verified by multiplication of both matrices. To compare this with the Lorentz transformation we rewrite above Eqs. (A-1, A-3) with Minkowski coordinates, i.e. with an imaginary time coordinate:

$$\begin{pmatrix} x'' \\ y'' \\ z'' \\ ict'' \end{pmatrix} = \mathbf{T} \begin{pmatrix} x' \\ y' \\ z' \\ ict' \end{pmatrix} \tag{A-4}$$

with

$$\mathbf{T} = \begin{pmatrix} \alpha & 0 & 0 & i\alpha\beta \\ 0 & 1 & 0 & 0 \\ 0 & 0 & 1 & 0 \\ 0 & 0 & 0 & \alpha \end{pmatrix} \tag{A-5}$$

and

$$\alpha := \sqrt{\frac{c^2 - v_1^2}{c^2 - v_2^2}}\,, \qquad \beta := \frac{v_2 - v_1}{c}\,. \tag{A-6}$$

Then we have in analogy to above:

$$\mathbf{T}^{-1} = \begin{pmatrix} \alpha^{-1} & 0 & 0 & -i\alpha^{-1}\beta \\ 0 & 1 & 0 & 0 \\ 0 & 0 & 1 & 0 \\ 0 & 0 & 0 & \alpha^{-1} \end{pmatrix} \tag{A-7}$$

The set of transformations $T(\alpha, \beta)$ is a commutative group. This is proven in the following by examining the group axioms.

1. Completeness
We define

$$\alpha_1 := \sqrt{\frac{c^2 - v_1^2}{c^2 - v_2^2}}\,, \qquad \beta_1 := \frac{v_2 - v_1}{c}\,, \tag{A-8}$$

$$\alpha_2 := \sqrt{\frac{c^2 - v_3^2}{c^2 - v_4^2}}\,, \qquad \beta_2 := \frac{v_4 - v_3}{c}\,. \tag{A-9}$$

Then we find for the concatenation of two transformations by matrix multiplication:

$$T(\alpha_1, \beta_1)\, T(\alpha_2, \beta_2) = T(\alpha_1\alpha_2, \beta_1 + \beta_2)\,. \tag{A-10}$$

2. Neutral element
The neutral element of the group is the unit matrix.

3. Inverse element
For each $T(\alpha, \beta)$ there is an inverse transformation $T^{-1} = T(\alpha^{-1}, -\beta)$.

4. Associativity
The law of associativity for the matrix multiplication holds:

$$\begin{aligned} T(\alpha_1, \beta_1) \left[T(\alpha_2, \beta_2)\, T(\alpha_3, \beta_3) \right] = \\ = \left[T(\alpha_1, \beta_1)\, T(\alpha_2, \beta_2) \right] T(\alpha_3, \beta_3)\,. \end{aligned} \tag{A-11}$$

5. Commutativity
From Eq. (A-10) directly follows

$$T(\alpha_1, \beta_1)\, T(\alpha_2, \beta_2) = T(\alpha_2, \beta_2)\, T(\alpha_1, \beta_1). \tag{A-12}$$

So the group axioms have been proven.

Submitted on January 17, 2009 / Accepted on January 26, 2009

References

1. Ruder H. and M. Die Spezielle Relativitätstheorie. Viewег-Verlag, 1993.
2. Schmelzer I. General ether theory. arXiv: gr-qc/0001101.
3. Meyl K. Elektromagnetische Umweltverträglichkeit. Teil 3: Umdruck zum informationstechnischen Seminar. Indel-Verlag, 2003.
4. Crothers S.J. On certain conceptual anomalies in Einstein's theory of relativity. *Progress in Physics*, 2008, v. 1, 52–57.
5. Nimtz G. Tunneln mit Überlichtgeschwindigkeit. *DLR Nachrichten*, 1998, v. 90.
6. Nimtz G. Evanescent modes ar not necessarily Einstein causal. *The European Physical Journal*, 1999, v. B7, 523.
7. Tangherlini F.R. The velocity of light in uniformly moving frame. PhD Thesis, Stanford Univ., Sept. 1958, 135 pages.
8. Tangherlini F.R. An inroduction to the General Theory of Relativity. *Suppl. Nuovo Cim.*, 1961, Ser. X, v. 20, 1–86.
9. Malykin G.B. Frank Robert Tangherlini — the founder of an alternative relativistic kinematics (on the occasion of his 85th birthday). *Progress in Physics*, 2009, v. 1, L9–L14.
10. Cahill R.T., Kitto K. Michelson-Morley experiments revisited and the Cosmic Background Radiation preferred frame. *Apeiron*, 2003, v. 10(2), 104–117.
11. Cahill R.T. A new light-speed anisotropy experiment: absolute motion and gravitational waves detected. *Progress in Physics*, 2006, v. 4, 73–92.
12. Cahill R.T. The Roland De Witte 1991 experiment (to the memory of Roland De Witte). *Progress in Physics*, 2006, v. 3, 60–65.
13. Cahill R.T. Unravelling Lorentz covariance and the spacetime formalism, *Progress in Physics*, 2008, v. 4, 19–24.
14. Thornhill C.K. Real and apparent invariants in the transformation of the equations governing wave-motion in the general flow of a general fluid. *Proc. R. Soc. Lond. A*, 1993, 442, 495–504.
15. Marinov S. Measurement of the laboratory's absolute velocity. *General Relativity and Gravitation*, 1980, v. 12(1), 57–66.
16. Marinov S. Repetition of Silvertooth's experiment for measuring the aether drift. *Speculations in Science and Technology*, 1989, v. 12(3), 187–179.
17. Robitaille P.-M. On the origins of the CMB: insight from the COBE, WMAP, and Relikt-1 satellites. *Progress in Physics*, 2007, v. 1, 19–23.
18. Evans M.W. Generally covariant unified field theory. Abramis, 2005–2009, vols. 1–6; see also http://www.aias.us
19. http://en.wikipedia.org/wiki/Cycloid

On the Field of a Stationary Charged Spherical Source

Nikias Stavroulakis

Solomou 35, 15233 Chalandri, Greece
E-mail: nikias.stavroulakis@yahoo.fr

The equations of gravitation related to the field of a spherical charged source imply the existence of an interdependence between gravitation and electricity [5]. The present paper deals with the joint action of gravitation and electricity in the case of a stationary charged spherical source. Let m and ε be respectively the mass and the charge of the source, and let k be the gravitational constant. Then the equations of gravitation need specific discussion according as $|\varepsilon| < m\sqrt{k}$ (source weakly charged) or $|\varepsilon| = m\sqrt{k}$ or $|\varepsilon| > m\sqrt{k}$ (source strongly charged). In any case the curvature radius of the sphere bounding the matter possesses a strictly positive greatest lower hound, so that the source is necessarily an extended object. Pointwise sources do not exist. In particular, charged black holes do not exist.

1 Introduction

We recall that the field of an isotropic stationary spherical charged source is defined by solutions of the Einstein equations related to the stationary $\Theta(4)$-invariant metric

$$ds^2 = \left(f(\rho)\,dt + f_1(\rho)\,(x dx)\right)^2 - \\ - \left[\left(l_1(\rho)\right)^2 dx^2 + \frac{\left(\left(l(\rho)\right)^2 - \left(l_1(\rho)\right)^2\right)}{\rho^2}\,(x dx)^2\right], \quad (1.1)$$

($\rho = \|x\| = \sqrt{x_1^2 + x_2^2 + x_3^2}$, $l(0) = l_1(0)$). The functions of one variable $f(\rho)$, $f_1(\rho)$, $l_1(\rho)$, $l(\rho)$ are supposed to be C^∞ with respect to $\rho = \|x\|$ on the half-line $[0, +\infty[$ (or, possibly, on the entire real line $]-\infty, +\infty[$), but since the norm $\|x\|$ is not differentiable at the origin with respect to the coordinates x_1, x_2, x_3, these functions are not either. So, in general, the origin will appear as a singularity without physical meaning. In order to avoid the singularity, the considered functions must be smooth functions of the norm in the sense of the following definition.

Definition 1.1. A function of the norm $\|x\|$, say $f(\|x\|)$, will be called smooth function of the norm, if:

a). $f(\|x\|)$ is C^∞ on $\mathbb{R}^3 - \{(0,0,0)\}$ with respect to the coordinates x_1, x_2, x_3.

b). Every derivative of $f(\|x\|)$ with respect to the coordinates x_1, x_2, x_3 at the points $x \in \mathbb{R}^3 - \{(0,0,0)\}$ tends to a definite value as $x \to (0,0,0)$.

Remark 1.1. In [3], [4] a smooth function of the norm is considered as a function C^∞ on $\mathbb{R}$. However this last characterisation neglects the fact that the derivatives of the function are not directly defined at the origin.

The proof of the following theorem appears in [3].

Theorem 1.1. $f(\|x\|)$ is a smooth function of the norm if and only if the function of one variable $f(u)$ is C^∞ on $[0, \infty[$ and its right derivatives of odd order at $u = 0$ vanish.

This being said, a significant simplification of the problem results from the introduction of the radial geodesic distance

$$\delta = \int_0^\rho l(u)\,du = \beta(\rho), \quad (\beta(0) = 0),$$

which makes sense in the case of stationary fields.

Since $\beta(\rho)$ is a strictly increasing C^∞ function tending to $+\infty$ as $\rho \to +\infty$, the inverse function $\rho = \gamma(\delta)$ is also a C^∞ strictly increasing function of δ tending to $+\infty$ as $\delta \to +\infty$. So to the distance δ there corresponds a transformation of space coordinates:

$$y_i = \frac{\delta}{\rho}\,x_i = \frac{\beta(\rho)}{\rho}\,x_i, \quad (i = 1,2,3),$$

with inverse

$$x_i = \frac{\rho}{\beta(\rho)}\,y_i = \frac{\gamma(\delta)}{\delta}\,y_i, \quad (i = 1,2,3).$$

As shown in [4], these transformations involve smooth functions of the norm and since

$$x dx = \sum_{i=1}^3 x_i dx_i = \frac{\gamma\gamma'}{\delta}\,(y dy),$$

$$dx^2 = \sum_{i=1}^3 dx_i^2 = \left(\frac{\gamma'^2}{\delta^2} - \frac{\gamma^2}{\delta^4}\right)(y dy)^2 + \frac{\gamma'^2}{\delta^2}\,dy^2$$

by setting

$$F(\delta) = f(\gamma(\delta)), \quad F_1(\delta) = f_1(\gamma(\delta))\frac{\gamma(\delta)\gamma'(\delta)}{\delta},$$

$$L_1(\delta) = l_1(\gamma(\delta))\frac{\gamma(\delta)}{\delta},$$

and taking into account that

$$L(\delta) = l(\gamma(\delta))\,\gamma'(\delta) = 1$$

we get the transformed metric:

$$ds^2 = (Fdt + F_1(ydy))^2 - \\ - \left(L_1^2 dy^2 + \frac{1 - L_1^2}{\delta^2}(ydy)^2\right). \quad (1.2)$$

Then $\delta = \|y\|$ and the curvature radius of the spheres $\delta = $ $=$ const, is given by the function

$$G = G(\delta) = \delta L_1(\delta).$$

Moreover, instead of $h = \rho f_1$, we have now the function

$$H = H(\delta) = \delta F_1(\delta).$$

This being said, we recall [5] that, with respect to (1.1), the field outside the charged spherical source is defined by the equations

$$fl = c\,\frac{dg}{d\rho},$$

$$\frac{dg}{d\rho} = l\sqrt{1 - \frac{2\mu}{g} + \frac{\nu^2}{g^2}} = l\,\frac{\sqrt{g^2 - 2\mu g + \nu^2}}{g},$$

($\mu = \frac{km}{c^2}$, $\nu = \frac{\sqrt{k}}{c^2}|\varepsilon|$, $g^2 - 2\mu g + \nu^2 > 0$, where k is the gravitational constant, m and ε being respectively the mass and the charge of the source).

The function $h = \rho f_1$ does not appear in these equations. Every function $h = \rho f_1$ satisfying the required conditions of differentiability and such that $|h| \leqslant l$ is allowable.

We obtain a simpler system of equations if we refer to the metric (1.2). Then

$$F = c\frac{dG}{d\delta} = c\sqrt{1 - \frac{2\mu}{G} + \frac{\nu^2}{G^2}}, \quad (1.3)$$

$$\frac{dG}{d\delta} = \sqrt{1 - \frac{2\mu}{G} + \frac{\nu^2}{G^2}} = \frac{\sqrt{G^2 - 2\mu G + \nu^2}}{G}, \quad (1.4)$$

$$|H| \leqslant 1.$$

So our problem reduces essentially to the definition of the curvature radius $G(\delta)$ by means of the equation (1.4) the study of which depends on the sign of the difference

$$\nu^2 - \mu^2 = \frac{k}{c^4}\left(\varepsilon^2 - km^2\right).$$

A concise approach to this problem appeared first in the paper [1].

2 Source weakly charged ($\nu^2 < \mu^2$ or $|\varepsilon| < m\sqrt{k}$)

$G^2 - 2\mu G + \nu^2 = (G - \mu)^2 + \nu^2 - \mu^2$ vanishes for $G = $ $= \mu - \sqrt{\mu^2 - \nu^2}$ and $G = \mu + \sqrt{\mu^2 - \nu^2}$. Moreover $G^2 - $ $- 2\mu G + \nu^2 < 0$ if $\mu - \sqrt{\mu^2 - \nu^2} < G < \mu + \sqrt{\mu^2 - \nu^2}$ and $G^2 - 2\mu G + \nu^2 > 0$ if $G < \mu - \sqrt{\mu^2 - \nu^2}$ or $G > \mu + $ $+ \sqrt{\mu^2 - \nu^2}$. Since negative values of G are not allowed and since the solution must be topologically connected, we have to consider two cases according as

$$0 < G \leqslant \mu - \sqrt{\mu^2 - \nu^2}$$

or

$$\mu + \sqrt{\mu^2 - \nu^2} \leqslant G < +\infty.$$

The first case gives an unphysical solution, because G cannot be bounded outside the source. So, it remains to solve the equation (1.4) when G describes the half-line $\left[\mu + \sqrt{\mu^2 - \nu^2}, +\infty\right[$. The value $\mu + \sqrt{\mu^2 - \nu^2}$ is the greatest lower bound of the values of G and is not reachable physically, because F vanishes, and hence the metric degenerates for this value. However the value $\mu + \sqrt{\mu^2 - \nu^2}$ must be taken into account for the definition of the mathematical solution. So, on account of (1.4) the function $G(\delta)$ is defined as an implicit function by the equation

$$\delta_0 + \int_{\mu + \sqrt{\mu^2 - \nu^2}}^{G} \frac{u\,du}{\sqrt{u^2 - 2\mu u + \nu^2}} = \delta, \quad (\delta_0 = \text{const}),$$

or, after integration,

$$\delta_0 + \sqrt{G^2 - 2\mu G + \nu^2} + \\ + \mu \ln \frac{G - \mu + \sqrt{G^2 - 2\mu G + \nu^2}}{\sqrt{\mu^2 - \nu^2}} = \delta \quad (2.1)$$

with $G > \mu + \sqrt{\mu^2 - \nu^2}$.

We see that the solution involves a new constant δ_0 which is not defined classically. To given mass and charge there correspond many possible values of δ_0 depending probably on the size of the source as well as on its previous history, namely on its dynamical states preceding the considered stationary one. From the mathematical point of view, the determination of δ_0 necessitates an initial condition, for instance the value of the curvature radius of the sphere bounding the matter.

Let us denote by $E(G)$ the left hand side of (2.1). The function $E(G)$ is a strictly increasing function of G such that $E(G) \to +\infty$ as $G \to +\infty$. Consequently (2.1) possesses a unique strictly increasing solution $G(\delta)$ tending to $+\infty$ as $\delta \to +\infty$

The equation (2.1) allows to obtain two significant relations:

a) Since

$$\delta - G(\delta) = E(G) - G =$$
$$= \delta_0 + \mu \ln \frac{G - \mu + \sqrt{G^2 - 2\mu G + \nu^2}}{\sqrt{\mu^2 - \nu^2}} +$$
$$+ \sqrt{G^2 - 2\mu G + \nu^2} - G =$$
$$= \delta_0 + \mu \ln \frac{G - \mu + \sqrt{G^2 - 2\mu G + \nu^2}}{\sqrt{\mu^2 - \nu^2}} +$$
$$+ \frac{-2\mu + \frac{\nu^2}{G}}{1 + \sqrt{1 - \frac{2\mu}{G} + \frac{\nu^2}{G^2}}} \to +\infty \quad \text{as} \quad G \to +\infty,$$

it follows that $\delta - G(\delta) \to +\infty$ as $\delta \to +\infty$.

b) Since

$$\frac{\delta}{G(\delta)} = \frac{E(G)}{G} = \frac{\delta_0}{G} + \sqrt{1 - \frac{2\mu}{G} + \frac{\nu^2}{G^2}} +$$
$$+ \mu \frac{\ln G}{G} + \frac{\mu}{G} \ln \frac{1 - \frac{\mu}{G} + \sqrt{1 - \frac{2\mu}{G} + \frac{\nu^2}{G^2}}}{\sqrt{\mu^2 - \nu^2}} \to 1$$
$$\text{as} \quad G \to +\infty,$$

it follows that $\frac{\delta}{G(\delta)} \to 1$ as $\delta \to +\infty$.

Moreover from (2.1), it follows that the greatest lower bound $\mu + \sqrt{\mu^2 - \nu^2}$ of the values of $G(\delta)$ is obtained for $\delta = \delta_0$. The characteristics of the solution depend on the sign of δ_0.

Suppose first that $\delta_0 < 0$. Since function $G(\delta)$ is strictly increasing, we have $G(0) > \mu + \sqrt{\mu^2 - \nu^2}$, which is physically impossible, because the physical solution $G(\delta)$ vanishes for $\delta = 0$. Consequently there exists a strictly positive value δ_1 (the radius of the sphere bounding the matter) such that the solution is valid only for $\delta \geqslant \delta_1$. So, there exists no vacuum solution inside the ball $\|x\| < \delta_1$. In other words, the ball $\|x\| < \delta_1$ lies inside the matter.

Suppose secondly that $\delta_0 = 0$. Then

$$G(0) = \mu + \sqrt{\mu^2 - \nu^2} > 0,$$

which contradicts also the properties of the globally defined physical solution. Consequently there exists a strictly positive value δ_1 (the radius of the sphere bounding the matter) such that the solution is valid for $\delta \geqslant \delta_1$.

Suppose thirdly that $\delta_0 > 0$. Since

$$G(\delta_0) = \mu + \sqrt{\mu^2 - \nu^2}\,,$$

the derivative

$$G'(\delta_0) = \frac{\sqrt{(G(\delta_0))^2 - 2\mu G(\delta_0) + \nu^2}}{G(\delta_0)}$$

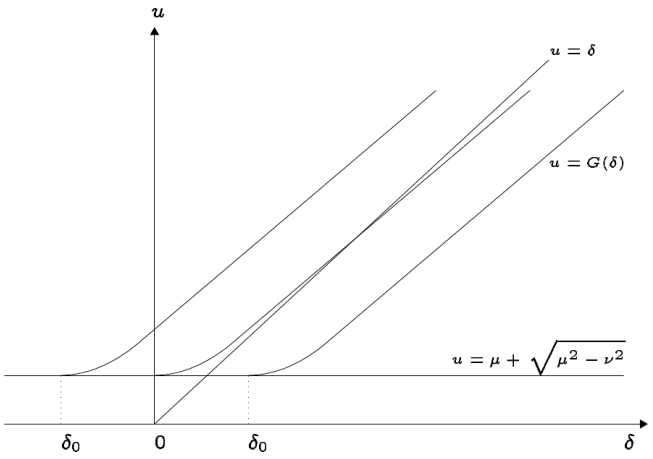

Fig. 1: Graph of G in the case where $\nu^2 < \mu^2$.

vanishes, so that $F(\delta_0) = c\,G'(\delta_0) = 0$. The vanishing of $F(\delta_0)$ implies the degeneracy of the spacetime metric for $\delta = \delta_0$ and since degenerate metrics have no physical meaning, there exists a value $\delta_1 > \delta_0$ such that the metric is physically valid for $\delta \geqslant \delta_1$. There exists no vacuum solution for $\delta \leqslant \delta_0$. The ball $\|x\| \leqslant \delta_0$ lies inside the matter.

From the preceding considerations it follows, in particular, that, whatever the case may be, a weakly charged source cannot be reduced to a point.

3 Source with $\mu^2 = \nu^2$ (or $|\varepsilon| = m\sqrt{k}$)

Since $\mu^2 = \nu^2$, we have $G^2 - 2\mu G + \nu^2 = (G - \mu)^2$, so that the equation (1.4) is written as

$$\frac{dG}{d\delta} = \frac{|G - \mu|}{G}\,.$$

Consider first the case where $G < \mu$. Then

$$\frac{dG}{d\delta} = \frac{G - \mu}{G} \quad \text{or} \quad \left(1 - \frac{\mu}{\mu - G}\right) dG = -\,d\delta\,,$$

whence

$$a_0 + G + \mu \ln \left(1 - \frac{G}{\mu}\right) = -\,\delta\,, \quad (a_0 = \text{const})\,.$$

If $G \to \mu$, then $\delta \to +\infty$, thus introducing a sphere with infinite radius and finite measure. This solution is unphysical. It remains to examine the case where $G > \mu$. Then

$$\left(1 + \frac{\mu}{G - \mu}\right) dG = d\delta\,,$$

whence

$$a_0 + G + \mu \ln \left(\frac{G}{\mu} - 1\right) = \delta\,, \quad (a_0 = \text{const})\,.$$

To the infinity of values of a_0 there correspond an infinity of solutions which results from one of them, for instance from

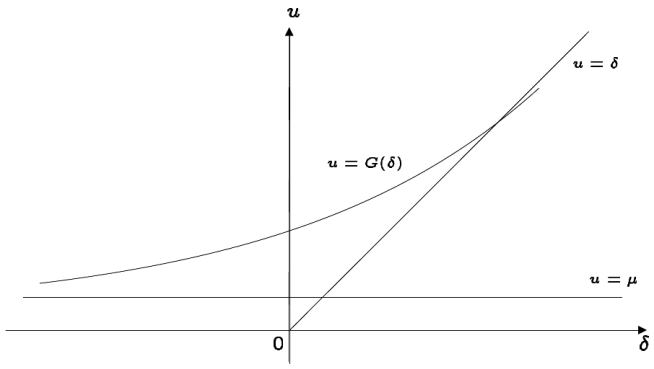

Fig. 2: Graph of G in the case where $\nu^2 = \mu^2$.

the solution obtained for $a_0 = 0$, by means of translations parallel to δ-axis.

For each value of a_0, we have $\delta \to +\infty$ as $G \to \mu$. The value μ is the unreachable greatest lower bound of the values of the corresponding solution $G(\delta)$ which is mathematically defined on the entire real line. If $\delta_1 > 0$ is the radius of the sphere bounding the matter, only the restriction of the solution to the half-line $[\delta_1, +\infty[$ is physically valid. In order to define the solution, we need the value of the corresponding constant a_0, the determination of which necessitates an initial condition, for instance the value $G(\delta_1)$. In any case, the values of $G(\delta)$ for $\delta \leqslant 0$ are unphysical.

Finally we remark that

$$\delta - G(\delta) \to +\infty \quad \text{and} \quad \frac{\delta}{G(\delta)} \to 1 \quad \text{as} \quad \delta \to +\infty.$$

4 Source strongly charged ($\nu^2 > \mu^2$ or $|\varepsilon| > m\sqrt{k}$)

Since $G^2 - 2\mu G + \nu^2 = (G - \mu)^2 + \nu^2 - \mu^2$, we have $G^2 - 2\mu G + \nu^2 > 0$ for every value of G. Regarding the function

$$\Phi(G) = 1 - \frac{2\mu}{G} + \frac{\nu^2}{G^2} = \frac{G^2 - 2\mu G + \nu^2}{G^2},$$

we have

$$\Phi(G) \to +\infty \text{ as } G \to 0 \quad \text{and} \quad \Phi(G) \to 1 \text{ as } G \to +\infty.$$

On the other hand the derivative

$$\Phi'(G) = \frac{2}{G^2}\left(\mu - \frac{\nu^2}{G}\right),$$

vanishes for

$$G = \frac{\nu^2}{\mu} = \frac{\varepsilon^2}{mc^2}$$

and moreover

$$\Phi'(G) < 0 \quad \text{for} \quad G < \frac{\nu^2}{\mu},$$

$$\Phi'(G) > 0 \quad \text{for} \quad G > \frac{\nu^2}{\mu}.$$

It follows that the function $\Phi(G)$ is strictly decreasing on the interval $]0, \frac{\nu^2}{\mu}[$, strictly increasing on the half-line $[\frac{\nu^2}{\mu}, +\infty[$, so that

$$\Phi\left(\frac{\nu^2}{\mu}\right) = 1 - \frac{\mu^2}{\nu^2} = 1 - \left(\frac{m\sqrt{k}}{\varepsilon}\right)^2$$

is the minimum of $\Phi(G)$.

The behaviour of the solution on the half-line $[\frac{\nu^2}{\mu}, +\infty[$ is quite different from that on the interval $]0, \frac{\nu^2}{\mu}[$. Several arguments suggest that only the restriction of the solution to the half-line $[\frac{\nu^2}{\mu}, +\infty[$ is physically valid.

a) Let δ_0 be the radius of the spherical source. In order to prove that the restriction of the solution to $]0, \frac{\nu^2}{\mu}[$ is unphysical, we have only to prove that $G(\delta_0) \geqslant \frac{\nu^2}{\mu}$. We argue by contradiction assuming that $G(\delta_0) < \frac{\nu^2}{\mu}$. Since $G(\delta)$ is unbounded, there exists a value $\delta_1 > \delta_0$ such that $G(\delta_1) = \frac{\nu^2}{\mu}$. On the other hand, since $G(\delta)$ satisfies the equation (1.4), namely

$$\frac{dG}{d\delta} = \sqrt{1 - \frac{2\mu}{G} + \frac{\nu^2}{G^2}} = \sqrt{\Phi(G)},$$

the function

$$F = c\frac{dG}{d\delta} = c\sqrt{\Phi(G)}$$

is strictly decreasing on the interval $]0, \frac{\nu^2}{\mu}[$, and strictly increasing on the half-line $[\frac{\nu^2}{\mu}, +\infty[$. Such a behaviour of the important function F, which is involved in the law of propagation of light, is unexplained. We cannot indicate a cause compelling the function F first to decrease and then to increase outside the spherical source. The solution cannot be valid physically in both intervals $]0, \frac{\nu^2}{\mu}[$ and $[\frac{\nu^2}{\mu}, +\infty[$, and since the great values of G are necessarily involved in the solution, it follows that only the half-line $[\frac{\nu^2}{\mu}, +\infty[$ must be taken into account. The assumption that $G(\delta_0) < \frac{\nu^2}{\mu}$ is to be rejected.

b) The non-Euclidean (or, more precisely, non-pseudo-Euclidean) properties of the spacetime metric are induced by the matter, and this is why they become more and more apparent in the neighbourhood of the spherical source. On the contrary, when δ (or G) increases the spacetime metric tends progressively to a pseudo-Euclidean form. This situation is expressed by the solution itself. In order to see this, we choose a positive value b_1 and integrate the equation (1.4) in the half-line $[b_1, +\infty[$,

$$b_0 + \int_{b_1}^{G} \frac{u\,du}{\sqrt{u^2 - 2\mu u + \nu^2}} = \delta\,, \quad (b_0 = \text{const}),$$

and then writing down the explicit expression resulting from the integration, we find, as previously, that

$$\delta - G(\delta) \to +\infty \quad \text{and} \quad \frac{\delta}{G(\delta)} \to 1 \text{ as } \delta \to +\infty.$$

But, since

$$L_1(\delta) = \frac{G(\delta)}{\delta} \to 1 \quad \text{and} \quad F = c\sqrt{\Phi(G(\delta))} \to c$$

as $\delta \to +\infty$, the metric (1.2) tends effectively to a pseudo-Euclidean form as $\delta \to +\infty$. Now, if δ decreases, the non-Euclidean properties become more and more apparent, so that the minimum $c\sqrt{1-\frac{\mu^2}{\nu^2}}$ of F, obtained for $G = \frac{\nu^2}{\mu}$, is related to the "strongest non-Euclidean character of the metric". For values of G less than $\frac{\nu^2}{\mu}$, the behaviour of the mathematical solution becomes unphysical. In fact, the metric loses progressively its non-Euclidean properties, and, in particular, for $G = \frac{\nu^2}{2\mu}$, we have

$$\Phi\left(\frac{\nu^2}{2\mu}\right) = 1 - \frac{4\mu^2}{\nu^2} + \frac{4\mu^2}{\nu^2} = 1,$$

hence $F\left(\frac{\nu^2}{2\mu}\right) = c$ and $\frac{dG}{d\delta} = 1$.

On account of $G = \delta L_1$, the last condition implies

$$1 = \frac{dG}{d\delta} = L_1 + \delta\,\frac{dL_1}{d\delta}$$

and since we have to do physically with very small values of δ (in the neighbourhood of the origin), we conclude that

$$L_1\left(\frac{\nu^2}{2\mu}\right) \approx 1.$$

and since $F\left(\frac{\nu^2}{2\mu}\right) = c$, the metric is almost pseudo-Euclidean, a phenomenon inadmissible physically in the neighbourhood of the source. So we are led to reject the restriction of the mathematical solution to the interval $[\frac{\nu^2}{2\mu}, \frac{\nu^2}{\mu}[$. For values less than $\frac{\nu^2}{2\mu}$, the function $F(G)$ increases rapidly and tends to $+\infty$ as G decreases, so that the restriction of the mathematical solution to the interval $]0, \frac{\nu^2}{2\mu}[$ is also physically inadmissible. It follows that the restriction of the solution to the entire interval $]0, \frac{\nu^2}{\mu}[$ is unphysical.

c) Another argument supporting the above assertion is given in [2].

Let δ_1 be the radius of the spherical source and assume that $G(\delta_1) > \frac{\nu^2}{\mu}$. A radiation emitted radially from the sphere bounding the matter is redshifted, and its redshift at the points of a sphere $\|x\| = \delta$ with $\delta > \delta_1$ is given by the formula

$$Z(\delta, \delta_1) = -1 + \frac{F(G(\delta))}{F(G(\delta_1))} = -1 + \sqrt{\frac{\Phi(G(\delta))}{\Phi(G(\delta_1))}}\,.$$

Suppose δ fixed and let us examine the variation of $Z(\delta, \delta_1)$ considered as function of δ_1. If δ_1 (or $G(\delta_1)$) decreases, $Z(\delta, \delta_1)$ increases and tends to its maximum, obtained for $G(\delta_1) = \frac{\nu^2}{\mu}$,

$$\max Z(\delta, \delta_1) = -1 + \sqrt{\frac{\Phi(G(\delta))}{1-\frac{\mu^2}{\nu^2}}}\,.$$

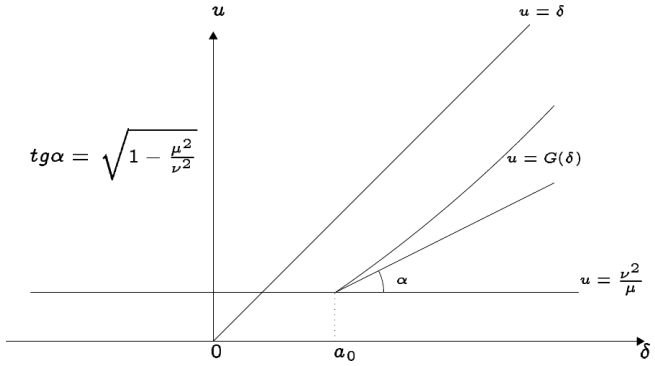

Fig. 3: Graph of G in the case where $\nu^2 > \mu^2$.

If $G(\delta_1)$ takes values less than $\frac{\nu^2}{\mu}$, the phenomenon is inverted: The redshift first decreases and then vanishes for a unique value $G(\delta_1) \in]\frac{\nu^2}{2\mu}, \frac{\nu^2}{\mu}[$ with $\Phi(G(\delta_1)) = \Phi(G(\delta))$. If $G(\delta_1)$ decreases further, instead of a redshift, we have a blueshift. This situation seems quite unphysical, inasmuch as the vanishing of the redshift depends on the position of the observer. In order to observe constantly a redshift, the condition $G(\delta_1) \geqslant \frac{\nu^2}{\mu}$ is necessary.

From the preceding considerations we conclude that the value

$$\frac{\nu^2}{\mu} = \frac{\varepsilon^2}{mc^2}$$

is the greatest lower bound of the curvature radius $G(\delta)$ outside the spherical strongly charged source. In particular, the curvature radius of the sphere bounding the matter is $\geqslant \frac{\varepsilon^2}{mc^2}$, so that a strongly charged source cannot be reduced to a point. Our study does not exclude the case where the solution $G(\delta)$ attains its greatest lower bound, namely the case where the curvature radius of the sphere bounding the matter is exactly equal to $\frac{\varepsilon^2}{mc^2}$. So, in order to take into account all possible cases, the equation (1.4) must be integrated as follows

$$a_0 + \int_{\nu^2/\mu}^{G} \frac{u\,du}{\sqrt{u^2 - 2\mu u + \nu^2}} = \delta\,, \quad (a_0 = \text{const})\,.$$

If $a_0 \leqslant 0$, there exists a value $\delta_1 > 0$ such that the solution is valid only for $\delta \geqslant \delta_1$.

If $a_0 > 0$, the solution is valid for $\delta \geqslant a_0$, only if the sphere bounding the matter has the curvature radius $\frac{\nu^2}{\mu}$. Otherwise there exists a value $\delta_1 > a_0$ such that the solution is valid for $\delta \geqslant \delta_1$.

The expression $\frac{\varepsilon^2}{mc^2}$ is also known in classical electrodynamics, but in the present situation it appears on the basis of new principles and with a different signification. Consider, for instance, the case of the electron. Then $\frac{|\varepsilon|}{m\sqrt{k}} = 2.02\times10^{21}$, so that the electron is strongly charged, and, from the point of view of the classical electrodynamics, is a spherical object with radius $\frac{\varepsilon^2}{mc^2} = 2.75\times10^{-13}$ cm.

Regarding the present theory, we can only assert that, if

the electron is a stationary spherical object, then it is a non-Euclidean ball such that the value 2.75×10^{-13} cm is the greatest lower bound of the possible values of the curvature radius of the sphere bounding it. The radius of the electron cannot be deduced from the present theory.

The proton is also strongly charged with $\frac{|\varepsilon|}{m\sqrt{k}}=1.1\times10^{18}$. The corresponding value $\frac{\varepsilon^2}{mc^2}=1.5\times10^{-16}$ cm is less than that related to the electron by a factor of the order 10^{-3}. So, if the proton is assumed to be spherical and stationary, it is not reasonable to accept that this value represents its radius. This last is not definable by the present theory.

Submitted on January 31, 2009 / Accepted on February 05, 2009

References

1. Stavroulakis N. Paramètres cachés dans les potentiels des champs statiques. *Annales Fond. Louis de Broglie*, 1981, v. 6 (4), 287–327.
2. Stavroulakis N. Particules et particules test en relativité générale. *Annales Fond. Louis de Broglie*, 1991, v. 16 (2), 129–175.
3. Stavroulakis N. Vérité scientifique et trous noires (deuxième partie) Symétries relatives au groupe des rotations. *Annales Fond. Louis de Broglie*, 2000, v. 25 (2), 223–266.
4. Stavroulakis N. Non-Euclidean geometry and gravitation. *Progress in Physics*, 2006, v. 2, 68–75.
5. Stavroulakis N. Gravitation and electricity. *Progress in Physics*, 2008, v. 2, 91–96.

Fractal Scaling Models of Resonant Oscillations in Chain Systems of Harmonic Oscillators

Hartmut Müller

Global Scaling Research Institute in memoriam Leonhard Euler, Munich, Germany
E-mail: info@globalscaling.de

Logarithmic scaling invariance is a wide distributed natural phenomenon and was proved in the distributions of physical properties of various processes — in high energy physics, chemistry, seismicity, biology, geology and technology. Based on the Gantmacher-Krein continued fraction method the present paper introduces fractal scaling models of resonant oscillations in chain systems of harmonic oscillators. These models generate logarithmic scaling spectra. The introduced models are not based on any statements about the nature of the link or interaction between the elements of the oscillating system. Therefore the model statements are quite generally, what opens a wide field of possible applications.

1 Introduction

Within the past 40 years many articles were published which show that logarithmic scaling invariance ("Scaling") is a wide distributed natural phenomenon.

In 1967/68 Feynman and Bjorken [1] discovered the scaling phenomenon in high energy physics, concrete in hadron collisions.

Simon E. Shnoll [2] found scaling in the distributions of macroscopic fluctuations of nuclear decay rates. Since 1967 his team discovers fractal scaling in the fluctuation distributions of different physical and chemical processes, as well as in the distributions of macroscopic fluctuations of different noise processes.

Within the fifties Beno Gutenberg and Charles Richter [3] have shown, that exists a logarithmic invariant (scaling) relationship between the energy (magnitude) and the total number of earthquakes in any given region and time period.

In 1981, Leonid L. Čislenko [4] published his extensive work on logarithmic invariance of the distribution of biological species, dependent on body size and weight of the organisms. By introducing a logarithmic scale for biologically significant parameters, such as mean body weight and size, Čislenko was able to prove that sections of increased specie representation repeat themselves in equal logarithmic intervals.

Knut Schmidt-Nielsen [5] (1984) was able to prove scaling in biological metabolic processes.

Alexey Zhirmunsky and Viktor Kuzmin [6] (1982) discovered process-independent scaling in the development stages of embryo-, morpho- and ontogenesis and in geological history.

In 1987–1989 we [7] have shown, that fractal scaling distributions of physical process properties can be understood as a consequence of resonant oscillations of matter. Based on a fractal scaling proton resonance model, we developed methods of optimization and prognostication of technical processes, which have got european and international patents [8].

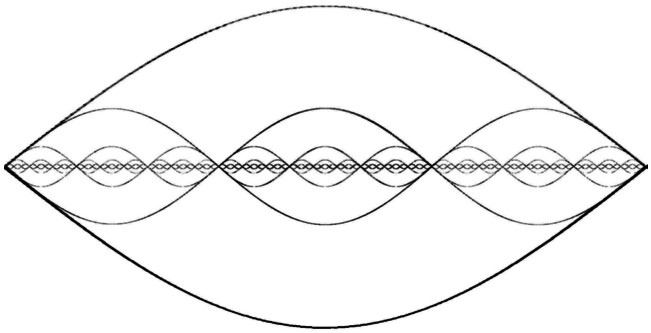

Fig. 1:

In the following we will show that Scaling is a fundamental property of any natural oscillation process. Therefore one can suspect, that natural oscillations of matter generate scaling distributions of physical properties in very different processes.

2 Fractal scaling as a fundamental property of resonant oscillations

A standing wave [9] in a homogeneous space arises only if in the direction of the wave penetration the space is finite and if the half wave length is equal to an integer part of the medium size L.

As a consequence we can find for any low enough resonant oscillation mode frequency f_0 a higher mode frequency f_1 with an integer relationship $n = f_1/f_0$. The frequencies of such resonant oscillation modes generate exponential series:

$$f_{n,p} = f_0 \cdot n^p. \qquad (1)$$

Fig. 1 illustrates the situation with $n = 3$ and $p = 0, 1, 2, \ldots$ for transversal oscillations.

Therefore, the complete resonant oscillation frequency spectrum can be represented as a set of logarithmic fractal spectra (1) with natural $n = 2, 3, 5, \ldots$ In this representation

the generation of the complete resonant oscillation frequency spectrum can be understood as an arithmetical task, what can be reduced to the fundamental theorem of arithmetic, that every natural number greater than 1 can be written as a unique product of prime numbers.

In the oscillation nodes of the logarithmic fractal oscillation modes the spectral density is maximum. Where the amplitudes of the oscillation modes are maximum, the medium particles have maximum kinetic energy, but near the oscillation nodes the kinetic energy is minimum. The distance between the ranges with maximum particle density (nodes) is the half of the oscillation mode wave length. As consequence, the distribution of the medium particle density will be fractal and exactly the same (isomorphism) as the distribution of the spectral density.

In the phases of spectral compression, where the spectral density increases, in the case of approach to any node arises a particle fusion trend, but in the phases of spectral decompression, where the spectral density decreases, in the case of distance from any node arises a particle dispersion trend. Logarithmic fractal change of spectral compression and decompression generates a logarithmic fractal change of high and low density structure areas inside the medium.

Resonant oscillations can be understood as the most probable forming-mechanism of fractal structures in nature, because the energy efficiency of resonant oscillations is very high.

In the works "About continued fractions" (1737) and "About oscillations of a string" (1748) Leonhard Euler [10] formulated tasks, the solution employed several generations of mathematicians the following 200 years. Euler investigated natural oscillations, based on a model of a massless flexible string with a finite or infinite set of similar pearls. Based on this task d'Alembert developed an intergration method of linear differencial equation systems. Daniel Bernoulli formulated the theorem, that the solution of the problem of the natural oscillations of a string can be represented as trigonometric series, what starts a discussion between Euler, d'Alembert and Bernoulli, and continued several decades.

Later Lagrange showed how can be realised the transition from the solution of the problem of the set with pearls string oscillations to the solution of the oscillations of a homogeneous string. In 1822 Fourier solved this task completely.

Though, big problems arisen with oscillations of strings with a finite set of different pearls. This task leads to functions with gaps. After 1893 Stieltjes [11] investigated such functions and found an integration method, what leads to continued fractions. But only in 1950 Gantmacher and Krein found the general solution of Euler's task about natural oscillations of a set with pearls string. Gantmacher and Krein interpreted the stretched string between the pearls as a broken line, what opened them a fractal vision of the problem. In the work „Oscillation matrixes, oscillation cores and low oscillations of mechanical systems" Gantmacher and Krein [12] showed that Stieltjes continued fractions are solutions of the Euler-Lagrange equation for low amplitude oscillations of chain systems. These continued fractions generate fractal spectra. Within the fifties and sixties the development of continued fraction analysis methods of oscillation processes in chain systems reaches a highlight. In 1950 Oskar Perron [13] publicated the book "The continued fraction theory". Achieser [14] investigated continued fractions in the work "The classic problem of moments and some questions of analysis" (1961). In the book "The continued fraction method" (1955) Terskich [15] generalized this method for analysis of oscillations of branched chain systems. In 1964 Khinchine [16] explained the importance of continued fractions in arithmetics and algebra. The works of Khintchine, Markov, Skorobogatko [17] and other mathematicians allowed the development of efficient addition and multiplication methods for continued fractions.

Based on the continued fraction method, in the following we will show, how one can generate scaling spectral models of natural oscillation processes which are not based on any statements about the nature of the link or interaction between the elements of the oscillating system.

3 Fractal scaling spectral models

Based on the continued fraction method we search the natural oscillation frequencies of a chain system of many similar harmonic oscillators in this form:

$$f = f_0 \exp(S)\,, \tag{2}$$

where f is a natural frequency of a chain system of similar harmonic oscillators, f_0 is the natural frequency of one isolated harmonic oscillator, S is a continued fraction with integer elements:

$$S = \frac{n_0}{z} + \cfrac{z}{n_1 + \cfrac{z}{n_2 + \ddots + \frac{z}{n_i}}}\,. \tag{3}$$

The partial numerator z, the free link n_0 and all partial denominators $n_1, n_2, \ldots, n_i$ are integer numbers: $z, n_0, n_i \in Z, i = \overline{1, \infty}$. The present paper follows the Terskich definition of a chain system (Terskich, p. 8) where the interaction between the elements proceeds only in their movement direction. In this connection we understand the concept "spectrum" as a discrete distribution or set of natural oscillation frequencies.

Spectra (2) are not only logarithmic-invariant, but also fractal, because the discrete hyperbolic distribution of natural frequencies repeats itself on each spectral level $i = 1, 2, \ldots$

Every continued fraction (3) with a partial numerator $z \neq 1$ can be changed into a continued fraction with $z = 1$.

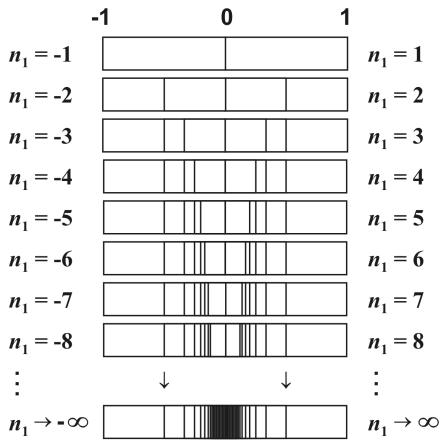

Fig. 2:

For this one can use the Euler equivalent transformation (Skorobogatko, p. 12) and present continued fractions (3) in the canonical form. With the help of the Lagrange [18] transformation (Perron, §40) every continued fraction with integer partial denominators can be represented as a continued fraction with natural partial denominators, what is allways convergent (Khintchine, §4). In this paper we will investigate spectra (2) which are generated by convergent continued fractions (3).

Every infinite continued fraction is irrational, and every irrational number can be represented in precisely one way as an infinite continued fraction (Khintchine, §5). An infinite continued fraction representation for an irrational number is useful because its initial segments provide the best possible rational approximations to the number (Khintchine, §6). These rational numbers are called the convergents of the continued fraction. This last property is quite important, and is not true of the decimal representation. The convergents are rational and therefore they generate a discrete spectrum. Furthermore we investigate continued fractions (3) with a finite quantity of layers $i = \overline{1,k}$ which generate discrete spectra. In the logarithmic representation each natural oscillation frequency can be written down as a finite set of integer elements of the continued fraction (3):

$$\ln(f/f_0) = \frac{n_0}{z} + \cfrac{z}{n_1 + \cfrac{z}{n_2 + \ddots + \frac{z}{n_k}}} = \left[z, n_0, n_1, n_2, \ldots, n_k\right]. \qquad (4)$$

Figure 2 shows the generation process of such fractal spectrum for $z = 1$ on the first layer $i = k = 1$ for $|n_1| = 1, 2, 3, \ldots$ and $n_0 = 0$ (logarithmic representation).

The partial denominators n_1 run through positive and negative integer values. Maximum spectral density ranges automatically arise on the distance of 1 logarithmic units, where $n_0 = 0, 1, 2, \ldots$ and $|n_1| \to \infty$. Figure 3 shows the spectrum on the first layer $i = k = 1$ for $|n_1| = 1, 2, 3, \ldots$ and $|n_0| = 0, 1, 2, \ldots$ (logarithmic representation):

Fig. 3:

The more layers $i = 1, 2, 3, \ldots$ are calculated, the more spectral details will be visible. In addition to the first spectral layer, Figure 4 shows the second layer $i = k = 2$ for $|n_2| = 1, 2, 3, \ldots$ and $|n_1| = 2$ (logarithmic representation):

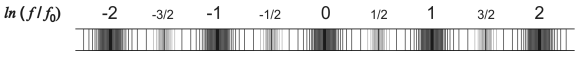

Fig. 4:

On each spectral layer i one can select ranges of relative low spectral density (spectral gaps) and ranges of relative high spectral density (spectral nodes). The highest spectral density corresponds to the nodes on the layer $i = 0$, where $|n_1| \to \infty$. The next (lower) spectral density level corresponds to the nodes on the layer $i = 1$, where $|n_2| \to \infty$, and so on. The largest spectral gaps are between the spectral node ranges on the layer n_0. On the spectral layers $i = 1, 2, 3, \ldots$ the gaps are corresponding smaller.

In 1795 Karl Friedrich Gauss discovered logarithmic scaling invariance of the distribution of prime numbers. Gauss proved, that the quantity of prime numbers $p(n)$ until the natural number n follows the law $p(n) \cong n/\ln(n)$. The equality symbol is correct for the limit $n \to \infty$. The logarithmic scaling distribution is the one and only nontrivial property of all prime numbers.

The free link n_0 and all partial denominators n_1, n_2, n_3, ..., n_k are integer numbers and therefore they can be represented as unique products of prime factors. On this base we distinguish spectral classes in dependence on the divisibility of the partial denominators by prime numbers. In addition, we will investigate continued fractions which correspond to the Markov [19] convergence requirement (Skorobogatko, p. 15):

$$|n_i| \geqslant |z_i| + 1\,. \qquad (5)$$

Continued fractions (3) with $z = 1$ and partial denominators divisible by 2 don't generate empty spectral gaps, because the alternating continued fraction [1, 0; +2, −2, +2, −2, ...] approximates the number 1 and [1, 0; −2, +2, −2, +2, ...] approximates the integer number −1.

Divisible by 3 partial denominators with $z = 2$ build the class of continued fractions (3) what generates the spectrum (4) with the smallest empty spectral gaps. Figure 5 shows fragments of spectra, which were generated by continued fractions (3) with divisible by 2, 3, 4, ... partial denominators and corresponding partial numerators $z = 1, 2, 3, \ldots$ on the first layer $i = 1$ for $n_0 = 0$ (logarithmic representation):

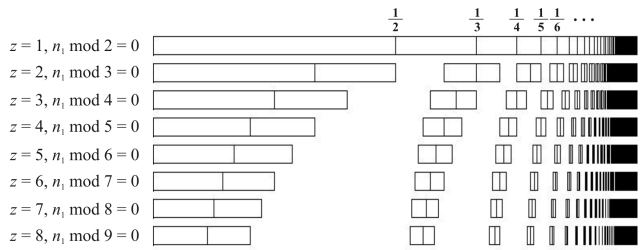

Fig. 5:

Figure 5 shows the spectral nodes on the first layer $i = 1$ and also the borders of the spectral node ranges, so the spectral gaps are visible clearly. The borders of the spectral empty gaps are determined by the following alternating continued fractions ($z \geqslant 1$):

$$\left.\begin{aligned} -1 &= \cfrac{z}{-z-1+\cfrac{z}{z+1+\cfrac{z}{-z-1+\ddots}}} \\ 1 &= \cfrac{z}{z+1+\cfrac{z}{-z-1+\cfrac{z}{z+1+\ddots}}} \end{aligned}\right\}. \quad (6)$$

More detailled we will investigate the second spectrum of the figure 5, what was generated by the continued fraction (3) with divisible by 3 partial denominators and the corresponding partial numerator $z = 2$. This spectrum is the most interesting one, because with $z = 2$ and $n_i \mod 3 = 0$ starts the generation process of empty gaps. Possibly, that the spectral ranges of these gaps are connected to fundamental properties of oscillation processes.

The partial denominators n_1 run through positive and negative integer values. The maximum spectral density areas arise automatically on the distance of 3/2 logarithmic units, where $n_0 = 3j$, $(j = 0, 1, 2, \dots)$ and $|n_1| \to \infty$. Figure 6 shows the spectrum on the first layer $i = k = 1$ for $|n_1| = 3, 6, 9, \dots$ and $|n_0| = 0, 3, 6, \dots$ (logarithmic representation):

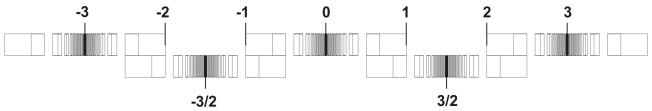

Fig. 6:

The alternating continued fraction [2, 0; +3, −3, +3, −3, ...] approximates the number 1, but the alternating continued fraction [2, 0; −3, +3, −3, +3, ...] approximates the number −1. In the consequence the spectral ranges between $|n_1| = 3 - 1$ and $|n_1| = 3 + 1$ are double occupied. The more layers $i = 1, 2, 3, \dots$ are calculated, the more spectral details are visible (see Figure 7).

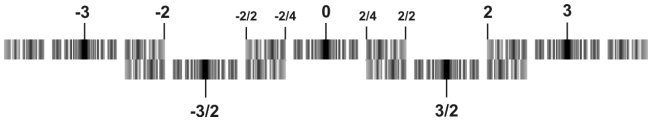

Fig. 7:

Divisible by three free links $|n_0| = 3j$, $(j = 0, 1, 2, \dots)$ of the continued fraction (3) mark the main spectral nodes, partial denominators divisible by three $|n_{i>0}| = 3j$, $(j = = 1, 2, \dots)$ mark spectral subnodes. All the other partial denominators $|n_i| \neq 3j$ mark borders of spectral gaps (see Figure 8):

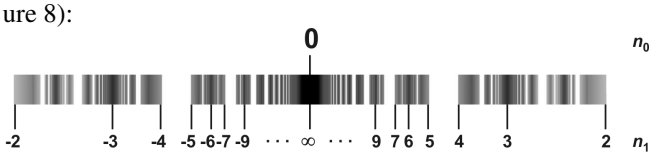

Fig. 8:

4 Local features of fractal scaling spectra and corresponding properties of oscillation processes

In the spectral node ranges, where the spectral density reachs local maximum, the resonance frequencies are distributed maximum densely, so that near a spectral node almost each frequency is a resonance frequency. The energy efficiency of resonant oscillations is very high. Therefore, if a frequency of an oscillation process is located near a node of the fractal spectrum (4), the process energy efficiency (degree of effectiveness) should be relative high. The highest process energy efficiency corresponds to the nodes on the layer $i = 0$. Near the spectral nodes on the layers $i = 1, 2, \dots$ the process energy efficiency should be corresponding lower. On the other hand, if a frequency of an oscillation process is located in a gap of the fractal spectrum (4), the process energy efficiency should be relative low. In the centre of a spectral node the spectral compression changes to spectral decompression (or reversed). Therefore the probability of the process trend change increases near a spectral node.

5 Fractal scaling spectral analysis

Based on the fractal scaling model (2) of resonant oscillations of chain systems one can execute fractal scaling spectral analyses of composite oscillation processes, if the connected oscillators are quite similar.

Corresponding to the logarithmic representation (5) the fractal scaling spectral analysis consists of the following steps:

a). Divide the lowest measured frequency f_{min} and the highest measured frequency f_{max} of an oscillating chain system by the resonance frequency f_0 of one isolated element of the chain system and calculate the natural logarithms $X_{min} = \ln(f_{min}/f_0)$ and $X_{max} = = \ln(f_{max}/f_0)$;

b). Use the Euclid's algorithm to find the free links n_0 and partial denominators n_1, n_2, ... of the corresponding to X_{min} and X_{min} continued fractions and determine the location of X_{min} and X_{min} in the spectrum (5);

c). Determine the highest/lowest spectral density ranges of the spectrum (5) between X_{min} and X_{min} which correspond to important properties of the composite oscillation processes;

d). Use the formula (4) to calculate the corresponding frequency ranges.

The fractal scaling spectral analysis is able to define following properties of of composite oscillation processes: turbulence probability, fluctuation probability, resonance probability, stability and sensibility.

6 Resume

The presented model is not based on any statements about the nature of the link or interaction between the elements of the oscillating chain system. Therefore the model statements are quite generally, what opens a wide field of possible applications. Based on the presented model one can use scaling spectral analyses of composite oscillation processes to find out spectral ranges where the process energy efficiency is relative high or low. Possibly, the scaling spectral analysis could be usefull not only in mechanical engineering, but also in nuclear physics and astrophysics.

The author is deeply grateful to O. M. Kalinin, A. I. Polovinkin, V. A. Kamaev and A. V. Petrukhin for valuable discussions. I wish to thank S. E. Shnoll, V. A. Panchelyuga and V. A. Kolombet for invaluable support.

Submitted on February 09, 2008 / Accepted on February 17, 2009

References

1. Feynman R.P. Very high-energy collisions of hadrons. *Phys. Rev. Lett.*, 1969, v. 23, 1415; Bjorken J.D. *Phys. Rev. D*, 1969, v. 179, 1547.
2. Shnoll S.E., Kolombet V.A., Pozharski E.V., Zenchenko T.A., Zvereva I.M., Konradov A.A., Realization of discrete states during fluctuations in macroscopic processes. *Physics Uspekhi*, 1998, v. 41(10), 1025–1035. (1998)
3. Gutenberg B., Richter C.F.. Seismicity of the Earth and associated phenomena. 2nd ed., Princeton University Press, Princeton, N.J., 1954; Corral A. Universal local versus unified global scaling laws in the statistics of seismicity. arXiv: cond-mat/0402555.
4. Čislenko L.L. The structure of the fauna and flora in connection with the sizes of the organisms. Moscow, 1981 (*in Russian*).
5. Schmidt-Nielsen K. Scaling. Why is the animal size so important? Cambridge University Press, 1984.
6. Zhirmunsky A.V., Kuzmin V.I. Critical levels in developmental processes of biological systems. Moscow, Nauka, 1982 (*in Rissian*).
7. Muller H. The general theory of stability and objective development trends of technology. *Applications of Developmental and Construction Laws of Technology in CAD*, Volgograd, VPI, 1987 (*in Russian*); Muller H. Superstability as a developmental law of technology. *Technology laws and their Applications*, Volgograd-Sofia, 1989 (*in Russian*).
8. Patents:
   Nr. 05700308.9-2206-CH2005000013,
   Nr. 05759820.3-1237-CH2005000427,
   Nr. 05759818.7-1267-CH2005000426,
   Nr. 05700352.7-2415-CH2005000057.
9. Tipler P.A. Physics for scientists and engineers. New York, 1991, p. 438ff.
10. Euler L. De oscillationibus fili flexilis quotcunque pondusculis onusti. Opera omnia, II–10, 35–49.
11. Stieltjes T. Recherches sur les fractions continues. *Ann. de Toulouse*, VIII–IX, 1894–1895.
12. Gantmacher F.R., Krein M.G. Oscillation matrixes, oscillation cores and low oscillations of mechanical systems. Leningrad, 1950 (*in Russian*).
13. Perron O. Die Lehre von den Kettenbruchen. 1950.
14. Achieser N.I. The classic problem of the momenta and some questions of the analysis which are connected. Moscow, 1961 (*in Russian*).
15. Terskich V.P. The continued fraction method. Leningrad, 1955 (*in Russian*).
16. Khintchine A.Ya. Continued fractions. University of Chicago Press, Chicago, 1964.
17. Skorobogatko V.Ya. The theory of branched continued fractions and mathematical applications. Moscow, Nauka, 1983.
18. Lagrange J.L. Additions aux elements d'algebre d'Euler. 1798.
19. Markov A.A. Selected work on the continued fraction theory and theory of functions which are minimum divergent from zero. Moscow–Leningrad, 1948.

On Dark Energy and Matter of the Expanding Universe

Bo Lehnert

Alfvén Laboratory, Royal Institute of Technology, S–10044 Stockholm, Sweden

E-mail: Bo.Lehnert@ee.kth.se

At present the expanding universe is observed to be dominated by the not fully understood concepts of dark energy and matter, in a conceived almost flat Euclidian geometry. As one of the possible efforts to understand the global behaviour of the expanding universe, the present paper attempts to explain these concepts in terms of the pressure force and gravity of a spherical photon gas cloud of zero point energy, in a flat geometry. A difficult point of the conventional theory concerns the frequency distribution of the zero point energy oscillations which leads to the unacceptable result of an infinite total energy per unit volume. A modification of this distribution is therefore proposed which results in finite energy density. A corresponding equilibrium state is investigated, as well as small dynamic deviations from it, to form a basis for a model of the expanding universe. Provided that the crucial points of the present approach hold true, the model satisfies the requirements of cosmic linear dimensions, results in an estimated acceleration of the expansion being of the order of the observed one, presents a possible solution of the coincidence problem of dark energy and matter, and provides one of the possible explanations of the observed excess of high-energy electrons and positrons in recent balloon and satellite experiments.

1 Introduction

From being a speculative subject of discussion, the features of the universe have during recent years become more of an area of strict scientific analysis. After Hubble's discovery of the cosmic expansion and the Big Bang hypothesis by Gamow, astronomical observations and associated theoretical work have resulted in a number of new points of view, as summarized in recent reviews such as those by Linde [1], Hogan, Kirshner and Suntzeff [2], Luminet, Starkman and Weeks [3], Turner [4], Perlmutter [5], Riess and Turner [6], Crease [7] and Linder and Perlmutter [8]. In particular, this includes the concepts of dark energy and dark matter as well as the newly discovered accelerated expansion of the universe and its possible theoretical explanation.

The Hubble redshift has not only been interpreted as the result of a real cosmic expansion. Recently Rabounski [9] has reconsidered the Hubble redshift in terms of General Relativity, thereby finding that a photon loses its proper energy due to the work against the field of the space non-holonomity.

There have so far been reported a number of efforts to understand the global behaviour of the universe. This paper presents one of the alternatives to be investigated for such a purpose. Here an investigation is made on the possible rôle of the zero point energy of quantum mechanical vacuum fluctuations as an origin of dark energy and matter. A summary of recent observations of the expanding universe is first presented in Section 2, with corresponding theoretical so far made considerations in Section 3, followed by a description of the basic reasons for the present approach in Section 4. The frequency distribution of the zero point energy is then reconsidered in Section 5, the cosmic equilibrium of a zero point energy photon gas is elaborated in Section 6, and the acceleration of the expansion is estimated in Section 7. The implications of the present approach are finally given in Section 8, as well as in the summary and conlusions of Section 9.

2 Observations of an expanding universe

As early as in 1900 Schwarzschild [10] considered the possible non-Euclidian structure of space. For a closed elliptical configuration the lower limit of its permissible radius of curvature was found to be about 6×10^{17} meters. At present it is often stated that observations indicate the universe just to be about flat on a scale of $R_0 = 10^{26}$ meters which is the radius of its observable parts [1], but the radius of the universe could be larger. With Hubble's discovery and the Big Bang model, a finite and growing radius can also form the basis of an expansion until the present time. Conventional wisdom says the universe is infinite, but it could be finite, merely giving the illusion of infinity [3]. On the other hand, a closed finite universe of curved space is certainly attractive from the conceptual point of view, but does not become reconcilable with an observed nearly flat geometry. The idea of a finite and flat universe runs then into its own obstacle of the apparent need for the "cut-off" at an edge defined by a radius $R \geqslant R_0$. Still these questions have not been settled, and will not be further touched upon in this paper.

In the 1990s it was realized that supernovae were promising candidates for measuring the cosmic expansion. This came out to be particularly fruitful when one kind of supernova, the type Ia, turned out to have the property of a "standard candle" [2, 5, 6, 8]. The method of surveying space-time with supernovae then became accurate enough even to measure the rate of change in the cosmic expansion. Many cosmologists had anticipated that the rate of expansion should

slow down due to the attractive force of the mass of the universe. It therefore became a news of utmost interest when the supernova measurements indicated that the expansion was in fact accelerating [2, 5, 6, 8].

The acceleration of the radius R_0 of the observable universe can be determined from the measurements of redshift, relative intensity of light, and relative distance [2, 5]. Here we consider very distant supernovae, near the radius of visibility where the redshift $z = \Delta\lambda/\lambda \cong 1$, $\Delta\lambda$ is the shift in wavelength, and λ stands for the wavelength of the light emitted by the supernova at its position. For a given intensity of light, the diagrams of the observations [2, 5] then yield a redshift $z_a \cong 0.8$ for an accelerated expansion instead of $z_0 \cong 1$ for a constant one. This shows that high-redshift supernovae are fainter than would be expected for a constant expansion [5]. The deviation of the redshift due to the acceleration thus corresponds to an additional increment $\Delta \mathrm{v} = (z_0 - z_a)c$ in velocity where c is the velocity of light. With a linear scale of $R_0/2$ relative to the universe of today [5], the corresponding time of passage becomes $\Delta t \cong R_0/2c$. This yields an acceleration $\Delta \mathrm{v}/\Delta t = 2(z_0 - z_a)c^2/R_0 \cong 4\times10^{-10}$ m/s^2 of the radius R_0.

Recent experiments with high-altitude balloons and satellites [11, 12] have further spotted an excess of high-energy electrons and positrons. These can become a possible signature of a decay of dark matter.

3 Theories on the present expansion

The period of acceleration has not prevailed during the entire expansion of the universe, but appears to have started about 5 billion years ago [8]. In order to account for the present acceleration, about 75 percent of the mass-energy content is then considered to be made of some weird gravitationally repulsive substance called dark energy [8], i.e. a "cosmological antigravity" which can drive the universe apart [2]. The remaining 25 percent has attractive gravitational interaction, but $5/6$ of this is not even normal matter but rather some additional unknown substance called dark matter [5].

An alternative description of the global behaviour of the universe has been presented by Rabounski [9]. In this theory the empirical Hubble law is explained in a static universe, as being due to the redshift produced by the global non-holonomity of the isotropic space in which a propagating photon loses its energy. Also the nonlinearity of the Hubble law which is observed at large distances is explained by the deduced form of the redshift.

A candidate to explain the effect of dark energy is further the vacuum energy which is mathematically equivalent to the cosmological constant introduced by Einstein in 1917. However, it appears to be a remarkable and implausible coincidence that the mass density, just in the present epoch, is within a factor of two of the vacuum energy density. This would need some kind of accelerating dark energy that, unlike the cosmological constant, does not become constant [5]. In addition, there are problems with the zero-point vacuum energy of the quantum fluctuations. Thus the standard model of particle physics has no place for a vacuum energy density of the modest magnitude required by astrophysical data, because the simplest estimates predict a vacuum energy being 10^{120} times greater [5]. We shall later return to this crucial point.

4 Exposition of reasons for the present approach

The investigation in this paper on the optional and possible rôle of the zero point energy as an origin of dark energy and matter, in particular during the later stages of the expansion, can be justified as follows:

- The concept of an expanding universe is accepted as a working hypothesis.
- The mass-energy content is mainly due to dark energy in the form of antigravity and to dark matter accounting for the attractive gravitational interaction, thereby dominating the general dynamics of the universe.
- From the observations the universe is here interpreted to have a nearly flat geometry. This supports a simple Euclidian approach in a first approximation, without the introduction of the curved space effects of General Relativity. This would not only hold for a strictly flat space, but also as an approximation for the limited observable part of a closed elliptical or spherical universe with a very large radius of curvature.
- The zero point energy represents the lowest quantum mechanical state. This is a "dark state" having no line radiation.

5 The zero point energy and its frequency distribution

We now turn to the zero point vibrational energy, as discussed by Terletskii [13], Milonni [14] and Loudon [15] among others. This energy can hardly be discarded since its effects have been revealed experimentally. Its infinite total amount per unit volume, as obtained from conventional theory, is on the other hand unacceptable and presents a so far unsolved dilemma.

5.1 Conventional deductions

It is known from quantum mechanics that the energy of a linear harmonic oscillator with the frequency ν only assumes the values [13–15]

$$E_k = h\nu\left(k + \frac{1}{2}\right) \qquad k = 0, 1, 2, \ldots \tag{1}$$

Utilizing the partition function and the Gibbs-Helmholtz equation [13], the mean energy of the ensemble of oscillators of all k-values, also including $k = 0$, then becomes

$$\bar{E} = \frac{1}{2}\, h\nu + \frac{h\nu}{\exp(h\nu/kT) - 1}\,, \tag{2}$$

where kT is the mean energy of a classical oscillator in thermal equilibrium at the temperature T.

The number of virtual field oscillators per unit volume with frequencies in the range $(\nu, \nu + d\nu)$ further becomes

$$dn(\nu) = (8\pi/c^3)\nu^2\, d\nu\,. \tag{3}$$

On the average the oscillators then have the energy density

$$du(\nu) = \bar{E}\, dn(\nu) = (8\pi\bar{E}/c^3)\nu^2\, d\nu \tag{4}$$

in the same range. The total energy density then becomes

$$u = u_0 + u_p \tag{5}$$

where

$$u_0 = \int_0^\infty (4\pi h/c^3)\nu^3\, d\nu\,, \tag{6}$$

$$u_p = \int_0^\infty (8\pi h/c^3)\frac{\nu^3}{\exp(h\nu/kT) - 1}\, d\nu\,, \tag{7}$$

(here u_0 is the infinite zero point energy contribution, and the finite contribution u_p originates from Planck's radiation law).

To obtain a finite total zero point energy, it has sometimes been suggested that the integral (6) should be truncated at a cut-off frequency corresponding either to the Planck length or to a high energy of 100 GeV. As compared to the magnitude of astrophysical data, this still leads to an excessive vacuum energy density being about 10^{120} or 10^{55} times greater than that which is required. The choice of cut-off also appears not to be rigorously motivated.

Even if the integral (6) leads to a physically unacceptable result, a straightforward illustration of vacuum effects can be obtained from a cavity configuration. In the latter a finite change in energy is obtained from the difference between two infinite integrals of forms being similar to that of equation (6). Thus, in 1948 a theoretical analysis was reported by Casimir [16] in which it was shown that two metal plates at narrow distance will attract each other slightly, due to the electromagnetic quantum fluctuations of the zero point energy. This force is due to the low-frequency part of the zero point energy pressure, because only the small high-frequency modes are allowed to squeeze in between the plates. Later, in 1997, the theory was experimentally confirmed within 5 percent accuracy by Lamoreaux [17] who used a torsional pendulum to measure the corresponding Casimir force between a spherical and a plane metal surface. He found that this generated a force up to about 10^{-9} N on a plate having a diameter of 2.54 centimetres, and at separation distances in the range 0.6 to 6 μm. The corresponding energy density was up to about 6×10^{-6} J/m^3. An experimental confirmation of Casimir's theory for parallel metal plates was further reported by Bressi et al. [18] who measured the force between a cantilever and a rigid surface. From data of the oscillating cantilever they obtained agreement with the calculated Casimir force with 15 percent accuracy for separation distances in the 0.5 to 3 μm range. Other experimental attempts to verify Casimir's prediction have also been reviewed by the same authors.

Consequently, the low-frequency part of the zero point frequency distribution has to be accepted as an experimental fact, whereas there arises a crucial problem with the high-frequency part.

5.2 A revised form of the high-frequency distribution

Several investigators have thrown doubt upon the conventional theory of vacuum energy and its related frequency distribution [6, 19]. Here the following points can be taken as an indication that some fundamental part of the theory may be lacking:

- In the conventional analysis the probability that an oscillator is excited to its k-th state is given by a Boltzmann factor. In this factor, however, the zero point energy cancels and disappears when expression (1) is substituted into the deductions [15];
- The energy values which an oscillator can assume at a given frequency ν are determined by expression (1), whereas expression (2) represents the mean energy values which an oscillator adopts in thermal equilibrium. Here $\bar{E}$ differs from E_k for $k \geqslant 1$ of the Planck radiation part which adapts itself to a probability distribution being in thermodynamic equilibrium at a temperature T. For the zero point energy part $k = 0$, however, conventional theory yields $\bar{E}_0 = E_0 = \frac{1}{2}\, h\nu$, which corresponds to the same probability for all frequencies ν. Such a distribution could be questioned and requires further investigation and explanation;
- In the conventional deduction of Planck's law, a finite mean energy kT of the oscillators is introduced as a given and independent parameter, as well as the resulting finite total energy. In the case of the zero point energy, a corresponding introduction becomes unclear in terms of the conventional theory. In other words, the Planck law part of equation (2) includes the disposable and independent parameter kT of the photon mean energy. However, for the zero point energy part of the same equation, the analogous situation is not fully determined because there is no corresponding and independent parameter which determines the average photon energy;
- In the limiting case $T = 0$ of a pure zero point energy photon gas, one would thus have to study an ensemble of continuous states, to search for the most probable distribution of frequency among the oscillators at a given total and finite energy per unit volume.

With these points in mind, it is here concluded that the zero point energy requires a separate statistical treatment. We thus limit the analysis to a state of zero temperature, in which there is an ensemble of photons, each having an energy E_0 of equation (1). The number of possible states of oscillation

is as before given by equation (3) in the range $(\nu, \nu + d\nu)$. Here the population of zero point energy photons due to the conventional theory is on the other hand put in question, as well as their corresponding average energy.

A simple proposal is now made to find a distribution in statistical equilibrium which results in a finite average photon energy. Following Kennard [20], the probability of any state of energy $E_0(\nu) = \frac{1}{2}\, h\nu$ becomes proportional to a Boltzmann factor

$$P_B = \exp(-E_0/\bar{E}) = \exp(-\nu/\bar{\nu}) \tag{8}$$

where

$$\bar{E} = \frac{1}{2}\, h\bar{\nu} \tag{9}$$

now stands for a finite average energy of a photon, and $\bar{\nu}$ is the corresponding average frequency. With this proposal the revised form of the density (4) of the zero point energy becomes

$$du(\nu) = (4\pi h/c^3)\nu^3 \exp(-\nu/\bar{\nu})\, d\nu \tag{10}$$

It results in a finite total energy density

$$u = 24\pi h\bar{\nu}^4/c^3 \tag{11}$$

where the frequency $\bar{\nu}$ is a so far undetermined quantity, like the arbitrary mean energy kT of the states for $k \geqslant 1$.

It is desirable to extend the studies on the Casimir effect also on the experimental side. Investigations on smaller plate distances do not become an easy task, and may involve advanced nanotechnological methods. Here we can only speculate about the possibility of deposing an extremely thin layer of insulating material on a flat metal plate, and placing another such plate on top of it. With layer thicknesses being much smaller than the so far studied plate distances in experiments, considerable mutual forces are expected to arise, as long as equation (4) applies. Observed deviations from this which reveal a smaller or even a saturated force, could provide a test of various theoretical approaches, also that of equations (10) and (11).

6 Equilibrium of a photon gas in its gravitational field

In a gas cloud of photons of zero point energy, there is an antigravity force due to the photon gas pressure gradient, and a gravitation force due to the intrinsic mass of the same photons as determined by the total energy according to Einstein's mass-energy relation. We now proceed to the steady-state balance of an isotropic photon gas of zero point energy, in which the pressure force is balanced by the gravitational force. A restriction is made to spherical symmetry in a flat space, as supported by the points given in Section 4, and based on the proposed model of frequency distribution given in Section 5.

With the radial coordinate r in a spherical frame of reference, the energy density u of equation (11) and the corresponding average photon energy $\bar{E}$ and frequency $\bar{\nu}$ of equation (9) then become functions of r only. The radially outward directed pressure force is given by

$$f_p = -\frac{dp}{dr} = -\frac{1}{3}\frac{du}{dr}\,. \tag{12}$$

With an average total mass $\bar{E}/c^2$ of each photon, the integrated mass of the photon gas within the radius r becomes

$$M(r) = \int_0^r 4\pi r^2 (u/c^2)\, dr = (4\pi/c^2)\int_0^r r^2 u\, dr\,. \tag{13}$$

This leads to a radially inward directed gravitational force

$$f_g = -GMnm_p/r^2 = -GMu/c^2 r^2 \tag{14}$$

where $G = 6.673\times10^{-11}$ m^3/kg$\cdot$s^2 is the Newtonian constant of gravitation.

A steady equilibrium is now determined by $f_p + f_g = 0$ which results in

$$-\frac{1}{3}\frac{du}{dr} = \frac{4\pi G}{c^4 r^2}\, u \int_0^r r^2 u\, dr\,. \tag{15}$$

This equation is normalized by introducing $\rho = r/r_c$ where r_c is a characteristic radius, and $u = u_c U(\rho)$ with u_c as a characteristic photon energy density. Multiplying eq. (15) by r^2/u and taking the derivative with respect to r,

$$\frac{d^2U}{d\rho^2} + \frac{2}{\rho}\frac{dU}{d\rho} - \frac{1}{U}\left(\frac{dU}{d\rho}\right)^2 + 2C_0U^2 = 0\,. \tag{16}$$

This relation includes the dimensionless characteristic parameter

$$C_0 = 6\pi G u_c r_c^2/c^4 = 3\pi n_c r_c^2 L_p^2/\bar{\lambda}\,. \tag{17}$$

Here $L_p = (Gh/c^3)^{1/2}$ is the Planck length, $n_c = u_c/\bar{E}$ a characteristic photon density, and $\bar{\lambda} = c/\bar{\nu}$.

A particular solution of eq. (16) can be found by means of the ansatz $U = \rho^{-\alpha}$ which leads to $2C_0 = \alpha\rho^{\alpha-2}$ and becomes satisfied when $\alpha = 2$. This yields $C_0 = 1$ and

$$u(r) = u_c\,(r_c/r)^2\,. \tag{18}$$

The equilibrium condition $C_0 = 1$ corresponds to a characteristic radius

$$r_c = \left(c^4/6\pi G u_c\right)^{1/2}\,. \tag{19}$$

The integrated mass at the distance r further becomes

$$M(r) = 2c^2 r/3G \tag{20}$$

from combination of relations (13), (18), and (19). The obtained results are now discussed as follows:

- In some respects the present analysis also applies to the equilibrium of a photon gas in the regime of Planck's radiation law at nonzero temperature;
- When being observed from the Earth, the surrounding parts of the universe appear on the average to be rather uniformly distributed over the sky. This is here taken as an indication that the position of the Earth and of an observer is deep inside the cloud of the universe, i.e. far

away from its "boundary". Consequently we take $r=r_c$ as the position of the Earth where the energy density has the characteristic value u_c, and have $r = R_0 \gg r_c$ as the radius of the observable parts of the universe. Due to relation (18) this implies that the energy density $u(r)$ decreases from u_c at $r=r_c$ to $u_c(r_c/R_0)^2 \ll u_c$ at $r=R_0$. A "halo" extending beyond the radius R_0 can also exist, as introduced in many cosmological versions [1];

- The Planck length $L_p \cong 4.05\times10^{-35}$ m is the smallest length appearing as a basic parameter in physics. To satisfy the equilibrium condition $C_0 = 1$, it is seen from eq. (17) that the characteristic radius r_c of eq. (19) has to be of cosmic dimensions for moderate values of u_c;
- Equation (19) further shows that a high energy density u_c requires a small radius r_c for a state being close to equilibrium, and does not lead to excessively large cloud dimensions;
- At the origin $r = 0$ the total mass (20) vanishes. The divergence at $r = 0$ of the energy density u in equation (18) can here be taken as a remnant of the earliest stage of a Big Bang. Further, even if each of the forces (12) and (14) diverges at $r = 0$, the total force vanishes at the origin in equilibrium;
- The mass (20) increases linearly with r, to $M(R_0) = 2c^2R_0/3G$ at the radius of the observable universe. This value is analogous to the solution by Einstein [21] for a steady quasi-Euclidian universe.

The parameter C_0 represents the ratio $\mid f_g/f_p \mid$ between the gravitation and pressure forces. Here f_g is proportional to u^2, and f_p to u. Small deviations from an equilibrium can in a first approximation be represented by values of C_0 which differ slightly from unity. This implies that $C_0 < 1$ corresponds to pressure-dominated accelerated expansion, and $C_0 > 1$ to gravitation-dominated accelerated compression. The deviations of C_0 from unity can therefore be used to identify the acceleration without considering a detailed equation of state as discussed elsewhere [4, 8]. This has some resemblance to the energy principle in fluid dynamics, where stability is studied in terms of virtual changes in energy, without analysing the dynamics of the corresponding normal modes in detail.

7 A simple discussion on the dynamics of the expansion

During the later stages of the expansion the equilibrium solution of Section 6 could provide a starting point also for a simple discussion on the related dynamics. As a working hypothesis we here adopt the often accepted view of a balance between the dark energy and matter forces corresponding to a constant expansion rate, whereas a force unbalance leads to an accelerated or retarded expansion. Only a crude estimation is made here of the order of the acceleration in the case of a slight deviation from the equilibrium treated in Section 6.

For this purpose we consider a volume element of thickness dr at the radius $r = R_0$. With the local force densities (12) and (14) the total forces on the layer become

$$(dF_p, dF_g) = 4\pi R_0^2 (f_g, f_p)\, dr\,. \tag{21}$$

From equations (12), (18) and (19)

$$f_p \cong 2u_c r_c^2/3R_0^3 \cong c^4/9\pi G R_0^3 \tag{22}$$

for small deviations from the equilibrium defined by $dF = dF_p + dF_g = 0$ and where

$$dF = (2\delta - 1)\, dF_p\,. \tag{23}$$

Here the fraction δ of the total mass-energy content is due to the pressure force dF_p, and δ is not far from the equilibrium value $\delta = 1/2$. The mass of the volume element further becomes

$$dM \cong (2c^2/3G)\, dr \tag{24}$$

due to equation (20). The acceleration of the radius R_0 is then roughly given by

$$d^2R_0/dt^2 \cong (2\delta - 1)\, dF_p/dM \cong (2\delta - 1)(2c^2/3R_0)\,. \tag{25}$$

In a rigorous dynamical approach the question would arise whether the photon gas cloud can be considered as a closed system or not, i.e. if the region $r > R_0$ of an undisturbed "background" has to be included in the analysis.

8 Implications of present approach

An attempt has been made here to understand at least part of the features of the expanding universe at its later stage. Among the obtained results, the order of magnitude of the characteristic radius (19) should first be mentioned. The experiments by Lamoreaux indicate that the possible "saturation" at a finite average frequency $\bar{\nu}$ of equations (9)–(11) would at least take place above an energy density of the order of 6×10^{-6} J/m^3. With $u_c \geqslant 6\times10^{-6}$ J/m^3 at the position $r=r_c$ of the Earth, we then have $r_c \lesssim 10^{24}$ m $= 0.01R_0$ with R_0 as the radius of the observable universe. Provided that there is not an excessively large average frequency $\bar{\nu}$ as compared to the frequency range in the experiments by Lamoreaux, and that the form (11) holds true, the linear dimensions of the present photon gas model should thus be consistent with cosmical dimensions. Since f_p is proportional to u and f_g to u^2, very large energy densities result in very small radii, and not in very large ones.

Concerning the present stage of an accelerated expansion, the radius of the outermost parts of the universe has been observed to expand at an acceleration of about 4×10^{-10} m/s^2 for a fraction $\delta = 0.75$, as described in Sections 2 and 3. The corresponding estimation (25) yields an acceleration of the order of 3×10^{-10} m/s^2, being of the same order as the observed value.

The generally discussed coincidence problem may have a solution in terms of the present theory. The vacuum energy density (dark energy) and its mass density (dark matter) are coupled here, because they originate from the same photon cloud. This coupling both exists in an equilibrium state, and in an accelerated state where the acceleration of the expansion is of the order of the ratio between the net pressure force and the mass of the cloud.

The spotted excess of high-energy electrons and positrons in recent balloon and satellite experiments [11, 12] may, among other possible explanations, also be due to electron-positron pair formation through the decay of energetic zero point energy photons. The latter then belong to the high-frequency part of the distribution, even in the proposed case of expression (10). The photon decay could be caused by impacts with other charged particles [22].

9 Summary and conlusions

The present expansion of the universe is dominated by the so far not fully understood concepts of dark energy and matter. An attempt has been made in this paper to explain these concepts in terms of the pressure force and gravity of a spherical photon gas cloud of zero point energy, treated in flat quasi-Euclidian geometry. Such an analysis requires a reconsideration to be made of the conventional concept of zero point energy and its frequency distribution, because this leads to an unacceptable infinite energy density. For this purpose a modified statistical approach has been proposed which results in a finite energy density. An equilibrium solution has then been found for a zero point energy photon gas confined in its own gravitational field. This also outlines the main behaviour of small dynamic deviations from an equilibrium, i.e. from a constant to an accelerated expansion of the universe.

A crucial point of the present analysis is the required finite energy density of the vacuum field. Provided that the present approach holds true, it would lead to the following features:

- The obtained linear dimensions seem to be consistent with observed cosmical ones;
- The observed and estimated values obtained for the acceleration of the present expansion are of the same order of magnitude;
- The generally discussed coincidence problem of dark energy and dark matter appears to have a solution, because these concepts originate from the same photon cloud in the present model;
- The observed excess of high-energy electrons and positrons in balloon and satellite experiments have one possible explanation in the decay of high-energy photons of the vacuum field.

Submitted on February 15, 2008
Accepted on February 26, 2009

References

1. Linde A. The self-reproducing inflatory universe. *Scientific American*, November 1994, 32–39.
2. Hogan C. J., Kirshner R. P., Suntzeff N.B. Surveying space-time with supernovae. *Scientific American*, January 1999, 28–33.
3. Luminet J.-P., Starkman G. D., Wecks J. R. Is space finite? *Scientific American*, April 1999, 68–75.
4. Turner M. S. Dark energy: just what theorists ordered. *Physics Today*, April 2003, 10–11.
5. Perlmutter S. Supernovae, dark energy, and the accelerating universe. *Physics Today*, April 2003, 53–60.
6. Riess A. G., Turner M. S. From slowdown to speedup. *Scientific American*, February 2004, 50–55.
7. Crease R. P. Critical point dark energy. *Physics World*, December 2007, 19–22.
8. Linder E., Perlmutter S. Dark energy: the decade ahead. *Physics World*, December 2007, 24–30.
9. Rabounski D. Hubble redshift due to the global non-holonomity of space. *The Abraham Zelmanov Journal*, 2009, v. 2, 11–28.
10. Schwarzschild K. Über das zulässige Krümmungsmaaß des Raumes. *Vierteljahrsschrift der Astronomische Gesellschaft*, 1900, Bd. 35, S. 337–347 (published in English as: Schwarzschild K. On the permissible numerical value of the curvature of space. *The Abraham Zelmanov Journal*, 2008, v. 1, 64–73).
11. Brumfiel G. Electric "bump" may confirm dark matter. *Nature*, 2008, v. 456, 290–291.
12. Chang J. et al. An excess of cosmic ray electrons at energies of 300–800 GeV. *Nature Letters*, 2008, v. 456, 362–365.
13. Terletskii Ya. P. Statistical physics. North-Holland Publishing Comp., Amsterdam, London, 1971, Ch V1.
14. Milonni P. W. The quantum vacuum. Academic Press Inc.,Boston, San Diego, New York, London, Sydney, Tokyo, Toronto, 1994.
15. Loudon R. The quantum theory of light. Oxford Univ. Press, 2000, Third Edition, Ch 1, Sec. 6.12.
16. Casimir H. B. G. On the attraction between two perfectly conducting plates. *Proc. Kon. Nederland. Akad. Wetensch.*, 1948, v. B51, 793–795.
17. Lamoreaux S. K. Demonstration of the Casimir force in the 0.6 to 6 μm range. *Phys. Rev. Letters*, 1997, v. 78, 5–8.
18. Bressi G., Carugno G., Onofrio R., Ruoso G. Measurement of the Casimir force between parallel metal plates. *Phys. Rev. Letters*, 2002, v. 88, 041804, 1–4.
19. Heitler W. The quantum theory of radiation. Clarendon Press, Oxford, 1954, pp 57 and 326.
20. Kennard E. H. Kinetic theory of gases. McGraw-Hill Book Comp., First Edition, New York and London, 1938, Sec. 226.
21. Einstein A. The meaning of relativity. Methuen and Co.Ltd., London, 1950, pp. 86 and 102.
22. Lehnert B. A model of electron-positron pair formation. *Progress in Physics*, 2008, v. 1, 16–20.

Regular Changes in the Fine Structure of Histograms Revealed in the Experiments with Collimators which Isolate Beams of Alpha-Particles Flying at Certain Directions

Simon E. Shnoll*† and Ilya A. Rubinstein‡

*Institute of Theor. and Experim. Biophysics, Russian Acad. of Sciences, Pushchino, Moscow Region, 142290, Russia
†Department of Physics, Moscow State University, Moscow 119992, Russia
‡Skobeltsin's Institute of Nuclear Physics, Moscow State University, Moscow 119991, Russia
E-mail: shnoll@mail.ru

As was shown in the works of 1951–1983, the fine structure of distributions of the results of measurements of processes of diverse nature is not casual. The changes in the shape of histograms corresponding to the distributions were called "macroscopic fluctuations". The universal character of the phenomenon and its independence of the nature of the process studied were demonstrated for various processes: biochemical and chemical reactions, movement of latex particles in the electric field, proton transverse relaxation in the inhomogeneous magnetic field, discharge in the neon-tube RC-generator and radioactive decay of various α- and β-isotopes. Since 1982, the main object chosen to study macroscopic fluctuations has been α-decay. The choice was based on the process being a priori independent of trivial factors and the possibility to conduct continuous long-term automatic measurements while storing the results in a computer archive (database). Started in 1982, these measurements have been carrying on, as unceasingly as possible, until now. Since July 2000, the measurements are conducted using devices designed by one of the coauthors of this review, I. A. Rubinstein. Application of these devices (especially, detectors with collimators which isolate beams of α-particles flying at certain directions), along with the use of Edwin Pozharsky's computer program, which eases histogram comparing by the expert, has allowed us to reveal a number of fundamentally new regularities. In the review, we describe these regularities, device constructions, and the methods of measurement and analysis of the results obtained.

1 Devices, measurement methods, and data analysis

The methods of histogram construction and analysis were described many times in our previous works [11–15]. We analyze the shape of "inconsistent" histograms [33, 34] — distributions of the results of consecutive measurements, the number of which is comparable with the selected number of digits (bins). Usually we cut the sequence of a time series of the results of measurements to equal, non-overlapping segments (60–100 segments in a series), with approximately the same number of bins. In the histograms constructed from such segments of time series, the number of results per bin will vary from 0 to 5. We analyze changes in the distribution of the number of results within a single bin depending on the position (order number) of the bin in the series, and the regularities become more evident (visible) after smoothing of the initially inconsistent histograms by moving summation. All the operations: registration of the quantities measured, their storing and sorting, histogram construction and processing (smoothing, superpositioning, mirroring) — are performed with the aid of a very handy program written by Edwin Pozharsky (see [12]). A weakness of our methodology is visual comparing of histogram shapes: the decision "similar/non-similar" is made by an expert, after evaluating a pair of histograms drawn on the computer monitor. There is a "radical" way to overcome subjectivity of expert's judgments: comparing histograms after randomization of their sequence. In this case, the expert knows nothing about the histograms compared. Using this approach, we checked all the principal results of our investigations. However, the approach is extremely laborious; the volume of work to do increases greatly. Another way to avoid expert's subjectivity, which was used in most cases, is pairwise comparing — *ceteris paribus* — of two series of measurements, "control" and "experiment", differing only in a single factor (e.g., comparing histograms constructed from the "direct" and "inverse" sequences of the same time series). This method, which has been conventional in science for 300 years, was used to obtain the results of last years.

It would be good to replace the expert with a computer program. We started such attempts about 20 years ago. This task turned out unexpectedly difficult for yet. The pattern-recognition specialists usually give it up, because what seems obvious for the expert appears vague for the computer program. Recently, however, some progress has been achieved. V. V. Strelkov has made a computer program which reprodu-

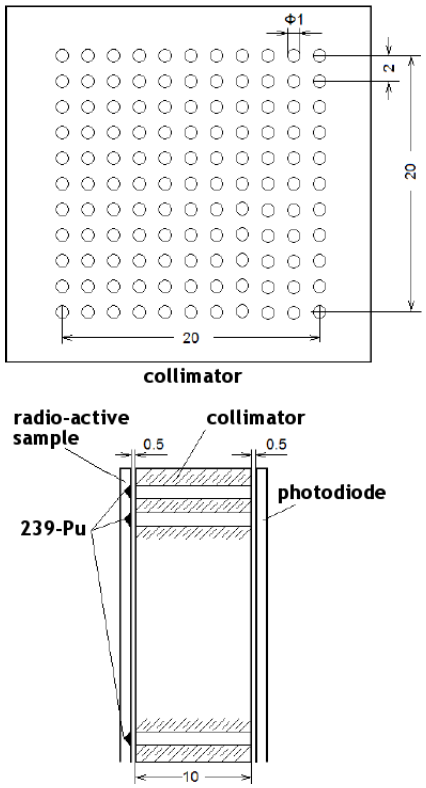

Fig. 1: — Fig. 1a: Collimator. Fig. 1b: Device assembly (radioactive sample, collimator, photodiode).

ces one of the main phenomena we study, namely, the "near-zone effect" [31, 32]. The effect means that the histograms constructed from the neighbor (non-overlapping!) segments of a time series are more probable to be similar than random far-apart histograms. Unfortunately, the program lacks user interface and is still accessible only by the author.

Despite the absence of a computer program and the laboriousness of visual histogram comparing, we have obtained much information on the phenomena studied, which is based on the "control-experiment" comparisons. Among those data, of special interest are the results of experiments, in which α-radioactivity was measured using a collimator-based setup.

Designing a collimator which would yield a narrow beam of α-particles (angle, $\leqslant 10^{\circ}$) represents a known difficulty. Since the mean range of 5-MeV α-particles in air is about 32 mm, the length of the collimator can be about 10 mm — then the particle's energy loss after passing the collimator will be about 20%. In this case, one can be sure that all the α-particles passed through the collimator will be registered, and no vacuumization of the "source-collimator-detector" system would be necessary.

With the collimator length 10 mm, the diameter of the hole for obtaining a narrow beam should not be more than 1 mm. The number of α-particles emitted by the radioactive source from a 1-mm spot cannot be substantially increased by raising the thickness of the ^{239}Pu layer. Hence, one can achieve a particle flux through a single collimator hole of 5–8 particles per second.

To enhance statistical significance of the experiment, we had to design a collimator in the form of a 120-hole grid (Fig. 1a), and use a larger-area detector.

The radioactive source itself is a grid with hollows filled up with ^{239}Pu. The centers of hollows are strictly coaxial with the centers of collimator holes. Fig. 1b shows the positional relationship between the source, collimator and detector, the latter being a photodiode with the area of sensor surface 400 mm^2.

2 Regular changes of the histogram shape with time

Regular changes with time is one of the main proofs of non-randomness of the fine structure of histograms obtained upon measuring processes of diverse nature. These regularities gradually emerged in the series of systematic many-year measurements of the rates of enzymatic and chemical reactions and the processes of radioactive decay [1–6]. The main results of those studies were reproduced and substantially extended in the experiments on α-activity measured using a line of new devices.

2.1 The "near-zone effect"

As shown in many our papers published earlier, changes in the histogram shape reveal an "effect of near zone", which states for a high probability of the histograms constructed from the non-overlapping neighbor segments of a time series to be similar. The nature of this effect remains mysterious, much because of its fractality: the effect manifests itself on different time scales, when histograms are constructed from hour, minute, second and 0.01-second segments of a time series [12, 14, 15].

2.2 Daily periods

The high quality of experimental setups and accurate determination of time intervals (and most of all, independence of the histogram shape of time series trends!) enabled us to see that the periods of appearance of a certain histogram shape split to the "sidereal" and "solar" ones. Now, with histograms constructed for 1-min segments, the daily period split to the "sidereal" (1436 min) and "solar" (1440 min) days. Determination of the yearly periods with the accuracy of 1 h also yielded two peaks: one equal to 365 average solar days (calendar year) and another equal to 365 days plus 6 h (sidereal year). When yearly periods were determined with the accuracy of 1 min (!), the calendar and sidereal periods, as expected from calculations, turned out to be 525599-525600 and 525969 min respectively. The calendar period seems to mean the recurring orientation of the laboratory relatively to the Sun, whereas the sidereal period reflects orientation in re-

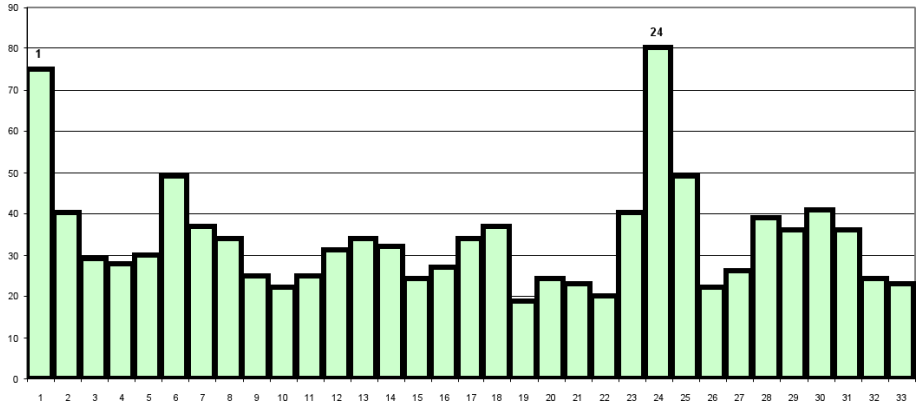

Fig. 2: A typical dependence of the probability of reappearance of histograms of a certain shape on the interval between them. The "near-zone" effect and the near-daily period of reappearance of similar 1-hour histograms in the measurements of ^{239}Pu α-activity at Novolazarevskaya station (Antarctic) on March 1–2, 2003. The measurements were made by A. V. Makarevich. In the figure, the number of similar histogram pairs (Y-axis) is plotted vs. the corresponding interval between histograms (X-axis, h) [20].

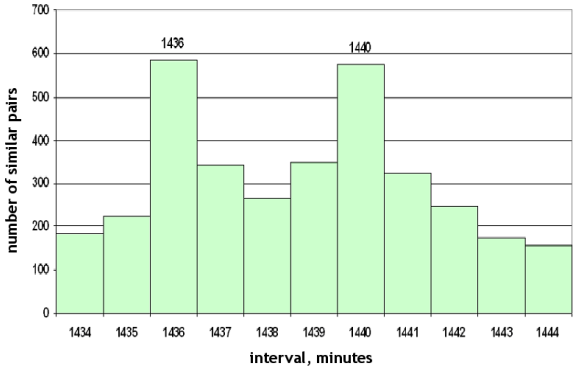

Fig. 3: When ^{239}Pu α-activity is measured with the detectors oriented in a plane parallel to the celestial equator, two distinct periods of the appearance of similar histograms can be seen: one equal to the sidereal day (1436 min) and another corresponding to the solar day (1440 min). The measurements were made in Pushchino on June–October, 2004. Axis legends as in Fig. 2 [22, 25].

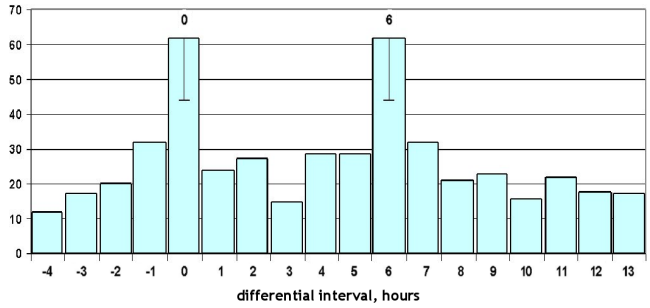

Fig. 4: Similar 1-hour histograms appear in the measurements of ^{239}Pu α-activity with the interval of exactly a year ("calendar year") and a year plus 6 hours ("sidereal year"). In the figure, the number of similar histogram pairs (Y-axis) is plotted vs. the corresponding interval between histograms minus the number of hours in a year (8760 h) (X-axis, h) [22, 25].

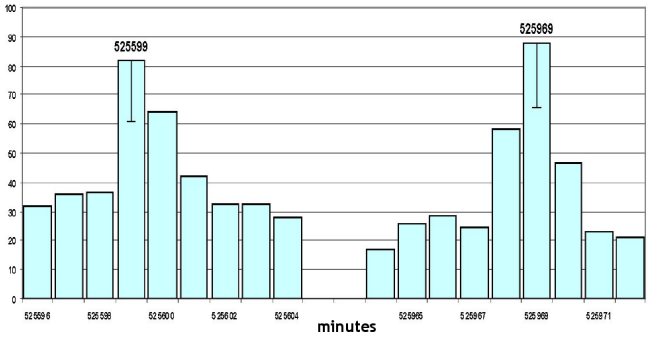

Fig. 5: With the accuracy of 1 min, similar histograms reappear after a year with two main periods: the double (split!) calendar (with 525599- and 525600-min peaks) and the sidereal, equal to 525969 min. The measurements of ^{239}Pu α-activity were made on November 24, 2001 and 2002. In the figure, the number of similar histogram pairs (Y-axis) is plotted vs. the corresponding interval between histograms (X-axis, min) [22, 25].

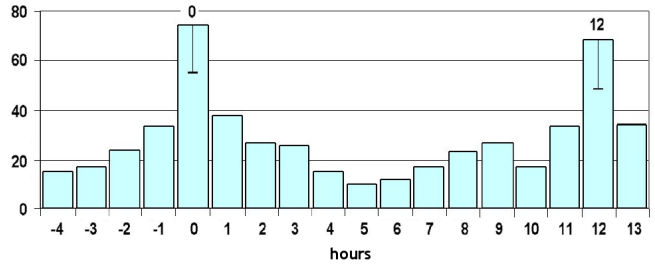

Fig. 6: With the accuracy of 1 h, similar histograms reappear with two periods: exactly 2 years and 2 years plus 12 h. The measurements of ^{239}Pu α-activity were made on August–September, 2000–2002. In the figure, the number of similar histogram pairs (Y-axis) is plotted vs. the corresponding interval between histograms minus the number of hours in two years (X-axis, h) [22, 25].

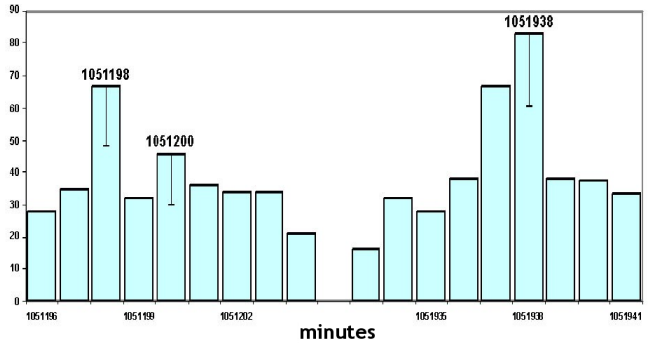

Fig. 7: When ^{239}Pu α-activity is measured with a 1-min resolution, similar histograms reappear with two main periods: calendar and sidereal. The calendar period consists of two subperiods: one is equal to the theoretical value (1051200 min) and another is 2 min shorter (1051198 min). The sidereal period exactly meets the theoretical value of 1051938 min. The measurements of ^{239}Pu α-activity were made on April 20, 2001–2003. In the figure, the number of similar histogram pairs (Y-axis) is plotted vs. the corresponding interval between histograms (X-axis, min) [22, 25].

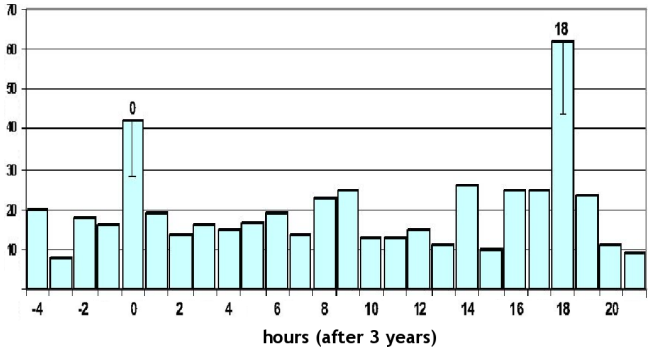

Fig. 8: With the accuracy of 1 h, similar histograms reappear exactly after 3 years and 3 years plus 18 h. The measurements of ^{239}Pu α-activity were made on August–October, 2000–2003. In the figure, the number of similar histogram pairs (Y-axis) is plotted vs. the corresponding interval between histograms minus the number of hours in three years (X-axis, h).

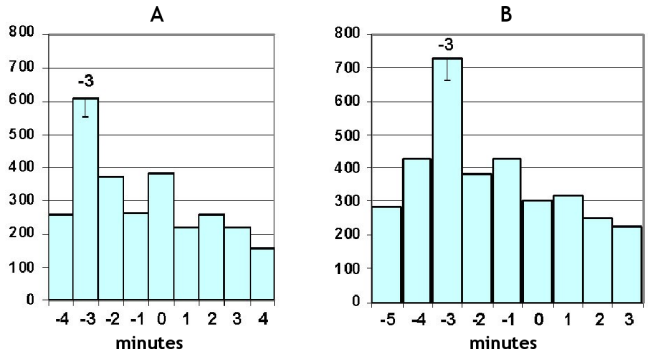

Fig. 9: When compared are histograms with a 3-year interval between them, the calendar period of reappearance of similar histograms is 3 min shorter than the theoretical value. The measurements of ^{239}Pu α-activity were made on the same dates of October (A) or August and November (B), 2000–2003. In the figure, the number of similar histogram pairs (Y-axis) is plotted vs. the corresponding interval between histograms minus the number of minutes in three years (1576800 min) (X-axis, h).

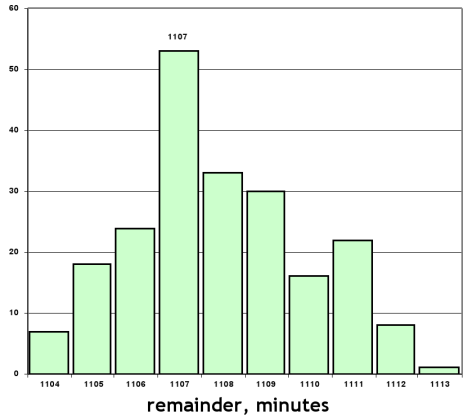

Fig. 10: When compared are histograms with a 3-year (1576800-min) interval between them, the sidereal period of reappearance of similar histograms is realized with a triple "leap shift", i.e. $369\times3 = 1107$ min later of the calculated calendar time. In the figure, the number of similar histogram pairs (Y-axis) is plotted vs. the corresponding interval between histograms minus the number of minutes in three years (1576800 min) (X-axis, h).

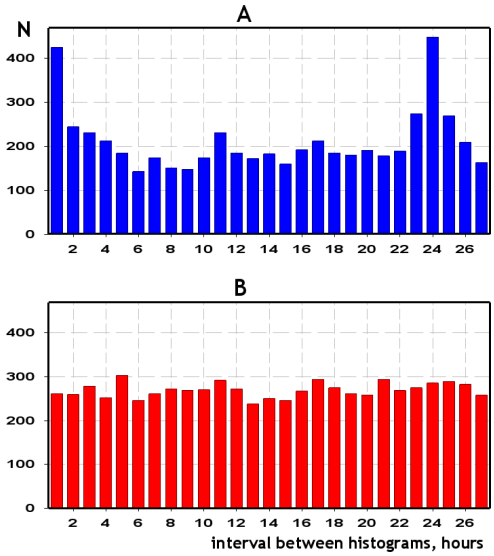

Fig. 11-1: The distribution of intervals between similar histograms depends on the direction that α-particles fly in upon ^{239}Pu radioactive decay. The measurements of ^{239}Pu α-activity were made on January–June, 2002. (A) α-Particles emitted by a flat sample are registered with a flat detector without collimator; (B) before registered by a detector, α-particles pass through a narrow collimator directed at the Pole Star. In the figure, the number of similar histogram pairs (Y-axis) is plotted vs. the corresponding interval between histograms (X-axis, h) [23, 26].

Fig. 11-2: Distribution of intervals between similar 1-hour histograms in the experiments with collimators aimed at the Pole Star (A) and directed west (B). The measurements of ^{239}Pu α-activity were made in Pushchino (at a latitude 54° north) on February–May, 2003 [23, 26].

lation to the sphere of fixed stars.

Apparently, the phenomenon of period splitting is underlain by the spatial anisotropy of factors that determine the shape of histograms. All the aforesaid is illustrated by Fig. 2–Fig. 9.

Fig. 2 shows a typical picture: a high probability of appearance of similar 1-h histograms in the nearest, neighbor intervals (the near-zone effect) and the increase of this probability after 24 h. We obtained analogous distributions with a pronounced near-zone effect and 24-h period many times — for processes of diverse nature measured at various geographical points.

Fig. 3. More accurate determination of the daily period in the appearance of similar histograms (with the 1-min resolution), undertaken on Yu. I. Galperin's advice, showed that the daily period is distinctly resolved to two peaks: the "sidereal day" (1436 min) and the "solar day" (1440 min).

2.3 Yearly periods

Fig. 4 shows that determined with the accuracy of 1 h, yearly periods split — like do daily periods determined with the 1-min accuracy — to two peaks: the "solar" (calendar) peak and the "star" (sidereal) one.

With the results of 1-s measurements collected for many years, yearly periods were determined with a 1-min accuracy. Then, apart from resolving the solar and sidereal yearly periods, we were able to see a surprising shift of the solar period by a minute per year: by one minute in the first, by two minutes in the second, and by three minutes in the third year. Strangely enough, the sidereal period did not shift; and since both observations were made in the same experiments, the shift of the solar period looked more reliable.

Constructing 1-h histograms after 3 years, we again obtained two periods: the "calendar" period, which was equal to the number of hours passed for 3 years, and the "sidereal" one, differing from the first by 18 h, i.e. by three "leap shifts". This can be seen in Fig. 8.

To obtain statistically significant values of the duration of "calendar period" after 3 year with a 1-min resolution, we compared about 200000 histogram pairs. The results are represented in Fig. 9.

It is also important that the 2nd "sidereal" period corresponds exactly to the leap shift and is equal to $369\times3 = 1107$ min (i.e., $1576800 + 1107 = 1577907$ min) — see Fig. 10. Analogous results were obtained time and again.

3 Dependence of the histogram shape on the direction in space

The use of collimators, isolating directed α-particle beams, allowed us to start studies on the spatial regularities in the change of the histogram shape.

3.1 The collimator is directed at the Pole Star [23, 26]

In 2002 we started measurements with collimators, which isolate directed beams of α-particles flying at different directions upon radioactive decay. The devices were constructed by I. A. Rubinstein. It was already in the first experiments, when we found that the histogram shape depended on the direction of α-particles escape. With the collimator directed North (at the Pole Star), we saw disappearance of the daily periods in the change of the histogram shape. The control measurements were conducted either without collimators or with a collimator directed west or east. These measurements lasted several months in 2002 and were repeated in 2003 and 2004 [23].

The dependence of the histogram shape on the direction of α-particles escape upon radioactive decay has quite a deep significance. The measurements were carried out in Pushchino laboratory (at the latitude 54° north and longitude 37° east), and the result was similar to that observed near the North Pole (at the latitude 80–82° north) [20]. In the air, α-Particles (^{239}Pu) will run a distance of $\sim$4 cm. Hence, the matter does not concern any factors of the Earth Pole region affecting the shape of histograms. Evidently, a suggestion of radioactive α-decay being influenced by something is out of consideration too. The measure of radioactive decay intensity (the number of decay events per time unit) is independent of the conditions of measurements and did not change in our experiments. The fluctuations of the radioactive decay intensity we observed were well-correspondent, according to the conventional criteria, to Poisson statistics. The only thing dependent on the orientation of the collimator was the change of the histogram shape in time, or rather the change associated with the daily rotation of the Earth. Considering the disappearance of that dependence in the experiments conducted near the North Pole, one could assume an interference of some local environmental factors. For the results of Pushchino experiments, when the collimator was directed at the Pole Star, no such explanation is possible, as daily periods did not disappear in the control, *ceteris paribus*, measurements. There remains only one conclusion: the phenomenon is a manifestation of sharp anisotropy of the space-time continuum. It should be noted here that this anisotropy reveals itself at the moment of α-particles escaping the nucleus. Given the nucleus diameter to be $\sim 10^{-13}$ cm, the spatial anisotropy should be of the same scale. With the energy of α-particles being several MeV, the fluctuations of the Earth magnetic field and its influence on the direction of α-particles run, let alone on the fine structure of histograms, may well be neglected.

3.2 Rotation of collimators [26, 27]

Following the experiments discussed above, we started, in 2004, measurements with collimators that were being rotated clockwise or counterclockwise with a special apparatus.

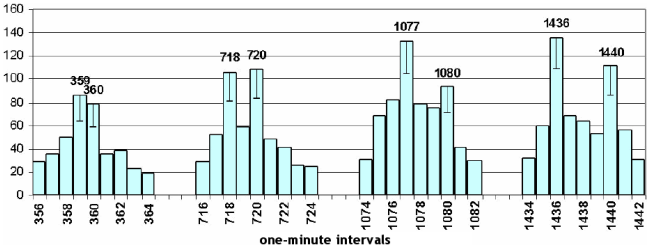

Fig. 12: When ^{239}Pu α-activity was measured with collimators being rotated counterclockwise in a plane parallel to the celestial equator, the probability of similar histograms to reappear periodically increased. These "artificial" periods turned out to be split to the sidereal and solar peaks too.

When the collimator was rotating counterclockwise (i.e., co-rotating with the Earth), the shape of histograms was changing with periods equal to the number of collimator rotations per day plus one rotation made by the Earth itself. We observed periods of 12, 8, 6, 4, 8, 3 and 1 h. When the collimator made one clockwise rotation a day, the Earth's rotation got compensated for, and the daily period in the change of histogram shape disappeared. All these results confirmed the conclusion on the dependence of histogram shape changes on "scanning" of the surrounding, sharply anisotropic, space. And again, we found that these "artificial" periods split to the "solar" and "sidereal" ones (Fig. 12) [26, 27].

Fig. 12 shows the results of an experiment, in which a collimator made three rotations per day counterclockwise. Together with one counterclockwise rotation made by the Earth itself, this amounts to four rotations per day, i.e., a period equal to 6 h (360 min). It can be seen that after the first rotation, the extremum consists of two unresolved peaks (359 and 360 min). After the second rotation, two distinct extrema (718 and 720 min) are visible, and they get to 1077 and 1080 min after the third rotation. After the forth rotation we finally see two extrema corresponding to the "normal" solar and sidereal day.

Analogous splitting was observed in the case of other "artificial" periods.

3.3 Collimators are directed west and east [27, 28]

The experiments, in which collimators were directed west and east, confirmed the main conclusions made before and revealed two new phenomena:

a). Simultaneous measurements with two collimators placed at the same point but counter-directed, aiming east and west, showed disappearance of similarity between histogram shapes. It was important, since earlier we considered similarity of histograms obtained at the same place and time as the main argument in favor of nonrandomness of the histogram shape;

b). Not less important was another phenomenon: there was a 12-hour difference in the appearance of similar his-

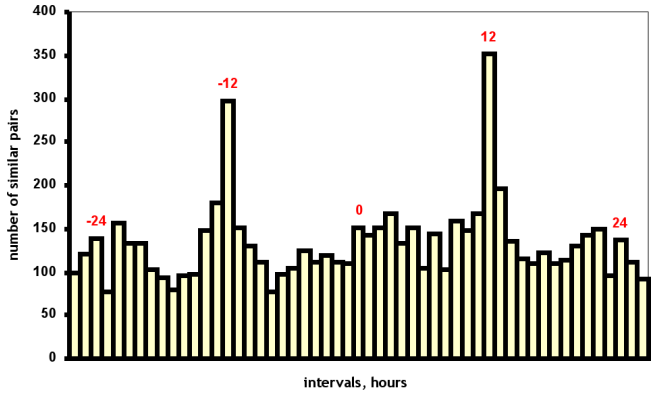

Fig. 13: With the collimators aimed at opposite directions, the probability of similar histograms to reappear sharply decreases. The histograms of a certain shape appear "in the west" exactly half a day later than "in the east". The measurements of ^{239}Pu α-activity were made in Pushchino on June 22 and October 13, 2003.

tograms in the series obtained with the "eastern" and "western" collimators. Essentially, this result was analogous to that obtained in the experiments with rotating collimators. Indeed, as the Earth rotates, the surrounding space is being scanned, and there should be a correspondence between histograms of a particular shape and certain directions in the space, which will consecutively appear in the collimator's "field of view" (Fig. 13).

3.4 A strange 1444-minute period emerging when the collimator is always aimed at the Sun

In the spring of 2004, we started continuous, 24/7 registration of ^{239}Pu α-activity with a collimator, which made one clockwise rotation per day — that is, it was always aimed at the Sun. The objective was to distinguish between changes dependent on the Earth's revolution around the Sun and changes caused by the Earth's movement in relation to the sphere of fixed stars. As expected, no daily periods was revealed in those measurements. The changes of the histogram shape seen under such conditions could, therefore, be only attributed to the Earth's movement along the circumsolar orbit. So it was even more surprising when in the second half of July 2005, we found a strange period equal to 1444 min. The similarity between histograms gradually grew, the peak became more distinct and reached its maximum on July 24–29, this followed by its rapid decline until complete disappearance by August. This phenomenon is illustrated in Fig. 14–Fig. 16.

Fig. 14 shows the distribution of the number of histogram pair matches for measurements with a "solar" collimator on July 25 and August 10, 2005. It can be seen that there are no distinct daily periods on August 10 — as well as on any other day, which is typical for measurements with the "solar" collimator. There is an exception though: on July 25 the probability of similar histograms to reappear jumped, the period

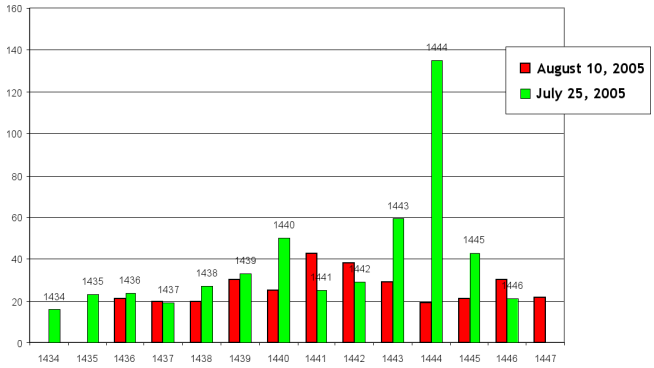

Fig. 14: The figure illustrates emergence of an "anomalous" period of similar histogram reappearance (July 25, 2005), which is equal to 1444 min. Usually, there are no marked daily periods in the experiments with the "solar" collimator — as can be seen on August 10, 2005.

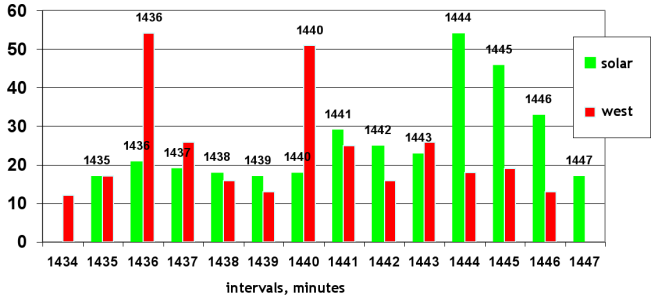

Fig. 15: The period of 1444 min emerges in the measurements with the "solar" collimator and is absent in the ceteris paribus measurements with the "western" collimator. In the experiments with a solar collimator, there is also no 1436- and 1440-min periods, which can be seen when a western collimator is used. The measurements of ^{239}Pu α-activity were made on July 24, 2005.

of appearance being 1444 min. Such a period does not correspond to any cosmophysical process we are aware of, and the fact of its emergence seems very strange.

It was important to ascertain that this period would emerge only in the experiments with the "solar" collimator. So we compared these data with the results obtained in parallel experiments with a "western" collimator. An example of the comparison is given in Fig. 15. The figure shows distributions of the number of histogram matches; compared are the results of simultaneous "solar" and "western" collimator-based measurements on July 24, 2005. It can be seen that in the "western collimator" measurements, there are distinct 1436-min and 1440-min periods and no 1444-min period. In the experiments with the "solar" collimator there is, *vice versa*, the 1444-min period and no the solar and sidereal daily periods. Thus, the phenomenon should be somehow related to the situation of α-particles running towards the Sun.

We tried to seek for this period on other days of the year, yet the search yielded no results — at first. We continued to register the period on the same July days in 2006 (incomplete data) and then in 2007 and 2008. Finally, a key step was

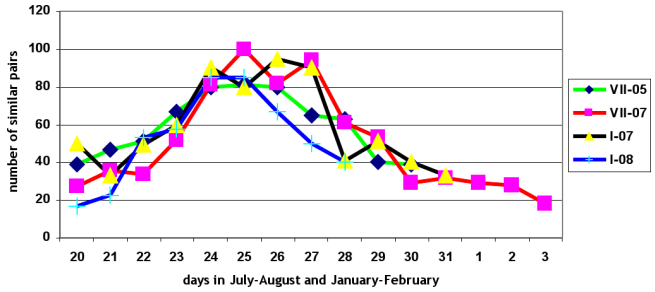

Fig. 16: In the experiments with a collimator directed at the Sun, the 1444-min period reappeared on the same dates of July and January, 2005–2008.

made: we found an analogous period in January, with the interval between the July and January peaks being exactly half a year, which meant they were right at the opposite points of a diameter of the circumsolar orbit.

As can be seen in Fig. 16, the July and January waves of the 1444-min period are quite synchronized to each other and also self-synchronized in different years (2005, 2007, 2008).

These results indicate that moving along the circumsolar orbit, the Earth will enter — at least twice a year — a spatial region with "anomalous characteristics", which change with a period of 1444 min. This spatial region represents an "anomalous band", crossing the center of the circumsolar orbit and stretched along the "July-January" line. It is remarkable that the characteristics of this anomaly are not shielded by the Sun, i.e., manifest themselves equally on both sides of the orbit. No analogy with the Doppler effect was revealed: the 1444-min period emerges "suddenly", does not change for several days (while the Earth is moving), and "suddenly" disappear. It should be stressed that the phenomenon is not observed in the parallel experiments without collimators or with collimators not aimed at the Sun. The "anomalous direction" crossed by the Earth on its way along the circumsolar orbit roughly corresponds to the direction from the constellation Cancer (July 21 — August 11) to the constellation Capricorn (January 19 — February 16). The nature of this period is enigmatic. The 1444-min period is 4 min longer than the daily period and, thus, cannot be explained by influence of any factors within the Solar system.

3.5 Effects of "half-day" and "half-year" palindromes [35, 36]

As follows from the data presented above, changes in the histogram shape depend on changes of the object's orientation in the space-time continuum. If we look in more detail at the path that the "laboratory" (the place where the measurements are performed) moves along over a day, we can see that during the "astronomical night" (i.e., from 18:00 to 6:00 by local time), the laboratory speeds up, since the Earth adds revolution about its own axis to the movement along the circumsolar orbit. From 6:00 to 18:00 (during the "astronomical day"), the laboratory, correspondingly, slows down, as the Earth's spinning is subtracted from its revolution around the Sun. In relation to the sphere of fixed stars, the objects studied will, correspondingly, move in the reverse order. Our investigations with V. A. Pancheluga showed that these circumstances would give rise to the "effect of half-day palindromes", which is a high probability of a series of "night histograms" to be similar with the inverted series of the correspondent "day histograms" [35]. As supposed by M. N. Kondrashova [39], an analogous palindrome effect should exist for the histogram series obtained from measurements at the "opposite sides" of the circumsolar orbit [2]. Subsequent studies confirmed this supposition. Indeed, in addition to the "half-day palindrome effect" we found the effect of "half-year palindromes". The half-year palindromes can be revealed when one takes into account the direction of night and day movement in relation to the sphere of fixed stars. At the opposite sides of the circumsolar orbit, the movement is counter-directional at day and night. That is, on vernal equinox the series of day histograms will be inverse to the day and similar to the night series on autumnal equinox. This proved valid for any opposite points of the circumsolar orbit. Therefore, the spatial characteristics that determine histogram shape must not change markedly over the year (the same being indicated by the existence of yearly periods). Holding true is also the converse: *histograms are a stable, regular characteristic of a direction (domain) of the space-time continuum* [36]. The aforesaid is illustrated by Fig. 17.

3.6 Collimators and the phenomenon of half-day and half-year palindromes

The effects of half-day and half-year palindromes are one of the most illustrative piece of evidence for the dependence of the phenomena under discussion on the movement of the objects studied in the space-time continuum. Of special interest is, thereby, palindromes that were revealed under the use of collimators. At the beginning of those experiments, we encountered an unexplainable irreproducibility of the results. In the experiments with a fixed west-oriented collimator, the half-day palindromes might either be seen quite clearly or be almost absent. Further studies with two collimators directed west and east correspondingly revealed a more complicated picture.

It turned out that this two-collimator setup yielded data series in which the orders of "day-night" and "night-day" were not equivalent. In the measurements with the eastern collimator, a clear palindrome was observed at comparing a sequence of day histograms with the *inverted* sequence of the *follow-up* night histograms. On the contrary, the western collimator gave series in which the *inverted* sequence of the *preceding* night histogram was a palindrome to the sequence of the *follow-up* day histograms.

The eastern collimator "faces the stream of time", the

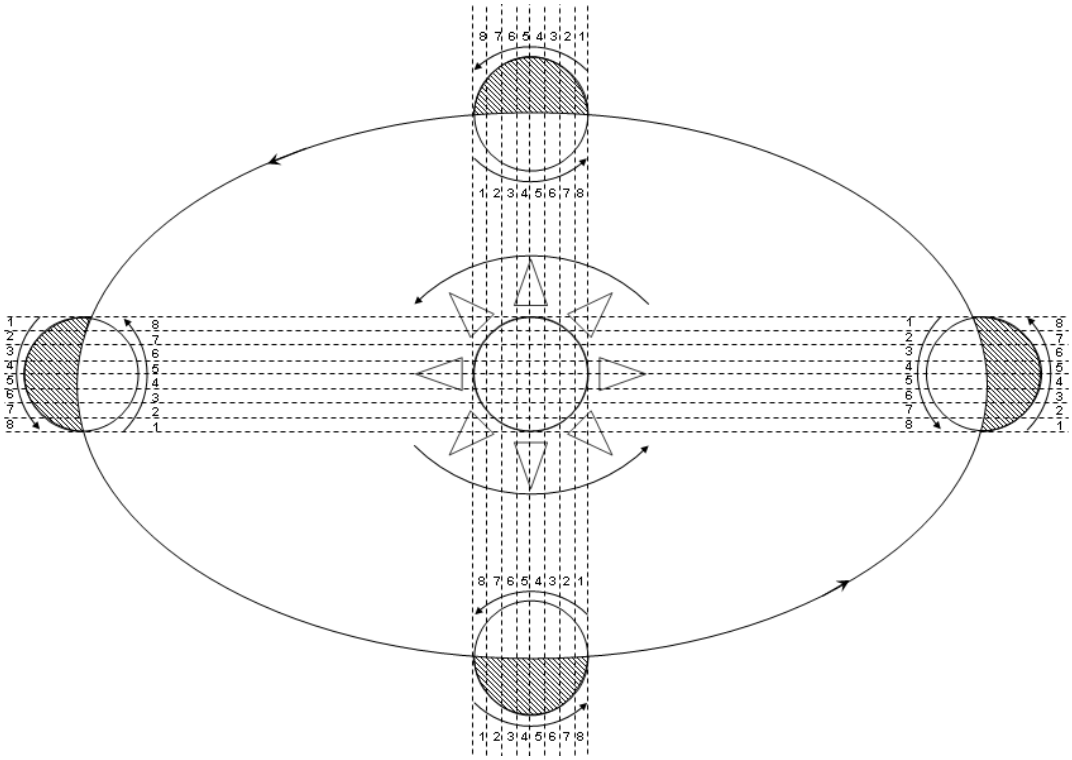

Fig. 17: A scheme illustrating the "palindrome effects". With the Sun in the center, the scheme shows four positions of the Earth on the circumsolar orbit. Both the Earth and the Sun are rotating counterclockwise; movement of the Earth along the circumsolar orbit is counterclockwise as well. As seen in the figure, the Earth's rotational movement in the nighttime is co-directional to its movement along the circumsolar orbit and to rotation of the Sun. In the daytime, the direction of these movements is opposite. Hence, in the case of "backward" movement (in the daytime), the object measured passes in the inverse order the same spatial regions that it has passed in the direct order in the nighttime. The effect of the "half-day palindrome" consists in the high probability of a "nighttime" histogram sequence to be similar to the inverted "daytime" sequence taken on the same day. Equally, the "daytime" sequence will be similar to the inverted "nighttime" one. For example, the 1–2–3–4–5 sequence of nighttime histograms is similar to the 5–4–3–2–1 sequence of the daytime ones. The effect of the "half-year" palindrome is determined by the fact that at the opposite points of the circumsolar orbit, the movements during the same halves of the day are opposite to each other. The effect consists in the high probability of a "nighttime" histogram sequence taken on one side of the circumsolar orbit to be similar to the "daytime" (not inverted) sequence taken on the opposite side. Correspondingly, nighttime (daytime) sequences on one side of the orbit will be similar to the inverted nighttime (daytime) sequences on the opposite side [36].

western one "looks after its flowing away"...

This strange effect still needs to be reproduced once and again, and many circumstances are to be clarified. We report it here due to its mysteriousness and, apparently, deep meaning.

3.7 The phenomenon of absolute-time synchronism in the measurements with collimators directed at the Pole Star and the Sun

The appearance of similar histograms in measurements at different geographical points at the same local time — the "local-time effect" — is quite regular. Sometimes, however, we obtained similar histograms at different geographical points not only at the same local but also at the same absolute time. The clearest observations of such an absolute-time synchronism were made during solar eclipses and new moons [37, 38]. At these moments, histograms of a certain shape appear simultaneously (with the accuracy of a few minutes) at different geographical points. We also observed absolute-time synchronism during the Antarctic expedition of 2001 (S. N. Shapovalov's measurements). Recently, we have compared the occurrences of absolute-time synchronism in the experiments without collimators and with collimators directed at the Sun and the Pole Star. Compared were data of simultaneous measurements made by S. N. Shapovalov in the Antarctic (Novolazarevskaya station) and data of Pushchino measurements. The results of comparison was unexpected: the extent of the "local-time effect" and absolute-time synchronism depended on the type of the measuring setup used. The local-time synchronism was clearly seen in the experiments without collimators or in the data obtained using the western Pushchino collimator; the absolute-time synchronism was almost absent. On the contrary, the measurements with Pushchino collima-

tors directed at the Pole Star or the Sun showed no local-time but good absolute-time synchronism (Fig. 18–20). This phenomenon also needs to be confirmed.

4 Discussion

Proving that the histograms obtained by measuring processes of diverse nature change regularly and in relation to the characteristics of the space-time continuum is the reason to pose questions on the nature of this relation. To answer these questions, additional studies are necessary.

The phenomena discovered are quite unusual and require alteration of conventional views. First of all, it applies to establishing the regular, non-casual character of the fine structure of amplitude fluctuation spectrum (histogram shape) for "quite stochastic", according to conventional criteria, processes. In fact, there is no contradiction here: the processes that are quite stochastic X-directionally can be absolutely non-stochastic Y-directionally. There is not — in principle — any determinate connection between the time course of a process and the spectrum of its amplitude fluctuations: the same histogram shape may correspond to many variations of time series.

Collecting the results of once-a-second measurements of ^{239}Pu α-activity for many years, which became possible after application of perfect enough detectors, and the use, upon necessity, of collimators — fixed or rotated by different ways — was extremely valuable for discovering and studying the phenomena discussed. The nature of many (most of) these phenomena is far from comprehension.

First of all, this is the *near-zone effect*. The statistically significant similarity of histograms constructed for different, independent segments of time series of the results of measurements is one of convincing indications of nonrandomness of the histogram shape. It seemed logical that the similarity of the nearest neighbor histograms should be the result of action of a common external "force" (cause). This cause changes in time, and while these changes are not significant, histograms remain similar. In other words, it would be natural to think that there is a "lifespan" of a certain "shape idea" [29]. However, the numerous attempts to determine even the order of magnitude of this "lifespan" were unsuccessful. Until now we failed to find such a small interval that the shape of histograms would not change (intervals were varied from minutes to tens of milliseconds).

The next mysterious phenomenon is the *splitting of the daily period* in change of the histogram shape to two peaks: the sidereal and solar days. Should only one of them be revealed, we would conclude that the shape of histograms is determined by the exposition (vector) of the object studied in relation to the Sun or the sphere of fixed stars. However, the fact that we observe two highly resolved extrema, with the periods of 1436 and 1440 min, seems quite unusual. The

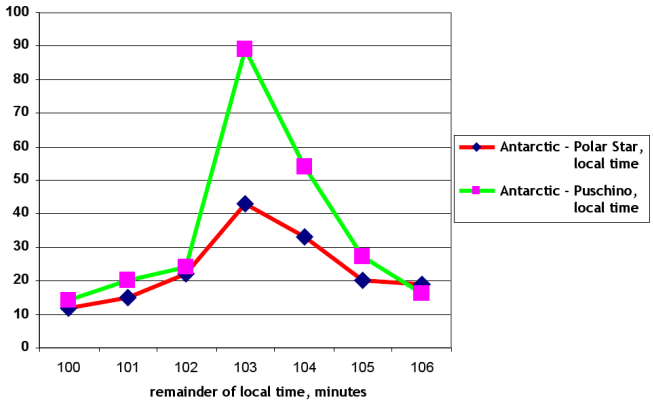

Fig. 18: Comparison of histograms corresponding to the parallel measurements of ^{239}Pu α-activity at Novolazarevskaya station (Antarctic) and in Pushchino shows that the effect of "local-time synchronism" is well-expressed when Pushchino measurements were performed with a west-directed collimator and it is weak when the collimator was directed at the Pole Star. The measurements were made by S. N. Shapovalov (in the Antarctic) and K.I. Zenchenko (in Pushchino) on March 19, 2003. The calculated difference in local time is 103 min. In the figure, the number of similar histogram pairs (Y-axis) is plotted vs. the corresponding interval between histograms (X-axis, min).

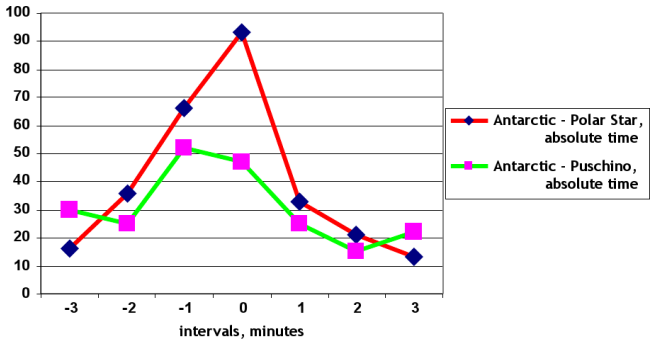

Fig. 19: In the Antarctic and Pushchino measurements, the absolute-time synchronism is more evident when measurements in Pushchino were made with a collimator aimed at the Pole Star, rather than a west-directed collimator. The measurements of ^{239}Pu α-activity were made on March 19, 2003.

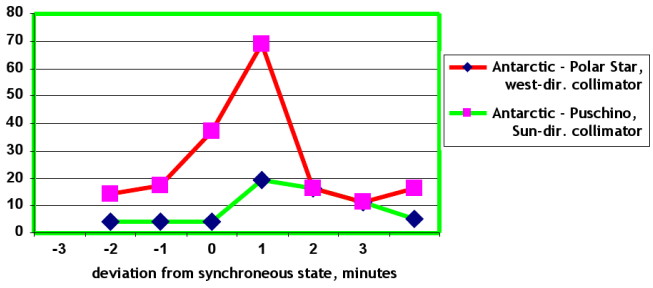

Fig. 20: In the Antarctic and Pushchino measurements, the absolute-time synchronism is more evident when measurements in Pushchino were made with a collimator aimed at the Sun, rather than a west-directed collimator. The measurements of ^{239}Pu α-activity were made on July 16, 2005.

time resolution of 1 min corresponds to the coelosphere resolution of 0.25° (15 angular minutes). And we can see this effect not only in the experiments with collimators but also in the measurements made with flat detectors, without collimators. This should be investigated in more details, yet even by now we have repeatedly registered the dependence of peak resolution on the orientation of the detectors. When flat detectors are positioned in the horizontal plane, one of the extrema (as a rule, the solar day) may not be seen. A good resolution was achieved when a flat detector was oriented in the plane of celestial equator. Also, we saw well-resolved sidereal and solar periods in the experiments with collimators, both fixed (directed east and west) and rotated counterclockwise. Phenomenology of these effects is far from being complete, and additional studies are necessary. The problem became more enigmatic after V. A. Pancheluga's experiments [40–43]. When measuring noise fluctuations in electronic circuits with frequency band up to 100 kHz, he determined the periods of reappearance of histograms of a certain shape. The splitting of extrema to the sidereal and solar days was found at a distance between the objects studied about several kilometers. The splitting corresponded to the period difference of several milliseconds, which in terms of angular units would mean an incredibly high resolution. Thus, the problem of period splitting grew even more paradoxical. This paradoxicality had long been noted by D. P. Kharakoz, who drew our attention to the fact that the collimator aperture allowed one to resolve coelosphere segments of approximately 5° (20 minutes), while we spoke about a second-order resolution ("Kharakoz's paradox" [44])! This paradox is, probably, seeming, as we use not single collimators but a setup in which 120 collimators are arranged on a small area. Perhaps, this is the cause of such a sharp "focusing".

All that was said about splitting of daily periods can be referred to the *splitting of yearly periods* as well. Now, what we see here are the same effects of discriminate orientation relative to the Sun and stars. And the same problems. Plus, what appears impossible at first glance — an extremely precise determination of yearly periods: with the accuracy of a minute, we determine the yearly period as equal to 525600 min! The accuracy is so high that we are able to register the diminishing of the "calendar" (solar) period by a minute (!) per year. One of possible explanations may be the movement of the solar system through the Galaxy. Any explanation, however, would still lack solid grounds.

It is necessary to emphasize that the largest puzzle, underlying all the observed phenomena, is the *nature of the histogram shape*. As follows from all our results in total, the shape is independent of the nature of the processes studied. The only cause common for all these processes can be the features of space-time. However, the nature of the relation between the shape of the histogram, i.e., the spectrum of amplitude fluctuations of the quantity measured, and the space-time fluctuations is absolutely unclear. What magnitude should these fluctuations be to affect the results of measurements? Why the sensitivity of different processes to these fluctuations ranges so much: the "scatter of the results of measurements" in piezoelectric quartz has an order of 10^{-6} of the measured magnitude, in chemical reactions the order is 10^{-2}, and in radioactive processes the scatter is proportional to $\sqrt{N}$?

Discovering the effect of daily and yearly palindromes substantially complements the mosaic of facts assembled earlier. The main conclusion, which can be drawn from the analysis of these effects, is that peculiarities of each region of the space-time continuum are rather stable; they keep unchanged for years, and the shape of histograms is, correspondingly, a stable characteristic of these peculiarities. It should be noted, however, that this stability is relative. The basic "local peculiarities" of the space-time continuum are overlaid with patterns of second, third etc. order: rotation of the Sun about its axis (near-27-day periods), revolution of the Moon round the Earth, changes in the relative positions of the Earth, Moon and Sun, effects of new moons, solar and lunar eclipses, solar flares etc. Perhaps, these "overlays" manifest themselves in the *effect of absolute-time synchronism*. For many years, we have mainly paid attention to the effect of local-time synchronism. The observations of a more distinct absolute synchronism in the experiments with collimators aimed at the Pole Star and the Sun bring hope that these questions will be answered.

The *effects of daily and yearly palindromes* essentially clarify the overall picture. Nevertheless, there remains a lot of work to do. The simplified picture of daily palindromes does not take into account the shift by 4 min per day in the course of the Earth's movement along the circumsolar orbit. Fig. 17 depicts movement of the Earth as a circle. It is still unclear how the picture would change with the "sidereal day" taken into consideration.

Finally, the recently found effect of *palindrome's time-vector asymmetry* in the measurements with the western and eastern collimators may happen to be — when reproduced and detailed — highly interesting.

Our works of the last years almost do not consider an important feature of "macroscopic fluctuations", which was found several decades ago: the shape, fine structure, of histograms and the average amplitude of fluctuations change independently of each other. The same "shape idea" may emerge in "narrow" and "wide" histograms. Comparing such histograms, we normalize them by abscissa. Regularities in the change of the average amplitude would also be very interesting to study, yet it is still in the future. A lot of work should be done to sort out all these problems.

Nevertheless, there is one conclusion we are certain of: *the apparently casual shape of histograms and its change over time are determined by the natural movement of the object studied through quite a complex space-time continuum.*

As for the nature of anisotropy and inhomogeneity of the space-time continuum, it is a matter of future research. Now

we may just adopt a notion of "interference pattern" resulting from the influence of numerous moving celestial bodies and radiant fluxes, whose effects are summed up in each point of the space.

Acknowledgements

The authors are thankful to M. N. Kondrashova and V. P. Tikhonov for valuable ideas, discussions, moral and financial support; V. A. Pancheluga for fruitful collaboration and joint research; V. A. Shlekhtarev for making devices used in the experiments with collimators.

We are grateful to D. D. Rabounski for valuable discussions and comments on the text of our manuscripts.

We express sincere gratitude to our colleagues from the Department of Biophysics of Physical Faculty of Moscow State University (Head of the Department, Prof. V. A. Tverdislov) and from the Laboratory of Physical Biochemistry at the Institute of Theoretical and Experimental Biophysics RAS (Head of the Laboratory, Prof. D. P. Kharakoz).

We thank Director of the Institute of Theoretical and Experimental Biophysics RAS, Corresponding Member of Russian Academy of Sciences G. R. Ivanitsky for his everlasting patience and goodwill.

We also highly appreciate T. A. Zenchenko and K. I. Zenchenko's help in conducting measurements and maintaining a computer archive of experimental results.

Submitted on Febrary 02, 2009 / Accepted on February 23, 2009

References

1. Shnoll S.E. On the spontaneous and synchronous transitions of actomyosin molecules in a solution from one state to another. *Problems of Medicinal Chemistry*, 1958, v. 4(6), 443–454 (*in Russian*).
2. Shnoll S.E., Namiot V.A., Zhvirblis V.E., Morozov V.N., Temnov A.V., Morozova T.Ya. A possible generality of macroscopic fluctuations of rates of biochemical and chemical reactions, cell electrophoretic mobility and fluctuations in measurements of radioactivity, absorbance and flicker noises. *Biophysics*, 1983, v. 28(1), 153–157 (*in Russian*).
3. Shnoll S.E. Macroscopic fluctuations with discrete distribution of amplitudes in the processes of diverse nature. In: *Results of Science and Engineering. Molecular Biology*, Ed. V. P. Skulachev, VINITI-Press, Moscow, 1985, v. 5, 130–200 (*in Russian*).
4. Udaltsova N.V., Kolombet V.A., Shnoll S.E. A possible cosmophysical conditionality of macroscopic fluctuations in the processes of diverse nature. Central Scientific Library Press, Pushchino, 1987 (*in Russian*).
5. Udaltzova N.V., Kolombet V.A. and Shnol' S.E. The possible gravitational nature of factor influencing discrete macroscopic fluctuations. In: *Proc. First Intern. Congress on Geo-cosmic Relations*, Wageningen, Netherlands, 1989, 174–180.
6. Shnol' S.E., Udaltzova N.V. and Bodrova N.B. Macroscopic fluctuations with discrete structure distributions as a result of universal causes including cosmophysical factors. In: *Proc. First Intern. Congress on Geo-cosmic Relations*, Wageningen, Netherlands, 1989, 181–188.
7. Shnoll S.E. Correlation of the shape of amplitude spectra of macroscopic fluctuations with the position of the Moon relative to the horizon. *Biophysics*, 1989, v. 34(5), 911–912 (*in Russian*).
8. Shnoll S.E., Kolombet V.A., Udaltzova N.V., Bodrova N.B., Namiot V.E. Regularities in the discrete distributions of the results of measurements (cosmophysical aspects). *Biophysics*, 1992, v. 37(3), 467–488 (*in Russian*).
9. Shnoll S.E. The shape of spectra of states realized in the course of macroscopic fluctuations depends on the rotation of the Earth about its axis. *Biophysics*, 1995, v. 40(4), 865–875 (*in Russian*).
10. Shnoll S.E., Agulova L.P., Zaikin A.N., Zenchenko T.A., Pozharskii E.V., and Konradov A.A. On the similarity of histograms fine structure for synchronized time series of different nature processes at different locations. *Annales Geophysicae*, Supplement 1 to Volume 16 Part 1 Society Symposia, Solid Earth Geophysics & Geodesy, 1998, C312.
11. Shnoll S.E., Kolombet V.A., Pozharsky E.V., Zenchenko T.A., Zvereva I.M., Konradov A.A. On the realization of discrete states in the course of fluctuations in macroscopic processes. *Advances in Physical Sciences*, 1998, v. 168(10), 1129–1140 (*in Russian*).
12. Shnoll S.E., Kolombet V.A., Pozharsky E.V., Zenchenko T.A., Zvereva I.M., Konradov A.A. On the cosmophysical conditionality of "macroscopic fluctuations". *Biophysics*, 1998, v. 43(5), 909–915 (*in Russian*).
13. Shnoll S.E., Pozharski E.V., Zenchenko T.A., Kolombet V.A., Zvereva I.M., Konradov A.A. Fine structure of distributions in measurements of different processes as affected by geophysical and cosmophysical factors. *Phys. Chem. Earth A*, 1999, v. 24, no. 8, 711–714.
14. Shnoll S.E., Zenchenko T.A., Zenchenko K.I., Pozharsky E.V., Kolombet V.A., Konradov A.A. Regular alteration of the fine structure of statistical distributions as a results of cosmophysical causes. *Advances in Physical Sciences*, 2000, v. 170(2), 214–218 (*in Russian*).
15. Shnoll S.E. Macroscopic fluctuations as a result of arithmetical and cosmophysical causes. The factors that determine the fine structure of histograms are, probably, beyond the bounds of the solar system. *Biophysics*, 2001, v. 46(5), 775–782 (*in Russian*.
16. Shnoll S.E., Zenchenko T.A., Zenchenko K.I., Fedorov M.V., Konradov A.A. The non-random character of fine structure of various measurement result distributions as a possible consequence of cosmophysical and arithmetical causes. In: *Gravitation & Cosmology*, 2002, v. 8, Supplement, 231–232.
17. Shnoll S.E. Paradoxes and problems in the interpretation of the phenomenon of macroscopic fluctuations. *Russian Chemical Journal*, 2002, v. 46(3), 3–8 (*in Russian*).
18. Fedorov M.V., Belousov L.V., Voeikov V.L., Zenchenko T.A., Zenchenko K.I., Pozharskii E.V., Konradov A.A., Shnoll S.E.

Synchronous changes in dark current fluctuations in two separate photomultipliers in relation to Earth rotation. *Astrophysics & Space Science*, 2003, no. 1, 105–112.

19. Shnoll S.E., Rubinstein I.A., Zenchenko K.I., Zenchenko T.A., Udaltsova N.V., Konradov A.A., Shapovalov S.N., Makarevich A.V., Gorshkov E.S., Troshichev O.A. Dependence of macroscopic fluctuations on geographical coordinates. *Biophysics*, 2003, v. 48(6), 1123–1131 (*in Russian*).
20. Shnoll S.E., Zenchenko K.I., Berulis I.I., Udaltsova N.V., Zhirkov S.S., Rubinstein I.A. Dependence of macroscopic fluctuations on cosmophysical factors. Spatial anisotropy. *Biophysics*, 2004, v. 49(1), 132–139 (in Russian).
21. Shnoll S.E., Zenchenko K.I., and Udaltsova N.V. Cosmophysical effects in the structure of daily and yearly periods of changes in the shape of histograms constructed from the measurements of ^{239}Pu alpha-activity. *Biophysics*, 2004, v. 49, Suppl. 1, 155–164.
22. Shnoll S.E., Zenchenko K.I., Berulis I.I., Udaltsova N.V. and Rubinstein I.A. Fine structure of histograms of alpha-activity measurements depends on direction of alpha particles flow and the Earth rotation: experiments with collimators. arXiv: physics/0412007.
23. Shnoll S.E., Zenchenko K.I., Shapovalov S.N., Gorshkov E.S., Makarevich A.V. and Troshichev O.A. The specific form of histograms presenting the distribution of data of alpha-decay measurements appears simultaneously in the moment of New Moon in different points from Arctic to Antarctic. arXiv: physics/0412152.
24. Shnoll S.E., Zenchenko K.I., and Udaltsova N.V. Cosmophysical effects in the structure of daily and yearly periods of changes in the shape of histograms constructed from the measurements of ^{239}Pu alpha-activity. arXiv: physics/0504092.
25. Shnoll S.E., Rubinstein I.A., Zenchenko K.I., Shlekhtarev V.A., Kaminsky A.V., Konradov A.A., Udaltsova N.V. Experiments with rotating collimators cutting out pencil of alpha-particles at radioactive decay of Pu-239 evidence sharp anisotropy of space. arXiv: physics/0501004.
26. Shnoll S.E., Rubinstein I.A., Zenchenko K.I., Shlekhtarev V.A., Kaminsky A.V., Konradov A.A., Udaltsova N.V. Experiments with rotating collimators cutting out pencil of alpha-particles at radioactive decay of Pu-239 evidence sharp anisotropy of space. *Progress in Physics*, 2005, v. 1, 81–84.
27. Shnoll S.E. Changes in fine structure of stochastic distributions as a consequence of space-time fluctuations. *Progress in Physics*, 2006, v. 2, 39–45.
28. Shnoll S.E. Fine structure of statistical distributions as a mirror of spatial and gravitational anisotropy of our world. *Russian Chemical Journal*, 2007, v. 51(1), 150–157.
29. Shnoll S.E. Cosmophysical nature of the "idea of shape" of histograms constructed from the results of measurements of processes of diverse nature. In: *Metaphysics. Century XXI*, Issue 2, Ed. Yu. S. Vladimirov, BINOM-S Press, 2007, 284–319 (*in Russian*).
30. Shnoll S.E. Reply to the letter by Gary C. Vezzoli. *Progress in Physics*, 2008, v. 2, 162–163.
31. Strelkov V.V. A new similarity measure for histogram comparison and its application in time series analysis. *Pattern Recognition Letters*, 2008, v. 29, no. 13, 1768–1774.
32. Strelkov V.V. The "near zone" effect in dynamic chaos. *Biophysics*, 2001, v. 46, 807–810 (*in Russian*).
33. Khmaladze E.V. *Probability Theory and Its Applications*, 1983, v. 28(3), 504 (*in Russian*).
34. Udaltsova N.V., Urinov I.K. Estimation of probability of the observed extrema in histograms constructed from small samples. Deposited at VINITI 08.02.89, no. 850-V89 (*in Russian*).
35. Shnoll S.E., Panchelyuga V.A., and Shnoll A.E. The palindrome effect. *Progress in Physics*, 2008, v. 2, 151–153.
36. Shnoll S.E. The "scattering of the results of measurements" of processes of diverse nature is determined by the Earth's motion in the inhomogeneous space-time continuum. The effect of "half-year palindromes". *Progress in Physics*, 2009, v. 1, 3–7.
37. Shnoll S.E., Zenchenko K.I., Shapovalov S.N., Gorshkov E.S., Makarevich A.V. and Troshichev O.A. The specific form of histograms presenting the distribution of data of alpha-decay measurements appears simultaneously in the moment of New Moon in different points from Arctic to Antarctic. arXiv: physics/0412152.
38. Shnoll S.E., Panchelyuga V.A. On the characteristic form of histograms appearing at the culmination of Solar eclipse. arXiv: physics/0603029.
39. Kondrashova M.N. Personal communication.
40. Pancheluga V.A., Kolombet V.A., Pancheluga M.S., Shnoll S.E. Studying the local-time effect on small spatial-temporal scales. *Hypercomplex Numbers in Geometry and Physics*, 2006, no. 1(5), v. 3, 116–121 (*in Russian*).
41. Panchelyuga V.A., Kolombet V.A., Pancheluga M.S., and Shnoll S.E. Local-time effect on small space-time scale. In: *Space-Time Structure*, collected papers, Moscow, Tetru, 2006, 344–350.
42. Panchelyuga V.A., Kolombet V.A., Pancheluga M.S., and Shnoll S.E. Experimental investigation of the existence of a local-time effect on the laboratory scale and the heterogeneity of spice-time. *Progress in Physics*, 2007, v. 1, 64–69.
43. Panchelyuga V.A. and Shnoll S.E. On the dependence of a local-time effect on spatial direction. *Progress in Physics*, 2007, v. 3, 51–54.
44. Kharakoz D.P. Personal communication.

4X1-Matrix Functions and Dirac's Equation

Gunn Alex Quznetsov

Chelyabinsk State University, Chelyabinsk, Ural, Russia
E-mail: quznets@yahoo.com, gunn@mail.ru

All 4X1-matrix square integrable functions with restricted domain obey slightly generalized Dirac's equations. These equations give formulas similar to some gluon and gravity ones.

1 Significations

Denote:

$$1_2 := \begin{bmatrix} 1 & 0 \\ 0 & 1 \end{bmatrix}, 0_2 := \begin{bmatrix} 0 & 0 \\ 0 & 0 \end{bmatrix},$$

$$\beta^{[0]} := -\begin{bmatrix} 1_2 & 0_2 \\ 0_2 & 1_2 \end{bmatrix} = -1_4,$$

the Pauli matrices:

$$\sigma_1 = \begin{pmatrix} 0 & 1 \\ 1 & 0 \end{pmatrix}, \sigma_2 = \begin{pmatrix} 0 & -\mathrm{i} \\ \mathrm{i} & 0 \end{pmatrix}, \sigma_3 = \begin{pmatrix} 1 & 0 \\ 0 & -1 \end{pmatrix}.$$

I call a set $\widetilde{C}$ of complex $n \times n$ matrices *a Clifford set of rank* n [1] if the following conditions are fulfilled:

— if $\alpha_k \in \widetilde{C}$ and $\alpha_r \in \widetilde{C}$ then $\alpha_k\alpha_r + \alpha_r\alpha_k = 2\delta_{k,r}$;

— if $\alpha_k\alpha_r + \alpha_r\alpha_k = 2\delta_{k,r}$ for all elements α_r of set $\widetilde{C}$ then $\alpha_k \in \widetilde{C}$.

If $n = 4$ then the Clifford set either contains 3 (*Clifford triplet*) or 5 matrices (*Clifford pentad*).

Here exist only six Clifford pentads [1]: one which I call

• *light pentad* β:

$$\beta^{[1]} := \begin{bmatrix} \sigma_1 & 0_2 \\ 0_2 & -\sigma_1 \end{bmatrix}, \quad \beta^{[2]} := \begin{bmatrix} \sigma_2 & 0_2 \\ 0_2 & -\sigma_2 \end{bmatrix}, \quad \beta^{[3]} := \begin{bmatrix} \sigma_3 & 0_2 \\ 0_2 & -\sigma_3 \end{bmatrix}, \tag{1}$$

$$\gamma^{[0]} := \begin{bmatrix} 0_2 & 1_2 \\ 1_2 & 0_2 \end{bmatrix}, \tag{2}$$

$$\beta^{[4]} := \mathrm{i} \cdot \begin{bmatrix} 0_2 & 1_2 \\ -1_2 & 0_2 \end{bmatrix}; \tag{3}$$

three *coloured* pentads:

• *the red pentad* ζ:

$$\zeta^{[1]} = \begin{bmatrix} -\sigma_1 & 0_2 \\ 0_2 & \sigma_1 \end{bmatrix}, \quad \zeta^{[2]} = \begin{bmatrix} \sigma_2 & 0_2 \\ 0_2 & \sigma_2 \end{bmatrix}, \tag{4}$$

$$\zeta^{[3]} = \begin{bmatrix} -\sigma_3 & 0_2 \\ 0_2 & -\sigma_3 \end{bmatrix},$$

$$\gamma_\zeta^{[0]} = \begin{bmatrix} 0_2 & -\sigma_1 \\ -\sigma_1 & 0_2 \end{bmatrix}, \quad \zeta^{[4]} = \mathrm{i}\begin{bmatrix} 0_2 & \sigma_1 \\ -\sigma_1 & 0_2 \end{bmatrix}; \tag{5}$$

• *the green pentad* η:

$$\eta^{[1]} = \begin{bmatrix} -\sigma_1 & 0_2 \\ 0_2 & -\sigma_1 \end{bmatrix}, \quad \eta^{[2]} = \begin{bmatrix} -\sigma_2 & 0_2 \\ 0_2 & \sigma_2 \end{bmatrix}, \tag{6}$$

$$\eta^{[3]} = \begin{bmatrix} \sigma_3 & 0_2 \\ 0_2 & \sigma_3 \end{bmatrix},$$

$$\gamma_\eta^{[0]} = \begin{bmatrix} 0_2 & -\sigma_2 \\ -\sigma_2 & 0_2 \end{bmatrix}, \quad \eta^{[4]} = \mathrm{i}\begin{bmatrix} 0_2 & \sigma_2 \\ -\sigma_2 & 0_2 \end{bmatrix}; \tag{7}$$

• *the blue pentad* θ:

$$\theta^{[1]} = \begin{bmatrix} \sigma_1 & 0_2 \\ 0_2 & \sigma_1 \end{bmatrix}, \quad \theta^{[2]} = \begin{bmatrix} -\sigma_2 & 0_2 \\ 0_2 & -\sigma_2 \end{bmatrix}, \tag{8}$$

$$\theta^{[3]} = \begin{bmatrix} -\sigma_3 & 0_2 \\ 0_2 & \sigma_3 \end{bmatrix},$$

$$\gamma_\theta^{[0]} = \begin{bmatrix} 0_2 & -\sigma_3 \\ -\sigma_3 & 0_2 \end{bmatrix}, \quad \theta^{[4]} = \mathrm{i}\begin{bmatrix} 0_2 & \sigma_3 \\ -\sigma_3 & 0_2 \end{bmatrix}; \tag{9}$$

• two *gustatory* pentads: *the sweet pentad* $\underline{\Delta}$:

$$\underline{\Delta}^{[1]} = \begin{bmatrix} 0_2 & -\sigma_1 \\ -\sigma_1 & 0_2 \end{bmatrix}, \quad \underline{\Delta}^{[2]} = \begin{bmatrix} 0_2 & -\sigma_2 \\ -\sigma_2 & 0_2 \end{bmatrix},$$

$$\underline{\Delta}^{[3]} = \begin{bmatrix} 0_2 & -\sigma_3 \\ -\sigma_3 & 0_2 \end{bmatrix},$$

$$\underline{\Delta}^{[0]} = \begin{bmatrix} -1_2 & 0_2 \\ 0_2 & 1_2 \end{bmatrix}, \quad \underline{\Delta}^{[4]} = \mathrm{i}\begin{bmatrix} 0_2 & 1_2 \\ -1_2 & 0_2 \end{bmatrix}.$$

• *the bitter pentad* $\underline{\Gamma}$:

$$\underline{\Gamma}^{[1]} = \mathrm{i}\begin{bmatrix} 0_2 & -\sigma_1 \\ \sigma_1 & 0_2 \end{bmatrix}, \quad \underline{\Gamma}^{[2]} = \mathrm{i}\begin{bmatrix} 0_2 & -\sigma_2 \\ \sigma_2 & 0_2 \end{bmatrix},$$

$$\underline{\Gamma}^{[3]} = \mathrm{i}\begin{bmatrix} 0_2 & -\sigma_3 \\ \sigma_3 & 0_2 \end{bmatrix},$$

$$\underline{\Gamma}^{[0]} = \begin{bmatrix} -1_2 & 0_2 \\ 0_2 & 1_2 \end{bmatrix}, \quad \underline{\Gamma}^{[4]} = \begin{bmatrix} 0_2 & 1_2 \\ 1_2 & 0_2 \end{bmatrix}.$$

If A is a 2×2 matrix then

$$A1_4 := \begin{bmatrix} A & 0_2 \\ 0_2 & A \end{bmatrix} \text{ and } 1_4A := \begin{bmatrix} A & 0_2 \\ 0_2 & A \end{bmatrix}.$$

And if B is a 4×4 matrix then

$$A + B := A1_4 + B,\ AB := A1_4 B$$

etc.

$$\underline{x} := \langle x_0, \mathbf{x} \rangle := \langle x_0, x_1, x_2, x_3 \rangle ,$$
$$x_0 := \mathrm{c}t,$$

with $\mathrm{c} = 299792458$.

2 Planck's functions

Let $\mathrm{h} = 6.6260755 \times 10^{-34}$ and $\underline{\Omega}$ ($\underline{\Omega} \subset R^{1+3}$) be a domain such that if $\underline{x} \in \underline{\Omega}$ then $|x_r| < \frac{\mathrm{c}\pi}{\mathrm{h}}$ for $r \in \{0, 1, 2, 3\}$.

Let $\Re_{\underline{\Omega}}$ be a set of functions such that for each element $\phi(\underline{x})$ of this set: if $\underline{x} \notin \underline{\Omega}$ then $\phi(\underline{x}) = 0$.

Hence:

$$\int_{(\underline{\Omega})} d\underline{x} \cdot \phi(\underline{x}) =$$
$$= \int_{-\frac{\mathrm{c}\pi}{\mathrm{h}}}^{\frac{\mathrm{c}\pi}{\mathrm{h}}} dx_0 \int_{-\frac{\mathrm{c}\pi}{\mathrm{h}}}^{\frac{\mathrm{c}\pi}{\mathrm{h}}} dx_1 \int_{-\frac{\mathrm{c}\pi}{\mathrm{h}}}^{\frac{\mathrm{c}\pi}{\mathrm{h}}} dx_2 \int_{-\frac{\mathrm{c}\pi}{\mathrm{h}}}^{\frac{\mathrm{c}\pi}{\mathrm{h}}} dx_3 \cdot \phi(\underline{x}) ,$$

and let for each element $\phi(\underline{x})$ of $\Re_{\underline{\Omega}}$ exist a number J_ϕ such that

$$J_\phi = \int_{(\underline{\Omega})} d\underline{x} \cdot \phi^*(\underline{x}) \phi(\underline{x}) .$$

Therefore, $\Re_{\underline{\Omega}}$ is unitary space with the following scalar product:

$$\widetilde{u} * \widetilde{v} := \int_{(\underline{\Omega})} d\underline{x} \cdot \widetilde{u}^*(\underline{x}) \widetilde{v}(\underline{x}) . \tag{10}$$

This space has an orthonormalised basis with the following elements:

$$\varsigma_{w,\mathbf{p}}(t, \mathbf{x}) :=$$
$$:= \left\{ \begin{array}{c} \left(\frac{\mathrm{h}}{2\pi \mathrm{c}}\right)^2 \exp(\mathrm{i}\mathrm{h}wt) \exp\left(-\mathrm{i}\frac{\mathrm{h}}{\mathrm{c}}\mathbf{px}\right) \text{ if} \\ -\frac{\pi \mathrm{c}}{\mathrm{h}} \leqslant x_k \leqslant \frac{\pi \mathrm{c}}{\mathrm{h}}; \\ 0, \text{ otherwise.} \end{array} \right| \tag{11}$$

with $k \in \{0, 1, 2, 3\}$ and $x_0 := \mathrm{c}t$, and with natural w, p_1, p_2, p_3 (here: $\mathbf{p}\langle p_1, p_2, p_3 \rangle$ and $\mathbf{px} = p_1 x_1 + p_2 x_2 + p_3 x_3$).

I call elements of the space with this basis *Planck's functions*.

Let $j \in \{1, 2, 3, 4\}$, $k \in \{1, 2, 3, 4\}$ and denote:

$$\sum_{\mathbf{k}} := \sum_{k_1=-\infty}^{\infty} \sum_{k_2=-\infty}^{\infty} \sum_{k_3=-\infty}^{\infty} .$$

Let a Fourier series for $\varphi_j(t, \mathbf{x})$ have the following form:

$$\varphi_j(t, \mathbf{x}) = \sum_{w=-\infty}^{\infty} \sum_{\mathbf{p}} c_{j,w,\mathbf{p}} \varsigma_{w,\mathbf{p}}(t, \mathbf{x}) . \tag{12}$$

If denote: $\varphi_{j,w,\mathbf{p}}(t, \mathbf{x}) := c_{j,w,\mathbf{p}} \varsigma_{w,\mathbf{p}}(t, \mathbf{x})$ then a Fourier series for $\varphi_j(t, \mathbf{x})$ has the following form:

$$\varphi_j(t, \mathbf{x}) = \sum_{w=-\infty}^{\infty} \sum_{\mathbf{p}} \varphi_{j,w,\mathbf{p}}(t, \mathbf{x}) . \tag{13}$$

Let $\langle t, \mathbf{x} \rangle$ be any space-time point.

Let us denote:

$$A_k := \varphi_{k,w,\mathbf{p}}|_{\langle t,\mathbf{x} \rangle} \tag{14}$$

the value of function $\varphi_{k,w,\mathbf{p}}$ in this point, and by

$$C_j := \left(\frac{1}{\mathrm{c}} \partial_t \varphi_{j,w,\mathbf{p}} - \sum_{s=1}^{4} \sum_{\alpha=1}^{3} \beta_{j,s}^{[\alpha]} \partial_\alpha \varphi_{s,w,\mathbf{p}} \right) \Bigg|_{\langle t,\mathbf{x} \rangle} \tag{15}$$

the value of function

$$\left(\frac{1}{\mathrm{c}} \partial_t \varphi_{j,w,\mathbf{p}} - \sum_{s=1}^{4} \sum_{\alpha=1}^{3} \beta_{j,s}^{[\alpha]} \partial_\alpha \varphi_{s,w,\mathbf{p}} \right) .$$

Here A_k and C_j are complex numbers. Hence, the following set of equations:

$$\left\{ \begin{array}{c} \sum_{k=1}^{4} z_{j,k,w,\mathbf{p}} A_k = C_j , \\ z^*_{j,k,w,\mathbf{p}} = -z_{k,j,w,\mathbf{p}} \end{array} \right| \tag{16}$$

is a system of 14 algebraic equations with complex unknowns $z_{j,k,w,\mathbf{p}}$.

Because

$$\partial_t \varphi_{j,w,\mathbf{p}} = \partial_t c_{j,w,\mathbf{p}} \varsigma_{w,\mathbf{p}} = \mathrm{i}\mathrm{h}w c_{j,w,\mathbf{p}} \varsigma_{w,\mathbf{p}} = \mathrm{i}\mathrm{h}w \varphi_{j,w,\mathbf{p}}$$

and for $k \neq 0$:

$$\partial_k \varphi_{j,w,\mathbf{p}} = -\mathrm{i}\frac{\mathrm{h}}{\mathrm{c}} p_k \varphi_{j,w,\mathbf{p}} .$$

then

$$C_j = \mathrm{i}\frac{\mathrm{h}}{\mathrm{c}} \left(w \varphi_{j,w,\mathbf{p}} + \sum_{s=1}^{4} \sum_{\alpha=1}^{3} \beta_{j,s}^{[\alpha]} p_\alpha \varphi_{s,w,\mathbf{p}} \right) \Bigg|_{\langle t,\mathbf{x} \rangle} .$$

Therefore, this system (16) has got the following form:

$$z_{1,1,w,\mathbf{p}} A_1 + z_{1,2,w,\mathbf{p}} A_2 + z_{1,3,w,\mathbf{p}} A_3 + z_{1,4,w,\mathbf{p}} A_4 =$$
$$= \mathrm{i}\frac{\mathrm{h}}{\mathrm{c}} (w + p_3) A_1 + \mathrm{i}\frac{\mathrm{h}}{\mathrm{c}} (p_1 - \mathrm{i}p_2) A_2 ,$$
$$z_{2,1,w,\mathbf{p}} A_1 + z_{2,2,w,\mathbf{p}} A_2 + z_{2,3,w,\mathbf{p}} A_3 + z_{2,4,w,\mathbf{p}} A_4 =$$
$$= \mathrm{i}\frac{\mathrm{h}}{\mathrm{c}} (w - p_3) A_2 + \mathrm{i}\frac{\mathrm{h}}{\mathrm{c}} (p_1 + \mathrm{i}p_2) A_1 ,$$
$$z_{3,1,w,\mathbf{p}} A_1 + z_{3,2,w,\mathbf{p}} A_2 + z_{3,3,w,\mathbf{p}} A_3 + z_{3,4,w,\mathbf{p}} A_4 =$$
$$= \mathrm{i}\frac{\mathrm{h}}{\mathrm{c}} (w - p_3) A_3 - \mathrm{i}\frac{\mathrm{h}}{\mathrm{c}} (p_1 - \mathrm{i}p_2) A_4 ,$$
$$z_{4,1,w,\mathbf{p}} A_1 + z_{4,2,w,\mathbf{p}} A_2 + z_{4,3,w,\mathbf{p}} A_3 + z_{4,4} A_{4,w,\mathbf{p}} =$$
$$= \mathrm{i}\frac{\mathrm{h}}{\mathrm{c}} (w + p_3) A_4 - \mathrm{i}\frac{\mathrm{h}}{\mathrm{c}} (p_1 + \mathrm{i}p_2) A_3 ,$$

$$z^*_{1,1,w,\mathbf{p}} = -z_{1,1,w,\mathbf{p}}\,,$$
$$z^*_{1,2,w,\mathbf{p}} = -z_{2,1,w,\mathbf{p}}\,,$$
$$z^*_{1,3,w,\mathbf{p}} = -z_{3,1,w,\mathbf{p}}\,,$$
$$z^*_{1,4,w,\mathbf{p}} = -z_{4,1,w,\mathbf{p}}\,,$$
$$z^*_{2,2,w,\mathbf{p}} = -z_{2,2,w,\mathbf{p}}\,,$$
$$z^*_{2,3,w,\mathbf{p}} = -z_{3,2,w,\mathbf{p}}\,,$$
$$z^*_{2,4,w,\mathbf{p}} = -z_{4,2,w,\mathbf{p}}\,,$$
$$z^*_{3,3,w,\mathbf{p}} = -z_{3,3,w,\mathbf{p}}\,,$$
$$z^*_{3,4,w,\mathbf{p}} = -z_{4,3,w,\mathbf{p}}\,,$$
$$z^*_{4,4,w,\mathbf{p}} = -z_{4,4,w,\mathbf{p}}\,.$$

This system can be transformed into a system of 8 linear real equations with 16 real unknowns $x_{s,k} := \mathrm{Re}\,(z_{s,k,w,\mathbf{p}})$ for $s < k$ and $y_{s,k} := \mathrm{Im}\,(z_{s,k,w,\mathbf{p}})$ for $s \leqslant k$:

$$\begin{aligned}
&-y_{1,1}b_1 + x_{1,2}a_2 - y_{1,2}b_2 + x_{1,3}a_3 -\\
&-y_{1,3}b_3 + x_{1,4}a_4 - y_{1,4}b_4 \;=\\
&= -\frac{\mathrm{h}}{\mathrm{c}}wb_1 - \frac{\mathrm{h}}{\mathrm{c}}p_3b_1 - \frac{\mathrm{h}}{\mathrm{c}}p_1b_2 + \frac{\mathrm{h}}{\mathrm{c}}p_2a_2\,,\\
&y_{1,1}a_1 + x_{1,2}b_2 + y_{1,2}a_2 + x_{1,3}b_3 +\\
&+y_{1,3}a_3 + x_{1,4}b_4 + y_{1,4}a_4 \;=\\
&= \frac{\mathrm{h}}{\mathrm{c}}wa_1 + hp_3a_1 + \frac{\mathrm{h}}{\mathrm{c}}p_1a_2 + hp_2b_2\,,\\
&-x_{1,2}a_1 - y_{1,2}b_1 - y_{2,2}b_2 + x_{2,3}a_3 -\\
&-y_{2,3}b_3 + x_{2,4}a_4 - y_{2,4}b_4 \;=\\
&= -\frac{\mathrm{h}}{\mathrm{c}}wb_2 - \frac{\mathrm{h}}{\mathrm{c}}p_1b_1 - \frac{\mathrm{h}}{\mathrm{c}}p_2a_1 + \frac{\mathrm{h}}{\mathrm{c}}p_3b_2\,,\\
&-x_{1,2}b_1 + y_{1,2}a_1 + y_{2,2}a_2 + x_{2,3}b_3 +\\
&+y_{2,3}a_3 + x_{2,4}b_4 + y_{2,4}a_4 \;=\\
&= \frac{\mathrm{h}}{\mathrm{c}}wa_2 + \frac{\mathrm{h}}{\mathrm{c}}p_1a_1 - \frac{\mathrm{h}}{\mathrm{c}}p_2b_1 - \frac{\mathrm{h}}{\mathrm{c}}p_3a_2\,,\\
&-x_{1,3}a_1 - y_{1,3}b_1 - x_{2,3}a_2 - y_{2,3}b_2 -\\
&-y_{3,3}b_3 + x_{3,4}a_4 - y_{3,4}b_4 \;=\\
&= -\frac{\mathrm{h}}{\mathrm{c}}wb_3 + \frac{\mathrm{h}}{\mathrm{c}}p_3b_3 + \frac{\mathrm{h}}{\mathrm{c}}p_1b_4 - \frac{\mathrm{h}}{\mathrm{c}}p_2a_4\,,\\
&-x_{1,3}b_1 + y_{1,3}a_1 - x_{2,3}b_2 + y_{2,3}a_2 +\\
&+y_{3,3}a_3 + x_{3,4}b_4 + y_{3,4}a_4 \;=\\
&= \frac{\mathrm{h}}{\mathrm{c}}wa_3 - \frac{\mathrm{h}}{\mathrm{c}}p_3a_3 - \frac{\mathrm{h}}{\mathrm{c}}p_1a_4 - \frac{\mathrm{h}}{\mathrm{c}}p_2b_4\,,\\
&-x_{1,4}a_1 - y_{1,4}b_1 - x_{2,4}a_2 - y_{2,4}b_2 -\\
&-x_{3,4}a_3 - y_{3,4}b_3 - y_{4,4}b_4 \;=\\
&= -\frac{\mathrm{h}}{\mathrm{c}}wb_4 + \frac{\mathrm{h}}{\mathrm{c}}p_1b_3 + \frac{\mathrm{h}}{\mathrm{c}}p_2a_3 - \frac{\mathrm{h}}{\mathrm{c}}p_3b_4\,,\\
&-x_{1,4}b_1 + y_{1,4}a_1 - x_{2,4}b_2 + y_{2,4}a_2 -\\
&-x_{3,4}b_3 + y_{3,4}a_3 + y_{4,4}a_4 \;=\\
&= \frac{\mathrm{h}}{\mathrm{c}}wa_4 - \frac{\mathrm{h}}{\mathrm{c}}p_1a_3 + \frac{\mathrm{h}}{\mathrm{c}}p_2b_3 + \frac{\mathrm{h}}{\mathrm{c}}p_3a_4\,;
\end{aligned}$$

(here $a_k := \mathrm{Re}A_k$ and $b_k := \mathrm{Im}A_k$).

This system has solutions according to the Kronecker-Capelli theorem (rank of this system augmented matrix and rank of this system basic matrix equal to 7). Hence, such complex numbers $z_{j,k,w,\mathbf{p}}|_{\langle t,\mathbf{x}\rangle}$ exist in all points $\langle t,\mathbf{x}\rangle$.

From (16), (14), (15):

$$\sum_{k=1}^{4} z_{j,k,w,\mathbf{p}}\varphi_{k,w,\mathbf{p}}|_{\langle t,\mathbf{x}\rangle} = \left(\frac{1}{\mathrm{c}}\,\partial_t\varphi_{j,w,\mathbf{p}} - \sum_{s=1}^{4}\sum_{\alpha=1}^{3}\beta^{[\alpha]}_{j,s}\partial_\alpha\varphi_{s,w,\mathbf{p}}\right)|_{\langle t,\mathbf{x}\rangle},$$

in every point $\langle t,\mathbf{x}\rangle$.

Therefore, from (16, 15, 14):

$$\frac{1}{\mathrm{c}}\,\partial_t\varphi_{j,w,\mathbf{p}} = \sum_{k=1}^{4}\left(\sum_{\alpha=1}^{3}\beta^{[\alpha]}_{j,k}\partial_\alpha\varphi_{k,w,\mathbf{p}} + z_{j,k,w,\mathbf{p}}\varphi_{k,w,\mathbf{p}}\right) \quad (17)$$

in every point $\langle t,\mathbf{x}\rangle$.

Let $\kappa_{w,\mathbf{p}}$ be linear operators on linear space, spanned of basic functions $\varsigma_{w,\mathbf{p}}(t,\mathbf{x})$, such that

$$\kappa_{w,\mathbf{p}}\varsigma_{w',\mathbf{p}'} := \begin{cases} \varsigma_{w',\mathbf{p}'}, \text{ if } w = w',\, \mathbf{p} = \mathbf{p}';\\ 0, \text{ if } w \neq w' \text{ and/or } \mathbf{p} \neq \mathbf{p}'. \end{cases}$$

Let

$$Q_{j,k}|_{\langle t,\mathbf{x}\rangle} := \sum_{w,\mathbf{p}}\left(z_{j,k,w,\mathbf{p}}|_{\langle t,\mathbf{x}\rangle}\right)\kappa_{w,\mathbf{p}}$$

in every point $\langle t,\mathbf{x}\rangle$.

Therefore, from (13) and (17), for every function φ_j here exists an operator $Q_{j,k}$ such that dependence of φ_j on t is described by the following differential equations:

$$\partial_t\varphi_j = \mathrm{c}\sum_{k=1}^{4}\left(\beta^{[1]}_{j,k}\partial_1 + \beta^{[2]}_{j,k}\partial_2 + \beta^{[3]}_{j,k}\partial_3 + Q_{j,k}\right)\varphi_k. \quad (18)$$

and

$$Q^*_{j,k} = \sum_{w,\mathbf{p}}\left(z^*_{j,k,w,\mathbf{p}}\right)\kappa_{w,\mathbf{p}} = \sum_{w,\mathbf{p}}\left(-z^*_{k,j,w,\mathbf{p}}\right)\kappa_{w,\mathbf{p}} = -Q_{k,j}\,.$$

Matrix form of formula (18) is the following:

$$\partial_t\varphi = \mathrm{c}\left(\beta^{[1]}\partial_1 + \beta^{[2]}\partial_2 + \beta^{[3]}\partial_3 + \widehat{Q}\right)\varphi \quad (19)$$

with

$$\varphi = \begin{bmatrix}\varphi_1\\ \varphi_2\\ \varphi_3\\ \varphi_4\end{bmatrix}$$

and

$$\widehat{Q} := \begin{bmatrix} \mathrm{i}\vartheta_{1,1} & Q_{1,2} & Q_{1,3} & Q_{1,4} \\ -Q^*_{1,2} & \mathrm{i}\vartheta_{2,2} & Q_{2,3} & Q_{2,4} \\ -Q^*_{1,3} & -Q^*_{2,3} & \mathrm{i}\vartheta_{3,3} & Q_{3,4} \\ -Q^*_{1,4} & -Q^*_{2,4} & -Q^*_{3,4} & \mathrm{i}\vartheta_{4,4} \end{bmatrix} \tag{20}$$

with $Q_{k,s} := \mathrm{i}\vartheta_{k,s} - \varpi_{k,s}$ if $k \neq s$, and with $\varpi_{s,k} := \mathrm{Re}\,(Q_{s,k})$ and $\vartheta_{s,k} := \mathrm{Im}\,(Q_{s,k})$.

Let $\vartheta_{s,k}$ and $\varpi_{s,k}$ be terms of $\widehat{Q}$ (20) and let Θ_0, Θ_3, Υ_0 and Υ_3 be the solution of the following sets of equations:

$$\left\{ \begin{array}{l} -\Theta_0 + \Theta_3 - \Upsilon_0 + \Upsilon_3 = \vartheta_{1,1}; \\ -\Theta_0 - \Theta_3 - \Upsilon_0 - \Upsilon_3 = \vartheta_{2,2}; \\ -\Theta_0 - \Theta_3 + \Upsilon_0 + \Upsilon_3 = \vartheta_{3,3}; \\ -\Theta_0 + \Theta_3 + \Upsilon_0 - \Upsilon_3 = \vartheta_{4,4} \end{array} \right|,$$

and Θ_1, Υ_1, Θ_2, Υ_2, M_0, M_4, $M_{\zeta,0}$, $M_{\zeta,4}$, $M_{\eta,0}$, $M_{\eta,4}$, $M_{\theta,0}$, $M_{\theta,4}$ be the solutions of the following sets of equations:

$$\left\{ \begin{array}{l} \Theta_1 + \Upsilon_1 = \vartheta_{1,2}; \\ -\Theta_1 + \Upsilon_1 = \vartheta_{3,4}; \end{array} \right| \left\{ \begin{array}{l} -\Theta_2 - \Upsilon_2 = \varpi_{1,2}; \\ \Theta_2 - \Upsilon_2 = \varpi_{3,4}; \end{array} \right|$$

$$\left\{ \begin{array}{l} M_0 + M_{\theta,0} = \vartheta_{1,3}; \\ M_0 - M_{\theta,0} = \vartheta_{2,4}; \end{array} \right| \left\{ \begin{array}{l} M_4 + M_{\theta,4} = \varpi_{1,3}; \\ M_4 - M_{\theta,4} = \varpi_{2,4}; \end{array} \right|$$

$$\left\{ \begin{array}{l} M_{\zeta,0} - M_{\eta,4} = \vartheta_{1,4}; \\ M_{\zeta,0} + M_{\eta,4} = \vartheta_{2,3}; \end{array} \right| \left\{ \begin{array}{l} M_{\zeta,4} - M_{\eta,0} = \varpi_{1,4}; \\ M_{\zeta,4} + M_{\eta,0} = \varpi_{2,3} \end{array} \right|.$$

Thus the columns of $\widehat{Q}$ are the following:

— the first and the second columns:

$$\begin{array}{c} -\mathrm{i}\Theta_0 + \mathrm{i}\Theta_3 - \mathrm{i}\Upsilon_0 + \mathrm{i}\Upsilon_3 \\ \mathrm{i}\Theta_1 + \mathrm{i}\Upsilon_1 - \Theta_2 - \Upsilon_2 \\ \mathrm{i}M_0 + \mathrm{i}M_{\theta,0} + M_4 + M_{\theta,4} \\ \mathrm{i}M_{\zeta,0} - \mathrm{i}M_{\eta,4} + M_{\zeta,4} - M_{\eta,0} \end{array} \quad \begin{array}{c} \mathrm{i}\Theta_1 + \mathrm{i}\Upsilon_1 + \Theta_2 + \Upsilon_2 \\ -\mathrm{i}\Theta_0 - \mathrm{i}\Theta_3 - \mathrm{i}\Upsilon_0 - \mathrm{i}\Upsilon_3 \\ \mathrm{i}M_{\zeta,0} + \mathrm{i}M_{\eta,4} + M_{\zeta,4} + M_{\eta,0} \\ \mathrm{i}M_0 - \mathrm{i}M_{\theta,0} + M_4 - M_{\theta,4} \end{array}$$

— the third and the fourth columns:

$$\begin{array}{c} \mathrm{i}M_0 + \mathrm{i}M_{\theta,0} - M_4 - M_{\theta,4} \\ \mathrm{i}M_{\zeta,0} + \mathrm{i}M_{\eta,4} - M_{\zeta,4} - M_{\eta,0} \\ -\mathrm{i}\Theta_0 - \mathrm{i}\Theta_3 + \mathrm{i}\Upsilon_0 + \mathrm{i}\Upsilon_3 \\ -\mathrm{i}\Theta_1 + \mathrm{i}\Upsilon_1 + \Theta_2 - \Upsilon_2 \end{array} \quad \begin{array}{c} \mathrm{i}M_{\zeta,0} - \mathrm{i}M_{\eta,4} - M_{\zeta,4} + M_{\eta,0} \\ \mathrm{i}M_0 - \mathrm{i}M_{\theta,0} - M_4 + M_{\theta,4} \\ -\mathrm{i}\Theta_1 + \mathrm{i}\Upsilon_1 - \Theta_2 + \Upsilon_2 \\ -\mathrm{i}\Theta_0 + \mathrm{i}\Theta_3 + \mathrm{i}\Upsilon_0 - \mathrm{i}\Upsilon_3 \end{array}$$

Hence

$$\begin{aligned} \widehat{Q} = {} & \mathrm{i}\Theta_0\beta^{[0]} + \mathrm{i}\Upsilon_0\beta^{[0]}\gamma^{[5]} + \\ & + \mathrm{i}\Theta_1\beta^{[1]} + \mathrm{i}\Upsilon_1\beta^{[1]}\gamma^{[5]} + \\ & + \mathrm{i}\Theta_2\beta^{[2]} + \mathrm{i}\Upsilon_2\beta^{[2]}\gamma^{[5]} + \\ & + \mathrm{i}\Theta_3\beta^{[3]} + \mathrm{i}\Upsilon_3\beta^{[3]}\gamma^{[5]} + \\ & + \mathrm{i}M_0\gamma^{[0]} + \mathrm{i}M_4\beta^{[4]} - \\ & - \mathrm{i}M_{\zeta,0}\gamma^{[0]}_{\zeta} + \mathrm{i}M_{\zeta,4}\zeta^{[4]} - \\ & - \mathrm{i}M_{\eta,0}\gamma^{[0]}_{\eta} - \mathrm{i}M_{\eta,4}\eta^{[4]} + \\ & + \mathrm{i}M_{\theta,0}\gamma^{[0]}_{\theta} + \mathrm{i}M_{\theta,4}\theta^{[4]}. \end{aligned}$$

From (19) the following equation is received:

$$\begin{aligned} & \sum_{k=0}^{3} \beta^{[k]} \left(\partial_k + \mathrm{i}\Theta_k + \mathrm{i}\Upsilon_k\gamma^{[5]} \right) \varphi + \\ & + \begin{pmatrix} +\mathrm{i}M_0\gamma^{[0]} + \mathrm{i}M_4\beta^{[4]} - \\ -\mathrm{i}M_{\zeta,0}\gamma^{[0]}_{\zeta} + \mathrm{i}M_{\zeta,4}\zeta^{[4]} - \\ -\mathrm{i}M_{\eta,0}\gamma^{[0]}_{\eta} - \mathrm{i}M_{\eta,4}\eta^{[4]} + \\ +\mathrm{i}M_{\theta,0}\gamma^{[0]}_{\theta} + \mathrm{i}M_{\theta,4}\theta^{[4]} \end{pmatrix} \varphi = 0 \end{aligned} \tag{21}$$

with real Θ_k, Υ_k, M_0, M_4, $M_{\zeta,0}$, $M_{\zeta,4}$, $M_{\eta,0}$, $M_{\eta,4}$, $M_{\theta,0}$, $M_{\theta,4}$and with

$$\gamma^{[5]} := \begin{bmatrix} 1_2 & 0_2 \\ 0_2 & -1_2 \end{bmatrix}. \tag{22}$$

Because

$$\zeta^{[k]} + \eta^{[k]} + \theta^{[k]} = -\beta^{[k]}$$

with $k \in \{1, 2, 3\}$ then from (21):

$$\begin{aligned} & \begin{pmatrix} -\left(\partial_0 + \mathrm{i}\Theta_0 + \mathrm{i}\Upsilon_0\gamma^{[5]}\right) + \\ \sum\limits_{k=1}^{3} \beta^{[k]} \left(\partial_k + \mathrm{i}\Theta_k + \mathrm{i}\Upsilon_k\gamma^{[5]} \right) \\ +2 \left(\mathrm{i}M_0\gamma^{[0]} + \mathrm{i}M_4\beta^{[4]} \right) \end{pmatrix} \varphi + \\ & + \begin{pmatrix} -\left(\partial_0 + \mathrm{i}\Theta_0 + \mathrm{i}\Upsilon_0\gamma^{[5]}\right) \\ -\sum\limits_{k=1}^{3} \zeta^{[k]} \left(\partial_k + \mathrm{i}\Theta_k + \mathrm{i}\Upsilon_k\gamma^{[5]} \right) \\ +2 \left(-\mathrm{i}M_{\zeta,0}\gamma^{[0]}_{\zeta} + \mathrm{i}M_{\zeta,4}\zeta^{[4]} \right) \end{pmatrix} \varphi + \\ & + \begin{pmatrix} \left(\partial_0 + \mathrm{i}\Theta_0 + \mathrm{i}\Upsilon_0\gamma^{[5]}\right) \\ -\sum\limits_{k=1}^{3} \eta^{[k]} \left(\partial_k + \mathrm{i}\Theta_k + \mathrm{i}\Upsilon_k\gamma^{[5]} \right) \\ +2 \left(-\mathrm{i}M_{\eta,0}\gamma^{[0]}_{\eta} - \mathrm{i}M_{\eta,4}\eta^{[4]} \right) \end{pmatrix} \varphi + \\ & + \begin{pmatrix} -\left(\partial_0 + \mathrm{i}\Theta_0 + \mathrm{i}\Upsilon_0\gamma^{[5]}\right) \\ -\sum\limits_{k=1}^{3} \theta^{[k]} \left(\partial_k + \mathrm{i}\Theta_k + \mathrm{i}\Upsilon_k\gamma^{[5]} \right) \\ +2 \left(\mathrm{i}M_{\theta,0}\gamma^{[0]}_{\theta} + \mathrm{i}M_{\theta,4}\theta^{[4]} \right) \end{pmatrix} \varphi = 0. \end{aligned}$$

It is a generalization of the Dirac equation with gauge field A:

$$\left(-\left(\partial_0+\mathrm{i}eA_0\right)+\sum_{k=1}^{3}\beta^{[k]}\left(\partial_k+\mathrm{i}eA_k\right)+\mathrm{i}m\gamma^{[0]}\right)\varphi=0.$$

Therefore, all Planck's functions obey to Dirac's type equations.

I call matrices $\gamma^{[0]},\beta^{[4]},\gamma_\zeta^{[0]},\zeta^{[4]},\gamma_\eta^{[0]},\eta^{[4]},\gamma_\theta^{[0]},\theta^{[4]}$ *mass elements of pentads*.

3 Colored equation

I call the following part of (21):

$$\left(\begin{array}{c}\beta^{[0]}\left(-\mathrm{i}\partial_0+\Theta_0+\Upsilon_0\gamma^{[5]}\right)+\\ \beta^{[1]}\left(-\mathrm{i}\partial_1+\Theta_1+\Upsilon_1\gamma^{[5]}\right)+\\ \beta^{[2]}\left(-\mathrm{i}\partial_2+\Theta_2+\Upsilon_2\gamma^{[5]}\right)+\\ \beta^{[3]}\left(-\mathrm{i}\partial_3+\Theta_3+\Upsilon_3\gamma^{[5]}\right)-\\ -M_{\zeta,0}\gamma_\zeta^{[0]}+M_{\zeta,4}\zeta^{[4]}+\\ -M_{\eta,0}\gamma_\eta^{[0]}-M_{\eta,4}\eta^{[4]}+\\ +M_{\theta,0}\gamma_\theta^{[0]}+M_{\theta,4}\theta^{[4]}\end{array}\right)\varphi=0. \qquad (23)$$

a coloured moving equation.

Here (5), (7), (9):

$$\gamma_\zeta^{[0]}=-\begin{bmatrix}0&0&0&1\\0&0&1&0\\0&1&0&0\\1&0&0&0\end{bmatrix},\quad \zeta^{[4]}=\begin{bmatrix}0&0&0&\mathrm{i}\\0&0&\mathrm{i}&0\\0&-\mathrm{i}&0&0\\-\mathrm{i}&0&0&0\end{bmatrix}$$

are mass elements of red pentad;

$$\gamma_\eta^{[0]}=\begin{bmatrix}0&0&0&\mathrm{i}\\0&0&-\mathrm{i}&0\\0&\mathrm{i}&0&0\\-\mathrm{i}&0&0&0\end{bmatrix},\quad \eta^{[4]}=\begin{bmatrix}0&0&0&1\\0&0&-1&0\\0&-1&0&0\\1&0&0&0\end{bmatrix}$$

are mass elements of green pentad;

$$\gamma_\theta^{[0]}=\begin{bmatrix}0&0&-1&0\\0&0&0&1\\-1&0&0&0\\0&1&0&0\end{bmatrix},\quad \theta^{[4]}=\begin{bmatrix}0&0&-\mathrm{i}&0\\0&0&0&\mathrm{i}\\-\mathrm{i}&0&0&0\\0&\mathrm{i}&0&0\end{bmatrix}$$

are mass elements of blue pentad.

I call:

- $M_{\zeta,0}$, $M_{\zeta,4}$ *red lower and upper mass members*;
- $M_{\eta,0}$, $M_{\eta,4}$ *green lower and upper mass members*;
- $M_{\theta,0}$, $M_{\theta,4}$ *blue lower and upper mass members*.

The mass members of this equation form the following matrix sum:

$$\widehat{M}:=\left(\begin{array}{c}-M_{\zeta,0}\gamma_\zeta^{[0]}+M_{\zeta,4}\zeta^{[4]}-\\ -M_{\eta,0}\gamma_\eta^{[0]}-M_{\eta,4}\eta^{[4]}+\\ +M_{\theta,0}\gamma_\theta^{[0]}+M_{\theta,4}\theta^{[4]}\end{array}\right)=$$

$$=\begin{bmatrix}0&0&-M_{\theta,0}&M_{\zeta,\eta,0}\\0&0&M^*_{\zeta,\eta,0}&M_{\theta,0}\\-M_{\theta,0}&M_{\zeta,\eta,0}&0&0\\M^*_{\zeta,\eta,0}&M_{\theta,0}&0&0\end{bmatrix}+$$

$$+\mathrm{i}\begin{bmatrix}0&0&-M_{\theta,4}&M^*_{\zeta,\eta,4}\\0&0&M_{\zeta,\eta,4}&M_{\theta,4}\\-M_{\theta,4}&-M^*_{\zeta,\eta,4}&0&0\\-M_{\zeta,\eta,4}&M_{\theta,4}&0&0\end{bmatrix}$$

with $M_{\zeta,\eta,0}:=M_{\zeta,0}-\mathrm{i}M_{\eta,0}$ and $M_{\zeta,\eta,4}:=M_{\zeta,4}-\mathrm{i}M_{\eta,4}$.

Elements of these matrices can be turned by formula of shape [2]:

$$\begin{pmatrix}\cos\frac{\theta}{2}&\mathrm{i}\sin\frac{\theta}{2}\\\mathrm{i}\sin\frac{\theta}{2}&\cos\frac{\theta}{2}\end{pmatrix}\begin{pmatrix}Z&X-\mathrm{i}Y\\X+\mathrm{i}Y&-Z\end{pmatrix}\times$$

$$\times\begin{pmatrix}\cos\frac{\theta}{2}&-\mathrm{i}\sin\frac{\theta}{2}\\-\mathrm{i}\sin\frac{\theta}{2}&\cos\frac{\theta}{2}\end{pmatrix}=$$

$$=\begin{pmatrix}Z\cos\theta-Y\sin\theta&X-\mathrm{i}\begin{pmatrix}Y\cos\theta\\+Z\sin\theta\end{pmatrix}\\X+\mathrm{i}\begin{pmatrix}Y\cos\theta\\+Z\sin\theta\end{pmatrix}&-Z\cos\theta+Y\sin\theta\end{pmatrix}.$$

Hence, if:

$$U_{2,3}(\alpha):=\begin{bmatrix}\cos\alpha&\mathrm{i}\sin\alpha&0&0\\\mathrm{i}\sin\alpha&\cos\alpha&0&0\\0&0&\cos\alpha&\mathrm{i}\sin\alpha\\0&0&\mathrm{i}\sin\alpha&\cos\alpha\end{bmatrix}$$

and

$$\widehat{M}':=\left(\begin{array}{c}-M'_{\zeta,0}\gamma_\zeta^{[0]}+M'_{\zeta,4}\zeta^{[4]}-\\ -M'_{\eta,0}\gamma_\eta^{[0]}-M'_{\eta,4}\eta^{[4]}+\\ +M'_{\theta,0}\gamma_\theta^{[0]}+M'_{\theta,4}\theta^{[4]}\end{array}\right):=U^\dagger_{2,3}(\alpha)\,\widehat{M}U_{2,3}(\alpha)$$

then

$$\begin{aligned}M'_{\zeta,0}&=M_{\zeta,0}\,,\\M'_{\eta,0}&=M_{\eta,0}\cos2\alpha+M_{\theta,0}\sin2\alpha\,,\\M'_{\theta,0}&=M_{\theta,0}\cos2\alpha-M_{\eta,0}\sin2\alpha\,,\\M'_{\zeta,4}&=M_{\zeta,4}\,,\\M'_{\eta,4}&=M_{\eta,4}\cos2\alpha+M_{\theta,4}\sin2\alpha\,,\\M'_{\theta,4}&=M_{\theta,4}\cos2\alpha-M_{\eta,4}\sin2\alpha\,.\end{aligned}$$

Therefore, matrix $U_{2,3}(\alpha)$ makes an oscillation between green and blue colours.

Let us consider equation (21) under transformation $U_{2,3}(\alpha)$ where α is an arbitrary real function of time-space variables ($\alpha=\alpha(t,x_1,x_2,x_3)$):

$$U^\dagger_{2,3}(\alpha)\left(\frac{1}{c}\partial_t+\mathrm{i}\Theta_0+\mathrm{i}\Upsilon_0\gamma^{[5]}\right)U_{2,3}(\alpha)\varphi=$$

$$= U^{\dagger}_{2,3}(\alpha) \begin{pmatrix} \beta^{[1]}\left(\partial_1 + \mathrm{i}\Theta_1 + \mathrm{i}\Upsilon_1\gamma^{[5]}\right) + \\ +\beta^{[2]}\left(\partial_2 + \mathrm{i}\Theta_2 + \mathrm{i}\Upsilon_2\gamma^{[5]}\right) + \\ +\beta^{[3]}\left(\partial_3 + \mathrm{i}\Theta_3 + \mathrm{i}\Upsilon_3\gamma^{[5]}\right) + \\ +\mathrm{i}M_0\gamma^{[0]} + \mathrm{i}M_4\beta^{[4]} + \widehat{M} \end{pmatrix} U_{2,3}(\alpha)\,\varphi\,.$$

Because

$$U^{\dagger}_{2,3}(\alpha)\,U_{2,3}(\alpha) = 1_4\,,$$
$$U^{\dagger}_{2,3}(\alpha)\,\gamma^{[5]}U_{2,3}(\alpha) = \gamma^{[5]}\,,$$
$$U^{\dagger}_{2,3}(\alpha)\,\gamma^{[0]}U_{2,3}(\alpha) = \gamma^{[0]}\,,$$
$$U^{\dagger}_{2,3}(\alpha)\,\beta^{[4]}U_{2,3}(\alpha) = \beta^{[4]}\,,$$
$$U^{\dagger}_{2,3}(\alpha)\,\beta^{[1]} = \beta^{[1]}U^{\dagger}_{2,3}(\alpha)\,,$$
$$U^{\dagger}_{2,3}(\alpha)\,\beta^{[2]} = \left(\beta^{[2]}\cos 2\alpha + \beta^{[3]}\sin 2\alpha\right)U^{\dagger}_{2,3}(\alpha)\,,$$
$$U^{\dagger}_{2,3}(\alpha)\,\beta^{[3]} = \left(\beta^{[3]}\cos 2\alpha - \beta^{[2]}\sin 2\alpha\right)U^{\dagger}_{2,3}(\alpha)\,,$$

then

$$\left(\frac{1}{\mathrm{c}}\,\partial_t + U^{\dagger}_{2,3}(\alpha)\,\frac{1}{\mathrm{c}}\,\partial_t U_{2,3}(\alpha) + \mathrm{i}\Theta_0 + \mathrm{i}\Upsilon_0\gamma^{[5]}\right)\varphi =$$

$$= \begin{pmatrix} \beta^{[1]}\begin{pmatrix}\partial_1 + U^{\dagger}_{2,3}(\alpha)\,\partial_1 U_{2,3}(\alpha) \\ +\mathrm{i}\Theta_1 + \mathrm{i}\Upsilon_1\gamma^{[5]}\end{pmatrix} + \beta^{[2]}\times \\ \times\begin{pmatrix} (\cos 2\alpha\cdot\partial_2 - \sin 2\alpha\cdot\partial_3) \\ +U^{\dagger}_{2,3}(\alpha)\begin{pmatrix}\cos 2\alpha\cdot\partial_2 \\ -\sin 2\alpha\cdot\partial_3\end{pmatrix}U_{2,3}(\alpha) \\ +\mathrm{i}\left(\Theta_2\cos 2\alpha - \Theta_3\sin 2\alpha\right) \\ +\mathrm{i}\left(\Upsilon_2\gamma^{[5]}\cos 2\alpha - \Upsilon_3\gamma^{[5]}\sin 2\alpha\right)\end{pmatrix} \\ +\beta^{[3]}\times \\ \times\begin{pmatrix} (\cos 2\alpha\cdot\partial_3 + \sin 2\alpha\cdot\partial_2) \\ +U^{\dagger}_{2,3}(\alpha)\begin{pmatrix}\cos 2\alpha\cdot\partial_3 \\ +\sin 2\alpha\cdot\partial_2\end{pmatrix}U_{2,3}(\alpha) \\ +\mathrm{i}\left(\Theta_2\sin 2\alpha + \Theta_3\cos 2\alpha\right) \\ +\mathrm{i}\left(\Upsilon_3\gamma^{[5]}\cos 2\alpha + \Upsilon_2\gamma^{[5]}\sin 2\alpha\right)\end{pmatrix} \\ +\mathrm{i}M_0\gamma^{[0]} + \mathrm{i}M_4\beta^{[4]} + \widehat{M}'\end{pmatrix}\varphi\,. \quad (24)$$

Let x'_2 and x'_3 be elements of other coordinate system such that:

$$\frac{\partial x_2}{\partial x'_2} = \cos 2\alpha,$$
$$\frac{\partial x_3}{\partial x'_2} = -\sin 2\alpha,$$
$$\frac{\partial x_2}{\partial x'_3} = \sin 2\alpha.$$
$$\frac{\partial x_3}{\partial x'_3} = \cos 2\alpha,$$
$$\frac{\partial x_0}{\partial x'_2} = \frac{\partial x_1}{\partial x'_2} = \frac{\partial x_0}{\partial x'_3} = \frac{\partial x_1}{\partial x'_3} = 0.$$

Hence:

$$\partial'_2 := \frac{\partial}{\partial x'_2} =$$
$$= \frac{\partial}{\partial x_0}\frac{\partial x_0}{\partial x'_2} + \frac{\partial}{\partial x_1}\frac{\partial x_1}{\partial x'_2} + \frac{\partial}{\partial x_2}\frac{\partial x_2}{\partial x'_2} + \frac{\partial}{\partial x_3}\frac{\partial x_3}{\partial x'_2} =$$
$$= \cos 2\alpha\cdot\frac{\partial}{\partial x_2} - \sin 2\alpha\cdot\frac{\partial}{\partial x_3} =$$
$$= \cos 2\alpha\cdot\partial_2 - \sin 2\alpha\cdot\partial_3\,,$$

$$\partial'_3 := \frac{\partial}{\partial x'_3} =$$
$$= \frac{\partial}{\partial x_0}\frac{\partial x_0}{\partial x'_3} + \frac{\partial}{\partial x_1}\frac{\partial x_1}{\partial x'_3} + \frac{\partial}{\partial x_2}\frac{\partial x_2}{\partial x'_3} + \frac{\partial}{\partial x_3}\frac{\partial x_3}{\partial x'_3} =$$
$$= \cos 2\alpha\cdot\frac{\partial}{\partial x_3} + \sin 2\alpha\cdot\frac{\partial}{\partial x_2} =$$
$$= \cos 2\alpha\cdot\partial_3 + \sin 2\alpha\cdot\partial_2\,.$$

Therefore, from (24):

$$\left(\frac{1}{\mathrm{c}}\,\partial_t + U^{\dagger}_{2,3}(\alpha)\,\frac{1}{\mathrm{c}}\,\partial_t U_{2,3}(\alpha) + \mathrm{i}\Theta_0 + \mathrm{i}\Upsilon_0\gamma^{[5]}\right)\varphi =$$

$$= \begin{pmatrix} \beta^{[1]}\begin{pmatrix}\partial_1 + U^{\dagger}_{2,3}(\alpha)\,\partial_1 U_{2,3}(\alpha) \\ +\mathrm{i}\Theta_1 + \mathrm{i}\Upsilon_1\gamma^{[5]}\end{pmatrix} \\ +\beta^{[2]}\begin{pmatrix}\partial'_2 + U^{\dagger}_{2,3}(\alpha)\,\partial'_2 U_{2,3}(\alpha) \\ +\mathrm{i}\Theta'_2 + \mathrm{i}\Upsilon'_2\gamma^{[5]}\end{pmatrix} \\ +\beta^{[3]}\begin{pmatrix}\partial'_3 + U^{\dagger}_{2,3}(\alpha)\,\partial'_3 U_{2,3}(\alpha) \\ +\mathrm{i}\Theta'_3 + \mathrm{i}\Upsilon'_3\gamma^{[5]}\end{pmatrix} \\ +\mathrm{i}M_0\gamma^{[0]} + \mathrm{i}M_4\beta^{[4]} + \widehat{M}'\end{pmatrix}\varphi\,.$$

with

$$\Theta'_2 := \Theta_2\cos 2\alpha - \Theta_3\sin 2\alpha\,,$$
$$\Theta'_3 := \Theta_2\sin 2\alpha + \Theta_3\cos 2\alpha\,,$$
$$\Upsilon'_2 := \Upsilon_2\cos 2\alpha - \Upsilon_3\sin 2\alpha\,,$$
$$\Upsilon'_3 := \Upsilon_3\cos 2\alpha + \Upsilon_2\sin 2\alpha\,.$$

Therefore, the oscillation between blue and green colours curves the space in the x_2, x_3 directions.

Similarly, matrix

$$U_{1,3}(\vartheta) := \begin{bmatrix} \cos\vartheta & \sin\vartheta & 0 & 0 \\ -\sin\vartheta & \cos\vartheta & 0 & 0 \\ 0 & 0 & \cos\vartheta & \sin\vartheta \\ 0 & 0 & -\sin\vartheta & \cos\vartheta \end{bmatrix}$$

with an arbitrary real function $\vartheta(t, x_1, x_2, x_3)$ describes the oscillation between blue and red colours which curves the space in the x_1, x_3 directions. And matrix

$$U_{1,2}(\varsigma) := \begin{bmatrix} e^{-\mathrm{i}\varsigma} & 0 & 0 & 0 \\ 0 & e^{\mathrm{i}\varsigma} & 0 & 0 \\ 0 & 0 & e^{-\mathrm{i}\varsigma} & 0 \\ 0 & 0 & 0 & e^{\mathrm{i}\varsigma} \end{bmatrix}$$

with an arbitrary real function $\varsigma(t, x_1, x_2, x_3)$ describes the oscillation between green and red colours which curves the space in the x_1, x_2 directions.

Now, let

$$U_{0,1}(\sigma) := \begin{bmatrix} \cosh\sigma & -\sinh\sigma & 0 & 0 \\ -\sinh\sigma & \cosh\sigma & 0 & 0 \\ 0 & 0 & \cosh\sigma & \sinh\sigma \\ 0 & 0 & \sinh\sigma & \cosh\sigma \end{bmatrix}.$$

and

$$\widehat{M}'' := \begin{pmatrix} -M''_{\zeta,0}\gamma^{[0]}_{\zeta} + M''_{\zeta,4}\zeta^{[4]} - \\ -M''_{\eta,0}\gamma^{[0]}_{\eta} - M''_{\eta,4}\eta^{[4]} + \\ +M''_{\theta,0}\gamma^{[0]}_{\theta} + M''_{\theta,4}\theta^{[4]} \end{pmatrix} := U^{\dagger}_{0,1}(\sigma)\,\widehat{M}U_{0,1}(\sigma)$$

then:

$$\begin{aligned} M''_{\zeta,0} &= M_{\zeta,0}\,, \\ M''_{\eta,0} &= (M_{\eta,0}\cosh 2\sigma - M_{\theta,4}\sinh 2\sigma)\,, \\ M''_{\theta,0} &= M_{\theta,0}\cosh 2\sigma + M_{\eta,4}\sinh 2\sigma\,, \\ M''_{\zeta,4} &= M_{\zeta,4}\,, \\ M''_{\eta,4} &= M_{\eta,4}\cosh 2\sigma + M_{\theta,0}\sinh 2\sigma\,, \\ M''_{\theta,4} &= M_{\theta,4}\cosh 2\sigma - M_{\eta,0}\sinh 2\sigma\,. \end{aligned}$$

Therefore, matrix $U_{0,1}(\sigma)$ makes an oscillation between green and blue colours with an oscillation between upper and lower mass members.

Let us consider equation (21) under transformation $U_{0,1}(\sigma)$ where σ is an arbitrary real function of time-space variables ($\sigma = \sigma(t, x_1, x_2, x_3)$):

$$U^{\dagger}_{0,1}(\sigma)\left(\frac{1}{\mathrm{c}}\partial_t + \mathrm{i}\Theta_0 + \mathrm{i}\Upsilon_0\gamma^{[5]}\right)U_{0,1}(\sigma)\,\varphi =$$

$$= U^{\dagger}_{0,1}(\sigma)\begin{pmatrix} \beta^{[1]}\left(\partial_1 + \mathrm{i}\Theta_1 + \mathrm{i}\Upsilon_1\gamma^{[5]}\right) + \\ +\beta^{[2]}\left(\partial_2 + \mathrm{i}\Theta_2 + \mathrm{i}\Upsilon_2\gamma^{[5]}\right) + \\ +\beta^{[3]}\left(\partial_3 + \mathrm{i}\Theta_3 + \mathrm{i}\Upsilon_3\gamma^{[5]}\right) + \\ +\mathrm{i}M_0\gamma^{[0]} + \mathrm{i}M_4\beta^{[4]} + \widehat{M} \end{pmatrix} U_{0,1}(\sigma)\,\varphi\,.$$

Since:

$$\begin{aligned} &U^{\dagger}_{0,1}(\sigma)\,U_{0,1}(\sigma) = \left(\cosh 2\sigma - \beta^{[1]}\sinh 2\sigma\right), \\ &U^{\dagger}_{0,1}(\sigma) = \left(\cosh 2\sigma + \beta^{[1]}\sinh 2\sigma\right)U^{-1}_{0,1}(\sigma), \\ &U^{\dagger}_{0,1}(\sigma)\,\beta^{[1]} = \left(\beta^{[1]}\cosh 2\sigma - \sinh 2\sigma\right)U^{-1}_{0,1}(\sigma), \\ &U^{\dagger}_{0,1}(\sigma)\,\beta^{[2]} = \beta^{[2]}U^{-1}_{0,1}(\sigma), \\ &U^{\dagger}_{0,1}(\sigma)\,\beta^{[3]} = \beta^{[3]}U^{-1}_{0,1}(\sigma), \\ &U^{\dagger}_{0,1}(\sigma)\,\gamma^{[0]}U_{0,1}(\sigma) = \gamma^{[0]}, \\ &U^{\dagger}_{0,1}(\sigma)\,\beta^{[4]}U_{0,1}(\sigma) = \beta^{[4]}, \\ &U^{-1}_{0,1}(\sigma)\,U_{0,1}(\sigma) = 1_4\,, \\ &U^{-1}_{0,1}(\sigma)\,\gamma^{[5]}U_{0,1}(\sigma) = \gamma^{[5]}\,, \\ &U^{\dagger}_{0,1}(\sigma)\,\gamma^{[5]}U_{0,1}(\sigma) = \gamma^{[5]}\left(\cosh 2\sigma - \beta^{[1]}\sinh 2\sigma\right), \end{aligned}$$

then

$$\left(\begin{array}{c} U^{-1}_{0,1}(\sigma)\begin{pmatrix}\cosh 2\sigma\cdot\frac{1}{\mathrm{c}}\partial_t \\ +\sinh 2\sigma\cdot\partial_1\end{pmatrix}U_{0,1}(\sigma) \\ +\left(\cosh 2\sigma\cdot\frac{1}{\mathrm{c}}\partial_t + \sinh 2\sigma\cdot\partial_1\right) \\ +\mathrm{i}\left(\Theta_0\cosh 2\sigma + \Theta_1\sinh 2\sigma\right) \\ +\mathrm{i}\left(\Upsilon_0\cosh 2\sigma + \sinh 2\sigma\cdot\Upsilon_1\right)\gamma^{[5]} - \\ -\beta^{[1]}\times \\ \times\left(\begin{array}{c} U^{-1}_{0,1}(\sigma)\begin{pmatrix}\cosh 2\sigma\cdot\partial_1 + \\ \sinh 2\sigma\cdot\frac{1}{\mathrm{c}}\partial_t\end{pmatrix}U_{0,1}(\sigma) \\ +\left(\cosh 2\sigma\cdot\partial_1 + \sinh 2\sigma\cdot\frac{1}{\mathrm{c}}\partial_t\right) \\ +\mathrm{i}\left(\Theta_1\cosh 2\sigma + \Theta_0\sinh 2\sigma\right) \\ +\mathrm{i}\left(\Upsilon_1\cosh 2\sigma + \Upsilon_0\sinh 2\sigma\right)\gamma^{[5]} \end{array}\right) \\ -\beta^{[2]}\begin{pmatrix}\partial_2 + U^{-1}_{0,1}(\sigma)\left(\partial_2 U_{0,1}(\sigma)\right) \\ +\mathrm{i}\Theta_2 + \mathrm{i}\Upsilon_2\gamma^{[5]}\end{pmatrix} \\ -\beta^{[3]}\begin{pmatrix}\partial_3 + U^{-1}_{0,1}(\sigma)\left(\partial_3 U_{0,1}(\sigma)\right) \\ +\mathrm{i}\Theta_3 + \mathrm{i}\Upsilon_3\gamma^{[5]}\end{pmatrix} \\ -\mathrm{i}M_0\gamma^{[0]} - \mathrm{i}M_4\beta^{[4]} - \widehat{M}'' \end{array}\right)\varphi = 0\,. \quad (25)$$

Let t' and x'_1 be elements of other coordinate system such that:

$$\left.\begin{aligned} \frac{\partial x_1}{\partial x'_1} &= \cosh 2\sigma \\ \frac{\partial t}{\partial x'_1} &= \frac{1}{\mathrm{c}}\sinh 2\sigma \\ \frac{\partial x_1}{\partial t'} &= \mathrm{c}\sinh 2\sigma \\ \frac{\partial t}{\partial t'} &= \cosh 2\sigma \\ \frac{\partial x_2}{\partial t'} &= \frac{\partial x_3}{\partial t'} = \frac{\partial x_2}{\partial x'_1} = \frac{\partial x_3}{\partial x'_1} = 0 \end{aligned}\right\}. \quad (26)$$

Hence:

$$\begin{aligned} \partial'_t &:= \frac{\partial}{\partial t'} = \frac{\partial}{\partial t}\frac{\partial t}{\partial t'} + \frac{\partial}{\partial x_1}\frac{\partial x_1}{\partial t'} + \frac{\partial}{\partial x_2}\frac{\partial x_2}{\partial t'} + \frac{\partial}{\partial x_3}\frac{\partial x_3}{\partial t'} = \\ &= \cosh 2\sigma\cdot\frac{\partial}{\partial t} + \mathrm{c}\sinh 2\sigma\cdot\frac{\partial}{\partial x_1} = \\ &= \cosh 2\sigma\cdot\partial_t + \mathrm{c}\sinh 2\sigma\cdot\partial_1\,, \end{aligned}$$

that is

$$\frac{1}{\mathrm{c}}\partial'_t = \frac{1}{\mathrm{c}}\cosh 2\sigma\cdot\partial_t + \sinh 2\sigma\cdot\partial_1$$

and

$$\partial'_1 := \frac{\partial}{\partial x'_1} =$$
$$= \frac{\partial}{\partial t}\frac{\partial t}{\partial x'_1} + \frac{\partial}{\partial x_1}\frac{\partial x_1}{\partial x'_1} + \frac{\partial}{\partial x_2}\frac{\partial x_2}{\partial x'_1} + \frac{\partial}{\partial x_3}\frac{\partial x_3}{\partial x'_1} =$$
$$= \cosh 2\sigma \cdot \frac{\partial}{\partial x_1} + \sinh 2\sigma \cdot \frac{1}{\mathrm{c}}\frac{\partial}{\partial t} =$$
$$= \cosh 2\sigma \cdot \partial_1 + \sinh 2\sigma \cdot \frac{1}{\mathrm{c}}\partial_t .$$

Therefore, from (25):

$$\left(\begin{array}{c} \beta^{[0]} \left(\begin{array}{c} \frac{1}{\mathrm{c}}\partial'_t + U^{-1}_{0,1}(\sigma)\frac{1}{\mathrm{c}}\partial'_t U_{0,1}(\sigma) \\ +\mathrm{i}\Theta''_0 + \mathrm{i}\Upsilon''_0\gamma^{[5]} \end{array} \right) \\ +\beta^{[1]} \left(\begin{array}{c} \partial'_1 + U^{-1}_{0,1}(\sigma)\partial'_1 U_{0,1}(\sigma) \\ +\mathrm{i}\Theta''_1 + \mathrm{i}\Upsilon''_1\gamma^{[5]} \end{array} \right) \\ +\beta^{[2]} \left(\begin{array}{c} \partial_2 + U^{-1}_{0,1}(\sigma)\partial_2 U_{0,1}(\sigma) \\ +\mathrm{i}\Theta_2 + \mathrm{i}\Upsilon_2\gamma^{[5]} \end{array} \right) \\ +\beta^{[3]} \left(\begin{array}{c} \partial_3 + U^{-1}_{0,1}(\sigma)\partial_3 U_{0,1}(\sigma) \\ +\mathrm{i}\Theta_3 + \mathrm{i}\Upsilon_3\gamma^{[5]} \end{array} \right) \\ +\mathrm{i}M_0\gamma^{[0]} + \mathrm{i}M_4\beta^{[4]} + \widehat{M}'' \end{array} \right) \varphi = 0$$

with

$$\Theta''_0 := \Theta_0 \cosh 2\sigma + \Theta_1 \sinh 2\sigma ,$$
$$\Theta''_1 := \Theta_1 \cosh 2\sigma + \Theta_0 \sinh 2\sigma ,$$
$$\Upsilon''_0 := \Upsilon_0 \cosh 2\sigma + \sinh 2\sigma \cdot \Upsilon_1 ,$$
$$\Upsilon''_1 := \Upsilon_1 \cosh 2\sigma + \Upsilon_0 \sinh 2\sigma .$$

Therefore, the oscillation between blue and green colours with the oscillation between upper and lower mass members curves the space in the t, x_1 directions.

Similarly, matrix

$$U_{0,2}(\phi) := \begin{bmatrix} \cosh\phi & \mathrm{i}\sinh\phi & 0 & 0 \\ -\mathrm{i}\sinh\phi & \cosh\phi & 0 & 0 \\ 0 & 0 & \cosh\phi & -\mathrm{i}\sinh\phi \\ 0 & 0 & \mathrm{i}\sinh\phi & \cosh\phi \end{bmatrix}$$

with an arbitrary real function $\phi(t, x_1, x_2, x_3)$ describes the oscillation between blue and red colours with the oscillation between upper and lower mass members curves the space in the t, x_2 directions. And matrix

$$U_{0,3}(\iota) := \begin{bmatrix} e^{\iota} & 0 & 0 & 0 \\ 0 & e^{-\iota} & 0 & 0 \\ 0 & 0 & e^{-\iota} & 0 \\ 0 & 0 & 0 & e^{\iota} \end{bmatrix}$$

with an arbitrary real function $\iota(t, x_1, x_2, x_3)$ describes the oscillation between green and red colours with the oscillation between upper and lower mass members curves the space in the t, x_3 directions.

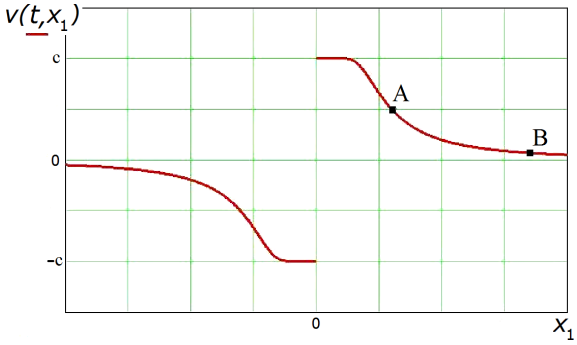

Fig. 1: It is dependency of $v(t, x_1)$ from x_1.

From (26):

$$\frac{\partial x_1}{\partial t'} = \mathrm{c}\sinh 2\sigma ,$$
$$\frac{\partial t}{\partial t'} = \cosh 2\sigma .$$

Because

$$\sinh 2\sigma = \frac{v}{\sqrt{1 - \frac{v^2}{\mathrm{c}^2}}} ,$$
$$\cosh 2\sigma = \frac{1}{\sqrt{1 - \frac{v^2}{\mathrm{c}^2}}}$$

with v is a velocity of system $\{t', x'_1\}$ as respects to system $\{t, x_1\}$ then

$$v = \tanh 2\sigma .$$

Let

$$2\sigma := \omega(x_1)\frac{t}{x_1}$$

with

$$\omega(x_1) = \frac{\lambda}{|x_1|} ,$$

where λ is a real constant bearing positive numerical value.

In that case

$$v(t, x_1) = \tanh\left(\omega(x_1)\frac{t}{x_1}\right)$$

and if g is an acceleration of system $\{t', x'_1\}$ as respects to system $\{t, x_1\}$ then

$$\mathrm{g}(t, x_1) = \frac{\partial v}{\partial t} = \frac{\omega(x_1)}{\left(\cosh^2 \omega(x_1)\frac{t}{x_1}\right) x_1} .$$

Figure 1 shows the dependency of a system $\{t', x'_1\}$ velocity $v(t, x_1)$ on x_1 in system $\{t, x_1\}$.

This velocity in point A is not equal to one in point B. Hence, an oscillator, placed in B, has a nonzero velocity in respect to an observer, placed in point A. Therefore, from the Lorentz transformations, this oscillator frequency for observer, placed in point A, is less than own frequency of this oscillator (*red shift*).

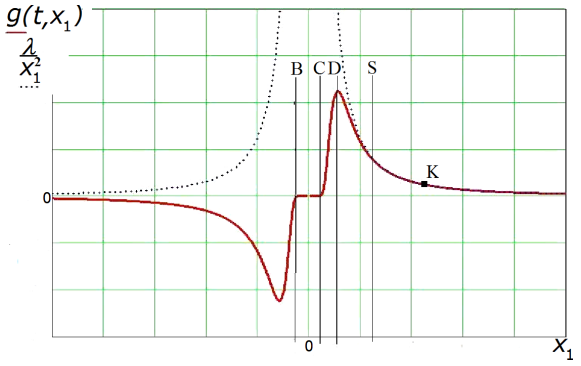

Fig. 2: It is dependency of $g(t, x_1)$ from x_1.

Figure 2 shows a dependency of a system $\{t', x_1'\}$ acceleration $g\,(t, x_1)$ on x_1 in system $\{t, x_1\}$.

If an object immovable in system $\{t, x_1\}$ is placed in point K then in system $\{t', x_1'\}$ this object must move to the left with acceleration g and $\mathrm{g} \simeq \frac{\lambda}{x_1^2}$.

I call:

- interval from S to ∞ the *Newton Gravity Zone*,
- interval from B to C the *the Asymptotic Freedom Zone*,
- and interval from C to D *the Confinement Force Zone*.

Now let

$$\widetilde{U}(\chi) := \begin{bmatrix} e^{\mathrm{i}\chi} & 0 & 0 & 0 \\ 0 & e^{\mathrm{i}\chi} & 0 & 0 \\ 0 & 0 & e^{2\mathrm{i}\chi} & 0 \\ 0 & 0 & 0 & e^{2\mathrm{i}\chi} \end{bmatrix}$$

and

$$\widehat{M}' := \begin{pmatrix} -M'_{\zeta,0}\gamma^{[0]}_{\zeta} + M'_{\zeta,4}\zeta^{[4]} - \\ -M'_{\eta,0}\gamma^{[0]}_{\eta} - M'_{\eta,4}\eta^{[4]} + \\ +M'_{\theta,0}\gamma^{[0]}_{\theta} + M'_{\theta,4}\theta^{[4]} \end{pmatrix} := \widetilde{U}^{\dagger}(\chi)\,\widehat{M}\widetilde{U}(\chi)$$

then:

$$\begin{aligned} M'_{\zeta,0} &= (M_{\zeta,0}\cos\chi - M_{\zeta,4}\sin\chi), \\ M'_{\zeta,4} &= (M_{\zeta,4}\cos\chi + M_{\zeta,0}\sin\chi), \\ M'_{\eta,4} &= (M_{\eta,4}\cos\chi - M_{\eta,0}\sin\chi), \\ M'_{\eta,0} &= (M_{\eta,0}\cos\chi + M_{\eta,4}\sin\chi), \\ M'_{\theta,0} &= (M_{\theta,0}\cos\chi + M_{\theta,4}\sin\chi), \\ M'_{\theta,4} &= (M_{\theta,4}\cos\chi - M_{\theta,0}\sin\chi). \end{aligned}$$

Therefore, matrix $\widetilde{U}(\chi)$ makes an oscillation between upper and lower mass members.

Let us consider equation (23) under transformation $\widetilde{U}(\chi)$ where χ is an arbitrary real function of time-space variables ($\chi = \chi(t, x_1, x_2, x_3)$):

$$\widetilde{U}^{\dagger}(\chi)\left(\frac{1}{\mathrm{c}}\partial_t + \mathrm{i}\Theta_0 + \mathrm{i}\Upsilon_0\gamma^{[5]}\right)\widetilde{U}(\chi)\,\varphi =$$

$$= \widetilde{U}^{\dagger}(\chi)\begin{pmatrix} \beta^{[1]}\left(\partial_1 + \mathrm{i}\Theta_1 + \mathrm{i}\Upsilon_1\gamma^{[5]}\right) + \\ +\beta^{[2]}\left(\partial_2 + \mathrm{i}\Theta_2 + \mathrm{i}\Upsilon_2\gamma^{[5]}\right) + \\ +\beta^{[3]}\left(\partial_3 + \mathrm{i}\Theta_3 + \mathrm{i}\Upsilon_3\gamma^{[5]}\right) + \\ +\widehat{M} \end{pmatrix}\widetilde{U}(\chi)\,\varphi.$$

Because

$$\begin{aligned} \gamma^{[5]}\widetilde{U}(\chi) &= \widetilde{U}(\chi)\gamma^{[5]}, \\ \beta^{[1]}\widetilde{U}(\chi) &= \widetilde{U}(\chi)\beta^{[1]}, \\ \beta^{[2]}\widetilde{U}(\chi) &= \widetilde{U}(\chi)\beta^{[2]}, \\ \beta^{[3]}\widetilde{U}(\chi) &= \widetilde{U}(\chi)\beta^{[3]}, \\ \widetilde{U}^{\dagger}(\chi)\,\widetilde{U}(\chi) &= 1_4, \end{aligned}$$

then

$$\left(\frac{1}{\mathrm{c}}\partial_t + \frac{1}{\mathrm{c}}\widetilde{U}^{\dagger}(\chi)\left(\partial_t\widetilde{U}(\chi)\right) + \mathrm{i}\Theta_0 + \mathrm{i}\Upsilon_0\gamma^{[5]}\right)\varphi =$$

$$= \begin{pmatrix} \beta^{[1]}\begin{pmatrix} \partial_1 + \widetilde{U}^{\dagger}(\chi)\left(\partial_1\widetilde{U}(\chi)\right) \\ +\mathrm{i}\Theta_1 + \mathrm{i}\Upsilon_1\gamma^{[5]} \end{pmatrix} + \\ +\beta^{[2]}\begin{pmatrix} \partial_2 + \widetilde{U}^{\dagger}(\chi)\left(\partial_2\widetilde{U}(\chi)\right) \\ +\mathrm{i}\Theta_2 + \mathrm{i}\Upsilon_2\gamma^{[5]} \end{pmatrix} + \\ +\beta^{[3]}\begin{pmatrix} \partial_3 + \widetilde{U}^{\dagger}(\chi)\left(\partial_3\widetilde{U}(\chi)\right) \\ +\mathrm{i}\Theta_3 + \mathrm{i}\Upsilon_3\gamma^{[5]} \end{pmatrix} + \\ +\widetilde{U}^{\dagger}(\chi)\,\widehat{M}\widetilde{U}(\chi) \end{pmatrix}\varphi.$$

Now let:

$$\widehat{U}(\kappa) := \begin{bmatrix} e^{\kappa} & 0 & 0 & 0 \\ 0 & e^{\kappa} & 0 & 0 \\ 0 & 0 & e^{2\kappa} & 0 \\ 0 & 0 & 0 & e^{2\kappa} \end{bmatrix}$$

and

$$\widehat{M}' := \begin{pmatrix} -M'_{\zeta,0}\gamma^{[0]}_{\zeta} + M'_{\zeta,4}\zeta^{[4]} - \\ -M'_{\eta,0}\gamma^{[0]}_{\eta} - M'_{\eta,4}\eta^{[4]} + \\ +M'_{\theta,0}\gamma^{[0]}_{\theta} + M'_{\theta,4}\theta^{[4]} \end{pmatrix} := \widehat{U}^{-1}(\kappa)\,\widehat{M}\widehat{U}(\kappa)$$

then:

$$\begin{aligned} M'_{\theta,0} &= (M_{\theta,0}\cosh\kappa - \mathrm{i}M_{\theta,4}\sinh\kappa), \\ M'_{\theta,4} &= (M_{\theta,4}\cosh\kappa + \mathrm{i}M_{\theta,0}\sinh\kappa), \\ M'_{\eta,0} &= (M_{\eta,0}\cosh\kappa - \mathrm{i}M_{\eta,4}\sinh\kappa), \\ M'_{\eta,4} &= (M_{\eta,4}\cosh\kappa + \mathrm{i}M_{\eta,0}\sinh\kappa), \\ M'_{\zeta,0} &= (M_{\zeta,0}\cosh\kappa + \mathrm{i}M_{\zeta,4}\sinh\kappa), \\ M'_{\zeta,4} &= (M_{\zeta,4}\cosh\kappa - \mathrm{i}M_{\zeta,0}\sinh\kappa). \end{aligned}$$

Therefore, matrix $\widehat{U}(\kappa)$ makes an oscillation between upper and lower mass members, too.

Let us consider equation (23) under transformation $\widehat{U}(\kappa)$ where κ is an arbitrary real function of time-space variables ($\kappa = \kappa(t, x_1, x_2, x_3)$):

$$\widehat{U}^{-1}(\kappa)\left(\frac{1}{\mathrm{c}}\partial_t + \mathrm{i}\Theta_0 + \mathrm{i}\Upsilon_0\gamma^{[5]}\right)\widehat{U}(\kappa)\varphi =$$
$$= \widehat{U}^{-1}(\kappa)\begin{pmatrix} \beta^{[1]}\left(\partial_1 + \mathrm{i}\Theta_1 + \mathrm{i}\Upsilon_1\gamma^{[5]}\right) + \\ +\beta^{[2]}\left(\partial_2 + \mathrm{i}\Theta_2 + \mathrm{i}\Upsilon_2\gamma^{[5]}\right) + \\ +\beta^{[3]}\left(\partial_3 + \mathrm{i}\Theta_3 + \mathrm{i}\Upsilon_3\gamma^{[5]}\right) + \\ +\widehat{M} \end{pmatrix}\widehat{U}(\kappa)\varphi$$

Because

$$\gamma^{[5]}\widehat{U}(\kappa) = \widehat{U}(\kappa)\gamma^{[5]},$$
$$\widehat{U}^{-1}(\kappa)\beta^{[1]} = \beta^{[1]}\widehat{U}^{-1}(\kappa),$$
$$\widehat{U}^{-1}(\kappa)\beta^{[2]} = \beta^{[2]}\widehat{U}^{-1}(\kappa),$$
$$\widehat{U}^{-1}(\kappa)\beta^{[3]} = \beta^{[3]}\widehat{U}^{-1}(\kappa),$$
$$\widehat{U}^{-1}(\kappa)\widehat{U}(\kappa) = 1_4,$$

then

$$\left(\frac{1}{\mathrm{c}}\partial_t + \widehat{U}^{-1}(\kappa)\left(\frac{1}{\mathrm{c}}\partial_t\widehat{U}(\kappa)\right) + \mathrm{i}\Theta_0 + \mathrm{i}\Upsilon_0\gamma^{[5]}\right)\varphi =$$
$$= \begin{pmatrix} \beta^{[1]}\begin{pmatrix} \partial_1 + \widehat{U}^{-1}(\kappa)\left(\partial_1\widehat{U}(\kappa)\right) \\ +\mathrm{i}\Theta_1 + \mathrm{i}\Upsilon_1\gamma^{[5]} \end{pmatrix} + \\ +\beta^{[2]}\begin{pmatrix} \partial_2 + \widehat{U}^{-1}(\kappa)\left(\partial_2\widehat{U}(\kappa)\right) \\ +\mathrm{i}\Theta_2 + \mathrm{i}\Upsilon_2\gamma^{[5]} \end{pmatrix} + \\ +\beta^{[3]}\begin{pmatrix} \partial_3 + \widehat{U}^{-1}(\kappa)\left(\partial_3\widehat{U}(\kappa)\right) \\ +\mathrm{i}\Theta_3 + \mathrm{i}\Upsilon_3\gamma^{[5]} \end{pmatrix} + \\ +\widehat{U}^{-1}(\kappa)\widehat{M}\widehat{U}(\kappa) \end{pmatrix}\varphi.$$

If denote:

$$\Lambda_1 := \begin{bmatrix} 0 & -1 & 0 & 0 \\ -1 & 0 & 0 & 0 \\ 0 & 0 & 0 & 1 \\ 0 & 0 & 1 & 0 \end{bmatrix},$$

$$\Lambda_2 := \begin{bmatrix} 0 & \mathrm{i} & 0 & 0 \\ \mathrm{i} & 0 & 0 & 0 \\ 0 & 0 & 0 & \mathrm{i} \\ 0 & 0 & \mathrm{i} & 0 \end{bmatrix},$$

$$\Lambda_3 := \begin{bmatrix} 0 & 1 & 0 & 0 \\ -1 & 0 & 0 & 0 \\ 0 & 0 & 0 & 1 \\ 0 & 0 & -1 & 0 \end{bmatrix},$$

$$\Lambda_4 := \begin{bmatrix} 0 & \mathrm{i} & 0 & 0 \\ -\mathrm{i} & 0 & 0 & 0 \\ 0 & 0 & 0 & -\mathrm{i} \\ 0 & 0 & \mathrm{i} & 0 \end{bmatrix},$$

$$\Lambda_5 := \begin{bmatrix} -\mathrm{i} & 0 & 0 & 0 \\ 0 & \mathrm{i} & 0 & 0 \\ 0 & 0 & -\mathrm{i} & 0 \\ 0 & 0 & 0 & \mathrm{i} \end{bmatrix},$$

$$\Lambda_6 := \begin{bmatrix} 1 & 0 & 0 & 0 \\ 0 & -1 & 0 & 0 \\ 0 & 0 & -1 & 0 \\ 0 & 0 & 0 & 1 \end{bmatrix},$$

$$\Lambda_7 := \begin{bmatrix} 1 & 0 & 0 & 0 \\ 0 & 1 & 0 & 0 \\ 0 & 0 & 2 & 0 \\ 0 & 0 & 0 & 2 \end{bmatrix},$$

$$\Lambda_8 := \begin{bmatrix} \mathrm{i} & 0 & 0 & 0 \\ 0 & \mathrm{i} & 0 & 0 \\ 0 & 0 & 2\mathrm{i} & 0 \\ 0 & 0 & 0 & 2\mathrm{i} \end{bmatrix},$$

then

$$U_{0,1}^{-1}(\sigma)\left(\partial_s U_{0,1}(\sigma)\right) = \Lambda_1\partial_s\sigma,$$
$$U_{2,3}^{-1}(\alpha)\left(\partial_s U_{2,3}(\alpha)\right) = \Lambda_2\partial_s\alpha,$$
$$U_{1,3}^{-1}(\vartheta)\left(\partial_s U_{1,3}(\vartheta)\right) = \Lambda_3\partial_s\vartheta,$$
$$U_{0,2}^{-1}(\phi)\left(\partial_s U_{0,2}(\phi)\right) = \Lambda_4\partial_s\phi,$$
$$U_{1,2}^{-1}(\varsigma)\left(\partial_s U_{1,2}(\varsigma)\right) = \Lambda_5\partial_s\varsigma,$$
$$U_{0,3}^{-1}(\iota)\left(\partial_s U_{0,3}(\iota)\right) = \Lambda_6\partial_s\iota,$$
$$\widehat{U}^{-1}(\kappa)\left(\partial_s\widehat{U}(\kappa)\right) = \Lambda_7\partial_s\kappa,$$
$$\widetilde{U}^{-1}(\chi)\left(\partial_s\widetilde{U}(\chi)\right) = \Lambda_8\partial_s\chi.$$

Let $\grave{U}$ be the following set:

$$\grave{U} := \left\{U_{0,1}, U_{2,3}, U_{1,3}, U_{0,2}, U_{1,2}, U_{0,3}, \widehat{U}, \widetilde{U}\right\}.$$

Because

$$U_{2,3}^{-1}(\alpha)\Lambda_1 U_{2,3}(\alpha) = \Lambda_1$$
$$U_{1,3}^{-1}(\vartheta)\Lambda_1 U_{1,3}(\vartheta) = (\Lambda_1\cos 2\vartheta + \Lambda_6\sin 2\vartheta)$$
$$U_{0,2}^{-1}(\phi)\Lambda_1 U_{0,2}(\phi) = (\Lambda_1\cosh 2\phi - \Lambda_5\sinh 2\phi)$$
$$U_{1,2}^{-1}(\varsigma)\Lambda_1 U_{1,2}(\varsigma) = \Lambda_1\cos 2\varsigma - \Lambda_4\sin 2\varsigma$$
$$U_{0,3}^{-1}(\iota)\Lambda_1 U_{0,3}(\iota) = \Lambda_1\cosh 2\iota + \Lambda_3\sinh 2\iota$$
$$\widehat{U}^{-1}(\kappa)\Lambda_1\widehat{U}(\kappa) = \Lambda_1$$
$$\widetilde{U}^{-1}(\chi)\Lambda_1\widetilde{U}(\chi) = \Lambda_1$$
========

$$\widetilde{U}^{-1}(\chi)\,\Lambda_2\widetilde{U}(\chi)=\Lambda_2$$
$$\widehat{U}^{-1}(\kappa)\,\Lambda_2\widehat{U}(\kappa)=\Lambda_2$$
$$U_{0,3}^{-1}(\iota)\,\Lambda_2U_{0,3}(\iota)=\Lambda_2\cosh 2\iota-\Lambda_4\sinh 2\iota$$
$$U_{1,2}^{-1}(\varsigma)\,\Lambda_2U_{1,2}(\varsigma)=\Lambda_2\cos 2\varsigma-\Lambda_3\sin 2\varsigma$$
$$U_{0,2}^{-1}(\phi)\,\Lambda_2U_{0,2}(\phi)=\Lambda_2\cosh 2\phi+\Lambda_6\sinh 2\phi$$
$$U_{1,3}^{-1}(\vartheta)\,\Lambda_2U_{1,3}(\vartheta)=\Lambda_2\cos 2\vartheta+\Lambda_5\sin 2\vartheta$$
$$U_{0,1}^{-1}(\sigma)\,\Lambda_2U_{0,1}(\sigma)=\Lambda_2$$
$$=========$$
$$U_{0,1}^{-1}(\sigma)\;\Lambda_3U_{0,1}(\sigma)=\Lambda_3\cosh 2\sigma-\Lambda_6\sinh 2\sigma$$
$$U_{2,3}^{-1}(\alpha)\;\Lambda_3U_{2,3}(\alpha)=\Lambda_3\cos 2\alpha-\Lambda_5\sin 2\alpha$$
$$U_{0,2}^{-1}(\phi)\;\Lambda_3U_{0,2}(\phi)=\Lambda_3$$
$$U_{1,2}^{-1}(\varsigma)\;\Lambda_3U_{1,2}(\varsigma)=\Lambda_3\cos 2\varsigma+\Lambda_2\sin 2\varsigma$$
$$U_{0,3}^{-1}(\iota)\;\Lambda_3U_{0,3}(\iota)=\;\Lambda_3\cosh 2\iota+\Lambda_1\sinh 2\iota$$
$$\widehat{U}^{-1}(\kappa)\;\Lambda_3\widehat{U}(\kappa)=\Lambda_3$$
$$\widetilde{U}^{-1}(\chi)\;\Lambda_3\widetilde{U}(\chi)=\Lambda_3$$
$$==========$$
$$\widetilde{U}^{-1}(\chi)\;\Lambda_4\widetilde{U}(\chi)=\Lambda_4$$
$$\widehat{U}^{-1}(\kappa)\;\Lambda_4\widehat{U}(\kappa)=\Lambda_4$$
$$U_{0,3}^{-1}(\iota)\;\Lambda_4U_{0,3}(\iota)=\Lambda_4\cosh 2\iota-\Lambda_2\sinh 2\iota$$
$$U_{1,2}^{-1}(\varsigma)\;\Lambda_4U_{1,2}(\varsigma)=\Lambda_4\cos 2\varsigma+\Lambda_1\sin 2\varsigma$$
$$U_{1,3}^{-1}(\vartheta)\;\Lambda_4U_{1,3}(\vartheta)=\Lambda_4$$
$$U_{2,3}^{-1}(\alpha)\;\Lambda_4U_{2,3}(\alpha)=\Lambda_4\cos 2\alpha-\Lambda_6\sin 2\alpha$$
$$U_{0,1}^{-1}(\sigma)\;\Lambda_4U_{0,1}(\sigma)=\Lambda_4\cosh 2\sigma+\Lambda_5\sinh 2\sigma$$
$$==========$$
$$U_{0,1}^{-1}(\sigma)\;\Lambda_5U_{0,1}(\sigma)\;=\Lambda_5\cosh 2\sigma+\Lambda_4\sinh 2\sigma$$
$$U_{2,3}^{-1}(\alpha)\;\Lambda_5U_{2,3}(\alpha)\;=\Lambda_5\cos 2\alpha+\Lambda_3\sin 2\alpha$$
$$U_{1,3}^{-1}(\vartheta)\;\Lambda_5U_{1,3}(\vartheta)\;=(\Lambda_5\cos 2\vartheta-\Lambda_2\sin 2\vartheta)$$
$$U_{0,2}^{-1}(\phi)\;\Lambda_5U_{0,2}(\phi)\;=\Lambda_5\cosh 2\phi-\Lambda_1\sinh 2\phi$$
$$U_{0,3}^{-1}(\iota)\;\Lambda_5U_{0,3}(\iota)\;=\Lambda_5$$
$$\widehat{U}^{-1}(\kappa)\;\Lambda_5\widehat{U}(\kappa)\;=\Lambda_5$$
$$\widetilde{U}^{-1}(\chi)\,\Lambda_5\widetilde{U}(\chi)\;=\Lambda_5$$
$$==========$$
$$\widetilde{U}^{-1}(\chi)\,\Lambda_6\widetilde{U}(\chi)\;=\Lambda_6$$
$$\widehat{U}^{-1}(\kappa)\,\Lambda_6\widehat{U}(\kappa)\;=\Lambda_6$$
$$U_{1,2}^{-1}(\varsigma)\,\Lambda_6U_{1,2}(\varsigma)\;=\Lambda_6$$
$$U_{0,2}^{-1}(\phi)\,\Lambda_6U_{0,2}(\phi)\;=\Lambda_6\cosh 2\phi+\Lambda_2\sinh 2\phi$$
$$U_{1,3}^{-1}(\vartheta)\,\Lambda_6U_{1,3}(\vartheta)\;=\Lambda_6\cos 2\vartheta-\Lambda_1\sin 2\vartheta$$
$$U_{2,3}^{-1}(\alpha)\,\Lambda_6U_{2,3}(\alpha)\;=\Lambda_6\cos 2\alpha+\Lambda_4\sin 2\alpha$$
$$U_{0,1}^{-1}(\sigma)\,\Lambda_6U_{0,1}(\sigma)=\Lambda_6\cosh 2\sigma-\Lambda_3\sinh 2\sigma$$
$$========$$
$$\widetilde{U}^{-1}(\chi)\;\Lambda_7\widetilde{U}(\chi)=\Lambda_7$$
$$U_{0,3}^{-1}(\iota)\;\Lambda_7U_{0,3}(\iota)=\Lambda_7$$
$$U_{1,2}^{-1}(\varsigma)\;\Lambda_7U_{1,2}(\varsigma)=\Lambda_7$$
$$U_{0,2}^{-1}(\phi)\;\Lambda_7U_{0,2}(\phi)=\Lambda_7$$
$$U_{1,3}^{-1}(\vartheta)\;\Lambda_7U_{1,3}(\vartheta)=\Lambda_7$$
$$U_{2,3}^{-1}(\alpha)\;\Lambda_7U_{2,3}(\sigma)=\Lambda_7$$
$$U_{0,1}^{-1}(\sigma)\;\Lambda_7U_{0,1}(\sigma)=\Lambda_7$$
$$=========$$
$$U_{0,1}^{-1}(\sigma)\;\Lambda_8U_{0,1}(\sigma)=\Lambda_8$$
$$U_{2,3}^{-1}(\alpha)\;\Lambda_8U_{2,3}(\alpha)=\Lambda_8$$
$$U_{1,3}^{-1}(\vartheta)\;\Lambda_8U_{1,3}(\vartheta)=\Lambda_8$$
$$U_{0,2}^{-1}(\phi)\;\Lambda_8U_{0,2}(\phi)=\Lambda_8$$
$$U_{1,2}^{-1}(\varsigma)\;\Lambda_8U_{1,2}(\varsigma)=\Lambda_8$$
$$U_{0,3}^{-1}(\iota)\;\Lambda_8U_{0,3}(\iota)=\Lambda_8$$
$$\widehat{U}^{-1}(\kappa)\;\Lambda_8\widehat{U}(\kappa)=\Lambda_8$$

then for every product U of $\grave{U}$'s elements real functions $G_s^r(t,x_1,x_2,x_3)$ exist such that

$$U^{-1}(\partial_s U)=\frac{g_3}{2}\sum_{r=1}^{8}\Lambda_r G_s^r$$

with some real constant g_3 (similar to 8 gluons).

4 Conclusion

Therefore, unessential restrictions on 4X1 matrix functions give Dirac's equations, and it seems that some gluon and gravity phenomena can be explained with the help of these equations.

Submitted on February 16, 2009 / Accepted on February 18, 2009

References

1. Madelung E. Die Mathematischen Hilfsmittel des Physikers. Springer Verlag, 1957, 29.
2. Ziman J.M. Elements of advanced quantum theory. Cambridge University Press, 1969, formula (6.59).

Key Notes on a Geometric Theory of Fields

Ulrich E. Bruchholz

Schillerstrasse 36, D-04808 Wurzen, Germany
http://www.bruchholz-acoustics.de

The role of potentials and sources in electromagnetic and gravitational fields is investigated. A critical analysis leads to the result that sources have to be replaced by integration constants. The existence of spatial boundaries gives reasons for this step. Potentials gain physical relevance first with it. The common view, that fields are "generated" by sources, appears as not tenable. Fields do exist by their own. These insights as well as results from numerical simulations force the conclusion that a Riemannian-geometrical background of electromagnetism and even quantum phenomena cannot be excluded. Nature could differ from abstract geometry in a way that distances and intervals never become infinitesimally small.

1 Introduction

In Physics a unified theory including all phenomena of nature is considered as the greatest challenge. All attempts founded on the present definition of matter have manifested to fail. It will require a redefinition of this term.

The traditional view consists on the assumption that matter "generates" fields. All effort aims at the description of this matter, detached from fields, at least from gravitation. This single-edged view led to the known problems and cannot bring more than stagnation. One had to unify different *methods* being used for handling of different physical situations. Also new mathematical procedures cannot help to master this unsolvable problem.

The traditional mathematical description puts the matter on the right-hand-side of partial differential equations, while the left-hand-side contains differential terms of the field quantities. However, practice demonstrates that only field quantities are measurable, never any form of matter terms. If we consider the practice impartially, the right-hand-sides of the field equations have to become zero. That means, there are no sources of fields.

There are severe caveats in physics against this conclusion. However, it will be demonstrated that any infinities like singular points are physically irrelevant. Connecting electromagnetism to gravitation without obstacles is only possible avoiding sources.

In this paper, solutions of known linear field equations (electromagnetism and gravitation) with and without sources are compared, in which, integration constants from source-free equations take the role of sources. Mass, spin, charge, magnetic momentum are first integration constants. The nonlinear case will validate the linear basic approach. Boundaries, introduced to solve linear source-free equations, reveal to be geometric limits in the space-time, described by nonlinear equations. This fact makes any artifacts unnecessary. The theory can be managed with exclusively classical mathematical methods.

These insights are not familiar in physics, because the present standard is the Quantum Field Theory [1, 2], in which the most known part, the Standard Model, is told to be very successful and precise [3, 4]. The existence of subatomic particles has been deduced from scattering experiments [3]. The field term, used in these theories, differs considerably from the classical field term. Actually, these theories are founded on building block models which more seem to aim at a phenomenology of a "particle zoo" than a description of nature based on first principles. In order to describe the interactions between particles respectively sub-particles, it needs the introduction of virtual particles like the Higgs, which have not been experimentally verified to date.* By principle, the subatomic particles cannot be observed directly. — Are the limits of classical methods really so narrow, that they would justify these less strict methods of natural philosophy?

The mathematical methods are more and more advanced (for example introducing several "gauge fields") according to the requirements by the building block models. However, these methods approach to limits [3, 4]. Gravitation must be handled external to the model and appears as an external force. The deeper reason is that the standard model is based on Special Relativity while gravitation is the principal item of General Relativity. These differences are inherent and do not lead to a comprehensive model which reflects the fact that gravitation and electromagnetism have analogous properties. Pursuing theories like string theory (quoted by [4]) do not really close this gap. Any predictions or conjectures are not validated, as demonstrated for example in [6].

The central question of modern physics is: How to quantize field theory? [4] In view of the looming limits, another question is proposed instead: Which quantities have discrete values? — In order to answer this alternative question, we

*Manfred Geilhaupt claims to "provide" a kind of "Higgs field" in his theory, called GR+QTD (General Relativity + Quantum Thermodynamics) by him [5]. It were a step beyond virtual particles "because they possess restmass itself due to TD principles. Second it also seems to be obvious that the fine structure constant of space fundamentally can be derived by GR but not without precursor extended by QTD" [5].

have to go back to the roots. That are Maxwell's theory and General Theory of Relativity as Einstein himself taught in his Four Lectures [7]. The simple approach of these basics should be a specific benefit, and a low standard by no means. We have to take notice of any proportions of forces (how extreme these may ever be), and to accept the direct consequences like the non-existence of sources (as explained in this paper) and the non-applicability of building block models. *We have to compare not forces but the fields with respect to metrics.*[*] The following lines will make General Relativity provide the basis which can describe all real forces of nature.

2 Electromagnetism

As known, electromagnetic fields in the vacuum can be described by Maxwell's equations, with tensor notation[†]

$$F_{ij,k} + F_{jk,i} + F_{ki,j} = 0\,, \tag{1}$$

$$F^{ia}{}_{;a} = S^i \tag{2}$$

where $\mathcal{S}$ is the vector of source terms. With Eq. (1), the field tensor is identically representable from a vector potential $\mathcal{A}$ with

$$F_{ik} = A_{i,k} - A_{k,i}\,. \tag{3}$$

The six independent components of the field tensor are reduced to four components of the vector potential. These four components can be put in the four equations (2).

If one changes the vector potential for the gradient of an arbitrary scalar

$$A_i \Longrightarrow A_i + \psi_{,i}\,, \tag{4}$$

field tensor and source $\mathcal{S}$ (currents and charges) do not change. These quantities are told to be gauge-invariant [9][‡].

The vector potential has been introduced to solve equations (2). It is at first an auxiliary quantity. Reasons for possible physical relevance are mentioned later. However, the Aharonov-Bohm effect (for example) does not give evidence for the physical relevance of vector potential and gauge, as Bruhn [10] demonstrated.

2.1 The Poisson equation

In order to get more close solutions, one can apply the Lorenz convention (see [9])

$$A^i{}_{;i} = 0\,. \tag{5}$$

One may not confuse the Lorenz convention with a gauge, because it is an *arbitrary* condition.[§] *This condition could reduce the possible set of solutions.*

Simplified equations result with Cartesian coordinates

$$\Box\mathcal{A} = -\mathcal{S}\,, \tag{6}$$

with the retarded potential

$$\mathcal{A} = \frac{1}{4\pi}\int \frac{\mathcal{S}(\mathbf{r}_0, ct - |\mathbf{r}-\mathbf{r}_0|)}{|\mathbf{r}-\mathbf{r}_0|}\,\mathrm{d}V_0 \tag{7}$$

as solution (without spatial boundaries).

Time-independent solutions

$$\mathcal{A} = \frac{1}{4\pi}\int \frac{\mathcal{S}(\mathbf{r}_0)}{|\mathbf{r}-\mathbf{r}_0|}\,\mathrm{d}V_0 \tag{8}$$

can be decomposed into several multipoles. As well, the term $1/|\mathbf{r}-\mathbf{r}_0|$ is developed in series. The vector potential results in

$$\mathcal{A} = \frac{1}{4\pi}\sum_{i=0}^{\infty}\frac{1}{r^{i+1}}\int {r_0}^i\,\mathsf{P}_i\left(\frac{\mathbf{r}\cdot\mathbf{r}_0}{r\,r_0}\right)\cdot\mathcal{S}(\mathbf{r}_0)\,\mathrm{d}V_0 \tag{9}$$

with $r = |\mathbf{r}|$, $r_0 = |\mathbf{r}_0|$. P_i are Legendre's polynoms (Wunsch [11]).

Introducing spherical coordinates with

$$x = r\sin\vartheta\sin\varphi\,,\ y = r\sin\vartheta\cos\varphi\,,\ z = r\cos\vartheta\,, \tag{10}$$

in which

$$x^1 = r\,,\ x^2 = \vartheta\,,\ x^3 = \varphi\,,\ x^4 = \mathsf{j}ct \tag{11}$$

(with $\mathsf{j}^2 = -1$), the argument is

$$\frac{\mathbf{r}\cdot\mathbf{r}_0}{r\,r_0} = \sin\vartheta\sin\vartheta_0\cos(\varphi-\varphi_0)\ +\ \cos\vartheta\cos\vartheta_0\,. \tag{12}$$

By this, the fixed volume integrals become functions of ϑ and φ. Rotationally symmetric ansatzes

$$\rho(r_0, \vartheta_0, \varphi_0) = \rho(r_0, \vartheta_0) \tag{13}$$

(charge density), and[¶]

$$J_\varphi(r_0, \vartheta_0, \varphi_0) = J_\varphi(r_0, \vartheta_0, \varphi)\cdot\cos(\varphi-\varphi_0) \tag{14}$$

(current density) lead to momenta that will be compared with the solutions from wave equations. The calculation of the first momenta, i.e. charge and magnetic momentum, is demonstrated in [12]. As well, the charge follows directly as a first approximation of the volume integral from Eq. (8). The magnetic momentum is calculated with a current loop model, see [12].

2.2 The wave equation

The wave equation follows from the Poisson equation if the sources vanish, i.e.

$$\Box\mathcal{A} = 0\,. \tag{15}$$

[*] See more Section 6.1

[†] The tensor equations have been normalized, see Kästner [8] and appendix.

[‡] Bruhn explains these basics with traditional notation.

[§] This condition is mostly met, but it is not ensured.

[¶] Condition (14) excludes the existence of magnetic monopoles.

2.2.1 The plane wave

A known solution is the plane wave, for propagation in direction of x^1 (with Cartesian coordinates, without gravitation)

$$A_2 = A_2(ct - x^1)\,. \tag{16}$$

One can take A_3 instead of A_2. However, A_1 and A_4 are irrelevant for the Lorenz convention, because this takes

$$A_4{}' = \mathrm{j}A_1{}'\,, \tag{17}$$

in which the apostrophe means the total derivative with respect to $ct - x^1$. The component F_{41} is always zero for that reason, and F_{23} vanishes anyway. It is the reason for the very fact that longitudinal electromagnetic waves (also called scalar waves) do not exist. The Lorenz convention is the prerequisite of the wave equation.

This solution is not physical, and has to be discussed in context with gravitation. A special kind of boundary could make plane waves physical. A possible context with Planck's constant is discussed in [17].

2.2.2 The spherical wave

The central symmetrical ansatz can be written for any scalar potential, and components treated by this means,

$$c^2\,\frac{\partial^2}{\partial r^2}(r\phi) = \frac{\partial^2}{\partial t^2}(r\phi) \tag{18}$$

with the solution

$$r\phi = Z(ct \mp r) \tag{19}$$

(Reichardt [13]), in which only the minus sign might be relevant here.

Transforming to the potential itself becomes problematical at $r = 0$. We shall see that this critical point proves to be physically irrelevant. Aware of this, one could take this solution as element of the retarded potential according to Eq. (7).

A spherical boundary around $r = 0$ does not change this solution at and outside of the boundary, and eliminates the mathematical problem. The solution is linked with the potential of the boundary then.

Since the boundary is part of the field, the question for cause and effect becomes irrelevant.

2.2.3 Time-independent solutions

Static solutions of the wave equation require the existence of spatial boundaries. That may be ideal conductors in electric fields, or hard bodies in sound fields. These problems are known as "marginal-problems" (for example [14, 15]). The values of integration constants in the solutions are linked with the potentials of the boundaries against infinity*. That may grant certain physical relevance to potentials. Of course, the wave equation is valid only out of the boundary. We shall see that regions within close boundaries are physically irrelevant.†

Let us confine the problem to a close boundary around $r = 0$. This restriction allows development of series (see [12, 16]), which were otherwise singular just at this point.

The wave equations for several components become for rotational symmetry with spherical coordinates

$$\frac{\partial^2 A_4}{\partial r^2} + \frac{2}{r}\frac{\partial A_4}{\partial r} + \frac{1}{r^2}\frac{\partial^2 A_4}{\partial \vartheta^2} + \frac{1}{r^2}\frac{\partial A_4}{\partial \vartheta}\cot\vartheta = 0 \tag{20}$$

(electric potential) and

$$\frac{\partial^2 A_3}{\partial r^2} + \frac{1}{r^2}\frac{\partial^2 A_3}{\partial \vartheta^2} - \frac{1}{r^2}\frac{\partial A_3}{\partial \vartheta}\cot\vartheta = 0 \tag{21}$$

(magnetic vector potential). The magnetic vector potential consists of only one component in direction of the azimuth

$$A_3 = A_\varphi\, r\sin\vartheta\,, \tag{22}$$

in which A_φ means the *physical* component.‡

The differently looking equations (20) and (21) follow from coordinate transformation.

Developments of series with ansatzes

$$A_4 = \sum_{i,k} a_{[4]\,i,k}\, r^i \cos^k\vartheta\,,$$

$$A_3 = \sum_{i,k} a_{[3]\,i,k}\, r^i \sin^k\vartheta \tag{23}$$

lead, by means of comparison of the coëfficients, to the performing laws

$$0 = a_{[4]\,i,k}\cdot[i(i+1) - k(k+1)] + a_{[4]\,i,k+2}\cdot(k+1)(k+2)\,,$$

$$0 = a_{[3]\,i,k}\cdot[i(i-1) - k(k-1)] + a_{[3]\,i,k+2}\cdot k(k+2)\,. \tag{24}$$

Physically meaningful are only the cases $i < 0$ and $k \geqslant 0$. With this, the series become

$$\begin{aligned} A_4 &= \frac{a_{[4]\,-1,0}}{r} + \frac{a_{[4]\,-2,1}}{r^2}\cdot\cos\vartheta + \\ &+ \frac{a_{[4]\,-3,2}}{r^3}\cdot\left(-\frac{1}{3} + \cos^2\vartheta\right) + \dots\,, \\ A_\varphi &= \sin\vartheta\cdot\left\{\frac{a_{[3]\,-1,2}}{r^2} + \frac{a_{[3]\,-2,3}}{r^3}\cdot\sin\vartheta + \right. \\ &\left. + \frac{a_{[3]\,-3,4}}{r^4}\cdot\left(-\frac{4}{5} + \sin^2\vartheta\right) + \dots\right\}. \end{aligned} \tag{25}$$

*as long as we have to do with a quasi flat space-time

†Who insists on sources may take these regions as source. Lastly the connection of electromagnetism with gravitation will show, that this step is illogical.

‡On physical components see Kästner [8].

A comparison of these solutions with static solutions of the Poisson equation results for the first integration constants in

$$a_{[4]-1,0} = -\mathrm{j}\,\frac{{\mu_0}^{\frac{1}{2}}\,Q}{4\pi} \tag{26}$$

(charge) and

$$a_{[3]-1,2} = -\,\frac{{\varepsilon_0}^{\frac{1}{2}}\,M}{4\pi} \tag{27}$$

(magnetic momentum).

Integration constants take the role of the sources. In more complex solutions, the $1/r$ field from point charges (for example) is assumed only for a large radius.

3 Gravitation

Another kind of potential can be derived from Einstein's [7] gravitation equations

$$R_{ik} - \frac{1}{2}\,g_{ik}\,R = -\kappa\,T_{ik}\,, \tag{28}$$

or

$$R_{ik} = -\kappa\,(T_{ik} - \frac{1}{2}\,g_{ik}\,T) = -\kappa\,{T_{ik}}^{*} \tag{29}$$

with $T = {T_a}^a$. These equations indicate the relations of the Ricci tensor with energy and momentum components. The Ricci tensor is a purely geometrical quantity of the spacetime. It contains differential terms of metrics components.

One can approximate metrics, with Cartesian coordinates, as

$$g_{ik} = \delta_{(ik)} + \gamma_{(ik)} \quad \text{with} \quad |\gamma_{(ik)}| \ll 1\,. \tag{30}$$

The $\gamma_{(ik)}$ are "physical components" of metrics and have the character of a potential.

The arbitrary conditions

$$0 = \frac{\partial\gamma_{(ia)}}{\partial x^a} - \frac{1}{2}\,\frac{\partial\gamma_{(aa)}}{\partial x^i} \tag{31}$$

may be the analogy of the Lorenz convention. These lead to Poisson equations

$$\Box\gamma_{(ik)} = 2\kappa\,{T_{ik}}^{*}\,, \tag{32}$$

with retarded potentials as solution

$$\gamma_{(ik)} = -\frac{\kappa}{2\pi}\int\frac{{T_{ik}}^{*}(\mathbf{r}_0, ct - |\mathbf{r}-\mathbf{r}_0|)}{|\mathbf{r}-\mathbf{r}_0|}\,\mathrm{d}V_0\,. \tag{33}$$

Using the energy-momentum tensor of the distributed mass

$$T^{ik} = \sigma\,\frac{\mathrm{d}x^i}{\mathrm{d}s}\,\frac{\mathrm{d}x^k}{\mathrm{d}s}\,, \tag{34}$$

in which σ be the mass density, static solutions result approximately in

$$\gamma_{(11)} = \gamma_{(22)} = \gamma_{(33)} = +\frac{\kappa}{4\pi}\int\frac{\sigma(\mathbf{r}_0)}{|\mathbf{r}-\mathbf{r}_0|}\,\mathrm{d}V_0\,, \tag{35}$$

$$\gamma_{(44)} = -\frac{\kappa}{4\pi}\int\frac{\sigma(\mathbf{r}_0)}{|\mathbf{r}-\mathbf{r}_0|}\,\mathrm{d}V_0\,, \tag{36}$$

the rest zero (Einstein [7]). This approximation is not more sufficient for the calculation of the spin.

The actual field quantity might be the curvature vector (Eisenhart [19]) of the world-line described by the test body

$$k^i = \frac{\mathrm{d}x^a}{\mathrm{d}s}\left(\frac{\mathrm{d}x^i}{\mathrm{d}s}\right)_{;a} = \frac{\mathrm{d}^2x^i}{\mathrm{d}s^2} + \left\{\begin{smallmatrix} a & i \\ & b \end{smallmatrix}\right\}\frac{\mathrm{d}x^a}{\mathrm{d}s}\,\frac{\mathrm{d}x^b}{\mathrm{d}s}\,, \tag{37}$$

because it acts as a force to the body by its mass.

With distributed mass, the force density becomes

$$K^i = {T^{ia}}_{;a} = \sigma k^i\,. \tag{38}$$

The force balance* is given only with $\sigma = 0$, unless one uses discrete masses. These are integration constants from $\Box\gamma_{(44)} = 0$. In this case, force balance is obtained with the equations of geodesics [19]

$$k^i = 0\,. \tag{39}$$

The curvature vector also contains accelerated motion, this is the most simple interpretation of the equivalence principle. The equations of geodesics become equations of motion with it.

The wave equations are analogous to those of electromagnetism, that means also analogous series and analogous integration constants (using spherical coordinates)

$$a_{[44]-1,0} = -\,\frac{\kappa\,m}{4\pi} \tag{40}$$

(mass) and

$$a_{[34]-1,2} = \mathrm{j}\,\frac{\kappa\,s}{4\pi c} \tag{41}$$

(spin). The analogy of the current loop is a spinning torus [12]. It must be explicitly pointed out that this model is *not* sufficient to represent the known proportions between mass and spin, or charge and magnetic momentum, respectively. This inconsistency is removed by integration constants.

Another derivation tries to omit boundaries [16], however, it is not supported by numerical simulations. The boundaries will have a direct geometrical meaning.

4 Connection of electromagnetism with gravitation

Electromagnetism can be connected with gravitation via the energy-momentum tensor of the electromagnetic field

$$T_{ik} = F_{ia}{F_k}^a - \frac{1}{4}\,g_{ik}F_{ab}F^{ab}\,, \tag{42}$$

with the force density

$$K^i = {T^{ia}}_{;a} = {F^i}_a S^a\,. \tag{43}$$

*Respectively energy conservation, mathematically expressed with the Bianchi identities [19] in Einstein's equations.

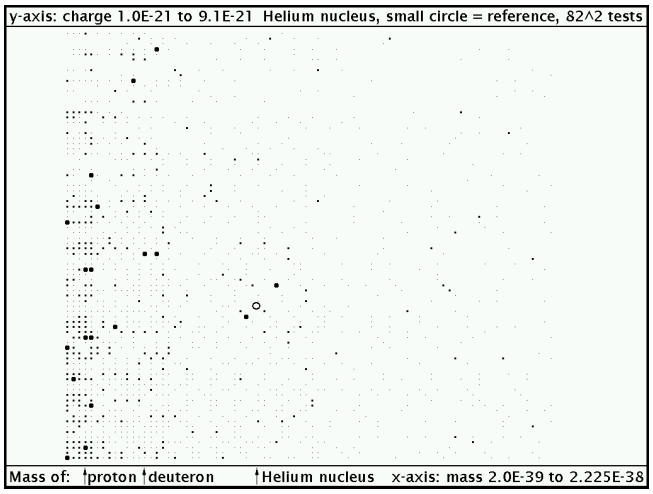

Fig. 1: Tests with parameters around the Helium nucleus

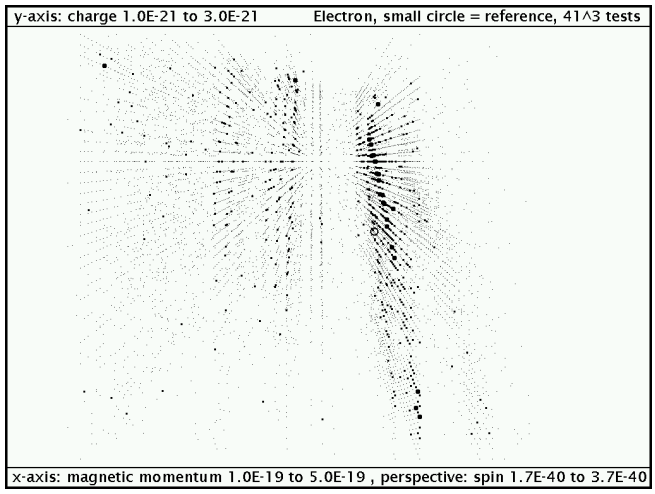

Fig. 2: Tests with parameters around the electron

Force balance is only given with $S^i = 0$. Using this energy-momentum tensor means, there is no choice: The sources *must* vanish, with them the divergences of the field tensor

$$F^{ia}{}_{;a} = 0\,. \tag{44}$$

Einstein stated this already in his Four Lectures [7]. This step is possible, as explained.

The necessity of this energy-momentum tensor to have just this form is also derived by Montesinos and Flores [21] based on Noether's theorem [22], but only without sources.

Numerical simulations according to source-free Einstein-Maxwell equations [18] demonstrate that the areas around possible formal singularities do not exist at all. Also known analytic solutions of Einstein's equations like the isotropic Schwarzschild solution [7], [19] indicate this. The event horizon here is the boundary. In general, a geometric boundary is given when physical components of metrics take an absolute value of 1. It is a kind of horizon in any case. We have to suppose it at the conjectural radius of the particle respectively nucleus, for chaos from the non-linear field equations (see next section).

However, any additional terms or extended methods cannot really repair the inconsistencies from the sources.

For $T = 0$ and $R = 0$, Einstein's equations now result in

$$R_{ik} = \kappa \left(\frac{1}{4}\, g_{ik} F_{ab} F^{ab} - F_{ia} F_k{}^a \right). \tag{45}$$

Equations (1), (44), and (45) involve a special Riemannian geometry of the space-time, as explained in [12] and [20]. The field tensor becomes a curve parameter of the world-lines like the curvature vector.

5 On numerical simulations

The precedingly explained insights are supported by numerical simulations according to equations (3), (44), and (45). Recent robust results can be seen at [23], including the Pascal code of the used program, and a program visualizing these results.

Algorithms and simulation techniques are discussed in [18], as well as the method of approximating the partial differential equations by discrete ones. The principle consists in going from the known (e.g. the distant field of a point charge) to the unknown. In this paper, two visualized samples are shown.

The particle quantities like mass, spin, charge, magnetic momentum are integration constants from mentioned tensor equations, and are inserted as parameters into the initial conditions. The initial conditions start from point charges, or analogous functions for the other integration constants respectively, and are assumed only for great radius.* The non-linearities are absolutely negligible at this place.

The number of iterations during the computation up to terminating the actual test means a degree of stability of the solution, and is marked in the graphs as a more or less fat "point". The reference point (according to literature [24]) is displayed as small circle.

In tests only with mass and charge (remaining parameters zero), masses of preferably small nuclei emerge significantly, together with the right charge at the Helium nucleus, Figure 1.† Unfortunately, the procedure is too inaccurate for the electron mass. In return, the other parameters emerge very significantly, see Figure 2.

Above mentioned stability could have to do with chaos. The author had to take notice of the fact, that the numerical solutions are fundamentally different from analytic solutions. Any singularities from analytic solutions are always replaced by boundaries, which can be interpreted as geometrical limits.

The non-linear equations (which behave chaotically) lead

*Concrete initial conditions see [23], also [18].

†The masses of proton and deuteron are in a sense an add-on of the Helium nucleus tests.

always to these geometrical boundaries, which are 1) finite and 2) outside of possible singular points. Areas with singular points do not exist, i.e. are irrelevant.

One could understand this fundamental contrast by the fact that the differences in time and length are never made zero in a numerical way. The results, exclusively achieved this way, support the view that one has to assume a discrete space-time that does not give reasons for action at a distance. The continuum is only defined with action from point to point, independently on distance or interval between adjacent points.

In order to correctly depict nature, it is apparently necessary to take into consideration the deviations, appearing during the calculation with finite differences. In nature apparently these deviations do not vanish with the transition to very small differences.

Konrad Zuse asked the question, if the possibility to arbitrarily subdivide quantities is "conceivable at all" in nature [25]. Common imagination of a consequent quantization leads to the problem of privileged coordinates, or a privileged frame [25]. Nature has never indicated it. However, it is successful practice in electrical engineering to adapt the coordinates to the actual problem (Wunsch [11]). Linear equations showed to be insensitive to the selection of coordinates. It requires intense research work to prove the chaotic behaviour of the non-linear equations dependent on the coordinates. The author was so fortunate to see the mentioned correlations with spherical coordinates. As well, the correlations became highly significant when the raster distances were the same tangentially as well as radially ($\mathrm{d}r = r\ \mathrm{d}\vartheta$) just at the conjectural particle radius.

6 Concluding remarks

If the obtained insights are right, all quantum phenomena should be understandable by them. At this place, tunnel effects are mentioned. This example is supplemented with very brief but essential remarks on causality.

6.1 On tunnel effects

Equations (1), (44), and (45) allow structures, in which a finite distance (as the outer observer sees it) can locally become zero, but metrics does not become singular. That were a real tunnel with an "inner" length of zero. An event at the one side is "instantaneously" seen at the other side. A known effect, that could be interpreted this way, is the EPR effect [26, 27]. Such tunnels might arise by accident.*

This view is supported with changes of metrics by electromagnetism. Distances are locally shortened (at electric fields in direction of the field strength), what can lead to a feedback. Trump and van de Graaf have measured the flashover in the vacuum, dependent on the distance of the electrodes (Kapcov [28]). As well, the product of voltage and field strength was nearly constant

$$U \cdot E \approx 10^{13}\mathrm{V}^2\ \mathrm{m}^{-1}\,. \tag{46}$$

That means

$$\frac{\partial g_{11}}{\partial r} \approx -2\times10^{-41}\ \mathrm{m}^{-1}\,. \tag{47}$$

One will not see these tiny changes, but they are apparently enough to release lightning etc.

On the whole, the influence of gravitation prevails, so that the space-time is macroscopically stable. Table 1 shows the arithmetical deviations of metrics at a radius of 10^{-15} m, that is roughly the conjectural radius of nuclei.

	proton	free electron
$\gamma_{(11)}(-\gamma_{(44)})$ from mass	2.48×10^{-39}	1.30×10^{-42}
$\gamma_{(11)}$ from charge	-1.85×10^{-42}	-1.85×10^{-42}
$\gamma_{(34)}$ from spin	$\mathrm{j}\,2.60\times10^{-40}$	$\mathrm{j}\,2.60\times10^{-40}$
$\gamma_{(34)}$ from charge times magn. momentum	$-\mathrm{j}\,5.57\times10^{-43}$	$-\mathrm{j}\,3.6\times10^{-40}$
$\gamma_{(33)}$ from magn. momentum (ambiguous)	-1.64×10^{-43}	-6.84×10^{-38}

Table 1: The arithmetical deviations of metrics at 10^{-15} m.

The influence by mass decreases with $1/r$, however, that by charge and spin with $1/r^2$, and that by magnetic momentum with $1/r^4$.

6.2 On causality

Firstly, equations (3), (44), and (45) provide 10 independent equations for 14 components g_{ik} , A_i . With it, causality is not given in principle. It is false to claim, a geometric approach would imply causality. Geometry has nothing to do with causality, because causality has not been geometrically defined at all.

If we see something causal, it comes from approximations by wave equations, as precedingly explained. These provide close solutions.

Appendix

"Classical" electric and magnetic fields in the vacuum are joined to an antisymmetric tensor of 2nd rank

$$\mathcal{D} = \varepsilon_0\mathcal{E} = \mathrm{j}\mu_0{}^{-\frac{1}{2}} \begin{pmatrix} F_{(14)} \\ F_{(24)} \\ F_{(34)} \end{pmatrix}\,,$$

$$\mathcal{B} = \mu_0\mathcal{H} = \varepsilon_0{}^{-\frac{1}{2}} \begin{pmatrix} F_{(23)} \\ F_{(31)} \\ F_{(12)} \end{pmatrix}\,. \tag{48}$$

*See also the joke with Mozart's Fortieth symphony by Nimtz.

Current density and charge density result in a source vector $\mathcal{S}$

$$\mathcal{J} = c\mu_0{}^{-\frac{1}{2}} \begin{pmatrix} S_{(1)} \\ S_{(2)} \\ S_{(3)} \end{pmatrix}, \qquad \rho = -\mathrm{j}\mu_0{}^{-\frac{1}{2}} S_{(4)}\,. \tag{49}$$

The indices in parentheses stand for physical components. See also Kästner [8].

Acknowledgement

The author owes interesting, partly controversy discussions, throwing light upon, to a circle with the gentlemen Prof. Manfred Geilhaupt, Wegberg (Germany), Dr. Gerhard Herres, Paderborn (Germany), and the psychologist Werner Mikus, Köln (Cologne, Germany). Special thanks are due to Prof. Arkadiusz Jadczyk, Castelsarrasin (France), who accompanied the article with critical questions and valuable hints, and Dr. Horst Eckardt, München (Munich, Germany), who carefully looked over this paper.

Submitted on February 19, 2009 / Accepted on February 23, 2009

References

1. Siegel W. Fields. arXiv: hep-th/9912205.
2. Wilczek F. Quantum field theory. *Review of Modern Physics*, 1999, v. 71, 85–S95; arXiv: hep-th/9803075.
3. Roy D.P. Basic constituents of matter and their interactions — a progress report. arXiv: hep-ph/9912523.
4. 't Hooft G. The conceptual basis of quantum field theory. Lectures given at Institute for Theoretical Physics, Utrecht University, and Spinoza Institute, Utrecht, the Netherlands, 2005, http://www.phys.uu.phys.nl/~thooft/lectures/basisqft.pdf
5. Geilhaupt M. Private information, 2008. See also: Geilhaupt M. and Wilcoxen J. Electron, universe, and the large numbers between. http://www.wbabin.net/physics/mj.pdf
6. Price J.C. et al. Upper limits to submillimetre-range forces from extra space-time dimensions. *Nature*, 2003, v. 421, 922–925.
7. Einstein A. Grundzüge der Relativitätstheorie. (A back-translation from the Four Lectures on Theory of Relativity.) Akademie-Verlag Berlin, Pergamon Press Oxford, Friedrich Vieweg & Sohn Braunschweig, 1969.
8. Kästner S. Vektoren, Tensoren, Spinoren. Akademie-Verlag, Berlin, 1960.
9. Bruhn G.W. Gauge theory of the Maxwell equations. Fachbereich Mathematik der TU Darmstadt, http://www.mathematik.tu-darmstadt.de/~bruhn/Elektrodynamik.html
10. Bruhn G.W. Zur Rolle des magnetischen Vektorpotentials beim Aharonov-Bohm-Effekt. Fachbereich Mathematik der TU Darmstadt, http://www.mathematik.tu-darmstadt.de/~bruhn/Elektrodynamik.html
11. Wunsch G. Theoretische Elektrotechnik. Lectures at Technische Universität Dresden, 1966–1968.
12. Bruchholz U. Zur Berechnung stabiler elektromagnetischer Felder. *Z. elektr. Inform.- u. Energietechnik*, Leipzig, 1980, v. 10, 481–500.
13. Reichardt W. Physikalische Grundlagen der Elektroakustik. Teubner, Leipzig, 1961.
14. Skudrzyk E. Die Grundlagen der Akustik. Wien, 1954.
15. Lenk A. Ausgewählte Kapitel der Akustik. Lectures at Technische Universität Dresden, 1969.
16. Bruchholz U. Berechnung elementarer Felder mit Kontrolle durch die bekannten Teilchengrößen. Experimentelle Technik der Physik, Jena, 1984, v. 32, 377–385.
17. Bruchholz U. Derivation of Planck's constant from Maxwell's electrodynamics. http://bruchholz.psf.net/h-article.pdf; http://UlrichBruchholz.homepage.t-online.de/HomepageClassic01/h-article.pdf
18. An obsolete report is to find at http://bruchholz.psf.net or http://UlrichBruchholz.homepage.t-online.de; See also a German-language textbook, Chapter 4.
19. Eisenhart L.P. Riemannian geometry. Princeton university press, 1949.
20. Bruchholz U. Ricci main directions in an EM vacuum. 2001. Look for improved articles at http://bruchholz.psf.net; http://UlrichBruchholz.homepage.t-online.de
21. Montesinos M. and Flores E. Symmetric energy-momentum tensor in Maxwell, Yang-Mills, and Proca theories obtained using only Noether's theorem. arXiv: hep-th/0602190.
22. Noether E. Invariante Variationsprobleme. *Nachr. d. König. Gesellsch. d. Wiss. zu Göttingen*, *Math-phys. Klasse*, 1918, 235–257 (English translation by M. A. Tavel in: *Transport Theory and Statistical Physics*, 1971, v. 1(3), 183–207; arXiv: physics/0503066).
23. Recent visible data are in the packages http://www.bruchholz-acoustics.de/robust.tar.gz; http://UlrichBruchholz.homepage.t-online.de/HomepageClassic01/robust.tar.bz2
24. The author took the reference values from: Gerthsen Ch. Physik. Springer-Verlag, Berlin-Heidelberg-New York, 1966 (regularly updated lists of the particle numbers are to find at http://pdg.lbl.gov/)
25. Zuse K. Rechnender Raum. *Elektronische Datenverarbeitung*, 1967, v. 8, 336–344; see also ftp://ftp.idsia.ch/pub/juergen/zuse67scan.pdf
26. Einstein A., Podolsky B., and Rosen N. Can quantum-mechanical description of physical reality be considered complete? *Phys. Rev.*, 1935, v. 47, 777–780.
27. Zeilinger A. Von Einstein zum Quantencomputer. *Neue Zürcher Zeitung*, v. 72, Nr. 148 vom 30.06.1999.
28. Kapcov S. Elektrische Vorgänge in Gasen und im Vakuum. Verlag der Wissenschaften, Berlin, 1955.

Numerical Solution of Quantum Cosmological Model Simulating Boson and Fermion Creation

Vic Christianto* and Florentin Smarandache†

*Present address: Institute of Gravitation and Cosmology, PFUR, Moscow, 117198
E-mail: vxianto@yahoo.com, admin@sciprint.org

†Chair of Department of Mathematics, University of New Mexico, Gallup, NM 87301, USA
E-mail: smarand@unm.edu

A numerical solution of Wheeler-De Witt equation for a quantum cosmological model simulating boson and fermion creation in the early Universe evolution is presented. This solution is based on a Wheeler-De Witt equation obtained by Krechet, Fil'chenkov, and Shikin, in the framework of quantum geometrodynamics for a Bianchi-I metric.

1 Introduction

It is generally aserted that in the early stage of Universe evolution, the quantum phase predominated the era. Therefore there are numerous solutions have been found corresponding to the Wheeler-DeWitt equation which governs this phase [2]. In the present paper we present another numerical solution of Wheeler-De Witt equation for a quantum cosmological model simulating boson and fermion creation in the early Universe evolution for a Bianchi-type I metric [1].

The solution is based on Wheeler-De Witt equation for a Bianchi-I metric obtained by Krechet, Fil'chenkov, and Shikin [1], in the framework of quantum geometrodynamics. Albeit the essence of the solution is quite similar from the solution given in [1] using Bessel function, in the present paper we present numerical result using Maxima. For comparison with other solutions of 1-d hydrogen problem, see [3] and [4].

2 Solution of Wheeler-DeWitt equation for boson and fermion creation

In the evolution of the Universe after inflation, a scalar field describing de Sitter vacuum was supposed to decay and its energy is converted into the energy of fermions and heavy vector-particles (the so-called X and Y bosons) [2].

In the framework of quantum geometrodynamics, and for a Bianchi-I metric, the Wheeler-De Witt equation has been obtained by Krechet, Fil'chenkov, and Shikin, which reduces to become (Eq. 23 in [1]):

$$T'' - \frac{2iC}{3\tau}\, T' - (E - V)\, T = 0. \tag{1}$$

where T'' and T' represent second and first differentiation of T with respect to r. The resulting equation appears quite similar to radial 1-dimensional Schrödinger equation for a hydrogen-like atom [3], with the potential energy is given by [1]:

$$U(r) = \frac{\beta}{\tau} + \frac{\varepsilon_o}{\tau^{4/3}}\,, \tag{2}$$

$$E = \frac{8}{3}\,\kappa \left(\frac{\Lambda}{\kappa} - \frac{M^2}{2\lambda} \right) \tag{3}$$

has here a continuous spectrum.

The solution of equation (1) has been presented in [1] based on modified Bessel function. Its interpretation is that in this quantum cosmological model an initial singularity is absent.

As an alternative to the method presented in [1], the numerical solution can be found using Maxima software package, as follows. All solutions are given in terms of E as constant described by (3).

(a) *Condition where* $V = 0$

```
'diff(y,r,2)−E*y−(2*%i*C/3/t)*y=0;   ode2(%o1,y,r);
```
(4)

The result is given by:

$$\mathrm{y{=}K1}\,\sin(\mathrm{a}){+}\mathrm{K2}\,\cos(\mathrm{a})\,, \tag{5}$$

where:

$$\mathrm{a{=}(r/}\sqrt{3})\,\sqrt{-3\mathrm{E}{-}2\mathrm{iC/t}}\,. \tag{6}$$

(b) *Condition where* $V \leqslant 0$

```
'diff(y,r,2)−E*y−(2*%i*C/3/t)*y−(b/t+e/t^4/3)*y=0;
ode2(%o2,y,r);
```
(7)

The result is given by:

$$\mathrm{y{=}K1}\,\sin(\mathrm{d}){+}\mathrm{K2}\,\cos(\mathrm{d})\,, \tag{8}$$

where:

$$\mathrm{d{=}(r/(}\sqrt{3}\,\mathrm{t}^{2/3})\,\sqrt{-3\mathrm{Et}^{4/3}{-}2\mathrm{iCt}^{1/3}{-}3\mathrm{e}{-}3\mathrm{bt}^{1/3}}\,. \tag{9}$$

As a result, the solution given above looks a bit different compared to the solution obtained in [1] based on the modified Bessel function.

3 A few implications

For the purpose of stimulating further discussions, a few implications of the above solution of Wheeler-DeWitt equation (in the form of 1-d Schrödinger equation) are pointed as follows:

(a) Considering that the Schrödinger equation can be used to solve the Casimir effect (see for instance Silva [5], Alvarez & Mazzitelli [6]), therefore one may expect that there exists some effects of Casimir effect in cosmological scale, in a sense that perhaps quite similar to Unruh radiation which can be derived from the Casimir effective temperature. Interestingly, Anosov [7] has pointed out a plausible deep link between Casimir effect and the fine structure constant by virtue of the entropy of coin-tossing problem. However apparently he did not mention yet another plausible link between the Casimir effective temperature and other phenomena at cosmological scale;

(b) Other implication may be related to the Earth scale effects, considering the fact that Schrödinger equation corresponds to the infinite dimensional Hilbert space. In other words one may expect some effects with respect to Earth eigen oscillation spectrum, which is related to the Earth's inner core interior. This is part of gravitational geophysical effects, as discussed by Grishchuk et al. [8]. Furthermore, this effect may correspond to the so-called Love numbers. Other phenomena related to variation to gravitational field is caused by the Earth inner core oscillation, which yields oscillation period $T \sim 3$–7 hours. Interestingly, a recent report by Cahill [9] based on the Optical fibre gravitational wave detector gave result which suggests oscillation period of around 5hours. Cahill concluded that this observed variation can be attributed to Dynamical 3-space. Nonetheless, the Figure 6c in [9] may be attributed to Earth inner core oscillation instead. Of course, further experiment can be done to verify which interpretation is more consistent.

Acknowledgements

One of the authors (VC) wishes to express his gratitude to Profs. A. Yefremov and M. Fil'chenkov for kind hospitality in the Institute of Gravitation and Cosmology, PFUR.

Submitted on February 06, 2009
Accepted on February 23, 2009

References

1. Krechet G., Fil'chenkov M., Shikin G.N. Quantum cosmological model simulating boson and fermion creation as a result of the primordial vacuum decay. *Grav. & Cosmology*, 2005, v. 11, no. 4(44), 373–375.
2. Grib A.A. Quantum vacuum effects in the strong external fields. St. Petersburg, St. Petersburg Univ. Publ., 1994.
3. Wolfram Project. Hydrogen orbital. http://demonstrations.wolfram.com/HydrogenOrbitals
4. Mavromatis H.A. Schrödinger equation solutions for small r and resulting functional relation. *Turkish J. Phys.*, 2001, v. 25, 175–179.
5. Silva P.R. Casimir force: an alternative treatment. arXiv: 0901.0908.
6. Alvarez E., Mazzitelli F.D. Long range Casimir force induced by transverse electromagnetic modes. arXiv: 0901.2641.
7. Anosov. Relation between fundamental constants. Physics Seminar held at Physics Faculty, MSU, Moscow, headed by Prof. Yu. S. Vladimirov, 18 Dec. 2008.
8. Grishchuk L. et al. *Grav. & Cosmology*, 2004, v. 10, no. 1–2.
9. Cahill R. Optical fibre detection of gravitation wave. *Prog. Phys.*, 2007, v. 4.

LETTERS TO PROGRESS IN PHYSICS

LETTERS TO PROGRESS IN PHYSICS

On the Earthly Origin of the Penzias-Wilson Microwave Background

Dmitri Rabounski and Larissa Borissova

E-mail: rabounski@yahoo.com; lborissova@yahoo.com

According to the experimental analysis conducted by P.-M. Robitaille, the 2.7 K microwave background, first detected by Penzias and Wilson, is not of cosmic origin, but originates from the Earth, and is generated by oceanic water. In examining this problem two fields must be considered: (1) the Earth Microwave Background, the EMB, present with the 2.7 K monopole and 3.35 mK dipole components; (2) the weak Intergalactic Microwave Background, the IMB, which is connected to the entire Metagalaxy. This conclusion meets our theoretical considerations. First, the field density of the EMB, being inversely proportional to the field volume, should decrease with the cube of the distance from the Earth's surface, while its dipole anisotropy, which is due to the motion of the entire field in common with the Earth, is independent from altitude. Therefore, the EMB monopole should not be found at the 2nd Lagrange point (1.5 mln km from the Earth), while the dipole anisotropy should remain the same as near the Earth. Second, according to General Relativity, the motion through the IMB in a referred direction manifests the three-dimensional rotation of the entire space of the Metagalaxy.

According to the experimental and observational analysis conducted by Pierre-Marie Robitaille, an expert in magnetic resonance imaging (MRI) [1], the 2.7 K monopole microwave background, first detected by Penzias and Wilson [2], is not of cosmic origin, but of the Earth, and is generated by the hydrogen bonds* in oceanic water.

Robitaille first advanced his concept in an open letter published in *The New York Times* in 2002 [3]. In the years which followed, he provided a detailed explanation in a series of journal publications [4–10].

Rabounski [11] then showed that the anisotropy of the Penzias-Wilson microwave background, observed through the 3.35 mK dipole component†, is due to the rapid motion of the whole field in common with its source, the Earth, with a velocity of 365 ± 18 km/sec through a weak intergalactic foreground, which is assignated to the Metagalaxy as a whole. So the anisotropy of the observed microwave background has a purely relativistic origin.

This conclusion is based on developments in the Special Theory of Relativity [12, 13]. Given a local (moving) inertial reference frame, the clocks of which are synchronized to the "preferred" (resting) intertial reference frame assigned to the Universe as a whole‡, an observer located in this local (moving) reference frame, should register an inverse $\left(1+\frac{\mathrm{v}}{c}\cos\theta\right)$ effect on the *physically observed velocity* of the light signals (photons) assigned to his (moving) reference frame, while the world-invariant of the velocity of light remains unchanged. This effect, directed toward the velocity v of the observer's (moving) reference frame, is manifested in the Tangherlini transformations in the Special Theory of Relativity [12, 13].

We assume that the photon source of an earthly microwave background moves in common the field's source, the Earth, with the velocity $\mathrm{v} = 365 \pm 18$ km/sec relative to the weak intergalactic microwave background, assigned to the Metagalaxy. In this case, according to the Tangherlini transformations, the spherical distribution of the velocities of the earthly origin microwave signals, being registered from the Earth or in an Earth-connected reference frame (such as the reference frame of a space mission moving in common with the Earth) should experience an anisotropy in the direction of the motion with respect to the weak intergalactic background. At the same time, the world-invariant of the velocity of light remains unchanged. Also, the distribution is still spherical if observed from the vewpoint of an observer connected to the Metagalaxy's background (i.e. in the "preferred" reference frame, which is resting with respect to the Metagalaxy as a whole). This anisotropic effect has the same formulation in temperature, $T = T_0/\left(1+\frac{\mathrm{v}}{c}\cos\theta\right)$, as the Doppler-effect, despite being generated by a different cause. We therefore refer to this effect as the *Doppler-like anisotropy*. Assume that the source of the earthly origin microwave photons, the Earth, moves through the weak intergalactic background with

*The vibration of a hydrogen atom in water weakly linked to an oxygen atom on another molecule.

†The 3.35 mK dipole (anisotropic) component of the Penzias-Wilson microwave background was first observed in 1969 by Conklin [14] in a ground-based observation. Then it was studied by Henry [15], Corey [16], and also Smoot, Gorenstein, and Muller (the latest team organized a stratosphere observation on board of a U2 aeroplane [17]). The history of the discovery and all the observations is given in detail in Lineweaver's paper of 1996 [18]. The weak anisotropic intergalactic field was found later, in the COBE space mission then verified by the WMAP space mission [19–23].

‡Such a synchronization can be done due to the "light-spot synchronization", which is by means of a phase-speed light spot, or due to the so-called "external synchronization". See [12, 13] or any encyclopaedic source, explaining the Tangherlini trasformations, for detail.

$\mathrm{v} = 365 \pm 18$ km/sec. We calculate the relative deviation of the temperature in the Earth's microwave background which is expected, due to the anisotropy, to be observed by an Earth-connected observer

$$\frac{\Delta T_{cal}}{T_{cal}} = \frac{\mathrm{v}}{c} = 0.122\,\% \pm 0.006\,\% .$$

According to the observations on board of the COBE satellite, the temperature of the Penzias-Wilson microwave background measured from the monopole component of it, is $T_{exp} = 2.730 \pm 0.001$ K. The dipole anisotropy, registered by the COBE satellite, is 3.353 ± 0.024 mK. The WMAP satellite gives approximately the same: 3.346 ± 0.017 mK. The anisotropic direction, in the Galactic longitude l and latitude b, is: $l = 264.26^\circ \pm 0.33^\circ$, $b = 48.22^\circ \pm 0.13^\circ$ as measured by COBE, a result confirmed by WMAP, $l = 263.85^\circ \pm 0.1^\circ$, $b = 48.25^\circ \pm 0.04^\circ$ [23]. So, the experimentally registered relative deviation of the temperature of the microwave background in the direction of the anisotropy is

$$\frac{\Delta T_{exp}}{T_{exp}} = 0.123\,\% \pm 0.001\,\%,$$

which is small number, but is significantly not zero due to the high precision of measurement. This is a systematic deviation with many years of observation.

In addition to this result, COBE initially registered a systematical deviation between the temperature of the monopole component of the microwave background, 2.730 ± 0.001 K, obtained by the direct measurements, and the temperature of the monopole 2.717 ± 0.003 K obtained from the 1st derivative of the monopole [24] (the 1st derivative was interpreted as the actual dipole component of the field). The average deviation $\Delta T_{exp} = 0.013 \pm 0.003$ K between these two results is a small number but is significantly not zero (this is due to the high precision of measurement). Thus, we obtain a minimal relative deviation between the temperature of the Penzias-Wilson microwave background from the monopole and from the 1st derivative of the monopole

$$\frac{\Delta T_{exp}}{T_{exp}} = 0.33\% \text{ at } 1\sigma, \qquad \frac{\Delta T_{exp}}{T_{exp}} = 0.18\,\% \text{ at } 2\sigma.$$

The aforementioned experimental results meet our theoretical calculation, $0.122\% \pm 0.006\%$. Therefore, our suggestion of the relativistic lowering of the temperature of the Penzias-Wilson microwave background due to the Doppler-like anisotropic effect on it [11], is in good agreement with that observed in the COBE and WMAP space missions.

With these, we have to suggest a model, in the framework of which two fields are under consideration (this classification meets the scenario suggested by Robitaille in [7]):

a). The Earth Microwave Background, the EMB, present with the 2.7 K monopole component and 3.35 mK dipole component. The EMB dipole anisotropy is explained due to the Tangherlini transformations in the Special Theory of Relativity: the spherical distribution of the earthly origin photons assigned to the EMB experiences the Doppler-like anisotropy toward the rapid motion of the Earth, with a velocity of 365 ± 18 km/sec, through the weak intergalactic background associated to the Metagalaxy as a whole (so the weak intergalactic background manifests the "preferred" reference frame connected to the entire Metagalaxy, and resting with respect to it). Such an anisotropy can be observed by an Earth-bound observer and any observer whose reference frame is connected to the Earth (for instance the observers located on board of the COBE satellite or the WMAP satellite), but the distribution of the earthly origin photons remains spherical being registered by an observer whose location is the reference frame resting with respect to the Metagalaxy as a whole;

b). A weak Intergalactic Microwave Background (IMB) exists. It is associated to the entire Metagalaxy, and is present with its monopole and dipole components. The dipole anisotropy of the IMB is explained due to the Doppler-effect on the IMB photons: the Earth moves through the IMB with a velocity of 365 ± 18 km/sec, so the IMB photons registered by an Earth-bound observer (or any observer who is connected to the reference frame of the Earth such as the observers on board of the COBE satellite or the WMAP satellite) bear different energies/frequencies toward and backward this motion that is manifest as the IMB anisotropy in this direction.

Our further considerations are focused on the additional theoretical proof in support to this conclusion.

Briefly, our theoretical considerations first suggest that, if the Penzias-Wilson microwave background is of earthly origin, it is approximated as a spherical field, distributed from the Earth into the outer space. In such a case, according to both classical and relativistic theory of fields, the density of the EMB is inversely proportional to the field volume

$$\rho \sim \frac{1}{V} \sim \frac{1}{R^3},$$

so it should decrease with the cube of the distance R from the field's sources, which are located on the surface of the Earth. In other word, the density of the EMB should decrease with the cube of the altitude from the Earth's surface. On the other hand, the dipole anisotropy of the EMB, being a purely relativistic effect due to the rapid motion of the field's source, the Earth, through the weak intergalactic field, is independent from altitude.

This conclusion provides an opportunity to simply verify the aforementioned theoretical suggestions. Naturally, if the Penzias-Wilson microwave background is the earthly origin, the monopole component should not be found at large distances from the Earth, while the dipole anisotropy remains the same as near the Earth.

The ground-bound measurements of the Penzias-Wilson

microwave background and the orbital measurements made with the COBE satellite, whose orbit is located at an altitude of 900 km, were obtained very near the oceans which are not point-like sources. Consequently, these observations were unable to manifest changes of the field density with altitude. However the 2nd Lagrange point is located 1.5 mln km from the Earth. It is the position of the WMAP satellite and the planned PLANCK satellite. Unfortunately, WMAP has only differential instruments on board: such an instrument registers only the difference between the number of photons in the channels. WMAP can therefore target measurements of the anisotropy of the field, but is unable to measure the field density. PLANCK is equipped with absolute instruments. Hence PLANCK will be able to measure the field density.

WMAP showed that the anisotropy of the Penzias-Wilson microwave background at the 2nd Lagrange point is the same as that measured by COBE, near the Earth. This agrees with our theory, but can occur if the background is of cosmic origin. Therefore the key probe, *experimentum crucis*, will be PLANCK, which targets the density of the field at the 2nd Lagrange point.

According to our theory, when PLANCK will arrive at the 2nd Lagrange point and start measurements, it shall manifest almost no photons associated to the Penzias-Wilson microwave background (at least a very small number of the photons), which is in very contrast to that was registered in the ground-based observations and in the COBE observations. This result should manifest the earthly origin of the Penzias-Wilson microwave background, and verify both Robitaille's phenomenological analysis and our theoretical considerations.

The second portion of our theory is specific to the General Theory of Relativity. Assume that the space of the Metagalaxy is a pseudo-Riemannian space with spherical geometry. Such a space is the surface of a hypersphere with the radius r (the curvature radius of the space). Now, suppose all the bodies located in the hyperspere's surface, have to travel, commonly, somewhere in a three-dimensional direction on the surface. This refers to the average common motion, because they all experience different motions with resect to each one, having however to travel on the average in the direction. Such an average "drift" of all bodies located in the hypersphere's surface manifests the three-dimensional rotation of the hypersphere. Therefore, in the framework of the views specific to the General Theory of Relativity, the presence of the weak Intergalactic Microwave Background, the IMB, which is associated to the Metagalaxy as a whole, through which the Earth moves, in common with the other space bodies (at different velocities, having however the average common velocity and direction in the space), manifests the three-dimensional rotation of the entire space of the Metagalaxy. The linear velocity of the rotation — the average velocity of all space bodies in the preferred direction, which is obviously different from the velocity 365 ± 18 km/sec specific to the Earth only — should arrive from observational astronomy, and be a world-invariant in the entire space (space-time) of the Metagalaxy.

Submitted on November 21, 2008 / Accepted on December 05, 2008
First published online on December 08, 2008

References

1. Robitaille P.-M. and Berliner L. J. Ultra high field magnetic resonance imaging. Springer, New York, 2006.
2. Penzias A. A. and Wilson R. W. A measurement of excess antenna temperature at 4080 Mc/s. *Astrophysical Journal*, 1965, v. 1, 419–421.
3. Robitaille P.-M. L. The collapse of the Big Bang and the gaseous Sun. *The New York Times*, March 17, 2002, page A10.
4. Robitaille P.-M. WMAP: a radiological analysis. *Progress in Physics*, 2007, v. 1, 3–18.
5. Robitaille P.-M. On the origins of the CMB: insight from the COBE, WMAP and Relikt-1 satellites. *Progress in Physics*, 2007, v. 1, 19–23.
6. Robitaille P.-M. On the Earth Microwave Background: absorption and scattering by the atmosphere. *Progress in Physics*, 2007, v. 3, pages 3–4.
7. Robitaille P.-M. On the nature of the microwave background at the Lagrange 2 Point. Part I. *Progress in Physics*, 2007, v. 4, 74–83.
8. Robitaille P.-M. The Earth Microwave Background (EMB), atmospheric scattering and the generation of isotropy. *Progress in Physics*, 2008, v. 2, 164–165.
9. Robitaille P.-M. Water, hydrogen bonding, and the microwave background. *Progress in Physics*, 2009, v. 1, L5–L8.
10. Robitaille P.-M. Global warming and the microwave background. *Progress in Physics*, 2009, v. 1, L9–L11.
11. Rabounski D. The relativistic effect of the deviation between the CMB temperatures obtained by the COBE satellite. *Progress in Physics*, 2007, v. 1, 19–21.
12. Tangherlini F.R. The velocity of light in uniformly moving frame. PhD Thesis, Stanford Univ., Sept. 1958, 135 pages.
13. Tangherlini F.R. An inroduction to the General Theory of Relativity. *Suppl. Nuovo Cim.*, 1961, Ser. X, v. 20, 1–86.
14. Conklin E. K. Velocity of the Earth with respect to the Cosmic Background Radiation. *Nature*, 1969, v. 222, 971–972.
15. Henry P. S. Isotropy of the 3 K background. *Nature*, 1971, v. 231, 516–518.
16. Corey B. E. and Wilkinson D. T. A measurement of the Cosmic Microwave Background Anisotropy at 19 GHz. *Bulletin of the American Astronomical Society*, 1976, v. 8, 351.
17. Smoot G. F., Gorenstein M. V. and Muller R. A. Detection of anisotropy in the Cosmic Blackbody Radiation. *Physical Review Letters*, 1977, v. 39, 898–901.
18. Lineweaver C.H. The CMB dipole: The most recent measurement and some history. In: *Microwave Background Anisotropies. Proceedings of the XVIth Moriond Astrophysics Meeting*, Les Arcs, Savoie, France, March 16–23, 1996, Gif-sur-Yvette: Editions Frontieres, 1997; see also arXiv: astro-ph/9609034.

19. Smoot G.F., et al. Preliminary results from the COBE differential microwave interferometers: large angular scale isotropy of the Cosmic Microwave Background. *Astrophys. J.*, 1991, v. 371, L1–L5.

20. Boggess N.W., et al. The COBE mission: its design and perfomance two years after launch. *Astrophys. J.*, 1992, v. 397, 420 – 429.

21. Page L., et al. The optical design and characterization of the Microwave Anisotropy Probe. *Astrophysical Journal*, 2003, v. 585, 566 – 586.

22. Bennett C.L., et al. The Microwave Anisotropy Probe mission. *Astrophys. J.*, 2003, v. 583(1), 1–23.

23. Bennett C.L., et al. First-year Wilkinson Microwave Anisotropy Probe (WMAP) observations: preliminary maps and basic results. *Astrophys. J. Suppl. Ser.*, 2003, v. 148(1), 1–27.

24. Fixsen D.J., et al. The Cosmic Microwave Background spectrum from the full COBE FIRAS data set. *Astrophys. J.*, 1996, v. 473, 576–587.

LETTERS TO PROGRESS IN PHYSICS

Water, Hydrogen Bonding, and the Microwave Background

Pierre-Marie Robitaille

Dept. of Radiology, The Ohio State University, 130 Means Hall, 1654 Upham Drive, Columbus, Ohio 43210, USA

E-mail: robitaille.1@osu.edu

In this work, the properties of the water are briefly revisited. Though liquid water has a fleeting structure, it displays an astonishingly stable network of hydrogen bonds. Thus, even as a liquid, water possesses a local lattice with short range order. The presence of hydroxyl (O−H) and hydrogen (H···OH$_2$) bonds within water, indicate that it can simultaneously maintain two separate energy systems. These can be viewed as two very different temperatures. The analysis presented uses results from vibrational spectroscopy, extracting the force constant for the hydrogen bonded dimer. By idealizing this species as a simple diatomic structure, it is shown that hydrogen bonds within water should be able to produce thermal spectra in the far infrared and microwave regions of the electromagnetic spectrum. This simple analysis reveals that the oceans have a physical mechanism at their disposal, which is capable of generating the microwave background.

While water is the best studied molecule on Earth [1], it remains one of the most mysterious. The unusual properties of this solvent are generated by its hydrogen bonding network [1–4]. In the condensed state, these relatively weak bonds (H···OH$_2$) interlink water into a local intermolecular lattice. Conversely, the robust intramolecular hydroxyl bond (O−H) permits water to be treated as a rigid unit. Water, in the solid state, can take up to one dozen possible crystal structures. Through hydrogen bonding, each molecule is incorporated into a structure wherein the oxygen atoms assume tetrahedral coordination as illustrated in Figure 1 [1]. As for the O−H···O bond angle, it deviates only slightly from linearity in ordinary ice, or ice Ih [1; p. 200].

Yet, it is the nature of liquid water which has largely captivated the interest of physical chemists. It has been said that: "the H-bond network of liquid water is, in the average, the same as that of ice" [1; p. 223]. In liquid water, the average tetrahedral geometry of the oxygen is maintained, but at the expense of tremendous dynamic bending of the hydrogen bonds [1; p. 223]. Nonetheless, to a first approximation, and for the purposes of the discussion which is to follow, the average O−H···O bond angle will not be considered to deviate substantially from linear. The energetic dynamic bending of hydrogen bonds will be neglected.

Liquid water has been tenacious in withholding its secrets. Still, scientists have not relented in the study of this universal solvent. Some of our knowledge has come from the study of the simple water dimer [5–9], the gaseous adduct of two molecules linked by a single hydrogen bond (see Figure 2). The structure of the dimer was first elucidated in 1977 by Dyke, Mack, and Muenter [7]. In its most stable form, the water dimer displays a *trans-linear* arrangement [7], where the O−H···O linkage deviates only slightly from a linear configuration. The stability of the *trans-linear* form has been confirmed repeatedly for this adduct, using both experimental and *ab initio* evaluations [5–9]. The energy of its hydrogen bond is ∼5 kcal/mol (∼21 kJ/mol; [6]).

Since the water molecules making up the dimer are somewhat rigid due to their strong hydroxyl bonds (∼119 kcal/mol or ∼497 kJ/mol [10; p. 9–74]), it is possible to treat this adduct as a monomer-monomer system. It is true that the dimer can undergo significant tunneling and rearrangements [5–9], but the resultant conformations do not produce the lowest energy species. As such, one can solely consider the *trans-linear* form [7] and treat each water molecule as a single, rigid unit. Under this scenario, the water dimer can be modeled as a harmonic oscillator [11–12] about the hydrogen bond. Dyke, Mack, and Muenter [7] have determined that the fundamental stretching frequency of the dimer corresponds to ∼143 cm^{-1} [7]. This frequency lies in the far infrared. It might be recalled, for instance, that NASA's COBE FIRAS (Far Infrared Absolute Spectrophotometer) instrument scanned the sky in a frequency range from 2 to 95 cm^{-1} [13].

Given a fundamental frequency at 143 cm^{-1}, it is possible to infer the force constant for the hydrogen bond in the water dimer [11–12]. The reduced mass, μ_r, of the dimer is equal to 1.495×10^{-23} g/molecule: $\mu_r = \frac{18\times18}{36\times(6.02\times10^{23})}$. The fundamental frequency of oscillation is related to the force constant, k, and reduced mass, μ_r, as follows:

$$\omega\ [\mathrm{cm}^{-1}] = \frac{1}{2\pi c}\left(\frac{k}{\mu_r}\right)^{1/2},$$

therefore, the force constant for the dimer corresponds to a very small 0.108×10^{5} dyn/cm. The force constant for the hydroxyl (O−H) bond within each molecule can be obtained from the literature [10]. It corresponds to 8.45 N/cm, which

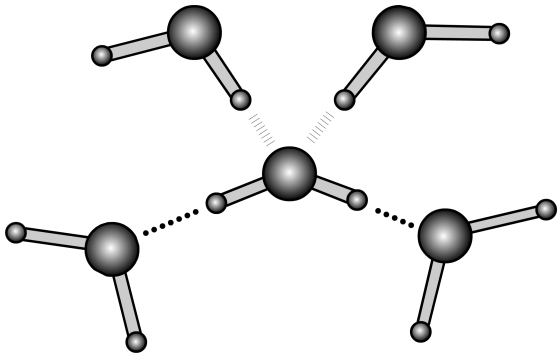

Fig. 1: Schematic representation of the water lattice. Each water molecule acts to accept and donate a total of four hydrogen bonds. Note the essentially linear O−H · · · O subunit.

is equivalent to 8.45×10^5 dyn/cm [10; p. 9–99].

In the ideal case, it should be possible to calculate the energy of each of these systems by considering the expression $E=\frac{1}{2}kx^2$, where k is the force constant and x is the infinitesimal displacement of the fundamental oscillation. The latter will be treated as an undetermined variable for each of these two subsystems.

Within the local water lattice, one can observe that the fundamental subunit of the dimer is also present (see Figure 1). That is, the linear O−H · · · O structure found within the *trans-linear* water dimer is constantly repeated. Indeed, if this were not the case, there would be little interest in studying the water dimer [5–9]. In this configuration, two bonds link every hydrogen atom to the adjacent oxygens (O−H · · · O): the hydrogen bond with a force constant of $\sim0.108\times10^5$ dyn/cm and the hydroxyl linkage with a force constant of $\sim8.45\times10^5$ dyn/cm. Since the grouping is a linear one, the displacement of the hydrogen atom must occur in the line linking the two oxygen atoms. If one isolates the hydrogen bonding system from this short range lattice, its energy will be roughly equal to $E_1=\frac{1}{2}k_1(x_1)^2$. Similarly, the energy for the hydroxyl system will be given by $E_2=\frac{1}{2}k_2(x_2)^2$. Thus, as there is a single hydrogen atom involved in the oscillation, it is immediately clear that $|x_1|=|x_2|$ and to a first approximation, $E_2/E_1=k_2/k_1$.

Water should then be capable of sustaining thermal emissions over two very distinct regions of the electromagnetic spectrum. The first of these regions occurs in the infrared and is generated by the hydroxyl bond. A second thermal emission region exists in the far infrared or microwave region. These emissions are produced by the hydrogen bond. They represent energies which are a factor of about 80 times ($k_2/k_1=78$) lower than the frequencies observed for the hydroxyl bonds. Although knowledge of emission frequencies cannot be easily correlated with temperatures, this result implies that the thermal photons produced by the hydrogen bonding network might be detectable at apparent temperatures which are 80 fold below the real temperatures of the water system.

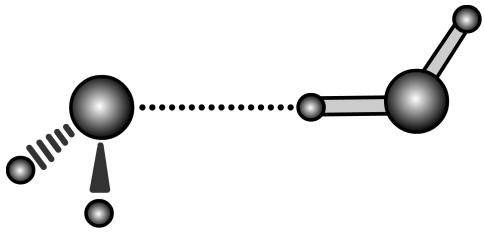

Fig. 2: Schematic representation of the *trans-linear* water dimer. Note the essentially linear O−H · · · O unit.

The thermodynamics of hydrogen bond rearrangements in the liquid phase have recently been examined [14]. This work gives a value of 1.5 ± 0.5 kcal/mol ($\sim$6.3 kJ/mol) for the rearrangement energy. As these energies are directly associated with the formation and breaking of hydrogen bonds, it implies that the true energy of these bonds is closer to 1.5 ± 0.5 kcal/mol in the liquid state, not the 5 kcal/mol obtained from dimer studies [6]. Therefore, the appropriate force constant for the hydrogen bond in liquid water could be nearly 3 fold lower, yielding a ratio of force constants (k_2/k_1) in a range of 80–240. Consequently, the hydrogen bonding system in water could produce a thermal spectrum reporting a temperature which is 80–240 fold lower than the true temperature of the water system.

An analysis of the hydrogen bonding system within water helps to explain how the oceans of the Earth could produce a thermal spectrum with an apparent temperature much lower than their physical temperature [15, 16]. This occurs despite the fact that sea water contains cations and anions [17, 18]. Note that the molar concentration and the physical influence of the salts in sea water (mostly NaCl at ~0.12 M) does not interfere significantly with the H-bonding network of $\sim$110 M hydrogen atoms [17, 18]. For instance, studies of the effects of cations and anions on the water system, tend to utilize ion concentrations which are more than 10 times those found in sea water [17, 18]. It is interesting however, that while the lifetimes of the first excited state for the hydroxyl (O−H · · ·) stretch in liquid water is on the order of $\sim$1 psec, this value increases to $\sim$2.6 psec in the vicinity of chloride ions [19, 20]. Nonetheless, it is unlikely that the presence of ions in the oceans will dramatically alter the conclusions reached herein, even though the presence of ions can produce small changes in the first solvation shell [17, 18].

Maréchal [1; p. 220] illustrates how liquid water displays strong hydroxyl absorption bands at 1644 cm^{-1} (H−O−H bending) and 3400 cm^{-1} (hydrogen bonded O−H stretch). Importantly, the spectra also revealed broad and powerful libration bands (hindered rotations about the hydrogen bond; O · · · H) at $\sim$700 cm^{-1} and hydrogen bond stretches (O · · · H) centered at $\sim$200 cm^{-1} which extend to lower frequencies. Since water is a good absorber in the far infrared, these studies were executed on samples which were only 1-μm thick. Consequently, it would not be unexpected that the supporting matrix and a small sample thickness could alter both the

position and amplitude of the hydrogen bonding stretching and libration bands. The findings reported by Maréchal [1; p. 220] are interesting, but inconclusive as related to the hydrogen bond itself.

Reflecting on the paucity of supportive data, in this very difficult experimental region of the far infrared, it seems that much more needs to be learned about the emissions due to hydrogen bonds in nature. In particular, the lack of a signal specifically assigned to hydrogen bonds from water on Earth gives cause for concern. This is because the microwave background [21] was assigned to the universe [22] when virtually nothing was known about the spectroscopic signature of the hydrogen bond.

Consideration of these findings reveals why the author has advanced [15, 16] that the microwave background [21] does not correspond to an astrophysical signal [22], but instead is generated by the oceans [15, 16, 23]. Water has the means to generate thermal emissions in the far infrared and microwave regions. The fundamental oscillator involved is best represented by the dimer subunit and its associated hydrogen bond within liquid water itself. In the gas phase, the dimer is known to have a fundamental frequency in the far infrared [7], very close to the region sampled by the COBE FIRAS instrument [13]. It is quite reasonable to expect that the emissions from the oceans occur in the same region.

In summary, the microwave background can be understood as follows: photons are being produced by the oceans and they are then scattered in the atmosphere such that a completely isotropic signal is observed [15]. The isotropy of the microwave background was first reported by Penzias and Wilson [21]. The signal is independent of temperature variations on the globe, since the hydrogen bonding energy system is already fully occupied at earthly temperatures. This explains why the microwave background is independent of seasonal changes [21]. Satellite data obtained by COBE strengthen the idea that the Earth does produce the microwave background [24, 25]. This hypothesis has not been refuted either by the three year [26] or five year WMAP findings.

Acknowledgements

The author would like to thank Luc Robitaille for assistance in figure preparation.

Dedication

This work is dedicated to my wife, Patricia.

Submitted on November 21, 2008 / Accepted on December 05, 2008
First published online on December 08, 2008

References

1. Maréchal Y. The hydrogen bond and the water molecule: The physics and chemistry of water, aqueous and bio-media. Elsevier, Amsterdam, 2007.
2. Jeffrey G.A. An introduction to hydrogen bonding. Oxford University Press, Oxford, 1997.
3. Schuster P., Zundel G., Sandorfy C. The hydrogen bond: Recent developments in theory and experiments (vols. 1–3). North-Holland Publishing Company. Amsterdam, 1976.
4. Smith J.D., Cappa C.D., Wilson K.R., Cohen R.C., Geissler P.L., Saykally R.J. Unified description of temperature-dependent hydrogen-bond rearrangements in liquid water. *Proc. Nat. Acad. Sci.*, 2005, v. 102, 14171–14174.
5. Dyke T.R., Muenter J.S. Microwave spectrum and structure of hydrogen bonded water dimer. *J. Chem. Phys.*, 1974, v. 60, 2929–2930.
6. Dyke T.R. Group theoretical classification of the tunneling-rotational energy levels of the water dimer. *J. Chem. Phys.*, 1977, v. 66, 492–497.
7. Dyke T.R., Mack K.M., Muenter J.S. The structure of water dimer from molecular beam electric resonance spectroscopy. *J. Chem. Phys.*, 1977, v. 66, 498–510.
8. Scheiner S. Ab initio studies of hydrogen bonds: The water dimer paradigm. *Ann. Rev. Phys. Chem.*, 1994, v. 45, 23–56.
9. Keutsch F.N., Goldman N., Harker H.A., Leforestier C., Saykally R.J. Complete characterization of the water dimer vibrational ground state and testing the VRT(ASP-W)III, SAPT-5st, and VRT(MCY-5f) surfaces. *Molecular Phys.*, 2003, v. 101, 3477–3492.
10. Lide D.R. CRC handbook of chemistry and physics. CRC Press, Boca Raton, 89th Edition, 2008.
11. Wilson E.B., Decius J.C., Cross P.C. Molecular vibrations: The theory of infrared and raman vibrational spectra. McGraw-Hill Book Company, New York, 1955.
12. Harris D.C., Bertolucci M.D. Symmetry and spectroscopy: An introduction to vibrational and electronic spectroscopy. Oxford University Press, Oxford, 1978.
13. Fixsen D.J., Cheng E.S., Cottingham D.A., Eplee R.E., Isaacman R.B., Mather J.C., Meyer S.S., Noerdlinger P.D., Shafer R.A., Weiss R., Wright E.L., Bennett C.L., Boggess N.W., Kelsall T., Moseley S.H., Silverberg R.F., Smoot G.F., Wilkinson D.T. Cosmic microwave background dipole spectrum measured by the COBE FIRAS instrument. *Astrophys. J.*, 2004, v. 420, 445–449.
14. Smith J.D., Cappa C.D., Wilson K.R., Messer B.M., Cohen R.C., Saykally R.J. Energetics of hydrogen bond network rearrangements in liquid water. *Science*, 2004, v. 306, 851–853.
15. Robitaille P.-M. The Earth microwave background (EMB), atmospheric scattering and the generation of isotropy. *Prog. in Phys.*, 2008, v. 2, 164–165.
16. Robitaille P.-M.L. A radically different point of view on the CMB. In: *Galilean Interviews on Cosmology*, M. D'Onofrio and C. Burigana, eds., Springer, New York, 2009.
17. Cappa C.D., Smith J.D., Messer B.M., Cohen R.C., Saykally R.J. Effects of cations on the hydrogen bond network of liquid water: New results from X-ray absorption spectroscopy of liquid microjets. *J. Phys. Chem. B*, 2006, v. 110, 5301–5309.

18. Smith J.D., Saykally R.J., Geissler P.L. The effects of dissolved halide anions on hydrogen bonding in liquid water. *J. Am. Chem. Soc.*, 2007, v. 129, 13847–13856.

19. Laenen R., Simeonidis K., and Laubereau A. Subpicosecond spectroscopy of liquid water in the infrared: Effect of deuteration on the structural and vibrational dynamics. *J. Phys. Chem. B*, 2002, v. 106, 408–417.

20. Kropman M.F., Bakker H.J. Femtosecond mid-infrared spectroscopy of aqueous solvation shells. *J. Chem. Phys.*, 2001, v. 115, 8942–8948.

21. Penzias A.A., Wilson R.W. A measurement of excess antenna temperature at 4080 Mc/s. *Astrophys. J.*, 1965, v. 1, 419–421.

22. Dicke R.H., Peebles P.J.E., Roll P.G., and Wilkinson D.T. Cosmic black-body radiation. *Astrophys. J.*, 1965, v. 1, 414–419.

23. Rabounski D., Borissova L. On the Earthly origin of the Penzias-Wilson microwave background. *Prog. in Phys.*, 2009, v. 2, L1–L4.

24. Robitaille P.-M. On the Origins of the CMB: Insight from the COBE, WMAP, and Relikt-1 Satellites. *Prog. in Phys.*, 2007, v. 1, 19–23.

25. Rabounski D. The relativistic effect of the deviation between the CMB temperatures obtained by the COBE satellite. *Prog. in Phys.*, 2007, v. 1, 24–26.

26. Robitaille P.-M. WMAP: A radiological analysis. *Prog. in Phys.*, 2007, v. 1, 3–18.

LETTERS TO PROGRESS IN PHYSICS

Global Warming and the Microwave Background

Pierre-Marie Robitaille

Dept. of Radiology, The Ohio State University, 130 Means Hall, 1654 Upham Drive, Columbus, Ohio 43210, USA

E-mail: robitaille.1@osu.edu

In the work, the importance of assigning the microwave background to the Earth is addressed while emphasizing the consequences for global climate change. Climate models can only produce meaningful forecasts when they consider the real magnitude of all radiative processes. The oceans and continents both contribute to terrestrial emissions. However, the extent of oceanic radiation, particularly in the microwave region, raises concerns. This is not only since the globe is covered with water, but because the oceans themselves are likely to be weaker emitters than currently believed. Should the microwave background truly be generated by the oceans of the Earth, our planet would be a much less efficient emitter of radiation in this region of the electromagnetic spectrum. Furthermore, the oceans would appear unable to increase their emissions in the microwave in response to temperature elevation, as predicted by Stefan's law. The results are significant relative to the modeling of global warming.

While controversy exits as to whether or not mankind has been an agent of global climate change, there is little dispute in the scientific community that the Earth is indeed warming [1–4]. Global warming may substantially alter the agricultural capacity and water cycles of our planet with dramatic human ramifications. With this in mind, if global warming is to be both understood and forecasted, climate modeling [5, 6] must be based on proper physical foundations. Through this letter, I wish to highlight that the modeling of the Earth's energy balance [5, 6] requires re-evaluation first of Kirchhoff's law of thermal emission [7–11] and its associated consequences for the application of Stefan's law [12], and second of the assignment of the microwave background [13, 14] to the oceans of the Earth [15, 16].

Regarding Kirchhoff's law [7], it is difficult to conceive that a central pillar of physics could be the subject of concern, both in its experimental formulation [8, 11] and in its theoretical proof [9, 10]. For those who have followed the arguments these past few years [8–11], it seems that a reconsideration of universality in blackbody radiation is in order. In short, there is no universality [9, 10] and each physical system must be treated with individualized care. The generalized application of Stefan's 4th power law [12] is unjustified in the analysis of global warming.

Relative to the microwave background, the reassignment is both unexpected and profound. Ever since its discovery [13] and assignment to the universe in 1965 [14], the microwave background has been considered a cornerstone of modern astrophysics. As such, the attributing of this background to the Earth brings consequences for physics [17]. Nonetheless, the global warming issue is of sufficient importance that its proper modeling [5, 6] should not be delayed by the continued misassignment of the true origin of the microwave background.

At the same time, it remains true that these are complex problems [1–21]. Kirchhoff's law of thermal emission has been in existence for nearly 150 years [7]. To question a fundamental law after many years [8–11] seems contrary to scientific logic, as scientists cannot be expected to verify the tenets of physics before any new advancement can be pursued. In this regard, the incorrect assignment of the microwave background to the universe [14] can be understood, although the accurate determination of temperatures from thermal emission spectra has always required thermal equilibrium with an enclosure [7–11]. This is something which could never be met in a cosmological origin for the microwave background, as I previously stated [18]. In the end, each signal requires a realistic physical origin [8, 9]. For the microwave background, the responsible physical entity will be the weak hydrogen bond between water molecules [15, 17].

With respect to the energy balance of the Earth [5, 6], its elucidation requires the determination of the relationship between absorbed (solar) and emitted (earthly) radiation. Usually, one is concerned with radiation in the infrared. However, substantial contributions can be made in the radio and microwave bands. While these energies are lower, their aggregate sums are non-negligible. Thus, in order to model climate change, the radiation balance of the Earth must be determined as a function of all frequencies from radio through the infrared.

In some climate models [5, 6], the radiation which the Earth emits is deduced by applying Stefan's law [12], at a given effective temperature, thereby treating the globe as a uniform blackbody source. In such an approach, oceanic contributions are undifferentiated from continental radiation. Yet, the thermal emission profiles of solid materials are dramat-

ically different from one another [20]. Few solids, if any, adhere to Stefan's law. Even various forms of graphite [20] differ in their ability to emit radiation as a function of the 4th power of the temperature [12]. Stefan's law simply does not apply to most materials [20] and certainly will not apply to land masses which are covered with extensive vegetation. The thermal emission from liquids, especially water, is even more complicated and much less understood. While Stefan's law might appear to hold over narrow spectral ranges within the infrared, such band-like emissions fall far short of producing the emissive power expected at all frequencies, through the application of the 4th power relationship.

Since there is no universality [8, 9], it is implausible that the Earth can be modeled as emitting at a single effective temperature. The oceans cannot be treated as simple blackbody emitters, producing Planckian thermal spectra reflecting an effective temperature near 300 K [5, 6]. In fact, while water can provide strong emission bands in the infrared, further study will reveal that the entire spectrum is far from blackbody or Planckian at 300 K. This is particularly important in the microwave region.

If the oceans had been able to emit with an effective temperature near 300 K, they would be expected to produce an extensive radiation in the microwave region of the electromagnetic spectrum. In actuality, the oceans mimic a 3K blackbody in this frequency range [13, 15]. The oceans remain powerful emitters of thermal radiation at these frequencies, but much less powerful than would have been predicted if they could be treated as 300 K sources. Note, in this regard, that Stefan's law invokes a 4th power temperature dependence [12]. As a result, the oceans, while still emitting ample radiation in the microwave region [13], are actually poor emitters in this spectral range. This is true, if one compares their actual emission [13] with the emission corresponding to an effective temperature of 300 K [12], as is currently expected. The lower than expected efficiency of the oceans to emit thermal radiation, particularly in the microwave region, appears to have dire consequences for global warming.

It is well known that global warming models invoke negative feedback mechanisms [5, pp.352–354]. The first of these predicts that, as the Earth warms, it becomes an even better emitter of radiation, because the use of Stefan's law [12] now applies a fourth power exponential to an even higher temperature. As a result, the production of even more thermal photons is expected. In practice, approximately 70% of the Earth is covered with water, and its thermal emissions in the microwave regions are not expected to increase in the slightest as a response to temperature elevation. Should the hydrogen bonding system within water actually be the oscillator responsible for the microwave background [15, 21], then this system cannot easily respond to increases in temperature, since the associated energy levels are already full at Earthly temperatures. This explains why the microwave background has always been observed to be independent of seasonal variations. For nearly 70% of the planet, the negative feedback mechanisms, brought by the application of Stefan's law, will not hold, at least in the microwave region of the spectrum.

It is well established that the inability of water bodies to efficiently emit radiation results in considerable retention of thermal energy within oceanic systems. Unable to dissipate heat through emission, the oceans turn to convection currents. This provides a driving force for oceanic currents and for hurricanes. Importantly, the secret to understanding oceanic behavior rests in large part with the microwave background. Its lack of seasonal variation constitutes a key parameter for modelers of global climate change and for the study of oceanic systems.

Given the centrality of global warming to human progress, it may be prudent to fully ascertain the Earth's emission profile, by using an array of satellites which continually monitor spectral emissions from the radio range through the infrared. Such an array, positioned in fixed orbit around the globe should be able to continuously monitor outgoing Earthly emissions. Using a satellite array, it should be possible to observe the ebb and flow of infrared radiation from the Earth in association with the diurnal cycle. In addition, the relative stability of microwave emission will once again be affirmed. Indeed, the latter has already been established long ago, by Penzias and Wilson [13]. Only when such findings are combined with increased direct solar, atmospheric, continental, and oceanic monitoring as a function of depth and global position, will scientists gain the insight required for the accurate analysis of climate change.

Dedication

This work is dedicated to my youngest sister, Mireille.

Submitted on November 21, 2008 / Accepted on December 05, 2008
First published online on December 08, 2008

References

1. Levitus S., Antonov J.I, Wang J., Delworth T.L., Dixon K.W., Broccoli A.J. Anthropogenic warming of Earth's climate system. *Science*, 2007, v. 292, 267–270.
2. Hansen J., Nazarenko L., Ruedy R., Sato M., Willis J., Genio A.D., Koch D., Lacis A., Lo K., Menon S., Novakov T., Perlwitz J., Russell G., Schmidt G.A, Tausnev N. Earth's energy imbalance: confirmation and implications. *Science*, 2005, v. 308, 1431–1435.
3. Levitus S., Antonov J.I., Boyer T.P., Stephens C. Warming of the world ocean. *Science*, 2000, v. 287, 2225–2229.
4. Gregory J.M., Banks H.T., Stott P.A., Lowe J.A., Palmer M.D. Simulated and observed decadal variability in ocean heat content. *Geophys. Res. Letters*, 2004, v. 31, L15312.
5. Kiehl J.T., Ramanathan V. Frontiers of climate modeling. Cambridge University Press, Cambridge, UK, 2006.

6. McGuffie K., Henderson-Sellers A. A climate modeling primer (2nd edition). John Wiley and Sons, New York, 1997.
7. Kirchhoff G. Über den Zusammenhang zwischen Emission und Absorption von Licht und. Wärme. *Monatsberichte der Akademie der Wissenschaften zu Berlin*, sessions of Dec. 1859, 1860, 783–787.
8. Robitaille P.M.L. On the validity of Kirchhoff's law of thermal emission. *IEEE Trans. Plasma Sci.*, 2003, v. 31(6), 1263–1267.
9. Robitaille P.-M. An analysis of universality in blackbody radiation. *Prog. in Phys.*, 2006, v. 2, 22–23.
10. Robitaille P.-M. A critical analysis of universality and Kirchhoff's law: A return to Stewart's law of thermal emission. *Prog. in Phys.*, 2008, v. 3, 30–35.
11. Robitaille P.-M. Blackbody radiation and the carbon particle. *Prog. in Phys.*, 2008, v. 3, 36–55.
12. Stefan J. Über die Beziehung zwischen der Warmestrahlung und der Temperature. *Sitzungsberichte der mathematischnaturwissenschaftlichen Classe der kaiserlichen Akademie der Wissenschaften*, Wien 1879, v. 79, 391–428.
13. Penzias A.A. and Wilson R.W. A measurement of excess antenna temperature at 4080 Mc/s. *Astrophys. J.*, 1965, v. 1, 419–421.
14. Dicke R.H., Peebles P.J.E., Roll P.G., and Wilkinson D.T. Cosmic black-body radiation. *Astrophys. J.*, 1965, v. 1, 414–419.
15. Robitaille P.M. The Earth microwave background (EMB), atmospheric scattering and the generation of isotropy. *Prog. in Phys.*, 2008, v. 2, 164–165.
16. Rabounski D. and Borissova L. On the Earthly origin of the Penzias-Wilson microwave background. *Prog. in Phys.*, 2009, v. 2, L1–L3.
17. Robitaille P.M.L. A radically different point of view on the CMB in: *Galilean Interviews on Cosmology*, M. D'Onofrio and C. Burigana, eds., Springer, New York, 2009.
18. Robitaille P.M.L. The collapse of the Big Bang and the gaseous Sun. *New York Times*, March 17, 2002, page A10 (available online: http://thermalphysics.org/pdf/times.pdf).
19. Robitaille P.M.L. The little heat engine: Heat transfer in solids, liquids, and gases. *Prog. in Phys.*, 2007, v. 4, 25–33.
20. Touloukian Y.S., DeWitt D.P. Thermal radiative properties of nonmetallic solids. Vol. 8 in: *Thermophysical Properties of Matter*, IFI/Plenum, New York, 1972.
21. Robitaille P.M.L. Water, hydrogen bonding and the microwave background. *Prog. in Phys.*, 2009, v. 2, L5–L8.

LETTERS TO PROGRESS IN PHYSICS

On the Upper Limit (Heaviest Element) in the Periodic Table of Elements, and the Periodic Table of Anti-Substances

Albert Khazan

E-mail: albkhazan@gmail.com

On the basis of the method involving equilateral hyperbolas developed by us with reference to the Periodic Table, its Top Limit has been established. It is the last element with atomic mass 411.66 and serial number 155. The great value, according to our calculation, has adjacent hyperbolas whose center is the point (0; 1). With the method, it has been possible to find just one element in the Periodic Table — Rhodium, which does not demand additional calculations involving the definition of the valid axes. Calculations towards updating the charge of a nucleus and the quantity of neutrons in end N-Z part of the diagram by means of the serial number 155 are herein executed. The variant of the Periodic Table of Elements with the eighth period is recommended. On the basis of symmetry, with the application of the Hyperbolic Law in the Periodic Table of Elements, the existence of Anti-Substances is herein indirectly proved.

In the Periodic Table, elements are in a static condition, which until now has not allowed us to reveal the dynamics of their contents in various chemical compounds. The regularity established by us represents equilateral hyperbolas $Y = K/X$, where Y is the content of any element K and X is the molecular mass of compounds taken according to one gram-atom of the defined element. The extreme conditions of the equation are attained when $Y \leqslant 1$, $K \leqslant X$. Mathematically speaking, if, for such hyperbolas, the peak is defined as $\sqrt{K}$, according to the theorem of Lagrange, on the basis of which the calculated factor of scaling ($M = 20.2895$) is applied, it shall allow us to pass from one system of coordinates to another. The square of this number (411.66) is equal to the maximal atomic mass of the last element, which is the crossing point of the valid axis of all hyperbolas whose ordinate is given by $Y = 1$. Its serial number is 155 [1].

Calculations of adjacent hyperbolas of the kind $Y = (X - K)/X$ whose center is the point 0; 1 have a simultaneous effect. Both versions of hyperbolas serve as additions with respect to each other. When in one curve Y decreases, in the second it increases. Each pair of hyperbolas of one element is crossed at the point ($X = 2K$, $Y = 0.5$) through which passes the axis of symmetry. Direct and adjacent hyperbolas of all elements are crossed among themselves. The hyperbolas of the last element are the right boundaries of existence for the compounds, and, at the left, they are bounded by the coordinate axes [2].

As a result of graphical constructions and voluminous calculations, it has been found that in the Periodic Table there is the element rhodium (Rh) to which it is not required to apply theorem Lagrange and the factor of scaling. On the basis of direct tabular data and adjacent hyperbolas, at a point of their crossing (205.811; 0.5), the valid axes which, on the X axis and along the line $Y = 1$, cut apiece with abscissa 411.622, are under construction. The divergence from the data described above is a few thousandths of percent. This fact manifests the validity of our theory [3].

It is thereby proved that the Top Limit of the Periodic Table is the element no. 155 with atomic mass 411.66. At present it is known that no. 118-th has been synthesized — last element of the seventh period (no. 117 does not exist yet). And, the above the serial number suggests that it is somehow difficult for the Table to receive a new element. So, accordingly, in nuclear reactions involving the synthesis of elements nos. 114, 115, 116, and 118, events 60, 24, 9 and 3 have been registered. In the known neutron-proton diagram of the nucleus (nearby 2500) which finishes with the element no. 114, it is seen that, in the end, its quantity of artificial isotopes sharply decreases [4]. To the number of the element with atomic mass 298, scientists have assigned special hopes as here isotopes should possess raised stability [5]. However, with the addition of the nucleus no. 155 to the diagram, a general line of new trends shows that the predicted element no. 114 should have 179 neutrons, instead of 175. Also expected by scientists are the twice-magic nucleus with a charge number 114 and atomic mass 298, which, according to our data, has a lack of 2 protons or, in other words, a surplus of 5 neutrons. The existing disorder in the parameters of the elements is caused by the fact that there enters a more long-living isotope into the table. Therefore the element no. 155 should be a reference point in nuclear reactions. It is necessary to consider it in new quantum theory calculations for the sake of filling the Periodic Table. There are different points of view on the quantity of elements in it: from 120 up to 218 and more. For example, G. Seaborg and V. Goldanskii have suggested adding 8-th and 9-th periods to 50 elements [6, 7]. But in constructing the total dependence of isotopes (more than 2500) on the charge of a nucleus, it is possible to

see that it has the parabolic form, and, in the end, its account goes by the units of the seventh period. It is also necessary to acknowledge that elements with numbers 94–103 have been discovered over the last 20 years, and 104–113–for 40.

In the world, hundreds of variants of the Periodic Table have been created, but no one never has been able to answer the question, whether it has a limit [8, 9]. We, for the first time, have given the parameters of the last element as belonging to the eighth period, the first group, having no. 155 and atomic mass 411.66 [10].

It is necessary to note that while our theory has been considered with reference to the first quadrant, the position of the second branches of equilateral hyperbolas in the third quadrant (where $K > 0$) has not been analyzed. However, it has appeared that they possess similar properties (similar to those in the first quadrant). Here too it is necessary to enter the factor for reduction of coordinate axes by one scale. If now around an imaginary axis we allow the overlapping of the third and the first quadrants, it is possible to see practically the full concurrence of curves, coordinates, and valid axes. However, it concerns only the central part of the hyperbolas, and their edges, observing a direction, fall outside the limits. Hence, here the principle of symmetry does not work. At $K < 0$ it is established, in the second and the fourth quadrants of the hyperbolas, that there is similar regularity which has been established by us for the first and the third quadrants. It is caused by equilateral hyperbolas having equal parameters with respect to the module, but with an opposite sign; namely, being mutually interfaced, they possess identical properties. Therefore, proceeding from the chemical concepts, they can be symmetric only after the change of scale of the X and Y axes. As in the third and fourth quadrants a negative ordinate (a degree of transformation of substance) is not allowable in Nature, we shall analyze only quadrants 1 and 2, in which $K > 0$ and $K < 0$. Here there is a full symmetry: the hyperbolas are congruent and all axes coincide. Hence, the Hyperbolic Law in the Periodic Table shall be applied to the second quadrant. At a positive value of Y, a negative value X, and $K < 0$, it is possible to assert that in it there are substances with a minus sign, i.e., Anti-Substances. Furnished with the analysis above, there arises the opportunity of constructing the Periodic Table of Anti-Substances similar to the one considered above.

Submitted on December 12, 2008 / Accepted on January 23, 2009

References

1. Khazan A. Upper limit in the Periodic System of Elements. *Progress in Physics*, 2007, v. 1, 38.
2. Khazan A. Effect from Hyperbolic law in Periodic Table of Elements. *Progress in Physics*, 2007, v. 2, 83.
3. Khazan A. The rôle of the element Rhodium in the Hyperbolic law of the Periodic Table of Elements. *Progress in Physics*, 2008, v. 3, 56.
4. Brookhaven National Laboratory. Table of Nuclides.
5. Ishhanov B.C. and Kebin E.I. Exotic nuclei. Moscow University Press, Moscow, 2002.
6. Seaborg G.T. and Bloom J.L. The synthetic elements. *Scientific American*, 1969, v. 220(4), 56.
7. Goldanskii V.I. About connections nuclear and chemical physics. *Progress Physical Sciences*, 1976, v. 118, issue 2.
8. Oganesyan Y. Islands of stability. *The World of Science*, March 2005, no. 3.
9. The Periodic Table: Into the 21st Century. D. H. Rouvray and R. B. King (Eds.), Research Studies Press, Baldock (UK).
10. Khazan A. Upper limit of the Periodic Table and synthesis of superheavy elements. *Progress in Physics*, 2007, v. 2, 104.

LETTERS TO PROGRESS IN PHYSICS

Corrections to the Biography of Frank Robert Tangherlini, Published in Progress in Physics, Vol. 1, 2009

Gregory B. Malykin

Inst. of Applied Physics, Russian Acad. of Sciences, Ulianova Str. 46, Nizhni Novgorod 603950, Russia
E-mail: malykin@ufp.appl.sci-nnov.ru

This short letter contains some additional information and actual corrections to the biography of Frank Robert Tangherlini, published by the author of the letter, Gregory B. Malykin, in *Progress in Physics*, v. 1, 2009.

Dear sir,

My recent publication [1] spent on the biography of Frank Robert Tangherlini (on the occasion of his 85th birthday) contained a minor lack of information in the field of mainly his family life, details of his military service during the World War II, and his private communications with some famous physicists of the 20th century. Due to the exceptional courtesy of Prof. Tangherlini who has read my recent paper [1], I would like to improve these, and also add several details, which could be interesting to a reader. Therefore I provide below some extractions from the comments made by Prof. Tangherlini himself on my topic in his private correspondence with me [2].

1. "...Thus: my maternal grandfather did not settle in New York, but in Chelsea, Massachusetts, a suburb of Boston, and later moved to Philadelphia. ... My oldest son Arne died in 1998 at the age of 37. However, he left me a wonderful granddaughter who will turn 18 in August."

2. "...Actually, I was not "set free" of military service, but rather, as with so many other engineering students, I received a "draft deferment", that enables the student to completer his technical education subject to government wishes. However, the engineering program I was enrolled in at Boston College (although it is a Jesuit institution, its name is just Boston College, not Boston Jesuit College) closed down, and I volunteered to be drafted in July 1943. After processing at Fort Devens in Ayer, Massachusetts, I was sent to Fort Benning, Georgia, to receive Basic Training. But I did not stay there a year. I had been placed in the Army Specialized Training Program (ASTP), and after completing my basic training, I along with others was sent to the University of Cincinnati, perhaps in early January of 1944. I completed two quarters of training there, and sometime in May, I arranged to be transferred to the regular ground forces that were preparing to be sent overseas. I received more infantry training in the summer of 1944 in Kentucky, and then volunteered to be sent to Fort Meade, Maryland to be shipped overseas. I was finally sent overseas on the Mauretania, perhaps in September 1944, and it was on board the ship that I met James Barlow and Joe Rhiley, who had been airforce cadets but were transferred to the infantry. After we arrived in Liverpool, we volunteered to join the 101st Airborne Division (only volunteers were in the Airborne, no one was forced to become a paratrooper, even when jumping, if someone didn't want to jump, they were asked to step aside, and let the next man jump; they then had to leave the Airborne). I made five training jumps in Hungerford before being flown over to Mourmelon, France, where we stayed for several weeks, before being sent to Bastogne, Belgium in TRUCKS, becasuse there was not enough time to arrange for a parachute jump. So I never parachuted into combat. If I had, I probably wouldn't be around today writing to you. The Germans had broken through in the Ardennes, and we were sent to halt their taking the key city of Bastogne, which we did. We eventually were surrounded, and the German commander asked our acting commander, Brig. Gen. MacAuliffe to surrender. He replied: nuts!* This became one of the famous stories from the Battle of the Bulge. At the end of the war, sometime late in August, I made another training jump, this time in France. It was part of our training for the so-called "Jump on Tokyo". The training jump took place even though the war had ended. It was the smoothest (and last!) parachute jump I ever made. I should also note that although I was a non-commissioned officer with the equivalent rank of a sergeant, the army designation of my rank was T-4 (i.e. technician 4th grade)."

3. "...I received a bronze medal in American history not world history. Incidentally, I still remember what the competition essay was about: It was about a comparison of Thomas Jefferson with Alexander Hamilton. ... Also, in colleges we do not speak of grade, so Robert F. Kennedy was in the same graduation class as myself, i.e., the class of 1948, but not "grade". I should emphasize that I never met him personally, and indeed only learned he was in my class many years later. I attended 60th reunion of the class of 1948 in June 2008. ... Skipping now to my post-doc training in Naples, I should mention that although Francis Halpern and Susum Okubo were there, Gell-Mann was not there. I think you may

*"Nuts" in the context MacAuliffe used it is not foul language, but rather an expression of contempt or derision as in "nuts to you", or "you must be crazy". It is also slang for testicles, but it was not being used in that sense.

have been confused by my reference to the Gell-Mann-Okubo elementary particle mass relations. ... I did not discuss the superluminal problem with Hermann Weyl, but wrote to him sometime in 1951–1952, but did not save his reply. See a comment he made in the letter I am sending you. Also, I did not discuss the problem with Pauli, although I did attend two colloquia he gave on Heisenberg's theory of elementary particles, the first at Berkeley, and the second at Stanford where I managed to ask him a question about Heisenberg's theory. Earlier, in 1994, while I was at Convair-General Dynamics, I corresponded with Feynman about my theory. Although he was very helpful (regretfully I didn't save his letters to me), he, as with Wentzel and Weyl, did not agree with my superluminal theory, which I eventually put aside after receiving further negative comments while I was at Stanford. as described in the enclosed letter to Fröman. One might say the TT represents an attempt to understand more deeply special relativity and the Lorentz Transformation rather than to replace it. I believe the concept of external synchronization helps enormously in this regard."

4. "...I should emphasize my marathon runs were not in California but in Boston, and on one occasion in New Mexico. I am a very, very slow marathoner. My last Boston Marathon was in 2006, and it took me 8 hrs and 35 minutes. This was an improved statement over my 2001 Boston Marathon which took me 9 hrs and 15 minutes. My first marathon was in 1989 while on sabbatical leave at Harvard, I ran it to celebrate my 65th birthday. It took me 9 hrs and 45 minutes. My best run was in the year I retired, 1994; it took me 7 hrs and 35 minutes."

In conclusion, I thank Frank Robert Tangherlini for his useful corrections to my biographic topic [1], which were emphasized by him in his private letter to me [2] after the topic has been published. I also thank Dr. Dmitri Rabounski, the Editor-in-Chief, for his courtesy agreement to publish the corrections (seem valuable to me), and also Edward G. Malykin who helped me in the preparation of this letter. This work was partly supported by the Council on President's Grants of the Russian Federation for Leading Scientific Schools (project no. NSh. 1931.2008.2).

Submitted on January 28, 2009 / Accepted on February 30, 2009

References

1. Malykin G.B. Frank Robert Tangherlini — the founder of an alternative relativistic kinematic (on the occasion of his 85th birthday). *Progress in Physics*, 2009, v. 1, L9–L14.
2. Tangherlini F.R. Private communication with the author, January 06, 2009.

The Journal on Advanced Studies in Theoretical and Experimental Physics, including Related Themes from Mathematics

PROGRESS IN PHYSICS

A quarterly issue scientific journal, registered with the Library of Congress (DC, USA). This journal is peer reviewed and included in the abstracting and indexing coverage of: Mathematical Reviews and MathSciNet (AMS, USA), DOAJ of Lund University (Sweden), Zentralblatt MATH (Germany), Scientific Commons of the University of St. Gallen (Switzerland), Open-J-Gate (India), Referativnyi Zhurnal VINITI (Russia), etc.

To order printed issues of this journal, contact the Editors. Electronic version of this journal can be downloaded free of charge:
http://www.ptep-online.com
http://www.geocities.com/ptep_online

Postal address

Chair of the Department
of Mathematics and Science,
University of New Mexico,
200 College Road,
Gallup, NM 87301, USA

This journal is powered by LaTeX

A variety of books can be downloaded free from the Digital Library of Science:
http://www.gallup.unm.edu/∼smarandache

ISSN: 1555-5534 (print)
ISSN: 1555-5615 (online)

Standard Address Number: 297-5092
Printed in the United States of America

JULY 2009 **VOLUME 3**

CONTENTS

Information for Authors and Subscribers

Progress in Physics has been created for publications on advanced studies in theoretical and experimental physics, including related themes from mathematics and astronomy. All submitted papers should be professional, in good English, containing a brief review of a problem and obtained results.

All submissions should be designed in LaTeX format using *Progress in Physics* template. This template can be downloaded from *Progress in Physics* home page http://www.ptep-online.com. Abstract and the necessary information about author(s) should be included into the papers. To submit a paper, mail the file(s) to the Editor-in-Chief.

All submitted papers should be as brief as possible. We usually accept brief papers, no larger than 8–10 typeset journal pages. Short articles are preferable. Large papers can be considered in exceptional cases to the section *Special Reports* intended for such publications in the journal. Letters related to the publications in the journal or to the events among the science community can be applied to the section *Letters to Progress in Physics*.

All that has been accepted for the online issue of *Progress in Physics* is printed in the paper version of the journal. To order printed issues, contact the Editors.

This journal is non-commercial, academic edition. It is printed from private donations. (Look for the current author fee in the online version of the journal.)

A New Cosmological Model: Black Hole Universe

Tianxi Zhang

Department of Physics, Alabama A & M University, Normal, Alabama
E-mail: tianxi.zhang@aamu.edu

A new cosmological model called black hole universe is proposed. According to this model, the universe originated from a hot star-like black hole with several solar masses, and gradually grew up through a supermassive black hole with billion solar masses to the present state with hundred billion-trillion solar masses by accreting ambient materials and merging with other black holes. The entire space is structured with infinite layers hierarchically. The innermost three layers are the universe that we are living, the outside called mother universe, and the inside star-like and supermassive black holes called child universes. The outermost layer is infinite in radius and limits to zero for both the mass density and absolute temperature. The relationships among all layers or universes can be connected by the universe family tree. Mathematically, the entire space can be represented as a set of all universes. A black hole universe is a subset of the entire space or a subspace. The child universes are null sets or empty spaces. All layers or universes are governed by the same physics - the Einstein general theory of relativity with the Robertson-walker metric of spacetime - and tend to expand outward physically. The evolution of the space structure is iterative. When one universe expands out, a new similar universe grows up from its inside. The entire life of a universe begins from the birth as a hot star-like or supermassive black hole, passes through the growth and cools down, and expands to the death with infinite large and zero mass density and absolute temperature. The black hole universe model is consistent with the Mach principle, the observations of the universe, and the Einstein general theory of relativity. Its various aspects can be understood with the well-developed physics without any difficulty. The dark energy is not required for the universe to accelerate its expansion. The inflation is not necessary because the black hole universe does not exist the horizon problem.

1 Introduction

In 1929, Edwin Hubble, when he analyzed the light spectra of galaxies, found that light rays from galaxies were all shifted toward the red [1, 2]. The more distant a galaxy is, the greater the light rays are shifted. According to the Doppler's effect, all the galaxies should be generally receding from us. The more distant a galaxy is, the faster it moves away from our Milky Way. This finding implies that our universe is expanding and thus had a beginning or an origin.

To explain the origin and evolution of the universe, Lemaitre [3–4] suggested that the universe began an explosion of a primeval atom. Around two decades later, George Gamow and his collaborators [5–9], when they synthesized elements in an expanding universe, devised the initial primordial fireball or big bang model based on the Lemaitre's superatom idea. To salvage the big bang model from some of its theoretical problems (e.g., flatness, relic particles, and event horizon), Guth [10] proposed the inflationary hypothesis based on the grand unification theory. The big bang model with an inflationary epoch has been widely accepted as the standard cosmological model because this model is the only one that can explain the three fundamental observations: the expansion of the universe, the 2.7°K cosmic microwave background radiation, and the abundances of helium and other light elements [11–15].

Although it has been declared to have successfully explained the three basic observations, the big bang theory is neither simple nor perfect because the explanations of the observations sensitively rely on many adjustable parameters and hypothesis that have not been or may never be tested [16–17]. In addition, the big bang theory has not yet told us a whole story for the origin and evolution of the universe with ninety-eight percent uncertainties of its composition. The past before 10^{-43} seconds, the outside, and the future of the universe are still unknown. As astronomers are able to observe the space deeper and deeper, the big bang theory may meet more and more severe difficulties with new evidences. In fact, that the newly observed distant quasars with a high fraction of heavy elements [18] has already brought the big bang model in a rather difficult situation. Cosmologists have being tried to mend this model for more than several decades. It is time for astronomers to open their minds to think the universe in different ways and develop a new model that is more convinced and competitive.

When the author was reading a paper [19] about the Mach principle and Brans-Dicke theory of gravity to develop his electric redshift mechanism in accord with the five-dimensional fully covariant Kaluza-Klein theory with a scalar field [20], an idea that the universe is a black hole came to his mind [21].

Upon this idea, a new cosmological model called black hole universe is then developed, which is consistent with the fundamental observations of the universe, the Mach principle, and the Einstein general theory of relativity. This new model provides us a simple and reasonable explanation for the origin, evolution, structure, and expansion of the universe. It also gives a better understanding of the 2.7°K cosmic microwave background radiation, the element abundances, and the high fraction of heavy elements in distant known quasars. Especially, the black hole universe model does not require new physics because the matter of the black hole universe would not be too dense and hot. Dark energy is not necessary for the universe to have an acceleration expansion. Inflation is not needed because there does not exist the horizon problem. Monopoles should not be created because it is not hot enough. Comparing to the standard big bang theory, the black hole universe model is more elegant, simple, and complete. The entire space is well structured hierarchically without outside, evolve iteratively forever without beginning and end, is governed by the simple well-developed physics, and does not exist other unable explained difficulties. The author has recently presented this new cosmological model on the 211th AAS meeting hold on January 7–11, 2008 at Austin, Texas [22] and the 213th AAS meeting hold on January 4–8, 2009 at Long Beach, California [23].

This paper gives a detail description of this new cosmological model. We will fully address why the universe behaves like a black hole, where the black hole universe originates from, how the entire space is structured, how the black hole universe evolves, why the black hole universe expands and accelerates, and what physics governs the black hole universe. Next studies will address how to explain the cosmic microwave background radiation, how quasars to form and release huge amount of energy, and how nuclear elements to synthesize, and so on.

2 Black hole universe

According to the Mach principle, the inertia of an object results as the interaction by the rest of the universe. A body experiences an inertial force when it accelerates relative to the center of mass of the entire universe. In short, mass there affects inertia here. In [24], Sciama developed a theoretical model to incorporate the Mach principle and obtained $GM_{\rm EF}/(c^2R_{\rm EF})\sim 1$, where $M_{\rm EF}$ and $R_{\rm EF}$ are the effective mass and radius of the universe (see also [19, 25]). Later on, it was shown by [26] that the Einstein general theory of relativity is fully consistent with the Sciama interpretation of the Mach principle and the relation between the effective mass and radius of the universe should be modified as $2GM_{\rm EF}/(c^2R_{\rm EF})\sim 1$.

According to the observations of the universe, the density of the present universe ρ_0 is about the critical density $\rho_0\sim\rho_c=3H_0^2/(8\pi G)\sim 9\times 10^{-30}\ \mathrm{g/cm^3}$ and the radius of the present universe is about $R_0\sim 13.7$ billion light years (or $\sim 1.3\times 10^{26}$ m). Here $G=6.67\times 10^{-11}\ \mathrm{N\,m^2\,kg^{-2}}$ is the gravitational constant and $H_0\sim 70\ \mathrm{km/s/Mpc}$ is the Hubble constant. Using the observed density (or the Hubble constant) and radius of the present universe, we have the total mass $M_0\sim 8\times 10^{52}$ kg and the mass-radius relation $2GM_0/(c^2R_0)=(H_0R_0/c)^2\sim 1$ for the present universe.

According to the Schwarzschild solution of the Einstein general theory of relativity [27], the radius of a black hole with mass $M_{\rm BH}$ is given by $R_{\rm BH}=2GM_{\rm BH}/c^2$ or by the relation $2GM_{\rm BH}/(c^2R_{\rm BH})=1$. For a black hole with mass equal to the mass of the present universe ($M_{\rm BH}=M_0$), the radius of the black hole should be about the radius of the present universe ($R_{\rm BH}\sim R_0$).

The results described above in terms of the Mach principle, the observations of the universe, and the Einstein general theory of relativity strongly imply that the universe is a Schwarzschild black hole, which is an extremely supermassive fully expanded black hole with a very big size and thus a very low density and temperature. The boundary of the universe is the Schwarzschild absolute event horizon described by

$$\frac{2GM}{c^2R}=1. \tag{1}$$

For convenience, this mass-radius relation (1) is named by Mach M-R relation. The black hole universe does not exist the horizon problem, so that it does not need an inflation epoch.

It is seen from equation (1) that the mass of a black hole including the universe is proportional to its radius ($M\propto R$). For a star-like black hole with 3 solar masses, its radius is about 9 km. For a supermassive black hole with 3 billion solar masses, its radius is about 9×10^9 km. For the present black hole universe with hundred billion-trillion solar masses, its radius is about 10^{23} km. Therefore, modeling the universe as a black hole is supported by the Mach principle, the observations of the universe, and the Einstein general theory of relativity.

The density of a black hole including the black hole universe can be determined as

$$\rho\equiv\frac{M}{V}=\frac{3c^6}{32\pi G^3M^2}=\frac{3c^2}{8\pi GR^2}, \tag{2}$$

i.e., $\rho R^2=\mathrm{constant}$ or $\rho M^2=\mathrm{constant}$. Here, we have used the Mach M-R relation (1) and $V=4\pi R^3/3$. It is seen that the density of a black hole including the black hole universe is inversely proportional to the square of the mass ($\rho\propto M^{-2}$) or to the square of the radius ($\rho\propto R^{-2}$). In other words, the mass of the black hole universe is proportional to its radius.

Figure 1 plots the density of a black hole as a function of its mass in the unit of the solar mass (the solid line) or a function of its radius in the unit of 3 kilometers (the same

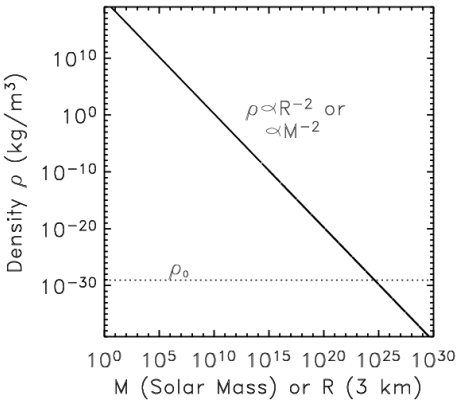

Fig. 1: The density of the black hole universe versus its mass or radius (solid line). The dotted line refers to $\rho = \rho_0$, so that the intersection of the two lines represents the density, radius, and mass of the present universe.

line). The dotted line marks the density of the present universe (ρ_0) and its intersection with the solid line shows the mass (M_0), density (ρ_0), and radius (R_0) of the present universe. Therefore, the black hole universe is not an isolated system because its mass increases as it expands. The density decreases by inversely proportional to the square of the radius (or the mass) of the black hole universe. Considering that matter can enter but cannot exit a black hole, we can suggest that the black hole universe is a semi-open system surrounded by outer space and matter.

In the black hole universe model, we have that the effective radius of the universe is about the actual radius of the universe (or $R_{\mathrm{EF}}/R \sim 1$) at all time. In the big bang theory, we have $R_{\mathrm{EF}}/R = [c^2 R/(2GM)]^{1/2}$ because $\rho R^3 = \mathtt{constant}$. This ratio R_{EF}/R increases as the universe expands and is equal to 1 only at the present time because the observation shows $2GM_0/(c^2 R_0) \sim 1$. In the past, the effective of radius is less than the radius of the universe ($R_{\mathrm{EF}} < R$). While, in future, the effective radius will be greater than the radius of the universe $R_{\mathrm{EF}} > R$, which is not physical, so that the Mach principle will lose its validity in future according to the big bang theory.

3 Origin, structure, and evolution of the black hole universe

In the black hole universe model, it is reasonable to suggest that the universe originated from a star-like black hole. According to the Einstein general theory of relativity, a star, if big enough, can form a star-like black hole when the inside thermonuclear fusion has completed. Once a star-like black hole is formed, an individual spacetime is created. The spacetime inside the event horizon is different from the outside, so that the densities and temperatures on both inside and outside are different. This origin of the universe is somewhat similar to the big bang model, in which the universe exploded from a singular point at the beginning, but the physics is quite different. Here, the star-like black hole with several solar masses (or several kilometers in radius) slowly grows up when it accretes materials from the outside and merges or packs with other black holes, rather than impulsively explodes from nothing to something in the big bang theory. It is also different from the Hoyle model, in which the universe expands due to continuous creation of matter inside the universe [28].

The star-like black hole gradually grows up to be a supermassive black hole as a milestone with billion solar masses and then further grows up to be one like the present universe, which has around hundred billion-trillion solar masses. It is generally believed that the center of an active galaxy exists a massive or supermassive black hole [29–32]. The present universe is still growing up or expanding due to continuously inhaling the matter from the outside called mother or parent universe. The star-like black hole may have a net angular momentum, an inhomogeneous and anisotropic matter distribution, and a net electric charge, etc., but all these effects become small and negligible when it sufficiently grows up.

The present universe is a fully-grown adult universe, which has many child universes such as the star-like and supermassive black holes as observed and one parent (or the mother universe). It may also have sister universes (some universes that are parallel to that we are living), aunt universes, grandmother universes, grand-grandmother universes, etc. based on how vast the entire space is. If the matter in the entire space is finite, then our universe will merge or swallow all the outside matter including its sisters, mother, aunts, grandmothers, and so on, and finally stop its growing. In the same way, our universe will also be finally swallowed by its children and thus die out. If the matter in the entire space is infinite, then the black hole universe will expand to infinitely large in size ($R \to \infty$), and infinitely low in both the mass density ($\rho \to 0$) and absolute temperature ($T \to 0$ K). In this case, the entire space has infinite size and does not have an edge. For completeness, we prefer the entire space to be infinite without boundary and hence without surroundings.

The entire space is structured with infinite layers hierarchically. The innermost three layers as plotted in Figure 2 include the universe that we are living, the outside called mother universe, and the inside star-like and supermassive black holes called child universes. In Figure 2, we have only plotted three child universes and did not plot the sister universes. There should have a number of child universes and may also have many sister universes.

The evolution of the space structure is iterative. In each iteration the matter reconfigures and the universe is renewed rather than a simple repeat or bouncing back. Figure 3 shows a series of sketches for the cartoon of the universe evolution in a single iteration from the present universe to the next similar one. This whole spacetime evolution process does not have the end and the beginning, which is similar to the Hawking's view of the spacetime [33]. As our universe expands,

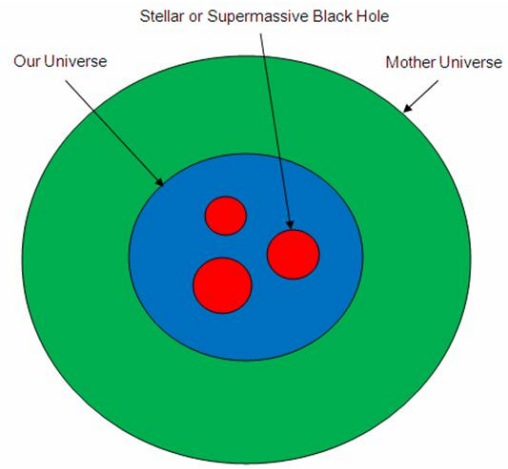

Fig. 2: The innermost three layers of the entire space that is structured hierarchically.

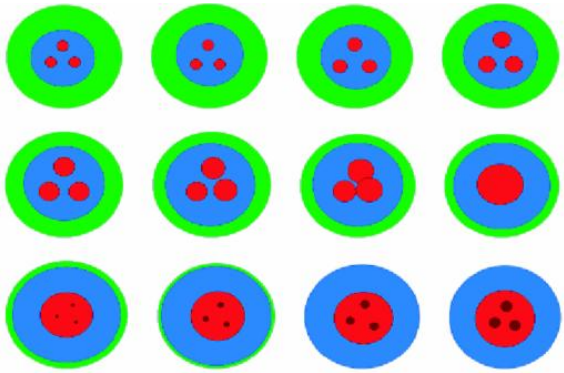

Fig. 3: A series of sketches (or a cartoon, from left to right and then top row to bottom row) for the black hole universe to evolve in a single iteration from the present universe to the next similar one. This is an irreversible process, in which matter and spacetime reconfigure rather than a simple repeat or bouncing back. One universe is expanded to die out and a new universe is born from inside.

the child universes (i.e., the inside star-like and supermassive black holes) grow and merge each other into a new universe. Therefore, when one universe expands out, a new similar universe is born from inside. As like the naturally living things, the universe passes through its own birth, growth, and death process and iterates this process endlessly. Its structure evolves iteratively forever without beginning and end.

To see the multi-layer structure of the space in a larger (or more complicate) view, we plot in Figure 4 the innermost four-layers of the black hole universe up to the grandmother universe. Parallel to the mother universe, there are aunt universes. Parallel to our universe, there are sister universes, which have their own child universes. Here again for simplicity, we have only plotted a few of universes for each layer. If the entire space is finite, then the number of layers is finite. Otherwise, it has infinite layers and the outermost layer corresponds to zero degree in the absolute temperature, zero in the density, and infinite in radius.

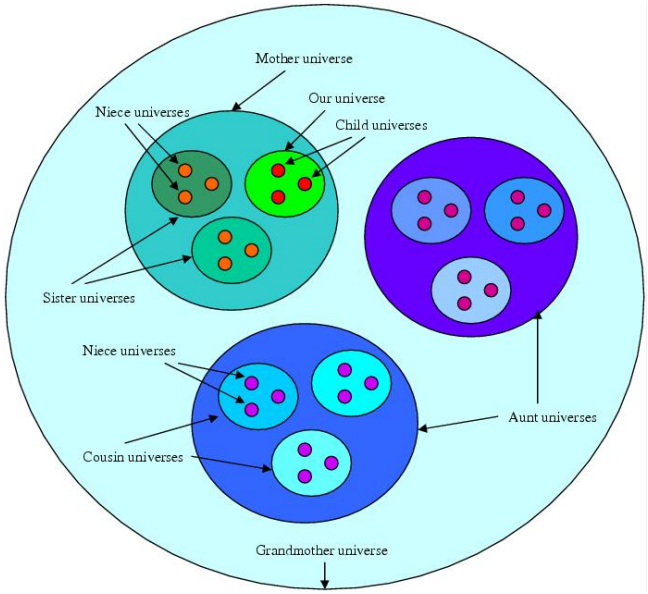

Fig. 4: A sketch of the innermost four layers of the black hole universe including grandmother universe, aunt universes, mother universe, sister universes, cousin universes, niece universes, and child universes.

This four generation universe family shown in Figure 4 can also be represented by a universe family tree (see Figure 5). The mother and aunt universes are children of the grandmother universe. The cousin universes are children of the aunt universes. Both our universe and the cousin universe have their own children, which are the star-like or supermassive black holes.

It is more natural to consider that the space is infinite large without an edge and has infinite number of layers. For the outermost layer, the radius tends to infinity, while the density and absolute temperature both tend to zero. We call this outermost layer as the entire space universe because it contains all universes. To represent this infinite layer structure of the entire space, we use the mathematical set concept (see Figure 6). We let the entire space universe be the set (denoted by U) of all universes; the child universes (also the niece universes) are null sets ($C = \{\}$ or $N = \{\}$); our universe is a set of the child universes ($O = \{C, C, C, \ldots, C\}$); the sister universes are sets of the niece universes $S = \{N, N, N, \ldots, N\}$); the mother universe is a set of our universe and the sister universes ($M = \{S, S, S, \ldots, O\}$); the aunt universes are sets of the cousin universes; the grandmother universe is a set of the aunt universes and the mother universe; and so on. The black hole universe model gives a fantastic picture of the entire space. All universes are self similar and governed by the same physics (the Einstein general theory of relativity with the Robertson-Walker metric) as shown later.

As a black hole grows up, it becomes nonviolent because its density and thus the gravitational field decrease. Matter being swallowed by a star-like black hole is extremely compressed and split into particles by the intense gravitational

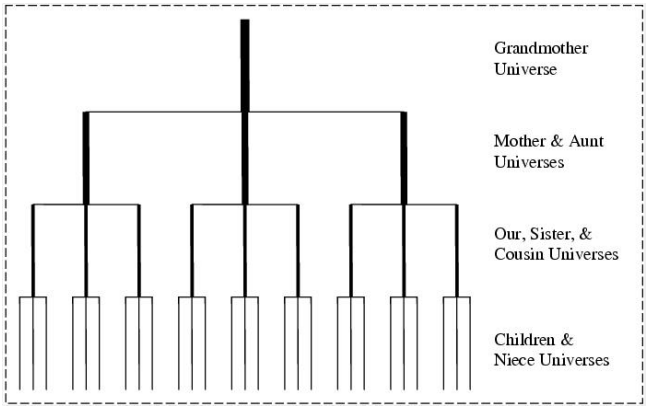

Fig. 5: A family tree for the youngest four generations of the universe family. The generation one includes the child and niece universes; the generation two includes our universe itself and the sister universes; the generation three includes the mother and aunt universes; and the generation four includes the grandmother universe.

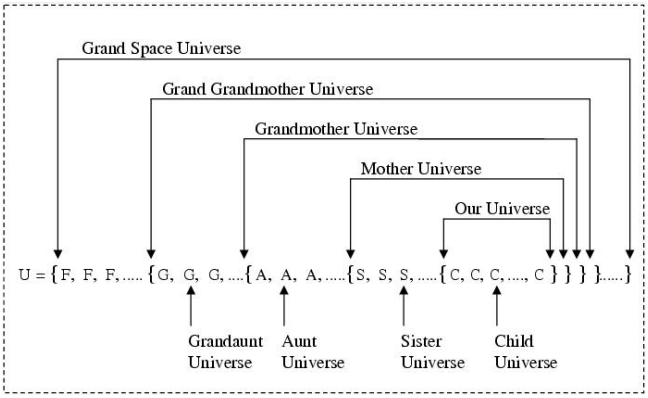

Fig. 6: Mathematical representation of sets of universes for an infinite large and layered space. An inner layer universe set is a subset of the outer layer universe set. The niece and child universes are null sets because they do not contain any sub-spacetime.

field; while that being swallowed by an extremely supermassive black hole (e.g., our universe) may not be compressed and even keeps the same state when it enters through the Schwarzschild absolute event horizon, because the gravitational field is very weak. To see more specifically on this aspect, we show, in Table 1, mass (M), radius (R), density (ρ), and gravitational field at surfaces (g_R) of some typical objects including the Earth, the Sun, a neutron star, a star-like black hole, a supermassive black hole, and the black hole universe. It is seen that the density of a star-like black hole is about that of a neutron star and 10^{14} times denser than the Sun and the Earth, while the density of supermassive black is less than or about that of water. The density of the black hole universe is only about 10^{-28} of supermassive black hole. The gravitational field of the supermassive black hole is only 10^{-8} of a star-like black hole. The gravitational field of the present universe at the surface is very weak ($g_R = c^2/(2R_0) \sim 3 \times 10^{-10}$N).

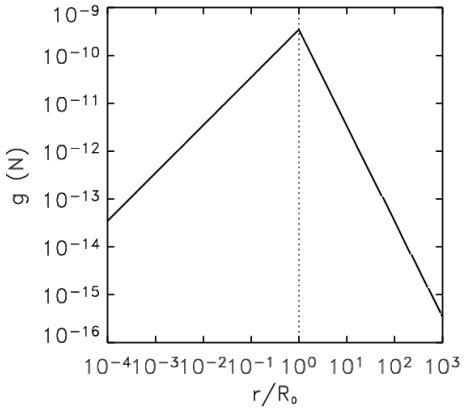

Fig. 7: The gravitational field of the present black hole universe. Inside the black hole universe, the gravity increases with the radial distance linearly from zero at the geometric center to the maximum value at the surface. While outside the black hole universe, the gravity decreases inversely with the square of the radial distance.

The total number of universes in the entire space is given by

$$n = \sum_{i=1}^{i=L} n_i \qquad (3)$$

where the subscript i is the layer number, n_i is the number of universes in the ith layer, and L refers to the number of layers in the entire space. For the four layer (or generation) black hole universe sketched in Figure 4 or 5, we have $L = 4$ and $n = 27 + 9 + 3 + 1 = 40$. If the entire space includes infinite number of layers (i.e., $L = \infty$), then the total number of universes is infinity.

The gravitational field of the black hole universe can be given by

$$g = \begin{cases} c^2 r/(2R_0^2) & \text{if} \quad r \leqslant R_0 \\ c^2 R_0/(2r^2) & \text{if} \quad r \geqslant R_0 \end{cases}, \qquad (4)$$

where r is the distance to the geometric center of the black hole universe. The gravity of the black hole universe increases linearly with r from zero at the center to the maximum (g_R) at the surface and then decreases inversely with r^2 (see Figure 7). In the present extremely expanded universe, the gravity is negligible (or about zero) everywhere, so that, physically, there is no special point (or center) in the black hole universe, which is equivalent to say that any point can be considered as the center. A frame that does not accelerate relative to the center of the universe is very like an inertial frame. The present universe appears homogeneous and isotropic.

4 The steady state and expansion of the black hole universe

In the black hole universe model, the physics of each universe is governed by the Einstein general theory of relativity. The matter density of each universe is inversely proportional to the square of the radius or, in other words, the mass

Object	M (kg)	R (m)	ρ (kg/m^3)	g_R (m/s^2)
Earth	6×10^{24}	6.4×10^6	5.5×10^3	9.8
Sun	2×10^{30}	7×10^8	1.4×10^3	270
Neutron Star	3×10^{30}	10^4	7.2×10^{17}	2×10^{12}
Starlike BH	10^{31}	3×10^3	8.8×10^{19}	7.4×10^{13}
Supermassive BH	10^{39}	3×10^{12}	22	7.4×10^3
Universe	10^{53}	1.4×10^{26}	8.7×10^{-27}	3.4×10^{-10}

Table 1: Mass, radius, density, and gravitational field at the surface of some typical objects.

is linearly proportional to the radius. The three dimensional space curvature of the black hole universe is positive, i.e., $k = 1$. The spacetime of each universe is described by the Robertson-Walker metric

$$ds^2 = c^2 dt^2 - a^2(t) \times \\ \times \left[\frac{1}{1 - r^2} dr^2 + r^2 d\theta^2 + r^2 \sin^2\theta \, d\phi^2 \right], \qquad (5)$$

where ds is the line element and $a(t)$ is the scale (or expansion) factor, which is proportional to the universe radius $R(t)$, and t is the time.

Substituting this metric into the field equation of the Einstein general relativity, we have the Friedmann equation [34]

$$H^2(t) \equiv \left[\frac{1}{R(t)} \frac{dR(t)}{dt} \right]^2 = \frac{8\pi G \rho(t)}{3} - \frac{c^2}{R^2(t)}, \qquad (6)$$

where $H(t)$ is the Hubble parameter (or the universe expansion rate) and $\rho(t)$ is the density of the universe. It should be noted that equation (6) can also be derived from the energy conservation in the classical Newton theory [35]. All layers or universes are governed by the same physics, i.e., the Einstein general theory of relativity with the Robertson-Walker metric, the Mach M-R relation, and the positive space curvature.

Substituting the density given by equation (2) into (6), we obtain

$$\frac{dR(t)}{dt} = 0, \qquad (7)$$

or $H(t) = 0$. Therefore, the black hole universe is usually in a steady state, although it has a positive curvature in the three dimensional space. The black hole universe is balanced when the mass and radius satisfy equation (1), or when the universe density is given by equation (2). The Einstein static universe model corresponds to a special case of the black hole universe model. The steady state remains until the black hole universe is disturbed externally, e.g., entering matter. In other words, when the universe is in a steady state, the Friedmann equation (6) reduces to the Mach M-R relation (1) or the density formula (2).

When the black hole universe inhales matter with an amount dM from the outside, we have

$$\frac{2G(M + dM)}{c^2 R} > 1. \qquad (8)$$

In this case, the black hole universe is not balanced. It will expand its size from R to $R + dR$, where the radius increment dR can be determined by

$$\frac{2G(M + dM)}{c^2(R + dR)} = 1, \qquad (9)$$

or

$$\frac{2G}{c^2} \frac{dM}{dR} = 1. \qquad (10)$$

Therefore, the black hole universe expands when it inhales matter from the outside. From equation (10), the expansion rate (or the rate of change in the radius of the universe) is obtained as

$$\frac{dR(t)}{dt} = \frac{2G}{c^2} \frac{dM(t)}{dt}, \qquad (11)$$

and the Hubble parameter is given by

$$H(t) = \frac{1}{R(t)} \frac{dR(t)}{dt} = \frac{1}{M(t)} \frac{dM(t)}{dt}. \qquad (12)$$

Equation (11) or (12) indicates that the rate at which a black hole including the black hole universe expands is proportional to the rate at which it inhales matter from its outside. Considering a black hole with three solar masses accreting 10^{-5} solar masses per year from its outside [36], we have $dR(t)/dt \sim 10^{-1}$ m/years and $H(t) \sim 10^7$ km/s/Mpc. Considering a supermassive black hole with one billion solar masses, which swallows one thousand solar masses in one year to run a quasar, we have $dR(t)/dt \sim 3 \times 10^3$ km/years and $H(t) \sim 10^6$ km/s/Mpc. When the black hole merges with other black holes, the growth rate should be larger. For our universe at the present state, the value of the Hubble parameter is measured as $H(t_0) \sim 70$ km/s/Mpc. If the radius of the universe is chosen as 13.7 billion light years, we have $dR(t_0)/dt \sim c$, which implies that our universe is expanding in about the light speed at present. To have such fast expansion, the universe must inhale about 10^5 solar masses in one second or swallows a supermassive black hole in about a few hours.

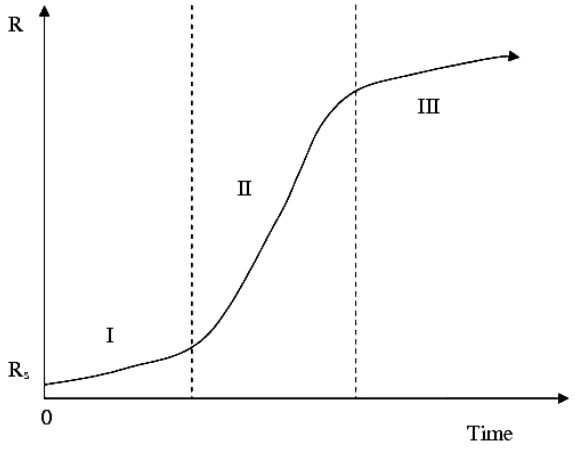

Fig. 8: A schematic sketch for the possible evolution of radius or mass of our black hole universe (solid line): R or M versus time. The two dashed vertical lines divide the plot into three regions, I: child universe, II: adult universe, and III: elder universe.

The whole life of our universe can be roughly divided into three time periods: I, II, and III (Figure 8). During the period I, the universe was a child (e.g., star-like or suppermassive black hole), which did not eat much and thus grew up slowly. During the period II, the universe is an adult (e.g., the present universe), which expands in the fastest speed. During the period III, the universe will become elder (e.g., the mother universe) and slow down the expansion till the end with an infinite radius, zero mass density, and zero absolute temperature. Figure 8 shows a possible variation of radius or mass of a black hole universe in its entire life. Since $dR(t)/dt < c$ in average, the age of the present universe must be greater than $R(t_0)/c$. The Hubble parameter represents the relative expansion rate, which decreases as the universe grows up.

The acceleration parameter is given by

$$q(t) \equiv \frac{1}{R^2(t)}\frac{d^2R(t)}{dt^2} = \frac{1}{M^2(t)}\frac{d^2M(t)}{dt^2}\,; \qquad (13)$$

therefore, if the universe inhales matter in an increasing rate ($d^2M(t)/dt^2 > 0$), the universe accelerates its expansion. Otherwise, it expands in a constant rate ($d^2M(t)/dt^2 = 0$) or expands in a decreasing rate ($d^2M(t)/dt^2 < 0$) or is at rest ($dM(t)/dt = 0$). In the black hole universe model, the dark energy is not required for the universe to accelerate. The black hole universe does not have the dark energy problem that exists in the big bang cosmological theory.

5 Discussions and conclusions

The black hole universe grows its space up by taking its mother's space as it inhales matter and radiation rather than by stretching the space of itself geometrically. As the black hole universe increases its size, the matter of the universe expands because its density must decrease according to equation (2). Since the planets are bound together with the Sun by the gravity, the solar system (also for galaxies and clusters) does not expand as the universe grows up. This is similar to that gases expand when its volume increases, but the atoms and molecules of the gases do not enlarge. Therefore, the expansion of the black hole universe is physical, not geometrical.

Conventionally, it has been suggested that, once a black hole is formed, the matter will further collapse into the center of the black hole, where the matter is crushed to infinitely dense and the pull of gravity is infinitely strong. The interior structure of the black hole consists of the singularity core (point-like) and the vacuum mantle (from the singularity core to the absolute even horizon). In the black hole universe model, our universe originated from a star-like black hole and grew up through a supermassive black hole. A star-like or supermassive black hole is just a child universe (or a mini spacetime). Physical laws and theories are generally applicable to all spacetimes or universes such as our universe, the mother universe, and the child universes (i.e., the star-like or supermassive black holes). The matter inside a black hole can also be governed by the Friedmann equation which is derived from the Einstein general relativity with the Robertson-Walker metric. Therefore, if a black hole does not inhale matter from its outside, it is in a steady state as described by equation (7). The matter inside a black hole distributes uniformly with a density given by equation (2). The highly curved spacetime of a black hole sustains its enormous gravity produced by the highly dense matter. If the black hole inhales the matter from its outside, it grows up and hence expands with a rate that depends on how fast it eats as described by equation (11) or (12).

A black hole, no matter how big it is, is an individual spacetime. From the view of us, a star-like black hole within our universe is a singularity sphere, from which the matter and radiation except for the Hawking radiation (a black body spectrum) cannot go out. Although it is not measurable by us, the temperature inside a star-like black hole should be higher than about that of a neutron star because the density of a star-like black hole is greater than about that of a neutron star, which may have a temperature as high as thousand billion degrees at the moment of its birth by following the explosion of a supernova and then be quickly cooled to hundred million degrees because of radiation [37]. A black hole can hold such high temperature because it does not radiate significantly. When a star-like black hole inhales the matter and radiation from its outside (i.e., the mother universe), it expands and cools down. From a star-like black hole to grow up to one as big as our universe, it is possible for the temperature to be decreased from thousand billion degrees (10^{12} K) to about 3 K. Therefore, in the black hole universe model, the cosmic microwave background radiation is the black body radiation of the black hole universe. In future study, we will explain the cosmic microwave background radiation in detail. We will analyze the nucleosynthesis of elements taken place

in the early (or child) black hole universe, which is dense and hot, grows slowly, and dominates by matter. The early black hole universe is hot enough for elements to synthesize, but not enough to create monopoles.

According to the Einstein general relativity, a main sequence star will, in terms of its mass, form a dwarf, a neutron star, or a black hole. After many stars in a normal galaxy have run out their fuels and formed dwarfs, neutron stars, and black holes, the galaxy will eventually shrink its size and collapse towards the center by gravity to form a supermassive black hole with billions of solar masses. This collapse leads to that extremely hot stellar black holes merge each other and further into the massive black hole at the center and meantime release intense radiation energies that can be as great as a quasar emits. Therefore, when the stellar black holes of a galaxy collapse and merge into a supermassive black hole, the galaxy is activated and a quasar is born. In the black hole universe model, the observed distant quasars can be understood as donuts from the mother universe. The observed distant quasars were formed in the mother universe as little sisters of our universe. When quasars entered our universe, they became children of our universe. The nearby galaxies are quiet at present because they are still very young. They will be activated with an active galactic nuclei and further evolve to quasars after billions of years. In future study, we will give a possible explanation for quasars to ignite and release huge amount of energy.

The black hole universe does not exist other significant difficulties. The dark energy is not necessary for the universe to accelerate its expansion. The expansion rate depends on the rate that the universe inhales matter from outside. When the black hole universe inhales the outside matter in an increasing rate, it accelerates its expansion. The boundary of the black hole universe is the Schwarzschild absolute event horizon, so that the black hole universe does not have the horizon problem. The inflation epoch is not required. The star-like or supermassive black holes are not hot enough to create monopoles. The present universe has been fully expanded and thus behaved as flat, homogeneous, and isotropic. The evolution and physical properties of the early universe are not critical to the present universe because matter and radiation of the present universe are mainly from the mother universe.

As a conclusion, we have proposed a new cosmological model, which is consistent with the Mach principle, the Einstein general theory of relativity, and the observations of the universe. The new model suggests that our universe is an extremely supermassive expanding black hole with a boundary to be the Schwarzschild absolute event horizon as described by the Mach M-R relation, $2GM/c^2R = 1$. The black hole universe originated from a hot star-like black hole with several solar masses, and gradually grew up (thus cooled down) through a supermassive black hole with billion solar masses as a milestone up to the present state with hundred billion-trillion solar masses due to continuously inhaling matter from its outside — the mother universe. The structure and evolution of the black hole universe are spatially hierarchical (or family like) and temporarily iterative. In each of iteration a universe passes through birth, growth, and death. The entire evolution of universe can be roughly divided into three periods with different expanding rates. The whole space is structured similarly and all layers of space (or universes) are governed by the same physics — the Einstein general relativity with the Robertson-Walker metric, the Mach M-R relation, and the positive space curvature. This new model brings us a natural, easily understandable, and reasonably expanding universe; thereby may greatly impact on the big bang cosmology. The universe expands physically due to inhaling matter like a balloon expands when gases are blown into instead of geometrically stretching. New physics is not required because the matter of the black hole universe does not go to infinitely dense and hot. The dark energy is not necessary for the universe to accelerate. There is not the horizon problem and thus not need an inflation epoch. The black hole universe is not hot enough to create monopoles. The black hole universe model is elegant, simple, and complete because the entire space is well structured, governed by the same physics, and evolved iteratively without beginning, end, and outside.

Acknowledgement

This work was supported by AAMU Title III. The author thanks Dr. Martin Rees for time in reading a draft of this paper.

Submitted on March 06, 2009 / Accepted on March 17, 2009

References

1. Hubble E. P. A clue to the structure of the Universe. *Leaflets of the Astronomical Society of the Pacific*, 1929, v. 1, 93–96.
2. Hubble E. P. A relation between distance and radial velocity among extra-galactic nebulae. *Proc. Nat. Acad. Sci.*, 1929, v. 15, 168–173.
3. Lemaitre G. *Annals of the Scientific Society of Brussels*, 1927, v. 47A, 41.
4. Lemaitre G. A homogeneous Universe of constant mass and growing radius accounting for the radial velocity of extragalactic nebulae. *MNRAS*, 1931, v. 91, 483–490.
5. Gamow G. The evolution of the Universe. *Nature*, 1948, v. 162, 680–682.
6. Gamow G. The origin of elements and the separation of galaxies. *Phys. Rev.*, 1948, v. 74, 505–506.
7. Alpher R. A., Bethe H. A., and Gamow G. The origin of chemical elements. *Phys. Rev.*, 1948, v. 73, 803–804.
8. Alpher R. A., Herman P., and Gamow G. Evolution of the Universe. *Nature*, 1948, v. 162, 774–775.
9. Alpher R. A., Herman P., and Gamow G. Thermonuclear reactions in the expanding Universe. *Phs. Rev.*, 1948, v. 74, 1198–1199.

10. Guth A. H. Iflationary universe: A possible solution to the horizon and flatness problems. *Phys. Rev. D* , 1981, v. 23, 347–356.
11. Dicke R. H., Peebles P. J. E., Roll P. G., and Wilkinson D. T. Cosmic black-body radiation. *Astrophys. J.*, 1965, v. 142, 414–419.
12. Penzias A., and Wilson R. W. A measurement of excess antenna temperature at 4080 Mc/s. *Astrophys. J.*, 1965, v. 142, 419–421.
13. Peebles P. J. E., and Yu J. T. Primeval adiabatic perturbation in an expanding universe. *Astrophys. J.*, 1970, v. 162, 815–836.
14. Boesgaard A. M. and Steigman G. Big bang nucleosynthesis — theories and observations. *ARA&A*, 1985, v. 23, 319–378.
15. Gilmore G., Edvardsson B., and Nissen P. E. First detection of beryllium in a very metal poor star — a test of the standard big bang model. *Astrophys. J.*, 1991, v. 378, 17–21.
16. Lerner E. J. et al. An open letter to the scientific community. *New Scientist*, 2004, v. 182, no. 2448, 20.
17. Alfvén H. Cosmology: myth or science. J. Astrophys. Astr., 1984, v. 5, 79–98.
18. Hasinger G., Schartel N., and Komossa S. Discovery of an ionized FeK edge in the Z=3.91 broad absorption line quasar APM 08279+5255 with XMM-Newton. *Astrophys. J.*, v. 573, L77–L80
19. Brans C. and Dicke R. H. Mach's principle and a relativistic theory of gravitation. Phys. Rev., 1961, v. 124, 925–935.
20. Zhang T. X. Electric redshift and quasars. *Astrophys. J.*, 2006, v. 636, L61–L64.
21. Zhang T. X. Black hole universe model. *Private Communication with Dr. Martin Rees*, 2005.
22. Zhang T. X. A new cosmological model: Black hole universe. *AAS 211th Meeting*, Jan. 7–11, 2008, Austin, Texas, 2007, Abstract no.: 152.04.
23. Zhang T. X. Anisotropic expansion of the black hole universe. *AAS 213th Meeting*, Jan. 4–8, 2009, Long Beach, California, 2008, Abstract no.: 357.03.
24. Sciama D. W. On the origin of inertia. *MNRAS*, 1953, v. 113, 34–42.
25. Dicke R. H. New research on old gravitation. *Science*, 1959, v. 129, 621–624.
26. Davidson W. General relativity and mach's principle. *MNRAS*, 1957, v. 117, 212–224.
27. Schwarzschild K. On the gravitational field of a mass point according to Einstein's theory. *Sitz. der Koniglich Preuss. Akad. der Wiss.*, 1916, v. 1, 189–196.
28. Hoyle F. A new model for the expanding universe. *MNRAS*, 1948, v. 108, 372–382.
29. Pringle J. E., Rees M. J., and Pacholczyk A. G. Accretion onto massive black holes. *Astron. Astrophys.*, 1973, v. 29, 179–184.
30. Gurzadian V. G. and Ozernoi L. M. Accretion on massive black holes in galactic nuclei. *Nature*, 1979, v. 280, 214–215.
31. Kormendy J. and Richstone D. Inward bound — The search for supermassive black holes in galactic nuclei. *ARA&A*, 1995, v. 33, 581–624.
32. Richstone D. et al. Supermassive black holes and the evolution of galaxies *Nature*, 1998, v. 395, 14–15.
33. Hawking S. W. Black hole explosions. *Nature*, 1974, v. 248, 30–31.
34. Friedmann A. On the curvature of space. *Z. Phys.*, 1922, v. 10, 377–386.
35. Duric N. Advanced Astrophysics. Cambridge Univ. Press, United Kingtom, 2004.
36. Shakura N. I., and Syunyaev R. A. Black holes in binary systems. Observational appearance. *Astron. Astrophys.*, 1973, v. 24, 337–355.
37. Yakovlev D. G., Gnedin O. Y., Kaminker A. D., Levenfish K. P., and Potekhin A. Y. Neutron star cooling: theoretical aspects and observational constraints. *Adv. Space Res.*, 2004, v. 33, 523–530.

Maxwell-Cattaneo Heat Convection and Thermal Stresses Responses of a Semi-infinite Medium due to High Speed Laser Heating

Ibrahim A. Abdallah

Department of Mathematics, Helwan University, Ain Helwan, 11795, Egypt
E-mail: iaawavelets@yahoo.com

Based on Maxwell-Cattaneo convection equation, the thermoelasticity problem is investigated in this paper. The analytic solution of a boundary value problem for a semi-infinite medium with traction free surface heated by a high-speed laser-pulses have Dirac temporal profile is solved. The temperature, the displacement and the stresses distributions are obtained analytically using the Laplace transformation, and discussed at small time duration of the laser pulses. A numerical study for Cu as a target is performed. The results are presented graphically. The obtained results indicate that the small time duration of the laser pulses has no effect on the finite velocity of the heat conductivity, but the behavior of the stress and the displacement distribution are affected due to the pulsed heating process and due to the structure of the governing equations.

1 Introduction

The induced thermoelastic waves in the material as a response to the pulsed laser heating becomes of great interest due to its wide applications inwelding, cutting, drilling surface hardening and machining of brittle materials. The classical linear theory of thermoelasticity [1] based on Fourier relation

$$q = -k\,\frac{\partial T}{\partial x} \tag{1}$$

together with the energy conservation produces the parabolic heat conduction equation;

$$\frac{\partial T}{\partial t} = \frac{k}{c}\,\frac{\partial T}{\partial x^2}\,. \tag{2}$$

Although this model solved some problems on the macroscale where the length and time scales are relatively large, but it have been proved to be unsuccessful in the microscales ($< 10^{-12}$ s) applications involving high heating rates by a short-pulse laser because Fourier's model implies an infinite speed for heat propagation and infinite thermal flux on the boundaries. To circumvent the deficiencies of Fourier's law in describing such problems involving high rate of temperature change; the concept of wave nature of heat transformation had been introduced [2, 3]. Beside the coupled thermoelasticity theory formulated by Biot [4], thermoelasticity theory with one relaxation time introduced by Lord and Shulman [5] and the two-temperature theory of thermoelasticity [6] which introduced to improve the classical thermoelasticity, there is the Maxwell-Cattaneo model of heat convection [9].

In the Maxwell-Cattaneo model the linkage between the heat conduction equation

$$q + \tau\,\frac{\partial q}{\partial t} = -k\,\frac{\partial T}{\partial x} \tag{3}$$

and the energy conservation introduces the hyperbolic equation

$$\tau\,\frac{\partial^2 T}{\partial t^2} + \frac{\partial T}{\partial t} = \frac{k}{c}\frac{\partial^2 T}{\partial x^2} \tag{4}$$

which describes a heat propagation with finite speed. The finiteness of heat propagation speed provided by the generalized thermoelasticity theories based on Maxwell- Cattaneo model of convection are supposed to be more realistic than the conventional theory to deal with practical problems with very large heat fluxes and/or short time duration.

Biot [4] formulated the theory of coupled thermoelasticity to eliminate the shortcoming of the classical uncoupled theory. In this theory, the equation of motion is a hyperbolic partial differential equation while the equation of energy is parabolic. Thermal disturbances of a hyperbolic nature have been derived using various approaches. Most of these approaches are based on the general notion of relaxing the heat flux in the classical Fourier heat conduction equation, thereby, introducing a non Fourier effect.

The first theory, known as theory of generalized thermoelasticity with one relaxation time, was introduced by Lord and Shulman [5] for the special case of an isotropic body. The extension of this theory to include the case of anisotropic body was developed by Dhaliwal and Sherief [7]. Recently, the author and co-workers investigated the problem of thermoelasticity, based on the theory of Lord and Shulman with one relaxation time, is used to solve a boundary value problem of one dimensional semiinfinite medium heated by a laser beam having a temporal Dirac distribution [8].

The purpose of the present work is to study the thermoelastic interaction caused by heating a homogeneous and isotropic thermoelastic semi-infinite body induced by a Dirac pulse having a homogeneous infinite cross-section by employing the theory of thermoelasticity with one relaxation time. The problem is solved by using the Laplace transform technique. Approximate small time analytical solutions to

stress, displacement and temperature are obtained. The convolution theorem is applied to get the spatial and temporal temperature distribution induced by laser radiation having a temporal Gaussian distribution. At the end of this work a numerical study for Cu as a target is performed and presented graphically and concluding remarks are given.

2 Formulation of the problem

We consider one-dimensional heating situation thermoelastic, homogeneous, isotropic semi-infinite target occupying the region $z \geqslant 0$, and initially at uniform temperature T_0. The surface of the target $z = 0$ is heated homogeneously by a leaser beam and assumed to be traction free. The Cartesian coordinates (x, y, z) are considered in the solution and z-axis pointing vertically into the medium. The governing equations are: The equation of motion in the absence of body forces

$$\sigma_{ji,j} = \rho\, \ddot{u}_i\,, \qquad i, j = x, y, z \tag{5}$$

where σ_{ij} is the components of stress tensor, u_i's are the displacement vector components and ρ is the mass density.

The Maxwell-Cattaneo convection equation

$$\frac{\partial \theta}{\partial t} + \tau\, \frac{\partial^2 \theta}{\partial t^2} = \frac{k}{\rho c_E} \frac{\partial^2 \theta}{\partial z^2} \tag{6}$$

where c_E is the specific heat at constant strain, τ is the relaxation time and k is the thermal conductivity.

The constitutive equation

$$\sigma_{ij} = (\lambda\, \mathrm{div}\, u - \gamma\, \theta)\, \delta_{ij} + 2\, \mu \epsilon_{ij} \tag{7}$$

where δ_{ij} is the delta Kronecker, $\gamma = \alpha_t(3\lambda + 2\mu)$, λ, μ are Lame's constants and α is the thermal expansion coefficient.

The strain-displacement relation

$$\epsilon_{ij} = \frac{1}{2}\,(u_{i,j} + u_{j,i})\,, \qquad i, j = x, y, z \tag{8}$$

The boundary conditions:

$$\sigma_{zz} = 0\,, \quad \text{at} \quad z = 0\,, \tag{9}$$

$$-k\, \frac{d\theta}{dz} = A_0\, q_0\, \delta(t)\,, \quad \text{at} \quad z = 0\,, \tag{10}$$

$$\sigma_{zz} = 0\,, \quad w = 0\,, \quad \theta = 0\,, \quad \text{as} \quad z \to \infty\,, \tag{11}$$

where A_0 is an absorption coefficient of the material, q_0 is the intensity of the laser beam and $\delta(t)$ is the Dirac delta function [10]. The initial conditions:

$$\left.\begin{aligned} &\theta(z,0) = \theta_0\,, \quad w(z,0) = 0\,, \quad \sigma_{ij}(z,0) = 0 \\ &\frac{\partial \theta}{\partial t} = \frac{\partial^2 \theta}{\partial t^2} = \frac{\partial w}{\partial t} = \frac{\partial^2 w}{\partial t^2} = \frac{\partial \sigma_{ij}}{\partial t} = \frac{\partial^2 \sigma_{ij}}{\partial t^2} = 0 \\ &\qquad\qquad\qquad\qquad \text{at} \quad t = 0\,, \ \forall z \end{aligned}\right\}. \tag{12}$$

Due to the symmetry of the problem and the external applied thermal field, the displacement vector u has the components:

$$u_x = 0\,, \quad u_y = 0\,, \quad u_z = w(z,t)\,. \tag{13}$$

From equation (12) the strain components ϵ_{ij}, read;

$$\left.\begin{aligned} &\epsilon_{xx} = \epsilon_{yy} = \epsilon_{xy} = \epsilon_{xz} = \epsilon_{yz} = 0 \\ &\epsilon_{zz} = \frac{\partial w}{\partial z} \\ &\epsilon_{ij} = \frac{1}{2}\,(u_{i,j} + u_{j,i})\,, \qquad i, j = x, y, z \end{aligned}\right\}. \tag{14}$$

The volume dilation e takes the form

$$e = \epsilon_{xx} + \epsilon_{yy} + \epsilon_{zz} = \frac{\partial w}{\partial z}\,. \tag{15}$$

The stress components in (8) can be written as:

$$\left.\begin{aligned} \sigma_{xx} = \sigma_{yy} &= \lambda\, \frac{\partial w}{\partial z} - \gamma\, \theta \\ \sigma_{zz} &= (2\,\mu + \lambda)\, \frac{\partial w}{\partial z} - \gamma\, \theta \end{aligned}\right\}, \tag{16}$$

where

$$\left.\begin{aligned} \sigma_{xy} &= 0 \\ \sigma_{xz} &= 0 \\ \sigma_{yz} &= 0 \end{aligned}\right\}. \tag{17}$$

The equation of motion (5) will be reduce to

$$\sigma_{xz,x} + \sigma_{yz,y} + \sigma_{zz,z} = \rho \ddot{u}_z\,. \tag{18}$$

Substituting from the constitutive equation (8) into the above equation and using $\theta = T - T_0$ we get,

$$(2\,\mu + \lambda)\, \frac{\partial^2 w}{\partial z^2} - \gamma\, \frac{\partial \theta}{\partial z} = \rho\, \frac{\partial^2 w}{\partial t^2} \tag{19}$$

where θ is the temperature change above a reference temperature T_0. Differentiating (19) with respect to z and using (15), we obtain

$$(2\,\mu + \lambda)\, \frac{\partial^2 e}{\partial z^2} - \gamma\, \frac{\partial^2 \theta}{\partial z^2} = \rho\, \frac{\partial^2 e}{\partial t^2} \tag{20}$$

after using (6) the energy equation can be written in the form:

$$(2\,\mu + \lambda)\, \frac{\partial^2 e}{\partial z^2} - \rho\, \frac{\partial^2 e}{\partial t^2} = \frac{\gamma \rho\, c_E}{k} \left(\frac{\partial}{\partial t} + \tau\, \frac{\partial^2}{\partial t^2}\right) \theta \tag{21}$$

by this equation one can determine the dilatation function e after determining θ which can be obtained by solving (6) using Laplace transformation; $\bar{f}(z,s) = \int_0^\infty e^{-st} f(z,t) dt$.

3 Analytic solution

In this section we introduce the analytical solutions of the system of equations (6), (16) and (19) based on the Laplace

transformation. Equation (6) after applying the Laplace transformation it will be;

$$\frac{d^2\bar{\theta}}{dz^2} - \alpha s\,(1+\tau s)\,\bar{\theta} = 0 \tag{22}$$

where $\alpha = \frac{\rho c_E}{k}$. By solving the above equation and using the boundary and the initial conditions (9)-(12); one can write the solution of equation (22) as

$$\bar{\theta} = \frac{A_0 q_0}{k f(s)} e^{-f(s)z}, \qquad \mathrm{Re}\,(f(s)) > 0\,. \tag{23}$$

Similarly the solution of equation (19) after Laplace transformation read;

$$\bar{w}(z,s) = B(s)\,e^{-asz} - \frac{\beta}{(f^2(s) - a^2 s^2)}\,e^{-f(s)z} \tag{24}$$

where

$$a^2 = \frac{\rho}{(2\mu+\lambda)}\,,\quad f(s) = \sqrt{\alpha s\,(1+\tau s)}\,,\quad \beta = \frac{\gamma A_0 q_0}{k(2\mu+\lambda)}\,,$$

$$B(s) = \frac{\beta f(s)}{sa\,(2\mu+\lambda)\,(f^2(s) - a^2 s^2)} - \frac{\beta}{asf(s)}\,.$$

Since we can use the Maclaurin series to write

$$\sqrt{s(1+\tau s)} = \sqrt{s^2\left(\tau + \frac{1}{s}\right)} \approx s\sqrt{\tau} + \frac{1}{2\sqrt{\tau}}\,. \tag{25}$$

Then the solution of the temperature distribution $\bar{\theta}$, and the displacement $\bar{w}$ can be written as

$$\bar{\theta}(z,s) = \left[\frac{C_1}{s} - \frac{C_2}{s^2} + \frac{C_3}{s^3}\right] e^{-z\left(s\sqrt{\alpha\tau} + \frac{1}{2}\sqrt{\frac{\alpha}{\tau}}\right)}, \tag{26}$$

$$\begin{aligned}\bar{w}(z,s) = &\left[\frac{w_1}{s} + \frac{w_2}{\frac{\alpha}{b}+s} + \frac{w_3}{s+\frac{1}{\tau}}\right] e^{-asz} - \\ &- \left[\frac{w_4}{s} + \frac{w_5}{\frac{\alpha}{b}+s}\right] e^{-z\left(s\sqrt{\alpha\tau} + \frac{1}{2}\sqrt{\frac{\alpha}{\tau}}\right)},\end{aligned} \tag{27}$$

therefore the stresses $\bar{\sigma}_{zz}$ and $\bar{\sigma}_{xx} = \bar{\sigma}_{yy}$ are obtained by applying the Laplace transformation to equation (16) and substituting by (26) and (27). Then using the inverse Laplace transformation, we obtain: the temperature θ

$$\begin{aligned}\theta(z,t) = &\Big[C_1 - C_2(t - \sqrt{\alpha\tau}z) + \\ &+ \frac{C_3}{2}(t - \sqrt{\alpha\tau}z)^2\Big] H(t - \sqrt{\alpha\tau}z) e^{-\frac{z}{2}\sqrt{\frac{\alpha}{\tau}}},\end{aligned} \tag{28}$$

the displacement w

$$\begin{aligned}w(z,t) = &\left[w_1 + \frac{w_2}{b}\,e^{-\frac{\alpha}{b}(t-az)} + w_3\,e^{-\frac{t-az}{\tau}}\right] H(t-az) - \\ &- \left[w_4 + \frac{w_5}{b}\,e^{-\frac{\alpha}{b}\left(t - \sqrt{\alpha\tau}z\right)}\right] H(t - \sqrt{\alpha\tau}\,z)\,e^{-\sqrt{\frac{\alpha}{\tau}}z},\end{aligned} \tag{29}$$

the stresses $\sigma_{xx} = \sigma_{yy}$

$$\begin{aligned}\sigma_{xx}(z,t) = &-a\lambda\Big[L_1\delta(t-az) - L_2 H(t-az)\,e^{-\frac{\alpha}{b}(t-az)} - \\ &- L_3 H(t-az) e^{-\frac{1}{\tau}(t-az)}\Big] + \\ &+ e^{-\frac{z}{2}\sqrt{\frac{\alpha}{\tau}}}\Big[L_4\delta(t - \sqrt{\alpha\tau}) + H(t - \sqrt{\alpha\tau}z) \times \\ &\times (L_5 + L_6 e^{-\frac{\alpha}{b}(t - \sqrt{\alpha\tau}z)})\Big] - \gamma\Big[C_1 - C_2(t - \sqrt{\alpha\tau}z) + \\ &+ \frac{C_3}{2}(t - \sqrt{\alpha\tau}z)^2\Big] H(t - \sqrt{\alpha\tau}z)\,e^{-\frac{z}{2}\sqrt{\frac{\alpha}{\tau}}},\end{aligned} \tag{30}$$

the stress σ_{zz}

$$\begin{aligned}\sigma_{zz}(z,t) = &-a(2\mu+\lambda)\Big[L_1\delta(t-az) - \\ &- L_2 H(t-az)\,e^{-\frac{\alpha}{b}(t-az)} - L_3 H(t-az)\,e^{-\frac{1}{\tau}(t-az)}\Big] + \\ &+ e^{-\frac{z}{2}\sqrt{\frac{\alpha}{\tau}}}\Big[L_4\delta(t - \sqrt{\alpha\tau}) + H(t - \sqrt{\alpha\tau}z) \times \\ &\times (L_5 + L_6\,e^{-\frac{\alpha}{b}(t - \sqrt{\alpha\tau}z)})\Big] - \gamma\Big[C_1 - C_2(t - \sqrt{\alpha\tau}z) + \\ &+ \frac{C_3}{2}(t - \sqrt{\alpha\tau}z)^2\Big] H(t - \sqrt{\alpha\tau}z)\,e^{-\frac{z}{2}\sqrt{\frac{\alpha}{\tau}}},\end{aligned} \tag{31}$$

$\delta(x)$ is Dirac delta function, and $H(x)$ is Heaviside unit step functions.

4 Results and discussions

We have calculated the spatial temperature, displacement and stress θ, w, σ_{xx}, σ_{yy} and σ_{zz} with the time as a parameter for a heated target with a spatial homogeneous laser radiation having a temporally Dirac distributed intensity with a width of (10^{-3} s). We have performed the computation for the physical parameters $T_0 = 293$ K, $\rho = 8954$ Kg/m^3, $A_0 = 0.01$, $c_E = 383.1$ J/kgK, $\alpha_t = 1.78\times10^{-5}$ K^{-1}, $k = 386$ W/mK, $\lambda = 7.76\times10^{10}$ kg/m sec^2, $\mu = 3.86\times10^{10}$ kg/m sec^2 and $\tau = 0.02$ sec for Cu as a target. Therefore the coefficients in the expressions (28)–(31)are

$$\left.\begin{array}{ll} C_1 = 1676.0\,, & C_2 = -83800.2 \\ C_3 = 1.57125\times10^6 & \\ w_1 = -5760.28\,, & w_2 = 44906.0 \\ \frac{w_2}{b} = 63506.0\,, & w_3 = 1.5589\times10^6 \\ w_4 = 0.1039\,, & w_5 = -0.7348 \\ \frac{\alpha}{b} = 1256.77\,, & L_1 = -3.0172\times10^{13} \\ L_2 = 1.4896\times10^5, & L_3 = 1.4547\times10^5 \\ L_4 = 2.7708\,, & L_5 = 34.6344 \\ L_6 = 1.7065\times10^3, & \frac{w_5}{b} = 0.103916 \end{array}\right\}. \tag{32}$$

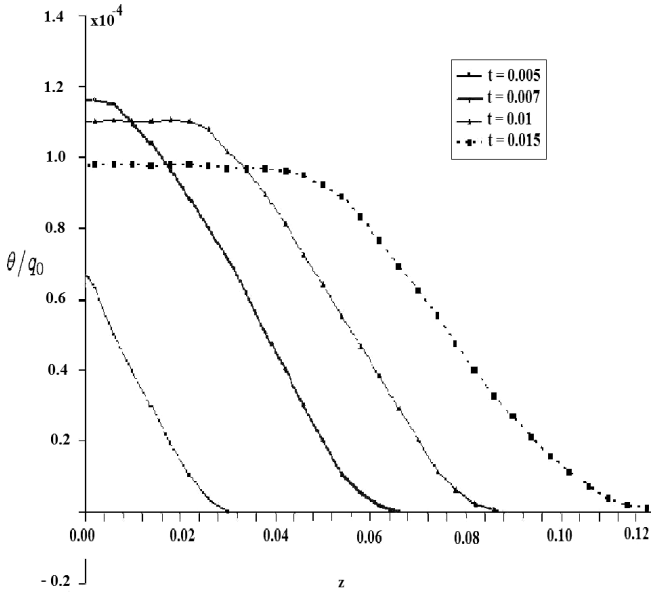

Fig. 1: The temperature distribution θ per unit intensity versus z with the time as a parameter.

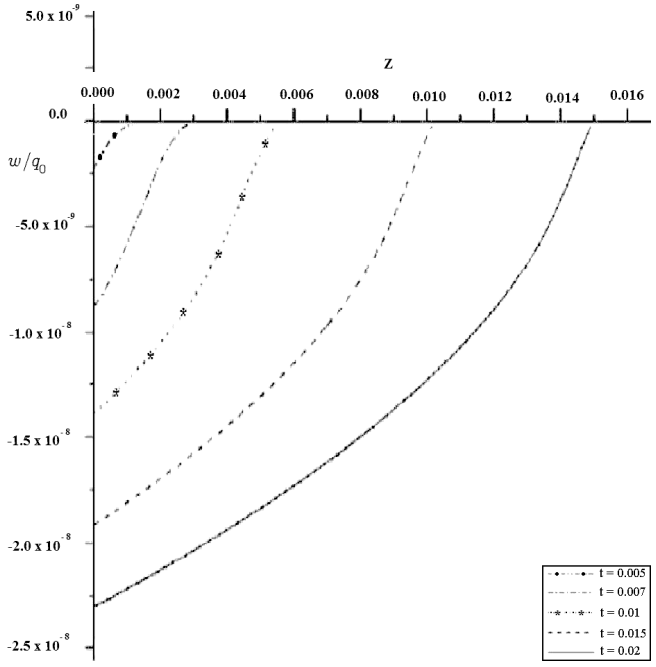

Fig. 2: The displacement distribution w per unit intensity versus z at different values of time as a parameter.

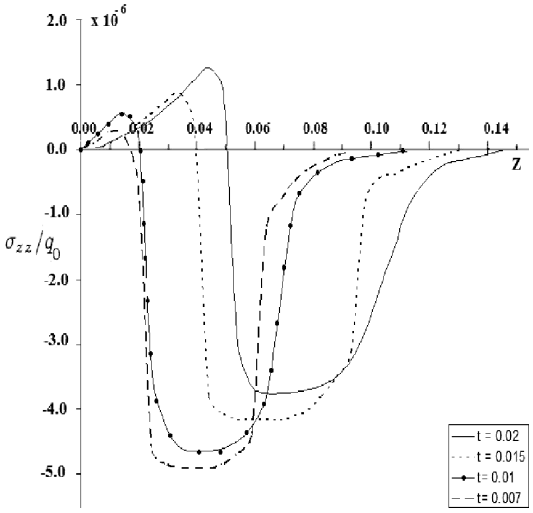

Fig. 3: The stress σ_{zz} distribution per unit intensity versus z with the time as a parameter.

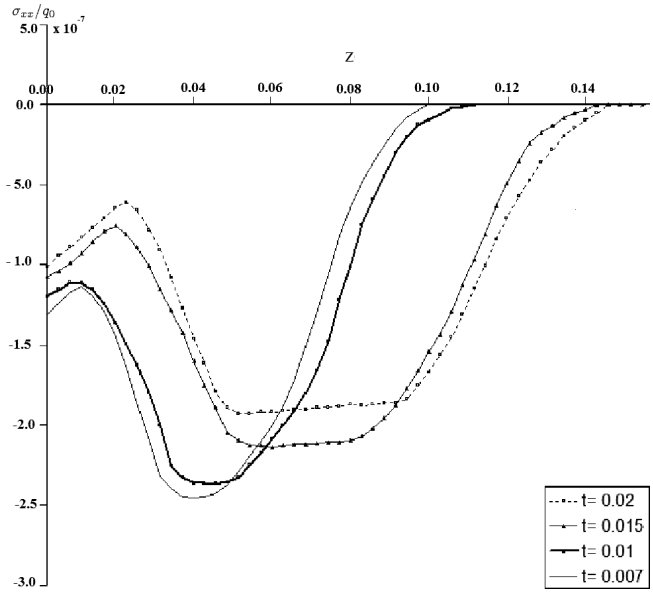

Fig. 4: The stress distribution $\sigma_{xx} = \sigma_{yy}$ per unit intensity versus z with the time as a parameter.

The obtained results are shown in the following figures.

Figure 1 illustrates the calculated spatial temperature distribution per unit intensity at different values of the time as a parameter $t = 0.005, 0.007, 0.01$ and 0.015. From the curves it is evident that the temperature has a finite velocity expressed through the strong gradient of the temperature at different locations which moves deeper in the target as the time increases.

Figure 2 represents the calculated spatial displacement per unit intensity for different values of time as a parameter. The displacement increases monotonically with increasing z. It Shows a smaller gradient with increasing z this behavior occurs at smaller z values than that of the temperature calculated at the corresponding time when it tends to zero. Both effects can be attributed to the temperature behavior and the finite velocity of the expansion which is smaller than that of the heat conduction. The negative displacement indicate the direction of the material expandion where the co-ordinate system is located at the front surface with positive direction of the $z-$axis pointing in the semi-infinite medium.

Figure 3 shows the calculated spatial stress σ_{zz} per unit intensity calculated at different times. It is given by $\sigma_{zz} = = \alpha e - \lambda_1 \theta$. For small z values and at the time $t = 0.005$ the temperature attains greater values than the gradient of the displacement, thus the stress in z direction becomes negative. After attaining z greater values both the temperature and the gradient of the displacement become smaller such that σ_{zz} takes greater values tending to zero. For $t = 0.007$ the effect of the temperature is dominant more than that of the gradient of the displacement this is leading to a more negative stress values shifted toward greater values of z. As the value $t = 0.01$ the effect of the gradient of the displacement over compensates that of the temperature leading to positive stress values lasting up to locations at which the gradient of the displacement and the temperature are practically equal. At this point the stress becomes maximum. As z takes greater values the gradient of the displacement decreases and the temperature becomes the upper hand leading to negative stress values. These behavior remains up to z values at which the temperature is practically zero where the stress tends also be zero. As t takes greater values the effect of the gradient will by more pronounced and thus the maximum of the stress becomes greater and shifts towards the greater z values.

Figure 4 depicts the calculated spatial stress distributions $\sigma_{xx} = \sigma_{yy}$ per unit intensity at different values of the time parameter. the same behavior as σ_{zz}. This is due to the same dependent relation of σ_{ij} on the strain and temperature except that the coefficient of the strain is different.

5 Conclusions

The thermoelastic waves in a semi infinite solid material indused by a Dirac pulsed laser heating are derived for non-Fourier effect based on the Maxwell-Cattaneo hyperbolic convection equation. Analytical solution for the temperature, the displacement and the stresses fields inside the material are derived using the Laplace transformation. The carried calculations enable us to model the thrmoelastic waves induced by a high speed Dirac laser pulse. From the figures it is evident that the temperature firstly increases with increasing the time this can be attributed to the increased absorbed energy which over compensates the heat losses given by the heat conductivity inside the material. As the absorbed power equals the conducted one inside the material the temperature attains its maximum value. the maximum of the temperature occurs at later time than the maximum of the radiation this is the result of the heat conductivity of Cu and the relatively small gradient of the temperature in the vicinity of $z = 0$. After the radiation becomes week enough such that it can not compensate the diffused power inside the material the temperature decreases monotonically with increasing time. Considering surface absorption the obtained results in Figure 1 shows the temperature θ, Figure 2 shows the displacement w, Figure 3 shows the the stress σ_{zz}, and Figure 4 shows the stresses $\sigma_{xx} = \sigma_{yy}$ respectively versus z. The solution of any of the considered function for this model vanishes identically to zero outside a bounded region. The response to the thermal effects by pulsed Laser heating does not reach infinity instantaneously but remains in a bounded region of z given by $0 < z < z^*(t)$ where t is the duration of the laser pulse used for heating. The stress exhibits like step-wise changes at the wave front. The stresses vanish quickly due to the dissipation of the thermal waves.

Submitted on February 25, 2009 / Accepted on March 18, 2009.

References

1. Chadwick L. P. Thermoelasticity: the dynamic theory. In: R. Hill and I. N. Sneddon (eds.), *Progress in Solid Mechanics*, v. I, North-Holland, Amsterdam, 1960, 263–328.
2. Müller L. and Rug-geri T. Extended thermodynamics. Springer, New York, 1993.
3. Özisik M. N. and Tzou D. Y. On the wave theory in heat conduction. *ASME J. of Heat Transfer*, 1994, v. 116, 526–535.
4. Biot M. Thermoelasticity and irreversible thermo-dynamics. *J. Appl. Phys.*, 1956, v. 27 240–253.
5. Lord H. and Shulman Y. A generalized dynamical theory of thermoelasticity. *J.Mech. Phys. Solid.*, 1967, v. 15 299–309.
6. Youssef H. M. and AlLehaibi E. A. State space approach of two temperature generalized thermoelasticity of one dimensional problem. *Intternational Journal of Solids and Structures*, 2007, v. 44, 1550–1562.
7. Dhaliwal R. and Sherief H. Generalized thermoelasticity for anisotropic media. *Quart. Appl. Math.*, 1980, v. 33, 1–8.
8. Abdallah I. A., Hassan A. F., and Tayel I. M. Thermoelastic property of a semi-infinite medium induced by a homogeneously illuminating laser radiation. *Progress In Physics*, 2008, v. 4, 44–50.

9. Andrea P. R., Patrizia B., Luigi M., and Agostino G. B. On the nonlinear Maxwell-Cattaneo equation with non-constant diffusivity: shock and discontinuity waves. *Int. J. Heat and Mass Trans.*, 2008, v. 51, 5327–5332.

10. Hassan A. F., et. al. Heating effects induced by a pulsed laser in a semi-infinite target in view of the theory of linear systems. *Optics and Laser Technology*, 1996, v. 28 (5), 337–343.

11. Hetnarski R. Coupled one-dimensional thermal shock problem for small times. *Arch. Mech. Stosow.*, 1961, v. 13, 295–306.

Relativistic Mechanics in Gravitational Fields Exterior to Rotating Homogeneous Mass Distributions within Regions of Spherical Geometry

Chifu Ebenezer Ndikilar*, Samuel Xede Kofi Howusu†, and Lucas Williams Lumbi‡

*Physics Department, Gombe State University, P.M.B. 127, Gombe, Gombe State, Nigeria
E-mail: ebenechifu@yahoo.com

†Physics Department, Kogi State University, Anyighba, Kogi State, Nigeria
E-mail: sxkhowusu@yahoo.co.uk

‡Physics Department, Nasarawa State University, Keffi, Nasarawa State, Nigeria
E-mail: williamslucas66@yahoo.com

General Relativistic metric tensors for gravitational fields exterior to homogeneous spherical mass distributions rotating with constant angular velocity about a fixed diameter are constructed. The coefficients of affine connection for the gravitational field are used to derive equations of motion for test particles. The laws of conservation of energy and angular momentum are deduced using the generalized Lagrangian. The law of conservation of angular momentum is found to be equal to that in Schwarzschild's gravitational field. The planetary equation of motion and the equation of motion for a photon in the vicinity of the rotating spherical mass distribution have rotational terms not found in Schwarzschild's field.

1 Introduction

General Relativity is the geometrical theory of gravitation published by Albert Einstein in 1915/1916 [1–3]. It unifies Special Relativity and Sir Isaac Newton's law of universal gravitation with the insight that gravitation is not due to a force but rather a manifestation of curved space and time, with the curvature being produced by the mass-energy and momentum content of the space time. After the publication of Einstein's geometrical field equations in 1915, the search for their exact and analytical solutions for all the gravitational fields in nature began [3].

The first method of approach to the construction of exact analytical solutions of Einstein's geometrical gravitational field equations was to find a mapping under which the metric tensor assumed a simple form, such as the vanishing of the off-diagonal elements. This method led to the first analytical solution — the famous Schwarzschild's solution [3]. The second method was to assume that the metric tensor contains symmetries — assumed forms of the associated Killing vectors. The assumption of axially asymmetric metric tensor led to the solution found by Weyl and Levi-Civita [4–11]. The fourth method was to seek Taylor series expansion of some initial value hyper surface, subject to consistent initial value data. This method has not proved successful in generating solutions [4–11].

We now introduce our method and approach to the construction of exact analytical solutions of Einstein's geometrical gravitational field equations [12, 13] as an extension of Schwarzschild analytical solution of Einstein's gravitational field equations. Schwarzschild's metric is well known to be the metric due to a static spherically symmetric body situated in empty space such as the Sun or a star [3, 12, 13]. Schwarzschild's metric is well known to be given as

$$g_{00} = 1 - \frac{2GM}{c^2 r}\,, \tag{1.1}$$

$$g_{11} = -\left[1 - \frac{2GM}{c^2 r}\right]^{-1}, \tag{1.2}$$

$$g_{22} = -r^2, \tag{1.3}$$

$$g_{33} = -r^2 \sin^2\theta\,, \tag{1.4}$$

$$g_{\mu\nu} = 0 \ \text{ otherwise}, \tag{1.5}$$

where $r > R$, the radius of the static spherical mass, G is the universal gravitational constant, M is the total mass of the distribution and c is the speed of light in vacuum. It can be easily recognized [12, 13] that the above metric can be written as

$$g_{00} = 1 + \frac{2f(r)}{c^2}\,, \tag{1.6}$$

$$g_{11} = -\left[1 + \frac{2f(r)}{c^2}\right]^{-1}, \tag{1.7}$$

$$g_{22} = -r^2, \tag{1.8}$$

$$g_{33} = -r^2 \sin^2\theta\,, \tag{1.9}$$

$$g_{\mu\nu} = 0 \ \text{ otherwise}, \tag{1.10}$$

where

$$f(r) = -\frac{GM}{r}\,. \tag{1.11}$$

We thus deduce that generally, $f(r)$ is an arbitrary function determined by the distribution. In this case, it is a function of the radial coordinate r only; since the distribution and hence its exterior gravitational field possess spherical symmetry. From the condition that these metric components should reduce to the field of a point mass located at the origin and contain Newton's equations of motion in the field of the spherical body, it follows that generally, $f(r)$ is approximately equal to the Newtonian gravitational scalar potential in the exterior region of the body, $\Phi(r)$ [12, 13].

Hence, we postulate that the arbitrary function f is solely determined by the mass or pressure distribution and hence possesses all the symmetries of the latter, a priori. Thus, by substituting the generalized arbitrary function possessing all the symmetries of the distribution in to Einstein's gravitational field equations in spherical polar coordinates, explicit equations satisfied by the single arbitrary function, $f(t, r, \theta, \phi)$, can be obtained. These equations can then be integrated exactly to obtain the exact expressions for the arbitrary function. Also, a sound and satisfactory approximate expression can be obtained from the well known fact of General Relativity [12, 13] that in the gravitational field of any distribution of mass;

$$g_{00} \approx 1 + \frac{2}{c^2}\,\Phi(t, r, \theta, \phi)\,. \tag{1.12}$$

It therefore follows that:

$$f(t, r, \theta, \phi) \approx \Phi(t, r, \theta, \phi)\,. \tag{1.13}$$

In a recent article [13], we studied spherical mass distributions in which the material inside the sphere experiences a spherically symmetric radial displacement. In this article, we now study general relativistic mechanics in gravitational fields produced by homogeneous mass distributions rotating with constant angular velocity about a fixed diameter within a static sphere placed in empty space.

2 Coefficients of affine connection

Consider a static sphere of total mass M and density ρ. Also, suppose the mass or pressure distribution within the sphere is homogeneous and rotating with uniform angular velocity about a fixed diameter. More concisely, suppose we have a static spherical object filled with a gas say and the gas is made to rotate with a constant velocity about a fixed diameter. In otherwords, the material inside the sphere is rotating uniformly but the sphere is static. Such a mass distribution might be hypothetical or exist physically or exist astrophysically. For this mass distribution, it is eminent that our arbitrary function will be independent of the coordinate time and azimuthal angle. Thus, the covariant metric for this gravitational field is given as

$$g_{00} = 1 + \frac{2f(r,\theta)}{c^2}\,, \tag{2.1}$$

$$g_{11} = -\left[1 + \frac{2f(r,\theta)}{c^2}\right]^{-1}, \tag{2.2}$$

$$g_{22} = -r^2, \tag{2.3}$$

$$g_{33} = -r^2\sin^2\theta\,, \tag{2.4}$$

$$g_{\mu\nu} = 0 \ \text{ otherwise}, \tag{2.5}$$

where $f(r,\theta)$ is an arbitrary function determined by the mass distribution within the sphere. It is instructive to note that our generalized metric tensor satisfy Einstein's field equations and the invariance of the line element; by virtue of their construction [1, 12]. An outstanding theoretical and astrophysical consequence of this metric tensor is that the resultant Einstein's field equations have only one unknown function, $f(r,\theta)$. Solutions to these field equations give explicit expressions for the function $f(r,\theta)$. In approximate gravitational fields, $f(r,\theta)$ can be conveniently equated to the gravitational scalar potential exterior to the homogeneous spherical mass distribution [1, 12–14]. It is most interesting and instructive to note that the rotation of the homogeneous mass distribution within the static sphere about a fixed diameter is taken care of by polar angle, θ in the function $f(r,\theta)$. Also, if the sphere is made to rotate about a fixed diameter, there will be additional off diagonal components to the metric tensor. Thus, in this analysis, the static nature of the sphere results in the vanishing of the off diagonal components of the metric.

The contravariant metric tensor for the gravitational field, obtained using the Quotient Theorem of tensor analysis [15] is given as

$$g^{00} = \left[1 + \frac{2f(r,\theta)}{c^2}\right]^{-1}, \tag{2.6}$$

$$g^{11} = -\left[1 + \frac{2f(r,\theta)}{c^2}\right], \tag{2.7}$$

$$g^{22} = -r^{-2}, \tag{2.8}$$

$$g^{33} = -\left(r^2\sin^2\theta\right)^{-1}, \tag{2.9}$$

$$g^{\mu\nu} = 0 \ \text{ otherwise}, \tag{2.10}$$

It is well known that the coefficients of affine connection for any gravitational field are defined in terms of the metric tensor [14, 15] as;

$$\Gamma^{\sigma}_{\mu\lambda} = \frac{1}{2}\,g^{\sigma\nu}\left(g_{\mu\nu,\lambda} + g_{\nu\lambda,\mu} - g_{\mu\lambda,\nu}\right), \tag{2.11}$$

$$\ddot{r} + \left[1 + \frac{2}{c^2} f(r,\theta)\right] \frac{\partial f(r,\theta)}{\partial r} \dot{t}^2 - \frac{1}{c^2} \left[1 + \frac{2}{c^2} f(r,\theta)\right]^{-1} \frac{\partial f(r,\theta)}{\partial r} \dot{r}^2 - \frac{2}{c^2} \left[1 + \frac{2}{c^2} f(r,\theta)\right]^{-1} \frac{\partial f(r,\theta)}{\partial \theta} \dot{r}\dot{\theta} - \\ - r \left[1 + \frac{2}{c^2} f(r,\theta)\right] \dot{\theta}^2 - r \sin^2\theta \left[1 + \frac{2}{c^2} f(r,\theta)\right]^{-2} \frac{\partial f(r,\theta)}{\partial \theta} \dot{\phi}^2 = 0 \tag{3.5}$$

where the comma as in usual notation designates partial differentiation with respect to x^λ, x^μ and x^ν. Thus, we construct the explicit expressions for the coefficients of affine connection in this gravitational field as;

$$\Gamma^0_{01} \equiv \Gamma^0_{10} = \frac{1}{c^2} \left[1 + \frac{2}{c^2} f(r,\theta)\right]^{-1} \frac{\partial f(r,\theta)}{\partial r}, \tag{2.12}$$

$$\Gamma^0_{02} \equiv \Gamma^0_{20} = \frac{1}{c^2} \left[1 + \frac{2}{c^2} f(r,\theta)\right]^{-1} \frac{\partial f(r,\theta)}{\partial \theta}, \tag{2.13}$$

$$\Gamma^1_{00} = \frac{1}{c^2} \left[1 + \frac{2}{c^2} f(r,\theta)\right] \frac{\partial f(r,\theta)}{\partial r}, \tag{2.14}$$

$$\Gamma^1_{11} = -\frac{1}{c^2} \left[1 + \frac{2}{c^2} f(r,\theta)\right]^{-1} \frac{\partial f(r,\theta)}{\partial r}, \tag{2.15}$$

$$\Gamma^1_{12} \equiv \Gamma^1_{21} = -\frac{1}{c^2} \left[1 + \frac{2}{c^2} f(r,\theta)\right]^{-1} \frac{\partial f(r,\theta)}{\partial \theta}, \tag{2.16}$$

$$\Gamma^1_{22} = -r \left[1 + \frac{2}{c^2} f(r,\theta)\right], \tag{2.17}$$

$$\Gamma^1_{33} = -r \sin^2\theta \left[1 + \frac{2}{c^2} f(r,\theta)\right]^{-2} \frac{\partial f(r,\theta)}{\partial \theta}, \tag{2.18}$$

$$\Gamma^2_{00} = \frac{1}{r^2 c^2} \frac{\partial f(r,\theta)}{\partial \theta}, \tag{2.19}$$

$$\Gamma^2_{11} = \frac{1}{r^2 c^2} \left[1 + \frac{2}{c^2} f(r,\theta)\right]^{-2} \frac{\partial f(r,\theta)}{\partial \theta}, \tag{2.20}$$

$$\Gamma^2_{12} \equiv \Gamma^2_{21} \equiv \Gamma^3_{13} \equiv \Gamma^3_{31} = -\frac{1}{r}, \tag{2.21}$$

$$\Gamma^2_{33} = -\frac{1}{2} \sin 2\theta, \tag{2.22}$$

$$\Gamma^3_{23} \equiv \Gamma^3_{32} = \cot\theta, \tag{2.23}$$

$$\Gamma^\sigma_{\mu\lambda} = 0 \text{ otherwise}, \tag{2.24}$$

Thus, the gravitational field exterior to a homogeneous rotating mass distribution within regions of spherical geometry has twelve distinct non zero affine connection coefficients. These coefficients are very instrumental in the construction of general relativistic equations of motion for particles of non-zero rest mass.

3 Motion of test particles

A test mass is one which is so small that the gravitational field produced by it is so negligible that it doesn't have any effect on the space metric. A test mass is a continuous body, which is approximated by its geometrical centre; it has nothing in common with a point mass whose density should obviously be infinite [16].

The general relativistic equation of motion for particles of non-zero rest masses is given [1, 12–14, 17] as

$$\frac{d^2 x^\mu}{d\tau^2} + \Gamma^\mu_{\nu\lambda} \left(\frac{dx^\nu}{d\tau}\right) \left(\frac{dx^\lambda}{d\tau}\right) = 0, \tag{3.1}$$

where τ is the proper time. To construct the equations of motion for test particles, we proceed as follows

Setting $\mu = 0$ in equation (3.1) and substituting equations (2.12) and (2.13) gives the time equation of motion as

$$\ddot{t} + \frac{2}{c^2} \left[1 + \frac{2}{c^2} f(r,\theta)\right]^{-1} \frac{\partial f(r,\theta)}{\partial r} \dot{t}\dot{r} + \\ + \frac{2}{c^2} \left[1 + \frac{2}{c^2} f(r,\theta)\right]^{-1} \frac{\partial f(r,\theta)}{\partial \theta} \dot{t}\dot{\theta} = 0, \tag{3.2}$$

where the dot denotes differentiation with respect to proper time. Equation (3.2) is the time equation of motion for particles of non-zero rest masses in this gravitational field. It reduces to Schwarzschild's time equation when $f(r,\theta)$ reduces to $f(r)$. The third term in equation (3.2) is the contribution of the rotation of the mass within the sphere; it does not appear in Schwarzschild's time equation of motion for test particles [1, 12–14, 17]. It is interesting and instructive to realize that equation (3.2) can be written equally as

$$\frac{d}{d\tau} \left(\ln \dot{t}\right) + \frac{d}{d\tau} \left[\ln \left(1 + \frac{2}{c^2} f(r,\theta)\right)\right] = 0. \tag{3.3}$$

Integrating equation (3.3) yields

$$\dot{t} = A \left(1 + \frac{2}{c^2} f(r,\theta)\right)^{-1}, \tag{3.4}$$

where A is the constant of integration (as $t \to \tau$, $f(r,\theta) \to 0$ and thus the constant A is equivalent to unity). Equation (3.4) is the expression for the variation of the time on a clock moving in this gravitational field. It is of same form as that in Schwarzschild's gravitational field [1, 12–14, 17].

Similarly, setting $\mu = 1$ in equation (3.1) gives the radial equation of motion as formula (3.5) on the top of this page.

For pure radial motion $\dot{\theta} \equiv \dot{\phi} = 0$ and hence equation (3.5) reduces to

$$\ddot{r} + \left[1 + \frac{2}{c^2} f(r,\theta)\right]^{-1} \frac{\partial f(r,\theta)}{\partial r} \left(1 - \frac{1}{c^2}\dot{r}^2\right) = 0 . \quad (3.6)$$

The instantaneous speed of a particle of non-zero rest mass in this gravitational field can be obtained from equations (3.5) and (3.6).

Also, setting $\mu = 2$ and $\mu = 3$ in equation (3.1) gives the respective polar and azimuthal equations of motion as

$$\ddot{\theta} + \frac{1}{r^2}\frac{\partial f(r,\theta)}{\partial \theta}\dot{t}^2 + \frac{1}{r^2 c^2}\left[1 + \frac{2}{c^2} f(r,\theta)\right]^{-2} \times \times \frac{\partial f(r,\theta)}{\partial \theta}\dot{r}^2 + \frac{2}{r}\dot{r}\dot{\theta} - \frac{1}{2}(\dot{\phi})^2 \sin 2\theta = 0 \quad (3.7)$$

and

$$\ddot{\phi} + \frac{2}{r}\dot{r}\dot{\phi} + 2\dot{\theta}\dot{\phi}\cot\theta = 0 . \quad (3.8)$$

It is instructive to note that equation (3.7) reduces satisfactorily to the polar equation of motion in Schwarzschild's gravitational field when $f(r,\theta)$ reduces to $f(r)$. Equation (3.8) is equal to the azimuthal equation of motion for particles of non-zero rest masses in Schwarzschild's field. Thus, the instantaneous azimuthal angular velocity from our field is exactly the same as that obtained from Newton's theory of gravitation [14] and Schwarzschild's metric [1, 12, 13, 17].

4 Orbits

The Lagrangian in the space time exterior to any mass or pressure distribution is defined as [17]

$$L = \frac{1}{c}\left(-g_{\alpha\beta}\frac{dx^\alpha}{d\tau}\frac{dx^\beta}{d\tau}\right)^{\frac{1}{2}} = 0 . \quad (4.1)$$

Thus, in our gravitational field, the Lagrangian can be written as

$$L = \frac{1}{c}\left[-g_{00}\left(\frac{dt}{d\tau}\right)^2 - g_{11}\left(\frac{dr}{d\tau}\right)^2\right]^{\frac{1}{2}} - - \frac{1}{c}\left[g_{22}\left(\frac{d\theta}{d\tau}\right)^2 - g_{33}\left(\frac{d\phi}{d\tau}\right)^2\right]^{\frac{1}{2}} = 0 . \quad (4.2)$$

Considering motion confined to the equatorial plane of the homogeneous spherical body, $\theta = \frac{\pi}{2}$ and hence $d\theta = 0$. Thus, in the equatorial plane, equation (4.2) reduces to

$$L = \frac{1}{c}\left[-g_{00}\left(\frac{dt}{d\tau}\right)^2 - - g_{11}\left(\frac{dr}{d\tau}\right)^2 - g_{33}\left(\frac{d\phi}{d\tau}\right)^2\right]^{\frac{1}{2}} = 0 . \quad (4.3)$$

Substituting the explicit expressions for the components of the metric tensor in the equatorial plane of the spherical body yields

$$L = \frac{1}{c}\left[-\left(1 + \frac{2}{c^2} f(r,\theta)\right)\dot{t}^2\right]^{\frac{1}{2}} + + \frac{1}{c}\left[\left(1 + \frac{2}{c^2} f(r,\theta)\right)^{-1}\dot{r}^2 + r^2\dot{\phi}^2\right]^{\frac{1}{2}} , \quad (4.4)$$

where the dot as in usual notation denotes differentiation with respect to proper time.

It is well known that the gravitational field is a conservative field. The Euler-lagrange equations of motion for a conservative system in which the potential energy is independent of the generalized velocities is written as [17]

$$\frac{\partial L}{\partial x^\alpha} = \frac{d}{d\tau}\left(\frac{\partial L}{\partial \dot{x}^\alpha}\right) , \quad (4.5)$$

but

$$\frac{\partial L}{\partial x^0} \equiv \frac{\partial L}{\partial t} = 0 , \quad (4.6)$$

by the time homogeneity of the field and thus from equation (4.5), we deduce that

$$\frac{\partial L}{\partial \dot{t}} = \text{constant} . \quad (4.7)$$

From equation (4.4), it can be shown using equation (4.7) that

$$\left(1 + \frac{2}{c^2} f(r,\theta)\right)\dot{t} = k , \qquad \dot{k} = 0 \quad (4.8)$$

where k is a constant. This the law of conservation of energy in the equatorial plane of the gravitational field [17]. It is of same form as that in Schwarzschild's field. Also, the Lagrangian for this gravitational field is invariant to azimuthal angular rotation (space is isotropic) and hence angular momentum is conserved, thus

$$\frac{\partial L}{\partial \phi} = 0 , \quad (4.9)$$

and from Lagrange's equation of motion and equation (4.4) it can be shown that

$$r^2\dot{\phi} = l , \qquad \dot{l} = 0 , \quad (4.10)$$

where l is a constant. This is the law of conservation of angular momentum in the equatorial plane of our gravitational field. It is equivalent to that obtained in Schwarzschild's gravitational field. Thus, we deduce that the laws of conservation of total energy and angular momentum are invariant in form in the two gravitational fields.

To describe orbits in Schwarzschild's space time, the Lagrangian for permanent orbits in the equatorial plane [17] is

given as;

$$L = \left\{ \left(1 - \frac{2GM}{c^2 r}\right)\left(\frac{dt}{d\tau}\right)^2 - \right. \\ \left. - \frac{1}{c^2}\left[\left(1 - \frac{2GM}{c^2 r}\right)^{-1}\left(\frac{dr}{d\tau}\right)^2 + r^2\left(\frac{d\phi}{d\tau}\right)^2\right]\right\}^{\frac{1}{2}}. \quad (4.11)$$

For time-like orbits, the Lagrangian gives the planetary equation of motion in Schwarzschild's space time as

$$\frac{d^2u}{d\phi^2} + u = \frac{GM}{h^2} + 3\frac{GM}{c^2}u^2, \quad (4.12)$$

where $u = \frac{1}{r}$ and h is a constant of motion. The solution to equation (4.12) depicts the famous perihelion precession of planetary orbits [1, 14, 17]. For null orbits, the equation of motion of a photon in the vicinity of a massive sphere in Schwarzschild's field is obtained as

$$\frac{d^2u}{d\phi^2} + u = 3\frac{GM}{c^2}u^2. \quad (4.13)$$

A satisfactory theoretical explanation for the deflection of light in the vicinity of a massive sphere in Schwarzschild's space time is obtained from the solution of equation (4.13).

It is well known [17] that the Lagrangian $L = \epsilon$, with $\epsilon = 1$ for time like orbits and $\epsilon = 0$ for null orbits. Setting $L = \epsilon$ in equation (4.4) and squaring yields the Lagrangian in the equatorial plane of the gravitational field exterior to a rotating mass distribution within regions of spherical geometry as

$$\epsilon^2 = \frac{1}{c^2}\left[-\left(1 + \frac{2}{c^2}f(r,\theta)\right)\dot{t}^2\right] + \\ + \frac{1}{c^2}\left[\left(1 + \frac{2}{c^2}f(r,\theta)\right)^{-1}\dot{r}^2 + r^2\dot{\phi}^2\right]. \quad (4.14)$$

Substituting equations (4.8) and (4.10) into equation (4.14) and simplifying yields

$$\dot{r}^2 + \left(1 + \frac{2}{c^2}f(r,\theta)\right)\frac{l^2}{r^2} - \\ - 2\epsilon^2 f(r,\theta) = c^2\epsilon^2 + k^2. \quad (4.15)$$

In most applications of general relativity, we are more interested in the shape of orbits (that is, as a function of the azimuthal angle) than in their time history [1, 14, 17]. Hence, it is instructive to transform equation (4.15) into an equation in terms of the azimuthal angle ϕ. Now, let us consider the following standard transformation

$$r = r(\phi) \quad \text{and} \quad u(\phi) = \frac{1}{r(\phi)}, \quad (4.16)$$

then

$$\dot{r} = -\frac{l}{1+u^2}\frac{du}{d\phi}. \quad (4.17)$$

Imposing the transformation equations (4.16) and (4.17) on (4.15) and simplifying yields

$$\left(\frac{l}{1+u^2}\frac{dt}{d\tau}\right)^2 + \left(1 + \frac{2}{c^2}f(u,\theta)\right)u^2 - \\ - 2\epsilon^2\frac{f(u,\theta)}{l^2} = \frac{c^2\epsilon^2 + k^2}{l^2}. \quad (4.18)$$

Equation (4.18) can be integrated immediately, but it leads to elliptical integrals, which are awkward to handle [14]. We thus differentiate this equation to obtain:

$$\frac{d^2u}{d\phi^2} - 2u\left(1+u^2\right)\frac{du}{d\phi} + u\left(1+u^2\right)^2 \times \\ \times\left(1 + \frac{2}{c^2}f(u,\theta)\right) = \left(\frac{2\epsilon^2}{l^2} - \frac{u^2}{c^2}\right)\left(1+u^2\right)^2\frac{\partial f}{\partial u}. \quad (4.19)$$

For time like orbits, equation (4.19) reduces to;

$$\frac{d^2u}{d\phi^2} - 2u\left(1+u^2\right)\frac{du}{d\phi} + u\left(1+u^2\right)^2 \times \\ \times\left(1 + \frac{2}{c^2}f(u,\theta)\right) = \left(\frac{2}{l^2} - \frac{u^2}{c^2}\right)\left(1+u^2\right)^2\frac{\partial f}{\partial u}. \quad (4.20)$$

This is the planetary equation of motion in the equatorial plane of this gravitational field. It can be solved to obtain the perihelion precision of planetary orbits. This equation has additional terms (resulting from the rotation of the mass distribution), not found in the corresponding equation in Schwarzschild's field. Light rays travel on null geodesics and thus equation (4.19) yields;

$$\frac{d^2u}{d\phi^2} - 2u\left(1+u^2\right)\frac{du}{d\phi} + u\left(1+u^2\right)^2 \times \\ \times\left(1 + \frac{2}{c^2}f(u,\theta)\right) = -\frac{u^2}{c^2}\left(1+u^2\right)^2\frac{\partial f}{\partial u}. \quad (4.21)$$

as the photon equation of motion in the vicinity of the homogeneous rotating mass distribution within a static sphere. The equation contains additional terms not found in the corresponding equation in Schwarzschild's field. In the limit of special relativity, some terms in equation (4.21) vanish and the equation becomes

$$\frac{d^2u}{d\phi^2} - 2u\left(1+u^2\right)\frac{du}{d\phi} + u\left(1+u^2\right)^2 = 0. \quad (4.22)$$

The solution of the special relativistic equation, (4.22), can be used to solve the general relativistic equation, (4.21). This can be done by taking the general solution of equation (4.21) to be a perturbation of the solution of equation (4.22). The immediate consequence of this analysis is that it will produce an expression for the total deflection of light grazing the massive sphere.

5 Conclusion

The equations of motion for test particles in the gravitational field exterior to a homogeneous rotating mass distribution within a static sphere were obtained as equations (3.2), (3.5), (3.7) and (3.8). Expressions for the conservation of energy and angular momentum were obtained as equations (4.8) and (4.10) respectively. The planetary equation of motion and the photon equation of motion in the vicinity of the mass where obtained as equations (4.19) and (4.20). The immediate theoretical, physical and astrophysical consequences of the results obtained in this article are three fold.

Firstly, the planetary equation of motion and the photon equation have additional rotational terms not found in Schwarzschild's gravitational field. These equations are opened up for further research work and astrophysical interpretations.

Secondly, in approximate gravitational fields, the arbitrary function $f(r,\theta)$ can be conveniently equated to the gravitational scalar potential exterior to the body. Thus, in approximate fields, the complete solutions for the derived equations of motion can be constructed.

Thirdly, Einstein's field equations constructed using our metric tensor have only one unknown function, $f(r,\theta)$. Solution to these field equations give explicit expressions for the function, $f(r,\theta)$, which can then be interpreted physically and used in our equations of motion. Thus, our method places Einstein's geometrical gravitational field theory on the same footing with Newton's dynamical gravitational field theory; as our method introduces the dependence of the field on one and only one dependent variable, $f(r,\theta)$, comparable to one and only one gravitational scalar potential function in Newton's theory [12, 13].

Submitted on March 12, 2009 / Accepted on March 24, 2009

References

1. Bergmann P. G. Introduction to the theory of relativity. Prentice Hall, New Delhi, 1987.
2. Einstein A. The foundation of the General Theory of Relativity. *Annalen der Physik*, 1916, Bd. 49, 12–34.
3. Schwarzschild K. Über das Gravitationsfeld eines Massenpunktes nach der Einsteinschen Theorie. *Sitzungsberichte der Königlich Preussischen Akademie der Wissenschaften*, 1916, 189–196 (published in English as: Schwarzschild K. On the gravitational field of a point mass according to Einstein's theory. *Abraham Zelmanov Journal*, 2008, v. 1, 10–19).
4. Finster F., et al. Decay of solutions of the wave equation in the Kerr geometry. *Communications in Mathematical Physics*, 2006, v. 264, 465–503.
5. Anderson L., et al. Assymptotic silence of generic cosmological singularities. *Physical Review Letters*, 2001, v. 94, 51–101.
6. Czerniawski J. What is wrong with Schwarzschild's coordinates. *Concepts of Physics*, 2006, v. 3, 309–320.
7. MacCallum H. Finding and using exact solutions of the Einstein equation. arXiv: 0314.4133.
8. Rendall M. Local and global existence theorems for the Einstein equations. *Living Reviews in Relativity*, 2005; arXiv: 1092.31.
9. Stephani H., et al. Exact solutions of Einstein's field equations. Cambridge Monographs Publ., London, 2003.
10. Friedrich H. On the existence of n-geodesically complete or future complete solutions of Einstein's field equations with smooth asmptotic structure. *Communications in Mathematical Physics*, 1986, v. 107, 587–609.
11. Berger B., et al. Oscillatory approach to the singularity in vacuum spacetimes with T^2 Isometry. *Physical Reviews D*, 2001, v. 64, 6–20.
12. Howusu S.X.K. The 210 astrophysical solutions plus 210 cosmological solutions of Einstein's geometrical gravitational field equations. Jos University Press, Jos, 2007 (also available on http://www.natphilweb.com).
13. Chifu E.N. and Howusu S.X.K. Gravitational radiation and propagation field equation exterior to astrophysically real or hypothetical time varying distributions of mass within regions of spherical geometry. *Physics Essays*, 2009, v. 22, no. 1, 73–77.
14. Weinberg S. Gravitation and cosmology, J. Wiley & Sons, New York, 1972.
15. Arfken G. Mathematical methods for physicists. Academic Press, New York, 1995.
16. Rabounski D. and Borissova L. Reply to the "Certain Conceptual Anomalies in Einstein's Theory of Relativity" and related questions. *Progress in Physics*. 2008, v. 2, 166–168.
17. Dunsby P. An introduction to tensors and relativity. Shiva, Cape Town, 2000.

Experimental Verification of a Classical Model of Gravitation

Pieter Wagener

Department of Physics, NMMU South Campus, Port Elizabeth, South Africa
E-mail: Pieter.Wagener@nmmu.ac.za

A previously proposed model of gravitation is evaluated according to recent tests of higher order gravitational effects such as for gravito-electromagnetic phenomena and the properties of binary pulsars. It is shown that the model complies with all the tests.

1 Introduction

In previous articles [1–3] in this journal we presented a model of gravitation, which also led to a unified model of electromagnetism and the nuclear force. The model is based on a Lagrangian,

$$L = -m_0(c^2 + v^2)\exp R/r, \tag{1}$$

where

m_0 = *gravitational rest mass* of a test body moving at velocity $\mathbf{v}$ in the vicinity of a massive, central body of mass M,
$\gamma = 1/\sqrt{1 - v^2/c^2}$,
$R = 2GM/c^2$ is the Schwarzschild radius of the central body.

The following conservation equations follow:

$$E = mc^2 e^{R/r} = \text{total energy} = \text{constant}, \tag{2}$$

$$\mathbf{L} = e^{R/r}\mathbf{M} = \text{constant}, \tag{3}$$

$$L_z = M_z e^{R/r} = e^{R/r} m_0 r^2 \sin^2\theta\, \dot{\phi}, \tag{4}$$

$$= z\text{-component of } \mathbf{L} = \text{constant},$$

where

$$m = m_0/\gamma^2 \tag{5}$$

and

$$\mathbf{M} = (\mathbf{r} \times m_0\mathbf{v}), \tag{6}$$

is the total angular momentum of the test body.

It was shown that the tests for perihelion precession and the bending of light by a massive body are satisfied by the equations of motion derived from the conservation equations.

The *kinematics* of the system is determined by assuming the local and instantaneous validity of special relativity (SR). This leads to an expression for gravitational redshift,

$$\nu = \nu_0 e^{-R/2r} \ (\nu_0 = \text{constant}), \tag{7}$$

which agrees with observation.

The model is further confirmed by confirmation of its electromagnetic and nuclear results.

Details of all calculations appear in the doctoral thesis of the author [4].

1.1 Lorentz-type force

Applying the associated Euler-Lagrange equations to the Lagrangian gives the following Lorentz-type force:

$$\dot{\mathbf{p}} = \mathbf{E}\, m + m_0\mathbf{v} \times \mathbf{H}, \tag{8}$$

where

$$\mathbf{p} = m_0\dot{\mathbf{r}} = m_0\mathbf{v}, \tag{9}$$

$$\mathbf{E} = -\hat{\mathbf{r}}\,\frac{GM}{r^2}, \tag{10}$$

$$\mathbf{H} = \frac{GM(\mathbf{v} \times \mathbf{r})}{c^2 r^3}. \tag{11}$$

1.2 Metric formulation

The above equations can also be derived from a metric,

$$ds^2 = e^{-R/r}dt^2 - e^{R/r}(dr^2 + r^2 d\theta^2 + r^2\sin^2\theta\, d\phi^2). \tag{12}$$

Comparing this metric with that of GR,

$$ds^2 = \left(1 - \frac{R}{r}\right)dt^2 - \\ - \frac{1}{1 - \frac{R}{r}}\,dr^2 - r^2 d\theta^2 - r^2\sin^2\theta\, d\phi^2, \tag{13}$$

we note that this metric is an approximation to our metric.

2 Higher order gravitational effects

Recent measurements of higher order gravitational effects have placed stricter constraints on the viability of gravitational theories. We consider some of these.

These effects fall in two categories: (i) Measurements by earth satellites and (ii) observations of binary pulsars.

2.1 Measurements by earth satellites

These involve the so-called gravito-electromagnetic effects (GEM) such as frame-dragging, or Coriolis effect, and the geodetic displacement. Surveys of recent research are given by Ruffini and Sigismondi [5], Soffel [6] and Pascual-Sànchez et.al. [7] A list of papers on these effects is given by Bini

and Jantzen [8], but we refer in particular to a survey by Mashoon. [9]

Mashhoon points out that for a complete GEM theory, one requires an analogue of the Lorentz force law. Assuming slowly moving matter ($v \ll c$) he derives a spacetime metric of GR in a GEM form (see (1.4) of reference [9]). Assuming further that measurements are taken far from the source, ($r \gg R$) (see (1.5) of reference [9]), he derives a Lorentz-type force (see (1.11) of reference [9]),

$$\mathbf{F} = -m\mathbf{E} - 2m\frac{\mathbf{v}}{c} \times \mathbf{B}, \tag{14}$$

where m in this case is a constant.

This equation is analogous to (8). The latter equation, however, is an *exact* derivation, whereas that of Mashhoon is an approximate one for weak gravitational fields and for particles moving at slow velocities. This difference can be understood by pointing out that GR, as shown above, is an approximation to our model. This implies that all predictions of GR in this regard will be accommodated by our model.

2.2 Binary pulsars

Binary pulsars provide accurate laboratories for the determination of higher order gravitational effects as tests for the viability of gravitational models. We refer to the surveys by Esposito-Farese [10] and Damour [11, 12].

The Parametric-Post-Newtonian (PPN) formulation provides a formulation whereby the predictions of gravitational models could be verified to second order in R/r. This formulation, initially developed by Eddington [13], was further developed by especially Will and Nordtvedt [14, 15]. According to this formulation the metric coefficients of a general metric, $ds^2 = -g_{00}dt^2 + g_{rr}dr^2 + g_{\theta\theta}r^2 d\theta^2 + g_{\phi\phi}r^2 \sin^2\theta\, d\phi^2$, can be represented by the following expansions (see eqs. 1a and 1b of reference [10]):

$$-g_{00} = 1 - \frac{R}{r} + \beta^{PPN}\frac{1}{2}\left(\frac{R}{r}\right)^2 + O\left(\frac{1}{c^6}\right), \tag{15}$$

$$g_{ij} = \delta_{ij}\left(1 + \gamma^{PPN}\frac{R}{r}\right) + O\left(\frac{1}{c^4}\right). \tag{16}$$

Recent observations place the parameters in the above equations within the limits of [16]:

$$|\beta^{PPN} - 1| < 6\times10^{-4}, \tag{17}$$

and [17]

$$\gamma^{PPN} - 1 = (2.1 \pm 2.3)\times10^{-6}. \tag{18}$$

We note that the coefficients of (12) fall within these limits. This implies that the predictions of our model will agree with observations of binary pulsars, or with other sources of higher order gravitational effects.

3 Other effects

Eqs. (2) and (5) show that gravitational repulsion occurs between bodies when their masses are increased by converting radiation energy into mass. We proposed in ref. [1] that this accounts for the start of the Big Bang and the accelerating expansion of the universe. It should be possible to demonstrate this effect in a laboratory.

Conversely, the conversion of matter into radiation energy ($v \to c$) as $r \to R$ describes the formation of a black hole without the mathematical singularity of GR.

4 Conclusion

The proposed model gives a mathematically and conceptually simple method to verify higher order gravitational effects.

Submitted on February 27, 2009 / Accepted on March 31, 2009

References

1. Wagener P. C. A classical model of gravitation. *Progress in Physics*, 2008, v. 3, 21–23.
2. Wagener P. C. A unified theory of interaction: gravitation and electrodynamics. *Progress in Physics*, 2008, v. 4, 3–9.
3. Wagener P. C. A unified theory of interaction: Gravitation, electrodynamics and the strong force. *Progress in Physics*, 2009, v. 1, 33–35.
4. Wagener P. C. Principles of a theory of general interaction. PhD thesis, University of South Africa, 1987. An updated version will be published as a book during 2009.
5. Ruffini R. J. and Constantino S. Nonlinear gravitodynamics: The Lense-Thirring effect. A documentary introduction to current research. World Scientific Publishing, 2003.
6. Soffel M. H. Relativity in astrometry, celestial mechanics and geodesy. Springer-Verlag, 1989.
7. Pascual-Sànchez J.F., Floria L., San Miguel A. and Vicente R. Reference frames and gravitomagnetism. World Scientific, 2001.
8. Bini D. and Jantzen R.T. A list of references on spacetime splitting and gravitoelectromagnetism. In: Pascual-Sànchez J.F., Floria L., San Miguel A. and Vicente R., editors. Reference frames and gravitomagnetism. World Scientific, 2001, 199–224.
9. Mashhoon B. Gravitoelectromagnetism: a brief review. In: Iorio L. editor. Measuring gravitomagnetism: a challenging enterprise. Nova Publishers, 2007, 29–39; arXiv: gr-qc/0311030.
10. Esposito-Farese G. Binary-pulsar tests of strong-field gravity and gravitational radiation damping. arXiv: gr-qc/0402007.
11. Damour T. Binary systems as test-beds of gravity theories. arXiv: gr-qc/0704.0749.
12. Damour T. Black hole and neutron star binaries: theoretical challenges. arXiv: gr-qc/0705.3109.
13. Eddington A. S. Fundamental theory. Cambridge Univ. Press, Cambridge, 1946, 93–94.

14. Nordvedt Jr. K. and Will C.M. Conservation laws and preferred frames in relativistic gravity. II: experimental evidence to rule out prefered-frame theories of gravity. *Astrophys. J.*, 1972, v. 177, 775–792.

15. Will C. M. Theory and experiment in gravitational physics. Revised edition, Cambridge Univ. Press, Cambridge, 1993.

16. Will C. M. *Living Rev. Rel.*, 2001, v. 4; arXiv: gr-qc/0103036.

17. Bertotti B., Iess I., and Tortora P. A test of General Relativity using radio links with the Cassini Spacecraft. *Nature*, 2003, v. 425, 374–376.

Limits to the Validity of the Einstein Field Equations and General Relativity from the Viewpoint of the Negative-Energy Planck Vacuum State

William C. Daywitt

National Institute for Standards and Technology (retired), Boulder, Colorado, USA
E-mail: wcdaywitt@earthlink.net

It is assumed in what follows that the negative-energy Planck vacuum (see the appendix) is the underlying "space" upon which the spacetime equations of General Relativity operate. That is, General Relativity deals with the spacetime aspects of the Planck vacuum (PV). Thus, as the PV appears continuous only down to a certain length ($l = 5r_*$ or greater, perhaps), there is a limit to which the differential geometry of the general theory is valid, that point being where the "graininess" ($l \sim r_* > 0$) of the vacuum state begins to dominate. This aspect of the continuity problem is obvious; what the following deals with is a demonstration that the Einstein equation is tied to the PV, and that the Schwarzschild line elements derived from this equation may be significantly limited by the nature of that vacuum state.

A spherical object of mass m and radius r exerts a relative curvature force

$$n_r = \frac{mc^2/r}{m_*c^2/r_*} \tag{1}$$

on the negative-energy PV and the spacetime of General Relativity, where m_* and r_* are the Planck particle (PP) mass and Compton radius respectively. For example: a white dwarf of mass 9×10^{32} gm and radius 3×10^{8} cm exerts a curvature force equal to 2.7×10^{45} dyne; while a neutron star of mass 3×10^{33} gm and radius 1×10^{6} cm exerts a force of 2.7×10^{48} dyne. Dividing these forces by the 1.21×10^{49} dyne force in the denominator leads to the n-ratios $n_r = 0.0002$ and $n_r = 0.2$ at the surface of the white dwarf and neutron star respectively. As the free PP curvature force m_*c^2/r_* is assumed to be the maximum such force that can be exerted on spacetime and the PV, the n-ratio is limited to the range $n_r < 1$.

The numerator in the first of the following two expressions for the Einstein field equation derived in the appendix

$$G_{\mu\nu} = \frac{8\pi T_{\mu\nu}}{m_*c^2/r_*} \qquad \text{and} \qquad \frac{G_{\mu\nu}/6}{1/r_*^2} = \frac{T_{\mu\nu}}{\rho_*c^2} \tag{2}$$

is normalized by this maximum curvature force. The second expression ties the Einstein equation to the PPs making up the degenerate PV, where $1/r_*^2$ and ρ_*c^2 are the PPs' Gaussian curvature and mass-energy density respectively. The denominators in the second expression represent the Planck limits for the maximum curvature and the maximum equivalent mass-energy density respectively, both limits corresponding to $n_r = 1$. For larger n_r, the equations of General Relativity, derived for a continuum using differential geometry, break down for the reasons already cited.

The limits on the Einstein equation carry over, of course, to results derived therefrom. A simple example is the case of Schwarzschild's point-mass derivation [1]. Its more general form [2] for a point mass m at $r = 0$ consists of the infinite collection ($n = 1, 2, 3, \cdots$) of Schwarzschild-like equations with continuous, non-singular metrics for $r > 0$:

$$ds^2 = \left(1 - \frac{\alpha}{R_n}\right) c^2 dt^2 - \frac{(r/R_n)^{2n-2}\, dr^2}{1 - \alpha/R_n} - \\ - R_n^2 \left(d\theta^2 + \sin^2\theta\, d\phi^2\right), \tag{3}$$

where

$$\alpha = \frac{2mc^2}{c^4/G} = 2\,\frac{mc^2}{m_*c^2/r_*} \tag{4}$$

and

$$R_n = \left(r^n + \alpha^n\right)^{1/n} = r\left(1 + 2^n n_r^n\right)^{1/n} = \\ = \alpha\left(1 + 1/2^n n_r^n\right)^{1/n}, \tag{5}$$

where n_r is given by (1) with r in this case being the *coordinate* radius from the point mass to the field point of interest. The original Schwarzschild solution [1] corresponds to $n = 3$. Here again, r is restricted to the range $r > r_*$ due to the previous continuity arguments leading to $n_r < 1$.

The plots of the time metric

$$g_{00} = g_{00}(n; n_r) = 1 - \frac{\alpha}{R_n} = 1 - \frac{2n_r}{\left(1 + 2^n n_r^n\right)^{1/n}} \tag{6}$$

as a function of n_r in Figure 1 show its behavior as n increases from 1 to 20. The vertical axis represents g_{00} from 0 to 1 and the horizontal axis n_r over the same range. The limiting case as n increases without limit yields

$$g_{00} = 1 - 2n_r \tag{7}$$

for $n_r \leqslant 0.5$. The same limit leads from (3) to the line element

$$ds^2 = \left(1 - 2n_r\right) c^2 dt^2 - \frac{dr^2}{\left(1 - 2n_r\right)} - \\ - r^2 \left(d\theta^2 + \sin^2\theta\, d\phi^2\right), \tag{8}$$

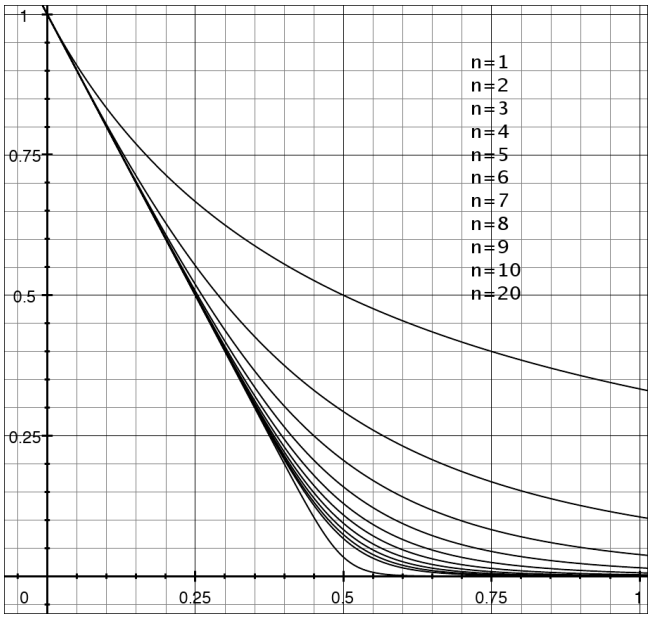

Fig. 1: The graph shows the time metric $g_{00} = g_{00}(n; n_r)$ plotted as a function of the n-ratio n_r for various indices n. Both axes run from 0 to 1. The "dog-leg" in the curves approaches the point (0.5,0) from above ($n_r > 0.5$) as n increases, the limiting case $n \to \infty$ yielding the metric $g_{00} = 1 - 2n_r$ for $n_r \leqslant 0.5$.

for $n_r \leqslant 0.5$. This is the same equation as the standard black-hole/event-horizon line element [3, p.360] except for the reduced range in n_r. Mathematically, the metrics in (3) are non-singular down to any $r > 0$, but we have already seen that this latter inequality should be replaced by $r > r_* > 0$ as $n_r < 1$.

As n_r increases from 0.5, it is assumed that a point is reached prior to $n_r = 1$ where the curvature stress on the PV is sufficient to allow energy to be released from the PV directly into the visible universe. A related viewpoint can be found in a closely similar, field-theoretic context:

> "[This release of energy] is in agreement with observational astrophysics, which in respect of high-energy activity is all of explosive outbursts, as seen in the QSOs, the active galactic nuclei, etc. The profusion of sites where X-ray and γ-ray activity is occurring are in the present [quasi-steady-state] theory sites where the creation of matter is currently taking place" [4, p. 340].

In summary: the obvious restraint on the Einstein field equations is that their time and space differentials be an order of magnitude or so greater than r_*/c and r_* respectively; and that $n_r < 1$, with some thought being given to the application of the equations in the region where $0.5 < n_r < 1$.

Appendix The Planck vacuum

The PV [5] is a uni-polar, omnipresent, degenerate gas of negative-energy PPs which are characterized by the triad (e_*, m_*, r_*), where e_*, m_*, and r_* ($\lambda_*/2\pi$) are the PP charge, mass, and Compton radius respectively. The vacuum is held together by van der Waals forces. The charge e_* is the bare (true) electronic charge common to all charged elementary particles and is related to the observed electronic charge e through the fine structure constant $\alpha = e^2/e_*^2$ which is a manifestation of the PV polarizability. The PP mass and Compton radius are equal to the Planck mass and length respectively. The particle-PV interaction is the source of the gravitational ($G = e_*^2/m_*^2$) and Planck ($\hbar = e_*^2/c$) constants, and the string of Compton relations

$$r_* m_* = \cdots = r_c m = \cdots = e_*^2/c^2 = \hbar/c \qquad \text{(A1)}$$

relating the PV and its PPs to the observed elementary particles, where the charged elementary particles are characterized by the triad (e_*, m, r_c), m and r_c being the mass and Compton radius ($\lambda_c/2\pi$) of the particle (particle spin is not yet included in the theory). The zero-point random motion of the PP charges e_* about their equilibrium positions within the PV, and the PV dynamics, are the source of the quantum vacuum [6] [7]. Neutrinos appear to be phonon packets that exist and propagate within the PV [8].

The Compton relations (A1) follow from the fact that an elementary particle exerts two perturbing forces on the PV, a curvature force mc^2/r and a polarization force e_*^2/r^2:

$$\frac{mc^2}{r} = \frac{e_*^2}{r^2} \qquad \Longrightarrow \qquad r_c = \frac{e_*^2}{mc^2} \qquad \text{(A2)}$$

whose magnitudes are equal at the particle's Compton radius r_c.

Equating the first and third expressions in (A1) leads to $r_* m_* = e_*^2/c^2$. Changing this result from Gaussian to MKS units yields the free-space permittivities

$$\epsilon_0 = \frac{1}{\mu_0 c^2} = \frac{e_*^2}{4\pi r_* m_* c^2} \quad \text{[mks]}, \qquad \text{(A3)}$$

where $\mu_0/4\pi = r_* m_*/e_*^2 = r_c m/e_*^2 = 10^{-7}$ in MKS units. Converting (A3) back into Gaussian units gives

$$\epsilon = \frac{1}{\mu} = \frac{e_*^2}{r_* m_* c^2} = 1 \qquad \text{(A4)}$$

for the permittivities.

A feedback mechanism in the particle-PV interaction leads to the Maxwell equations and the Lorentz transformation [5] [9].

General Relativity describes the spacetime-curvature aspects of the PV. The ultimate curvature force

$$\frac{c^4}{G} = \frac{m_* c^2}{r_*} \qquad \text{(A5)}$$

that can be exerted on spacetime and the PV is due to a free PP. An astrophysical object of mass m exerts a curvature force equal to mc^2/r at a coordinate distance r from the center of the mass. Equation (A5) leads to the ratio

$$\frac{c^4}{8\pi G} = \frac{1}{6}\,\frac{\rho_* c^2}{1/r_*^2}, \qquad \text{(A6)}$$

where $\rho_* \equiv m_*/(4\pi r_*^3/3)$ is the PP mass density and $1/r_*^2$ is its Gaussian curvature. The Einstein equation including the cosmological constant Λ can then be expressed as

$$\frac{(G_{\mu\nu} + \Lambda g_{\mu\nu})/6}{1/r_*^2} = \frac{T_{\mu\nu}}{\rho_* c^2} \qquad \text{(A7)}$$

tying the differential geometry of Einstein to the PPs in the negative-energy PV. In this form both sides of the equation are dimensionless.

Submitted on April 12, 2009 / Accepted on April 28, 2009

References

1. Schwarzschild K. Über das Gravitationsfeld eines Massenpunktes nach der Einsteinschen Theorie. *Sitzungsberichte der Königlich Preussischen Akademie der Wissenschaften*, 1916, 189–196 (published in English as: Schwarzschild K. On the gravitational field of a point mass according to Einstein's theory. *Abraham Zelmanov Journal*, 2008, v. 1, 10–19).
2. Crothers S. J. On the general solution to Einstein's vacuum field and its implications for relativistic degeneracy. *Progress in Physics*, 2005, v. 1, 68.
3. Carroll B. W., Ostlie D. A. An introduction to modern astrophysics. Addison-Wesley, San Francisco — Toronto, 2007.
4. Narlikar J. V. An introduction to cosmology. Third edition, Cambridge Univ. Press, Cambridge, UK, 2002.
5. Daywitt W. C. The planck vacuum. *Progress in Physics*, 2009, v. 1, 20.
6. Daywitt W. C. The source of the quantum vacuum. *Progress in Physics*, 2009, v. 1, 27.
7. Milonni P. W. The quantum vacuum — an introduction to quantum electrodynamics. Academic Press, New York, 1994.
8. Daywitt W. C. The neutrino: evidence of a negative-energy vacuum state. *Progress in Physics*, 2009, v. 2, 3.
9. Pemper R. R. A classical foundation for electrodynamics. Master Dissertation, U. of Texas, El Paso, 1977. Barnes T.G. Physics of the future — a classical unification of physics. Institute for Creation Research, California, 1983, 81.

The Planck Vacuum and the Schwarzschild Metrics

William C. Daywitt

National Institute for Standards and Technology (retired), Boulder, Colorado, USA
E-mail: wcdaywitt@earthlink.net

The Planck vacuum (PV) is assumed to be the source of the visible universe [1, 2]. So under conditions of sufficient stress, there must exist a pathway through which energy from the PV can travel into this universe. Conversely, the passage of energy from the visible universe to the PV must also exist under the same stressful conditions. The following examines two versions of the Schwarzschild metric equation for compatability with this open-pathway idea.

The first version is the general solution to the Einstein field equations [3, 4] for a point mass m at $r = 0$ and consists of the infinite collection ($n = 1, 2, 3, \cdots$) of Schwarzschild-like equations with continuous, non-singular metrics for all $r > 0$:

$$ds^2 = \left(1 - \frac{\alpha}{R_n}\right) c^2 dt^2 - \frac{(r/R_n)^{2n-2}\, dr^2}{1 - \alpha/R_n} - \\ - R_n^2 \left(d\theta^2 + \sin^2\theta\, d\phi^2\right), \tag{1}$$

where

$$\alpha = \frac{2mc^2}{m_* c^2/r_*} = 2rn_r\,, \tag{2}$$

$$R_n = \left(r^n + \alpha^n\right)^{1/n} = r\left(1 + 2^n n_r^n\right)^{1/n} = \\ = \alpha\left(1 + 1/2^n n_r^n\right)^{1/n}, \tag{3}$$

and

$$n_r = \frac{mc^2/r}{m_* c^2/r_*}\,, \tag{4}$$

where r is the *coordinate* radius from the point mass to the field point of interest, and m_* and r_* are the Planck particle mass and Compton radius respectively. The n-ratio n_r is the relative stress the point mass exerts on the PV, its allowable range being $0 < n_r < 1$ which translates into $r > r_*$. The original Schwarzschild line element [5] corresponds to $n = 3$.

The magnitude of the relative coordinate velocity of a photon approaching or leaving the point mass in a radial direction is calculated from the metrics in (1) (by setting $ds = 0$, $d\theta = 0$, $d\phi = 0$) and leads to

$$\beta_n(n_r) = \left|\frac{dr}{c\,dt}\right| = \left(\frac{g_{00}}{-g_{11}}\right)^{1/2} = \\ = \left(1 + 2^n n_r^n\right)^{(1-1/n)} \left(1 - \frac{2n_r}{\left(1 + 2^n n_r^n\right)^{1/n}}\right) \tag{5}$$

whose plot as a function of n_r in Figure 1 shows β_n's behavior as n increases from 1 to 20. The vertical and horizontal axes run from 0 to 1. The limiting case as n increases without limit is

$$\beta_\infty(n_r) = \begin{cases} 1 - 2n_r, & 0 < n_r \leqslant 0.5 \\ 0, & 0.5 \leqslant n_r < 1\,. \end{cases} \tag{6}$$

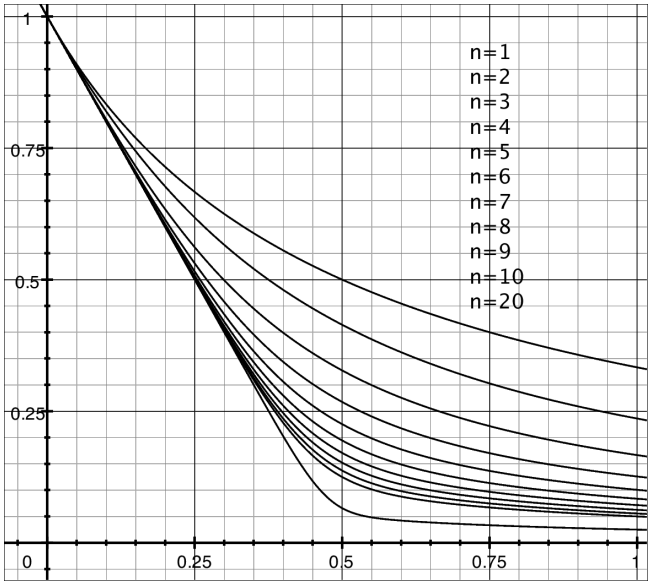

Fig. 1: The graph shows the relative photon velocity $\beta_n(n_r)$ plotted as a function of the n-ratio n_r for various indices n. Both axes run from 0 to 1. The limiting case $n \to \infty$ yields $\beta_n(n_r) = 1 - 2n_r$ for $n_r \leqslant 0.5$.

That is, the photon does not propagate ($\beta_\infty(n_r) = 0$) in the region $0.5 \leqslant n_r < 1$ for the limiting case. So if photon propagation is expected for n_r in this range, i.e., if energy transfer between the stressed PV and the visible universe is assumed, then the "$n = \infty$" solution must be discarded.

The second version of the Schwarzschild line element [6, p. 634]

$$ds^2 = \left(1 - 2n_r\right) c^2 dt^2 - \frac{dr^2}{\left(1 - 2n_r\right)} - \\ - r^2 \left(d\theta^2 + \sin^2\theta\, d\phi^2\right) \tag{7}$$

is the standard black-hole line element universally employed to interpret various astrophysical observations, where $2n_r = 1$ leads to the so-called Schwarzschild radius

$$R_s = \frac{2mc^2}{m_* c^2/r_*} = 2rn_r \tag{8}$$

the interior ($r < R_s$) of which is called the black hole. Within this black hole is the naked singularity at the coordinate radius $r = 0$ where the black-hole mass is assumed to reside—hiding this singularity is the event-horizon sphere with the Schwarzschild radius. It should be noted that this version is the same as the previous version with $n \to \infty$ except that there the coordinate radius is restricted to $r > r_*$ as $n_r < 1$. Equations (1) and (7) are functionally identical if one assumes that $R_n = r$, this being the assumption (for $n = 3$) that led to the standard version of the Schwarzschild equation.

The photon velocity calculated from (7) is the same as (6). That is, there is no energy propagation ($\beta = 0$) in the region $0.5 \leqslant n_r < 1$; so the standard Schwarzschild solution to the Einstein equation is not compatible with the assumed existence of the PV as a source for the visible universe, and thus must be discarded in the PV scenario.

Submitted on April 18, 2009 / Accepted on April 28, 2009

References

1. Daywitt W. C. The Planck vacuum. *Progress in Physics*, 2009, v. 1, 20.
2. Daywitt W. C. The source of the quantum vacuum. *Progress in Physics*, 2009, v. 1, 27.
3. Crothers S. J. On the general solution to Einstein's vacuum field and its implications for relativistic degeneracy. *Progress in Physics*, 2005, v. 1, 68.
4. Daywitt W. C. Limits to the validity of the Einstein field equations and General Relativity from the viewpoint of the negative-energy Planck vacuum state. *Progress in Physics*, 2009, v. 3, 27.
5. Schwarzschild K. Über das Gravitationsfeld eines Massenpunktes nach der Einsteinschen Theorie. *Sitzungsberichte der Königlich Preussischen Akademie der Wissenschaften*, 1916, 189–196 (published in English as: Schwarzschild K. On the gravitational field of a point mass according to Einstein's theory. *Abraham Zelmanov Journal*, 2008, v. 1, 10–19).
6. Carroll B. W., Ostlie D. A. An introduction to modern astrophysics. Addison-Wesley, San Francisco — Toronto, 2007.

Higgsless Glashow's and Quark-Gluon Theories and Gravity without Superstrings

Gunn Alex Quznetsov

Chelyabinsk State University, Chelyabinsk, Ural, Russia
E-mail: gunn@mail.ru, quznets@yahoo.com

This is the probabilistic explanation of some laws of physics (gravitation, red shift, electroweak, confinement, asymptotic freedom phenomenons).

1 Introduction

I do not construct any models because Physics does not need any strange hypotheses. Electroweak, quark-gluon, and gravity phenomenons are explained purely logically from spinor expression of probabilities:

Denote:

$$1_2 := \begin{bmatrix} 1 & 0 \\ 0 & 1 \end{bmatrix}, 0_2 := \begin{bmatrix} 0 & 0 \\ 0 & 0 \end{bmatrix},$$

$$\beta^{[0]} := -\begin{bmatrix} 1_2 & 0_2 \\ 0_2 & 1_2 \end{bmatrix} = -1_4,$$

the Pauli matrices:

$$\sigma_1 = \begin{bmatrix} 0 & 1 \\ 1 & 0 \end{bmatrix}, \sigma_2 = \begin{bmatrix} 0 & -\mathrm{i} \\ \mathrm{i} & 0 \end{bmatrix}, \sigma_3 = \begin{bmatrix} 1 & 0 \\ 0 & -1 \end{bmatrix}.$$

A set $\widetilde{C}$ of complex $n \times n$ matrices is called *a Clifford set of rank* n if the following conditions are fulfilled [1]:
if $\alpha_k \in \widetilde{C}$ and $\alpha_r \in \widetilde{C}$ then $\alpha_k\alpha_r + \alpha_r\alpha_k = 2\delta_{k,r}$;
if $\alpha_k\alpha_r + \alpha_r\alpha_k = 2\delta_{k,r}$ for all elements α_r of set $\widetilde{C}$ then $\alpha_k \in \widetilde{C}$.

If $n = 4$ then a Clifford set either contains 3 (*a Clifford triplet*) or 5 matrices (*a Clifford pentad*).

Here exist only six Clifford pentads [1]: one which I call *light pentad* β:

• *light pentad* β:

$$\beta^{[1]} := \begin{bmatrix} \sigma_1 & 0_2 \\ 0_2 & -\sigma_1 \end{bmatrix}, \quad \beta^{[2]} := \begin{bmatrix} \sigma_2 & 0_2 \\ 0_2 & -\sigma_2 \end{bmatrix}, \quad \beta^{[3]} := \begin{bmatrix} \sigma_3 & 0_2 \\ 0_2 & -\sigma_3 \end{bmatrix}, \tag{1}$$

$$\gamma^{[0]} := \begin{bmatrix} 0_2 & 1_2 \\ 1_2 & 0_2 \end{bmatrix}, \tag{2}$$

$$\beta^{[4]} := \mathrm{i} \cdot \begin{bmatrix} 0_2 & 1_2 \\ -1_2 & 0_2 \end{bmatrix}; \tag{3}$$

three *coloured* pentads:

• *the red pentad* ζ:

$$\zeta^{[1]} := \begin{bmatrix} -\sigma_1 & 0_2 \\ 0_2 & \sigma_1 \end{bmatrix}, \quad \zeta^{[2]} := \begin{bmatrix} \sigma_2 & 0_2 \\ 0_2 & \sigma_2 \end{bmatrix}, \quad \zeta^{[3]} := \begin{bmatrix} -\sigma_3 & 0_2 \\ 0_2 & -\sigma_3 \end{bmatrix},$$

$$\gamma_\zeta^{[0]} := \begin{bmatrix} 0_2 & -\sigma_1 \\ -\sigma_1 & 0_2 \end{bmatrix}, \zeta^{[4]} := \mathrm{i}\begin{bmatrix} 0_2 & \sigma_1 \\ -\sigma_1 & 0_2 \end{bmatrix}; \tag{4}$$

• *the green pentad* η:

$$\eta^{[1]} := \begin{bmatrix} -\sigma_1 & 0_2 \\ 0_2 & -\sigma_1 \end{bmatrix}, \quad \eta^{[2]} := \begin{bmatrix} -\sigma_2 & 0_2 \\ 0_2 & \sigma_2 \end{bmatrix}, \quad \eta^{[3]} := \begin{bmatrix} \sigma_3 & 0_2 \\ 0_2 & \sigma_3 \end{bmatrix},$$

$$\gamma_\eta^{[0]} := \begin{bmatrix} 0_2 & -\sigma_2 \\ -\sigma_2 & 0_2 \end{bmatrix}, \quad \eta^{[4]} := \mathrm{i}\begin{bmatrix} 0_2 & \sigma_2 \\ -\sigma_2 & 0_2 \end{bmatrix}; \tag{5}$$

• *the blue pentad* θ:

$$\theta^{[1]} := \begin{bmatrix} \sigma_1 & 0_2 \\ 0_2 & \sigma_1 \end{bmatrix}, \quad \theta^{[2]} := \begin{bmatrix} -\sigma_2 & 0_2 \\ 0_2 & -\sigma_2 \end{bmatrix}, \quad \theta^{[3]} := \begin{bmatrix} -\sigma_3 & 0_2 \\ 0_2 & \sigma_3 \end{bmatrix},$$

$$\gamma_\theta^{[0]} := \begin{bmatrix} 0_2 & -\sigma_3 \\ -\sigma_3 & 0_2 \end{bmatrix}, \quad \theta^{[4]} := \mathrm{i}\begin{bmatrix} 0_2 & \sigma_3 \\ -\sigma_3 & 0_2 \end{bmatrix}; \tag{6}$$

two *gustatory* pentads (about these pentads in detail, please, see in [2]):

• *the sweet pentad* $\underline{\Delta}$:

$$\underline{\Delta}^{[1]} := \begin{bmatrix} 0_2 & -\sigma_1 \\ -\sigma_1 & 0_2 \end{bmatrix}, \quad \underline{\Delta}^{[2]} := \begin{bmatrix} 0_2 & -\sigma_2 \\ -\sigma_2 & 0_2 \end{bmatrix}, \quad \underline{\Delta}^{[3]} := \begin{bmatrix} 0_2 & -\sigma_3 \\ -\sigma_3 & 0_2 \end{bmatrix},$$

$$\underline{\Delta}^{[0]} := \begin{bmatrix} -1_2 & 0_2 \\ 0_2 & 1_2 \end{bmatrix}, \quad \underline{\Delta}^{[4]} := \mathrm{i}\begin{bmatrix} 0_2 & 1_2 \\ -1_2 & 0_2 \end{bmatrix}.$$

• *the bitter pentad* $\underline{\Gamma}$:

$$\underline{\Gamma}^{[1]} := \mathrm{i}\begin{bmatrix} 0_2 & -\sigma_1 \\ \sigma_1 & 0_2 \end{bmatrix}, \quad \underline{\Gamma}^{[2]} := \mathrm{i}\begin{bmatrix} 0_2 & -\sigma_2 \\ \sigma_2 & 0_2 \end{bmatrix}, \quad \underline{\Gamma}^{[3]} := \mathrm{i}\begin{bmatrix} 0_2 & -\sigma_3 \\ \sigma_3 & 0_2 \end{bmatrix},$$

$$\underline{\Gamma}^{[0]} := \begin{bmatrix} -1_2 & 0_2 \\ 0_2 & 1_2 \end{bmatrix}, \quad \underline{\Gamma}^{[4]} := \begin{bmatrix} 0_2 & 1_2 \\ 1_2 & 0_2 \end{bmatrix}.$$

Denote: if A is a 2×2 matrix then

$$A1_4 := \left[\begin{array}{cc} A & 0_2 \\ 0_2 & A \end{array}\right] \text{ and } 1_4 A := \left[\begin{array}{cc} A & 0_2 \\ 0_2 & A \end{array}\right].$$

And if B is a 4×4 matrix then

$$A+B := A1_4 + B,\ AB := A1_4 B$$

etc.

$$\underline{x} := \langle x_0, \mathbf{x}\rangle := \langle x_0, x_1, x_2, x_3\rangle,$$
$$x_0 := ct,$$

with $\mathtt{c} = 299792458$.

2 Probabilities' movement equations

Let $\rho_{\mathtt{A}}(\underline{x})$ be a probability density [4] of a point event $\mathtt{A}(\underline{x})$. And let real functions

$$u_{\mathtt{A},1}(\underline{x}), u_{\mathtt{A},2}(\underline{x}), u_{\mathtt{A},3}(\underline{x})$$

satisfy conditions

$$u_{\mathtt{A},1}^2 + u_{\mathtt{A},2}^2 + u_{\mathtt{A},3}^2 < \mathtt{c}^2,$$

and if $j_{\mathtt{A},s} := \rho_{\mathtt{A}} u_{\mathtt{A},s}$ then

$$\rho_{\mathtt{A}} \to \rho'_{\mathtt{A}} = \frac{\rho_{\mathtt{A}} - \frac{v}{\mathtt{c}^2} j_{\mathtt{A},k}}{\sqrt{1-\left(\frac{v}{\mathtt{c}}\right)^2}},$$
$$j_{\mathtt{A},k} \to j'_{\mathtt{A},k} = \frac{j_{\mathtt{A},k} - v\rho_{\mathtt{A}}}{\sqrt{1-\left(\frac{v}{\mathtt{c}}\right)^2}},$$
$$j_{\mathtt{A},s} \to j'_{\mathtt{A},s} = j_{\mathtt{A},s} \text{ for } s \neq k$$

for $s \in \{1,2,3\}$ and $k \in \{1,2,3\}$ under the Lorentz transformations:

$$\begin{aligned} t &\to t' = \frac{t - \frac{v}{\mathtt{c}^2} x_k}{\sqrt{1-\frac{v^2}{\mathtt{c}^2}}}, \\ x_k &\to x'_k = \frac{x_k - vt}{\sqrt{1-\frac{v^2}{\mathtt{c}^2}}}, \\ x_s &\to x'_s = x_s, \text{ if } s \neq k. \end{aligned}$$

In that case $\mathbf{u}_{\mathtt{A}}\langle u_{\mathtt{A},1}, u_{\mathtt{A},2}, u_{\mathtt{A},3}\rangle$ is called *a vector of local velocity* of an event $\mathtt{A}$ *probability propagation* and

$$\mathbf{j}_{\mathtt{A}}\langle j_{\mathtt{A},1}, j_{\mathtt{A},2}, j_{\mathtt{A},3}\rangle$$

is called *a current vector* of an event $\mathtt{A}$ probability.

Let us consider the following set of four real equations with eight real unknowns:

$$b^2 \text{ with } b>0, \alpha, \beta, \chi, \theta, \gamma, \upsilon, \lambda:$$

$$\left.\begin{array}{l} b^2 = \rho_{\mathtt{A}} \\ b^2\left(\begin{array}{c}\cos^2(\alpha)\sin(2\beta)\cos(\theta-\gamma)\\ -\sin^2(\alpha)\sin(2\chi)\cos(\upsilon-\lambda)\end{array}\right) = -\frac{j_{\mathtt{A},1}}{\mathtt{c}} \\ b^2\left(\begin{array}{c}\cos^2(\alpha)\sin(2\beta)\sin(\theta-\gamma)\\ -\sin^2(\alpha)\sin(2\chi)\sin(\upsilon-\lambda)\end{array}\right) = -\frac{j_{\mathtt{A},2}}{\mathtt{c}} \\ b^2\left(\begin{array}{c}\cos^2(\alpha)\cos(2\beta)\\ -\sin^2(\alpha)\cos(2\chi)\end{array}\right) = -\frac{j_{\mathtt{A},3}}{\mathtt{c}} \end{array}\right\}. \quad (7)$$

This set has solutions for any $\rho_{\mathtt{A}}$ and $j_{\mathtt{A},k}$. For example, one of these solutions is placed in [4].

If

$$\begin{aligned} \varphi_1 &:= b\cdot\exp(\mathrm{i}\gamma)\cos(\beta)\cos(\alpha), \\ \varphi_2 &:= b\cdot\exp(\mathrm{i}\theta)\sin(\beta)\cos(\alpha), \\ \varphi_3 &:= b\cdot\exp(\mathrm{i}\lambda)\cos(\chi)\sin(\alpha), \\ \varphi_4 &:= b\cdot\exp(\mathrm{i}\upsilon)\sin(\chi)\sin(\alpha) \end{aligned} \quad (8)$$

then

$$\begin{aligned} \rho_{\mathtt{A}} &= \sum_{s=1}^{4} \varphi_s^* \varphi_s, \\ \frac{j_{\mathtt{A},r}}{\mathtt{c}} &= -\sum_{k=1}^{4}\sum_{s=1}^{4} \varphi_s^* \beta_{s,k}^{[r]} \varphi_k \end{aligned} \quad (9)$$

with $r \in \{1,2,3\}$. These functions φ_s are called *functions of event* $\mathtt{A}$ *state*.

If $\rho_{\mathtt{A}}(\underline{x}) = 0$ for all $\underline{x}$ such that $|\underline{x}| > (\pi\mathtt{c}/\mathtt{h})$ with $\mathtt{h} := 6.6260755\cdot 10^{-34}$ then $\varphi_s(\underline{x})$ are Planck's functions [3]. And if

$$\varphi := \left[\begin{array}{c}\varphi_1\\ \varphi_2\\ \varphi_3\\ \varphi_4\end{array}\right]$$

then these functions obey [5] the following equation:

$$\begin{aligned} &\sum_{k=0}^{3} \beta^{[k]}\left(\partial_k + \mathrm{i}\Theta_k + \mathrm{i}\Upsilon_k \gamma^{[5]}\right)\varphi + \\ &+\left(\begin{array}{c} +\mathrm{i}M_0\gamma^{[0]} + \mathrm{i}M_4\beta^{[4]} - \\ -\mathrm{i}M_{\zeta,0}\gamma_\zeta^{[0]} + \mathrm{i}M_{\zeta,4}\zeta^{[4]} - \\ -\mathrm{i}M_{\eta,0}\gamma_\eta^{[0]} - \mathrm{i}M_{\eta,4}\eta^{[4]} + \\ +\mathrm{i}M_{\theta,0}\gamma_\theta^{[0]} + \mathrm{i}M_{\theta,4}\theta^{[4]} \end{array}\right)\varphi = 0 \end{aligned} \quad (10)$$

with real $\Theta_k(\underline{x})$, $\Upsilon_k(\underline{x})$, $M_0(\underline{x})$, $M_4(\underline{x})$, $M_{\zeta,0}(\underline{x})$, $M_{\zeta,4}(\underline{x})$, $M_{\eta,0}(\underline{x})$, $M_{\eta,4}(\underline{x})$, $M_{\theta,0}(\underline{x})$, $M_{\theta,4}(\underline{x})$ and with

$$\gamma^{[5]} := \left[\begin{array}{cc} 1_2 & 0_2 \\ 0_2 & -1_2 \end{array}\right]. \quad (11)$$

2.1 Lepton movement equation

If $M_{\zeta,0}(\underline{x}) = 0$, $M_{\zeta,4}(\underline{x}) = 0$, $M_{\eta,0}(\underline{x}) = 0$, $M_{\eta,4}(\underline{x}) = 0$, $M_{\theta,0}(\underline{x}) = 0$, $M_{\theta,4}(\underline{x}) = 0$ then the following equation is deduced from (10):

$$\left(\begin{array}{c} \beta^{[0]} \left(\frac{1}{c} i\partial_t - \Theta_0 - \Upsilon_0 \gamma^{[5]} \right) \\ + \sum\limits_{\alpha=1}^{3} \beta^{[\alpha]} \left(i\partial_\alpha - \Theta_\alpha - \Upsilon_\alpha \gamma^{[5]} \right) \\ - M_0 \gamma^{[0]} - M_4 \beta^{[4]} \end{array} \right) \widetilde{\varphi} = 0 \qquad (12)$$

I call it *lepton movement equation* [6].

If similar to (9):

$$j_{\mathcal{A},5} := -c \cdot \varphi^{\dagger} \gamma^{[0]} \varphi \text{ and } j_{\mathcal{A},4} := -c \cdot \varphi^{\dagger} \beta^{[4]} \varphi$$

and:

$$u_{\mathcal{A},4} := j_{\mathcal{A},4} / \rho_{\mathcal{A}} \text{ and } u_{\mathcal{A},5} := j_{\mathcal{A},5} / \rho_{\mathcal{A}} \qquad (13)$$

then from (8):

$$-\frac{u_{\mathcal{A},5}}{c} = \sin 2\alpha \left(\begin{array}{c} \sin\beta \sin\chi \cos(-\theta + \upsilon) \\ + \cos\beta \cos\chi \cos(\gamma - \lambda) \end{array} \right),$$

$$-\frac{u_{\mathcal{A},4}}{c} = \sin 2\alpha \left(\begin{array}{c} -\sin\beta \sin\chi \sin(-\theta + \upsilon) \\ + \cos\beta \cos\chi \sin(\gamma - \lambda) \end{array} \right).$$

Hence from (7):

$$u_{\mathcal{A},1}^2 + u_{\mathcal{A},2}^2 + u_{\mathcal{A},3}^2 + u_{\mathcal{A},4}^2 + u_{\mathcal{A},5}^2 = c^2.$$

Thus only all five elements of a Clifford pentad provide an entire set of speed components and, for completeness, yet two "space" coordinates x_5 and x_4 should be added to our three x_1, x_2, x_3. These additional coordinates can be selected so that

$$-\frac{\pi c}{h} \leqslant x_5 \leqslant \frac{\pi c}{h}, \quad -\frac{\pi c}{h} \leqslant x_4 \leqslant \frac{\pi c}{h}.$$

Coordinates x_4 and x_5 are not coordinates of any events. Hence, our devices do not detect them as actual space coordinates.

Let us denote:

$$\widetilde{\varphi}(t, x_1, x_2, x_3, x_5, x_4) := \varphi(t, x_1, x_2, x_3) \times$$
$$\times \left(\exp\left(i \left(x_5 M_0(t, x_1, x_2, x_3) + x_4 M_4(t, x_1, x_2, x_3) \right) \right) \right).$$

In this case a lepton movement equation (12) shape is the following:

$$\left(\sum_{s=0}^{3} \beta^{[s]} \left(i\partial_s - \Theta_s - \Upsilon_s \gamma^{[5]} \right) - \gamma^{[0]} i\partial_5 - \beta^{[4]} i\partial_4 \right) \widetilde{\varphi} = 0$$

This equation can be transformated into the following form [7]:

$$\left(\begin{array}{c} \sum_{s=0}^{3} \beta^{[s]} \left(i\partial_s + F_s + 0.5 g_1 Y B_s \right) \\ -\gamma^{[0]} i\partial_5 - \beta^{[4]} i\partial_4 \end{array} \right) \widetilde{\varphi} = 0 \qquad (14)$$

with real F_s, B_s, a real positive constant g_1, and with *charge matrix* Y:

$$Y := -\left[\begin{array}{cc} 1_2 & 0_2 \\ 0_2 & 2 \cdot 1_2 \end{array} \right]. \qquad (15)$$

If $\chi(t, x_1, x_2, x_3)$ is a real function and:

$$\widetilde{U}(\chi) := \left[\begin{array}{cc} \exp\left(i\frac{\chi}{2} \right) 1_2 & 0_2 \\ 0_2 & \exp(i\chi)\, 1_2 \end{array} \right]. \qquad (16)$$

then equation (14) is invariant under the following transformations [8]:

$$\begin{array}{l} x_4 \to x_4' := x_4 \cos\frac{\chi}{2} - x_5 \sin\frac{\chi}{2}; \\ x_5 \to x_5' := x_5 \cos\frac{\chi}{2} + x_4 \sin\frac{\chi}{2}; \\ x_\mu \to x_\mu' := x_\mu \text{ for } \mu \in \{0, 1, 2, 3\}; \\ \widetilde{\varphi} \to \widetilde{\varphi}' := \widetilde{U} \widetilde{\varphi}, \\ B_\mu \to B_\mu' := B_\mu - \frac{1}{g_1} \partial_\mu \chi, \\ F_\mu \to F_\mu' := \widetilde{U} F_s \widetilde{U}^{\dagger}. \end{array} \qquad (17)$$

Therefore, B_μ are similar to components of the Standard Model gauge field B.

Further $\Im_{\mathbf{J}}$ is the space spanned by the following basis [9]:

$$\mathbf{J} := \left\langle \begin{array}{c} \frac{h}{2\pi c} \exp\left(-i\frac{h}{c}(s_0 x_4) \right) \epsilon_k, \ldots \\ \frac{h}{2\pi c} \exp\left(-i\frac{h}{c}(n_0 x_5) \right) \epsilon_r, \ldots \end{array} \right\rangle \qquad (18)$$

with some integer numbers s_0 and n_0 and with

$$\epsilon_1 := \left[\begin{array}{c} 1 \\ 0 \\ 0 \\ 0 \end{array} \right], \ \epsilon_2 := \left[\begin{array}{c} 0 \\ 1 \\ 0 \\ 0 \end{array} \right], \ \epsilon_3 := \left[\begin{array}{c} 0 \\ 0 \\ 1 \\ 0 \end{array} \right], \ \epsilon_4 := \left[\begin{array}{c} 0 \\ 0 \\ 0 \\ 1 \end{array} \right].$$

Further in this subsection U is any linear transformation of space $\Im_{\mathbf{J}}$ so that for every $\widetilde{\varphi}$: if $\widetilde{\varphi} \in \Im_{\mathbf{J}}$ then:

$$\begin{array}{c} \int\limits_{-\frac{\pi c}{h}}^{\frac{\pi c}{h}} dx_4 \int\limits_{-\frac{\pi c}{h}}^{\frac{\pi c}{h}} dx_5 \cdot (U\widetilde{\varphi})^{\dagger} (U\widetilde{\varphi}) = \rho_{\mathrm{A}}, \\ \int\limits_{-\frac{\pi c}{h}}^{\frac{\pi c}{h}} dx_4 \int\limits_{-\frac{\pi c}{h}}^{\frac{\pi c}{h}} dx_5 \cdot (U\widetilde{\varphi})^{\dagger} \beta^{[s]} (U\widetilde{\varphi}) = -\frac{j_{\mathrm{A},s}}{c} \end{array} \qquad (19)$$

for $s \in \{1, 2, 3\}$.

Matrix U is factorized as the following:

$$U = \exp(i\varsigma)\, \widetilde{U} U^{(-)} U^{(+)}$$

with real ς, with $\widetilde{U}$ from (16), and with

$$U^{(+)} := \begin{bmatrix} 1_2 & 0_2 & 0_2 & 0_2 \\ 0_2 & (u+iv)\,1_2 & 0_2 & (k+is)\,1_2 \\ 0_2 & 0_2 & 1_2 & 0_2 \\ 0_2 & (-k+is)\,1_2 & 0_2 & (u-iv)\,1_2 \end{bmatrix} \quad (20)$$

and

$$U^{(-)} := \begin{bmatrix} (a+ib)\,1_2 & 0_2 & (c+iq)\,1_2 & 0_2 \\ 0_2 & 1_2 & 0_2 & 0_2 \\ (-c+iq)\,1_2 & 0_2 & (a-ib)\,1_2 & 0_2 \\ 0_2 & 0_2 & 0_2 & 1_2 \end{bmatrix} \quad (21)$$

with real a, b, c, q, u, v, k, s.

Matrix $U^{(+)}$ refers to antiparticles (About antiparticles in detail, please, see [10] and about neutrinos - [11]). And transformation $U^{(-)}$ reduces equation (14) to the following shape:

$$\left(\begin{array}{c} \sum_{\mu=0}^{3} \beta^{[\mu]} i \begin{pmatrix} \partial_\mu - i0.5 g_1 B_\mu Y \\ -i\frac{1}{2} g_2 W_\mu - iF_\mu \end{pmatrix} \\ +\gamma^{[0]} i\partial_5 + \beta^{[4]} i\partial_4 \end{array} \right) \widetilde{\varphi} = 0. \quad (22)$$

with a real positive constant g_2 and with

$$W_\mu := \begin{bmatrix} W_{0,\mu}\,1_2 & 0_2 & (W_{1,\mu} - iW_{2,\mu})\,1_2 & 0_2 \\ 0_2 & 0_2 & 0_2 & 0_2 \\ (W_{1,\mu} + iW_{2,\mu})\,1_2 & 0_2 & -W_{0,\mu}\,1_2 & 0_2 \\ 0_2 & 0_2 & 0_2 & 0_2 \end{bmatrix}$$

with real $W_{0,\mu}$, $W_{1,\mu}$ and $W_{2,\mu}$.

Equation (22) is invariant under the following transformation:

$$\varphi \to \varphi' := U\varphi,$$
$$x_4 \to x'_4 := (\ell_\circ + \ell_*)\, a x_4 + (\ell_\circ - \ell_*)\, \sqrt{1-a^2}\, x_5,$$
$$x_5 \to x'_5 := (\ell_\circ + \ell_*)\, a x_5 - (\ell_\circ - \ell_*)\, \sqrt{1-a^2}\, x_4,$$
$$x_\mu \to x'_\mu := x_\mu, \text{ for } \mu \in \{0,1,2,3\},$$
$$B_\mu \to B'_\mu := B_\mu,$$
$$W_\mu \to W'_\mu := U W_\mu U^\dagger - \frac{2i}{g_2} (\partial_\mu U)\, U^\dagger$$

with

$$\ell_\circ := \frac{1}{2\sqrt{(1-a^2)}} \times$$
$$\times \begin{bmatrix} \left(b + \sqrt{(1-a^2)}\right) 1_4 & (q - ic)\,1_4 \\ (q + ic)\,1_4 & \left(\sqrt{(1-a^2)} - b\right) 1_4 \end{bmatrix},$$
$$\ell_* := \frac{1}{2\sqrt{(1-a^2)}} \times$$
$$\times \begin{bmatrix} \left(\sqrt{(1-a^2)} - b\right) 1_4 & (-q + ic)\,1_4 \\ (-q - ic)\,1_4 & \left(b + \sqrt{(1-a^2)}\right) 1_4 \end{bmatrix}.$$

Hence W_μ behaves the same way as components of the weak field W of Standard Model.

Field $W_{0,\mu}$ obeys the following equation [12]:

$$\left(-\frac{1}{c^2}\,\partial_t^2 + \sum_{s=1}^{3} \partial_s^2 \right) W_{0,\mu} =$$
$$= g_2^2 \left(\widetilde{W}_0^2 - \widetilde{W}_1^2 - \widetilde{W}_2^2 - \widetilde{W}_3^2 \right) W_{0,\mu} + \Lambda \quad (23)$$

with

$$\widetilde{W}_\nu := \begin{bmatrix} W_{0,\nu} \\ W_{1,\nu} \\ W_{2,\nu} \end{bmatrix}$$

and Λ is the action of other components of field W on $W_{0,\mu}$.

Equation (23) looks like the Klein-Gordon equation of field $W_{0,\mu}$ with mass

$$m := \frac{h}{c}\, g_2 \sqrt{\widetilde{W}_0^2 - \sum_{s=1}^{3} \widetilde{W}_s^2} \quad (24)$$

and with additional terms of the $W_{0,\mu}$ interactions with other components of $\widetilde{W}$. Fields $W_{1,\mu}$ and $W_{2,\mu}$ have similar equations.

The "mass" (24) is invariant under the Lorentz transformations

$$\widetilde{W}'_0 := \frac{\widetilde{W}_0 - \frac{v}{c}\widetilde{W}_k}{\sqrt{1 - \left(\frac{v}{c}\right)^2}}, \quad \widetilde{W}'_k := \frac{\widetilde{W}_k - \frac{v}{c}\widetilde{W}_0}{\sqrt{1 - \left(\frac{v}{c}\right)^2}},$$

$$\widetilde{W}'_s := \widetilde{W}_s, \text{ if } s \neq k,$$

is invariant under the turns of the $\left\langle \widetilde{W}_1, \widetilde{W}_2, \widetilde{W}_3 \right\rangle$ space

$$\left\{ \begin{array}{l} \widetilde{W}'_r := \widetilde{W}_r \cos\lambda - \widetilde{W}_s \sin\lambda \\ \widetilde{W}'_s := \widetilde{W}_r \sin\lambda + \widetilde{W}_s \cos\lambda \end{array} \right.$$

and invariant under a global weak isospin transformation $U^{(-)}$:

$$W_\nu \to W'_\nu := U^{(-)} W_\nu U^{(-)\dagger},$$

but is not invariant for a local transformation $U^{(-)}$. But local transformations for $W_{0,\mu}$, $W_{1,\mu}$ and $W_{2,\mu}$ are insignificant since all three particles are very short-lived.

The form (24) can vary in space, but locally acts like mass - i.e. it does not allow particles of this field to behave the same way as massless ones.

If

$$Z_\mu := (W_{0,\mu} \cos\alpha - B_\mu \sin\alpha),$$
$$A_\mu := (B_\mu \cos\alpha + W_{0,\mu} \sin\alpha)$$

with

$$\alpha := \arctan \frac{g_1}{g_2}$$

then masses of Z and W fulfill the following ratio:

$$m_Z = \frac{m_W}{\cos\alpha}\,.$$

If

$$\mathrm{e} := \frac{g_1 g_2}{\sqrt{g_1^2 + g_2^2}}\,,$$

and

$$\widehat{Z}_\mu := Z_\mu \frac{1}{\sqrt{g_2^2 + g_1^2}} \times$$

$$\times \begin{bmatrix} \left(g_2^2 + g_1^2\right) 1_2 & 0_2 & 0_2 & 0_2 \\ 0_2 & 2g_1^2 1_2 & 0_2 & 0_2 \\ 0_2 & 0_2 & \left(g_2^2 - g_1^2\right) 1_2 & 0_2 \\ 0_2 & 0_2 & 0_2 & 2g_1^2 1_2 \end{bmatrix},$$

$$\widehat{W}_\mu := g_2 \times$$

$$\times \begin{bmatrix} 0_2 & 0_2 & \left(W_{1,\mu} - \mathrm{i}W_{2,\mu}\right) 1_2 & 0_2 \\ 0_2 & 0_2 & 0_2 & 0_2 \\ \left(W_{1,\mu} + \mathrm{i}W_{2,\mu}\right) 1_2 & 0_2 & 0_2 & 0_2 \\ 0_2 & 0_2 & 0_2 & 0_2 \end{bmatrix},$$

$$\widehat{A}_\mu := A_\mu \begin{bmatrix} 0_2 & 0_2 & 0_2 & 0_2 \\ 0_2 & 1_2 & 0_2 & 0_2 \\ 0_2 & 0_2 & 1_2 & 0_2 \\ 0_2 & 0_2 & 0_2 & 1_2 \end{bmatrix}.$$

then equation (22) has the following form:

$$\begin{pmatrix} \sum_{\mu=0}^{3} \beta^{[\mu]} \mathrm{i} \begin{pmatrix} \partial_\mu + \mathrm{i}\mathrm{e}\widehat{A}_\mu \\ -\mathrm{i}0.5\left(\widehat{Z}_\mu + \widehat{W}_\mu\right) \end{pmatrix} \\ +\gamma^{[0]}\mathrm{i}\partial_5 + \beta^{[4]}\mathrm{i}\partial_4 \end{pmatrix} \widetilde{\varphi} = 0. \quad (25)$$

Here [13] the vector field A_μ is similar to *the electromagnetic potential* and $\left(\widehat{Z}_\mu + \widehat{W}_\mu\right)$ is similar to *the weak potential*.

2.2 Colored equations

The following part of (10) I call *colored movement equation* [3]:

$$\begin{pmatrix} \sum_{k=0}^{3} \beta^{[k]} \left(-\mathrm{i}\partial_k + \Theta_k + \Upsilon_k \gamma^{[5]}\right) - \\ -M_{\zeta,0}\gamma_\zeta^{[0]} + M_{\zeta,4}\zeta^{[4]} + \\ -M_{\eta,0}\gamma_\eta^{[0]} - M_{\eta,4}\eta^{[4]} + \\ +M_{\theta,0}\gamma_\theta^{[0]} + M_{\theta,4}\theta^{[4]} \end{pmatrix} \varphi = 0. \quad (26)$$

Here (4), (5), (6):

$$\gamma_\zeta^{[0]} = -\begin{bmatrix} 0 & 0 & 0 & 1 \\ 0 & 0 & 1 & 0 \\ 0 & 1 & 0 & 0 \\ 1 & 0 & 0 & 0 \end{bmatrix}, \quad \zeta^{[4]} = \begin{bmatrix} 0 & 0 & 0 & \mathrm{i} \\ 0 & 0 & \mathrm{i} & 0 \\ 0 & -\mathrm{i} & 0 & 0 \\ -\mathrm{i} & 0 & 0 & 0 \end{bmatrix}$$

are mass elements of red pentad;

$$\gamma_\eta^{[0]} = \begin{bmatrix} 0 & 0 & 0 & \mathrm{i} \\ 0 & 0 & -\mathrm{i} & 0 \\ 0 & \mathrm{i} & 0 & 0 \\ -\mathrm{i} & 0 & 0 & 0 \end{bmatrix}, \quad \eta^{[4]} = \begin{bmatrix} 0 & 0 & 0 & 1 \\ 0 & 0 & -1 & 0 \\ 0 & -1 & 0 & 0 \\ 1 & 0 & 0 & 0 \end{bmatrix}$$

are mass elements of green pentad;

$$\gamma_\theta^{[0]} = \begin{bmatrix} 0 & 0 & -1 & 0 \\ 0 & 0 & 0 & 1 \\ -1 & 0 & 0 & 0 \\ 0 & 1 & 0 & 0 \end{bmatrix}, \quad \theta^{[4]} = \begin{bmatrix} 0 & 0 & -\mathrm{i} & 0 \\ 0 & 0 & 0 & \mathrm{i} \\ -\mathrm{i} & 0 & 0 & 0 \\ 0 & \mathrm{i} & 0 & 0 \end{bmatrix}$$

are mass elements of blue pentad.

I call:

- $M_{\zeta,0}$, $M_{\zeta,4}$ *red lower and upper mass members*;
- $M_{\eta,0}$, $M_{\eta,4}$ *green lower and upper mass members*;
- $M_{\theta,0}$, $M_{\theta,4}$ *blue lower and upper mass members*.

The mass members of this equation form the following matrix sum:

$$\widehat{M} := \begin{pmatrix} -M_{\zeta,0}\gamma_\zeta^{[0]} + M_{\zeta,4}\zeta^{[4]} - \\ -M_{\eta,0}\gamma_\eta^{[0]} - M_{\eta,4}\eta^{[4]} + \\ +M_{\theta,0}\gamma_\theta^{[0]} + M_{\theta,4}\theta^{[4]} \end{pmatrix} =$$

$$= \begin{bmatrix} 0 & 0 & -M_{\theta,0} & M_{\zeta,\eta,0} \\ 0 & 0 & M^*_{\zeta,\eta,0} & M_{\theta,0} \\ -M_{\theta,0} & M_{\zeta,\eta,0} & 0 & 0 \\ M^*_{\zeta,\eta,0} & M_{\theta,0} & 0 & 0 \end{bmatrix} +$$

$$+\mathrm{i}\begin{bmatrix} 0 & 0 & -M_{\theta,4} & M^*_{\zeta,\eta,4} \\ 0 & 0 & M_{\zeta,\eta,4} & M_{\theta,4} \\ -M_{\theta,4} & -M^*_{\zeta,\eta,4} & 0 & 0 \\ -M_{\zeta,\eta,4} & M_{\theta,4} & 0 & 0 \end{bmatrix}$$

with $M_{\zeta,\eta,0} := M_{\zeta,0} - \mathrm{i}M_{\eta,0}$ and $M_{\zeta,\eta,4} := M_{\zeta,4} - \mathrm{i}M_{\eta,4}$.

Elements of these matrices can be turned by formula of shape [14]:

$$\begin{pmatrix} \cos\frac{\theta}{2} & \mathrm{i}\sin\frac{\theta}{2} \\ \mathrm{i}\sin\frac{\theta}{2} & \cos\frac{\theta}{2} \end{pmatrix} \begin{pmatrix} Z & X - \mathrm{i}Y \\ X + \mathrm{i}Y & -Z \end{pmatrix} \times$$

$$\times \begin{pmatrix} \cos\frac{\theta}{2} & -\mathrm{i}\sin\frac{\theta}{2} \\ -\mathrm{i}\sin\frac{\theta}{2} & \cos\frac{\theta}{2} \end{pmatrix} =$$

$$= \begin{pmatrix} Z\cos\theta - Y\sin\theta & X - \mathrm{i}\begin{pmatrix} Y\cos\theta \\ +Z\sin\theta \end{pmatrix} \\ X + \mathrm{i}\begin{pmatrix} Y\cos\theta \\ +Z\sin\theta \end{pmatrix} & -Z\cos\theta + Y\sin\theta \end{pmatrix}.$$

Hence, if:

$$U_{2,3}(\alpha) := \begin{bmatrix} \cos\alpha & \mathrm{i}\sin\alpha & 0 & 0 \\ \mathrm{i}\sin\alpha & \cos\alpha & 0 & 0 \\ 0 & 0 & \cos\alpha & \mathrm{i}\sin\alpha \\ 0 & 0 & \mathrm{i}\sin\alpha & \cos\alpha \end{bmatrix}$$

and

$$\widehat{M}' := \begin{pmatrix} -M'_{\zeta,0}\gamma^{[0]}_{\zeta} + M'_{\zeta,4}\zeta^{[4]} - \\ -M'_{\eta,0}\gamma^{[0]}_{\eta} - M'_{\eta,4}\eta^{[4]} + \\ +M'_{\theta,0}\gamma^{[0]}_{\theta} + M'_{\theta,4}\theta^{[4]} \end{pmatrix} := U^{-1}_{2,3}(\alpha)\,\widehat{M}U_{2,3}(\alpha)$$

then

$$\begin{aligned} M'_{\zeta,0} &= M_{\zeta,0}\,,\\ M'_{\eta,0} &= M_{\eta,0}\cos 2\alpha + M_{\theta,0}\sin 2\alpha\,,\\ M'_{\theta,0} &= M_{\theta,0}\cos 2\alpha - M_{\eta,0}\sin 2\alpha\,,\\ M'_{\zeta,4} &= M_{\zeta,4}\,,\\ M'_{\eta,4} &= M_{\eta,4}\cos 2\alpha + M_{\theta,4}\sin 2\alpha\,,\\ M'_{\theta,4} &= M_{\theta,4}\cos 2\alpha - M_{\eta,4}\sin 2\alpha\,. \end{aligned}$$

Therefore, matrix $U_{2,3}(\alpha)$ makes an oscillation between green and blue colours.

If α is an arbitrary real function of time-space variables ($\alpha = \alpha(t, x_1, x_2, x_3)$) then the following expression is received from equation (10) under transformation $U_{2,3}(\alpha)$ [3]:

$$\left(\frac{1}{\mathrm{c}}\partial_t + U^{-1}_{2,3}(\alpha)\,\frac{1}{\mathrm{c}}\,\partial_t U_{2,3}(\alpha) + \mathrm{i}\Theta_0 + \mathrm{i}\Upsilon_0\gamma^{[5]}\right)\varphi =$$

$$= \begin{pmatrix} \beta^{[1]}\begin{pmatrix} \partial_1 + U^{-1}_{2,3}(\alpha)\,\partial_1 U_{2,3}(\alpha) \\ +\mathrm{i}\Theta_1 + \mathrm{i}\Upsilon_1\gamma^{[5]} \end{pmatrix} \\ +\beta^{[2]}\begin{pmatrix} \partial'_2 + U^{-1}_{2,3}(\alpha)\,\partial'_2 U_{2,3}(\alpha) \\ +\mathrm{i}\Theta'_2 + \mathrm{i}\Upsilon'_2\gamma^{[5]} \end{pmatrix} \\ +\beta^{[3]}\begin{pmatrix} \partial'_3 + U^{-1}_{2,3}(\alpha)\,\partial'_3 U_{2,3}(\alpha) \\ +\mathrm{i}\Theta'_3 + \mathrm{i}\Upsilon'_3\gamma^{[5]} \end{pmatrix} \\ +\mathrm{i}M_0\gamma^{[0]} + \mathrm{i}M_4\beta^{[4]} + \widehat{M}' \end{pmatrix}\varphi\,.$$

Here

$$\begin{aligned} \Theta'_2 &:= \Theta_2\cos 2\alpha - \Theta_3\sin 2\alpha\,,\\ \Theta'_3 &:= \Theta_2\sin 2\alpha + \Theta_3\cos 2\alpha\,,\\ \Upsilon'_2 &:= \Upsilon_2\cos 2\alpha - \Upsilon_3\sin 2\alpha\,,\\ \Upsilon'_3 &:= \Upsilon_3\cos 2\alpha + \Upsilon_2\sin 2\alpha\,, \end{aligned}$$

and x'_2 and x'_3 are elements of an another coordinate system so that:

$$\begin{aligned} \frac{\partial x_2}{\partial x'_2} &= \cos 2\alpha\,,\\ \frac{\partial x_3}{\partial x'_2} &= -\sin 2\alpha\,,\\ \frac{\partial x_2}{\partial x'_3} &= \sin 2\alpha\,,\\ \frac{\partial x_3}{\partial x'_3} &= \cos 2\alpha\,,\\ \frac{\partial x_0}{\partial x'_2} &= \frac{\partial x_1}{\partial x'_2} = \frac{\partial x_0}{\partial x'_3} = \frac{\partial x_1}{\partial x'_3} = 0\,. \end{aligned}$$

Therefore, the oscillation between blue and green colours curves the space in the x_2, x_3 directions.

Similarly, matrix

$$U_{1,3}(\vartheta) := \begin{bmatrix} \cos\vartheta & \sin\vartheta & 0 & 0 \\ -\sin\vartheta & \cos\vartheta & 0 & 0 \\ 0 & 0 & \cos\vartheta & \sin\vartheta \\ 0 & 0 & -\sin\vartheta & \cos\vartheta \end{bmatrix}$$

with an arbitrary real function $\vartheta(t, x_1, x_2, x_3)$ describes the oscillation between blue and red colours which curves the space in the x_1, x_3 directions. And matrix

$$U_{1,2}(\varsigma) := \begin{bmatrix} e^{-\mathrm{i}\varsigma} & 0 & 0 & 0 \\ 0 & e^{\mathrm{i}\varsigma} & 0 & 0 \\ 0 & 0 & e^{-\mathrm{i}\varsigma} & 0 \\ 0 & 0 & 0 & e^{\mathrm{i}\varsigma} \end{bmatrix}$$

with an arbitrary real function $\varsigma(t, x_1, x_2, x_3)$ describes the oscillation between green and red colours which curves the space in the x_1, x_2 directions.

Now, let

$$U_{0,1}(\sigma) := \begin{bmatrix} \cosh\sigma & -\sinh\sigma & 0 & 0 \\ -\sinh\sigma & \cosh\sigma & 0 & 0 \\ 0 & 0 & \cosh\sigma & \sinh\sigma \\ 0 & 0 & \sinh\sigma & \cosh\sigma \end{bmatrix}.$$

and

$$\widehat{M}'' := \begin{pmatrix} -M''_{\zeta,0}\gamma^{[0]}_{\zeta} + M''_{\zeta,4}\zeta^{[4]} - \\ -M''_{\eta,0}\gamma^{[0]}_{\eta} - M''_{\eta,4}\eta^{[4]} + \\ +M''_{\theta,0}\gamma^{[0]}_{\theta} + M''_{\theta,4}\theta^{[4]} \end{pmatrix} := U^{-1}_{0,1}(\sigma)\,\widehat{M}U_{0,1}(\sigma)$$

then:

$$\begin{aligned} M''_{\zeta,0} &= M_{\zeta,0}\,,\\ M''_{\eta,0} &= \left(M_{\eta,0}\cosh 2\sigma - M_{\theta,4}\sinh 2\sigma\right)\,,\\ M''_{\theta,0} &= M_{\theta,0}\cosh 2\sigma + M_{\eta,4}\sinh 2\sigma\,,\\ M''_{\zeta,4} &= M_{\zeta,4}\,,\\ M''_{\eta,4} &= M_{\eta,4}\cosh 2\sigma + M_{\theta,0}\sinh 2\sigma\,,\\ M''_{\theta,4} &= M_{\theta,4}\cosh 2\sigma - M_{\eta,0}\sinh 2\sigma\,. \end{aligned}$$

Therefore, matrix $U_{0,1}(\sigma)$ makes an oscillation between green and blue colours with an oscillation between upper and lower mass members.

If σ is an arbitrary real function of time-space variables ($\sigma = \sigma(t, x_1, x_2, x_3)$) then the following expression is received from equation (10) under transformation $U_{0,1}(\sigma)$ [3]:

$$\left(\begin{array}{l} \beta^{[0]} \left(\begin{array}{l} \frac{1}{\mathrm{c}} \partial'_t + U^{-1}_{0,1}(\sigma) \frac{1}{\mathrm{c}} \partial'_t U_{0,1}(\sigma) \\ + \mathrm{i}\Theta''_0 + \mathrm{i}\Upsilon''_0 \gamma^{[5]} \end{array} \right) \\ + \beta^{[1]} \left(\begin{array}{l} \partial'_1 + U^{-1}_{0,1}(\sigma) \partial'_1 U_{0,1}(\sigma) \\ + \mathrm{i}\Theta''_1 + \mathrm{i}\Upsilon''_1 \gamma^{[5]} \end{array} \right) \\ + \beta^{[2]} \left(\begin{array}{l} \partial_2 + U^{-1}_{0,1}(\sigma) \partial_2 U_{0,1}(\sigma) \\ + \mathrm{i}\Theta_2 + \mathrm{i}\Upsilon_2 \gamma^{[5]} \end{array} \right) \\ + \beta^{[3]} \left(\begin{array}{l} \partial_3 + U^{-1}_{0,1}(\sigma) \partial_3 U_{0,1}(\sigma) \\ + \mathrm{i}\Theta_3 + \mathrm{i}\Upsilon_3 \gamma^{[5]} \end{array} \right) \\ + \mathrm{i}M_0 \gamma^{[0]} + \mathrm{i}M_4 \beta^{[4]} + \widehat{M}'' \end{array} \right) \varphi = 0$$

with

$$\begin{aligned} \Theta''_0 &:= \Theta_0 \cosh 2\sigma + \Theta_1 \sinh 2\sigma , \\ \Theta''_1 &:= \Theta_1 \cosh 2\sigma + \Theta_0 \sinh 2\sigma , \\ \Upsilon''_0 &:= \Upsilon_0 \cosh 2\sigma + \Upsilon_1 \sinh 2\sigma , \\ \Upsilon''_1 &:= \Upsilon_1 \cosh 2\sigma + \Upsilon_0 \sinh 2\sigma \end{aligned}$$

and t' and x'_1 are elements of an another coordinate system so that:

$$\left. \begin{array}{l} \dfrac{\partial x_1}{\partial x'_1} = \cosh 2\sigma \\ \dfrac{\partial t}{\partial x'_1} = \dfrac{1}{\mathrm{c}} \sinh 2\sigma \\ \dfrac{\partial x_1}{\partial t'} = \mathrm{c} \sinh 2\sigma \\ \dfrac{\partial t}{\partial t'} = \cosh 2\sigma \\ \dfrac{\partial x_2}{\partial t'} = \dfrac{\partial x_3}{\partial t'} = \dfrac{\partial x_2}{\partial x'_1} = \dfrac{\partial x_3}{\partial x'_1} = 0 \end{array} \right\} . \qquad (27)$$

Therefore, the oscillation between blue and green colours with the oscillation between upper and lower mass members curves the space in the t, x_1 directions.

Similarly, matrix

$$U_{0,2}(\phi) := \begin{bmatrix} \cosh\phi & \mathrm{i}\sinh\phi & 0 & 0 \\ -\mathrm{i}\sinh\phi & \cosh\phi & 0 & 0 \\ 0 & 0 & \cosh\phi & -\mathrm{i}\sinh\phi \\ 0 & 0 & \mathrm{i}\sinh\phi & \cosh\phi \end{bmatrix}$$

with an arbitrary real function $\phi(t, x_1, x_2, x_3)$ describes the oscillation between blue and red colours with the oscillation between upper and lower mass members curves the space in the t, x_2 directions. And matrix

$$U_{0,3}(\iota) := \begin{bmatrix} e^{\iota} & 0 & 0 & 0 \\ 0 & e^{-\iota} & 0 & 0 \\ 0 & 0 & e^{-\iota} & 0 \\ 0 & 0 & 0 & e^{\iota} \end{bmatrix}$$

with an arbitrary real function $\iota(t, x_1, x_2, x_3)$ describes the oscillation between green and red colours with the oscillation between upper and lower mass members curves the space in the t, x_3 directions.

From (27):

$$\begin{aligned} \frac{\partial x_1}{\partial t'} &= \mathrm{c} \sinh 2\sigma , \\ \frac{\partial t}{\partial t'} &= \cosh 2\sigma . \end{aligned}$$

Because

$$\begin{aligned} \sinh 2\sigma &= \frac{v}{\sqrt{1 - \frac{v^2}{\mathrm{c}^2}}} , \\ \cosh 2\sigma &= \frac{1}{\sqrt{1 - \frac{v^2}{\mathrm{c}^2}}} \end{aligned}$$

where v is a velocity of system $\{t', x'_1\}$ as respects system $\{t, x_1\}$ then

$$v = \tanh 2\sigma .$$

Let

$$2\sigma := \omega(x_1) \frac{t}{x_1}$$

with

$$\omega(x_1) := \frac{\lambda}{|x_1|} ,$$

where λ is a real constant bearing positive numerical value.

In that case

$$v(t, x_1) = \tanh\left(\omega(x_1) \frac{t}{x_1} \right)$$

and if g is an acceleration of system $\{t', x'_1\}$ as respects system $\{t, x_1\}$ then

$$g(t, x_1) = \frac{\partial v}{\partial t} = \frac{\omega(x_1)}{x_1 \cosh^2\left(\omega(x_1) \frac{t}{x_1} \right)} .$$

Figure 1 shows the dependency of a system $\{t', x'_1\}$ velocity $v(t, x_1)$ on x_1 in system $\{t, x_1\}$.

This velocity in point A is not equal to one in point B. Hence, an oscillator, placed in B has a nonzero velocity in respects an observer placed in point A. Therefore, from the Lorentz transformations this oscillator frequency for observer placed in point A is less than own frequency of this oscillator (*red shift*).

Figure 2 shows the dependency of a system $\{t', x'_1\}$ acceleration $g(t, x_1)$ on x_1 in system $\{t, x_1\}$.

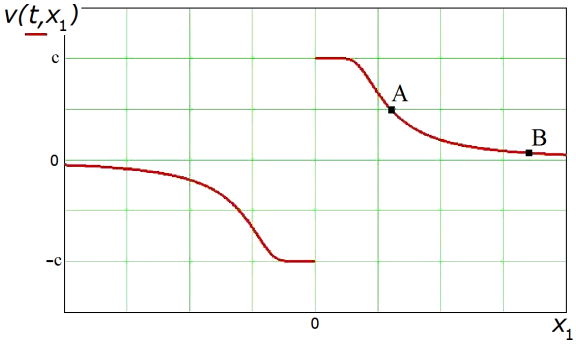

Fig. 1: Dependency of $v(t, x_1)$ from x_1 [3].

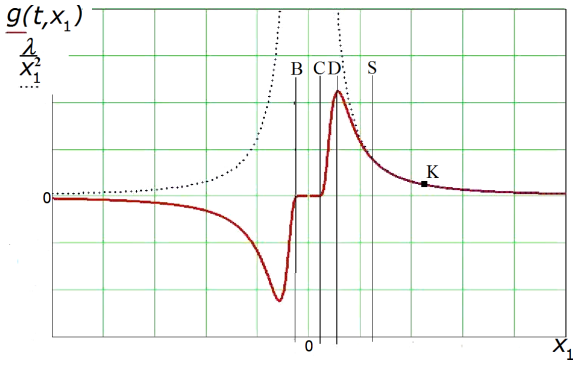

Fig. 2: Dependency of $g(t, x_1)$ from x_1 [3].

If an object immovable in system $\{t, x_1\}$ is placed in point K then in system $\{t', x_1'\}$ this object must move to the left with acceleration g and $g \simeq \lambda / x_1^2$.

I call:

- interval from S to ∞: *Newton Gravity Zone*,
- interval from B to C: *Asymptotic Freedom Zone*,
- and interval from C to D: *Confinement Force Zone*.

Now let

$$\widetilde{U}(\chi) := \begin{bmatrix} e^{i\chi} & 0 & 0 & 0 \\ 0 & e^{i\chi} & 0 & 0 \\ 0 & 0 & e^{2i\chi} & 0 \\ 0 & 0 & 0 & e^{2i\chi} \end{bmatrix}$$

and

$$\widehat{M'} := \begin{pmatrix} -M'_{\zeta,0}\gamma_\zeta^{[0]} + M'_{\zeta,4}\zeta^{[4]} - \\ -M'_{\eta,0}\gamma_\eta^{[0]} - M'_{\eta,4}\eta^{[4]} + \\ +M'_{\theta,0}\gamma_\theta^{[0]} + M'_{\theta,4}\theta^{[4]} \end{pmatrix} := \widetilde{U}^{-1}(\chi)\,\widehat{M}\widetilde{U}(\chi)$$

then:

$$\begin{aligned} M'_{\zeta,0} &= (M_{\zeta,0}\cos\chi - M_{\zeta,4}\sin\chi), \\ M'_{\zeta,4} &= (M_{\zeta,4}\cos\chi + M_{\zeta,0}\sin\chi), \\ M'_{\eta,4} &= (M_{\eta,4}\cos\chi - M_{\eta,0}\sin\chi), \\ M'_{\eta,0} &= (M_{\eta,0}\cos\chi + M_{\eta,4}\sin\chi), \\ M'_{\theta,0} &= (M_{\theta,0}\cos\chi + M_{\theta,4}\sin\chi), \\ M'_{\theta,4} &= (M_{\theta,4}\cos\chi - M_{\theta,0}\sin\chi). \end{aligned}$$

Therefore, matrix $\widetilde{U}(\chi)$ makes an oscillation between upper and lower mass members.

If χ is an arbitrary real function of time-space variables ($\chi = \chi(t, x_1, x_2, x_3)$) then the following expression is received from equation (26) under transformation $\widetilde{U}(\chi)$ [3]:

$$\left(\frac{1}{c}\partial_t + \frac{1}{c}\widetilde{U}^{-1}(\chi)\left(\partial_t\widetilde{U}(\chi)\right) + i\Theta_0 + i\Upsilon_0\gamma^{[5]}\right)\varphi =$$
$$= \left(\begin{array}{c} \sum_{k=1}^{3}\beta^{[k]}\left(\begin{array}{c}\partial_k + \widetilde{U}^{-1}(\chi)\left(\partial_k\widetilde{U}(\chi)\right) \\ + i\Theta_k + i\Upsilon_k\gamma^{[5]}\end{array}\right) + \\ + \widetilde{U}^{-1}(\chi)\,\widehat{M}\widetilde{U}(\chi)\end{array}\right)\varphi.$$

Now let:

$$\widehat{U}(\kappa) := \begin{bmatrix} e^{\kappa} & 0 & 0 & 0 \\ 0 & e^{\kappa} & 0 & 0 \\ 0 & 0 & e^{2\kappa} & 0 \\ 0 & 0 & 0 & e^{2\kappa} \end{bmatrix}$$

and

$$\widehat{M'} := \begin{pmatrix} -M'_{\zeta,0}\gamma_\zeta^{[0]} + M'_{\zeta,4}\zeta^{[4]} - \\ -M'_{\eta,0}\gamma_\eta^{[0]} - M'_{\eta,4}\eta^{[4]} + \\ +M'_{\theta,0}\gamma_\theta^{[0]} + M'_{\theta,4}\theta^{[4]} \end{pmatrix} := \widehat{U}^{-1}(\kappa)\,\widehat{M}\widehat{U}(\kappa)$$

then:

$$\begin{aligned} M'_{\theta,0} &= (M_{\theta,0}\cosh\kappa - iM_{\theta,4}\sinh\kappa), \\ M'_{\theta,4} &= (M_{\theta,4}\cosh\kappa + iM_{\theta,0}\sinh\kappa), \\ M'_{\eta,0} &= (M_{\eta,0}\cosh\kappa - iM_{\eta,4}\sinh\kappa), \\ M'_{\eta,4} &= (M_{\eta,4}\cosh\kappa + iM_{\eta,0}\sinh\kappa), \\ M'_{\zeta,0} &= (M_{\zeta,0}\cosh\kappa + iM_{\zeta,4}\sinh\kappa), \\ M'_{\zeta,4} &= (M_{\zeta,4}\cosh\kappa - iM_{\zeta,0}\sinh\kappa). \end{aligned}$$

Therefore, matrix $\widehat{U}(\kappa)$ makes an oscillation between upper and lower mass members, too.

If κ is an arbitrary real function of time-space variables ($\kappa = \kappa(t, x_1, x_2, x_3)$) then the following expression is received from equation (26) under transformation $\widehat{U}(\kappa)$ [3]:

$$\left(\frac{1}{c}\partial_t + \widehat{U}^{-1}(\kappa)\left(\frac{1}{c}\partial_t\widehat{U}(\kappa)\right) + i\Theta_0 + i\Upsilon_0\gamma^{[5]}\right)\varphi =$$
$$= \left(\begin{array}{c} \sum_{s=1}^{3}\beta^{[s]}\left(\begin{array}{c}\partial_s + \widehat{U}^{-1}(\kappa)\left(\partial_s\widehat{U}(\kappa)\right) \\ + i\Theta_s + i\Upsilon_s\gamma^{[5]}\end{array}\right) \\ + \widehat{U}^{-1}(\kappa)\,\widehat{M}\widehat{U}(\kappa)\end{array}\right)\varphi.$$

Denote: $U_{0,1} := U_1$, $U_{2,3} := U_2$, $U_{1,3} := U_3$, $U_{0,2} := U_4$, $U_{1,2} := U_5$, $U_{0,3} := U_6$, $\widehat{U} := U_7$, $\widetilde{U} := U_8$.

In that case for every natural k ($1 \leqslant k \leqslant 8$) there a 4×4 constant complex matrix Λ_k exists [3] so that:

$$U_k^{-1}(\beta)\,\partial_s U_k(\beta) = \Lambda_k \partial_s \beta$$

and if $r \neq k$ then for every natural r ($1 \leqslant r \leqslant 8$) there real functions $a_s^{k,r}(\alpha)$ exist so that:

$$U_k^{-1}(\alpha)\,\Lambda_r U_k(\alpha) = \sum_{s=1}^{8} a_s^{k,r}(\alpha) \cdot \Lambda_s.$$

Hence, if $\grave{U}$ is the following set:

$$\grave{U} := \left\{ U_{0,1}, U_{2,3}, U_{1,3}, U_{0,2}, U_{1,2}, U_{0,3}, \widehat{U}, \widetilde{U} \right\}$$

then for every product U of $\grave{U}$'s elements real functions $G_s^r(t, x_1, x_2, x_3)$ exist so that

$$U^{-1}(\partial_s U) = \frac{g_3}{2} \sum_{r=1}^{8} \Lambda_r G_s^r$$

with some real constant g_3 (similar to 8 gluons).

3 Conclusion

Therefore, higgsless electroweak and quark-gluon theories and gravity without superstrings can be deduced from properties of probability.

Submitted on April 14, 2009 / Accepted on April 29, 2009

References

1. For instance, Madelung E. Die Mathematischen Hilfsmittel des Physikers Springer Verlag, 1957, p. 29.
2. Quznetsov G. Logical foundation of theoretical physics. Nova Sci. Publ., NY, 2006, p. 107
3. Quznetsov G. *Progress in Physics*, 2009, v. 2, 96–106
4. Quznetsov G. Probabilistic treatment of gauge theories. In series *Contemporary Fundamental Physics*, Nova Sci. Publ., NY, 2007, pp. 29, 40–41.
5. Ibidem, p. 61.
6. Ibidem, p. 62.
7. Ibidem, p. 63.
8. Ibidem, pp. 64–68.
9. Ibidem, pp. 96–100.
10. Ibidem, pp. 91–94.
11. Ibidem, pp. 100–117.
12. Ibidem, p. 127.
13. Ibidem, pp. 130–131.
14. For instance, Ziman J. M. Elements of advanced quantum theory. Cambridge University Press, 1969, formula (6.59).

A Heuristic Model for the Active Galactic Nucleus Based on the Planck Vacuum Theory

William C. Daywitt

National Institute for Standards and Technology (retired), Boulder, Colorado, USA
E-mail: wcdaywitt@earthlink.net

The standard explanation for an active galactic nucleus (AGN) is a "central engine" consisting of a hot accretion disk surrounding a supermassive black hole [1, p. 32]. Energy is generated by the gravitational infall of material which is heated to high temperatures in this dissipative accretion disk. What follows is an alternative model for the AGN based on the Planck vacuum (PV) theory [2, Appendix], where both the energy of the AGN and its variable luminosity are explained in terms of a variable photon flux emanating from the PV.

The Einstein field equation

$$\frac{G_{\mu\nu}/6}{1/r_*^2} = \frac{T_{\mu\nu}}{\rho_* c^2} \tag{1}$$

is probably invalid in much of the region of interest ($0.5 < n_r < 1$) to the AGN modeling process, especially as n_r gets closer to unity [2]. Ignoring this concern, though, there is a non-black-hole Schwarzschild line element for an extended mass [3, 4] available for consideration. Unfortunately, this incompressible-fluid model is incompatible with the PV theory (see Appendix B). The following calculations provide a rough heuristic way around these modeling problems.

The expression to be used to estimate the mass of an AGN can be derived from the relation between a spherical mass m and its mass density ρ_0

$$m = \frac{4\pi r^3}{3}\,\rho_0 = \frac{8\pi}{6}\,\rho_0 r^3 \tag{2}$$

where $r\,(\leqslant r_0)$ is the radius of the sphere and ρ_0 is assumed to be constant. This can be expressed as

$$S_r = \frac{mc^2}{r} = \frac{8\pi}{6}\,\frac{\rho_0 c^2}{1/r^2} \tag{3}$$

in terms of the curvature stress S_r exerted on the PV at the mass' surface. The maximum stress S_* that can be exerted on the PV is given by the first ratio in

$$S_* = \frac{m_* c^2}{r_*} = \frac{8\pi}{6}\,\frac{\rho_* c^2}{1/r_*^2} \tag{4}$$

which can be transformed to the second ratio by recognizing $\rho_* = m_*/(4\pi r_*^3/3)$ as the mass density of the individual PPs making up the degenerate PV. Dividing equation (3) by (4) leads to

$$\frac{n_r(1/r^2)}{1/r_*^2} = \frac{\rho_0 c^2}{\rho_* c^2} \tag{5}$$

where the n-ratio

$$n_r = \frac{S_r}{S_*} = \frac{mc^2/r}{m_* c^2/r_*} < 1 \tag{6}$$

is the relative stress exerted by m. The curvature stress in (3) is infinite if r is allowed to vanish, but the PV theory restricts r to $r > r_*$ [2]. The surface of the AGN is at $r = r_0$ where $m = m_0$.

As an aside, it is interesting to note that the result in (5) can be made to resemble the Einstein equation in (1)

$$\frac{G_{00}/6}{1/r_*^2} = \frac{T_{00}}{\rho_* c^2} \tag{7}$$

by defining $G_{00} \equiv 6n_r(1/r^2)$ and $T_{00} \equiv \rho_0 c^2$. That G_{00} is proportional to the n-ratio n_r demonstrates in a simple way that the Einstein equation is physically related to stresses in the PV.

The time varying luminosity of an AGN can be used to estimate the AGN's radius. A simplified calculation for a typical AGN [5, p.1110] leads to the radius $r_0 = 1.1\times10^{14}$cm. From (5) with $r = r_0$, this radius can be related to the AGN mass density ρ_0 via

$$\frac{\rho_0}{\rho_*} = n_0\left(\frac{r_*}{r_0}\right)^2 \tag{8}$$

where $n_0 = (m_0 c^2/r_0)/(m_* c^2/r_*)$. From previous investigations [2, 6], a reasonable n-ratio to assume for the AGN might be $n_0 = 0.5$, leading from (8) to

$$\frac{\rho_0}{\rho_*} = 0.5\left(\frac{1.62\times10^{-33}}{1.1\times10^{14}}\right)^2 = 1.1\times10^{-94} \tag{9}$$

for the relative mass density. Then the absolute density is

$$\begin{aligned}\rho_0 &= 1.1\times10^{-94}\rho_* = \\ &= 1.1\times10^{-94}\,1.22\times10^{93} = 0.13\,[\mathrm{gm/cm^3}]\end{aligned} \tag{10}$$

which yields

$$m_0 = \frac{4\pi r_0^3\,\rho_0}{3} = \\ = \frac{4\pi(1.1\times10^{14})^3(0.13)}{3} = 7.2\times10^{41}[\mathrm{gm}] \tag{11}$$

for the mass of the AGN.

The standard calculation uses the black-hole/mass-accretion paradigm to determine the AGN mass and leads to the estimate $m_0 > 6.6\times10^{41}$gm for the typical calculation referenced above. This result compares favorably with the 7.2×10^{41}gm estimate in (11) and yields the n-ratio $n_r = 0.44$.

Currently there is no generally accepted theory for the time variability in the luminosity of an AGN [1, 7]. As mentioned above, there is also no PV-acceptable line element to be used in the AGN modeling. As a substitute, the line elements for the generalized Schwarzschild solution of a point mass will be used to address the luminosity variability. Furthermore, because the differential geometry of the General theory is certainly not applicable for $r < r_* = 1.62\times10^{-33}$ [2], the point-mass solution will be treated as a model for a "hole" of radius r_* that leads from the visible universe into the PV.

If it assumed that the luminosity of the AGN is due to a large photon flux from the PV, through the "hole", and into the visible universe, then the corresponding luminosity will be proportional to the *coordinate* velocity of this flux. If it is further assumed that the flux excites material that has collected between the coordinate radii corresponding to the n-ratios $n_r = 0.5$ and $n_r = 1$, then both the variable luminosity and its uniformity at the surface of the AGN can be explained by the model, the uniformity resulting from the compact nature of the variable-flux source at the surface $r = r_*$. (The distortion of the PV by the collection of material between 0.5 and 1 is ignored in the rough model being pursued.)

The general solution [8, 9] to the Einstein field equations leading to the Schwarzschild line elements mentioned above is given in Appendix A. The magnitude of the relative coordinate velocity of a photon approaching or leaving the area of the point mass in a radial direction can be calculated from this solution as ($n = 1, 2, 3, \ldots$)

$$\beta_n(n_r) = \left|\frac{dr}{c\,dt}\right| = \left(\frac{g_{00}}{-g_{11}}\right)^{1/2} = \\ = \left(1+2^n n_r^n\right)^{(1-1/n)}\left(1-\frac{2n_r}{\left(1+2^n n_r^n\right)^{1/n}}\right) \tag{12}$$

whose plot as a function of n_r in Figure 1 shows β_n's behavior for $n = 3, 10, 20$. The vertical and horizontal axes run from 0 to 1. The approximate n-ratios for various astrophysical bodies are labeled on the $n = 3$ curve and include white dwarfs, neutron stars, and AGNs. The free Planck particle is labeled PP.

The existence of multiple solutions ($n = 1, 2, 3, \ldots$) in the spacetime geometry suggests a dynamic condition implying the possibility of a variable n or a composite solution "oscillating" between various values of n. For example, consider a solution oscillating between the $n = 10$ and $n = 20$ indices in the figure, where the relative flux velocities at $n_r = 0.5$ are 0.125 and 0.066 respectively. Since the luminosity is proportional to these flux velocities, the variation in luminosity changes by a factor of $0.125/0.066 \sim 2$ over the period of the oscillation. Again, as the source of the flux is the compact "hole" leading from the PV, the surface of the AGN is uniformly brightened by the subsequent flux scattered by the material intervening between the "hole" and the AGN surface at $n_r = 0.5$ where from (6)

$$r_0 = \frac{2m_0c^2}{m_*c^2/r_*} \tag{13}$$

as $m = m_0$ at $r = r_0$.

"Earlier studies of galaxies and their central black holes in the nearby Universe revealed an intriguing linkage between the masses of the black holes and of the central 'bulges' of stars and gas in the galaxies.The ratio of the black hole and the bulge mass is nearly the same for a wide range of galactic sizes and ages. For central black holes from a million to many billions of times the mass of our sun, the black hole's mass is about one one-thousandth of the mass of the surrounding galactic bludge. ... This constant ratio indicates that the black hole and the bulge affect each others' growth in some sort of interactive relationship. ... The big question has been whether one grows before the other or if they grow together, maintaining their mass ratio throughout the entire process." [10] Recent measurements suggest that the constant ratio seen in nearby galaxies may not hold in the early more distant galaxies. The black holes in these young galaxies are much more massive compared to the bulges in the nearby galaxies, implying that the black holes started growing first.

The astrophysical measurements described in the preceding paragraph in terms of black holes could just as well be described by the PV model of the present paper, suggesting that the PV is the source of the energy and variability of the AGN and probably the primary gases (electrons and protons) of its galactic bulge.

Acknowledgment

The author takes pleasure in thanking a friend, Gerry Simonson, for bringing reference [10] to the author's attention.

Appendix A Crothers point mass

The general solution [6,8,9] to the Einstein field equations for a point mass m at $r = 0$ consists of the infinite collection ($n = 1, 2, 3, \ldots$) of Schwarzschild-like equations with continuous, non-singular met-

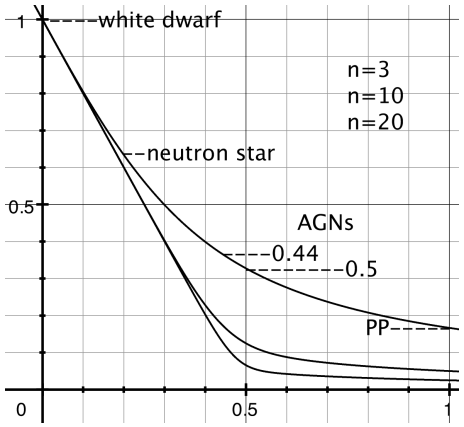

Fig. 1: The graph shows the relative coordinate velocity $\beta_n(n_r)$ plotted as a function of the n-ratio n_r for various indices n. Both axes run from 0 to 1. The approximate n-ratios corresponding to various astrophysical bodies are labeled on the $n = 3$ curve and include white dwarfs ($n_r \sim 0.0002$), neutron stars (~ 0.2), and AGNs (the 0.44 value calculated from the black-hole model and the 0.5 assumed by the PV model). The free Planck particle is represented by PP (1). The intersections of the $n = 10$ and $n = 20$ curves with the 0.5 ordinate result in the relative velocities $\beta_{10}(0.5) = 0.125$ and $\beta_{20}(0.5) = 0.066$ respectively.

rics for $r > 0$:

$$ds^2 = g_{00}\, c^2 dt^2 + g_{11}\, dr^2 - R_n^2 \left(d\theta^2 + \sin^2\theta\, d\phi^2\right) \tag{A1}$$

where

$$g_{00} = (1 - \alpha/R_n) \qquad \text{and} \qquad g_{11} = -\frac{(r/R_n)^{2n-2}}{g_{00}} \tag{A2}$$

$$\alpha = \frac{2mc^2}{m_* c^2/r_*} = 2r n_r \tag{A3}$$

$$R_n = \left(r^n + \alpha^n\right)^{1/n} = r(1 + 2^n n_r^n)^{1/n} = \\ = \alpha(1 + 1/2^n n_r^n)^{1/n} \tag{A4}$$

and

$$0 < n_r \left(= \frac{mc^2/r}{m_* c^2/r_*}\right) < 1 \tag{A5}$$

where r is the *coordinate* radius from the point mass to the field point of interest, and m_* and r_* are the PP mass and Compton radius respectively.

The metrics in (A2) yield

$$g_{00} = 1 - \frac{2n_r}{(1 + 2^n n_r^n)^{1/n}} \longrightarrow 1 \tag{A6}$$

$$-g_{11} = \frac{(1 + 2^n n_r^n)^{(2-2n)/n}}{g_{00}} \longrightarrow 1 \tag{A7}$$

with

$$R_n = r(1 + 2^n n_r^n)^{1/n} \longrightarrow r \tag{A8}$$

where the arrows lead to the far-field results for $n_r \to 0$. As expected, the n-ratio n_r in these equations is the sole variable that expresses the relative distortion of the PV due to the mass at $r = 0$.

Appendix B Incompressible fluid

Outside a spherical mass of incompressible fluid (or any static mass of the same shape), the Schwarzschild line elements [3, 4] are the same as (A1) and (A2) except that for the fluid model

$$\alpha = \left(\frac{3}{\kappa\rho_0 c^2}\right)^{1/2} \sin^3\chi_0 \tag{B1}$$

where $\kappa = 8\pi G/c^4 = 6(1/r_*^2)/\rho_* c^2$ [2]

$$R_n = (r^n + \epsilon^n)^{1/n} \tag{B2}$$

$$\sin\chi_0 = \left(\frac{\kappa\rho_0 c^2}{3}\right)^{1/2} (r_0^3 + \rho)^{1/3} \tag{B3}$$

and $\epsilon = \epsilon(\rho_0, \chi_0)$ and $\rho = \rho(\rho_0, \chi_0)$ are constants, where ρ_0 represents the constant density of the fluid. The ratios in (B1) and (B3) can be expressed as

$$\frac{3}{\kappa\rho_0 c^2} = \frac{\rho_* r_*^2}{2\rho_0} \tag{B4}$$

where $\rho_* \left(= m_*/(4\pi r_*^3/3)\right)$ is the PP mass density.

Dividing (B1) by (B2) and using (B3) leads to

$$\frac{\alpha}{R_n} = \left(\frac{\kappa\rho_0 c^2}{3}\right) \frac{r_0^3(1 + \rho/r_0^3)}{r(1 + \epsilon^n/r^n)^{1/n}}\,. \tag{B5}$$

Inserting (B4) into (B5) then gives

$$\frac{\alpha}{R_n} = 2n_r \frac{1 + \rho/r_0^3}{(1 + \epsilon^n/r^n)^{1/n}} \tag{B6}$$

after some manipulation, where the n-ratio

$$n_r = \frac{m_0 c^2/r}{m_* c^2/r_*}\,. \tag{B7}$$

Here m_0 is defined in terms of the fluid density ρ_0 and the coordinate radius r_0, where $m_0 = (4\pi r_0^3/3)\rho_0$. The radius r_0 corresponds to the coordinate radius r_a in equation (32) of reference [4].

As pointed out in Appendix A, α/R_n (which is related to the PV distortion *exterior* to the mass) should be solely a function of the variable n_r as n_r is the only relative stress the static spherical mass as a whole can exert on the exterior vacuum. Consequently the variable r can only appear within the variable n_r. Therefor the denominator in (B6), and thus the incompressible-fluid model, are incompatible with the PV model.

Submitted on May 06, 2009 / Accepted on May 11, 2009

References

1. Peterson B.M. An introduction to active galactic nuclei. Cambridge Univ. Press, Cambridge UK, 1997.
2. Daywitt W.C. Limits to the validity of the Einstein field equations and General Relativity from the viewpoint of the negative-energy Planck vacuum state. *Progress in Physics*, 2009, v. 3, 27.
3. Crothers S.J. On the vacuum field of a sphere of incompressible fluid. *Progress in Physics*, 2005, v. 12, 76.

4. Schwarzschild K. Über das Gravitationsfeld einer Kugel aus incompressiebler Flüssigkeit nach der Einsteinschen Theorie. *Sitzungsberichte der Königlich Preussischen Akademie der Wissenschaften*, 1916, 424–435 (published in English as: Schwarzschild K. On the gravitational field of a sphere of incompressible liquid, according to Einstein's theory. *Abraham Zelmanov Journal*, 2008, v. 1, 20–32).
5. Carroll B.W., Ostlie D.A. An introduction to modern astrophysics. Addison-Wesley, San Francisco — Toronto, 2007.
6. Daywitt W.C. The Planck vacuum and the Schwarzschild metrics. *Progress in Physics*, 2009, v. 3, 30.
7. Kembhavi A.K., Narlikar J.V. Quasars and active galactic nuclei — an introduction. Cambridge Univ. Press, Cambridge UK, 1999.
8. Crothers S.J. On the general solution to Einstein's vacuum field and its implications for relativistic degeneracy. *Progress in Physics*, 2005, v. 1, 68.
9. Schwarzschild K. Über das Gravitationsfeld eines Massenpunktes nach der Einsteinschen Theorie. *Sitzungsberichte der Königlich Preussischen Akademie der Wissenschaften*, 1916, 189–196 (published in English as: Schwarzschild K. On the gravitational field of a point mass according to Einstein's theory. *Abraham Zelmanov Journal*, 2008, v. 1, 10–19).
10. National Radio Astronomy Observatory: Black holes lead galaxy growth, new research shows. Socorro, NM 87801, USA, Jan. 6, 2009.

Solution of Einstein's Geometrical Gravitational Field Equations Exterior to Astrophysically Real or Hypothetical Time Varying Distributions of Mass within Regions of Spherical Geometry

Chifu Ebenezer Ndikilar* and Samuel Xede Kofi Howusu†

*Physics Department, Gombe State University, P.M.B. 127, Gombe, Gombe State, Nigeria
E-mail: ebenechifu@yahoo.com

†Physics Department, Kogi State University, Anyighba, Kogi State, Nigeria
E-mail: sxkhowusu@yahoo.co.uk

Here, we present a profound and complete analytical solution to Einstein's gravitational field equations exterior to astrophysically real or hypothetical time varying distributions of mass or pressure within regions of spherical geometry. The single arbitrary function f in our proposed exterior metric tensor and constructed field equations makes our method unique, mathematically less combersome and astrophysically satisfactory. The obtained solution of Einstein's gravitational field equations tends out to be a generalization of Newton's gravitational scalar potential exterior to the spherical mass or pressure distribution under consideration.

1 Introduction

After the publication of Einstein's geometrical gravitational field equations in 1915, the search for their exact and analytical solutions for all the gravitational fields in nature began [1]. In recent publications [2–4], we have presented a standard generalization of Schwarzschild's metric to obtain the mathematically most simple and astrophysically most satisfactory metric tensors exterior to various mass distributions within regions of spherical geometry. Our method of generating metric tensors for gravitational fields is unique as it introduces the dependence of the field on one and only one dependent function f and thus the geometrical field equations for a gravitational field exterior to any astrophysically real or hypothetical massive spherical body has only one unknown f.

In this article, the equation satisfied by the function f in the gravitational field produced at an external point by a time varying spherical mass distribution situated in empty space is considered and an analytical solution for it proposed. A possible astrophysical example of such a distribution is when one considers the vacuum gravitational field produced by a spherically symmetric star in which the material in the star experiences radial displacement or explosion.

2 Gravitational radiation and propagation field equation exterior to a time varying spherical mass distribution

The covariant metric tensor exterior to a homogeneous time varying distribution of mass within regions of spherical geometry [2] is

$$g_{00} = 1 + \frac{2}{c^2} f(t,r)\,, \tag{2.1}$$

$$g_{11} = -\left[1 + \frac{2}{c^2} f(t,r)\right]^{-1}, \tag{2.2}$$

$$g_{22} = -r^2, \tag{2.3}$$

$$g_{33} = -r^2 \sin^2\theta\,, \tag{2.4}$$

$$g_{\mu\nu} = 0;\ \text{otherwise.} \tag{2.5}$$

The corresponding contravariant metric tensor for this field, is then constructed trivially using the Quotient Theorem of tensor analysis and used to compute the affine coefficients, given explicitly as

$$\Gamma^0_{00} = \frac{1}{c^3}\left[1 + \frac{2}{c^2} f(t,r)\right]^{-1} \frac{\partial f(t,r)}{\partial t}\,, \tag{2.6}$$

$$\Gamma^0_{01} \equiv \Gamma^0_{10} = \frac{1}{c^2}\left[1 + \frac{2}{c^2} f(t,r)\right]^{-1} \frac{\partial f(t,r)}{\partial r}\,, \tag{2.7}$$

$$\Gamma^0_{11} = -\frac{1}{c^3}\left[1 + \frac{2}{c^2} f(t,r)\right]^{-3} \frac{\partial f(t,r)}{\partial t}\,, \tag{2.8}$$

$$\Gamma^1_{00} = \frac{1}{c^2}\left[1 + \frac{2}{c^2} f(t,r)\right] \frac{\partial f(t,r)}{\partial r}\,, \tag{2.9}$$

$$\Gamma^1_{01} \equiv \Gamma^1_{10} = -\frac{1}{c^3}\left[1 + \frac{2}{c^2} f(t,r)\right]^{-1} \frac{\partial f(t,r)}{\partial t}\,, \tag{2.10}$$

$$\Gamma^1_{11} = -\frac{1}{c^2}\left[1 + \frac{2}{c^2} f(t,r)\right]^{-1} \frac{\partial f(t,r)}{\partial r}\,, \tag{2.11}$$

$$\Gamma^1_{22} = -r\left[1 + \frac{2}{c^2} f(t,r)\right], \tag{2.12}$$

$$\Gamma^1_{33} = -r\sin^2\theta\left[1 + \frac{2}{c^2} f(t,r)\right], \tag{2.13}$$

$$R_{00} = \frac{4}{c^6}\left[1+\frac{2}{c^2}f(t,r)\right]^{-2}\left(\frac{\partial f}{\partial t}\right)^2 - \frac{1}{c^4}\left[1+\frac{2}{c^2}f(t,r)\right]^{-1}\frac{\partial^2 f}{\partial t^2} - \\ - \frac{1}{c^2}\left[1+\frac{2}{c^2}f(t,r)\right]\frac{\partial^2 f}{\partial r^2} - \frac{2}{rc^2}\left(1+\frac{2}{c^2}f(t,r)\right)\frac{\partial f}{\partial r} \tag{2.18}$$

$$R_{11} = -\frac{4}{c^6}\left[1+\frac{2}{c^2}f(t,r)\right]^{-4}\left(\frac{\partial f}{\partial t}\right)^2 + \frac{1}{c^4}\left[1+\frac{2}{c^2}f(t,r)\right]^{-3}\frac{\partial^2 f}{\partial t^2} + \\ + \frac{1}{c^2}\left[1+\frac{2}{c^2}f(t,r)\right]^{-1}\frac{\partial^2 f}{\partial r^2} + \frac{2}{rc^2}\left[1+\frac{2}{c^2}f(t,r)\right]^{-1}\frac{\partial f}{\partial r} \tag{2.19}$$

$$R_{22} = \frac{2}{c^2}\left[1+\frac{2}{c^2}f(t,r)\right] \tag{2.20}$$

$$R_{33} = \frac{2}{c^2}\sin^2\theta\left(r\frac{\partial f}{\partial r}+f(t,r)\right) \tag{2.21}$$

$$R_{\alpha\beta} = 0;\ \text{otherwise} \tag{2.22}$$

$$R = \frac{8}{c^6}\left[1+\frac{2}{c^2}f(t,r)\right]^{-3}\left(\frac{\partial f}{\partial t}\right)^2 - \frac{2}{c^4}\left[1+\frac{2}{c^2}f(t,r)\right]^{-2}\frac{\partial^2 f}{\partial t^2} - \frac{2}{c^2}\frac{\partial^2 f}{\partial r^2} - \frac{8}{rc^2}\frac{\partial f}{\partial r} - \frac{4f(t,r)}{r^2c^2} \tag{2.23}$$

$$\nabla^2 f(t,r) + \frac{\partial}{\partial t}\left\{\frac{1}{c^2}\left[1+\frac{2}{c^2}f(t,r)\right]^{-2}\frac{\partial f(t,r)}{\partial t}\right\} = 0 \tag{2.25}$$

$$\nabla^2 f(t,r) + \frac{1}{c^2}\left[1+\frac{2}{c^2}f(t,r)\right]^{-2}\frac{\partial^2 f(t,r)}{\partial t^2} - \frac{4}{c^4}\left[1+\frac{2}{c^2}f(t,r)\right]^{-3}\left(\frac{\partial f(t,r)}{\partial t}\right)^2 = 0 \tag{2.26}$$

$$\Gamma^2_{12} \equiv \Gamma^2_{21} \equiv \Gamma^3_{13} \equiv \Gamma^3_{31} = r^{-1}, \tag{2.14}$$

$$\Gamma^2_{33} = -\frac{1}{2}\sin 2\theta\,, \tag{2.15}$$

$$\Gamma^3_{23} \equiv \Gamma^3_{32} = \cot\theta\,, \tag{2.16}$$

$$\Gamma^\alpha_{\beta\gamma} = \quad 0;\ \text{otherwise}. \tag{2.17}$$

The Riemann-Christoffel or curvature tensor for the gravitational field is then constructed and the Ricci tensor obtained from it as (2.18)–(2.22).

From the Ricci tensor, we construct the curvature scalar R as (2.23).

Now, with the Ricci tensor and the curvature scalar, Einstein's gravitational field equations for a region exterior to a time varying spherical mass distribution is eminent. The field equations are given generally as

$$R_{\alpha\beta} - \frac{1}{2}Rg_{\alpha\beta} = 0\,. \tag{2.24}$$

Substituting the expressions for the Ricci tensor, curvature scalar and the covariant metric tensor; the R_{22} and R_{33} equations reduce identically to zero. The R_{00} and R_{11} field equations reduce identically to the single equation (2.25), or equivalently (2.26).

It is interesting and instructive to note that to the order of c^0, the geometrical wave equation (2.26) reduces to

$$\nabla^2 f(t,r) + \frac{\partial^2 f(t,r)}{\partial t^2} = 0\,. \tag{2.27}$$

Equation (2.27) admits a wave solution with a phase velocity v given as

$$v = i\ \mathrm{m\,s^{-1}}, \tag{2.28}$$

where $i = \sqrt{-1}$. Thus, such a wave exists only in imagination and is not physically or astrophysically real.

It is also worth noting that, to the order of c^2, the geometrical wave equation (2.26) reduces, in the limit of weak gravitational fields, to

$$\nabla^2 f(t,r) + \frac{1}{c^2}\frac{\partial^2 f(t,r)}{\partial t^2} = 0 \tag{2.29}$$

and equation (2.28) is the wave equation of a wave propagating with an imaginary speed *ic* in vacuum.

We now, present a profound and complete analytical solution to the field equation (2.26).

$$\frac{\partial^2}{\partial r^2} f(t,r) + \frac{2}{r}\frac{\partial}{\partial r} f(t,r) - \frac{1}{c^2}\frac{\partial}{\partial t}\left\{\left[1 - \frac{4}{c^2} f(t,r) + \frac{12}{c^4} f^2(t,r) + \ldots\right]\frac{\partial}{\partial t} f(t,r)\right\} = 0 \tag{3.1}$$

$$\frac{\partial^2}{\partial r^2} f(t,r) + \frac{2}{r}\frac{\partial}{\partial r} f(t,r) - \frac{1}{c^2}\frac{\partial^2}{\partial t^2} f(t,r) + \frac{4}{c^4} f(t,r)\frac{\partial^2}{\partial t^2} f(t,r) + \frac{4}{c^4}\left[\frac{\partial}{\partial t} f(t,r)\right]^2 + \ldots = 0 \tag{3.2}$$

$$\frac{\partial^2}{\partial r^2} f(t,r) = \sum_{n=0}^{\infty}\left[R_n''(r) - \frac{2ni\omega}{c} R_n'(r) + \frac{n^2 i^2 \omega^2}{c^2} R_n(r)\right] \exp ni\omega\left(t - \frac{r}{c}\right) \tag{3.4}$$

$$\frac{2}{r}\frac{\partial}{\partial r} f(t,r) = \sum_{n=0}^{\infty}\frac{2}{r}\left(R_n'(r) - \frac{ni\omega}{r}\right) \exp ni\omega\left(t - \frac{r}{c}\right) \tag{3.5}$$

$$\frac{1}{c^2}\frac{\partial^2}{\partial t^2} f(t,r) = \frac{1}{c^2}\sum_{n=0}^{\infty} n^2 i^2 \omega^2 R_n \exp\ ni\omega\left(t - \frac{r}{c}\right) \tag{3.6}$$

$$\begin{aligned} f(t,r)\frac{\partial^2 f(t,r)}{\partial t^2} = {} & i^2\omega^2 R_0 R_1 \exp i\omega\left(t - \frac{r}{c}\right) + \left[2^2 i^2 \omega^2 R_0 R_2 + i\omega^2 R_1^2\right] \exp 2i\omega\left(t - \frac{r}{c}\right) + \\ & + \left[3^2 i^2 \omega^2 R_0 R_3 + 2^2 i^2 \omega^2 R_1 R_2 + i^2 \omega^2 R_1 R_2\right] \exp 3i\omega\left(t - \frac{r}{c}\right) + \ldots \end{aligned} \tag{3.7}$$

$$\left(\frac{\partial}{\partial t} f(t,r)\right)^2 = \left[i\omega R_1(r) \exp i\omega\left(t - \frac{r}{c}\right) + 2i\omega R_2(r) \exp 2i\omega\left(t - \frac{r}{c}\right) + \ldots\right]^2 \tag{3.8}$$

$$R_2''(r) + 2\left(\frac{1}{r} - \frac{2i\omega}{c}\right) R_2'(r) - \frac{4}{c}\left(\frac{i\omega}{r} + \frac{4\omega}{c^3} R_0\right) R_2(r) - \frac{8\omega^2}{c^4} R_1^2(r) = 0\,. \tag{3.13}$$

3 Formulation of analytical solution to Einstein's geometrical gravitational field equation

The field equation for the gravitational field exterior to a time varying mass distribution within regions of spherical geometry are found to be given equally as equation (2.25) or (2.26).

For small gravitational fields (weak fields), the geometrical wave equation (1.1) reduces to (3.1) or equally (3.2).

We now seek a possible solution of equation (3.2) in the form

$$f(t,r) = \sum_{n=0}^{\infty} R_n(r)\ \exp\ ni\omega\left(t - \frac{r}{c}\right), \tag{3.3}$$

where R_n are functions of r only. Thus, by evaluating the first and second partial derivatives of our proposed solution for $f(t,r)$ in equation (3.3); it can be trivially shown that the separate terms of our expanded field equation (3.2) can be written as (3.4), (3.5), (3.6), (3.7), and (3.8), where the primes on the function R denote differentiation with respect to r. Now, substituting equations (3.4) to (3.8) into our field equation (3.2) and equating coefficients on both sides yields the following:

Equating coefficients of $\exp(0)$ gives

$$R_0'' + \frac{2}{r} R_0' = 0\,. \tag{3.9}$$

Thus, we can conveniently choose the best astrophysical solution for equation (3.9) as

$$R_0(r) = -\frac{k}{r} \tag{3.10}$$

where $k = GM_0$; by deduction from Schwarzschild's metric and Newton's theory of gravitation; with G being the universal gravitational constant and M_0 the total mass of the spherical body. Thus at this level, we note that the field equation yields a value for the arbitrary function f in our field equal to that in Schwarzschild's field. This is profound and interesting indeed as the link between our solution, Schwarzschild's solution and Newton's dynamical theory of gravitation becomes quite clear and obvious.

Equating coefficients of $\exp i\omega\left(t - \frac{r}{c}\right)$ gives

$$\begin{aligned} & R_1''(r) + 2\left(\frac{1}{r} - \frac{i\omega}{c}\right) R_1' + \\ & \quad + \frac{2\omega}{c}\left(-\frac{i}{r} - \frac{2\omega}{c^3} R_0\right) R_1 = 0\,. \end{aligned} \tag{3.11}$$

This is our exact differential equation for R_1 and it determines R_1 in terms of R_0. Thus, the solution admits an exact wave solution which reduces in the order of c^0 to:

$$f(t,r) \approx -\frac{k}{r} \exp i\omega\left(t - \frac{r}{c}\right). \tag{3.12}$$

Equating coefficients of $\exp 2i\omega\left(t - \frac{r}{c}\right)$ gives (3.13).

This is our exact equation for $R_2(r)$ in terms of $R_0(r)$ and $R_1(r)$. Similarly, all the other unknown functions $R_n(r)$, $n > 2$ are determined in terms of $R_0(r)$ by the other recurrence differential equations. Hence we obtain our unique astrophysically most satisfactory exterior solution of order c^4.

4 Conclusion

Interestingly, we note that the terms of our unique series solution (3.10), (3.11), (3.12) and (3.13) converge everywhere in the exterior space-time. Similarly, all the solutions of the other recurrence differential equations will also converge everywhere in the exterior space-time.

Instructively, we realize that our solution has a unique link to the pure Newtonian gravitational scalar potential for the gravitational field and thus puts Einstein's geometrical gravitational field on same footing with the Newtonian dynamical theory. This method introduces the dependence of geometrical gravitational field on one and only one dependent function f, comparable to one and only one gravitational scalar potential in Newton's dynamical theory of gravitation [4].

Hence, we have obtained a complete solution of Einstein's field equations in this gravitational field. Our metric tensor, which is the fundamental parameter in this field is thus completely defined.The door is thus open for the complete study of the motion of test particles and photons in this gravitational field introduced in the articles [5] and [6].

Submitted on April 29, 2009 / Accepted on May 12, 2009

References

1. Weinberg S. Gravitation and cosmology. J. Wiley, New York, 1972, p. 175–188.
2. Howusu S.X.K. The 210 astrophysical solutions plus 210 cosmological solutions of Einstein's geometrical gravitational field equations. Jos University Press, Jos, 2007.
3. Chifu E.N. and Howusu S.X.K. Einstein's equation of motion for a photon in fields exterior to astrophysically real or imaginary spherical mass distributions who's tensor field varies with azimuthal angle only. *Journal of the Nigerian Association of Mathematical Physics*, 2008, v. 13, 363–366.
4. Chifu E.N., Howusu S.X.K. and Lumbi L.W. Relativistic mechanics in gravitational fields exterior to rotating homogeneous mass distributions within regions of spherical geometry. *Progress in Physics*, 2009, v. 3, 18–23.
5. Chifu E.N., Howusu S.X.K. and Usman A. Motion of photons in time dependent spherical gravitational fields. *Journal of Physics Students*, 2008, v. 2(4), L10–L14.
6. Chifu E.N., Usman A. and Meludu O.C. Motion of particles of non-zero rest masses exterior to a spherical mass distribution with a time dependent potential field. *Pacific Journal of Science and Technology*, 2008, v. 9(2), 351–356.

Orbits in Homogeneous Oblate Spheroidal Gravitational Space-Time

Chifu Ebenezer Ndikilar*, Adams Usman†, and Osita C. Meludu†

*Physics Department, Gombe State University, P.M.B. 127, Gombe, Gombe State, Nigeria
E-mail: ebenechifu@yahoo.com

†Physics Department, Federal University of Technology, Yola, Adamawa State, Nigeria
E-mail: aausman@yahoo.co.uk, omeludu@yahoo.co.uk

The generalized Lagrangian in general relativistic homogeneous oblate spheroidal gravitational fields is constructed and used to study orbits exterior to homogenous oblate spheroids. Expressions for the conservation of energy and angular momentum for this gravitational field are obtained. The planetary equation of motion and the equation of motion of a photon in the vicinity of an oblate spheroid are derived. These equations have additional terms not found in Schwarzschild's space time.

1 Introduction

It is well known experimentally that the Sun and planets in the solar system are more precisely oblate spheroidal in geometry [1–6]. The oblate spheroidal geometries of these bodies have corresponding effects on their gravitational fields and hence the motion of test particles and photons in these fields.

It is also well known that satellite orbits around the Earth are governed by not only the simple inverse distance squared gravitational fields due to perfect spherical geometry. They are also governed by second harmonics (pole of order 3) as well as fourth harmonics (pole of order 5) of gravitational scalar potential not due to perfect spherical geometry. Therefore, towards the more precise explanation and prediction of satellite orbits around the Earth, Stern [3] and Garfinkel [4] introduced the method of quadratures for approximating the second harmonics of the gravitational scalar potential of the Earth due to its spheroidal Earth. This method was improved by O'Keefe [5]. Then in 1960, Vinti [6] suggested a general mathematical form of the gravitational scalar potential of the spheroidal Earth and how to estimate some of the parameters in it for use in the study of satellite orbits. Recently [1], an expression for the scalar potential exterior to a homogeneous oblate spheroidal body was derived. Most recently, Ioannis and Michael [3] proposed the Sagnac interferometric technique as a way of detecting corrections to the Newton's gravitational scalar potential exterior to an oblate spheroid.

In this article, we formulate the metric tensor for the gravitational field exterior to massive homogeneous oblate spheroidal bodies as a direct extension of Schwarzschild's metric. This metric tensor is then used to study orbits in homogeneous oblate spheroidal space time.

2 Metric tensor exterior to a homogeneous oblate spheroid

The invariant world line element in the exterior region of all possible static spherical distributions of mass is given [1, 7] as

$$c^2 d\tau^2 = c^2 \left[1 + \frac{2f(r,\theta,\phi)}{c^2}\right] dt^2 - \\ - \left[1 + \frac{2f(r,\theta,\phi)}{c^2}\right]^{-1} dr^2 - r^2 d\theta^2 - r^2 \sin^2\theta \, d\phi^2 \quad (2.1)$$

where $f(r,\theta,\phi)$ is a generalized arbitrary function determined by the distribution of mass or pressure and possess all the symmetries of the mass distribution. It is a well known fact of general relativity that $f(r,\theta,\phi)$ is approximately equal to Newton's gravitational scalar potential in the space-time exterior to the mass or pressure distributions within regions of spherical geometry [1, 7]. For a static homogeneous spherical body ("Schwarzschild's body") the arbitrary function takes the form $f(r)$.

Now, let "Schwarzschild's body" be transformed, by deformation, into an oblate spheroidal body in such a way that its density and total mass remain the same and its surface parameter is given in oblate spheroidal coordinates [1] as

$$\xi = \xi_0 \,;\ \text{constant}. \quad (2.2)$$

The general relativistic field equation exterior to a homogeneous static oblate spheroidal body is tensorially equivalent to that of a static homogeneous spherical body ("Schwarzschild's body") [1, 7] hence, is related by the transformation from spherical to oblate spheroidal coordinates. Therefore, to get the corresponding invariant world line element in the exterior region of a static homogeneous oblate spheroidal mass, we first replace the arbitrary function in Schwarzschild's field, $f(r)$ by the corresponding arbitrary function exterior to static homogenous oblate spheroidal bodies, $f(\eta,\xi)$. Thus, the function $f(\eta,\xi)$ is approximately equal to the gravitational potential exterior to a homogeneous spheroid. The gravitational scalar potential exterior to a homogeneous static oblate spheroid [1] is given as

$$f(\eta,\xi) = B_0 Q_0(-i\xi) P_0(\eta) + B_2 Q_2(-i\xi) P_2(\eta) \quad (2.3)$$

$$g_{00} = \left(1 + \frac{2}{c^2} f(\eta, \xi)\right) \tag{2.10}$$

$$g_{11} = -\frac{a^2}{1+\xi^2-\eta^2}\left[\eta^2\left(1+\frac{2}{c^2}f(\eta,\xi)\right)^{-1} + \frac{\xi^2(1+\xi^2)}{(1-\eta^2)}\right] \tag{2.11}$$

$$g_{12} \equiv g_{21} = -\frac{a^2\eta\xi}{1+\xi^2-\eta^2}\left[1-\left(1+\frac{2}{c^2}f(\eta,\xi)\right)^{-1}\right] \tag{2.12}$$

$$g_{22} = -\frac{a^2}{1+\xi^2-\eta^2}\left[\xi^2\left(1+\frac{2}{c^2}f(\eta,\xi)\right)^{-1} + \frac{\eta^2(1-\eta^2)}{(1+\xi^2)}\right] \tag{2.13}$$

$$g_{33} = -a^2(1+\xi^2)(1-\eta^2) \tag{2.14}$$

$$g_{\mu\nu} = 0; \text{ otherwise} \tag{2.15}$$

$$g^{00} = \left[1 + \frac{2}{c^2} f(\eta, \xi)\right]^{-1} \tag{2.16}$$

$$g^{11} = \frac{-\left(1-\eta^2\right)\left(1+\xi^2-\eta^2\right)\left[\eta^2\left(1-\eta^2\right)+\xi^2\left(1+\xi^2\right)\left(1+\frac{2}{c^2}f(\eta,\xi)\right)^{-1}\right]}{a^2\left(1+\frac{2}{c^2}f(\eta,\xi)\right)^{-1}\left[\eta^2(1-\eta^2)+\xi^2(1+\xi^2)\right]^2} \tag{2.17}$$

$$g^{12} \equiv g^{21} = \frac{-\eta\xi\left(1-\eta^2\right)\left(1+\xi^2\right)\left(1+\xi^2-\eta^2\right)\left[1-\left(1+\frac{2}{c^2}f(\eta,\xi)\right)^{-1}\right]}{a^2\left(1+\frac{2}{c^2}f(\eta,\xi)\right)^{-1}\left[\eta^2(1-\eta^2)+\xi^2(1+\xi^2)\right]^2} \tag{2.18}$$

$$g^{22} = \frac{-\left(1+\xi^2\right)\left(1+\xi^2-\eta^2\right)\left[\xi^2\left(1+\xi^2\right)+\eta^2\left(1-\eta^2\right)\left(1+\frac{2}{c^2}f(\eta,\xi)\right)^{-1}\right]}{a^2\left(1+\frac{2}{c^2}f(\eta,\xi)\right)^{-1}\left[\eta^2(1-\eta^2)+\xi^2(1+\xi^2)\right]^2} \tag{2.19}$$

$$g^{33} = -\left[a^2\left(1+\xi^2\right)\left(1-\eta^2\right)\right]^{-1} \tag{2.20}$$

$$g^{\mu\nu} = 0; \text{ otherwise} \tag{2.21}$$

where Q_O and Q_2 are the Legendre functions linearly independent to the Legendre polynomials P_0 and P_2 respectively. B_0 and B_2 are constants.

Secondly, we transform coordinates from spherical to oblate spheroidal coordinates;

$$(ct, r, \theta, \phi) \to (ct, \eta, \xi, \phi) \tag{2.4}$$

on the right hand side of equation (2.1).

From the relation between spherical polar coordinates and Cartesian coordinates as well as the relation between oblate spheroidal coordinates and Cartesian coordinates [8] it can be shown trivially that

$$r(\eta, \xi, \phi) = a(1+\xi^2-\eta^2)^{\frac{1}{2}} \tag{2.5}$$

and

$$\theta(\eta, \xi, \phi) = \cos^{-1}\left[\frac{\eta\xi}{(1+\xi^2-\eta^2)^{\frac{1}{2}}}\right] \tag{2.6}$$

where a is a constant parameter. Therefore,

$$dr = a(1+\xi^2-\eta^2)^{-\frac{1}{2}}(\xi d\xi - \eta d\eta) \tag{2.7}$$

and

$$d\theta = -\frac{\xi(1+\xi^2)^{\frac{1}{2}}}{(1-\eta^2)^{\frac{1}{2}}(1+\xi^2-\eta^2)}\,d\eta - \\ -\frac{\eta(1-\eta^2)^{\frac{1}{2}}}{(1+\xi^2)^{\frac{1}{2}}(1+\xi^2-\eta^2)}\,d\xi\,. \tag{2.8}$$

Also,

$$\sin^2\theta = \frac{(1+\xi^2)(1-\eta^2)}{(1+\xi^2-\eta^2)}\,. \tag{2.9}$$

Substituting equations (2.5), (2.7), (2.8) and (2.9) into equation (2.1) and simplifying yields the following components of the covariant metric tensor in the region exterior to a

$$L = \frac{1}{c}\left(-g_{00}\left(\frac{dt}{d\tau}\right)^2 - g_{11}\left(\frac{d\eta}{d\tau}\right)^2 - 2g_{12}\left(\frac{d\eta}{d\tau}\right)\left(\frac{d\xi}{d\tau}\right) - g_{22}\left(\frac{d\xi}{d\tau}\right)^2 - g_{33}\left(\frac{d\phi}{d\tau}\right)^2\right)^{\frac{1}{2}} \tag{3.1}$$

$$L = \frac{1}{c}\left[-\left(1+\frac{2}{c^2}f(\eta,\xi)\right)\dot{t}^2 - \frac{a^2\xi^2}{1+\xi^2}\left(1+\frac{2}{c^2}f(\eta,\xi)\right)^{-1}\dot{\xi}^2 + a^2(1+\xi^2)\dot{\phi}^2\right]^{\frac{1}{2}} \tag{3.2}$$

static homogeneous oblate spheroid in oblate spheroidal coordinates (2.10)–(2.15).

The covariant metric tensor, equations (2.10) to (2.15) is the most fundamental geometric parameter required to study general relativistic mechanics in static homogeneous oblate spheroidal gravitational fields. The covariant metric tensor obtained above for gravitational fields exterior to oblate spheroidal masses has two additional non-zero components g_{12} and g_{21} not found in Schwarzschild field [7]. Thus, the extension from Schwarzschild field to homogeneous oblate spheroidal gravitational fields has produced two additional non-zero tensor components and hence this metric tensor field is unique. This confirms the assertion that oblate spheroidal gravitational fields are more complex than spherical fields and hence general relativistic mechanics in this field is more involved [6].

The contravariant metric tensor for this gravitational field is found to be given explicitly as (2.16)–(2.21).

It can be shown that the coefficients of affine connection for the gravitational field exterior to a homogenous oblate spheroidal mass are given in terms of the metric tensors for the gravitational field as

$$\Gamma^0_{01} \equiv \Gamma^0_{10} = \frac{1}{2}\,g^{00}g_{00,1}\,, \tag{2.22}$$

$$\Gamma^0_{02} \equiv \Gamma^0_{20} = \frac{1}{2}\,g^{00}g_{00,2}\,, \tag{2.23}$$

$$\Gamma^1_{00} = -\frac{1}{2}\,g^{11}g_{00,1} - \frac{1}{2}\,g^{12}g_{00,2}\,, \tag{2.24}$$

$$\Gamma^1_{11} = \frac{1}{2}\,g^{11}g_{11,1} + \frac{1}{2}\,g^{12}\left(2g_{12,1} - g_{11,2}\right)\,, \tag{2.25}$$

$$\Gamma^1_{12} \equiv \Gamma^1_{21} = \frac{1}{2}\,g^{11}g_{11,2} + \frac{1}{2}\,g^{12}g_{22,1}\,, \tag{2.26}$$

$$\Gamma^1_{22} = \frac{1}{2}\,g^{11}\left(2g_{12,2} - g_{22,1}\right) + \frac{1}{2}\,g^{12}g_{22,2}\,, \tag{2.27}$$

$$\Gamma^1_{33} = -\frac{1}{2}\,g^{11}g_{33,1} - \frac{1}{2}\,g^{12}g_{33,2}\,, \tag{2.28}$$

$$\Gamma^2_{00} = -\frac{1}{2}\,g^{21}g_{00,1} - \frac{1}{2}\,g^{22}g_{00,2}\,, \tag{2.29}$$

$$\Gamma^2_{11} = \frac{1}{2}\,g^{21}g_{11,1} + \frac{1}{2}\,g^{22}\left(2g_{12,1} - g_{11,2}\right)\,, \tag{2.30}$$

$$\Gamma^2_{12} \equiv \Gamma^2_{21} = \frac{1}{2}\,g^{21}g_{11,2} + \frac{1}{2}\,g^{22}g_{22,1}\,, \tag{2.31}$$

$$\Gamma^2_{22} = \frac{1}{2}\,g^{21}\left(2g_{12,2} - g_{22,1}\right) + \frac{1}{2}\,g^{22}g_{22,2}\,, \tag{2.32}$$

$$\Gamma^2_{33} = -\frac{1}{2}\,g^{21}g_{33,1} - \frac{1}{2}\,g^{22}g_{33,2}\,, \tag{2.33}$$

$$\Gamma^3_{13} \equiv \Gamma^3_{31} = \frac{1}{2}\,g^{33}g_{33,1}\,, \tag{2.34}$$

$$\Gamma^3_{23} \equiv \Gamma^3_{32} = \frac{1}{2}\,g^{33}g_{33,2}\,, \tag{2.35}$$

$$\Gamma^\delta_{\alpha\beta} = 0;\ \text{otherwise}, \tag{2.36}$$

where comma as in usual notation denotes partial differentiation with respect to $\eta(1)$ and $\xi(2)$.

3 Conservation of total energy and angular momentum

Many physical theories start by specifying the Lagrangian from which everything flows. We would adopt the same attitude with gravitational fields exterior to homogenous oblate spheroidal masses. The Lagrangian in the space time exterior to our mass or pressure distribution is defined explicitly in oblate spheroidal coordinates using the metric tensor as (3.1) [7, 9], where τ is the proper time.

For orbits confined to the equatorial plane of a homogenous oblate spheroidal mass [1, 8]; $\eta \equiv 0$ (or $d\eta \equiv 0$) and substituting the explicit expressions for the components of metric tensor in the equatorial plane yields (3.2), where the dot denotes differentiation with respect to proper time.

It is well known that the gravitational field is a conservative field. The Euler-Lagrange equations for a conservative system in which the potential energy is independent of the generalized velocities is written as [7, 9];

$$\frac{\partial L}{\partial x^\alpha} = \frac{d}{d\tau}\left(\frac{\partial L}{\partial \dot{x}^\alpha}\right) \tag{3.3}$$

but

$$\frac{\partial L}{\partial x^0} \equiv \frac{\partial L}{\partial t} = 0 \tag{3.4}$$

and thus from equation (3.3), we deduce that

$$\frac{\partial L}{\partial \dot{t}} = \text{constant}. \tag{3.5}$$

From equation (3.3), it can be shown using equation (3.5) that

$$\left(1+\frac{2}{c^2}\,f(\eta,\xi)\right)\dot{t} = k, \quad \dot{k} = 0 \tag{3.6}$$

where k is a constant. This is the law of conservation of energy in the equatorial plane of the gravitational field exterior to an oblate spheroidal mass [7, 9].

The law of conservation of total energy, equation (3.6) can also be obtained by constructing the coefficients of affine connection for this gravitational field and evaluating the time equation of motion for particles of non-zero rest masses. The general relativistic equation of motion for particles of non-zero rest masses in a gravitational field are given by

$$\frac{d^2x^\mu}{d\tau^2} + \Gamma^\mu_{\nu\lambda}\left(\frac{dx^\nu}{d\tau}\right)\left(\frac{dx^\lambda}{d\tau}\right) = 0 \tag{3.7}$$

where $\Gamma^\mu_{\nu\lambda}$ are the coefficients of affine connection for the gravitational field.

Setting $\mu = 0$ in equation (3.7) and substituting the explicit expressions for the affine connections Γ^0_{01} and Γ^0_{02} gives

$$\ddot{t} + \frac{2}{c^2}\left(1 + \frac{2}{c^2}f(\eta,\xi)\right)^{-1} \times \times \left(\dot{\eta}\frac{\partial f(\eta,\xi)}{\partial \eta} + \dot{\xi}\frac{\partial f((\eta,\xi))}{\partial \xi}\right)\dot{t} = 0\,. \tag{3.8}$$

Integrating equation (3.8) yields

$$\dot{t} = k\left(1 + \frac{2}{c^2}f(\eta,\xi)\right)^{-1} \tag{3.9}$$

where k is a constant of integration. Thus, the two methods yield same results.

Also, the Lagrangian for this gravitational field is invariant to azimuthal angular rotation and hence angular momentum is conserved, thus;

$$\frac{\partial L}{\partial \phi} = 0 \tag{3.10}$$

and from Lagrange's equation of motion,

$$\left(1 + \xi^2\right)\dot{\phi} = l, \quad \dot{l} = 0 \tag{3.11}$$

where l is a constant. This is the law of conservation of angular momentum in the equatorial plane of the gravitational field exterior to a static homogeneous oblate spheroidal body.

This expression can also be obtained by solving the azimuthal equation of motion for particles of non-zero rest masses in this gravitational field. Setting $\mu = 3$ in equation (3.7) and substituting the relevant affine connection coefficients gives the azimuthal equation of motion as

$$\frac{d}{d\tau}\left(\ln\dot{\phi}\right) + \frac{d}{d\tau}\left(\ln\left(1-\eta^2\right)\right) + + \frac{d}{d\tau}\left(\ln\left(1+\xi^2\right)\right) = 0\,. \tag{3.12}$$

Thus, by integrating equation (3.12), it can be shown that the azimuthal equation of motion for our gravitational field is given as

$$\dot{\phi} = \frac{l}{\left(1-\eta^2\right)\left(1+\xi^2\right)}\,, \tag{3.13}$$

where l is a constant of motion. l physically corresponds to the angular momentum and hence equation (3.13) is the Law of Conservation of angular momentum in this gravitational field [7, 9]. It does not depend on the gravitational potential and is of same form as that obtained in Schwarzschild's Field and Newton's dynamical theory of gravitation [7, 9]. Note that equation (3.13) reduces to equation (3.11) if the particles are confined to move in the equatorial plane of the oblate spheroidal mass.

4 Orbits in homogeneous oblate spheroidal gravitational fields

It is well known [7, 9] that the Lagrangian $L = \epsilon$, with $\epsilon = 1$ for time like orbits and $\epsilon = 0$ for null orbits. Setting $L = \epsilon$ in equation (3.2), substituting equations (3.6) and (3.11) and simplifying yields;

$$\frac{a^2\xi^2}{\left(1+\xi^2\right)}\dot{\xi}^2 + \frac{a^2l^2}{\left(1+\xi^2\right)}\left(1 + \frac{2}{c^2}f(\eta,\xi)\right) - - 2\epsilon^2 f(\eta,\xi) = c^2\epsilon^2 + 1\,. \tag{4.1}$$

In most applications of general relativity, we are more interested in the shape of orbits (that is, as a function of the azimuthal angle) than in their time history [7]. Hence, it is instructive to transform equation (4.1) into an equation in terms of the azimuthal angle ϕ. Now, let us consider the following transformation;

$$\xi = \xi(\phi) \text{ and } u(\phi) = \frac{1}{\xi(\phi)}\,, \tag{4.2}$$

thus,

$$\dot{\xi} = -\frac{l}{1+u^2}\frac{du}{d\phi}\,. \tag{4.3}$$

Now, imposing equations (4.2) and (4.3) on equation (4.1) and simplifying yields (4.4). Differentiating equation (4.4) gives (4.5).

For time like orbits $(\epsilon = 1)$, equation (4.5) reduces to (4.6).

This is the planetary equation of motion in this gravitational field. It can be solved to obtain the perihelion precision of planetary orbits. It has additional terms (resulting from the oblateness of the body), not found in the corresponding equation in Schwarzschild's field [7].

Light rays travel on null geodesics $(\epsilon = 0)$ and hence equation (4.5) becomes (4.7).

In the limit of special relativity, some terms in equation (4.7) vanish and the equation becomes (4.8).

Equation (4.7) is the photon equation of motion in the vicinity of a static massive homogenous oblate spheroidal body. The equation contains additional terms not found in the corresponding equation in Schwarzschild's field. The solution of the special relativistic case, equation (4.8) can be used to solve the general relativistic equation, (4.7). This can

$$\frac{1}{\left(1+u^2\right)^3}\left(\frac{du}{d\phi}\right)^2+\frac{u^2}{1+u^2}\left(1+\frac{2}{c^2}f(u)\right)-\frac{2\epsilon^2 f(u)}{a^2l^2}=\frac{c^2\epsilon^2+1}{a^2l^2}\,. \tag{4.4}$$

$$\frac{d^2u}{d\phi^2}-3u\left(1+u^2\right)\frac{du}{d\phi}+\frac{\left(u+u^2\right)}{2}\left(u^2-u+2\right)\left(1+\frac{2}{c^2}f(u)\right)=\left(\frac{1+u^2}{acl}\right)^2\left(a^2c^2l^2-\epsilon^2-\epsilon^2u^2\right)\frac{d}{du}f(u)\,. \tag{4.5}$$

$$\frac{d^2u}{d\phi^2}-3u\left(1+u^2\right)\frac{du}{d\phi}+\frac{\left(u+u^2\right)}{2}\left(u^2-u+2\right)\left(1+\frac{2}{c^2}f(u)\right)=\left(\frac{1+u^2}{acl}\right)^2\left(a^2c^2u^2-1-u^2\right)\frac{d}{du}f(u)\,. \tag{4.6}$$

$$\frac{d^2u}{d\phi^2}-3u\left(1+u^2\right)\frac{du}{d\phi}+\frac{\left(u+u^2\right)}{2}\left(u^2-u+2\right)\left(1+\frac{2}{c^2}f(u)\right)=\frac{u^2}{c^2}\left(1+u^2\right)^2\frac{d}{du}f(u)\,. \tag{4.7}$$

$$\frac{d^2u}{d\phi^2}-3u\left(1+u^2\right)\frac{du}{d\phi}+\frac{\left(u+u^2\right)}{2}\left(u^2-u+2\right)=0\,. \tag{4.8}$$

be done by taking the general solution of equation (4.7) to be a perturbation of the solution of equation (4.8). The immediate consequence of this analysis is that it will produce an expression for the total deflection of light grazing a massive oblate spheroidal body such as the Sun and the Earth.

5 Remarks and conclusion

The immediate consequences of the results obtained in this article are:

1. The equations derived are closer to reality than those in Schwarzschild's gravitational field. In Schwarzschild's space time, the Sun is assumed to be a static perfect sphere. The Sun has been proven to be oblate spheroidal in shape and our analysis agrees perfectly with this shape;
2. The planetary equation of motion and the photon equation of motion have additional spheroidal terms not found in Schwarzschild's field. This equations are opened up for further research work and astrophysical interpretation.
3. In approximate oblate spheroidal gravitational fields, the arbitrary function $f(\eta,\xi)$ can be conveniently equated to the gravitational scalar potential exterior to an oblate spheroid [7]. Thus for these fields, the complete solutions for our equations of motion can be constructed;
4. Einstein's field equations constructed using our metric tensor has only one unknown, $f(\eta,\xi)$. A solution of these field equations will give explicit expressions for the function, $f(\eta,\xi)$ which can then be used in our equations of motion.

Submitted on April 29, 2009 / Accepted on May 12, 2009

References

1. Howusu S.X.K. The 210 astrophysical solutions plus 210 cosmological solutions of Einstein's geometrical gravitational field equations. Jos University Press, Jos, 2007.
2. Haranas I.I. and Harney M. Detection of the relativistic corrections to the gravitational potential using a Sagnac interferometer. *Progress in Physics*, 2008, v. 3, 3–8.
3. Stern T.E. Theory of satellite orbits. *Astronomical Journal*, 1957, v. 62, 96.
4. Garfinkel B. Problem of quadratures. *Astronomical Journal*, 1958, v. 63, 88.
5. O'Keefe J.A, Ann E., and Kenneth S.R. The gravitational field of the Earth. *Astronomical Journal*, 1959, v. 64, 245.
6. Vinti J.P. New approach in the theory of satellite orbits. *Physical Review Letters*, 1960, v. 3(1), 8.
7. Chifu E.N., Howusu S.X.K. and Lumbi L.W. Relativistic mechanics in gravitational fields exterior to rotating homogeneous mass distributions within regions of spherical geometry. *Progress in Physics*, 2009, v. 3, 18–23.
8. Arfken G. Mathematical methods for physicists. 5th edition, Academic Press, New York, 1995.
9. Peter K.S.D. An introduction to tensors and relativity. Cape Town, 2000, 51–110.

Primes, Geometry and Condensed Matter

Riadh H. Al Rabeh
University of Basra, Basra, Iraq
E-mail: alrabeh_rh@yahoo.com

Fascination with primes dates back to the Greeks and before. Primes are named by some "the elementary particles of arithmetic" as every nonprime integer is made of a unique set of primes. In this article we point to new connections between primes, geometry and physics which show that primes could be called "the elementary particles of physics" too. This study considers the problem of closely packing similar circles/spheres in 2D/3D space. This is in effect a discretization process of space and the allowable number in a pack is found to lead to some unexpected cases of prime configurations which is independent of the size of the constituents. We next suggest that a non-prime can be considered geometrically as a symmetric collection that is separable (factorable) into similar parts- six is two threes or three twos for example. A collection that has no such symmetry is a prime. As a result, a physical prime aggregate is more difficult to split symmetrically resulting in an inherent stability. This "number/physical" stability idea applies to bigger collections made from smaller (prime) units leading to larger stable prime structures in a limitless scaling up process. The distribution of primes among numbers can be understood better using the packing ideas described here and we further suggest that differing numbers (and values) of distinct prime factors making a nonprime collection is an important factor in determining the probability and method of possible and subsequent disintegration. Disintegration is bound by energy conservation and is closely related to symmetry by Noether theorems. Thinking of condensed matter as the packing of identical elements, we examine plots of the masses of chemical elements of the periodic table, and also those of the elementary particles of physics, and show that prime packing rules seem to play a role in the make up of matter. The plots show convincingly that the growth of prime numbers and that of the masses of chemical elements and of elementary particles do follow the same trend indeed.

1 Introduction

Primes have been a source of fascination for a long time- as far back as the Greeks and much before. One reason for this fascination is the fact that every non-prime is the product of a unique set of prime numbers, hence the name *elementary particles of arithmetic*, and that although primes are distributed seemingly randomly among other integers, they do have regular not fully understood patterns (see [1] for example). The literature is rich in theories on primes but one could say that none-to-date have managed to make the strong connection between primes and physics that is intuitively felt by many. One recent attempt in this direction is [2], wherein possible connections between the atomic structure and the zeros of the Zeta function — closely connected to primes — are investigated. We quote from this reference, "Why the periodicity of zeros from the Riemann-Zeta function would match the spacing of energy levels in high-Z nuclei still remains a mystery".

In the present work we attempt to relate primes to both geometry and physics. We start with the packing of circles in a plane (or balls on a plane)- all of the same size, and pose a question; *In a plane, what is the condition for packing an integral number of identical circles to form a larger circle- such that both the diameter and circumference of the larger circle contain an integral numbers of the small circle*? The problem is essentially the same when the 2D circles are replaced with balls on a tray. A surprising result here is the appearance of only two prime numbers 2 and 3 in the answer and *only one of them is nontrivial- the number 3*. This gives such numbers a fundamental and natural importance in geometry. We may view this number as a "discretization number of the continuous $3D$ spaces". We further study this matter and shed light (using balls to represent integers) on bounds on the growth of primes- namely the well known logarithmic law in the theory of primes. Still further, we coin the notion that distinct prime factors in the packing of composite collections/grouping can have a profound influence on the behaviour of such collections and the manner they react with other collections built of some different or similar prime factors. As many physics models of condensed matter assume identical elements for simple matter (photons, boson and fermion statistics and the MIT bag model [3, 6] are examples) we examine the applicability of our packing rules in such case and conclude that condensed matter do seem to follow the packing rules discussed here.

2 Theory

Consider the case of close packing of circles on a plane so as to make a bigger circle (Figure 1). The ratio of the radius of the large circle to that of the small circle is; $R/r = 1+1/\sin t$,

1	**7**	**13**	**19**	25	**31**	**37**	**43**	49	55	**61**	**67**	**73**	**79**	85	91	**97**...
2	8	14	20	26	32	38	44	50	56	62	68	74	80	86	92	98...
3	9	15	21	27	33	39	45	51	57	63	69	75	81	87	93	99...
4	10	16	22	28	34	40	46	52	58	64	70	76	82	88	94	100...
5	**11**	**17**	**23**	**29**	35	**41**	**47**	**53**	**59**	65	**71**	77	**83**	**89**	95	**101**...
6	12	18	24	30	36	42	48	54	60	66	72	78	84	90	96	102...

Table 1: Integers arranged in columns of six.

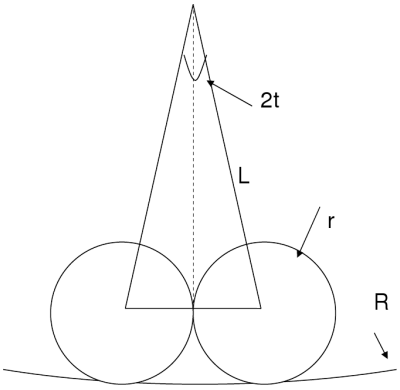

Fig. 1: Close packing of an integral number of circles/balls on a plane have one nontrivial solution- 6 balls, plus one at the centre (see also Figure 2). Here in Fig. 1: $L\sin t = r$; $t = \pi/n$; $R = L + r$; $R/r = 1 + 1/\sin t$. For integral ratio R/r, t must be $\pi/2$ or $\pi/6$ and $L/r = 2, 3$.

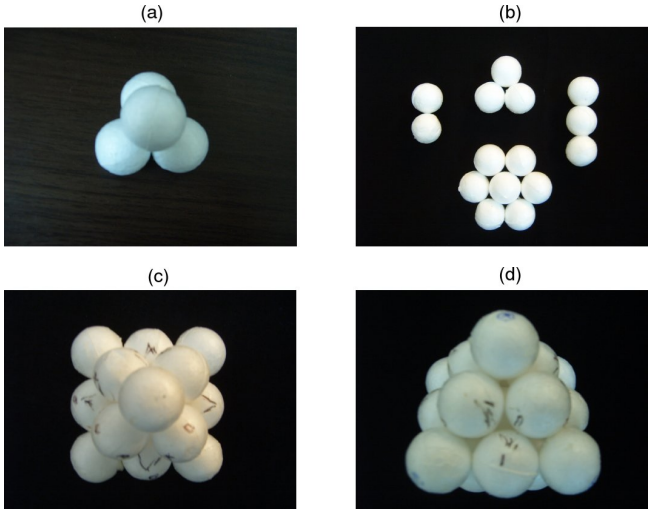

Fig. 2: Packing of 2, 3, 4, 7 & 19 (=7+(3+3)+(3+3)) balls in 3D (a, b). The 19 ball case possesses six side and eight side symmetries (c, d).

where t is half the angle between radial lines through the centers of any two adjacent circles. For this number to be an integer, the quantity $(1/\sin t)$ must be an integer and hence the angle t must be either 30 or 90 degrees. Thus R/r should be either three or two (see Figure 2b). That is; the diameter can be either two or three circles wide. The number 3 is nontrivial, and gives six circles touching each other, and all in turn tangent to a seventh circle at the centre.

Clearly the arrangement of balls on a plane does follow exactly the same pattern leading to six balls touching in pairs and surrounding a seventh ball (touching all other six) at the center. This result is unique and is independent of the size of the balls involved. It is rather remarkable as it gives the number 6 a special stature in the physics of our 3D space, parallel to that of the number π in geometry. Such stature must have been realized in the past by thinkers as far back as the Babylonian times and the divine stature given to such a number in the cultures of many early civilizations- six working days in a week and one for rest is one example, the six prongs of the star of David and the seven days of creation as well as counting in dozens might have also been inspired by the same. Before this, the Bees have discovered the same fact and started building their six sided honey combs accordingly.

Consider now the set of prime numbers. It is known that every prime can be written as $6n \pm 1$, where n is an integer. *That is* the number six is a generator of all primes. Further, we note that whereas the number six is divisible into 2 (threes) or 3 (twos), an addition of one unit raises the number to seven- a prime and not divisible into any smaller symmetric entities. Put differently, an object composed of six elements can easily break into smaller symmetrical parts, whereas an object made of 7 is more stable and not easily breakable into symmetric parts. We know from physics that symmetry in interactions is demanded by many conservation laws. In fact symmetry and conservation are tightly linked by Noether theorems- such that symmetry can always be translated to a conservation law and vice versa. When we have a group of highly symmetric identical items, the addition of one at the centre of the collection can make it a prime.

Now if we arrange natural numbers in columns of six as shown in Table 1, we see clearly that all primes fall along two lines- top line for the $6n + 1$ type and the bottom line for the case of $6n - 1$ type primes (text in bold). If these are balls arranged physically on discs six each and on top of each other, the two lines will appear diametrically opposite on a long cylinder. Thus there are two favourite lines along which all primes fall in a clear display of a sign of the close connection between primes geometry and physics.

We see then that the connection between primes and geometry is an outcome of how the plane and the space lend themselves to discretization, when we pair such blocks with

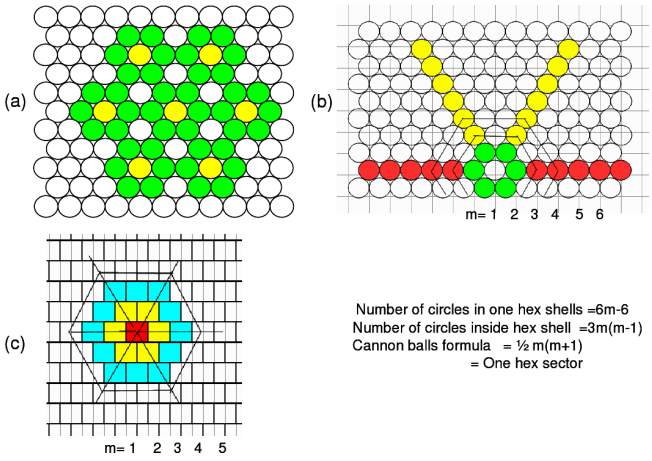

Fig. 3: (a) Scaling up using small blocks of seven to make larger blocks of seven; (b) Tight packing of circles naturally resulting in hex objects made of hex layers. The number of circles in each layer strip increases in steps of 6. Note that each hex sector has cannon balls (or conical) packing structure; (c) Easy to construct (square) brick structure to formally replace circles.

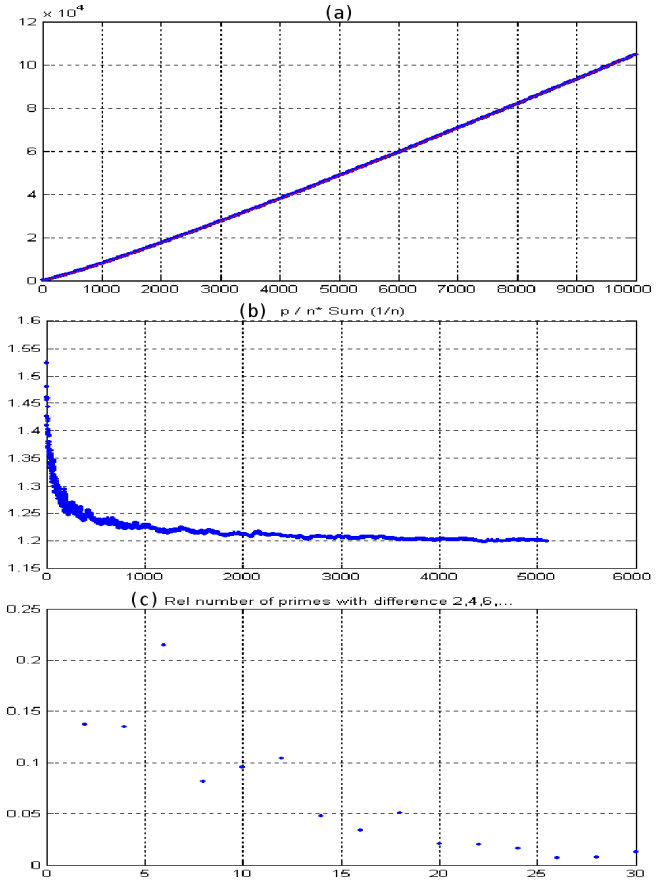

Fig. 4: (a) Two overlapping plots of the first 104 primes: (1, 2, 3, 5, $\cdots$, 104729) compared to fitting plot (–), $y = (\ln \pi) \cdot n \cdot \ln n$ (n = serial positions of prime numbers) (.); (b) Ratio of a prime (p) to $n \sum 1/n$; (c) Relative number of primes with differences of 2, 4, 6, $\cdots$ 30. Peaks occur at differences of 6, 12, 18, 24, 30.

the set of positive integers. We may note also that the density of $6n-1$ and $6n+1$ type primes is the same with respect to the integers. Moreover, if we take the difference between prime pairs, the distribution of the difference peaks at 6 and all multiples of it, but diminishes as the difference increases (Figure 4c).

In a violent interaction between two prime groups, one or more of the groups could momentarily loose a member or more leaving a non-prime group which then become less stable and divisible into symmetric parts according to the factors making the collection. Clearly in this case, the few none primes neighbouring a prime also become important, and would contribute to the rules of break-up, to the type of products and to the energy required in each case.

Our packing endeavour can continue beyond 7 to make larger 3D objects (Figure 2). A stable new arrangement can result from the addition of 6 balls- 3 on each side (top and bottom) making an object of 13 balls- a new prime figure. Further 6 balls can be put symmetrically secured on top and bottom to give an object of 19 balls. This last case in addition to being a prime collection has an interesting shape feature. It has six and eight face symmetries and fairly smooth faces as shown in Figures 2(c, d), which could give rise to two different groups of 19 ball formations. Further addition of 6's is possible, but the resulting object appears less strong. To go a different direction, we can instead consider every 7, 13 or 19 ball objects as the new building unit and use it to form further new collections of objects of prime grouping. Clearly this can be continued in an endless scaling up process (Figure 3b). Scaling is a prominent phenomenon in physical structures. Fig. 3b shows that, in a plane, our packing problem and also that of the packing of cannon-balls [5] are only subsets of the general densest packing problem and thus it truly is a discretization process of space. We note also that circles can be replaced with squares placed in a brick like structure provided we only think of the centres of these squares.

In the process of adding new rings of circles to form larger objects, both prime and nonprime numbers are met. A prime is formed every time we have highly symmetric combination with one to be added or subtracted to it to break the symmetry and produce a prime. If we consider the number of circles added in each ring in the case of circular geometry (the same applies to hex geometry with small modification), the radius of a ring is given by $mr+m$, where m is the number of layers and r is the radius of one small circle set to unity. The number of circles in each ring is estimated by the integer part of $2\pi m$. For the next ring we substitute $(m+1)$ for m in the above expressions and obtain $2\pi(m+1)$ for a ring. The *relative* increase in the number of circles is the difference between these two divided by the circumference which gives $1/m$. The relative (or probable) number of primes for m-th ring should be taken to come from the contribution of all the items in the ring and this is proportional to $\sum 1/m$ for large m. The actual number of primes is an integral of this given by $m \sum 1/m$

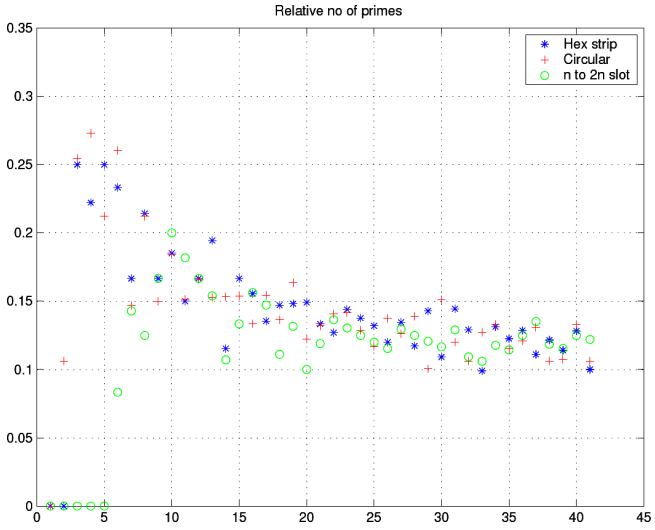

Fig. 5: Relative number of primes in (50000 integer sample): Hex strips $m : m+1$ (*); Circular rings $m : m+1$, m is the number of rings of circles around the centre (+); Interval $n : 2n$, n is the serial number of a prime (○).

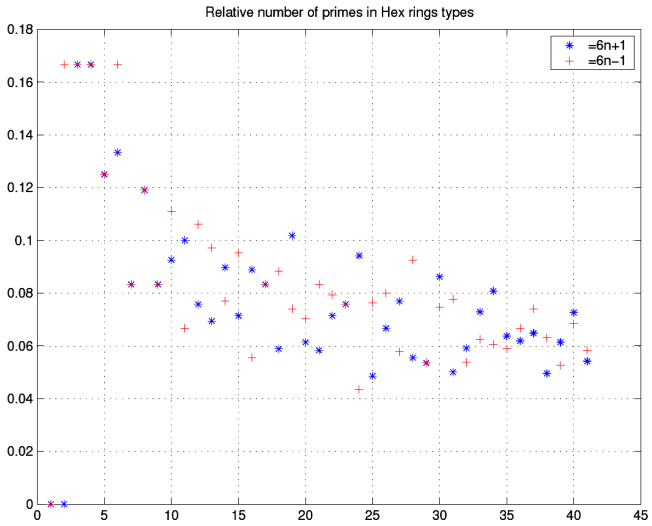

Fig. 6: Relative number of primes in hex strips (see Figure 3b); primes of the form $6n+1$ (*); primes of the form $6n-1$, n is the number of prims around the centre (+).

since both the radius of a circular strip and the number of circles in that strip are proportional to m. Fig. 5 gives the relative number of primes in one strip and the trend is of the form $a/\log m$, thus confirming the reasoning used above.

Figure 4b gives a plot of the ratio $p/(n\sum 1/n)$ where p is the value of the n-th prime for some 50000 primes sample which, for large n, equals the number of integers/circles in the whole area. Since $\sum 1/n \sim \ln(n)$ for large n, we see that this ratio tends to a constant in agreement with the results of the prime number theory (see [1] for example).

Further, there are few results from the theory of primes that can also be interpreted in support of the above arguments. For example the well known conjectures suggesting that there is always a prime between m and $2m$ and also between m^2 and $(m+1)^2$ [7] can respectively be taken to correspond to the symmetrical duplication of an area and to the ring regions between two concentric circles must contain at least one prime. That is if the original area or sector can produce a prime, then duplicating it symmetrically or adding one more sector to it will produce at least one prime. The number of primes in each of the above cases and that of a hex region are of course more than one and the results from a sample of (1–50000) integers are plotted in Figure 5. The data is generated using a simple Excel-Basic program shown below;

```
%Open excel > Tools > micro > Basic Editor > paste and run
subroutine prime( )
kk=0:
% search divisibility up to square root
for ii=1 to 1e6: z=1: iis=int(sqr(ii+1)+1):
% test divisibility
for jj=2 to iis: if ii-int(ii/jj)*jj=0 then z=0: next jj:
% write result in excel sheet
if z=1 then kk=kk+1: if z=1 then cells(kk,1)=ii: next ii:
end sub:
```

Concentric circles can be drawn on top of the hexagons shown in Figure 3, and the number of smaller circles tangent to the large circles then occur in a regular and symmetrical way when the number of circular layers is a prime. Some attempt was made by one researcher to explain this by forming and solving the associated Diophantine equations. It is noted here that potential energy and forces are determined by radial distances- that is the radii of the large circles. Also it is known that the solution of sets of Diophantine equations is a generator of primes.

None prime numbers can be written in a unique set of primes. Thus for any number P we have;

$$P = p_1^a\, p_2^b\, p_3^c \cdots \quad \text{and}$$
$$\log P = a\log p_1 + b\log p_2 + c\log p_3 \cdots$$

where a, b, c are integral powers of the prime factors $p_1\ p_2 \cdots p_n$. Ref. [8] have observed that this relation is equivalent to energy conservation connecting the energy of one large object to the energy of its constituents- where energy is to be associated with $(\log P)$. Further, if the values of a, b, c are unity, the group would only have one energy state (structure), and could be the equivalent of fermions in behaviour. When the exponents are not unity (integer > 1), the group would behave as bosons and would be able to exist in multiple equivalent energy states corresponding to the different combination values of the exponents. Note that $\log p$ would correspond to the derivative of the prime formula $(n\log n)$ for large n accept for a negative sign.

Still in physics, we note that the size of the nucleus of chemical elements is proportional to the number of nucleons [3, 6] inside it. Since many of the physical and statistical models of the nucleus assume identical constituents, we may think of testing the possibility of condensed matter fol-

I – Elementary particles;	II – Particle mass/electron mass;				III – Nearest primes					
I-	e	μ	π^0	$\pi^{\pm}$	$K^{\pm}$	K^0	η	ρ	ω	K^*
II-	1	206.7	264.7	274.5	966.7	974.5	1074.5	1506.8	1532.3	1745.5
III-	1	211	263	277	967	977	1069	1511	1531	1747
I-	p	n	η'	φ	Λ	Σ^+	Σ^0	Σ^-	Δ	Ξ^0
II-	1836.2	1838.7	1873.9	1996.1	2183.2	2327.5	2333.6	2343.1	2410.9	2573.2
III-	1831	1831	1877	2003	2179	2333	2339	2347	2417	2579
I-	Ξ^-	Σ^*	Ξ^*	Ω^-	τ	D^0	$D^{\pm}$	$F^{\pm}$	D^*	Λ_c^-
II-	2585.7	2710.4	3000	3272	3491.2	3649.7	3657.5	3857.1	3933.4	4463.8
III-	2591	2713	3001	3271	3491	3643	3671	3863	3931	4463

Table 2: Relative masses of well known elementary particles and their nearest primes.

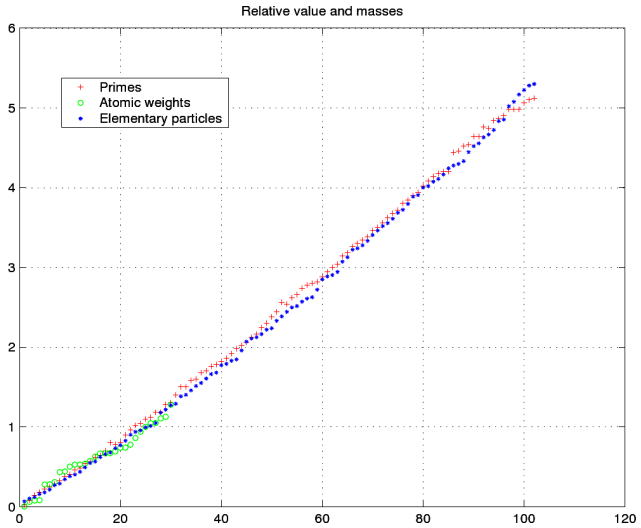

Fig. 7: Three normalized plots in ascending order of the relative atomic weight of 102 elements (+); 30 elementary particles (○); the first 102 prime numbers (*), starting with number 7. Each group is divided by entry number 25 of the group.

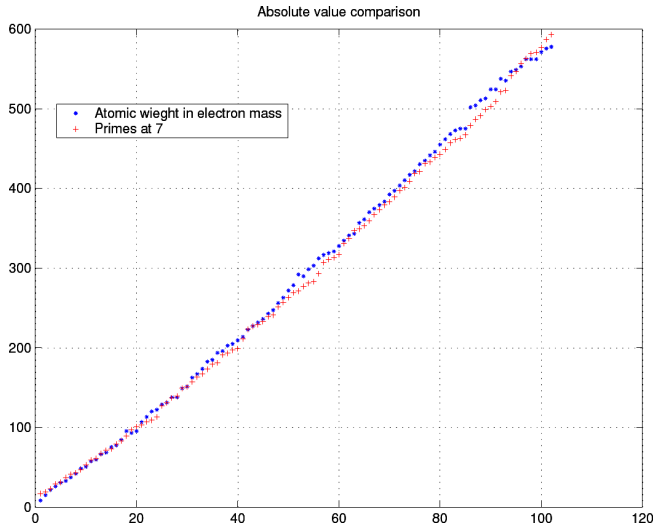

Fig. 8: Absolute-value comparison of the masses of chemical elements and primes. Primes starting from 7 (+) and relative masses of the chemical elements of the periodic table in units of Electron mass divided by (137×6) (*).

lowing the prime packing patterns as a result. We may also repeat the same for the masses of the *elementary particles* of physics which have hitherto defied many efforts to put a sense in the interpretation of their mass spectrum. To do this we shall arrange the various chemical elements of the periodic table (102 in total) and most of the elementary particles (30 in totals) in an ascending order of their masses (disregarding any other chemical property). We shall divide the masses of the chemical elements by the mass of the element say, number 25, in the list of ascending mass- which is Manganese (mass 55 protons) in order to get a relative value picture. The same is done with the group of elementary particles and these are divided by the mass of particle number 25 in the list namely the (Tau) particle (mass 1784 in MeV/c^2 units). Actual units do not matter here as we are only considering ratios. We then compare these with the list of primes arranged in ascending order too. Table 2 contains the data for the case of elementary particles. Masses of the chemical elements can be taken from any periodic table. The nearest prime figures in the table are for information and not used in the plots. In Figure 8 an absolute value comparison for the elements is shown. The primes starts at 7 and the masses of the elements (in electron mass) are divided by 137×6 in order to get the two curves matching at the two ends.

For better fitting, the prime number series had to be started at number 7, not 1 as one might normally do. Comparison results are given in Figures 7 and 8. The trends are strikingly similar. The type of agreement must be a strong indication that the same packing rules are prevailing in all the cases.

3 Concluding remarks

We noticed that primes are closely connected to geometry and physics and this is dictated by the very properties of discrete space geometry like you can closely pack on a plane only seven balls to form a circle. This result and that of the cannon ball packing problem are found to be subsets of the dense packing problem. One clear link between primes and geom-

etry comes from the fact that all primes are generated by the formula $6n \pm 1$. When integers are associated with balls, this formula can be represented in the form of a long cylinder with primes lying along two opposite generator of the cylindrical surface.

Highly energetic particles bound together dynamically are more likely to have circular/spherical structures, and thus can follow the packing arrangements discussed in this article. It may be said now that the source of discreteness frequently observed in the energy levels of atoms and the correspondence between energy levels and prime numbers are only manifestations of this fact. The number of elements (balls) in each circular area or spherical leaf in the building up of a collection is proportional to n^2. The energy of each would naturally be proportional n^2 too. Each constituent will thus carry $1/n^2$ of the energy and the jump of one constituent from one level to the other gives an energy change of $(1/n_1^2 - 1/n_2^2)$ as in the Ballmer series. The Bohr model for the atom relies on an integral number of wavelengths around a circumference, which in this case can be interpreted as integral number of balls, which makes the present model more realistic and easier to digest. The Bohr model was originally intended for the electrons, but later studies took this to concern the whole nucleus [8].

If the packing picture is carried down to the level of very elementary particles, we could speculate that the 2 and 3 circle solutions of the packing problem correspond to the 2 and 3 quarks constituent evidence found in experimental work and stated in the quark theory of elementary particles. Fast particles crossing the nucleus are normally used to probe the nucleus. The 6 pack with 3 balls along any diameter could very well be responsible for the conclusions of such measurements.

The plots of the mass growth (packing) of chemical elements and elementary particles (and hence all massive bodies), as shown here, follow very closely the rules of packing of spheres and also those of the prime numbers. Prime numbers or prime collections appear when it is not possible to divide a collection into symmetric (equal) parts and are hence more stable in structure. This makes the growth of primes to be naturally tied to the growth in the masses of condensed matter in its different phases. We also note that the prime character of a number is an independent property- more of an abstract physical property, and it is not a function of the base of the number system in use or the physical case that number might represent.

The eight fold rules frequently found in the behaviour pattern of chemical elements and elementary particles [4, 8] may now be suspected to be a consequence of the packing rules of similar spheres in space. We might even suggest that the successes of the Bohr Theory for the atom, the Ballmer series formula for energy levels and indeed the Schrödinger equation itself in predicting discrete behaviour in atoms and other entities, might be mainly due to the discretization of space implied in their formulations. In fact while Schrödinger equation has many solutions, those deemed correct have to obey the integrability condition which is essentially a discretization (normalization) of space condition. We mention also that in the solutions of Schrödinger equation, the main interest when finding a solution (the wave function) is the resulting number of discrete states along any radial or circumferential direction and not the actual form (function) of the solution. Not forgetting also that the most fruitful solutions of Schrödinger equation are those in circular no-Cartesian coordinates anyway.

4 Recommendations

More work is needed to reach more concrete, verifiable and useful results. Such work might investigate the origin of the various properties that distinguish groups of elementary particles like strangeness, charm etc in relation to the possible geometric shape/packing of their constituents. The circles and spheres in the present investigation are not referring to a static picture, but one formed by very fast moving particles that generated such shapes as a result of their own dynamic rules. Detailed position-energy calculations of various arrangements, as done on crystals for example, could be done here to pin point the reasons behind an elementary particle to become stable or unstable in the presence of external disturbances, and also the explanation of the various probabilities associated with different break-up scenarios of unstable particles.

Acknowledgement

The author acknowledges very fruitful discussions with Dr. J. Hemp (Oxford). Most of the literature and information used are obtained through the generous contribution of their authors by allowing their free consultation on the open domain. This work was stimulated first by an article by J. Gilson of QMC, attempting to discover the origin of the fine structure constant 137 (approximately a prime number by itself) using algebraic expressions and geometry. The present quest did not get there and the matter will be left for the next inline.

Submitted on May 07, 2009 / Accepted on May 14, 2009

References

1. Wells D. Prime numbers. Whiley, 2005.
2. Harney M. *Progress in Physics*, 2008, v. 1.
3. Finn A. Fundamental university physics. Quantum and statistical physics. Addison-Wesley, 1968.
4. Bohr N. *Nature*, March 24, 1921.
5. Hales T. C. *Notices of the AMS*, 2000, v. 47(4).
6. Griffiths D. Introduction to elementary particles. Wiley, 2004.
7. Hassani M. arXiv: math/0607096.
8. Sugamoto A. *OCHA-PP-277*, arXiv: 0810.4434.

Dual Phase Lag Heat Conduction and Thermoelastic Properties of a Semi-Infinite Medium Induced by Ultrashort Pulsed Laser

Ibrahim A. Abdallah

Department of Mathematics, Helwan University, Ain Helwan, 11795, Egypt
E-mail: iaawavelets@yahoo.com

In this work the uncopled thermoelastic model based on the Dual Phase Lag (DPL) heat conduction equation is used to investigate the thermoelastic properties of a semi-infinite medium induced by a homogeneously illuminating ultrashort pulsed laser heating. The exact solution for the temperature, the displacement and the stresses distributions obtained analytically using the separation of variables method (SVM) hybrid with the source term structure. The results are tested numerically for Cu as a target and presented graphically. The obtained results indicate that at very small time duration disturbance by the pulsed laser the behavior of the temperature, stress and the displacement distribution have wave like behaviour with finite speed.

1 Introduction

Heat transport and thermal stresses response of the medium at small scales becomes recently in the spot of interest due to application in micro-electronics [1] and biology [2, 3] and due to its wide applications in welding, cutting, drilling surface hardening, machining of brittle materials. Because of the unique capability of very high precision control of the ultrashort pulsed laser it is interesting to investigate the thermoelastic properties of the medium due to the ultrashort pulsed laser heating. The different models of thermoelasticity theory based on the equation of heat convection and the elasticity equations. The main categories of these models are the coupled thermoelasticity theory formulated by abd-2-04 [4], and the coupled thermoelasticity theory with one relaxation time [5], the two-temperature theory of thermoelasticity [6], the uncoupled classical linear theory of thermoelasticity based on Fourier'a law [7], the uncoupled thermoelasticity theory based on the Maxwell-Cattaneo modification of heat convection to include one time lag between heat flux and the temperature gradient [8, 9].

The coupled and uncoupled models have been used to solve some problems on the macroscale where the length and time scales are relatively large. The technological needs of a high precision control of the ultrashort pulsed laser applications processes at the microscales ($< 10^{-12}$ s), with high heating rates processes are not compatible with the Fourier's model of heat conduction because it implies to an infinite speed for heat propagation and infinite thermal flux on the boundaries. To overcome the deficiencies of Fourier's law in describing high rate heating processes the concept of wave nature of heat convection had been introduced [10]. Tzou [11, 12] had introduced another modification to Fourier law, by inventing two time lags, Dual Phase Lag (DPL), between the heat flux and the temperature gradient namely the heat flux time lag and the temperature gradient time lag. Therefore he had used the dual phase lag heat convection equation with the energy conservation law to obtain the dual phase lag model for heat convection.

The purpose of the present work is to study the induced thermoelastic waves in a homogeneous isotropic semi-infinite medium caused by an ultrashort pulsed laser heating exponentially decay, based on the dual phase lag modification of Fourier's law. The problem is formulated in the dimensionless form and then solved analytically by inventing a new sort of the separation of variables hybridized by the source structure function. The stress, the displacement and the temperature solutions are obtained and tested by a numerical study using the parameters of Cu as a target. The results performed and presented graphically and concluding remarks are given.

2 Problem formulation

In this investigation I considered a homogeneous isotropic semi-infinite medium with mass density ρ, specific heat c_E, thermal conductivity k, and thermal diffusivity $\alpha = \frac{k}{\rho c_E}$. The medium occupy the half space region $z \geqslant 0$ considering the Cartesian coordinates (x, y, z). the medium is assumed to be traction free, initially at uniform temperature T_0, and subjected to heating process by a ultrashort pulsed laser heat source its structure function; $g(z,t) = \frac{I_0(1-R)}{t_p \phi \sqrt{\pi}} e^{-\frac{z}{\varphi}} e^{-\left|\frac{t-t_p}{t_p}\right|}$, at the surface $z = 0$ as in Fig. 1. where the constants characterize this laser pulse are: I_0, the laser intensity, R the reflectivity of the irradiated surface of the medium, ϕ the absorption depth, and t_p the laser pulse duration. The Cartesian coordinates (x, y, z) are considered and z-axis pointing vertically into the medium. Therefore the governing equations are: The equation of motion in the absence of body forces

$$\sigma_{ji,j} = \rho \ddot{u}_i \qquad i, j = x, y, z\,, \tag{1}$$

where σ_{ij} is the stress tensor components, $u_i = (0, 0, w)$ are the displacement vector components. The constitutive rela-

tion

$$\sigma_{ij} = \left[\lambda\, div\, u_i - \gamma(T - T_0)\right]\delta_{ij} + 2\mu e_{ij} \tag{2}$$

by which the stress components are

$$\begin{aligned} &\sigma_{xx} = \sigma_{yy} = \lambda w_z - \gamma(T - T_0) \\ &\sigma_{zz} = (\lambda + 2\mu) w_z - \gamma(T - T_0) \\ &\sigma_{xy} = 0, \qquad \sigma_{xz} = 0, \qquad \sigma_{yz} = 0\,. \end{aligned} \tag{3}$$

The volume dilation e takes the form

$$e = e_{xx} + e_{yy} + e_{zz} = \frac{\partial w}{\partial z}\,. \tag{4}$$

Where the strain-displacement components e_{ij}, read;

$$\begin{aligned} &e_{ij} = \frac{1}{2}\left(u_{i,j} + u_{j,i}\right) \qquad i, j = x, y, z\,, \\ &e_{zz} = \frac{\partial w}{\partial z}\,, \quad e_{xx} = e_{yy} = e_{xy} = e_{xz} = e_{yz} = 0\,, \end{aligned} \tag{5}$$

substituting from the constitutive relation into the equation of motion using the equation of motion we get:

• The displacement equation

$$(\lambda + 2\mu)\, w_{zz} - \gamma(T - T_0)_z = \rho\, \ddot{w}\,; \tag{6}$$

• The energy conservation

$$-\rho\, c_E \dot{T} = q_z\,. \tag{7}$$

Since the response of the medium to external heating effect comes later after the pulsed laser heating interacts with the medium surface then there is a time lag, and by using the dual phase lag modification of the Fourier's law as invented by Tzou;

$$\begin{aligned} &q(z, t + \tau_q) = -\,k\, T_z(z, t + \tau_T)\,, \\ &q + \tau_q \dot{q} = -\,k\, T_z - k\, \tau_T \dot{T}_z\,. \end{aligned} \tag{8}$$

Then the energy transport equation of hyperbolic type can be obtained by substituting in the energy conservation law and considering the laser heat source

$$\frac{\tau_q}{\alpha}\ddot{T} + \frac{1}{\alpha}\dot{T} = T_{zz} + \tau_T \dot{T}_{zz} - \frac{1}{\rho c_E}\, g(z, t) - \tau_q\, \dot{g}(z, t)\,. \tag{9}$$

This equation shows that the dual lagging should be considered for the processes whose characteristic time are scale comparable to τ_q and τ_T. It describes a heat propagation with finite speed. where τ_q is represents the effect of thermal inertia, it is the delay in heat flux and the associated conduction through the medium, and τ_T is represents the delay in the temperature gradient across the medium during which conduction occurs through its microstructure. For $\tau_T = 0$ one obtain the Maxwell-Cattaneo model, and Fourier law obtained if $\tau_T = \tau_q = 0$.

The boundary conditions are;

$$\begin{aligned} &-k\, T_z(z, t) = g(z, t)\,,\ w = 0\,,\ \sigma_{zz} = 0, \ \text{at}\ z = 0\,, \\ &\sigma_{zz} = 0, \quad w = 0\,, \quad T = 0\,, \quad \text{as} \quad z \to \infty\,. \end{aligned} \tag{10}$$

Introducing the dimensionless transformations $z^* = \frac{z}{\sqrt{\alpha\tau_q}}$, $w^* = \frac{w}{\sqrt{\alpha\tau_q}}$, $\sigma_{ij}^* = \frac{\sigma_{ij}}{\mu}$, $t^* = \frac{t}{\tau_q}$, $t_p^* = \frac{t_p}{\tau_q}$, $\varphi^* = \frac{\varphi}{\sqrt{\alpha\tau_q}}$, $\tau^* = \frac{\tau_T}{\tau_q}$, $\theta_0\theta^* = T - T_0$, $\lambda_1^* = \frac{\lambda}{\mu}$, $\lambda_2^* = \frac{\lambda+2\mu}{\mu}$, $\gamma_0 = \frac{\gamma\theta_0}{\mu}$, $\theta_0 = \frac{I_0(1-R)}{k}\sqrt{\frac{\alpha}{\pi\tau_q}}$, substituting in the governing equations and in boundary conditions of the problem by the above dimensionless transformations and then omitting the $(^*)$ from the resulting equations we obtain the dimensionless set of the governing equations and boundary conditions:

• The dimensionless temperature equation

$$\ddot{\theta} + \dot{\theta} = \theta_{zz} + \tau\dot{\theta}_{zz} + \left(\frac{1 - t_p}{t_p^2\,\varphi}\right) e^{-\frac{z}{\varphi}} e^{-\left|\frac{t-2t_p}{t_p}\right|}\,; \tag{11}$$

• The dimensionless displacement equation

$$w_{zz} - B^2\ddot{w} = G\,\theta_z\,, \tag{12}$$

where $B^2 = \frac{\rho\alpha}{\tau_q t_p^2(\lambda+2\mu)}$ and $G = \frac{\gamma_0\theta_0}{(\lambda+2\mu)}$;

• The dimensionless stresses equations

$$\begin{aligned} &\sigma_{zz} = \lambda_2 w_z - \gamma_0\,\theta\,, \\ &\sigma_{xx} = \sigma_{yy} = \lambda_1 w_z - \gamma_0\,\theta\,; \end{aligned} \tag{13}$$

• Dimensionless boundary conditions

$$\begin{aligned} &w = 0\,, \quad \sigma_{zz} = 0\,, \quad \text{at} \quad z = 0\,, \\ &\theta_z(z, t) = -\frac{1}{k\sqrt{\alpha\tau_q}}\, e^{-\left|\frac{t-2t_p}{t_p}\right|}, \quad \text{at} \quad z = 0\,, \\ &\sigma_{zz} = 0\,, \quad w = 0\,, \quad T = 0\,, \quad \text{as} \quad z \to \infty\,. \end{aligned} \tag{14}$$

3 Solution of the problem

In this section I introduced the hybrid separation of variables method (HSVM) to get the solution of equations (11) and (12). Using this method one can construct the analytic solution for some type of nonhomogeneous partial differential equations (or system). Its idea based on using the structure of the nonhomogeneous term to invent the form of separation of variables. Therefore the PDE (or system) will reduced to ODE (or system) which can be solved. To illustrate the (HSVM) we use it to solve the problem in this paper. Introducing the following separation of variables based on the structure of the source function, which represents the inhomogeneous term,

$$\theta(z, t) = Z(z)\, e^{-\left|\frac{t-2t_p}{t_p}\right|}, \quad w(z, t) = W(z)\, e^{-\left|\frac{t-2t_p}{t_p}\right|} \tag{15}$$

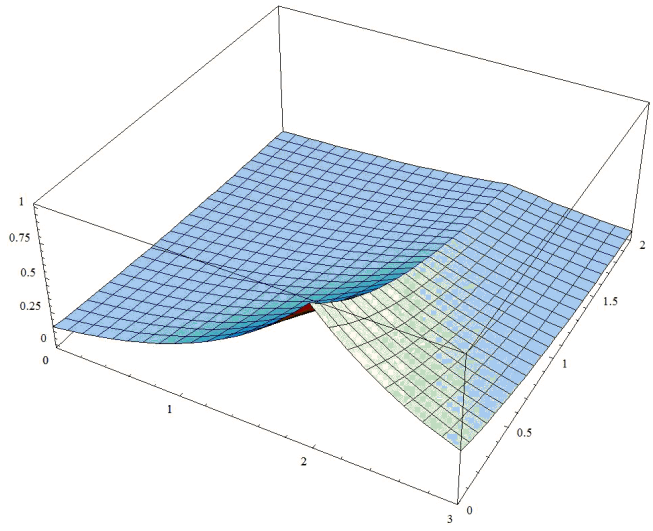

Fig. 1: The strcture function of the ultrashort pulsed laser of exponentially decay.

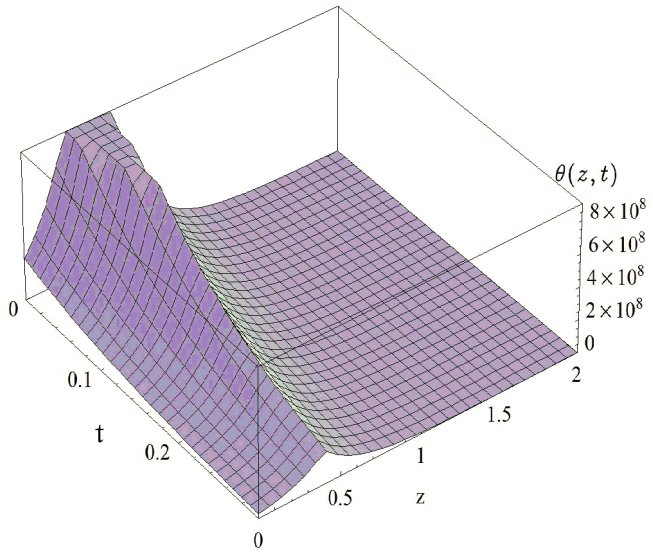

Fig. 2: The dimensionless temperature distribution.

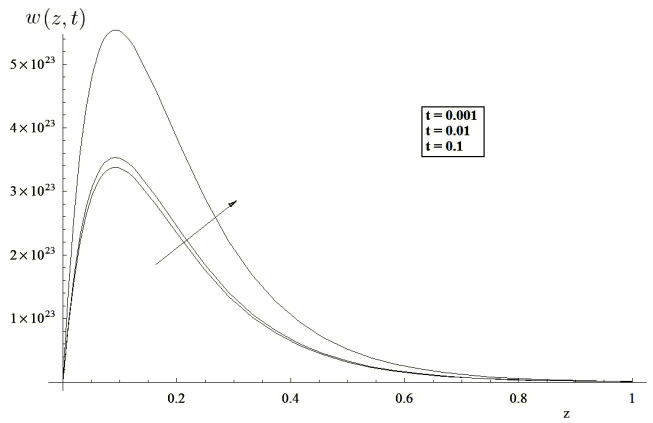

Fig. 3: The dimensionless w-displacement distribution.

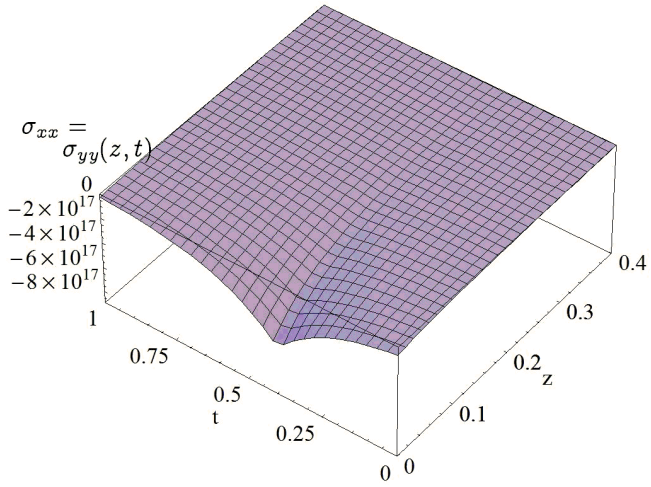

Fig. 4: The dimensionless stresses $\sigma_{xx} = \sigma_{yy}$ distributions.

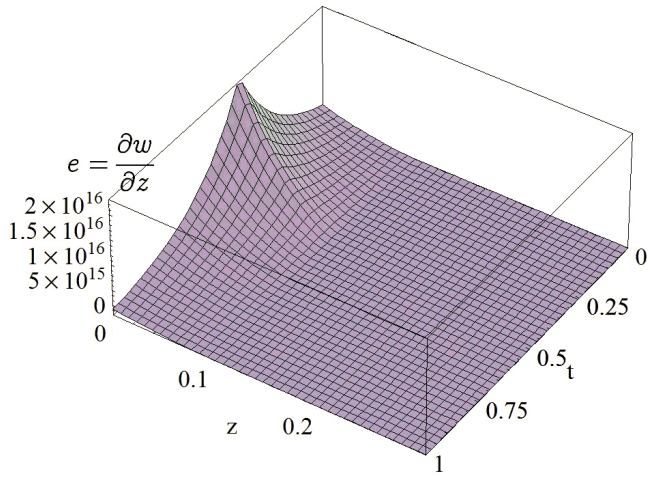

Fig. 5: The dimensionless volume dilation e.

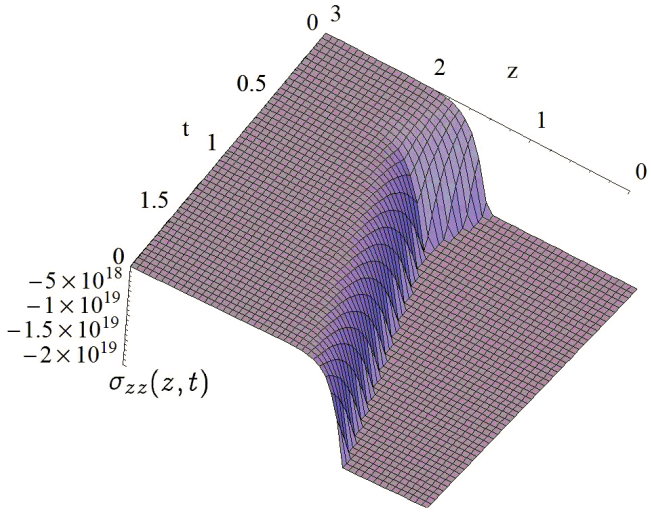

Fig. 6: The dimensionless stresses σ_{zz} distributions.

the equations (11) and (12) will be reduced to a separable form and can be solved directly and therefore using the dimensionless boundary conditions we obtain:

• The solution of the dimensionless temperature equation

$$\theta(z,t) = \left[\vartheta_1 e^{-Az} + \vartheta_2 e^{-\frac{z}{\varphi}}\right] e^{-\left|\frac{t-2t_p}{t_p}\right|}; \qquad (16)$$

where $A^2 = \frac{(1-t_p)}{t_p(t_p-\tau)}$, $H = \frac{(t_p-1)}{t_p\varphi}$,
$\vartheta_1 = \left[\frac{1}{At_p\varphi\sqrt{\alpha\tau_p}} - \frac{H}{A\varphi(\frac{1}{\varphi^2}-A^2)}\right]$, $\vartheta_2 = \frac{H}{(\frac{1}{\varphi^2}-A^2)}$;

• The solution of the dimensionless displacement equation

$$w(z,t) = \left[W_1 e^{-Bz} + W_2 e^{-Az} + W_3 e^{-\frac{z}{\varphi}}\right] e^{-\left|\frac{t-2t_p}{t_p}\right|}, \quad (17)$$

where $W_1 = \left[\frac{GA\vartheta_1}{(A^2-\frac{B^2}{t_p^2})} + \frac{G\vartheta_2}{\varphi(A^2-\frac{B^2}{t_p^2})}\right]$, $W_2 = -\frac{GA\vartheta_1}{(A^2-\frac{B^2}{t_p^2})}$,
$W_3 = -\frac{G\vartheta_2}{\varphi(\frac{1}{\varphi^2}-\frac{B^2}{t_p^2})}$;

• The solution of the dimensionless stresses equation

$$\sigma_{xx} = \sigma_{yy} = -e^{-\left|\frac{t-2t_p}{t_p}\right|}\left[\gamma_0\left(\vartheta_1 e^{-Az} + \vartheta_2 e^{-\frac{z}{\varphi}}\right) + \right.$$
$$\left. + \lambda_1\left(W_1 B e^{-Bz} + W_2 A e^{-Az} + W_3\frac{1}{\varphi}e^{-\frac{z}{\varphi}}\right)\right], \qquad (18)$$

$$\sigma_{zz} = -e^{-\left|\frac{t-2t_p}{t_p}\right|}\left[\gamma_0(\vartheta_1 e^{-Az} + \vartheta_2 e^{-\frac{z}{\varphi}}) + \right.$$
$$\left. + \lambda_2\left(W_1 B e^{-Bz} + W_2 A e^{-Az} + W_3\frac{1}{\varphi}e^{-\frac{z}{\varphi}}\right)\right], \qquad (19)$$

where $\lambda = 7.76\times10^{10}$ kg/m sec^2,
$\rho = 8954$ Kg/m^3, $\mu = 3.86\times10^{10}$ kg/m sec^2,
$\alpha_t = 1.78\times10^{-5}$, $c_E = 383.1$ J/kgK, $t_p = 0.1$ sec,
$k = 386$ W/mK, $\lambda + 2\mu = 1.548\times10^{11}$ kg/m sec^2,
$\tau_q = 0.7\times10^{-12}$ sec, $\tau_\theta = 89\times10^{-12}$ sec,
$\varphi = 0.2$ m, $\gamma = (3\lambda + 2\mu)\alpha_t = 5.518\times10^6$ kg/m sec^2,
$\beta = 2\times10^{13}$, $\delta = 1.7\times10^{-6}$, $A = \beta\tau_q = 14$,
$I_1 = I_0(1-R) = 1\times10^{13}$ W/m^2.

4 Discussion and conclusion

In this paper the thermoelastic waves in a homogeneous isotropic semi-infinite medium caused by an ultrashort pulsed laser heating having exponentially decay, based on the dual phase lag modification of Fourier's law have been investigated. The problem formulated in the dimensionless form and then solved analytically for the temperature, the stress, and the displacement by inventing a new sort of the hybridized separation of variables by the source structure function. The obtained analytical solutions are tested numerically using for Cu as a target medium.

The results are presented graphically. The obtained results indicated that due to the very high power of the laser pulse at the surface in a very short duration the temperature distribution possessing a wave nature with finite speed as in Fig. 2. The medium responses to the laser heating by increasing change in the displacement distribution with increasing time duration as in Fig. 3. The thermoelastic characteristics (stresses components $\sigma_{xx} = \sigma_{yy}$ and volume dilation $e = \frac{\partial w}{\partial z}$) of the medium possess wave nature as in Fig. 4 and Fig. 5. Fig. 6. depicts that the stress component σ_{zz} have wave nature with wave front has its maximum at the average of the laser pulse duration. By these results it is expected that the dual phase lag heat conduction model will serve to be more realistic to handle practically the laser problems with very high heat flux and/or ultrashort time heating duration.

Submitted on May 06, 2009 / Accepted on May 15, 2009

References

1. Kulish V.V., Lage J.L., Komarov P.L., and Raad P.E., *ASME J. Heat Transfer*, 2001, v. 123(6), 1133–1138.
2. Kuo-Chi Liu and Han-Taw Chen. *Int. J. Heat and Mass Transfer*, 2009, v. 52, 1185–1192.
3. Zhou J., Chen J.K., Zhang Y. *Computers in Biology and Medicine*, 2009, v. 39, 286–293.
4. abd-2-04 M. *J. Appl. Phys.*, 1956, v. 27, 240–253.
5. Lord H. and Shulman Y. *J. Mech. Phys. Solid.*, 1967, v. 15, 299–309.
6. Youssef H.M. and Al Lehaibi A. Eman. *I. J. of Sol. and Struct.*, 2007, v. 44, 1550–1562.
7. Chadwick 1.P. Thermoelasticity: the dynamic theory. In: *Prog. in Sol. Mech.*, v. I, Hill R. and Sneddon I.N. (eds.), North-Holland, Amsterdam, 1960, 263–328.
8. Abdallah A.I. *Progress in Physics*, 2009, v. 2, 12–17.
9. Andrea P.R., Patrizia B., Luigi M., and Agostino G.B. *Int. J. Heat and Mass Trans.*, 2008, v. 51, 5327–5332.
10. Özisik M.N. and Tzou D.Y. *ASME J. of Heat Transfer*, 1994, v. 116, 526–535.
11. Tzou D.Y. *ASME J. of Heat Transfer*, 1995, v. 117, 8–16.
12. Tzou D.Y. Macro-to-micro scale heat transfer: the lagging behavior. Taylor and Francis, Washington (DC), 1997.

The Missing Measurements of the Gravitational Constant

Maurizio Michelini
ENEA — Casaccia Research Centre, Rome, Italy
E-mail: m_michelini@alice.it

G measurements are made with torsion balance in "vacuum" to the aim of eliminating the air convection disturbances. Nevertheless, the accuracy of the measured values appears unsatisfying. In 2000 J. Luo and Z. K. Hu first denounced the presence of some unknown systematic error in high vacuum G measurements. In this work a new systematic effect is analyzed which arises in calm air from the non-zero balance of the overall momentum discharged by the air molecules on the test mass. This effect is negligible at vacuum pressures higher than a millibar. However in the interval between the millibar and the nanobar the disturbing force is not negligible and becomes comparable to the gravitational force when the chamber pressure drops to about 10^{-5} bar. At the epoch of Heyl's benchmark measurement at 1–2 millibar (1927), the technology of high vacuum pumps was developed, but this chance was not utilized without declaring the reason. The recent G measurements use high vacuum techniques up to 10^{-10} and 10^{-11} bar, but the effect of the air meatus is not always negligible. We wonder whether the measurements in the interval between the millibar and the nanobar have been made. As a matter of fact, we were not able to find the related papers in the literature. A physical explanation of the denounced unknown systematic error appears useful also in this respect.

1 Introduction

Everyone knows the simple experience of two flat microscopy glasses which cannot be separated from each other when their surfaces touch. Obviously this effect is due to the pressure of the air whose molecules penetrate with difficulty between the corrugations of the polished surfaces generating within the small meatus a considerable air depression. The mean free path of the air molecules at normal pressure is about 10^{-7} metres, that is of the same order of magnitude of the polished surface corrugations. In general, the molecules are not able to freely penetrate within a meatus whose thickness is reduced to about 1 mean free path. When we consider the meatus facing the test mass of a gravitational torsion balance placed in a vacuum chamber, the very little air depression within the meatus originates a disturbing force on the test mass, which adds to the gravitational force. This disturbing force is negligible at normal pressure, but when the pressure within the vacuum chamber is reduced beyond the millibar (for instance to avoid other disturbances due to air convection or to minimize the air friction on the oscillating pendulum) the meatus optical thickness further reduces, so as to attain the above condition about 1 mean free path. It appears opportune to investigate this phenomenon to obtain a semi-quantitative prediction of the disturbing drawing force arising on the gravitational balance. This research takes into account the results of some experimenters which denounced the presence of some unknown systematic effect in the G measurements.

2 Historical background

The torsion balance apparatus was first used by Cavendish in 1798 in a very simple form which permitted him to reach an unexpected accuracy. In the following two centuries the torsion balance was used by several experimenters which substantially improved the technique, but the level of accuracy did not show a dramatic enhancement. Several methods were devised in the XXth century to measure G. In a Conference organized by C. C. Speake and T. J. Quinn [1] at London in 1998 — two centuries after Cavendish — a variety of papers described the methods of measurement and their potential accuracy related to the disturbances and systematic errors. In Table 1 we report the most accurate values presented at the Conference [$G \times 10^{-11}$ kg/m^{3}s^2]:

Author	Method	G	Accur. (ppm)
PTB	torsion balance	6.7154	68
MSL	torsion balance (a)	6.6659	90
MSL	idem (re-evaluation)	6.6742	90
MSL	torsion balance (b)	6.6746	134
BIPM	torsion-streap bal.	6.683	1700
JILA	absolute gravimeter	6.6873	1400
Zurich	beam balance	6.6749	210
Wuppertal	double-pendulum	6.6735	240
Moscow	torsion pendulum	6.6729	75

Table 1: Measurements of G, according to [1].

Among the methods described there are: a torsion balance where the gravitational torque is balanced by an electrostatic torque produced by an electrometer; a torsion-strip balance where the fibre is substituted by a strip; a dynamic method based on a rotating torsion pendulum with angular acceleration feedback; a free fall method where the determination of G depends on changes in acceleration of the falling object, etc. Notwithstanding the technological improvement, up to now the gravitational constant is the less accurately known among the physical constants. The uncertainty has been recognized to depend on various experimental factors. To eliminate the air thermal convection on the test mass, in 1897 K. F. Braun made a torsion balance measurement after extracting the air from the ampule. The level of vacuum ob-

tained with his technique is not known. In 1905 W. Gaede invented the rotary pumps reaching the void level of 10^{-6} bar. Subsequently Gaede developed the molecular drag pumps (1915) using Hg vapour. In 1923 the mercury was substituted by refined or synthetic oil, which enabled to reach void levels around 10^{-9} bar.

In 1927 Heyl [2] made a benchmark measurement with a heavy torsion balance to the aim of establishing a firm value of G. Although the high vacuum technology was available, he adopted a chamber pressure equal to 1–2 millibar. The molecule mean free path at 1 millibar is about 10^{-4} metres, a quantity much smaller than the thickness of the meatus. From our present investigation it appears that the air pressure effect does not alter the accuracy of the classical G measurements performed at pressures higher than some millibars. But this fact was unknown at the epoch. In any case the choice of high vacuum was compelling against the air convection disturbance. After 1958 the development of turbomolecular pumps and the improved molecular drag pumps made available an ultra-high-vacuum up to 10^{-13} bar. Also this spectacular jumping was apparently disregarded by the G experimenters. In 1987 G. T. Gillies published an Index of measurements [3] containing over 200 experiments, which does not report vacuum pressures between the millibar and the nanobar. At the end of ninety the unsatisfying values of G became publicly discussed.

3 First report of a new unknown systematic error

A status of the recent G measurements was published in 2000 by J. Luo and Z. K. Hu [4] in which the presence of some unknown systematic effect was first denounced: "This situation, with a disagreement far in excess to the estimate, suggests the presence of unknown systematic problems".

In 2003 R. Kritzer [5] concluded that "the large spread in G measurements compared to small error estimates, indicates that there are large systematic errors in various results".

Among the last experiments, some of them used new sophisticated methods with technologies coupled to very low pressures within the test chamber. This fact shows a new attention to the problems of possible unknown air effects.

J. H. Gundlach and S. M. Merkowitz [6] made a measurement where a flat pendulum is suspended by a torsion fiber without torque since the accelerated rotation of the attracting masses equals the gravitational acceleration of the pendulum.

To minimize the air dynamic effect, the pressure was lowered to 10^{-7} Torr ($p_0 \approx 10^{-10}$ bar). At this pressure the classical mean free path $l = m/\sigma\,\delta_0$ within a large homogeneous medium is of the order of 1000 metres. Hence within the vacuum chamber the lack of flux homogeneity is everywhere present.

Another accurate measurement was performed in 2002 by M. L. Gershteyn et al. [7] in which the pendulum feels a unique drawing mass fixed at different distances from the test mass. The change of the oscillation period determines G. To minimize the air disturbance, the pressure in the vacuum chamber was lowered to 10^{-6} Pascal (i.e. $p_0 = 10^{-11}$ bar). The reason for such a dramatic lowering is not discussed. The authors revealed the presence of a variation of G with the orientation (regard to the fixed stars) amounting to 0.054%. Incidentally, the anisotropy of G is predicted by the gravitational-inertial theory discussed in [8].

In 2004 a new torsion balance configuration with four attracting spheres located within the vacuum chamber ($p_0 = = 1.5\times10^{-10}$ bar) was described by Z. K. Hu and J. Luo [9]. The four masses are aligned and each test mass oscillates between a pair of attracting masses. Each test mass determines with the adjacent spheres a small meatus (estimated about 4 mm) and a large meatus (about 16 mm). During the experiment the authors found the presence of an abnormal period of the torsion pendulum, which resulted independent of the material wire, test mass, torsion beam and could not be explained with external magnetic or electric fields. Adopting a magnetic damper system, the abnormal mode was suppressed, but the variance of the fundamental period of the pendulum introduced an uncertainty as large as 1400 ppm, testifying the presence of a systematic disturbance in determining G.

We applied to this problem the analysis carried out in this paper. From the air density in the vacuum chamber, we calculate the optical thickness of the small meatus and the related air depression, Eq. (5), which substituted in Eq. (7) gives upon the test mass a disturbing force rising up to $F(p_0) \approx \approx 10^{-14}$ Newton, equivalent to about 10^{-4} times the gravitational force, which alters the pendulum period. This fact agrees with the author conclusions [9] that the torsion balance configuration would have an inherent accuracy of about 10 ppm in determining G, but the uncertainty in the fundamental period reduces this accuracy to 1400 ppm.

The presence of an abnormal disturbance was previously described (1998) by Z. K. Hu, J. Luo, X. H. Fu et al. [10] in dealing with the time-of-swing method. They found the presence of "important non-linear effects in the motion of the pendulum itself, independent of any defect in the detector, caused by the finite amplitude of the swing". Their configuration consisted in a torsion balance with heavy masses external to the vacuum chamber, where the pressure was lowered to $p_0 = 2\times10^{-10}$ bar. The test mass, diameter about 19 mm, was suspended within a stainless vacuum tube placed between two heavy masses distant 60 mm apart. Since the test mass oscillates up to 8 mm from the centre of the vacuum tube, the optical thickness of the small meatus can be deduced. The smaller this thickness, the greater the disturbing force $F(p_0)$. Repeating the analysis carried out for the preceding experiment, we found a force $F(p_0)$ which represents a lower fraction of the gravitational force thanks to the heavy attractor masses. Comparing with many measurements made in last decades with high vacuum technology [11–19] we notice that the vacuum pressures (when reported) were not

comprised between the millibar and the nanobar. The reasons for this avoidance do not appear to have been discussed.

4 Scattering of molecules upon smooth surfaces

The scattering of gas molecules hitting a smooth surface does not generally follow the optical reflection because that which collide about orthogonally may interact with a few atoms of the lattice. As it happens when two free particles come in collision, these molecules may be scattered randomly. Conversely, the molecules hitting the surface from a nearly parallel direction interact softly with the field of the atomic lattice. In fact these molecules, whose momentum $q = mv$ makes an angle $\alpha = \pi/2$ with the vertical axis, receive from the lattice field a small vertical momentum $\Delta q \approx 2\,mv\cos\alpha$ which redirects the molecules along a nearly optical reflection. It is usefull to recall that the momentum hv/c of the UV rays (which observe the reflection law) is comparable to the momentum of air molecules at normal temperature.

To resume: after scattering on a smooth surface a fraction of the nearly orthogonal molecules becomes quasi parallel.

As a consequence an isotropic flux ϕ_0 of molecules hitting a smooth surface, after scattering becomes non-isotropic. This condition may be described by the relationship

$$\psi_0(\alpha) \backsimeq \phi_0\left(1 - \Delta_1\cos\alpha + \Delta_2\sin\alpha\right) \tag{1}$$

where the parameters Δ_1, Δ_2 satisfy the total flux condition $\int_0^{\pi/2}\sin\alpha\,\psi_w(\alpha)\,d\alpha = \phi_0$. Moreover we assume that about χ percent of the nearly orthogonal molecules become quasi-parallel after scattering on the wall. Applying these two conditions one obtains the figures $\Delta_1 \simeq 1.46\,\chi$, $\Delta_2 \simeq 2\Delta_1/\pi \simeq$ $\simeq 0.928\,\chi$, where χ may range between 0.10 down to 0,0001 for smoothed glass walls. This physical condition makes easy to understand the molecular flux depression within the meatus around the test mass. This phenomenon becomes particularly evident at low air pressures. For instance when the vacuum pressure is about a millibar, then 99.99% molecules hitting the test mass, Fig. 1, come from scattering with other molecules within the meatus, whereas 0.01% molecules come directly from the scattering on the chamber wall. To feel a sensible flux depression in the meatus it is necessary that the molecules coming from wall-scattering be about a half of the total. Within an air meatus of thickness "s" this happens when the optical thickness $\Sigma s = s\sigma\delta_0/m \simeq 10^7 s\,\delta_0$ equals 1 mean free path, i.e. when the air density equals $\delta_0 \simeq 10^{-7}/s$. For usual torsion balances the critical vacuum pressure which maximizes the flux depression is $p_0 \approx 1\times10^{-5} \div 3\times10^{-5}$ bar.

The old G measurements adopted a torsion balance at atmospheric pressure, so the meatus effect took place between the test mass and the attracting sphere. This happens also to G measurements in vacuum when the heavy masses are comprised within the chamber. But in general the G measurements in vacuum are made with the heavy masses outside the chamber. In this case we define "meatus" the air comprised between the test mass and the adjacent wall of the vacuum chamber (Fig. 1). At pressures higher than some millibars the molecular flux upon the moving mass is highly uniform, so the sum of every momentum discharged by the molecules on the sphere is null for any practical purpose. However, when the pressure in the chamber is further reduced, the molecular flux begins to show a little depression in the meatus. The flux depression in the circular meatus may be expressed along the radial direction x

$$\phi(x) \backsimeq \phi_m\left(1 + kx^2\right), \tag{2}$$

where ϕ_m is the minimum figure the flux takes on the meatus centre. Since the flux on the boundary, i.e. $x = L$, is the unperturbed flux ϕ_0, then one gets $\phi_m\left(1 + kL^2\right) = \phi_0$ which shows that k is linked to the flux parameters of the meatus

$$k = \left(\phi_0/\phi_m - 1\right)/L^2, \tag{3}$$

where $L \backsimeq R\cos\beta$ is the radius of the area of the test mass experiencing the flux depression. The angle β, defined by $\sin\beta = R/(R+s)$ (where R is the radius of the moving mass, s is the minimum thickness of the meatus), plays a fundamental role since it describes (Fig. 1) the "shadow" of the moving mass on the adjacent chamber wall. Choosing spherical co-ordinates with the same axis of the meatus and origin (Fig. 1) in the point B, the monokinetic transport theory gives us the angular flux of incident molecules $\psi_B(\alpha)$ integrating the scattered molecules along the meatus thickness $s(\alpha)$ and adding the flux $\psi_s(\alpha)$ of uncollided molecules scattered on the surface of the moving mass

$$\psi_B(\alpha) = \int_0^{s(\alpha)} \Sigma\phi(r)\exp(-\Sigma r)dr + \\ + \psi_s(\alpha)\exp\left[-\Sigma s(\alpha)\right], \tag{4}$$

where Σ is the air macroscopic cross section, $\Sigma\phi(r)$ is the density of isotropically scattered molecules, $s(\alpha)$ is the meatus thickness along α. This angular flux holds for $\alpha \leqslant \beta$. The above presentation of the problem has only an instructive character denoting the complexity of the problem, because the fluxes $\phi(r)$ and $\psi_s(\alpha)$ are unknown.

5 Calculation of the molecular flux in the meatus

To solve the problem of calculating the molecular flux within the meatus we adopt the principle of superposition of the effects. Let's consider the test sphere surrounded by the air in the vacuum chamber at pressure p_0. To obtain the disturbing force $F(p_0)$ on the test mass we must calculate the flux in the point A of the sphere and in the point C diametrically opposite (Fig. 1). Let's now remove the sphere and substitute an equal volume of air at pressure p_0, so to fill the chamber with the uniform molecular flux ϕ_0. Let's calculate the flux incident on both sides of the point A considering a spherical coordinates system with origin in this point (Fig. 1). The

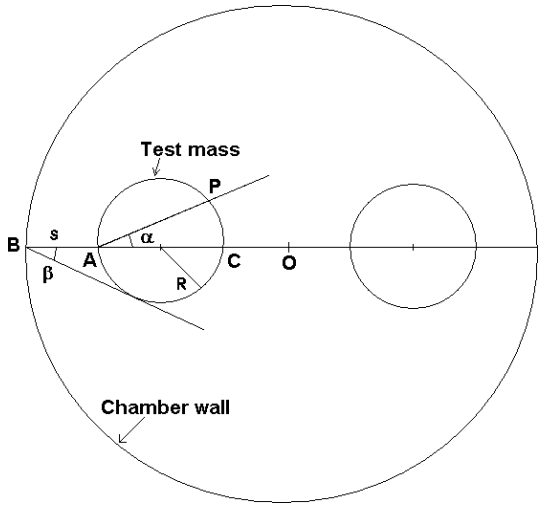

Fig. 1: Schematic drawing of a torsion balance in a vacuum chamber (meatus thickness arbitrarily large).

angular flux on the right-side of the point A is due to the scattering on the molecules within the sphere volume and to the uncollided molecules coming from the surface of the sphere (point P) where there is the uniform flux ϕ_0

$$\psi_A(\alpha) = \int_0^{t(\alpha)} \Sigma\phi_0 \exp(-\Sigma r)dr + \phi_0 \exp\left[-\Sigma t(\alpha)\right] \quad (5)$$

where $t(\alpha) = 2R\cos\alpha$ is the distance between the points A and P (Fig. 1) placed on the (virtual) surface of the removed mass. Let's notice that the first term in Eq. (3) represents the flux due to the scattering source occupying the sphere volume. When we cancel this source term (for instance reintroducing the test mass), Eq. (5) gives the flux

$$\psi_{A+}(\alpha) = \phi_0 \exp(-2\Sigma R\cos\alpha). \quad (6)$$

On the left-side of the point A the flux comes from scattering on the air within the meatus and from the uncollided molecules coming from the chamber wall

$$\psi_{A-}(\alpha) = \phi_0\left[1 - \exp(-\Sigma z(\alpha))\right] + \\ + \psi_w(\alpha)\exp(-\Sigma z(\alpha)), \quad (7)$$

where $z(\alpha)$ is the wall distance and $\phi_w(\alpha)$ is the flux scattered on the chamber wall, as defined by Eq. (1). Since in general the size of the chamber is much larger than R, one may assume the distance $z(\alpha) \simeq s/\cos\alpha$. Subtracting the flux $\psi_{A+}(\alpha)$ from $\psi_{A-}(\alpha)$ gives the actual flux on the point A of the test mass

$$\psi_A(\alpha) \simeq \phi_0\left[1 - \exp(-2\Sigma R\cos\alpha)\right] - \\ - \left[\phi_0 - \psi_w(\alpha)\right]\exp(-\Sigma s/\cos\alpha). \quad (8)$$

Now we calculate with the same procedure the incident flux on the point C

$$\psi_C(\alpha) \cong \phi_0\left[1 - \exp(-2\Sigma R\cos\alpha)\right] - \\ - \left[\phi_0 - \psi_w(\alpha)\right]\exp(-\Sigma(s+2R)/\cos\alpha). \quad (9)$$

The disturbing force on the moving mass is linked to the different pressures on the points A and C due to the momentum discharged by the molecular flux on these points. The molecular flux shows the following difference across the test mass diameter $\phi_C - \phi_A = \phi_0 \int_0^{\pi/2} \sin\alpha\left[\psi_C(\alpha) - \psi_A(\alpha)\right] d\alpha$.

Substituting and putting $w(\alpha) = \psi_w(\alpha)/\phi_0$, one gets the flux difference

$$\Delta\phi_0 = \phi_0 \int_0^{\pi/2} \sin\alpha\left[1 - w(\alpha)\right]\left[\exp(-\Sigma s/\cos\alpha) - \right. \\ \left. - \exp(-\Sigma(s+2R)/\cos\alpha)\right] d\alpha, \quad (10)$$

which confirms that the flux depression depends on the anisotropy of the flux $\psi_w(\alpha)$ scattered on the wall. Through Eq. (1) we also have $w(\alpha) = 1 - \Delta_1\cos\alpha + \Delta_2\sin\alpha$ which, substituting in the above equation gives the air depression

$$\Delta p_0/p_0 = \Delta\phi_0/\phi_0 = \\ = \Delta_1\Gamma(\Sigma s,\ \Sigma R) - \Delta_2\Omega(\Sigma s,\ \Sigma R), \quad (11)$$

where the functions

$$\Gamma(\Sigma s,\ \Sigma R) = \int_0^{\pi/2} \sin\alpha\cos\alpha\left[\exp(-\Sigma s/\cos\alpha) - \right. \\ \left. - \exp(-\Sigma(s+2R)/\cos\alpha)\right] d\alpha \quad (12)$$

and

$$\Omega(\Sigma s,\ \Sigma R) = \int_0^{\pi/2} \sin^2\alpha\left[\exp(-\Sigma s/\cos\alpha) - \right. \\ \left. - \exp(-\Sigma(s+2R)/\cos\alpha)\right] d\alpha \quad (13)$$

depend on the meatus geometry and on the air density δ_0 in the vacuum chamber. These functions do not appear to have been already tabulated. Fitting functions have been used for calculations, whose accuracy is not completely satisfying.

To give a quantitative idea of the phenomenon, the relative depression $\Delta p_0/p_0$ has been calculated assuming the usual size of a torsion balance, as specified in Table 2. Substituting in Eq. (12) the macroscopic cross section $\Sigma = \sigma\delta_0/m$ for any air density δ_0, one obtains the depressions $\Delta p_0/p_0$ reported in Table 2. Notice the high uniformity of the molecular flux within the meatus at 1 millibar vacuum level.

Conversely, the chamber pressure $p_0 = 10^{-5}$ bar corresponds to a sensible depression $\Delta p_0/p_0 \approx 3.4\times10^{-3}$ which may alter the gravitational force between the gravitational masses.

The disturbing force due to the small depression within the meatus $\Delta p(r) = mv\left[\phi_0 - \phi(r)\right]$ is defined by

$$F = \int_0^L 2\pi\, r\, \Delta p(r)\, dr, \quad (14)$$

where $L = R\cos\beta$ is the radius of the meatus periphery where $p(L) = p_0$. Substituting the flux distribution given by Eq. (2) one gets the corresponding depression within the meatus

$$p_0 - p(r) = p_0\left[1 - (\phi_m/\phi_0)\left(1 + kr^2\right)\right]. \quad (15)$$

Vacuum pressure p_0 Pascal	Air density δ_0 kg/m^3	Meatus optical width Σs m.f.p.	Flux depression $\Delta\phi_0/\phi_0$	Disturbing force $F(p_0)$ Newton
100	10^{-3}	40	1.4×10^{-22}	3.6×10^{-25}
50	5×10^{-4}	20	1.2×10^{-11}	1.5×10^{-14}
10	10^{-4}	4	2.8×10^{-6}	7.2×10^{-10}
1	10^{-5}	0.4	3.4×10^{-5}	8.4×10^{-10}
0.1	10^{-6}	4×10^{-2}	6.8×10^{-5}	1.7×10^{-10}
10^{-2}	10^{-7}	4×10^{-3}	1.8×10^{-5}	4.5×10^{-12}
10^{-3}	10^{-8}	4×10^{-4}	4.4×10^{-6}	1.1×10^{-13}
10^{-4}	10^{-9}	4×10^{-5}	1.1×10^{-6}	2.8×10^{-15}
10^{-5}	10^{-10}	4×10^{-6}	2.8×10^{-7}	7×10^{-17}
10^{-6}	10^{-11}	4×10^{-7}	8×10^{-8}	2×10^{-18}

Table 2: Calculation of the disturbing force due to the air molecules within the vacuum chamber of a gravitational torsion balance. The assumed geometrical characteristics are: meatus thickness $s = 4$ mm, moving mass radius $R = 5$ mm.

Substituting the expression of k by Eq. (3) one obtains

$$p_0 - p(r) = p_0 \left[1 - \phi_m/\phi_0\right]\left(1 - r^2/L^2\right) \qquad (16)$$

which, substituted in Eq. (15), gives us the force

$$F(p_0) = (\pi/2)\, p_0 L^2 \left(\Delta p_0/p_0\right) \qquad (17)$$

where the relative depression is given by Eq. (12). Assuming for smoothed chamber walls a value $\xi = 0.001$ we obtain the disturbing force reported in Table 2. One can notice that in the assumed torsion balance apparatus with light test mass ($R = 5$ mm) the disturbing force $F(p_0)$ takes a maximum at a pressure $p_0 \approx 2$ Pascal $= 2\times10^{-5}$ bar which makes the optical thickness of the meatus about equal to 1. This maximum is estimated to be comparable to the measured gravitational force F_{gr}. Even taking into account the questionable accuracy of the fitting functions, the values of the disturbing force explain "ad abundantiam" why the region of the intermediate pressures between millibar and nanobar was avoided by the experimenters. Obviously, what is of interest in the measurements is the systematic error due to $F(p_0)$. For instance in the Gershteyn's light torsion balance (where F_{gr} may be of the order of 10^{-11} Newton) the measurement was made at a pressure $p_0 = 10^{-11}$ bar (10^{-6} Pascal), so the disturbing force $F(p_0)$ gives a negligible systematic error $\epsilon \approx 2\times10^{-7}$.

In the Heyl's heavy balance experiment (where the measured F_{gr} was of the order of 10^{-9} Newton) the disturbing force $F(p_0)$ at a pressure $p_0 = 1$ millibar (100 Pascal) gives $\epsilon \approx 10^{-16}$. However the random error due to the air convection was probably around $\epsilon \approx 10^{-4}$, that is much larger than the systematic error due to the vacuum pressure.

Submitted on February 07, 2009 / Accepted on May 18, 2009

References

1. Speake C.C., Quinn T.J. The gravitational constant: theory and experiment 200 years after Cavendish. *Meas. Sci. Technol.*, 1999, v. 10, 420.
2. Heyl P.R. A determination of the Newtonian constant of gravitation. *Proc. Nat. Acad. Sci.*, 1927, v. 13, 601–605.
3. Gillies G.T. The Newtonian gravitational constant: an index of measurements. *Metrologia*, 1987, v. 24, 1–56.
4. Luo J., Hu Z.K. Status of measurement of the Newtonian gravitational constant. *Class. Quant. Grav.*, 2000, v. 17, 2351–2363.
5. Kritzer R. The gravitational constant. http://www.physics.uni-wuerzburg.de
6. Gundlach J.H., Merkowitz S.M. Mesurement of Newton's constant using a torsion balance with angular acceleration feedback. arXiv: gr-qc/0006043.
7. Gershteyn M.L. et al. Experimental evidence that the gravitational constant varies with orientation. arXiv: physics/0202058.
8. Michelini M. The common physical origin of the gravitational, strong and weak forces. *Apeiron*, 2008, v.15, no. 4, 440.
9. Hu Z.K., Luo J. Progress in determining the gravitational constant with four acttracting masses. *Journal Korean Phys. Soc.*, 2004, v. 45, 128–131.
10. Luo J., Hu Z.K., Fu X.H., Fan S.H., Tang M.X. Determination of the Newtonian constant with a non linear fitting method. *Phys. Rev. D*, 1998, v. 59, 042001.
11. Luther G.G., Towler W.R. Redetermination of the Newtonian G. *Phys. Rev. Lett.*, 1981, v. 48, 121–123.
12. Gundlach J.H., Smith G.L., Adelberger E.G. et al. Short-range test of the Equivalence Principle. *Phys. Rev. Lett.*, 1997, v. 78, 2523.
13. Su Y., Heckel B.R., Adelberger H.G., Gundlach J.H. et al. New tests of the universality of free fall. *Phys. Rev. D*, 1994, v. 50, 3614.
14. Sanders A.J., Deeds W.E. Proposed new determination of G and test of Newtonian gravitation. *Phys. Rev. D*, 1991, v. 46, 489.
15. More G.I., Stacey F.D., Tuck G.J. et al. *Phys. Rev. D*, 1991, v. 38, 1023.
16. Karagioz O.V., Izmailov V.P., Gillies V.P. Gravitational constant measurement using a four-position procedure. *Grav. and Cosmol.*, 1998, v. 4, 239.
17. Ritter R.C., Winkler L.I., Gillies G.T. Precision limits of the modern Cavendish device. *Meas. Sci. Technol.*, 1999, v. 10, 499–507.
18. Fitzgerald M.P., Armstrong T.R. The measurement of G using the MSL torsion balance. *Meas. Sci. Technol.*, 1999, v. 10, 439–444.
19. Gundlach J.H. A rotating torsion balance experiment to measure Newton's constant. *Meas. Sci. Technol.*, 1999, v. 10, 454–459.

LETTERS TO PROGRESS IN PHYSICS

Additional Explanations to "Upper Limit in Mendeleev's Periodic Table — Element No. 155". A Story How the Problem was Resolved

Albert Khazan

E-mail: albkhazan@gmail.com

This paper gives a survey for the methods how a possible upper limit in Mendeleev's Periodic Table can be found. It is show, only the method of hyperbolas leads to exact answering this question.

True number of elements in Mendeleev's Periodic Table is the most important problem to the scientists working on the theory of the Periodic Table. The theory is based in the core on our views about the properties of the electron shells and sub-shells in atoms, which obviously change with increasing nuclear change (the nuclei themselves remains unchanged in chemical reactions). The electron shells change due to redistribution of electrons among the interacting atoms. Therefore, it is important that we know the limits of stability of the electron shells in the heavy elements (high numbers in the Periodic Table); the stability limits are the subjects of calculation in the modern quantum theory which takes into account the wave properties of electron and nucleons. To do it, the scientists employ a bulky mathematical technics, which gives calculations for the 8th and 9th periods of the Table (a hundred new elements are joined there).

Already 40 years ago the physicists proved that no chemical elements with mass higher than 110 can exists. Now, 118th element is known (117th element, previous to it, is still non-discovered). In the last time, the scientists of Joint Institute for Nuclear Research, Dubna, talked that the Periodic Table ends with maybe 150th element, but they did not provided any theoretical reason to this claim. As is probable, the regular method of calculation, based on the quantum theory, gives no exact answer to the question about upper limit of the Table.

It should be noted that 10 new elements were synthesed during the last 25 years: 5 elements were synthesed in GSI*, 4 elements were synthesed in JINR† (2 of these — in common with LLNL‡), and 1 element was synthesed in LBNL§. All the laboratories produced new elements as a result of nuclear reactions in accelerators: new elements were found after analysis of the products of the reactions. This is a very simplified explanation, however the essence of the process is so: problem statement, then components for the nuclear reaction and the necessary physics condition, then — identification of the obtained products after the reaction. This method gives new elements, of course, but it gives no answer to the question about their total number in the Periodic Table.

In contrast to this approach, when I tackled this problem, I used neither calculation for the limits of stability of the electron shells in atoms, nor experiments on synthesis of new elements, but absolutely another theoretical approach which allowed me for formulation of a new law in the Periodic Table and, as a result, the upper limit in it. Here I explain how. (I published all the results, in detail, in a series of papers [1–6], then collected in a book [7]).

First. Contents Y of every single element (say, of a K-th element in the Table) in a chemical compound of a molecular mass X can be given by the equation of an equilateral hyperbola $Y = K/X$, according to which Y (in parts of unit) decreases with increasing X.

Second. After as I created the hyperbolic curves for not only all known elements, but also for the hypothetical elements, expected by the aforementioned experimentalists, I looked how the hyperbolas change with molecular mass. To do it, I determined the tops of the hyperbolas, then paved a line connecting the tops.

Third. The line comes from the origin of the coordinates, then crosses the line $Y = 1$ in a point, where the top of one of the hyperbolas meets atomic mass of element, $K = X$, that is the boundary condition in the calculation. The calculated coordinates of the special point are $X = 411.663243$ and $Y = 1$. Because no elements can be above the point (contents Y of an element in a chemical compound is taken in parts of unit), the element with mass $X = 411.663243$ is the heaviest in the Periodic Table, so the Table ends with this element.

Fourth. In the next stage of this research, I was focused on the functions of atomic mass of element from its number along the Periodic Table. As a result, I have deduced the number of the last (heaviest) element in the Table. It is No. 155.

Thus, the last (heaviest) element in the Periodic Table was proved and its parameters were calculated without calculation of the stability of the electron shells in atoms on the basis of the quantum theory, but proceeding only from the general considerations of theoretical chemistry.

Of course, the methods of theoretical chemistry I applied in this reseach do not cancel the regular methods of the quan-

*Gesellschaft für Schwrionenforshung — Helmholtz Centre for Heavy Ion Research, Darmstadt, Germany.

†JINR — Joint Institute for Nuclear Research, Dubna, Russia.

‡LLNL — Lawrence Livermore National Laboratory, USA.

§LBNL — Lawrence Berkeley National Laboratory, USA.

tum theory; both methods are also not in competition to each other. Meanwhile calculations for the stability of the electronic shells of super-heavy elements can be resultative only in the case where the last element is known. Also, the experimentalists may get a new super-heavy element in practice, but, in the absence of theory, it is unnecessary that the element is the last in the Periodic Table. Only the aforementioned theory, created on the basis of the hyperbolic law in the Periodic Table, provides proper calculation for the upper limit in the Periodic Table, for characteristics of the last (heaviest) element, and hence sets a lighthouse for all futher experimental search for super-heavy elements.

P.S. This short paper was written due to the readers who, after reading my papers and just published book, asked me about the rôle of the calculations for the stability of the electron shells in my theory.

Submitted on April 03, 2009 / Accepted on May 20, 2009

References

1. Khazan A. Upper limit in the Periodic Table of Elements. *Progress in Physics*, 2007, v. 1, 38–41.
2. Khazan A. Effect from hyperbolic law in Periodic Table of Elements. *Progress in Physics*, 2007, v. 2, 83–86.
3. Khazan A. The rôle of the element Rhodium in the hyperbolic law of the Periodic Table of Elements. *Progress in Physics*, 2008, v. 3, 56–58.
4. Khazan A. Upper limit of the Periodic Table and synthesis of superheavy elements. *Progress in Physics*, 2007, v. 2, 104–109.
5. Khazan A. Introducing the Table of the Elements of Anti-Substance, and theoretical grounds to it. *Progress in Physics*, 2009, v. 2, 19–23.
6. Khazan A. On the upper limit (heaviest element) in the Periodic Table of Elements, and the Periodic Table of Anti-Elements. 2009, v. 2, L12–L13.
7. Khazan A. Upper limit in Mendeleev's Periodic Table — element No. 155. Svenska fysikarkivet, Stockholm, 2009.

LETTERS TO PROGRESS IN PHYSICS

Nikolai A. Kozyrev (1908–1983) — Discoverer of Lunar Volcanism

(On the 100th Anniversary of His Birth)

Alexander N. Dadaev*

Central Astronomical Observatory of the Russian Academy of Sciences at Pulkovo, Russia

This paper draws biography of Nikolai A. Kozyrev (1908–1983), the Russian astronomer who was one of the founders of theoretical astrophysics in the 1930's, and also discovered Lunar volcanism in 1958.

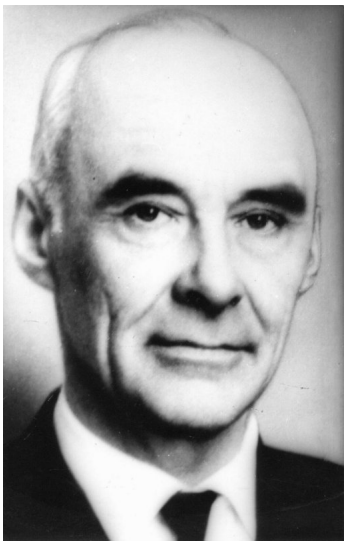

Nikolai A. Kozyrev, the 1970's

Of theories of the internal structure of stars and stellar energy sources scientists nowadays do not show as much interest as in the twenties and thirties of the past century. Interest at that time is explained by the situation then, when thinking about the nature of stellar energy was grounded in the study of the tremendous energy of the atomic nucleus, then new. Already, at the beginning of that century, hypotheses about the structure of the atom had been put forward. That encouraged physicists to study the deep secrets of the atom and its energy. By the end of the 1920's it became a widespread notion amongst astrophysicists that the generation of energy in stars is connected with sub-atomic processes in the chemical elements of which a star is composed. By the end of the 1930's, theoretical physicists had advanced some schemes for nuclear reactions which might explain energy generation in stars, to account for the energy expenditure of a star through radiation into space. Kozyrev's university study and the beginning of his scientific activity was undertaken in the 1920's. Very soon he became known as a serious physicist, and also as an outstanding planetologist. The young scientist had taken a keen interest in the fashionable problem of the origin of stellar energy, but he solved this problem more generally, encompassing not only stars, but also planets and their satellites. He proposed the hypothesis that the genesis of the internal energy of celestial bodies is the result of an interaction of *time with substance*. The discovery of volcanic activity in the Moon, made by Kozyrev when aged fifty, served to confirm his hypothesis. This discovery holds an important place in astronomical history, since a period of some 300 years of telescopic observations until then had not revealed volcanic activity on the Moon; the Moon being regarded as a "dead" heavenly body. Nikolai Kozyrev is rightly considered to be the discoverer of lunar volcanism.

Nikolai Aleksandrovich Kozyrev was born on August, 20 (2nd of September by the New Calendar) 1908, in St. Petersburg, into the family of an engineer, Alexander Adrianovich Kozyrev (1874–1931), a well-known expert in his field, at the Ministry of Agriculture, and who served in the Department of Land Management engaged in the hydrology of Kazakhstan. Originating from peasants of the Samara province, Kozyrev senior, who was born in Samara, was appointed to the rank of Valid State Councillor, in accordance with the 'tables of ranks' in Imperial Russia, which gave to him, and to his family, the rights of a hereditary nobleman. N. A. Kozyrev's mother, Julia Nikolaevna (1882–1961), came from the family of Samara merchants, Shikhobalov. A. A. Kozyrev had three more children: two daughters — Julia (1902–1982); Helena (1907–1985); and a son, Alexei (1916–1989).

Upon finishing high school in 1924, Nikolai Kozyrev went on up to the Pedagogical Institute, and thence, under the insistence of professors at the Institute, was admitted to the Physical and Mathematical Science faculty of Leningrad University, to become an astronomer. He finished university in 1928 and went on to postgraduate study at Pulkovo Observatory.

At the same time two other Leningrad University graduates went on to postgraduate study at Pulkovo — Victor A. Ambartsumian and Dmitri I. Eropkin. Academician Aristarch A. Belopolsky became the supervisor of studies of all three.

The "inseparable trinity" has left its imprint on the Pulkovo Observatory. Each of them was endowed with much talent,

*Submitted through Markian S. Chubey, Pulkovo Observatory. E-mail: mchubey@gao.spb.ru

but they differed in character. Life at Pulkovo proceeded separately from "this world", monotonously and conservatively, as in a monastery: astronomical observations, necessary relaxation, processing of observations, rest before observations, and the constant requirement of silence. The apartments of the astronomers were located in the main building of an observatory, in the east and west wings, between which there were working offices and premises for observations — meridian halls and towers with rotating domes.

The low salary was a principal cause of latent discontent. The protests of the three astrophysicists supported many employees of the Observatory, including the oldest — Aristarch A. Belopolsky.

After postgraduate study, in 1931, Ambartsumian and Kozyrev were appointed to the staff of the observatory as scientific experts category 1. The direction taken by the work of their supervisor is reflected in the character of the publications of the young scientists. But an independent approach was also outlined in these works in the solving of solar physics problems. Their work in the field of theoretical astrophysics was already recognized thanks to the writings of Milne, Eddington, and Zanstr, which they quickly developed on the basis of the successes of quantum mechanics, of the theory of relativity and of atomic and nucleus physics, was quite original. Ambartsumian and Kozyrev closely connected to a group of young theoretical physicists working at universities and physico-technical institutes: George A. Gamov (1904–1968), Lev D. Landau (1908–1968), Dmitri D. Ivanenko (1904–1994), Matwey P. Bronstein (1906–1938). Gamov, Landau and Ivanenko, along with their works on physics, were publishing articles on astrophysics. Ivanenko and Bronstein frequently visited Pulkovo for 'free discussions' of the essential problems of theoretical physics and astrophysics [1]. It was an original "school of talent".

Ambartsumian taught university courses in theoretical physics (for astrophysicists) and theoretical astrophysics. Kozyrev read lectures on the theory of relativity at the Pedagogical Institute. Both participated in working out the problems of a developing new science — theoretical astrophysics.

Courses of study in physics and astrophysics are essentially various. The study of the physics of elementary processes of interaction of matter and radiation is in astrophysics a study of the total result of processes in huge systems that stellar atmospheres as a whole represent. In such difficult systems the process of elementary interaction is transformed into the process of transfer of radiation (energy) from a star's internal layers to external ones, whence radiation leaves for space. The study methods are also various. In physics, a directed action of radiation on matter is possible, and the researcher operates by this action, and the studied process can be modified by the intervention of the researcher. In astrophysics intervention is impossible: the researcher can only observe the radiations emitted into space, and by the properties of observable radiation conjecture as to the internal processes of a star, applying the physical laws established in terrestrial conditions. Meaningful conclusions can be made by means of correctly applied theory. Study within these constraints is of what theoretical astrophysics consists.

The problem cannot be solved uniformly for all objects because astrophysical objects are very diverse. The process of transfer of radiation (energy) in stars of different spectral classes does not occur by a uniform scheme. Still more diversity is represented by stars of different types: stationary, variable, and non-stationary. Besides the stars, astrophysical objects include the planetary nebula, diffuse nebula (light and dark), white dwarfs, pulsars, etc. Theoretical astrophysics is a science with many branches.

From Kozyrev's early publications it is necessary to single out articles about the results of spectro-photometrical studies of the solar faculae and spots on the basis of his own observations. One work dealt with the temperature of sun spots, another the interpretation of the depth of dark spots, and Kozyrev proved that sun spots extend to much deeper layers of the solar atmosphere than was generally believed at that time. Kozyrev's arguments have since found verification.

In 1934 Kozyrev published in *Monthly Notices of the Royal Astronomical Society* a solid theoretical research paper concerning the radiant balance of the extended photospheres of stars [2]. Concerning the problem of transfer of radiant energy, atmospheric layers are usually considered as plane-parallel, for stars with extended atmospheres (photospheres), but such a simplification is inadmissible. Considering the sphericity of the photospheric layers, Kozyrev made the assumption that the density in these layers changes in inverse proportion to the square of the distance from the star's centre and corresponds to the continuous emanation of matter from the star's surface. He used available data on observations of stars of the Wolf-Rayet type and of P Cygni and theoretically explained observable anomalies, namely appearance in their spectral lines of high ionization potentials, which demands the presence of considerably more heat than actually observed on the surface of these stars. In the issue of the above-mentioned Journal, S. Chandrasekar's paper, containing the more common view of the same problem, was published, although received by the Journal half a year after Kozyrev's paper. The theory is called the "theory of Kozyrev-Chandrasekar".

A considerable part of the work during the Pulkovo period was carried out by Kozyrev and Ambartsumian. Together with Eropkin, Kozyrev published two articles containing the results of their expedition research work on polar lights by a spectral method; luminescence of the night sky and zodiac light. Research on the terrestrial atmosphere in those years was rather physical. However, works of a geophysical character stood outside the profile of the astronomical observatory; besides, these works demanded considerable expenditure that led to conflict with observatory management.

In May 1934, Belopolsky died — to the end a defender

Nikolai Kozyrev, 1934

of his pupils. Ambartsumian, in the autumn of 1935, had moved to Leningrad university. The "trinity" has broken up. The Director of Pulkovo Observatory, Boris P. Gerasimovich (1889–1937) decided to remove the two remaining "infractors of calmness". An infringement of financial management during the Tadjik expedition was fashioned into a reason for the dismissal of Dmitri Eropkin and Nikolai Kozyrev. In those years appointment and dismissal of scientific personnel of the observatory were made not by the director, but only with the permission of the scientific secretary of the Academy of Sciences, who upheld the action of the Director. A subsequent investigation for the reinstatement of Eropkin and Kozyrev conducted by the National Court and the commission of the Presidium of the Academy of Sciences occupied more than half a year.

In the meantime, in October, 1936, in Leningrad, arrests of scientists, teachers of high schools, and scientific officers had begun. One of the first to be arrested was the corresponding member of the USSR Academy of Sciences, Boris V. Numerov (1891–1941), the director of the Astronomical Institute, an outstanding scientist in the field of astronomy and geodesy. He was accused of being the organizer of a terrorist anti-Soviet group amongst intellectuals [3].

The wave of arrests reached Pulkovo. Kozyrev was arrested on the solemn evening of the 19th anniversary of October revolution, in the House of Architects (the former Jusupovsky palace). The choice of the date and the place of the repressive operation was obviously made for the purpose of intimidation of the inhabitants. On the night of December 5th (Day of the Stalin Constitution, the "most democratic in the world") Eropkin was arrested in Leningrad. These "red dates" are not forgotten in Pulkovo: all victims of the repression are not forgotten.

The Director of the observatory, Boris P. Gerasimovich was arrested at night, between the 29th and 30th of June 1937, in a train between Moscow and Leningrad. On November 30, 1937, Gerasimovich was sentenced to death and was shot that same day.

The Pulkovo astronomers, arrested between November and the following February, were tried in Leningrad on May 25, 1937. Seven of them, Innokentiy A. Balanovsky, Nikolai I. Dneprovsky, Nikolai V. Komendantov, Peter I. Jashnov, Maximillian M. Musselius, Nikolai A. Kozyrev, Dmitri I. Eropkin; were each sentenced to 10 years imprisonment. The hearings lasted only minutes, without a presentation of charges, without legal representation, with confessions of "guilt" extracted by torture — no hearings, only sentence.

According to the legal codes at the time, the 10 year imprisonment term was the maximum, beyond which was only execution. However, almost all the condemned, on political grounds, were died before the expiry of the sentences. Of the condemned Pulkoveans, only Kozyrev survived.

Boris V. Numerov was sentenced 10 years imprisonment and whilst serving time in the Oryol prison, was shot, on September, 15th, 1941, along with other prisoners, under the threat of occupation of Oryol by the advancing fascist army.

In Pulkovo arrests of the wives of the "enemies of the people", and other members of their families, had begun. It is difficult to list all arrested persons. They were condemned and sentenced to 5 year terms of imprisonment.

Until May 1939, Kozyrev was in the Dmitrovsk prison and in the Oryol prison in the Kursk area, then afterwards he was conveyed through Krasnoyarsk into the Norilsk camps. Until January 1940, he laboured on public works, and then, for health reasons, he was sent to the Dudinsky Permafrost Station, as a geodesist. In the spring of 1940 he made topographical readings of Dudinka and its vicinities, for what Kozyrev was permitted free activity, for to escape there was no possibility: the surrounds were only tundra.

In the autumn of 1940 he worked as an engineer-geodesist, and from December 1940 was appointed to Chief of Permafrost Station. On October 25, 1941, "for engaging in hostile counter-revolutionary propaganda amongst the prisoners" he was again arrested, and on January 10, 1942, he was sentenced to an additional 10 years imprisonment. On the same charges, Dmitri I. Eropkin had been condemned repeatedly, and was shot in Gryazovetsky prison of the Vologda area, on January 20, 1938 [3].

The Supreme Court of the Soviet Russia reconsidered the sentence on Kozyrev as liberal one and replaced it with death execution. But the Chief of the Noril-Lag (a part of the well-known GULAG) tore up the order of execution before the eyes of Kozyrev, referring to the absence in the regional centre, Dudinka, of any "executive teams". Probably, in all reality, this was a theatrical performance. Simply, Kozyrev was

needed, as an expert, for the building of a copper-nickel integrated facility, as another nickel mine near the Finnish border was then located within a zone of military action.

After the court hearing Kozyrev was transported to Norilsk and directed to work on a metallurgical combine as a thermo-control engineer. By spring of 1943, owing to his state of poor health, Kozyrev was transferred to work at the Norilsk Combine Geological Headquarters as an engineer-geophysicist. Until March 1945, he worked as the construction superintendent for the Hantaysky lake expedition and as the Chief of the Northern Magneto-Research Group for the Nizhne-Tungus geology and prospecting expedition.

Some episodes of the prison and camp life of Nikolai A. Kozyrev testify to his intense contemplations during this period. Certainly, some stories, originating from Kozyrev himself, in being re-told, have sometimes acquired a fantastic character.

The episode concerning Pulkovo's *Course of Astrophysics and Stellar Astronomy* [4] whilst being held in Dmitrovsky Central (the primary prison in Dmitrov city), is an example. Being in a cell for two people, Kozyrev thought much of scientific problems. His mind went back to the problem of the source of stellar energy. His cell-mate had been sent to solitary confinement for five days and when he returned he was very ill, and died. Kozyrev was then alone in his cell. He was troubled by the death of this cell-mate and his thoughts ceased to follow a desirable direction. A deadlock was created: there were no scientific data which could drive his thoughts. He knew that the necessary data were contained in the second volume of the *Course of Astrophysics*. Suddenly, in a day of deep meditation, through the observation port of his cell was pushed the book most necessary — from the *Course of Astrophysics*.

By different variants in the re-telling of the tale, the prisoner used the book for between one and three days, thumbing through it and memorising the necessary data. Then the book was noticed by a prison guard, and as it was deemed that the use of such specialist material literature was not allowed, the book was taken from him. Kozyrev thought that this book ,which so casually appeared, was from the prison library. That is almost impossible: someone delivered to the prison the special reference book, published in such a small circulation? Was there really a book in the hands of the prisoner or it was a figment of his tormented and inflamed imagination? Most likely mental exertion drew from his memory the necessary data. Something similar happens, sometimes, to theoreticians, when some most complicated problems steadfastly occupying the brain, are solved in unusual conditions, for example, as in a dream.

Another episode: consumed by his thoughts, Kozyrev began to pace his cell, from corner to corner. This was forbidden: in the afternoon the prisoner should sit on a stool, and at night lie on his bunk. For infringement of the rules Kozyrev was sent to solitary confinement for five days, in February 1938. The temperature in the confinement cell where daylight did not penetrate, was about zero degrees. There the prisoners wore only underwear, barefooted. For a meal they got only a piece of black bread and a mug of hot water per a day. With the mug it was possible to warm one's freezing hands but not the body. Kozyrev began to intensely pray to God from which he derived some internal heat, owing to which he survived.

Upon his release from solitary, Kozyrev reflected, from where could the internal heat have come? Certainly he understood that in a live organism the heat is generated by various vital processes and consumption of food. And it happens that a person remains vigorous and efficient, rather long term, without consumption of food, and "lives by the Holy Spirit"? What is Holy Spirit? If He pours in energy then energy can appear through Him, in a lifeless body. What factor of universal character can generate the energy? So Kozyrev's "time theory", advanced by him twenty years later, thus arose.

Both episodes contain mystical elements, but the mysticism accompanied Kozyrev both in imprisonment and in freedom, both in his life and in his scientific activity.

In June 1945 Kozyrev was moved from Norilsk to Moscow for "choice jugée revision". According to the official enquiry [3], choice judgée revision was made under the petition of academician Grigory A. Shayn, requesting liberation of the exiled Kozyrev, for his participation in restoration of astronomical observatories that were destroyed during the war; in Pulkovo, Simeis, Nikolaev, and Kharkov. However the petition of the academician was too weak an argument. Previously, in 1939, the academicians Sergey I. Vavilov and Grigoriy A. Shayn petitioned for revision of the choice jugées of the Pulkovo astronomers, not knowing that some of them were then already dead. The petition by the outstanding academicians was of no consequence.

The petition which was sent to the Minister of Internal Affairs, in August 1944, and registered with the judicial-investigatory bodies as the "letter of academician Shayn", but had actually been signed by three persons [5], namely, the full members of the Academy of Sciences of the USSR, Sergei I. Vavilov and Gregory A. Shayn, and by the correspondent-member of the Academy, Alexander A. Mihailov, the Chairman of the Astronomical Council of the Academy. This petition concerned only Kozyrev. The fate other condemned astronomers was known only to elements of the People's Commissariat of Internal Affairs. The petition for liberation of Kozyrev was obviously initiated those elements of the People's Commissariat of Internal Affairs. How to explain this?

When the Soviet intelligence agencies had received information about research by the USA on the creation of nuclear weapons, the State Committee of defence of the USSR made, in 1943, a secret decision on the beginning of such works in the USSR. As the head of the programme had been appointed Laurentiy P. Beriya, the National Commissar of Internal Affairs [6, p. 57]. Many physicists were in custody. Many were already dead. Those who still lived in prison camps it was

necessary to rehabilitate. Kozyrev numbered amongst them.

The "choice jugée revision" is an unusual process, almost inconceivable then. It was a question of overturning the decision of Military Board of the Supreme Court of the USSR, the sentences of which then were not reconsidered, but categorically carried out. The decision was made in the special prison of the People's Commissariat of Internal Affairs on Lubyanka (called then the "Felix Dzerzhinsky Square", in the centre of Moscow) where Kozyrev was held for one and a half years. At last, by decision of a Special Meeting of the KGB of the USSR on December 14, 1946, Kozyrev was liberated "conditionally ahead of schedule". This meant that over Kozyrev's head still hung the sentence of the Taymyrsky court, and with the slightest pretext he could appear again behind bars. Only on February 21, 1958, was the sentence of the Taymyrsky court overruled and Kozyrev completely rehabilitated.

After liberation Kozyrev has spent some days in Moscow that were connected mainly with an employment problem. Gregory A. Shayn, appointed in December 1944 as the Director of the Crimean Astrophysical Observatory (CrAO) then under construction, invited him to work in the Crimea. Kozyrev agreed. He devoted himself once again to scientific work.

But first he went to Leningrad for a meeting with kinsfolk and old friends, for restoration of scientific communications and, primarily, to complete work on his doctoral thesis, the defence of which took at Leningrad University on March 10th, 1947, i.e. only two and a half of months after his liberation. Many colleagues were surprised; when did he have time to write the dissertation? But he had more or less composed the dissertation during his ten years in prison. The strange episodes which occurred in Dmitrovsky Central had been connected with its theme. Kozyrev had some free time in Taymyr, when he was free to wander there for the one and a half years he worked as the Chief of the Topographical Group, and as the senior manager of the Permafrost Station. Besides, during his stay in Lubyanka, the possibility of being engaged within a year on the dissertation with use of the specialist literature been presented itself to him. Then he could write down all that at he had collected in his head. After liberation, possibly, it was only necessary to "brush" the draft papers.

Defence of the dissertation by Kozyrev occurred at the Department of Mathematics and Mechanics of Leningrad University: the dissertation theme, *Sources of Stellar Energy and the Theory of the Internal Constitution of Stars*. Attending as official examiners were the corresponding member of the Academy of Sciences of the USSR, Victor A. Ambartsumyan, professor Cyrill F. Ogorodnikov, and Alexander I. Lebedinsky. As a person working, after demobilization, at the Astronomical Observatory of Leningrad University, I was permitted to be present at this defence. Discussion was rather animated, because, beyond the modest name of his dissertation, Kozyrev put forward a new idea as to the source of the stellar energy, subverting the already widespread conviction that thermonuclear reactions are the source of energy in the entrails of stars. The discussion ended with a voting in favour of the Author's dissertation. On this basis the Academic Council of the University conferred upon Kozyrev the award of Doctor of Physical and Mathematical Sciences (the Soviet ScD), subsequently ratified by the Supreme Certifying Commission.

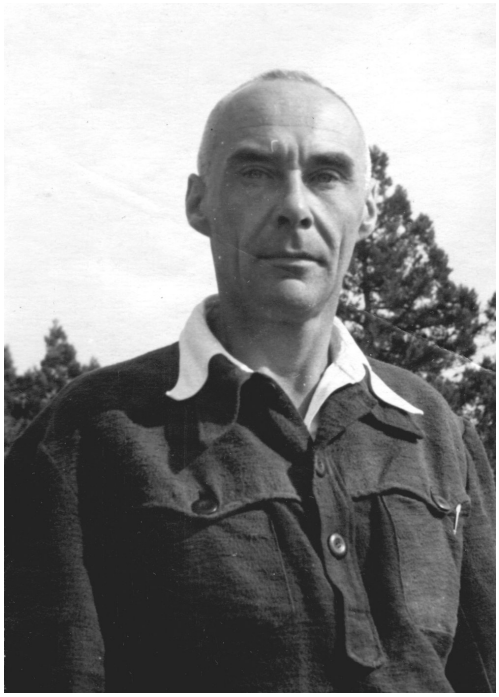

Kozyrev in Crimean Observatory, after the liberation

Kozyrev's dissertation was published in two parts, in the *Proceedings of the CrAO* [8], in 1948 (a part I), and in 1951 (a part II).

With scheme for nuclear reactions in the Sun and stars proposed by the German theoretical physicist Hans Bethe, in 1939, the question of stellar energy sources seemed to have been solved, and so nobody, except Kozyrev, reconsidered the problem.

Arguing by that the age of the Earth means that the Sun has already existed for some billions of years, and intensity of its radiation has not changed for some millions of years, which geological and geophysical research testifies, Kozyrev concluded the Sun is in a rather steady state, both in its mechanical and its thermodynamic aspects. This necessitates a study of the sources of its energy by which it is able to operate continuously for millions, even billions, of years.

Certainly the character of the source depends on the internal structure of the Sun (a star). Theories of the internal structure of stars are constructed on the basis of many assumptions about a star's chemical composition (percentage of hydrogen and other chemical elements), about the ionization conditions, about the quantity of developed energy per unit mass per second, about the nature of absorption of radiation,

etc. The reliability of all these assumptions is determined by comparison of the theoretical conclusions with the data of observations.

The key parameters of a star are its luminosity L, its mass M and its radius R. Kozyrev deduced theoretical dependencies of type M-L and L-R, and compared them with observable statistical dependencies "mass-luminosity" and "luminosity — spectral class" (Herzsprung-Russell diagram). The spectral class is characterized by the star's temperature, and the temperature is connected through luminosity with the star's radius (Stefan-Boltzman's law), i.e. the observable dependence of type L-R obtains. Comparison of the theoretically derived dependencies with observations statistically leads to the conclusion that the temperature at the centres of stars of the same type as the Sun does not exceed 6 million degrees, whereas the temperature necessary for reactions of nuclear synthesis is over 20 million degrees.

Moreover, by comparison of theoretical indicators of energy generation in a star and the emitted energy, these indicators are cancelled out by a star. Hence, in the thermal balance of a star, the defining factor is the energy emitted. But the estimated energy generation of thermonuclear reactions (if they operate in a star) far exceeds the observed emitted energy. Thus, reactions of nuclear synthesis are impossible because of insufficient heat in the stellar core (a conclusion drawn in the first part of Kozyrev's dissertation), and are not necessary (a conclusion of the second part).

Kozyrev drew the following conclusions: 1) a star is not a reactor, not a nuclear furnace; 2) stars are machines that develop energy, the emitted radiation being only a regulator for these machines; 3) the source of stellar energy is not Einstein's mass-energy interconversion, but of some other combination of the physical quantities. He also wrote that the "third part of this research will be devoted to other relations". Kozyrev held that stellar energy must be of a non-nuclear source, and must be able to operate for billions years without spending the mass of a star. The energy generation should not depend on temperature, i.e. the source should work both in stars, and in planets and their satellites, generating the internal energy of these cooler bodies as well. Accordingly, Kozyrev carried out observations, in order to obtain physical substantiation of his fundamental assumptions.

Kozyrev paid special attention to observations of the Moon and planets. About that time the 50-inch reflector, which Kozyrev grew so fond of, had been installed at the Crimean Observatory.

In 1954 Kozyrev published the paper *On Luminescence of the Night Sky of Venus* on the basis of spectral observations made at the Crimean Observatory in 1953. The observations for the purpose of recording the spectrogram of the night sky of a planet possessing a substantial atmosphere, required great skill: it was necessary to establish and keep on a slit of the spectrograph the poorly lighted strip to be completely fenced off from the reflected light of the day side of the planet, the brightness of which is 10,000 times the luminescence of the night sky. Dispersion of light from the horns of the bright crescent extend far into the night part, and can serve as the source of various errors, as the exposure must be long, to embody on a photographic plate the spectrum of the weak luminescence of the atmosphere of the planet. His observations went well; their processing and interpretation led to the detection of nitrogen in the atmosphere of Venus in the form of molecules N_2 and N_2^+.

The English astrophysicist Bryan Warner, in 1960, on the basis of a statistical analysis of Kozyrev's observations, proved identification of nitrogen and, additionally, that part of the spectral lines belong to neutral and ionized oxygen [9]. The presence of nitrogen and oxygen on Venus was definitely verified by direct measurements of its atmosphere by the interplanetary space missions "Venus-5", "Venus-6" (1969) and in the subsequent missions.

The observations of Mars in opposition, 1954 and 1956, inclined Kozyrev to the new conclusions concerning the Martian atmosphere and polar caps. Studying the spectral details of the planet's surface, he has come to the conclusion that observable distinction of the colour of continents and the seas on Mars can be explained by optical properties of the Martian atmosphere. This contention drew sharp objections from Gabriel A. Tihov, the well-known researcher of Mars. The scientific dispute remained unresolved. Kozyrev reasoned, that the polar cap observed in 1956 was an atmospheric formation, similar to "hoarfrost in air". Independently, Nikolai P. Barabashev and Ivan K. Koval (1956), and later also Alexander I. Lebedinsky and Galina I. Salova (1960), came to similar conclusions.

Kozyrev systematically surveyed with spectrograph various sites on the Moon's surface. The purpose of such inspections was to look for evidence of endogenetic (internal) activity which, as Kozyrev believed, should necessarily exist in the Moon. With the help of spectrographs it is possible to locate on the surface the sites of gas ejection, and he was sure that, sooner or later, he would see such phenomena.

In the beginning of the 19th century, William Hershel had reported observation of volcanoes on the Moon. François Arago later showed that visual observations do not permit detection of eruption of a lunar volcano as in the absence of atmosphere the eruption is not accompanied by ignition and luminescence. Kozyrev however approached the question with a belief in the existence of a "cold source" of energy in stars and planets.

His dissertation is devoted to the energy sources of stars. Concerning accumulation and action of the internal energy of planets, Kozyrev had expounded in the years 1950–1951 in the articles *Possible Asymmetry in Llanetary Figures* [10] and *On the Internal Structure of the Major Planets* [11].

The Moon does not differ from the planets in that the non-nuclear energy source should exist in the Moon as well. Its continuous operation should lead to accumulation of energy

which will inevitably erupt onto the surface, together with volcanic products, including gas. The gas can be observed with the help of the spectrograph. Before Kozyrev nobody used such methods of observation of the Moon. Difficulties in the observations are due to the necessity of catching the moment of emission because the ejected gas will quickly dissipate. The gases ejected by terrestrial volcanoes consist of molecules and molecular composites. The temperature of eruptions on the Moon cannot be higher. At successful registration the spectrogram should embody the linear spectrum of the Sun, reflected by the Moon, and molecular bands superimposed upon this spectrum, in accordance with the structure of the emitted gas.

Kozyrev found that luminescent properties are inherent to the white substance of the beam systems on the Moon. Supporters of the theory of a volcanic origin of craters on the Moon consider that the beam systems are recent formations of volcanic origins. One night in 1955 the crater Aristarkh differed in luminescence, exceeding the usual by approximately four times. It was possible to explain the strengthening of the luminescence by the action of a corpuscular stream as the light stream from the Sun depends only on inclination of the solar beams to the Moon's surface. As a stream of the charged corpuscles is deviated by a magnetic field, the luminescence should be observed on a dark part of the lunar disc that was not marked. Hence, "the Moon does not have a magnetic field" [12].

Kozyrev had drawn this conclusion three to four years prior to spacecraft missions to the Moon (1959). The discovery of an absence of a magnetic field for the Moon is considered an important achievement of astronautics. But in those years the prediction made by Kozyrev, went unnoticed, as did the results of his research on the atmosphere of Venus.

Also went unacknowledged was his doctoral dissertation which concluded an absence of thermonuclear synthesis in stars. It would seem that his work should have drawn the attention of physicists and astrophysicists in connection with Raymond Davis' experiments on the detection of the solar neutrino.

In 1946 Bruno Pontekorvo described a technique of neutrino detection through physical and chemical reaction of transformation of chlorine in argon. Any thermonuclear reactions are accompanied by emission of neutrino or antineutrino. R. Davis organized, in the 1950's, a series of experiments on the basis of Pontekorvo's method. The observations revealed little evidence for the expected reaction, in accordance with an absence of thermonuclear reactions in the Sun's entrails as had been predicted by Kozyrev.

Throughout the years 1967–1985, Davis continued experiments to measure neutrino streams from the Sun, with an advanced technique. Results were no better: the quantity of detected neutrinos did not surpass one third of the theoretically calculated stream. In the 1990's the experiments were performed in other research centres by other means, reaffirming Davis' results. The Nobel Prize [13] was awarded to Raymond Davis in 2002.

From August 15th, 1957, Kozyrev began to work at Pulkovo Observatory in the same post of senior scientific researcher. He had received a small apartment in Leningrad, on the Moscow Prospect, on a straight line connecting the city with Pulkovo. Twice a year he went to the Crimea to carry out observations, in the spring and autumn, with the 50-inch reflector.

In August, 1958 Kozyrev published his book *Causal or Asymmetrical Mechanics in the Linear Approximation* [14], where he generalized the results of laboratory experiments and astrophysical observations to a conclusion on the non-nuclear energy source of stars. It was a continuation of his thesis for his doctor's degree. Thus, this third part is in style and character very unlike the first two. Discussion of this book began before the death of Kozyrev, and continues.

The non-nuclear energy source of stars and planets is attributed in Part III to time. Kozyrev however did not explain what time is, but asserted that time proceeds by physical properties, and he tried to reveal them. He believed that in rotating celestial bodies, time makes energy, which he tried to prove experimentally by weighing of gyroscopes at infringement of the usual relationships between cause and effect.

To consolidate his ideas about transformation of time into energy Kozyrev tried to create a corresponding theory. Postulating an infinitesimal spatial interval between cause and effect, and the same time interval between them, he defines the relation of these intervals as the velocity of transition of a reason into a consequence. After a series of postulates, Kozyrev defined the course of time as the speed of transition of a reason in a consequence, and designates it c_2, unlike the velocity of light c_1. He considered that c_2 is a universal constant, as well as c_1; the value of c_2 he finds experimentally and theoretically, as $c_2 = 1/137 c_1$, where 1/137 is dimensionless value equal to Sommerfeld's fine structure constant. Besides that

$$c_2 = a\,\frac{e^2}{h} = a \cdot 350 \text{ km/sec},$$

where e is the elementary charge, h is Planck's constant, a a dimensionless multiplier which is subject to definition.

To describe the character of interaction of the causes and effects by means of mathematical formulae, Kozyrev gave to these phenomena the sense of mechanical forces: reason is active force, and effect is passive force. Thereby Kozyrev *materialized* these concepts just as the definition of force includes mass. Though cause and effect phenomena had already been *materialized* by postulation of the spatial and time intervals between them, Kozyrev used representations about the compactness of bodies and the impossibility of the simultaneous location of two bodies at one point of space. In the same manner Kozyrev also materialized time, or the *course of time*, owing to which there is an intermediate force $\frac{mdv}{dt}$ between the active and passive forces. Values of m and v are not

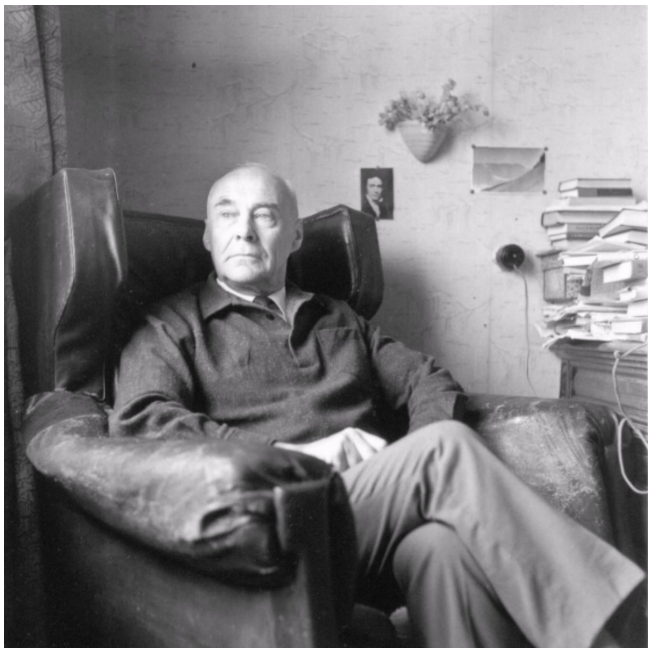

Kozyrev at home, in Leningrad

explained. Nor does Kozyrev explain how the course of time causes the occurrence of the additional force. It was simply a postulate, which he had not formulated. The *materialization* of causes and effects is also just postulated.

The long chain of postulates included in the long theoretical reasoning is reduced to a statement about the subliminal *flow of time* which exists from extreme antiquity. Directly about the flow Kozyrev does not write; but if the *course of time* proceeds by mechanical force, then the force, over some distance, does work. So the river flow actuates a water-mill.

That is why, according to Kozyrev's theory, energy is created at the expense of time only in rotating bodies. To prove this thesis experimentally, Kozyrev engaged in experiments with gyroscopes, to which a separate chapter in his book is devoted. Later, Kozyrev reconstructed the theory on the basis of Einstein's theory.

The physical essence of the *course of time* nobody has been able to elucidate. However there are no bases to deny that time action promotes energy generation in stars and planets, as Kozyrev's theory specifies. Kozyrev's discovery of lunar volcanism, as a result of his persevering research on the basis of his own theory, also specifies that.

On November 3, 1958, at the Crimean observatory, Kozyrev was observing a region on the surface of the Moon for the purpose of its detecting endogenetic activity. This time Kozyrev concentrated his attention on the crater Alphons, in the central part of the lunar disc. According to American astronomer Dinsmor Alter, a haze observed in the crater Alphons prevented clarification of the details of crater [15].

Kozyrev made a pair of spectrograms. On one of them, in the background of the solar spectrum, with its specific dark lines, the light bands of molecular carbon C_2 and carbon dioxide gas CO_2 were visible. On the other spectrogram taken half an hour after the first, the bands were absent. The slit of the spectrograph crossed the crater through the central hill of the crater. Hence, the gas eruption occurred from the central hill of the crater Alphons. So the discovery was made.

Soon Kozyrev published a short letter in *The Astronomical Circular* (No. 197, 1958) and an article containing the detailed description of a technique and circumstances of the observations, with a reproduction of the unique spectrogram, in *Sky and Telescope* (vol. 18, No. 4, 1959). In response to this article the well-known astronomer and planetologist, Gerard Kuiper, sent a letter to the Director of Pulkovo Observatory in which he declared that Kozyrev's spectrogram was a fake.

From December 6 to December 10, 1960, in Leningrad and Pulkovo, there was held an international symposium on lunar research by ground-based and rocket means (the Symposium No. 14 "Moon"), assembled in accordance with the calendar schedule of the International Astronomical Union (IAU). Well-known planetologists took part in the Symposium sessions and scientists from many countries were present: Gerard Kuiper, Garald Jurys, John Grey (USA), Zdenek Copal (Great Britain), Auduin Dolfus (France), Nicola Bonev (Bulgaria), Nikolai A. Kozyrev, Alexander V. Markov, Nadezhda N. Sytinskaja (USSR), etc.

Kozyrev's report *Spectroscopic Proofs for the Existence of Volcanic Processes on the Moon* [16], with presentation of the original spectrogram, was favourably received. Concerning the decoding of the emittance spectrum which had appeared when photographing the lunar crater Alphons, the skilled spectroscopists Alexander A. Kalinjak and Lydia A. Kamionko reported. Their identification of the spectrum proved the authenticity of the spectrogram. G. Kuiper was also convinced of the validity of the spectrogram, and withdrew his claims of forgery.

Kozyrev's detection of endogenetic activity in the "dead" Moon has not received either due consideration or support in relation to his search for a "cold source" of the energy of the Earth and in stars. Kozyrev's book *Causal Mechanics*, putting forward the flow of time as an energy source, has received inconsistent responses in the press. The first was by the Leningrad publicist and physicist Vladimir Lvov, who published in the newspaper *Evening Leningrad*, from December 20, 1958, the article *New Horizons of Science*. The article's title indicates a positive reception of Kozyrev's book. Subsequently, Lvov repeatedly published in newspapers and periodicals, strengthening the arguments in favour of statements that Kozyrev's theory, in essence, amounts to discovery of a third origin of thermodynamics, which counteracts thermal death of the Universe.

In the same spirit, in *The Literary Newspaper*, from November 3rd of 1959, an article by the well-known writer Marietta Shaginyan, entitled 'Time from the big letter', was published. Meanwhile, in Pulkovo Observatory, Kozyrev's lab-

oratory experiments, which he conducted to substantiate the conclusions of *Causal Mechanics* and his "time theory", had been organized. It was found that the experimental data did not exceed the "level of noise" and so did not reveal the effects predicted by the theory. On the basis of these results, the full members of Academy, Lev A. Artsimovich, Peter L. Kapitsa and Igor E. Tamm reported in the newspaper *Pravda*, on November 22, 1959, in the article *On the Turn in Pursuit of Scientific Sensations*, in which they condemned the article by M. Shaginjan as an "impetuously laudatory" account of the "revolution in science" made by professor Kozyrev.

The Branch of General Physics and Astronomy of the Academy of Sciences organized another more careful check of the experiments and Kozyrev's theory. The examination and analysis was made by scientists in Leningrad and Moscow, appointed by the Branch, with involvement of some Leningrad institutes. The results were discussed by the Academic Council of Pulkovo Observatory on July 1, 1961. Kozyrev's theory, detailed in the book *Causal Mechanics*, was deemed insolvent, and recommendations to improve equipment and to raise the accuracy of experimental data were given.

The book *Causal Mechanics* met with a negative reception, although it deserved some measure of positive evaluation. Kozyrev's theory as it is presented in the book is an investigation, which, before Kozyrev, nobody had undertaken. The investigation occurred in darkness, blindly, groping, producing an abundance of postulates and inconsistent reasoning. Before Kozyrev, time was mostly perceived subjectively as sensation of its flow, from birth to death. The great philosopher Immanuel Kant considered time to be the form of our perception of the external world. It is defined still now as the form of existence of matter. The modern theory of relativity has fixed this concept also, having defined time as one of the dimensions of four-dimensional space-time, by which it amplifies the idea that space and time are the *essence of the form* of the physical world. Kozyrev searched not for formal time, but for time that is actively operating.

Despite criticism of his efforts, Kozyrev continued his investigations in the same direction, following his intuition. He did not change his belief that time generates energy, only his methods of inquiry. After July 1961, Kozyrev almost entirely disengaged from experiments of mechanical character.

Kozyrev was carried along by a great interest in the laboratory study of irreversible processes which might visually reveal time action. For this purpose he designed a torsion balance, with an indicating arm rotating in a horizontal plane and reacting to external processes. Having isolated the device from thermal influences, Kozyrev interpreted any deviations of an arm from its "zero" position as the effect of time. Generally speaking, all processes in Nature are irreversible, by which the orientation of time manifests. This orientation should cause a deviation of the balance arm in one and the same direction, though deviations are possible to different angles, depending on the intensity of the process. In Kozyrev's experiments the deviation of the arm occurred in both directions (to the right and to the left), for which he devised explanations.

Intensive irreversible processes are especially evident. Cases Kozyrev used included the cooling of a heated wire or a piece of metal; the evaporation of spirit or aether; the dissolution of sugar in water; the withering of vegetation. Processes carried out near the device caused deviations the arm which could occur from electromagnetic influence, or waves in the range of ultrasonic or other. Such influences Kozyrev did not study, but any deviations of the arm he considered to be produced by time. He introduced the concept of "time density" in the space surrounding the device. He explained the balance arm deviations in both directions as the passing of a radiant time process ("time density" arises) or the absorption of time ("density" in the surrounding space goes down). What is "time density" Kozyrev did not explain. In some experiments the same irreversible process yielded different results on different days (deviations in opposite directions). Kozyrev explained this by the action of a remote powerful process deforming the laboratory experiment.

In studying irreversible processes by the methods described above, Kozyrev investigated the possibility of time shielding. Kozyrev conjectured that if time signals come from space, these signals can be captured by means of aluminium coated telescopic mirrors. This offered a method for "astronomical observations by means of the physical properties of time". In February, 1963, Victor Vasilevich Nassonov (1931–1986), a skilled engineer and expert in electronics with work experience at a radio engineering factory, visited Kozyrev's laboratory. Nassonov expressed his desire to work as a voluntary assistant to Kozyrev. As such he worked in laboratory until Kozyrev died. Nassonov immediately began improvement of equipment and introduced automatic data recordings which raised their accuracy. Nassonov usually went to laboratory in the evenings, after his work at the radio factory. Kozyrev too worked mainly in the evenings. When Kozyrev was away on observations in the Crimea, Nassonov took holiday leave from the radio factory and, at his own expense, accompanied Kozyrev. Nassonov became Kozyrev's irreplaceable assistant and close colleague.

Kozyrev worked not only in the laboratory or at home behind a desk. He did not alter his periodic trips to the Crimean Observatory where he used the 50-inch reflector. Planets and the Moon were primary objects of his observations. At any opportunity he undertook spectrographic surveys of the lunar surface for the purpose of detection of any changes characterizing endogenic activity. He noted some minor indications but did not again obtain such an expressive spectrogram as on November 3, 1958 — that was a unique find by good luck.

For observations of planets he used the configurations (opposition, elongation), most convenient for the tasks he had in mind. He took every opportunity; adverse weather the only

Nassonov and Kozyrev in front of Pulkovo Observatory

hindrance. In April 1963, Kozyrev conducted observations of Mercury when the planet was at elongation — the most remote position from the Sun, visible from the Earth. He aimed to determine whether or not hydrogen is present in the Mercurian atmosphere. Such an atmosphere could be formed by Mercury's capture of particles which constitute the solar wind; basically protons and electrons. The captured particles, by recombination, form atomic and molecular hydrogen. The task was a very difficult one. First, observations of Mercury are possible only after sunset or before sunrise, when the luminescence of the terrestrial atmosphere is weak. However Mercury is then close to horizon, and noise from the terrestrial atmosphere considerably amplified. Second, Mercury shines by reflected sunlight, in the spectrum of which the hydrogen lines are embedded. It is possible to observe the hydrogen lines formed in the atmosphere of a planet by taking into account the shift of lines resulting from the planet's motion (toward the red when receding from the observer, toward the violet on approach). This shift can be seen as distortion of a contour of the solar line from the corresponding side. In April 1963, Mercury was to the west of the Sun and was visible after sunset. Kozyrev detected the presence of an atmosphere on Mercury. In autumn of the same year, Mercury was east of the Sun, and it was observed before sunrise; its atmosphere was not detected (details are given in [17]).

By means of observations of the passage of Mercury across the Sun's disc on November 10th of 1973, Kozyrev again detected signs of an atmosphere on Mercury [18]. However his conclusion contradicted the results of direct measurements by the spacecraft "Mariner-10", in 1974–1975. This spacecraft, first sent to Venus, and then to Mercury, during a flight around the Sun, took three sets of measurements as it approached Mercury. Concerning the atmosphere of the planet, the gathered data had demonstrated that it contains helium and oxygen in minute quantities, and almost no hydrogen.

Kozyrev's disagreement with the Mariner-10 data can be explained by the instability of hydrogen in the atmosphere because of the great temperature of Mercury's Sun-facing surface (above 500°C) and by Mercury's small force of gravitational attraction (escape velocity 4.2 km/s). Observations of Kozyrev fell to the periods of capture of a corpuscular solar stream; soon the grasped volume of a stream dissipated. Anyway, Kozyrev's observations and conclusions to write-off there are no bases.

Observing Saturn in 1966, Kozyrev detected the presence of water vapour in its rings [19]. Emergence of the water bands in the spectrum of the planet, which is so removed from the Sun, Kozyrev explained as the "photosublimation" process (the term coined by Kozyrev), i.e. by the direct transformation of crystals of ice into water vapour under the influence of solar radiation. G. Kuiper an opponent, argued that the Saturnean rings consist not of the usual ice, but of ammoniac, upon which Kuiper's objections were been based, but subsequently retracted by him.

Only in 1969 did Kozyrev's discovery of lunar volcanism receive official recognition, owing to findings made by the American Apollo-11 mission on the Moon in July, 1969. Astronauts Neil Armstrong, Buzz Aldrin and Michael Collins brought back to Earth a considerable quantity of lunar soils, which consisted mainly of volcanic rocks; proving intensive lunar volcanic activity in the past, possibly occurring even

now. Kozyrev's discovery has thus obtained an official recognition.

The International Academy of Astronautics (IAA, Paris, France) at its annual meeting in late September, 1969, in Cloudcroft (New Mexico, USA), made the resolution to award Kozyrev a nominal gold medal with interspersed seven diamonds in the form of constellation of the Ursa Major: "For remarkable telescopic and spectral observations of luminescent phenomena on the Moon, showing that the Moon remains a still active body, and stimulating development of the methods of luminescent researches world wide". Kozyrev was invited to Moscow for the award ceremony, where, in solemnity, the academician Leonid I. Sedov, vice-president of the International Astronautic Federation (a part of which is the IAA) gave Kozyrev the medal.

In December 1969, the State Committee for Affairs of Discovery and Inventions at the Ministerial Council of the USSR, awarded Kozyrev the diploma for discovery for "tectonic activity of the Moon".

Despite the conferring of medal and diploma, the question of a non-nuclear stellar energy source was not acknowledged. To Kozyrev the recognition of his discovery was also recognition of his work on the source of stellar energy. His theoretical research was amplified by his publication of a series of articles detailing his results, along with the formulation of his new considerations about the physical properties of time.

He no longer spoke about time generating energy in celestial bodies. In experiments with irreversible processes the properties of bodies to "emit" or to "absorb" time, forming around bodies a raised or lowered "time density" seemed to have been established, though Kozyrev did not explain how this is to be understand; but he nonetheless used the idea. It is especially strange that in works after 1958 he avoided the interpretation of time as material essence. In the seventies he gradually passed to the representation of immaterial time.

Upon the idea of time "emitting" and "absorption" is based Kozyrev's work *Features of the Physical Structure of the Double Stars Components* [20]. Therein Kozyrev did not investigate the interaction of double star components by light and other kinds of electromagnetic and corpuscular radiation; he postulated the presence of "time radiations" — the main star (primary star) radiates time in the direction of the companion-star (secondary star) owing to which the time density in the vicinity of both stars becomes identical, which finally leads to the alignment of the temperatures of both stars and their spectral classes in accordance with statistical studies of double stars.

By a similar method, Kozyrev investigated the mutual influence of tectonic processes on the Earth and on the Moon [21]. In consideration of tectonic processes Kozyrev could not neglect their gravitational interaction and put forward two kinds of interaction: 1) a trigger mechanism of tidal influences; 2) a direct causal relationship which is effected "through the material properties of time".

For comparison of lunar processes with terrestrial ones Kozyrev used the catalogue of recorded phenomena on the Moon, published by Barbara Middlherst et al. [22]. It is conditionally possible to suppose that all considerable phenomena on the Moon, observed from the Earth, are caused by tectonic processes. Records of the same phenomena on the Earth for the corresponding period (1964–1977) are easy to find. From comparison of the records Kozyrev drew the conclusion that there are both types of communication of the phenomena on the Earth and on the Moon, "independently of each other", though they are inseparable. To reinforcement his conclusions about the existence of relationships "through the material properties of time", Kozyrev referred to such relationships established for double stars, although alternative and quite obvious relations for double stars systems were not considered.

Some words are due about appearance and habits of Kozyrev. Since the age of fifty, when Kozyrev worked in Pulkovo, his appearance did not change much. He was of tall stature, well-built, gentlemanly, with a high forehead, short haircut and clean shaven, and proudly held his head high. He resembled a military man although he never served in the army, and went about his business in an army style, quickly, and at meetings with acquaintances kindly bowed whilst on the move or, if not so hastened, stopped for a handshake. He was always polite, with everybody. When operating a telescope and other laboratory devices Kozyrev displayed soft and dexterous movements. He smoked much, especially when not observing. In the laboratory he constantly held the hot tea pot and cookies: a stomach ulcer, acquired in prison (which ultimately caused his death), compelled him to take often of any food.

When at the Crimean Observatory, he almost daily took pedestrian walks in the mountains and woods surrounding the settlement of Nauchny (Scientific). He walked mostly alone, during which he reflected. Every summer, whilst on holiday, he took long journeys. He was fond of kayaking the central rivers of Russia for days on end. On weekends he travelled by motorbike or bicycle along the roads of the Leningrad region. On one occasion he travelled by steam-ship, along a tourist route, from Moscow, throughout the Moscow Sea, then downwards across the Volga to Astrakhan. He loved trips to Kiev and in to places of Russian antiquity. In the summer of 1965 Kozyrev took a cruise by steam-ship, around Europe, visiting several capitals and large cities. Separately he visited Bulgaria, Czechoslovakia, and Belgium.

In scientific work, which consumed his life, Kozyrev, even in the days of his imprisonment and exile, he, first of all, *trusted in himself*, in his own intuition, and considered, in general, that intuition is theomancy emanating from God. According to Kozyrev, postulates should represent the facts which are not the subject to discussion. Truth certainly sometime, will appear in such a form that it becomes clear to all who aspire to it.

Nikolai Aleksandrovich Kozyrev died on February 27, 1983. He is buried in the Pulkovo astronomer's memorial cemetery. Victor Vasilevich Nassonov continued some laboratory experiments with irreversible processes relating to biology. Nassonov, through overwork that could not be sustained, died on March 15th 1986, at the age of fifty-five.

Submitted on March 27, 2009 / Accepted on May 20, 2009

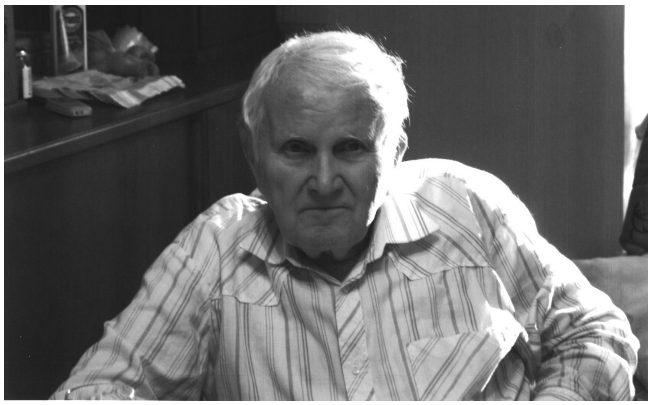

About the Author: Alexander Nikolaevich Dadaev was born on October 5, 1918 in Petrograd (now — St. Petersburg), Russia. In 1941 he completed his education, as astronomer-astrophysicists, at Leningrad University. He participated in the World War II, in 1941–1945, and was wounded in action. During 1948–1951 he continued PhD studies at Pulkovo Observatory, where he defended his PhD thesis *Nature of Hot Super-Giants* in 1951. He was the Scientific Council of Pulkovo Observatory in 1953–1965, and Chief of the Laboratory of Astrophysics in 1965–1975. Alexander N. Dadaev is a member of the International Astronomical Union (IAU) commencing in 1952. The Author would like to express his gratitude to Dr. Markian S. Chubey, the astronomer of Pulkovo Observatory who friendly assisted in the preparation of this paper.

References

1. Martynov D. Ja. The Pulkovo observatory 1926–1928. *Historical Astronomical Research*, issue 17, Nauka, Moscow, 1984 (*in Russian*).
2. Kozyrev N. A. Radiative equilibrium of the extended photosphere. *Monthly Notices of the Royal Astron. Society*, 1934, v. 94, 430–443.
3. Official data about the destiny of the Pulkovo astronomers. *Historical Astronomical Research*, issue 22, Nauka, Moscow, 1990, 482–490 (*in Russian*).
4. Course of astrophysics and stellar astronomy. Ed. by B. P. Gerasimovich. Part I. Methods of astrophysical and astrophotographic researches. ONTI, Leningrad, 1934; Part II. Physics of the Solar system and stellar astronomy. ONTI, Leningrad, 1936 (*in Russian*).
5. In protection of the condemned astronomers. *Historical Astronomical Research*, issue 22, Nauka, Moscow, 1990, 467–472 (*in Russian*).
6. Zalessky K. A. Stalin's empire. Biographic encyclopedia. "Veche" Publ., Moscow, 2000, 120 (*in Russian*).
7. Kozyrev N. A. Sources of stellar energy and he theory of the internal constitution of stars. *Proceedings of the Crimean Astron. Observatory*, 1948, v. 2, 3–13 (*in Russian*).
8. Kozyrev N. A. The theory of the internal structure of stars and sources of stellar energy. *Proceedings of the Crimean Astron. Observatory*, 1951, v. 6, 54–83 (*in Russian*).
9. Warner B. The emission spectrum of the night side of Venus. *Monthly Notices of the Royal Astron. Society*, 1960, v. 121, 279–289.
10. Kozyrev N. A. Possible asymmetry in figures of planets. *Priroda*, 1950, no. 8, 51–52 (*in Russian*).
11. Kozyrev N. A. On the internal structure of major planets. *Doklady Akademii Nauk USSR*, 1951, v. 79, no. 2, 217–220 (*in Russian*).
12. Kozyrev N. A. Luminescence of the lunar surface and intensity of corpuscular radiation of the Sun. *Proceedings of the Crimean Astron. Observatory*, 1956, v. 16, 148–158 (*in Russian*).
13. Davis R., Jr. Solar neutrinos, and the Solar neutrino problem. http://www.osti.gov/accomplishments/davis.html
14. Kozyrev N. A. Causal or asymmetrical mechanics in the linear approximation. Pulkovo Observatory, Pulkovo, 1958 (*in Russian*).
15. Alter D. A suspected partial obscuration of the floor of Alphonsus. *Publications of the Astronomical Society of the Pacific*, v. 69, no. 407, 158–161.
16. Kozyrev N. A. Spectroscopic proofs for the existence of volcanic processes in the Moon. *The Moon*, Proceedings from IAU Symposium No. 14 held in Leningrad, Pulkovo, December 1960, 263–271.
17. Kozyrev N. A. The atmosphere of Mercury. *Sky and Telescope*, 1964, v. 27, no. 6, 339–341.
18. Kozyrev N. A. The atmosphere of Mercury in observations of its passage cross the Sun's disc on November 10, 1973. *Astron. Circular*, 1974, no. 808, 5–6 (*in Russian*).
19. Kozyrev N. A. Water vapour in a ring of Saturn and its hothouse effect on a planet's surface. *Izvestiya Glavnoy Astronomicheskoy Observatorii*, 1968, no. 184, 99–107 (*in Russian*).
20. Kozyrev N. A. Relation masse-luminosité et diagramme H-R dans le cas des binaires: Physical peculiarities of the components of double stars. *On the Evolution of Double Stars*, Proceedings of a Colloquium organiced under the Auspices of the International Astronomical Union, in honor of Professor G. Van Biesbroeck. Edited by J. Dommanget. *Communications Obs. Royal de Belgique*, ser. B, no. 17, 197–202.
21. Kozyrev N. A. On the interaction between tectonic processes of the Earth and the Moon. *The Moon*, Proceedings from IAU Symposium No. 47 held at the University of Newcastle-Upon-Tyne England, 22–26 March, 1971. Edited by S. K. Runcorn and Harold Clayton Urey, Dordrecht, Reidel, 1971, 220–225.
22. Middlehurst B. M., Burley J. M., Moore P., Welther B. L. Chronological catalogue of reported lunar events. *NASA Techn. Rep.*, 1968, R-277, 55+IV pages.

The Journal on Advanced Studies in Theoretical and Experimental Physics, including Related Themes from Mathematics

PROGRESS IN PHYSICS

A quarterly issue scientific journal, registered with the Library of Congress (DC, USA). This journal is peer reviewed and included in the abstracting and indexing coverage of: Mathematical Reviews and MathSciNet (AMS, USA), DOAJ of Lund University (Sweden), Zentralblatt MATH (Germany), Scientific Commons of the University of St. Gallen (Switzerland), Open-J-Gate (India), Referativnyi Zhurnal VINITI (Russia), etc.

To order printed issues of this journal, contact the Editors. Electronic version of this journal can be downloaded free of charge:
http://www.ptep-online.com

Postal address

Department of Mathematics and Science,
University of New Mexico,
200 College Road,
Gallup, NM 87301, USA

This journal is powered by LaTeX

A variety of books can be downloaded free from the Digital Library of Science:
http://www.gallup.unm.edu/∼smarandache

ISSN: 1555-5534 (print)
ISSN: 1555-5615 (online)

Standard Address Number: 297-5092
Printed in the United States of America

OCTOBER 2009 **VOLUME 4**

CONTENTS

Information for Authors and Subscribers

Progress in Physics has been created for publications on advanced studies in theoretical and experimental physics, including related themes from mathematics and astronomy. All submitted papers should be professional, in good English, containing a brief review of a problem and obtained results.

All submissions should be designed in LaTeX format using *Progress in Physics* template. This template can be downloaded from *Progress in Physics* home page http://www.ptep-online.com. Abstract and the necessary information about author(s) should be included into the papers. To submit a paper, mail the file(s) to the Editor-in-Chief.

All submitted papers should be as brief as possible. We accept brief papers, no larger than 8 typeset journal pages. Short articles are preferable. Large papers can be considered in exceptional cases to the section *Special Reports* intended for such publications in the journal. Letters related to the publications in the journal or to the events among the science community can be applied to the section *Letters to Progress in Physics*.

All that has been accepted for the online issue of *Progress in Physics* is printed in the paper version of the journal. To order printed issues, contact the Editors.

This journal is non-commercial, academic edition. It is printed from private donations. (Look for the current author fee in the online version of the journal.)

Kirchhoff's Law of Thermal Emission: 150 Years

Pierre-Marie Robitaille

Department of Radiology, The Ohio State University, 395 W. 12th Ave, Suite 302, Columbus, Ohio 43210, USA

E-mail: robitaille.1@osu.edu

In this work, Kirchhoff's law (Kirchhoff G. *Monatsberichte der Akademie der Wissenschaften zu Berlin*, sessions of Dec. 1859, 1860, 783–787) is being revisited not only to mark its 150th anniversary but, most importantly, to highlight serious overreaching in its formulation. At the onset, Kirchhoff's law correctly outlines the equivalence between emission and absorption for an opaque object under thermal equilibrium. This same conclusion had been established earlier by Balfour Stewart (Stewart B. *Trans. Royal Soc. Edinburgh*, 1858, v. 22(1), 1–20). However, Kirchhoff extends the treatment beyond his counterpart, stating that cavity radiation must always be black, or normal: depending only on the temperature and the frequency of observation. This universal aspect of Kirchhoff's law is without proper basis and constitutes a grave distortion of experimental reality. It is readily apparent that cavities made from arbitrary materials ($\varepsilon < 1$) are never black. Their approach to such behavior is being driven either by the blackness of the detector, or by black materials placed near the cavity. Ample evidence exists that radiation in arbitrary cavities is sensitive to the relative position of the detectors. In order to fully address these issues, cavity radiation and the generalization of Kirchhoff's law are discussed. An example is then taken from electromagnetics, at microwave frequencies, to link results in the resonant cavity with those inferred from the consequences of generalization.

1 Introduction

Kirchhoff's law is one of the simplest and most misunderstood in thermodynamics [1, 2]. It is widely considered to be the first of the laws of thermal emission [3–7]. In simple mathematical terms, Kirchhoff's law can take on several formulations, which stem from the equivalence between the coefficients of emission, ε, and absorption, α, at thermal equilibrium. The most general expression of Kirchhoff's law for opaque objects is, in fact, a statement of Stewart's law [6], namely, $\varepsilon = 1 - \rho$, where ρ corresponds to the coefficient of reflection. However, Kirchhoff's law [1, 2] is much farther reaching than Stewart's [6], in requiring that radiation within an enclosure, or cavity, must always be black, or normal [5]. Kirchhoff conceives that the ratio of emissive power, e, to absorptive power, a, of all bodies can be described by a universal function, f, common to all radiation within enclosures: $e/a = f(T, \lambda)$. Furthermore, this must be the case in a manner which is independent of the nature and shape of the enclosure, and which depends only on the temperature, T, of the system and the wavelength, λ, of observation [1, 2, 5, 7].

Kirchhoff's law constitutes an attempt to summarize the state of knowledge in radiative heat transfer during the mid-1800's. At the time, physicists created blackbodies from graphite plates, by lining the interior of cavities with soot, or by coating objects with black paint containing soot [8]. Contrary to Gustav Kirchhoff [1, 2], Balfour Stewart, in 1858 [6], stated that radiation in thermal equilibrium depends on the constituents involved and his treatment did not lead to a universal function. If Kirchhoff's law can be expressed as $e/a = f(T, \lambda)$, then Stewart's would be $e/a = f'(T, \lambda, N)$, where N represents all factors linked to the nature of the emitter itself and f' is not universal. Like Kirchhoff, Stewart based his ideas on Prévost's theory of exchanges [9, 10], which was ultimately linked to the study of radiation within enclosures. The distinctions between Stewart's formulation and Kirchhoff's are profound [11, 12]. Kirchhoff's ideas advocate a universal function [5]. Stewart's do not [6, 11, 12].

Today, 150 years after its formulation [1, 2], the foundation of Kirchhoff's law still rests on condensed matter physics. Blackbodies continue to be highly specialized objects [13–25] constructed from absorbers which are nearly perfect over the frequency range of interest. Yet, if Kirchhoff was correct about the nature of radiation within cavities, it should be possible to assemble a blackbody from any material. Surely, the presence of the universal function, f, dictates that cavity radiation must always be black, or normal [5]. All that should be theoretically required is thermal equilibrium with the walls of an enclosure. The attributes of the walls, or its contents, should be inconsequential. However, the body of experimental knowledge, relative to the assembly of blackbodies in the laboratory, stands firmly opposed to this concept [13–25]. True blackbodies [13–25] are extremely difficult to produce and testify against Kirchhoff's universal formulation [1, 2, 5]. Stewart's law [6] alone, not Kirchhoff's [1, 2], is supported by a careful consideration of experimental reality [8, 12–41]. Still, a cursory review of the literature, relative to cavity emission, would suggest that arbitrary cavities can appear black. Furthermore, the trend towards blackness appears to increase as "truer" cavities are produced. This seems to

be the case, irrespective of the emissivity of the cavity walls. The subject is a fascinating problem in physics.

2 Cavity radiation

While ideal blackbodies do not exist in nature, laboratory examples approach theoretical performances, especially when narrow frequency and temperature ranges are considered [8, 13–25]. Typically, the best laboratory blackbodies are constructed from highly absorbing walls ($\alpha \approx 1$) usually containing soot, carbon black, or graphite [8, 13–25]. Cavities which operate in the far infrared may also be lined with metals, metal blacks, or metal oxides [35–41]. Blackbody enclosures are often made isothermal using water, oil, or molten metal baths. Alternatively, metal freezing point techniques or electrical heating elements may ensure isothermal operation. The vast body of the laboratory evidence supports the idea that standard blackbodies are always made from highly absorbing materials set to function in an isothermal state.

Nonetheless, in treating cavity radiation from a theoretical standpoint, Planck invokes the perfectly reflecting enclosure [7, 8]. This is an interesting approach, since perfectly reflecting enclosures are adiabatic by definition and cannot therefore participate in the exchange of heat, either through emission or absorption. Planck, though, requires that the interior of such cavities contains black radiation [7; §51–52], in conformity with Kirchhoff's law [1, 2]. In so insisting, Planck makes constant recourse [8] to a minute particle of carbon [7; §51–52]. He inserts the particle into the cavity, in order to ensure that the latter appropriately holds black radiation. Planck invokes carbon, despite the fact that Kirchhoff's law should have ensured the presence of the radiation sought. In the end, and though carbon particles are perfect absorbers, Planck treats them simply as catalysts, and ignores their importance to the blackbody problem [7, 8].

It remains commonly acknowledged that all cavity radiation must be black. This is the case even though cavities with arbitrary walls of low emissivity are never used as laboratory blackbody standards [13–25]. Clearly, there is more to the understanding of arbitrary cavities than the belief that they are black [1, 2, 5]. In any case, when arbitrary cavities are analyzed with radiometric detectors, they do appear to become black, as seen in classic texts [i.e. 28] and the references they contain [29–34, 42–48]. Ample theoretical work reinforces this position [i.e. 42–48]. Monte Carlo calculations on lambertian spherical arbitrary cavities constructed from walls of low emissivity provide a good example [28]. Such calculations lead to apparent cavity emissivities approaching 1 [28]. These amazing results hint at proof, at least on the surface, that Kirchhoff's law is fully valid. Unfortunately, it can be shown that such conclusions are erroneous.

Let us return for a moment to Planck's treatment [7] and the perfectly reflecting cavity containing a carbon particle [8]. A schematic representation of this situation is presented in Figure 1A. Since the cavity wall is perfectly reflecting, one can treat it as an adiabatic boundary producing no radiation of its own. All of the radiation which comes to fill the cavity is being produced by the carbon particle [12]. As a result, if one examines the contents of the cavity through a small hole, the radiation it contains will obviously be black. Now, let us displace the carbon particle, such that it is located just outside the aperture leading to the cavity (see Fig. 1B). From this position, the particle will once again be able to fill the cavity with photons, and the observer will find that its interior contains black radiation. Finally, let us place the carbon particle well outside the cavity itself, such that its radiation can still penetrate the cavity (see Fig. 1C). In this instance, the observer will record that the cavity is black, but not because it was able to become black on its own. It is black simply because the carbon particle has filled the cavity with radiation.

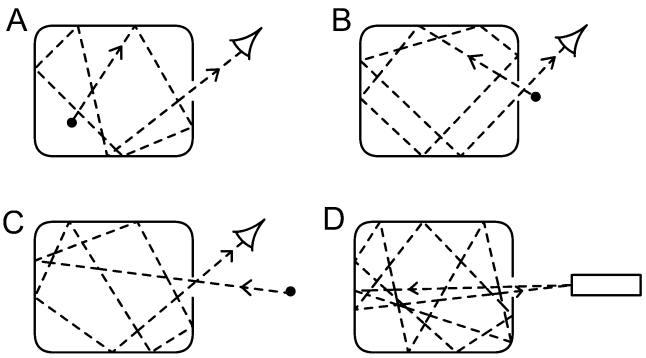

Fig. 1: Schematic representation of a perfectly reflecting cavity A) containing a carbon particle, B) with a carbon particle near the aperture, C) with a carbon particle farther from the aperture, and D) with the carbon particle replaced by a physical detector. The eye represents a point of detection. Note that if perfectly reflecting cavities contain any radiation whatsoever, it is solely because they have been filled with photons either from the carbon particle or the detector.

Returning to the days of Kirchhoff, it is evident that limited experimental means existed. As a result, cavity radiation was monitored through a combination of prisms, for frequency differentiation, and thermometers, for energy detection. These thermometers were always blackened with soot, as Langley reminds us in 1888: "*I may reply that we have lately found an admirable check on the efficiency of our optical devices in the behavior of that familiar substance lampblack, which all physicists use either on the thermometers, thermopiles, or bolometers*" [49]. Consequently, by sampling the cavity with a thermometer coated with lampblack, every experimentalist brought about for himself the result which he sought. All cavities appeared black, because all cavities were being filled unintentionally with black radiation. Adding the carbon particle directly to the interior of the cavity simply helped to bring about the desired experimental scenario.

In Fig. 1D, a cavity is represented along with a radiometric detector. In order to maintain a logical progression, let us assume that the cavity is perfectly reflecting in its interior.

In this case, the cavity itself cannot emit any photons [12]. A small hole is made into the cavity, and the radiation contained within it can be sampled with the radiometer. The cavity will be found to contain black radiation [12]. Yet, if the cavity was a perfect reflector, then how could its interior be black? The answer, of course, is similar to what Planck had done with the small carbon particle. A carbon particle, no matter how tiny [8, 12], will instantly fill an experimental cavity with black radiation. Planck, in fact, relies on this reality [7; §51–52]. Now, consider our radiometric detector. This instrument must have high photon capture rates. That is to say, it must possess an elevated absorptivity. As a result, by Stewart's law [6], it must also possess a high emissivity. Thus, if the cavity appears black, it is only because it has been filled with black radiation by the detector. Again, the experimentalist inadvertently produced the expected result.

In order to more fully appreciate the role of the detector in generating black radiation within cavities, let us consider the classic works by De Vos [32, 33] and Ono [28, 34]. Even though he is addressing arbitrary cavities, De Vos emphasizes that: "*The radiation emerging from the hole of observation in the blackbody should be an approximation, as well as possible, to the theoretical blackbody radiation*" [32]. A cursory examination of these studies would lead one to believe that all arbitrary cavities are indeed black. However, upon closer analysis, these investigators have not distinguished themselves from their predecessors. De Vos elegantly links mathematical and experimental results obtained from cavities [32]. If the cavities appear black under certain viewing conditions, it is simply because black radiation has been injected into them using detectors. De Vos notes that in order to sample black radiation in a spherical cavity of arbitrary construction: "*It is necessary to take care that the surface element observed is not perpendicular to the direction of observation*" [32]. The reason for this statement is evident. If the surface element was perpendicular, most of the radiation introduced by the detector into the cavity would undergo normal specular reflection back out of the cavity and the latter would not appear black. In subsequently describing the tubular blackbody (see Figure 2A), De Vos states that: "*The actual value of the quality will be better than calculated in this way but only slightly better since the radiant intensity decreases rapidly towards the ends of the tube*" [32]. Of course, the detector is pumping radiation into the hole at the center of the tube. It is, therefore, simple to understand why radiation must fall rapidly towards the ends of the tube. Clearly, the tubular cavity is manifesting the performance of the detector. In fact, De Vos himself unintentionally makes the point: "*Owing to the small hole in the tungsten tube a small quantity of energy was available only. Hence it was necessary to use radiation receivers of high sensitivity*" [33]. De Vos might have more appropriately written that it was important for the detector to provide an ample supply of photons. For his part, Ono has demonstrated that the apparent emission of the tubular cavity depends on the position of the detector itself. Ono writes: "*The apparent emissivity has deep minima around $\theta = 0^\circ$ at which specularly reflected radiation escapes through the lateral hole. The shallow minima around 30° are also due to specular reflection effects where incident radiation escapes after two successive specular reflections*" [28, p. 605]. This situation is reproduced schematically in Fig. 2B. Of course, the incident radiation arises from the detector. It alone is filling the cavity with black radiation. The cavity itself is not producing this radiation for, if it did, the position of the detector would be immaterial. This is certain proof that Kirchhoff's law does not hold. Much depends on the detector, not on the cavity.

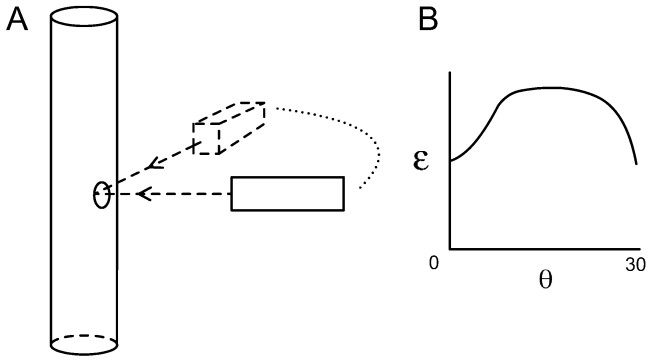

Fig. 2: A) Schematic representation of a tubular cavity and a detector. B) Illustration of the type of result seen with the detector as a function of angle from the normal. Note how there is less emission measured at 0° and 30°.

The point is further amplified by considering the work of Sparrow and Heinisch [30]. The authors demonstrate that the normal emission from a cylindrical cavity is absolutely dependent on the distance of the detector from the cavity. They fail to examine the cavity as a function of detector angle. Still, it is obvious that distance variations should not be occurring. Again, the detector is critically important in flooding the cavity with radiation.

Vollmer's studies [29] help us to understand that arbitrary cavities are not black, despite the fact that, at least on the surface, they point to the contrary. His work is particularly interesting, as it aims to reconcile theoretical foundations, stemming from Buckley's classic paper [42], with experimental data. Surprising agreement is obtained between theory and experiment. In the limit, these results appear to re-emphasize that cylindrical cavities of sufficient size, made from arbitrary materials, will indeed behave as blackbodies. Everything seems to rest on solid footing, until the experimental setup is carefully examined. In order to reach agreement with theory, the apparatus used not only supplied the typical detector radiation, but also a black bellows, a black water cooled shutter, and a black water cooled cylinder [42]. Given these many possible sources of black radiation in front of the cavity opening, there can be little wonder that the cavity begins to appear black. In reality, the contrary position should have

been adopted. How surprising that, bombarded with black radiation, some cavities still fail to be able to appear fully black.

R. E. Bedford, though he believes in the validity of Kirchhoff's law, re-emphasizes the point that arbitrary cavities are simply not black [28; p. 678]: "*A blackbody is a lambertian emitter; with the exception of a spherical cavity, none of the blackbody simulators we will discuss will radiate directionally as does a blackbody*". Yet, as seen above for the spherical cavity, "*It is necessary to take care that the surface element observed is not perpendicular to the direction of observation*" [32]. Consequently, when these two excerpts are taken together, Bedford's statement constitutes a direct refutation of Kirchhoff's law. The situation deteriorates further: "*At some angle of view away from the normal to the cavity aperture (the angle depending on the particular cavity shape), the cavity radiance will begin to drop sharply from its axial value as that part of the wall becomes visible where $\varepsilon_a(y)$ near the aperture is much lower than $\varepsilon_a(x)$ deep within the cavity. In most cases this deficiency in emitted energy will be significant only at angles of view larger than are subtended by most pyrometers*" [28; p. 678]. In any event, the point is made. None of the cavities modeled can ever truly be considered blackbodies. Arbitrary materials are not lambertian and their emissivity can never be black [5]. Spherical cavities must be monitored with careful attention to the angle of observation. This should not occur if they were truly blackbodies.

If Monte Carlo simulations and other calculations reveal that arbitrary cavities move to blackness independent of wall emissivities, it is strictly because such methods fill the cavities with black radiation [42–48]. Once again, blackbodies are unique in possessing lambertian surfaces. Thus, models which utilize lambertian surfaces of low emissivity represent situations which have no counterparts in nature. In addition, there can be no difference between placing a carbon particle in a cavity, in order to ensure the presence of black radiation, and simply filling the cavity with black radiation without physically making recourse to carbon. Monte Carlo simulations introduce black photons into cavities. Hence, they become black. The process is identical to placing a highly emitting carbon particle, or radiometer, at the opening of a cavity. No proof is provided by computational methods that arbitrary cavities contain black radiation.

It can be stated that Monte Carlo simulations obtain similar answers by modeling the repeated emission of photons directly from the cavity walls. In this case, computational analysis relies on internal reflection to arrive at a cavity filled with black radiation. The problem is that this scenario violates the first law of thermodynamics and the conservation of energy. It is not mathematically possible to maintain an isothermal cavity while, at the same time, enabling its walls to lose a continual stream of photons. Such approaches build up the photon density in the cavity at the expense of wall cooling. These methods must therefore be forbidden on grounds that they violate the 1st law of thermodynamics.

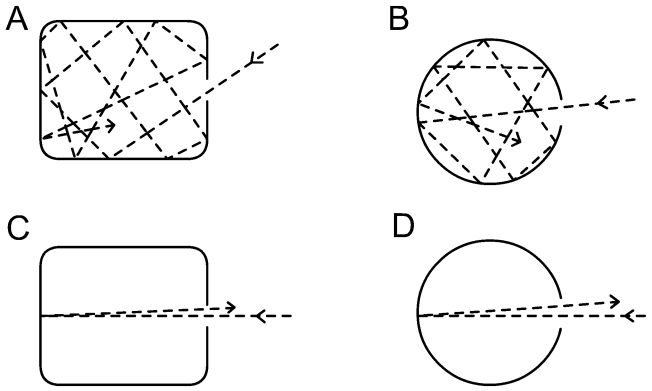

Fig. 3: Schematic representations typically used to argue that cavity radiation is always black. Figure A is similar to Figure 6.1 in [50]. Figure B is similar to 5.6 in [51]. Note that figures illustrating immediate reflection back out of the cavity (C and D) are never invoked. This is precisely because they represent direct physical proof that arbitrary cavities are not black.

It is commonly argued [50, 51] that a cavity with a sufficiently small hole contains black radiation. For example, in his classic text on the photosphere D. F. Gray writes: "*Let us begin with a container that is completely closed except for a small hole in one wall. Any light entering the hole has a very small probability of finding its way out again, and eventually will be absorbed by the walls of the container or the gas inside the container... We have constructed a perfect absorber*" [50; p. 100]. In reality, the maintenance of thermal equilibrium requires that if a photon enters the cavity, another photon must exit. The experimentalist will never be able to discern whether the exiting photon was 1) the same, 2) a photon that was newly emitted without reflection, 3) a photon that had previously undergone several reflections before exiting the cavity, or 4) a photon that had undergone a nearly infinite number of internal reflections before exiting the cavity. Each of these cases corresponds to different types of cavities, made either from arbitrary walls, perfectly absorbing walls, or perfectly reflecting walls. In any case, a photon must exit to maintain thermal equilibrium and nothing has been learned about the internal nature of the cavity. Clearly, given thermal equilibrium and the first law of thermodynamics, we cannot be sure that the radiation inside the cavity was black. Such arguments [50; p. 100–101] are unsound *a priori*. Notice, for instance, the types of figures typically associated with such rhetoric: the photon is usually drawn such that normal and immediate specular reflection back out of the cavity is discounted (see Figure 3A–B). This is precisely because immediate specular reflection of the photon back out of the cavity provides a sound logical defeat of such arguments (see Figure 3C–D).

In summary, the radiation contained inside arbitrary cavities is not black and depends exclusively on 1) the nature of the cavity, and 2) the nature of the radiation which is permitted to enter. If excellent radiometers are used, they will be

good emitters, and will act to fill the cavities with black radiation. As such, it seems logical, although counterintuitive, that the sampling of cavity radiation should be performed with suboptimal radiometers. Radiometers for these studies should not have high photon capture rates. Such devices would provide lower photon emission towards the cavity. In so doing, they would minimally alter the true nature of the radiation they seek to measure. Perhaps, by using cryogenic devices, it might be possible to build detectors which retain adequate sensitivity. By maintaining lower detector emissions, the true nature of radiation within cavities might be ascertained. The proper result should echo Stewart, as previously demonstrated mathematically [12].

3 The generalization of Kirchhoff's law

The proofs of Kirchhoff's law are usually limited to the realm of geometrical optics. In his classic paper [2], Kirchhoff states in a footnote: "*The effect of the diffraction of the rays by the edges of opening 1 is here neglected. This is allowable if openings 1 and 2, though infinitely small in comparison with their distance apart, be considered as very great in comparison with the length of a wave*." Since Planck's treatment of Kirchhoff's law is also based on geometric optics, Planck writes: "*Only the phenomena of diffraction, so far at least as they take place in space of considerable dimensions, we shall exclude on account of their rather complicated nature. We are therefore obliged to introduce right at the start a certain restriction with respect to the size of the parts of space to be considered. Throughout the following discussion it will be assumed that the linear dimensions of all parts of space considered, as well as the radii of curvature of all surfaces under consideration, are large compared to the wave lengths of the rays considered. With this assumption we may, without appreciable error, entirely neglect the influence of diffraction caused by the bounding surfaces, and everywhere apply the ordinary laws of reflection and refraction of light. To sum up: We distinguish once for all between two kinds of lengths of entirely different orders of magnitudes — dimensions of bodies and wave lengths. Moreover, even the differentials of the former, i.e., elements of length, area and volume, will be regarded as large compared with the corresponding powers of wave lengths. The greater, therefore, the wave length of the rays we wish to consider, the larger must be the parts of space considered. But, inasmuch as there is no other restriction on our choice of size of the parts of space to be considered, this assumption will not give rise to any particular difficulty*" [7; §2]. Kirchhoff and Planck specifically excluded diffraction. They do so as a matter of mathematical practicality. The problem of diffraction greatly increases the mathematical challenges involved. As a result, Kirchhoff and Planck adapt a physical setting where its effects could be ignored. This is not a question of fundamental physical limitation.

Nonetheless, the first section of Kirchhoff's law, namely the equivalence between the absorption and emission of energy by an opaque material at thermal equilibrium, has been generalized to include diffraction. Correctly speaking, this constitutes an extension of Stewart's law, as will be discussed below.

Much of the effort in generalizing Kirchhoff's (Stewart's) law can be attributed to Sergi M. Rytov, the Russian physicist. Indeed, it appears that efforts to generalize Kirchhoff's law were largely centered in Russia [52–55], but did receive attention in the West [56, 57]. Though Rytov's classic work appears initially in Russian [52], later works have been translated into English [53]. In describing their theoretical results relative to the generalization of Kirchhoff's law, Rytov and his associates [53; §3.5] write: "*Equations (3.37-39) can be termed Kirchhoff's form of the FDT (fluctuation-dissipation theorem), as they are a direct generalization of Kirchhoff's law in the classical theory of thermal radiation. This law is known to relate the intensity of the thermal radiation of a body in any direction to the absorption in that body when exposed to a plane wave propagating in the opposite direction...*" The authors continue: "*and most important, (3.37–39) contain no constraints on the relationships between the wavelength λ and characteristic scale l of the problem (the size of the bodies, the curvature radii of their surfaces, the distances from the body to an observation point, etc.). In other words, unlike the classical theory of thermal radiation, which is bound by the constraints of geometrical optics, we can now calculate the second moments of the fluctuational field, that is to say both the wave part (taking into account all the diffraction phenomena), and the nonwave (quasistationary) part for any λ vs l ratio*" [53; §3.5].

A discussion of the fluctuation-dissipation theorem (FTD), as it applies to thermal radiation, can also be found in the book by Klyshko [54]. This text provides a detailed presentation of the generalization of Kirchhoff's law [54; §4.4 and 4.5]. Apresyan and Kravtsov also address generalization in their work on radiative heat transfer [55]. They summarize the point as follows: "*In this formulation, the Kirchhoff statement — that the radiating and absorbing powers of a body are proportional to each other — as was initially derived in the limit of geometrical optics, is valid also for bodies with dimension below or about the wavelength*" [55; p. 406].

It appears that the generalized form of Kirchhoff's law has been adapted by the astrophysical community [57]. Like the Russians before them, Linsky and Mount [56] assume that the equality between emissivity and absorptivity at thermal equilibrium is a sufficient statement of Kirchhoff's law [1, 2]. They refer to a Generalized Kirchhoff's Law (GKL) as $E(\mu_0) = 1 - \rho(\mu_0)$, where $E(\mu_0)$ is the directional spectral emissivity and $\rho(\mu_0)$ corresponds to the directional hemispherical reflectivity [56]. This statement should properly be referred to as Stewart's law [6], since Stewart was the first to argue for the equality between the emissivity and absorptiv-

ity of an opaque material under conditions of thermal equilibrium. Furthermore, Stewart's law makes no claim that the radiation within opaque cavities must be black, or normal [5]. Seigel [11] speaks for physics when he outlines the important distinction between Stewart's law [6] and Kirchhoff's [1, 2]. He writes: "*Stewart's conclusion was correspondingly restricted and did not embrace the sort of connection between the emissive and absorptive powers of different materials, through a universal function of wavelength and temperature which Kirchhoff established*" [11; p. 584]. Herein, we find the central difference between Stewart and Kirchhoff. It is also the reason why Kirchhoff's law must be abandoned. In fact, since universality is not valid, there can be no more room for Kirchhoff's law in physics.

Returning to Rytov and his colleagues, following their presentation of the generalization of Kirchhoff's law [53; §3.5], they move rapidly to present a few examples of its use [53; §3.6] and even apply the treatment to the waveguide [53; §3.7]. Interestingly, though the authors fail to discuss the microwave cavity, from their treatment of the waveguide, it is certain that the radiation within the cavity cannot be black. It must depend on the dimensions of the cavity itself. Such a result is a direct confirmation of Stewart's findings [6], not Kirchhoff's [1, 2]. As a consequence, the generalization of Kirchhoff's law brings us to the conclusion that the radiation within cavities is not black, and the second portion of Kirchhoff's law is not valid.

These questions now extend to ultra high field magnetic resonance imaging [58, 59], and hence the problem of radiation within cavities should be reexamined in the context of the generalization of Kirchhoff's law [52–55]. Since generalization extends to situations where cavity size is on the order of wavelength, it is appropriate to turn to this setting in magnetic resonance imaging. In fact, this constitutes a fitting end to nearly 10 years of searching to understand why microwave cavities are not black, as required by Kirchhoff's law.

4 Cavity radiation in magnetic resonance imaging

Prior to treating the resonant microwave cavity, it is important to revisit Kirchhoff's claims. In his derivation, Kirchhoff initially insists that his treatment is restricted to the study of heat radiation. He reminds the reader that: "*All bodies emit rays, the quality and intensity of which depend on the nature and temperature of the body themselves*" [2]. Then, he immediately eliminates all other types of radiation from consideration: "*In addition to these, however, there may, under certain circumstances, be rays of other kinds, — as, for example, when a body is sufficiently charged with electricity, or when it is phosphorescent or fluorescent. Such cases are, however, here excluded*" [2]. Kirchhoff then proceeds to provide a mathematical proof for his law. Surprisingly, he then reintroduces fluorescence. This is precisely to make the point that, within cavities, all radiation must be of a universal nature. Moreover, this occurs in a manner which is completely independent of the objects they contain, even if fluorescent, or any other processes. Kirchhoff writes: "*The equation $E/A = e$ cannot generally be true of such a body, but it is true if the body is enclosed in a black covering of the same temperature as itself, since the same considerations that led to the equation in question on the hypothesis that the body C was not fluorescent, avail in this case even if the body C be supposed to be fluorescent*" [2]. Kirchhoff deliberately invokes the all encompassing power of universality and its independence from all processes, provided enclosure is maintained.

Consequently, two important extensions exist. First, given the generalization of Kirchhoff's law [52–55], it is appropriate to extend these arguments to the microwave cavity. In this experimental setting, the wavelengths and the size of the object are on the same order. Furthermore, assuming thermal equilibrium, it is proper to consider steady state processes beyond thermal radiation. This is provided that a cavity be maintained. In any event, it is established that thermal loses exist within microwave devices. Thus, we can examine the electromagnetic resonant cavity in light of Kirchhoff's law.

When the use of the blackbody resonator in UHFMRI was advanced [60], it was not possible to reconcile the behavior of such a coil, given the conflict between Kirchhoff's law [1, 2] and the known performance of cavities in electromagnetics [61, 62]. A photograph of a sealed blackbody resonator for UHFMRI [60] is presented in Figure 4. In the simplest sense, this resonant cavity is an enclosure in which radiation can solely enter, or exit through, at a single drive point. The radiation within such cavities should be black, according to Kirchhoff [1, 2]. Nonetheless, measurements of the real cavity show that it does not contain black radiation, as demonstrated experimentally in Figure 5. Resonant cavities are well known devices in electromagnetics [61, 62]. Their radiation is determined purely by the constituent properties of the cavity and its dimensions [61, 62]. This point is affirmed in Figure 5. In its current form, Kirchhoff's law [1, 2] stands at odds against practical microwave techniques [61, 62]. Since this knowledge should not be discounted, something must be incorrect within Kirchhoff's law. Everything about the blackbody resonator presented in Figure 4 echoes Planck, yet the radiation it contains is not black [5]. The type of radiation within this cavity is being determined by electromagnetics [61, 62], not by Kirchhoff's law. Only the attributes of any substance present and that of the enclosed resonant elements, along with the size and shape of the enclosure itself, govern the type of radiation. For example, as seen in Figs. 4 and 5, the simple addition of echosorb acts to significantly alter the resonances within such cavities. The associated loses are thermal. Of course, at these frequencies, echosorb is not a perfect absorber and the radiation inside the cavity cannot easily be made black. Still, in partial deference to Kirchhoff, if a perfect absorber could be found, the radiation within cav-

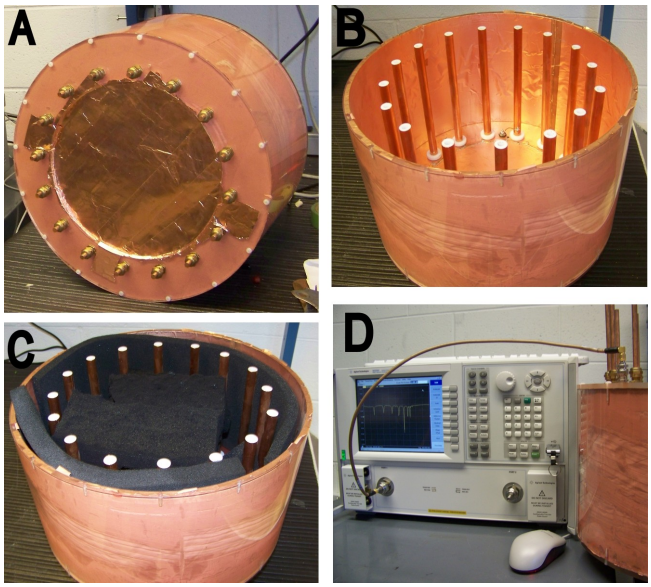

Fig. 4: A) End-view photograph of a sealed blackbody resonator [60] for use in UHFMRI studies. This device behaves as a resonant cavity [61, 62] and is constructed by sealing both ends of the well-known TEM resonator [63, 64]. In this particular case, one of the ends of the resonator was made by sealing an acrylic ring with a thin copper sheet which was then re-enforced with copper tape on the inner and outer surfaces. All other assembly details are as previously reported [60]. When a resonator is sealed at both ends to make a cavity [61, 62], radiation can solely enter or leave the device through a single drive port. As such, the blackbody resonator can be regarded as the electromagnetic equivalent of Kirchhoff's blackbody [1, 2, 5, 7], with the important difference, of course, that the radiation inside such a device is never black. This constitutes a direct refutation of Kirchhoff's law of thermal emission as demonstrated experimentally in Fig. 5. B) Photograph of the interior of the blackbody coil illustrating the TEM rods, the interior lined with copper, and the drive point. Note that for these studies, a matching capacitor [60] was not utilized, as the measurement of interest does not depend on matching a given resonance to 50 ohms. It is the resonant nature of the coil itself which is of interest, not the impedance matching of an individual resonant frequency. C) Photograph of the blackbody coil filled with pieces of Echosorb. D) Photograph of the blackbody coil connected to an Agilent Technologies N5230C 300kHz – 6 GHz PNA-L Network Analyzer using an RG400 cable and SMA connectors. Since the RF coil was assembled with a BNC connector, an SMA/BNC adaptor was utilized to close the RF chain. The calibration of the analyzer was verified from 200–400 MHz using a matched load of 50 ohms placed directly on the network analyzer port. In this case, the return loss (S11) was less than -40 dB over the frequency range of interest. The matched load was also placed on the end of the test cable used for these studies and in this case the return loss (S11) was less than -25 dB from 200–400 MHz. The network analyzer provides a continuous steady state coherent source of radiation into the cavity. The coherence of this radiation is critical to the proper analysis of the returned radiation by the network analyzer. This does not alter the conclusions reached. Only the ability to properly monitor cavity behavior is affected by the use of incoherent radiation. The cavity, of course, is indifferent to whether or not the radiation incident upon it is coherent.

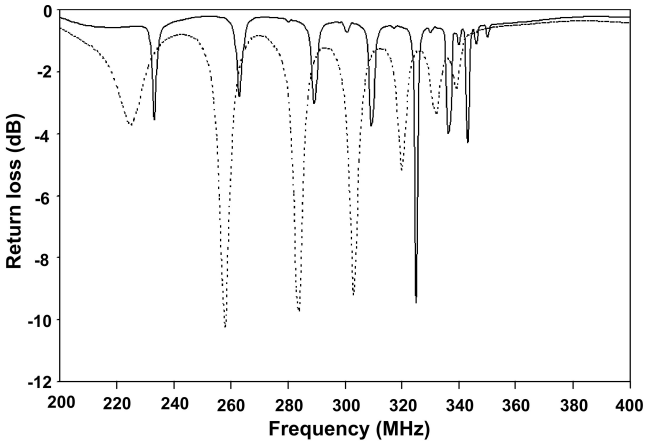

Fig. 5: Plot of the return loss (S11) for the blackbody coil (solid line) as measured from 200–400 MHz. Note that even though this cavity is completely closed, the radiation within this device is not black. Several sharp resonances are observed whose resonant position depend on the nature of the resonant cavity itself (dimension of the cavity, quality of the inner copper lining, dimensions of the TEM resonant elements, degree of insertion of the struts into the TEM elements, etc.). It is the presence of such resonances within cavities that forms the basis of practical electromagnetics and enables the use of resonant cavities in both EPR and MRI [61, 62]. If Kirchhoff's law of thermal emission had been correct, such a resonant device would not exist. The problem is easily rectified if one adopts Stewart's formulation for the treatment of thermal emission [6]. The dashed line displays the return loss (S11) for the blackbody coil filled with the carbon-foam Echosorb as measured from 200–400 MHz. Note that Echosorb is not a perfect absorber of radiation at these frequencies. But since this foam is somewhat absorbing, the resonance lines are broadened substantially. The return losses at several frequencies are lower, as is to be expected from the introduction of an absorbing object within a resonant cavity. If a perfect absorber could be found at these frequencies, the return loses would become extremely low across the entire frequency range of interest. Given these measurements and access to resonant devices, network analyzers and microwave technology, it is likely that Kirchhoff would have reconsidered the formulation of his law of thermal emission.

ities containing such objects would be black. Nonetheless, only Stewart's law [6] is formulated in such a way as to conform with results from electromagnetics [61, 62].

5 Conclusions

Tragically, if Kirchhoff believed in universality, it was because he did not properly treat both reflection and absorption, as previously highlighted [12]. The correct treatment of radiation at thermal equilibrium was first performed by Stewart, in 1858 [6]. Stewart properly addresses reflection [6, 8, 12], and does not arrive at universality. Unfortunately, Stewart's formulation lacked mathematical rigor [6, 12] and this did not help in drafting a central law of thermal emission. At the same time, in deriving Kirchhoff's law in his treatise, Planck fails to fully treat reflection [7; §6]. Like Kirchhoff

his teacher, Planck is thereby lead erroneously to the concept that all enclosures contain black radiation. Planck begins his derivation of Kirchhoff's law by considering elements $d\tau$ within an extended substance. He then analyzes the radiation emitted by these elements, but ignores the coefficient of reflection, ρ_ν. He writes: "*total energy in a range of frequency from ν to $\nu + d\nu$ emitted in the time dt in the direction of the conical element $d\Omega$ by a volume element $d\tau$*" [7; §6] is equal to $dt\, d\tau\, d\Omega\, d\nu\, 2\varepsilon_\nu$. As a result, he is brought to a universal function, which is independent of the nature of the object, and affirms the validity of Kirchhoff's law: $\varepsilon_\nu / a_\nu = f(T, \nu)$. In this equation, the coefficient of emission, ε_ν, the coefficient of absorbance, a_ν, the temperature, T, and the frequency, ν, alone are considered. Had Planck properly addressed the coefficient of reflection, ρ_ν, and recognized that the total radiation which leaves an element is the sum produced by the coefficients of emission, ε_ν, and reflection, ρ_ν, he would have obtained $(\varepsilon_\nu + \rho_\nu)/(a_\nu + \rho_\nu) = f'(T, \nu, N)$, where the nature of the object, N, determined the relative magnitudes of ε_ν, a_ν, and ρ_ν. By moving to the interior of an object and neglecting reflection, Planck arrives at Kirchhoff's law, but the consequence is that his derivation ignores the known truth that opaque objects possess reflection.

Given thermal equilibrium, the equivalence between the absorptivity, a_ν, and emissivity, ε_ν, of an object was first recognized by Stewart [6]. Stewart's formulation preserves this central equivalence. Only, it does not advance the universality invoked by Kirchhoff [1, 2]. At the same time, it remains fortunate for human medicine that Kirchhoff's law of thermal emission does not hold. If it did, MRI within cavities [60] would not be possible. Devices containing solely black radiation would be of no use, either as microwave components, or as antenna for human imaging. Physics and medicine should return thereby, by necessity, to Stewart's formulation [6] and the realization that radiation within cavities depends not uniquely on frequency and temperature, as stated by Kirchhoff [1, 2], but also on the attributes of the cavity itself and the materials it contains. This contribution was first brought to physics by Balfour Stewart [6]. Stewart's law, not Kirchhoff's, properly describes physical reality as observed in the laboratory across all subdisciplines of physics and over the entire span of the electromagnetic spectrum.

Practical blackbodies are always made from specialized substances which are nearly perfect absorbers over the frequency range of interest [13–25]. Accordingly, the nature of the enclosure is important, in opposition to Kirchhoff's law which claims independence from the properties of the walls and its contents. Through the formulation of his law of thermal emission, Balfour Stewart [6], unlike Kirchhoff, recognized the individualized behavior of materials in thermal equilibrium. In addition, it is well-established that the radiation within microwave cavities is not necessarily black. Rather, it depends on the nature, shape, contents, and dimensions of the enclosure itself. This is in accordance with Stewart's law. Alternatively, if Kirchhoff's law was correct, cavities should strictly contain blackbody radiation and their use in radio and microwave circuitry would be pointless. Network analyzer measurements of return losses for a sealed enclosure, or blackbody resonator [60], from 200–400 MHz, confirm that Kirchhoff's law of thermal emission does not hold within arbitrary resonant cavities.

At the same time, the physics community is justified in taking a cautious approach in these matters. After all, it was Planck [5] who provided the functional form contained in Kirchhoff's law [1, 2]. As a result, there is an understandable concern, that revisiting Kirchhoff's law will affect the results of Planck himself and the foundation of quantum physics [5]. There is cause for concern. The loss of the universal function brings about substantial changes not only in astrophysics, but also in statistical thermodynamics.

Relative to Planck's equation itself, the solution remains valid. It does however, become strictly limited to the problem of radiation within cavities which are known to be black (i.e. made of graphite, lined with soot, etc). Universality is lost. As for the mathematical value of Planck's formulation for the perfectly absorbing cavity, it is preserved. In describing blackbody radiation, Planck consistently invokes the presence of a perfect absorber. In his treatise [7], he repeatedly calls for a minute particle of carbon [8]. Planck views this particle as a simple catalyst, although it can be readily demonstrated that this is not the case: the carbon particle acted as a perfect absorber [12]. As a result, I have stated that Kirchhoff's law is not universal [8, 12, 26, 27] and is restricted to the study of cavities which are either made from, or contain, perfect absorbers. Arbitrary cavity radiation is not black [12]. There can be no universal function. Planck's equation presents a functional form which, far from being universal, is highly restricted to the emission of bodies, best represented on Earth by materials such as graphite, soot, and carbon black [8].

In closing, though 150 years have now elapsed since Kirchhoff and Stewart dueled over the proper form of the law of thermal emission [11, 12], little progress has been made in bringing closure to this issue. Experimentalists continue to unknowingly pump black radiation into arbitrary cavities using their detectors. Theorists replicate the approach with Monte Carlo simulations. At the same time, astrophysicists apply with impunity the laws of thermal emission [1–7] to the stars and the universe. Little pause is given relative to the formulation of these laws [1–7] using condensed matter. The fact that all of electromagnetics stands in firm opposition to the universality, instilled in Kirchhoff's law, is easily dismissed as science unrelated to thermal emission [61, 62]. Losses in electromagnetics are usually thermal in origin. Nonetheless, electromagnetics is treated almost as an unrelated discipline. This occurs despite the reality that Kirchhoff himself specifically included other processes, such as fluorescence, provided enclosures were maintained. Though the generalization of Kirchhoff's law is widely recognized

as valid [52–55], its application to the microwave cavity has been strangely omitted [52], even though it is used in treating the waveguide. This is the case, even though waveguides and cavities are often treated in the same chapters in texts on electromagnetics. All too frequently, the simple equivalence between apparent spectral absorbance and emission is viewed as a full statement of Kirchhoff's law [57, 65], adding further confusion to the problem. Kirchhoff's law must always be regarded as extending much beyond this equivalence. It states that the radiation within all true cavities made from arbitrary walls is black [1, 2]. The law of equivalence [57, 65] is Stewart's [6].

Most troubling is the realization that the physical cause of blackbody radiation remains as elusive today as in the days of Kirchhoff. Physicists speak of mathematics, of Planck's equation, but nowhere is the physical mechanism mentioned. Planck's frustration remains: "*Therefore to attempt to draw conclusions concerning the special properties of the particles emitting rays from the elementary vibrations in the rays of the normal spectrum would be a hopeless undertaking*" [7; §111]. In 1911, Einstein echoes Planck's inability to link thermal radiation to a physical cause: "*Anyway, the h-disease looks ever more hopeless*" [66; p. 228]. Though he would be able to bring a ready derivation of Planck's theorem using his coefficients [67], Einstein would never be able to extract a proper physical link [68]. In reality, we are no closer to understanding the complexities of blackbody radiation than scientists were 150 years ago.

Acknowledgements

William F. Moulder from the Electrosciences Laboratory is recognized for measuring return losses specific to this experiment. Brief access to the Agilent Technologies network analyzer was provided by the Electrosciences Laboratory. Luc Robitaille is acknowledged for figure preparation.

Dedication

This work is dedicated to my eldest sister, Christine.

Submitted on May 27, 2009 / Accepted on May 29, 2008
First published online on June 19, 2009

References

1. Kirchhoff G. Über den Zusammenhang zwischen Emission und Absorption von Licht und. Wärme. *Monatsberichte der Akademie der Wissenschaften zu Berlin*, sessions of Dec. 1859, 1860, 783–787.
2. Kirchhoff G. Über das Verhältnis zwischen dem Emissionsvermögen und dem Absorptionsvermögen. der Körper für Wärme und Licht. *Poggendorfs Annalen der Physik und Chemie*, 1860, v. 109, 275–301. (English translation by F. Guthrie: Kirchhoff G. On the relation between the radiating and the absorbing powers of different bodies for light and heat. *Phil. Mag.*, 1860, ser. 4, v. 20, 1–21).
3. Wien W. Über die Energieverteilung in Emissionspektrum eines schwarzen Körpers. *Ann. Phys.*, 1896, v. 58, 662–669.
4. Stefan J. Über die Beziehung zwischen der Warmestrahlung und der Temperature. *Sitzungsberichte der mathematischnaturwissenschaftlichen Classe der kaiserlichen Akademie der Wissenschaften*, Wien 1879, v. 79, 391–428.
5. Planck M. Über das Gesetz der Energieverteilung im Normalspektrum. *Annalen der Physik*, 1901, v. 4, 553–563 (English translation by ter Haar D.: Planck M. On the theory of the energy distribution law in the normal spectrum. The old quantum theory. Pergamon Press, 1967, 82–90; also Planck's December 14, 1900 lecture Zur Theorie des Gesetzes der Energieverteilung in Normalspectrum, which stems from this paper, can be found in either German, or English, in: Kangro H. Classic papers in physics: Planck's original papers in quantum physics. Taylor & Francis, London, 1972, 6–14 or 38–45).
6. Stewart B. An account of some experiments on radiant heat, involving an extension of Prévost's theory of exchanges. *Trans. Royal Soc. Edinburgh*, 1858, v. 22(1), 1–20 (also found in Harper's Scientific Memoirs, edited by J. S. Ames: The Laws of Radiation and Absorption: Memoirs of Prévost, Stewart, Kirchhoff, and Kirchhoff and Bunsen, translated and edited by D. B. Brace, American Book Company, New York, 1901, 21–50).
7. Planck M. The theory of heat radiation. P. Blakiston's Son & Co., Philadelphia, PA, 1914.
8. Robitaille P. M. L. Blackbody radiation and the carbon particle. *Prog. in Phys.*, 2008, v. 3, 36–55.
9. Prévost P. Mémoire sur l'équilibre du feu. *Journal de Physique*, 1791, v. 38, 314–322 (translated in Harper's Scientific Memoirs (J. S. Ames, Ed.) — The Laws of Radiation and Absorption: Memoirs of Prévost, Stewart, Kirchhoff, and Kirchhoff and Bunsen. Translated and edited by D. B. Brace, American Book Company, New York, 1901, 1–13).
10. Prévost P., Du calorique rayonnant. J. J. Paschoud, Geneva & Paris 1809 (Sections are translated in Harper's Scientific Memoirs (J. S. Ames, Ed.) — The Laws of Radiation and Absorption: Memoirs of Prévost, Stewart, Kirchhoff, and Kirchhoff and Bunsen. Translated and edited by D. B. Brace, American book company, New York, 1901, 15–20).
11. Siegel D. M. Balfour Stewart and Gustav Robert Kirchhoff: two independent approaches to Kirchhoff's law. *Isis*, 1976, v. 67(4), 565–600.
12. Robitaille P. M. L. A critical analysis of universality and Kirchhoff's law: a return to Stewart's law of thermal emission. *Prog. in Phys.*, 2008, v. 3, 30–35; arXiv: 0805.1625.
13. Quinn T. J. and Martin J. E. Cryogenic radiometry, prospects for further improvements in accuracy. *Metrologia*, 1991, v. 28, 155–161.
14. Sakuma F. and Hattori S. A practical-type fixed point blackbody furnace. *Temperature and Its Measurement and Control in Science and Industry*, 1982, v. 5, part 1, 535–539.

15. Murphy A. V., Tsai B. K., Saunders R. D. Comparative calibration of heat flux sensors in two blackbody facilities. *J. Res. Nat. Inst. Stand. Technol.*, 1999, v. 104, 487–494.
16. Murphy A. V., Tsai B. K., Saunders R. D. Transfer calibration validation tests on a heat flux sensor in the 51 mm hightemperature blackbody. *J. Res. Nat. Inst. Stand. Technol.*, 2001, v. 106, 823–831.
17. Navarro N., Bruce S. S., Carol Johnson B., Murphy A. V, Saunders R. D. Vacuum processing techniques for development of primary standard blackbodies. *J. Res. Nat. Inst. Stand. Technol.*, 1999, v. 104, 253–259.
18. Chahine K., Ballico M., Reizes J., Madadnia J. Optimization of a graphite tube blackbody heater for a thermogage furnace. *Int. J. Thermophys.*, 2008, v. 29, 386–394.
19. Hanssen L. M., Mekhontsev S. N., Zeng J., Prokhorov A. V. Evaluation of blackbody cavity emissivity in the infrared using total integrated scatter measurements. *Int. J. Thermophys.*, 2008, v. 29, 352–369.
20. Fowler J. B. A third generation water bath based blackbody source. *J. Res. Nat. Inst. Stand. Technol.*, 1995, v. 100, 591–599.
21. Schalles M., Bernhard F. Triple-fixed-point blackbody for the calibration of radiation thermometers. *Int. J. Thermophys.*, 2007, v. 28, 2049–2058.
22. Fowler J. B., Carol Johnson B., Rice J. P., Lorenz S. R. The new cryogenic vacuum chamber and black-body source for infrared calibrations at the NIST's FARCAL facility. *Metrologia*, 1998, v. 35, 323–327.
23. Fowler J. B. An oil-bath-based 293 K to 473 K blackbody source. *J. Res. Natl. Inst. Stand. Technol.*, 1996, v. 101, 629–637.
24. Geist J. Note on the quality of freezing point blackbodies. *Applied Optics*, 1971, v. 10(9), 2188–2190.
25. Geist J. Theoretical analysis of laboratory blackbodies 1: a generalized integral equation. *Applied Optics*, 1973, v. 12(6), 1325–1330.
26. Robitaille P. M. L. On the validity of Kirchhoff's law of thermal emission. *IEEE Trans. Plasma Sci.*, 2003, v. 31(6), 1263–1267.
27. Robitaille P. M. L. An analysis of universality in blackbody radiation. *Prog. in Phys.*, 2006, v. 2, 22–23; arXiv: physics/0507007.
28. DeWitt D. P. and Nutter G. D. Theory and practice of radiation thermometry. John Wiley and Sons, New York, 1988.
29. Vollmer J. Study of the effective thermal emittance of cylindrical cavities. *J. Opt. Soc. Am.*, 1957, v. 47(10), 926–932.
30. Sparrow E. M. and Heinisch R. P. The normal emittance of circular cylindrical cavities. *Appl. Opt.*, 1970, v. 9(11), 2569–2572.
31. Bauer G. and Bischoff K. Evaluation of the emissivity of a cavity source by reflection measurements. *Appl. Opt.*, 1971, v. 10(12), 2639–2643.
32. De Vos J. C. Evaluation of the quality of a blackbody. *Physica*, 1954, v. 20, 669–689.
33. De Vos J.C. A new determination of the emissivity of tungsten ribbon. *Physica*, 1954, v. 20, 690–714.
34. Ono A., Trusty R. E., and DeWitt D. P. Experimental and theoretical study on the quality of reference blackbodies formed by lateral holes on a metallic tube. *Temperature and Its Measurement and Control in Science and Industry*, 1982, v. 5, part 1, 541–550.
35. Harris L. The optical properties of metal blacks and carbon blacks. MIT and The Eppley Foundation for Research, Monograph Ser., 1, New Port, R.I., Dec. 1967.
36. Harris L., McGuiness R. T., Siegel B. M. The preparation and optical properties of gold black. *J. Opt. Soc. Am.*, 1948, v. 38, 582.
37. Paschen F. Ueber das Strahlungsgesetz des schwarzen Körpers. *Ann. Phys.*, 1901, v. 4, 277-298; Paschen F. On the distribution of energy in the spectrum of the black body at high temperatures. *Astrophys. J.*, 1900, v. 11, 288–306.
38. Lummer O. and Pringsheim E. Kritisches zur schwarzen Strahlung. *Annalen der Physik*, 1901, v. 6, 192–210.
39. Rubens H. and Kurlbaum F. Anwendung der Methode der Reststrahlen zur Prüfung der Strahlungsgesetzes. *Annalen der Physik*, 1901, v. 2, 649–666.
40. Rousseau B., Sin A., Odier P., Weiss F., Echegut P. Black body coating by spray pyrolysis. *Journal de Physique*, 2001, v. 91, Pr11.277–Pr11.281.
41. Rousseau B. Chabin M., Echegut P., Sin A., Weiss F., and Odier P. High emissivity of a rough Pr_2NiO_4 coating. *Appl. Phys. Lett.*, 2001, v. 79(22), 3633–3635.
42. Buckley H. On the radiation from the inside of a circular cylinder. *Phil. Mag.*, Ser. 7, 1927, v. 4(23), 753-762.
43. Sparrow E. M., Albers L. U., and Eckert E. R. G. Thermal radiation characteristics of cylindrical enclosures. *J. Heat Trans.*, 1962, v. 84C, 73–79.
44. Lin S. H., Sparrow E. M. Radiant interchange among curved specularly reflecting surfaces — application to cylindrical and conical cavities. *J. Heat Trans.*, 1965, v. 87C, 299–307.
45. Treuenfels E. W. Emissivity of isothermal cavities. *J. Opt. Soc. Am.*, 1963, v. 53(10), 1162–1171.
46. Sparrow E. M. and Jonsson V. K. Radiation emission characteristics of diffuse conical cavities. *J. Opt. Soc. Am.*, 1963, v. 53(7), 816–821.
47. Chandos R. J. and Chandos R. E. Radiometric properties of isothermal, diffuse wall cavity sources. *Appl. Opt.*, 1974, v. 13(9), 2142–2152.
48. Peavy B. A. A note on the numerical evaluation of thermal radiation characteristics of diffuse cylindrical and conical cavities. *J. Res. Nat. Bur. Stand. — C* (*Eng. and Instr.*), 1966, v. 70C(2), 139–147.
49. Langley S. P. The invisible solar and lunar spectrum. *Am. J. Science*, 1888, v. 36(216), 397–410.
50. Gray D. F. The observation and analysis of stellar photospheres. 2nd edition, Cambridge University Press, Cambridge, U.K., 1992, p. 101.
51. Kreith F. Principles of heat transfer. Harper & Row Publishers, New York, 1973, p. 228.
52. Rytov S. M. A theory of electrical fluctuations and thermal radiation. USSR Academy of Sciences, Moscow, 1953.

53. Rytov S. M, Kravtsov Y. A., Tatarskii V. I., Principles of statistical radiophysics, v. 3. Springer Verlag, Berlin, 1978.
54. Klyshko D. N. Photons and nonlinear optics. Gordon and Breach Scientific Publishers, New York, 1988.
55. Apresyan L. A. and Kravtsov Y. A., Radiation transfer: statistical and wave aspects. Gordon and Breach Publishers, Australia, 1996.
56. Richter F., Florian M., Henneberger K. Generalized radiation law for excited media in a nonequilibrium steady state. *Phys. Rev. B*, 2008, 205114.
57. Linsky J. L. and Mount G. H. On the validity of a generalized Kirchhoff's law for a nonisothermal scattering and absorptive medium. *Icarus*, 1972, v. 17, 193–197.
58. Robitaille P. M. L., Abduljalil A.M., Kangarlu A., Zhang X., Yu Y., Burgess R., Bair S., Noa P., Yang L., Zhu H., Palmer B., Jiang Z.,Chakeres D.M., and Spigos D. Human magnetic resonance imaging at eight tesla. *NMR Biomed.*, 1998, v. 11, 263–265.
59. Robitaille P. M. L. and Berliner L.J. Ultra high field magnetic resonance imaging. Springer, New York, 2006.
60. Robitaille P. M. L. Black-body and transverse electromagnetic (TEM) resonators operating at 340 MHz: volume RF coils for UHFMRI. *J. Comp. Assist. Tomogr.*, 1999, v. 23, 879–890.
61. Pozar D. M. Microwave engineering. John Wiley and Sons, New York, 1998.
62. Argence E. Theory of waveguides and cavity resonators. Hart Pub. Co., Oxford, 1968.
63. Roschmann P. K. High-frequency coil system for a magnetic resonance imaging apparatus. US Patent, 1988, no. 4,746,866.
64. Vaughn J. T., Hetherington H., Otu J., Pan J., Pohost G. High frequency volume coils for clinical NMR imaging and spectroscopy. *Magn. Reson. Med.*, 1994, v. 32, 206–218.
65. Kelley F. J. On Kirchhoff's law and its generalized application to absorption and emission by cavities. *J. Res. Nat. Bur. Stand. B* — (*Math. Math. Phys.*), 1965, v. 69B(3), 165–171.
66. Einstein A. The collected papers of Albert Einstein, v. 5. The Swiss years: Correspondence 1902–1914. Princeton University Press, Princeton, N.J., 1995, p. 105.
67. Einstein A. Strahlungs-emission und absorption nach der quantentheorie. *Verhandlunger der Deutschen Physikalischen Gesellschaft*, 1916, v. 18, 318–323; Einstein A. *Phys. Zs.*, 1917, v. 18, 121 (English translation by ter Haar D.: Einstein A. On the quantum theory of radiation. The old quantum theory, Pergamon Press, 1967, 167–183).
68. Robitaille P. M. L. Comment to the NRC committee on condensed matter and material physics. January 20, 2005. http://www7.nationalacademies.org/bpa/CMMP2010_Robitaille.pdf

Blackbody Radiation and the Loss of Universality: Implications for Planck's Formulation and Boltzman's Constant

Pierre-Marie Robitaille

Department of Radiology, The Ohio State University, 395 W. 12th Ave, Suite 302, Columbus, Ohio 43210, USA

E-mail: robitaille.1@osu.edu

Through the reevaluation of Kirchhoff's law (Robitaille P. M. L. *IEEE Trans. Plasma Sci.*, 2003, v. 31(6), 1263–1267), Planck's blackbody equation (Planck M. *Ann. der Physik*, 1901, v. 4, 553–356) loses its universal significance and becomes restricted to perfect absorbers. Consequently, the proper application of Planck's radiation law involves the study of solid opaque objects, typically made from graphite, soot, and carbon black. The extension of this equation to other materials may yield apparent temperatures, which do not have any physical meaning relative to the usual temperature scales. Real temperatures are exclusively obtained from objects which are known solids, or which are enclosed within, or in equilibrium with, a perfect absorber. For this reason, the currently accepted temperature of the microwave background must be viewed as an apparent temperature. Rectifying this situation, while respecting real temperatures, involves a reexamination of Boltzman's constant. In so doing, the latter is deprived of its universal nature and, in fact, acts as a temperature dependent variable. In its revised form, Planck's equation becomes temperature insensitive near 300 K, when applied to the microwave background.

With the formulation of his law of thermal emission [1], Planck brought to science a long sought physical order. Though individual materials varied widely in their radiative behaviors, Kirchhoff's law of thermal emission [2, 3] had enabled him to advance dramatic simplifications in an otherwise chaotic world [1]. Given thermal equilibrium and enclosure, the blackbody cavity seemed to impart upon nature a universal property, far removed from the confusion prevailing outside its walls [4]. Universality produced conceptual order and brought rapid and dramatic progress in mathematical physics.

In his "Theory of Heat Radiation" [4], Planck outlines the prize: the existence of the universal constants, h and k. Moreover, he is able to introduce natural units of length, mass, time, and temperature [4; §164]. He writes: "*In contrast with this it might be of interest to note that, with the aid of the two constants h and k which appear in the universal law of radiation, we have the means of establishing units of length, mass, time, and temperature, which are independent of special bodies or substances, which necessarily retain their significance for all time and for all environments, terrestrial and human or otherwise, and which may, therefore, be described as 'natural units'*" [4; §164]. Planck then presents the values of the four fundamental constants [4; §164]:

Planck's constant $h = 6.415 \times 10^{-27}$ g cm^2/sec,

Boltzman's constant $k = 1.34 \times 10^{-16}$ g cm^2/sec^2 degree,

the speed of light $c = 3.10 \times 10^{10}$ cm/sec,

the gravitational constant $f = 6.685 \times 10^{-8}$ cm^3/g sec^2.

Finally, he reveals basic units of:

$$\text{length} \quad \sqrt{fh/c^3} = 3.99 \times 10^{-33} \text{ cm},$$

$$\text{mass} \quad \sqrt{ch/f} = 5.37 \times 10^{-5} \text{ g},$$

$$\text{time} \quad \sqrt{fh/c^5} = 1.33 \times 10^{-43} \text{ s},$$

$$\text{temperature} \quad \frac{1}{k}\sqrt{c^5 h/f} = 3.60 \times 10^{32} \text{ degree}.$$

Planck continues: "*These quantities retain their natural significance as long as the law of gravitation and that of the propagation of light in a vacuum and the two principles of thermodynamics remain valid; they therefore must be found always the same, when measured by the most widely differing intelligences according to the most widely differing methods*" [4; §164].

The real triumph of Planck's equation [1] rested not solely on solving the blackbody problem, but rather on the universal nature of h and k. The four fundamental units of scale for time, length, mass, and temperature profoundly altered physics. It is in this light, that concern over any fundamental change in Kirchhoff's law [2, 3] and Planck's equation [1] must be viewed.

The notion that the microwave background [5] is being produced directly by the oceans of the Earth [6–9], brings with it an immediate realization that universality is lost, and Kirchhoff's law is invalid [10–14]. Blackbody radiation is not a universal process [10–14], as Planck so adamantly advocated [4]. Yet, if the microwave background truly arises from oceanic emissions [5–8], then it is not simple to reconcile a temperature at ∼3 K with a source known to have a physical temperature of ∼300 K [10]. Let us examine more closely the problem at hand, by considering Planck's formulation (1):

$$\frac{\varepsilon_\upsilon}{\alpha_\upsilon} = \frac{2h\upsilon^3}{c^2} \frac{1}{e^{h\upsilon/kT} - 1}. \qquad (1)$$

In order to properly fit the microwave background using this equation, the problem rests in the kT term. It is possible, for instance, to make that assumption that an apparent temperature exists [10] and to keep the meaning of Boltzman's constant. In fact, this was the course of action initially proposed [10]. In this way, nothing was lost from the universal nature of h and k [10]. But, upon further consideration, it is clear that such an approach removes all physical meaning from temperature itself. The one alternative is to alter Boltzman's constant directly, and accept the full consequences of the loss of universality. The issue involves a fundamental understanding of how energy is distributed within matter. For the microwave background, this must focus on water [8].

Thus, let us consider a very primitive description of how energy enters, or becomes distributed, within water [8]. Water possesses many degrees of freedom and must be viewed as a complex system. At low temperatures, some of the first degrees of freedom to be fully occupied will be associated with the weak intermolecular hydrogen bond ($H_2O \cdots HOH$) [8]. These involve both stretching and bending processes, resulting in several vibrational-rotational modes. The hydrogen bond ($H_2O \cdots HOH$) has been advanced as responsible for the microwave background [8], particularly as a result of its predicted bond strength. As energy continues to enter the water system, it will start to populate other degrees of freedom, including those associated with the direct translation and rotation of individual molecules. This is in sharp contrast to graphite, for instance, because the latter never undergoes a solid-liquid phase transition [15]. Eventually, other degrees of freedom, associated with the vibrational and bending modes of the intramolecular hydroxyl bonds (H–OH) themselves, will become increasingly populated. Hydrogen bonds ($H_2O \cdots HOH$) have bond strengths which are on the order of 100 times lower than hydroxyl bonds (H–OH) [8]. Considering these complexities, it is unreasonable to believe that energy will enter the water system in a manner which ignores the existence of these degrees of freedom, particularly those associated with the liquid state.

Contrary to what Kirchhoff and Planck require for universality [1–3], these complex issues extend throughout nature. Each material is unique relative to the degrees of freedom it has available as a function of temperature [15]. Water possesses two distinct oscillators, the intermolecular hydrogen bond ($H_2O \cdots HOH$) and the intramolecular hydroxyl bond (H–OH) [7]. These two oscillatory systems have very distinct energies [8] and provide a situation which is quite removed from graphite. Kirchhoff and Planck had no means of anticipating such complexity. In fact, they were relatively unaware of the tremendous atomic variability found at the level of the lattice. As such, it is somewhat understandable that they might seek universal solutions.

In any case, it has been amply demonstrated that Kirchhoff's law is not valid [10–14]. There can be no universality. In addition, it is extremely likely that the microwave background is being produced by thermal photons emitted directly from the oceanic surface and then scattered in the Earth's atmosphere [6]. This implies that a ~300 K source is able to behave, at least over a region of the electromagnetic spectrum, as a ~3 K source. However, since the oceans are not at ~3 K, an inconsistency has been revealed in the determination of temperatures using the laws of thermal emission. The problem stems from the weakness of the hydrogen bond and the associated ease with which water enters the liquid state. Furthermore, it is evident that energy can enter the water system and be directed into its translational degrees of freedom, thereby becoming unavailable for thermal emission. This is a significant problem, which Kirchhoff and Planck did not need to consider, and of which they were unaware, when treating graphite boxes [1–4, 10]. Graphite, unlike water, cannot support convection.

In any event, the central issue remains that a ~3 K temperature has been obtained from a ~300 K source. As mentioned above, it is possible to essentially ignore the consequences of this finding by simply treating the microwave background as an apparent temperature [10], devoid of physical meaning. In this way, Planck's equation and the universal constants, survive quite nicely [10]. Conversely, if one refuses to abandon the real temperature scale, then a problem arises. In order to properly fit the microwave background with Planck's equation and a real temperature at ~300 K, then Boltzman's constant must change. In fact, it must become a temperature dependent variable, $k'(T)$. This variable must behave such that when it is multiplied by a range of temperatures near 300 K, it results in a perfectly constant value independent of temperature ($k'(T) \cdot T = P$, where P is a constant). Planck's equation thereby becomes completely insensitive to temperature fluctuations over the temperature and frequency ranges of interest, as seen in Eq. (2):

$$\frac{\varepsilon_\upsilon}{\alpha_\upsilon} = \frac{2h\upsilon^3}{c^2} \frac{1}{e^{h\upsilon/P} - 1} . \qquad (2)$$

As a result, relative to the microwave background, we move from a universal constant, k, to a temperature sensitive variable, $k'(T)$, which acts to render Planck's equation temperature insensitive. The modern value of the constant, P, for the microwave background, is approximately 3.762×10^{-16} ergs. The move away from graphite, into another Planckian system, has resulted in a profound re-evaluation of the science of thermodynamics. Boltzman's constant, therefore, remains valid only for graphite, soot, or carbon black, and those materials approaching their performance at a given frequency. Outside a certain range of temperatures, or frequencies, or materials, then other constants and/or variables, which are material specific, exist. The measure of how much energy a system can hold at a given temperature, or how temperature changes as a function of energy, is directly determined by the makeup of the system itself. The flow of heat within a system depends on all of the degrees of freedom which eventually

become available [15]. In this regard, phase transitions bring with them additional degrees of freedom, either translational or rotational, which are simply not available to the solid state [15]. Herein is found the central reason for the loss of universality: phase transitions exist. Nothing is universal, since phase transitions and any available degrees of freedom [15] are strictly dependent on the nature of matter. Hence, each material must be treated on its own accord. This is the primary lesson of the water/microwave background findings.

Physics cannot maintain a proper understanding of temperature without abandoning the universal attributes of Boltzman's constant. Otherwise, the temperature scale itself loses meaning. In order to specifically address the microwave background, Boltzman's constant, in fact, can become a temperature dependent variable. At the same time, since many materials contain covalent bonds with bond strengths near those found within graphite, it is likely that many material specific constants will, in fact, approach Boltzman's. Nonetheless, relative to the microwave background, a temperature dependent variable exists which acts to completely remove all temperature sensitivity from Planck's equation at earthly temperatures. This explains why Penzias and Wilson [5] first reported that the microwave background was devoid of seasonal variations.

As regards to Planck's constant, and the fundamental units of time, mass, and length, they appear to remain unaltered by the findings prompted by the microwave background. Perhaps they will be able to retain their universal meaning. However, a careful analysis of individual physical processes is in order, such that the consequences of the loss of universality can be fully understood.

Dedication

This work is dedicated to my wife, Patricia Anne, and to our sons, Jacob, Christophe, and Luc.

Submitted on May 28, 2009 / Accepted on June 02, 2008
First published online on June 20, 2009

References

1. Kirchhoff G. Über den Zusammenhang zwischen Emission und Absorption von Licht und Wärme. *Monatsberichte der Akademie der Wissenschaften zu Berlin*, sessions of Dec. 1859, 1860, 783–787.
2. Kirchhoff G. Über das Verhältnis zwischen dem Emissionsverögen und dem Absorptionsvermögen. der Körper für Wärme und Licht. *Poggendorfs Annalen der Physik und Chemie*, 1860, v. 109, 275–301. (English translation by F. Guthrie: Kirchhoff G. On the relation between the radiating and the absorbing powers of different bodies for light and heat. *Phil. Mag.*, 1860, ser. 4, v. 20, 1–21).
3. Planck M. Über das Gesetz der Energieverteilung im Normalspektrum. *Annalen der Physik*, 1901, v. 4, 553–563. (English translation by ter Haar D.: Planck M. On the theory of the energy distribution law in the normal spectrum. The old quantum theory. Pergamon Press, 1967, 82–90; also Planck's December 14, 1900 lecture Zur Theorie des Gesetzes der Energieverteilung in Normalspectrum, which stems from this paper, can be found in either German, or English, in: Kangro H. Classic papers in physics: Planck's original papers in quantum physics. Taylor & Francis, London, 1972, 6–14 or 38–45).
4. Planck M. The theory of heat radiation. P. Blakiston's Son & Co., Philadelphia, PA, 1914.
5. Penzias A. A. and Wilson R. W. A measurement of excess antenna temperature at 4080 Mc/s. *Astrophys. J.*, 1965, v. 1, 419–421.
6. Robitaille P. M. L. The Earth microwave background (EMB), atmospheric scattering and the generation of isotropy. *Progr. in Phys.*, 2008, v. 2, L7–L8.
7. Rabounski D. The relativistic effect of the deviation between the CMB temperatures obtained by the COBE satellite. *Progr. in Phys.*, 2007, v. 1, 24–26.
8. Robitaille P. M. L. Water, hydrogen bonding, and the microwave background. *Prog. in Phys.*, 2009, v. 2, L5–L7.
9. Rabounski D. and Borissova L. On the earthly origin of the Penzias-Wilson microwave background. *Prog. in Phys.*, 2009, v. 2, L1–L4.
10. Robitaille P. M. L. Blackbody radiation and the carbon particle. *Prog. in Phys.*, 2008, v. 3, 36–55.
11. Robitaille P. M. L. On the validity of Kirchhoff's law of thermal emission. *IEEE Trans. Plasma Sci.*, 2003, v. 31(6), 1263–1267.
12. Robitaille P. M. L. An analysis of universality in blackbody radiation. *Prog. in Phys.*, 2006, v. 2, 22–23; arXiv: physics/0507007.
13. Robitaille P. M. L. A critical analysis of universality and Kirchhoff's law: a return to Stewart's law of thermal emission. Prog. in Phys. 2008, v. 3, 30–35; arXiv: 0805.1625.
14. Robitaille P. M. L. Kirchhoff's law of thermal emission: 150 years. *Prog. in Phys.*, 2009, v. 4, 3–13.
15. Robitaille P. M. L. The little heat engine: Heat transfer in solids, liquids, and gases. *Prog. in Phys.*, 2007, v. 4, 25–33.

COBE: A Radiological Analysis

Pierre-Marie Robitaille

Department of Radiology, The Ohio State University, 395 W. 12th Ave, Suite 302, Columbus, Ohio 43210, USA

E-mail: robitaille.1@osu.edu

The COBE Far Infrared Absolute Spectrophotometer (FIRAS) operated from ∼30 to ∼3,000 GHz (1–95 cm^{-1}) and monitored, from polar orbit (∼900 km), the ∼3 K microwave background. Data released from FIRAS has been met with nearly universal admiration. However, a thorough review of the literature reveals significant problems with this instrument. FIRAS was designed to function as a differential radiometer, wherein the sky signal could be nulled by the reference horn, Ical. The null point occurred at an Ical temperature of 2.759 K. This was 34 mK above the reported sky temperature, 2.725±0.001 K, a value where the null should ideally have formed. In addition, an 18 mK error existed between the thermometers in Ical, along with a drift in temperature of ∼3 mK. A 5 mK error could be attributed to Xcal; while a 4 mK error was found in the frequency scale. A direct treatment of all these systematic errors would lead to a ∼64 mK error bar in the microwave background temperature. The FIRAS team reported ∼1 mK, despite the presence of such systematic errors. But a 1 mK error does not properly reflect the experimental state of this spectrophotometer. In the end, all errors were essentially transferred into the calibration files, giving the appearance of better performance than actually obtained. The use of calibration procedures resulted in calculated Ical emissivities exceeding 1.3 at the higher frequencies, whereas an emissivity of 1 constitutes the theoretical limit. While data from 30–60 GHz was once presented, these critical points are later dropped, without appropriate discussion, presumably because they reflect too much microwave power. Data obtained while the Earth was directly illuminating the sky antenna, was also discarded. From 300–660 GHz, initial FIRAS data had systematically growing residuals as frequencies increased. This suggested that the signal was falling too quickly in the Wien region of the spectrum. In later data releases, the residual errors no longer displayed such trends, as the systematic variations had now been absorbed in the calibration files. The FIRAS team also cited insufficient bolometer sensitivity, primarily attributed to detector noise, from 600–3,000 GHz. The FIRAS optical transfer function demonstrates that the instrument was not optimally functional beyond 1,200 GHz. The FIRAS team did not adequately characterize the FIRAS horn. Established practical antenna techniques strongly suggest that such a device cannot operate correctly over the frequency range proposed. Insufficient measurements were conducted on the ground to document antenna gain and field patterns as a full function of frequency and thereby determine performance. The effects of signal diffraction into FIRAS, while considering the Sun/Earth/RF shield, were neither measured nor appropriately computed. Attempts to establish antenna side lobe performance in space, at 1,500 GHz, are well outside the frequency range of interest for the microwave background (<600 GHz). Neglecting to fully evaluate FIRAS prior to the mission, the FIRAS team attempts to do so, on the ground, in highly limited fashion, with a duplicate Xcal, nearly 10 years after launch. All of these findings indicate that the satellite was not sufficiently tested and could be detecting signals from our planet. Diffraction of earthly signals into the FIRAS horn could explain the spectral frequency dependence first observed by the FIRAS team: namely, too much signal in the Jeans-Rayleigh region and not enough in the Wien region. Despite popular belief to the contrary, COBE has not proven that the microwave background originates from the universe and represents the remnants of creation.

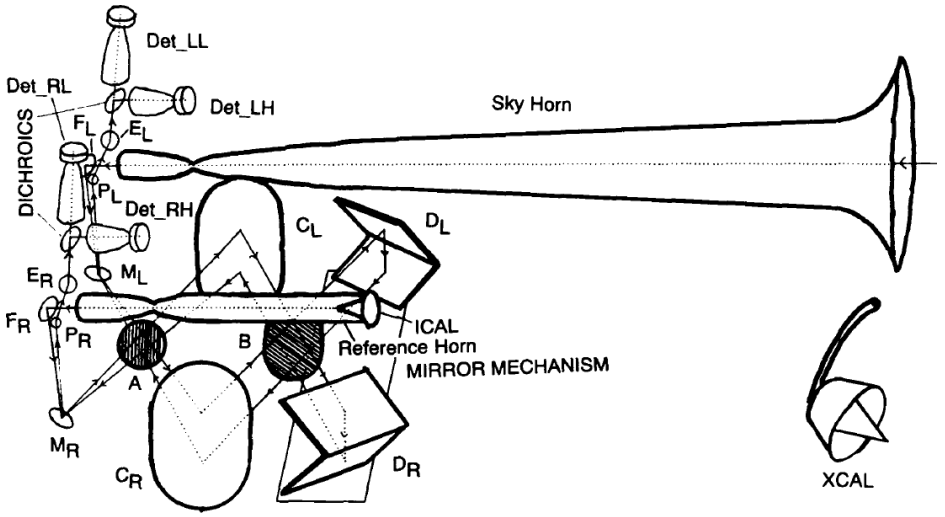

Fig. 1: Schematic representation of the COBE FIRAS instrument reproduced from [38]. The spectrometer is based on an interferometer design wherein the signal from the sky horn is being compared with that provided by the reference horn. Each of the input signals is split by grid polarizers, reflected by mirrors, and sent down the arms of the interferometer. Two output ports receive the resultant signal. An internal calibrator, Ical, equipped with two germanium resistance thermometers (GRT), provides signal to the reference horn. During calibration, the external calibrator, Xcal, is inserted into the sky horn. Xcal is monitored by three GRTs. The interferometer assembly includes a single mirror transport mechanism (MTM). Specific details can be found in [38]. No knowledge about the functioning of FIRAS, beyond that contained in this figure legend, is required to follow this work. The central elements are simply that FIRAS is made up of a sky horn, a reference horn, Ical (2 thermometers), and Xcal (3 thermometers). Reproduced by permission of the AAS.

1 Introduction

Conceding that the microwave background [1] must arise from the cosmos [2], scientists have dismissed the idea that the Earth itself could be responsible for this signal [3–7]. Most realize that the astrophysical claims are based on the laws of thermal emission [8–12]. Yet, few have ever personally delved into the basis of these laws [13–17]. At the same time, it is known that two satellites, namely COBE [18] and WMAP [19], support the cosmological interpretation [2]. As such, it seems impossible that an alternative explanation of the findings could ever prevail.

In late 2006, I prepared a detailed review of WMAP which uncovered many of the shortcomings of this instrument [20]. A range of issues were reported, including: 1) the inability to properly address the galactic foreground, 2) dynamic range issues, 3) a lack of signal to noise, 4) poor contrast, 5) yearly variability, and 6) unjustified changes in processing coefficients from year to year. In fact, WMAP brought only sparse information to the scientific community, related to the dipole and to point sources.

Nonetheless, the COBE satellite, launched in 1989, continues to stand without challenge in providing empirical proof that the microwave background did come from the universe. If COBE appears immune to criticism, it is simply because scientists outside the cosmological community have not taken the necessary steps to carefully analyze its results. Such an analysis of COBE, and specifically the Far Infrared Absolute Spectrophotometer, FIRAS, is provided in the pages which follow. Significant problems exist with FIRAS. If anything, this instrument provides tangential evidence for an earthly source, but the data was discounted. A brief discussion of the Differential Microwave Radiometers, DMR, outlines that the anisotropy maps, and the multipoles which describe them, are likely to represent a signal processing artifact.

1.1 The microwave background

When the results of the Cosmic Background Explorer (COBE) were first announced, Stephen Hawking stated that this "*was the scientific discovery of the century, if not of all time*" [21, book cover], [22, p. 236]. The Differential Microwave Radiometers (DMR) were said to have detected "*wrinkles in time*", the small anisotropies overlaid on the fabric of a nearly isotropic, or uniform, microwave background [21]. As for the COBE Far Infrared Absolute Spectrophotometer, FIRAS (see Figure 1), it had seemingly produced the most perfect blackbody spectrum ever recorded [23–45]. The blackbody curve deviated from ideality by less than 3.4×10^{-8} ergs cm^{-2} s^{-1} sr^{-1} cm [35] from $\sim$60–600 GHz. Eventually, the FIRAS team would publish that the "*rms deviations are less than 50 parts per million of the peak of the cosmic microwave background radiation*" [39]. As seen in Figure 2, the signal was so powerful that the error bars in its detection would form but a slight portion of the line used to draw the spectrum [39]. For its part, the Differential Microwave Radiometers (DMR), beyond the discovery of the anisotropies [21], had also confirmed the motion of the Earth through the

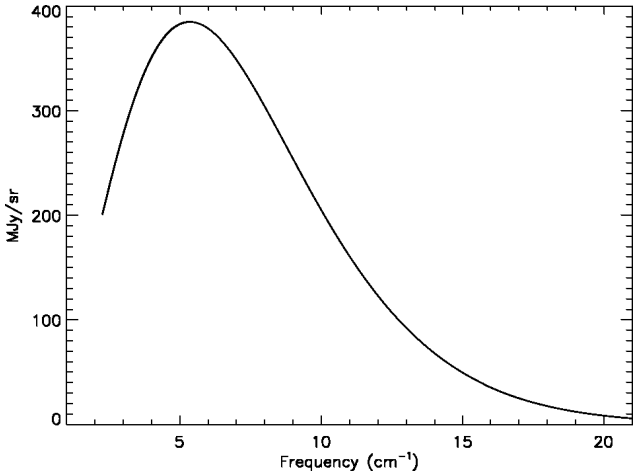

Fig. 2: Spectrum of the microwave background reproduced from [39]. This figure is well known for the claim that the error bars it contains are but a small fraction of the line width used to draw the spectrum. While this curve appears to represent a blackbody, it should be recalled that FIRAS is only sensitive to the difference between the sky and Xcal. This plot therefore reflects that the signal from the sky, after extensive calibration, is indistinguishable from that provided by Xcal. Since the latter is presumed to be a perfect blackbody, then such a spectrum is achieved for the sky. Note that the frequency axis is offset and all data below 2 cm^{-1} have been excluded. Reproduced by permission of the AAS.

local group, as established by a microwave dipole [46–49].

Over one thousand professional works have now appeared which directly utilize, or build upon, the COBE results [22, p. 247]. Yet, sparse concern can be found relative to any given aspect of the COBE project. Eventually, George Smoot and John Mather, the principle investigators for the DMR and FIRAS projects, would come to share the 2006 Nobel Prize in physics. Less than 30 years had elapsed since Arno Penzias and Robert Wilson received the same honor, in 1978, for the discovery of the $\sim$3 K microwave background [1].

Before the background was officially reported in the literature [1], the origin of the signal had already been advanced by Dicke et al. [2]. The interpretive paper [2] had immediately preceded the publication of the seminal discovery [1]. If the microwave background was thermal in origin [8–12], it implied a source at $\sim$3 K. Surely, such a signal could not come from the Earth. For the next 40 years, astrophysics would remain undaunted in the pursuit of the spectrum, thought to have stemmed from the dawn of creation. Smoot writes: "*Penzias and Wilson's discovery of the cosmic microwave background radiation was a fatal blow to the steady state theory*" [21, p. 86]. The steady state theory of the universe [50, 51] was almost immediately abandoned and astrophysics adopted Lemaître's concept of the primordial atom [52], later known as the Big Bang. Cosmologists advanced that mankind knew the average temperature of the entire universe. Thanks to COBE, cosmology was thought to have become a precision science [53, 54].

Throughout the detection history of the microwave background, it remained puzzling that the Earth itself never provided interference with the measurements. Water, after all, acts as a powerful absorber of microwave radiation. This is well understood, both at sea aboard submarines, and at home, within microwave ovens. As such, it seemed unlikely that the surface of our planet was microwave silent in every CMB experiment which preceded COBE. The only interference appeared to come from the atmosphere [55–57]. The latter was recognized as a powerful emitter of microwave radiation. The presence of water absorption/emission lines and of the water continuum, within the atmosphere, was well documented [55–57]. Nonetheless, emission from the Earth itself was overlooked.

The microwave signal is isotropic [1], while the Earth is anisotropic. The Earth experiences a broad range of real temperatures, which vary according to location and season. Yet, the background is found to be independent of seasonal variation [1]. The signal is definitely thermal in origin [9–17]. Most importantly, it is completely free from earthly contamination. The background appears to monitor a source temperature near $\sim$3 K. Earthly temperatures average $\sim$300 K and seldom fall below $\sim$200 K, even at the poles. It seems impossible that the Earth could constitute the source of this signal [3–7]. Everything can be reconsidered, only if the temperature associated with the microwave background signature is not real. Namely, that the source temperature is much higher than the temperature reported by the photons it emits. Insight in this regard can be gained by returning to the laws of thermal emission [8–12], as I have outlined [13–17].

1.2 Kirchhoff's law

One hundred and fifty years have now passed, since Kirchhoff first advanced the law upon which the validity of the microwave background temperature rests [9]. His law of thermal emission stated that radiation, at equilibrium with the walls of an enclosure, was always black, or normal [9, 10]. This was true in a manner independent of the nature of the enclosure. Kirchhoff's law was so powerful that it would become the foundation of contemporary astrophysics. By applying this formulation, the surface temperatures of all the stars could be evaluated, with the same ease as measuring the temperature of a brick-lined oven. Planck would later derive the functional form of blackbody radiation, the right-hand side of Kirchhoff's law, and thereby introduce the quantum of action [10]. However, since blackbody radiation only required enclosure and was independent of the nature of the walls, Planck did not link this process to a specific physical cause [13–17]. For astrophysics, this meant that any object could produce a blackbody spectrum. All that was required was mathematics and the invocation of thermal equilibrium. Even the requirement for enclosure was soon discarded. Processes occurring far out of equilibrium, such as the radiation of a star, and the alleged

expansion of the universe, were thought to be suitable candidates for the application of the laws of thermal emission [2]. To aggravate the situation, Kirchhoff had erred in his claim of universality [13–17]. In actuality, blackbody radiation was not universal. It was limited to an idealized case which, at the time, was best represented by graphite, soot, or carbon black [13–17]. Nothing on Earth has been able to generate the elusive blackbody over the entire frequency range and for all temperatures. Silver enclosures could never produce blackbody spectra. Kirchhoff's quest for universality was futile [13–17]. The correct application of the laws of thermal emission [8–12] requires the solid state. Applications of the laws to other states of matter, including liquids, gases, stars, and primordial atoms, constitute unjustified extensions of experimental realities and theoretical truths [13–17].

Since the source of the microwave background [1] could not possibly satisfy Kirchhoff's requirement for an enclosure [9], its $\sim$3 K temperature might only be apparent [13–17]. The temperature of the source could be very different than the temperature derived from its spectrum. Planck, indeed, advanced the same idea relative to using the laws of thermal emission to measure the surface temperature of the Sun. He wrote: "*Now the apparent temperature of the sun is obviously nothing but the temperature of the solar rays, depending entirely on the nature of the rays, and hence a property of the rays and not a property of the sun itself. Therefore it would be, not only more convenient, but also more correct, to apply this notation directly, instead of speaking of a fictitious temperature of the sun, which can be made to have a meaning only by the introduction of an assumption that does not hold in reality*" [58, §101]. Without a known enclosure, spectra appearing Planckian in nature do not necessarily have a direct link to the actual temperature of the source. The Sun operates far out of thermal equilibrium by every measure, as is evident by the powerful convection currents on its surface [59]. Furthermore, because it is not enclosed within a perfect absorber, its true surface temperature cannot be derived from the laws of thermal emission [59]. These facts may resemble the points to which Planck alludes.

1.3 The oceans of the Earth

The COBE team treats the Earth as a blackbody source of emission at $\sim$280 K [48]. Such a generalization seems plausible at first, particularly in the near infrared, as revealed by the remote sensing studies [60, 61]. However, FIRAS is making measurements in the microwave and far-infrared regions of the spectrum. It is precisely in this region that these assumptions fail. Furthermore, the FIRAS team is neglecting the fact that 70% of the planet is covered with water. Water is far from acting as a blackbody, either in the infrared or in the microwave. Using remote sensing, it has been well established that rainfall causes a pronounced drop in terrestrial brightness temperatures in a manner which is proportional to the rate of precipitation. In the microwave region, large bodies of water, like the oceans, display brightness temperatures which vary from a few Kelvin to $\sim$300 K, as a function of angle of observation, frequency, and polarization (see Figure 11.45 in [62]). Since the oceans are not enclosed, their thermal emission profiles do not necessarily correspond to their true temperatures. The oceans of the Earth, like the Sun, sustain powerful convection currents. Constantly striving for equilibrium, the oceans also fail to meet the requirements for being treated as a blackbody [13–17].

In order to understand how the oceans emit thermal radiation, it is important to consider the structure of water itself [6]. An individual water molecule is made up of two hydroxyl bonds, linking a lone oxygen atom with two adjacent hydrogens (H$-$O$-$H). These are rather strong bonds, with force constants of $\sim 8.45 \times 10^5$ dyn/cm [6]. In the gas phase, it is known that the hydroxyl bonds emit in the infrared region. The O$-$H stretch can thus be found near 3,700 cm^{-1}, while the bending mode occurs near 1,700 cm^{-1} [63]. In the condensed state, liquid water displays corresponding emission bands, near 3,400 cm^{-1} and 1,644 cm^{-1} [63, p. 220]. The most notable change is that the O$-$H stretching mode is displaced to lower frequencies [63]. This happens because water molecules, in the condensed state (liquid or solid), can interact weakly with one another, forming hydrogen bonds [63]. The force constant for the hydrogen bond ($H_2O \cdots HOH$) has been determined in the water dimer to be on the order of $\sim 0.108 \times 10^5$ dyn/cm [6, 64, 65]. But, in the condensed state, a study of rearrangement energetics points to an even lower value for the hydrogen bond force constant [66]. In any event, water, through the action of the hydrogen bond, should be emitting in the microwave and far-IR regions [6, 63]. Yet, this emission has never been detected. Perhaps, the oceanic emission from hydrogen bonds has just been mistaken for a cosmic source [2].

1.4 Ever-present water

1.4.1 Ground-based measurements

From the days of Penzias and Wilson [1], ground-based measurements of the microwave background have involved a correction for atmospheric water contributions (see [56] for an in-depth review). By measuring the emission of the sky at several angles (at least two), a correction for atmospheric components was possible. Further confidence in such procedures could be provided through the modeling of theoretical atmospheres [55, 56]. Overall, ground-based measurements were difficult to execute and corrections for atmospheric contributions could overwhelm the measurement of interest, particularly as higher frequencies were examined. The emission from atmospheric water was easy to measure, as Smoot recalls in the "parking lot testing" of a radiometer at Berkeley: "*An invisible patch of water vapor drifted overhead; the scanner showed a rise in temperature. Good: this meant the*

instrument was working, because water vapor was a source of stray radiation" [21, p. 132].

The difficulty in obtaining quality measurements at high frequencies was directly associated with the presence of the water continuum, whose amplitude displays powerful frequency dependence [55, 56]. As a result, experiments were typically moved to locations where atmospheric water was minimized. Antarctica, with its relatively low atmospheric humidity, became a preferred monitoring location [55]. The same was true for mountain tops, places like Mauna Kea and Kitt Peak [55]. Many ground-based measurements were made from White Mountain in California, at an elevation of 3800 m [55]. But, there was one circumstance which should have given cosmologists cause for concern: measurements located near the oceans or a large body of water. These were amongst the simplest of all to perform. Weiss writes: "*Temperature, pressure, and constituent inhomogeneities occur and in fact are the largest source of random noise in ground-based experiments. However, they do not contribute systematic errors unless the particular observing site is anisotropic in a gross manner — because of a large lake or the ocean in the direction of the zenith scan, for example. The atmospheric and CBR contributions are separable in this case without further measurement or modeling*" [67, p. 500]. Surely, it might be of some importance that atmospheric contributions are always a significant problem which is only minimized when large bodies of condensed water are in the immediate scan direction.

The interesting interplay between atmospheric emissions and liquid surfaces is brought to light, but in a negative fashion, in the book by Mather [22]. In describing British work in the Canary Islands, Mather writes: "*Their job was unusually difficult because Atlantic weather creates patterns in the air that can produce signals similar to cosmic fluctuations. It took the English scientists years to eliminate this atmospheric noise...*" [22, p. 246–247]. As such, astronomers recognized that the Earth was able to alter their measurements in a substantial manner. Nonetheless, the possibility that condensed water itself was responsible for the microwave background continued to be overlooked.

1.4.2 U2 planes, rockets, and balloons

As previously outlined, the presence of water vapor in the lower atmosphere makes all measurements near the Wien maximum of the microwave background extremely difficult, if not impossible, from the ground. In order to gain more elevation, astrophysicists carried their instruments skywards using U2 airplanes, rockets, and balloons [21, 22]. All too often, these measurements reported elevated microwave background temperatures. The classic example is given by the Berkeley-Nagoya experiments, just before the launch of COBE [68]. Reflecting on these experiments, Mather writes: "*A greater shock to the COBE science team, especially to me since I was in charge of the FIRAS instrument, was an announcement made in early 1987 by a Japanese-American team headed by Paul Richards, my old mentor and friend at Berkeley, and Toshio Matsumoto of Nagoya University. The Berkeley-Nagoya group had launched from the Japanese island of Kyushu a small sounding rocket carrying a spectrometer some 200 miles high. During the few minutes it was able to generate data, the instrument measured the cosmic background radiation at six wavelengths between 0.1 millimeter and 1 millimeter. The results were quite disquieting, to say the least: that the spectrum of the cosmic microwave background showed an excess intensity as great as 10 percent at certain wavelengths, creating a noticeable bump in the blackbody curve. The cosmological community buzzed with alarm*" [22, p. 206]. The results of the Berkeley-Nagoya group were soon replaced by those from COBE. The origin of the strange "bump" on the blackbody curve was never identified. However, condensation of water directly into the Berkeley-Nagoya instrument was likely to have caused the interference. In contrast, the COBE satellite was able to operate in orbit, where any condensed water could be slowly degassed into the vacuum of space. COBE did not have to deal with the complications of direct water condensation and Mather could write in savoring the COBE findings: "*Rich and Ed recognized at once that the Berkeley-Nagoya results had been wrong*" [22, p. 216]. Nonetheless, the Berkeley-Nagoya experiments had provided a vital clue to the astrophysical community.

Water seemed to be constantly interferring with microwave experiments. At the very least, it greatly increased the complexity of studies performed near the Earth. For instance, prior to flying a balloon in Peru, Smoot reports: "*It is much more humid in the tropics, and as the plane descended from the cold upper air into Lima, the chilly equipment condensed the humidity into water. As a result, water collected into the small, sensitive wave guides that connect the differential microwave radiometer's horns to the receiver. We had to take the receiver apart and dry it... Our equipment had dried, so we reassembled it and tested it: it worked*" [21, p. 151].

Still, little attention has been shown in dissecting the underlying cause of these complications [6]. Drying scientific equipment was considered to be an adequate solution to address this issue. Alternatively, scientists simply tried to protect their antenna from condensation and added small monitoring devices to detect its presence. Woody makes this apparent, relative to his experiments with Mather: "*On the ground and during the ascent, the antenna is protected from atmospheric condensation by two removable windows at the top of the horn... At the same time, a small glass mirror allows us to check for atmospheric condensation in the antenna by taking photographs looking down the throat of the horn and cone*" [69, p. 16]. Indeed, monitoring condensation has become common place in detecting the microwave background using balloons. Here is a recent excerpt from the 2006 flight of the ARCADE 2 balloon: "*A video camera mounted*

on the spreader bar above the dewar allows direct imaging of the cold optics in flight. Two banks of light-emitting diodes provide the necessary illumination. The camera and lights can be commanded on and off, and we do not use data for science analysis from times when they are on" [70]. They continue: "*The potential problem with a cold open aperture is condensation from the atmosphere. Condensation on the optics will reflect microwave radiation adding to the radiometric temperature observed by the instrument in an unknown way. In the course of an ARCADE 2 observing flight, the aperture plate and external calibrator are maintained at cryogenic temperatures and exposed open to the sky for over four hours. Figure 12 shows time averaged video camera images of the dewar aperture taken two hours apart during the 2006 flight. No condensation is visible in the 3 GHz horn aperture despite the absence of any window between the horn and the atmosphere. It is seen that the efflux of cold boiloff helium gas from the dewar is sufficient to reduce condensation in the horn aperture to below visibly detectable levels*" [70].

The fact that condensation is not visible does not imply that it is not present. Microscopic films of condensation could very well appear in the horn, in a manner undetectable by the camera. In this regard, claims of strong galactic microwave bursts, reported by ARCADE 2 [70, 71] and brought to the attention of the public [72], must be viewed with caution. This is especially true, since it can be deduced from the previous discussion, that the camera was not functional during this short term burst. In any event, it is somewhat improbable that an object like the galaxy would produce bursts on such a short time scale. Condensation near the instrument is a much more likely scenario, given the experimental realities of the observations.

It remains puzzling that greater attention is not placed on understanding why water is a source of problems for microwave measurements. Singal et al. [70], for instance, believe that condensed water is a good reflector of microwave radiation. In contrast, our naval experiences, with signal transmission by submarines, document that water is an extremely powerful absorber of microwave radiation. Therefore, it must be a good emitter [8–12].

It is interesting to study how the Earth and water were treated as possible sources of error relative to the microwave background. As a direct precursor to the COBE FIRAS horn, it is most appropriate to examine the Woody-Mather instrument [69, 73]. Woody provides a detailed error analysis, associated with the Mather/Woody interferometer-based spectrometer [69]. This includes virtually every possible source of instrument error. Both Mather and Woody view earthshine as originating from a $\sim$300 K blackbody source. They appear to properly model molecular species in the atmosphere (H_2O, O_2, ozone, etc...), but present no discussion of the expected thermal emission profile of water in the condensed state on Earth. Woody [69, p. 99] and Mather [73, p. 121] do attempt to understand the response of their antenna to the Earth. Woody places an upper limit on earthshine [69, p. 104] by applying a power law continuum to model the problem. In this case, the Earth is modeled as if it could only produce 300 K photons. Such a treatment generates an error correction which grows with increasing frequency. Woody reaches the conclusion that, since the residuals on his fits for the microwave background are relatively small, even when earthshine is not considered, then its effect cannot be very significant [69, p. 105]. It could be argued that continental emission is being modeled. Yet, the function selected to represent earthly effects overtly dismisses that the planet itself could be producing the background. The oceans are never discussed.

Though Mather was aware that the water dimer exists in the atmosphere [73, p. 54], he did not extend this knowledge to the behavior of water in the condensed state. The potential importance of the hydrogen bond to the production of the microwave background was not considered [73]. At the same time, Mather realized that condensation of water into his antenna created problems. He wrote: "*The effect of air condensing into the antenna were seen...*" [73, p. 140]. He added: "*When the second window was opened, the valve which controls the gas flow should have been rotated so that all the gas was forced out through the cone and horn. When this situation was corrected, emissions from the horn were reduced as cold helium has cooled the surfaces on which the air had condensed, and the signal returned to its normal level*" [73, p. 140–141]. Mather does try to understand the effect of diffraction for this antenna [73, p. 112–121]. However, the treatment did not model any objects beyond the horn itself.

Relative to experiments with balloons, U2 airplanes, and rockets, the literature is replete with complications from water condensation. Despite this fact, water itself continues to be ignored as the underlying source of the microwave background. It is in this light that the COBE project was launched.

1.4.3 The central question

In studying the microwave background, several important conclusions have been reached as previously mentioned. First, the background is almost perfectly isotropic: it has essentially the same intensity, independent of observation angle [1]. Second, the background is not affected by seasonal variations on Earth [1]. Third, the signal is of thermal origin [8–17]. Finally, the background spectrum (see Figure 2) is clean: it is free from earthly interference. Over a frequency range spanning nearly 3 orders of magnitude ($\sim$1–660 GHz), the microwave background can be measured without any contaminating effect from the Earth. The blackbody spectrum is "perfect" [39]. But, as seen above, liquid water is a powerful absorber of microwave radiation. Thus, it remains a complete mystery as to why cosmology overlooked that the surface of the Earth could not produce any interference in these measurements. The only issue of concern for astrophysics is the atmosphere [55, 56] and its well-known absorption in the mi-

crowave and infrared bands. The contention of this work is that, if the Earth's oceans cannot interfere with these measurements, it is precisely because they are the primary source of the signal.

2 COBE FIRAS

For this analysis, the discussion will be limited primarily to the FIRAS instrument. Only a brief treatment of the DMR will follow in section 3. The DIRBE instrument, since it is unrelated to the microwave background, will not be addressed.

2.1 General concerns

Beginning in the late 1980's, it appeared that NASA would utilize COBE as a much needed triumph for space exploration [22, 24]. This was understandable, given the recent Challenger explosion [22, 24]. Visibility and a sense of urgency were cast upon the FIRAS team. COBE, now unable to use a shuttle flight, was faced with a significant redesign stage [22, 24]. Mather outlined the magnitude of the task at hand: "*Every pound was crucial as the engineers struggled to cut the spacecraft's weight from 10,594 pounds to at most 5,025 pounds and its launch diameter from 15 feet to 8 feet*" [22, p. 195]. This urgency to launch was certain to have affected prelaunch testing. Mather writes: "*Getting COBE into orbit was now Goddard's No. 1 priority and one of NASA's top priorities in the absence of shuttle flights. In early 1987 NASA administrator Jim Fletcher visited Goddard and looked over the COBE hardware, then issued a press release stating that COBE was the centerpiece of the agency's recovery*" [22, p. 194–195]. Many issues surfaced. These are important to consider and have been highlighted in detail [22, chap. 14].

After the launch, polite open dissent soon arose with a senior group member. The entire premise of the current paper can be summarized in the discussions which ensued: "*Dave Wilkinson, the FIRAS team sceptic, argued effectively at numerous meetings that he did not believe that Ned*" (Wright) "*and Al*" (Kogut) "*had proven that every systematic error in the data was negligible. Dave's worry was that emissions from the earth might be shinning over and around the spacecraft's protective shield*" [22, p. 234]. As will be seen below, Wilkinson never suspected that the Earth could be emitting as a $\sim$3 K source. Nonetheless, he realized that the FIRAS horn had not been adequately modeled or tested. Despite these challenges, the FIRAS team minimized Wilkinson's unease. Not a single study examines the interaction of the COBE shield with the FIRAS horn. The earthshine issue was never explored and Wilkinson's concerns remain unanswered by the FIRAS team to this day.

2.2 Preflight testing

A review of the COBE FIRAS prelaunch data reveals that the satellite was not adequately tested on the ground. These concerns were once brought to light by Professor Wilkinson, as mentioned above. He writes: "*Another concern was the magnitude of 300 K Earth emission that diffracted over, or leaked through, COBE's ground screen. This had not been measured in preflight tests, only estimated from crude (by today's standards) calculations*" [74]. Unfortunately, Professor Wilkinson does not give any detailed outline of the question and, while there are signs of problems with the FIRAS data, the astrophysical community itself has not published a thorough analysis on this subject.

Professor Wilkinson focused on the Earth as a $\sim$300 K blackbody source, even if the established behavior of the oceans in the microwave and far-infrared suggested that the oceans were not radiating in this manner [62]. Wilkinson never advanced that the Earth could be generating a signal with an apparent temperature of $\sim$3 K. This means that the diffraction problems could potentially be much more important than he ever suspected. Mather did outline Wilkinson's concerns in his book as mentioned above [22, p. 234], but did not elaborate further on these issues.

Beyond the question of diffraction, extensive testing of FIRAS, assembled in the flight dewar, did not occur. Mather stated that each individual component of FIRAS underwent rigorous evaluation [22, chap. 14], however testing was curtailed for the fully-assembled instrument. For instance, Hagopian described optical alignment and cryogenic performance studies for FIRAS in the test dewar [29]. These studies were performed at room and liquid nitrogen temperatures and did not achieve the cryogenic values, $\sim$1.4 K, associated with FIRAS [29]. Furthermore, Hagopian explained: "*Due to schedule constraints, an abbreviated version of the alignment and test plan developed for the FIRAS test unit was adopted*" [29]. Vibration testing was examined in order to simulate, as much as possible, the potential stresses experienced by FIRAS during launch and flight. The issue centered on optical alignments: "*The instrument high frequency response is however, mainly a function of the wire grid beam splitter and polarizer and the dihedrals of the MTM. The instrument is sensitive to misalignments of these components on the order of a few arc seconds*" [29]. In these studies, a blackbody source was used at liquid nitrogen temperatures to test FIRAS performance, but not with its real bolometers in place. Instead, Golay cell IR detectors were fed through light pipes mounted on the dewar output ports. It was noted that: "*Generally, the instrument behaved as expected with respect to performance degradation and alignment change... These results indicate that the instrument was successfully flight qualified and should survive cryogenic and launch induced perturbations*" [29]. These experiments did not involve FIRAS in its final configuration within the flight dewar and did not achieve operational temperatures.

A description of the preflight tests undergone by COBE was also presented by L. J. Milam [26], Mosier [27], and Co-

ladonato et al. [28]. These accounts demonstrate how little testing COBE actually underwent prior to launch. Concern rested on thermal performance and flight readiness. There obviously were some RF tests performed on the ground. In Mather [22, p. 216], it was reported that the calibration file for Xcal had been obtained on Earth. This was the file utilized to display the first spectrum of the microwave background with FIRAS [22, p. 216]. Nonetheless, no RF tests for sensitivity, side lobe performance, or diffraction were discussed for the FIRAS instrument. Given that Fixsen et al. [38] cite work by Mather, Toral, and Hemmati [25] for the isolated horn, as a basis for establishing side lobe performance, it is clear that these tests were never conducted for the fully-assembled instrument. Since such studies were difficult to perform in the contaminating microwave environments typically found on the ground, the FIRAS team simply chose to bypass this aspect of preflight RF testing.

As a result, the scientific community believes that COBE was held to the highest of scientific standards during ground testing when, in fact, a careful analysis suggests that some compromises occurred. However, given the scientific nature of the project, the absence of available preflight RF testing reports implies that little took place. Wilkinson's previously noted statement echoes this belief [74].

2.2.1 Bolometer performance

The FIRAS bolometers were well designed, as can be gathered from the words of Serlemitsos [31]: "*The FIRAS bolometers were optimized to operate in two frequency ranges. The slow bolometers cover the range from 1 to 20 Hz (with a geometric average of 4.5 Hz), and the fast ones cover the range from 20–100 Hz (average 45 Hz).*" Serlemitsos continues: "*The NEP's for the FIRAS bolometers are* $\sim 4.5\times10^{-15}$ *W/Hz*$^{1/2}$ *at 4.5 Hz for the slow bolometers and* $\sim 1.2\times10^{-14}$ *W/Hz*$^{1/2}$ *at 45 Hz for the fast ones*" [31], where NEP stands for "noise equivalent power". The FIRAS bolometers were made from a silicon wafer "*doped with antimony and compensated with boron*" [31]. Serlemitsos also outlined the key element of construction: "*IR absorption was accomplished by coating the back side of the substrate with metallic film...*" made "*of 20 Å of chromium, 5 Å of chromium-gold mixture, and 30–35 Å of gold*" [31]. Such vaporized metal deposits, or metal blacks, were well known to give good blackbody performance in the far IR [75,76]. Thus, if problems existed with FIRAS, it was unlikely that they could be easily attributed to bolometer performance.

2.2.2 Grid polarizer performance

The FIRAS team also fully characterized the wire grid polarizer [30]. While the grids did "*not meet the initial specification*" their spectral performance did "*satisfy the overall system requirements*" [30].

2.2.3 Emissivity of Xcal and Ical

The FIRAS team essentially makes the assumption that the two calibrators, Xcal and Ical, function as blackbodies over the entire frequency band. Xcal and Ical are represented schematically in Figure 3 [38, 42]. Both were manufactured from Eccosorb CR-110 (Emerson and Cuming Microwave Products, Canton, MA, 1980 [77]), a material that does not possess ideal attenuation characteristics. For instance, CR-110 provides an attenuation of only 6 dB per centimeter of material at 18 GHz [78]. In Hemati et al. [79], the thermal properties of Eccosorb CR-110 are examined in detail over the frequency range for FIRAS. The authors conduct transmission and reflection measurements. They demonstrate that Eccosorb CR-110 has a highly frequency dependent decrease in the transmission profile, which varies by orders of magnitude from $\sim$30–3,000 GHz [79]. Hemati et al. [79] also examine normal specular reflection, which demonstrate less variation with frequency. Therefore, when absorption coefficients are calculated using the transmission equation [79], they will have frequency dependence. Consequently, Hemati et al. [79] report that the absorption coefficients for Eccosorb CR-110 vary by more than one order of magnitude over the frequency range of FIRAS.

In addition, it is possible that even these computed absorption coefficients are too high. This is because Hemati et al. [79] do not consider diffuse reflection. They justify the lack of these measurements by stating that: "*For all samples the power response was highly specular; i.e., the reflected power was very sensitive with respect to sample orientation*" [79]. As a result, any absorption coefficient which is derived from the transmission equation [79], is prone to being overestimated. It is unlikely that Eccosorb CR-110 allows no diffuse reflection of incoming radiation. Thus, Eccosorb CR-110, at these thicknesses, does not possess the absorption characteristics of a blackbody. It is only through the construction of the "trumpet mute" shaped calibrator that blackbody behavior is thought to be achieved [38].

When speaking of the calibrators, Fixsen et al. [39] state: "*The other input port receives emission from an internal reference calibrator (emissivity* ≈ 0.98*)*" and "*During calibration, the sky aperture is completely filled by the external calibrator with an emissivity greater than 0.99997, calculated and measured*" [39]. Practical experience, in the construction of laboratory blackbodies, reveals that it is extremely difficult to obtain such emissivity values over a wide frequency range. Measured emissivity values should be presented in frequency dependent fashion, not as a single value for a broad frequency range [80]. In the infrared, comparable performance is not easily achievable, even with the best materials [15, 80]. The situation is even more difficult in the far infrared and microwave.

The emissivity of the calibrators was measured, at 34 and 94 GHz, using reflection methods as described in de-

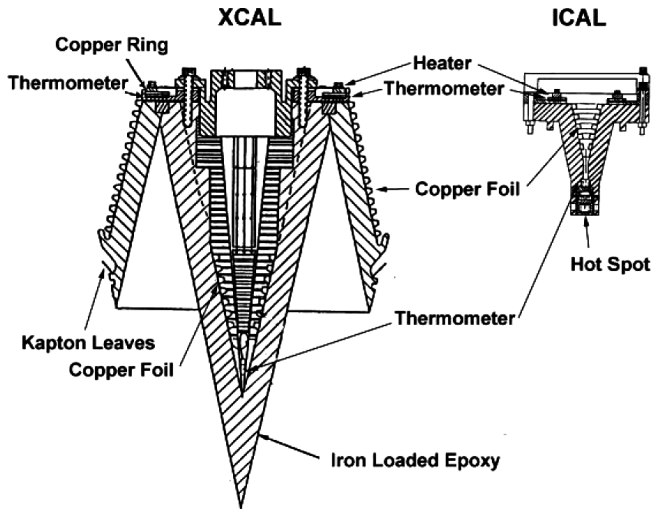

Fig. 3: Schematic representation of Xcal and Ical reproduced from [42]. Note that the calibrators are made from Eccosorb CR-110 which is backed with copper foil. Xcal, which contains three GRTs, is attached to the satellite with a movable arm allowing the calibrator to be inserted into, or removed from, the sky horn. The internal calibrator, Ical, is equipped with two GRTs and provides a signal for the reference horn. Reproduced by permission of the AAS.

tail [42]. However, these approaches are not appropriate for devices like the calibrators. In examining Figure 3, it is evident that Xcal is cast from layers of Eccosorb CR-110, backed with copper foil. For reflection methods to yield reliable results, they must address purely opaque surfaces. Eccosorb CR-110 is not opaque at these thicknesses [79] and displays significant transmission. The problem is worthy of further discussion.

In treating blackbody radiation, it is understood, from the principle of equivalence [8], that the emission of an object must be equal to its absorption at thermal and radiative equilibrium. Emission and absorption can be regarded as quantum mechanical processes. Therefore, it is most appropriate to state that, for a blackbody, or any body in radiative equilibrium, the probability of absorption, P_α, must be equal to the probability of emission, P_ε, $(P_\alpha = P_\varepsilon)$. But, given the combination of the transmittance for Eccosorb CR-110, the presence of a copper lining and the calibrator geometry, the FIRAS team has created a scenario wherein $P_\alpha \neq P_\varepsilon$. This is an interesting situation, which is permitted to exist because the copper backing on the calibrator provides a conductive path, enabling Xcal to remain at thermal equilibrium through non-radiative processes. Under these test conditions, Xcal is in thermal equilibrium, but not in radiative equilibrium. It receives incoming photons from the test signal, but can dissipate the heat, using conduction, through the copper backing. Xcal does not need to use emission to balance absorption.

If the FIRAS calibrators provide excellent reflection measurements [42], it is because of their "trumpet mute" shape and the presence of a copper back lining. Radiation incident to the device, during reflectance measurements, which is not initially absorbed, will continue to travel through the Eccosorb and strike the back of the casing. Here it will undergo normal specular reflection by the copper foil present at this location. The radiation can then re-enter the Eccosorb, where it has yet another chance of being absorbed. As a result, P_α can be effectively doubled as a consequence of this first reflection. Because of the shape of the calibrators, along with the presence of normal specular reflection on the copper, the radiation is essentially being pushed further into the calibrator where its chances of being absorbed are repeated. Consequently, P_α continues to increase with each reflection off the copper wall, or because photons are being geometrically forced to re-enter the adjacent Eccosorb wall. The situation moves in the opposite direction for P_ε and this probability therefore drops under test conditions.

Note that the copper foil has a low emissivity in this frequency range. Therefore, it is reasonable to assume that it cannot contribute much to the generation of photons. These must be generated within the Eccosorb CR-110 layers. Now, given the geometry of the "trumpet mute", there exists no means of increasing the probability of emission, P_ε. Indeed, some of the photons emitted will actually travel in the direction of the copper foil. This will lengthen their effective path out of the Eccosorb, since they exit and immediately re-enter, and increases the chance that they are absorbed before ever leaving the surface of the calibrator. Thus, P_ε experiences an effective decrease, because of the presence of the copper foil. The net result is that $P_\alpha \neq P_\varepsilon$ and the FIRAS team has not properly measured the emissivity of their calibrators using reflective methods [42]. In fact, direct measures of emissivity for these devices would demonstrate that they are not perfectly black across the frequencies of interest. Nonetheless, the devices do appear black in reflection measurements. But this is an illusion which does not imply that the calibrators are truly black when it comes to emission. Reflection measurements cannot establish the blackness of such a device relative to emission if the surface observed is not opaque. Geometry does matter in treating either emission or absorption under certain conditions. The problem is reminiscent of other logical errors relative to treating Kirchhoff's first proof for universality [16].

The FIRAS group asserts that they have verified the blackness of their calibrators with computational methods. Yet, these methods essentially "inject photons" into cavities, which otherwise might not be present [17]. Much like the improper use of detectors and reflection methods (on non-opaque surfaces), they can ensure that all cavities appear black [17]. The FIRAS calibrators are not perfectly black, but it is not clear what this implies relative to the measurements of the microwave background.

2.2.4 Leaks around Xcal

The acquisition of a blackbody spectrum from the sky is based on the performance of Xcal. For instance, Fixsen and Mather write: "*It is sometimes stated that this is the most perfect blackbody spectrum ever measured, but the measurement is actually the difference between the sky and the calibrator*" [43]. Mathematically, the process is as follows:

$$(\text{Sky} - \text{Ical}) - (\text{Xcal} - \text{Ical}) = (\text{Sky} - \text{Xcal}) .$$

Thus, Ical and all instrumental factors should ideally be negligible, contrary to what the FIRAS team experiences. Furthermore, if the calibration file with Xcal perfectly matches the sky, then a null result occurs. Since Xcal is thought to be a perfect blackbody, the derived sky spectrum is also ideal, as seen in Figure 2. It is extremely important that the calibration file, generated when Xcal is within the horn, does not contain any contamination from the sky. In the limit, should the sky dominate the calibration, a perfect blackbody shape will be recorded. This would occur because the sky is effectively compared against itself, ensuring a null.

The FIRAS team reminds us that: "*When the Xcal is in the sky horn it does not quite touch it. There is a 0.6 mm gap between the edge of the Xcal and the horn, so that the Xcal and the sky horn can be at different temperatures. Although the gap is near the flare of the horn and not in the direct line of sight of the detectors, it would result in undesirable leakage at long wavelengths because of diffraction. To ensure a good optical seal at all wavelengths, two ranks of aluminized Kapton leaves attached to the Xcal make a flexible contact with the horn*" [38] (see Figure 3). The claim that the Kapton leaves make a flexible contact with the horn, at operating temperatures, does not seem logical. The horn is operating at cryogenic temperatures ($\sim$2.7 K) and, thus, the Kapton leaves should not be considered flexible, but rather rigid, perhaps brittle. This might cause a poor contact with the horn during critical calibration events in space. The FIRAS team continues: "*An upper limit for leakage around the Xcal was determined in ground tests with a warm cryostat dome by comparing signals with the Xcal in and out of the horn. Leakage is less than 1.5×10^{-4} in the range $5 < \nu < 20$ cm^{-1} and 6.0×10^{-5} in the range $25 < \nu < 50$ cm^{-1}*" [38]. The issue of leakage around Xcal is critical to the proper functioning of FIRAS. Consequently, Mather et al. revisit the issue at length in 1999 (see section 3.5.1 in [42]). The seal does indeed appear to be good [42], but it is not certain that these particular ground tests are valid in space.

It is not clear if RF leak testing occurred while FIRAS was equipped with its specialized bolometers. As seen in section 2.2, in some preflight testing, Golay cell IR detectors had been fed through light pipes mounted on the dewar output ports. Such detectors would be unable to properly detect signals at the lowest frequencies. In fact, the FIRAS bolometers were made from metal blacks [31, 75, 76] in order to specifically provide sensitivity in the difficult low frequency range. As a result, any leak testing performed with the Golay cell IR detectors might be subject to error, since these may not have been sensitive to signal, in the region most subject to diffraction.

The FIRAS group also makes tests in flight and states: "*The Kapton levels sealing the gap between the sky horn and Xcal were tested by gradually withdrawing the Xcal from the horn. No effect could be seen in flight until it had moved 1.2 cm*" [38]. This issue is brought up, once again, by Mather et al.: "*A test was also done in flight by removing the calibrator 12 steps, or 17 mm, from the horn. Only a few interferograms were taken, but there was no sign of a change of signal level*" [42]. It is interesting that Fixsen et al. [38] claim that no effect could be seen until the horn had moved 1.2 cm. This implies that effects were seen at 1.2 cm. Conversely, Mather et al. assert that no effects were seen up to 17 mm [42]. In any case, identical results could have been obtained, even if the seal was inadequate. Perhaps this is why Fixsen et al. write: "*During calibration, the sky acts as a backdrop to the external calibrator, so residual transmission is still nearly 2.73 K radiation*" [39]. Clearly, if the seal was known to be good, there should not be any concern about "residual transmission" from the sky.

Fixsen et al. [39] rely on the sky backdrop providing a perfect blackbody spectrum behind Xcal. However, if the signal was originating from the Earth, the sky signal could be distorted as a function of frequency. This would bring error into the measurements, should the sky signal leak into the horn. From their comments, a tight seal by the Kapton leaves cannot be taken for granted. While in-flight tests, slowly removing Xcal, indicate that the spectrum changes as the calibrator was lifted out of the horn, they may not exclude that leakage exists when it is inside the horn.

It is also interesting that Mather describes significant problems with Xcal prior to launch, as follows: "*Now without gravity to help hold it in place, the calibrator popped out of the horn every time the test engineers inserted it by means of the same electronic commands they would use once COBE was in orbit. Nothing the engineers tried would keep it in place*" [22, p. 202]. In the end, the problem was caused by the flexible cable to the Xcal [22]. The cable was replaced with three thin ribbons of Kapton [22, p. 202–204]. COBE underwent one more cryogenic test, with the liquid helium dewar at 2.8 K, lasting a total of 24 days ending in June 1989 [26]. Milan's report does not provide the results of any RF testing [26], but everything must have worked. The satellite was prepared for shipment to the launch site [22, p. 202–204].

In 2002, Mather reminds us of the vibration problems with COBE: "*There were annoying vibrations at 57 and ~ 8 Hz*" [43]. On the ground, the Xcal could "pop out" of the horn if the satellite was turned on its side [22, p. 202]. Only gravity was holding Xcal in place. Still, in orbit, COBE experiences very little gravity. As such, the effects of the vi-

brations in knocking Xcal out of the horn, or in breaking the contact between the Kapton leaves and the horn, are not the same in space. A small vibration, in space, could produce a significant force against Xcal, pushing it out of the horn. Thus, all leak testing on the ground has little relevance to the situation in orbit, since both gravity and vibrations affect the Xcal position in a manner which cannot be simulated in the laboratory. The FIRAS team simply cannot be assured that Xcal did not allow leakage from the sky into the horn during calibration.

2.2.4.1 Conclusive proof for Xcal performance

When FIRAS first begins to transfer data to the Earth, a calibration file using Xcal had not been collected in space [22, p. 216]. Nonetheless, a calibration file existed which had been measured on the ground. Mather provides a wonderful account of recording the first blackbody spectrum from the microwave background [22, p. 216]. The text is so powerfully convincing that it would be easy to dismiss the search for any problems with FIRAS. Using the ground-based calibration file, the FIRAS team generates an "*absolutely perfect blackbody curve*" [22, p. 216]. However, considering all of the errors present in orbit, it is not clear how the calibration file gathered on Earth differed, if at all, from the one obtained in space. If the FIRAS team had wanted to bring forth the most concrete evidence that the situation in space, relative to Xcal, was identical to that acquired on the ground, then they could have easily displayed the difference spectrum between these two files. Ideally, no differences should be seen. But, if differences were observed, then either temperature variations, or leakage, must be assumed. In fact, the difference between the two files could have provided a clue as to the nature of the leakage into the FIRAS horn. Mather et al. feel compelled to verify the performance of Xcal on the ground 10 years after launch [42]. This suggests that the calibration files taken prior to launch did not agree with those acquired in flight.

2.2.5 Design of the FIRAS horn

In examining the FIRAS horn (see Figure 1), it is apparent that this component does not conform to accepted practices in the field of antenna design [81–83]. This device is unique, meant to operate over a phenomenal range from ∼30 to 3,000 GHz [32–45]. Since broadband horns generally span no more than 1 or 2 decades in frequency [84, 85], it is doubtful that a comparable antenna can be found in the electromagnetics literature. Even the most modern broadband horns tend to cover very limited frequency ranges and, typically, at the expense of variable gains across the band [84, 85]. Unfortunately, insufficient ground tests were conducted, to demonstrate the expected performance from 30–3,000 GHz. It is highly unlikely that FIRAS was ever able to perform as intended. The FIRAS team provides no test measurements to the contrary. These would have included gain and side lobe performances spanning the frequency spectrum. Moreover, as will be seen below (see section 2.4.3.1), FIRAS is operating less than optimally over all wavelengths. The idea of using an interferometer for these studies was elegant [32–45]. But, broadband horns with demonstrated performances, over such a range of frequencies, simply do not exist [81–85]. It is interesting in this light, that the WMAP [19] and PLANCK [86] missions have both reverted to the use of narrow band devices to sample the microwave background. As for FIRAS, it functions primarily from ∼30–600 GHz. However, even in this region, the instrument must deal with horn/shield interactions and the effects of diffraction. These effects were never appropriately considered by the FIRAS team.

The testing of the COBE FIRAS antenna pattern was inadequate. Proper tests were never performed to document the interaction of the FIRAS horn with the Sun/Earth/RFI shield. Furthermore, the team conducted no computational modeling of the horn-shield interaction as a function of frequency. This type of documentation would have been central in establishing the reliability of the FIRAS findings. Without it, the FIRAS team did not eliminate the possibility that the Earth itself is producing the microwave background. The RF shield on COBE could accomplish little more than prevent terrestrial/solar photons, in the visible or near-infrared range, from directly illuminating the dewar which contains FIRAS. The central issue for the Sun/Earth shield appears to be the conservation of helium in the dewar, not the elimination of RF interference [87]. The shield is not corrugated [81, p. 657–659] and has no special edges to prevent diffraction in the far infrared. Given that the FIRAS horn is broadband, it is extremely difficult, if not impossible, to build a good RF shield for such a device. The FIRAS team has not established that an adequate shield was constructed to prevent RF interference from the Earth. The Sun/Earth shield simply prevents direct heating of the dewar, by visible or near infrared light [87]. They comment: "*a large external conical shield protects the cryostat and instruments from direct radiation from the Sun and the Earth. The Sun never illuminates the instruments or cryostat, but the COBE orbit inclination combined with the inclination of the Earth's equator to the ecliptic do allow the Earth limb to rise a few degrees above the plane of the instrument and sunshade apertures during about one-sixth of the orbit for one-fourth of the year. During this period, the sky horn could not be cooled to 2.7 K because of the Earth limb heating*" [42]. Nowhere, in the COBE literature, is the RF performance of the "sunshade" analyzed.

2.3 FIRAS in flight

2.3.1 Side lobe performance

Fixsen et al. [38] argue that the FIRAS horn "*provides a 7° field of view with low side lobes*". They base this statement on work by Mather, Toral, and Hemmati [25]. In this paper, Mather et al. present measured and theoretical evaluations of

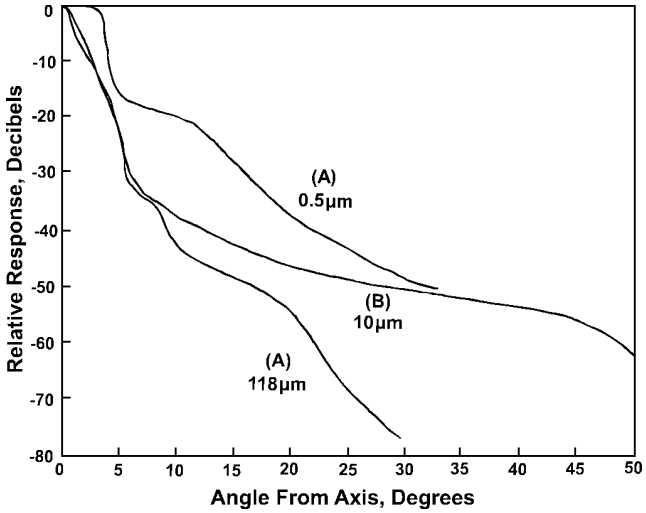

Fig. 4: Plot of the side lobe response for the FIRAS horn, without the presence of the COBE ground shield as reproduced from [25]. The sky lobe response, in preflight testing, was evaluated at three wavelengths, namely 118, 10, and 0.5 μm. Note that only the first measurement at 118 μm ($\sim$2,540 GHz) is within the frequency range of the instrument (30–3000 GHz). The latter two occur in the optical band. The side lobe performance is best at the longer wavelength, in opposition to the expected theoretical result. The FIRAS team also measures the FIRAS horn at 31.4 and 90 GHZ [25], with excellent performance (data is not reproduced herein). However, once again, these results were obtained without the interfering effects of the ground shield. Reproduced with permission of the Optical Society of America from: Mather J.C., Toral M., Hemmati H. Heat trap with flare as multimode antenna. *Appl. Optics*, 1986, v. 25(16), 2826–2830 [25].

side lobe data at 31.4 and 90 GHz [25]. As expected, the side lobes are lower at the higher frequency. The measurements conform to expected performance, at least at these frequencies. But, these tests were conducted without the RF shield and consequently have limited relevance to the actual situation in flight.

A careful examination of Figure 4 [25] is troubling. In this figure, Mather et al. [25] characterize the antenna pattern of the isolated FIRAS horn, without the COBE RF shield, at infrared and optical wavelengths (118, 10, and 0.5 μm). It is not evident why the authors present this data, as only the first wavelength, 118 μm ($\sim$2,540 GHz), is within the usable bandwidth of the instrument. Nonetheless, in Figure 4, the antenna has the strongest side lobes at the highest frequencies. For instance, at a wavelength of 0.5 μm, the antenna shows a relative response that is decreased by only 20 dB at 10° [25], as shown in Figure 4. At 118 μm, the antenna response is decreased by nearly 50 db. The authors are demonstrating that the FIRAS horn has better side lobe behavior at longer wavelengths rather than at short wavelengths. This is opposed to the expected performance. Mathematical modeling may well be impossible at these elevated frequencies. Once again, the shield was never considered.

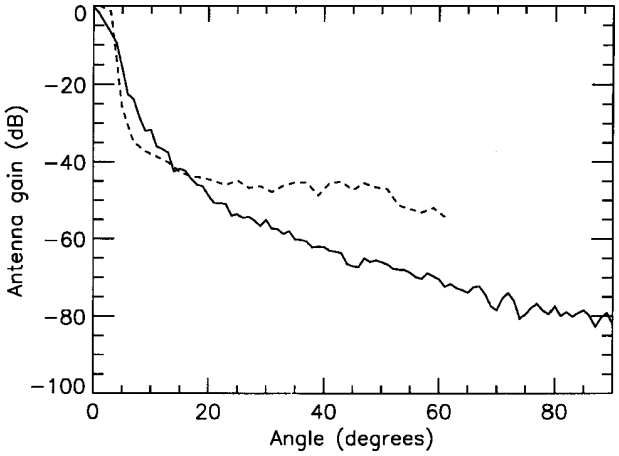

Fig. 5: Plot of the side lobe response obtained for the FIRAS shield on the ground, at 3 cm^{-1} (solid line), and in orbit, using the Moon as a source of signal, at 50 cm^{-1} (dashed line). This figure is reproduced from [38]. A detailed discussion is provided in section 2.3.1. Reproduced by permission of the AAS.

Neglecting to characterize the horn-shield interaction on the ground, the FIRAS team attempts to do so in flight. In Fixsen et al. [38], they publish Figure 5. They attempt to determine the antenna pattern in space by monitoring the Moon as a function of angle. Using this approach at 50 cm^{-1}, they conclude that the satellite provides a maximum side lobe response of "*less −38 dB beyond 15° from the center of the beam*" [38]. Such a performance is reasonable, at least at this frequency. However, the FIRAS team then compares side lobe performance at 50 cm^{-1} ($\sim$1,500 GHz) with data obtained on the ground at 3 cm^{-1} ($\sim$90 GHz). In referring to this figure in their paper, the FIRAS team writes: "*Preliminary results are shown in Figure 4, along with preflight measurements at 1 and 1.77 cm^{-1}*" [38]. Yet the figure legend itself states the following: "*Antenna pattern for the FIRAS horn as measured on the ground before launch at 3 cm^{-1} (solid line) and as measured from in flight Moon data at $\sim$50 cm^{-1} (dashed line)*" [38]. Beyond the inconsistency between the text and the figure legend, there are at least five concerns relative to this figure.

First, the data on the ground appears to have measured the FIRAS horn exclusively, not the horn with the RF shield. Second, they are comparing data at frequencies which differ by more than one order of magnitude. Third, they display none of the critical in-flight data for the lowest frequencies, namely those frequencies where one would expect the strongest effects from diffraction. Fourth, they fail to present ground data at 50 cm^{-1}. Finally, the data from Fixsen et al. [38] is also puzzling. It reveals much stronger side lobes at 50 cm^{-1} than one would have predicted at this frequency ($\sim$1,500 GHz). Note, in Figure 5, that the Moon data displays a plateau at approximately -45 dB in the range from 20–50°. This is higher than would be expected, based on the excellent side lobe response, even at a much lower 90 GHz, reported for the free

horn on the ground [25]. This plateau may simply be caused by a lack of sensitivity for the Moon at these angles. It is impossible to determine whether the plateau achieved in detection is a result of this effect. The FIRAS Explanatory Supplement suggests that the Moon can contaminate the microwave background at all frequencies [40, p. 61]. The FIRAS team does not adequately confront the issue and does not publish a work focused on side lobe behavior. Comparing ground data at ∼30 GHz, or even ∼90 GHz, with in-flight data at 1,500 GHz, has no value relative to addressing the side lobe issue.

It is also true that a loss of "Moon signal", as a function of angle, could account for the appearance of good side lobe performance. The possibility that the Moon could be reflecting terrestrial, or even solar, signals back into the FIRAS horn, through normal specular reflection, is not discussed. This process would be angle dependent and might create the illusion of reasonable side lobe behavior. The FIRAS team provides no supportive evidence from the literature that the Moon behaves as a lambertian emitter at 50 cm^{-1}. The Moon does have phases, which result in differential heating across its surface. Should the Moon not act as a lambertian emitter, the side lobe performance was not properly evaluated. This would be true, unless the satellite was rapidly turned away from the Moon while maintaining a single orbital position. But, this is unlikely to have been the case, since COBE did not have a propulsion system [22, p. 195]. Thus, the satellite was simply permitted to continue in its orbit, and the angle to the Moon thereby increased. Such a protocol might not accurately assay side lobe behavior. This is because it would depend on the absence of specular reflection from the Earth and the Sun, while requiring that the Moon is lambertian. In the end, experiments in space cannot replace systematic testing on the ground in establishing side lobe behavior.

Perhaps more troubling is that the frequencies of interest, relative to the microwave background, extend from less than 1 cm^{-1} to ∼22 cm^{-1} (<30 to ∼660 GHz). For example, the initial Penzias and Wilson measurements were made near 4 GHz [1]. Consequently, the FIRAS team is showing side lobe performance for a region outside the frequencies of interest. In fact, 1,500 GHz is the region wherein galactic dust would be sampled, not the microwave background [23]. The side lobe performance at this frequency is not relevant to the problem at hand. Furthermore, if there are problems with diffraction, they are being manifested by a distortion of signal, primarily in the lower frequency ranges. Hence, it would be critical for the FIRAS team to display in-flight data, or ground data including the shield, in order to fully document side lobe performance in this region. The data, unfortunately, is not provided.

Should access be available to the exact dimensions of the FIRAS horn and the COBE shield, it would, in principle, be possible for an independent group to verify the performance of the satellite relative to this instrument. It is true that the problem of modeling the FIRAS horn/shield interaction is extremely complex, even at 30 GHz. Nonetheless, given current computational methods, using the Geometric Theory of Diffraction, it is difficult to reconcile that the true directional sensitivity of the FIRAS horn was not modeled at any frequency. These studies would depend on obtaining the exact configuration, for the FIRAS horn/shield, and then treating the problem using computational methods. The issue cannot be treated analytically. Furthermore, this is a difficult task. It is achievable perhaps, only at the lowest frequencies of operation.

In 2002, Fixsen and Mather give a summary of the FIRAS results [43], wherein they also describe how a new instrument might be constructed. In order to address the lack of side lobe characterization, they advance that: "*we would surround the entire optical system with segmented blackbody radiators to measure the side lobe responses and ensure that the source of every photon is understood*" [43]. With COBE, the source of every photon was not understood. The side lobes were never measured in the presence of the shield. The idea of surrounding the optical system with blackbody calibrators is less than optimal. It would be best to simply analyze the horn/shield performance with preflight testing.

2.3.2 Establishing temperatures

The FIRAS team presents a dozen values for the microwave background temperature, using varying methods, as shown in Table 1. This occurs over a span of 13 years. Each time, there is a striking recalculation of error bars. In the end, the final error on the microwave background temperature drops by nearly two orders of magnitude from 60 mK to 0.65 mK. Yet, as will be seen below, in sections 2.3.3 and 2.3.4, FIRAS was unable to yield proper nulls, either with the sky and Ical, or with Xcal and Ical. Despite the subsequent existence of systematic errors, the FIRAS team minimizes error bars.

The problems with correctly establishing temperatures for Xcal and Ical were central to the mission, as these investigators recognized: "*There were two important problems. One was that the thermometers on both the Ical and Xcal did not at all agree. In fact, the disagreement among different Xcal thermometers was 3 mK at 2.7 K*" [38]. They continue: "*The disagreement between the Ical thermometers was 18 mK at 2.7 K. The heat sinking of the Ical thermometer leads was inadequate, and some of the applied heat flowed through part of the Ical*" [38].

They try to overcome the reality that the temperature monitors on the external calibrator report a systematic error. The temperature errors on Xcal are fitted with an "*arbitrary offset in the Xcal thermometer and the result was* -7.4 ± 0.2 *mK for this offset*" [38]. The FIRAS team realizes that this was "*considerably larger than the ∼1 mK expected from the preflight calibration of the thermometers*" [38]. They attribute the problem either to having improperly calibrated the thermometers before flight, or due to an unknown systematic

Reference	Temperature	Error (mK)*	Frequency (cm^{-1})
Mather et al., *ApJ*, 1990, v. 354, L37–40 [32]	2.735§	±60	1–20#
Mather et al., *ApJ*, 1994, v. 420, 439–444 [35]	2.726§	±10	2–20#
Fixsen et al., *ApJ*, 1996, v. 473, 576–587 [39]	2.730§	±1	2–21†
Fixsen et al., *ApJ*, 1996, v. 473, 576–587 [39]	2.7255¶	±0.09	2–21†
Fixsen et al., *ApJ*, 1996, v. 473, 576–587 [39]	2.717¥	±7	2–21†
Fixsen et al., *ApJ*, 1996, v. 473, 576–587 [39]	2.728**	±4	2–21†
Mather et al., *ApJ*, 1999, v. 512, 511–520 [42]	2.725§	±5	2–20‡
Mather et al., *ApJ*, 1999, v. 512, 511–520 [42]	2.7255¶	±0.085	2–21†
Mather et al., *ApJ*, 1999, v. 512, 511–520 [42]	2.722¥	±12	2–20‡
Mather et al., *ApJ*, 1999, v. 512, 511–520 [42]	2.725**	±2	2–20‡
Fixsen & Mather, *ApJ*, 2002, v. 581, 817–822 [43]	2.725	±0.65	2–20‡
Fixsen & Mather, *ApJ*, 2002, v. 581, 817–822 [43]	2.725	±1	2–20‡

* 95% confidence intervals.
§ Measurement using FIRAS microwave background lineshape. Calibration sensitive to the thermometers of the external calibrator, Xcal.
¶ Measurement using FIRAS microwave background frequency. Calibration relies on CO and C+ lines at 7.69, 11.53, 15.38, and 16.42 cm^{-1} [39].
¥ Measurement using a fit of the dipole spectrum to the 1st derivative of a Planckian function describing the microwave background with T_{cmbr} set to 2.728 K.
** Composite value obtained from analysis of three previous entries.
# Frequency range used is formally stated.
† Frequency range used is not formally stated but appears to be 2–21 cm^{-1}.
‡ Frequency range used is not formally stated but appears to be 2–20 cm^{-1}.

Table 1: Summary of microwave background temperatures obtained by the COBE FIRAS instrument.

error. They therefore assign a -4 mK offset to Xcal and raise to 5 mK its 1σ error. Though this might seem negligible, the FIRAS team is sufficiently concerned about Xcal that they attempt to recalibrate it on the ground, using a duplicate experiment, nearly ten years after launch [42]. For the present discussion, an error of at least 5 mK can be attributed to Xcal.

The FIRAS Explanatory Supplement outlines an enhanced picture relative to Ical performance [40, p. 42]. An optical temperature drift is modeled as follows:

$$T' = T + A \exp\left(t/\tau_{\mathrm{Ical}}\right) + T_{\mathrm{offset}}$$

where T' is the "raw" Ical temperature, $A = 4.26$ mK, $T_{\mathrm{offset}} = -3.054$ mK, and $\tau_{\mathrm{Ical}} = 104.3$ days [40, p. 42]. Given that FIRAS was operational for ∼259 days [40, p. 28], the drift model accounts for a 48 mK error in Ical by the time the instrument is decommissioned. Yet, in 1999, Mather et al. [42] offer a different view [40, p. 42]. While treating Ical, they write: "*An additional drift of ∼3 mK was noted in the early part of the mission*" [42]. Thus, it is likely that the equation in the supplement is simply missing a negative sign in the exponent. As a result, the ∼3 mK drift, discussed by Mather et al., can be attributed to Ical [42] along with errors of 18 mK for temperature differences between thermometers. In addition, as demonstrated in Figure 6, the emissivity modeled for Ical can exceed the theoretical upper limit of 1 over much of the FIRAS frequency range. This illustrates that the calibration model adopted by the FIRAS team contains significant shortcomings.

2.3.3 Achieving a sky null

As represented in Figure 1, FIRAS functions as a differential spectrometer, wherein the sky or the external reference, Xcal, are being constantly compared to an internal reference blackbody, Ical. When the system is functioning properly and all temperatures are equal, then a perfect null should be measured in the interferogram. This should take place whether 1) the sky is being compared to Ical set at the temperature of the sky, or 2) the external reference calibrator, Xcal, is being compared to Ical set at the same temperature.

Once COBE finally reaches orbit, the first finding is that FIRAS is unable to achieve a null when the internal reference Ical is set to the sky temperature. This is demonstrated in Figure 7 [32]. Years later, the FIRAS team discuss the situation: "*If both the sky and the Ical were blackbodies, and the interferometer were perfectly symmetrical, one could in principle null the signal from the former simply by adjusting the temperature of the latter. The temperature of the CMBR could then be read from the reference body thermometers. Unfortunately, neither of those conditions prevails*" [38]. The FIRAS team continues: "*Our Ical and instrument asymmetry com-*

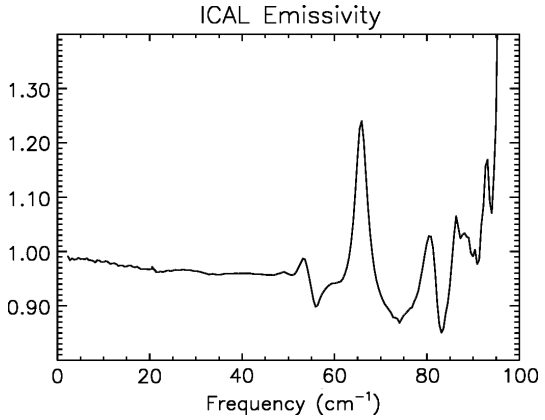

Fig. 6: Calculated emissivity for Ical as a result of calibration reproduced from the FIRAS Explanatory Supplement [40]. Note that emissivity exceeds 1, the theoretical maximum, at many frequencies. Reprinted with permission of John Mather.

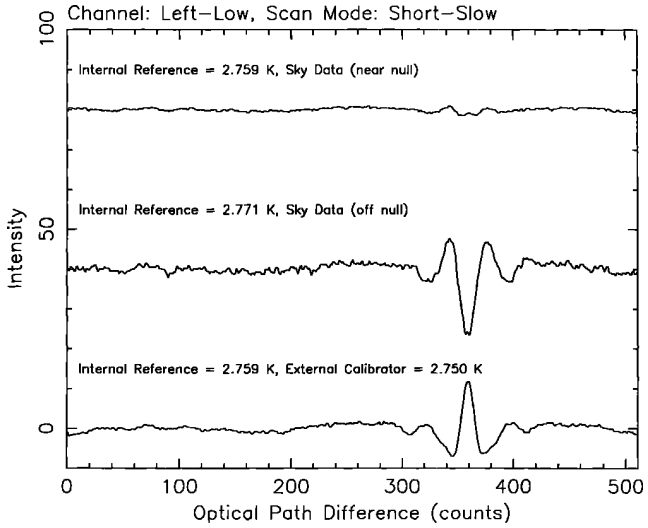

Fig. 7: Interferograms obtained in flight with the FIRAS instrument, as reproduced from [32]. The upper trace demonstrates the null condition between the sky (final reported temperature = 2.725±0.001 K [43]) and Ical set at 2.759 K. This trace is not plotted with the same vertical scaling factor as the one displayed in the central portion of the figure. Such a plot creates the illusion that a better result was achieved than actually obtained. The middle trace displays the interferogram recorded when Ical was set at 2.771 K. This indicates the magnitude of signal "off the null". The bottom interferogram was measured when comparing the two calibrators set at nearly the same temperature (Xcal = 2.759; Ical = 2.750). A null should have been obtained under these conditions, but did not occur. Once again, the vertical scale does not correspond to that used for the central trace. A correction of a factor of 3–5 should be applied to place the upper and lower interferograms on scale with the central one. This was not mentioned in the original text [32], but points to deviations from the theoretically expected results. Reproduced by permission of the AAS.

bine to produce a net reflectance of ∼4%, and Galactic emission from gas and dust contributes to the observed signal. To measure these effects, we must calibrate the instrument" [38]. Note that since the sky temperature would end up being assigned as 2.725±0.001 K [43], the upper trace in Figure 7 indicates that the null point appears with Ical at nearly 34 mK above the sky temperature (2.759–2.725 K = 34 mK). Consequently, COBE is faced with a 34 mK systematic error based on this fact. It is not clear how much of this error can be attributed to Galactic emissions. These should be primarily sensed at frequencies beyond 20 cm^{-1} [23], the cutoff of the low frequency channel [38]. As such, it is doubtful that galactic contributions can fully account for the lack of a proper null in these channels. By the end of the mission, Ical is spending most of its time near the null, at ∼2.758 K and toggling to a temperature 12 mK higher, ∼2.770 K [40, p. 28]. The FIRAS team writes: "*In addition, the temperature of Ical was toggled between a "sky null" setting to a setting 12 mK hotter, every 3–4 days, to allow instrumental gain errors to be distinguished*" [40, p. 19]. The latter is 45 mK above the temperature reported for the microwave background.

Unable to attain the expected null, the FIRAS team begins to target instrumental problems and calibration [38]. They do not envision that a null could not be achieved, because the sky was not acting as anticipated. Consider, for instance, that the Earth is producing the microwave background and that its diffracted signal is coming over the shield of the satellite. In this case, one can assume that the Earth was producing a signal with a nearly perfect Planckian [10] shape. But, at lower frequencies, the microwave background will experience more diffraction at the shield. Hence, FIRAS will be most sensitive to low frequency signals. As frequencies are increased, progressively less diffraction will occur at the shield and the FIRAS horn will become more forward directional. In so doing, it will be less sensitive to signals arising from beneath the shield. Thus, FIRAS may not sense a true Planckian curve, but a distorted spectrum displaying too much signal at the lower frequencies, and not enough signal at the higher frequencies. There may be less than the expected signal instensity along with constructive/destructive interference effects. The situation is illustrated schematically in an exaggerated fashion in Figure 8. This scenario would make it impossible to reach a null. The issue is not simply a question of temperature, but of lineshape. If two signals, arising from the sky and Ical, do not have the same lineshape, they can never be nulled. A proper null is never displayed. The underlying cause cannot be ascertained, given the nature of preflight testing, instrumental drift, and incoming signal.

In re-examining Figure 7 [32], note that the trace determining the null point is not a good null. The top trace in this figure is not plotted on the same scale as the bottom two traces, as can be deduced by examining the noise power. It needs to be multiplied by a factor of 3–5 to match the noise seen in the central trace. This gives the illusion that a better null is achieved than is actually obtained in practice. The second trace has much more noise. In fact, an analysis of noise

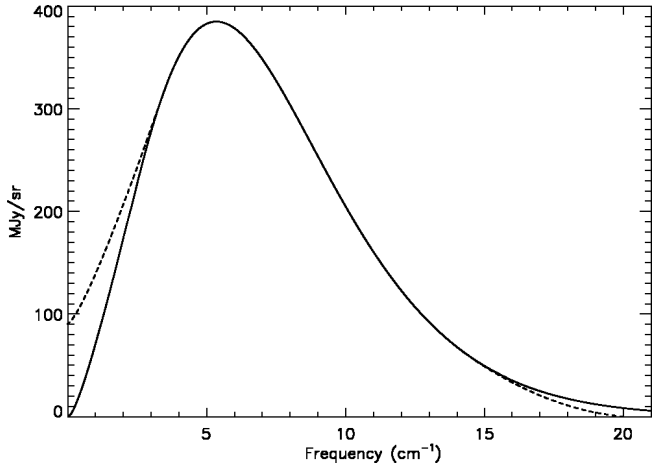

Fig. 8: Schematic representation of an ideal blackbody at 2.725 K (solid line). The dashed line is an exaggerated representation of the distortions that might occur if an earthly signal was diffracting over the FIRAS ground shield. Since diffraction might be expected to have the greatest effects at the lowest frequencies, the points in this region would be elevated. Conversely, as frequencies are increased, less diffraction should occur off the ground shield. The FIRAS horn should become more forward directional at elevated frequencies. As a result, a decreased signal might be sensed in this region. It is difficult to deduce the exact appearance of the effects from diffraction. For instance, there could actually be signs of constructive and destructive interference on the acquired spectrum. The nature of the spectrum acquired by FIRAS would also depend on the extent that the sky signal was diffracting into the FIRAS horn during calibration with Xcal, due to leakage. In the limit of severe leakage, FIRAS would report a perfect blackbody spectrum from the sky, even with diffraction occurring at the ground shield. Further details are provided in the text.

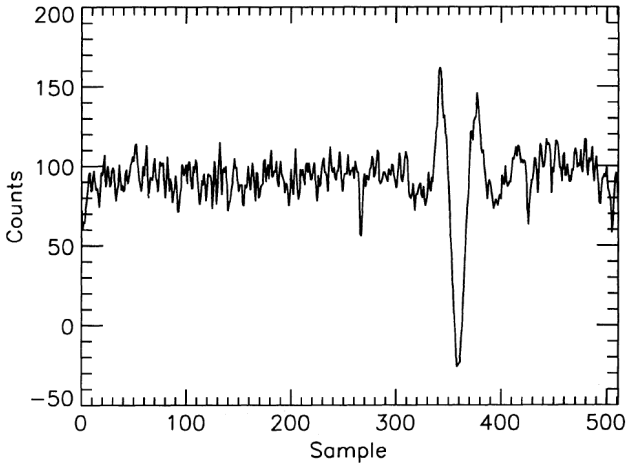

Fig. 9: FIRAS interferogram acquired between the sky and Ical, as reproduced from [38]. The signal is being generated just slightly "off the null". Apparently, the point at 355 can be perfectly nulled [38], but it is doubtful that such a result can be obtained while maintaining the null condition over all other points. The FIRAS team does not present a perfect null. A spectrum acquired "just off the null" yields little scientific information. Reproduced by permission of the AAS.

power from these traces establishes that the FIRAS team is not maintaining a constant vertical amplification. This should not have escaped the eye of the reviewers. Correct scaling factors should have been provided in the figure legend.

In any case, the null is not clean. The FIRAS team, for instance, shows a second interferogram in Fixsen et al. [38], reproduced herein as Figure 9. In the figure legend, they state that the peak at 355 can be nulled within detector noise levels. However, they fail to demonstrate the corresponding interferogram. It is certain that the point at 355 can be nulled. But, it is essential that all the points in the spectrum are simultaneously nulled. The FIRAS team has never been able to present such an interferogram. Moreover, if a proper null exists, they should not display data "just off the null". These interferograms are not useful as measures of instrument performance. The issue is not simply one of temperature match. For, if two blackbodies are brought to the same temperature, then ideally, the null must be perfect. Lineshape differences, generated by diffraction on the shield, could account for the discrepancies noted.

Unable to reach a perfect null with the sky and dismissing lineshape effects, the FIRAS team is left to implicate instrument design [38]. This is because they believe that a perfectly Planckian background must be found in the sky in front of FIRAS. The idea that an ideal blackbody spectrum, produced by the Earth, could have been distorted by diffraction over the shield, is not entertained. As a result, they cite that the Ical provides a 4% reflectance, to partially account for the lack of a proper null [38].

2.3.4 Achieving a null when $T_{\mathrm{Ical}} = T_{\mathrm{Xcal}}$

In analyzing the bottom trace in Figure 7, it is evident that a null cannot be achieved, when Xcal is set at nearly the same temperature as Ical (Xcal = 2.750 K, Ical = 2.759 K). Unfortunately, the FIRAS team does not publish a sufficient number of interferograms to enable the complete dissection of this question. On the surface, failure to locate a null, when $T_{\mathrm{Ical}} = T_{\mathrm{Xcal}}$, would support the idea that the problem was instrumental. After all, a second failure to establish a solid null is being reported. The FIRAS team might have been able to supply proof of this contention, using a combination of interferograms with Xcal and Ical at differing temperatures. As it is, no proof exists that Ical was the sole problem with FIRAS. Again, failure to attain a null, when $T_{\mathrm{Ical}} = T_{\mathrm{Xcal}}$, could also be supported by technical issues with leakage around Xcal.

It is vital to understand the exact temperatures for Xcal and Ical, when a null spectrum is achieved by the two calibrators. However, such data is not presented by the FIRAS team. Furthermore, it is not certain that they were ever able to obtain a null. In order to properly address this issue, the critical data is found in the null spectrum between Xcal and Ical on the ground. It is not known if the null imbalance was documented for FIRAS using preflight tests. The data have

not been published, but are critical to understanding the inability to reach a null between the sky and Ical, as discussed in section 2.3.3. Without it, the FIRAS team cannot defend the hypothesis that galactic contributions, for instance, were responsible for this shortcoming. It is obvious that the galaxy may not be invoked for the lack of a null between the two reference blackbodies. Therefore, for a proper evaluation of these questions, ground data, obtained between Xcal and Ical, should be provided.

2.4 Data processing

Initially, the FIRAS team publishes a spectrum from 1–21 cm^{-1} [32]. That spectrum was said to deviate from the intensity of a blackbody by less than 1%. Then, in 1994, Mather et al. [35] advance a new set of data, wherein the intensity deviates from a blackbody by less than 0.03%. The error bar in setting the absolute temperature, using Xcal, drops precipitously from 60 mK to 10 mK (see Table 1). Fixsen et al. [39], in 1996, then report that the "*rms deviations are less than 50 parts per million of the peak of the cosmic microwave background radiation*". In 1999, Mather et al. apparently again increase the rms deviation and assert that the deviation of the CMB from the theoretical blackbody is less than 0.01% [42]. Finally, in 2002, Fixsen and Mather [43] advance that "*the measured deviation from this spectrum are 50 parts per million (PPM, rms) of the peak brightness of the CMBR spectrum, within the uncertainty of the measurement*". Using technology established in the 1970's, the FIRAS team reported a spectral precision well beyond that commonly achievable today in the best radiometry laboratories of the world.

Figure 2 [39] is famous for the observation that the uncertainties are a small fraction of the line thickness. This figure is unusually drawn, as the frequency axis is offset. This makes it less apparent that data is not being shown below 2 cm^{-1}. The final result was obtained with the calibration procedures outlined by Fixsen et al. [38]. In the end, the FIRAS team transfers the error from the spectrum of interest into the calibration file, as will be discussed in detail below. Using this approach, it would be possible, in principle, to attain no deviations whatsoever from the perfect theoretical blackbody. Given enough degrees of freedom and computing power, errors begin to lose physical meaning. The calibration file became a repository for everything that did not work with FIRAS. The only problem was that it was now impossible to dissect what the FIRAS microwave background spectrum really looked like. Along these lines, the most serious concern was the omission of data, as discussed in section 2.4.3.

2.4.1 FIRAS calibration

In order to provide data for in-flight calibration, the FIRAS team controls the temperature of four key sources of emission, 1) the internal calibrator, 2) the external calibrator, 3) the sky horn, and 4) the reference horn. The emissivity of each of these devices could be modified on demand in the temperature range from 2–25 K [38]. Other parts of the instrument are approximated as Planckian functions [10], presumably because they are isothermal [38]. Cheng describes the calibration process: "*Calibration is accomplished by removing all known instrument effects from the raw spectra. This requires a model of the instrument, with all known imperfections, and sufficient calibration data to establish the model parameters. The measured instrument state for the sky data can then be used to predict the instrument characteristics based on the model which is then used to calibrate the sky data... The emissivity of various internal components in the instrument are determined by varying their temperatures while observing a constant input signal (e.g. from the external calibrator). These components include the sky horn, reference horn, internal reference load, dihedral mirrors, collimator, and the detector itself. The temperature of the first three components can be varied by command so that determining their emissivity is straightforward. The emissivity of the other components are determined by temperature variations during several cryostat temperature transients which occurred early on in the mission*" [34].

A critical aspect of the calibration procedure is that the external calibrator, Xcal, is treated as providing a perfect blackbody signal to the rest of the instrument. This approximation may not be justified, given the discussion in section 2.2.3. There are also complications, if the seal between the horn and the calibrator is not perfect, due to vibration, as addressed in section 2.2.4. The idea of approximating the thermal behavior of the dihedral mirrors, collimator, and detectors with Planck functions, as Fixsen describes [38], does not rest on solid grounds. Each material should ideally have been measured in the laboratory, as real materials do not behave as blackbody sources [80]. For instance, the FIRAS team describes harmonic responses in the instrument when radiation passes through the system more than once. This proves that the interior components of the instrument cannot be modeled as perfect blackbodies. They do provide reflective surfaces. It is noted that $\sim$20% of the input signal fails to reach the output [38]. This is a large number, which represents frequency dependent losses. However, no frequency dependence is mentioned, presumably because the loss for each interferogram cannot be dissected in these terms. Both second and third order harmonics were thought to be significant at the 0.1% level [38]. They also report that the frequency scale for FIRAS does not quite agree with that determined using known spectral lines. In order to correct the situation, they make a 0.5% adjustment with "*the remainder being absorbed by a 4 mK adjustment in the absolute temperature scale*" [38].

The discussion relative to the bolometers highlights how modeling can misrepresent the actual behavior of a device. The FIRAS team writes: "*The total of nine parameters with their uncertainties and covariance matrix were determined*

from these tests. The agreement with the determination of the parameters from the FIRAS in-orbit calibration is poor, with normalized χ^2's of 80 to 800 in various fits for 9 DOF (degrees of freedom). This is probably due to a deficit in the bolometer model" [38]. In the final analysis, the in-flight calibration procedure is viewed as correct, and the disagreement with pre-flight data appears to be disregarded. This demonstrates how the COBE calibration procedures have become essentially detached from any experimental findings recorded on the ground before flight.

The calibration process brings many more degrees of freedom for setting error bars and temperatures. Mather et al. thus write: "*However, the calibration process corrects other effects of the error to the first order...*" [42]. Calibration involves: "*comparison of the sky with an ideal movable external blackbody calibrator (Xcal) that can fill the aperture of the sky horn. The rest of the calibration process is used to measure gains and offsets that apply if the calibrator spectrum does not match the sky spectrum*" [43]. As a result, the FIRAS team can achieve a perfect fit to the sky spectrum. They have sufficient degrees of freedom to accomplish the task by invoking the calibration procedure. The inversion matrix required for the calibration fits is "*of such large rank (∼4,000)*" that it "*is not generally tractable*" [38]. The FIRAS team was "*able to invert this matrix by taking advantage of its special form... This made inversion possible, though still not speedy*" [38].

Relative to error analysis, very large degrees of freedom (DOF) were invoked. The FIRAS team writes: "*The normalized χ^2 resulting from this fit is 2.8218 (27873 DOF) for the left low detector, short slow stroke data ($2.27 < \nu < 21.54$ cm^{-1}), and 4.53 for (159353 DOF) for the right high detector, short slow stroke data ($2.27 < \nu < 96.28$ cm^{-1})*" [38]. Moreover, it can be deduced that the values are rather high for χ^2/DOF, particularly when operating away from the null position. Cheng [34] reports higher than expected χ^2/DOF values, of 4 to 10, for the low and high frequency channels when discussing the calibration data. Apparently [34], it is only when considering calibration files near the null condition that χ^2/DOF values near 1 are reached [39]. Of course, it is easier to fit data near the null, for the precise reason that the spectrum contains little power in this range. It is solely by examining the performance of the calibration model away from the null, that any real insight can be harnessed relative to the reliability of this method. However, such data appears to give even higher χ^2/DOF values than obtained near the null [34]. This is not a good sign, relative to the validity of this approach. The inability to find good χ^2/DOF values off the null might be reflecting leakage around Xcal, for instance. This could become more apparent when Xcal and Ical are at very different temperatures.

Fixsen et al. [39] do describe excellent χ^2/DOF performance in their Figure 1 (not reproduced herein). An analysis of Table 1 in [39] reveals that χ^2/DOF are generally on the order of 2 or more. Nonetheless, it is noticeable that the χ^2/DOF, listed in this work (see Table 1 in [39]), have improved substantially over those found 2 years earlier (see Table 2 in [38]). It is not clear if this represents anything but better insight into how χ^2/DOF values could be minimized. In the end, there is too much flexibility in these approaches. This places at risk all physically meaningful experimental findings, reflecting systematic errors.

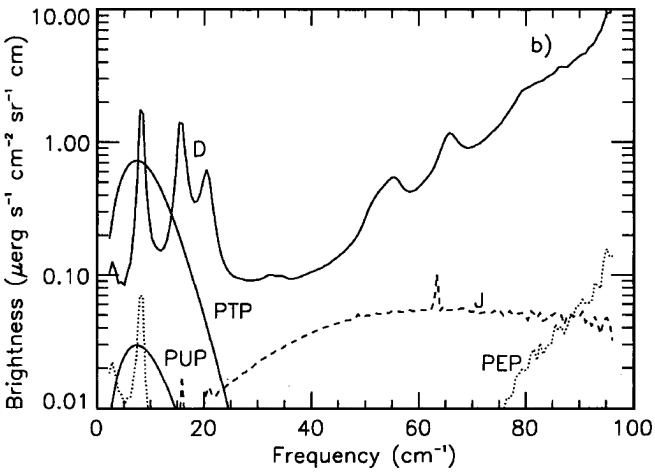

Fig. 10: Plot of various error terms for the FIRAS high frequency channel for a typical sky point, as reproduced from [38]. Separate fits are obtained for each point in the sky. This allows for far too many degrees of freedom in the FIRAS calibration stage. Curve D represents the error arising from detector sensitivity. Note the resonances at ∼7, 16, and 20 cm^{-1}. These may correspond to CO lines in the galaxy. Such resonances should not be found on functions representing detector sensitivity. They are not found in the detector functions at low frequency [38]. The dashed line, which is not labeled in the original work, represents the calculated errors from the galaxy as can be established using Figure 13. Note that there is little error contribution from the galaxy, below 20 cm^{-1}. As such, the FIRAS team cannot attribute the failure to achieve a proper null to the presence of contaminating galactic signal in this frequency region. The dotted line, PEP, accounts for error associated with various temperatures within the instrument. Once again, a resonance line is observed at ∼7 cm^{-1}. Such a resonance line should not be found on this function. It would, however, permit the FIRAS team to vary the error in this region when trying to correct for contributions from galactic CO. PTP accounts for errors in the absolute temperature scale. PUP error depends on the absolute temperature state of the instrument and is most sensitive to Ical. PUP and PTP are given a blackbody appearance without proper justification by the FIRAS team (see text for additional details). Reproduced by permission of the AAS.

A treatment by Fixsen et al. [38] of the error terms for FIRAS reveals that the FIRAS team considered nearly every possible source of instrumental contribution, while discounting the possibility that errors existed in the shape of the blackbody provided by the sky itself. Such a systematic error could exist if diffraction effects were important.

Figure 10 is a reproduction of Figure 9b in [38]. For

the low frequency channel (figure not displayed), the major term is referred to as PTP. It represents the uncertainty in the absolute temperature scale. The peak brightness of a 2.7 K blackbody is approximately 120 μergs cm^{-2} s^{-1} sr^{-1} cm [38]. As a result, this error term absorbs about 0.5% of the deviation from the peak of a blackbody. The most important error term for the high frequency channel, D, accounts for detector noise. The PUP error is linked to the temperature state of the instrument and is primarily dependent on Ical. The PEP error depends on the temperatures of various emitters in the instrument. "*These are: Ical 2.76±0.006 K, MTM 2.0±0.4 K, horns 2.75±0.005 K, mirrors 1.56±0.02 K, and bolometers 1.52±0.017 K*" [38]. The FIRAS team writes that the PEP and PUP error terms are well approximated by Planckian functions. This claim, however, is without foundation. In fact, there are no references provided for assigning a Planckian shape [10] to either PTP or PUP. Assigning such shapes to these two terms will help determine the appearance of the other terms. The entire procedure is without scientific basis [80]. It is particularly concerning that the FIRAS team generates such error functions for each point in the sky. Instrument error should not be dependent on the scan direction. At the same time, it is true that the instrument experiences temperature fluctuations over time: "*Further tests of the calibration are obtained by searching the calibrated map of the sky for features relating to changes of the instrument state. The largest such changes occurred during the time from 1990 May to August. In this time period, it was impossible to keep both the Earth and the Sun below the Sun screen, and the Earth illuminated the top of the instrument during part of the orbit. The data taken with the Earth above the instrument were rejected in the maps, but the thermal transient produced by the heat of the Earth was large and long. As a result, we raised the set point of the horn temperature controllers to as high as 6 K to achieve stability*" [38]. Direct visualization of the Earth did impact the COBE results, but the data were rejected. Yet, if the Earth was truly silent over the frequency of interest, there could be no reason to reject this data. Heating by the Earth could simply be accounted for in a manner similar to that used for other parts of the orbit. The FIRAS team believes that the heat transient in the instrument, as a consequence of direct infrared heating, was the only effect. However, it would have been most interesting to examine the resulting sky interferograms. Perhaps these actually contained direct physical proof that the Earth had emitted the microwave background.

In any case, note the nature of the error term, D, for the high frequency channels. Essentially, there are resonance lines at ∼7, ∼16, and ∼20 cm^{-1}. These features seem to correspond to the presence of the CO lines in the galaxy [39]. Such lines should not be found within detector noise error. In addition, curve D for the high frequency channels approaches 10 μergs cm^{-2} s^{-1} sr^{-1} cm, at 95 cm^{-1}. This is an extremely powerful contribution from this term, given that the maximal power of the microwave background itself is on the order of 120 μergs cm^{-2} s^{-1} sr^{-1} cm.

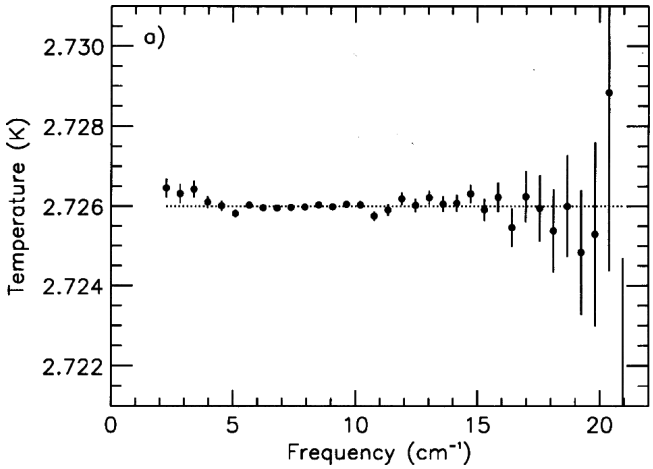

Fig. 11: Calculated residual errors in the microwave background, as reproduced from [35]. These residuals were generated, using a conservative approach, by increasing the statistical errors, forcing χ^2 to 32 [35]. Nonetheless, note the systematic increase in the residuals beyond 15 cm^{-1}. There is a slight trend towards signal loss in this region as well. In addition, the points below 5 cm^{-1}, slowly begin to rise away from the reported temperature, and represent signs of excessive signal in this region of the spectrum. The residuals are presented once again in 2001 [44]. At this time, systematic variations have been absorbed by the calibration files and the residuals are now random and of insignificant importance. Reproduced by permission of the AAS.

2.4.2 Analysis of residual errors

When Mather et al. [35] publish the 1994 FIRAS data release, several unexpected findings are revealed. Figure 1 of this work [35], a presentation of the CMBR residuals, is reproduced as Figure 11. There are two interesting aspects of this figure. First, there is a pronounced increase in the error bars associated with the residuals, as the frequencies are raised beyond 15 cm^{-1}. This increase in variability is systematic, and consequently may represent a real finding. In fact, there is a slight trend towards decreased temperatures as a function of frequency beyond 15 cm^{-1}. Second, at the lower frequencies, the data points begin to rise. The FIRAS team comments as follows: "*pending further detailed study of possible instrument faults at these low frequencies, we cannot speculate on their nature. We emphasize that the size of the apparent deviations is greatest at those frequencies where diffractive effects, interferogram baseline curvature, and very low spectral resolving power and wide spectral sidebands cause the greatest difficulties in calibration*" [35]. The authors therefore "*conservatively increase the statistical errors by a factor, forcing χ^2 to exactly 32, the number of degrees of freedom in the fit*" [35]. Nonetheless, they eventually publish

new residuals [44], which have now lost the systematic variations displayed in Figure 11. This shows the power of the fitting methods applied.

The FIRAS team believes that they fully understand all systematic errors and that their fits are justified. However, this is not the case. The fact that an excellent fit can be found, given sufficient degrees of freedom, is well recognized in science. The question remains how well justified were the bases for the fits. Adequate justification is based on a complete understanding of the instrument on the ground with calibrated test procedures. This approach was not utilized. Instead, fits are obtained by adjusting gains, offsets, and functions, which have a weak foundation, other than their ability to result in minimal residual errors for the sky. Furthermore, the FIRAS team has not shown that it can minimize residuals, using their final calibrations across all ranges of temperatures for Xcal, Ical, the sky horn, and the reference horn. Without explicit demonstration that the final calibrations apply to all possible interferograms, the analysis of residuals for the sky alone have little value. It is a complement of all residuals, for all conditions, which is important to visualize, for this alone might help establish the reliability of the approach in the absence of sufficient pre-flight testing.

2.4.3 Data omission

The FIRAS data set from 1994 contains a more serious concern: all of the observations at frequencies below 2 cm^{-1} are now excluded [35]. Moreover, there is a rise in the residuals below 4 cm^{-1} which cannot be accounted for by their error bars. This region is usually the easiest to monitor due to the low frequency range. Never again is the data below 2 cm^{-1} re-included in the FIRAS data set. It is only through reading the accompanying calibration work by Fixsen et al. [38], that one might postulate on the causes behind the loss of this data. A single sentence is presented when discussing the reference horn: "*However, the measured emission is higher than predicted, particularly at the lowest frequencies*" [38].

Though FIRAS was designed to cover the region from 1–2 cm^{-1}, the FIRAS team omits the data below 2 cm^{-1} and ignores the excessive signal. They do not discuss the cause of this anomaly, unless Wilkinson's concerns about earthshine were a reaction to this problem [74]. At the same time, given the use of calibration files to correct FIRAS, it may have been that the FIRAS team could not envision a means to account for the spectral behavior below 2 cm^{-1}. On the surface, ignoring this data might not appear so serious. After all, the entire spectrum beyond 2 cm^{-1} was reported.

Given that diffraction of a terrestrial signal would produce distortions in the measurement of the microwave background, which include excessive signal at low frequencies and decreased signal as frequencies increase, the dismissal of this data cannot be taken lightly. The FIRAS team also forsakes all data acquired when the Earth was directly illuminating FIRAS [38], as previously discussed in section 2.4.1. While infrared heating of the instrument did occur at this time, it is not evident that such heating could not be modeled. This is the type of evidence that may have pointed to an earthly source for the microwave background.

2.4.4 Error bars

Despite the presence of systematic errors, the FIRAS team is able to essentially sidestep the recordings of their thermometers and overcome their inaccuracy. E. S. Cheng summarizes the overall approach of the group: "*Since the FIRAS is a far more sensitive thermometer that the GRT's (germanium resistance thermometers), especially at temperatures above 3 K, the thermometer readings can be adjusted, using the calibration data, to provide maximal internal consistency and a refined temperature calibration*" [34]. As such, the readings of the physical thermometers could be given less weight.

Initially, it is not evident if they are aware that errors in the thermometers limit the ultimate temperature that can be reported for the microwave background. In 1996, Fixsen et al. arrive at a microwave background temperature of 2.730 ± 0.001 K (see Table 1), which relies on Xcal (see page 581, section 4.1, in [39]). Then, three years later, in 1999, the FIRAS team writes: "*A 5 mK error in the temperature determination of Xcal leads directly to a 5 mK error in the temperature determination of the CMBR*" [42]. The team apparently realized that it was impossible for Fixsen et al. [39] to claim a 1 mK error bar for this measurement in 1996. But, they continue to discount the 18 mK error between the Ical thermometers [38].

In order to fully restrict the error bars on the determination of the microwave background, the COBE group therefore moves to adopt two additional methods which, at least on the surface, are independent of Xcal. In the first instance, they determine the temperature by calibrating the frequencies of the background, using lines from CO and C+ [39]. Few details are provided relative to this approach; however, it may rely on accurately defining a Wien maximum and extracting the temperature from Wien's law [11]. The method is solid, on the surface at least. Nonetheless, it will depend on correctly setting the peak in the microwave background data, which may in turn depend on Ical and/or Xcal. The ability to detect a proper Wien maximum [11] would also be sensitive to interference effects caused by diffraction on the COBE shield, should the signal originate from the Earth. As a result, it is not clear that the frequency method holds any less systematic error than that directly relying on Xcal.

Alternatively, the group also uses the existence of a dipole to extract a monopole temperature [39]. In this way, they can build on the findings of the DMR relative to the dipole value [46–49]. Once again, the method may appear more accurate, but is also subject to many of the same problems as that based on Xcal. If the use of frequency calibration, or of

the dipole, seems less prone to systematic error, it may simply be because these have escaped detection by the FIRAS team. It is well established, not only in physics, but across the sciences, that systematic errors can be extremely difficult, even impossible, to detect [88]. Consequently, one must not dismiss those systematic errors which are evident.

Using a combination of these three methods, the FIRAS team finally arrives at a microwave background temperature of 2.725±.00065 K [43]. Beyond undetected systematic errors, this number circumvents much of the planning built into Xcal and Ical. It also neglects the excessive signal detected below 2 cm^{-1}. Relative to error bars, the result obtained, using an average of many methods, was analogous to ignoring the existence of known temperature error in the reference calibrators Xcal and Ical. The existence of imperfect nulls was also dismissed, as were all interferograms obtained while the Earth was directly illuminating FIRAS.

In the absence of proper pre-flight testing, it is impossible to account, with certainty, for all possible source of systematic errors associated with inability to find a null. Data processing methods do not address the fundamental issue. The FIRAS team believes that it has fully understood all systematic errors and that they can be removed from the final error report. But, systematic errors are best treated through the proper design and testing of scientific instruments on the ground. This was not achieved. The calibration procedure creates the illusion that all systematic error can be taken into account, after completion of data acquisition. This is not a prudent approach to systematic error, especially since they can be nearly impossible to identify [88, p. 93–95]. It is best to report all known systematic errors within the final error bar.

In failing to achieve a clear null, FIRAS is pointing to something on the order of a 34 mK error. The overall error in Xcal was ∼5 mK. The error difference between the Ical thermometers is 18 mK and the drift for Ical is 3 mK. A frequency correction of ∼4 mK exists. Some of these errors may be related and could be added quadratically [88, p. 93–95]. Direct addition provides a worse case scenario of ∼64 mK [88, p. 93–95]. As such, using direct addition, ∼64 mK appears to be a good lower limit on the accuracy of the FIRAS data set, from 2–20 cm^{-1}. This treatment would discount attempts to lower the error bar to 1 mK in the final FIRAS report [43]. In fact, ∼64 mK is not far from the 60 mK error initially used by the FIRAS team [32]. At the same time, the group asserts that their data is "*indistinguishable from a blackbody*" [37]. A cursory examination would suggest that this was the case (see Figure 2). An understanding of calibration process has provided the explanation.

2.4.5 The optical transfer function

The FIRAS team first presents the optical transfer function in the Explanatory Supplement, in 1997 [40]. This function is critical in processing FIRAS data files [40, p. 50] and it is reproduced herein as Figure 12. For an ideal spectrometer, the optical transfer function would be unity over the entire frequency range. That is, for every photon which enters the system, one photon is recorded by the detector. This situation does not occur in practice, and transfer functions will deviate from ideality. But, the transfer function for FIRAS is much less than ideal. At the lowest frequencies (<20 cm^{-1}), the transfer function contains a very strange and unexplained oscillation. The FIRAS team does not comment on the cause of this feature. Nonetheless, since the reciprocal of the transfer function is used to process data, this oscillation is significant. Although difficult to ascertain, this feature might be a sign of signal diffraction into the horn. In any event, the discontinuity near 20 cm^{-1} is due to the filter cutoff between the low and high frequency channels.

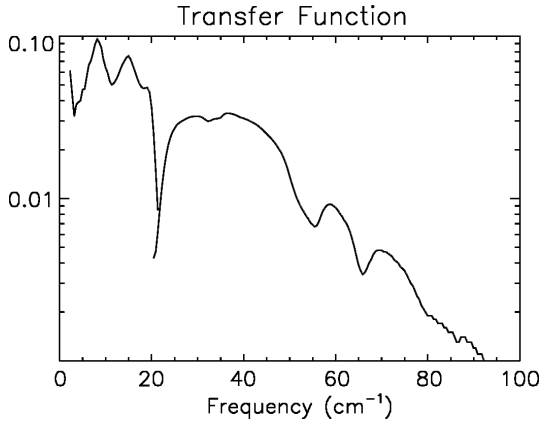

Fig. 12: Illustration of the Optical Transfer Function for FIRAS, as reproduced from the Explanatory Supplement [40]. The features near 20 cm^{-1} are due to the position of the filter cutoff. Nonetheless, this does act to provide a substantial correction for signal beyond the Wien maximum and between 15 and 20 cm^{-1}. Note the oscillation present below this frequency range. It is not clear why such features should be present on this optical transfer function. These might represent the effect of constructive and destructive interference. It is impossible to truly ascertain their cause with the data provided. Most importantly, the optical transfer function is decreasing exponentially. This is not characteristic of a properly functioning spectrophotometer. This figure reveals that the FIRAS instrument is suboptimal, beyond ∼30 cm^{-1}. Reprinted with permission of John Mather.

The most noteworthy feature of the optical transfer function for FIRAS is that only 1 photon in 10 is being detected, at best. In addition, the plot is on a logarithmic scale. Such behavior is highly unusual and demonstrates that the FIRAS instrument is not linear. It is also not sensitive at the higher frequencies. As a result, when the optical transfer function is applied to process data beyond 30 cm^{-1}, it results in a pronounced amplification of spectral noise. This is revealed in Figure 13 [41], where noise in the fits is amplified beyond 40 cm^{-1}. This constitutes a solid illustration that the FIRAS instrument, for practical purposes, is subfunctional in this frequency range.

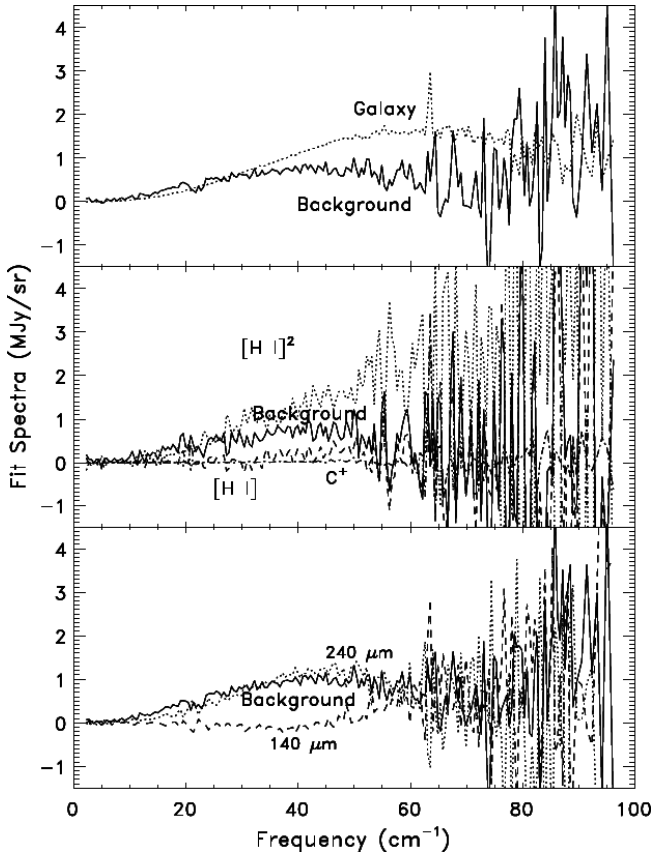

Fig. 13: Fit spectra calculated across the high frequency region using the FIRAS instrument, as reproduced from [41]. Note the tremendous increase in random errors beyond 30 cm^{-1}. This indicates that the spectrometer is suboptimal, in this frequency range. Reproduced by permission of the AAS.

2.4.6 Comments made by other authors

Several Italian authors [89–91] have been interested in the calibration of the FIRAS instrument as Fixsen and Mather highlight [42]. Giorgi, for instance, suggests that there could be an asymmetry of as much as 5% in the two input arms of FIRAS [89]. Fixsen and Mather point out that the measured asymmetry is only 1–3% [42]. In defending FIRAS data, Fixsen and Mather write: "*However, one must also consider the source of any reflection. The Xcal is part of a closed cavity composed of the calibrator, the sky horn, a small gap between the calibrator and the sky, and a small aperture leading to the spectrometer horn. Consequently, the radiation reflected by the calibrator must have originated either from itself, the sky horn, the sky through the gap, or the small aperture to the spectrometer. Three of these sources are effectively at the temperature of the CMB. As the most emissive of the four, the source of most of the reflected radiation is the calibrator itself... Moreover, since both the horn and the Xcal temperatures were set to match the CMB temperature, the only source of radiation that could be reflected by the calibrator and that was not at the CMB temperature is the small aperture leading to the spectrometer*" [42]. Such a statement cannot be justified. It is not clear that the sky is at the temperature of the CMB. Should the signal originate from the Earth, it would undergo differential diffraction as a function of frequency, as it travels over the RF shield and into the horn. This would lead to a spectrum which is not blackbody, and the measured sky spectrum would not be at the exact temperature of the microwave background. It would be distorted. Fixsen and Mather cannot assume that the sky is a blackbody at the temperature of the CMB. That is what they are trying to determine.

Work by Battistelli et al. [90] is centered on a computational analysis of Xcal, in order to further refine cosmological parameters. The text does not constitute a criticism of FIRAS. The emissivity values obtained for Xcal, are nearly ideal. Salvaterra and Burigana [91] examine a range of issues in detail, but the text does not raise any real concerns relative to FIRAS.

3 The Differential Microwave Radiometers (DMR)

The COBE satellite is also equipped with Differential Microwave Radiometers, the DMR. These constitute three pairs of narrow band antennae operating at 31.5, 53, and 90 GHz [46]. The DMR are mounted directly on the sides of the helium dewar containing the FIRAS and DIRBE instruments [45]. A detailed treatment of the DMR will not be presented, as many of the issues relative to the DMR have already been addressed relative to the WMAP satellite [20]. It is clear that the DMR has measured a dipole. This result is highly significant.

Of all the concerns which the DMR shares with WMAP, the central issue remains the processing of data and the extraction of the multipoles [20]. These are the "*wrinkles on the fabric of time*" [21]. Before the multipoles can be analyzed, the signal from both the dipole and galactic foreground must be removed. Importantly, as Smoot discusses in his popular book [21], these investigators also remove the quadrupole signal from the underlying maps. It is only at this stage that the multipoles become visible. Smoot writes: "*We were confident that the quadrupole was a real cosmic signal... By late January and early February, the results were beginning to gel, but they still did not quite make sense. I tried all kinds of different approaches, plotting data in every format I could think of, including upside down and backwards, just to try a new perspective and hoping for a breakthrough. Then I thought, why not throw out the quadrupole — the thing I'd been searching for all those years — and see if nature had put anything else there!*" [21, 276–277]. After removing the quadrupole, the multipoles finally appeared. Smoot then comments [21, 279]: "*Why, I puzzled, did I have to remove the quadrupole to see the wrinkles?*"

The answer to this question is one of data processing.

The raw maps do not contain any systematic signal variations on their own [21, 276–279]. The signals were random in nature. However, when Smoot and his colleagues imposed a systematic removal of signal, they produced a systematic remnant. In essence, the act of removing the quadrupole created the multipoles and the associated systematic anisotropy. Once the quadrupole was removed, the multipoles appeared as extremely consistent variations on the maps. As previously mentioned, these findings have no relevance to cosmology and are purely an artifact of signal processing. Citing from previous work [20]: "*Apparent anisotropy must not be generated by processing*". The sky does have anisotropy. But this anisotropy is likely to remain random, as Smoot initially observed in his data set, before removal of the quadrupole.

4 Conclusion

Through this analysis, unexpected problems with FIRAS and the DMR data have been brought to light. With regard to FIRAS, many issues exist. They include: 1) lack of gain and side lobe characterization for the FIRAS horn, 2) absence of diffraction modeling involving the interaction between FIRAS and the shield, 3) rudimentary pre-flight testing, 4) failure to document side lobe performance, in space, at frequencies relevant to the microwave background, 5) inappropriate evaluation of Xcal emissivities, 6) inability to ensure that leakage did not occur around Xcal in flight, given the vibrations present, the lack of gravity, and the nature of the Kapton leaves, 7) existence of a suboptimal transfer function for the instrument, 8) the presence of systematic errors, for the Xcal and Ical thermometers, 9) inability to achieve a proper null between the sky and Ical, 10) inability to reach a proper null between Xcal and Ical, 11) excessive degrees of freedom during the calibration process, 12) lack of justification for the error functions PTP and PUP, 13) inappropriate minimization of error bars, 14) omission of data below 2 cm^{-1} from all final data releases, and 15) omission of data when the Earth was directly illuminating FIRAS.

Given the systematic errors on Xcal, Ical, the frequency drift, and the null temperature, it is reasonable to ascertain that the FIRAS microwave background temperature has a significant error bar. As such, an error on the order of 64 mK represents a best case scenario, especially in light of the dismissal/lack of data at low frequency. The report of a microwave temperature of 2.725 ± 0.001 K [43] does not accurately reflect the extent of the problems with the FIRAS instrument. Furthermore, the absolute temperature of the microwave background will end up being higher than 2.725 K, when measured without the effect of diffraction, and when data below 2 cm^{-1} is included. Contrary to popular belief, the FIRAS instrument did not record the most perfect blackbody spectrum in the history of science.

Relative to the DMR, the problems mirror, to a large extent, those I voiced earlier with WMAP [20]. The most pressing questions are centered on the ability to remove the quadrupole from the maps of the sky. In so doing, it is clear that a systematic residual will be created, which can easily be confounded for true multipoles. In the end, the methods to process the anisotropy maps are likely to be "creating anisotropy" where none previously existed.

It also remains fascinating that the astrophysical community has not expressed greater anxiety relative to the difficulties produced by water, in the lower atmosphere. This is perhaps the most serious area of concern. It is certainly true that the Earth is bathed in a field with an apparent temperature near 3 K. The existence of the dipole is also firmly established. Cosmology holds that the monopole signal [1] represents a remnant of creation. Conversely, I maintain, along with my colleagues [5, 7], that it is being produced by the oceans of the Earth. Through this work, it is my hope that others will begin to see that there are legitimate issues with the FIRAS and DMR results on COBE. The thermal emission of water, in the microwave and far infrared, remains incompletely characterized. Our planet has never been eliminated as the source of the microwave background. In the end, the PLANCK satellite [86] should reveal that the Penzias and Wilson monopole [1] was never present in the depth of the Cosmos. The signal belongs to the Earth.

Acknowledgement

John Mather is recognized for granting permission to reproduce figures on behalf of the COBE team.

Dedication

This work is dedicated to Professor A. J. Christoforidis for the faith he demonstrated relative to my work these many years and for conferring upon me the privilege of becoming a professor of radiology.

Submitted on June 24, 2009 / Accepted on July 03, 2009
First published online on July 16, 2009

References

1. Penzias A.A. and Wilson R.W. A measurement of excess antenna temperature at 4080 Mc/s. *Astrophys. J.*, 1965, v. 1, 419–421.
2. Dicke R.H., Peebles P.J.E., Roll P.G., and Wilkinson D.T. Cosmic black-body radiation. *Astrophys. J.*, 1965, v. 1, 414–419.
3. Robitaille P.-M.L. A radically different point of view on the CMB. In: *Questions of Modern Cosmology — Galileo's Legacy*, ed. by M. D'Onofrio and C. Burigana, Springer, New York, N.Y., 2009.
4. Robitaille P.M.L. The Earth microwave background (EMB), atmospheric scattering and the generation of isotropy. *Prog. in Phys.*, 2008, v. 2, L7–L8.

5. Rabounski D. The relativistic effect of the deviation between the CMB temperatures obtained by the COBE satellite. *Prog. in Phys.*, 2007, v. 1, 24–26.
6. Robitaille P.M.L. Water, hydrogen bonding, and the microwave background. *Prog. in Phys.*, 2009, v. 2, L5–L7.
7. Rabounski D. and Borissova L. On the earthly origin of the Penzias-Wilson microwave background. *Prog. in Phys.*, 2009, v. 2, L1–L4.
8. Stewart B. An account of some experiments on radiant heat, involving an extension of Prévost's theory of exchanges. *Trans. Royal Soc. Edinburgh*, 1858, v. 22(1), 1–20 (also found in Harper's Scientific Memoirs, edited by J. S. Ames: The Laws of Radiation and Absorption: Memoirs of Prévost, Stewart, Kirchhoff, and Kirchhoff and Bunsen, translated and edited by D. B. Brace, American Book Company, New York, 1901, 21–50).
9. Kirchhoff G. Über das Verhältnis zwischen dem Emissionsvermögen und dem Absorptionsvermögen. der Körper für Wärme und Licht. Poggendorfs Annalen der Physik und Chemie, 1860, v. 109, 275–301 (English translation by F. Guthrie: Kirchhoff G. On the relation between the radiating and the absorbing powers of different bodies for light and heat. *Phil. Mag.*, 1860, ser. 4, v. 20, 1–21).
10. Planck M. Über das Gesetz der Energieverteilung im Normalspektrum. *Annalen der Physik*, 1901, v. 4, 553–563 (English translation by ter Haar D.: Planck M. On the theory of the energy distribution law in the normal spectrum. The old quantum theory. Pergamon Press, 1967, 82–90; also Planck's December 14, 1900 lecture *Zur Theorie des Gesetzes der Energieverteilung in Normalspectrum*, which stems from this paper, can be found in either German, or English, in: Kangro H. Classic papers in physics: Planck's original papers in quantum physics. Taylor & Francis, London, 1972, 6–14 or 38–45).
11. Wien W. Über die Energieverteilung in Emissionspektrum eines schwarzen Körpers. *Ann. Phys.*, 1896, v. 58, 662–669.
12. Stefan J. Über die Beziehung zwischen der Warmestrahlung und der Temperature. *Sitzungsberichte der mathematischnaturwissenschaftlichen Classe der kaiserlichen Akademie der Wissenschaften Wien*, 1879, v. 79, 391–428.
13. Robitaille P.M.L. On the validity of Kirchhoff's law of thermal emission. *IEEE Trans. Plasma Sci.*, 2003, v. 31(6), 1263–1267.
14. Robitaille P.M.L. An analysis of universality in blackbody radiation. *Prog. in Phys.*, 2006, v. 2, 22–23; arXiv: physics/0507007.
15. Robitaille P.M.L. Blackbody radiation and the carbon particle. *Prog. in Phys.*, 2008, v. 3, 36–55.
16. Robitaille P.M.L. A critical analysis of universality and Kirchhoff's law: a return to Stewart's law of thermal emission. *Prog. in Phys.*, 2008, v. 3, 30–35; arXiv: 0805.1625.
17. Robitaille P.M.L. Kirchhoff's law of thermal emission: 150 years. *Prog. in Phys.*, 2009, v. 4, 3–13.
18. COBE website, http://lambda.gsfc.nasa.gov/product/cobe
19. WMAP website, http://map.gsfc.nasa.gov
20. Robitaille P.-M.L. WMAP: A radiological analysis. *Prog. in Phys.*, 2007, v. 1, 3–18.
21. Smoot G. and Davidson K. Wrinkles in time: witness to the birth of the Universe. Harper Perennial, New York, N.Y., 1993.
22. Mather J.C. and Boslough J. The very first light. Basic Books, New York, N.Y., 1996.
23. Mather J.C. COBE-explorer of the primeval explosion. *Astronautics & Aeronautics*, 1978, v. 16, 60–66.
24. NASA. Redesign of the Cosmic Background Explorer (COBE), Academy of Program/Project & Engineering Leadership (available online through NASA).
25. Mather J.C., Toral M., Hemmati H. Heat trap with flare as multimode antenna. *Appl. Optics*, 1986, v. 25(16), 2826–2830.
26. Milan L.J. Test facility requirements for the thermal vacuum thermal balance test of the cosmic background explorer. *Journal IES*, 1991, March/April, 27–33.
27. Mosier C.L. Thermal design of the cosmic background explorer cryogenic optical assembly. *AIAA*, *Aerospace Sciences Meeting*, 29th, Reno, NV, Jan. 7–10, 1991, 1–6.
28. Coladonato R.J., Irish S.M, and Mosier C.L. Cryogenic Optical Assembly (COA) cooldown analysis for the Cosmic Background Explorer (COBE). *Third Air Force/NASA Symposium on Recent Advances in Multidisciplinary Analysis and Optimization*, 1990, 370–377.
29. Hagopian J.G. FIRAS optical alignment and performance during vibration qualification and cryogenic cycling. *Cryogenic Optical Systems and Instruments III*: Proceedings of the SPIE, 1989, v. 973, 117–131.
30. Barney R.D. and Magner T.J. FIRAS wire grid characterization techniques. *Cryogenic Optical Systems and Instruments III*: Proceedings of the SPIE, 1989, v. 973, 139–146.
31. Serlemitos A.T. Flight worthy infrared bolometers with high throughput and low NEP. *Cryogenic and Optical Systems III*: *Proceedings of the SPIE*, 1989, v. 973, 314–321.
32. Mather J.C., Cheng E.S., Eplee R.E., Isaacman R.B., Meyer S.S., Shafer R.A., Weiss R., Wright E.L., Bennett C.L., Boggess N., Dwek E., Gulkis S., Hauser M.G., Janssen M., Kelsall T., Lubin P.M., Moseley S.H., Murdock T.L., Silverberg R.F., Smoot G.F., and Wilkinson D.T. A preliminary measurement of the cosmic microwave background spectrum by the cosmic background explorer (COBE) satellite. *Astrophys. J.*, 1990, v. 354, L37–L40.
33. Mather J.C., Fixsen D.J., and Shafer R.A. Design for the COBE Far Infrared Absolute Spectrophotometer (FIRAS). *Proc. SPIE*, 1993, v. 2019, 168–179; http://lambda.gsfc.nasa.gov/data/cobe/firas/doc/FES4_APP_B.PS
34. Cheng E.S. Far-infrared cosmology measurements — the FIRAS spectrum and other curious results. *Astronomical Soc. Pac. Conf. Ser. Observational Cosmology*, 1993, v. 51, 501–511.
35. Mather J.C., Cheng E.S., Cottingham D.A., Eplee R.E., Fixsen D.J., Hewagama T., Isaacman R.B, Jensen K.A., Meyer S.S., Noerdlinger P.D., Read S.M., Rosen L.P., Shafer R.A., Wright E.L., Bennett C.L., Boggess N.W., Hauser M.G., Kelsall T., Moseley S.H., Silverberg R.F., Smoot G.F., Weiss R, and Wilkinson D.T. Measurement of the cosmic microwave background spectrum by the COBE FIRAS Instrument. *Astrophys. J.*, 1994, v. 420, 439–444.

36. Fixsen D.J.,Cheng E.S., Cottingham D.A., Eplee R.E., Isaacman R.B., Mather J.C., Meyer S.S., Noerdlinger P.D., Shafer R.A., Weiss R., Wright E.L., Bennett C.L., Boggess N.W., Kelsall T., Moseley S.H., Silverberg R.F., Smoot G.F., and Wilkinson D.T. Cosmic microwave background dipole spectrum measured by COBE FIRAS. *Astrophys. J.*, 1994, v. 420, 445–449.
37. Wright E.L., Mather J.C., Fixsen D.J., Kogut A., Shafer R.A., Bennett C.L., Boggess N.W., Cheng E.S., Silverberg R.F., Smoot G.F., and Weiss R. Interpretation of the COBE FIRAS CMBR spectrum. *Astrophys. J.*, 1994, v. 420, 450–456.
38. Fixsen D.J., Cheng E.S., Cottingham D.A., Eplee R.E., Hewagama T., Isaacman R.B, Jensen K.A., Mather J.C., Massa D.L., Meyer S.S., Noerdlinger D.P., Read S.M., Rosen L.P., Shafer R.A., Trenholme A.R., Weiss R., Bennett C.L., Boggess N.W., Wilkinson D.T., and Wright E.L. Calibration of the COBE FIRAS instrument. *Astrophys. J.*, 1994, v. 420, 457–473.
39. Fixsen D.J., Cheng E.S., Gales J.M, Mather J.C., and Shafer R.A., and Wright E.L. The cosmic microwave background spectrum from the full COBE FIRAS data set. *Astrophys. J.*, 1996, v. 473, 576–587.
40. Brodd S., Fixsen D.J., Jensen K.A., Mather J.C., and Shafer R.A. Cosmic background explorer (COBE) Far Infrared Absolute Spectrophotometer (FIRAS) Explanatory Supplement. NASA, 1997; lambda.gsfc.nasa.gov/data/cobe/firas/doc/FES4_ABSPREF.PS
41. Fixsen D.J., Dwek E., Mather J.C., Bennett C.L., Shafer R.A. The spectrum of the extragalactic far-infrared background from the COBE FIRAS observations. *Astrophys. J.*, 1998, v. 508, 123–128.
42. Mather J.C., Fixsen D.J., Shafer R.A., Mosier C., and Wilkinson D.T. Calibrator design for the COBE far infrared absolute spectrometer (FIRAS). *Astrophys. J.*, 1999, v. 512, 511–520.
43. Fixsen D.J. and Mather J.C. The spectral results of the far-infrared absolute spectrophotometer instrument on COBE. *Astrophys. J.*, 2002, v. 581, 817–822.
44. Wright E. Cosmic microwave background. Encyclopedia of Astronomy and Astrophysics (Paul Murdin, Ed.), Institute of Physics Publishing, Bristol, U.K., 2001, v. 1, 524–530.
45. Boggess N.W., Mather J.C., Weiss R., Bennett C.L., Cheng E.S., Dwek E., Gulkis S., Hauser M.G., Janssen M.A., Kelsall T., Meyer S.S., Moseley S.H., Murdock T.L., Shafer R.A., Silverberg R.F., Smoot G.F., Wilkinson D.T., and Wright E.L. The COBE mission: its design and performance two years after launch. *Astrophys. J.*, 1992, v. 397, 420–429.
46. Smoot G., Bennett C., Weber R., Maruschak J., Ratliff R., Janssen M., Chitwood J., Hilliard L., Lecha M., Mills R., Patschke R., Richards C., Backus C., Mather J., Hauser M., Weiss R., Wilkinson D., Gulkis S., Boggess N., Cheng E., Kelsall T., Lubin P., Meyer S., Moseley H., Murdock T., Shafer R., Silverberg R., and Wright E. COBE Differential Microwave Radiometers: Instrument design and implementation. *Astrophys. J.*, 1990, v. 360, 685–695.
47. Smoot G.F., Bennett C.L., Kogut A., Wright E.L., Aymon J., Boggess N.W., Cheng E.S., de Amici G., Gulkis S., Hauser M.G., Hinshaw G., Jackson P.D., Janssen M., Kaita E., Kelsall T., Keegstra P., Lineweaver C., Loewenstein K., Lubin P., Mather J., Meyer S.S., Moseley S.H., Murdock T., Rokke L., Silverberg R.F., Tenorio L., Weiss R., and Wilkinson D.T. Structure in the COBE differential microwave radiometer first-year maps. *Astrophys. J. Letters*, 1992, v. 396(1), L1–L5.
48. Bennett C.L., Kogut A., Hinshaw G., Banday A.J., Wright E.L., Gorski K.M., Wilkinson D.T., Weiss R., Smoot G.F., Meyer S.S., Mather J.C., Lubin P., Loewenstein K., Lineweaver C., Keegstra P., Kaita E., Jackson P.D., and Cheng E.S. Cosmic temperature fluctuations from two years of COBE differential microwave radiometers observations. *Astrophys. J.*, 1994, v. 436, 423–442.
49. Bennett C.L., Banday A.J., Gorski K.M., Hinshaw G., Jackson P., Keegstra P., Kogut A., Smoot G.F., Wilkinson D.T., and Wright E.L. Four-Year COBE DMR Cosmic Microwave Background Observations: Maps and Basic Results. *Astrophys. J.*, 1996, v. 464, L1–L4 and plates L1–L3.
50. Hoyle F. A new model for the expanding universe. *Monthly Not. Roy. Astron. Soc.*, 1948, v. 108(5), 372–382.
51. Bondi H. and Gold T. The steady-state theory of the expanding universe. *Monthly Not. Roy. Astron. Soc.*, 1948, v. 108(3), 252–270.
52. Lemaitre G. Un univers homogène de masse constante et de rayon croissant, rendant compte de la vitesse radiale des nébuleuses extragalactiques. *Annales de la Société scientifique de Bruxelles*, 1927, v. 47, 49–59.
53. Guth A.H. Inflation and the new era of high precision cosmology. *MIT Physics Annual*, 2002, 28–39.
54. Smoot G.F. Our age of precision cosmology. *Proceedings of the 2002 International Symposium on Cosmology and Particle Astrophysics* (CosPA 02), X.G. He and K.W. Ng, Editors, World Scientific Publications, London, U.K., 2003, 314–326.
55. Danese L. and Partidge R.B. Atmospheric Emission Models: Confrontation between Observational Data and Predictions in the 2.5–300 GHz Frequency Range. *Astrophys. J.*, 1989, v. 342, 604–615.
56. Partridge R.B. 3 K: the Cosmic Microwave Background Radiation. Cambridge University Press, Cambridge, 1995, p. 103–160.
57. Lay O.P and Halverson N.W. The Impact of Atmospheric Fluctuations on Degree-Scale Imaging of the Cosmic Microwave Background. *Astrophys. J.*, 2000, v. 543, 787–798.
58. Planck M. The theory of heat radiation. P. Blakiston's Son & Co., Philadelphia, PA, 1914.
59. Robitaille P.-M.L. The solar photosphere: evidence for condensed matter. *Prog. in Phys.*, 2006, v. 2, 17–21.
60. Sabins F.F. Remote sensing: principles and applications. W. H. Freeman and Company, San Francisco, CA, 1978.
61. Lillesand T.M., Kiefer R.W., and Chipman J.W. Remote sensing and image interpretation (6th Edition). John Wiley and Sons, Hoboken, N.J., 2008.
62. Ulaby F.T., Moore R.K., and Fung A.K. Microwave remote sensing active and passive — Volume 2: Radar remote sensing and surface scattering and emission theory. London, Addison-Wesley Publishing Company, 1982, p. 880–884.

63. Maréchal Y. The hydrogen bond and the water molecule: the physics and chemistry of water, aqueous and bio-media. Elsevier, Amsterdam, 2007.
64. Dyke T.R. and Muenter J.S. Microwave spectrum and structure of hydrogen bonded water dimer. *J. Chem. Phys.*, 1974, v. 60, 2929–2930.
65. Dyke T.R., Mack K.M., and Muenter J.S. The structure of water dimer from molecular beam electric resonance spectroscopy. *J. Chem. Phys.*, 1977, v. 66, 498–510.
66. Smith J.D., Cappa C.D., Wilson K.R., Messer B.M., Cohen R.C., and Saykally R.J. Energetics of hydrogen bond network rearrangements in liquid water. *Science*, 2004, v. 306, 851–853.
67. Weiss R. Measurements of the cosmic background radiation. *Ann. Rev. Astron. Astrophys.*, 1980, v. 18, 489–535.
68. Matsumoto T., Hayakawa S., Matsuo H., Murakami H., Sato S., Lange A.E., and Richards P.L. The submillimeter spectrum of the cosmic background radiation. *Astrophys. J.*, 1988, v. 329, 567–571.
69. Woody D.P. An observation of the submillimeter cosmic background spectrum. University of California, Berkeley, 1975.
70. Singal J., Fixsen D.J., Kogut A., Levin S., Limon M., Lubin P., Mirel P., Seiffert M. Villela T., Wollack E. and Wuensche C.A. The ARCADE 2 instrument. arXiv: 0901.0546.
71. 71.Kogut A., Fixsen D.J., Levin S.M., Limon M., Lubin P.M., Mirel P., Seiffert M., Singal J., Villela T., Wollack E., and Wuensche C.A. ARCADE 2 observations of galactic radio emission. arXiv: 0901.0562.
72. Atkinson N. Cosmic radio noise booms six times louder than expected. Universe Today, January 7, 2000, http://www.universetoday.com/2009/01/07/cosmic-radio-noise-booms-six-times-louder-than-expected/
73. Mather J.C. Far infrared spectrometry of the Cosmic Background Radiation. University of California, 1974.
74. Wilkinson D. The microwave background anisotropies: observations. *PNAS*, 1998, v. 95(1), 29–34.
75. Harris L. The optical properties of metal blacks and carbon blacks. MIT and The Eppley Foundation for Research, Monograph Ser. 1, New Port, R.I., Dec. 1967.
76. Harris L., McGuiness R.T., and Siegel B.M. The preparation and optical properties of gold black. *J. Opt. Soc. Am.*, 1948, v. 38, 582.
77. Emerson and Cuming Microwave Products (Canton, MA). Technical Bulletin 2–6 (revised).
78. Emerson and Cuming Microwave Products. Technical Reference: ECCOSORB® CR Two-Part Castable Load Absorber Series. http://www.eccosorb.com/file/958/cr.pdf
79. Hemmati H., Mather J.C., and Eichhorn W.L. Submillimeter and millimeter wave characterization of absorbing materials. *Appl. Optics*, 1985, v. 24, 4489–4492.
80. Touloukian Y.S. and DeWitt D.P. Thermal radiative properties of nonmetallic solids. Vol. 8. In: *Thermophysical Properties of Matter*, IFI/Plenum, New York, N.Y., 1972.
81. Kraus J.D. Antennas. McGraw-Hill Book Company, New York, N.Y., 1988.
82. Balanis C. Modern antenna handbook. John Wiley and Sons, Inc., Hoboken, N.J., 2008.
83. Johnson R.C. Antenna engineering handbook. McGraw-Hill Company, New York, N.Y., 1993.
84. Shen Z. and Feng C. A new dual-polarized broadband horn antenna. *IEEE Ant. Wireless Prop. Lett.*, 2005, v. 4, 270–273.
85. Bruns C., Leuchtmann P., and Vahldieck R. Analysis and simulation of a 1–18 GHz broadband double-ridged horn antenna. *IEEE Trans. Electromagn. Comp.*, 2003, v. 45(1), 55–60.
86. PLANCK website, http://www.rssd.esa.int/index.php?project=PLANCK&page=index.
87. Bard S., Stein J., and Petrick S.W. Advanced radiative cooler with angled shields. Spacecraft radiative transfer and temperature control (T.E. Horton, Ed). *Prog. Astronautics & Aeronautics*, 1982, v. 83, 249–258.
88. Taylor J.R. An introduction to error analysis: the study of uncertainties in physical measurements. University Science Books, Mill Valley, CA, 1982.
89. Giorgi P.G. Influence of the angular response on Fourier absolute spectrometry the case of COBE-FIRAS. *Infrared Phys. Tech.*, 1995, v. 36, 749–753.
90. Battistelli E.S., Fulcoli V., and Macculi C. The CMBR spectrum: new upper limits for the distortion parameters y and μ. *New Astronomy*, 2000, v. 5, 77–90.
91. Salvatera R. and Burigana C. A joint study of early and late spectral distortions of the cosmic microwave background and of the millimetric foreground. *Mon. Not. Royal Astron. Soc.*, 2002, v. 336(2), 592–610.

Active Galactic Nuclei: the Shape of Material Around Black Holes and the Witch of Agnesi Function. Asymmetry of Neutrino Particle Density

Gary C. Vezzoli

Department of Science and Mathematics, Lebanon College, Hanover Street, Lebanon, NH 03766, USA
Senior Research Consultant Physicist, Institute for the Basic Sciences, West Windsor, VT 05089, USA

E-mail: vezzoli2005@yahoo.com

A mathematical representation is given and physically described for the shape of the very hot material that immediately surrounds a black hole and the warm material located at a greater distance from the black hole, as related to active galactic nuclei. The shape of the material surrounding the black hole is interpreted in terms of asymmetry of the neutrino flux. Detailed experimental measurements on radioactive decay influenced by astrophysical events are given to support this interpretation.

1 Introduction

Recent work [1] that examined over 200 active galactic nuclei has shown that all have a common shape of the material surrounding the black hole core, and that this shape seems to be independent of the size of the black hole. The Active galactic nuclei (AGN) are cores of galaxies that are energized by disks of hot material that act as ingress/feeder to supermassive black holes. the shape of the hot material that surrounds the black hole was inferred from the observation of x-rays that emanate from very hot material that is close to the black hole, and from infra-red radiation that derives from warm material much further from the core of the black hole.

Through comparing the ratio of x-rays to infrared radiation, the contour shape of the black hole is indirectly mapped [1]. The results are shown in Fig. 1. Inspection of the inferred topology of the surrounding material indicates that although approximate symmetry is shown across the vertical axis, the horizontal axis shows no indication whatsoever of mirror plane symmetry, and thus the upper and lower regions of the 2-d projection must derive from very different functional representations. Stars, planets, and moons do not show a significant asymmetry, other than equatorial bulge. The non-symmetry of the material surrounding the black hole appears thus at first surprising, however, when considered in terms of a collision-induced gravity model [2], the asymmetry could be hypothesized to be a consequence of observing the black hole from a location closer to the centre of the universe where the neutrino flux density is far greater than at position coordinates that are associated with the expansion of the periphery region of the universe, even though that locus of positions is considered unbounded. Asymmetries, such as shown in Fig. 1 are generally thought to be associated with tidal effects — and in the case at hand, this would mean gravitational interactions, such as a form of lensing. Although there is a consideration of the red shift associated with the receding of the galaxies, the cores of which are powered by disks of very hot material "feeding" the supper massive black hole, I do not think that the asymmetry shown in Fig. 1 arises purely from considerations of Relativity, but instead arises at least to some significant level from collision criteria [2].

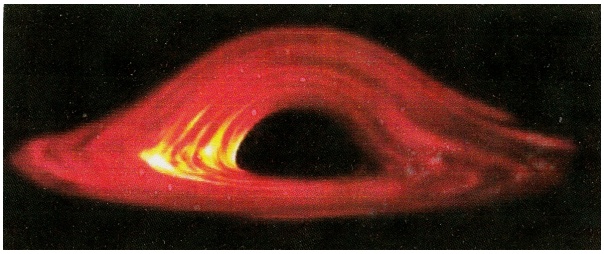

Fig. 1: Material shape near black hole. Courtesy of Anna Morton, moderator of 4D WorldX Yahoo Science Groups. See [1].

2 Analysis and interpretation

The event horizon associated with a black hole refers to the surface that surrounds the black hole, having the property that any visible light cannot escape from the super dense mass because of the strength of the gravitational field [3]. In terms of collision-induced gravity, the term "field" is *not* employed because gravity is considered to be particle-based and the escape-inability of photons at energies less than x-rays is due the increase in collision cross-section between neutrinos and photons that accompanies the super dense packing of mass in a black hole that has developed from a neutron star. The accretion disc of a black hole refers to how accretion onto a neutron star takes place from from a matter input from the Roche lobe of a primary star in the binary system. This passing of matter when occurring from the primary to the secondary star through a Lagrangian point [4] establishes a non-symmetry, but of a different form than that of the black hole shown in Fig. 1, yet these asymmetries may be ultimately related through the physical processes associated with the involvement of the black hole. The vertical asymmetry of the material that surrounds the black hole may also arise from the phenomena that are associated with the periodic ejecta of

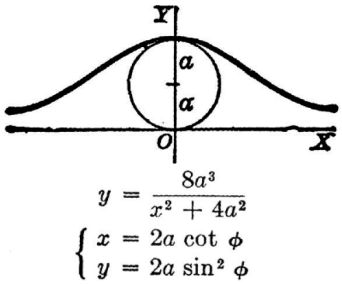

Fig. 2: The Witch of Agnesi function.

material from the black hole, which may be influenced by the magnetic properties of the super dense collapsed star. The comparatively slight asymmetry in the horizontal direction must relate to inhomogeneous temperatures and non-isotropic mass distributions of the black hole because of specific local conditions at the $xyzt$ spatial-temporal location of the highly dense aggregating of matter.

The 2-d geometry shown in Fig. 1 above the horizontal axis that passes through the extrema of the inferred contoured distribution of mass, shows the appearance of the mathematical function known as the Witch of Agnesi. (The term "witch" is an involvement of a misnomer, caused by an incorrect translation of the work of Maria Agnesi who developed the function geometrically in 1768). The Agnesi function (Fig. 2) is generally given by, $y = [(8a^3)/(x^2 + 4a^2)]$, where a is the radius of the circle that is utilized to geometrically form the functional curve. In polar coordinates the Agnesi function is given by $x = 2a \cot \phi$, and $y = 2 \sin^2 \phi$. The function can be generated geometrically by rotating the radius of the circle whereby the y-coordinate of the function is the y-value of the radial vector as it sweeps the associated circle, and the x-coordinate is the x-value of the ordered pair that represents the intersection of the extrapolation of the radial vector with the line, $y = a$. Although many world class mathematicians explored the geometric development of this function, including Fermat, no application in astrophysics to the author's knowledge was established for what became known as the Witch of Agnesi function, until now — general applications of the function being confined to probability theory.

Some properties of the Agnesi function are associated with gravitational criteria, such as the x-squared term appearing in the denominator, and suggestive of an inverse square relationship, which in Newtonian gravity derives from Newton's postulate of a central force, which he interpreted from Kepler's First Law of Planetary Action-namely that the orbits of the planet must be elliptical from consideration of years of visual data of Tycho Brahe. The inverse square relationship in the collision-induced gravity model/theory derives from the properties of a flux, as in the photon inverse-square light intensity fall-off, or the equivalent for the distance dependency of the amplitude/intensity of magnetic or electrostatic properties. The relationship of the sweeping rotating radius of the function-forming circle, and its extension to intersect the line

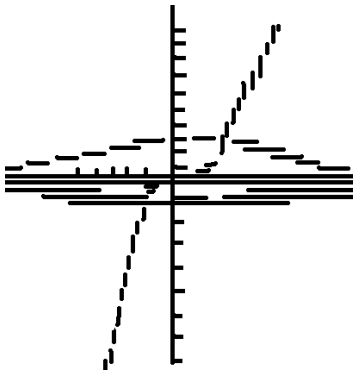

Fig. 3: Representation of the shape of material near a black hole using Agnesi function contours and quadratic function.

$y = a$ can be arguably topologically associated with the notion of accretion and event horizon, and *continuous* processes. The asymptotes of the function (the positive and negative x-axes) relate to the convergence of the shape of the constituent material as temperature decreases because of distance from the "donut" core of the black hole.

The region of Fig. 1 below the horizontal axis can in 2-d projection be well represented by a wide parabola that opens upward. Thus the combined representation of the 2-d geometry shown in Fig. 1 requires the use of a two-function coalescence, and implies the involvement of two different physical phenomena, whereby the quadratic is typically associated with gravitational interactions but the Agnesi function is not.

Using the Agnesi function, and varying the value of the radius, a, combined with the parabola, $y = ax^2 - k$, where a is a very small positive constant $\ll 1$, the contoured representation shown in Fig. 3 is readily developed. The knee shaped curve given also in Fig. 3 represents the calculation of volume of integration of the region surrounding the black hole as a function of the position coordinate, x, showing a threshold effect above which the volume increases rapidly with high slope. The volume function involves an arc tangent term which which is consistent with involvement of an event horizon.

It has been proposed [5] that when emission from an inner accretion disk around a black hole is occulted by a companion star, the observed light curve becomes asymmetric at ingress and egress on a time scale of 0.1–1 sec. The light-curve analysis is claimed [5] to provide a means of verifying the relativistic properties of the accretion flow which is based on both the Special Relativity and General Relativity that is associated with black holes. It is reported [5] that the "skewness" for the eclipsing light curve is approximately zero for what are called slim disks because the innermost part is self-occulted by the outer rim of the disk. This self occulting is a very important property of the black hole, yet these criteria do not uniquely and exclusively seem capable of explaining the major asymmetry shown in the geometry inferred from the x-ray and infra-red data [1] given in Fig. 1.

1	425
2	415
2	390
4	462
5	420
6	420
7	405
8	406
9	421
10	429
11	410
12	415
13	392
14	420
15	430
16	412
17	411
18	418
19	420
20	410
21	391
22	420
23	440
24	421
25	395
26	421
27	422
28	437
29	437
30	402
31	404
32	402
33	430

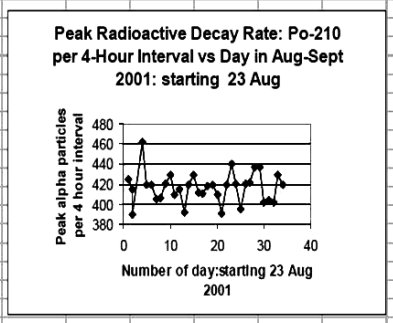

Fig. 4: Radioactive decay data for Po-210 during August-September 2001 measured at Harvard University using the Rad-7 solid-state detector.

On the other hand, it has been reported [6] that propagation of fermions in curved space-time generates gravitational interaction due to the coupling of its spin with space time curvature connection, and causes a CPT violating term in the Lagrangian, generating an asymmetry between the left-handed and the right-handed partners under the CPT transformation. (CPT refers to charge conjugation, space reversal, and time interval, and thus deals with parity). It is interpreted [6] that in the case of neutrinos this property can generate neutrino asymmetry in the Universe, causing the dispersion energy relation for the neutrino and its anti-neutrino to be different giving rise to differences in their number density, and associated with the left-hand helicity of the neutrino. These effects may have an influence in contributing to the asymmetry shown in Fig. 1. It has also been shown [7] that particle interactions in the black-hole accretion disks cause an excess production of positrons as compared to electrons, however, this disparity alone, without emission directionality considerations, does not constitute a non-conservation of parity.

Although the behaviour of each type of galaxy or AGN is *dependent* upon the angle of observation relative to the accretion plane of the black hole core, the asymmetry shown in Fig. 1 is common to all 200 AGN's that were studied in [1], yet the angles of observation relative to the accretion zones had to be different, and the azimuths from the observation coordinates also had to be different.

Our own work [8] has suggested that near the periphery of the current universe, gravitational interactions must have a net repulsive, rather than attractive, dependence — this owing to the far lower neutrino flux in the far distant regions of the universe ($\sim 10^{50}$ km). Thus, though arguably at very small length scales ($\ll 0.1$ mm), gravitational interactions may be described by an inverse fourth dependence [9], and at typical solar system and galactic length scales by inverse square dependence, yet at length scales of 10^n km (where $n > 40$), the dependence is likely *not* to be attractive at all, and instead repulsive near the outer zones of the universe. Thus, relative to the line of centres (a curved Riemannian arc) of the earth born measurement laboratory and the very distant black holes, the neutrino flux that is emanating from the outer regions of the universe, and opposing the escape of both x-rays and infra-red radiation toward the observer, has a higher particle density, than the neutrino flux that is *opposing* (due to collisions and associated net exchange of total momenta) the escape of electromagnetic radiation in the direction of the periphery of the universe. This higher level of particles per square centimetre per second escaping toward the periphery of the universe diffuses in curved directions because of the collision basis of gravity, and the net result contributes to the asymmetry detected by the observer, as in Fig. 1, and shown functionally in Figs. 2 and 3.

3 Supporting evidence for the significance of the neutrino flux

In a work previously published in this journal [10] I presented the explanation of the physical cause of the decades of radioactive decay data histograms determined by Shnoll et al. [11–13] which reported characteristic histograms for the decay of Pu-239 which were periodic over a 24 h interval (the solar day, thus the spin of the Earth), a ∼28 day interval (the lunar month, thus the period of the Moon), and the sidereal year, and also reported characteristic histograms of radioactive decay rate associated with a New Moon and a total solar eclipse. My explanation [10] was based on the Moon and/or the Earth periodically interrupting through scattering and capture some of the neutrinos that emanated from the Sun, and which would have otherwise transferred their momentum to the radioactive source, the decay rate of which was being studied in the experiments (taking place in Moscow, and aboard two research ships that travelled all over the world, including the polar regions). Also, the Sun and Moon intercept neutrinos emanating from deep space.

The Shnoll work [11–13] prompted me to lease a Rad-7 solid-state detector through Dr. Derek Lane-Smith at Durridge Corporation (Bedford, MA) for the purpose of exploring further the Shnoll conclusions. The Rad-7 detector is utilized worldwide as the principle detector of alpha particles decaying from radon gas, and as such is ideally suited also to study the daughter isotopes of Radon. Amongst these, Po-210 has the ideal half life compatible with the purposes of my work. The detector was set up for a 4 week period at the Farlow Herbarium at Harvard University, where I was a research affiliate at the time, conducting work at the Arnold Ar-

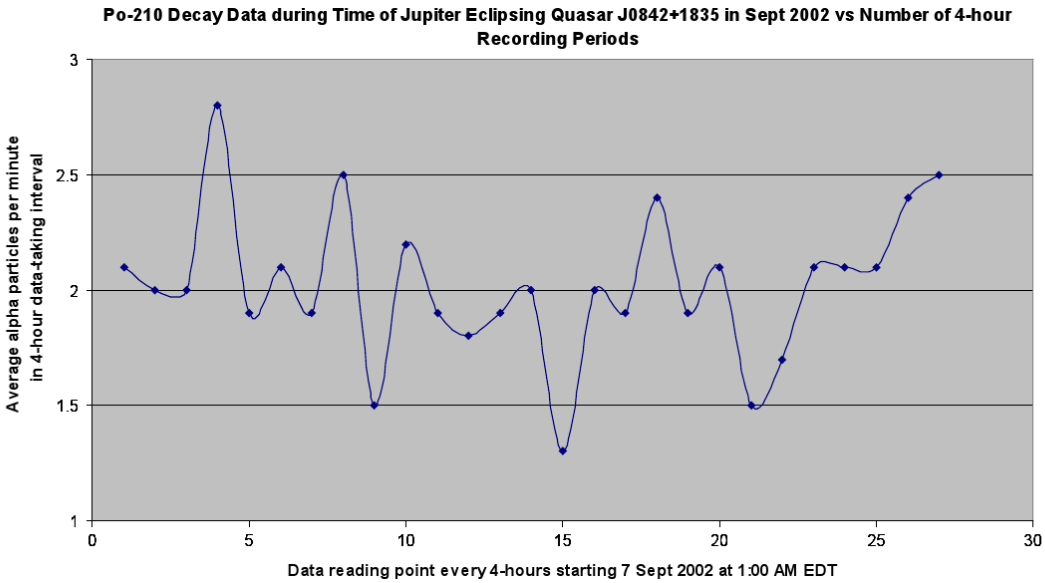

Fig. 5: Data showing three decreases in radioactive decay data of Po-210, 24 hours apart, corresponding to period of 6–10 AM Sept. 7–10 during time interval of Jupiter eclipsing quasar JO842+1835. Reproduced from [16].

boretum, studying the negative geotropism of a heavy vine, Aristolochia macrophylla. Although, conclusions could not be definitely established regarding a diurnal variation of the radioactive decay, a clear peak was observed in the 12:00–4:00 PM time interval on 26 August 2001, far exceeding two-sigma in alpha particles per 4 hour interval. These data are given in Fig. 4, and are digitally reproduced from [14]. It was not until over a year later that I learned that on 26–27 August 2001, radiation from the explosion of supernova SN 2001 dz (in UGC 47) reached the Earth [15]. A supernova explosion is associated with a very significant release of neutrinos, and I interpret that the radioactive alpha particle decay rate peak, shown in Fig. 4, is a consequence of the impingement of the neutrinos, associated with the supernova explosion burst, upon the radioactive isotope source which then pertubed and further de-stabilized a nucleus that was already unstable due to the ratio of neutrons to protons.

During the period September 7–11, 2002, the planet Jupiter eclipsed the deep space quasar JO842+1835, and measurements of alpha particle decay rate were conducted by Dr. Lane-Smith in the Boston area at my request. The averaged data are given in Fig. 5 (digitally reproduced from [16]), showing a decrease in decay rate from approximately 6:00AM to 10:00 AM every 24 hours during the 3-day time interval of the eclipsing event. This variation is attributed to the rotation of the Earth such that once per day Jupiter, interrupted the particle-path from the deep-space quasar to the earth laboratory where the radioactive source was located for the experiment. This interruption of neutrinos, due to the nucleons of Jupiter scattering and inelastically capturing some small, but non-trivial, proportion of particles and/or radiation causes a decrease in radioactive decay rate because of the consequent decrease in the particle flux transferring momentum to the nuclei of Po-210. The x-axis scale is the number of four-hour periods in to the experiment starting at 1:00 AM EDT Sept 7, 2002, and showing decreases at abscissa values of 9, 15, and 21 — these being six 4-hr intervals (24 h) apart.

On 4 Dec 2002, a total solar eclipse occurred, during which the radioactive decay rate of Co-60 was measured at Pittsburg State University in southeastern Kansas [17], and the radioactive decay rate of Po-210 [18] was measured in the Boston area, both at/near the time of totality in southern Australia. The decay data [14] are plotted in Fig. 6, and show dips in decay rate at the time when the umbra of the eclipse was closest to the location of the source isotopes (on the opposite side of the Earth from totality). The inset shows very recent data [19] on the decay of Cs-137 during the annular solar eclipse of 26 January 2009, also in southeast Kansas, at the time when the eclipse was at peak darkness in Australia, also showing a dip in decay rate when the umbra passed closest to the source isotope (time = 4.06 days into the experiment). The 2009 data plot (inset) shows also the envelope of the negative percent changes. The circled data points are analogous to the leading-edge signal and the trailing-edge signal that corresponded to dips in gravity upon first contact and upon last contact associated with the total solar eclipse in China in March 1997 (see [20, 20]). These consistent decreases in decay rate (using three different isotopes) during two different solar eclipses can only be explained by the mass of the Moon and the mass of the Earth interupting the flux of neutrinos coming from the Sun, and thus some of the neutrinos associated with the flux, never reaching the source isotope. Hence these scattered and captured neutrinos do *not* cause any further de-stabilization of the weak cohesive interaction of mesons and of gluons that hold the nucleus intact/together, normally ascribed to the weak force — an internal interaction

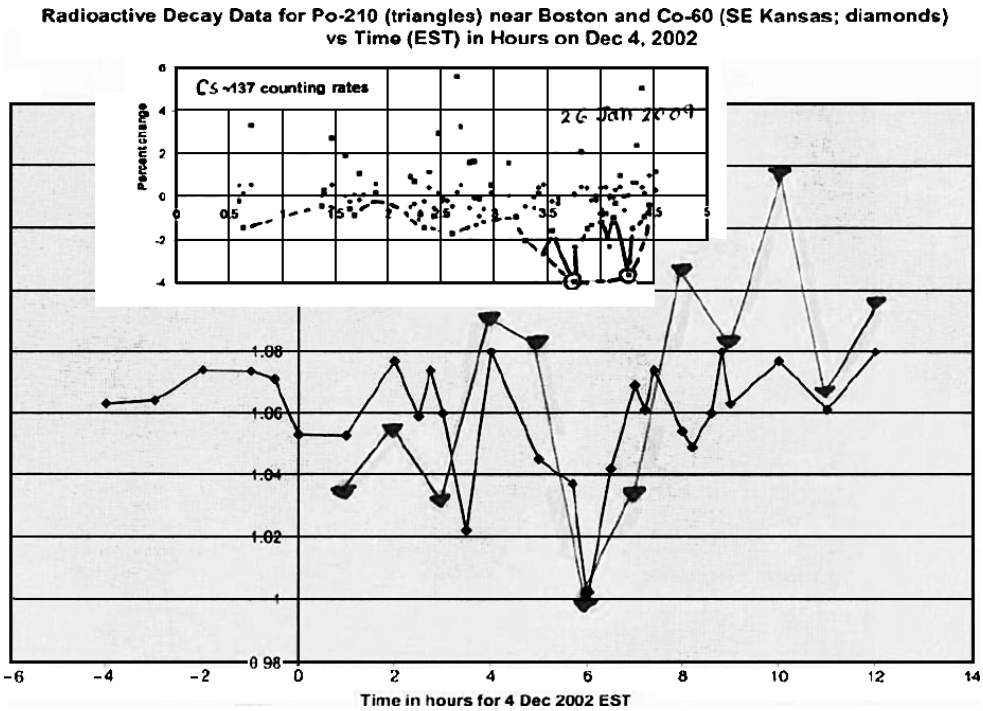

Fig. 6: Decrease in radioactive decay rate for Co-60 and for Po-210 during total eclipse of 4 Dec. 2002, and decrease in radioactive decay rate for Cs-137 during annular solar eclipse of 26 Jan. 2009.

— but now shown to depend upon momenta transfer from externally impinging particles including primarily the muon neutrino and the electron neutrino.

Additional supporting data regarding the significance of the neutrino flux on radioactivity, and highly supportive of my own work and interpretations given herein, are as follows:

1. A major multi-year study by Purdue University researchers at Brookhaven National Laboratory clearly show that the radioactive decay rates of many isotopes correlate very well with the distance of the source isotope from the Sun, as well as changes in radioactive decay rate correlated with major solar flares [22].
2. Positron annihilation measurements [23] that show periodic variation with the phases of the Moon, yielding peaks associated with the New Moon (which approximates a solar eclipse), and troughs correlated with the presence of the Full Moon. The source of positrons in this study was Na-22, and the dependent variable of the experiment measured the yield of molecular iodine (I_2). Thus the peaks in $I_2\%$ correlated with the presence of the New Moon, and hence the interference by the Moon of a flow of particles from the Sun and from space. The data also showed a general trend increase in I_2 production over the course of the months of the experiment (November through February), that the authors tentatively attribute to seasonal changes of the distance between the Earth and the Sun. The exact phenomena causing the peaks is not yet established since in this case an interruption of neutrino flow by the Moon enhances positronium production. It is possible that the peaks are due to more molecular iodine being produced associated with a different collision cross-section caused by change-in-flavor of the neutrino due to collision with nucleons of the Moon.
3. Periodic oscillations have been reported [24] in Pm-142 which show an oscillating sinusoidal decay for electron capture (as contrasted to a conventionally established exponential decay) which the authors attribute to modulations caused by the oscillation of neutrinos between two different mass states (flavors), that of the electron neutrino emitted in the original decay, and that of the muon neutrino which is observed in decays of the muon (a particle 200 times more massive than the electron).
4. The standard deviation of decay rate of radioactive isotopes is periodic with respect to the phases of the Moon, being maximum at Full Moon (whereby external particle impingement from the Sun is unobstructed) and minimum at New Moon (whereby external particle impingement is obstructed by the Moon [25]), akin an eclipse condition.

4 Conclusion

Thus based on all of the above considerations, in the current work, the asymmetry in neutrino flux is identified as the prin-

cipal cause of the non-symmetry shown in Fig. 1, owing to neutrino-photon collisions in the AGN or black hole regimes where the collision cross-sections of neutrinos and photons is many orders of magnitude higher than in the solar system regime. This conclusion is supported by our previous experimental work using both very-close-proximity gravitational pendula, and a magnetic pendulum system, interrogated by laser scattering, showing asymmetry in gravitational particle/wave impinging flux in the X-Y plane as compared to the zed (Z) direction [16].

Note added in proof

Recent work by G. C. Vezzoli and R. Morgan has shown that the 1444 minute annually periodic histogram reported by Shnol and Rubenstein in this journal for the period 24 July 2005 into August correlates with the NASA report of the Sun beginning the occulting of Saturn on that date; and thus also correlates with the work of Vezzoli reporting a dip in gravity on 18 May 2001 when earth, Sun, and Saturn were in syzygy [15]. The Morgan-Vezzoli work will be reported in a Letter-to-the-Editor of this journal authored by Morgan.

Acknowledgements

The author wishes to gratefully acknowledge the assistance, collegial cooperation, fruitful discussions of Prof. C. Blatchley, Dr. Derek Lane-Smith, Dr. William Stanley, Sandra Smalling, and the faculty, administration, staff, and students at Lebanon College.

Submitted on February 24, 2009 / Accepted on June 03, 2009

References

1. McKernan B. American Museum of Natural History and Manhattan Community College, City University of New York, 17 Dec 2008 See also Kaku M. and Thompson J. Beyond Einstein. Anchor, Random House, New York, 1995.
2. Stanley W. and Vezzoli G.C. Induced gravity model based on external impinging neutrinos: calculation of G in terms of collision phenomena and inferences to inertial mass and atomic-quantization. *arXiV: astro-ph/0102109*
3. The new physics. Ed. by P. Davies, Cambridge University Press, 1989.
4. Longair M. *Ibid.*, p.141
5. Watarai K-Y. Ecipsing light-curve asymmetry for black hole accretion flows. *Publ. Astron. Soc. Jpn.*, 2005, v. 57(5), 827–833.
6. Banibrata M. Neutrino asymmetry around black holes. *Modern Physics Letters A*, 2005, v. 20(28), 2145–2155.
7. Akujar C.E. Contribution of black hole accretion disks to symmetric lepton production. *Astrophysics and Space Science*, 1984, v. 100, 1–2, 413–415.
8. Vezzoli G.C. Note on indication of nano local short range order in liquid iron from analysis of recovered products from molten state: geophysical inferences from the materials science, *Mat. Res. Innov.*, 2002, v. 5, 222–225.
9. Hoyle C.D. *Phys. Rev. Lett.*, 2001, v. 86(8), 1418.
10. Vezzoli G.C. On the explaination of the physical cause of the Shnoll characteristic histograms and observed fluctuations. *Progress in Physics*, 2008, v. 2, 158–161.
11. Shnoll S., Kolombet V., Pozharski E., Zenchenko T., Zvereva I., and Konradov A. Realization of discrete states during fluctuations in macroscopic processes. *Physics-Uspekhi*, 1998, v. 162(10), 1139–1140.
12. Shnoll S., Zenchenko T., Zenchenko K., Pozharski E., Kolombet V., and Konradov A. Regular variation of the fine structure of statistical distributions as a consequence of cosmophysical agents. *Physics-Uspekhi*, 2000, v. 43(2), 205–209.
13. Shnoll S., Zenchenko K., Shapovalov S., Gorshkov S., Makarevich., and Troshichev O.A. The specific form of histograms presenting the distribution of data of alpha decay measurements appears simultaneously in the moment of New Moon in different points from Artic to Antartic. arXiv: physics/0412152.
14. Vezzoli G.C. Radioactive decay of Po-210 and Co-60 at two U.S. Observation Stations in the Path of the Umbra/Penumbra of the total eclipse of the Sun of December 4, 2002 in Southern Australia. *Infinite Energy*, 2005, v. 11(61), 48–53.
15. Photograph of this supernova was taken by T. Boles and G. M. Hurst in Basingstoke, England, August 27–28 2001. The supernova SN 2001 is described at website http://www.theastronomer.org/supernovae.html. Code symbols are SN 2001dw-20010825-tb.jpg or SN 2001dz.
16. Vezzoli G.C. Gravitational data during the syzygy of May 18, 2001 and related studies. *Infinite Energy*, 2004, v. 9(53), 18–27.
17. Co-60 was conducted by Professor C. Blatchley at Pittsburg State University during time interval of total solar eclipse of 4 Dec 2002 showing a decrease in decay rate at the time of totality in Southern Australia. Dr. Blatchley asked me to point out in this citation that he is not certain whether his data are supportive of my conclusions because of inherent noise effects and barometric effects that relate to these type of radioactive decay measurements.
18. Po-210 study was conducted by Dr. Derek Lane-Smith of Durridge Corporation in Bedford, MA, during time interval of total solar eclipse of 4 Dec 2002 showing a decrease in radioactive decay rate at the time of totality in southern Australia.
19. Cs-137 decay study was conducted by Professor C. Blatchley at Pittsburg State University during the time interval of the annular solar eclipse of 26 January 2009, indicating a small decrease in decay rate at the time of totality in Australia, corresponding to 4.06 days since the beginning of the experimental measurements. Dr. Blatchley does not share the same opinion as the author regarding the significance of the Cs-137 radioactive decay data as related to the total physics of a solar eclipse, partly because the detected signal does not show a variation exceding two-sigma. However, it must be pointed out that the variation in the measuring of a property such as radioactive decay, or gravity, during totality of a solar eclipse must indeed necessarily

be extremely small. Regarding gravity, this variation was measured to be about 10 microgal (see Refs. 21 and 22).

20. Wang Q., Yang X., Wu C., Guo H., Liu H., and Hua C. Precise measurement of gravity variation during a total solar eclipse. *Phys. Rev. D.*, 2000, v. 62, 041101R.
21. Yang X. and Wang Q. Gravity anomaly during the Mohe total solar eclipse and new constraint on gravitational shielding parameter. *Astrophysics and Space Science*, 2002, v. 285, 245–253; Yang X. Private communications, 2005–2007.
22. Jenskin J., Fischbach E., Buncher J., Gruenwald J., Krause D., and Mattes J. Evidence for correlations between nuclear decay rates and earth-Sun distance. arXiv: 00808.3283.
23. Vikin B.P. Gravitational pertubations as a possible cause for instability in the measurements of positron annihilation. *Progress in Physics*, 2008, v. 2, 76–77.
24. Litvinov Y.A. et al. *Phys. Rev. Lett.*, 2008, v. 664, 162–168.
25. Goleminov N. Private communications, 2006.

Combining NASA/JPL One-Way Optical-Fiber Light-Speed Data with Spacecraft Earth-Flyby Doppler-Shift Data to Characterise 3-Space Flow

Reginald T. Cahill

School of Chemistry, Physics and Earth Sciences, Flinders University, Adelaide 5001, Australia
E-mail: Reg.Cahill@flinders.edu.au

We combine data from two high precision NASA/JPL experiments: (i) the one-way speed of light experiment using optical fibers: Krisher T.P., Maleki L., Lutes G.F., Primas L.E., Logan R.T., Anderson J.D. and Will C.M. *Phys. Rev. D*, 1990, v. 42, 731–734, and (ii) the spacecraft earth-flyby Doppler shift data: Anderson J.D., Campbell J.K., Ekelund J.E., Ellis J. and Jordan J.F. *Phys. Rev. Lett.*, 2008, v. 100, 091102, to give the solar-system galactic 3-space average speed of 486 km/s in the direction RA $= 4.29^{\rm h}$, Dec $= -75.0^{\circ}$. Turbulence effects (gravitational waves) are also evident. Data also reveals the 30 km/s orbital speed of the Earth and the Sun inflow component at 1AU of 42 km/s and also 615 km/s near the Sun, and for the first time, experimental measurement of the 3-space 11.2 km/s inflow of the Earth. The NASA/JPL data is in remarkable agreement with that determined in other light speed anisotropy experiments, such as Michelson-Morley (1887), Miller (1933), Torr and Kolen (1981), DeWitte (1991), Cahill (2006), Munera (2007), Cahill and Stokes (2008) and Cahill (2009).

1 Introduction

In recent years it has become clear, from numerous experiments and observations, that a dynamical 3-space* exists [1, 2]. This dynamical system gives a deeper explanation for various observed effects that, until now, have been successfully described, but not explained, by the Special Relativity (SR) and General Relativity (GR) formalisms. However it also offers an explanation for other observed effects not described by SR or GR, such as observed light speed anisotropy, bore hole gravity anomalies, black hole mass spectrum and spiral galaxy rotation curves and an expanding universe without dark matter or dark energy. Herein yet more experimental data is used to further characterise the dynamical 3-space, resulting in the first direct determination of the inflow effect of the Earth on the flowing 3-space. The 3-space flow is in the main determined by the Milky Way and local galactic cluster. There are also components related to the orbital motion of the Earth and to the effect of the Sun, which have already been extracted from experimental data [1].

The postulate of the invariance of the free-space speed of light in all inertial frames has been foundational to the physics of the 20th Century, and so to the prevailing physicist's paradigm. Not only did it provide computational means essential for the standard model of particle physics, but also provided the spacetime ontology, which physicists claim to be one of the greatest of all discoveries, particularly when extended to the current standard model of cosmology, which assumes a curved spacetime account of not only gravity but also of the universe, but necessitating the invention of dark matter and dark energy.

*The nomenclature *3-space* is used to distinguish this dynamical 3-dimensional space from other uses of the word *space*.

It s usually assumed that the many successes of the resulting Special Theory of Relativity mean that there could be very little reason to doubt the validity of the invariance postulate. However the spacetime formalism is just that, a formalism, and one must always be careful in accepting an ontology on the basis of the postulates, as in the case of the speed of light, because the postulate never stipulated how the speed of light was to be measured, in particular how clock retardation and length contraction effects were to be corrected. In contrast to the spacetime formalism Lorentz gave a different neo-Galilean formalism in which space and time were not mixed, but where the special relativity effects were the consequence of absolute motion with respect to a real 3-space. Recently [3] the discovery of an exact linear mapping between the Minkowski-Einstein spacetime class of coordinates and the neo-Galilean class of time and space coordinates was reported. In the Minkowski-Einstein class the speed of light is invariant by construction, while in the Galilean class the speed is not invariant. Hence statements about the speed of light are formalism dependent, and the claim that the successes of SR implies that the speed of light is invariant is bad logic. So questions about of the speed of light need to be answered by experiments.

There have been many experiments to search for light speed anisotropy, and they fall generally into two classes — those that successfully detected anisotropy and those that did not. The reasons for this apparent disparity are now understood, for it is important to appreciate that because the speed of light is invariant in SR — as an essential part of that formalism, then SR cannot be used to design or analyse data from light speed anisotropy experiments. The class of experiments that failed to detect anisotropy, such as those using vacuum Michelson interferometers, say in the form of reso-

nant vacuum cavities [4], suffer a design flaw that was only discovered in 2002 [5,6]. Essentially there is a subtle cancellation effect in the original Michelson interferometer, in that two unrelated effects exactly cancel unless the light passes through a dielectric. In the original Michelson interferometer experiments the dielectric happened, fortuitously, to be a gas, as in [7–11,15], and then the sensitivity is reduced by the factor $k^2 = n^2 - 1$, where n is the refractive index of the gas, compared to the sensitivity factor $k^2 = 1$ used by Michelson in his calculation of the instrument's calibration constant, using Newtonian physics. For air, with $n = 1.00029$, this factor has value $k^2 = 0.00058$ which explained why the original Michelson-Morley fringe shifts were much smaller than expected. The physics that Michelson was unaware of was the reality of the Lorentz-Fitzgerald contraction effect. Indeed the null results from the resonant vacuum cavities [4] experiments, in comparison with their gas-mode versions, gives explicit proof of the reality of the contraction effect*. A more sensitive and very cheap detector is to use optical fibers as the light carrying medium, as then the cancellation effect is overcome [16]. Another technique to detect light speed anisotropy has been to make one-way speed measurements; Torr and Kolen [12], Krisher *et al.* [18], DeWitte [13] and Cahill [14]. Another recently discovered technique is to use the Doppler shift data from spacecraft earth-flybys [19]. Using the spacetime formalism results in an unexplained earth-flyby Doppler shift anomaly, Anderson *et al.* [20], simply because the spacetime formalism is one that explicitly specifies that the speed of the EM waves is invariant, but only wrt a peculiar choice of space and time coordinates.

Here we combine data from two high precision NASA/JPL experiments: (i) the one-way speed of light experiment using optical fibers: Krisher *et al.* [18], and (ii) the spacecraft earth-flyby Doppler shift data: Anderson *et al.* [20], to give the solar-system galactic 3-space average speed of 486 km/s in the direction RA $= 4.29^{\rm h}$, Dec $= -75^\circ$. Turbulence effects (gravitational waves) are also evident. Various data reveal the 30 km/s orbital speed of the Earth and the Sun inflow component of 615 km/s near the Sun, and 42 km/s at 1AU, and for the first time, experimental evidence of the 3-space inflow of the Earth, which is predicted to be 11.2 km/s at the Earth's surface. The optical-fiber and restricted flyby data give, at this stage, only an average of 12.4 ± 5 km/s for the Earth inflow — averaged over the spacecraft orbits, and so involving averaging wrt distance from earth and RF propagation angles wrt the inflow†. The optical fiber — flyby data is in remarkable agreement with the spatial flow characteristics as determined in other light speed anisotropy experiments, such as Michelson-Morley (1887), Miller (1933), DeWitte (1991), Torr and Kolen (1981), Cahill (2006), Munera (2007), Cahill and Stokes (2008) and Cahill (2009). The NASA data enables an independent calibration of detectors for use in light speed anisotropy experiments and related gravitational wave detectors. These are turbulence effects in the flowing 3-space. These fluctuations are in essence gravitational waves, and which were apparent even in the Michelson-Morley 1887 data [1,2,21].

2 Flowing 3-space and emergent quantum gravity

We give a brief review of the concept and mathematical formalism of a dynamical flowing 3-space, as this is often confused with the older dualistic space and aether ideas, wherein some particulate aether is located and moving through an unchanging Euclidean space — here both the space and the aether were viewed as being ontologically real. The dynamical 3-space is different: here we have only a dynamical 3-space, which at a small scale is a quantum foam system without dimensions and described by fractal or nested homotopic mappings [1]. This quantum foam is not embedded in any space — the quantum foam is all there is and any metric properties are intrinsic properties solely of that quantum foam. At a macroscopic level the quantum foam is described by a velocity field $\mathbf{v}(\mathbf{r}, t)$, where $\mathbf{r}$ is merely a 3-coordinate within an embedding space. This space has no ontological existence — it is merely used to (i) record that the quantum foam has, macroscopically, an effective dimension of 3, and (ii) to relate other phenomena also described by fields, at the same point in the quantum foam. The dynamics for this 3-space is easily determined by the requirement that observables be independent of the embedding choice, giving, for zero-vorticity dynamics and for a flat embedding space‡

$$\left.\begin{aligned} &\nabla\cdot\left(\frac{\partial\mathbf{v}}{\partial t}+(\mathbf{v}\cdot\nabla)\mathbf{v}\right)+\\ &\qquad+\frac{\alpha}{8}\left((\mathrm{tr}D)^2-\mathrm{tr}(D^2)\right)=-4\pi G\rho\,,\\ &\nabla\times\mathbf{v}=\mathbf{0}, \qquad D_{ij}=\frac{1}{2}\left(\frac{\partial v_i}{\partial x_j}+\frac{\partial v_j}{\partial x_i}\right),\end{aligned}\right\} \quad (1)$$

where $\rho(\mathbf{r}, t)$ is the matter and EM energy densities expressed as an effective matter density. Borehole g measurements and astrophysical blackhole data has shown that $\alpha \approx 1/137$ is the fine structure constant to within observational errors [1, 2, 24, 25]. For a quantum system with mass

*As well the null results from the LIGO-like and related vacuum-mode Michelson interferometers are an even more dramatic confirmation. Note that in contrast the LISA space-based vacuum interferometer does not suffer from the Lorentz contraction effect, and as a consequence would be excessively sensitive.

†A spacecraft in an eccentric orbit about the Earth would permit, using the high-precision Doppler shift technology, a detailed mapping of the 3-space inflow.

‡It is easy to re-write (1) for the case of a non-flat embedding space, such as an S^3, by introducing an embedding 3-space-metric $g_{ij}(\mathbf{r})$, in place of the Euclidean metric δ_{ij}. A generalisation of (1) has also been suggested in [1] when the vorticity is not zero. This vorticity treatment predicted an additional gyroscope precession effect for the GPB experiment, R. T. Cahill, *Progress in Physics*, 2007, v. 3, 13–17.

m the Schrödinger equation is uniquely generalised [24] with the new terms required to maintain that the motion is intrinsically wrt to the 3-space, and not wrt to the embedding space, and that the time evolution is unitary

$$i\hbar\frac{\partial\psi(\mathbf{r},t)}{\partial t}=-\frac{\hbar^2}{2m}\nabla^2\psi(\mathbf{r},t)- -i\hbar\left(\mathbf{v}\cdot\nabla+\frac{1}{2}\nabla\cdot\mathbf{v}\right)\psi(\mathbf{r},t)\,. \tag{2}$$

The space and time coordinates $\{t,x,y,z\}$ in (1) and (2) ensure that the separation of a deeper and unified process into different classes of phenomena — here a dynamical 3-space (quantum foam) and a quantum matter system, is properly tracked and connected. As well the same coordinates may be used by an observer to also track the different phenomena. However it is important to realise that these coordinates have no ontological significance — they are not real. The velocities $\mathbf{v}$ have no ontological or absolute meaning relative to this coordinate system — that is in fact how one arrives at the form in (2), and so the "flow" is always relative to the internal dynamics of the 3-space. A quantum wave packet propagation analysis of (2) gives the acceleration induced by wave refraction to be [24]

$$\mathbf{g}=\frac{\partial\mathbf{v}}{\partial t}+(\mathbf{v}\cdot\nabla)\mathbf{v}+(\nabla\times\mathbf{v})\times\mathbf{v}_R\,, \tag{3}$$

$$\mathbf{v}_R(\mathbf{r}_\circ(t),t)=\mathbf{v}_\circ(t)-\mathbf{v}(\mathbf{r}_\circ(t),t)\,, \tag{4}$$

where $\mathbf{v}_R$ is the velocity of the wave packet relative to the 3-space, and where $\mathbf{v}_\circ$ and $\mathbf{r}_\circ$ are the velocity and position relative to the observer, and the last term in (3) generates the Lense-Thirring effect as a vorticity driven effect. Together (2) and (3) amount to the derivation of gravity as a quantum effect, explaining both the equivalence principle ($\mathbf{g}$ in (3) is independent of m) and the Lense-Thirring effect. Overall we see, on ignoring vorticity effects, that

$$\nabla\cdot\mathbf{g}=-4\pi G\rho-\frac{\alpha}{8}\left((\mathrm{tr}D)^2-\mathrm{tr}(D^2)\right), \tag{5}$$

which is Newtonian gravity but with the extra dynamical term whose strength is given by α. This new dynamical effect explains the spiral galaxy flat rotation curves (and so doing away with the need for "dark matter"), the bore hole g anomalies, the black hole "mass spectrum". Eqn. (1), even when $\rho=0$, has an expanding universe Hubble solution that fits the recent supernovae data in a parameter-free manner without requiring "dark matter" nor "dark energy", and without the accelerating expansion artifact [25,26]. However (5) cannot be entirely expressed in terms of $\mathbf{g}$ because the fundamental dynamical variable is $\mathbf{v}$. The role of (5) is to reveal that if we analyse gravitational phenomena we will usually find that the matter density ρ is insufficient to account for the observed $\mathbf{g}$. Until recently this failure of Newtonian gravity has been explained away as being caused by some unknown and undetected "dark matter" density. Eqn. (5) shows that to the contrary it is a dynamical property of 3-space itself. Here we determine various properties of this dynamical 3-space from the NASA optical-fiber and spacecraft flyby Doppler anomaly data.

Significantly the quantum matter 3-space-induced "gravitational" acceleration in (3) also follows from maximising the elapsed proper time wrt the wave-packet trajectory $\mathbf{r}_\circ(t)$, see [1],

$$\tau=\int dt\sqrt{1-\frac{\mathbf{v}_R^2(\mathbf{r}_\circ(t),t)}{c^2}} \tag{6}$$

and then taking the limit $v_R/c\to 0$. This shows that (i) the matter 'gravitational' geodesic is a quantum wave refraction effect, with the trajectory determined by a Fermat least proper-time principle, and (ii) that quantum systems undergo a local time dilation effect — which is used later herein in connection with the Pound-Rebka experiment. A full derivation of (6) requires the generalised Dirac equation.

3 3-space flow characteristics and the velocity superposition approximation

This paper reports the most detailed analysis so far of data from various experiments that have directly detected the 3-space velocity field $\mathbf{v}(\mathbf{r},t)$. The dynamics in (1) is necessarily time-dependent and having various contributing effects, and in order of magnitude: (i) galactic flows associated with the motion of the solar system within the Milky Way, as well as flows caused by the supermassive black hole at the galactic center and flows associated with the local galactic cluster, (ii) flows caused by the orbital motion of the Earth and of the inflow caused by the Sun, and (iii) the inflow associated with the Earth. An even smaller flow associated with the Moon is not included in the analysis. It is necessary to have some expectations of the characteristics of the flow expected for an earth based observer. First consider an isolated spherical mass density $\rho(r)$, with total mass M, then (1) has a stationary flow solution, for $r>R$, i.e outside of the mass,

$$\mathbf{v}(\mathbf{r})=-\hat{\mathbf{r}}\sqrt{\frac{2GM(1+\frac{\alpha}{2}+\dots)}{r}} \tag{7}$$

which gives the matter acceleration from (3) to be

$$\mathbf{g}(\mathbf{r})=-\hat{\mathbf{r}}\frac{GM(1+\frac{\alpha}{2}+\dots)}{r^2} \tag{8}$$

corresponding to a gravitational potential, via $\mathbf{g}=-\nabla\mathbf{\Phi}$,

$$\Phi(\mathbf{r})=-\frac{GM(1+\frac{\alpha}{2}+\dots)}{r}\,. \tag{9}$$

This special case is Newton's law of gravity, but with some 0.4% of the effective mass being caused by the α- dynamics term. The inflow (7) would be applicable to an isolated and stationary sun or earth. At the surface of the Sun

this predicts an inflow speed of 615 km/s, and 42 km/s at the Earth distance of 1AU. For the Earth itself the inflow speed at the Earth's surface is predicted to be 11.2 km/s. When both occur and when both are moving wrt the asymptotic 3-space, then numerical solutions of (1) are required. However an approximation that appears to work is to assume that the net flow in this case may be approximated by a vector superposition [27]

$$\mathbf{v} = \mathbf{v}_{galactic} + \mathbf{v}_{sun} - \mathbf{v}_{orbital} + \mathbf{v}_{earth} + \dots \qquad (10)$$

which are, in order, translational motion of the Sun, inflow into the Sun, orbital motion of the Earth (the orbital motion produces an apparent flow in the opposite direction — hence the -ve sign; see Fig. 4), inflow into the Earth, etc. The first three have been previously determined from experimental data, and here we more accurately and using new data determine all of these components. However this superposition cannot be completely valid as (1) is non-linear. So the superposition may be at best approximately valid as a time average only. The experimental data has always shown that the detected flow is time dependent, as one would expect, as with multi-centred mass distributions no stationary flows are known. This time-dependence is a turbulence effect — it is in fact easily observed and is seen in the Michelson-Morley 1887 data [2]. This turbulence is caused by the presence of any significant mass, such as the galaxy, sun, earth. The NASA/JPL data discussed herein again displays very apparent turbulence. These wave effects are essentially *gravitational waves*, though they have characteristics different from those predicted from GR, and have a different interpretation. Nevertheless for a given flow $\mathbf{v}(\mathbf{r}, t)$, one can determine the corresponding induced spacetime metric $g_{\mu\nu}$ which generates the same matter geodesics as from (5), with the proviso that this metric is not determined by the Hilbert-Einstein equations of GR. Significantly vacuum-mode Michelson interferometers cannot detect this phenomenon, which is why LIGO and related detectors have not seen these very large wave effects.

4 Gas-mode Michelson interferometer

The Michelson interferometer is a brilliant instrument for measuring $\mathbf{v}(\mathbf{r}, t)$, but only when operated in dielectric mode. This is because two different and independent effects exactly cancel in vacuum mode; see [1, 2, 5]. Taking account of the geometrical path differences, the Fitzgerald-Lorentz arm-length contraction and the Fresnel drag effect leads to the travel time difference between the two arms, and which is detected by interference effects*, is given by

$$\Delta t = k^2 \frac{L v_P^2}{c^3} \cos\big(2(\theta - \psi)\big), \qquad (11)$$

*The dielectric of course does not cause the observed effect, it is merely a necessary part of the instrument design physics, just as mercury in a thermometer does not *cause* temperature.

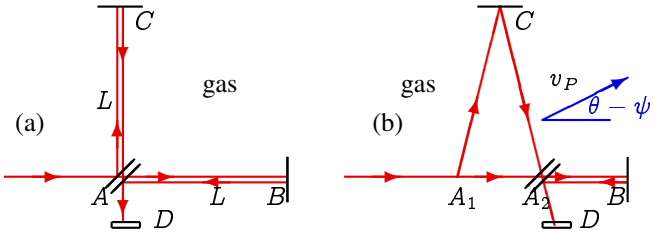

Fig. 1: Schematic diagrams of the gas-mode Michelson Interferometer, with beamsplitter/mirror at A and mirrors at B and C mounted on arms from A, with the arms of equal length L when at rest. D is the detector screen. In (a) the interferometer is at rest in space. In (b) the 3-space is moving through the gas and the interferometer with speed v_P in the plane of the interferometer and direction $\delta = \theta - \psi$ relative to AB arm. Interference fringes are observed at D when mirrors C and D are not exactly perpendicular. As the interferometer is rotated in the plane shifts of the fringes are seen in the case of absolute motion, but only if the apparatus operates in a gas. By measuring fringe shifts the speed v_P may be determined. In general the v_P direction has angle θ wrt the local meridian, and the arm AB has angle ψ relative to the local meridian, so that $\delta = \theta - \psi$ is angle between $\mathbf{v}_P$ and one-arm. The difference in travel times Δt is given in (11), but with temperature changes and non-orthogonal mirrors by (12). In vacuum the fringes do not shift during rotation .

where ψ specifies the direction of $\mathbf{v}(\mathbf{r}, t)$ projected onto the plane of the interferometer, giving projected value v_P, relative to the local meridian, and where $k^2 = (n^2 - 2) \times \times (n^2 - 1)/n$. Neglect of the relativistic Fitzgerald-Lorentz contraction effect gives $k^2 \approx n^3 \approx 1$ for gases, which is essentially the Newtonian theory that Michelson used.

However the above analysis does not correspond to how the interferometer is actually operated. That analysis does not actually predict fringe shifts, for the field of view would be uniformly illuminated, and the observed effect would be a changing level of luminosity rather than fringe shifts. As Michelson and Miller knew, the mirrors must be made slightly non-orthogonal with the degree of non-orthogonality determining how many fringe shifts were visible in the field of view. Miller experimented with this effect to determine a comfortable number of fringes: not too few and not too many. Hicks [22] developed a theory for this effect – however it is not necessary to be aware of the details of this analysis in using the interferometer: the non-orthogonality reduces the symmetry of the device, and instead of having period of 180° the symmetry now has a period of 360°, so that to (11) we must add the extra term $a \cos(\theta - \beta)$ in

$$\Delta t = k^2 \frac{L(1 + e\theta) v_P^2}{c^3} \cos\big(2(\theta - \psi)\big) + \\ + a(1 + e\theta) \cos(\theta - \beta) + f\,. \qquad (12)$$

The term $1 + e\theta$ models the temperature effects, namely that as the arms are uniformly rotated, one rotation taking several minutes, there will be a temperature induced change in the length of the arms. If the temperature effects are linear

in time, as they would be for short time intervals, then they are linear in θ. In the Hick's term the parameter a is proportional to the length of the arms, and so also has the temperature factor. The term f simply models any offset effect. Michelson and Morley and Miller took these two effects into account when analysing his data. The Hick's effect is particularly apparent in the Miller and Michelson-Morley data.

The interferometers are operated with the arms horizontal. Then in (12) θ is the azimuth of one arm relative to the local meridian, while ψ is the azimuth of the absolute motion velocity projected onto the plane of the interferometer, with projected component v_P. Here the Fitzgerald-Lorentz contraction is a real dynamical effect of absolute motion, unlike the Einstein spacetime view that it is merely a spacetime perspective artifact, and whose magnitude depends on the choice of observer. The instrument is operated by rotating at a rate of one rotation over several minutes, and observing the shift in the fringe pattern through a telescope during the rotation. Then fringe shifts from six (Michelson and Morley) or twenty (Miller) successive rotations are averaged to improve the signal to noise ratio, and the average sidereal time noted. Some examples are shown in Fig. 2, and illustrate the incredibly clear signal. The ongoing claim that the Michelson-Morely experiment was a null experiment is disproved. And as well, as discussed in [1, 2, 21], they detected gravitational waves, *viz* 3-space turbulence in 1887. The new data analysed herein is from one-way optical fiber and Doppler shift spacecraft experiments. The agreement between these and the gas-mode interferometer techniques demonstrate that the Fitzgerald-Lorentz contraction effect is a real dynamical effect. The null results from the vacuum-mode interferometers [4] and LIGO follow simply from having $n = 1$ giving $k^2 = 0$ in (11).

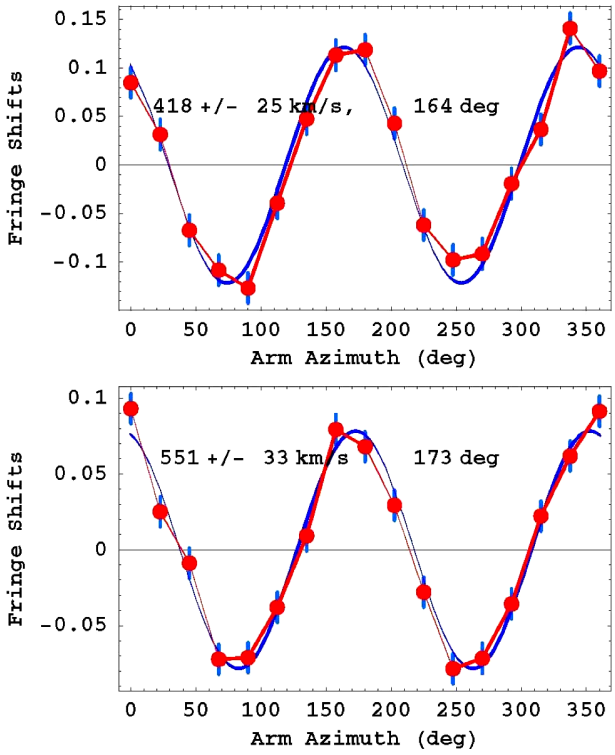

Fig. 2: (a) A typical Miller averaged-data from September 16, 1925, $4^{\rm h}40'$ Local Sidereal Time (LST) — an average of data from 20 turns of the gas-mode Michelson interferometer. Plot and data after fitting using (12), and then subtracting both the temperature drift and Hicks effects from both, leaving the expected sinusoidal form. The error bars are determined as the rms error in this fitting procedure, and show how exceptionally small were the errors, and which agree with Miller's claim for the errors. (b) Best result from the Michelson-Morley 1887 data — an average of 6 turns, at $7^{\rm h}$ LST on July 11, 1887. Again the rms error is remarkably small. In both cases the indicated speed is v_P — the 3-space speed projected onto the plane of the interferometer. The angle is the azimuth of the 3-space speed projection at the particular LST. The speed fluctuations from day to day significantly exceed these errors, and reveal the existence of 3-space flow turbulence — i.e gravitational waves.

5 Sun 3-space inflow from Miller interferometer data

Miller was led to the conclusion that for reasons unknown the existing theory of the Michelson interferometer did not reveal true values of v_P, and for this reason he introduced the parameter k, with $\overline{k}$ herein indicating his numerical values. Miller had reasoned that he could determine both $\mathbf{v}_{galactic}$ and $\overline{k}$ by observing the interferometer-determined v_P and ψ over a year because the known orbital speed of the Earth about the Sun of 30 km/s would modulate both of these observables, giving what he termed an aberration effect as shown in Fig. 11, and by a scaling argument he could determine the absolute velocity of the solar system. In this manner he finally determined that $|\mathbf{v}_{galactic}| = 208$ km/s in the direction $(\alpha = 4^{\rm h}54^{\rm m}, \delta = -70^\circ 33')$. However now that the theory of the Michelson interferometer has been revealed an anomaly becomes apparent. Table 2 shows $v = v_M/k_{air}$, the speed determined using (11), for each of the four epochs. However Table 3 also shows that $\overline{k}$ and the speeds $\overline{v} = v_M/\overline{k}$ determined by the scaling argument are considerably different. We denote by v_M the notional speeds determined from (11) using the Michelson Newtonian-physics value of $k = 1$. The v_M values arise after taking account of the projection effect. That $\overline{k}$ is considerably larger than the value of k_{air} indicates that another velocity component has been overlooked. Miller of course only knew of the tangential orbital speed of the Earth, whereas the new physics predicts that as-well there is a 3-space radial inflow $\mathbf{v}_{sun} = 42$ km/s at 1AU. We can approximately re-analyse Miller's data to extract a first approximation to the speed of this inflow component. Clearly it is $v_R = \sqrt{v_{sun}^2 + v_{orbital}^2}$ that sets the scale, see Fig. 4 and not $v_{orbital}$, and because $\overline{k} = v_M/v_{orbit}$ and $k_{air} = v_M/v_R$ are the scaling relations, then

$$v_{sun} = v_{orbital}\sqrt{\frac{v_R^2}{v_{orbital}^2} - 1} = v_{orbital}\sqrt{\frac{\overline{k}^2}{k_{air}^2} - 1}\,. \quad (13)$$

Epoch 1925/26	v_M	$\overline{k}$	$v = v_M/k_{air}$	$\overline{v} = v_M/\overline{k}$	$v = \sqrt{3}\overline{v}$	v_{sun}
February 8	9.3 km/s	0.048	385.9 km/s	193.8 km/s	335.7 km/s	51.7 km/s
April 1	10.1	0.051	419.1	198.0	342.9	56.0
August 1	11.2	0.053	464.7	211.3	366.0	58.8
September 15	9.6	0.046	398.3	208.7	361.5	48.8

Table 1: The $\overline{k}$ anomaly: $\overline{k} \gg k_{air} = 0.0241$, as the 3-space inflow effect. Here v_M and $\overline{k}$ come from fitting the interferometer data using Newtonian physics (with $v_{orbital} = 30$ km/s used to determine $\overline{k}$), while v and $\overline{v}$ are computed speeds using the indicated scaling. The average of the Sun inflow speeds, at 1AU, is $v_{sun} = 54 \pm 6$ km/s, compared to the predicted inflow speed of 42 km/s from (7). From column 4 we obtain the average galactic flow of $v = 417 \pm 50$ km/s, compared with the NASA-data determined flow of 486 km/s.

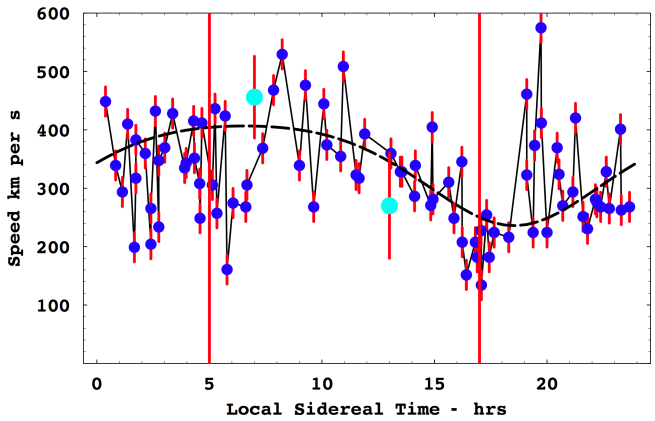

Fig. 3: Speeds v_P, of the 3-space velocity $\mathbf{v}$ projected onto the horizontal plane of the Miller gas-mode Michelson interferometer located atop Mt.Wilson, plotted against local sidereal time in hours, for a composite day, with data collected over a number of days in September 1925, [8]. The data shows considerable fluctuations, from hour to hour, and also day to day, as this is a composite day. The dashed curve shows the non-fluctuating best-fit variation over one day, as the Earth rotates, causing the projection onto the plane of the interferometer of the velocity of the average direction of the space flow to change. The maximum projected speed of the curve is 417 km/s (using the STP air refractive index of $n = 1.00029$ in (11) (atop Mt. Wilson the better value of $n = 1.00026$ is suggested by the NASA data), and the min/max occur at approximately 5hrs and 17hrs local sidereal time (Right Ascension). Note from Fig. 11 and Table 2 that the Cassini flyby in August gives a RA$= 5.15^{\text{h}}$, close to the RA apparent in the above plot. The error bars are determined by the method discussed in Fig. 2. The green data points, with error bars, at 7^{h} and 13^{h} are from the Michelson-Morley 1887 data, from averaging (excluding only the July 8 data for 7^{h} because it has poor S/N), and with same rms error analysis. The fiducial time lines at 5^{h} and 17^{h} are the same as those shown in Figs. 6 and 11. The speed fluctuations are seen to be much larger than the statistically determined errors, confirming the presence of turbulence in the 3-space flow, i.e gravitational waves, as first seen in the Michelson-Morley experiment.

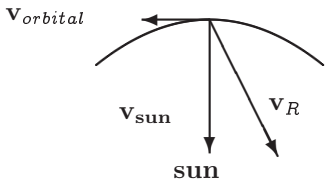

Fig. 4: Orbit of earth about the Sun defining the plane of the ecliptic with tangential orbital velocity $\mathbf{v}_{orbital}$ and the Sun inflow velocity $\mathbf{v}_{sun}$. Then $\mathbf{v}_R = \mathbf{v}_{sun} - \mathbf{v}_{orbital}$ is the velocity of the 3-space relative to the Earth, but not showing the $\mathbf{v}_{galactic}$ contribution.

Using the $\overline{k}$ values in Table 1 and the value* of k_{air} we obtain the v_{sun} speeds shown in Table 1, which give an averaged speed of 54 ± 6 km/s, compared to the predicted inflow speed of 42 km/s. Of course this simple re-scaling of the Miller results is not completely valid because the direction of $\mathbf{v}_R$ is of course different to that of $\mathbf{v}_{orbital}$, nevertheless the Sun inflow speed of $v_{sun} = 54 \pm 5$ km/s at 1AU from this analysis is reasonably close to the predicted value of 42 km/s.

6 Generalised Maxwell equations and the Sun 3-space inflow light bending

One of the putative key tests of the GR formalism was the gravitational bending of light by the Sun during the 1915 solar eclipse. However this effect also immediately follows from the new 3-space dynamics once we also generalise the Maxwell equations so that the electric and magnetic fields are excitations of the dynamical space. The dynamics of the electric and magnetic fields must then have the form, in empty space,

$$\left.\begin{aligned} \nabla \times \mathbf{E} &= -\mu \left(\frac{\partial \mathbf{H}}{\partial t} + \mathbf{v} \cdot \nabla \mathbf{H} \right), \quad \nabla \cdot \mathbf{E} = \mathbf{0}, \\ \nabla \times \mathbf{H} &= \epsilon \left(\frac{\partial \mathbf{E}}{\partial t} + \mathbf{v} \cdot \nabla \mathbf{E} \right), \quad \nabla \cdot \mathbf{H} = \mathbf{0}, \end{aligned}\right\} \tag{14}$$

*We have not modified this value to take account of the altitude effect or temperatures atop Mt.Wilson. This weather information was not recorded by Miller. The temperature and pressure effect is that $n = 1.0 + 0.00029 \frac{P}{P_0} \frac{T_0}{T}$, where T is the temperature in 0 K and P is the pressure in atmospheres. $T_0 = 273$K and $P_0 =$1atm. The NASA data implies that atop Mt. Wilson the air refractive index was probably close to $n = 1.00026$.

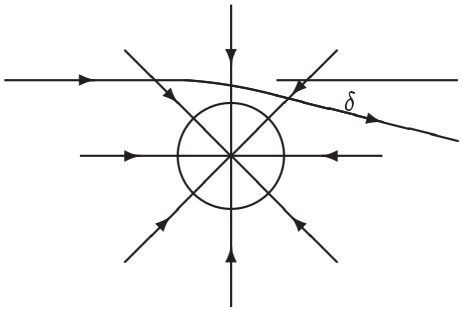

Fig. 5: Shows bending of light through angle δ by the inhomogeneous spatial inflow, according to the minimisation of the travel time in (18). This effect permits the inflow speed at the surface of the Sun to be determined to be 615 km/s. The inflow speed into the Sun at the distance of the Earth from the Sun has been extracted from the Miller data, giving 54 ± 6 km/s.

which was first suggested by Hertz in 1890 [23], but with $\mathbf{v}$ being a constant vector field. Suppose we have a uniform flow of space with velocity $\mathbf{v}$ wrt the embedding space or wrt an observer's frame of reference. Then we can find plane wave solutions for (14):

$$\mathbf{E}(\mathbf{r},t) = \mathbf{E}_0 e^{i(\mathbf{k}\cdot\mathbf{r}-\omega t)} \quad \mathbf{H}(\mathbf{r},t) = \mathbf{H}_0 e^{i(\mathbf{k}\cdot\mathbf{r}-\omega t)} \qquad (15)$$

with

$$\omega(\mathbf{k},\mathbf{v}) = c|\vec{\mathbf{k}}| + \mathbf{v}\cdot\mathbf{k} \quad \text{where} \quad c = 1/\sqrt{\mu\epsilon}\,. \qquad (16)$$

Then the EM group velocity is

$$\mathbf{v}_{EM} = \vec{\nabla}_k\,\omega(\mathbf{k},\mathbf{v}) = c\hat{\mathbf{k}} + \mathbf{v}\,. \qquad (17)$$

So the velocity of EM radiation $\mathbf{v}_{EM}$ has magnitude c only with respect to the space, and in general not with respect to the observer if the observer is moving through space. These experiments show that the speed of light is in general anisotropic, as predicted by (17). The time-dependent and inhomogeneous velocity field causes the refraction of EM radiation. This can be computed by using the Fermat least-time approximation. Then the EM ray paths $\mathbf{r}(t)$ are determined by minimising the elapsed travel time:

$$\tau = \int_{s_i}^{s_f} \frac{ds\left|\dfrac{d\mathbf{r}}{ds}\right|}{|c\hat{\mathbf{v}}_R(s) + \mathbf{v}(\mathbf{r}(\mathbf{s}),\mathbf{t}(\mathbf{s})|}\,, \qquad (18)$$

$$\mathbf{v}_R = \left(\frac{d\mathbf{r}}{dt} - \mathbf{v}(\mathbf{r}(\mathbf{t}),\mathbf{t})\right), \qquad (19)$$

by varying both $\mathbf{r}(s)$ and $t(s)$, finally giving $\mathbf{r}(t)$. Here s is a path parameter, and $\mathbf{v}_R$ is the 3-space vector tangential to the path. For light bending by the Sun inflow (7) the angle of deflection is

$$\delta = 2\,\frac{v^2}{c^2} = \frac{4GM(1+\frac{\alpha}{2}+\dots)}{c^2 d} + \dots \qquad (20)$$

where v is the inflow speed at distance d and d is the impact parameter. This agrees with the GR result except for the α correction. Hence the observed deflection of 8.4×10^{-6} radians is actually a measure of the inflow speed at the Sun's surface, and that gives $v = 615$ km/s, in agreement with (7). These generalised Maxwell equations also predict gravitational lensing produced by the large inflows associated with the new "black holes" in galaxies.

7 Torr and Kolen RF one-way coaxial cable experiment

A one-way coaxial cable experiment was performed at the Utah University in 1981 by Torr and Kolen [12]. This involved two rubidium vapor clocks placed approximately 500 m apart with a 5 MHz sinewave RF signal propagating between the clocks via a nitrogen filled coaxial cable buried in the ground and maintained at a constant pressure of $\sim$2 psi. Torr and Kolen observed variations in the one-way travel time, as shown in Fig. 7 by the data points. The theoretical predictions for the Torr-Kolen experiment for a cosmic speed of 480 km/s in the direction ($\alpha = 5^{\mathrm{h}}, \delta = -70^\circ$), and including orbital and in-flow velocities, are shown in Fig. 7. The maximum/minimum effects occurred, typically, at the predicted times. Torr and Kolen reported fluctuations in both the magnitude, from 1–3 ns, and time of the maximum variations in travel time, just as observed in all later experiments — namely wave effects.

8 Krisher *et al.* one-way optical-fiber experiment

The Krisher *et al.* one-way experiment [18] used two hydrogen maser oscillators with light sent in each direction through optical fiber of length approximately 29 km. The optical fiber was part of the NASA DSN Deep Space Communications Complex in the Mojave desert at Goldstone, California. Each maser provided a stable 100-MHz output frequency. This signal was split, with one signal being fed directly into one channel of a Hewlett-Packard Network Analyzer. The other signal was used to modulate a laser carrier signal propagated along a 29 km long ultrastable fiber optics link that is buried five feet underground. This signal was fed into the second channel of the other Network Analyzer at the distant site. Each analyzer is used to measure the relative phases of the masers, ϕ_1 and ϕ_2. The data collection began on November 12 1988 at 20:00:00 (UTC), with phase measurements made every ten seconds until November 17 1988 at 17:30:40 (UTC). Figs. 6(a) and (f) shows plots of the phase difference $\phi_1 - \phi_2$ and phase sum $\phi_1 + \phi_2$, in degrees, after removing a bias and a linear trend, as well as being filtered using a Fast Fourier Transform. The data is plotted against local sidereal time. In analysing the phase data the propagation path was taken to be along a straight line between the two masers, whose longitude and latitude are given by $(243^\circ 12' 21''.65,\ 35^\circ 25' 33''.37)$ and $(243^\circ 06' 40''.37,\ 35^\circ 14' 51''.82)$. Fig. 6

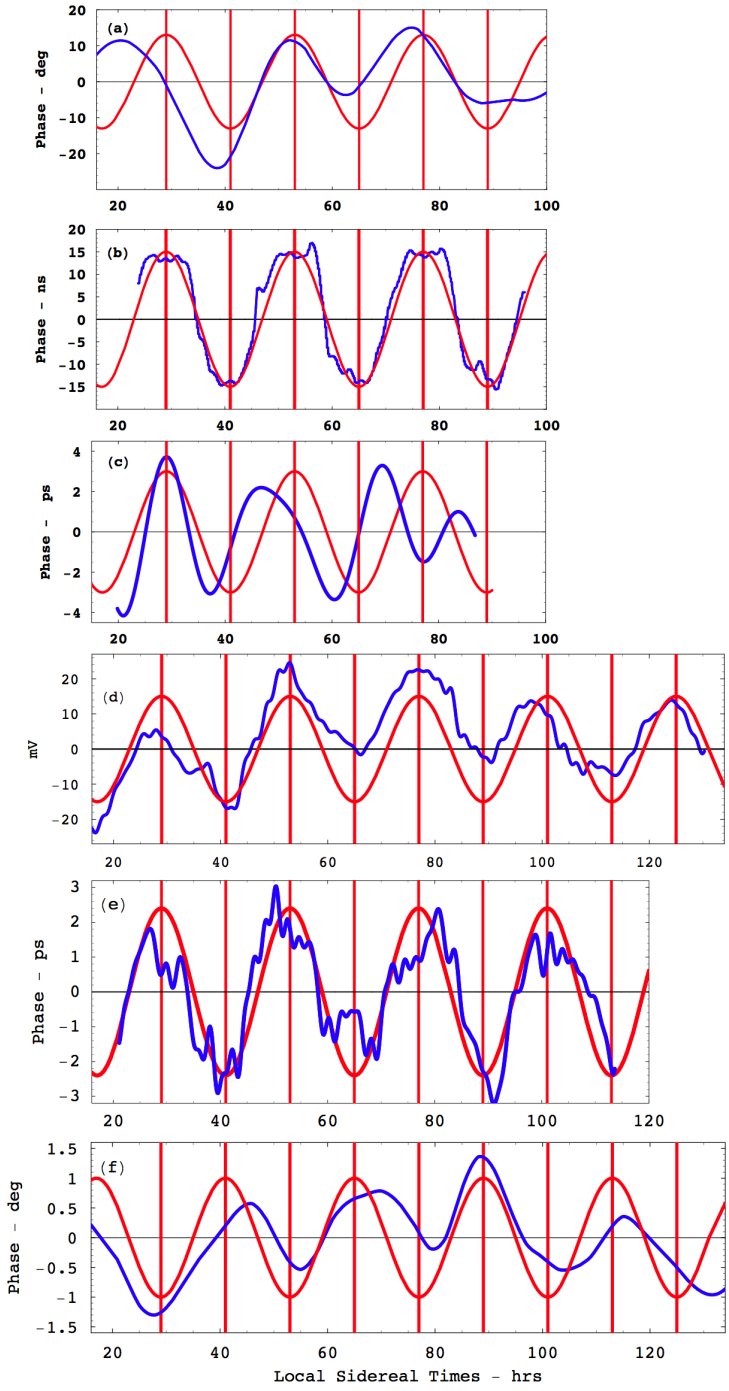

Fig. 6: Data from five different EM speed anisotropy experiments showing earth rotation wrt local preferred frame, as shown by sidereal time phasing, together with wave effects. In all cases a zero bias was removed and low-pass filtering was applied. **(a)**: Krisher [18] optical fiber phase difference data $\phi_1 - \phi_2$, in degrees. **(b)**: DeWitte [13] RF coaxial cable phase data, in ns. The DeWitte cable ran NS. **(c):** Cahill [14] hybrid optical-fiber/RF coaxial-cable data, in ps, from August 2006. Cable ran NS. **(d):** Cahill [16, 17] optical-fiber Michelson interferometer, in photodiode mV, from September 18, 2007. **(e):** Cahill RF coaxial-cable data, in ps, from May 2009. Cable ran NS. **(f)**: Krisher [18] optical fiber phase sum data $\phi_1 + \phi_2$, in degrees. In each case the (red) sinusoidal curves shows the phase expected for a RA of 5^{h}, but with arbitrary magnitudes. The vertical lines are at local sidereal times of 5^{h} and 17^{h}, on successive days, corresponding to the RAs shown in red in Fig. 11. The Krisher data gives a local sidereal time of 4.96^{h}, corresponding to a RA of 6.09^{h} for November — caused by the 42° azimuth angle of the optical fiber to the local meridian. This RA was used in combination with the spacecraft earth-flyby Doppler shift data. Note the amplitude and phase fluctuations in all the data — these are gravitational wave effects.

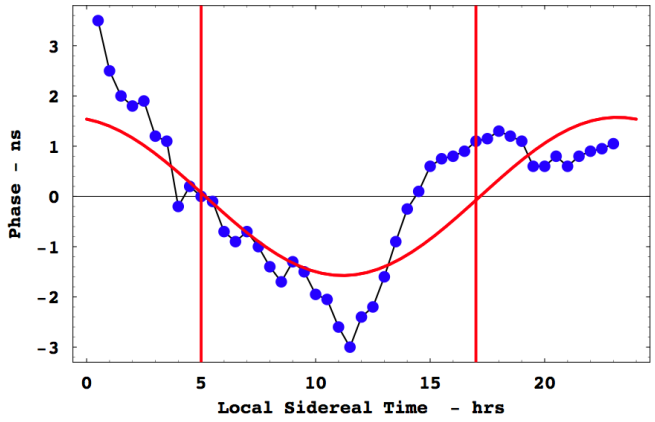

Fig. 7: Data from the 1981 Torr-Kolen experiment at Logan, Utah [12]. The data shows variations in travel times (ns), for local sidereal times, of an RF signal travelling through 500 m of coaxial cable orientated in an EW direction. Actual days are not indicated but the experiment was done during February-June 1981. Results are for a typical day. For the 1st of February the local time of 12:00 corresponds to 13:00 sidereal time. The predictions are for February, for a cosmic speed of 480 km/s in the direction ($\alpha = 5.0^{\mathrm{h}}, \delta = -70^{\circ}$), and including orbital and in-flow velocities but without theoretical turbulence. The vertical lines are at local sidereal times of 5^{h} and 17^{h}, corresponding to the RAs shown in red in Figs. 6 and 11.

shows as well the corresponding phase differences from other experiments. Krisher only compared the phase variations with that of the Cosmic Microwave Background (CMB), and noted that the phase relative to the local sidereal time differed from CMB direction by 6 hrs, but failed to notice that it agreed with the direction discovered by Miller in 1925/26 and published in 1933 [8]. The phases from the various experiments show that, despite very different longitudes of the experiments and different days in the year, they are in phase when plotted against local sidereal times. This demonstrates that the phase cycles are caused by the rotation of the Earth relative to the stars — that we are observing a galactic phenomenon, being that the 3-space flow direction is reasonably steady wrt the galaxy*. Nevertheless we note that all the phase data show fluctuations in both the local sidereal time for maxima/minima and also fluctuations in magnitude. These wave effects first appeared in experimental data of Michelson and Morley in 1887.

From the November Krisher data in Figs. 6(a) and (f) the Right Ascension of the 3-space flow direction was obtained from the local sidereal times of the maxima and minima, giving a RA of 6.09^{h}, after correcting the apparent RA of 4.96^{h} for the 42° inclination of the optical fiber to the local meridian. This RA was used in combination with the spacecraft earth-flyby Doppler shift data, and is shown in Fig. 11.

The magnitudes of the Krisher phases are not used in determining the RA for November, and so are not directly used in this report. Nevertheless these magnitudes provide a check on the physics of how the speed of light in optical fibers is affected by the 3-space flow. The phase differences $\phi_1 - \phi_2$ in Fig. 6a, which correspond to a 1st order in v/c experiment in which the Fresnel drag effect must be taken into account, are shown to be consistent with the determined speed for November, noting that the use of phase comparators does not allow the determination of multiple 360° contributions to the phase differences. The analysis of the Krisher phase sum $\phi_1 + \phi_2$ in Fig. 6f, which correspond to a 2nd order in v/c experiment, requires the Lorentz contraction of the optical fibers. as well as the Fresnel drag effect, to be taken into account. The physics of optical fibers in relation to this and other 3-space physics will be discussed more fully elsewhere.

*The same effect is observed in Ring Lasers [29] — which detect a sidereal period of rotation of the Earth, and not the solar period. Ring Lasers cannot detect the 3-space direction, only a rate of rotation.

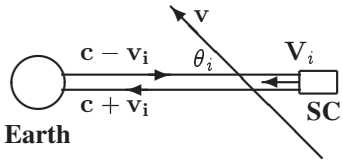

Fig. 8: Asymptotic flyby configuration in earth frame-of-reference, with spacecraft (SC) approaching Earth with velocity $\mathbf{V}_i$. The departing asymptotic velocity will have a different direction but the same speed, as no force other than conventional Newtonian gravity is assumed to be acting upon the SC. The dynamical 3-space velocity is $\mathbf{v}(\mathbf{r}, t)$, though taken to be time independent during the Doppler shift measurement, which causes the outward EM beam to have speed $c - v_i(r)$, and inward speed $c + v_i(r)$, where $v_i(r) = v(r)\cos(\theta_i)$, with θ_i the angle between $\mathbf{v}$ and $\mathbf{V}$. A similar description applies to the departing SC, labeled $i \to f$.

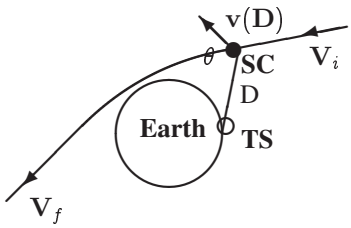

Fig. 9: Spacecraft (SC) earth flyby trajectory, with initial and final asymptotic velocity $\mathbf{V}$, differing only by direction. The Doppler shift is determined from Fig. 8 and (32). The 3-space flow velocity at the location of the SC is $\mathbf{v}$. The line joining Tracking Station (TS) to SC is the path of the RF signals, with length D. As SC approaches earth $\mathbf{v}(D)$ changes direction and magnitude, and hence magnitude of projection $v_i(D)$ also changes, due to earth component of 3-space flow and also because of RF direction to/from Tracking Station. The SC trajectory averaged magnitude of this earth in-flow is determined from the flyby data and compared with theoretical prediction.

9 3-space flow from Earth-flyby Doppler shifts

The motion of spacecraft relative to the Earth are measured by observing the direction and Doppler shift of the transponded RF transmissions. This gives another technique to determine

the speed and direction of the dynamical 3-space as manifested by the light speed anisotropy [19]. The repeated detection of the anisotropy of the speed of light has been, until recently, ignored in analysing the Doppler shift data, causing the long-standing anomalies in the analysis [20]. The use of the Minkowski-Einstein choice of time and space coordinates does not permit the analysis of these Doppler anomalies, as they mandate that the speed of the EM waves be invariant.

Because we shall be extracting the Earth inflow effect we need to take account of a spatially varying, but not time-varying, 3-space velocity. In the Earth frame of reference, see Fig. 8, and using clock times from earth-based clocks, let the transmitted signal from earth have frequency f. The time for one RF maximum to travel distance D to SC from earth is, see Fig. 9,

$$t_1 = \int_0^D \frac{dr}{c - v_i(r)} \,. \tag{21}$$

The next RF maximum leaves time $T = 1/f$ later and arrives at SC at time, taking account of SC motion,

$$t_2 = T + \int_0^{D-VT} \frac{dr}{c - v_i(r)} \,. \tag{22}$$

The period at the SC of the arriving RF is then

$$T' = t_2 - t_1 = T + \int_D^{D-VT} \frac{dr}{c - v_i(r)} \approx \approx \frac{c - v_i(D) - V}{c - v_i(D)}\, T \,. \tag{23}$$

Essentially this RF is reflected* by the SC. Then the 1st RF maximum takes time to reach the Earth

$$t_1' = -\int_{D-VT}^0 \frac{dr}{c + v_i(r)} \tag{24}$$

and the 2nd RF maximum takes time

$$t_2' = T' - \int_{D-VT-VT'}^0 \frac{dr}{c + v_i(r)} \,. \tag{25}$$

Then the period of the returning RF at the Earth is

$$\begin{aligned} T'' &= t_2' - t_1' = \\ &= T' + \int_{D-VT}^{D-VT-VT'} \frac{dr}{c + v_i(r)} \approx \\ &\approx \frac{c + v_i(D) - V}{c + v_i(D)}\, T' . \end{aligned} \tag{26}$$

Then overall we obtain the return frequency to be†

$$f'' = \frac{1}{T''} = \frac{c + v_i(D)}{c + v_i(D) - V} \cdot \frac{c - v_i(D)}{c - v_i(D) - V}\, f \,. \tag{27}$$

*In practice a more complex protocol is used.

†This corrects the corresponding expression in [19], but without affecting the final results.

Ignoring the projected 3-space velocity $v_i(D)$, that is, assuming that the speed of light is invariant as per the usual literal interpretation of the Einstein 1905 light speed postulate, we obtain instead

$$f'' = \frac{c^2}{(c - V)^2}\, f \,. \tag{28}$$

The use of (28) instead of (27) is the origin of the putative anomalies. Expanding (28) we obtain

$$\frac{\Delta f}{f} = \frac{f'' - f}{f} = \frac{2V}{c} \,. \tag{29}$$

However expanding (27) we obtain, for the same Doppler shift,

$$\frac{\Delta f}{f} = \frac{f'' - f}{f} = \left(1 + \frac{v(D)^2}{c^2}\right) \frac{2V}{c} + \dots \tag{30}$$

It is the prefactor to $2V/c$ missing from (29) that explains the spacecraft Doppler anomalies, and also permits yet another determination of the 3-space velocity $\mathbf{v}(D)$, *viz* at the location of the SC. The published data does not give the Doppler shifts as a function of SC location, so the best we can do at present is to use a SC trajectory-averaged $v(D)$, namely $\overline{v}_i$ and $\overline{v}_f$, for the incoming and outgoing trajectories, as further discussed below.

From the observed Doppler shift data acquired during a flyby, and then best fitting the trajectory, the asymptotic hyperbolic speeds $V_{i\infty}$ and $V_{f\infty}$ are inferred from (29), but incorrectly so, as in [20]. These inferred asymptotic speeds may be related to an inferred asymptotic Doppler shift

$$\frac{\Delta f_{i\infty}}{f} = \frac{f'_\infty - f}{f} = \frac{2V_{i\infty}}{c} + \dots \tag{31}$$

which from (30) gives

$$V_{i\infty} \equiv \frac{\Delta f_{i\infty}}{f} \cdot \frac{c}{2} = \left(1 + \frac{\overline{v}_i^2}{c^2}\right) V + \dots \tag{32}$$

where V is the actual asymptotic speed. Similarly after the flyby we obtain

$$V_{f\infty} \equiv \frac{\Delta f_{f\infty}}{f} \cdot \frac{c}{2} = \left(1 + \frac{\overline{v}_f^2}{c^2}\right) V + \dots \tag{33}$$

and we see that the "asymptotic" speeds $V_{i\infty}$ and $V_{f\infty}$ must differ, as indeed reported in [20]. We then obtain the expression for the so-called flyby anomaly

$$\Delta V_\infty = V_{f\infty} - V_{i\infty} = \frac{\overline{v}_f^2 - \overline{v}_i^2}{c^2}\, V \tag{34}$$

where here $V \approx V_\infty$ to sufficient accuracy, where V_∞ is the average of $V_{i\infty}$ and $V_{f\infty}$, The existing data on $\mathbf{v}$ permits *ab*

initio predictions for ΔV_∞. As well a separate least-squares-fit to the individual flybys permits the determination of the average speed and direction of the 3-space velocity, relative to the Earth, during each flyby. These results are all remarkably consistent with the data from the various laboratory experiments that studied $\mathbf{v}$. We now indicate how $\overline{v}_i$ and $\overline{v}_f$ were parametrised during the best-fit to the flyby data. In (10) $\mathbf{v}_{galactic} + \mathbf{v}_{sun} - \mathbf{v}_{orbital}$ was taken as constant during each individual flyby, with $\mathbf{v}_{sun}$ inward towards the Sun, with value 42 km/s, and $\mathbf{v}_{orbital}$ as tangential to earth orbit with value 30 km/s — consequentially the directions of these two vectors changed with day of each flyby. The earth inflow $\mathbf{v}_{earth}$ in (10) was taken as radial and of an unknown fixed trajectory-averaged value. So the averaged direction but not the averaged speed varied from flyby to flyby, with the incoming and final direction being approximated by the (α_i, δ_i) and (α_f, δ_f) asymptotic directions shown in Table 2. The predicted theoretical variation of $v_{earth}(R)$ is shown in Fig. 10. To best constrain the fits to the data the flyby data was used in conjunction with the RA from the Krisher optical fiber data. This results in the aberration plot in Fig. 11, the various flyby data in Table 2, and the Earth in-flow speed determination in Fig. 12. The results are in remarkable agreement with the results from Miller, showing the extraordinary skill displayed by Miller in carrying out his massive interferometer experiment and data analysis in 1925/26. The only effect missing from the Miller analysis is the spatial in-flow effect into the Sun, which affected his data analysis, but which has been partially corrected for in Sect. 5. Miller obtained a galactic flow direction of $\alpha = 4.52$ hrs, $\delta = -70.5^\circ$, compared to that obtained herein from the NASA data of $\alpha = 4.29$ hrs, $\delta = -75.0^\circ$, which differ by only $\approx 5^\circ$.

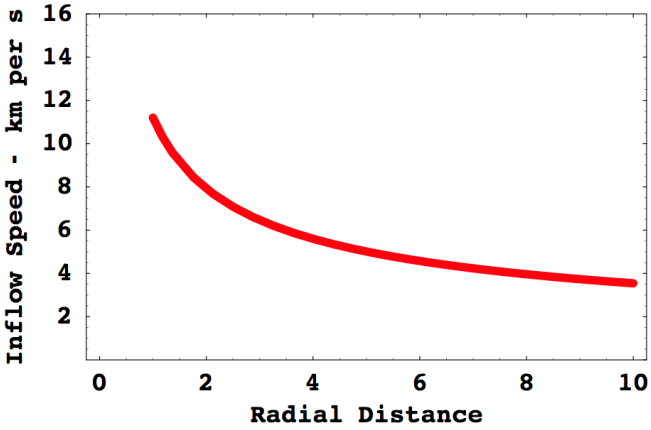

Fig. 10: Earth 3-space inflow speed vs distance from earth in earth radii, as given in (7), plotted only for $R > 1.0$. Combining the NASA/JPL optical fiber RA determination and the flyby Doppler shift data has permitted the determination of the angle- and distance-averaged inflow speed, to be 12.4 ± 5km/s.

10 Earth 3-space inflow: Pound and Rebka experiment

The numerous EM anisotropy experiments discussed herein demonstrate that a dynamical 3-space exists, and that the speed of the earth wrt this space exceeds 1 part in 1000 of c, namely a large effect. Not surprisingly this has indeed been detected many times over the last 120 years. The speed of nearly 500 km/s means that earth based clocks experience a real, so-called, time dilation effect from (6) of approximately 0.12 s per day compared to cosmic time. However clocks may be corrected for this clock dilation effect because their speed v though space, which causes their slowing, is measurable by various experimental methods. This means that the absolute or cosmic time of the universe is measurable. This very much changes our understanding of time. However because of the inhomogeneity of the Earth 3-space in-flow component the clock slowing effect causes a differential effect for clocks at different heights above the Earth's surface. It was this effect that Pound and Rebka reported in 1960 using the Harvard tower [28]. Consider two clocks at heights h_1 and h_2, with $h = h_2 - h_1$, then the frequency differential follows from (6),

$$\begin{aligned}
\frac{\Delta f}{f} &= \sqrt{1 - \frac{v^2(h_2)}{c^2}} - \sqrt{1 - \frac{v^2(h_1)}{c^2}} \approx \\
&\approx \frac{v^2(h_1) - v^2(h_2)}{2c^2} + \cdots = \\
&= \frac{1}{2c^2}\frac{dv^2(r)}{dr}\,h + \cdots = \\
&= \frac{g(r)\,h}{c^2} + \cdots = \\
&= -\frac{\Delta\Phi}{c^2} + \ldots
\end{aligned} \tag{35}$$

using (3) with $\mathbf{v}\cdot\nabla\mathbf{v} = \nabla\left(\frac{v^2}{2}\right)$ for zero vorticity $\nabla\times\mathbf{v} = \mathbf{0}$, and ignoring any time dependence of the flow, and where finally, $\Delta\Phi$ is the change in the gravitational potential. The actual process here is that, say, photons are emitted at the top of the tower with frequency f and reach the bottom detector with the same frequency f — there is no change in the frequency. This follows from (23) but with now $V = 0$ giving $T = T'$. However the bottom clock is running slower because the speed of space there is faster, and so this clock determines that the falling photon has a higher frequency, ie. appears blue shifted. The opposite effect is seen for upward travelling photons, namely an apparent red shift as observed by the top clock. In practice the Pound-Rebka experiment used motion induced Doppler shifts to make these measurements using the Mössbauer effect. The overall conclusion is that Pound and Rebka measured the derivative of v^2 wrt to height, whereas herein we have measured that actual speed, but averaged wrt the SC trajectory measurement protocol. It is important to note that the so-called "time dilation" effect is really a "clock slowing" effect — clocks are simply slowed by their movement through 3-space. The Gravity Probe A

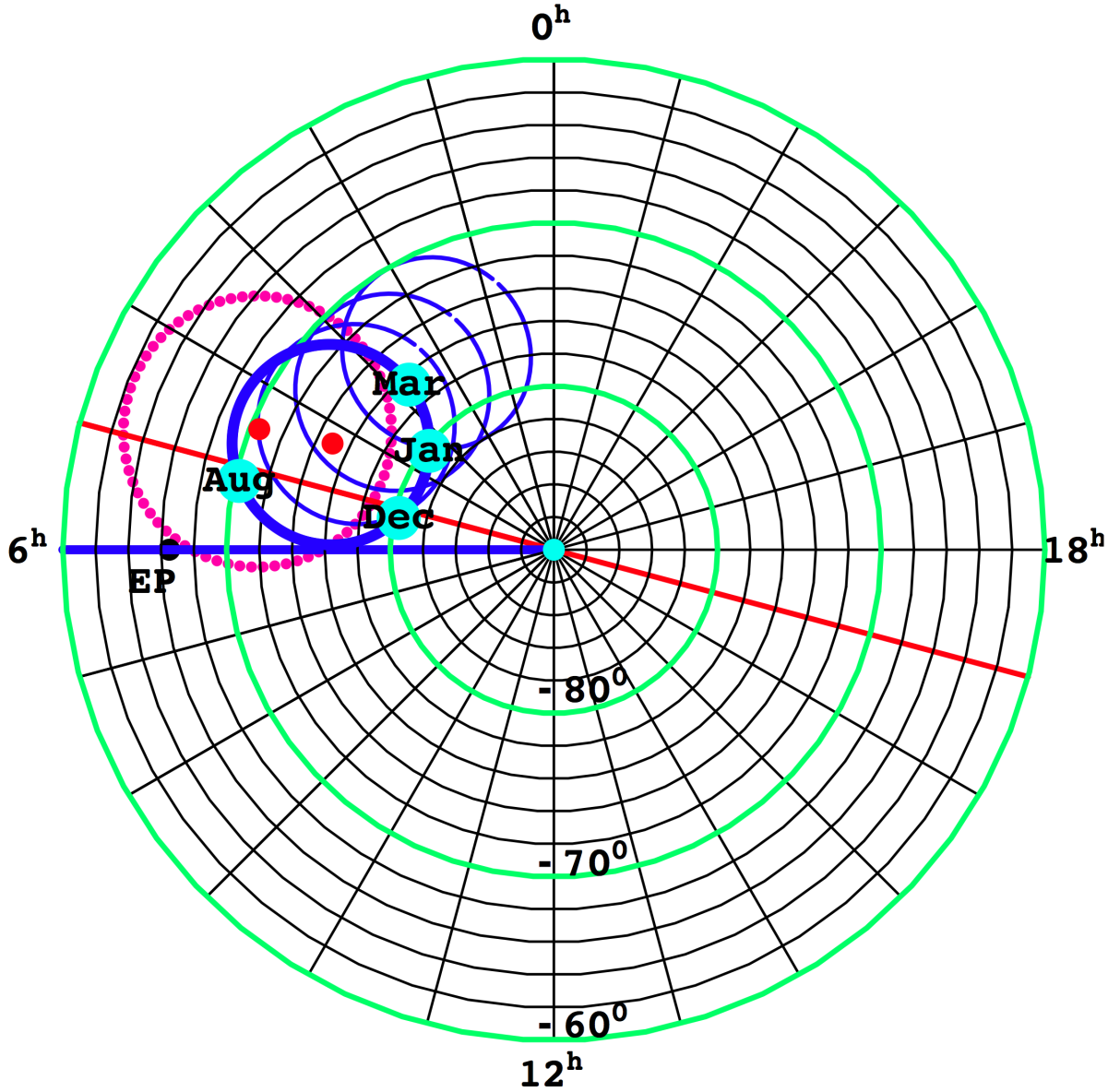

Fig. 11: South celestial sphere with RA and Dec shown. The red dotted circle shows the Miller aberration path discovered in 1925/26, from [8]. The red point at $\alpha = 4.52$ hrs, $\delta = -70.5^\circ$ shows the galactic flow direction determined by Miller, after removing earth-orbit aberration effect. The dark blue circle shows the aberration path from best-fitting the Earth-flyby Doppler shift data and using the optical-fiber RA data point for November from Krisher [18], see Fig. 12. This corresponds to a best fit averaged earth inflow speed of 12.4 ± 5km/s. The blue aberration paths show the best-fit if (a) upper circle: earth inflow speed = 0 km/s, (b) = 4.0 km/s, (c) = 8.0 km/s and (d) = 12.4 km/s (thick blue circle). The actual 3-space flow directions are shown by light-blue background to labels for the flybys in Aug, Dec, Jan and Mar, and given in Table 2. The red point at $\alpha = 4.29$ hrs, $\delta = -75.0^\circ$ shows the optical-fiber/earth-flyby determined galactic flow direction, also after removal of earth-orbit aberration effect, and is only 5° from the above mentioned Miller direction. The miss-fit angle $\Delta\theta$ between the best-fit RA and Dec for each flyby is given in Table 2, and are only a few degrees on average, indicating the high precision of the fit. This plot shows the remarkable concordance between the NASA/JPL determined 3-space flow characteristics and those determined by Miller in 1925/26. It must be emphasised that the optical-fiber/flyby aberration plot and galactic 3-space flow direction is obtained completely independently of the Miller data. The blue line at $6.09^{\rm h}$ is the orientation corrected Krisher RA, and has an uncertainty of $\pm 1^{\rm h}$, caused by wave/turbulence effects. The fiducial RA of $5^{\rm h}$ and $17^{\rm h}$, shown in red, are the fiducial local sidereal times shown in Figs. 3, 6 and 7. The point EP is the pole of the ecliptic. The speed and declination differences between the Miller and NASA data arise from Miller being unaware of the Sun 3-space inflow effect — correcting for this and using an air refractive index of $n = 1.00026$ atop Mt. Wilson increases the Miller data determined speed and moves the declination slightly southward, giving an even better agreement with the NASA data. Here we have merely reproduced the Miller aberration plot from [8].

Parameter	GLL-I	GLL-II	NEAR	Cassini	Rosetta	M'GER
Date	Dec 8, 1990	Dec 8, 1992	Jan 23, 1998	Aug 18, 1999	Mar 4, 2005	Aug 2, 2005
V_∞ km/s	8.949	8.877	6.851	16.010	3.863	4.056
α_i deg	266.76	219.35	261.17	334.31	346.12	292.61
δ_i deg	-12.52	−34.26	−20.76	−12.92	−2.81	31.44
α_f deg	219.97	174.35	183.49	352.54	246.51	227.17
δ_f deg	−34.15	−4.87	−71.96	−4.99	−34.29	−31.92
α_v hrs	5.23	5.23	3.44	5.18	2.75	4.89
δ_v deg	−80.3	−80.3	−80.3	−70.3	−76.6	−69.5
v km/s	490.6	490.6	497.3	478.3	499.2	479.2
(O) ΔV_∞ mm/s	3.92±0.3	−4.6±1.0	13.46±0.01	−2±1	1.80±0.03	0.02±0.01
(P) ΔV_∞ mm/s	4.07	−5.26	13.45	−0.76	0.86	−4.56
(P) $\Delta\theta$ deg	1	1	2	4	5	—

Table 2: Earth flyby parameters from [20] for spacecraft Galileo (GLL: flybys I and II), NEAR, Cassini, Rosetta and MESSENGER (M'GER). V_∞ is the average osculating hyperbolic asymptotic speed, α and δ are the right ascension and declination of the incoming (i) and outgoing (f) osculating asymptotic velocity vectors, and (O) ΔV_∞ is the putative "excess speed" anomaly deduced by assuming that the speed of light is isotropic in modeling the Doppler shifts, as in (31). The observed (O) ΔV_∞ values are from [20], and after correcting for atmospheric drag in the case of GLL-II, and thruster burn in the case of Cassini. (P) ΔV_∞ is the predicted "excess speed", using (34), after least-squares best-fitting that data using (34): α_v and δ_v and v are the right ascension, declination and the 3-space flow speed for each flyby date, which take account of the Earth-orbit aberration and earth inflow effects, and correspond to a galactic flow with $\alpha = 4.29$ hrs, $\delta = -75.0^\circ$ and $v = 486$ km/s in the solar system frame of reference. $\Delta\theta$ is the error, in the best fit, for the aberration determined flow direction, from the nearest flyby flow direction. In the fitting the MESSENGER data is not used, as the data appears to be anomalous.

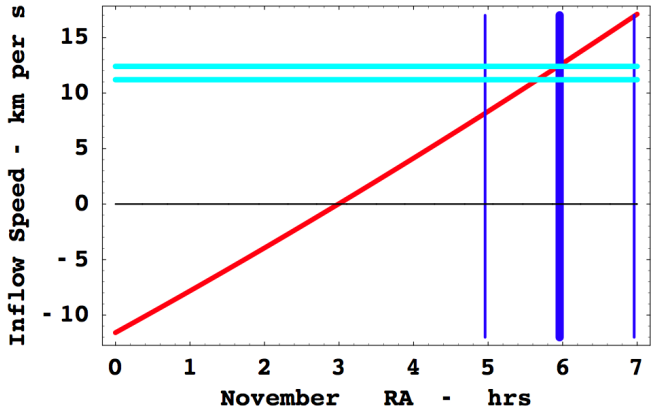

Fig. 12: The weighted angle- and distance-averaged earth 3-space inflow speed v_{earth}, see Fig. 10, as determined from NASA data, upper green plot. Uses the averaged Right Ascension from the Krisher *et al.* data for November, $\alpha = 4.96^{\rm h}$, but corrected to $\alpha = 6.09^{\rm h}$ for orientation effect of the optical fiber, shown by the thick blue line, with uncertainty range from wave effects shown by two thin blue lines, compared with the predicted RA from fitting the flyby data, as shown in Fig. 11. The red plot shows that prediction for various averaged inflow speeds, with +ve speeds being an inflow, while -ve speeds are an outflow. The earth flyby aberration fits for $v_{earth} = 0, +4.0, +8.0$ and $+12.4$ km/s are shown in Fig. 11. Theory gives that the inflow speed is $+11.2$km/s at the Earth's surface — shown by lower green plot. So the detected averaged inflow speed seems to be in good agreement with an expected averaged value. This is the first detection of the Earth's spatial inflow, and the acceleration of this flow is responsible for the Earth's gravity. Note that the flyby data clearly mandates an inflow (+ve values in this figure and not an out-flow — having -ve values).

experiment [33] also studied the clock slowing effect, though again interpreted differently therein, and again complicated by additional Doppler effects.

11 CMB direction

The Cosmic Microwave Background (CMB) velocity is often confused with the Absolute Motion (AM) velocity or light-speed anisotropy velocity as determined in the experiments discussed herein. However these are unrelated and in fact point in very different directions, being almost at 90° to each other, with the CMB velocity being 369 km/s in direction $(\alpha = 11.2^{\rm h}, \delta = -7.22^\circ)$. The CMB velocity vector was first determined in 1977 by Smoot *et al.* [30].

The CMB velocity is obtained by defining a frame of reference in which the thermalised CMB 3°K radiation is isotropic, that is by removing the dipole component, and the CMB velocity is the velocity of the Earth in that frame. The CMB velocity is a measure of the motion of the solar system relative to the last scattering surface (a spherical shell) of the universe some 13.4Gyrs in the past. The concept here is that at the time of decoupling of this radiation from matter that matter was on the whole, apart from small observable fluctuations, on average at rest with respect to the 3-space. So the CMB velocity is not motion with respect to the *local* 3-space now; that is the AM velocity. Contributions to the AM velocity would arise from the orbital motion of the solar system within the Milky Way galaxy, which has a speed of some 250 km/s, and contributions from the motion of the Milky

Way within the local cluster, and so on to perhaps super clusters, as well as flows of space associated with gravity in the Milky Way and local galactic cluster etc. The difference between the CMB velocity and the AM velocity is explained by the spatial flows that are responsible for gravity at the galactic scales.

12 Conclusions

We have shown that the NASA/JPL optical fiber and spacecraft earth flyby data give another independent determination of the velocity of the solar system through a dynamical 3-space. The resulting direction is in remarkable agreement with the direction determined by Miller in 1925/26 using a gas-mode Michelson interferometer. The Miller speed requires a better knowledge of the refractive index of the air atop Mt. Wilson, where Miller performed his experiments, but even using the STP value we obtain reasonable agreement with the NASA/JPL determined speed. Using an air refractive index of 1.00026 in place of the STP value of 1.00029 would bring the Miller speed into agreement with the NASA data determined speed. As well the NASA/JPL data has permitted the first direct measurement of the flow of 3-space into the Earth, albeit averaged over spacecraft trajectory during their flybys. This is possible because the inflow component is radially inward and so changes direction relative to the other flow components during a flyby, making the flyby Doppler shifts sensitive to the inflow speed.

It must be emphasised that the long-standing and repeated determinations of the anisotropy of vacuum EM radiation is not in itself in contradiction with the Special Relativity formalism — rather SR uses a different choice of space and time variables from those used herein, a choice which by construction mandates that the speed of EM radiation in vacuum be invariant wrt to that choice of coordinates [3]. However that means that the SR formalism cannot be used to analyse EM radiation anisotropy data, and in particular the flyby Doppler shift data.

The discovery of absolute motion wrt a dynamical 3-space has profound implications for fundamental physics, particularly for our understanding of gravity and cosmology. It shows that clocks, and all oscillators, whether they be classical or quantum, exhibit a slowing phenomenon, determined by their absolute speed though the dynamical 3-space. This "clock slowing" has been known as the "time dilation" effect — but now receives greater clarity. It shows that there is an absolute or cosmic time, and which can be measured by using any clock in conjunction with an absolute speed detector — many of which have been mentioned herein, and which permits the "clock slowing" effect to be compensated. This in turn implies that the universe is a far more coherent and non-locally connected process than previously realised, although a model for this has been proposed [1]. It also shows that the now standard discussion of the limitations of simultaneity were really misleading — being based on the special space and time coordinates invoked in the SR formalism, and that simultaneity is a fact of the universe, albeit an astounding one.

As well successful absolute motion experiments have always shown wave or turbulence phenomena, and at a significant scale. This is a new phenomena that is predicted by the dynamical theory of 3-space. Ongoing development of new experimental techniques to detect and characterise these wave phenomena will be reported elsewhere.

Submitted on June 18, 2009 / Accepted on July 10, 2009

References

1. Cahill R.T. Process physics: from information theory to quantum space and matter. Nova Science Pub., New York, 2005.
2. Cahill R.T. Dynamical 3-space: a review. In: *Ether Space-time and Cosmology: New Insights into a Key Physical Medium*, Duffy M. and Lévy J., eds., *Apeiron*, 2009, 135–200.
3. Cahill R.T. Unravelling Lorentz covariance and the spacetime formalism. *Progress in Physics*, 2008, v. 4, 19–24.
4. Braxmaier C. *et al. Phys. Rev. Lett.*, 2002, v. 88, 010401; Müller H. *et al. Phys. Rev. D*, 2003, v. 68, 116006-1-17; Müller H. *et al. Phys. Rev. D*, 2003, v. 67, 056006; Wolf P. *et al. Phys. Rev. D*, 2004, v. 70, 051902-1-4; Wolf P. *et al. Phys. Rev. Lett.*, 2003, v. 90, 060402; Lipa J.A. *et al. Phys. Rev. Lett.*, 2003, v. 90, 060403.
5. Cahill R.T. and Kitto K. Michelson-Morley experiments revisited. *Apeiron*, 2003, v. 10(2), 104–117.
6. Cahill R.T. The Michelson and Morley 1887 experiment and the discovery of absolute motion. *Progress in Physics*, 2005, v. 3, 25–29.
7. Michelson A.A. and Morley E.W. *Am. J. Sc.*, 1887, v. 34, 333–345.
8. Miller D.C. *Rev. Mod. Phys.*, 1933, v. 5, 203–242.
9. Illingworth K.K. *Phys. Rev.*, 1927, v. 3, 692–696.
10. Joos G. *Ann. d. Physik*, 1930, v. 7, 385.
11. Jaseja T.S. *et al. Phys. Rev. A*, 1964, v. 133, 1221.
12. Torr D.G. and Kolen P. In: *Precision Measurements and Fundamental Constants*, Taylor, B.N. and Phillips, W.D. eds. *Natl. Bur. Stand. (U.S.), Spec. Pub.*, 1984, 617, 675.
13. Cahill R.T. The Roland DeWitte 1991 experiment. *Progress in Physics*, 2006, v. 3, 60–65.
14. Cahill R.T. A new light-speed anisotropy experiment: absolute motion and gravitational waves detected. *Progress in Physics*, 2006, v. 4, 73–92.
15. Munéra H.A. *et al.* In: *Proceedings of SPIE*, 2007, v. 6664, K1–K8, eds. Roychoudhuri C. *et al.*
16. Cahill R.T. Optical-fiber gravitational wave detector: dynamical 3-space turbulence detected. *Progress in Physics*, 2007, v. 4, 63–68.
17. Cahill R.T. and Stokes F. Correlated detection of sub-mHz gravitational waves by two optical-fiber interferometers. *Progress in Physics*, 2008, v. 2, 103–110.

18. Krisher T.P., Maleki L., Lutes G.F., Primas L.E., Logan R.T., Anderson J.D. and Will C.M. Test of the isotropy of the one-way speed of light using hydrogen-maser frequency standards. *Phys. Rev. D*, 1990, v. 42, 731–734.

19. Cahill R.T. Resolving spacecraft Earth-flyby anomalies with measured light speed anistropy. *Progress in Physics*, 2008, v. 4, 9–15.

20. Anderson J.D., Campbell J.K., Ekelund J.E., Ellis J. and Jordan J.F. Anomalous orbital-energy changes observed during spacecraft flybys of Earth. *Phys. Rev. Lett.*, 2008, v. 100, 091102.

21. Cahill R.T. Quantum foam, gravity and gravitational waves. In: *Relativity, Gravitation, Cosmology: New Developments*, Dvoeglazov V., ed., Nova Science Pub., New York, 2009.

22. Hicks W.M. *Phil. Mag.*, 1902, v. 3, 9–42.

23. Hertz H. On the fundamental equations of electro-magnetics for bodies in motion. *Wiedemann's Ann.*, 1890, v. 41, 369; Electric waves. Collection of scientific papers. Dover Publ., New York, 1962.

24. Cahill R.T. Dynamical fractal 3-space and the generalised Schrödinger equation: equivalence principle and vorticity effects. *Progress in Physics*, 2006, v. 1, 27–34.

25. Cahill R.T. A quantum cosmology: no dark matter, dark energy nor accelerating Universe. arXiv: 0709.2909.

26. Cahill R.T. Unravelling the dark matter — dark energy paradigm. *Apeiron*, 2009, v. 16, no. 3, 323–375.

27. Cahill, R.T. The dynamical velocity superposition effect in the quantum-foam theory of gravity. In: *Relativity, Gravitation, Cosmology: New Developments*, Dvoeglazov V., ed., Nova Science Pub., New York, 2009.

28. Pound R.V. and Rebka Jr. G.A. *Phys. Rev. Lett.*, 1960, v. 4(7), 337–341.

29. Schreiber K.U., Velikoseltsev A., Rothacher M., Klügel T., Stedman G.E. and Wilsthire D.L. Direct measurement of diurnal polar motion by ring laser gyroscopes. *J. Geophys. Res.*, 2004, v. 109, B06405; arXiv: physics/0406156.

30. Smoot G.F., Gorenstein M.V. and Muller R.A. *Phys. Rev. Lett.*, 1977, v. 39(14), 898.

31. Cahill R.T. 3-space inflow theory of gravity: boreholes, black-holes and the fine structure constant. *Progress in Physics*, 2006, v. 2, 9–16.

32. Cahill R.T. Dark matter as a quantum foam in-flow effect. In: *Trends in Dark Matter Research*, ed. J. Val Blain, Nova Science Pub., NY, 2005, 95–140.

33. Vessot R.F.C. *et al.* Test of relativistic gravitation with a space-borne hydrogen maser. *Rev. Mod. Phys.*, 1980, v. 45, 2081.

Geometry of Space-Time

Ulrich E. Bruchholz

Schillerstrasse 36, D-04808 Wurzen, Germany

E-mail: Ulrich.Bruchholz@t-online.de; http://www.bruchholz-acoustics.de

The geometry of the space-time is deduced from gravitational and electromagnetic fields. We have to state that Rainich's "already unified field theory" is the ground work of the proposed theory. The latter is deduced independently on Rainich. Rainich's analogies are brilliantly validated. His formulae are verified this way. Further reaching results and insights demonstrate that Rainich's theory is viable. In final result, we can formulate an enhanced equivalence principle. It is the equivalence of Newton's force with the Lorentz force.

To the memory of John Archibald Wheeler, who foresaw this simple idea.

1 The predecessor

George Yuri Rainich already saw the analogies of the electromagnetic with the gravitational field. Since Einstein's equivalence principle implies a geometric approach of gravitation [1], electromagnetism has to be geometry too. Not enough, Rainich also saw that the electromagnetic field tensor is performed from the congruences of two dual surfaces. It is the analogy of the curvature vector of the current path, performed from the main normal, see on generalized Frenet formulae in [2].

One can well pursue Rainich's way in his papers from 1923 to 1924. First, he tried to find a non-Riemannian geometry for the electromagnetic vacuum field [3]. Later, he saw that Riemannian geometry is sufficient to describe electromagnetism [4, 5]. Rainich's identities (also called algebraic Rainich conditions) are deduced without special techniques in [6]. Present paper provides a further derivation of Rainich's identities, additionally identifying the concrete geometry.

Since a full geometric approach precludes sources, Rainich concluded a central role of singularities. However, it is deduced in [7] that this role is commonly overestimated. The singularities pass for a bar to the geometric approach. It is shown in [7] that formal singularities are in areas (according to observer's coordinates), which are not locally imaged. The related boundaries specify the discrete values of the integration constants from field equations [7].

2 The derivation

The first precursor is to see in [8]. The derivation follows the steps according to the chapter "Geometric interpretation of the Ricci tensor — the Ricci main directions" in [2]. As well, we shall see that the space-time involves a vital difference to other manifolds.

The known source-free Einstein-Maxwell equations

$$R_{ik} = \kappa \left(\frac{1}{4}\, g_{ik} F_{ab} F^{ab} - F_{ia} F_k{}^a \right), \tag{1}$$

$$F^{ia}{}_{;a} = 0\,, \tag{2}$$

$$F_{ij,k} + F_{jk,i} + F_{ki,j} = 0 \tag{3}$$

involve a special kind of Riemannian geometry, what is explained as follows.

The Ricci main directions (written in terms according to Eisenhart [2]) follow from

$$\det \left| R_{ik} + \rho g_{ik} \right| = 0 \tag{4}$$

with the solutions*

$$\rho_{|1} = \rho_{|4} = +\rho_0\,, \quad \rho_{|2} = \rho_{|3} = -\rho_0 \tag{5}$$

with

$$\rho_0{}^2 = R_1{}^a R^1{}_a = R_2{}^a R^2{}_a = R_3{}^a R^3{}_a = R_4{}^a R^4{}_a\,, \tag{6}$$

what leads directly to Rainich's identities

$$R_i{}^a R^k{}_a = \delta_i^k \rho_0{}^2 = \frac{1}{4}\, \delta_i^k R_a{}^b R^a{}_b\,. \tag{7}$$

Characteristical are the two double-roots, that means: There are two dual surfaces of the congruences

$$e_{|1}{}^i e_{|4}{}^k - e_{|1}{}^k e_{|4}{}^i \quad \text{and} \quad e_{|2}{}^i e_{|3}{}^k - e_{|2}{}^k e_{|3}{}^i$$

with minimal and maximal mean Riemannian curvature. $e_{|1} \ldots e_{|4}$ are the vectors of an orthogonal quadruple (vierbein) in those "main surfaces". At single roots we had 4 main directions. But we will see that the main surfaces are a spe-

*Where ρ_0 has a negative value, what has to do with the special signature of the space-time.

ciality of the space-time. With the obtained solutions we get

$$\left.\begin{aligned} g_{ik} &= e_{|1\_i}e_{|1\_k} + e_{|2\_i}e_{|2\_k} + \\ &\quad + e_{|3\_i}e_{|3\_k} - e_{|4\_i}e_{|4\_k}\,, \\ \frac{R_{ik}}{\rho_0} &= -e_{|1\_i}e_{|1\_k} + e_{|2\_i}e_{|2\_k} + \\ &\quad + e_{|3\_i}e_{|3\_k} + e_{|4\_i}e_{|4\_k}\,. \end{aligned}\right\} \tag{8}$$

If we set

$$c_{|ik} = -c_{|ki} = F_{ab}e_{|i}{}^{a}e_{|k}{}^{b} \tag{9}$$

follows from elementary calculations

$$\left.\begin{aligned} &-\kappa\left((c_{|23})^2 + (c_{|14})^2\right) = 2\rho_0\,, \\ &c_{|12} = c_{|34} = c_{|13} = c_{|24} = 0\,. \end{aligned}\right\} \tag{10}$$

With it, the field tensor

$$\begin{aligned} F_{ik} = &-c_{|14}\left(e_{|1\_i}e_{|4\_k} - e_{|1\_k}e_{|4\_i}\right) + \\ &+ c_{|23}\left(e_{|2\_i}e_{|3\_k} - e_{|2\_k}e_{|3\_i}\right) \end{aligned} \tag{11}$$

is performed from the main surfaces. Rainich knew also these relations [4, 5].

3 Conclusions

Montesinos and Flores [9] deduce the electromagnetic energy-momentum tensor via Noether's theorem [10]. That means, the Ricci tensor must have just the form according to Eqn. (1). Therefore, the geometry with the main surfaces is necessary for the space-time. Since the electromagnetic field tensor is performed by the main surfaces, it is a curve parameter of the current path like the curvature vector (which is performed by the main normal, and is the geometric expression of both gravitation and accelerated motion), as Rainich already saw. We can formulate an enhanced equivalence principle this way. It is the equivalence of the Lorentz force with Newton's force. Because the test body means a current point on the path, i.e. all forces to the test body come from curve parameters.

Montesinos and Flores [9] derived a symmetric energy-momentum tensor from three different theories, with the result that sources have to vanish in each case. That means:

1. The Maxwell theory is sufficient, because it runs as demonstrated in [7], even also regarding quantization. Non-Riemannian ansatzes are not needed;
2. Any ansatz with distributed charges or masses is false in principle. This error was helpful in classical theories before Einstein, which were separately handled. Now, such error turns up to be counterproductive.

It appears inviting to specify metrics first via Eqn. (7) (see [6]), but this method has narrow limits. The electromagnetic integration constants (charge, magnetic momentum) come from Maxwell's equations. The geometric theory of fields [7] unifies electromagnetism with gravitation natural way.

Submitted on June 23, 2009 / Accepted on July 17, 2009

References

1. Einstein A. Grundzüge der Relativitätstheorie. A back-translation from the Four Lectures on Theory of Relativity. Akademie-Verlag Berlin, Pergamon Press Oxford, Friedrich Vieweg & Sohn Braunschweig, 1969.
2. Eisenhart L.P. Riemannian geometry. Princeton University Press, Princeton, 1949.
3. Rainich G.Y. The electromagnetic field and curvature. *Proc. N.A.S.*, 1923, v. 9, 404–406.
4. Rainich G.Y. Electrodynamics in the general relativity theory. *Proc. N.A.S.*, 1924, v. 10, 124–127.
5. Rainich G.Y. Second note on electrodynamics in the general relativity theory. *Proc. N.A.S.*, 1924, v. 10, 294–298.
6. Caltenco Franca J.H., López-Bonilla J.L., Peña-Rivero R. The algebraic Rainich conditions. *Progress in Physics*, 2007, v. 3, 34–35.
7. Bruchholz U.E. Key notes on a geometric theory of fields. *Progress in Physics*, 2009, v. 2, 107–113.
8. Bruchholz U. Zur Berechnung stabiler elektromagnetischer Felder. *Z. elektr. Inform.- u. Energietechnik*, Leipzig, 1980, Bd. 10, 481–500.
9. Montesinos M. and Flores E. Symmetric energy-momentum tensor in Maxwell, Yang-Mills, and Proca theories obtained using only Noether's theorem. arXiv: hep-th/0602190.
10. Noether E. Invariante Variationsprobleme. *Nachr. d. König. Gesellsch. d. Wiss. zu Göttingen, Math-phys. Klasse*, 1918, 235–257 (English translation by M. A. Tavel in: *Transport Theory and Statistical Physics*, 1971, v. 1(3), 183–207; arXiv: physics/0503066).

Derivation of Planck's Constant from Maxwell's Electrodynamics

Ulrich E. Bruchholz

Schillerstrasse 36, D-04808 Wurzen, Germany

E-mail: Ulrich.Bruchholz@t-online.de; http://www.bruchholz-acoustics.de

Like Planck deduced the quantization of radiation energy from thermodynamics, the same is done from Maxwell's theory. Only condition is the existence of a geometric boundary, as deduced from author's Geometric theory of fields.

Let us go from Maxwell's equations of the vacuum that culminate in wave equations for the electric potential

$$\Box\varphi = 0 \tag{1}$$

and

$$\Box\mathcal{A} = 0 \tag{2}$$

for the magnetic vector potential.

Take the wave solution from Eqn. (2), in which the vector potential consists of a single component vertical to the propagation direction

$$A_y = A_y\Big(\omega\cdot(t-x)\Big), \tag{3}$$

where $c = 1$ (normalization), ω is a constant (identical with the circular frequency at the waves), x means the direction of the propagation, A_y is an *arbitrary* real function of $\omega\cdot(t-x)$ (independent on y, z).

The field strengthes respectively flow densities (which are the same in the vacuum) become

$$E_y = \frac{\partial A_y}{\partial t} = \omega {A_y}'\Big(\omega\cdot(t-x)\Big), \tag{4}$$

and

$$B_z = -\frac{\partial A_y}{\partial x} = \omega {A_y}'\Big(\omega\cdot(t-x)\Big), \tag{5}$$

where ${A_y}'$ means the total derivative.

The energy density of the field results in

$$\eta = \frac{\varepsilon_\circ}{2}\cdot({E_y}^2 + {B_z}^2) = \omega^2\varepsilon_\circ {A_y}'^2\Big(\omega\cdot(t-x)\Big), \tag{6}$$

where $\varepsilon_\circ$ means the vacuum permitivity.

The geometric theory of fields allows geometric boundaries from the non-linearities in the equations of this theory [1]. If one assumes such a boundary, like those in stationary solutions of the non-linear equations, the included energy becomes the volume integral within this boundary

$$\iiint \eta\,\mathrm{d}(t-x)\,\mathrm{d}y\,\mathrm{d}z = \\ = \omega\,\varepsilon_\circ \iiint {A_y}'^2\Big(\omega\cdot(t-x)\Big)\,\mathrm{d}\Big(\omega\cdot(t-x)\Big)\,\mathrm{d}y\,\mathrm{d}z\,. \tag{7}$$

This volume integral would be impossible without the boundary, because the linear solution, being alone, is not physically meaningful for the infinite extension.

We can write the last equation as

$$E = \omega\,\hbar \tag{8}$$

(E means here energy), or

$$E = h\,\nu\,, \tag{9}$$

because the latter volume integral has a constant value. The known fact that this value is always the same means also that only one solution exists with ω as a parameter.

Keep the calculation for the concrete value. This can be done only in numerical way, and might be a great challenge. The value of the above volume integral has to become $\hbar/\varepsilon_\circ$. With it, the fundamental relation of Quantum Mechanics follows from classical fields.

Summarizingly, the derivation involves two predictions:

1. Photon has a geometric boundary. That may be the reason that photon behaves as a particle;
2. There is only one wave solution.

Submitted on June 23, 2009 / Accepted on July 23, 2009

References

1. Bruchholz U.E. Key notes on a geometric theory of fields. *Progress in Physics*, 2009, v. 2, 107–113.

Changes in the Shape of Histograms Constructed from the Results of ^{239}Pu Alpha-Activity Measurements Correlate with the Deviations of the Moon from the Keplerian Orbit

Sergei N. Shapovalov*, Ilya A. Rubinstein†, Oleg A. Troshichev*, and Simon E. Shnoll‡

*St. Petersburg Arctic and Antarctic Institute, 38 Bering Str., St. Petersburg 199397, Russia
†Skobeltsin's Institute of Nuclear Physics, Moscow State University, Moscow 119991, Russia
‡Department of Physics, Moscow State University, Moscow 119992, Russia
‡Inst. of Theor. and Experim. Biophysics, Russian Acad. of Sci., Pushchino, Moscow Region, 142290, Russia
‡Puschino State University, Prospect Nauki 3, Pushchino, Moscow Region, 142290, Russia

E-mail: shapovalov@aari.nw.ru; shnoll@mail.ru

We have found that the shape of the histograms, constructed on the basis of the results of radioactivity measurements, changes in correlation with the distortions of the lunar Keplerian orbit (due to the gravitational influence of the Sun). Taking into account that the phenomenon of "macroscopic fluctuations" (regular changes in the fine structure of histograms constructed from the results of measurements of natural processes) does not depend on the nature of the process under study, one can consider the correlation of the histogram shape with the Moon's deviations from the Keplerian orbit to be independent from the nature of the process the histograms were obtained on.

1 Introduction

In the last decades, the studies of solar-terrestrial relations, which were initiated by A. L. Chizhevsky [1, 2], rest upon the concept that these relations have an electromagnetic origin [3–9]. A supposition that the solar-terrestrial relations could be of gravitational nature — when the matter at issue are *physico-chemical*, *chemical* and *biochemical* processes — would raise objections, as the energy change upon gravitational disturbances is much less than that observed in the processes mentioned. As for correlations of *physiological* processes with tidal forces (see, for example, [10–12]), they can be explained on the basis of complex indirect mechanisms.

Nevertheless, there were reports [13–21] on a strong correlation between variation of some physical and biochemical processes and deviations of the Moon from the Keplerian orbit (evection, variation and annual inequality; see [30]). The conclusion was that gravitational disturbances should play an essential role in these phenomena. The processes that correlations were revealed for were very different in their nature: there were fluctuations of "computer time", ^{239}Pu α-activity, the rate of a model chemical redox reaction, the content of haemoglobin in erythrocytes, and urea secretion.

There is no trivial explanation to the fact that physical and biochemical processes, which are little affected by tidal forces, correlate with changes of the lunar orbit.

As shown for the processes of diverse nature, the spectrum of their amplitude fluctuations (i.e., the shape of the corresponding histograms) correlates with a number of cosmophysical factors [22–28]. The change of energy in those processes (noise in electronic circuits, α-decay, chemical reactions) varies by tens orders of magnitude, yet the correlations are the same. Evidently, we deal with correlations of a non-energy nature. So we can suggest that the correlations of various processes with the distortions of the lunar orbit reported in [13–21] have a non-energy nature as well.

Thereby we have checked if changes in the shape of histograms constructed from the results of ^{239}Pu α-activity measurements correlate with the deviations of the Moon from the Keplerian orbit. The measurements were carried out at Novo-Lazarevskaya station (Antarctida) and in Pushchino in 2003–2008. Analysing regularities in the change of the histogram shape, we found periods corresponding to the periodical deviations of the Moon from the Keplerian orbit: variation (14.8 days) and evection (31.8 days). The correlations are analogous to those reported earlier [13–21], which suggests a common and very general nature of all these phenomena.

2 Materials and methods

The measurements of ^{239}Pu α-activity were performed at Novo-Lazarevskaya station (Antarctida) and in Pushchino in 2003–2008. α-Activity was monitored continuously, with a second interval, using devices constructed by one of the authors (I. A. Rubinstein). The analysis of data consists in pairwise comparing of histograms constructed from the results of measurements. Histograms were constructed either for 60-point segments of one-second measurements (1-min histograms) or for 60-point segments of one-minute measurements (1-h histograms). All the operations of histogram construction and analysis, as well as calculation of intervals between similar histograms and plotting the corresponding dis-

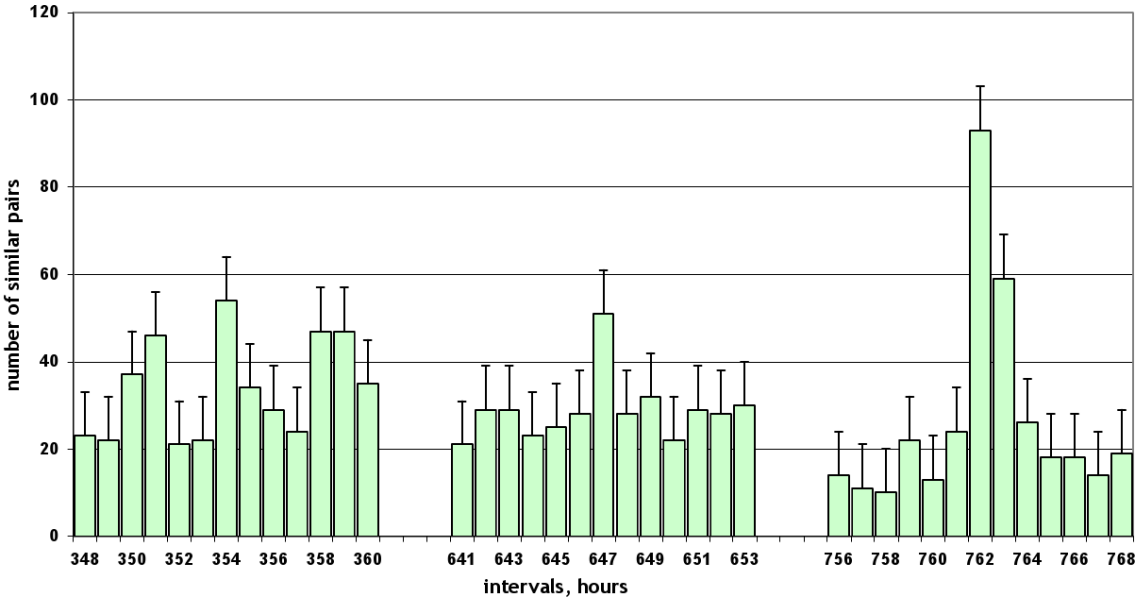

Fig. 1: Comparing 1-h histograms reveals periods equal to 350–354 h (in the region of variation, 14.8 days), 647 h (in the region of the 27-day period) and 762 h (in the region of evection, 31.8 days). In the figure, the number of similar histogram pairs (y-axis) is plotted versus the interval between similar histograms (x-axis, h).

tributions, were conducted with the aid of a computer program written by E. V. Pozharsky [22]. The decision of two histograms to be or not to be similar was made by an expert upon visual evaluation. A detailed description of all the procedures (measurements, histogram construction and analysis) can be found in [22].

3 Results

3.1 The shape of histograms changes with the periods of evection and variation

Figs. 1 and 2 show the results of our search for periodical changes in the shape of histograms constructed from the Antarctic data (Novo-Lazarevskaya station; since May 26, 2005 till the end of the year). We compared series of both 1-min and 1-h histograms in the regions of the putative periods: 762±6 h (a 31-day period, evection), 648±6 h (a 27-day period) and 355±6 h (a 15-day period, variation).

All the expected periods can be seen in Fig. 1. However, the period that corresponds to evection is, *ceteris paribus*, much more pronounced. To be sure that the periods revealed are not artefacts, we repeated the analysis many times with different data. Fig. 2 shows the summary result of five other experiments, in which we compared 1-h histograms constructed from the data obtained on April–October, 2004.

Along with 1-h histograms, we also compared 1-min ones. Fig. 3 shows the results of this analysis, which was made in the region of evection period.

As can be seen in Fig. 3, the 60-fold increase in "resolution" does not change the character of the distribution: there is a sharp extremum, which corresponds to the evection period. It is very surprising. Evection is a rather slow process: its period equals to 31.8 days. Naturally, one minute (out of 45779!) is by no means enough for evection to manifest itself — the distortion of the Keplerian orbit will be negligible. So we believe that the clear periodicity in the alteration of the histogram shape cannot be explained by a slow change of the "effecting force".

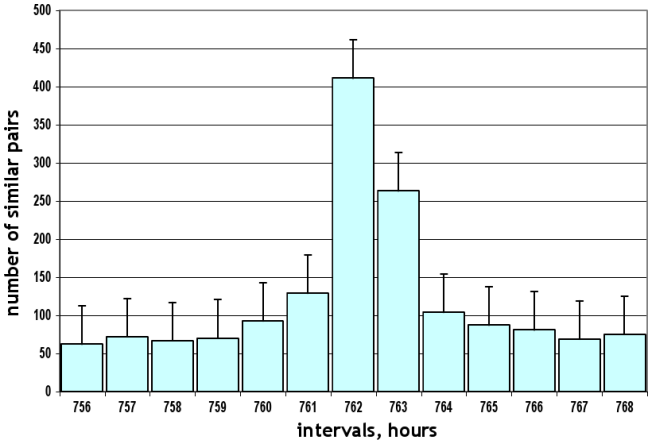

Fig. 2: Determination of the evection period by comparing 1-h histograms constructed from the results of ^{239}Pu α-activity measurements on April–October, 2004 (a summary result of five experiments). Axes are defined as in Fig. 1.

3.2 "Palindrome effects" in the evection periods

It seems that the apparently paradoxal narrowness of the extrema we see in the above figures has a relation to the sharp spatial anisotropy of our world [26–29]. Many observations

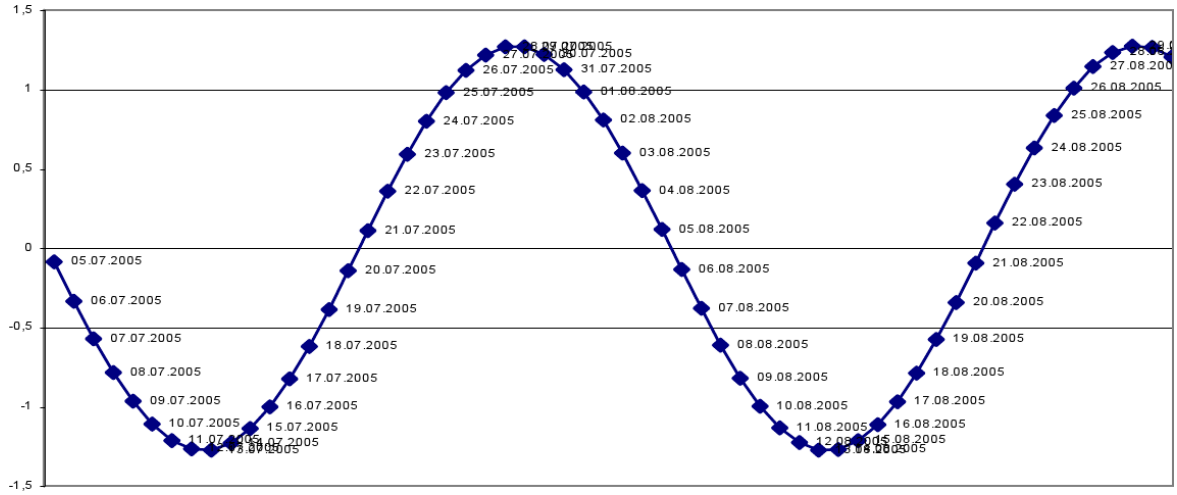

Fig. 4: Evection phenomenon (periodical change of the extent of distortion of the lunar Keplerian orbit) on July–August, 2005. Evection maxima in 2005: May 26, June 26, July 27, August 28–29, September 29–30, November 1 and December 2. Evection minima in 2005: June 10, July 11–12, August 12–13, September 13–14, October 15–16 and November 16.

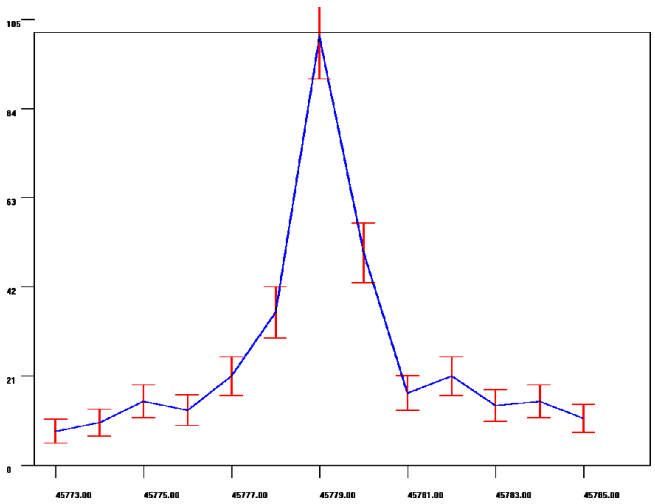

Fig. 3: Comparing 1-min histograms gave an evection period equal to 45779 min (31.79 days). Axes are defined as in Fig. 1.

confirmed this supposition — in particular, the experiments that made use of collimators, isolating narrowly directed beams of α-particles [24–25]. This anisotropy is stable, which is evidenced by the high probability of a certain histogram shape to reappear every time the laboratory has the same orientation towards the sphere of fixed stars. With the Earth rotating about its axis and moving along the circumsolar orbit, the laboratory will repeatedly pass through such points of the same star-related orientation. A manifestation of stable anisotropy of our space is the phenomenon of "palindromes", which is the high probability of a series of "daytime" histograms to be similar to the inverse series of the "nighttime" ones. In the nighttime, the rotation of the Earth is co-directed with its movement along the sircumsolar orbit, this being the opposite in the daytime. As a result, the sequence of "star-orientation points" that the laboratory passes through in the nighttime will be reversibly scanned by the laboratory in the daytime. Accordingly, series of daytime histograms were found to be opposite to the correspondent series of the nighttime ones [27, 28], with the "day-" and "nighttime" being accurately defined as the local time since 6:00 to 18:00 (daytime) and since 18:00 to 6:00 of the next day (nighttime). Figuratively speaking, the rotating Earth consecutively reads the same text first in the direct and then in the inverse order, and the result is the same — as in the phrase "step on no pets".

As it turned out, the histogram series that correspond to the "direct" and "inverse" halfs of the evection cycle are also "palindromes".

The periodical changes of the lunar Keplerian orbit in the evection cycles that correspond to the periods of our measurements are given in Fig. 4. According to this graph, we prepared series of 1-h histograms constructed from the results of ^{239}Pu α-activity measurements. The series were divided into the "odd" and "even" ones, corresponding to the descending and ascending halfs of the evection periods respectively (each half lasting 381.6 h or, more precisely, 22896 min). Then we compared the "odd" series to the "even" ones pairwise, with the even series being of two types: direct and inverse (with the direct and inverse sequence of histograms).

As shown in Fig. 5, there is a high probability of an "even" histogram to be similar to the "odd" one of the same order number when the series of "odd" histograms is inverse. Without inversion, the similarity is much less probable. This is a typical palindrome.

4 Discussion

Thus, the shape of histograms constructed from the results of radioactivity measurements changes in correlation with the distortions of the lunar Keperian orbit caused by the gravita-

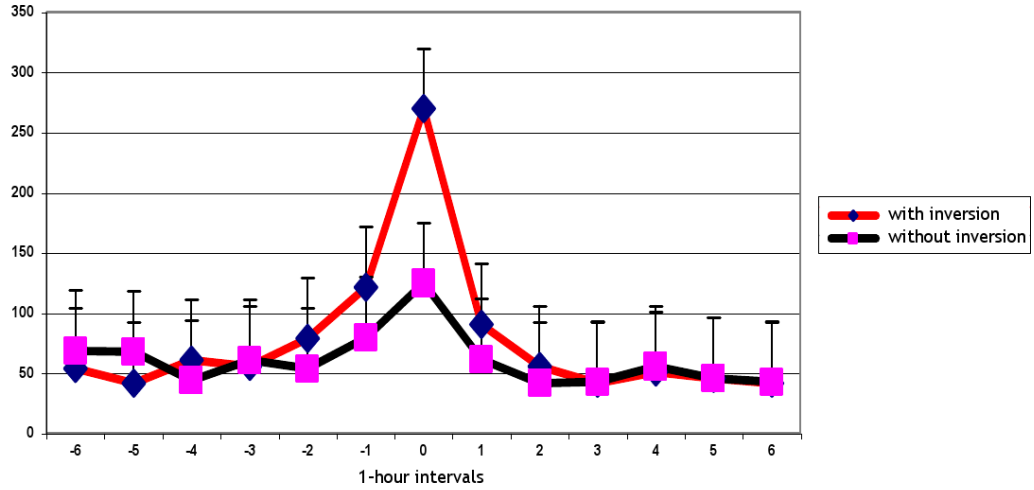

Fig. 5: The palindrome effect. When a series of consecutive 1-h histograms of the 1st (descending) half of the evection period is compared to the corresponding series of the 2nd (ascending) half, the high probability of histograms of the same order number to be similar is observed only in the case of *inversion* of the 2nd histogram series. The figure shows a summary result of analysis of four different sets of data obtained in the period since May 26 to October 1, 2005 at Novo-Lazarevskaya station.

tional influence of the Sun. It changes in the same manner as the processes reported in [13–21]. Taking into account that the phenomenon of "macroscopic fluctuations" (i.e., regular changes in the fine structure of histograms constructed from the results of measurements of natural processes) does not depend on the nature of the process studied [26, 28], one can consider the correlation of the histogram shape with the deviations of the Moon from the Keplerian orbit to be independent of the process nature as well. Since gravitational forces would have no direct impact on physico-chemical and biological processes in terms of energy, the correlations revealed can be considered as resulting from gravitation-induced disturbances in the space geometry. These disturbances, changes of space curvature — to formulate in general, changes of the spacial-temporal scale — should equally manifest themselves in the processes of any nature. The data on strong correlations revealed for the fluctuations of "computer time" [13–21] might be an illustration of such alterations of the spacial-temporal scale.

The phenomena of half-day and half-year palindromes were explained by the repetition of a certain orientation of the Earth towards the Sun [27] and the sphere of fixed stars [28] respectively. Adopting an analogous explanation to the palindrome with the period equal to that of evection (31.8 days) assumes a strong spatial anisotropy caused by the Moon.

Acknowledgements

S. E. Shnoll is thankful to M. N. Kondrashova for permanent discussions and spiritual support. The authors thank their colleagues for valuable discussions. We also appreciate help from the side of T. A. Zenchenko and K. I. Zenchenko, in conducting measurements and maintaining a computer bank of experimental results. We are pleased to thank A. V. Agafonoff for creative English translation. S. E. Shnoll is greatly indebted to D. Rabounski for deep understanding of our results and mental support.

Submitted on July 02, 2009 / Accepted on July 28, 2009

References

1. Chizhevsky A.L. Physical factors of the historical process. Kaluga, 1924 (*in Russian*).
2. Chizhevsky A.L. Terrestrial echo of solar storms. Mysl' Press, Moscow, 1976 (*in Russian*).
3. Vladimirsky B.M. Solar activity and the biosphere: an interdisciplinary problem. *Priroda*, 1994, v. 9, 15–19 (*in Russian*).
4. Solar activity and life. Zinante Press, Riga, 1967 (*in Russian*).
5. Effect of solar activity on the Earth's biosphere. Gnevyshev M. N. and Ol' A. I. (eds.), Nauka Press, Moscow, 1971 (*in Russian*).
6. Sidyakin V.T., Temur'yants N.A., Makeev V.B. and Vladimirsky B.M. Cosmic ecology. Naukova Dumka Press, Kiev, 1985 (*in Russian*).
7. Vladimirsky B.M. and Temur'yants N.A. Effect of solar activity on the biosphere-noosphere. MNEPU Press, Moscow, 2000 (*in Russian*).
8. See numerous papers in *Biofizika* (*in Russian*): no. 3 and 4 (1992); no. 4 and 5 (1995); no. 4 and 5 (1998); no. 7 (2004).
9. Glybin L.Ya. Cosmo-physical aspects of diurnal cyclicity: a concept of temporal organization of the life of human society. *Biofizika*, 1992, v. 37(3), 559–565 (*in Russian*).
10. Dubrov A.P. Lunar rhythms in a human: a brief essay on selenomedicine. Meditsina Press, Moscow, 1990 (*in Russian*).
11. Raybstein B.A., Voinov V.I., Kydryashev V.E. and Chepasov V.I. On the correlation of medical characterisitics with fluc-

tuations of natural gravitational fields. *Biofizika*, 1992, v. 7(3), 524–532 (*in Russian*).

12. Bortnikova G.I. The effect of tidal forces on the periodicity of adrenocortical and thyroidal activity in dogs. *Biofizika*, 1992, v. 7(3), 533–540 (*in Russian*)
13. Gorshkov E.S., Shapovalov S.N., Sokolovsky V.V. and Troshichev O.A. On the detection of impulse cosmophysical radiation. *Biofizika*, 2000, v. 45(5), 947–949 (*in Russian*).
14. Gorshkov E.S., Shapovalov S.N., Sokolovsky V.V. and Troshichev O.A. On the gravitational conditionality of rate fluctuations in the reaction of unithiol oxidation by nitrite ions. *Biofizika*, 2000, v. 45(4), 631–635 (*in Russian*).
15. Shapovalov S.N., Gorshkov E.S., Troshichev O.A., Borisova T.D. and Frank-Kamenetsky A.V. Stochastic fluctuations in the readings of measuring devices: effects of cosmophysical influence? *Biofizika*, 2001, v. 46(6), 819–822 (*in Russian*).
16. Shapovalov S.N. Principles of physical indication of cosmogeophysical ecological factors of non-electromagnetic nature. PhD Thesis, AANII and RGGMU Press, St. Petersburg, 2003 (*in Russian*).
17. Shapovalov S.N., Gorshkov E.S., Troshichev O.A., Borisova T.D., Frank-Kamenetsky A.V. Effects of non-electromagnetic disturbances from the Sun in "computer time" instability. *Biophysics*, 2004, v. 49(1), S79–S84.
18. Sokolovsky V.V., Gorshkov E.S., Ivanov V.V., Shapovalov S.N. and Troshichev O.A. Relation of the regular gravitational field variations to biochemical processes observed in vitro and in vivo. *Biophysics*, 2004, v. 49(1), S85–S91.
19. Shapovalov S.N., Gorshkov E.S., Troshichev O.A. Cosmophysical effects observed in impulses of the microphotocolorimeter current. *Biophysics*, 2004, v. 49(1), S119–S122.
20. Troshichev O.A., Gorshkov E.S., Shapovalov S.N., Sokolovskii V.V. , Ivanov V.V., Vorobeitchikov V.M. Variation of the gravitational field as a motive power for rhythmics of biochemical processes. *Advances in Space Research*, 2004, v. 34, 1619–1624.
21. Shapovalov S.N., Troshichev O.A., Povazhny V.I., Sokolovsky V.V., Vorobeychikov V.M., Gorshkov E.S., Lozovsky V.T. and Alexandrova A.B. Cosmophysical regularities in the photoeffect experiment. *Meteorologichesky Vestnik*, 2008, v. 1(1), 1–23 (*in Russian*).
22. Shnoll S.E., Kolombet V.A., Pozharsky E.V., Zenchenko T.A., Zvereva I.M. and Konradov A.A. On the cosmophysical conditionality of "macroscopic fluctuations". *Biofizika*, 1998, v. 43(5), 909–915 (*in Russian*).
23. Shnoll S.E., Rubinstein I.A., Zenchenko K.I., Zenchenko T.A., Udaltsova N.V., Konradov A.A., Shapovalov S.N., Makarevich A.V., Gorshkov E.S. and Troshichev O.A. Dependence of "macroscopic fluctuations" on geographical coordinates (on the basis of materials of the Arctic (2000) and Antarctic (2001) expeditions). *Biofizika*, 2003, v. 48(6), 1123–1131 (*in Russian*).
24. Shnoll S.E., Zenchenko K.I., Berulis I.I., Udaltsova N.V., Zhirkov S.S. and Rubinstein I.A. Dependence of "macroscopic fluctuations" on cosmophisical factors. Space anisotropy. *Biofizika*, 2004, v. 49(1), 132–139 (*in Russian*)
25. Shnoll S.E., Rubinshtejn I.A., Zenchenko K.I., Shlekhtarev V.A., Kaminsky A.V., Konradov A.A. and Udaltsova N.V. Experiments with rotating collimators cutting out pencil of alpha-particles at radioactive decay of Pu-239 evidence sharp anisotropy of space. *Progress in Physics*, 2004, v. 1, 81–84.
26. Shnoll S.E. Changes in fine structure of stochastic distributions as a consequence of space-time fluctuations. *Progress in Physics*, 2006, v. 2, 39–45.
27. Shnoll S.E., Pancheluga V.A. and Shnoll A.E. The palindrom effect. *Progress in Physics*, 2008, v. 2, 151–153.
28. Shnoll S.E. The "scattering of the results of measurements" of processes of diverse nature is determined by the Earth's motion in the inhomogeneous space-time continuum. The effect of "half-year palindromes". *Progress in Physics*, 2009, v. 1, 3–7.
29. Shnoll S.E. and Rubinstein I.A. "Regular changes in the fine structure of histograms reaveled in the experiments with collimators which isolate beams of alpha-particles flying at certain directions". *Progress in Physics*, 2009, v. 2, 33–95.
30. Astronomical calendar (invariant part). Nauka Press, Moscow, 1981 (*in Russian*).

Astrophysically Satisfactory Solutions to Einstein's R-33 Gravitational Field Equations Exterior/Interior to Static Homogeneous Oblate Spheroidal Masses

Chifu Ebenezer Ndikilar

Physics Department, Gombe State University, P.M.B. 127, Gombe, Gombe State, Nigeria
E-mail: ebenechifu@yahoo.com

In this article, we formulate solutions to Einstein's geometrical field equations derived using our new approach. Our field equations exterior and interior to the mass distribution have only one unknown function determined by the mass or pressure distribution. Our obtained solutions yield the unknown function as generalizations of Newton's gravitational scalar potential. Thus, our solution puts Einstein's geometrical theory of gravity on same footing with Newton's dynamical theory; with the dependence of the field on one and only one unknown function comparable to Newton's gravitational scalar potential. Our results in this article are of much significance as the Sun and planets in the solar system are known to be more precisely oblate spheroidal in geometry. The oblate spheroidal geometries of these bodies have effects on their gravitational fields and the motions of test particles and photons in these fields.

1 Introduction

After the publication of A. Einstein's geometrical theory of gravitation in 1915/1916, the search for exact solutions to its inherent geometrical field equations for various mass distributions began [1]. Four well known approaches have so far been proposed.

The first approach is to seek a mapping under which the metric tensor assumed a simple form, such as the vanishing of the off-diagonal components.With sufficiently clever assumptions of this sort, it is often possible to reduce the Einstein field equations to a much simpler system of equations, even a single partial differential equation (as in the case of stationary axisymmetric vacuum solutions, which are characterised by the Ernst equation) or a system of ordinary differential equations (this led to the first exact analytical solution — the famous Schwarzschild's solution [2]). A special generalization of the Schwarzschild's metric is the Kerr metric. This metric describes the geometry of space time around a rotating massive body.

The second method assumes that the metric tensor has symmetries-assumed forms of the Killing vectors. This led to the solution found by Weyl and Levi-Civita [3–6]. The third approach required that the metric tensor leads to a particular type of the classifications of Weyl and Riemann — Christoffel tensors. These are often stated interms of Petrov classification of the possible symmetries of the Weyl tensor or the Segre classification of the possible symmetries of the Ricci tensor. This leds to plane fronted wave solutions [3–6]. It is worth remarking that even after the symmetry reductions in the three methods above, the reduced system of equations is often difficult to solve. The fourth approach is to seek Taylor series expansion of some initial value hyper surface, subject to consistent initial value data. This method has not proved successful in generating solutions [3–6].

Recently [7–12], we introduced our own method and approach to formulation of exact analytical solutions as an extension of Schwarzschild's method. In this article, we show how exact analytical solutions of order c^{-2} (where c is the speed of light in vacuum) can be constructed in gravitational fields interior and exterior to static homogeneous oblate spheroids placed in empty space. For the sake of mathematical convenience we choose to use the 3rd (R_{33}) field equation [7].

2 Exterior field equation

The covariant metric tensor in the gravitational field of a static homogeneous oblate spheroid in oblate spheroidal coordinates (η, ξ, ϕ) has been obtained [7, 12] as

$$g_{00} = \left(1 + \frac{2}{c^2} f(\eta, \xi)\right), \tag{2.1}$$

$$g_{11} = -\frac{a^2}{1+\xi^2-\eta^2} \times \times \left[\eta^2 \left(1 + \frac{2}{c^2} f(\eta, \xi)\right)^{-1} + \frac{\xi^2(1+\xi^2)}{(1-\eta^2)}\right], \tag{2.2}$$

$$g_{12} \equiv g_{21} = -\frac{a^2\eta\xi}{1+\xi^2-\eta^2}\left[1 - \left(1 + \frac{2}{c^2} f(\eta, \xi)\right)^{-1}\right], \tag{2.3}$$

$$g_{22} = -\frac{a^2}{1+\xi^2-\eta^2} \times \times \left[\xi^2 \left(1 + \frac{2}{c^2} f(\eta, \xi)\right)^{-1} + \frac{\eta^2(1-\eta^2)}{(1+\xi^2)}\right], \tag{2.4}$$

$$g_{33} = -a^2(1+\xi^2)(1-\eta^2), \tag{2.5}$$

$$g_{\mu\nu} = 0; \text{ otherwise}, \tag{2.6}$$

$$g^{00}=\left[1+\frac{2}{c^2}f(\eta,\xi)\right]^{-1} \tag{2.7}$$

$$g^{11}=\frac{-\left(1-\eta^2\right)\left(1+\xi^2-\eta^2\right)\left[\eta^2\left(1-\eta^2\right)+\xi^2\left(1+\xi^2\right)\left(1+\frac{2}{c^2}f(\eta,\xi)\right)^{-1}\right]}{a^2\left(1+\frac{2}{c^2}f(\eta,\xi)\right)^{-1}\left[\eta^2\left(1-\eta^2\right)+\xi^2\left(1+\xi^2\right)\right]^2} \tag{2.8}$$

$$g^{12}\equiv g^{21}=\frac{-\eta\xi\left(1-\eta^2\right)\left(1+\xi^2\right)\left(1+\xi^2-\eta^2\right)\left[1-\left(1+\frac{2}{c^2}f(\eta,\xi)\right)^{-1}\right]}{a^2\left(1+\frac{2}{c^2}f(\eta,\xi)\right)^{-1}\left[\eta^2\left(1-\eta^2\right)+\xi^2\left(1+\xi^2\right)\right]^2} \tag{2.9}$$

$$g^{22}=\frac{-\left(1+\xi^2\right)\left(1+\xi^2-\eta^2\right)\left[\xi^2\left(1+\xi^2\right)+\eta^2\left(1-\eta^2\right)\left(1+\frac{2}{c^2}f(\eta,\xi)\right)^{-1}\right]}{a^2\left(1+\frac{2}{c^2}f(\eta,\xi)\right)^{-1}\left[\eta^2\left(1-\eta^2\right)+\xi^2\left(1+\xi^2\right)\right]^2} \tag{2.10}$$

$$g^{33}=-\left[a^2\left(1+\xi^2\right)\left(1-\eta^2\right)\right]^{-1} \tag{2.11}$$

$$g^{\mu\nu}=0 \text{ otherwise} \tag{2.12}$$

$$\begin{aligned}
&-g^{00}g^{00}g_{00,12}-g^{00}g^{11}{}_{,2}\,g_{00,1}-g^{00}g^{12}g_{00,22}-g^{00}g^{12}{}_{,2}\,g_{00,2}-g^{00}g^{21}{}_{,2}\,g_{00,1}-\\
&-g^{00}g^{22}g_{00,22}-g^{00}g^{22}{}_{,2}\,g_{00,2}-g^{00}g^{11}g^{22}g_{00,1}g_{22,1}-g^{00}g^{11}g^{33}g_{00,1}g_{33,1}-\\
&-g^{00}g^{12}g^{12}g_{00,2}g_{12,1}-g^{00}g^{12}g^{33}g_{00,2}g_{33,1}-g^{00}g^{11}g^{21}g_{00,1}g_{11,2}-\\
&-g^{00}g^{21}g^{12}g_{00,1}g_{12,2}-g^{00}g^{21}g^{33}g_{00,1}g_{33,2}-\tfrac{1}{2}\,g^{00}g^{22}g^{33}g_{00,2}g_{33,2}-\\
&-g^{00}g^{11}g_{00,11}-g^{11}g^{00}{}_{,1}\,g_{00,1}-g^{11}g^{12}{}_{,1}\,g_{11,2}-2g^{11}g^{22}g_{22,11}-g^{11}g^{22}{}_{,1}\,g_{22,1}-\\
&-g^{11}g^{33}{}_{,1}\,g_{33,1}+4g^{11}g^{21}g_{11,12}+g^{11}g^{21}{}_{,2}\,g_{11,1}+4g^{11}g^{22}g_{12,12}-2g^{11}g^{22}g_{11,22}+\\
&+g^{11}g^{22}{}_{,2}\,g_{11,2}-g^{11}g^{11}g^{22}g_{11,2}g_{12,1}+g^{00}g^{11}g^{22}g_{00,2}g_{12,1}-g^{00}g^{11}g^{22}g_{00,2}g_{11,2}+\\
&+g^{11}g^{22}g^{22}g_{12,1}g_{22,1}-\tfrac{1}{2}\,g^{11}g^{22}g^{22}g_{11,2}g_{22,1}+g^{11}g^{22}g^{33}g_{12,1}g_{33,2}-\\
&-\tfrac{1}{2}\,g^{11}g^{22}g^{33}g_{11,2}g_{33,2}+\tfrac{1}{2}\,g^{11}g^{21}g^{22}g_{11,1}g_{22,1}-g^{11}g^{21}g^{21}g_{11,2}g_{11,2}+\\
&+g^{11}g^{21}g^{12}g_{11,2}g_{12,1}-g^{22}g^{00}g_{00,12}-g^{22}g^{00}{}_{,2}\,g_{00,1}-g^{22}g^{11}{}_{,2}\,g_{00,1}-g^{22}g^{11}{}_{,2}\,g_{11,2}-\\
&-g^{22}g^{12}{}_{,2}\,g_{22,1}-g^{22}g^{33}g_{33,22}-g^{22}g^{33}{}_{,2}\,g_{33,2}+g^{22}g^{12}{}_{,1}\,g_{22,2}+g^{22}g^{11}{}_{,1}\,g_{12,2}-\\
&-g^{22}g^{11}{}_{,1}\,g_{22,1}+\tfrac{1}{2}\,g^{00}g^{22}g^{22}g_{00,2}g_{22,2}-g^{12}g^{12}g^{22}g_{11,2}g_{22,2}+\\
&+\tfrac{1}{2}\,g^{00}g^{12}g^{22}g_{00,1}g_{22,2}+\tfrac{1}{2}\,g^{11}g^{12}g^{22}g_{11,1}g_{22,2}+\tfrac{1}{2}\,g^{12}g^{22}g^{33}g_{22,2}g_{33,1}-\\
&-g^{11}g^{22}g^{22}g_{12,2}g_{22,1}+g^{00}g^{11}g^{22}g_{00,1}g_{12,2}+g^{11}g^{11}g^{22}g_{11,1}g_{12,2}+g^{11}g^{22}g^{33}g_{12,2}g_{33,1}+\\
&+\tfrac{1}{2}\,g^{11}g^{22}g^{22}g_{11,2}g_{22,2}+g^{12}g^{12}g^{22}g_{12,2}+\tfrac{1}{2}\,g^{12}g^{12}g^{22}g_{22,1}g_{22,1}-\\
&-\tfrac{1}{2}\,g^{12}g^{22}g^{33}g_{12,2}g_{33,2}+\tfrac{1}{2}\,g^{12}g^{22}g^{33}g_{22,1}g_{33,2}+g^{33}g^{11}{}_{,1}\,g_{33,1}+g^{33}g^{12}{}_{,1}\,g_{33,2}+\\
&+2g^{21}g^{33}g_{33,12}-g^{33}g^{21}{}_{,2}\,g_{33,1}-g^{22}g^{33}g_{33,22}-g^{33}g^{22}{}_{,2}\,g_{33,2}-g^{11}g^{22}g^{33}g_{22,1}g_{33,1}-\\
&-g^{12}g^{12}g^{33}g_{12,1}g_{33,2}-\tfrac{1}{2}\,g^{12}g^{22}g^{33}g_{22,1}g_{33,2}-g^{21}g^{21}g^{33}g_{12,2}g_{33,1}-\\
&-\tfrac{1}{2}\,g^{21}g^{22}g^{33}g_{22,2}g_{33,1}-\tfrac{1}{2}\,g^{00}g^{22}g^{33}g_{00,2}g_{33,2}-\tfrac{1}{2}\,g^{11}g^{22}g^{33}g_{11,2}g_{33,2}+\\
&+g^{00}g^{12}g_{00,12}+2g^{12}g^{00}{}_{,2}\,g_{00,1}+2g^{12}g^{11}{}_{,2}\,g_{11,1}+4g^{12}g^{12}g_{12,12}+4g^{12}g^{12}{}_{,2}\,g_{12,1}-2g^{12}g^{12}g_{11,22}-\\
&-2g^{12}g^{12}{}_{,2}\,g_{11,2}+2g^{12}g^{33}{}_{,2}\,g_{33,1}+2g^{12}g^{11}{}_{,1}\,g_{11,2}+2g^{12}g^{12}g_{22,11}+2g^{12}g^{12}{}_{,1}\,g_{22,1}+\\
&+g^{00}g^{11}g^{12}g_{00,1}g_{11,2}+g^{00}g^{12}g^{12}g_{00,1}g_{22,1}+g^{00}g^{12}g^{21}g_{00,2}g_{11,2}+g^{11}g^{12}g^{21}g_{11,2}g_{11,2}+\\
&+g^{12}g^{12}g^{12}g_{11,2}g_{22,1}+g^{12}g^{21}g^{33}g_{11,2}g_{33,2}+g^{12}g^{12}g^{33}g_{22,1}g_{33,1}-g^{11}g^{12}g^{21}g_{11,1}g_{12,2}-\\
&-g^{12}g^{21}g^{12}g_{11,1}g_{22,2}-g^{12}g^{21}g^{22}g_{12,1}g_{22,2}-g^{11}g^{12}g^{22}g_{11,2}g_{22,1}+g^{12}g^{12}g^{22}g_{11,2}g_{22,2}=0
\end{aligned} \tag{2.18}$$

and the contravariant metric tensor is as shown in formulas (2.7)–(2.12), where $f(\eta,\xi)$ is an unknown function determined by the mass distribution. From this covariant metric tensor, we can then construct our field equations for the gravitational field after formulating the Coefficients of affine connection, Riemann Christoffel tensor, Ricci tensor and the Einstein tensor [7–12]. After the above steps, it can be shown that the exterior R_{33} field equation in this gravitational field is given as;

$$R_{33} - \frac{1}{2} R g_{33} = 0 . \tag{2.13}$$

or more explicitly interms of the affine connections, Ricci tensor and covariant metric tensor as;

$$\begin{aligned} &-\Gamma^1_{33}\Gamma^0_{10} - \Gamma^2_{33}\Gamma^0_{20} - \Gamma^1_{33,1} - \Gamma^1_{33}\Gamma^1_{11} - \Gamma^2_{33}\Gamma^1_{21}\Gamma^3_{31}\Gamma^1_{33} - \\ &- \Gamma^2_{33,2} - \Gamma^1_{33}\Gamma^2_{12} - \Gamma^2_{33}\Gamma^2_{22} + \Gamma^3_{32}\Gamma^2_{33} - \frac{1}{2} R g_{\alpha\beta} = 0 \end{aligned} \tag{2.14}$$

with the symbols and numbers having their usual meaning and

$$R = g^{00}R_{00} + g^{11}R_{11} + 2g^{12}R_{12} + g^{22}R_{22} + g^{33}R_{33} . \tag{2.15}$$

Now, multiplying equation (2.13) by $2g^{33}$ and using the fact that $g^{33}g_{33} = 1$ yields

$$2g^{33}R_{33} - R = 0 . \tag{2.16}$$

Writing the expression for the curvature scalar,R as in equation (2.15) gives;

$$\begin{aligned} &-g^{00}R_{00} - g^{11}R_{11} - 2g^{12}R_{12} - \\ &- g^{22}R_{22} + g^{33}R_{33} = 0 . \end{aligned} \tag{2.17}$$

Writing the various terms of the field equation (2.17) explicitly in terms of the metric tensor gives our field equation explicitly as (2.18).

Now, we realize that our covariant metric tensor (2.1)–(2.6) can be written equally as

$$g_{\mu\nu}(\eta,\xi) = h_{\mu\nu}(\eta,\xi) + f_{\mu\nu}(\eta,\xi) , \tag{2.19}$$

where $h_{\mu\nu}$ are the well known pure empty space components and $f_{\mu\nu}$ are the contributions due to the oblate spheroidal mass distribution. Consequently, as the mass distribution decays out; $f_{\mu\nu} \to 0$ and hence $g_{\mu\nu} \to h_{\mu\nu}$. Therefore, the metric tensor reduces to the pure empty space metric tensor as the distribution of mass decays out. Also,

$$g^{\mu\nu}(\eta,\xi) = h^{\mu\nu}(\eta,\xi) + f^{\mu\nu}(\eta,\xi) , \tag{2.20}$$

where $h^{\mu\nu}$ are the well known pure empty space components and $f^{\mu\nu}$ are the contributions due to the oblate spheroidal mass distribution. Thus it can be shown that for this field, the non zero metric components can be written as;

$$h_{00} = 1 , \tag{2.21}$$

$$h_{11} = -\frac{a^2\left(\eta^2+\xi^2\right)}{1-\eta^2} , \tag{2.22}$$

$$h_{22} = -\frac{a^2\left(\eta^2+\xi^2\right)}{1+\eta^2} , \tag{2.23}$$

$$h_{33} = -a^2\left(1+\eta^2\right)\left(1+\xi^2\right) , \tag{2.24}$$

$$f_{00} = \frac{2}{c^2} f , \tag{2.25}$$

$$f_{11} = -\frac{a^2\eta^2}{\left(1-\eta^2+\xi^2\right)} \sum_{n=1}^{\infty} \binom{-1}{n} \frac{2^n}{c^n} f^n , \tag{2.26}$$

$$f_{12} \equiv f_{21} = -\frac{a^2\eta\xi}{\left(1-\eta^2+\xi^2\right)} \sum_{n=1}^{\infty} \binom{-1}{n} \frac{2^n}{c^n} f^n , \tag{2.27}$$

$$f_{22} = -\frac{a^2\xi^2}{\left(1-\eta^2+\xi^2\right)} \sum_{n=1}^{\infty} \binom{-1}{n} \frac{2^n}{c^n} f^n , \tag{2.28}$$

also,

$$h^{00} = \frac{1}{h_{00}} , \tag{2.29}$$

$$h^{11} = \frac{1}{h_{11}} , \tag{2.30}$$

$$h^{22} = \frac{1}{h_{22}} , \tag{2.31}$$

$$h^{33} = \frac{1}{h_{33}} , \tag{2.32}$$

$$f^{00} = \sum_{n=1}^{\infty} \binom{-1}{n} \frac{2^n}{c^n} f^n , \tag{2.33}$$

$$f^{11} = -\frac{f_{11}}{(h_{11})^2} + 0\left(c^{-4}\right) , \tag{2.34}$$

$$f^{12} \equiv f^{21} = -\frac{f_{12}}{h_{11}h_{22}} + 0\left(c^{-4}\right) , \tag{2.35}$$

$$f^{22} = -\frac{f_{22}}{(h_{22})^2} + 0\left(c^{-4}\right) . \tag{2.36}$$

To begin the explicit formulation of the R_{33} field equation we note, first of all, that all the terms of order c^0 cancel out identically since the empty space time metric tensor $h_{\mu\nu}$ independently satisfies the homogeneous R_{33} field equation. Therefore the lowest order of terms we expect in the exterior R_{33} field equation is c^{-2}. Hence in order to formulate the exterior R_{33} field equation of order c^{-2}, let us decompose our covariant metric tensor $g_{\mu\nu}$ into pure empty space part $h_{\mu\nu}$ (of order c^0 only) and the nonempty space part $f_{\mu\nu}$ (of order c^{-2} or higher). Similarly, let our contravariant metric tensor $g^{\mu\nu}$ be decomposed into pure empty space part $h^{\mu\nu}$ (of order c^0 only) and the nonempty space part $f^{\mu\nu}$ (of order c^{-2} or higher). Substituting explicit expressions for equations (2.19) and (2.20) into equation (2.18) and neglecting all terms of order c^0, the exterior R_{33} field equation can be written as (2.37), where the coefficients are given as (2.38)–(2.58).

$$S_1(\eta,\xi)\,f_{22,11}+S_2(\eta,\xi)\,f_{00,11}+S_3(\eta,\xi)\,f_{12,12}+S_4(\eta,\xi)\,f_{00,12}+S_5(\eta,\xi)\,f_{11,22}+$$
$$+S_6(\eta,\xi)\,f_{00,22}+S_7(\eta,\xi)\,f_{00,1}+S_8(\eta,\xi)\,f_{12,1}+S_9(\eta,\xi)\,f_{22,1}+S_{10}(\eta,\xi)\,f^{11},_1+$$
$$+S_{11}(\eta,\xi)\,f^{12},_1+S_{12}(\eta,\xi)\,f^{22},_1+S_{13}(\eta,\xi)\,f_{00,2}+S_{14}(\eta,\xi)\,f_{11,2}+S_{15}(\eta,\xi)\,f_{12,2}+ \tag{2.37}$$
$$+S_{16}(\eta,\xi)\,f_{22,2}+S_{17}(\eta,\xi)\,f^{12},_2+S_{18}(\eta,\xi)\,f^{22},_2+S_{19}(\eta,\xi)\,f^{11}+S_{20}(\eta,\xi)\,f^{12}+$$
$$+S_{21}(\eta,\xi)\,f^{22}=0$$

$$S_1(\eta,\xi)=-2h^{11}h^{22} \tag{2.38}$$

$$S_2(\eta,\xi)=-h^{11} \tag{2.39}$$

$$S_3(\eta,\xi)=4h^{11}h^{22} \tag{2.40}$$

$$S_4(\eta,\xi)=-h^{11}-h^{22} \tag{2.41}$$

$$S_5(\eta,\xi)=-2h^{11}h^{22} \tag{2.42}$$

$$S_6(\eta,\xi)=-h^{22} \tag{2.43}$$

$$S_7(\eta,\xi)=-h^{11},_2-h^{11}h^{22}h_{22,1}-h^{11}h^{33}h_{33,1} \tag{2.44}$$

$$S_8(\eta,\xi)=h^{11}h^{22},_2+h^{11}h^{22}\left(h^{33}h_{33,2}+h^{22}h_{22,1}-h^{11}h_{11,2}\right) \tag{2.45}$$

$$S_9(\eta,\xi)=-h^{11}h^{22}\left(h^{33}h_{33,1}+\tfrac{1}{2}\,h^{22}h_{11,2}\right)-h^{22}h^{11},_1-h^{11}h^{22},_1 \tag{2.46}$$

$$S_{10}(\eta,\xi)=-h^{22}h_{22,1}+h^{33}h_{33,1} \tag{2.47}$$

$$S_{11}(\eta,\xi)=h^{22}h_{22,2}+h^{33}h_{33,2} \tag{2.48}$$

$$S_{12}(\eta,\xi)=-h^{11}h_{22,1} \tag{2.49}$$

$$S_{13}(\eta,\xi)=-h^{22},_2-h^{22}h^{33}h_{33,2}+\tfrac{1}{2}\,h^{22}h^{22}h_{22,2}-h^{11}h^{22}h_{11,2} \tag{2.50}$$

$$S_{14}(\eta,\xi)=-h^{11}h^{22},_2-h^{22}h^{11},_2+\frac{1}{2}\,h^{11}h^{22}\left(-h^{22}h_{22,1}+h^{22}h_{22,2}-h^{33}h_{33,2}\right) \tag{2.51}$$

$$S_{15}(\eta,\xi)=h^{22}h^{11},_1+h^{11}h^{22}\left(h^{33}h_{33,1}+h^{11}h_{11,1}-h^{22}h_{22,1}\right) \tag{2.52}$$

$$S_{16}(\eta,\xi)=\tfrac{1}{2}\,h^{11}h^{22}h^{22}h_{11,2} \tag{2.53}$$

$$S_{17}(\eta,\xi)=h^{11}h_{11,1}-h^{22}h_{22,1}-h^{33}h_{33,1} \tag{2.54}$$

$$S_{18}(\eta,\xi)=-h^{11}h_{11,1}-h^{33}h_{33,2} \tag{2.55}$$

$$S_{19}(\eta,\xi)=-h^{22}h^{33}h_{33,2}-h^{22}h^{33}h_{33,1}+h^{22}h^{22}h_{11,2}h_{22,2}-$$
$$-h^{22}h^{33}h_{11,2}h_{33,2}-\tfrac{1}{2}\,h^{22}h^{22}h_{11,2}h_{22,1}-h^{22},_2\,h_{11,2}-2h^{22}h_{11,22}-h^{33},_1\,h_{33,1}- \tag{2.56}$$
$$-h^{22},_1\,h_{22,1}-2h^{22}h_{22,11}$$

$$S_{20}(\eta,\xi)=4h^{11}h_{11,12}+\tfrac{1}{2}\,h^{11}h^{22}h_{11,1}\left(h_{22,1}+h_{22,2}\right)+$$
$$+\tfrac{1}{2}\,h^{22}h^{33}h_{22,1}h_{33,2}+2h^{33}h_{33,12}-\tfrac{1}{2}\,h^{22}h^{33}h_{22,1}+2h^{11},_2\,h_{11,1}+2h^{33},_2\,h_{33,1}+ \tag{2.57}$$
$$+2h^{11},_1\,h_{11,2}-h^{11}h^{22}h_{11,2}h_{22,1}$$

$$S_{21}(\eta,\xi)=-\tfrac{1}{2}\,h^{11}h^{33}h_{33,2}+h^{11}h^{22}h_{11,2}h_{22,2}-h^{11}h^{22}h_{11,2}h_{22,1}-$$
$$-\tfrac{1}{2}\,h^{11}h^{33}h_{11,2}h_{33,2}-2h^{33}h_{33,22}-h^{11}h^{33}h_{33,1}-h^{11},_2\,h_{11,2}-h^{33},_2\,h_{33,2}- \tag{2.58}$$
$$-h^{11},_1\,h_{22,1}-2h^{11}h_{22,11}-2h^{11}h_{11,22}\,.$$

$$K_1(\eta,\xi) f_{\eta\eta} + K_2(\eta,\xi) f_{\eta\xi} + K_3(\eta,\xi) f_{\xi\xi} + K_4(\eta,\xi) f_\eta + K_5(\eta,\xi) f_\xi + K_6(\eta,\xi) f = 0 \tag{2.59}$$

$$K_1(\eta,\xi) = \frac{2\left(1-\eta^2\right)\left(1-\eta^2+\xi^2\right) - 2a^4\xi^2\left(\eta^2+\xi^2\right)}{a^2c^2\left(\eta^2+\xi^2\right)\left(1-\eta^2+\xi^2\right)} \tag{2.60}$$

$$K_2(\eta,\xi) = \frac{4\left(\eta^2+\xi^2\right)\left(1-\eta^2+\xi^2\right) - 8\eta\xi\left(1-\eta^4\right)}{a^2c^2\left(\eta^2+\xi^2\right)^2\left(1-\eta^2+\xi^2\right)} \tag{2.61}$$

$$K_3(\eta,\xi) = \frac{2\left(1+\eta^2\right)}{a^2c^2\left(\eta^2+\xi^2\right)} \tag{2.62}$$

$$\begin{aligned} K_4(\eta,\xi) = {} & \frac{-8a^2\eta\xi^2 S_1(\eta,\xi) + 2a^2\xi^2 S_9(\eta,\xi)}{c^2\left(1-\eta^2+\xi^2\right)^2} - \frac{8\xi\left(1-\eta^4\right)\left(1-\eta^2-\xi^2\right)}{a^2c^2\left(\eta^2+\xi^2\right)^2\left(1-\eta^2+\xi^2\right)^2} + \\ & + \frac{2a^2\eta^2 S_{10}(\eta,\xi)}{c^2\left(h_{11}\right)^2\left(1-\eta^2+\xi^2\right)} + \frac{2a^2\eta\xi S_{11}(\eta,\xi)}{c^2 h_{11}h_{22}\left(1-\eta^2+\xi^2\right)} - \frac{2a^2\xi^2 S_{12}(\eta,\xi)}{c^2\left(h_{22}\right)^2\left(1-\eta^2+\xi^2\right)} \end{aligned} \tag{2.63}$$

$$\begin{aligned} K_5(\eta,\xi) = {} & \frac{-8\xi\left(1+\eta^2+\xi^2\right)}{a^2c^2\left(\eta^2+\xi^2\right)^2\left(1-\eta^2+\xi^2\right)^2} + \frac{16\eta^2\xi\left(1-\eta^4\right)}{a^2c^2\left(\eta^2+\xi^2\right)^2\left(1-\eta^2+\xi^2\right)} + \frac{2\left[S_9(\eta,\xi)+S_{13}(\eta,\xi)\right]}{c^2} + \\ & + \frac{2a^2\eta\xi\left[-S_8(\eta,\xi) - S_{15}(\eta,\xi) + \xi S_{16}(\eta,\xi)\right]}{c^2\left(h_{11}\right)^2\left(1-\eta^2+\xi^2\right)} + + \frac{2a^2\eta\xi S_{17}(\eta,\xi)}{c^2 h_{11}h_{22}\left(1-\eta^2+\xi^2\right)} - \frac{2a^2\xi^2 S_{17}(\eta,\xi)}{c^2\left(h_{22}\right)^2\left(1-\eta^2+\xi^2\right)} \end{aligned} \tag{2.64}$$

$$\begin{aligned} K_6(\eta,\xi) = {} & \frac{-4a^2\xi^2\left(1+3\eta^2+\xi^2\right)}{c^2\left(1-\eta^2+\xi^2\right)^3} - \frac{8\left(1-\eta^4\right)\left(1-\eta^4-\xi^4-10\eta^2\xi^2\right)}{a^2c^2\left(\eta^2+\xi^2\right)^2\left(1-\eta^2+\xi^2\right)^3} + \frac{8\eta^2\left(1-\eta^2\right)}{a^2c^2\left(\eta^2+\xi^2\right)\left(1-\eta^2+\xi^2\right)^2} + \\ & + \frac{2a^2\left[-\eta\left(1+\eta^2+\xi^2\right)S_8(\eta,\xi) + 2\eta\xi^2 S_9(\eta,\xi) - \eta\left(1-\eta^2-\xi^2\right)S_{15}(\eta,\xi) + 2\xi\left(1-\eta^2\right)S_{16}(\eta,\xi)\right]}{c^2\left(1-\eta^2+\xi^2\right)^2} - \\ & - \frac{-2a^2\eta^2\left(h_{11}\right)^2{}_{,1}\,S_{10}(\eta,\xi)}{c^2\left(h_{11}\right)^4\left(1-\eta^2+\xi^2\right)} + \frac{2a^2\eta^2\left[2\left(1+\xi^2\right)S_{10}(\eta,\xi) - S_{19}(\eta,\xi)\right]}{c^2\left(h_{11}\right)^2\left(1-\eta^2+\xi^2\right)} + \frac{2a^2\xi\left(1+\eta^2+\xi^2\right)S_{11}(\eta,\xi)}{c^2 h_{11}h_{22}} - \\ & - \frac{2a^2\eta\xi\left[\left(h_{11}h_{22}\right)_{,1}\,S_{11}(\eta,\xi)\right]}{c^2\left(h_{11}h_{22}\right)^2\left(1-\eta^2+\xi^2\right)} + \frac{2a^2\xi\left[\left(h_{22}\right)^2{}_{,1}\,S_{12}(\eta,\xi) - \xi\left(h_{22}\right)^2{}_{,2}\,S_{18}(\eta,\xi)\right]}{c^2\left(h_{22}\right)^4\left(1-\eta^2+\xi^2\right)} + \\ & + \frac{2a^2\left[\left(1-\eta^2-\xi^2\right)S_{17}(\eta,\xi) - \eta\xi\left(1-\eta^2+\xi^2\right)S_{20}(\eta,\xi)\right]}{c^2\left(h_{11}h_{22}\right)\left(1-\eta^2+\xi^2\right)^2} - \\ & - \frac{2a^2\xi\left[\eta\xi S_{12}(\eta,\xi) - 2\left(1-\xi^2\right)^2 S_{18}(\eta,\xi) - \xi S_{21}(\eta,\xi)\right]}{c^2\left(h_{22}\right)^2\left(1-\eta^2+\xi^2\right)^2} \end{aligned} \tag{2.65}$$

Substituting the explicit expressions for the nonempty space parts $f_{\mu\nu}$ and $f^{\mu\nu}$ into equation (2.37), simplifying and grouping like terms yields (2.59), where the terms consisting it are (2.60)–(2.65).

Equation (2.59) is thus our exact explicit R_{33} exterior field equation to the order c^{-2}. We can now conveniently formulate astrophysical solutions for the equation in the next section; which are convergent in the exterior space time of a homogeneous massive oblate spheroid placed in empty space.

3 Formulation of R-33 exterior solution

In the exterior oblate spheroidal space time [7]:

$$\xi \geqslant \xi_0 \quad \text{and} \quad -1 \leqslant \eta \leqslant 1; \quad \xi_0 = constant \tag{3.1}$$

Let us now seek a solution for the R_{33} field equation (2.59) in the form of the power series

$$f(\eta,\xi) = \sum_{n=0}^{\infty} P_n^+(\xi)\,\eta^n. \tag{3.2}$$

where P_n^+ is a function to be determined for each value of n. Substituting the proposed function into the field equation and taking into consideration the fact that $\{\eta^n\}_{n=0}^{\infty}$ is a linearly independent set, we can thus equate the coefficients of η^n on both sides of the obtained equation. From the coefficients of η^0, we obtain the equation

$$\begin{aligned} 0 = {} & K_1(\eta,\xi) P_2^+(\xi) + K_2(\eta,\xi)\left[P_1^+(\xi)\right]' + \\ & + K_3(\eta,\xi)\left[P_0^+(\xi)\right]'' + K_4(\eta,\xi) P_1^+(\xi) + \\ & + K_5(\eta,\xi)\left[P_0^+(\xi)\right]' + K_6(\eta,\xi) P_0^+(\xi) \end{aligned} \tag{3.3}$$

or more explicitly

$$\begin{aligned} 0 = {} & a^3\xi^3\left(1+\xi^2-a^2\xi^4\right)P_2^+(\xi) + \\ & + 2a^3\xi^3\left(1+\xi^2\right)^2\left[P_1^+(\xi)\right]' + a^3\xi^2\left(1+\xi^2\right)P_1^+(\xi) + \\ & + a^3\xi^3\left(1+\xi^2\right)^2\left[P_0^+(\xi)\right]'' + \left(1+\xi^2\right)\times \\ & \times\left(-1-2a^2\xi^2-\xi^2-a^2\xi^3+4a^2\xi^5\right)\left[P_0^+(\xi)\right]' + \\ & + \left[2a^3\xi\left(4-2\xi^2-a^4\xi^4-a^4\xi^6\right)\right]P_0^+(\xi). \end{aligned} \tag{3.4}$$

Equation (3.4) is the first recurrence differential equation for the unknown functions. All the other recurrence differential equations can thus follow, yielding infinitely many recurrence differential equations that can be used to determine all the unknown functions.

The following profound points can thus be made. Firstly, equation (3.4) determines P_2^+ in terms of P_0^+ and P_1^+, similarly the other recurrence differential equations will determine the other unknown functions $P_3^+, \dots$ in terms of P_0^+ and P_1^+. Secondly, we note that we have the freedom to choose our arbitrary functions to satisfy the physical requirements or needs of any particular distribution or area of application.

Let us now recall that for any gravitational field [7, 13],

$$g_{00} \cong 1 + \frac{2}{c^2}\,\Phi \tag{3.5}$$

where Φ is Newton's gravitational scalar potential for the field under consideration. Thus we can then deduce that the unknown function in our field equation can be given approximately as

$$f(\eta,\xi) \cong \Phi^+(\eta,\xi) \tag{3.6}$$

where $\Phi^+(\eta,\xi)$ is Newton's gravitational scalar potential exterior to a homogeneous oblate spheroidal mass. Recently [14], it has been shown that

$$\Phi^+(\eta,\xi) = B_0 Q_0(-i\xi)\,P_0(\eta) + B_2 Q_2(-i\xi)\,P_2(\eta) \tag{3.7}$$

where Q_0 and Q_2 are the Legendre functions linearly independent to the Legendre polynomials P_0 and P_2 respectively; B_0 and B_2 are constants.

Let us now seek our exact analytical exterior solution (3.4) to be as close as possible to the approximate exterior solution (3.7). Now since the approximate solution possesses no term in the first power of η, let us choose

$$P_0^+(\xi) = B_0 Q_0(-i\xi)\,P_0 + B_2 Q_2(-i\xi) \tag{3.8}$$

and

$$P_1^+(\xi) \equiv 0\,. \tag{3.9}$$

Hence, we can write P_2^+ in terms of P_0^+ as

$$\begin{aligned} P_2^+(\xi) = &-\frac{\left(1+\xi^2\right)^2}{\left(1+\xi^2-a^2\xi^4\right)}\left[P_0^+(\xi)\right]'' - \\ &-\frac{2\left(1+\xi^2\right)\left(3a^2\xi^2+4a^2\xi^5-\xi^2-1\right)}{a^2\xi^3}\left[P_0^+(\xi)\right]' - \\ &-2\left[\frac{1-2a^3\xi^2-a^7\xi^4-a^7\xi^6+a^3}{a^3\xi^2\left(1+\xi^2-a^2\xi^4\right)}\right]P_0^+(\xi)\,. \end{aligned} \tag{3.10}$$

We now remark that the first three terms of our series solution converge everywhere in the exterior space time. We also remark that our solution of order c^0 may be written as

$$f(\eta,\xi) = \Phi^+(\eta,\xi) + \Phi_0^+(\eta,\xi) \tag{3.11}$$

where $\Phi^+(\eta,\xi)$ is the corresponding Newtonian gravitational scalar potential given by (3.7) and $\Phi_0^+(\eta,\xi)$ is the pure Einsteinian or general relativistic or post Newtonian correction of order c^0.

Hence, we deduce that our exterior analytical solution is of the general form

$$f(\eta,\xi) = \Phi^+(\eta,\xi) + \Phi_0^+(\eta,\xi) + \sum_{n=1}^{\infty}\Phi_{2n}^+(\eta,\xi)\,. \tag{3.12}$$

4 Formulation of interior R-33 field equation and solution

For the interior space time, Einstein's field equations are well known to be given as;

$$R_{\mu\nu} - \frac{1}{2}\,R g_{\mu\nu} = -\frac{8\pi G}{c^4}\,T_{\mu\nu} \tag{4.1}$$

where $T_{\mu\nu}$ is the energy momentum tensor.

Now, let us assume that the homogeneous mass distribution is a "perfect fluid". Thus, we can define the energy momentum tensor as

$$T_{\mu\nu} = (\rho_0 + P_0)\,u_\mu u_\nu - P_0 g_{\mu\nu} \tag{4.2}$$

where ρ_0 is the proper mass density and P_0 is the proper pressure and u_μ is the velocity four vector. Hence, the five non trivial interior field equations can be written as;

$$R_{00} - \frac{1}{2}\,R g_{00} = -\frac{8\pi G}{c^4}\left[(\rho_0 + P_0)\,u_0 u_0 - P_0 g_{00}\right], \tag{4.3}$$

$$R_{11} - \frac{1}{2}\,R g_{11} = \frac{8\pi G}{c^4}\,P_0 g_{11}\,, \tag{4.4}$$

$$R_{12} - \frac{1}{2}\,R g_{12} = \frac{8\pi G}{c^4}\,P_0 g_{12}\,, \tag{4.5}$$

$$R_{22} - \frac{1}{2}\,R g_{22} = \frac{8\pi G}{c^4}\,P_0 g_{22}\,, \tag{4.6}$$

$$R_{33} - \frac{1}{2}\,R g_{33} = \frac{8\pi G}{c^4}\,P_0 g_{33}\,. \tag{4.7}$$

Now, we formulate the solution of (4.7). For the sake of mathematical convenience, we assume in this article that the pressure is negligible compared to the mass density and hence

$$P_0 \cong 0\,. \tag{4.8}$$

Multiplying equation (4.7) by $2g^{33}$ and using the fact that $g^{33}g_{33} = 1$ we obtain precisely as in the section 2;

$$-g^{00}R_{00} - g^{11}R_{11} - g^{22}R_{22} + g^{33}R_{33} - 2g^{12}R_{12} = 0\,. \tag{4.9}$$

Similarly, we obtain the interior equation explicitly as

$$\begin{aligned} &K_1(\eta,\xi)\,f_{\eta\eta} + K_2(\eta,\xi)\,f_{\eta\xi} + K_3(\eta,\xi)\,f_{\xi\xi} + \\ &+ K_4(\eta,\xi)\,f_\eta + K_5(\eta,\xi)\,f_\xi + K_6(\eta,\xi)\,f = 0\,. \end{aligned} \tag{4.10}$$

We now remark that, for the interior field we are required to formulate interior solutions of (4.10) convergent in the range

$$0 \leqslant \xi \leqslant \xi_0 , \qquad -1 \leqslant \eta \leqslant 1. \tag{4.11}$$

Let us thus seek a series solution of the form;

$$f^- (\eta, \xi) = \sum_{n=0}^{\infty} Z_n^- (\eta) \, \xi^n. \tag{4.12}$$

where Z_n^- are unknown functions to be determined. Now, using the fact that $\{\xi^n\}_{n=0}^{\infty}$ is a linearly independent set, we may equate coefficients on both sides and hence obtain the equations satisfied by Z_n^-. We proceed similarly as in the case of the exterior solution to obtain recurrence differential equations that determine the explicit expression for our exact analytical solution. Equating the coefficients of ξ^0, we obtain the first recurrence differential equation as

$$\begin{aligned} & K_1 (\eta, \xi) \left[Z_0^- (\eta) \right]'' + K_2 (\eta, \xi) \left[Z_1^- (\eta) \right]' + \\ & + K_3 (\eta, \xi) \, Z_2^- (\eta) + K_4 (\eta, \xi) \left[Z_0^- (\eta) \right]' + \\ & + K_5 (\eta, \xi) \, Z_1^- (\eta) + K_6 (\eta, \xi) \, Z_0^- (\eta) = 0 . \end{aligned} \tag{4.13}$$

In a similar manner, the other recurrence differential equations follow.

We can now proceed as in the previous section to choose the most astrophysically satisfactory solution to be as close as possible to the approximate solution. The gravitational scalar potential interior to a homogeneous oblate spheroid is well known [14] to be given as

$$\Phi^- (\eta, \xi) = \left[A_0 - \frac{1}{2} A_2 P_2(\eta) \right] - 3/2 A_2 P_2(\eta) \, \xi^2, \tag{4.14}$$

where P_2 is Legendre's polynomial of order 2 and A_0, A_2, are constants.

Since (4.14) converges for all values in the interval (4.11), it is very satisfactory for us to choose;

$$Z_0^- (\eta) = A_0 - \frac{1}{2} A_2 P_2(\eta) \tag{4.15}$$

and

$$Z_1^- (\eta) \equiv 0 . \tag{4.16}$$

Thus the first recurrence differential equation determines Z_2^- in terms of Z_0^-. Similarly, all the other recurrence differential equations will determine all the other functions in terms of Z_0^-. Hence we obtain our unique astrophysically most satisfactory interior solution. It is obvious that this unique solution will converge, precisely as the first two terms. Moreover, it is obvious that our unique solution reduces to the corresponding pure Newtonian gravitational scalar potential in the limit of the first two terms. This solution may be written as

$$f^- (\eta, \xi) = \Phi^- (\eta, \xi) + \Phi_0^- (\eta, \xi) \tag{4.17}$$

where $\Phi^- (\eta, \xi)$ is the corresponding Newtonian gravitational scalar potential given by (4.14) and $\Phi_0^- (\eta, \xi)$ is the pure instructively Einstenian (or general relativistic or post Newtonian correction) of order c^0.

Proceeding exactly as above we may derive all the corresponding solutions of all the other non-trivial interior Einstein's field equations for the sake of mathematical completeness, comparison with those of the R_{33} equation and theoretical applications where and when necessary in Physics. It is clearly obvious how to extend the derivation of the interior Einstein field equations above to include any given pressure function $P_0 (\eta, \xi)$, wherever and whenever necessary and useful in physical theory.

5 Conclusions

Interestingly, the single dependent function f in our mathematically most simple and astrophysically most satisfactory solution turns out as the corresponding well known pure Newtonian exterior/interior gravitational scalar potential augmented by hitherto unknown pure Einsteinian (or general relativistic or post-Newtonian) gravitational scalar potential terms of orders c^0, c^{-2}, c^{-4}, ... Hence, this article has revealed a hitherto unknown sense in which the exterior/interior Einstein's geometrical gravitational field equations are obtained as a generalization or completion of Newton's dynamical gravitational field equations.

With the formulation of our mathematically most simple and astrophysically most satisfactory solutions in this article, the way is opened up for the formulation and solution of the general relativistic equations of motion for all test particles in the gravitational fields of all static homogeneous distributions of mass within oblate spheroidal regions in the universe. And precisely because these equations contain the pure Newtonian as well as post-Newtonian gravitational scalar potentials all their predictions shall be most naturally comparable to the corresponding predictions from the pure Newtonian theory. This is most satisfactory indeed.

It is now obvious how our work in this article may by emulated to (i) derive a mathematically most simple structure for all the metric tensors in the space times exterior or interior to any distribution of mass within any region having any of the 14 regular geometries in nature, (ii) formulate all the nontrivial Einstein geometrical gravitational field equations and derive all their general solutions and (iii) derive astrophysically most satisfactory unique solutions for application to the motions of all test particles and comparison with corresponding pure Newtonian results and applications. Therefore our goal in this article has been completely achieved: to use the case of a spheroidal distribution of mass to show how the much vaunted Einstein's geometrical gravitational field equations may be solved exactly and analytically for any given distribution of mass within any region having any geometry.

Finally, we conclude that at very long last — 93 years after the publication of the laws of General Relativity by Einstein in 1915 — we have found a method and process for (1) deriving a unique approximate astrophysically most satisfactory solutions for the space times exterior and interior to every distribution of mass within any region having any of the 14 regular geometries in nature, in terms of the corresponding pure Newton's gravitational scalar potential, without even formulating the field equation; and (2) systematically formulating and solving the geometrical gravitational field equations in the space times of all distributions of mass in nature.

Acknowledgenent

The author is highly indebted to Prof. S. X. K. Howusu of the Physics Department, Kogi State University, Nigeria for his immense inspiration, guidance; and for the use of his R_{11} solution method to formulate the solution in this article.

Submitted on June 29, 2009 / Accepted on August 03, 2009

References

1. Bergmann P.G. Introduction to the Theory of Relativity. Prentice Hall, New Delhi, 1987.
2. Schwarzschild K. Über das Gravitationsfeld eines Massenpunktes nach der Einsteinschen Theorie. *Sitzungsberichte der Koniglich Preussischen Akademie der Wissenschaften*, 1916, 189–196 (published in English as: Schwarzschild K. On the gravitational field of a point mass according to Einstein's theory. *The Abraham Zelmanov Journal*, 2008, v. 1, 10–19).
3. Finster F., Kamran N., Smoller J. and Yau S.T. Decay of solutions of the wave equation in the Kerr geometry. *Communications in Mathematical Physics*, 2006, v. 264, 465–503.
4. Anderson L., Elst V., Lim W.C. and Uggla C. Assymptotic silence of generic cosmological singularities. *Physical Review Letters*, 2001, v. 94, 51–101.
5. MacCallum M.A.H. Finding and using exact solutions of the Einstein equation. arxiv: 0314.4133.
6. Stephani H., Kramer D., MacCallum M.A.H., Hoenselars C., Herlt E. Exact solutions of Einstein's field equations. 2nd ed., Cambridge Univ. press, London, 2003.
7. Howusu S.X.K. The 210 astrophysical solutions plus 210 cosmological solutions of Einstein's geometrical gravitational field equations. Jos University Press, Jos, 2007.
8. Chifu E.N. and Howusu S.X.K. Gravitational radiation and propagation field equation exterior to astrophysically real or hypothetical time varying distributions of mass within regions of spherical geometry. *Physics Essays*, 2009, v. 22(1), 73–77.
9. Chifu E.N. and Howusu S.X.K. Einstein's equation of motion for a photon in fields exterior to astrophysically real or imaginary spherical mass distributions who's tensor field varies with azimuthal angle only. *Journal of the Nigerian Association of Mathematical Physics*, 2008, v. 13, 363–366.
10. Chifu E.N., Howusu S.X.K. and Lumbi L.W. Relativistic mechanics in gravitational fields exterior to rotating homogeneous mass distributions within regions of spherical geometry. *Progress in Physics*, 2009, v. 3, 18–23.
11. Chifu E.N and Howusu S.X.K. Solution of Einstein's geometrical field equations exterior to astrophysically real or hypothetical time varying distributions of mass within regions of spherical geometry. *Progress in Physics*, 2009 v. 3,45–48.
12. Chifu E.N., Usman A. and Meludu O.C. Orbits in homogeneous oblate spheroidal gravitational space time. *Progress in Physics*, 2008, v. 3, 49–53.
13. Weinberg S. Gravitation and cosmology. J. Wiley, New York, 1972, p. 175–188.
14. Howusu S.X.K. Gravitational fields of spheroidal bodies-extension of gravitational fields of spherical bodies. *Galilean Electrodynamics*, 2005, v. 16(5), 98–100.

A New Finslerian Unified Field Theory of Physical Interactions

Indranu Suhendro
E-mail: spherical_symmetry@yahoo.com

In this work, we shall present the foundational structure of a new unified field theory of physical interactions in a geometric world-space endowed with a new kind of Finslerian metric. The intrinsic non-metricity in the structure of our world-geometry may have direct, genuine connection with quantum mechanics, which is yet to be fully explored at present. Building upon some of the previous works of the Author, our ultimate aim here is yet another quantum theory of gravity (in just four space-time dimensions). Our resulting new theory appears to present us with a novel Eulerian (intrinsically motion-dependent) world-geometry in which the physical fields originate.

1 Introduction

This work is a complementary exposition to our several previous attempts at the geometrization of matter and physical fields, while each of them can be seen as an independent, self-contained, coherent unified field theory.

Our primary aim is to develop a new foundational world-geometry based on the intuitive notion of a novel, fully naturalized kind of Finsler geometry, which extensively mimics the Eulerian description of the mechanics of continuous media with special emphasis on the world-velocity field, in the sense that the whole space-time continuum itself is taken to be globally dynamic on both microscopic and macroscopic scales. In other words, the world-manifold itself, as a whole, is not merely an ambient four-dimensional geometric background, but an open (self-closed, yet unbounded), co-moving, self-organizing, self-projective entity, together with the individual particles (objects) encompassed by its structure.

2 Elementary construction of the new world-geometry

Without initial recourse to the common structure of Finsler geometry, whose exposition can easily be found in the literature, we shall build the essential geometric world-space of our new theory somewhat from scratch.

We shall simply start with an intuitive vision of intrinsically motion-dependent objects, whose fuzzy Eulerian behavior, on the microscopic scale, is generated by the structure of the world-geometry in the first place, and whose very presence, on the macroscopic scale, affects the entire structure of the world-geometry. In this sense, the space-time continuum itself has a dynamic, non-metric character at heart, such that nothing whatsoever is intrinsically "fixed", including the defining metric tensor itself, which evolves, as a structural entity of global coverage, in a self-closed (self-inclusive) yet unbounded (open) manner.

In the present theory, the Universe is indeed an evolving, holographic (self-projective) four-dimensional space-time continuum U_4 with local curvilinear coordinates x^α and an intrinsically fuzzy (quantum-like), possibly degenerate, non-metric field ψ. As such, U_4 may encompass all possible metric-compatible (sub-)universes, especially those of the General Theory of Relativity. In this sense, U_4 may be viewed as a Meta-Universe, possibly without admitting any apparent boundary between its microscopic (interior) and macroscopic (exterior) mechanisms, as we shall see.

If we represent the metric-compatible part of the geometric basis of U_4 as $g_\alpha(x)$, then, following our unification scenario, the total geometric basis of our generally non-metric manifold shall be given by

$$\begin{aligned} g_\alpha(x,u) &= g_\alpha(x) + \psi_\alpha u \\ g^\alpha(x,u) &= \left(g_\alpha(x,u)\right)^{-1} \\ \left\langle g_\alpha(x,u), g^\beta(x,u)\right\rangle &= \delta^\beta_\alpha \end{aligned}$$

where $u = \frac{dx^\alpha}{ds} g_\alpha(x,u)$ is the world-velocity field along the world-line

$$s(x,u) = \int \sqrt{g_{\alpha\beta}(x,u)\, dx^\alpha dx^\beta}$$

(with $g_{\alpha\beta}(x,u)$ being the components of the generalized metric tensor to be subsequently given below), and where δ^β_α are the components of the Kronecker delta. (Needless to say, the Einstein summation convention is applied throughout this work as usual.) Here the inner product is indicated by $\langle \dots, \dots \rangle$. We then have

$$\frac{\partial}{\partial x^\beta} g_\alpha(x,u) = \frac{\partial}{\partial x^\beta} g_\alpha(x) + u \frac{\partial \psi_\alpha}{\partial x^\beta} + \psi_\alpha \nabla_\beta u,$$

where ∇ denotes the gradient, that is, the covariant derivative.

The components of the symmetric, bilinear metric tensor $g(x,u)$ for the given geometric basis are readily given by

$$\begin{aligned} g_{\alpha\beta}(x,u) &= \langle g_\alpha(x,u), g_\beta(x,u)\rangle \\ g_{\alpha\lambda}(x,u)\, g^{\beta\lambda}(x,u) &= \delta^\beta_\alpha . \end{aligned}$$

As such, we obtain

$$g_{\alpha\beta}(x,u) = g_{\alpha\beta}(x) + 2\,\hat{u}_{(\alpha}\psi_{\beta)} + \phi^2(x,u)\,\psi_\alpha\,\psi_\beta .$$

As usual, round brackets enclosing indices indicate symmetrization; subsequently, anti-symmetrization shall be indicated by square brackets. In the above relation, $\hat{u}_\alpha = \langle u, g_\alpha(x)\rangle$ and

$$\phi^2(x,u) = g_{\alpha\beta}(x,u)\, u^\alpha u^\beta$$

is the squared length of the world-velocity vector, which varies from point to point in our world-geometry. As we know, this squared length is equal to unity in metric-compatible Riemannian geometry.

The connection form of our world-geometry is obtained through the inner product

$$\Gamma^\lambda_{\alpha\beta}(x,u) = \left\langle g^\lambda(x,u), \frac{\partial}{\partial x^\beta} g_\alpha(x,u)\right\rangle.$$

In an explicit manner, we see that

$$\Gamma^\lambda_{\alpha\beta}(x,u) = \Gamma^\lambda_{\alpha\beta}(x) + \left(\frac{\partial \psi_\alpha}{\partial x^\beta}\right) u^\lambda + \psi_\alpha \nabla_\beta u^\lambda.$$

In accordance with our previous unified field theories (see, for instance, [1–5]), the above expression must generally be asymmetric, with the torsion being given by the anti-symmetric form

$$\Gamma^\lambda_{[\alpha\beta]}(x,u) = \Gamma^\lambda_{[\alpha\beta]}(x) + \frac{1}{2}\left(\frac{\partial \psi_\alpha}{\partial x^\beta} - \frac{\partial \psi_\beta}{\partial x^\alpha}\right) u^\lambda + \frac{1}{2}\left(\psi_\alpha \nabla_\beta u^\lambda - \psi_\beta \nabla_\alpha u^\lambda\right).$$

In contrast to the case of a Riemannian manifold (without background embedding), we have the following unique case:

$$\nabla_\beta g_\alpha(x,u) \equiv \frac{\partial}{\partial x^\beta} g_\alpha(x,u) - \Gamma^\lambda_{\alpha\beta}(x,u)\, g_\lambda(x,u) = \frac{1}{2}\psi_\alpha \psi_\lambda \left(\nabla_\beta u^\lambda\right)\psi$$

for which, additionally, $\Gamma^\lambda_{\alpha\beta}(x)\ \psi_\lambda = 0$. Consequently, the covariant derivative of the world-metric tensor fails to vanish in the present theory, as we obtain the following non-metric expression:

$$\nabla_\lambda g_{\alpha\beta}(x,u) = \psi_\alpha \psi_\beta \psi_\sigma \nabla_\lambda u^\sigma.$$

At this point, in order to correspond with Finsler geometry in a manifest way, we shall write

$$\nabla_\lambda g_{\alpha\beta}(x,u) = \Phi_{\alpha\beta\sigma} \nabla_\lambda u^\sigma$$

and

$$g_{\alpha\beta}(x,u) = \frac{1}{2}\frac{\partial^2}{\partial u^\alpha \partial u^\beta}\phi^2(x,u)$$

in such a way that the following conditions are satisfied:

$$\Phi_{\alpha\beta\lambda} = \psi_\alpha \psi_\beta \psi_\lambda,$$

$$\frac{1}{2}\Phi_{\alpha\beta\lambda} = \frac{1}{2}\Phi_{(\alpha\beta\lambda)} = \frac{1}{2}\frac{\partial}{\partial u^\lambda} g_{\alpha\beta}(x,u) = \frac{1}{4}\frac{\partial^3}{\partial u^\alpha \partial u^\beta \partial u^\lambda}\phi^2(x,u),$$

$$\Phi_{\alpha\beta\lambda}\, u^\lambda = 0,$$

$$\psi_\alpha\, u^\alpha = 0.$$

Once the velocity field is known, the Hessian form of the metric tensor enables us to write, in the momentum representation for a geometric object with mass m (initially at rest, locally),

$$g_{\alpha\beta}(x,u) = \frac{1}{2} m^2 \frac{\partial^2}{\partial p^\alpha \partial p^\beta}\phi^2(x,u),$$

$$p^\alpha = m\, u^\alpha$$

such that, with $\phi^2(x,u)$ being expressed in parametric form, physical geometry, that is, the existence of a geometric object in space-time, is essentially always related to mass and its energy content.

Taking into account the projective angular tensor given by

$$\Omega_{\alpha\beta}(x,u) = g_{\alpha\beta}(x,u) - \frac{1}{\phi^2(x,u)} u_\alpha u_\beta,$$

$$\Omega_{\alpha\lambda}(x,u)\ \Omega^{\beta\lambda}(x,u) = \delta^\beta_\alpha - \frac{1}{\phi^2(x,u)} u_\alpha u^\beta,$$

$$\Omega_{\alpha\beta}(x,u)\ u^\beta = 0,$$

where n is the number of dimensions of the geometric space (in our case, of course, $n = 4$), in the customary Finslerian way, it can easily be shown that

$$\Phi_{\alpha\beta\lambda} = \frac{1}{n}\left(\Omega_{\alpha\beta}(x,u)\ \Phi_\lambda + \Omega_{\beta\lambda}(x,u)\ \Phi_\alpha + \Omega_{\lambda\alpha}(x,u)\ \Phi_\beta - \frac{1}{\Phi_\sigma \Phi^\sigma}\Phi_\alpha \Phi_\beta \Phi_\lambda\right),$$

$$\Phi_\alpha = g^{\sigma\rho}(x,u)\ \Phi_{\sigma\rho\alpha} = 2\frac{\partial}{\partial u^\alpha}\ln\sqrt{\det\left(g(x,u)\right)},$$

$$\frac{\partial}{\partial u^\alpha}\ln\sqrt{\det\left(g(x,u)\right)} = \frac{1}{2} g^{\rho\sigma}(x,u)\frac{\partial}{\partial u^\alpha} g_{\rho\sigma}(x,u)$$

for which, in our specific theory, we have, with $\psi^2 = g_{\alpha\beta}(x,u)\ \psi^\alpha \psi^\beta$,

$$\Phi_{\alpha\beta\lambda} = \frac{\psi^2}{n}\left(\Omega_{\alpha\beta}(x,u)\ \psi_\lambda + \Omega_{\beta\lambda}(x,u)\ \psi_\alpha + \Omega_{\lambda\alpha}(x,u)\ \psi_\beta - \frac{1}{\psi^2}\psi_\alpha \psi_\beta \psi_\lambda\right).$$

We may note that, along the world-line, for the intrinsic geodesic motion of a particle given by the parallelism

$$\frac{Du^\alpha}{Ds} = \left(\nabla_\beta u^\alpha\right) u^\beta = 0,$$

the Finslerian condition

$$\frac{D}{Ds}\, g_{\alpha\beta}\,(x,u) = 0$$

is always satisfied, along with the supplementary condition

$$\frac{D}{Ds}\, \phi^2\,(x,u) = 0\,.$$

Consequently, we shall also have

$$\frac{D}{Ds}\, \Omega_{\alpha\beta}\,(x,u) = 0\,.$$

It is essential to note that, unlike in Weyl geometry, we shall not expect to arrive at the much simpler gauge condition $\nabla_\lambda\, g_{\alpha\beta}\,(x,u) = g_{\alpha\beta}\,(x,u)\; A_\lambda\,(\psi)$. Instead, we shall always employ the following alternative general form:

$$\nabla_\lambda\, g_{\alpha\beta}\,(x,u) = \frac{1}{\phi^2\,(x,u)}\left(\delta_u\, g_{\alpha\beta} - 2\,\hat{u}_{(\alpha}\;\psi_{\beta)}\right)\;\psi_\sigma\,\nabla_\lambda\, u^\sigma$$

where, as we can easily see, the diffeomorphic structure of the metric tensor for the condition of non-metricity of our world-geometry is manifestly given by

$$\delta_u\, g_{\alpha\beta} \equiv g_{\alpha\beta}\,(x,u) - g_{\alpha\beta}\,(x) =$$
$$= 2\,\hat{u}_{(\alpha}\,\psi_{\beta)} + \phi^2\,(x,u)\;\psi_\alpha\,\psi_\beta$$

3 Explicit physical (Eulerian) structure of the connection form

Having recognized the structural non-metric character of our new world-geometry in the preceding section, we shall now seek to outline the explicit physical structure of the connection form for the purpose of building a unified field theory.

We first note that the non-metric connection form of our theory can always be given by the general expression

$$\Gamma^\lambda_{\alpha\beta}\,(x,u) = \frac{1}{2}\, g^{\lambda\sigma}\,(x,u)\left(\frac{\partial}{\partial\, x^\beta}\, g_{\sigma\alpha}\,(x,u) -\right.$$
$$- \frac{\partial}{\partial x^\sigma}\, g_{\alpha\beta}\,(x,u) + \frac{\partial}{\partial\, x^\alpha}\, g_{\beta\sigma}\,(x,u)\Big) +$$
$$+\; \Gamma^\lambda_{[\alpha\beta]}\,(x,u) - g^{\lambda\sigma}\,(x,u)\left(g_{\alpha\rho}\,(x,u)\,\Gamma^\rho_{[\sigma\beta]}\,(x,u) +\right.$$
$$+\; g_{\beta\rho}\,(x,u)\,\Gamma^\rho_{[\sigma\alpha]}\,(x,u)\Big) +$$
$$+\; \frac{1}{2}\, g^{\lambda\sigma}\,(x,u)\left(\nabla_\beta\, g_{\sigma\alpha}\,(x,u) -\right.$$
$$-\; \nabla_\sigma\, g_{\alpha\beta}\,(x,u) + \nabla_\alpha\, g_{\beta\sigma}\,(x,u)\Big)\,.$$

Then, using the results given in the previous section, in direct relation to our previous metric-compatible unification theory of gravity, electromagnetism, material spin, and the nuclear interaction [4], where the electromagnetic field and material spin are generated by the torsion field, we readily obtain

$$\Gamma^\lambda_{\alpha\beta}\,(x,u) = \frac{1}{2}\, g^{\lambda\sigma}\,(x,u)\left(\frac{\partial}{\partial\, x^\beta}\, g_{\sigma\alpha}\,(x,u) -\right.$$
$$- \frac{\partial}{\partial\, x^\sigma}\, g_{\alpha\beta}\,(x,u) + \frac{\partial}{\partial\, x^\alpha}\, g_{\beta\sigma}\,(x,u)\Big) +$$
$$+\; \frac{e}{2\, m\, c^2}\,\phi^2\,(x,u)\left(F_{\alpha\beta}\, u^\lambda - F^\lambda{}_\alpha\, u_\beta - F^\lambda{}_\beta\, u_\alpha\right) +$$
$$+\; S^\lambda_{\alpha\beta} - g^{\lambda\sigma}\,(x,u)\left(g_{\alpha\rho}\,(x,u)\; S^\rho_{\sigma\beta} + g_{\beta\rho}\,(x,u)\; S^\rho_{\sigma\alpha}\right) +$$
$$+\; \frac{1}{2}\, g^{\lambda\sigma}(x,u)\,\psi_\rho(\psi_\sigma\,\psi_\alpha\,\nabla_\beta\, u^\rho - \psi_\alpha\,\psi_\beta\,\nabla_\sigma\, u^\rho +$$
$$+\; \psi_\beta\,\psi_\sigma\,\nabla_\alpha\, u^\rho)\,.$$

Here it is interesting to note that even when $\psi = 0$, which gives a metric-compatible ("classical") case, our connection form already explicitly depends on the world-velocity (in addition to position), hence the unified field theory of physical interactions outlined in [4] can somehow already be considered as being a Finslerian one despite the fact that it is metric-compatible.

We recall, still from [4], that the electromagnetic field F and the material spin field S have a common geometric origin, which is the structural torsion of the space-time manifold, and are essentially given by the following expressions:

$$F_{\alpha\beta} = 2\,\frac{m\, c^2}{e}\,\Gamma^\lambda_{[\alpha\beta]}\, u_\lambda\,,$$
$$S^\lambda_{\alpha\beta} = S^\lambda{}_\alpha\, u_\beta - S^\lambda{}_\beta\, u_\alpha\,,$$
$$S^{\alpha\beta}\, u_\beta = 0,\, S^{\alpha\beta} = S^{[\alpha\beta]}\,,$$
$$\Gamma^\lambda_{[\alpha\beta]} = \frac{e}{2\, m\, c^2}\, F_{\alpha\beta}\, u^\lambda + S^\lambda_{\alpha\beta}\,,$$

where m is the (rest) mass, e is the electric charge, and c is the speed of light in vacuum, such that the physical fields are intrinsic to the space-time geometry itself, as manifest in generalized geodesic equation of motion $\frac{Du^\alpha}{Ds} = 0$, which naturally yields the general relativistic equation of motion of a charged, massive particle in the gravitational field

$$m\, c^2\left(\frac{du^\alpha}{ds} + \Delta^\alpha_{\beta\lambda}\, u^\beta\, u^\lambda\right) = e\, F^\alpha_\beta\, u^\beta\,,$$
$$\Delta^\alpha_{\beta\lambda} = \frac{1}{2}\, g^{\alpha\sigma}\left(\frac{\partial\, g_{\sigma\beta}}{\partial\, x^\lambda} - \frac{\partial\, g_{\beta\lambda}}{\partial\, x^\sigma} + \frac{\partial\, g_{\lambda\sigma}}{\partial\, x^\beta}\right).$$

In other words, the physical fields other than gravity (chiefly, the electromagnetic field) can also be represented as part of the internal structure of the free-fall of a particle. Just like gravity, being fully geometrized in our theory, these non-holonomic (vortical) fields are no longer external entities merely added into the world-picture in order to interact with

gravity and the structure of space-time itself, thereby essentially fulfilling the geometrization program of physics as stated, for example, in [6].

Correspondingly, the nuclear (Yang-Mills) interaction is essentially given in our theory as an internal electromagnetic interaction by

$$F^i_{\alpha\beta} = 2\,\omega^i_\lambda\,\Gamma^\lambda_{[\alpha\beta]}\,,$$

$$F_{\alpha\beta} = \frac{m\,c^2}{e}\,F^i_{\alpha\beta}\,u_i\,(i=1,2,3)\,,$$

where ω^i_α are the components of the tetrad (projective) field relating the global space-time to the internal three-dimensional space of the nuclear interaction.

In this direction, we may also define the extended electromagnetic field, which explicitly depends on the world-velocity, through

$$\tilde{F}_{\alpha\beta}\,(x,u) = \phi^2\,(x,u)\,F_{\alpha\beta} = 2\,\phi^2\,(x,u)\,\frac{mc^2}{e}\,\Gamma^\lambda_{[\alpha\beta]}\,u_\lambda\,.$$

4 Substantial structure of covariant differentiation in $\mathbf{U_4}$

Given an arbitrary world-tensor $T\,(x,u)$ at any point in our Finslerian world-geometry, we have the following elementary substantial derivatives:

$$\frac{d}{d\tau}\,T^{\alpha\beta\ldots\gamma}_{\rho\sigma\ldots\lambda}\,(x,u) =$$
$$= \frac{\partial}{\partial x^\eta}\left(T^{\alpha\beta\ldots\gamma}_{\rho\sigma\ldots\lambda}\,(x,u)\right)\frac{dx^\eta}{d\tau} + \frac{\partial}{\partial u^\eta}\left(T^{\alpha\beta\ldots\gamma}_{\rho\sigma\ldots\lambda}\,(x,u)\right)\frac{\partial u^\eta}{\partial\tau}\,,$$

$$\frac{d}{dx^\eta}T^{\alpha\beta\ldots\gamma}_{\rho\sigma\ldots\lambda}\,(x,u) =$$
$$= \frac{\partial}{\partial x^\eta}T^{\alpha\beta\ldots\gamma}_{\rho\sigma\ldots\lambda}\,(x,u) + \frac{\partial}{\partial u^\delta}\left(T^{\alpha\beta\ldots\gamma}_{\rho\sigma\ldots\lambda}\,(x,u)\right)\frac{\partial u^\delta}{\partial x^\eta}\,,$$

where τ is a global parameter.

In this way, the substantial structure of covariant differentiation in U_4 shall be given by

$$\tilde{\nabla}_\eta\,T^{\alpha\beta\ldots\gamma}_{\rho\sigma\ldots\lambda}\,(x,u) =$$
$$= \frac{\partial}{\partial\,x^\eta}\,T^{\alpha\beta\ldots\gamma}_{\rho\sigma\ldots\lambda}\,(x,u) + \frac{\partial}{\partial\,u^\varsigma}\left(T^{\alpha\beta\ldots\gamma}_{\rho\sigma\ldots\lambda}\,(x,u)\right)\frac{\partial\,u^\varsigma}{\partial\,x^\eta} +$$
$$+\,\Gamma^\alpha_{\delta\eta}\,(x,u)\,T^{\delta\beta\ldots\gamma}_{\rho\sigma\ldots\lambda}\,(x,u) + \Gamma^\beta_{\delta\eta}\,(x,u)\,T^{\alpha\delta\ldots\gamma}_{\rho\sigma\ldots\lambda}\,(x,u) + \ldots +$$
$$+\,\Gamma^\gamma_{\delta\eta}\,(x,u)\,T^{\alpha\beta\ldots\delta}_{\rho\sigma\ldots\lambda}\,(x,u) - \Gamma^\delta_{\rho\eta}\,(x,u)\,T^{\alpha\beta\ldots\gamma}_{\delta\sigma\ldots\lambda}\,(x,u) -$$
$$-\,\Gamma^\delta_{\sigma\eta}\,(x,u)\,T^{\alpha\beta\ldots\gamma}_{\rho\delta\ldots\lambda}\,(x,u) - \ldots - \Gamma^\delta_{\lambda\eta}\,(x,u)\,T^{\alpha\beta\ldots\gamma}_{\rho\sigma\ldots\delta}\,(x,u)$$

along with the more regular (point-oriented) form

$$\nabla_\eta\,T^{\alpha\beta\ldots\gamma}_{\rho\sigma\ldots\lambda}\,(x,u) = \frac{\partial}{\partial\,x^\eta}\,T^{\alpha\beta\ldots\gamma}_{\rho\sigma\ldots\lambda}\,(x,u) +$$
$$+\,\Gamma^\alpha_{\delta\eta}\,(x,u)\,T^{\delta\beta\ldots\gamma}_{\rho\sigma\ldots\lambda}\,(x,u) + \Gamma^\beta_{\delta\eta}\,(x,u)\,T^{\alpha\delta\ldots\gamma}_{\rho\sigma\ldots\lambda}\,(x,u) + \cdots +$$
$$+\,\Gamma^\gamma_{\delta\eta}\,(x,u)\,T^{\alpha\beta\ldots\delta}_{\rho\sigma\ldots\lambda}\,(x,u) - \Gamma^\delta_{\rho\eta}\,(x,u)\,T^{\alpha\beta\ldots\gamma}_{\delta\sigma\ldots\lambda}\,(x,u) -$$
$$-\,\Gamma^\delta_{\sigma\eta}\,(x,u)\,T^{\alpha\beta\ldots\gamma}_{\rho\delta\ldots\lambda}\,(x,u) - \cdots - \Gamma^\delta_{\lambda\eta}\,(x,u)\,T^{\alpha\beta\ldots\gamma}_{\rho\sigma\ldots\delta}\,(x,u)\,.$$

Turning our attention to the world-metric tensor, we see that the expression

$$\tilde{\nabla}_\lambda\,g_{\alpha\beta}\,(x,u) = \frac{\partial}{\partial\,x^\lambda}\,g_{\alpha\beta}\,(x,u) + \frac{\partial}{\partial\,u^\sigma}\,(g_{\alpha\beta}\,(x,u))\,\frac{\partial\,u^\sigma}{\partial\,x^\lambda} -$$
$$-\,\Gamma^\rho_{\alpha\lambda}\,(x,u)\,g_{\rho\beta}\,(x,u) - \Gamma^\rho_{\beta\lambda}\,(x,u)\,g_{\alpha\rho}\,(x,u)$$

may enable us to establish a rather indirect metricity-like condition. This can be done by invoking the condition

$$\Phi_{\alpha\beta\sigma}\Gamma^\sigma_{\rho\lambda}\,(x,u)\,u^\lambda = 0$$

and by setting

$$\tilde{\nabla}_\lambda\,g_{\alpha\beta}\,(x,u) = 0\,.$$

Now, with the help of the already familiar relations

$$\frac{\partial}{\partial\,u^\lambda}\,g_{\alpha\beta}\,(x,u) = \Phi_{\alpha\beta\lambda}\,,$$

$$g^{\alpha\beta}\,(x,u)\,\frac{\partial}{\partial\,u^\lambda}\,g_{\alpha\beta}\,(x,u) = 2\frac{\partial}{\partial\,u^\lambda}\ln\sqrt{\det\left(g\,(x,u)\right)}$$

we shall again have

$$\nabla_\lambda\,g_{\alpha\beta}\,(x,u) = \Phi_{\alpha\beta\sigma}\,\nabla_\lambda\,u^\sigma\,.$$

5 Generalized curvature forms

We are now equipped enough with the basic structural relations to investigate curvature forms in our theory. In doing so, we shall derive a set of generalized Bianchi identities corresponding to a peculiar class of field equations, including some possible conservation laws (in rather special circumstances).

In a direct customary manner, we have the extended expression

$$\left(\tilde{\nabla}_\nu\,\tilde{\nabla}_\mu - \tilde{\nabla}_\mu\,\tilde{\nabla}_\nu\right)T^{\alpha\beta\ldots\gamma}_{\rho\sigma\ldots\lambda}\,(x,u) =$$
$$= \left(\nabla_\nu\,\nabla_\mu - \nabla_\mu\,\nabla_\nu\right)T^{\alpha\beta\ldots\gamma}_{\rho\sigma\ldots\lambda}\,(x,u) +$$
$$+\,\frac{\partial}{\partial\,u^\eta}\left(\nabla_\mu T^{\alpha\beta\ldots\gamma}_{\rho\sigma\ldots\lambda}\,(x,u)\right)\frac{\partial\,u^\eta}{\partial\,x^\nu} -$$
$$-\,\frac{\partial}{\partial\,u^\eta}\left(\nabla_\nu T^{\alpha\beta\ldots\gamma}_{\rho\sigma\ldots\lambda}\,(x,u)\right)\frac{\partial\,u^\eta}{\partial\,u^\mu} +$$
$$+\,\nabla_\nu\left(\frac{\partial}{\partial\,u^\eta}\left(T^{\alpha\beta\ldots\gamma}_{\rho\sigma\ldots\lambda}\,(x,u)\right)\frac{\partial\,u^\eta}{\partial\,x^\mu}\right) -$$
$$-\,\nabla_\mu\left(\frac{\partial}{\partial\,u^\eta}\left(T^{\alpha\beta\ldots\gamma}_{\rho\sigma\ldots\lambda}\,(x,u)\right)\frac{\partial\,u^\eta}{\partial\,x^\nu}\right) +$$
$$+\,\frac{\partial}{\partial\,u^\delta}\left(\frac{\partial}{\partial\,u^\eta}\left(T^{\alpha\beta\ldots\gamma}_{\rho\sigma\ldots\lambda}\,(x,u)\right)\frac{\partial\,u^\eta}{\partial\,x^\mu}\right)\frac{\partial\,u^\delta}{\partial\,x^\nu} -$$
$$-\,\frac{\partial}{\partial\,u^\delta}\left(\frac{\partial}{\partial\,u^\eta}\left(T^{\alpha\beta\ldots\gamma}_{\rho\sigma\ldots\lambda}\,(x,u)\right)\frac{\partial\,u^\eta}{\partial\,x^\nu}\right)\frac{\partial\,u^\delta}{\partial\,x^\mu}$$

for which the essential part is

$$(\nabla_\nu \nabla_\mu - \nabla_\mu \nabla_\nu) T^{\alpha\beta\ldots\gamma}_{\rho\sigma\ldots\lambda}(x,u) =$$
$$= R^\eta{}_{\rho\mu\nu}(x,u) T^{\alpha\beta\ldots\gamma}_{\eta\sigma\ldots\lambda}(x,u) +$$
$$+ R^\eta{}_{\sigma\mu\nu}(x,u) T^{\alpha\beta\ldots\gamma}_{\rho\eta\ldots\lambda}(x,u) + \ldots +$$
$$+ R^\eta{}_{\lambda\mu\nu}(x,u) T^{\alpha\beta\ldots\gamma}_{\rho\sigma\ldots\eta}(x,u) -$$
$$- R^\alpha{}_{\eta\mu\nu}(x,u) T^{\eta\beta\ldots\gamma}_{\rho\sigma\ldots\lambda}(x,u) -$$
$$- R^\beta{}_{\eta\mu\nu}(x,u) T^{\alpha\eta\ldots\gamma}_{\rho\sigma\ldots\lambda}(x,u) -$$
$$- \ldots - R^\gamma{}_{\eta\mu\nu}(x,u) T^{\alpha\beta\ldots\eta}_{\rho\sigma\ldots\lambda}(x,u) -$$
$$- 2\,\Gamma^\eta_{[\mu\nu]}(x,u) \nabla_\eta T^{\alpha\beta\ldots\gamma}_{\rho\sigma\ldots\lambda}(x,u).$$

Here the world-curvature tensor, that is, the generalized, Eulerian Riemann tensor, is given by

$$R^\alpha{}_{\beta\rho\sigma}(x,u) = \frac{\partial}{\partial x^\rho}\Gamma^\alpha_{\beta\sigma}(x,u) - \frac{\partial}{\partial x^\sigma}\Gamma^\alpha_{\beta\rho}(x,u) +$$
$$+ \Gamma^\lambda_{\beta\sigma}(x,u)\Gamma^\alpha_{\lambda\rho}(x,u) - \Gamma^\lambda_{\beta\rho}(x,u)\Gamma^\alpha_{\lambda\sigma}(x,u)$$

for which the corresponding curvature form of mobility may simply be given by

$$\tilde{R}^\alpha{}_{\beta\rho\sigma}(x,u) = \frac{\partial}{\partial x^\rho}\Gamma^\alpha_{\beta\sigma}(x,u) + \frac{\partial}{\partial u^\lambda}\left(\Gamma^\alpha_{\beta\sigma}(x,u)\right)\frac{\partial u^\lambda}{\partial x^\rho} -$$
$$- \frac{\partial}{\partial x^\sigma}\Gamma^\alpha_{\beta\rho}(x,u) - \frac{\partial}{\partial u^\lambda}\left(\Gamma^\alpha_{\beta\rho}(x,u)\right)\frac{\partial u^\lambda}{\partial x^\sigma} +$$
$$+ \Gamma^\lambda_{\beta\sigma}(x,u)\Gamma^\alpha_{\lambda\rho}(x,u) - \Gamma^\lambda_{\beta\rho}(x,u)\Gamma^\alpha_{\lambda\sigma}(x,u).$$

We can now write the following fundamental decomposition:

$$R^\alpha{}_{\beta\rho\sigma}(x,u) = B^\alpha{}_{\beta\rho\sigma}(x,u) + M^\alpha{}_{\beta\rho\sigma}(x,u) +$$
$$+ N^\alpha{}_{\beta\rho\sigma}(x,u) + U^\alpha{}_{\beta\rho\sigma}(x,u),$$
$$B^\alpha{}_{\beta\rho\sigma}(x,u) = \frac{\partial}{\partial x^\rho}\Delta^\alpha_{\beta\sigma}(x,u) - \frac{\partial}{\partial x^\sigma}\Delta^\alpha_{\beta\rho}(x,u) +$$
$$+ \Delta^\lambda_{\beta\sigma}(x,u)\Delta^\alpha_{\lambda\rho}(x,u) - \Delta^\lambda_{\beta\rho}(x,u)\Delta^\alpha_{\lambda\sigma}(x,u),$$
$$M^\alpha{}_{\beta\rho\sigma}(x,u) = \overset{\smile}{\nabla}_\rho K^\alpha_{\beta\sigma}(x,u) - \overset{\smile}{\nabla}_\sigma K^\alpha_{\beta\rho}(x,u) +$$
$$+ K^\lambda_{\beta\sigma}(x,u)K^\alpha_{\lambda\rho}(x,u) - K^\lambda_{\beta\rho}(x,u)K^\alpha_{\lambda\sigma}(x,u),$$
$$N^\alpha{}_{\beta\rho\sigma}(x,u) = \overset{\smile}{\nabla}_\rho Q^\alpha_{\beta\sigma}(x,u) - \overset{\smile}{\nabla}_\sigma Q^\alpha_{\beta\rho}(x,u) +$$
$$+ Q^\lambda_{\beta\sigma}(x,u)Q^\alpha_{\lambda\rho}(x,u) - Q^\lambda_{\beta\rho}(x,u)Q^\alpha_{\lambda\sigma}(x,u),$$
$$U^\alpha{}_{\beta\rho\sigma}(x,u) = K^\lambda_{\beta\sigma}(x,u)Q^\alpha_{\lambda\rho}(x,u) - K^\lambda_{\beta\rho}(x,u)Q^\alpha_{\lambda\sigma}(x,u) +$$
$$+ Q^\lambda_{\beta\sigma}(x,u)K^\alpha_{\lambda\rho}(x,u) - Q^\lambda_{\beta\rho}(x,u)K^\alpha_{\lambda\sigma}(x,u),$$

where the Eulerian Levi-Civita connection, the Eulerian contorsion tensor, and the connection of non-metricity are respectively given by

$$\Delta^\lambda_{\alpha\beta}(x,u) = \frac{1}{2}g^{\lambda\sigma}(x,u)\left(\frac{\partial}{\partial x^\beta}g_{\sigma\alpha}(x,u) - \frac{\partial}{\partial x^\sigma}g_{\alpha\beta}(x,u) +\right.$$
$$\left. + \frac{\partial}{\partial x^\alpha}g_{\beta\sigma}(x,u)\right),$$
$$K^\lambda_{\alpha\beta}(x,u) = \Gamma^\lambda_{[\alpha\beta]}(x,u) -$$
$$- g^{\lambda\sigma}(x,u)\left(g_{\alpha\rho}(x,u)\,\Gamma^\rho_{[\sigma\beta]}(x,u) + g_{\beta\rho}(x,u)\,\Gamma^\rho_{[\sigma\alpha]}(x,u)\right),$$
$$Q^\lambda_{\alpha\beta}(x,u) = \frac{1}{2}g^{\lambda\sigma}(x,u)\left(\nabla_\beta g_{\sigma\alpha}(x,u) - \nabla_\sigma g_{\alpha\beta}(x,u) +\right.$$
$$\left. + \nabla_\alpha g_{\beta\sigma}(x,u)\right),$$

such that $\overset{\smile}{\nabla}$ represents covariant differentiation with respect to the symmetric connection $\Delta(x,u)$ alone. The curvature tensor given by $B(x,u)$ is, of course, the Eulerian Riemann-Christoffel tensor, generalizing the one of the General Theory of Relativity which depends on position alone.

Of special interest, for the world-metric tensor, we note that

$$(\nabla_\sigma \nabla_\rho - \nabla_\rho \nabla_\sigma) g_{\alpha\beta}(x,u) = R_{\alpha\beta\rho\sigma}(x,u) + R_{\beta\alpha\rho\sigma}(x,u) -$$
$$- 2\,\Gamma^\lambda_{[\rho\sigma]}(x,u)\nabla_\lambda g_{\alpha\beta}(x,u)$$

where, with the usual notation, $R_{\alpha\beta\rho\sigma}(x,u) = g_{\alpha\lambda}(x,u)R^\lambda{}_{\beta\rho\sigma}(x,u)$. That is, more specifically, while keeping in mind that

$$\Phi_{\alpha\beta\lambda} = \frac{\partial}{\partial u^\lambda}g_{\alpha\beta}(x,u) = \psi_\alpha \psi_\beta \psi_\lambda,$$

we have

$$(\nabla_\sigma \nabla_\rho - \nabla_\rho \nabla_\sigma) g_{\alpha\beta}(x,u) = R_{\alpha\beta\rho\sigma}(x,u) +$$
$$+ R_{\beta\alpha\rho\sigma}(x,u) - 2\,\Gamma^\lambda_{[\rho\sigma]}(x,u)\Phi_{\alpha\beta\gamma}\nabla_\lambda u^\gamma.$$

As such, we have a genuine homothetic curvature given by

$$H_{\alpha\beta}(x,u) = R^\lambda{}_{\lambda\alpha\beta}(x,u) =$$
$$= \overset{\smile}{\nabla}_\alpha Q_\beta(x,u) - \overset{\smile}{\nabla}_\beta Q_\alpha(x,u) =$$
$$= \frac{\partial}{\partial x^\alpha}Q_\beta(x,u) - \frac{\partial}{\partial x^\beta}Q_\alpha(x,u),$$
$$Q_\alpha(x,u) = Q^\lambda_{\lambda\alpha}(x,u) = \frac{1}{2}g^{\lambda\beta}(x,u)\nabla_\alpha g_{\lambda\beta}(x,u) =$$
$$= \psi^2 \psi_\beta \nabla_\alpha u^\beta.$$

Upon setting

$$\theta_\alpha(x,u) = \frac{1}{2}\psi_\beta \nabla_\alpha u^\beta,$$

we have

$$H_{\alpha\beta}(x,u) = \psi^2\left(\frac{\partial}{\partial x^\alpha}\theta_\beta(x,u) - \frac{\partial}{\partial x^\beta}\theta_\alpha(x,u) -\right.$$
$$\left. - 2\left(\theta_\alpha(x,u)\frac{\partial \ln\psi}{\partial x^\beta} - \theta_\beta(x,u)\frac{\partial \ln\psi}{\partial x^\alpha}\right)\right).$$

At this point, the generalized, Eulerian Ricci tensor is given in the form

$$R_{\alpha\beta}(x,u) = R^{\lambda}{}_{\alpha\lambda\beta}(x,u) = Z_{\alpha\beta}(\Delta(x,u), K(x,u)) +$$
$$+ N_{\alpha\beta}(Q(x,u)) + X_{\alpha\beta}(K(x,u), Q(x,u)),$$
$$Z_{\alpha\beta}(\Delta(x,u), K(x,u)) = B^{\lambda}{}_{\alpha\lambda\beta}(x,u) + M^{\lambda}{}_{\alpha\lambda\beta}(x,u),$$
$$N_{\alpha\beta}(Q(x,u)) = N^{\lambda}_{\alpha\lambda\beta}(x,u),$$
$$X_{\alpha\beta}(K(x,u), Q(x,u)) = U^{\lambda}{}_{\alpha\lambda\beta}(x,u),$$

which admits the peculiar anti-symmetric part

$$R_{[\alpha\beta]}(x,u) = \frac{1}{2}\left(\frac{\partial}{\partial x^{\alpha}} K^{\lambda}_{\beta\lambda}(x,u) - \frac{\partial}{\partial x^{\beta}} K^{\lambda}_{\alpha\lambda}(x,u)\right) +$$
$$+ \frac{1}{2}\left(\frac{\partial}{\partial x^{\alpha}} Q_{\beta}(x,u) - \frac{\partial}{\partial x^{\beta}} Q_{\alpha}(x,u)\right) +$$
$$+ \breve{\nabla}_{\lambda}\Gamma^{\lambda}_{[\alpha\beta]}(x,u) +$$
$$+ \Gamma^{\lambda}_{[\alpha\beta]}(x,u) K^{\sigma}_{\lambda\sigma}(x,u) + \Gamma^{\lambda}_{[\alpha\beta]}(x,u) Q_{\lambda}(x,u) +$$
$$+ \Gamma^{\lambda}_{[\beta\sigma]}(x,u) Q^{\sigma}_{\alpha\lambda}(x,u) - \Gamma^{\lambda}_{[\alpha\sigma]}(x,u) Q^{\sigma}_{\beta\lambda}(x,u) +$$
$$+ \frac{1}{2}\left(K^{\lambda}_{\alpha\sigma}(x,u) K^{\sigma}_{\lambda\beta}(x,u) - K^{\lambda}_{\beta\sigma}(x,u) K^{\sigma}_{\lambda\alpha}(x,u)\right),$$

where we have made use of the fact that $K^{\lambda}_{[\alpha\beta]}(x,u) = \Gamma^{\lambda}_{[\alpha\beta]}(x,u)$. Let us also keep in mind that the explicit physical structure of the connection form forming our various curvature expressions, as it relates to gravity, electromagnetism, material spin, and the nuclear interaction, is given in Section 3 of this work, naturally following [4].

We can now obtain the complete Eulerian generalization of the first Bianchi identity as follows:

$$R_{\alpha\beta\rho\sigma}(x,u) + R_{\alpha\rho\sigma\beta}(x,u) + R_{\alpha\sigma\beta\rho}(x,u) =$$
$$= -2\, g_{\alpha\lambda}(x,u)\left(\frac{\partial}{\partial x^{\sigma}}\Gamma^{\lambda}_{[\beta\rho]}(x,u) + \frac{\partial}{\partial x^{\beta}}\Gamma^{\lambda}_{[\rho\sigma]}(x,u) +\right.$$
$$\left. + \frac{\partial}{\partial x^{\rho}}\Gamma^{\lambda}_{[\sigma\beta]}(x,u)\right) -$$
$$- 2\, g_{\alpha\lambda}(x,u)\left(\Gamma^{\lambda}_{\gamma\beta}(x,u)\Gamma^{\gamma}_{[\rho\sigma]}(x,u) +\right.$$
$$\left. + \Gamma^{\lambda}_{\gamma\rho}(x,u)\Gamma^{\gamma}_{[\sigma\beta]}(x,u) + \Gamma^{\lambda}_{\gamma\sigma}(x,u)\Gamma^{\gamma}_{[\beta\rho]}(x,u)\right) +$$
$$+ 2\,\Phi_{\alpha\lambda\gamma}\left(\Gamma^{\lambda}_{[\rho\sigma]}(x,u)\nabla_{\beta}u^{\gamma} + \Gamma^{\lambda}_{[\sigma\beta]}(x,u)\nabla_{\rho}u^{\gamma} +\right.$$
$$\left. + \Gamma^{\lambda}_{[\beta\rho]}(x,u)\nabla_{\sigma}u^{\gamma}\right).$$

Similarly, after a somewhat lengthy calculation, we obtain, for the generalization of the second Bianchi identity,

$$\nabla_{\lambda} R_{\alpha\beta\rho\sigma}(x,u) + \nabla_{\rho} R_{\alpha\beta\sigma\lambda}(x,u) + \nabla_{\sigma} R_{\alpha\beta\lambda\rho}(x,u) =$$
$$= 2\left(\Gamma^{\gamma}_{[\rho\sigma]}(x,u) R_{\alpha\beta\gamma\lambda}(x,u) + \Gamma^{\gamma}_{[\sigma\lambda]}(x,u) R_{\alpha\beta\gamma\rho}(x,u) +\right.$$
$$\left. + \Gamma^{\gamma}_{[\lambda\rho]}(x,u) R_{\alpha\beta\gamma\sigma}(x,u)\right) +$$
$$+ \Gamma^{\gamma}_{\beta\rho}(x,u)\left(\left(\nabla_{\lambda}\Phi_{\alpha\gamma\eta}\right)\nabla_{\sigma}u^{\eta} - \left(\nabla_{\sigma}\Phi_{\alpha\gamma\eta}\right)\nabla_{\lambda}u^{\eta}\right) +$$
$$+ \Gamma^{\gamma}_{\beta\sigma}(x,u)\left(\left(\nabla_{\rho}\Phi_{\alpha\gamma\eta}\right)\nabla_{\lambda}u^{\eta} - \left(\nabla_{\lambda}\Phi_{\alpha\gamma\eta}\right)\nabla_{\rho}u^{\eta}\right) +$$
$$+ \Gamma^{\gamma}_{\beta\lambda}(x,u)\left(\left(\nabla_{\sigma}\Phi_{\alpha\gamma\eta}\right)\nabla_{\rho}u^{\eta} - \left(\nabla_{\rho}\Phi_{\alpha\gamma\eta}\right)\nabla_{\sigma}u^{\eta}\right) -$$
$$- \Gamma^{\gamma}_{\beta\rho}(x,u)\Phi_{\alpha\gamma\eta}\left(R^{\eta}{}_{\mu\sigma\lambda}(x,u)u^{\mu} + 2\Gamma^{\mu}_{[\sigma\lambda]}(x,u)\nabla_{\mu}u^{\eta}\right) -$$
$$- \Gamma^{\gamma}_{\beta\sigma}(x,u)\Phi_{\alpha\gamma\eta}\left(R^{\eta}{}_{\mu\lambda\rho}(x,u)u^{\mu} + 2\Gamma^{\mu}_{[\lambda\rho]}(x,u)\nabla_{\mu}u^{\eta}\right) -$$
$$- \Gamma^{\gamma}_{\beta\lambda}(x,u)\Phi_{\alpha\gamma\eta}\left(R^{\eta}{}_{\mu\rho\sigma}(x,u)u^{\mu} + 2\Gamma^{\mu}_{[\rho\sigma]}(x,u)\nabla_{\mu}u^{\eta}\right) +$$
$$+ \Phi_{\alpha\gamma\eta}\left(\nabla_{\rho}u^{\eta}\right)\left(\nabla_{\sigma}\Gamma^{\gamma}_{\beta\lambda}(x,u) - \nabla_{\lambda}\Gamma^{\gamma}_{\beta\sigma}(x,u)\right) +$$
$$+ \Phi_{\alpha\gamma\eta}\left(\nabla_{\sigma}u^{\eta}\right)\left(\nabla_{\lambda}\Gamma^{\gamma}_{\beta\rho}(x,u) - \nabla_{\rho}\Gamma^{\gamma}_{\beta\lambda}(x,u)\right) +$$
$$+ \Phi_{\alpha\gamma\eta}\left(\nabla_{\lambda}u^{\eta}\right)\left(\nabla_{\rho}\Gamma^{\gamma}_{\beta\sigma}(x,u) - \nabla_{\sigma}\Gamma^{\gamma}_{\beta\rho}(x,u)\right),$$

where

$$\nabla_{\sigma}\Gamma^{\lambda}_{\alpha\beta}(x,u) - \nabla_{\beta}\Gamma^{\lambda}_{\alpha\sigma}(x,u) = -R^{\lambda}{}_{\alpha\beta\sigma}(x,u) +$$
$$+ \Gamma^{\rho}_{\alpha\beta}(x,u)\Gamma^{\lambda}_{\rho\sigma}(x,u) - \Gamma^{\rho}_{\alpha\sigma}(x,u)\Gamma^{\lambda}_{\rho\beta}(x,u) -$$
$$- 2\,\Gamma^{\rho}_{[\beta\sigma]}(x,u)\Gamma^{\lambda}_{\alpha\rho}(x,u).$$

By contraction, we may extract a physical density field as follows:

$$J_{\alpha}(x,u) =$$
$$= -\nabla_{\beta}\left(\frac{1}{2}\left(R^{\beta}{}_{\alpha}(x,u) + {}^{*}R^{\beta}{}_{\alpha}(x,u)\right) - \frac{1}{2}\delta^{\beta}_{\alpha} R(x,u)\right),$$

where ${}^{*}R^{\alpha}{}_{\beta}(x,u) = R^{\alpha\lambda}_{\beta\lambda}(x,u)$ are the components of the generalized Ricci tensor of the second kind and $R(x,u) = R^{\lambda}{}_{\lambda}(x,u) = {}^{*}R^{\lambda}{}_{\lambda}(x,u)$ is the generalized Ricci scalar. As we know, the Ricci tensor of the first kind and the Ricci tensor of the second kind coincide only when the connection form is metric-compatible. The asymmetric, generally non-conservative world-entity given by

$$G^{\alpha}{}_{\beta}(x,u) = \frac{1}{2}\left(R^{\alpha}{}_{\beta}(x,u) + {}^{*}R^{\alpha}{}_{\beta}(x,u)\right) - \frac{1}{2}\delta^{\alpha}_{\beta} R(x,u)$$

will therefore represent the generalized Einstein tensor, such that we may have a corresponding geometric object given by

$$C^{\alpha}(x,u) \equiv -g^{\alpha\beta}(x,u) J_{\beta}(x,u) =$$
$$= \nabla_{\beta} G^{\beta\alpha}(x,u) - G^{\beta}{}_{\lambda}(x,u)\nabla_{\beta} g^{\lambda\alpha}(x,u).$$

6 Quantum gravity from the physical vacuum of $\mathbf{U_4}$

We are now in a position to derive a quantum mechanical wave equation from the underlying structure of our present theory. So far, our field equations appear too complicated to handle for this particular purpose. It is quite enough that

we know the structural content of the connection form, which encompasses the geometrization of the known classical fields. However, if we deal with a particular case, namely, that of physical vacuum, we shall immediately be able to speak of one type of emergent quantum gravity.

Assuming now that the world-geometry U_4 is devoid of "ultimate physical substance" (that is, intrinsic material confinement on the most fundamental scale) other than, perhaps, primordial radiation, the field equation shall be given by

$$R_{\alpha\beta}(x,u) = 0$$

for which, in general, $R^{\alpha}_{\beta\mu\nu}(x,u) = W^{\alpha}_{\beta\mu\nu}(x,u) \neq 0$, where $W(x,u)$ is the generalized Weyl conformal tensor. In this way, all physical fields, including matter, are mere appearances in our geometric world-structure. Consequently, from $R_{(\alpha\beta)}(x,u) = 0$, the emergent picture of gravity is readily given by the symmetric Eulerian Ricci tensor for the composite structure of gravity, that is, explicitly,

$$B_{\alpha\beta}(\Delta(x,u)) = -\Big(M_{\alpha\beta}\big(K(x,u)\big) + N_{\alpha\beta}\big(Q(\psi)\big) + U_{\alpha\beta}\big(K(x,u), Q(\psi)\big)\Big),$$

where we have written $Q(x,u) = Q(\psi)$, such that, in this special consideration, gravity can essentially be thought of as exterior electromagnetism as well as arising from the quantum fuzziness of the background non-metricity of the world-geometry. In addition, from $R_{[\alpha\beta]}(x,u) = 0$, we also have the following anti-symmetric counterpart:

$$R_{[\alpha\beta]}(\Delta(x,u), K(x,u)) = \frac{\partial}{\partial x^{\beta}} Q_{\alpha}(\psi) - \frac{\partial}{\partial x^{\alpha}} Q_{\beta}(\psi) - \Gamma^{\lambda}_{[\alpha\beta]}(x,u) Q_{\lambda}(\psi) + \Gamma^{\lambda}_{[\alpha\sigma]}(x,u) Q^{\sigma}_{\beta\lambda}(\psi) - \Gamma^{\lambda}_{[\beta\sigma]}(x,u) Q^{\sigma}_{\alpha\lambda}(\psi),$$

$$Q_{\alpha}(\psi) = \frac{1}{2}\psi^2 \psi_{\beta} \nabla_{\alpha} u^{\beta}.$$

Correspondingly, we shall set, for the "quantum potential",

$$Q_{\alpha}(\psi) = \frac{\partial}{\partial x^{\alpha}} \ln \bar{\psi}$$

such that the free, geodesic motion of a particle along the fuzzy world-path $s(x,u) = \tau\left(\psi\left(\bar{\psi}\right)\right)$ in the empty U_4 can simultaneously be described by the pair of dynamical equations

$$\frac{Du^{\alpha}}{Ds} = 0,$$
$$\frac{D\bar{\psi}}{Ds} = 0,$$

since, as we have previously seen, $Q_{\alpha}\left(\psi\left(\bar{\psi}\right)\right) u^{\alpha} = 0$.

Immediately, we obtain the geometrically non-linear wave equation

$$\frac{1}{\sqrt{\det(g(x,u))}} \frac{\partial}{\partial x^{\alpha}} \left(g^{\alpha\beta}(x,u) \sqrt{\det(g(x,u))} \frac{\partial \bar{\psi}}{\partial x^{\beta}} \right) = \left(R(\Delta(x,u), K(x,u)) + \Lambda(Q(\psi))\right) \bar{\psi}$$

that is,

$$\left(\Delta^2_B - \widehat{R}(x,u)\right) \bar{\psi} = 0,$$

where

$$\Delta^2_B = \frac{1}{\sqrt{\det(g(x,u))}} \frac{\partial}{\partial x^{\alpha}} \left(g^{\alpha\beta}(x,u) \sqrt{\det(g(x,u))} \frac{\partial}{\partial x^{\beta}} \right)$$

is the covariant four-dimensional Beltrami wave operator and, with the explicit dependence of ψ on $\bar{\psi}$,

$$\widehat{R}(x,u) = R(\Delta(x,u), K(x,u)) + \Lambda\left(Q\left(\psi\left(\bar{\psi}\right)\right)\right)$$

is the emergent curvature scalar of our quantum field, for which

$$\Lambda(Q(\psi)) = \widehat{N}\left(Q\left(\psi\left(\bar{\psi}\right)\right)\right) - \frac{1}{\bar{\psi}^2} g^{\alpha\beta}(x,u) \frac{\partial \bar{\psi}}{\partial x^{\alpha}} \frac{\partial \bar{\psi}}{\partial x^{\beta}},$$

$$\widehat{N}\left(Q\left(\psi\left(\bar{\psi}\right)\right)\right) = N\left(Q\left(\psi\left(\bar{\psi}\right)\right)\right) + U\left(K(x,u), Q\left(\psi\left(\bar{\psi}\right)\right)\right) - g^{\alpha\beta}(x,u) \breve{\nabla}_{\beta} Q_{\alpha}\left(\psi\left(\bar{\psi}\right)\right).$$

In terms of the Eulerian Ricci scalar, which is now quantized by the wave equation, we have a quantum gravitational wave equation with two quantized intrinsic sources, namely, the torsional source $M(x,u)$, which combines the electromagnetic and material sources, and the quantum mechanical source $\Lambda\left(Q\left(\psi\left(\bar{\psi}\right)\right)\right) = \Lambda(Q(x,u))$,

$$\left(\Delta^2_B - B(x,u)\right) \bar{\psi} = M(x,u) \bar{\psi} + \Lambda\left(Q\left(\psi\left(\bar{\psi}\right)\right)\right) \bar{\psi}$$

thereby completing the quantum gravitational picture at an elementary stage.

7 Special analytic form of geodesic paths

Here we are interested in the derivation of the generalized geodesic equation of motion such that our geodesic paths correspond to the formal solution of the quantum gravitational wave equation in the preceding section. Indeed, owing to the wave function $\bar{\psi} = \bar{\psi}(x,u)$, these geodesic paths shall be conformal ones.

For our purpose, let $\Psi(x) = const.$ represent a family of hypersurfaces in U_4 such that with respect to a mobile hypersurface Σ, for $\frac{\partial}{\partial x^{\alpha}}(\Psi(x)) \delta x^{\alpha} = 0$, there exists a genuine unit normal velocity vector, given by $n^{\alpha} = \frac{dx^{\alpha}}{d\tau}$, at some point whose extended path can be parametrized by $\tau = \tau(s)$, that is

$$n_{\alpha} = \zeta\left(x, \frac{\partial}{\partial x}\Psi(x)\right) \frac{\partial}{\partial x^{\alpha}} \Psi(x)$$

$$g_{\alpha\beta}(x,u)\, n^{\alpha} \delta n^{\beta} = 0.$$

The essential partial differential equation representing any quantum gravitational hypersurface Σ_{ψ} can then

simply be represented by the arbitrary parametric form $\zeta\left(x, \frac{\partial}{\partial x}\,\Psi(x)\right) = \zeta\left(\bar{\psi}\right) = const$ such that

$$\int_a^b \left(\phi(x,u) - \zeta\left(\bar{\psi}\right)\frac{d}{d\tau}\,\Psi(x)\right) d\tau \geqslant 0$$

where a and b are two points in Σ_ψ.

Keeping in mind once again that $\psi_\alpha\, u^\alpha = 0$ and that

$$u_\alpha = \frac{1}{2}\frac{\partial}{\partial u^\alpha}\,\phi^2(x,u)$$

$$\frac{\partial}{\partial x^\lambda}\,g_{\alpha\beta}(x,u) =$$

$$= \Gamma_{\alpha\beta\lambda}(x,u) + \Gamma_{\beta\alpha\lambda}(x,u) + \psi_\alpha\,\psi_\beta\,\psi_\sigma\,\nabla_\lambda u^\sigma$$

the generalized Euler-Lagrange equation corresponding to our situation shall then be given by

$$\frac{d}{ds}\left(\frac{\partial}{\partial u^\alpha}\,\phi^2(x,u)\right) - \frac{\partial}{\partial x^\alpha}\,\phi^2(x,u) +$$

$$+ \frac{\partial}{\partial u^\beta}\left(\phi^2(x,u)\right)\frac{\partial u^\beta}{\partial x^\alpha} + b_\alpha(x,u) = 0\,,$$

where the "external" term is given by

$$b_\alpha(x,u) = 4\,\Gamma^\lambda_{[\alpha\beta]}(x,u)\,u_\lambda\,u^\beta.$$

As a matter of straightforward verification, we have

$$\frac{du_\alpha}{ds} - \Gamma_{\beta\alpha\lambda}(x,u)\,u^\beta\,u^\lambda = 0$$

A unique general solution to the above equation corresponding to the quantum displacement field $\psi = \psi\left(\bar{\psi}\right)$, which, in our theory, generates the non-metric nature of the world-manifold U_4, can now be obtained as

$$s(x,u) = s\left(\psi\left(\bar{\psi}\right)\right) = C_1 + C_2\int \exp\left(\int H\left(\psi\left(\bar{\psi}\right)ds\right)\right)ds$$

where C_1 and C_2 are integration constants. This is such that, at arbitrary world-points a and b, we have the conformal relation (for $C = C_2$)

$$ds_b = \exp\left(C\int H\left(\psi\left(\bar{\psi}\right)\right)ds\right)\,ds_a\,,$$

which sublimely corresponds to the case of our previous quantum theory of gravity [3].

8 Geometric structure of the electromagnetic potential

As another special consideration, let us now attempt to extensively describe the geometric structure of the electromagnetic potential in our theory.

Due to the degree of complicatedness of the detailed general coordinate transformations in U_4, let us, for the sake of tangibility, refer a smoothly extensive coordinate patch $P(x)$ to the four-dimensional tangent hyperplane $M_4(y)$, whose metric tensor η is Minkowskian, such that an ensemble of Minkowskian tangent hyperplanes, that is,

$$\sum\nolimits_{a\,=\,1,2,\ldots,N} M_4^{(a)}(y)$$

cannot globally cover the curved manifold U_4 without breaking analytic continuity (smoothness), at least up to the third order. Denoting the "invariant derivative" by $\nabla_A = E^\alpha_A(x,u)\,\frac{\partial}{\partial x^\alpha}$, this situation can then basically be described by

$$g_{\alpha\beta}(x,u) = E^A_\alpha(x,u)\,E^B_\beta(x,u)\,\eta_{AB}\,,$$

$$E^A_\alpha(x,u) = \frac{\partial y^A}{\partial x^\alpha}, E^\alpha_A(x,u) = \left(E^A_\alpha(x,u)\right)^{-1},$$

$$y^A = y^A(x,u)\,, x^\alpha = x^\alpha(y)\,,$$

$$E^A_\alpha(x,u)\,E^\beta_A(x,u) = \delta^\beta_\alpha, E^\alpha_A(x,u)\,E^B_\alpha(x,u) = \delta^B_A\,,$$

$$\Gamma^\lambda_{\alpha\beta}(x,u) = E^\lambda_A(x,u)\,\frac{\partial}{\partial x^\beta}E^A_\alpha(x,u) =$$

$$= E^\lambda_A(x,u)\,E^B_\beta(x,u)\,\nabla_B E^A_\alpha(x,u)\,.$$

Of fundamental importance in our unified field theory are, of course, the torsion tensor given by

$$\Gamma^\lambda_{[\alpha\beta]}(x,u) = \frac{1}{2}\,E^\lambda_A(x,u)\left(\frac{\partial}{\partial x^\beta}\,E^A_\alpha(x,u) - \frac{\partial}{\partial x^\alpha}\,E^A_\beta(x,u)\right)$$

and the curvature tensor given by

$$R^\lambda{}_{\sigma\alpha\beta}(x,u) =$$

$$= -E^\lambda_A(x,u)\left(\left(\frac{\partial}{\partial x^\beta}\frac{\partial}{\partial x^\alpha} - \frac{\partial}{\partial x^\alpha}\frac{\partial}{\partial x^\beta}\right)E^A_\sigma(x,u)\right) =$$

$$= E^A_\sigma(x,u)\left(\left(\frac{\partial}{\partial x^\beta}\frac{\partial}{\partial x^\alpha} - \frac{\partial}{\partial x^\alpha}\frac{\partial}{\partial x^\beta}\right)E^\lambda_A(x,u)\right).$$

Additionally, we can also see that

$$R_{\rho\sigma\alpha\beta}(x,u) =$$

$$= E^A_\sigma(x,u)\left(\left(\frac{\partial}{\partial x^\beta}\frac{\partial}{\partial x^\alpha} - \frac{\partial}{\partial x^\alpha}\frac{\partial}{\partial x^\beta}\right)E_{A\rho}(x,u)\right) +$$

$$+ \left(\frac{\partial}{\partial x^\beta}\frac{\partial}{\partial x^\alpha} - \frac{\partial}{\partial x^\alpha}\frac{\partial}{\partial x^\beta}\right)g_{\rho\sigma}(x,u)\,.$$

Immediately, we obtain

$$R^\lambda{}_{\sigma\alpha\beta}(x,u) = E^\lambda_A(x,u)\,E^B_\alpha(x,u)\,E^C_\beta(x,u)\,\times$$

$$\times\left(\left(\nabla_B\nabla_C - \nabla_C\nabla_B\right)E^A_\sigma(x,u)\right) - 2\,\Gamma^\lambda_{\sigma\rho}(x,u)\,\Gamma^\rho_{[\alpha\beta]}(x,u)\,.$$

Introducing a corresponding internal ("isotopic") curvature form through

$$\bar{R}^\alpha{}_{\beta AB}(x,u) = E^\alpha_C(x,u)\left(\left(\nabla_A\nabla_B - \nabla_B\nabla_A\right)E^C_\beta(x,u)\right),$$

we can write

$$R^{\lambda}{}_{\sigma\alpha\beta}(x,u) = E^{A}_{\alpha}(x,u)\, E^{B}_{\beta}(x,u)\, \bar{R}^{\lambda}{}_{\sigma AB}(x,u) -$$
$$- 2\,\Gamma^{\lambda}_{\sigma\rho}(x,u)\,\Gamma^{\rho}_{[\alpha\beta]}(x,u)\ .$$

In physical terms, we therefore see that

$$R^{\lambda}{}_{\sigma\alpha\beta}(x,u) = E^{A}_{\alpha}(x,u)\, E^{B}_{\beta}(x,u)\, \bar{R}^{\lambda}{}_{\sigma AB}(x,u) -$$
$$- 2\,\Gamma^{\lambda}_{\sigma\rho}(x,u)\, S^{\rho}_{\alpha\beta} - \frac{e}{mc^2}\,\phi^2(x,u)\,\Gamma^{\lambda}_{\sigma\rho}(x,u)\, F_{\alpha\beta}\, u^{\rho}\ ,$$

where the electromagnetic field tensor can now be expressed by the extended form (given in Section 3)

$$\tilde{F}_{\alpha\beta}(x,u) = 2\,\frac{mc^2}{e}\,\phi^2(x,u)\ \Gamma^{\lambda}_{[\alpha\beta]}(x,u)\, u_{\lambda}\ ,$$

that is,

$$\tilde{F}_{\alpha\beta}(x,u) = \frac{mc^2}{e}\,\phi^2(x,u)\left(\frac{\partial\, u_{\alpha}}{\partial\, x^{\beta}} - \frac{\partial\, u_{\beta}}{\partial\, x^{\alpha}} -\right.$$
$$\left. -\ E^{A}_{\alpha}(x,u)\, E^{B}_{\beta}(x,u)\,(\nabla_B\, u_A - \nabla_B\, u_A)\right).$$

An essential feature of the electromagnetic field in our unified field theory therefore manifests as a field of vorticity, somewhat reminiscent of the case of fluid dynamics, that is,

$$\tilde{F}_{\alpha\beta}(x,u) =$$
$$= 2\,\frac{mc^2}{e}\,\phi^2(x,u)\left(\omega_{\alpha\beta} - E^{A}_{\alpha}(x,u)\, E^{B}_{\beta}(x,u)\,\Theta_{AB}\right),$$

where the vorticity field is given in two referential forms by

$$\omega_{\alpha\beta} = \frac{1}{2}\left(\frac{\partial\, u_{\alpha}}{\partial\, x^{\beta}} - \frac{\partial\, u_{\beta}}{\partial\, x^{\alpha}}\right),$$

$$\Theta_{AB} = \frac{1}{2}\left(\nabla_B\, u_A - \nabla_A\, u_B\right).$$

For our regular Eulerian electromagnetic field, we simply have

$$F_{\alpha\beta} = F_{\alpha\beta}(x,u) = 2\,\frac{mc^2}{e}\left(\omega_{\alpha\beta} - E^{A}_{\alpha}(x,u)\, E^{B}_{\beta}(x,u)\,\Theta_{AB}\right).$$

After some algebraic (structural) factorization, a profound physical solution to our most general Eulerian expression for the electromagnetic field can be obtained in integral form as

$$\varphi_{\alpha}(x,u) = \frac{mc^2}{e}\oint_{C}\phi^2(x,u)\left(\frac{\partial}{\partial\, x^{\beta}}\, E^{A}_{\alpha}(x,u)\right) u_A\, dx^{\beta}$$

such that $\tilde{F}_{\alpha\beta}(x,u) = \frac{\partial}{\partial\, x^{\beta}}\,\varphi_{\alpha}(x,u) - \frac{\partial}{\partial\, x^{\alpha}}\,\varphi_{\beta}(x,u)$, that is, in order to preserve the customary gauge invariance, our electromagnetic field shall manifestly be a "pure curl". This structural form is, of course, given in the domain of a vortical path C covered by a quasi-regular surface spanned in two directions and essentially given by the form $d\,\sigma^{AB} = d_1\, y^{A}(x,u)\, d_2\, y^{B}(x,u) \ - \ d_1\, y^{B}(x,u)\, d_2\, y^{A}(x,u)$. Upon using Gauss theorem, we therefore see that.

$$\varphi_{\alpha}(x,u) = \frac{1}{2}\,\frac{mc^2}{e}\,\times$$
$$\times\iint_{\sigma}\phi^2(x,u)\left(\left(\nabla_B\,\nabla_A - \nabla_A\,\nabla_B\right) E^{C}_{\alpha}(x,u)\right) u_C\, d\,\sigma^{AB}.$$

In other words, we have

$$\varphi_{\alpha}(x,u) = -\frac{1}{2}\,\frac{mc^2}{e}\int\int_{\sigma}\phi^2(x,u)\,\bar{R}^{\lambda}{}_{\alpha AB}(x,u)\, u_{\lambda}\, d\,\sigma^{AB}$$

or, with $d\,\sigma^{\alpha\beta} = E^{\alpha}_{A}(x,u)\, E^{\beta}_{B}(x,u)\, d\,\sigma^{AB}$,

$$\varphi_{\alpha}(x,u) = -\frac{1}{2}\,\frac{mc^2}{e}\int\int_{\sigma}\phi^2(x,u)\,\times$$
$$\times\left(R^{\lambda}{}_{\alpha\beta\sigma}(x,u) + 2\,\Gamma^{\lambda}_{\alpha\rho}(x,u)\,\Gamma^{\rho}_{[\beta\sigma]}(x,u)\right) u_{\lambda}\, d\,\sigma^{\beta\sigma},$$

which means that

$$\varphi_{\alpha}(x,u) = -\frac{1}{2}\,\frac{mc^2}{e}\int\int_{\sigma}\phi^2(x,u)\,\times$$
$$\times\left(R^{\lambda}{}_{\alpha\beta\sigma}(x,u) + 2\,\Gamma^{\lambda}_{\alpha\rho}(x,u)\, S^{\rho}_{\beta\sigma}(x,u)\right) u_{\lambda}\, d\,\sigma^{\beta\sigma} -$$
$$-\frac{1}{2}\int\int_{\sigma}\Gamma^{\lambda}_{\alpha\rho}(x,u)\, F_{\beta\sigma}(x,u)\, u^{\rho}\, u_{\lambda}\, d\,\sigma^{\beta\sigma}.$$

Combining the above expression with the geodesic equation of motion given by $\frac{du_{\alpha}}{ds} = \Gamma^{\lambda}_{\alpha\beta}(x,u)\, u_{\lambda}\, u^{\beta}$, we finally obtain the integral equation of motion

$$\varphi_{\alpha}(x,u) = -\frac{1}{2}\,\frac{mc^2}{e}\int\int_{\sigma}\phi^2(x,u)\,\times$$
$$\times\left(R^{\lambda}{}_{\alpha\beta\sigma}(x,u) + 2\,\Gamma^{\lambda}_{\alpha\rho}(x,u)\, S^{\rho}_{\beta\sigma}(x,u)\right) u_{\lambda}\, d\,\sigma^{\beta\sigma} -$$
$$-\frac{1}{2}\int\int_{\sigma}\left(\frac{du_{\alpha}}{ds}\right) F_{\beta\sigma}(x,u)\, d\,\sigma^{\beta\sigma},$$

which shows, for the first time, the explicit dependence of the electromagnetic potential on world-velocity (as well as local acceleration), global curvature, and the material spin field.

9 Closing remarks

In the foregoing presentation, we have created a new kind of Finsler space, from which we have built the foundation of a unified field theory endowed with propagating torsion and curvature. Previously [1, 5], we have done it without the "luxury" of killing the metricity condition of Riemannian geometry; at present, the asymmetric connection form of our world-geometry, in addition to the metric and curvature, is a function of both position and world-velocity. Therefore,

looking back on our previous works, we may conclude that, in particular, the theories outlined in [3,4], as a whole, appear to be a natural bridge between generalized Riemannian and Finslerian structures.

A very general presentation of my own version of the theory of non-linear connection has also been given in [3], where, in immediate relation to [4], the enveloping evolutive world-structure can be seen as some kind of conformal Finsler space with torsion. The union between [3] and [4] has indeed already given us the essence of a fully geometric quantum theory of gravity, with electromagnetism and the Yang-Mills gauge field included. The present work mainly serves to complement and enrich this purely geometric union.

Submitted on June 27, 2009 / Accepted on August 06, 2009

References

1. Suhendro I. A four-dimensional continuum theory of space-time and the classical physical fields. *Progress in Physics*, 2007, v. 4, 34–46.
2. Suhendro I. A new semi-symmetric unified field theory of the classical fields of gravity and electromagnetism. *Progress in Physics*, 2007, v. 4, 47–62.
3. Suhendro I. A new conformal theory of semi-classical quantum general relativity. *Progress in Physics*, 2007, v. 4, 96–103.
4. Suhendro I. A unified field theory of gravity, electromagnetism, and the Yang-Mills gauge field. *Progress in Physics*, 2008, v. 1, 31–37.
5. Suhendro I. Spin-curvature and the unification of fields in a twisted space. Svenska fysikarkivet, Stockholm, 2008.
6. Borissova L. and Rabounski D. Fields, vacuum, and the mirror Universe. 2nd edition, Svenska fysikarkivet, Stockholm, 2009, p. 26–29.

Physical Consequences of Mathematical Principles

Eliahu Comay

Characteell Ltd., PO Box 39019, Tel-Aviv, 61390, Israel

E-mail: elicomay@post.tau.ac.il

Physical consequences are derived from the following mathematical structures: the variational principle, Wigner's classifications of the irreducible representations of the Poincaré group and the duality invariance of the homogeneous Maxwell equations. The analysis is carried out within the validity domain of special relativity. Hierarchical relations between physical theories are used. Some new results are pointed out together with their comparison with experimental data. It is also predicted that a genuine Higgs particle will not be detected.

1 Introduction

Physics aims to describe processes which are observed in the real world. For this purpose, mathematical formulations of physical theories are constructed. Mathematical elements of a physical theory can be divided into three sets: elements that play a relative fundamental role and are regarded as cornerstones of the theory's structure, elements used as a derivation tool and final formulas that describe the behavior of a given system. This kind of classification is used here for the convenience of the presentation. In particular, what is regarded here as a fundamental element may, in principle, be derived from more profound mathematical elements.

This work regards the following mathematical structures as cornerstones of the discussion. The variational principle and its relevant Lagrangian density; Wigner's analysis of the irreducible representations of the Poincaré group; the duality invariance of the homogeneous Maxwell equations. Some well known results of these elements are pointed out alongside others that are not very well known. Boldface numbers are used for marking the latter kind of results. It is shown that some of these results fit experimental data whereas others are used as a prediction of yet unknown experimental data.

The discussion is carried out within a framework that is based on the following theoretical elements. First, Special Relativity is regarded as a covering theory and all expressions must be consistent with relativistic covariance. The De Broglie relation between the particle's wave properties and its energy-momentum is used. Another issue is related to the hierarchical relations between physical theories. (A good discussion of this issue can be found in [1], pp. 1–6.) The following lines explain this issue in brief.

Every physical theory applies to a limited set of processes. For example, let us take the problem of moving bodies. It is well known that physical theories yield very good predictions for the motion of planets around the sun. On the other hand, nobody expects that a physical theory be able to predict the specific motion of an eagle flying in the sky. This simple example proves that the validity of a physical theory should be evaluated only with respect to a limited set of experiments. The set of experiments which can be explained by a physical theory is called its domain of validity. The relations between domains of validity define hierarchical relations between the corresponding theories. For example, given theories A, B and A's domain of validity is a subset of B's domain of validity then B's rank is higher than that of A.

An examination of Newtonian mechanics and relativistic mechanics illustrates the notion of hierarchical relations between theories. Newtonian mechanics is good for low velocity experiments (because its predictions are consistent with the error range of measurements). On the other hand, relativistic mechanics is good even for velocities that approach the speed of light. Two conclusions can be derived from these properties of the theories: First, relativistic mechanics has a more profound basis because it is valid for all experiments where Newtonian mechanics holds *and* for many other experiments where Newtonian mechanics fails. Another aspect of the relations between Newtonian mechanics and relativistic mechanics is that Newtonian mechanics imposes constraints on the form of the low velocity limit of relativistic mechanics. Indeed, the low velocity limit of relativistic mechanics is (and must be) consistent with Newtonian formulas. Below, this kind of constraint is called *constraint imposed by a lower rank theory*. Some of the theoretical derivations included below rely on this principle.

The Lorentz metric used is diagonal and its entries are $(1,-1,-1,-1)$. Greek indices run from 0 to 3. Expressions are written in units where $\hbar = c = 1$. In this system of units there is just one dimension. Here it is taken to be that of length. Therefore, the dimension of a physical quantity is a power of length and is denoted by $[L^n]$. In particular, energy and momentum take the dimension $[L^{-1}]$. The symbol $Q_{,\mu}$ denotes the partial derivative of the quantity Q with respect to x^μ. An upper dot denotes a differentiation with respect to time.

The second section discusses quantum mechanical consequences of the variational principle. The Dirac equation is examined in the third section. The fourth section shows incon-

sistencies of the Klein-Gordon (KG) and the Higgs equations. The fifth section examines results obtained from Wigner's classification of the irreducible representations of the Poincare group. Consequences of the duality invariance of the homogeneous Maxwell equations together a regular charge-monopole theory are discussed in the sixth section. The seventh section contains concluding remarks.

2 The Variational Principle

This section is dedicated to the form of a quantum theory of a *massive particle*. Let us examine the pattern obtained in a two slit interference experiment. Here one finds bright and dark strips. A completely dark interference point indicates that a full anti-phase destruction takes place there. Obviously, this property should be obtained in every Lorentz frame of reference. It follows that the phase must depend on a Lorentz scalar.

The quantity which is suitable for this purpose is the action of the system. Thus, let us examine a Lagrangian density of the system and its action

$$S = \int \mathcal{L}(\psi, \psi_{,\mu})\, d^4x^\mu . \tag{1}$$

Now, if the Lagrangian density is a Lorentz scalar then also the action is a Lorentz scalar. Therefore, it is concluded that

1. A relativistically consistent quantum theory may be derived from a Lagrangian density which is a Lorentz scalar.

Another issue is related to the dimension of the quantities. The phase is an argument of an exponent. Therefore, it must be dimensionless. Thus, in the system of units used here the action is dimensionless and satisfies this requirement. It follows that

2. An acceptable Lagrangian density must have the dimension $[L^{-4}]$.

This conclusion means that the wave function ψ acquires a well defined dimension.

Remark:

The foregoing arguments indicate that if one wishes to take an alternative way for constructing a relativistically self-consistent quantum theory, then one must find another physically meaningful quantity that is a dimensionless Lorentz scalar and is suitable for taking the role of the particle's phase. Apparently, such a quantity does not exist. If this claim is correct then the variational principle is also a necessary condition for constructing a self-consistent relativistic quantum theory.

Another point is related to the independent variables x^μ of the wave function

$$\psi(x^\mu) \tag{2}$$

which is a *single set* of four space-time coordinates. Therefore (2) cannot describe a composite particle, because such a particle requires, besides a description of the space-time location of its center of energy, additional coordinates for describing its internal structure. Therefore,

3. The wave function $\psi(x^\mu)$ describes an elementary structureless pointlike particle.

This result is consistent with the nature of an elementary classical particle (see [2], pp. 46, 47). Below it is applied as a useful criterion for evaluating experimental data.

The Lagrangian density is used here as the cornerstone of the theory. Hence, the particle's equations of motion are the corresponding Euler-Lagrange equations (see [3], p. 14; [4], p. 16)

$$\frac{\partial}{\partial x^\mu}\frac{\partial \mathcal{L}}{\partial \frac{\partial \psi}{\partial x^\mu}} - \frac{\partial \mathcal{L}}{\partial \psi} = 0 . \tag{3}$$

On this basis it is concluded that

4. The particle's equations of motion are the Euler-Lagrange equations derived from the Lagrangian density.

Obviously, different kinds of Lagrangian density yield different equations of motion. This point is discussed later.

Another issue is the consistency of a quantum theory of a massive particle with the classical theory, where the latter provides an example of constraints imposed by a lower rank theory. The classical limit of quantum mechanics is discussed in the literature (see [5], pp. 19–21 and elsewhere; [6], pp. 25–27, 137–138).

In order to do that, the quantum theory should provide expressions for the energy and the momentum of the particle. As a matter of fact, having an appropriate expression for the energy at the system's rest frame is enough. Indeed, a Lorentz boost guarantees that the theory provides appropriate expressions for the energy and momentum in any reference frame. Therefore, the following lines examine the construction of an expression for the energy of a massive quantum mechanical particle *in its rest frame*. For this end, let us take the Lagrangian density and construct the following second rank tensor (see [4], p. 19)

$$\mathcal{T}_{\mu\nu} = \frac{\partial \mathcal{L}}{\partial \frac{\partial \psi}{\partial x_\mu}}\frac{\partial \psi}{\partial x^\nu} - \mathcal{L} g_{\mu\nu} . \tag{4}$$

Now, density is a 0-component of a 4-vector and the same is true for energy. Hence, energy density is a (0,0) component of a second rank tensor. Moreover, like the dimension of the Lagrangian density, the dimension of $\mathcal{T}_{\mu\nu}$ of (4) is $[L^{-4}]$. This is also the dimension of energy density. Now, in quantum mechanics, the Hamiltonian is regarded as the energy operator. Thus, the entry $\mathcal{T}_{00}$ of (4) is regarded as an expression for the Hamiltonian density

$$\mathcal{H} = \dot{\psi}\frac{\partial \mathcal{L}}{\partial \dot{\psi}} - \mathcal{L} . \tag{5}$$

It is explained below why an expression for density is required. Here, density properties can be readily taken from electrodynamics (see [2], pp. 73–75). Density must have the dimension $[L^{-3}]$ and be a 0-component of a 4-vector satisfying the continuity equation

$$j^{\mu}_{,\mu} = 0\,. \tag{6}$$

At this point, one may take either of the following alternatives:

A. Use the Hamiltonian density $\mathcal{H}$ together with the density expression and extract the Hamiltonian differential operator H, operating on ψ. The energy is an eigenvalue of this operator:

$$H\psi = E\psi\,, \tag{7}$$

Now the De Broglie relation

$$i\,\frac{\partial\psi}{\partial t} = E\psi\,, \tag{8}$$

yields the differential equation

$$i\,\frac{\partial\psi}{\partial t} = H\psi\,. \tag{9}$$

At this point one can construct a Hilbert space that includes all eigenfunctions of the Hamiltonian H.

B. Use the expression for density as an inner product for ψ and construct an orthonormal basis for the corresponding Hilbert space. Next construct the Hamiltonian matrix. For the i, j functions of the Hilbert space basis, the Hamiltonian matrix element is

$$H_{ij} = \int \mathcal{H}(\psi_i, \psi_{i,\mu}, \psi_j, \psi_{j,\nu})\, d^3x\,. \tag{10}$$

At this point, the Hamiltonian matrix is diagonalized and its energy eigenfunctions and eigenvalues are obtained.

Obviously, the mathematical structures of A and B are relevant to the same data. Therefore, both methods construct one and the same Hilbert space.

Equation (9) makes the following problem. As stated above, the Euler-Lagrange equation (3) is the system's equation of motion. On the other hand, (9) is *another* differential equation. Hence, the following requirement should be satisfied.

5. Requirement 1: The first order differential equation (9) should be consistent with the Euler-Lagrange equation of the theory (3).

The next two sections are devoted to two specific kinds of Lagrangian density of massive particles.

3 The Dirac field

It is shown here that the Dirac field satisfies the requirements derived above and that experimental data support the theory. The formulas are written in the standard notation [3,7].

The Dirac Lagrangian density is

$$\mathcal{L} = \bar{\psi}\left[\gamma^{\mu}(i\partial_{\mu} - eA_{\mu}) - m\right]\psi\,. \tag{11}$$

A variation with respect to $\bar{\psi}$ yields the corresponding Euler-Lagrange equation

$$\gamma^{\mu}(i\partial_{\mu} - eA_{\mu})\psi = m\psi\,. \tag{12}$$

As stated in section 2, the dimension of a Lagrangian density is $[L^{-4}]$. Therefore, the dimension of ψ is $[L^{-3/2}]$ and the Dirac 4-current

$$j^{\mu} = \bar{\psi}\gamma^{\mu}\psi \tag{13}$$

satisfies the required dimension and the continuity equation (6) (see [7], p. 9). Thus, the density is the 0-component of (13)

$$\rho_{Dirac} = \psi^{\dagger}\psi\,. \tag{14}$$

Substituting the Dirac Lagrangian density (11) into the general formula (5), one obtains the Dirac Hamiltonian density

$$\mathcal{H} = \psi^{\dagger}\left[\boldsymbol{\alpha}\cdot(-i\nabla - e\mathbf{A}) + \beta m + eV\right]\psi\,. \tag{15}$$

The density $\psi^{\dagger}\psi$ can be factored out from (15) and the expression enclosed within the square brackets is the Dirac Hamiltonian written as a differential operator. Its substitution into (9) yields the well known Dirac quantum mechanical equation

$$i\,\frac{\partial\psi}{\partial t} = \left[\boldsymbol{\alpha}\cdot(-i\nabla - e\mathbf{A}) + \beta m + eV\right]\psi\,. \tag{16}$$

It is also interesting to note that due to the linearity of the Dirac Lagrangian density (11) with respect to $\dot{\psi}$, the Dirac Hamiltonian density (15) as well as the Dirac Hamiltonian *do not contain a derivative of ψ with respect to time.* Hence, (16) is an explicit first order differential equation. It is easily seen that (16) agrees completely with the Euler-Lagrange equation (12) of the Dirac field. It follows that Requirement 1 which is written near the end of section 2 is satisfied.

A Hilbert space can be constructed from the eigenfunctions obtained as solutions of the Dirac equation (16). Here the inner product of the Hilbert space is based on the density of the Dirac function (14). The eigenfunctions of the Hamiltonian are used for building an orthonormal basis

$$\delta_{ij} = \int \psi_i^{\dagger}\psi_j\, d^3x\,. \tag{17}$$

Now, the form of an energy eigenfunction is

$$\psi(\mathbf{x}, t) = e^{-iEt}\chi(\mathbf{x}). \tag{18}$$

This form enables a construction of a Hilbert space based on $e^{-iEt}\chi(\mathbf{x})$ (the Schrödinger picture) *or* on $\chi(\mathbf{x})$ (the Heisenberg picture). Here, in the Heisenberg picture, wave functions of the Hilbert space are time independent.

As is well known, the non-relativistic limit of the Dirac equation agrees with the Pauli equation of a spinning electron (see [7], pp. 10–13). Hence, in accordance with the discussion presented in the first section, the Dirac relativistic quantum mechanical equation is consistent with the constraint imposed by the lower rank theory of the non-relativistic quantum mechanical equations. A related aspect of this constraint is the density represented by the Dirac wave function (14). Indeed, in the non-relativistic limit of Dirac's density, (14) reduces to the product of the "large" components of Dirac's ψ (see [7], pp. 10–13). Hence, (14) agrees with the density of the Pauli-Schrödinger equations $\Psi^{\dagger}\Psi$. This agreement also proves the compatibility of the Hilbert space of the Pauli-Schrödinger equations with that of the non-relativistic limit of the Dirac equation.

Beside the satisfactory status of Dirac's theory, his equation has an extraordinary success in describing experimental results of electrons and muons in general and in atomic spectroscopy in particular. Moreover, experiments of very high energy prove that quarks are spin-1/2 particles. In particular, high energy experimental data are consistent with the *point-like* nature of electrons, muons and quarks (see [8], pp. 271, 272; [9], p. 149). Hence, the Dirac equation satisfies item 3 of section 2.

4 Lagrangian density of second order equations

This section discusses second order quantum equations of motion (denoted here by SOE) which are derived from a Lagrangian density. The presentation is analogous to that of the previous section where the Dirac equation is discussed. The analysis concentrates on terms containing the highest order derivatives. Thus, the specific form of terms containing lower order derivatives is not written explicitly and all kinds of these terms are denoted by the acronym for Low Order Terms LOT. Second order quantum differential equations are derived from Lagrangian densities of the following form:

$$\mathcal{L} = \phi^{*}_{,\mu}\phi_{,\nu}g^{\mu\nu} + LOT. \tag{19}$$

This form of the Lagrangian density is used for the KG (see [3], p. 38) and the Higgs (see [4], p. 715) fields.

Applying the Euler-Lagrange variational principle to the Lagrangian density (19) one obtains a second order differential equation that takes the following form

$$g^{\mu\nu}\partial_{\mu}\partial_{\nu}\phi = LOT. \tag{20}$$

Here, unlike the case of the Dirac field, the dimension of ϕ is L^{-1}. Hence, in order to satisfy dimensional requirements, the expression for density must contain a derivative with respect to a coordinate. Thus, the 4-current takes the following form (see [3], p. 40; [10], p. 199)

$$j_{\mu} = i\left(\phi^{*}\phi_{,\mu} - \phi^{*}_{,\mu}\phi\right) + LOT \tag{21}$$

and the density is

$$\rho = i\left(\phi^{*}\dot{\phi} - \dot{\phi}^{*}\phi\right) + LOT. \tag{22}$$

The left hand side of (21) is a 4-vector. Therefore, ϕ of SOE is a Lorentz scalar.

Using the standard method (5), one finds that the Hamiltonian density takes the following form (see [3], p. 38; [10], p. 198)

$$\mathcal{H} = \dot{\phi}^{*}\dot{\phi} + (\nabla\phi^{*})\cdot(\nabla\phi) + LOT. \tag{23}$$

An analysis of these expressions shows that, unlike the case of the Dirac equation, SOE theories encounter problems. Some of these problems are listed below.

a. One cannot obtain a differential operator representing the Hamiltonian. Indeed, the highest order time derivative of the SOE density (22) is *anti-symmetric* with respect to $\dot{\phi}^{*}, \dot{\phi}$ whereas the corresponding term of the Hamiltonian density (23) is *symmetric* with respect to these functions (see [11], section 3, which discusses the KG equation). Hence, in the case of SOE theories, one cannot use method A of section 2 for constructing a Hilbert space for the system.

b. The density associated with the wave function ϕ is an indispensable element of the Hilbert space. The dependence of the SOE density (22) on time-derivatives proves that a SOE Hilbert space *is built on functions of the four space-time coordinates* x^{μ}. Hence, SOE cannot use the Heisenberg picture where the functions of the Hilbert space are time independent $\psi_H = \psi_S(t_0)$ (see [3], p. 7).

c. In the Schrödinger theory $\Psi^{*}\Psi$ represents density. It follows that like the case of the Dirac field, the dimension of this Ψ is $[L^{-3/2}]$. On the other hand, the dimension of the SOE function ϕ is $[L^{-1}]$. Therefore, the nonrelativistic limit of SOE theories is inconsistent with the Schrödinger theoretical structure.

d. Unlike the Dirac Hamiltonian, which is independent of time-derivatives of ψ, the SOE Hamiltonian density has a term containing the *bilinear product* $\dot{\phi}^{*}\dot{\phi}$. Hence, it is not clear how a SOE analogue of the fundamental quantum mechanical equation (9) can be created. Moreover, it should be proved that this *first order implicit nonlinear differential equation* is consistent with the corresponding *second order explicit differential equation* (20) of SOE, as stated by requirement 1 which is formulated near the end of section 2. Without substantiating the validity of the Hamiltonian, SOE

theories violate a constraint imposed by a lower rank theory which is explained in the lines that precede (4).

e. Some SOE theories apply to *real* fields (see [3], p. 26; [4], p. 19 etc.). New problems arise for these kinds of physical objects. Indeed, density cannot be defined for these particles (see [12], pp. 41–43). Moreover, a massive particle may be at rest. In this case its amplitude should be independent of time. But a *real* wave function has no phase. Therefore, in the case of a motionless real particle, *the time-derivative of its wave function vanishes identically*. For this reason, its physical behavior cannot be described by a differential equation with respect to time. Thus, a real SOE particle *cannot* be described by the SOE equation of motion (20) and it cannot have a Hamiltonian.

f. Another problem arises for a charged SOE particle. As stated in item *a* above, this particle cannot have a differential operator representing the Hamiltonian. Hence, method *A*, discussed near (7)-(9), cannot be used for a Hilbert space construction. Moreover, the inner product of a time-dependent Hilbert space is destroyed in the case of an external charge that approaches a charged SOE particle (see [13], pp. 59–61). Hence, method *B* does not hold either. It follows that a charged SOE particle has no Hamiltonian. Therefore, a charged SOE particle does not satisfy a constraint imposed by a lower rank theory.

This discussion points out theoretical difficulties of SOE fields. The experimental side responds accordingly. Point 3 of section 2 is useful for evaluating the data. Thus, a field $\psi(x^\mu)$ used in a Lagrangian density describes *an elementary point-like particle*. It turns out that as of today, no scalar pointlike particle has been detected.

In the history of physics, the three π-mesons have been regarded as KG particles and the electrically neutral π^0 member of this triplet was regarded as a Yukawa particle, namely, a real (pseudo) scalar KG particle. However, it has already been established that π-mesons are not elementary pointlike particles but composite particles made of $q\bar{q}$ and they occupy a nonvanishing spatial volume. Thus, as of today, there is no experimental support for an SOE particle. The theoretical and experimental SOE problems mentioned above are regarded seriously here. On the basis of the foregoing analysis, it is predicted here that no genuine elementary SOE particle will be detected. A special case is the following statement: a genuine Higgs particle will not be detected.

5 Irreducible representations of the Poincaré group

The profound significance of Wigner's analysis of the irreducible representations of the Poincaré group (see [14]; [15], pp. 44–53; [16], pp. 143–150) is described by the following words: "It is difficult to overestimate the importance of this paper, which will certainly stand as one of the great intellectual achievements of our century" (see [16], p. 149). Wigner's work shows that there are two physically relevant classes of irreducible representations of the Poincaré group. One class is characterized by a mass $m > 0$ and a spin s. The second class consists of cases where the self mass $m = 0$, the energy $E > 0$ and two values of helicity. (Helicity is the projection of the particle's spin in the direction of its momentum.) Two values of helicity $\pm s$ correspond to a spin s. Thus, each massive particle makes a basis for a specific irreducible representation that is characterized by the pair of values (m, s). A massless particle (like the photon) has a zero self mass, a finite energy and two values of helicity (for a photon, the helicity is ± 1).

A result of this analysis is that a system that is stable for a long enough period of time is a basis for an irreducible representation of the Poincaré group (see [15], pp. 48–50). Let us take a photon. Cosmic photons are detected by measuring devices on earth after traveling in space for a very very long time, compared to the duration of an electromagnetic interaction. Therefore, photons must belong to a unique irreducible representation of the Poincaré group. This conclusion is inconsistent with the idea of Vector Meson Dominance (VMD). VMD regards the photon as a linear combination of a massless real photon *and* a massive vector meson. (For a presentation of VMD see [9], pp. 296–303; [17].)

The VMD idea has been suggested in order to explain experimental results of scattering of energetic photons on nucleons. The main points of the data are:

i. The overall charge of a proton is $+e$ whereas the overall charge of a neutron vanishes. Therefore, charge constituents of a proton and a neutron are different.

ii. In spite of the data of the previous item, interaction of a hard photon with a proton is nearly the same as its interaction with a neutron.

The theoretical analysis of Wigner's work shows that VMD is unacceptable. Other inconsistencies of VMD with experimental data have also been published [18]. This state of affairs means that the currently accepted Standard Model has no theoretical explanation for the photon-nucleon interaction. This point is implicitly recognized by the PACS category of VMD which does not belong to a theoretical PACS class. Thus, on July 2009, VMD is included in the class of "Other models for strong interactions". Hence, the Standard Model does not provide a theoretical explanation for the scattering data of hard photons on nucleons.

6 Duality transformations of electromagnetic fields

Electromagnetic fields travel in vacuum at the speed of light. Therefore, the associated particle, namely — the photon, is massless. For this reason, it cannot be examined in a frame where it is motionless. This result means that the argument of

point e of section 4 does not hold for electromagnetic fields. It follows that, unlike the wave function of a massive particle, electromagnetic fields can be described by a Lagrangian density that depends on *real functions*. This well known fact is another aspect of the inherent difference between massive and massless particles, which has been obtained by Wigner and discussed in the previous section.

Thus, the system consists of electromagnetic fields whose equations of motion (Maxwell equations) are derived from a Lagrangian density and charge carrying massive particles whose equation of motion (the Lorentz force) is derived from a classical Lagrangian. Below, this theory is called ordinary electrodynamics. All quantities are described by real functions. The action of the system is (see [2], p. 75)

$$S = -\int m\sqrt{1-v^2}\,dt - \int A_\mu j^\mu_{(e)}\,d^4x - \\ - \frac{1}{16\pi}\int F_{\mu\nu}F^{\mu\nu}d^4x\,, \qquad (24)$$

where the subscript $_{(e)}$ indicates that j^μ is a current of electric charges, A_μ denotes the 4-potential of the electromagnetic fields, and $F^{\mu\nu}$ is the corresponding fields tensor

$$F_{\mu\nu} = A_{\nu,\mu} - A_{\mu,\nu}\,. \qquad (25)$$

The explicit form of this tensor is

$$F^{\mu\nu} = \begin{pmatrix} 0 & -E_x & -E_y & -E_z \\ E_x & 0 & -B_z & B_y \\ E_y & B_z & 0 & -B_x \\ E_z & -B_y & B_x & 0 \end{pmatrix}. \qquad (26)$$

These expressions enable one to derive Maxwell equations (see [2], pp. 78, 79 and 70, 71)

$$F^{\mu\nu}_{\ \ ,\nu} = -4\pi j^\mu_{(e)};\quad F^{*\mu\nu}_{\ \ ,\nu} = 0\,. \qquad (27)$$

Here $F^{*\mu\nu}$ is the dual tensor of $F^{\mu\nu}$

$$F^{*\mu\nu} = \begin{pmatrix} 0 & -B_x & -B_y & -B_z \\ B_x & 0 & E_z & -E_y \\ B_y & -E_z & 0 & E_x \\ B_z & E_y & -E_x & 0 \end{pmatrix}. \qquad (28)$$

These tensors satisfy the following relation

$$F^{*\mu\nu} = \frac{1}{2}\,\varepsilon^{\mu\nu\alpha\beta}F_{\alpha\beta}\,, \qquad (29)$$

where $\varepsilon^{\mu\nu\alpha\beta}$ is the completely antisymmetric unit tensor of the fourth rank.

The Lorentz force, which describes the motion of a charged particle, is obtained from a variation of the particle's coordinates (see [2], pp. 49–51)

$$ma^\mu_{(e)} = eF^{\mu\nu}v_\nu\,. \qquad (30)$$

The foregoing expressions describe the well established theoretical structure of ordinary electrodynamics. Let us see the results of introducing duality transformations. Duality transformations (also called duality rotations by $\pi/2$) of electromagnetic fields take the following form (see [19], pp. 252, 551; [20], p. 1363)

$$\mathbf{E} \to \mathbf{B},\quad \mathbf{B} \to -\mathbf{E}\,. \qquad (31)$$

These transformations can be put into the following tensorial form

$$F^{\mu\nu} \to F^{*\mu\nu};\quad F^{*\mu\nu} \to -F^{\mu\nu}. \qquad (32)$$

An examination of the *homogeneous* Maxwell equations

$$F^{\mu\nu}_{\ \ ,\nu} = 0;\quad F^{*\mu\nu}_{\ \ ,\nu} = 0, \qquad (33)$$

proves that they are invariant under the duality transformations (32). On the other hand, an inequality is obtained for the inhomogeneous Maxwell equation

$$F^{*\mu\nu}_{\ \ ,\nu} \neq -4\pi j^\mu_{(e)}. \qquad (34)$$

This problem can be settled by the introduction of the notion of magnetic monopoles (called briefly monopoles). Thus, duality transformations of the electromagnetic fields (32) are augmented by the following transformation that relates charges and monopoles

$$e \to g;\quad g \to -e\,, \qquad (35)$$

where g denotes the monopole strength.

Two things are established at this point:

1. The theoretical foundation of ordinary electrodynamics (24), and its equations of motion (27) and (30).
2. The mathematical form of duality transformations (32) and (35).

Now, a theory for a system of monopoles and electromagnetic fields (called below monopole electrodynamics) is obtained from the application of duality transformations to ordinary electrodynamics. The action principle of this system is

$$S = -\int m\sqrt{1-v^2}\,dt - \int A_{(m)\mu}j^\mu_{(m)}\,d^4x - \\ - \frac{1}{16\pi}\int F^*_{(m)\mu\nu}F^{*\mu\nu}_{(m)}\,d^4x\,, \qquad (36)$$

where the subscript (m) denotes that the quantities pertain to monopole electrodynamics. Here the fields are derived from a 4-potential

$$F^*_{(m)\mu\nu} = A_{(m)\nu,\mu} - A_{(m)\mu,\nu}\,, \qquad (37)$$

which is analogous to (25). Maxwell equations of monopole electrodynamics are

$$F^*_{(m)}{}^{\mu\nu}_{\ \ ,\nu} = -4\pi j^\mu_{(m)};\quad F_{(m)}{}^{\mu\nu}_{\ \ ,\nu} = 0 \qquad (38)$$

and the Lorentz force is

$$ma^{\mu}_{(m)} = g F^{*\mu\nu}_{(m)} v_{\nu} \,. \tag{39}$$

Thus, we have two theories for two distinct systems: ordinary electrodynamics for a system of charges and fields and monopole electrodynamics for a system of monopoles and fields. The first system does not contain monopoles and the second system does not contain charges. The problem is to find the form of a unified theory that describes the motion of charges, monopoles and fields. Below, such a theory is called a charge-monopoly theory. The charge-monopole theory is a higher rank theory whose domain of validity includes those of ordinary electrodynamics and of monopole electrodynamics as well. On undertaking this assignment, one may examine two postulates:

1. Electromagnetic fields of ordinary electrodynamics are identical to electromagnetic fields of monopole electrodynamics.
2. The limit of the charge-monopole theory for a system that does not contain monopoles agrees with ordinary electrodynamics and limit of the charge-monopole theory for a system that does not contain charges agrees with monopole electrodynamics.

It turns out that these postulates are mutually contradictory.

A charge-monopole theory that relies (implicitly) on the first postulate has been published by Dirac many years ago [21, 22]. (Ramifications of Dirac monopole theory can be found in the literature [20].) This theory shows the need to define physically unfavorable irregularities along strings. Moreover, the form of its limit that applies to a system of monopoles without charges is inconsistent with the theory of monopole electrodynamics, which is derived above from the duality transformations. Therefore, it does not satisfy the constraint imposed by a lower rank theory. The present experimental situation is that in spite of a long search, there is still no confirmation of the existence of a Dirac monopole (see [23], p. 1209).

The second postulate was used for constructing a different charge-monopole electrodynamics [24, 25]. This postulate guarantees that the constraints imposed by the two lower rank theories are satisfied. Moreover, this theory does not introduce new irregularities into electrodynamics. Thus, it is called below regular charge-monopole theory. The following statements describe important results of the regular charge-monopole theory: The theory can be derived from an action principle, whose limits take the form of (24) and (36), respectively. Charges do not interact with bound fields of monopoles; monopoles do not interact with bound fields of charges; radiation fields (namely, photons) of the systems are identical and charges as well as monopoles interact with them. Another result of this theory is that the size of an elementary monopole g is a free parameter. Hence, the theory is relieved from the huge and unphysical Dirac's monopole size $g^2 = 34.25$.

The regular charge-monopole theory is constructed on the basis of the second postulate. This point means that it is not guided by new experimental data. However, it turns out that it explains the important property of hard photon-nucleon interaction which is mentioned in the previous section. Indeed, just assume that quarks carry a monopole and postulate that the elementary monopole unit g is much larger then the electric charge e (probably $|g| \simeq 1$). This property means that photon-quark interaction depends mainly on monopoles and that the photon interaction with the quarks' electric charge is a small perturbation. Therefore, the very similar results of photon-proton and photon-neutron scattering are explained. (Note also that all baryons have a core which carries three units of magnetic charge that attracts the three valence quarks. The overall magnetic charge of a hadron vanishes.) Other kinds of experimental support for the regular charge-monopole theory have been published elsewhere [26].

7 Concluding remarks

This work is based on the main assumption of theoretical physics which states that results derived from physically relevant mathematical structures are expected to fit experimental data [27]. Three well known mathematical structures are used here: the variational principle, Wigner's analysis of the irreducible representations of the Poincaré group and duality transformations of electromagnetic fields.

The paper explains and uses three points which are either new or at least lack an adequate discussion in textbooks.

1. Constraints are imposed by a lower rank theory on properties of the corresponding limit of a higher rank theory (see a discussion in the Introduction).
2. The need to prove consistency between the Euler-Lagrange equation obtained from a Lagrangian density and the quantum mechanical equation $i\,\partial\psi/\partial t = H\psi$ which holds for the corresponding Hamiltonian.
3. The field function $\psi(x^{\mu})$ describes an elementary pointlike particle (see the discussion near (2)).

Points 1 and 2 are useful for a theoretical evaluation of the acceptability of specific physical ideas. Point 3 is useful for finding an experimental support for these ideas.

The main results of the analysis presented in this work are as follows: Dirac equation is theoretically consistent and has an enormous experimental support. Second order quantum mechanical equations (like the Klein-Gordon and the Higgs equations) suffer from many theoretical problems and have no experimental support. (π-mesons are not pointlike, therefore, they are not genuine Klein-Gordon particles.) Real fields cannot be used for a description of massive particles. The idea of Vector Meson Dominance is inconsistent with Wigner's analysis of the irreducible representations of the Poincaré group.

Therefore, VMD is unacceptable and the Standard Model has no theoretical explanation for the data of a scattering process of an energetic photon on nucleon. Monopole theories that introduce irregularities along strings are inconsistent with point 1 of this section and have no experimental support. The regular charge monopole theory [24–26] is consistent with point 1 and has experimental support.

Submitted on August 02, 2009 / Accepted on August 06, 2009

References

1. Rohrlich F. Classical charged particles. Addison-Wesley, Reading (Mass), 1965.
2. Landau L. D., Lifshitz E. M. The classical theory of fields. Elsevier, Amsterdam, 2005.
3. Bjorken J. D., Drell S. D. Relativistic quantum fields. McGraw-Hill, New York, 1965.
4. Peskin M. E., Schröder D. V. An introduction to quantum field theory. Addison-Wesley, Reading (Mass), 1995.
5. Landau L. D., Lifshitz E. M. Quantum Mechanics. Pergamon, London, 1959.
6. Schiff L. I. Quantum Mechanics. McGraw-Hill, New York, 1955.
7. Bjorken J. D., Drell S. D. Relativistic Quantum Mechanics. McGraw-Hill, New York, 1964.
8. Perkins D. H. Introduction to high energy physics. Addison-Wesley, Menlo Park (CA), 1987.
9. Frauenfelder H., Henley E. M. Subatomic physics. Prentice Hall, Englewood Cliffs, 1991.
10. Pauli W., Weisskopf V. The quantization of the scalar relativistic wave equation. *Helv. Phys. Acta*, 1934, v. 7, 709–731. English translation: Miller A. I. Early Quantum Electrodynamics. University Press, Cambridge, 1994. pp. 188–205. (In the text, page references apply to the English translation.)
11. Comay E. Further diffculties with the Klein-Gordon equation. *Apeiron*, 2005, v. 12, 26–46.
12. Berestetskii V. B., Lifshitz E. M., Pitaevskii L. P., Quantum Electrodynamics. Pergamon, Oxford, 1982.
13. Comay E. The significance of density in the structure of quantum theories. *Apeiron* 2007, v. 14, 50–64.
14. Wigner E. On unitary representations of the inhomogeneous Lorentz group. *Ann. Math.* 1939, v. 40, 149–204.
15. Schweber S. S. An introduction to relativistic quantum field theory. Harper & Row, New York, 1964.
16. Sternberg S. Group theory and physics. Cambridge University Press, Cambridge, 1994.
17. Bauer T. H., Spital R. D., Yennie D. R., Pipkin F. M. The hadronic properties of the photon in high-energy interactions. *Rev. Mod. Phys.* 1978, v. 50, 261–436.
18. Comay E. Remarks on photon-hadron interactions. *Apeiron* 2003, v. 10, 87–103.
19. Jackson J. D. Classical Electrodynamics. John Wiley, New York, 1975.
20. Goddard P., Olive D. I. Magnetic monopoles in gauge field theories. *Rep. Prog. Phys.*, 1978, v. 41, 1357–1437.
21. Dirac P. A. M. Quantized singularities in the electromagnetic field. *Proc. Royal Soc. A*, 1931, v. 133, 60–72.
22. Dirac P. A. M. The theory of magnetic poles. *Phys. Rev.*, 1948, v. 74, 817–830.
23. Amsler C. et al. Review of particle physics. *Phys. Lett. B*, 2008, v. 667, 1–1340.
24. Comay E. Axiomatic deduction of equations of motion in classical electrodynamics. *Nuovo Cimento B*, 1984, v. 80, 159–168.
25. Comay E. Charges, monopoles and duality relations. *Nuovo Cimento B*, 1995, v. 110, 1347–1356.
26. Comay E. A regular theory of magnetic monopoles and its implications. Published in *Has the Last Word Been Said on Classical Electrodynamics?* Editors: A. Chubykalo, V. Onoochin, A. Espinoza, and R. Smirnov-Rueda. Rinton Press, Paramus (NJ), 2004.
27. Wigner E. P. The unreasonable effectiveness of mathematics in the natural sciences. *Comm. in Pure and Appl. Math.*, 1960, v. 13, 1–14.

Progress in Physics **is an American scientific journal on advanced studies in physics, registered with the Library of Congress (DC, USA): ISSN 1555-5534 (print version) and ISSN 1555-5615 (online version). The journal is peer reviewed and listed in the abstracting and indexing coverage of: Mathematical Reviews of the AMS (USA), DOAJ of Lund University (Sweden), Zentralblatt MATH (Germany), Scientific Commons of the University of St. Gallen (Switzerland), Open-J-Gate (India), Referential Journal of VINITI (Russia), etc.** ***Progress in Physics*** **is an open-access journal published and distributed in accordance with the Budapest Open Initiative: this means that the electronic copies of both full-size version of the journal and the individual papers published therein will always be acessed for reading, download, and copying for any user free of charge. The journal is issued quarterly (four volumes per year).**

Electronic version of this journal:
http://www.ptep-online.com

Postal address for correspondence:

Department of Mathematics and Science
University of New Mexico
200 College Road, Gallup, NM 87301, USA

Printed in the United States of America